

Accumulation and Transformation of Halogenated Biphenyl and Diphenyl Ethers in Urban Sediments

BY

AZIVY CHE AZIZ

B.S., University of Wisconsin-Madison, 2007

M.S., University of Illinois at Chicago, 2011

THESIS

Submitted in partial fulfillment of the requirement
for the degree of Doctor of Philosophy in Civil Engineering
in the Graduate College of
the University of Illinois at Chicago, 2014

Chicago, Illinois

Defense Committee:

Karl J. Rockne, Chair and Advisor

Amid Khodadoust

An Li, Environmental and Occupational Health Sciences

Neil Sturchio, Earth and Environmental Sciences

Asha Rani, College of Medicine

Erik Christensen, University of Wisconsin-Milwaukee

This thesis is dedicated to my husband, Steven Schwanbeck, who loves me unconditionally, to my parents, Aziz Ismail and Ivy Aimi Abdullah, who taught me to be humble in everything except my ambitions, to my in-law family, who have kept my focus on the future, and to Pendek, who stayed up with me every night.

Thank you!

ACKNOWLEDGEMENT

I would like to take this opportunity to thank my advisor, Dr. Karl Rockne for the guidance and support throughout my graduate career. Dr. Karl Rockne has been an excellent mentor who always encourages career and personal development, and provided advice where needed the most. I would like to thank my thesis committee members, Professor Amid Khodadoust, Professor An Li, Professor Neil Sturchio, Dr. Asha Rani, and Professor Erik Christensen for their time, valuable discussions, and constructive feedback. I am especially grateful to Professor An Li for the opportunity to work in a dynamic and supportive research group, Professor Neil Sturchio for discussion on radionuclide data interpretation, Professor Erik Christensen for valuable suggestions in source apportionment and analysis, and Dr. Asha Rani for excellent molecular biology input.

I am eternally grateful to Dr. Hua Wei for providing accurate chemical data, Dr. Yonghong Zou for providing multivariate linear regression input and sampling help, and Meg Corcoran and Armen Phogosyan for radionuclide data measurement and analysis. I am fortunate to have the friendship of my fellow lab-mates Dr. Kelly Granberg, Dr. Priscilla Viana, Solidea Bonina, Raja Kaliappan, Gregory Bourgon, Soheil Hosseini, Kamel Babaeiveli, Michael Bolouri, Dr. Jayashree Jayaraj, Dr. Ke Yin, and Dr. Xiuhong Zhao.

Finally, I extend my heartfelt thank you to my husband, family, in-law family, and friends for their love and support throughout this journey. I would not have come this far without you!

Table of Content

CHAPTER 1. INTRODUCTION	1
CHAPTER 2. LITERATURE REVIEW	4
2.1.1. Polybrominated Diphenyl Ethers (PBDEs)	4
2.1.2. Polychlorinated Biphenyls (PCBs)	6
2.2. PBDE and PCB Chemical Properties.....	7
2.3. PBDE and PCB Environmental Releases	14
2.4. PBDEs and PCBs in Sediments.....	16
2.5. Microbial Facilitated PBDE and PCB Transformation	20
2.5.1. Microbial Facilitated PCB Transformation	20
2.5.2. Microbial Facilitated PBDE Transformation.....	24
2.6. PBDE and PCB Transport Processes In The Sediment Phase.....	30
2.6.1. Partitioning between solute and solid phase.....	31
2.6.2. Chemical Diffusion Process.....	34
2.6.3. Advection process.....	35
2.6.4. Adsorption To Black Carbon.....	37
CHAPTER 3. CHARACTERIZATION OF URBAN CHICAGO SEDIMENTS CONTAMINATED WITH POLYBROMINATED DIPHENYL ETHERS (PBDEs) AND POLYCHLORINATED BIPHENYLS (PCBs)	40
3.0. Abstract.....	40
3.1. Introduction.....	41
3.2. Objectives.....	42
3.3. Experimental Section.....	44
3.3.1. Sampling Sites	44
3.3.2. Physical Characterization	48
3.3.3. Sediment Dating	50
3.2.4. Chemical Characterization	50
3.4. Results and Discussion.....	52
3.4.1. Field Measurement	52
3.4.2. Physical Characterization	54
3.4.3. PBDEs and PCBs in The Metropolitan Chicago Sediment Cores	59
3.4.4. Evaluating evidence of <i>in-situ</i> degradation of PBDEs and PCBs	81
3.5. Conclusion	93

CHAPTER 4. INDIGINEOUS MICROBIAL COMMUNITY IN PBDE AND PCB IMPACTED SEDIMENTS IN METROPOLITAN CHICAGO AND ARKANSAS	96
4.0. Abstract.....	96
4.1. Introduction.....	97
4.2. Objectives and Hypotheses.....	98
4.3. Experimental Method	99
4.4. Results and Discussion.....	103
4.4.1. Indigenous Microbial Community In Surface Sediments	103
4.4.1.1. General Sequence Statistics In Surface Sediments	103
4.4.1.2. Species Richness and Abundance In Surface Sediments.....	104
4.4.1.3. Dominant Microbial Community Distribution In Surface Sediments	107
4.4.1.4. Similarity In Microbial Community Composition In Surface Sediments	126
4.4.1.5. Microorganisms With Confirmed PBDE and PCB Degradation Capability	131
4.4.1.6. Composition of PBDE and PCB Potential Degradars In Surface Sediments	135
4.4.1.7. Composition of Unclassified <i>Bacteria</i> In Surface Sediments.....	143
4.4.2. Indigenous Microbial Community In AMW Sediment Segments.....	146
4.4.2.1. General Sequence Statistics.....	146
4.4.2.2. Microbial Species Richness and Abundance In AMW Sediment Segments.....	147
4.4.2.3. Dominant Microbial Community Composition In AMW Sediment Segments	148
4.4.2.4. Similarity in Microbial Community Composition In AMW Sediment Segments.....	162
4.4.2.5. Potential PBDE and PCB Degradars In AMW Sediment Segments	166
4.4.2.6. Unclassified <i>Bacteria</i> Composition In AMW Sediment Segments.....	174
4.5. Conclusion	177
CHAPTER 5. MODELLING POLYBROMINATED DIPHENYL ETHER (PBDE) AND POLYCHLORINATED BIPHENYL (PCB) <i>IN-SITU</i> MASS TRANSPORT IN NATURAL SEDIMENT COLUMNS.....	185
5.0. Abstract.....	185
5.1. Introduction.....	186
5.2. Objective and Hypotheses	187
5.3. Materials and Methods.....	188
5.3.1. Overview	188
5.3.2. Mathematical Model Development.....	190
5.3.3. Model Parameterization.....	193
5.3.3.1. Sorbate Properties	193

5.3.3.2. Sorbent Properties	199
5.3.3.3. Initial Sediment Concentration.....	201
5.4. Results and Discussion.....	201
5.4.1. Sorbate Properties	201
5.4.2. Sorbent Properties	204
5.4.3. Sediment Porewater Partitioning Coefficient (K_d)	207
5.4.4. PBDE and PCB Diffusion And Advection-Diffusion Transport Processes	221
5.4.4.1. Observed Diffusivities (D_{obs}).....	221
5.4.4.2. Advective Velocity (v)	231
5.4.4.3. Drivers Of Diffusion And Advection-Diffusion Transport Processes.	240
5.4.4.4. PBDE and PCB Aqueous Phase Breakthrough Under Diffusion and Advection-Diffusion Conditions.....	242
5.5. PBDE and PCB Mass Removal From The Sediment Columns	281
5.6. The Impact of PBDE and PCB In-Situ Mass Flux On Sediment Contaminant Profile	324
5.7. Conclusion	355
CHAPTER 6. CONCLUSION	359
Appendix A	376
Appendix B	401
Appendix C	419
Appendix D	423
CURRICULUM VITAE.....	593

List of Tables

Table 2.1. Reported production of TBBPA, HBCD, and PBDEs in the Americas, Europe, and Asia in metric tons in the year 2001.....	5
Table 2.2. Physical properties of selected PBDE congeners.	9
Table 2.3 (Cont.). Physical properties of selected PCB congeners.....	10
Table 2.4: Reported PBDE concentrations in surface sediments in the U.S.....	18
Table 2.5. PBDE and PCB concentrations in the U.S. surface sediments reported in selected recent studies.	20
Table 2.6. Summary of reported empirical correlations to estimate KOC values from KOW values for hydrophobic and halogenated compounds. Number of compound (n), regression coefficient (R^2), and standard error (SE) is included when available.	33
Table 3.1. Site identifiers and latitude and longitude for sampling sites in Chicago (CBC, CWP, CLC) and IGC (IGC09 and IGC13).	45
Table 3.2. Summary of PBDE and PCB concentrations in Chicago and IGC sediment cores.	61
Table 3.3. Sedimentation and chemical loading for Chicago, IGC and Arkansas sample sites. Shown are net deposition rates of black carbon (BC), Σ_{49} PBDEs, and Σ_{132} PCBs in surface sediment, and inventories for core depth as shown.	69
Table 3.4. PBDE and PCB concentrations in selected recent studies of surface sediments in the U.S.	71
Table 3.5. Multiple linear square regression (MLSR) predicted loading for PBDE TMs and PCB Aroclor mixtures, PBDE and PCB MLSR residuals and MLSR fit in Chicago metropolitan and AMW sediment cores.	90
Table 3.6. Indicators of PBDE and PCB <i>in-situ</i> transformation.	95
Table 4.1. Physicochemical properties of sediment segments selected for DNA extractions.	100
Table 4.2. Barcode sequences for primers Gray28f and Gray519R used in Roche 454 pyrosequencing.	102
Table 4.3. Pre- and post-quality control sequence statistics for surface sediments.	104
Table 4.4. A summary of reported microorganisms and the associated microbial taxa with confirmed PBDE degradation capability under laboratory simulations.	132
Table 4.5. A summary of reported microorganisms and the associated microbial taxa with confirmed PCB degradation capability under laboratory conditions.....	134
Table 4.6: Sequence statistic for AMW sediment segments.....	146
Table 4.7a: Overview of potential PBDE and PCB degraders in all surface sediments in relations to other <i>in-situ</i> microbial facilitated dehalogenation indicators.	179
Table 4.7b: Overview of potential PBDE and PCB degraders in AMW sediment segments in relations to other <i>in-situ</i> microbial facilitated dehalogenation indicators.	183
Table 5.1. Summary of 79 and 111 discrete log K_{OW} values for PBDEs and PCBs used to guide Monte Carlo simulations for mass transport modeling.	194
Table 5.2: C_{Sat} values (ug/L) predicted by USEPA EPI v4.11 software. Comparison to literature values is included when available.....	196
Table 5.3. Predicted D_{mol} ($m^2/year$) at 25°C for PBDE and PCB homologs as calculated by the Hayduk-Laudie method. When available, predicted values were compared to literature value.	198
Table 5.4. Sediment column properties used to guide the Monte Carlo simulations.....	199

Table 5.5. Range of silt and sand composition in the sediment columns (as determined by agglomerate particle size distribution analysis and USDA particle size classification) and predicted range of K_h values (assuming linear proportionality to agglomerate particle size).....	200
Table 5.6. Distribution of \sum_{49} PBDEs and \sum_{132} PCBs concentrations (ng/g) in the sediment samples at specific percentile.	201
Table 5.7a (Cont.): PBDE and PCB Monte Carlo predicted log K_d values at the 95th percentile for organic carbon (OC) only sorption, and organic carbon and black carbon (OCBC) sorption.	208
Table 5.8. Monte Carlo predicted PBDE and PCB log K_{BC} values at the 95 th percentile in all sediment cores.	218
Table 5.9 (Cont.): The 95 th percentile Monte Carlo predicted PBDE and PCB observe diffusivity (D_{obs}) values for organic carbon only sorption (OC), and organic carbon and black carbon co-sorption (OCBC).	223
Table 5.10 (Cont): Monte Carlo predicted PBDE and PCB ν values at the 95th percentile for organic carbon only sorption (OC), and organic carbon and black carbon (OCBC) co-sorption.....	232
Table 5.13. PBDE and PCB homologs that reached 10% (non-underlined) and 1% (underlined) C/C_o breakthrough under diffusion with organic carbon only sorption (D(OC)) (black), diffusion with organic carbon and black carbon co-sorption (D(OCBC)) (charcoal), advection-diffusion with organic carbon only sorption (A(OC)) (dark grey), and advection-diffusion with organic carbon and black carbon co- sorption (A(OCBC)) (light grey).	266
Table 5.12: Summary of PBDE and PCB transport process dominance as predicted by the Monte Carlo 95 th percentile transport parameter values. The black dots indicate advection dominance and hollow dots indicate diffusion dominance. Organic carbon only sorption processes are signified by no line whereas organic carbon and black carbon co-sorption is signified by an underline below the dots.....	280
Table 5.13. Multivariate least square regression (MLSR) and multivariate least median square regression (MLMS) analyses for PBDE homolog and z-transformed composition in select sediment cores.....	330
Table 5.14: Summary of the fraction of mass leaving the sediment boundary layer relative to initial mass in the sediment phase under advection-diffusion with organic carbon only sorption for transport time of 40 years.	354

List of Figures

Figure 2.1: Homolog distribution in the three PBDE technical mixtures (Saytex 102E, DE-79, and DE-71) manufactured in North America.	5
Figure 2.2: Homolog distribution in eight selected PCB Aroclor mixtures manufactured in North America.....	7
Figure 2.3: Structure of a) decachlorobiphenyl (PCB-209) and b) decabromodiphenyl ether (BDE-209). These are the complete halogenated structure of PCBs and PBDEs with the maximum ten chlorine or bromine substitutions, respectively. PBDE and PCB congeners can have 0 to 10 bromine or chlorine substitutions. Structure was generated in National Center for Biotechnology Information (NCBI) PubChem Sketcher. ⁽¹⁷⁾	8
Figure 2.4: PBDE and PCB predicted log K_{OW} values as a function of homolog number from QSPR empirical correlations.....	13
Figure 2.3: An illustration of the isotherm sorption model. Adapted from Alvarez and Illman (2005). ⁽¹⁴⁰⁾	38
Figure 3.1: a) Sampling sites located in the metropolitan Chicago area and b) land use categorization by the United States Geological Services 2006 National Land Cover Database. Higher levels of development correspond to darker hue. Land use map was generated using ArcMap version 10.	44
Figure 3.2: Oxidation reduction potential (ORP) in sediment cores CBC, CWP, and CLC. Shaded areas represent ORP levels consistent with anaerobic metabolism and non-shaded areas represent ORP levels consistent with facultative metabolism.	53
Figure 3.4: Wet and dry densities (ρ_w and ρ_d , respectively) (a-e), and solids and water content (% Solid and % Water, respectively) (f-j) in cores CBC (a,f), CWP (b,g), CLC (c,h), IGC09 (d,i), and IGC13 (e,j). Error bars represent the standard deviation of triplicate measurements. These error bars were typically smaller than the data symbol.....	56
Figure 3.5: Organic matter (OM), organic carbon (OC), and black carbon (BC) concentrations in CBC(a,e), CWP (b,g), CLC (c,h), IGC09 (d,i), and IGC13 (e,j). Error bars represent the standard deviation of triplicate measurements. These error bars were typically smaller than the data symbol.	57
Figure 3.7b: a-e) Concentrations of PCB homologs ($\Sigma H1-3$, $\Sigma H4-6$, $\Sigma H7-9$, and H10) and f-j) homolog compositions in cores a,f) CBC, b,g) CWP, c,h) CLC, d,i) IGC09, and e,j) IGC13. The lower x-axes scales in panels a-e are for H10 concentration.....	63
Figure 3.8: a-c) Σ_{49} PBDEs and Σ_{132} PCBs in 1960-2010 and d-f) Saytex 102E, DE-71, and DE-79 TMs in cores a,d) CWP, b,e) IGC13, and c,f) AMW. DE-71 TM contains congeners 17, 28/33, 47, 49, 66, 85, 99, 100, 126/155, 138, 139, and 154. DE-79 TM contains congeners 138, 153, 183, 196, 197, 201, 203, 207, and 208. Saytex 102E TM contains congeners 206 and 209. Statistically significant regressions at the 95% CI are in bold and 90% CI are non-bold. Regressions were split between periods of active pond use (pre-1989) and non-active use (post-1989) in AMW. Note the different scale on the y-axes in panels a-f.	76
Figure 3.9: a) Compositions and b) BDE-209 normalized compositions of tetra-, penta-, hexa-, and hepta-PBDE homologs in Chicago, IGC, AR, MC, and Great Lakes surface sediments. In a) Σ_{10} PBDEs represent sum of commonly analyzed PBDE congeners in all the studies (BDE-28, 47, 66, 100, 99, 85, 154, 153, 183, and 209). In the Great Lakes, composition values shown represent average of all sampling sites within the lake. References: (1) ⁽¹⁵¹⁾ ; (2) ⁽¹⁹⁴⁾ ; (3) ⁽⁴⁵⁾ ; (4) ⁽⁴⁹⁾ ; and (5): ⁽⁴⁷⁾	79

Figure 3.10: Ratio of Σ_{10} PBDEs and Σ_8 PCBs concentrations in sediments from the metropolitan Chicago, AR, and the Great Lakes. Σ_{10} PBDEs represent sum of commonly analyzed PBDE congeners in all the studies (BDE-28, 47, 66, 100, 99, 85, 154, 153, 183, and 209). URB-W are Chicago metropolitan waterborne deposition-dominated cores (CBC, CLC, and IGC13), URB-Atm is Chicago metropolitan atmospheric-deposition dominated core (CWP), AR-W is AR waterborne deposition-dominated cores (AMW), AR-Source are southern AR production area cores (AED and ACL), AR-Atm are northeastern AR atmospheric-deposition impacted cores (AJL, AOT, and AFR), and the Great Lakes. Lines represent 1:1 and 10:1 ratios of Σ_{10} PBDE: Σ_8 PCBs.	80
Figure 3.11: Weighted average PBDE congener mole fractions at a) CBC, b) CWP, c) CLC, and d) IGC13 compared to PBDE TMs congener mole fractions in e) DE-71, f) DE-79, and g) Saytex 102E. BDE-209 is shown on right y-axes; note different left y-axes for a) to d) and e) to g).	84
Figure 3.12: PBDE MLSR residuals calculated as site average congener mole fraction minus MLSR regression model assuming LMM in cores a) CBC, b) CWP, c) CLC, d) IGC13, and e) AMW. Note that BDE-209 is shown on the right y-axes at a 10x scale.	85
Figure 3.14: PCB MLSR residual values calculated as site average congener mole fraction minus MLSR regression model assuming LMM in cores a) CBC, b) CWP, c) CLC, d) IGC13, and e) AMW.	88
Figure 3.15: Concentration of <i>ortho</i> - (red), <i>meta</i> - (blue), and <i>para</i> - (green) chlorines (a-e) and bromines (f-j) in non-co-eluting PCB/PBDE congeners, as well as mean Cl/PCB or Br/PBDE molecule (yellow) as a function of depth in cores a, f) CBC, b, g) CWP, c, h) CLC, d,i) IGC13, and e, j) AMW. Co-eluting congeners are not included as their substitution pattern is not certain. Note the different scale on the x-axis for cores IGC13 and AMW.	92
Figure 4.1: Distribution of unassigned and unclassified sequences, and unclassified <i>Bacteria</i> in selected sediment samples as identified by a) SSU, b) RDP, c) m5RNA, and d) Greengenes databases in MGRAST.	103
Figure 4.2: Rarefaction curves measuring microbial species richness in all surface sediments.	105
Figure 4.3: Microbial species diversity, as alpha diversity based on RDP database classification ⁽²⁰⁴⁾ in a) AR and b) Chicago metropolitan surface sediments. Grey bar indicates primarily atmospheric- deposition-dominated cores, hollow bar indicates primarily hydraulic-deposition-dominated cores, and patterned bar indicates likely mixed exposure pathways. AR sites are in order of increasing distance from PBDE source zone.	106
Figure 4.6a: Overview of the microbial community in ACL surface sediment as characterized by the RDP database ⁽²⁰⁴⁾ . Visualization was generated in Krona. ⁽²⁰⁵⁾	112
Figure 4.6b: Overview of the microbial community in AED surface sediment as characterized by the RDP database ⁽²⁰⁴⁾ . Visualization was generated in Krona. ⁽²⁰⁵⁾	113
Figure 4.6c: Overview of the microbial community in AFR surface sediment as characterized by the RDP database. ⁽²⁰⁴⁾ Visualization was generated in Krona. ⁽²⁰⁵⁾	114
Figure 4.6d: Overview of the microbial community in AJL surface sediment as characterized by the RDP database. ⁽²⁰⁴⁾ Visualization was generated in Krona. ⁽²⁰⁵⁾	115
Figure 4.6e: Overview of the microbial community in AMW surface sediment as characterized by the RDP database. ⁽²⁰⁴⁾ Visualization was generated in Krona. ⁽²⁰⁵⁾	116
Figure 4.6f: Overview of the microbial community in AOT surface sediment as characterized by the RDP database. ⁽²⁰⁴⁾ Visualization was generated in Krona. ⁽²⁰⁵⁾	117
Figure 4.6g: Overview of the microbial community in CBC surface sediment as characterized by the RDP database. ⁽²⁰⁴⁾ Visualization was generated in Krona. ⁽²⁰⁵⁾	118

Figure 4.6h: Overview of the microbial community in CLC surface sediment as characterized by the RDP database. ⁽²⁰⁴⁾ Visualization was generated in Krona. ⁽²⁰⁵⁾	119
Figure 4.6i: Overview of the microbial community in CWP surface sediment as characterized by the RDP database. ⁽²⁰⁴⁾ Visualization was generated in Krona. ⁽²⁰⁵⁾	120
Figure 4.6j: Overview of the microbial community in IGC09 surface sediment as characterized by the RDP database. ⁽²⁰⁴⁾ Visualization was generated in Krona. ⁽²⁰⁵⁾	121
Figure 4.6k: Overview of the microbial community in IGC13 surface sediment as characterized by the RDP database. ⁽²⁰⁴⁾ Visualization was generated in Krona. ⁽²⁰⁵⁾	122
Figure 4.7: Visual comparison of the microbial phylum composition in all surface sediments as classified by the RDP database ⁽²⁰⁴⁾ through MGRAST interface. ⁽²⁰³⁾ The unclassified notation in the legend refers to unclassified sequences of the <i>Bacteria</i> origin.	125
Figure 4.8: Hierarchical cluster map analysis performed in MGRAST ⁽²⁰³⁾ and microbial community composition at the class operational taxonomic unit (OTU) level for all surface sediments. The hierarchical cluster map used the Manhattan method to cluster and measure distance or similarity in the microbial community composition in the surface sediments.	129
Figure 4.9: Result of principal component analysis (PCA) of microbial community distribution performed in MGRAST. ⁽²⁰³⁾ Arrow points in the direction of average increased distance between four AR sites to two PBDE manufacturing facilities. Dotted lines reflect surface sediment grouping in the hierarchical cluster map shown in Figure 4.8.	130
Figure 4.10: a) Abundance of potential PBDE degraders by the microbial class operational taxonomic unit (OTU) level, b) \sum_{49} PBDEs concentration and total abundance of potential PBDE degraders, and c) residual value of multiple linear square regression (MLSR) between three PBDE technical mixtures (DE-71, DE-79, and Saytex 102E TMs) versus total abundance of potential PBDE degraders in surface sediments. Note that the surface sediments in the x-axis of panel a) are arranged by hierarchical cluster map in Figure 4.7. In b) and c), vertical bold lines represent the 50 th percentile value of the abundance of potential PBDE degraders and horizontal lines represent the 50 th percentile value for \sum_{49} PBDEs concentration and PBDE MLSR residual value, respectively, in all surface sediments.	136
Figure 4.11: a) Abundance of \sum_{LMW} PBDE and \sum_{HMW} PBDE potential degraders, b) $\sum_{LMW/HMW}$ PBDE potential degraders ratio, c) \sum_{49} PBDEs concentration versus $\sum_{LMW/HMW}$ PBDE potential degraders, d) \sum_{HI-6} PBDEs versus $\sum_{LMW/HMW}$ PBDE potential degraders, e) MLSR residual value versus $\sum_{LMW/HMW}$ PBDE potential degraders, and f) a scale-up of the region surrounded by bold grey oval in e) in all surface sediments. In c) through f), vertical bold lines represent the 50 th percentile value of ratio of \sum_{1-6Br} PBDE potential degraders over $\sum_{>6Br}$ PBDE potential degraders and horizontal lines represent the 50 th percentile value of $\sum_{LMW/HMW}$ PBDE potential degraders ratio, \sum_{HI-6} PBDEs composition, and MLSR residual value (e-f). Note the different scales on the x and y-axes.	140
Figure 4.12: a) Abundance of potential PCB degraders by the microbial class operational taxonomic unit (OTU) level, b) \sum_{132} PCBs concentration and abundance of potential PCB degraders, and c) PCB MLSR residual value and abundance of potential PCB degraders in all surface sediments. Note that surface sediments in a) were arranged by hierarchical cluster map in Figure 4.7. In b) and c), vertical bold lines represent the 50 th percentile value of PBDE potential degraders abundance and horizontal lines represent the 50 th percentile value for \sum_{132} PBDEs concentrations and MLSR residual values, respectively, in all surface sediments.	142
Figure 4.13: Abundance of potential PBDE and PCB degraders OTUs in all surface sediments. Also shown are the 1:2, 1:1 and 2:1 slopes as bold lines.	143

Figure 4.14: a) Abundance of unclassified <i>Bacteria</i> , b) microbial alpha diversity as a function of unclassified <i>Bacteria</i> abundance, c) \sum_{49} PBDEs concentration as a function of unclassified <i>Bacteria</i> abundance, d) \sum_{132} PCBs concentration as a function of unclassified <i>Bacteria</i> abundance, e) PBDE MLSR residual value versus unclassified <i>Bacteria</i> abundance, and f) PCB MLSR residual value versus unclassified <i>Bacteria</i> abundance in all surface sediment samples. Y-axes on c) and d) are in log scale. Note the different scale of the x and y-axes.	145
Figure 4.15: Rarefaction curves for a) the upper AMW sediment segments with sediment age of 2010 to 1995, and b) the lower AMW sediment segments with sediment age of 1990 to 1965.	147
Figure 4.15: Microbial species diversity as measured by the alpha diversity index for the AMW sediment segments.	148
Figure 4.16a: Overview of the microbial community in AMW 2005(8-10cm) sediment segments as identified by the RDP database. ⁽²⁰⁴⁾ Visualization was generated in Krona. ⁽²⁰⁵⁾	153
Figure 4.16c: Overview of the microbial community in AMW 1995 (24-26cm) sediment segments as identified by the RDP database. ⁽²⁰⁴⁾ Visualization was generated in Krona. ⁽²⁰⁵⁾	155
Figure 4.16d: Overview of the microbial community in AMW 1990 (30-32cm) sediment segments as identified by the RDP database. ⁽²⁰⁴⁾ Visualization was generated in Krona. ⁽²⁰⁵⁾	156
Figure 4.16e: Overview of the microbial community in AMW 1985 (34-36cm) sediment segments as identified by the RDP database. ⁽²⁰⁴⁾ Visualization was generated in Krona. ⁽²⁰⁵⁾	157
Figure 4.16f: Overview of the microbial community in AMW 1980 (38-40cm) sediment segments as identified by the RDP database. ⁽²⁰⁴⁾ Visualization was generated in Krona. ⁽²⁰⁵⁾	158
Figure 4.16g: Overview of the microbial community in AMW 1975 (42-44cm) sediment segments as identified by the RDP database. ⁽²⁰⁴⁾ Visualization was generated in Krona. ⁽²⁰⁵⁾	159
Figure 4.16h: Overview of the microbial community in AMW 1970 (46-48cm) sediment segments as identified by the RDP database. ⁽²⁰⁴⁾ Visualization was generated in Krona. ⁽²⁰⁵⁾	160
Figure 4.16i: Overview of the microbial community in AMW 1965 (48-50cm) sediment segments as identified by the RDP database. ⁽²⁰⁴⁾ Visualization was generated in Krona. ⁽²⁰⁵⁾	161
Figure 4.17: Hierarchical cluster map analysis performed in MGRAS ⁽²⁰³⁾ and microbial community structure at the class operational taxonomic unit (OTU) level for AMW sediment segments. The hierarchical cluster map used the Manhattan method to cluster and measure distance or similarity in the microbial community structure in the surface sediments.	163
Figure 4.18: Principal component analysis (PCA) of the microbial community structure in AMW sediment segments. Dotted hollow spheres reflect the grouping based on microbial community clustering (Figure 4.17). Dark grey shaded area represents the upper sediment segments (AMW 2010 to AMW 1995) and light grey shaded area represents the lower sediment segments (AMW 1990 to AMW 1965).	164
Figure 4.19: a) Abundance of potential PBDE degraders at the class operational taxonomic unit (OTU) level, b) \sum_{49} PBDEs concentration and total abundance of potential PBDE degraders, and c) PBDE MLSR residual value versus total abundance of potential PBDE potential degraders in AMW sediment segments. In b) and c), vertical bold lines represent the 50 th percentile value of the potential PBDE degraders abundance and horizontal lines represent the 50 th percentile value for \sum_{49} PBDEs concentration and MLSR residual value, respectively, in all AMW sediment segments.	168
Figure 4.20: a) Abundance of \sum_{LMW} PBDE and \sum_{HMW} PBDE potential degraders, b) ratio of \sum_{LMW}/\sum_{HMW} PBDE potential degraders, c) \sum_{49} PBDEs concentration versus ratio of \sum_{LMW}/\sum_{HMW} PBDE potential degraders, d) \sum_{H1-6} PBDEs composition versus ratio of \sum_{LMW}/\sum_{HMW} PBDE potential degraders, e) PBDE	

MLSR residual value versus ratio of $\sum_{\text{LMW/HMW}}$ PBDE potential degraders, and f) a scale-up of the region surrounded by bold grey oval in e) for all AMW sediment segments. In c) through f), vertical bold lines represent the 50 th percentile value of ratio of $\sum_{\text{LMW/HMW}}$ PBDE potential degraders and horizontal lines represent the 50 th percentile value for \sum_{49} PBDEs concentration (c), $\sum_{\text{H1-6}}$ PBDEs composition (d), and MLSR residual value (e-f). Y-axes in c) is in the log scale. Note the different scales on the x and y-axes in c) through f).	170
Figure 4.21: a) Abundance of potential PCB degraders by the microbial class operational taxonomic unit (OTU) level, b) \sum_{132} PCBs concentrations and total abundance of potential PCB degraders, and c) PCB MLSR residual value versus total abundance of potential PCB degraders in all surface sediments. In b) and c), vertical bold lines represent the 50 th percentile value of the potential PCB degraders abundance and horizontal bold lines represent the 50 th percentile value for \sum_{132} PBDEs concentration and MLSR residual value, respectively, in all AMW sediment segments.	173
Figure 4.22: a) Abundance of PBDE and PCB potential degraders in all surface sediments, and b) a scale up of the area bounded by the bold grey oval in a). Also shown are the 1:2, 1:1 and 2:1 slopes in bold lines. Note the different scale in x- and y-axes in a) and b).	174
Figure 4.23: a) Abundance of unclassified <i>Bacteria</i> , b) alpha diversity as a function of unclassified <i>Bacteria</i> abundance, c) \sum_{49} PBDEs concentration as a function of unclassified <i>Bacteria</i> abundance, d) \sum_{132} PCBs concentration as a function of unclassified <i>Bacteria</i> abundance, e) PBDE MLSR residual value versus unclassified <i>Bacteria</i> abundance, and f) PCB MLSR residual value versus unclassified <i>Bacteria</i> abundance in AMW sediment segments. Y-axes on c) and d) are in log scale. Note that the y-axes in e) and f) and x-axes on c) and d) are not in the same scale.	176
Figure 5.1: Schematic showing the hypothetical scenario used to model PBDE and PCB mass transport through diffusion and advection-diffusion transport in natural sediment column provided with the most mobile mass transport conditions. Boundary conditions are shown on the left and segment boundary layers are bounded by the box with dotted lines. It is assumed that contaminants move equally in both upward and downward directions.	189
Figure 5.2: Application of known transport processes equations to evaluate PBDE and PCB in-situ mass transport in natural sediment columns. Note that diffusion and advection-diffusion can occur in both upward and downward directions.	193
Figure 5.3: Molecular diffusivities (D_{mol}) at 25°C for PBDE and PCB homologs as predicted by Hayduk-Laudie method compared to literature PCB molecular diffusivities at 15°C. ⁽²²⁷⁾ Molecular diffusivities (D_{mol}) values for phenanthrene, pyrene, tetrachlorobiphenyl, dodecane, and tetradecane were indicated by horizontal lines. ^(120, 121, 222)	198
Figure 5.4: Distribution of log K_{OW} (a-b) and log K_{OC} (c-d) as predicted by 50,000 Monte Carlo simulations for PBDEs (a,c) and PCBs (b,d). The 5 th and 95 th percentiles are shown by the error bars, the box covers the 25 th to 75 th percentiles, and the middle vertical bar in the box is the 50 th percentile. For log K_{OW} , average values used in Monte Carlo simulations are denoted by a hollow triangle. Log K_{OW} values predicted by empirical correlations are denoted by * and ^x (* is Equation 2.1 and ^x is Equation 2.2 for PBDEs; * is Equation 2.3 and ^x is Equation 2.4 for PCBs). USEPA EPI predicted log K_{OW} values are denoted by hollow sphere. Average literature log K_{OW} values are denoted by hollow diamond. For log K_{OC} , ^x are values predicted by EPI MCI method and * are values predicted by EPI KOW method.	203
Figure 5.6: Distribution range of fraction organic carbon (f_{OC}) (a) and fraction black carbon (f_{BC}) (b) in the sediment columns as predicted by 50,000 Monte Carlo simulations.	205

Figure 5.7: Porosity (a) and particle density (b) distribution range in the sediment columns as predicted by 50,000 Monte Carlo simulations.	206
Figure 5.8: Hydraulic conductivity (K_h) distributions in the sediment columns as predicted by 50,000 Monte Carlo simulation.	207
Figure 5.9a: The 95 th percentile PBDE log K_d values as predicted by 50,000 Monte Carlo simulations for organic carbon only sorption (K_d (OC)) and organic carbon and black carbon co-sorption (K_d (OCBC)) in AR sediment columns. Y-axes are homologs 1 through 10 (H1-H10).	210
Figure 5.9b: The 95 th percentile PBDE log K_d values as predicted by 50,000 Monte Carlo simulations for organic carbon only sorption (K_d (OC)) and organic carbon and black carbon co-sorption (K_d (OCBC)) in Chicago and IGC sediment columns. Y-axes are homologs 1 through 10 (H1-H10).	211
Figure 5.9c: The 95 th percentile PCB log K_d values as predicted by 50,000 Monte Carlo simulations for organic carbon only sorption (K_d (OC)) and organic carbon and black carbon co-sorption (K_d (OCBC)) in AR sediment columns. Y-axes are homologs 1 through 10 (H1-H10).	212
Figure 5.9d: The 95 th percentile PCB log K_d values as predicted by 50,000 Monte Carlo simulations for organic carbon only sorption (K_d (OC)) and organic carbon and black carbon co-sorption (K_d (OCBC)) in Chicago and IGC sediment columns. Y-axes are homologs 1 through 10 (H1-H10).	213
Figure 5.10a: Ratios of PBDE and PCB sediment porewater partitioning coefficient under sorption to organic carbon only and organic carbon and black carbon co-sorption ($\log K_d$ (OCBC)/ $\log K_d$ (OC)) in AR sediment cores	216
Figure 5.10b: Ratios of PBDE and PCB sediment porewater partitioning coefficient under sorption to organic carbon only and organic carbon and black carbon co-sorption ($\log K_d$ (OCBC)/ $\log K_d$ (OC)) in Chicago and IGC sediment cores.	217
Figure 5.11a: The 95 th percentile PBDE and PCB black carbon-porewater partitioning coefficient ($\log K_{BC}$) as predicted by Monte Carlo simulation in AR sediment cores.	219
Figure 5.11b: The 95 th percentile PBDE and PCB black carbon-porewater partitioning coefficient ($\log K_{BC}$) as predicted by Monte Carlo simulation in Chicago and IGC sediment cores.	220
Figure 5.12a: The Monte Carlo 95 th percentile predicted PBDE D_{obs} (m ² /yr) values for organic carbon only sorption (D_{obs} (OC)), and organic carbon and black carbon co-sorption (D_{obs} (OCBC)) in AR sediment columns.	225
Figure 5.12b: The Monte Carlo 95 th percentile predicted PBDE D_{obs} (m ² /yr) values for organic carbon only sorption (D_{obs} (OC)), and organic carbon and black carbon co-sorption (D_{obs} (OCBC)) in Chicago and IGC sediment columns.	226
Figure 5.12c: The Monte Carlo 95 th percentile predicted PCB D_{obs} (m ² /yr) values for organic carbon only sorption (D_{obs} (OC)), and organic carbon and black carbon co-sorption (D_{obs} (OCBC)) in AR sediment columns.	227
Figure 5.12d: The Monte Carlo 95 th percentile predicted PCB D_{obs} (m ² /yr) values for organic carbon only sorption (D_{obs} (OC)), and organic carbon and black carbon co-sorption (D_{obs} (OCBC)) in Chicago and IGC sediment columns.	228
Figure 5.13a: Ratios of observed diffusivity under organic carbon and black carbon co-sorption (D_{obs} (OCBC)) to observed diffusivity under organic carbon only sorption (D_{obs} (OC)) for PBDE and PCB homologs in AR sediment columns.	229
Figure 5.13b: Ratios of observed diffusivity under organic carbon and black carbon co-sorption (D_{obs} (OCBC)) to observed diffusivity under organic carbon only sorption (D_{obs} (OC)) for PBDE and PCB homologs in Chicago and IGC sediment columns.	230

Figure 5.14a: Monte Carlo predicted 95 th percentile PBDE ν values for organic carbon only sorption (ν (OC)), and organic carbon and black carbon co-sorption (ν (OCBC)) in AR sediment columns.....	234
Figure 5.14b: Monte Carlo predicted 95 th percentile PBDE ν values for organic carbon only sorption (ν (OC)), and organic carbon and black carbon co-sorption (ν (OCBC)) in Chicago and IGC sediment columns.....	235
Figure 5.14c: Monte Carlo predicted 95 th percentile PCB ν values for organic carbon only sorption (ν (OC)), and organic carbon and black carbon co-sorption (ν (OCBC)) in AR sediment columns.....	236
Figure 5.14d: Monte Carlo predicted 95 th percentile PCB ν values for organic carbon only sorption (ν (OC)), and organic carbon and black carbon co-sorption (ν (OCBC)) in Chicago and IGC sediment columns.....	237
Figure 5.15a: Ratio of advective velocity under organic carbon and black carbon co-sorption (ν (OCBC)) to advective velocity under organic carbon sorption (ν (OC)) for PBDE and PCB homologs in AR sediment columns.....	238
Figure 5.15b: Ratios of advective velocity under organic carbon and black carbon co-sorption (ν (OCBC)) to advective velocity under organic carbon sorption (ν (OC)) for PBDE and PCB homologs in Chicago and IGC sediment columns.....	239
Figure 5.16: Transport parameter component loadings in factors 1, 2, and 3 (F1, F2, and F3) which explained 45.35, 24.07, and 16.24% of the variance, respectively. Negative component loading indicates an inverse relationship between the transport parameter and factor.	240
Figure 5.17: Factor loadings plot for the transport parameters as generated in SYSTAT version 13.	241
Figure 5.18a: PBDE breakthrough (C/C_o) in core ACL under the 95 th percentile transport parameter values for diffusion with organic carbon only sorption (D(OC)), and organic carbon and black carbon co-sorption (D(OCBC)) and under advection-diffusion with organic carbon only sorption (A(OC)), and organic carbon and black carbon co-sorption (A(OCBC)). Horizontal bold line marks the 10% C/C_o breakthrough and horizontal dotted line marks the 1% C/C_o breakthrough. Data not shown indicates that C/C_o breakthrough is below 1E-18%.	244
Figure 5.18b: PBDE breakthrough (C/C_o) in core AED under the 95 th percentile transport parameter values for diffusion with organic carbon only sorption (D(OC)), and organic carbon and black carbon co-sorption (D(OCBC)) and under advection-diffusion with organic carbon only sorption (A(OC)), and organic carbon and black carbon co-sorption (A(OCBC)). Horizontal bold line marks the 10% C/C_o breakthrough and horizontal dotted line marks the 1% C/C_o breakthrough. Data not shown indicates that C/C_o breakthrough is below 1E-18%.	245
Figure 5.18c: PBDE breakthrough (C/C_o) in core AFR under the 95 th percentile transport parameter values for diffusion with organic carbon only sorption (D(OC)), and organic carbon and black carbon co-sorption (D(OCBC)) and under advection-diffusion with organic carbon only sorption (A(OC)), and organic carbon and black carbon co-sorption (A(OCBC)). Horizontal bold line marks the 10% C/C_o breakthrough and horizontal dotted line marks the 1% C/C_o breakthrough. Data not shown indicates that C/C_o breakthrough is below 1E-18%.	246
Figure 5.18d: PBDE breakthrough (C/C_o) in core AJL under the 95 th percentile transport parameter values for diffusion with organic carbon only sorption (D(OC)), and organic carbon and black carbon co-sorption (D(OCBC)) and under advection-diffusion with organic carbon only sorption (A(OC)), and organic carbon and black carbon co-sorption (A(OCBC)). Horizontal bold line marks the 10% C/C_o breakthrough and horizontal dotted line marks the 1% C/C_o breakthrough. Data not shown indicates that C/C_o breakthrough is below 1E-18%.	247

Figure 5.17e: PBDE breakthrough (C/C_o) in core AMW under the 95 th percentile transport parameter values for diffusion with organic carbon only sorption (D(OC)), and organic carbon and black carbon co-sorption (D(OCBC)) and under advection-diffusion with organic carbon only sorption (A(OC)), and organic carbon and black carbon co-sorption (A(OCBC)). Horizontal bold line marks the 10% C/C_o breakthrough and horizontal dotted line marks the 1% C/C_o breakthrough. Data not shown indicates that C/C_o breakthrough is below 1E-18%.	248
Figure 5.18f: PBDE breakthrough (C/C_o) in core AOT under the 95 th percentile transport parameter values for diffusion with organic carbon only sorption (D(OC)), and organic carbon and black carbon co-sorption (D(OCBC)) and under advection-diffusion with organic carbon only sorption (A(OC)), and organic carbon and black carbon co-sorption (A(OCBC)). Horizontal bold line marks the 10% C/C_o breakthrough and horizontal dotted line marks the 1% C/C_o breakthrough. Data not shown indicates that C/C_o breakthrough is below 1E-18%.	249
Figure 5.18g: PBDE breakthrough (C/C_o) in core CBC under the 95 th percentile transport parameter values for diffusion with organic carbon only sorption (D(OC)), and organic carbon and black carbon co-sorption (D(OCBC)) and under advection-diffusion with organic carbon only sorption (A(OC)), and organic carbon and black carbon co-sorption (A(OCBC)). Horizontal bold line marks the 10% C/C_o breakthrough and horizontal dotted line marks the 1% C/C_o breakthrough. Data not shown indicates that C/C_o breakthrough is below 1E-18%.	250
Figure 5.18j: PBDE breakthrough (C/C_o) in core IGC09 under the 95 th percentile transport parameter values for diffusion with organic carbon only sorption (D(OC)), and organic carbon and black carbon co-sorption (D(OCBC)) and under advection-diffusion with organic carbon only sorption (A(OC)), and organic carbon and black carbon co-sorption (A(OCBC)). Horizontal bold line marks the 10% C/C_o breakthrough and horizontal dotted line marks the 1% C/C_o breakthrough. Data not shown indicates that C/C_o breakthrough is below 1E-18%.	253
Figure 5.18k: PBDE breakthrough (C/C_o) in core IGC13 under the 95 th percentile transport parameter values for diffusion with organic carbon only sorption (D(OC)), and organic carbon and black carbon co-sorption (D(OCBC)) and under advection-diffusion with organic carbon only sorption (A(OC)), and organic carbon and black carbon co-sorption (A(OCBC)). Horizontal bold line marks the 10% C/C_o breakthrough and horizontal dotted line marks the 1% C/C_o breakthrough. Data not shown indicates that C/C_o breakthrough is below 1E-18%.	254
Figure 5.18l: PCB breakthrough (C/C_o) in core ACL under the 95 th percentile transport parameter values for diffusion with organic carbon only sorption (D(OC)), and organic carbon and black carbon co-sorption (D(OCBC)) and under advection-diffusion with organic carbon only sorption (A(OC)), and organic carbon and black carbon co-sorption (A(OCBC)). Horizontal bold line marks the 10% C/C_o breakthrough and horizontal dotted line marks the 1% C/C_o breakthrough. Data not shown indicates that C/C_o breakthrough is below 1E-18%.	255
Figure 5.18m: PCB breakthrough (C/C_o) in core AED under the 95 th percentile transport parameter values for diffusion with organic carbon only sorption (D(OC)), and organic carbon and black carbon co-sorption (D(OCBC)) and under advection-diffusion with organic carbon only sorption (A(OC)), and organic carbon and black carbon co-sorption (A(OCBC)). Horizontal bold line marks the 10% C/C_o breakthrough and horizontal dotted line marks the 1% C/C_o breakthrough. Data not shown indicates that C/C_o breakthrough is below 1E-18%.	256
Figure 5.18n: PCB breakthrough (C/C_o) in core AFR under the 95 th percentile transport parameter values for diffusion with organic carbon only sorption (D(OC)), and organic carbon and black carbon co-	

sorption (D(OCBC)) and under advection-diffusion with organic carbon only sorption (A(OC)), and organic carbon and black carbon co-sorption (A(OCBC)). Horizontal bold line marks the 10% C/Co breakthrough and horizontal dotted line marks the 1% C/Co breakthrough. Data not shown indicates that C/Co breakthrough is below 1E-18%. 257

Figure 5.18o: PCB breakthrough (C/Co) in core AJL under the 95th percentile transport parameter values for diffusion with organic carbon only sorption (D(OC)), and organic carbon and black carbon co-sorption (D(OCBC)) and under advection-diffusion with organic carbon only sorption (A(OC)), and organic carbon and black carbon co-sorption (A(OCBC)). Horizontal bold line marks the 10% C/Co breakthrough and horizontal dotted line marks the 1% C/Co breakthrough. Data not shown indicates that C/Co breakthrough is below 1E-18%. 258

Figure 5.18p: PCB breakthrough (C/Co) in core AMW under the 95th percentile transport parameter values for diffusion with organic carbon only sorption (D(OC)), and organic carbon and black carbon co-sorption (D(OCBC)) and under advection-diffusion with organic carbon only sorption (A(OC)), and organic carbon and black carbon co-sorption (A(OCBC)). Horizontal bold line marks the 10% C/Co breakthrough and horizontal dotted line marks the 1% C/Co breakthrough. Data not shown indicates that C/Co breakthrough is below 1E-18%. 259

Figure 5.18q: PCB breakthrough (C/Co) in core AOT under the 95th percentile transport parameter values for diffusion with organic carbon only sorption (D(OC)), and organic carbon and black carbon co-sorption (D(OCBC)) and under advection-diffusion with organic carbon only sorption (A(OC)), and organic carbon and black carbon co-sorption (A(OCBC)). Horizontal bold line marks the 10% C/Co breakthrough and horizontal dotted line marks the 1% C/Co breakthrough. Data not shown indicates that C/Co breakthrough is below 1E-18%. 260

Figure 5.18r: PCB breakthrough (C/Co) in core CBC under the 95th percentile transport parameter values for diffusion with organic carbon only sorption (D(OC)), and organic carbon and black carbon co-sorption (D(OCBC)) and under advection-diffusion with organic carbon only sorption (A(OC)), and organic carbon and black carbon co-sorption (A(OCBC)). Horizontal bold line marks the 10% C/Co breakthrough and horizontal dotted line marks the 1% C/Co breakthrough. Data not shown indicates that C/Co breakthrough is below 1E-18%. 261

Figure 5.18s: PCB breakthrough (C/Co) in core CLC under the 95th percentile transport parameter values for diffusion with organic carbon only sorption (D(OC)), and organic carbon and black carbon co-sorption (D(OCBC)) and under advection-diffusion with organic carbon only sorption (A(OC)), and organic carbon and black carbon co-sorption (A(OCBC)). Horizontal bold line marks the 10% C/Co breakthrough and horizontal dotted line marks the 1% C/Co breakthrough. Data not shown indicates that C/Co breakthrough is below 1E-18%. 262

Figure 5.18t: PCB breakthrough (C/Co) in core CWP under the 95th percentile transport parameter values for diffusion with organic carbon only sorption (D(OC)), and organic carbon and black carbon co-sorption (D(OCBC)) and under advection-diffusion with organic carbon only sorption (A(OC)), and organic carbon and black carbon co-sorption (A(OCBC)). Horizontal bold line marks the 10% C/Co breakthrough and horizontal dotted line marks the 1% C/Co breakthrough. Data not shown indicates that C/Co breakthrough is below 1E-18%. 263

Figure 5.18u: PCB breakthrough (C/Co) in core IGC09 under the 95th percentile transport parameter values for diffusion with organic carbon only sorption (D(OC)), and organic carbon and black carbon co-sorption (D(OCBC)) and under advection-diffusion with organic carbon only sorption (A(OC)), and organic carbon and black carbon co-sorption (A(OCBC)). Horizontal bold line marks the 10% C/Co

breakthrough and horizontal dotted line marks the 1% C/C_o breakthrough. Data not shown indicates that C/C_o breakthrough is below $1E-18\%$	264
Figure 5.18v: PCB breakthrough (C/C_o) in core IGC13 under the 95 th percentile transport parameter values for diffusion with organic carbon only sorption (D(OC)), and organic carbon and black carbon co-sorption (D(OCBC)) and under advection-diffusion with organic carbon only sorption (A(OC)), and organic carbon and black carbon co-sorption (A(OCBC)). Horizontal bold line marks the 10% C/C_o breakthrough and horizontal dotted line marks the 1% C/C_o breakthrough. Data not shown indicates that C/C_o breakthrough is below $1E-18\%$	265
Figure 5.19a: PBDE breakthrough (C/C_o) (a-c) and change of breakthrough rate ($\Delta (C/C_o)$) (d-f) at $x=0.02m$ in cores ACL (a,d), AED (b,e), and AFR (c,f) predicted from the Monte Carlo 95 th percentile transport parameter values for diffusion with organic carbon only sorption (D(OC)), diffusion with organic carbon and black carbon co-sorption (D(OCBC)), advection-diffusion with organic carbon only sorption (A(OC)), and advection-diffusion with organic carbon and black carbon co-sorption (A(OCBC)).	269
Figure 5.19b: PBDE breakthrough (C/C_o) (a-c) and change of breakthrough rate ($\Delta (C/C_o)$) (d-f) at $x=0.02m$ in cores AJL (a,d), AMW (b,e), and AOT (c,f) predicted from the Monte Carlo 95 th percentile transport parameter values for diffusion with organic carbon only sorption (D(OC)), diffusion with organic carbon and black carbon co-sorption (D(OCBC)), advection-diffusion with organic carbon only sorption (A(OC)), and advection-diffusion with organic carbon and black carbon co-sorption (A(OCBC)).	270
Figure 5.19c: PBDE breakthrough (C/C_o) (a-c) and change of breakthrough rate ($\Delta (C/C_o)$) (d-f) at $x=0.02m$ in cores CBC (a,d), CLC (b,e), and CWP (c,f) predicted from the Monte Carlo 95 th percentile transport parameter values for diffusion with organic carbon only sorption (D(OC)), diffusion with organic carbon and black carbon co-sorption (D(OCBC)), advection-diffusion with organic carbon only sorption (A(OC)), and advection-diffusion with organic carbon and black carbon co-sorption (A(OCBC)).	271
Figure 5.19d: PBDE breakthrough (C/C_o) (a-b) (left panels) and change of breakthrough rate ($\Delta (C/C_o)$) (c-d) at $x=0.02m$ in cores IGC09 (a,c) and IGC13 (b,d) predicted from the Monte Carlo 95 th percentile transport parameter values for diffusion with organic carbon only sorption (D(OC)), diffusion with organic carbon and black carbon co-sorption (D(OCBC)), advection-diffusion with organic carbon only sorption (A(OC)), and advection-diffusion with organic carbon and black carbon co-sorption (A(OCBC)).	272
Figure 5.19e: PCB breakthrough (C/C_o) (a-c) and change of breakthrough rate ($\Delta (C/C_o)$) (d-f) at $x=0.02m$ in cores ACL (a,c), AED (b,e), and AFR (c,f) predicted from the Monte Carlo 95 th percentile transport parameter values for diffusion with organic carbon only sorption (D(OC)), diffusion with organic carbon and black carbon co-sorption (D(OCBC)), advection-diffusion with organic carbon only sorption (A(OC)), and advection-diffusion with organic carbon and black carbon co-sorption (A(OCBC)).	273
Figure 5.19f: PCB breakthrough (C/C_o) (a-c) and change of breakthrough rate ($\Delta (C/C_o)$) (d-f) at $x=0.02m$ in cores AJL (a,c), AMW (b,e), and AOT (c,f) predicted from the Monte Carlo 95 th percentile transport parameter values for diffusion with organic carbon only sorption (D(OC)), diffusion with organic carbon and black carbon co-sorption (D(OCBC)), advection-diffusion with organic carbon only sorption (A(OC)), and advection-diffusion with organic carbon and black carbon co-sorption (A(OCBC)).	274

Figure 5.19g: PCB breakthrough (C/C_o) (a-c) and change of breakthrough rate ($\Delta (C/C_o)$) (d-f) at $x=0.02\text{m}$ in cores CBC (a,d), CLC (c,e), and CWP (c,f) predicted from the Monte Carlo 95th percentile transport parameter values for diffusion with organic carbon only sorption (D(OC)), diffusion with organic carbon and black carbon co-sorption (D(OCBC)), advection-diffusion with organic carbon only sorption (A(OC)), and advection-diffusion with organic carbon and black carbon co-sorption (A(OCBC)).

..... 275
 Figure 5.19h: PCB breakthrough (C/C_o) (a-b) and change of breakthrough rate ($\Delta (C/C_o)$) (c-d) at $x=0.02\text{m}$ in cores IGC09 (a,c) and IGC13 (b,d) predicted from the Monte Carlo 95th percentile transport parameter values for diffusion with organic carbon only sorption (D(OC)), diffusion with organic carbon and black carbon co-sorption (D(OCBC)), advection-diffusion with organic carbon only sorption (A(OC)), and advection-diffusion with organic carbon and black carbon co-sorption (A(OCBC)). 276

Figure 5.20: Cumulative C/C_o under diffusion with organic carbon sorption (D(OC)), diffusion with organic carbon and black carbon co-sorption (D(OCBC)), advection-diffusion with organic carbon sorption (A(OC)), and advection-diffusion with organic carbon and black carbon co-sorption (A(OCBC)) in all sediment cores as predicted from the Monte Carlo 95th percentile transport parameter values for 1000 years simulation period. 277

Figure 5.21: Cumulative Peclet number in all sediment cores under advection-diffusion with organic carbon only sorption (A(OC)) (a,c) and organic carbon and black carbon co-sorption (A(OCBC)) (b,d) predicted by the Monte Carlo 95th percentile transport parameter values for PBDE (a,b) and PCB (c,d) homologs. 279

Figure 5.22a: Predicted flux of PBDE homologs in core ACL under advection-diffusion with organic carbon only sorption (A(OC)) conditions for initial sediment concentration of 36100, 60, and 0.2 ng/g at 40, 100, and 1000 years. Panels a,c, and e show aqueous phase concentration leaving the sediment boundary layer ($C_{aq|x=0.02\text{m},t}$), aqueous phase breakthrough percentage ($C_{aq|x=0.02\text{m},t}/C_{aq|x=0\text{m},t=0\text{year}}$) (%BT), and ratio of aqueous phase concentration under local equilibrium assumption to saturation concentration ($C_{aq|x=0\text{m},t}/C_{\text{sat}}$) (%Sat) represented as grey triangle with vertical lines, hollow sphere, and star, respectively. Panels b,d, and f show mass leaving the sediment boundary layer at specific time ($M_{t|t}$) and ratio of mass leaving the sediment boundary layer to initial starting mass ($M_{t|t}/M_{\text{sed}|t=0\text{year}}$) represented as grey triangle with vertical lines and hollow sphere, respectively. For $C_{aq|x=0.02\text{m},t}$ and $M_{t|t}$, median values as predicted by the 50th percentile transport parameters values are represented by the grey triangle while upper and lower boundaries as predicted by the 95th and 5th percentile transport parameters values are indicated by the vertical lines. Lines that did not appear in figure are below the minimum y-axes values. X-axes are homologs 1 to 10 (H1 to H10). 283

Figure 5.22b: Predicted flux of PBDE homologs in core AED under advection-diffusion with organic carbon only sorption (A(OC)) conditions for initial sediment concentration of 36100, 60, and 0.2 ng/g at 40, 100, and 1000 years. Panels a,c, and e show aqueous phase concentration leaving the sediment boundary layer ($C_{aq|x=0.02\text{m},t}$), aqueous phase breakthrough percentage ($C_{aq|x=0.02\text{m},t}/C_{aq|x=0\text{m},t=0\text{year}}$) (%BT), and ratio of aqueous phase concentration under local equilibrium assumption to saturation concentration ($C_{aq|x=0\text{m},t}/C_{\text{sat}}$) (%Sat) represented as grey triangle with vertical lines, hollow sphere, and star, respectively. Panels b,d, and f show mass leaving the sediment boundary layer at specific time ($M_{t|t}$) and ratio of mass leaving the sediment boundary layer to initial starting mass ($M_{t|t}/M_{\text{sed}|t=0\text{year}}$) represented as grey triangle with vertical lines and hollow sphere, respectively. For $C_{aq|x=0.02\text{m},t}$ and $M_{t|t}$, median values as predicted by the 50th percentile transport parameters values are represented by the grey triangle while upper and lower boundaries as predicted by the 95th and 5th percentile transport parameters values are

indicated by the vertical lines. Lines that did not appear in figure are below the minimum y-axes values. X-axes are homologs 1 to 10 (H1 to H10). 284

Figure 5.22c: Predicted flux of PBDE homologs in core AFR under advection-diffusion with organic carbon only sorption (A(OC)) conditions for initial sediment concentration of 36100, 60, and 0.2 ng/g at 40, 100, and 1000 years. Panels a,c, and e show aqueous phase concentration leaving the sediment boundary layer ($C_{aq|x=0.02m,t}$), aqueous phase breakthrough percentage ($C_{aq|x=0.02m,t}/C_{aq|x=0m,t=0year}$) (%BT), and ratio of aqueous phase concentration under local equilibrium assumption to saturation concentration ($C_{aq|x=0m,t}/C_{sat}$) (%Sat) represented as grey triangle with vertical lines, hollow sphere, and star, respectively. Panels b,d, and f show mass leaving the sediment boundary layer at specific time ($M_{t|t}$) and ratio of mass leaving the sediment boundary layer to initial starting mass ($M_{t|t}/M_{sed|t=0year}$) represented as grey triangle with vertical lines and hollow sphere, respectively. For $C_{aq|x=0.02m,t}$ and $M_{t|t}$, median values as predicted by the 50th percentile transport parameters values are represented by the grey triangle while upper and lower boundaries as predicted by the 95th and 5th percentile transport parameters values are indicated by the vertical lines. Lines that did not appear in figure are below the minimum y-axes values. X-axes are homologs 1 to 10 (H1 to H10). 285

Figure 5.22d: Predicted flux of PBDE homologs in core AJL under advection-diffusion with organic carbon only sorption (A(OC)) conditions for initial sediment concentration of 36100, 60, and 0.2 ng/g at 40, 100, and 1000 years. Panels a,c, and e show aqueous phase concentration leaving the sediment boundary layer ($C_{aq|x=0.02m,t}$), aqueous phase breakthrough percentage ($C_{aq|x=0.02m,t}/C_{aq|x=0m,t=0year}$) (%BT), and ratio of aqueous phase concentration under local equilibrium assumption to saturation concentration ($C_{aq|x=0m,t}/C_{sat}$) (%Sat) represented as grey triangle with vertical lines, hollow sphere, and star, respectively. Panels b,d, and f show mass leaving the sediment boundary layer at specific time ($M_{t|t}$) and ratio of mass leaving the sediment boundary layer to initial starting mass ($M_{t|t}/M_{sed|t=0year}$) represented as grey triangle with vertical lines and hollow sphere, respectively. For $C_{aq|x=0.02m,t}$ and $M_{t|t}$, median values as predicted by the 50th percentile transport parameters values are represented by the grey triangle while upper and lower boundaries as predicted by the 95th and 5th percentile transport parameters values are indicated by the vertical lines. Lines that did not appear in figure are below the minimum y-axes values. X-axes are homologs 1 to 10 (H1 to H10). 286

Figure 5.22e: Predicted flux of PBDE homologs in core AMW under advection-diffusion with organic carbon only sorption (A(OC)) conditions for initial sediment concentration of 36100, 60, and 0.2 ng/g at 40, 100, and 1000 years. Panels a,c, and e show aqueous phase concentration leaving the sediment boundary layer ($C_{aq|x=0.02m,t}$), aqueous phase breakthrough percentage ($C_{aq|x=0.02m,t}/C_{aq|x=0m,t=0year}$) (%BT), and ratio of aqueous phase concentration under local equilibrium assumption to saturation concentration ($C_{aq|x=0m,t}/C_{sat}$) (%Sat) represented as grey triangle with vertical lines, hollow sphere, and star, respectively. Panels b,d, and f show mass leaving the sediment boundary layer at specific time ($M_{t|t}$) and ratio of mass leaving the sediment boundary layer to initial starting mass ($M_{t|t}/M_{sed|t=0year}$) represented as grey triangle with vertical lines and hollow sphere, respectively. For $C_{aq|x=0.02m,t}$ and $M_{t|t}$, median values as predicted by the 50th percentile transport parameters values are represented by the grey triangle while upper and lower boundaries as predicted by the 95th and 5th percentile transport parameters values are indicated by the vertical lines. Lines that did not appear in figure are below the minimum y-axes values. X-axes are homologs 1 to 10 (H1 to H10). 287

Figure 5.22f: Predicted flux of PBDE homologs in core AOT under advection-diffusion with organic carbon only sorption (A(OC)) conditions for initial sediment concentration of 36100, 60, and 0.2 ng/g at 40, 100, and 1000 years. Panels a,c, and e show aqueous phase concentration leaving the sediment

boundary layer ($C_{aq|x=0.02m,t}$), aqueous phase breakthrough percentage ($C_{aq|x=0.02m,t}/C_{aq|x=0m,t=0year}$) (%BT), and ratio of aqueous phase concentration under local equilibrium assumption to saturation concentration ($C_{aq|x=0m,t}/C_{sat}$) (%Sat) represented as grey triangle with vertical lines, hollow sphere, and star, respectively. Panels b,d, and f show mass leaving the sediment boundary layer at specific time ($M_{t|t}$) and ratio of mass leaving the sediment boundary layer to initial starting mass ($M_{t|t}/M_{sed|t=0year}$) represented as grey triangle with vertical lines and hollow sphere, respectively. For $C_{aq|x=0.02m,t}$ and $M_{t|t}$, median values as predicted by the 50th percentile transport parameters values are represented by the grey triangle while upper and lower boundaries as predicted by the 95th and 5th percentile transport parameters values are indicated by the vertical lines. Lines that did not appear in figure are below the minimum y-axes values. X-axes are homologs 1 to 10 (H1 to H10). 288

Figure 5.22g: Predicted flux of PBDE homologs in core CBC under advection-diffusion with organic carbon only sorption (A(OC)) conditions for initial sediment concentration of 36100, 60, and 0.2 ng/g at 40, 100, and 1000 years. Panels a,c, and e show aqueous phase concentration leaving the sediment boundary layer ($C_{aq|x=0.02m,t}$), aqueous phase breakthrough percentage ($C_{aq|x=0.02m,t}/C_{aq|x=0m,t=0year}$) (%BT), and ratio of aqueous phase concentration under local equilibrium assumption to saturation concentration ($C_{aq|x=0m,t}/C_{sat}$) (%Sat) represented as grey triangle with vertical lines, hollow sphere, and star, respectively. Panels b,d, and f show mass leaving the sediment boundary layer at specific time ($M_{t|t}$) and ratio of mass leaving the sediment boundary layer to initial starting mass ($M_{t|t}/M_{sed|t=0year}$) represented as grey triangle with vertical lines and hollow sphere, respectively. For $C_{aq|x=0.02m,t}$ and $M_{t|t}$, median values as predicted by the 50th percentile transport parameters values are represented by the grey triangle while upper and lower boundaries as predicted by the 95th and 5th percentile transport parameters values are indicated by the vertical lines. Lines that did not appear in figure are below the minimum y-axes values. X-axes are homologs 1 to 10 (H1 to H10). 289

Figure 5.22h: Predicted flux of PBDE homologs in core CLC under advection-diffusion with organic carbon only sorption (A(OC)) conditions for initial sediment concentration of 36100, 60, and 0.2 ng/g at 40, 100, and 1000 years. Panels a,c, and e show aqueous phase concentration leaving the sediment boundary layer ($C_{aq|x=0.02m,t}$), aqueous phase breakthrough percentage ($C_{aq|x=0.02m,t}/C_{aq|x=0m,t=0year}$) (%BT), and ratio of aqueous phase concentration under local equilibrium assumption to saturation concentration ($C_{aq|x=0m,t}/C_{sat}$) (%Sat) represented as grey triangle with vertical lines, hollow sphere, and star, respectively. Panels b,d, and f show mass leaving the sediment boundary layer at specific time ($M_{t|t}$) and ratio of mass leaving the sediment boundary layer to initial starting mass ($M_{t|t}/M_{sed|t=0year}$) represented as grey triangle with vertical lines and hollow sphere, respectively. For $C_{aq|x=0.02m,t}$ and $M_{t|t}$, median values as predicted by the 50th percentile transport parameters values are represented by the grey triangle while upper and lower boundaries as predicted by the 95th and 5th percentile transport parameters values are indicated by the vertical lines. Lines that did not appear in figure are below the minimum y-axes values. X-axes are homologs 1 to 10 (H1 to H10). 290

Figure 5.22i: Predicted flux of PBDE homologs in core CWP under advection-diffusion with organic carbon only sorption (A(OC)) conditions for initial sediment concentration of 36100, 60, and 0.2 ng/g at 40, 100, and 1000 years. Panels a,c, and e show aqueous phase concentration leaving the sediment boundary layer ($C_{aq|x=0.02m,t}$), aqueous phase breakthrough percentage ($C_{aq|x=0.02m,t}/C_{aq|x=0m,t=0year}$) (%BT), and ratio of aqueous phase concentration under local equilibrium assumption to saturation concentration ($C_{aq|x=0m,t}/C_{sat}$) (%Sat) represented as grey triangle with vertical lines, hollow sphere, and star, respectively. Panels b,d, and f show mass leaving the sediment boundary layer at specific time ($M_{t|t}$) and ratio of mass leaving the sediment boundary layer to initial starting mass ($M_{t|t}/M_{sed|t=0year}$) represented as

grey triangle with vertical lines and hollow sphere, respectively. For $C_{aq|x=0.02m,t}$ and $M_{t|t}$, median values as predicted by the 50th percentile transport parameters values are represented by the grey triangle while upper and lower boundaries as predicted by the 95th and 5th percentile transport parameters values are indicated by the vertical lines. Lines that did not appear in figure are below the minimum y-axes values. X-axes are homologs 1 to 10 (H1 to H10). 291

Figure 5.22j: Predicted flux of PBDE homologs in core IGC09 under advection-diffusion with organic carbon only sorption (A(OC)) conditions for initial sediment concentration of 36100, 60, and 0.2 ng/g at 40, 100, and 1000 years. Panels a,c, and e show aqueous phase concentration leaving the sediment boundary layer ($C_{aq|x=0.02m,t}$), aqueous phase breakthrough percentage ($C_{aq|x=0.02m,t}/C_{aq|x=0m,t=0year}$) (%BT), and ratio of aqueous phase concentration under local equilibrium assumption to saturation concentration ($C_{aq|x=0m,t}/C_{sat}$) (%Sat) represented as grey triangle with vertical lines, hollow sphere, and star, respectively. Panels b,d, and f show mass leaving the sediment boundary layer at specific time ($M_{t|t}$) and ratio of mass leaving the sediment boundary layer to initial starting mass ($M_{t|t}/M_{sed|t=0year}$) represented as grey triangle with vertical lines and hollow sphere, respectively. For $C_{aq|x=0.02m,t}$ and $M_{t|t}$, median values as predicted by the 50th percentile transport parameters values are represented by the grey triangle while upper and lower boundaries as predicted by the 95th and 5th percentile transport parameters values are indicated by the vertical lines. Lines that did not appear in figure are below the minimum y-axes values. X-axes are homologs 1 to 10 (H1 to H10). 292

Figure 5.22k: Predicted flux of PBDE homologs in core IGC13 under advection-diffusion with organic carbon only sorption (A(OC)) conditions for initial sediment concentration of 36100, 60, and 0.2 ng/g at 40, 100, and 1000 years. Panels a,c, and e show aqueous phase concentration leaving the sediment boundary layer ($C_{aq|x=0.02m,t}$), aqueous phase breakthrough percentage ($C_{aq|x=0.02m,t}/C_{aq|x=0m,t=0year}$) (%BT), and ratio of aqueous phase concentration under local equilibrium assumption to saturation concentration ($C_{aq|x=0m,t}/C_{sat}$) (%Sat) represented as grey triangle with vertical lines, hollow sphere, and star, respectively. Panels b,d, and f show mass leaving the sediment boundary layer at specific time ($M_{t|t}$) and ratio of mass leaving the sediment boundary layer to initial starting mass ($M_{t|t}/M_{sed|t=0year}$) represented as grey triangle with vertical lines and hollow sphere, respectively. For $C_{aq|x=0.02m,t}$ and $M_{t|t}$, median values as predicted by the 50th percentile transport parameters values are represented by the grey triangle while upper and lower boundaries as predicted by the 95th and 5th percentile transport parameters values are indicated by the vertical lines. Lines that did not appear in figure are below the minimum y-axes values. X-axes are homologs 1 to 10 (H1 to H10). 293

Figure 5.22l: Predicted flux of PCB homologs in core ACL under advection-diffusion with organic carbon only sorption (A(OC)) conditions for initial sediment concentration of 1640, 262, and 19 ng/g at 40, 100, and 1000 years. Panels a,c, and e show aqueous phase concentration leaving the sediment boundary layer ($C_{aq|x=0.02m,t}$), aqueous phase breakthrough percentage ($C_{aq|x=0.02m,t}/C_{aq|x=0m,t=0year}$) (%BT), and ratio of aqueous phase concentration under local equilibrium assumption to saturation concentration ($C_{aq|x=0m,t}/C_{sat}$) (%Sat) represented as grey triangle with vertical lines, hollow sphere, and star, respectively. Panels b,d, and f show mass leaving the sediment boundary layer at specific time ($M_{t|t}$) and ratio of mass leaving the sediment boundary layer to initial starting mass ($M_{t|t}/M_{sed|t=0year}$) represented as grey triangle with vertical lines and hollow sphere, respectively. For $C_{aq|x=0.02m,t}$ and $M_{t|t}$, median values as predicted by the 50th percentile transport parameters values are represented by the grey triangle while upper and lower boundaries as predicted by the 95th and 5th percentile transport parameters values are indicated by the vertical lines. Lines that did not appear in figure are below the minimum y-axes values. X-axes are homologs 1 to 10 (H1 to H10). 294

Figure 5.22m: Predicted flux of PCB homologs in core AED under advection-diffusion with organic carbon only sorption (A(OC)) conditions for initial sediment concentration of 1640, 262, and 19 ng/g at 40, 100, and 1000 years. Panels a,c, and e show aqueous phase concentration leaving the sediment boundary layer ($C_{aq|x=0.02m,t}$), aqueous phase breakthrough percentage ($C_{aq|x=0.02m,t}/C_{aq|x=0m,t=0year}$) (%BT), and ratio of aqueous phase concentration under local equilibrium assumption to saturation concentration ($C_{aq|x=0m,t}/C_{sat}$) (%Sat) represented as grey triangle with vertical lines, hollow sphere, and star, respectively. Panels b,d, and f show mass leaving the sediment boundary layer at specific time ($M_{t|t}$) and ratio of mass leaving the sediment boundary layer to initial starting mass ($M_{t|t}/M_{sed|t=0year}$) represented as grey triangle with vertical lines and hollow sphere, respectively. For $C_{aq|x=0.02m,t}$ and $M_{t|t}$, median values as predicted by the 50th percentile transport parameters values are represented by the grey triangle while upper and lower boundaries as predicted by the 95th and 5th percentile transport parameters values are indicated by the vertical lines. Lines that did not appear in figure are below the minimum y-axes values. X-axes are homologs 1 to 10 (H1 to H10). 295

Figure 5.22n: Predicted flux of PCB homologs in core AFR under advection-diffusion with organic carbon only sorption (A(OC)) conditions for initial sediment concentration of 1640, 262, and 19 ng/g at 40, 100, and 1000 years. Panels a,c, and e show aqueous phase concentration leaving the sediment boundary layer ($C_{aq|x=0.02m,t}$), aqueous phase breakthrough percentage ($C_{aq|x=0.02m,t}/C_{aq|x=0m,t=0year}$) (%BT), and ratio of aqueous phase concentration under local equilibrium assumption to saturation concentration ($C_{aq|x=0m,t}/C_{sat}$) (%Sat) represented as grey triangle with vertical lines, hollow sphere, and star, respectively. Panels b,d, and f show mass leaving the sediment boundary layer at specific time ($M_{t|t}$) and ratio of mass leaving the sediment boundary layer to initial starting mass ($M_{t|t}/M_{sed|t=0year}$) represented as grey triangle with vertical lines and hollow sphere, respectively. For $C_{aq|x=0.02m,t}$ and $M_{t|t}$, median values as predicted by the 50th percentile transport parameters values are represented by the grey triangle while upper and lower boundaries as predicted by the 95th and 5th percentile transport parameters values are indicated by the vertical lines. Lines that did not appear in figure are below the minimum y-axes values. X-axes are homologs 1 to 10 (H1 to H10). 296

Figure 5.22o: Predicted flux of PCB homologs in core AJL under advection-diffusion with organic carbon only sorption (A(OC)) conditions for initial sediment concentration of 1640, 262, and 19 ng/g at 40, 100, and 1000 years. Panels a,c, and e show aqueous phase concentration leaving the sediment boundary layer ($C_{aq|x=0.02m,t}$), aqueous phase breakthrough percentage ($C_{aq|x=0.02m,t}/C_{aq|x=0m,t=0year}$) (%BT), and ratio of aqueous phase concentration under local equilibrium assumption to saturation concentration ($C_{aq|x=0m,t}/C_{sat}$) (%Sat) represented as grey triangle with vertical lines, hollow sphere, and star, respectively. Panels b,d, and f show mass leaving the sediment boundary layer at specific time ($M_{t|t}$) and ratio of mass leaving the sediment boundary layer to initial starting mass ($M_{t|t}/M_{sed|t=0year}$) represented as grey triangle with vertical lines and hollow sphere, respectively. For $C_{aq|x=0.02m,t}$ and $M_{t|t}$, median values as predicted by the 50th percentile transport parameters values are represented by the grey triangle while upper and lower boundaries as predicted by the 95th and 5th percentile transport parameters values are indicated by the vertical lines. Lines that did not appear in figure are below the minimum y-axes values. X-axes are homologs 1 to 10 (H1 to H10). 297

Figure 5.22p: Predicted flux of PCB homologs in core AMW under advection-diffusion with organic carbon only sorption (A(OC)) conditions for initial sediment concentration of 1640, 262, and 19 ng/g at 40, 100, and 1000 years. Panels a,c, and e show aqueous phase concentration leaving the sediment boundary layer ($C_{aq|x=0.02m,t}$), aqueous phase breakthrough percentage ($C_{aq|x=0.02m,t}/C_{aq|x=0m,t=0year}$) (%BT), and ratio of aqueous phase concentration under local equilibrium assumption to saturation concentration

($C_{aq|x=0m,t}/C_{sat}$) (%Sat) represented as grey triangle with vertical lines, hollow sphere, and star, respectively. Panels b,d, and f show mass leaving the sediment boundary layer at specific time ($M_{t|t}$) and ratio of mass leaving the sediment boundary layer to initial starting mass ($M_{t|t}/M_{sed|t=0year}$) represented as grey triangle with vertical lines and hollow sphere, respectively. For $C_{aq|x=0.02m,t}$ and $M_{t|t}$, median values as predicted by the 50th percentile transport parameters values are represented by the grey triangle while upper and lower boundaries as predicted by the 95th and 5th percentile transport parameters values are indicated by the vertical lines. Lines that did not appear in figure are below the minimum y-axes values. X-axes are homologs 1 to 10 (H1 to H10). 298

Figure 5.22q: Predicted flux of PCB homologs in core AOT under advection-diffusion with organic carbon only sorption (A(OC)) conditions for initial sediment concentration of 1640, 262, and 19 ng/g at 40, 100, and 1000 years. Panels a,c, and e show aqueous phase concentration leaving the sediment boundary layer ($C_{aq|x=0.02m,t}$), aqueous phase breakthrough percentage ($C_{aq|x=0.02m,t}/C_{aq|x=0m,t=0year}$) (%BT), and ratio of aqueous phase concentration under local equilibrium assumption to saturation concentration ($C_{aq|x=0m,t}/C_{sat}$) (%Sat) represented as grey triangle with vertical lines, hollow sphere, and star, respectively. Panels b,d, and f show mass leaving the sediment boundary layer at specific time ($M_{t|t}$) and ratio of mass leaving the sediment boundary layer to initial starting mass ($M_{t|t}/M_{sed|t=0year}$) represented as grey triangle with vertical lines and hollow sphere, respectively. For $C_{aq|x=0.02m,t}$ and $M_{t|t}$, median values as predicted by the 50th percentile transport parameters values are represented by the grey triangle while upper and lower boundaries as predicted by the 95th and 5th percentile transport parameters values are indicated by the vertical lines. Lines that did not appear in figure are below the minimum y-axes values. X-axes are homologs 1 to 10 (H1 to H10). 299

Figure 5.22r: Predicted flux of PCB homologs in core AMW under advection-diffusion with organic carbon only sorption (A(OC)) conditions for initial sediment concentration of 1640, 262, and 19 ng/g at 40, 100, and 1000 years. Panels a,c, and e show aqueous phase concentration leaving the sediment boundary layer ($C_{aq|x=0.02m,t}$), aqueous phase breakthrough percentage ($C_{aq|x=0.02m,t}/C_{aq|x=0m,t=0year}$) (%BT), and ratio of aqueous phase concentration under local equilibrium assumption to saturation concentration ($C_{aq|x=0m,t}/C_{sat}$) (%Sat) represented as grey triangle with vertical lines, hollow sphere, and star, respectively. Panels b,d, and f show mass leaving the sediment boundary layer at specific time ($M_{t|t}$) and ratio of mass leaving the sediment boundary layer to initial starting mass ($M_{t|t}/M_{sed|t=0year}$) represented as grey triangle with vertical lines and hollow sphere, respectively. For $C_{aq|x=0.02m,t}$ and $M_{t|t}$, median values as predicted by the 50th percentile transport parameters values are represented by the grey triangle while upper and lower boundaries as predicted by the 95th and 5th percentile transport parameters values are indicated by the vertical lines. Lines that did not appear in figure are below the minimum y-axes values. X-axes are homologs 1 to 10 (H1 to H10). 300

Figure 5.22s: Predicted flux of PCB homologs in core CBC under advection-diffusion with organic carbon only sorption (A(OC)) conditions for initial sediment concentration of 1640, 262, and 19 ng/g at 40, 100, and 1000 years. Panels a,c, and e show aqueous phase concentration leaving the sediment boundary layer ($C_{aq|x=0.02m,t}$), aqueous phase breakthrough percentage ($C_{aq|x=0.02m,t}/C_{aq|x=0m,t=0year}$) (%BT), and ratio of aqueous phase concentration under local equilibrium assumption to saturation concentration ($C_{aq|x=0m,t}/C_{sat}$) (%Sat) represented as grey triangle with vertical lines, hollow sphere, and star, respectively. Panels b,d, and f show mass leaving the sediment boundary layer at specific time ($M_{t|t}$) and ratio of mass leaving the sediment boundary layer to initial starting mass ($M_{t|t}/M_{sed|t=0year}$) represented as grey triangle with vertical lines and hollow sphere, respectively. For $C_{aq|x=0.02m,t}$ and $M_{t|t}$, median values as predicted by the 50th percentile transport parameters values are represented by the grey triangle while

upper and lower boundaries as predicted by the 95th and 5th percentile transport parameters values are indicated by the vertical lines. Lines that did not appear in figure are below the minimum y-axes values. X-axes are homologs 1 to 10 (H1 to H10). 301

Figure 5.22t: Predicted flux of PCB homologs in core CWP under advection-diffusion with organic carbon only sorption (A(OC)) conditions for initial sediment concentration of 1640, 262, and 19 ng/g at 40, 100, and 1000 years. Panels a,c, and e show aqueous phase concentration leaving the sediment boundary layer ($C_{aq|x=0.02m,t}$), aqueous phase breakthrough percentage ($C_{aq|x=0.02m,t}/C_{aq|x=0m,t=0year}$) (%BT), and ratio of aqueous phase concentration under local equilibrium assumption to saturation concentration ($C_{aq|x=0m,t}/C_{sat}$) (%Sat) represented as grey triangle with vertical lines, hollow sphere, and star, respectively. Panels b,d, and f show mass leaving the sediment boundary layer at specific time ($M_{t|t}$) and ratio of mass leaving the sediment boundary layer to initial starting mass ($M_{t|t}/M_{sed|t=0year}$) represented as grey triangle with vertical lines and hollow sphere, respectively. For $C_{aq|x=0.02m,t}$ and $M_{t|t}$, median values as predicted by the 50th percentile transport parameters values are represented by the grey triangle while upper and lower boundaries as predicted by the 95th and 5th percentile transport parameters values are indicated by the vertical lines. Lines that did not appear in figure are below the minimum y-axes values. X-axes are homologs 1 to 10 (H1 to H10). 302

Figure 5.22u: Predicted flux of PCB homologs in core IGC09 under advection-diffusion with organic carbon only sorption (A(OC)) conditions for initial sediment concentration of 1640, 262, and 19 ng/g at 40, 100, and 1000 years. Panels a,c, and e show aqueous phase concentration leaving the sediment boundary layer ($C_{aq|x=0.02m,t}$), aqueous phase breakthrough percentage ($C_{aq|x=0.02m,t}/C_{aq|x=0m,t=0year}$) (%BT), and ratio of aqueous phase concentration under local equilibrium assumption to saturation concentration ($C_{aq|x=0m,t}/C_{sat}$) (%Sat) represented as grey triangle with vertical lines, hollow sphere, and star, respectively. Panels b,d, and f show mass leaving the sediment boundary layer at specific time ($M_{t|t}$) and ratio of mass leaving the sediment boundary layer to initial starting mass ($M_{t|t}/M_{sed|t=0year}$) represented as grey triangle with vertical lines and hollow sphere, respectively. For $C_{aq|x=0.02m,t}$ and $M_{t|t}$, median values as predicted by the 50th percentile transport parameters values are represented by the grey triangle while upper and lower boundaries as predicted by the 95th and 5th percentile transport parameters values are indicated by the vertical lines. Lines that did not appear in figure are below the minimum y-axes values. X-axes are homologs 1 to 10 (H1 to H10). 303

Figure 5.22v: Predicted flux of PCB homologs in core IGC13 under advection-diffusion with organic carbon only sorption (A(OC)) conditions for initial sediment concentration of 1640, 262, and 19 ng/g at 40, 100, and 1000 years. Panels a,c, and e show aqueous phase concentration leaving the sediment boundary layer ($C_{aq|x=0.02m,t}$), aqueous phase breakthrough percentage ($C_{aq|x=0.02m,t}/C_{aq|x=0m,t=0year}$) (%BT), and ratio of aqueous phase concentration under local equilibrium assumption to saturation concentration ($C_{aq|x=0m,t}/C_{sat}$) (%Sat) represented as grey triangle with vertical lines, hollow sphere, and star, respectively. Panels b,d, and f show mass leaving the sediment boundary layer at specific time ($M_{t|t}$) and ratio of mass leaving the sediment boundary layer to initial starting mass ($M_{t|t}/M_{sed|t=0year}$) represented as grey triangle with vertical lines and hollow sphere, respectively. For $C_{aq|x=0.02m,t}$ and $M_{t|t}$, median values as predicted by the 50th percentile transport parameters values are represented by the grey triangle while upper and lower boundaries as predicted by the 95th and 5th percentile transport parameters values are indicated by the vertical lines. Lines that did not appear in figure are below the minimum y-axes values. X-axes are homologs 1 to 10 (H1 to H10). 304

Figure 5.23a: PBDE homolog 1 sediment concentration (C_{sed}) (a-c), percent porewater saturation ($C_{aq|x=0m}/C_{sat}$) (d-f), and fraction of mass leaving the sediment boundary layer relative to initial starting

mass (M_t/M_{sed}) (g-i) as a function of time in cores ACL (a,d,g), AED (b,e,h), and AFR (c,f,i) as predicted by the Monte Carlo 95 th percentile transport parameters values under advection-diffusion with organic carbon only sorption (A(OC)) mass transport condition.....	308
Figure 5.23b: PBDE homolog 1 sediment concentration (C_{sed}) (a-c), percent porewater saturation ($C_{aq/x=0m}/C_{sat}$) (d-f), and fraction of mass leaving the sediment boundary layer relative to initial starting mass (M_t/M_{sed}) (g-i) as a function of time in cores AJL (a,d,g), AMW (b,e,h), and AOT (c,f,i) as predicted by the Monte Carlo 95 th percentile transport parameters values under advection-diffusion with organic carbon only sorption (A(OC)) mass transport condition.....	309
Figure 5.23c: PBDE homolog 1 sediment concentration (C_{sed}) (a-c), percent porewater saturation ($C_{aq/x=0m}/C_{sat}$) (d-f), and fraction of mass leaving the sediment boundary layer relative to initial starting mass (M_t/M_{sed}) (g-i) as a function of time in cores CBC (a,d,g), CLC (b,e,h), and CWP (c,f,i) as predicted by the Monte Carlo 95 th percentile transport parameters values under advection-diffusion with organic carbon only sorption (A(OC)) mass transport condition.....	310
Figure 5.23d: PBDE homolog 1 concentration (C_{sed}) (a-c), percent porewater saturation ($C_{aq/x=0m}/C_{sat}$) (d-f), and fraction of mass leaving the sediment boundary layer relative to initial starting mass (M_t/M_{sed}) (g-i) as a function of time in cores IGC09 (a,c,e) and IGC13 (b,d,f), and CWP (c,f,i) as predicted by the Monte Carlo 95 th percentile transport parameters values under advection-diffusion with organic carbon only sorption (A(OC)) mass transport condition.	311
Figure 5.23e: PCB homologs 1 and 2 sediment concentration (C_{sed}) (a-c), percent porewater saturation ($C_{aq/x=0m}/C_{sat}$) (d-f), and fraction of mass leaving the sediment boundary layer relative to initial starting mass (M_t/M_{sed}) (g-i) as a function of time in cores ACL (a,d,g), AED (b,e,h), and AFR (c,f,i) as predicted by the Monte Carlo 95 th percentile transport parameters values under advection-diffusion with organic carbon only sorption (A(OC)) mass transport condition.....	312
Figure 5.23f: PCB homologs 1 and 2 sediment concentration (C_{sed}) (a-c), percent porewater saturation ($C_{aq/x=0m}/C_{sat}$) (d-f), and fraction of mass leaving the sediment boundary layer relative to initial starting mass (M_t/M_{sed}) (g-i) as a function of time in cores AJL (a,d,g), AMW (b,e,h), and AOT (c,f,i) as predicted by the Monte Carlo 95 th percentile transport parameters values under advection-diffusion with organic carbon only sorption (A(OC)) mass transport condition.....	313
Figure 5.23g: PCB homologs 1 and 2 sediment concentration (C_{sed}) (a-c), percent porewater saturation ($C_{aq/x=0m}/C_{sat}$) (d-f), and fraction of mass leaving the sediment boundary layer relative to initial starting mass (M_t/M_{sed}) (g-i) as a function of time in cores CBC (a,d,g), CLC (b,e,h), and CWP (c,f,i) as predicted by the Monte Carlo 95 th percentile transport parameters values under advection-diffusion with organic carbon only sorption (A(OC)) mass transport condition.....	314
Figure 5.23h: PCB homologs 1 and 2 sediment concentration (C_{sed}) (a-c), percent porewater saturation ($C_{aq/x=0m}/C_{sat}$) (d-f), and fraction of mass leaving the sediment boundary layer relative to initial starting mass (M_t/M_{sed}) (g-i) as a function of time in cores IGC09 (a,c,e) and IGC13 (b,d,f), as predicted by the Monte Carlo 95 th percentile transport parameters values under advection-diffusion with organic carbon only sorption (A(OC)) mass transport condition.	315
Figure 5.24a: Sediment phase concentrations (C_{sed}) of PBDE (a-b, e-f, i-j) and PCB (c-d, g-h, k-l) homologs that result in local equilibrium aqueous phase concentration equals to saturation concentration ($C_{aq/x=0m}=C_{sat}$) predicted from sediment-porewater partitioning coefficient for organic carbon only sorption (K_d (OC)) (PBDEs: a,e,i ; PCBs: c,g,k) and organic carbon and black carbon co-sorption (K_d (OCBC)) (PBDEs: b,f,j ; PCBs: d,h,l) at the 5 th , 50 th , and 95 th percentile values in cores ACL(a-d), AED	

(e-h), and AFR (i-l). C_{sed} values predicted from the 50th percentile log K_d values are marked by the grey triangle and C_{sed} values predicted from the 5th and 95th percentile are shown as the bold vertical lines...318

Figure 5.24b: Sediment phase concentrations (C_{sed}) of PBDE (a-b, e-f, i-j) and PCB (c-d, g-h, k-l) homologs that result in local equilibrium aqueous phase concentration equals to saturation concentration ($C_{aq/x=0m}=C_{sat}$) predicted from sediment-porewater partitioning coefficient for organic carbon only sorption (K_d (OC)) (PBDEs:a,e,i ; PCBs: c,g,k) and organic carbon and black carbon co-sorption (K_d (OCBC)) (PBDEs:b,f,j ; PCBs: d,h,l) at the 5th, 50th, and 95th percentile values in cores AJL(a-d), AMW (e-h), and AOT (i-l). C_{sed} values predicted from the 50th percentile log K_d values are marked by the grey triangle and C_{sed} values predicted from the 5th and 95th percentile are shown as the bold vertical lines...319

Figure 5.24c: Sediment phase concentrations (C_{sed}) of PBDE (a-b, e-f, i-j) and PCB (c-d, g-h, k-l) homologs that result in local equilibrium aqueous phase concentration equals to saturation concentration ($C_{aq/x=0m}=C_{sat}$) predicted from sediment-porewater partitioning coefficient for organic carbon only sorption (K_d (OC)) (PBDEs:a,e,i ; PCBs: c,g,k) and organic carbon and black carbon co-sorption (K_d (OCBC)) (PBDEs:b,f,j ; PCBs: d,h,l) at the 5th, 50th, and 95th percentile values in cores CBC(a-d), CLC (e-h), and CWP (i-l). C_{sed} values predicted from the 50th percentile log K_d values are marked by the grey triangle and C_{sed} values predicted from the 5th and 95th percentile are shown as the bold vertical lines...320

Figure 5.24d: Sediment phase concentrations (C_{sed}) of PBDE (a-b, e-f, i-j) and PCB (c-d, g-h, k-l) homologs that result in local equilibrium aqueous phase concentration equals to saturation concentration ($C_{aq/x=0m}=C_{sat}$) predicted from sediment-porewater partitioning coefficient for organic carbon only sorption (K_d (OC)) (PBDEs:a,e,i ; PCBs: c,g,k) and organic carbon and black carbon co-sorption (K_d (OCBC)) (PBDEs:b,f,j ; PCBs: d,h,l) at the 5th, 50th, and 95th percentile values in cores IGC09(a-d) and IGC13 CLC (e-h). C_{sed} values predicted from the 50th percentile log K_d values are marked by the grey triangle and C_{sed} values predicted from the 5th and 95th percentile are shown as the bold vertical lines...321

Figure 5.25: The fraction of PCB homolog 1 (a-c), PBDE homolog 1 (d-f), and PCB homolog 2 (g-i) leaving the sediment segment relative to initial sediment concentration at the 95th percentile concentration (1640 and 36100 ng/g for PCB homologs 1 and 2, and PBDE homolog 1, respectively)($M_{t/t}/M_{sed,t=0year}$) in all sediment cores at 40 (a,d,g), 100 (b,e,h) and 1000 (c,f,i) years. Size of the hollow circle represent the % $M_{t/t}/M_{sed,t=0year}$ 323

Figure 5.25a: DE-71 and DE-79 (a-c), and Saytex 102E (d-f) coefficients and residual ($\sum Res$) (g-i) as determined by multivariate least square regression analysis for cores ACL (a,d,g), AED (b,e,h), and AMW (c,f,i). 326

Figure 5.25b: DE-71 and DE-79 (a-h), and Saytex 102E (e-h) coefficients and residuals ($\sum Res$) (i-l) as determined by multivariate least square regression analysis for cores CBC (a,e,i), CLC (b,f,j), CWP (c,g,k) and IGC13 (d,h,l)..... 327

Figure 5.25c: Aroclors 1016, 1248, 1254, and 1260 coefficients and residuals ($\sum Res$) (g-i) as determined by multivariate least square regression analysis for cores a)CBC, b) CLC, c) CWP,d) AMW , and e)IGC13. 328

Figure 5.26a: Flux (a-c) and flux contribution (d-f) of DE-71, DE-79, and Saytex 102E PBDE technical mixtures as predicted by the linear mixing model for cores ACL (a,d), AED (b,e), and AMW (c,f)..... 333

Figure 5.26b: Flux (a-d) and flux contribution (d-f) of DE-71, DE-79, and Saytex 102E predicted by the linear mixing model for cores CBC (a,e), CLC (b,f), CWP (c,g), and IGC13(d,h). 334

Figure 5.26c: Flux (a-e) and flux contribution (f-j) of Aroclors 1016, 1248, 1254, and 1260 predicted by the linear mixing model for cores a,f) CBC, b,g) CLC, c,h) CWP, d,i) AMW, and e,j) IGC13..... 335

Figure 5.27a: Comparison of measured PBDE homolog concentrations to the linear mixing model predicted concentrations in cores ACL (a), AED (b), and AMW (c). Also shown are the 1:1, 10:1, and 1:10 lines. Note log scale on axes	337
Figure 5.27b: Comparison of measured PBDE homolog concentrations to the linear mixing model predicted concentrations in cores CBC (a), CLC (b), CWP (c), AMW (d), and IGC13(e). Also shown are the 1:1, 10:1, and 1:10 lines. Note log scale on axes	338
Figure 5.27c: Comparison of measured PCB homolog concentrations to the linear mixing model predicted concentrations in cores CBC (a), CLC (b), CWP (c), AMW(d), IGC09 (e), and IGC13(f). Also shown are the 1:1, 10:1, and 1:10 lines. Note log scale on axes.	339
Figure 5.28a: LMM predicted and measured PBDE homologs (H1-H10: homolog 1 to homolog 10) concentrations in core ACL. Lines that do not show up are below the minimum concentration level. Error bars, representing the maximum amount of mass percentage moving out of the sediment boundary layer relative to initial sediment mass at 40 years ($M_{t=40 \text{ years}} M_{sed t=0 \text{ year}}$) under advection with organic carbon only sorption (A(OC)) were added to the measured PBDE homologs. Note that error bars are at a 10x scale. In most cases, predicted $M_{t=40 \text{ years}} M_{sed t=0 \text{ year}}$ were very low and error bars are not visible. X-axes are in the log scale.....	341
Figure 5.28b: LMM predicted and measured PBDE homologs (H1-H10: homolog 1 to homolog 10) concentrations in core AED. Lines that do not show up are below the minimum concentration level. Error bars, representing the maximum amount of mass percentage moving out of the sediment boundary layer relative to initial sediment mass at 40 years ($M_{t=40 \text{ years}} M_{sed t=0 \text{ year}}$) under advection with organic carbon only sorption (A(OC)) were added to the measured PBDE homologs. Note that error bars are at a 10x scale. In most cases, predicted $M_{t=40 \text{ years}} M_{sed t=0 \text{ year}}$ were very low and error bars are not visible. X-axes are in the log scale.....	342
Figure 5.28c: LMM predicted and measured PBDE homologs (H1-H10: homolog 1 to homolog 10) concentrations in core AMW. Lines that do not show up are below the minimum concentration level. Error bars, representing the maximum amount of mass percentage moving out of the sediment boundary layer relative to initial sediment mass at 40 years ($M_{t=40 \text{ years}} M_{sed t=0 \text{ year}}$) under advection with organic carbon only sorption (A(OC)) were added to the measured PBDE homologs. Note that error bars are at a 10x scale. In most cases, predicted $M_{t=40 \text{ years}} M_{sed t=0 \text{ year}}$ were very low and error bars are not visible. X-axes are in the log scale.	343
Figure 5.28d: LMM predicted and measured PBDE homologs (H1-H10: homolog 1 to homolog 10) concentrations in core CBC. Lines that do not show up are below the minimum concentration level. Error bars, representing the maximum amount of mass percentage moving out of the sediment boundary layer relative to initial sediment mass at 40 years ($M_{t=40 \text{ years}} M_{sed t=0 \text{ year}}$) under advection with organic carbon only sorption (A(OC)) were added to the measured PBDE homologs. Note that error bars are at a 10x scale. In most cases, predicted $M_{t=40 \text{ years}} M_{sed t=0 \text{ year}}$ were very low and error bars are not visible. X-axes are in the log scale.....	344
Figure 5.28e: LMM predicted and measured PBDE homologs (H1-H10: homolog 1 to homolog 10) concentrations in core CLC. Lines that do not show up are below the minimum concentration level. Error bars, representing the maximum amount of mass percentage moving out of the sediment boundary layer relative to initial sediment mass at 40 years ($M_{t=40 \text{ years}} M_{sed t=0 \text{ year}}$) under advection with organic carbon only sorption (A(OC)) were added to the measured PBDE homologs. Note that error bars are at a 10x scale. In most cases, predicted $M_{t=40 \text{ years}} M_{sed t=0 \text{ year}}$ were very low and error bars are not visible. X-axes are in the log scale.....	345

Figure 5.28f: LMM predicted and measured PBDE homologs (H1-H10: homolog 1 to homolog 10) concentrations in core CWP. Lines that do not show up are below the minimum concentration level. Error bars, representing the maximum amount of mass percentage moving out of the sediment boundary layer relative to initial sediment mass at 40 years ($M_{t=40 \text{ years}}|M_{sed|t=0 \text{ year}}$) under advection with organic carbon only sorption (A(OC)) were added to the measured PBDE homologs. Note that error bars are at a 10x scale. In most cases, predicted $M_{t=40 \text{ years}}|M_{sed|t=0 \text{ year}}$ were very low and error bars are not visible. X-axes are in the log scale..... 346

Figure 5.28g: LMM predicted and measured PBDE homologs (H1-H10: homolog 1 to homolog 10) concentrations in core IGC13. Lines that do not show up are below the minimum concentration level. Error bars, representing the maximum amount of mass percentage moving out of the sediment boundary layer relative to initial sediment mass at 40 years ($M_{t=40 \text{ years}}|M_{sed|t=0 \text{ year}}$) under advection with organic carbon only sorption (A(OC)) were added to the measured PBDE homologs. Note that error bars are at a 10x scale. In most cases, predicted $M_{t=40 \text{ years}}|M_{sed|t=0 \text{ year}}$ were very low and error bars are not visible. X-axes are in the log scale. 347

Figure 5.28h: LMM predicted and measured PBDE homologs (H1-H10: homolog 1 to homolog 10) concentrations in core CBC. Lines that do not show up are below the minimum concentration level. Error bars, representing the maximum amount of mass percentage moving out of the sediment boundary layer relative to initial sediment mass at 40 years ($M_{t=40 \text{ years}}|M_{sed|t=0 \text{ year}}$) under advection with organic carbon only sorption (A(OC)) were added to the measured PBDE homologs. Note that error bars are at a 10x scale. In most cases, predicted $M_{t=40 \text{ years}}|M_{sed|t=0 \text{ year}}$ were very low and error bars are not visible. X-axes are in the log scale..... 348

Figure 5.28i: LMM predicted and measured PBDE homologs (H1-H10: homolog 1 to homolog 10) concentrations in core CLC. Lines that do not show up are below the minimum concentration level. Error bars, representing the maximum amount of mass percentage moving out of the sediment boundary layer relative to initial sediment mass at 40 years ($M_{t=40 \text{ years}}|M_{sed|t=0 \text{ year}}$) under advection with organic carbon only sorption (A(OC)) were added to the measured PBDE homologs. Note that error bars are at a 10x scale. In most cases, predicted $M_{t=40 \text{ years}}|M_{sed|t=0 \text{ year}}$ were very low and error bars are not visible. X-axes are in the log scale..... 349

Figure 5.28j: LMM predicted and measured PBDE homologs (H1-H10: homolog 1 to homolog 10) concentrations in core CWP. Lines that do not show up are below the minimum concentration level. Error bars, representing the maximum amount of mass percentage moving out of the sediment boundary layer relative to initial sediment mass at 40 years ($M_{t=40 \text{ years}}|M_{sed|t=0 \text{ year}}$) under advection with organic carbon only sorption (A(OC)) were added to the measured PBDE homologs. Note that error bars are at a 10x scale. In most cases, predicted $M_{t=40 \text{ years}}|M_{sed|t=0 \text{ year}}$ were very low and error bars are not visible. X-axes are in the log scale..... 350

Figure 5.28k: LMM predicted and measured PBDE homologs (H1-H10: homolog 1 to homolog 10) concentrations in core AMW. Lines that do not show up are below the minimum concentration level. Error bars, representing the maximum amount of mass percentage moving out of the sediment boundary layer relative to initial sediment mass at 40 years ($M_{t=40 \text{ years}}|M_{sed|t=0 \text{ year}}$) under advection with organic carbon only sorption (A(OC)) were added to the measured PBDE homologs. Note that error bars are at a 10x scale. In most cases, predicted $M_{t=40 \text{ years}}|M_{sed|t=0 \text{ year}}$ were very low and error bars are not visible. X-axes are in the log scale. 351

Figure 5.28l: LMM predicted and measured PBDE homologs (H1-H10: homolog 1 to homolog 10) concentrations in core IGC13. Lines that do not show up are below the minimum concentration level.

Error bars, representing the maximum amount of mass percentage moving out of the sediment boundary layer relative to initial sediment mass at 40 years ($M_{t=40 \text{ years}}/M_{\text{sed}|t=0 \text{ year}}$) under advection with organic carbon only sorption (A(OC)) were added to the measured PBDE homologs. Note that error bars are at a 10x scale. In most cases, predicted $M_{t=40 \text{ years}}/M_{\text{sed}|t=0 \text{ year}}$ were very low and error bars are not visible. X-axes are in the log scale. 352

List of Acronyms

AEBL.....	Applied Environmental and Biotechnology Laboratory
BC.....	Black carbon
BFR.....	Brominated flame retardant
CB.....	Chlorobenzene
CE.....	Chloroethene
CSO.....	Combined sewage outfall
DCE.....	Dichloroethylene
EPI.....	Estimation program interface
GAC.....	Granular activated carbon
HBCD.....	Hexabromocyclododecane
HMW.....	High molecular weight
HOC.....	Hydrophobic organic contaminant
HSD.....	Hammond Sanitary District
IHC.....	Indiana Harbor Canal
LEA.....	Local equilibrium assumption
LFER.....	Linear free energy relationship
LMM.....	Linear mixing model
LMW.....	Low molecular weight
MLMS.....	Multivariate least median square
MLSR.....	Multiple least square regression
NCBI.....	National Center for Biotechnology Information
NSOC.....	Non-soot organic carbon
OC.....	Organic carbon
OECD.....	Organization for Economic Cooperation and Development
OM.....	Organic matter
ORP.....	Oxidation reduction potential
PAH.....	Polyaromatic hydrocarbon

PBB.....	Polybrominated Biphenyl
PBDE.....	Polybrominated Diphenyl Ether
PCB.....	Polychlorinated biphenyl
PCD.....	Polychlorinated dibenzodioxin
QSAR.....	Quantitative structure activity relationship
QSPR.....	Quantitative structure property relationship
RAPS.....	Racine Avenue Pumping Station
TBBPA.....	Tetrabromobisphenol A
TM.....	Technical Mixture
TRI.....	Toxic Release Inventory
TSCA.....	Toxic Control and Substances Act
USDA.....	United States Department of Agriculture
USGS.....	United States Geological Services
V.....	Volume
VC.....	Vinyl Chloride
WBGCR.....	West Branch of the Grand Calumet River
WDS.....	Weight of dry sediment
WWS.....	Weight of wet sediment
WWTP.....	Wastewater treatment plant

CHAPTER 1. INTRODUCTION

In the United States, flammability standards such as defined in the California Technical Bulletin 117, were imposed on consumer products to better protect life and properties from fire hazards. Polybrominated diphenyl ethers (PBDEs) are one of the halogenated flame retardants incorporated into various consumer products and can be found in common household items including textile, couches and mattress foams, and electronic components.⁽¹⁾ PBDEs, as well as other flame retardants have played an important role in minimizing life and economic losses due to fire; however, the mass production and incorporation of PBDEs into many consumer products have resulted in environmental dissemination which can pose human and/or ecological health risks.^(2,3)

The structural similarities between PBDEs and hormones suggest that PBDEs may act as endocrine disruptors in addition to acute health impacts.⁽²⁾ In response to toxicology studies showing higher toxicity and bioaccumulative potential of some low molecular weight (LMW) PBDE congeners, the DE-71 and DE-79 technical mixtures (TM) (composed primarily of penta- and octa-PBDE congeners, respectively) were banned by the State of California in 2003 resulting in voluntary industry withdrawal in the United States by 2004.⁽²⁾ The most prevalent PBDE TM formulation, Saytex 102E is composed primarily of the deca-PBDE congener. Saytex 102E TM formulation is argued to be safer due to its low bioavailability and apparent stability; however, potential environmental transformation of deca-PBDE to more toxic PBDE compounds has fueled public health concerns and controversies into its continued usage. In 2007, the Saytex 102E formulation was banned in Sweden and partial bans have followed in four U.S. states by 2010.⁽³⁾

Polychlorinated biphenyls (PCBs) were commercially produced starting in the 1930s and were widely used as coolant fluid in transformers, dielectric fluids, and solvents owing to their high heat resistance and stable properties. Despite industry-related incidences demonstrating compelling evidences of the detrimental health effects of PCB exposures, commercial use of PCBs continued into the 1970s

with an overall estimate of 570 million kg sold in the U.S.⁽⁴⁾ Public concerns grew from a multitude of studies demonstrating high PCB body burdens in biota finally resulting in a U.S. PCB production ban in 1979.⁽⁴⁾ It is important to note that the production ban did not remove PCB-containing products in use at the time of the ban. The result is that PCBs continue to be a legacy problem especially in sites exposed to high level of PCBs. As but one example, sediments from the Hudson River which received more than 680,000 kg of PCBs from 1947 to 1977 via waste discharge streams still contained PCB levels that exceeded the Toxic Control and Substances Act (TSCA) standards.⁽⁵⁾

Discharges of PCB-laden waste streams directly into the aquatic systems were not deemed problematic as PCBs were previously not legally classified as a toxic contaminant. Often, when the toxicity of a contaminant is not properly understood and/or characterized, fewer regulations are enforced to control the disposal, as was the case for PCBs. This resulted in the global-scale dissemination of PCBs. PCBs provide a precautionary tale against the manufacture and release of synthetic chemical without an effective waste stream capture and treatment plan for end of life product disposal. Similar to the case of PCBs, PBDEs have also been mass produced and incorporated into various consumer products prior to proper toxicological and environmental risk assessment analyses. Large data gaps still exist on PBDE physico-chemical properties, rendering environmental fate modeling inaccurate, and with high uncertainty.

Sediments can act as the final reservoir for hydrophobic contaminants that have been released into the environment. In the sediment phase, both PBDEs and PCBs are susceptible to transformation and transport processes which have implications on the final fate and exposure risk. Applying a multidisciplinary approach, the unifying theme of this thesis is to characterize sediment phase PBDE and PCB contamination from urban and rural geographical locations to investigate the potential of sediment phase microbial facilitated transformation and *in-situ* mass transport. The overall objectives of this thesis are listed below:

- A) Characterize PBDE and PCB distributions in sediments from the Metropolitan Chicago area and AR (near and distant from PBDE manufacturing facilities) to determine if location characteristics (urban versus rural, production versus non-production area, dissipative versus point source) have an impact on the contaminants' distributions.
- B) Determine the potential for transformation of sediment phase PBDEs and PCBs by evaluating geochemical properties (e.g., organic matter level, oxidation-reduction potential) in tandem with interpretation of multivariate least square regression (MLSR) analysis quantifying the disparity between observed sediment phase PBDE and PCB distributions to PBDE TMs and PCB Aroclor mixtures, respectively.
- C) Using high yield pyrosequencing technology to investigate the microbial community structure in PBDE and PCB contaminated sediments. Of particular interest is to track the abundance of known dehalorespirers (or lack thereof) in sediment segments with potential PBDE and PCB transformation processes inferred from geochemical and physico-chemical properties to provide some insight into the role of microorganisms in transforming sediment phase PBDEs and PCBs.
- D) Quantifying the magnitude of diffusion, advection, and black carbon (BC) adsorption on *in-situ* mass transport of PBDEs and PCBs in the sediment column by applying the diffusion and advection-diffusion transport models. The results are used to evaluate the contribution of *in-situ* PBDE and PCB mass transport in shaping the observed PBDE and PCB sediment profiles. Mass transport modeling result will also evaluate if *in-situ* PBDE and PCB mass transport can shift the deposited PBDE and PCB distributions in the sediment.

CHAPTER 2. LITERATURE REVIEW

2.1.1. Polybrominated Diphenyl Ethers (PBDEs)

Flame retardants are chemicals added or bound to plastics, polymers, textiles, and coatings to inhibit or impede the spread of fire during combustion. There are four steps in the combustion process; preheating, volatilization or decomposition, combustion, and propagation.⁽⁶⁾ Halogenated flame retardants work by capturing highly oxidizing free radicals thus inhibiting the flame propagation process.⁽⁷⁾ All halogens are effective at capturing free radicals; however, their stability and radical trapping efficiency are key factors in determining their suitability as flame retardants.⁽⁷⁾ For example, iodide is not stable and decomposes under very low temperature.⁽⁷⁾ In contrast, the high stability of fluoride results in late halogen delivery which is ineffective in impeding flame propagation.⁽⁷⁾ The combination of stability and high trapping efficiency of both bromine and chlorine render these two halogens appropriate as flame retardant. Currently, there are more than 75 different aliphatic, aromatic, and cyclo-aromatic brominated, and chlorinated compounds synthesized as flame retardant chemicals.⁽⁷⁾ These include polybrominated diphenyl ethers (PBDEs), hexabromocyclododecane (HBCD), tetrabromobisphenol A (TBBPA), and polybrominated biphenyls (PBBs). Among these chemicals, PBDEs represent the highest flame retardant in North America as of 2001 (Production volume is shown in Table 2.1).⁽⁸⁾

Transporting large quantity of bromine whether in gaseous or bromide form presents a large hazardous waste spill risk; therefore, brominated compounds are synthesized in the vicinity of their source.⁽⁷⁾ Given the reactivity of bromide, it exists naturally as salts and alkali/alkaline earth metals.⁽⁷⁾ The Organization for Economic Cooperation and Development (OECD) reported that the Arkansas (AR) bromine brine has 0.38 to 0.5% bromine concentration. The high level of bromine coupled with accessibility have led to the mass production of PBDEs in El Dorado, AR by Albermarle Corp. (formerly Ethyl Corp.) and Great Lakes Chemical Company.⁽⁹⁾ PBDEs are manufactured in three technical mixtures

(TMs); the Saytex 102E TM comprised mostly of the deca-PBDE congener (BDE209), the DE-79 TM comprised mostly of octa-PBDE congeners, and the DE-71 TM comprised mostly of penta-PBDE congeners.⁽¹⁰⁾ Detailed TM compositions as reported in La Guardia et al.(2006) are shown in Table A2.1 and Figure 2.1.

Table 2.1. Reported production of TBBPA, HBCD, and PBDEs in the Americas, Europe, and Asia in metric tons in the year 2001.

Compound	Production (metric tons)		
	Americas	Europe	Asia
TBBPA	18000	11600	89400
HBCD	2800	9500	3900
PBDEs	33100	8360	24650

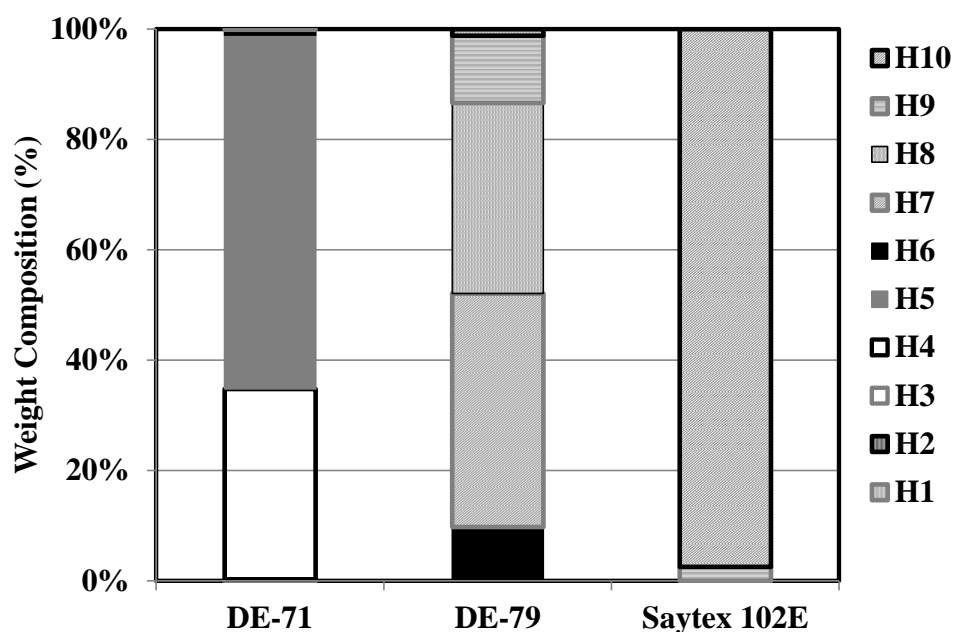


Figure 2.1: Homolog distribution in the three PBDE technical mixtures (Saytex 102E, DE-79, and DE-71) manufactured in North America.

PBDEs are synthesized from diphenyl ethers in the presence of a Friedel-Craft catalyst in brominated solvents such as dibromomethane.^(7, 9) Larger homologs are synthesized by subsequent bromination. The DE-71 TM is almost exclusively incorporated into polyurethane foam found in beddings, furniture and vehicle upholstery^(1, 7, 9, 11, 12) while the DE-79 TM is commonly used in electrical wiring and similar products.^(7, 9, 11) Saytex 102E TM is a general purpose flame retardant mixture and is incorporated into various polymers used in electronic equipment such as polycarbonate, polyester resins, polyolefins, polyamides, and polyvinyl chloride.^(7, 9, 11, 12)

2.1.2. Polychlorinated Biphenyls (PCBs)

From 1929 to 1970, polychlorinated biphenyls (PCBs) were widely used as coolants, dielectric fluids, solvents, and lubricants in electrical equipment such as transformers and capacitors owing to their ability to resist high heat and high thermal heat capacity.⁽¹³⁾ However, PCBs have been found to be toxic and potentially carcinogenic to humans and wildlife.⁽¹⁴⁾ In addition to suspected carcinogenicity, occupational and inadvertent exposure to PCBs have resulted in adverse health impacts including liver damage, thyroid gland injuries, compromised immunities, and impaired reproduction.⁽¹⁴⁾ Because of their toxicity and environmental recalcitrance, PCBs have been classified as a persistent organic pollutant. Concerns on PCB toxicity and its environmental persistence have led to the ban of PCB production in the U.S. in 1970, followed by a worldwide ban by the Stockholm Convention on Persistent Organic Pollutants in 2001.⁽¹³⁾

In North America, Monsanto Corp (St. Louis, MO) was the primary PCB manufacturer.^(4, 13) Of the 570 million kg of PCBs that were sold in the U.S. up to 1975, approximately 68 million kg are estimated to be mobile in the environment and 130 million kg are estimated to be in landfills.⁽⁴⁾ Similar to PBDEs, PCBs were manufactured as formulation trade-named as Aroclor. Specific PCB Aroclor mixture

is identified by a series of four numbers; the first two numbers generally denote the number of carbon atoms in the PCB structure (12 carbons) and the latter two numbers denote the mass percent of chlorine in the mixture.^(15,16) The composition of eight PCB Aroclor mixtures manufactured in North America is shown in Table A2.2 and illustrated in Figure 2.2.

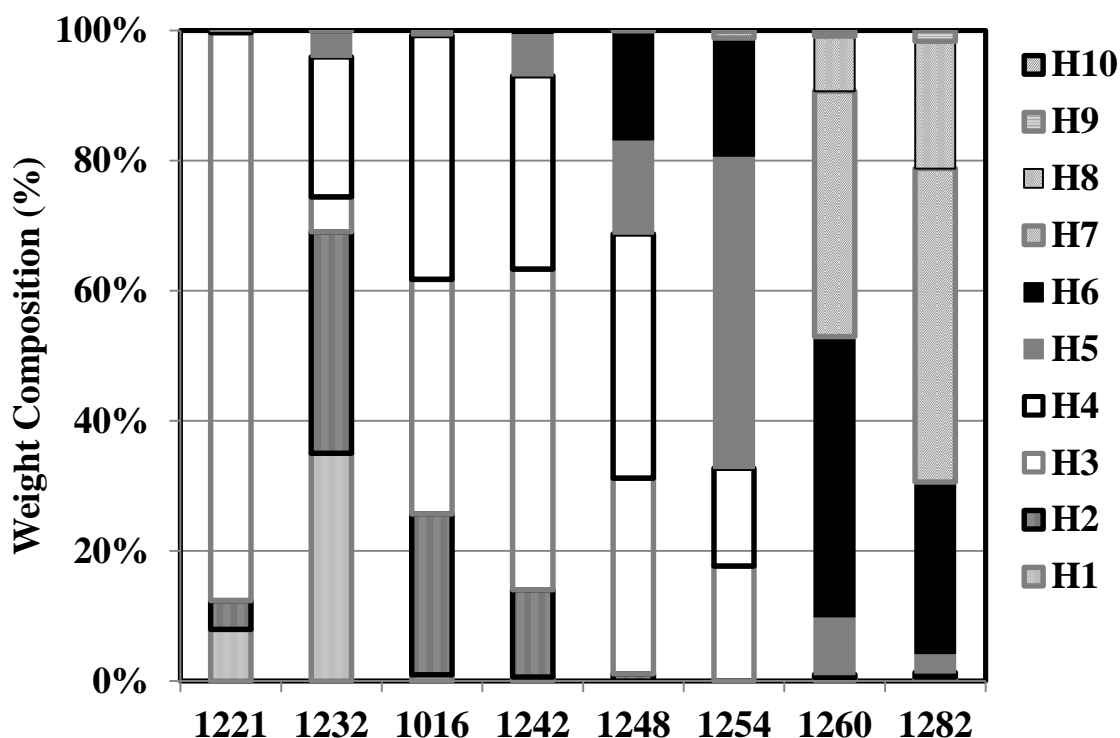


Figure 2.2: Homolog distribution in eight selected PCB Aroclor mixtures manufactured in North America.

2.2. PBDE and PCB Chemical Properties

PBDEs and PCBs each have 209 different congeners; the congeners from these two classes of polyhalogenated aromatic compounds followed the naming convention stipulated by The International

Union of Pure and Applied Chemistry (IUPAC).⁽¹⁵⁾ The phenyl rings are connected by an ether and carbon linkage in PBDEs and PCBs, respectively. The deca-PBDE and deca-PCB structures are shown in Figure 2.3 below.

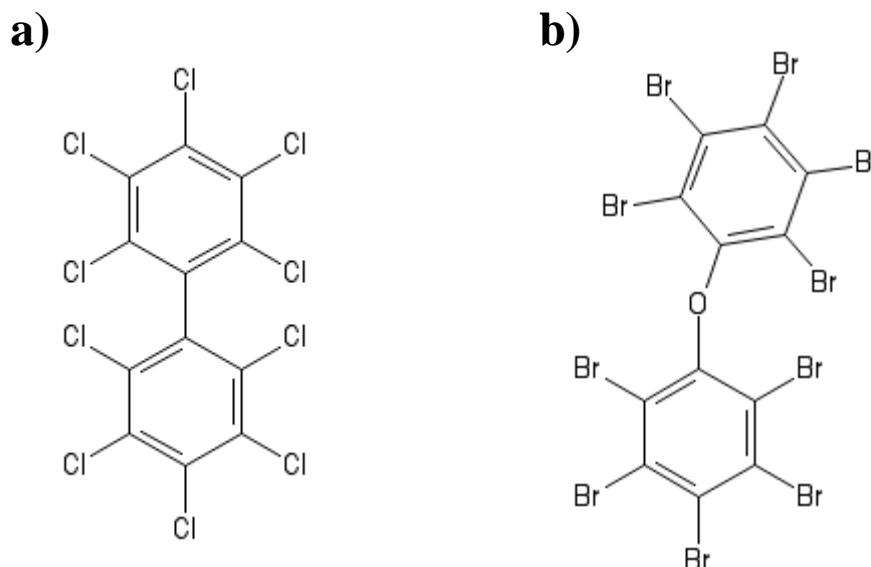


Figure 2.3: Structure of a) decachlorobiphenyl (PCB-209) and b) decabromodiphenyl ether (BDE-209). These are the complete halogenated structure of PCBs and PBDEs with the maximum ten chlorine or bromine substitutions, respectively. PBDE and PCB congeners can have 0 to 10 bromine or chlorine substitutions. Structure was generated in National Center for Biotechnology Information (NCBI) PubChem Sketcher.⁽¹⁷⁾

As with other polyhalogenated aromatic compounds, PBDEs and PCBs physical and chemical properties are influenced by the number of halogens on the molecule. Several studies have measured the physicochemical properties of selected PBDE congeners. In Tittlemeir et al. (2002), the melting temperature (T_m), enthalpies of vaporization (h), solid aqueous solubility at 25°C (C_{SOL25}), and Henry's law constant at 25°C (H_{25}) of select PBDE congeners were experimentally measured using the gas-chromatography column retention and generator column techniques.⁽¹⁸⁾ Braekevelt et al. (2003) employed the slow stir technique to experimentally measure the octanol-water partition coefficient (K_{OW}) of several

PBDE congeners.⁽¹⁹⁾ The measured physicochemical properties of selected PBDE congeners are summarized in Table 2.2.

Table 2.2. Physical properties of selected PBDE congeners.

Congener	$T_m(^{\circ}\text{C})$	$h(\text{kJ/mol})^{(18)}$	$C_{\text{SOL25}}(\text{g/L})^{(18)}$	$H_{25}(\text{Pa m}^3/\text{mol})^{(18)}$	$\text{Log } K_{\text{OW}}^{(19)}$
15	57-58	48	$1.3 \times 10^{-4} \pm 2 \times 10^{-5}$	21	na
28	64-65	80	$7.0 \times 10^{-5} \pm 1 \times 10^{-5}$	5.1	5.94 ± 0.55
47	84-85	95	$1.5 \times 10^{-4} \pm 2 \times 10^{-6}$	1.5	6.81 ± 0.08
66	104-108	98	$1.8 \times 10^{-4} \pm 3 \times 10^{-6}$	0.5	na
77	97-98	99	$6.0 \times 10^{-5} \pm 1 \times 10^{-7}$	1.2	na
85	119-121	110	$6.0 \times 10^{-5} \pm 1 \times 10^{-7}$	0.11	7.37 ± 0.12
99	91-95	108	$9.4 \times 10^{-4} \pm 1 \times 10^{-5}$	0.23	7.32 ± 0.14
100	100-101	102	$4.0 \times 10^{-5} \pm 1 \times 10^{-5}$	0.069	7.24 ± 0.16
153	160-163	110	$8.7 \times 10^{-7} \pm 6 \times 10^{-8}$	0.067	7.90 ± 0.14
154	131-133	113	$8.7 \times 10^{-7} \pm 9 \times 10^{-8}$	0.24	7.82 ± 0.16
183	171-173	118	$1.5 \times 10^{-6} \pm 3 \times 10^{-7}$	0.0074	8.27 ± 0.26

na: Not available

As a legacy contaminant with many decades of research interest, a much larger body of physical property measurements are available for PCBs. A summary of the T_m , C_{SOL25} , H_{25} , and $\log K_{\text{OW}}$ for select PCB congeners are provided in Table 2.3.

Table 2.3 (Cont.). Physical properties of selected PCB congeners.

Congener	$T_m(^{\circ}\text{C})^{(4)}$	$C_{\text{SOL25}}(\text{mmol/m}^3)^{(4)}$	$H_{25}(\text{Pa m}^3/\text{mol})^{(4)}$	$\text{Log } K_{ow}^{(4)}$
1	307	29.5 ± 2.6	74.58	4.30 ± 0.50
2	298	13.3 ± 6.4	62.11	4.60 ± 0.31
3	351	6.4 ± 1.6	58.06	4.50 ± 0.30
4	334	4.5 ± 0.9	22.29	4.91 ± 0.50
6			21.28	4.80 ± 0.30
7	297	5.6 ± 0.7	96.66	5.00 ± 0.30
8	316	4.5 ± 1.8		5.10 ± 0.40
9		8.9 ± 0.5		5.10 ± 0.20
10	308	6.3 ± 0.04		5.00 ± 0.20
11	302			5.30 ± 0.10
12	323			5.30 ± 0.20
14	304			5.40 ± 0.20
15	422	0.3 ± 0.1		
16	301			5.60 ± 0.40
17				5.60 ± 0.10
18	317	1.6 ± 0.8	20.06	5.60 ± 0.10
19				5.60 ± 0.60
20				5.60 ± 0.50
22	346			5.60 ± 0.50
24				5.50 ± 0.50
26				5.50 ± 0.50
28	330	0.6 ± 0.4		5.80 ± 0.20
29	351	0.5 ± 0.2		5.60 ± 0.30
30	335.5			5.50 ± 0.20
31	340		20.26	5.70 ± 0.20
32				5.80 ± 0.30
33	333	0.3 ± 0.08	15.21	5.80 ± 0.30
36				5.70 ± 0.50
37	360	0.06 ± 0.04		5.90 ± 0.20
40	394	0.1 ± 0.01		5.60 ± 0.30
41				6.00 ± 0.30
44	320	0.3 ± 0.2	24.32	6.00 ± 0.30
47	356	0.3 ± 0.1		5.90 ± 0.30
49	337	0.06 ± 0.002	20.27	6.10 ± 0.20
52	360	0.1 ± 0.07	22.29	6.10 ± 0.20
53			30.40	
54				5.90 ± 0.20
60	415			5.90 ± 0.30
61	365	0.07 ± 0.07		5.90 ± 0.30
66	397	0.1 ± 0.1		
70		0.1 ± 0.03	20.26	
74	398			6.10 ± 0.30
77	453	0.003 ± 0.003		6.10 ± 0.40
80	437			6.10 ± 0.40
82			20.27	
84				6.10 ± 0.40
85				6.20 ± 0.40
86	373	0.06 ± 0.03		6.20 ± 0.40

Table 2.3 (Cont.). Physical properties of selected PCB congeners.

Congener	$T_m(^{\circ}\text{C})^{(4)}$	$C_{\text{SOL25}}(\text{mmol/m}^3)^{(4)}$	$H_{25}(\text{Pa m}^3/\text{mol})^{(4)}$	$\text{Log } K_{\text{OW}}^{(4)}$
87	387	0.01 ± 0.03	33.44	6.50 ± 0.40
88	373	0.04 ± 0.003		6.50 ± 0.40
91				6.30 ± 0.50
92				6.50 ± 0.50
95				6.40 ± 0.50
97	354			6.60 ± 0.60
99				6.60 ± 0.60
101	350	0.03 ± 0.03	35.46	6.40 ± 0.50
116	397	0.01 ± 0.006		6.30 ± 0.30
118	378		40.53	6.40 ± 0.30
128	423	0.001 ± 0.001	50.66	6.30 ± 0.30
129	358	0.0006 ± 0.001		7.30 ± 0.50
130				7.30 ± 0.50
134	373	0.001 ± 0.001	57.76	7.30 ± 0.50
135				7.30 ± 0.60
136	387	0.002 ± 0.0006		6.70 ± 0.20
137	350			7.0 ± 0.60
138	352		48.64	7.0 ± 0.50
141			40.53	
144			60.8	
149			30.4	6.80 ± 0.50
151			30.4	
153	376	0.003 ± 0.001	35.46	6.90 ± 0.20
155	387	0.002 ± 0.0005		7.00 ± 0.40
156			88.15	
157			58.77	
158			64.85	
163	361	0.01 ± 0.006		
165				7.00 ± 0.50
171	395	0.005 ± 0.002		6.70 ± 0.40
179				7.00 ± 0.60
183			63.84	
185	422	0.001 ± 0.0005		7.00 ± 0.50
194	432	0.0005 ± 0.0002		7.10 ± 0.50
202	435	0.0007 ± 0.0002		7.10 ± 0.20
206	479	0.0002 ± 0.00007		7.20 ± 1.0
208	456	0.00004 ± 0.000002		8.16 ± 0.10
209	579	0.000002 ± 0.000001		8.26 ± 0.20

As is clear in the data from Tables 2.2 and 2.3, PBDEs and PCBs are highly hydrophobic compounds with low water solubility that are characterized by high K_{OW} values ($\log K_{\text{OW}} > 5$ for most

homologs). These characteristics are similar to other flame retardants such as TBBPA ($\log K_{OW} = 4.5-5.3$)^[20] and HBCD ($\log K_{OW} = 5.8$).^(21,22) T_m and $\log K_{OW}$ increase with increasing bromine substitution in PBDEs whereas C_{SOL25} , h , and H_{25} decrease with increasing bromine substitution. PCBs also showed similar trend for T_m , $\log K_{OW}$, SW_{25} , and H_{25} with increasing halogenation.

While more experimental values are reported for PCB congeners relative to PBDE congeners, there are still data gaps in PCB physical properties. Not all PBDE and PCB congeners can be individually synthesized for experimental measurement. Measurement of parameters such as C_{SOL25} and $\log K_{OW}$ for highly hydrophobic organic contaminants (HOCs) can also be experimentally challenging and produce erroneous results with high uncertainty.

Unfortunately, knowledge of these physicochemical properties is necessary to accurately predict partitioning, degradation rate, and environmental fate of these contaminants. Quantitative structure-property relationships (QSPRs) that exist between molecular structure and chemical property is a commonly utilized technique to fill in the data gaps in physicochemical properties of PBDE and PCB congeners. Primary among them is $\log K_{OW}$, perhaps the most important parameter in assessing the fate of PBDEs in the environment, especially in the sediment medium. Several QSPR equations have been developed to predict the $\log K_{OW}$ values for PBDEs (Equations 2.1-2.2) and PCBs (Equations 2.3-2.4).^(4, 19, 23,24)

$$\text{Log } K_{OW} = 0.0051M_m + 3.8091 \quad (2.1)$$

$$\text{Log } K_{OW} = 0.621N_{Br} + 4.12 \quad (2.2)$$

$$\text{Log } K_{OW} = 0.45N_{Cl} + 4.36 \quad (2.3)$$

$$\text{Log } K_{OW} = 0.40N_{Cl} + 4.33 \quad (2.4)$$

In Equations 2.1 to 2.4, M_m is molecular mass, N_{Br} is number of bromines, and N_{Cl} is number of chlorines. Equations 2.1 to 2.4 were derived at 25°C from the linear free energy relationship (LFER) observed between experimental PBDE and PCB $\log K_{OW}$ values.^(23,19) Predicted $\log K_{OW}$ values from the QSPR empirical correlations in Equation 2.1 to 2.4 are shown in Figure 2.4.

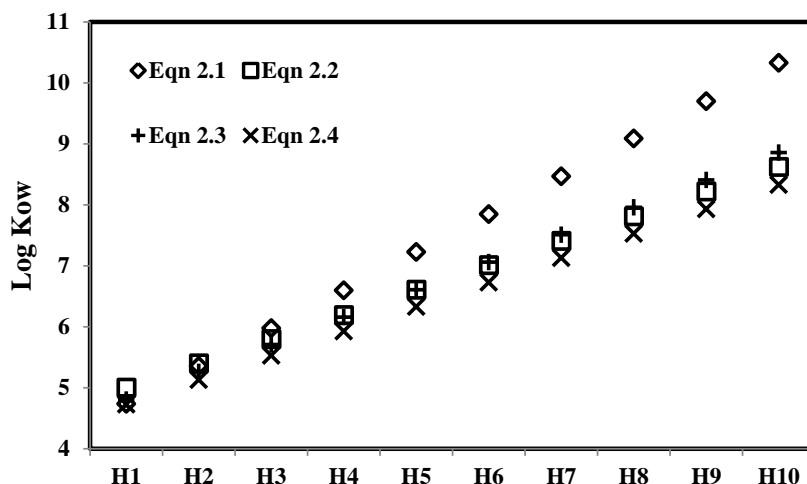


Figure 2.4: PBDE and PCB predicted log K_{OW} values as a function of homolog number from QSPR empirical correlations.

For LMW PBDEs and PCBs (homologs 1 to 3), all QSPR empirical correlations predicted relatively similar log K_{OW} values. With increasing homolog however, the predicted log K_{OW} values showed greater deviation between Equations 2.1 to 2.2 and Equations 2.3 to 2.4, respectively. Overall, the deviation in predicted log K_{OW} values was larger for PBDE homologs relative to PCB homologs.

Estimation software such as the Estimation Program Interface (EPI) can also be used to determine the physicochemical properties of PBDEs and PCBs in lieu of experimentally measured and QSPR derived values.⁽²⁵⁾ The EPI was developed by the USEPA Office of Pollution Prevention Toxics and Syracuse Research Corporation.⁽²⁵⁾ EPI can estimate a suite of environmentally relevant parameters such as C_{SOL} , K_{OW} , and H using estimation methods published in scientific literature. Estimated environmental parameters from the EPI have been used in several scientific publications, particularly for experimentally data-sparse compounds such as PBDEs and PCBs.^(26,27)

The EPI Suite Version 4.11 has 11,200 built in chemical compounds including BDE209. Other PBDE congeners not included in the library can be inputted using the Simplified Molecular Input Line Entry System (SMILES). The SMILES system was developed by Weininger (1988) specifically for coding molecular structure into computers.⁽²⁸⁾ With SMILES, the two dimensional molecular structure is

depicted similar to the way it is drawn on paper.⁽²⁸⁾ Selected PBDE and PCB environmental parameters estimated from the EPI program are shown in Tables A2.3 and A2.4.

2.3. PBDE and PCB Environmental Releases

Among the primary sources of PBDE environmental releases are effluents and emissions from PBDE manufacturing facilities.⁽²⁹⁻³¹⁾ For example, sediments from the River Skerne and River Tees in the UK that receive effluent from a brominated flame retardant (BFR) manufacturer (the main producer of penta-BDE TM in the UK and the sole producer of octa-BDE TM in the European Union) have high concentrations of both penta and octa-BDEs.⁽²⁹⁾ However, the ubiquitous detection of PBDEs in various environmental media^(7,11,32) indicates that effluents and emissions from PBDE manufacturing facilities are not the only sources of PBDEs contamination.

Secondary manufacturing facilities that incorporate PBDE technical products into polymer, textile, and final consumer products can also be a significant source for PBDE environmental release.^(11, 31) For example, Sellstrom et al. (1998) collected sediment samples from the River Viskan upstream and downstream of several textile manufactures that use PBDEs in their final product.⁽³³⁾ Among the main observations of this study is that PBDE levels in the sediment increased progressively downstream as more textile manufacturers were passed. Manufacturing facilities that incorporate PBDEs into various consumer products are more widely distributed relative to PBDE or BFR manufacturing facilities⁽¹¹⁾ and can contribute towards the widespread contamination of PBDEs in the environment.

Another source that contributes towards PBDEs widespread contamination is the post-manufacture use of consumer products. PBDEs can reach up to 14600, 16400, 19400, and 109000 ppm in mattress pads, pillows, sofas, and computer housings, respectively.⁽¹⁾ As PBDEs are additives, they can separate or leach out from product surfaces⁽⁹⁾ and can continue to be released throughout the entire

products' life cycle^(11, 31) PBDEs are released indoors directly from consumer products⁽³⁴⁾ and up to 85% can be distributed into the environment via air advection.⁽³⁵⁾ In Massachusetts, PBDE concentrations in house dust reportedly ranged from non-detect to 10, 23, and 3 ug/g for BDE-47, 99, and 100, respectively.^(36,37) These values are much lower than those reported in a California study with reported dust PBDE concentrations ranging (median [range] in ng/g) from 2700 [112 to 10700], 3800 [102 to 107000], and 684 [non-detect to 30900] for BDE-47, 99, and 100 respectively.^(36,37) The higher levels in the California study were attributed to the higher furniture flammability standard imposed by the state of California;^(36, 37) this suggest that levels of PBDEs in indoor house dust is dependent on amount of bound-PBDEs present in the household. PBDE use patterns not only affect concentrations in indoor house dust, but also affect the congener composition. In the U.K., house dust was dominated by BDE209; in contrast PBDEs in U.S. house dust was enriched in penta-PBDE congeners.⁽³⁸⁾ Furthermore, principal components analysis (PCA) indicated that PBDEs in U.S. house dust originated from penta- and deca-PBDE TMs whereas PBDEs in U.K. house dust originated primarily from the deca-PBDE TM.⁽³⁸⁾ These observations are consistent with the ban on penta- and octa-PBDE TM placed by the European Union since early 2004.

Wastewater treatment plant (WWTP) aqueous discharges and application of sludge as land disposal can also result in widespread PBDE release.^(11, 39-42) In aqueous phase WWTP influent and effluent, PBDEs are bound to suspended particulate matters, consistent with their high K_{OW} values.⁽⁴²⁾ It is estimated that 0.9 kg/year of PBDEs are discharged into the San Francisco Estuary via the Palo Alto WWTP aqueous effluent.⁽⁴⁰⁾ Oros et al. (2005) found that sediment collected near the WWTP discharges had the highest total PBDE concentration in the San Francisco Bay Estuary area.⁽⁴³⁾ This finding formed the hypothesis of the present study that anthropogenic hydraulic discharges such as WWTP effluents can be significant source of PBDEs release into the environment. With a treatment capacity of 22 million gallons per day (MGD),⁽³⁹⁾ the Palo Alto WWTP capacity is >50 times smaller than the capacities of the two main WWTPs in the Chicago area. It is possible that the amount of PBDEs discharged via WWTP aqueous effluent increases with treatment capacity, rendering larger WWTPs serving large metropolitan areas as an important release source of PBDEs to the environment.

Although PCB production has been banned in the U.S. in 1970s, PCBs are still present prominently in the environment. Production and manufacturing facilities that use PCBs are no longer the source of PCB environmental emission since they were globally banned in the late 1970s. Continued use of PCB-containing products resulting in subsequent transport to WWTPs has been identified as a source of PCB environmental release. Releases of PCB into the environment from PCB-containing products are mostly inadvertent.⁽⁴⁴⁾ Plasticizers with PCBs are estimated to release 1000 to 2000 tonnes of PCBs annually.⁽⁴⁴⁾ Up to 1970, almost 60% of the PCB produced by Monsanto Corp. (St. Louis, MO) was used in dielectric, coolant, or conductor applications in closed systems such as transformers that could still be in active use.⁽⁴⁴⁾ It is estimated that PCB release into the environment due to leaks and improper disposal of PCB-containing products is between 4000 to 5000 tonnes per year.⁽⁴⁴⁾

Overall, studies point towards various PBDE and PCB release mechanisms and sources; either via direct releases from chemical manufacturing facilities and industrial effluents from manufacturing facilities that incorporate PBDEs in its production, or from indirect releases from post-manufacture use in consumer products and releases from WWTPs. These various release mechanisms result in the ubiquitous detection of PBDEs and PCBs in the environment.

2.4. PBDEs and PCBs in Sediments

Organic-rich sediments are highly susceptible to PBDE and PCB contamination given the hydrophobic nature of the contaminants. While PBDEs and PCBs are environmentally ubiquitous, this research focuses primarily on sediment contamination, and thus my focus here is on the level of PBDEs and PCBs in sediments, particularly in the North America geographic region.

In Lake Ontario, \sum_{10} PBDEs surface concentrations ranged from 216 to 248 ng/g; 4 to 40 times higher than concentrations reported in the other Laurentian Great Lakes.^(45,46) These high concentrations

were attributed to proximity to several urban areas such as Toronto, Hamilton, Buffalo, and Rochester on the Lake Ontario shoreline. In 1998, BDE209 surface concentration in the west basin of Lake Ontario of 112 ng/g; in 2002, BDE209 surface concentration at the same spot was observed.⁽⁴⁷⁾ In Samara et al. (2006), as high as 148 ng/g of LMW PBDE congeners were reported in the sediments of the Niagara River.⁽⁴⁸⁾ Given that the Niagara River flows into Lake Ontario, it is probable that municipal and industrial discharges into the Niagara River contribute to the accumulation of PBDEs in Lake Ontario,⁽⁴⁸⁾ consistent with the claim that anthropogenic aqueous discharges can disperse PBDEs in the aquatic environment. Lake Michigan had the second highest reported PBDE surface concentrations (\sum_{10} PBDEs ranging from 48 to 98 ng/g).⁽⁴⁹⁾ The effects of urbanization and industrialization on PBDE concentrations are well illustrated in Lake Michigan sampling sites.⁽⁴⁹⁾ In Lake Michigan, the two sampling sites closest to the cities of Chicago, IL and Green Bay, WI have the highest PBDE surface concentrations.⁽⁴⁹⁾ The site in the northern basin located furthest away from Chicago and Green Bay had lower reported \sum_{10} PBDEs surface concentrations.⁽⁴⁹⁾ Lake Erie, surrounded by urbanized areas such as Toledo, OH, Detroit, MI, and Cleveland, OH also had high \sum_{10} PBDEs surface concentrations.⁽⁴⁷⁾ The \sum_{10} PBDEs surface concentrations in Lake Michigan and Lake Erie reported by Song et al. (2005a and 2005b) is in agreement with concentrations reported by Zhu and Hites (2005).^(47, 49, 50) Lake Huron and Lake Superior had relatively lower PBDE concentrations compared to the other Great Lakes.^(47, 49) Studies in other sediment sites in the United States including the Saginaw River Watershed, MI, San Francisco Bay Estuary, CA, and Hadley Lake, IN have reported similar surface PBDE concentrations to those reported for the Great Lakes.^(43, 51, 52) A summary of the surface sediment PBDE concentrations reported in the literature is shown in Table 2.4.

Table 2.4: Reported PBDE concentrations in surface sediments in the U.S.

Location	Sampling Locations ⁽¹⁾	Analyzed Congeners ⁽²⁾	Concentration (ng/g d.w)		
			ΣPBDE ⁽³⁾	BDE-209	Total
Great Lakes					
Lake Michigan ⁽⁴⁹⁾	3	10	1.67-3.97	43.9-95.6	47.87-97.57
Lake Huron ⁽⁴⁹⁾	3	10	1.02-1.87	21.5-36.0	23.15-37.87
Lake Superior ⁽⁴⁵⁾	6	10	0.49-3.14	4.3-17.5	5.3-20.64
Lake Erie ⁽⁴⁵⁾	2	10	1.83-1.95	50.2-55.4	51.83-57.35
Lake Ontario ⁽⁴⁵⁾	2	10	4.85-6.33	211.2-242.0	216.05-248.33
Inland Lake Michigan ⁽⁵³⁾					
White Lake	1	23	2.10	NAN	2.10
Muskegon Lake	1	23	2.10	NAN	2.10
Saginaw River MI ⁽⁵¹⁾	153				
Shiawassee River		10	0.03-3.57	0.15-12.8	NR
Saginaw River		10	0.04-2.54	0.17-49.44	NR
Saginaw Bay		10	0.01-0.92	0.05-6.51	NR
Niagara River ⁽⁴⁸⁾	11	9	0.72-148	NAN	0.72-148
San Francisco Estuary ⁽⁴³⁾					
		22	0.2-211.8	BDL	0.2-211.8
Hadley Lake, IN ⁽⁵²⁾	4	7	5 to 38	19-36	24-71

⁽¹⁾ Number of sampling locations

⁽²⁾ Number of congeners analyzed

⁽³⁾ PBDE concentration except BDE-209

In contrast to the relatively recent scientific study of PBDEs in the Laurentian Great Lakes, the accumulation of PCBs in the Laurentian Great Lakes sediments has been documented since the late 1960s.⁽⁵⁴⁻⁵⁷⁾ In more recent studies, PCBs can still be detected at significant levels in the Great Lakes sediments⁽⁵⁸⁾ four decades after the U.S. PCBs ban. This exemplifies the persistent nature of PCBs. Although PCB levels were high in the Great Lakes sediments in the 1970s, in more recent studies, PCB

concentrations in the Great Lakes surface sediments were less than the archived PBDE concentrations. For example, 19 to 42 ng/g in Lake Michigan, 8 to 19 ng/g in Lake Huron, 3 to 28 ng/g in Lake Superior, 23 to 28 ng/g in Lake Erie, and 58 to 64 ng/g in Lake Ontario.⁽⁵⁸⁾ As was the case with PBDEs, the highest PCB concentrations were observed in Lake Ontario. Although PCBs are still detected in the Great Lakes sediments, several studies have shown reduction in the inventory of sediment and water phase PCBs attributed to *in-situ* degradation and air volatilization, respectively.^(58,59)

While PCB levels in the Great Lakes are lower than PBDE levels, different results have been observed in industrialized areas and historically contaminated sites. For example, total PCB concentrations in the Indiana Harbor and Canal (IHC) was 1200 ng/g.⁽⁶⁰⁾ In the Houston Ship Canal, total PCB concentration peaked at 4600 ng/g in active and heavily trafficked area. PCB discharges to the Hudson River in New York State by General Electric Inc. from 1947 to 1977 resulted in PCB hot-spot locations in the Thompson Island Pool; recent surveys showed that PCB concentrations in the Thompson Island Pool were greater than 20000 ng/g.⁽⁵⁾ Table 2.5 provides a summary of PCB concentrations reported in surface sediments in recent literature.

Table 2.5. PBDE and PCB concentrations in the U.S. surface sediments reported in selected recent studies.

Contaminant	Area	Location	Sampling locations ⁽¹⁾	Analyzed congeners ⁽²⁾	Concentration (ng/g d.w.)
PCBs	Great Lakes Texas New York	Lake Michigan ⁽⁵⁸⁾	3	38	18.6-41.6
		Lake Huron ⁽⁵⁸⁾	3	38	7.8-18.7
		Lake Superior ⁽⁵⁸⁾	4	19	3.4-27.5
		Lake Erie ⁽⁵⁸⁾	2	38	23-28.3
		Lake Ontario ⁽⁵⁸⁾	2	38	58.3-63.6
		Houston Ship Canal ⁽⁶¹⁾	98	209	4 to 4601
		Thompson Island Pool ⁽⁵⁾	1	28	20,140
		Indiana Harbor and Canal ⁽⁶⁰⁾	2	209	1200
	Indiana				

⁽¹⁾ Number of sampling locations ; ⁽²⁾ Number of analyzed congeners

2.5. Microbial Facilitated PBDE and PCB Transformation

In the sediment phase, PBDEs and PCBs can be transformed by selected microorganisms with partial and/or full degradation capability verified in numerous laboratory scale studies of biostimulation, bioaugmentation, and biomimetry experiments; these studies are reviewed in the sections that follow.

2.5.1. Microbial Facilitated PCB Transformation

The potential for *in-situ* PCB dechlorination can be deduced from the distribution of PCB concentrations and congeners in the sediment column.⁽⁶²⁾ For example, comparison of PCB contaminated sediments collected from 16 locations in Canada, Japan, the Netherlands, and United States showed that there were significant decreased in PCB concentrations in the older sediments from recent collection compared to archived sediment data indicating natural attenuation of PCBs was occurring.⁽⁶²⁾ Various studies have shown that PCB congeners deposited in sediments are different than the Aroclor mixtures

either via the presence of congeners absent in the Aroclor mixtures and/or disproportionate presence of congeners.^(58,63, 64) The differences in PCB congeners in sediment to Aroclor mixtures can be quantified using positive matrix factorization⁽⁶⁵⁾ and multiple least square regression (MLSR). To date, most identified microorganisms capable of PCB dechlorination preferentially favors *meta*- and *para*-chlorine removal whereas *ortho*-chlorines are more recalcitrant towards biotransformation.^(58,63) Distribution and relative abundance of *meta*-, *para*-, and *ortho*-chlorine congeners can also be used to evaluate *in-situ* PCB degradation.^(58,63) For example, in Lake Ontario and Lake Hartwell, the decrease in *meta*- and *para*-chlorine fractions with increasing sediment depth was interpreted as strong indication of *in-situ* PCB degradation.^(58,63)

PCBs can be biotransformed by both aerobic and anaerobic microorganisms.^(70-83,87,88,92-96) Under aerobic conditions, PCB degradation typically occurs via the formation of chlorinated dihydro-dihydroxybiphenyl through a dioxygenase attack on an unsubstituted biphenyl ring.⁽⁶⁶⁻⁶⁹⁾ Further enzymatic cleavage of the dihydro-dihydroxybiphenyl compound into chlorobenzoic acid and biphenyl yields a compound that can be mineralized by indigenous microorganisms.^(70,71) Hence, aerobic PCB degradation is sometimes referred to as aerobic PCB mineralization. Research to date suggests that aerobic PCB degradation is more common for PCB congeners with five or fewer chlorine branches due to the necessity of having open carbons for oxygenase attack.^(68,69)

Among the isolated aerobic PCB degraders are *Burkholderia* spp., *Acinetobacter* spp., *Alcaligene* spp., *Ralstonia* spp., *Pseudomonas* spp., and *Rhodococcus* spp.;⁷⁵⁻⁸³ the *Burkholderia xenovorans* strain LB400 which has been genetically and phenotypically characterized⁽⁷²⁾ is among the most well studied microorganism capable of PCB degradation. Inoculation of *Burkholderia xenovorans* strain LB400 was shown to be capable of removing 54 and 57% of the spiked Aroclor 1242 in a two stage anaerobic/aerobic process.⁽⁷³⁾ Another study found that degradation was retarded using PCB as the sole carbon source and addition of sodium pyruvate was necessary to increase the degradation rate of Aroclor 1242 by *Burkholderia xenovorans*, resulting in 85% removal.⁽⁷⁴⁾ *Acinetobacter* spp. strain P6 was shown to be

capable of reducing PCB Aroclor mixtures composed primarily of tetra- and smaller PCBs (Kaneclors 200 and 400) after only four hours incubation.⁽⁷⁵⁾ However, no dehalogenation of PCB Aroclor mixtures composed of high molecular weight (HMW) PCBs was observed (Kaneclor 500 composed primarily of penta-PCB).⁽⁷⁵⁾ Examination of 31 PCB congeners degraded by *Alcaligenes* spp. strain Y42 and *Acinetobacter* spp. strain P6 consistently showed that PCB aerobic dechlorination increases with decreasing PCB molecular weight.⁽⁷⁶⁾ Several *Pseudomonas* spp. strains have been identified as capable of LMW PCB aerobic degradation.⁽⁷⁷⁾ This includes *Pseudomonas aeruginosa* which is capable of cell growth on di- to hexa-PCB as the sole carbon source.⁽⁷⁷⁾ Another study showed that *Pseudomonas* spp. strain LB400 has a more diverse PCB degrading capability compared to *Pseudomonas pseudoalcaligenes* strain KF707.^(78,79) The broad PCB degradation capability of *Pseudomonas* spp. has led to the demonstration of successful *ex-situ* bioremediation in soils and sediments through surfactant washing process.⁽⁸⁰⁾ *Ralstonia* spp. strain SA-3 and *Ralstonia* spp. strain SA-4 were shown to prefer *meta*-chlorine removal; consistent with other studies.⁽⁸¹⁾ Similar to strain LB400, the *Rhodococcus* spp. strain RHA1 was found to be capable of di- to hexa-PCB congeners in PCB Aroclors (Kaneclors 200,300,400, and 500).⁽⁸²⁾ *Rhodococcus erythropolis* and *Rhodococcus ruber* extracted from marine sediments were also capable of substantial PCB degradation.⁽⁸³⁾ Genetic studies showed that all these aerobic microorganisms capable of aerobic mineralization of LMW PCBs share the bphA gene cluster.^(73,84) Interestingly, identified PCBs degraders such as *Rhodococcus* spp. and *Pseudomonas* spp. are quite common and abundant in natural sediment and soil environments.^(85,86)

Under anaerobic conditions, PCBs degrade via sequential reductive dehalogenation where a chlorine accepts an electron from an electron donor and is replaced with a hydrogen.⁽⁸⁷⁾ In contrast to aerobic mineralization, HMW PCB congeners are found to be more amenable to degradation under anaerobic conditions.^(69,87,88) Anaerobic degradation also preferentially favors *meta*- and *para*-chlorine removal.^(66,69,71,87,88) While *ortho*-chlorines are more recalcitrant towards removal, *ortho*-dechlorination is not entirely impossible.⁽⁸⁹⁻⁹¹⁾ Indigenous microorganisms from Baltimore Harbor, Wood Ponds

(Housatonic River, Lenox, MA), and Silver Lake (Pittsfield, MA) can remove *ortho*-chlorine from selected PCB congeners (PCB-26, 32, and 73).⁽⁸⁹⁻⁹²⁾ However it is worth mentioning that these microbial consortia did not show substantial amounts of *ortho*-chlorine removal from Aroclor 1260 congeners.⁽⁸⁹⁻⁹¹⁾

Among the first study to evaluate anaerobic dehalogenation of PCBs was by Quensen et al. (1988); indigenous microorganisms from the PCB-contaminated Hudson River sediments were enriched into a reduced medium with PCB-free sediment.⁽⁹³⁾ Dechlorination of HMW PCB congeners in Aroclor 1242 into mono- and di-PCBs were observed after a 16 weeks incubation period (53% removal) with highest dechlorination rate observed in the consortium spiked with the highest total PCB concentration (700 ppm).⁽⁹³⁾ As expected, *meta*- and *para*-chlorine removal were the primary reduction pathways.

Dehalococcoides spp. from the *Chloroflexi* phylum in particular have been shown to have a very diverse ability to degrade PCBs.⁹²⁻⁹⁷ *Dehalococcoides* derived from Woods Pond (Housatonic River, Lenox, MA) was able to dechlorinate 64 PCB congeners in Aroclor 1260 in sediment-free culture.⁽⁹²⁾ In a more recent publication, *Dehalococcoides* spp. strain CBDB1 was shown to extensively degrade 43 congeners from Aroclors 1248 and 1260.⁽⁹⁴⁾ Competitive polymerase chain reaction (PCR), denaturing high performance liquid chromatography (HPLC), and denaturing gradient gel electrophoresis (DGGE) of enriched microbial communities from contaminated sediments (Grasse and Buffalo River, NY and Anacostia River, DC,⁽⁹⁵⁾ and Baltimore Harbor, Palos Verdes, and Hudson River sediments⁽⁹⁶⁾) indicated the presence of *Dehalococcoides*-like microorganisms. It is possible that yet unidentified microorganisms capable of extensive PCB degradation could still exist in the sediment phase. In addition to *Dehalococcoides* spp., some sulfate reducers can also anaerobically reduce PCBs.⁽⁹⁷⁾ *Desulfovibrio* spp. was shown to be capable of reducing weathered Aroclor 1260 under anaerobic conditions.⁽⁹⁷⁾ All of the anaerobic microorganisms discussed here preferentially removed *meta*- and *para*-chlorines.⁹²⁻⁹⁷

PCB degradation is a very beneficial process from the standpoint of risk and toxicity. Anaerobic reductive dehalogenation favors *meta*- and *para*-removal, thus “dioxin-like” PCB congeners (i.e., PCB

congeners with *meta*- and *para*-chlorine) are more likely to be removed through biotransformation mechanisms.^(62,67) As an added benefit, reductive dechlorination of HMW PCB congeners result in the formation of LMW PCB congeners that are more amenable to aerobic mineralization.^(62,67)

2.5.2. Microbial Facilitated PBDE Transformation

Many laboratory scale studies have focused on identifying microorganisms capable of reductive dehalogenation for their potential PBDE degradation. He et al. (2006) investigated PBDE debromination by *Sulfurospirillum multivorans*, a strain capable of dechlorinating perchloroethylene (PCE) to trichloroethene (TCE),^(98,99) *Dehalococcoides ethenogenes* strain 195 which has been shown to dechlorinate chloroethenes (CEs), chlorobenzenes (CBs), and polychlorinated dibenzodioxins (PCDs),^(100,101) and *Dehalococcoides* strain BAV1 which can degrade dichloroethylenes (DCEs) and vinyl chloride (VC).⁽¹⁰²⁾ Deca- and octa-BDE mixtures in 500 uM TCE solvent were added to initial growth medium with H₂/CO₂ (80/20% v/v).⁽¹⁰²⁾ While *Sulfurospirillum multivorans* culture showed reduction of TCE to cis-dichloroethene (cis-DCE) and acetate within one week, no PBDE debromination was observed. After 2 months, deca-BDE was no longer detected without additional TCE. With the octa-BDE mixture, no new debromination product was observed even after one year of incubation. In the *Dehalococcoides ethenogenes* strain 195 culture, TCE solvent was completely dechlorinated after 8 weeks. The lower rate of TCE dechlorination by *Dehalococcoides ethenogenes* strain 195 compared to *Sulfurospirillum multivorans* suggests that the deca- and octa-BDE mixtures inhibited TCE degradation reaction. After 6 months of incubation, octa-BDE mixture containing hexa- through nona-BDE congeners were debrominated to hepta-, hexa-, and penta-BDE congeners. Debromination of the deca-BDE mixture was not observed even after 1 year of incubation. In *Dehalococcoides* strain BAV1 amendment, no debromination of octa- or deca-BDE mixture was observed after 1 year of incubation period; however addition of *Dehalococcoides* strain BAV1 to *Dehalococcoides ethenogenes* strain 195 promoted further

debromination of octa-BDE mixture indicating that *Dehalococcoides ethenogenes* can degrade HMW PBDE congeners whereas *Dehalococcoides* strain BAV1 can degrade LMW PBDE congeners. In addition, the lack of accumulation of hexa- and penta-BDE congeners showed that *Dehalococcoides* strain BAV1 reduction rate was faster. In all cultures, chromatograms observation suggested sequential reductive debromination of PBDE congeners.

The anaerobic degradation pathway of seven PBDE congeners (BDE-196, 203, 197, 183, 153, 99, and 47) was studied in Robrock et al. (2008) using three TCE enriched consortia of *Dehalococcoides* spp. strain ANAS195, *Dehalobacter restrictus* strain PER-K23, and *Desulfitobacterium hafniense* strain PCP-1.⁽¹⁰³⁾ All seven congeners were reduced to LMW PBDE congeners within three months of incubation. While extent of debromination varies by congeners and cultures, similar kinetic pathway was observed. The *Dehalococcoides* spp. ANAS195, *Dehalobacter restrictus* PER-K23, and *Desulfitobacterium hafniense* PCP-1 often share similar reduction pathways; however, several degradation pathways were unique to specific culture. For example, the *Dehalococcoides* spp. ANAS195 was the sole culture in this study capable of reducing BDE-153 to BDE-118, and BDE-47 to BDE-28, whereas the *Dehalobacter restrictus* strain PER-K23 was found to be capable of reducing BDE-196 to BDE-191, and BDE-183 to BDE-139. BDE-197 was debrominated in equal amounts into BDE-183, 184, and 176 by *ortho*, *meta*, and *para*-substitution, respectively. Debromination of BDE-203 however, had *meta* and *para*-debromination bias, as evidenced by the production of large amounts of BDE-183 and 187 relative to BDE-180 (the *ortho*-substitution product). Debromination of BDE-196 to BDE-183, 182, and 175 in all three cultures were observed. An additional *ortho*-product, BDE-180, was also produced in BDE-196 debromination with *Desulfitobacterium hafniense* and *Dehalococcoides* strain ANAS 195. Debromination of BDE-183 to BDE-154 (through *meta*-removal), BDE-153 (through *ortho*-removal), and BDE-149 and 144 (through *para*-removal) were observed in all three cultures. *Dehalobacter restrictus* was also able to produce BDE-139 through *meta*-removal. All three cultures debrominated BDE-153 to BDE-99 and 101. BDE-118 formation was observed in the *Dehalococcoides* ANAS195 culture

incubation. BDE-99 was debrominated to BDE-47 and 49 by *meta*- and *para*-removal. *Dehalobacter restrictus* and *Desulfitobacterium hafniense* produced BDE-48 via *para*-debromination of BDE-99. *Ortho*-debromination of BDE-99 to BDE-66 was only observed in *Dehalococcoides* strain ANAS195 and *Desulfitobacterium hafniense* cultures. *Desulfitobacterium hafniense* and *Dehalobacter restrictus* debrominate BDE-47 to BDE-17 and sequentially to BDE-4.

Overall, the first order PBDE debromination rate typically decreases with increasing bromine substitution.^{102,103} To date, most anaerobic microbial facilitated reduction pathways suggest favorable *para*- and *meta*-bromine removal with preferences defined as relatively higher congener production resulting from *para*- and/or *meta*-bromine removal.^{102,103} Bromines located in doubly-flanked position are more susceptible to debromination, consistent with increased in enthalpies of formation resulting from repulsion between adjacent bromines.^{102,103} While *ortho*-bromine removal does occur, the kinetic rate is much lower than *para*- and *meta*-bromine removal, as evidenced by lack of substantial formation of *ortho*-substituted products.^{102,103} Preferential removal of *para*- and *meta*-substituted halogens over *ortho*-debromination is similar to the case of PCBs.^(104,105)

In the case of PCBs, biphenyls with three to six chlorines are widely known to be aerobically mineralized by common soil microorganisms.^(85,86,101,106) In contrast, although aerobic oxidation typically yields more energy than anaerobic catabolism, little is known about aerobic PBDE degradation. Among the first identified aerobic bacterium capable of PBDE degradation was *Sphingomonas* spp. strain SS3, which is capable of degrading monobromodiphenyl ether.⁽¹⁰⁷⁾ A different strain, *Sphingomonas* spp. SS33 was later isolated that can aerobically reduce di-BDE congeners.⁽¹⁰⁷⁾ Aerobic degradation of HMW PBDEs was not confirmed until recently.⁽¹⁰⁸⁾ Robrock et al. (2009) investigated the debromination potential of mono- to hexa-BDE congeners by several aerobic strains; *Rhodococcus jostii* strain RHA1, *Burkholderia xenovorans* strain LB400, and *Pseudonocardia dioxanivorans* strain CB1190.⁽¹⁰⁸⁾ The first two bacteria are known PCB degraders and the last strain is an ether degrader. *Rhodococcus jostii* strain RHA1 and *Burkholderia xenovorans* strain LB400 transformed more than 90% of the mono- and di-BDE

within three days. Over the same time, only 10 to 45% of the penta-BDE was transformed. The most resistant PBDE congeners were the hexa-BDEs. LB400 was capable of reducing 18% of BDE-138, but was not able to degrade other hexa congeners (BDE-153 and 149). *Rhodococcus jostii* strain RHA1 was only able to degrade mono-BDEs and BDE-7. Only 16% of the mono-BDEs were reduced by *Pseudonocardia dioxanivorans* strain CB1190. *Rhodococcus jostii* strain RHA1 appeared to be most versatile in terms of PBDE degradation capability based upon studies of its debromination activity with DE-71 TM. Results showed the same general pattern as observed in individual PBDE congeners experiment; 95, 78, and 45% of BDE-47, 99, and 100 were removed, respectively. In general, transformation of mono to hexa-BDE was inversely proportional to the degree of bromination. This is expected as PBDE congeners are expected to be less bioavailable with the increasing size and hydrophobicity of higher brominated congeners. A similar trend has been observed in aerobic PCB degradation by *Rhodococcus jostii* strain RHA1 and *Burkholderia xenovorans* strain LB400.^(79,84)

Deng et al. (2011) evaluated the aerobic degradation potential of BDE-209.⁽¹⁰⁹⁾ Out of the 155 bacterial colonies isolated from sediments contaminated with high levels of PBDEs, *Lysinibacillus fusiformis* strain DB-1 showed the highest efficiency for BDE-209 degradation. Accumulation of bromide ion was observed within four weeks of incubation. While this strain can grow on acetate and pyruvate, the highest growth rate was observed with lactate as carbon source. Isolation of a bacterial strain from PBDE-contaminated sediments suggests that PBDE degradation can take place *in-situ* in the environment. While environmental conditions may not be favorable, bacterial adaptation can lead to significant *in-situ* debromination.

In-situ microbial degradation reaction is likely a more complex process than just one bacterial species or strain reducing a particular PBDE congener. Bioreactors, such as the fixed-film plug flow biological reactor is often used for enrichment of wild-type microbial consortia to stimulate the natural biodegradation process. Several studies have demonstrated the efficacy of the bioreactor to reduce chlorinated organic pollutants such as PCBs and chlorophenols under anaerobic conditions.^(110- 113) Rayne

et al. (2003) was among the earliest to evaluate PBDE degradation potential in wild-type microbial consortia. In this study, indigenous microbial community from a wetland located down-gradient of a historical munitions dump was colonized in a bioreactor to quantify the microbial degradation of BDE-15. The possibility of bromine transfer was eliminated by extensive analysis of 32 congeners from the same or lower homolog group. The study found substantial ratios of BDE-3 and diphenyl ether (non-brominated form of PBDE congeners) with respect to BDE-15 initial concentration which suggests increasing debromination rate with decreasing bromination; it is postulated that debromination rate increased due to less steric hindrance in smaller compounds which makes the bromine atom more susceptible to microbial attack.^(112,113)

Although Rayne et al. (2003) demonstrated the reductive debromination of a di-PBDE congener, the possibility for microbial reduction of HMW PBDE congeners by microbial consortia was not demonstrated until Gerecke et al. (2005).^(114, 115) They demonstrated that BDE-209 in sewage sludge can be reduced under anaerobic conditions after 238 days incubation period.⁽¹¹⁵⁾ In the presence of five different set of possible dehaloprimers (4-bromobenzoic acid 2, 6-dibromobiphenyl, tetrabromobisphenol A, hexabromocyclododecane, and decabromobiphenyl), approximately 30% of amended BDE-209 concentration was removed at a pseudo first order reaction rate constant of $1 \times 10^{-3} \text{ d}^{-1}$. Analysis of gas production showed that reduction reaction took place under methanogenic conditions. Formation of two nona- and six octa-BDE congeners was observed. Although incubation in the absence of primers resulted in a 50% slower reaction rate, the same nona- and octa-BDE congeners were observed after the same incubation period. In both the presence and absence of primers, removal of bromine from the *meta*- and *para*-positions were favored whereas *ortho*-removal was insignificant.

The low bioavailability of PBDEs is also likely a limiting factor in their biotransformation potential. Both Rayne et al. (2003) and Gerecke et al. (2005) spiked the microbial cultures with PBDEs.^(114, 115) Bioavailability however, is not the only factor affecting microbial PBDE degradation process. Presence of the appropriate electron donors and competing electron acceptors could also affect PBDE

degradation kinetics. For example, Lee and He (2010) collected 28 sediment samples from 3 regions (Wuhan in Hubei, China; Guiyu in Guangdong, China; Singapore and San Francisco in California, North America) with different characteristics. The samples were enriched with three electron donors (lactate, pyruvate, and acetate) prior to addition of octa-BDE TM in TCE or nonane solvent.⁽¹¹⁶⁾ The octa-BDE in nonane solvent enabled the investigation of PBDE debromination without any external electron acceptors. In microcosms supplied with octa-BDE in TCE, debromination products were observed in 20 out of 28 microcosms within one month, as measured by appearance of new product peaks in gas chromatography. Penta- and tetra-BDE congeners were also detected in most samples whereas tri- and di-BDE were rarely detected. The large number of microcosms with debromination activity indicates that PBDE-reducing bacteria can be found in sediment samples from various regions. For microcosms supplied with octa-BDE TM in nonane, only 11 out of 28 microcosms had active debromination. After two months, hexa-BDE was detected in all active samples whereas penta- and tetra-BDEs were only detected in five samples. The smaller amount of active microcosms coupled with the less extensive debromination (as compared to microcosms enriched with octa-BDE TM in TCE) suggested that the presence of external electron acceptors other than PBDEs can stimulate degradation. Interestingly, microcosms with high debromination rate in octa-BDE TM in TCE showed no activity when enriched with octa-BDE TM in nonane. The reverse trend was also true for microcosms with high degradation rate in octa-BDE TM in nonane. Electron donors also played a key role in PBDE degradation; microcosms enriched with acetate showed a wider range of debromination products compared to microcosm enriched with lactate and pyruvate. Lee and He (2010) transferred the most active microcosm enrichment to sediment-free culture for further study. After 42 days, concentrations of octa-BDE decreased; however no debromination beyond tetra-BDE was observed, even after eight months of incubation. PBDEs in the sediment-free culture had a faster degradation rate, although with a limited degradation ability. This suggests that certain components exist within the sediment matrix that can limit the PBDE degradation rate. On the other hand, microbial components that can enhance the degradation of smaller PBDE congeners are

potentially present in the sediment matrix, as evidenced by the wider ability of PBDE degradation in sediment culture relative to sediment-free culture.

Thus far, studies summarized in this section have focused on the changes in contaminant composition due to specific microorganism and/or microbial consortia activities. Complete characterization of the microbial community structure in a contaminated environment was previously an experimentally challenging and time consuming process.⁽¹¹⁷⁾ This typically required PCR of denaturing gradient gel electrophoresis bands followed by extraction, purification, and amplification of the genomic DNA.⁽¹¹⁷⁾ In the advent of next generation sequencing technology such as pyrosequencing, complete microbial community characterization can be accomplished rapidly while providing higher resolution data.⁽¹¹⁷⁾ The research in this thesis was designed to take advantage of rapid and high throughput next generation sequencing technology to characterize the microbial community composition in PBDE and PCB contaminated sediments and shed some light on the potential of *in-situ* microbial facilitated diphenyl and biphenyl ether degradation.

2.6. PBDE and PCB Transport Processes In The Sediment Phase

Transport processes in saturated sediment environment driven by partitioning, chemical gradients, and porewater advection promote the movement of contaminants such as PBDEs and PCBs in the sediment phase.⁽¹¹⁸⁾ In the sediment phase, PBDEs and PCBs can migrate from one contaminated sediment segment to another sediment segment. Of particular interest in this study is the vertical migration of PBDEs and PCBs in the sediment column obtained from core sampling in depositional environments. These samples are sectioned and dated as a proxy measurement of age. This section provides an overview of the known mechanisms for PBDE and PCB movement and/or transport in the sediment column.

2.6.1. Partitioning between solute and solid phase

Partitioning of contaminants between the pore water and solid phase can have a substantial effect on the mobility, fate, and transport potential of pollutants.⁽¹¹⁸⁾ Sorption to sediment particles can retard migration and is typically the most significant control on mobility⁽¹¹⁸⁻¹²¹⁾ Equation 2.5 can be used to express the equilibrium partition coefficient of an organic chemical between the porewater and sediment particle phases (K_d).⁽¹¹⁸⁾

$$K_d = \frac{C_s}{C_w} \quad (2.5)$$

In Equation 2.5, C_s is the sediment phase concentration (g/g) and C_w is the aqueous phase concentration (g/cm³).⁽¹¹⁸⁾ This K_d has units of volume/mass (cm³/g). For HOCs, K_d value can be approximated by the sorption to the organic carbon (OC) and mineral phases of the sediment⁽¹¹⁸⁾ as expressed in Equation 2.6 below.

$$K_d = f_{min}S_AK_{d,min} + f_{oc}K_{OC} \quad (2.6)$$

In Equation 2.6, f_{min} and f_{oc} are mineral and OC fraction in the sediment and the sum of f_{min} and f_{oc} equals 1, S_A is the specific surface area (cm²/g), $K_{d,min}$ (cm³/g) is the mineral equilibrium partition coefficient and K_{OC} (unitless) is the OC partition coefficient. In sediment with high OC content ($f_{oc}>0.1\%$), the mineral sorption can be neglected (i.e., $f_{min}S_AK_{d,min} \ll f_{oc}K_{OC}$) which simplifies Equation 2.6 to the equation below.

$$K_d = f_{oc}K_{OC} \quad (2.7)$$

Current understanding of HOCs transport in sediments typically assumes that Equation 2.7 governs partitioning in the absence of detailed characterization. Thus, K_{OC} values can be obtained from the literature. When experimental K_{OC} values are not available, K_{OC} values can be estimated from K_{OW} values using linear free energy (LFER) empirical correlations. Table 2.6 provides a comprehensive

summary of the empirical correlations that can be used to estimate K_{OC} values for PBDEs and PCBs. LFERs shown in Table 2.6 are for compounds that share structural, hydrophobicity, and/or aromaticity similarity to PBDEs and PCBs. In addition, K_{OC} values can also be estimated from quantitative structure activity relationship (QSAR) as utilized in the USEPA Estimation Program Interface Suite (EPI) in the KOCWIN™ program.⁽¹²²⁾ K_{OC} values estimated by the USEPA EPI program for PBDE and PCB congeners are summarized in Tables A2.3 to A2.4.

Table 2.6. Summary of reported empirical correlations to estimate KOC values from KOW values for hydrophobic and halogenated compounds. Number of compound (n), regression coefficient (R²), and standard error (SE) is included when available.

Correlation⁽¹⁾	Description
$\text{Log } K_{OC} = 0.81 \text{ Log } K_{OW} + 0.09$ (n=118; R ² =-.89, SE= ± 0.42) ⁽¹²³⁾	Regression analysis of aggregated literature data for various HOCs
$\text{Log } K_{OC} = 1.08 \text{ Log } K_{OW} + 0.41$ ⁽¹²³⁾	Recommended upper limit from statistical analysis of aggregated literature data for various HOCs
$\text{Log } K_{OC} = 0.99 \text{ Log } K_{OW} - 0.81$ ⁽¹²³⁾	Recommended lower limit from statistical analysis of aggregated literature data for various HOCs
$\text{Log } K_{OC} = 0.90 \text{ Log } K_{OW} + 0.09$ (n=72, R ² =0.91) ⁽¹²⁴⁾	Regression analysis for 11 classes of organic chemicals including 6 PCB congeners
$\text{Log } K_{OC} = 0.68 \text{ Log } K_{OW} + 0.66$ (n=419, R ² =0.83) ⁽¹²⁵⁾	Regression analysis for >400 compounds including aromatic halogenated compounds
$\text{Log } K_{OC} = 0.72 \text{ Log } K_{OW} + 0.42$ (R ² =0.86) ⁽¹²⁵⁾	Regression analysis for aromatic halogenated compounds
$\text{Log } K_{OC} = 0.54 \text{ Log } K_{OW} + 1.38$ (n=45, R ² =0.74) ⁽¹²⁶⁾	Regression analysis for pesticides including organochlorine pesticides
$\text{Log } K_{OC} = 0.81 \text{ Log } K_{OW} + 0.10$ (n=81, R ² =0.89) ⁽¹²⁷⁾	Regression analysis for hydrophobic compounds including aromatic halogenated compounds
$\text{Log } K_{OC} = 0.63 \text{ Log } K_{OW} + 0.90$ (n=54, R ² =0.87) ⁽¹²⁷⁾	Correlation for phenolic, anilines, nitrobenzenes, and chlorinated benzonitriles
$\text{Log } K_{OC} = 0.90 \text{ Log } K_{OW} - 0.54$ (n=12, R ² =0.99) ⁽¹²⁸⁾	Correlation for PAHs and chlorinated hydrocarbons
$\text{Log } K_{OC} = 1.00 \text{ Log } K_{OW} - 0.21$ (n=10, R ² =1.00) ⁽¹²⁹⁾	Regression analysis for chlorinated hydrocarbons and pesticides
$\text{Log } K_{OC} = 0.72 \text{ Log } K_{OW} + 0.46$ (n=65, R ² =0.93, SE=0.44) ⁽¹³⁰⁾	Multiparameter regression analysis on polychlorinated organic compound
$\text{Log } K_{OC} = 0.99 \text{ Log } K_{OW} - 0.35$ (R ² =0.98) ⁽¹³¹⁾	Regression analysis for 7 class of compounds including chlorinated hydrocarbons
$\text{Log } K_{OC} = 0.72 \text{ Log } K_{OW} + 0.49$ (R ² =0.95) ⁽¹³²⁾	Regression analysis for methylated and halogenated benzenes

⁽¹⁾Log K_{OC} when expressed as A*log K_{OW} ± b have A value ranging from 0.63 to 1 (average ± standard deviation as 0.96±0.60) and b value ranging from -0.81 to 1.38 (average ± standard deviation as 0.22±0.58).

2.6.2. Chemical Diffusion Process

Once in the porewater, contaminants move through the sediment via diffusion and bulk advection. Chemical diffusion is driven by a concentration gradient between defined transport boundaries.^(118, 133) The sediment phase is a highly porous and tortuous medium.⁽¹¹⁸⁾ As a general rule, compounds with LMW has a higher diffusive mobility.^(133, 134) Additionally, a larger concentration gradient will drive faster diffusion.^(133, 134) Chemical diffusion flux occurs through random Brownian motion of ions and/or molecules in the sediment phase and can be mathematically expressed using Fick's first law shown in Equation 2.8.⁽¹³⁴⁾

$$J_{diff} = -D \frac{\partial C}{\partial x} \quad (2.8)$$

In Equation 2.8, the J_{diff} is the mass flux density ($\text{g m}^{-2} \text{s}^{-1}$), D is the diffusion coefficient ($\text{m}^2 \text{s}^{-1}$) and the differential $\frac{\partial C}{\partial x}$ is the change in concentration over diffusive path length. The chemical flux through a defined segment of length x over a defined period of time t can be mathematically described by differentiating the flux with time as in Fick's second law of diffusion shown in Equation 2.9.^(133, 134)

$$\frac{\partial C}{\partial t} = D \frac{\partial^2 C}{\partial x^2} \quad (2.9)$$

In cases where boundary conditions are defined as $C_w(x,0) = C_w(\infty,t)=0$ and $C_w(0,t)=C_0$, the close form solution for Equation 2.9 can be expressed as shown in Equation 2.10.⁽¹³⁵⁾

$$\frac{C}{C_0} = \text{erfc}\left(\frac{x}{\sqrt{4D_{obs}t}}\right) \quad (2.10)$$

In Equation 2.10, C_0 is the initial aqueous phase concentration (g/cm^3), erfc is the complimentary error function, and D_{obs} is the observed diffusion coefficient (m^2/year) defined in Equation 2.11.⁽¹³⁵⁾

$$D_{obs} = \frac{D_{eff}}{R} \quad (2.11)$$

In Equation 2.11, R is the retardation factor (unitless) which represents the slower rate of chemical diffusion relative to water given sorption or partitioning into solid phase and D_{eff} is the effective diffusion coefficient ($m^2/year$) in porous media of tortuosity (τ). D_{eff} captures the slower diffusion process relative to molecular diffusion (D_{mol}) ($m^2/year$) attributed by diffusion occurring over a tortuous path.^(118,134) The sediment matrix is an example of a media where tortuosity has an impact on the chemical diffusion process.¹³² D_{eff} can be obtained by correcting D_{mol} as shown in Equation 2.12.⁽¹³⁵⁾

$$D_{eff} = D_{mol}\tau \quad (2.12)$$

In Equation 2.12, τ is the tortuosity of the diffusion path length (m/m) in the porous medium. τ is difficult to measure, and is typically estimated from porosity. One of the most widely used is the empirical correlation shown in Equation 2.13.⁽¹³⁵⁾ The R term in Equation 2.11 can be estimated from K_d , dry bulk density (ρ_{dry}), and ϕ_e as in Equation 2.14.

$$\tau = \phi_e^{4/3} \quad (2.13)$$

$$R = 1 + K_d \frac{\rho}{\phi_e} \quad (2.14)$$

Substitution of Equations 2.11 through 2.14 into Equation 2.10 results in an expanded equation for diffusive concentration as a function of distance and time as shown below.

$$\frac{C}{C_o} = \text{erfc}\left(\frac{x}{2\sqrt{D_{mol}\phi_e^{7/3}}} \frac{\sqrt{\phi_e + \rho K_d}}{\sqrt{t}}\right) \quad (2.15)$$

2.6.3. Advection process

Advection describes the movement of chemical species in the sediment phase induced by bulk porewater movement.^(118, 133, 134) When both advection and molecular diffusion are occurring, J_{diff} through

the bulk fluid movement typically exceed that of molecular diffusion.⁽¹¹⁸⁾ In one dimensional (1D) flow, the advection-diffusion process can be incorporated into Fick's second law to yield the 1D advection-diffusion equation shown in Equation 2.16.

$$\frac{\partial C}{\partial t} + v \frac{\partial C}{\partial x} = D \frac{\partial^2 C}{\partial x^2} \quad (2.16)$$

In Equation 2.16, the term $v \frac{\partial C}{\partial x}$ represents the advection process where v is the porewater chemical velocity (m/s). The porewater velocity is calculated using hydraulic gradient ($\frac{dh}{dx}$), hydraulic conductivity (K_h), R , and ϕ_e from Darcy's law as shown in Equation 2.17.

$$v = \frac{K_h \frac{dh}{dx}}{R \phi_e} \quad (2.17)$$

K_h is a function of particle size and distribution where K_h increases with more coarse and well-sorted sediment particles.[118] When introducing chemical mass in a uniform vertical sediment column to initial boundary condition of $C_w(0,t) = C_0$, the closed form analytical solution for Equation 2.18 is as shown below.

$$\frac{C}{C_0} = \frac{1}{2} \left[\operatorname{erfc} \left(\frac{x-vt}{\sqrt{4D_{\text{obs}}}} \right) + \exp \left(\frac{xv}{D_{\text{obs}}} \right) \operatorname{erfc} \left(\frac{x-vt}{\sqrt{4D_{\text{obs}}}} \right) \right] \quad (2.18)$$

Equation 2.18 can be expanded to measurable parameters by substituting Equation 2.11 through 2.14 into Equation 2.18.

$$\begin{aligned} \frac{C}{C_0} = & \frac{1}{2} \left(\operatorname{erfc} \left(\frac{x \sqrt{\phi_e + \rho K_d}}{2 \sqrt{D_{\text{mol}} \phi_e^{7/3}}} \sqrt{t} - \frac{K_h}{\sqrt{\phi_e + \rho K_d}} \frac{\frac{dh}{dx}}{2 \sqrt{D_{\text{mol}} \phi_e^{7/3}}} \sqrt{t} \right) + \dots \right. \\ & \left. \exp \left(\frac{x K_h \left(\frac{dh}{dx} \right)}{D_{\text{mol}} \phi_e^{7/3}} \right) \operatorname{erfc} \left(\frac{x \sqrt{\phi_e + \rho K_d}}{2 \sqrt{D_{\text{mol}} \phi_e^{7/3}}} \sqrt{t} + \frac{K_h}{\sqrt{\phi_e + \rho K_d}} \frac{\frac{dh}{dx}}{2 \sqrt{D_{\text{mol}} \phi_e^{7/3}}} \sqrt{t} \right) \right) \end{aligned} \quad (2.19)$$

2.6.4. Adsorption To Black Carbon

OC structure plays a key role in partitioning that is not characterized by simple f_{OC} equations shown in Table 2.6.⁽¹³⁶⁾ In particular, condensed phase soots, chars and cenospheres, collectively known as black carbon (BC) act as a “super sorbent” to HOCs.⁽¹³⁶⁾ Diffusion and advection-diffusion processes are also affected by adsorption to the BC. Partition coefficients of HOCs to BC (K_{BC}) can be expressed using the non-linear Freundlich sorption isotherm shown in Equation 2.20.⁽¹³⁷⁻¹³⁹⁾

$$K_{BC} = f_{BC} K_{F_{BC}} C_w^{NF-1} \quad (2.20)$$

In Equation 2.20, f_{BC} is black carbon fraction, $K_{F_{BC}}$ is the Freundlich constant accounting for non-linear adsorption to BC, C_w is the dissolved aqueous concentration as before, and NF is the Freundlich number.⁽¹³⁷⁻¹³⁹⁾ Regression analysis of PBDEs and PCBs between porewater and the sediment phase provided $K_{F_{BC}}$ estimation from K_{OW} via Equations 2.21 and 2.22 for PBDEs and PCBs, respectively.⁽¹³⁹⁾

$$\text{Log } K_{F_{BC}} = 1.088 * \text{Log } K_{OW} - 1.365 \quad (2.21)$$

$$\text{Log } K_{F_{BC}} = 0.928 * \text{Log } K_{OW} + 0.080 \quad (2.22)$$

Absorption of PBDEs and PCBs to organic matter phase of the sediment is expected to be linear. In contrast, PBDE and PCB adsorption to BC is expected to follow a non-linear Freundlich isotherm.⁽¹³⁷⁻¹³⁹⁾ In linear sorption, the NF value equals one.⁽¹⁴⁰⁾ The affinity for sorption to the solid and aqueous phase depends on the NF value; when NF value is larger than 1, the sorbate will have a larger affinity for the solid phase, whereas when NF value is smaller than 1, the sorbate will have a larger affinity for the aqueous phase.⁽¹⁴⁰⁾ Sorption can also be limited by surface saturation, which is modeled using the Langmuir isotherm.⁽¹⁴⁰⁾ Due to the low levels of HOCs in sediments relative to sorption sites, it is unlikely that saturation will be approached in the sediment environment. Illustrations of these concepts are shown in Figure 2.3.

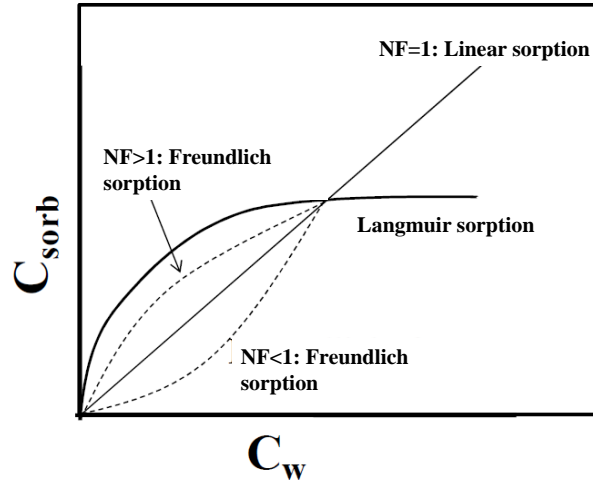


Figure 2.3: An illustration of the isotherm sorption model. Adapted from Alvarez and Illman (2005).⁽¹⁴⁰⁾

When considering both absorption to OC and adsorption to BC, the K_d expression can be expanded as shown in Equation 2.23 to include HOCs partitioning to BC.

$$K_{d|Total} = f_{OC}K_{OC} + f_{BC} * KF_{BC} * C_w^{NF-1} \quad (2.23)$$

To model diffusion and diffusion-advection vertical migration that take into consideration both the OC and BC portions, Equation 2.23 can be substituted in lieu of Equation 2.7. As part of this thesis, I will model PBDE and PCB vertical migration using established transport models. There are substantial uncertainties due to data gaps in PBDE and PCB physicochemical properties needed for these models, as well as variability in sorbent (sediment column) properties. Therefore, I will employ a Monte Carlo approach to deal with these uncertainties. With Monte Carlo, a set of values (e.g. range, average, standard deviation) can be used to guide random resampling or bootstrapping to obtain a distribution for each parameter. The results for the vertical migration modeling will be a distribution of output reflecting the probability associated with its predicted value.

Monte Carlo approach has been used successfully to model mass transport of HOCs^(120, 121) and organo-metals^(119, 141) from contaminated underlying sediment across different capping materials. In Viana

et al. (2008), Monte Carlo approach was used to model diffusion and advection-diffusion of a suite of heavy metals (Cadmium, chromium, lead, silver, arsenic, barium, mercury, methyl mercury, and cyanide) across several different capping materials including sand, granular activated carbon (GAC) , organoclay, shredded tires, and apatite.^(118,140) Under diffusion only conditions, the lowest breakthrough for all heavy metals was observed in the sand cap. This was attributed to longer diffusive path length in sand. Organoclay and apatite showed high affinity for different heavy metals under the advection-diffusion conditions. Mass transport of silver, arsenic, barium, methyl mercury, and cyanide was best controlled by organoclay whereas apatite showed high affinity for cadmium, chromium, and lead. The main drivers for heavy metals mass transport across the cap material were K_d and K_h . Using similar modeling approach, shredded tires was predicted as the best cap material among sand, GAC, organoclay, and apatite to control the mass transport of twelve HOCs (benzene, toluene, ethylbenzene, naphthalene, phenanthrene, pyrene, dichlorobiphenyl, tetrachlorobiphenyl, hexachlorobiphenyl, octane, dodecane, and tetradecane) under diffusion conditions.^(120, 121) The increased performance of shredded tires under diffusion condition was attributed to thickness of the shredded tire active caps (conventionally, shredded tire active caps are thicker compared to the other cap materials) and higher R values. Predicted HOCs mass transport was lowest in the organoclay and GAC caps under the advection-diffusion condition due to the low K_h in these cap materials. The Monte Carlo approach has enabled the mass transport prediction of data-spare HOCs and organometals under diffusion and advection-diffusion conditions. Adopting this approach, one of the goal of this research is to gain better insight into the drivers of *in-situ* PBDE and PCB mass transport in the sediment column.

CHAPTER 3. CHARACTERIZATION OF URBAN CHICAGO SEDIMENTS CONTAMINATED WITH POLYBROMINATED DIPHENYL ETHERS (PBDEs) AND POLYCHLORINATED BIPHENYLS (PCBs)

3.0. Abstract

Urban areas can be susceptible to polybrominated diphenyl ether (PBDE) and polychlorinated biphenyl (PCB) contamination. In this study, characterization of five cores from the Chicago metropolitan area showed elevated PBDE and PCB levels. PBDE concentrations peaked at ~2500 ng/g and were higher than reported values for the Great Lakes and other areas in North America.^(45,47,49) PCB concentrations peaked at >2000 ng/g. PCB concentrations in the Chicago metropolitan sediments were comparable to reported value from other industrial areas;^(60, 61) however, these concentrations were still lower than PCB-historically contaminated sites.⁽⁵⁾ Relative enrichment of tetra- and penta-PBDE congeners were observed in Chicago sediment cores exposed to anthropogenic hydraulic discharges such as wastewater treatment plant (WWTP) effluent, stormwater discharges, and combined sewage outfalls (CSOs).

Multiple least-square regression (MLSR) analysis was performed to quantify the differences between PBDE and PCB sediment profiles to PBDE technical mixtures (TMs) and PCB Aroclor mixtures, respectively. The site with the highest PBDE and PCB MLSR residuals also experienced increase in low molecular weight (LMW) PBDE and PCB homologs concomitant with decrease in high molecular weight (HMW) PBDE or PCB homologs; this observation is consistent with *in-situ* dehalogenation. Additionally, analysis of *ortho*, *meta*, and *para*-substitution pattern showed increase in *ortho*-PCBs concomitant with a decrease in *meta*-PCBs provides strong evidence in support of microbial facilitated PCB dehalogenation.

3.1. Introduction

Rapid urbanization surrounding the Pearl River Delta area in China rendered the soil, air, sediment, and even biota with high levels of various persistent organic and inorganic pollutants.⁽¹⁴²⁻¹⁴⁴⁾ The Pearl River Delta is not a single case study; a multitude of environmental studies showed that many urban areas across the globe are also facing the threat of declining environmental quality stemming from the accumulation of various synthetic, organic, and in-organic contaminants.⁽¹⁴⁵⁻¹⁵⁰⁾ Rapid urban development, along with historical and on-going presence of various industries such as refineries, chemicals, and consumer goods manufacturers in the Chicago metropolitan area make it susceptible to accumulation of various hydrophobic organic contaminants (HOCs) such as polybrominated diphenyl ethers (PBDEs) and polychlorinated biphenyls (PCBs).

PBDEs are brominated bicyclic compounds used as additive flame retardants incorporated into various consumer products in the textile, plastic, and electronic industries that have been used since the early 1970s.⁽⁷⁾ Historically, PBDEs were manufactured in three forms of technical mixtures (TMs): DE-71 comprised mostly of penta-BDE congeners, DE-79 comprised mostly of the octa-BDE congeners, and Saytex102E comprised mostly of deca-BDE (BDE-209) congener⁽¹⁰⁾ by the Albermarle and Chemtura Corp.⁽¹⁵¹⁾ in two facilities in southern Arkansas (AR). Productions of DE-71 and DE-79 TMs were voluntarily ceased in 2004 in response to concerns about the higher toxicity and bio-accumulative potential of several small BDE congeners.^(152,153) The discovery that BDE-209 can rapidly form lower brominated BDE congeners when exposed to sunlight^(154,156) and the demonstrated ability of certain microorganisms to partially or completely debrominate BDE-209 into smaller congeners under laboratory conditions^(102,103,108) has fueled the controversies on the continued use of the Saytex 102E TM.

PCBs are a suite of chlorinated semi-volatile bicyclic compounds used as early as the 1920s as dielectric and coolant fluid in transformers and electric systems.⁽¹⁶⁾ Historically, PCBs were manufactured as Aroclors;⁽¹⁶⁾ the first two digits in the Aroclor mix generally refers to the number of carbon atoms in the phenyl ring and the last two digits generally refers to the average percent chlorination in the mixture

by weight. Studies have established the adverse health effects from incidental and occupational exposures to PCBs;⁽¹⁴⁾ in response, active production of PCBs in the USA ceased in the 1970s. However, PCBs continued to be released into the environment from past usage and are continuously detected in various environmental media.^(157,163)

In this study, sediment cores collected from five urban waterways impacted by storm and sanitary sewage outfalls, urban/industrial runoff, and air deposition were characterized in an effort to understand the recent depositional trends of the so-called “emerging pollutant” PBDEs and the “legacy pollutant” PCBs in the metropolitan Chicago area. This study compliments our previous study on PBDE production area in southern AR⁽¹⁵¹⁾ with the ultimate goal of understanding the distribution, trends, potential sources, and fate of PBDEs in the metropolitan Chicago aquatic environment.

3.2. Objectives

This study is a continuation of a previous study characterizing the magnitude of PBDE and PCB contamination across AR including in locations proximate to two PBDE manufacturing facilities.⁽¹⁵¹⁾ For the purpose of this study, five urban waterways in the metropolitan Chicago area were characterized for PBDE and PCB contamination. Contaminant levels were interpreted in light off the previous study with an overall goal to identify drivers for PBDE and PCB contamination in the metropolitan Chicago area and to evaluate the potential for *in-situ* sediment transformation. There are four objectives for this study:

- Understand the extent of PBDE and PCB sediment phase contamination in the metropolitan Chicago area. Land use characterization by the United States Geological Services (USGS) showed that the metropolitan Chicago area is highly urbanized and industrialized (see Figure 3.1b); this is hypothesized to drive high levels of sediment phase PBDE and PCB contamination. PBDEs in Chicago sediments are expected to originate from diffusive sources. In contrast, the dominant sources for PBDEs contamination in southern AR sediments are large point sources

(i.e., emissions from PBDEs manufacturing facilities).⁽¹⁵¹⁾ While a high level of sediment-phase PBDE concentrations are expected in the metropolitan Chicago area, it is hypothesized to be relatively lower than southern AR sediments. Given the more robust urbanization and industrialization in the metropolitan Chicago area, sediment phase PCB concentrations are expected to be relatively higher than AR.

- Examine the recent PBDE and PCB depositional trends in the metropolitan Chicago area. PBDEs are still actively manufactured and used in various consumer products, while PCBs are no longer manufactured. As an emerging contaminant, PBDE depositional rates are hypothesized to have increased rapidly in recent years. On the other hand, given its status as a legacy contaminant, PCB depositional rates are hypothesized to substantially decline in recent years.
- Compare PBDE and PCB congener distributions in the metropolitan Chicago area sediments to the AR sediments. The metropolitan Chicago area sediments are expected to have two pathways for PBDE and PCB exposures; through anthropogenic waterborne deposition (i.e., storm and sanitary sewage outfalls, urban/industrial runoff) and through atmospheric deposition. PBDE and PCB congener distributions are hypothesized to differ reflecting the exposure pathways and sources (i.e., diffusive versus point sources and waterborne versus atmospheric deposition).
- Evaluate PBDE and PCB *in-situ* sediment transformation potential by interpreting trends in PBDE and PCB homolog fractions, assessment of changes in *ortho*, *meta*, and *para* (OMP) distributions, and multivariate least square regression (MLSR) comparing sediment phase PBDE and PCB distributions to PBDE TM or PCB Aroclor profiles. Given the stronger carbon to chlorine chemical bond relative to carbon to bromine chemical bond, PBDE *in-situ* degradation is hypothesized to be more likely and to a larger extent than PCB *in-situ* degradation.

3.3. Experimental Section

3.3.1. Sampling Sites

Several criteria were used to guide the selection of the sampling locations. Sampling sites should: (I) be within the Chicago metropolitan region in urbanized and industrialized areas to obtain sediment samples with high PBDE and PCB concentrations, (II) have high sedimentation rates to provide accurate sediment dating resolution, (III) have no known sediment disturbance events such as dredging and/or large scale remediation for the past ~50 years, (IV) have no or minimal bioturbation, and (V) have a sediment-water interface below the sunlight penetration depth as determined by Secchi disk. These guiding characteristics represent the ideal for the sampling locations; compromises are often necessary as some sampling locations do not fulfill all the ideal characteristics listed above. The sampling locations are shown in Figure 3.1.

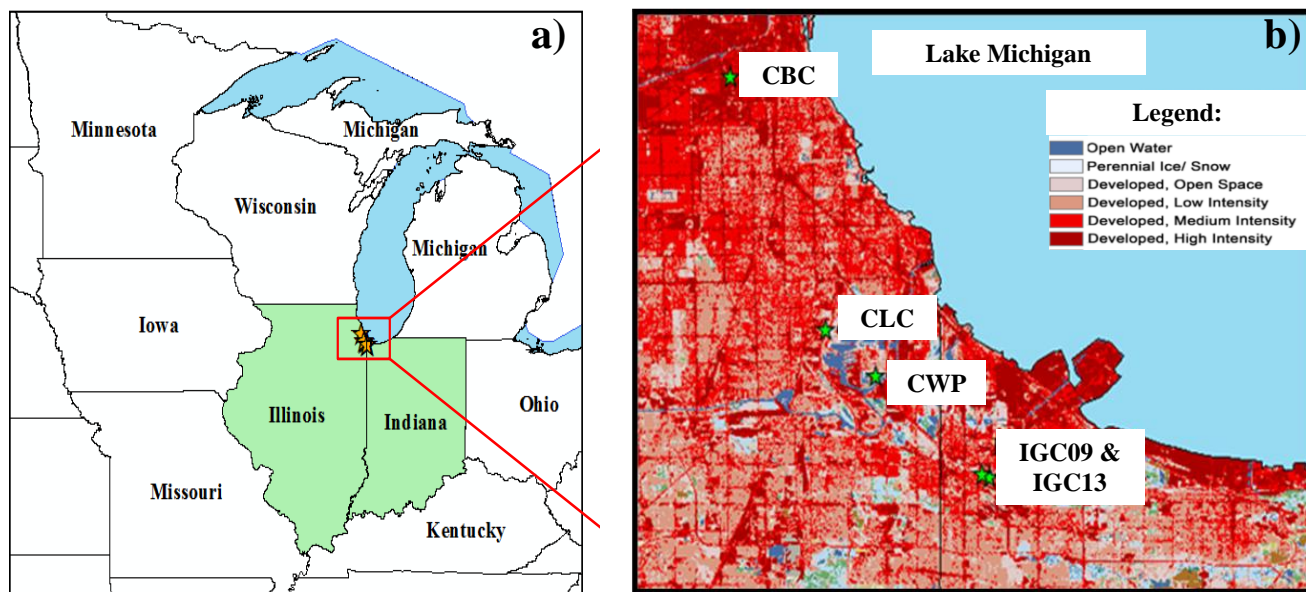


Figure 3.1: a) Sampling sites located in the metropolitan Chicago area and b) land use categorization by the United States Geological Services 2006 National Land Cover Database. Higher levels of development correspond to darker hue. Land use map was generated using ArcMap version 10.

Coordinates and sampling dates are summarized in Table 3.1. Information and detailed map (including recorded sampling coordinates) for each site are provided below and in Figure B3.2.

Table 3.1. Site identifiers and latitude and longitude for sampling sites in Chicago (CBC, CWP, CLC) and IGC (IGC09 and IGC13).

ID	Site	Latitude	Longitude	Sampling Dates
CBC	Bubbly Creek	41.8325	-87.6583	8/14/2008
CWP	Calumet Wetland Pond	41.6706	-87.5656	9/11/2008
CLC	Lake Calumet	41.6957	-87.5964	5/7/2009
IGC09	Grand Calumet Site 09	41.6159	-87.4914	3/9/2010
IGC13	Grand Calumet Site 13	41.6174	-87.4964	3/9/2010

Bubbly Creek (CBC): Site CBC is the south branch of the Chicago River and has a long contamination history. The Chicago Union Stockyard which is no longer operational used CBC as a main discharge point since 1865 for a little over a century.^(119,141,164) Previous studies have characterized high levels of heavy metals, PCBs, and polycyclic aromatic hydrocarbons (PAHs) contamination in CBC.^(119,141,164) Currently, various industrial facilities line the banks of CBC including metal plating, scrap metal yards, and trucking yards. CBC is largely quiescent except during large volume release events from the Racine Avenue Pumping Station (RAPS), the largest pumping station in the world. High volume release events occurred on average 13 times per year.^(119,141,164) Sediment cores for this study were collected 300 m north of the RAPS discharge point.

Lake Calumet (CLC) and Calumet Wetland Pond (CWP): Located 24 km southeast of Chicago, CLC and CWP are located in the Calumet area in the midst of a heavily populated and industrialized area. Among the prominent industrial activities in the area include active and inactive coke mills, coke ovens, petroleum refineries, chemical plants, building material companies, grain processing facilities,

incinerators, and landfills. Pullman Creek is a tributary into Lake Calumet carrying runoff from nearby expressways, industries, and landfills into the northwest corner of the lake.^(166,167) The sediment is known to be highly contaminated with PAHs and PCBs.^(166,167) Site CWP, also known as Gun Club Pond, is ~4 km east of site CLC. This pond receives no continuous inflow and is bordered by rail tracks and a wastewater treatment sludge drying bed. An active municipal solid waste landfill is also nearby. CWP is approximately ~3000 m² and the sampling spot is near the center of the pond. The Calumet water reclamation plant (CWRP) is located on the west of both sampling sites. CWRP serves a 777 km² area in Chicago and southern suburbs, and on average processes 238 MGD.⁽¹⁶⁸⁾

Grand Calumet River site 09 (IGC09) and site 13 (IGC13): Sites IGC09 and IGC13 are located on the west branch of the Grand Calumet River (WBGCR), a heavily polluted waterway with documented polyaromatic hydrocarbons (PAHs), PCBs, metal, mercury, and arsenic contaminations.^(169,170) The WBGCR flows through heavily industrialized areas in Gary and Hammond, IN and receives substantial recharge from the Hammond Sanitary District Wastewater Treatment Plant (HSD WWTP) before draining into Lake Michigan via the Indiana Harbor Canal (IHC). The HSD WWTP treats wastewater originating from mixed municipal and industrial sources.⁽¹⁷¹⁾

In this study, sites CBC, CLC, and CWP located within the Chicago city limit boundary are collectively referred as Chicago sites whereas sites IGC09 and IGC13 situated on the WBGCR are collectively referred as IGC sites.

Sediment coring and extrusion: Whenever possible, sediment cores were obtained from the center or at known deepest water depth. Sampling personnel on a boat operated a hand push corer with a 6.6 cm I.D. polycarbonate tube to obtain the sediment cores at all sites except for core CLC, which was obtained using the vibra-core and box core located on board of the EPA *R/V Mudpuppy*. We would like to

acknowledge the EPA R/V Mudpuppy crew for their assistance. Four to five sediment cores were collected per site. Sediment cores remained in the vertical position and were brought to shore for extrusion using hydraulic pressure extruder. Sediment cores were extruded into 0.5 to 5 cm sections. Sections from the same depth were combined and homogenized in amber glass jars. Sediment sample jars were kept on dry-ice during transport to UIC laboratory, where they were stored at -4°C until analysis.

Oxidation reduction potential (ORP): One sediment core from each site was used for oxidation reduction potential (ORP) measurement. An electrode probe (Jensen Instruments, Tacoma, WA) was used with a reference electrode HI5312 (Hanna Instrument, Woonsocket, RI). Measurements were made using a portable pH/ORP/ISE HI98185 meter (Hanna Instrument, Woonsocket, RI). ORP measurement followed the vertical electrode insertion method described in a previous study.⁽¹⁷²⁾ Sediment cores remained vertical at all times. A scale was placed on the side of the polycarbonate core tube to mark depth. Electrode probe was inserted in the middle of the sediment core to the desired depth in 0.5 to 2 cm intervals. Measurement was recorded after stabilization before inserting the electrode probe deeper. Care was taken to minimize sediment disturbance when inserting and removing the electrode probe.

Sulfide Measurement: Sulfide measurement followed the method recommended in another study.⁽¹⁷³⁾ 2 mL aliquot from the extruded and homogenized sediment sample was used for sulfide measurement. The sample was mixed with an equivolume sulfite antioxidant buffer solution HI4015 (Hanna Instrument, Woonsocket, RI). Sulfide was measured using the portable pH/ORP/ISE meter HI98185 (Hanna Instrument, Woonsocket, RI) with a silver/sulfide combination ISE electrode HI4115 (Hanna Instrument, Woonsocket, RI).

3.3.2. Physical Characterization

Physical characterization of the sediments included wet and dry density (ρ_w and ρ_D), solid and moisture content, and particle density (ρ_p), total organic carbon (OC), black carbon (BC), non-soot organic carbon (NSOC), organic matter (OM), and particle size distribution (PSD). All methods for bulk sediment properties and carbon measurement were commonly employed in the Applied Environmental and Biotechnology Laboratory (AEBL, Department of Civil and Materials Engineering, University of Illinois in Chicago) described in previous studies,^(45-47, 49, 174, 175) methods are briefly described below.

Bulk measurement: Sediment samples in amber jars were first homogenized using a clean spatula. A clean spatula was used for each sediment sample. Using an open ended syringe (1 or 3 cm³ for bottom and top sediment segment, respectively), sediment samples were volumetrically sub-sampled. Aliquots were placed on a clean, tared aluminum boat for weighing. Sediment samples were then dried in an oven at 100°C until no change in weight was observed. For quality control purposes, measurement was conducted in triplicate.

The ρ_w and ρ_D were calculated using Equations 3.1 and 3.2 whereas solid and water contents were calculated using Equations 3.3 and 3.4.

$$\rho_{PD} = \frac{WWS}{V} \quad (3.1)$$

$$\rho_{DD} = \frac{WDS}{V} \quad (3.2)$$

$$Water\ Content\ (\%) = \frac{WWS - WDS}{WDS} \times 100\% \quad (3.3)$$

$$Solid\ Content(\%) = 100\% - Moisture\ Content\ (\%) \quad (3.4)$$

In Equations 3.1 to 3.4, WWS is weight of wet sediment (g/ cm³), V is volume (cm³), and WDS is weight of dry sediment (g/ cm³).

Carbon measurement: Two out of the triplicate set of dried sediment samples were used for OC measurement and one was used for BC measurement. For BC measurement, sediment samples pulverized with a clean mortar and pestle were further combusted at 375°C for 24 hours in a muffle furnace to remove NSOC through low temperature oxidation using a modified version of the Gustaffson et al. (1996, 1998) methods.^(176, 177) The mass of combusted sediment sample was recorded.

Sediment samples for both OC and BC measurements were pulverized using a glass mortar which was cleaned thoroughly between samples. A small aliquot of the pulverized sediment samples (between 5-10 mg for OC and 10-20 mg for BC) was weighed and sealed in a 10X12mm tin capsule (ThermoQuest/CE Elantech, Lakewood, NJ) for carbon measurement on the Flash EA1112 (ThermoQuest/CE Elantech, Lakewood, NJ). Analysis was conducted using automated combustion/reduction at 900°C followed by molecular sieve gas chromatography and thermal conductivity detection system at 60°C. Carbon peak areas were compared to a six point acetanilide standard curve with size integration performed using the Eager version 5.0 software. A new standard curve was made every 80 to 100 samples to protect against run-to-run inaccuracies. For quality control, at least one of ten sediment samples and acetanilide were analyzed as unknowns to determine the accuracy and precision. The carbon measurement has bias value ranging from 3 to 8% and precision between 4 to 8% yielding a 95th percentile total uncertainty of 5 to 11% in all the sediment columns.

Particle size distribution (PSD): PSD of suspended dried sediment agglomerates was determined by laser diffraction on the Mastersizer 2000 (Malvern Instrument, Worcestershire, UK). Dried sediment samples (5 to 30 mg) were suspended and homogenized in 1 L beaker filled with clean, aerated water until the rarefraction index reading was stable. It is recognized that this measurement reflect the agglomerate nature of sediment due to particle to particle attraction. No attempt was made to chemically remove organic matter to more accurately characterize the *in-situ* PSD for mass transport modeling.

3.3.3. Sediment Dating

I would like to acknowledge our collaborators at the Earth and Environmental Sciences Department, University of Illinois in Chicago for performing sediment dating measurement and analysis. Air dried sediment samples were weighed (0.70 to 8.07 g) and sealed in aluminum counting cans prior to gamma activity measurement of selected radionuclides (^{210}Pb , ^{137}Cs , and ^{226}Ra at 46.5, 186.2 and 661.6 keV, respectively) using the GR3020 reverse-electrode intrinsic Ge detector system interfaced with a DSA-2000 digital spectrum analyzer. Both the Constant Initial Concentration (CIC) and Constant Rate of Supply (CRS) were used to determine sedimentation date.⁽¹⁷⁸⁾

3.2.4. Chemical Characterization

I would like to acknowledge that chemical characterization was performed by collaborators at the School of Public Health, University of Illinois in Chicago. 49 PBDE congeners and 132 PCB congeners were measured; target analytes are summarized in Table B3.1 to B3.2.

Chemical purchase. PBDE and PCB congeners, as well as analytical standards, were purchased from Accu Standard (New Haven, CT) and Cambridge Isotope Libraries (Andover, MA). HPLC-GC/MS and OptimaP grade solvents, silica gel (100-200 mesh, Davisil grade 644) and anhydrous sodium sulfate (Na_2SO_4) were purchased from Fisher Scientific (Pittsburgh, PA). Bio-beads S-X3 (200 – 400 mesh) were purchased from Bio-Rad Laboratories (Richmond, CA).

Sample pretreatment. Sediment samples were thawed, air dried, and mixed with Na_2SO_4 (drying agent) prior to spiking with surrogate analytes. Soxhlet extraction used 150 mL hexane-DCM (1:1,v/v) for 20 hours. Elemental sulfur was removed by addition of granular copper. Soxhlet extracts were concentrated to 2 mL using a rotary evaporator and cleaned with solvent elution through a glass column (40 cm length,

11 mm I.D.) packed with 1 g neutral, 2 g basic, 4 g acidic, and 1 g neutral silica gel cleanup. Elution solvents were 80 mL hexane for silica gel cleanup and 140 mL hexane/DCM (1:1,v/v) for gel permeation column. Eluent volume was reduced to 2 mL with the rotary evaporator. Internal standards of PCB-209L and BB-209 were added prior to instrumental analysis.

Instrumental analysis. PBDEs, PCBs, and DBDPE were analyzed on the Agilent 6890 GC coupled with 5973N MS with electron capture negative ionization (ECNI) using gas chromatography/mass spectrometry (GC/MS) parameters optimized in previous studies.^(45,47,49,58)

BDE-30 and 190 were surrogate analytes for PBDE analysis. A 20 μ L extract with a total of 3 injections was introduced to the programmable temperature vaporization injection port in solvent vent mode. Injection port temperature was 40°C and was increased to 300°C at a rate of 600°C/minute with 1.5 minute holding time. Flow was maintained at 100 mL/minute for 1.4 minute and purged at 50 mL/min from 2.75 to 10 minutes. Separation with helium gas carrier at flow of 1.5 mL/minute was introduced in an Rtx-1614 capillary column with dimensions of 30 m length, 0.25 mm I.D., and 0.10 μ m film thickness. The oven was set to 90°C for 3 minutes followed by a temperature ramp to 200°C at 10°C/minute to 300°C at 2°C/minute for 15 minutes. MS ion source, quadrupole, and interface temperatures were 200, 106, and 280°C, respectively. Analysis was in selected ion monitoring mode, with m/z 486.6 and 488.6 (BDE-209), 79 and 81 (other BDEs, DBDPE, and BB-209), and 510, and 512(PCB-209L), respectively.

For PCB analysis, two sediment standard reference materials (SRM1941b and SRM1944; NIST Office of Reference Materials, Gaithersburg, MD US) were used. 2 μ L extracts were injected in pulsed splitless injection mode and separated on a DB-5MS capillary column (60 m length X 0.25 mm I.D. X 0.25 μ m film thickness) with helium carrier gas at a constant flow of 1.2 mL/minute. The initial oven temperature was 50°C for 3 minute, and then increased to 140°C at 15 °C/minute, and further to 290°C at 1.5°C/minute. The total run time is 109 minute. The MS ion source, quadrupole, and interface temperatures were 200, 106, and 280°C, respectively. The MS was operated with multiple reaction monitoring mode in electron impact. The MS ion source, quadrupole, and interface temperatures were

230, 150, and 300°C, respectively. Nitrogen was used as the collision gas at 1.5 mL/minute and helium as quenching gas at 2.25 mL/minute.

3.4. Results and Discussion

3.4.1. Field Measurement

Oxidation Reduction Potential (ORP). ORP characterizes the oxidation-reduction status of the sediment and can be used as a diagnostic to predict the predominant microbial metabolism process occurring in the respective sediment segments. It has been reported that anaerobic metabolism has ORP below -150 mV, facultative metabolism has ORP between -150 to 400 mV, and aerobic metabolism has ORP above 400 mV.⁽¹⁷⁹⁾ Chicago surface sediments have ORP consistent with facultative metabolism; ORP gradually decreased into the anaerobic metabolism region at approximately 15, 20, and 23 cm in CBC, CWP, and CLC sediment columns, respectively (Figure 3.2, Table B3.3). Interestingly, the Chicago sediment columns have ORP levels that were comparatively lower than ORP levels observed in AR sediment columns which were all in the facultative region (Figure B3.3); these results were consistent with expectation given the darker black color, organic texture, and frequently-observed sulfide smell (from metal-sulfides) in the Chicago sediments. In the ACL sediment column, ORP increased with increased sediment depth (Figure B3.3c); this trend was unexpected as sediment columns generally shift towards anaerobic metabolism region with increased depth. In other AR sediment columns, ORP levels were relatively similar with increased sediment depth possibly indicating that the upper and lower sediment segments of these columns remained in the facultative region.

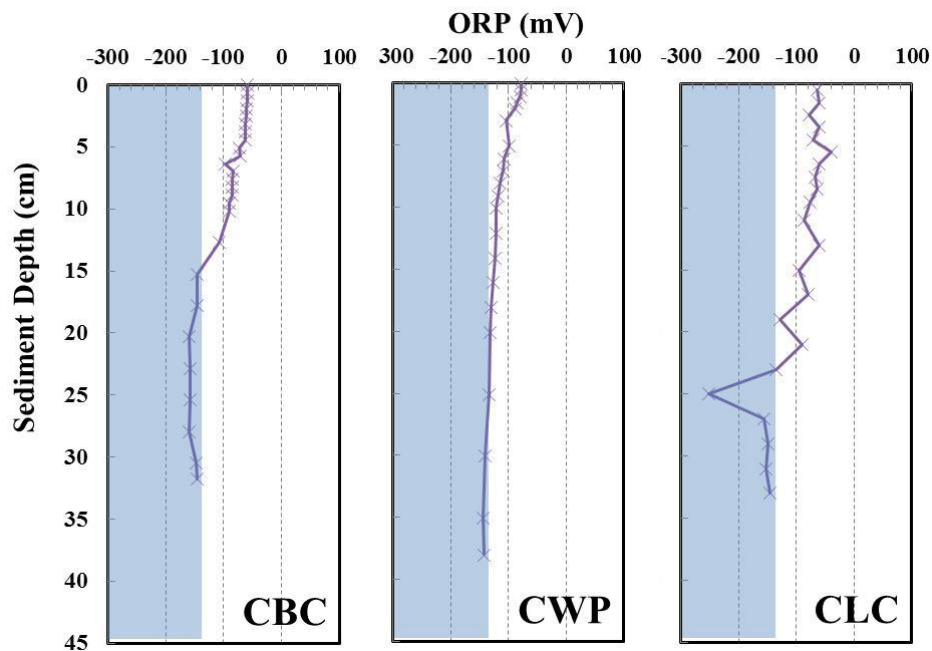


Figure 3.2: Oxidation reduction potential (ORP) in sediment cores CBC, CWP, and CLC. Shaded areas represent ORP levels consistent with anaerobic metabolism and non-shaded areas represent ORP levels consistent with facultative metabolism.

Sulfide concentration. Sulfide concentrations in the Chicago and IGC cores varied greatly (Figure 3.3). In CBC sediment column, sulfide concentrations increased between surface sediments to near mid-core where sulfide concentration peak values exceeded 300 ppm. Sulfide concentration gradually decreased between ~12 cm to ~25 cm and remained relatively constant in sediment segment deeper than 25 cm in CBC sediment column. In contrast, sulfide concentration was relatively similar at ~100 ppm throughout CLC sediment column. Sulfide concentration peak value exceeded 400 ppm in deep CWP sediment segment (~27 cm). In general, sulfide concentration in the IGC sediment columns which ranged from 15 to 40 ppm were relatively lower than the Chicago sediment columns. The presence of heavy hydrocarbon as evidenced by the strong gasoline smell and “black mayonnaise” appearance of the IGC sediment columns could be interfering with the sulfide electrode probe sensing probe which was coated with sheen of oil during sulfide measurement.

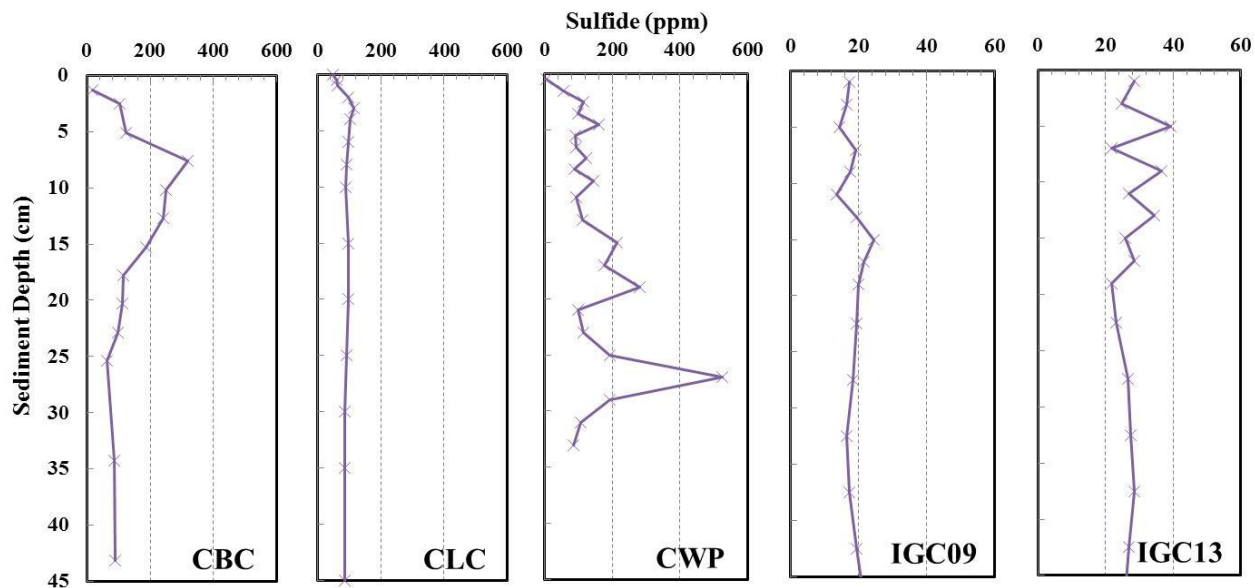


Figure 3.3: Sulfide concentrations in cores CBC, CWP, CLC, IGC09, and IGC13. Note the different scale on the x-axes for cores CBC, CLC, and CWP compare to cores IGC09 and IGC13.

In AR sediments, sulfide concentrations generally increased rapidly from the surface sediment to ~5 to 8 cm to reach peak sulfide concentrations (Figure B3.4). Peak sulfide concentrations do not exceed 150 ppm in all AR cores. Sulfide concentrations remain relatively constant in deeper sediment depth in all AR cores. The relatively lower sulfide concentration in AR cores compared to Chicago cores is consistent with the lower ORP in AR cores.

3.4.2. Physical Characterization

Bulk sediment characteristics in Chicago and IGC sediment cores. Generally, ρ_w and ρ_D do not change appreciably with depth in the Chicago and IGC sediment cores (Figure 3.4a-e). In general, the Chicago and IGC sediments were low in solids content at the surface and become more compacted with depth (Figure 3.4f-j). The high water content in the Chicago and IGC sediment cores reflect high porosity with great implications for porewater transport (discussed in Chapter 5). CBC core was an exception to trend observed in ρ_w , ρ_D , and solids and water content (Figure 3.4a and f). The increased in ρ_w , ρ_D , and

water content and decreased in solids content suggest differences in the sediment particle composition in the 10 to 15 cm region in core CBC.

ρ_w and ρ_D in core AMW and AOT also do not change appreciably with depth (Figure B3.5b and e). Cores AED, ACL, and AJL have higher ρ_w and ρ_D in the lower sediment segments compared to the upper sediment segments whereas core AFR have lower ρ_w and ρ_D in the lower sediment segments compared to the upper sediment segments (Figure B3.5a, c, d, and f). Solids and water content in AMW was relatively constant with depth (Figure B3.6b). Solids content in the upper sediment segment of cores AED, ACL, AJL, and AOT were substantially higher compared to the lower sediment segment (Figure B3.6 a, c, d, and e). In core AFR, solids content exceeded water content throughout the sediment column (Figure B3.6f).

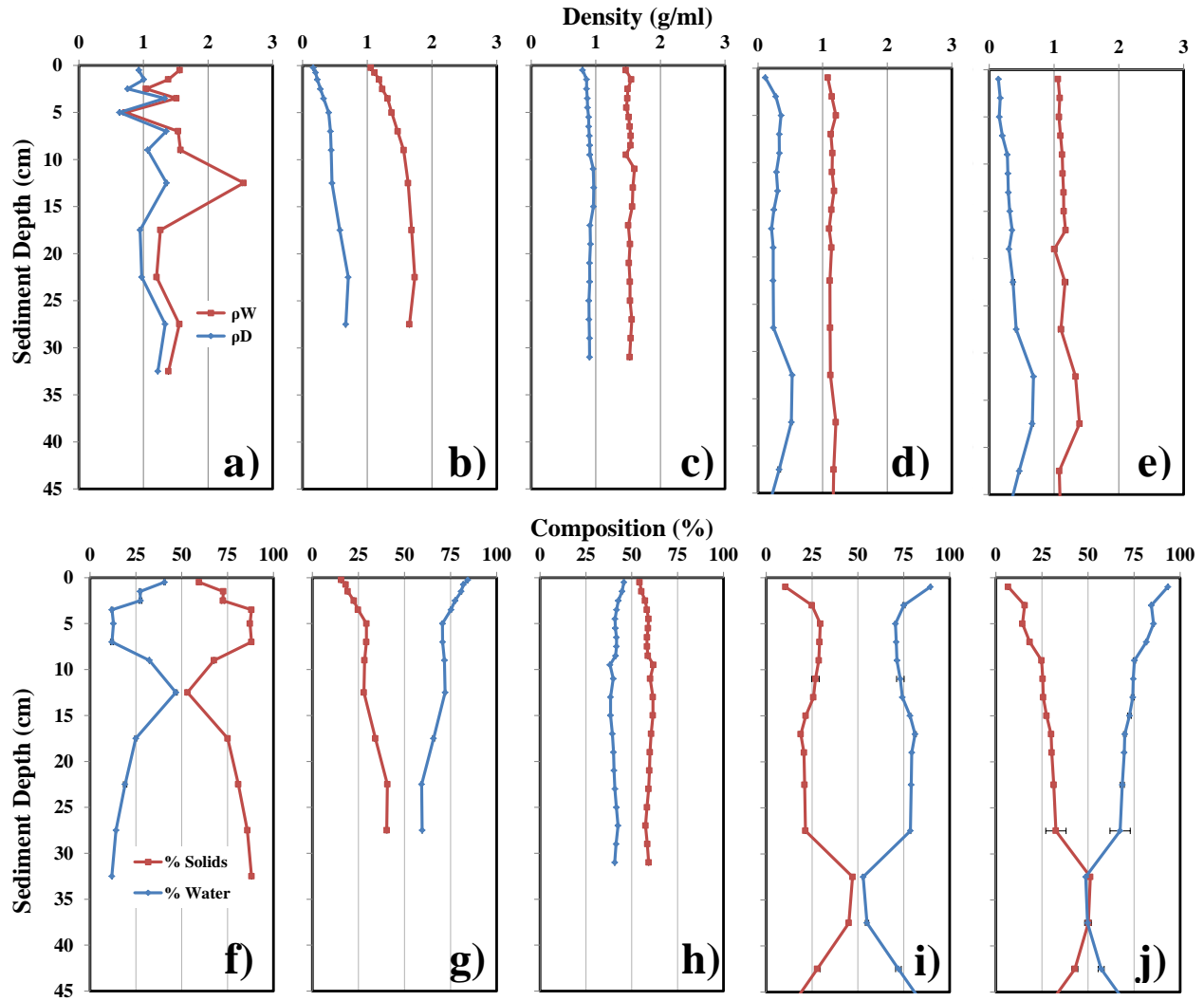


Figure 3.4: Wet and dry densities (ρ_W and ρ_D , respectively) (a-e), and solids and water content (% Solid and % Water, respectively) (f-j) in cores CBC (a,f), CWP (b,g), CLC (c,h), IGC09 (d,i), and IGC13 (e,j). Error bars represent the standard deviation of triplicate measurements. These error bars were typically smaller than the data symbol.

Carbon Concentration. OM and OC concentrations in IGC cores were higher than Chicago cores (Figure 3.5b-e). CBC had fairly low levels of OM and OC except for the peak at 10 to 15 cm; interestingly, this corresponded to a large increase in ρ_W and water content at this depth. This result together with the ρ_W and water content data, indicate the presence of a sediment layer of significantly different composition at site CBC in the 10 to 15 cm depth region. Almost no change in OC and OM was observed in cores CWP and CLC except for a higher level in OC and OM concentrations in CWP surface

sediment. IGC09 and IGC13 sediment cores have higher OC and OM concentrations relative to Chicago sediments. There does not appear to be any significant trend in BC with depth in the Chicago and IGC columns indicating that BC deposition has been largely unchanged in the sedimentary record (Figure 3.5 a-j). The BC level in cores CWP and CLC were ~ two times higher than cores CBC, IGC09, and IGC13.

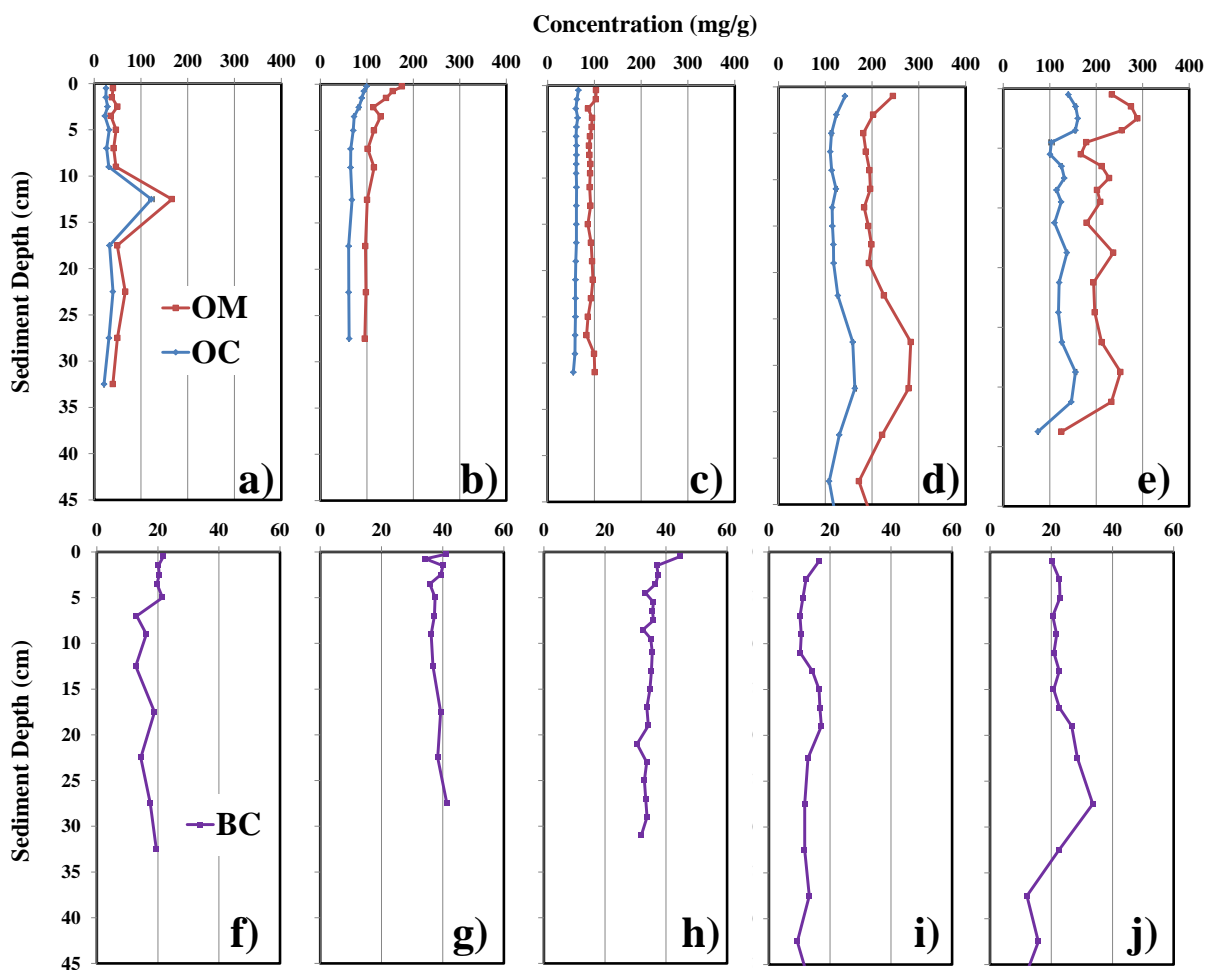


Figure 3.5: Organic matter (OM), organic carbon (OC), and black carbon (BC) concentrations in CBC(a,e), CWP (b,g), CLC (c,h), IGC09 (d,i), and IGC13 (e,j). Error bars represent the standard deviation of triplicate measurements. These error bars were typically smaller than the data symbol.

In general, the OC and OM levels in AR sediment cores decreased with increased depth (Figure B3.7a-f). OC and OM levels in the upper sediment segments of core AED and AOT were two to four

times higher than the lower sediment segments. While OC and OM levels decreased with depth in cores AMW and AOT, the difference in the upper and lower sediment segments was not as pronounced as observed in cores AED and AOT. In core ACL, OC and OM levels generally decreased with depth; however, OC and OM levels increased and peaked between 15 to 25 cm depth. In core AFR, the OC and OM levels were relatively constant with depth. BC level only showed small variation with depth in cores AED, AMW, AJL, and AFR (Figure B3.8a, b, d, and f). In core ACL, BC increased between the surface sediment to approximately 20 cm before gradually decreasing to constant level of ~2 mg/g in deeper sediment segment (Figure B3.8c). In core AOT, the upper sediments have BC levels two to four times higher than the lower sediments (Figure B3.8e).

The BC levels in the Chicago and IGC cores were statistically significantly higher than BC levels in the AR cores; average BC concentration in Chicago and IGC cores was ~25 mg/g (n=85) whereas average BC concentration in AR cores was ~ 3 mg/g (n=2.18). This observation was consistent with the higher level of urbanization in metropolitan Chicago and IGC relative to AR (as can be observed in differences in USGS land use categorization in Figure 3.1 and Figure B3.1).

Agglomerate Particle Size Distribution (PSD): Sediment particles are not expected to be uniformly size particularly in fluvial systems like sites CBC, IGC09, and IGC13. Although sediment particles are not homogenous in terms of size, the size of the sediment particles can be described by the PSD. The agglomerate PSD data were classified using the United States Department of Agriculture (USDA) soil classification criteria which state that particles smaller than 2 μm are clay, between 2 to 63 μm are silt, between 63 to 250 μm are fine sand, and larger than 500 μm are coarse sand. Cores CLC and CWP primarily from lacustrine sites (Figure 3.6b and c), have a very homogenous PSD dominated by some clay and >80 % silt. As expected, cores IGC09, IGC13, and CBC (riverine sites with major CSO sources and flows) have highly graded PSDs with depth. Changes in particle characteristics mid-depth at site CBC are consistent with the PSD data (Figures 3.4a and f, Figures 3.5a). The 10 to 15 cm sediment

segment is quite different from all other segments, with nearly equal amounts of silt and sand, and large amounts of coarse sands. This trend of marked changes in PSD with depth was also observed at IGC09 and IGC13. Again, sand made up a large percentage of the sediment particles (up to 80 %) at these fluvial sites.

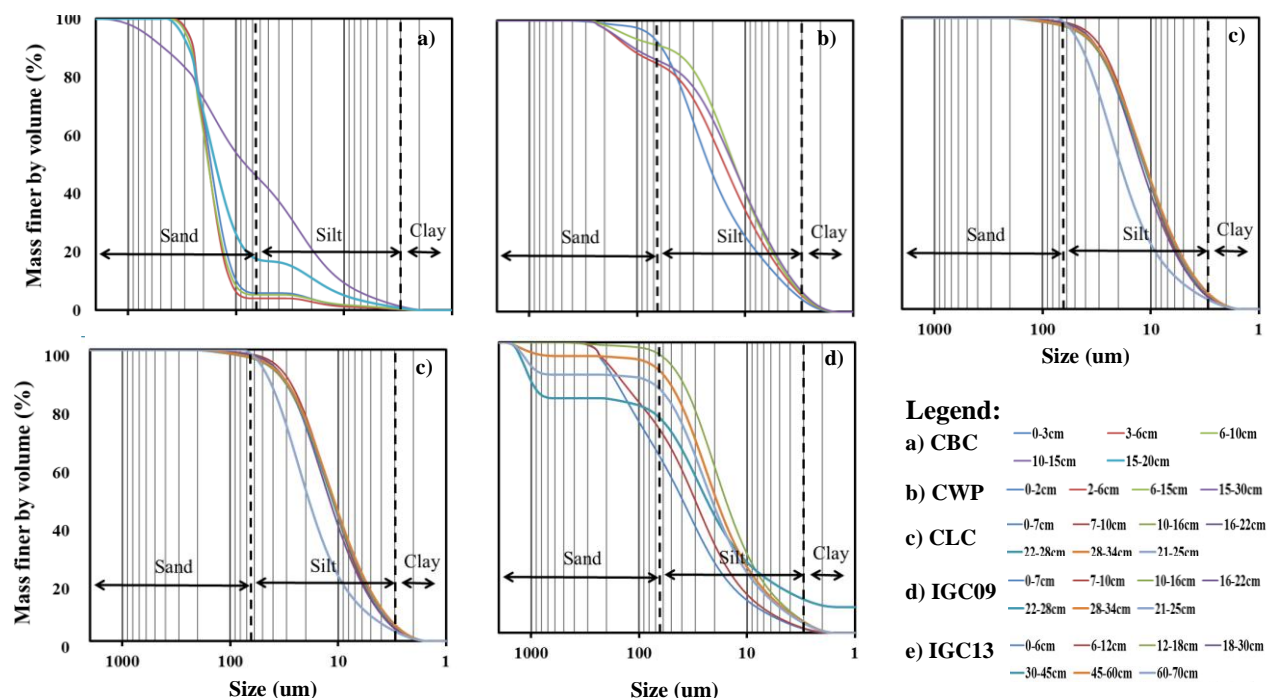


Figure 3.6: Particle size distributions in cores a) CBC, b) CWP, c) CLC, d) IGC09, and e) IGC13. Particle sizes for sand, silt, and clay were based on United States Department of Agriculture (USDA) classification.

3.4.3. PBDEs and PCBs in The Metropolitan Chicago Sediment Cores

PBDE and PCB concentrations vary with depth and location. PBDE and PCB concentrations vary with depth and location in the metropolitan Chicago and IGC cores (Figure 3.7a and b). PBDE concentrations generally increased towards the sediment-water interface (Figure 3.7a, panels a-e). PBDE surface concentrations increased in the order of CLC < CWP < CBC < IGC09 < IGC13 (Table 3.2). In contrast to other sites, CBC had higher PBDE concentrations in sediment segments deeper than 10 cm.

However, the previous discussion of the physical and chemical characteristics of CBC sediments provided strong evidence for sediment mixing in the 10 to 15 cm sediment zone. If that were the case, the PBDE data are likely an artifact of sediment mixing (perhaps from RAPS combined sewage outfall (CSO) high volume discharge event). It is known that one had occurred less than 24 hours prior to sampling. Further details on evidence of sediment mixing in core CBC is discussed in a later section. Although PBDE concentrations in the metropolitan Chicago cores vary substantially between cores, similarities were observed in the ratio of PBDE congeners (Figure 3.7a, panels f-j; PBDE congeners grouped into homologs 1-4(Σ H1-4), homologs 5-7(Σ H5-7), homologs 8-9(Σ H8-9), and homolog 10 (H10)) in cores CBC, CLC, CWP, IGC09, and IGC13. BDE-209 was the dominant congener except in mid-core of IGC09 (10-17 cm) and bottom sediment segments of IGC13 (sediment deeper than 25 cm). The relative congener variation in these samples was driven from the lack of BDE-209 rather than changes in the other PBDE homologs.

Similar to the case with PBDEs, PCBs also vary with depth and location in the metropolitan Chicago cores. However, PCB concentrations generally decreased toward the sediment water interface in marked contrast to the case with PBDEs. The higher PCB concentrations in the mid to bottom sediment segments was apparent in cores CBC and CLC, and to a certain extent in core IGC13 (Figure 3.7b, panels a-e). PCB surface concentrations increased in the order of CWP < CLC < CBC < IGC09 < IGC13 (Table 3.2). Unlike PBDEs (which were clearly dominated by BDE-209), PCBs were more enriched in the LMW homologs (Figure 3.7b, panels f-j, PCBs grouped into Σ H1-3, Σ H4-6, Σ H7-9, and H10). Generally, concentrations of homologs decreased in the order Σ H4-6 > Σ H7-9 > Σ H1-3 > H10 in all metropolitan Chicago sediment cores. A deviation from this trend was observed in core IGC09 between 10 to 30 cm depth, where concentrations of Σ H4-6 < Σ H7-9. This may have been due to sediment mixing or changes in historical PCB Aroclors usage. Overall, more than 90% of the PCBs were composed of Σ H1-3 and Σ H4-6. The higher composition of LMW PCB homologs in surface sediments was reflective of the composition of some known PCB Aroclors. For example, Aroclors 1221, 1232, 1016, and 1242 are

composed of more than 90% PCB homologs 1-4, Aroclors 1248 and 1254 are composed of more than 90% PCB homologs 1-7, and Aroclor 1260 is composed of more than 90 % PCB homologs 5-7.⁽¹⁶⁾

In IGC09, deviation in ratio of Σ H1-4, Σ H5-7, and Σ H8-9BDEs homologs were observed between 5 to 20 cm sediment segment (Figure 3.7a, panel i). As mentioned previously, PCB homolog composition between 10 to 30 cm sediment segment in IGC09 was different than the other Chicago cores and IGC13 (between 10 to 30 cm sediment segment in IGC09: Σ H4-6 < Σ H7-9PCBs; other sediment cores: Σ H4-6 > Σ H7-9PCBs). Interestingly, in IGC09 sediment segment deeper than 30 cm, the homolog composition was reversed where Σ H4-6 < Σ H7-9PCBs. These deviations were not observed in IGC13, located in very close proximity to IGC09 (~400 m). Given the oddity in PBDE and PCB homolog composition in in-depth IGC09 sediment core, it is suspected that the PBDE and PCB concentrations in IGC09 do not reflect the actual PBDE and PCB depositions nature in the metropolitan Chicago area. IGC09 is excluded from further discussion in subsequent sections.

Table 3.2. Summary of PBDE and PCB concentrations in Chicago and IGC sediment cores.

Core	Average Concentration $\pm 1\sigma$ (ng/g)		Peak concentration ng/g (depth in cm)	
	Σ_{49} BDEs	Σ_{132} PCBs	Σ_{49} PBDEs	Σ_{132} PCBs
CBC	207 \pm 114	820 \pm 650	3440 (15-20)	2220 (10-15)
CWP	120 \pm 120	57 \pm 6	404 (0-1)	70 (15-20)
CLC	65 \pm 21	400 \pm 100	96 (26-28)	580 (32-34)
IGC09	328 \pm 910	989 \pm 676	3461 (0-2)	2062 (4-6)
IGC13	1195 \pm 940	2410 \pm 2540	2630 (2-4)	11,300 (35-40)

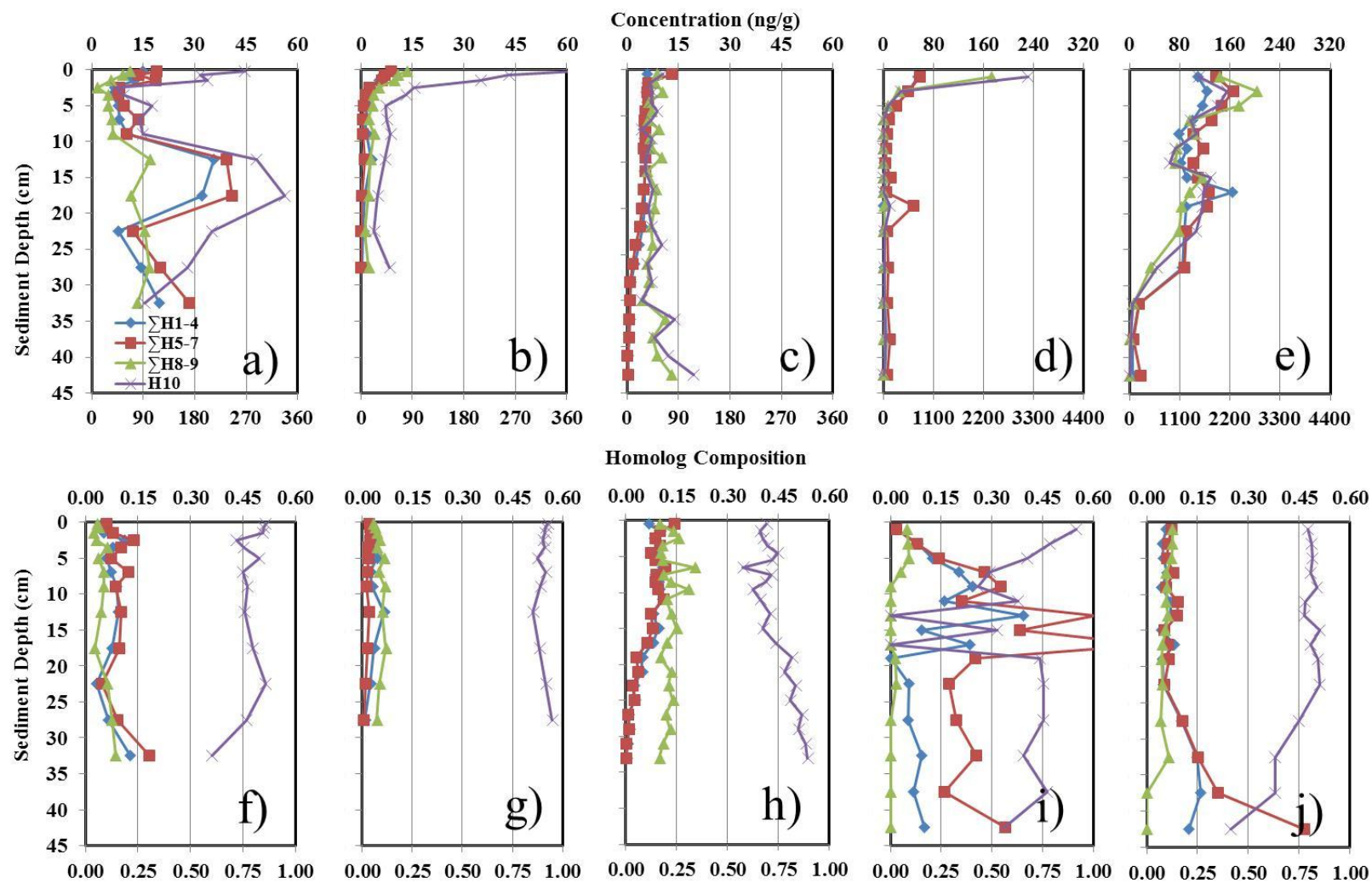


Figure 3.7a: a-e) Concentrations of PBDE homologs (Σ H1-4, Σ H5-7, Σ H8-9, and H10) and f-j) homolog compositions in cores a,f) CBC, b,g) CWP, c,h) CLC, d,i) IGC09, and e,j) IGC13. The lower x-axes scales in panels a-e and f-j are for H10 concentration and composition, respectively. Note the different upper and lower x-axes scales for panels a-c and d-e.

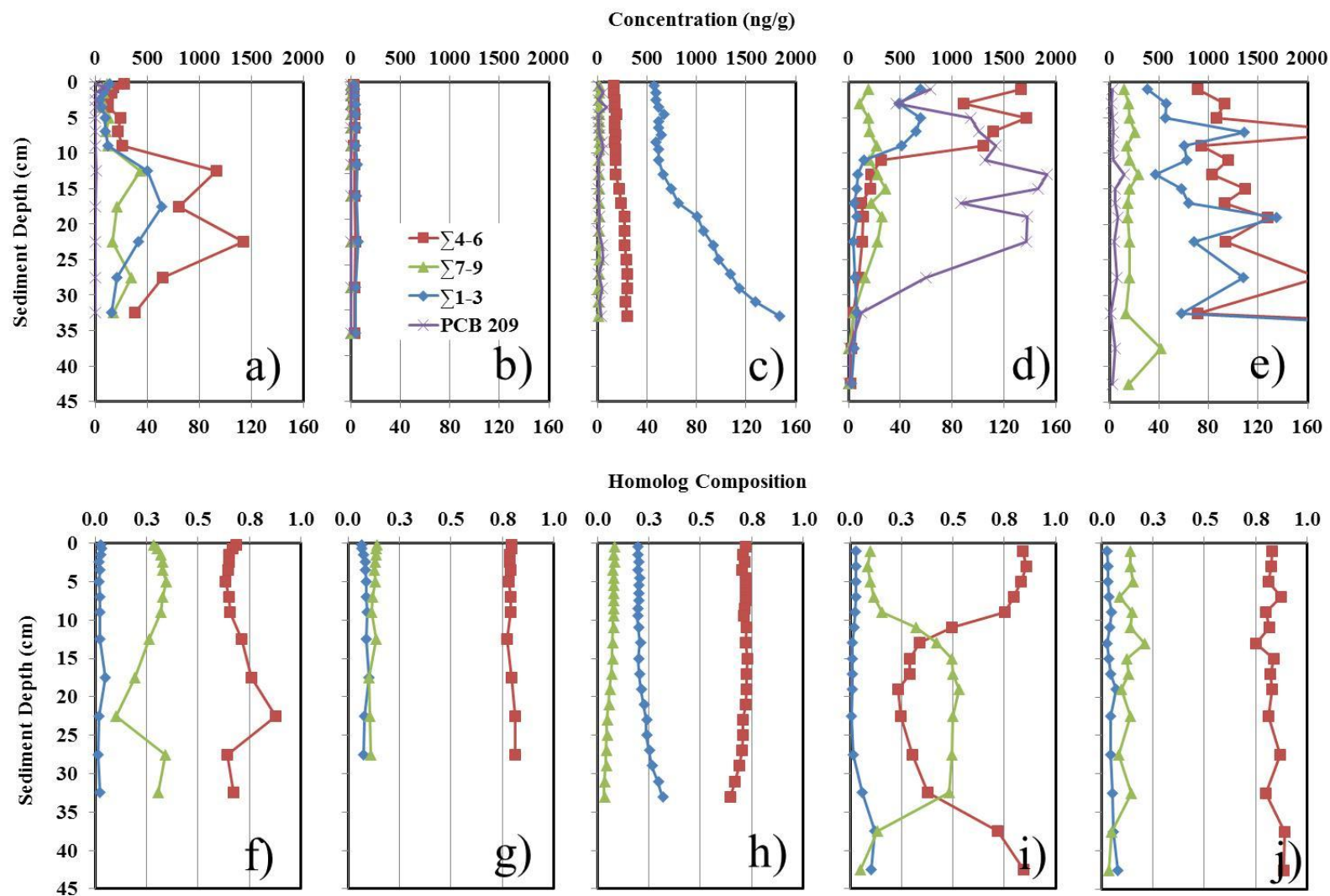


Figure 3.7b: a-e) Concentrations of PCB homologs ($\Sigma H1-3$, $\Sigma H4-6$, $\Sigma H7-9$, and $H10$) and f-j) homolog compositions in cores a,f) CBC, b,g) CWP, c,h) CLC, d,i) IGC09, and e,j) IGC13. The lower x-axes scales in panels a-e are for $H10$ concentration.

High amounts of PCB-209 (peak concentration of 153 ng/g) was observed in IGC09 between 5 to 30 cm (Figure 3.7b, panel d); interestingly, PCB-209 concentration was low ranging only from 1 to 12 ng/g in the nearby IGC13 (Figure 3.7b, panel e). PCB-209 was only present in Aroclor 1268 in low amounts (4.8% by mass)^(16,180) and only accounted <0.5% of the total U.S. produced PCB.⁽¹³⁾ Despite the small historical usage of Aroclor 1268, several studies found high sediment phase PCB-209 concentrations in several industrial areas in the U.S. For example, PCB-209 accounted for approximately 10% of \sum_{209} PCBs in a sediment sample from the Houston Ship Channel, and was also detected in water and biota samples from the same location.⁽⁶¹⁾ Marsh sediment in a Superfund site in coastal Georgia has PCB-209 concentration up to 2500 ng/g suspected due to application of Aroclor 1268 to electrical equipment in a chlor-alkali manufacturing facility.⁽¹⁸⁰⁾ A titanium dioxide purification plant was suspected to be the source of high PCB-209 concentrations in suspended solid from the Delaware River.⁽¹⁸¹⁾ Recently, PCB-209 was reported to account for 66, 33, and 50% of \sum_{209} PCBs in commercial paints containing phthalocyanine green pigment in Sherwin Williams, PPG, and Vogel brand, respectively.⁽¹⁸²⁾ Coincidentally, it is possible between 1970 to 1992 the HSD WWTP treated wastewater originating from various industries⁽¹⁷¹⁾ which could include a former paint manufacturer. As PCB-209 is not expected to occur in high amount in the environment, it is often used as a surrogate for PCB analysis^(58,183) The results reported here build upon other recent studies^(61,180,181) and questions the validity of using PCB-209 as a surrogate congener in chromatography analysis especially for urban and/or industrially exposed environmental samples.

Inverse relationship between net deposition of PBDEs and PCBs. Radionuclides activities of ^{210}Pb , ^{137}Cs , and ^{226}Ra as a function of depth are shown in Figure B3.10. Cores CWP and IGC13 had an expected trend of decreasing ^{210}Pb activity level to ^{226}Ra activity level at depth (i.e., achieving fully supported ^{210}Pb). CBC did not have a discernible trend in $^{210}\text{Pb}/^{226}\text{Ra}$ ratio, consistent with a suspected mid-core mixing/scouring event at this site in the 1980 to 2000 time frame. PBDE and PCB

concentrations and composition also support the notion of a mid-core mixing/scouring event in CBC (Figure 3.7a-b, panels a and e). The trend in $^{210}\text{Pb}/^{226}\text{Ra}$ in CLC was inconclusive for dating purposes consistent with a suspected mixing in deeper sediment depth (Figure B3.10c).

Whole core net sedimentation rates estimated from CRS method were larger than rates estimated from the CIC methods for cores CBC, CLC, and IGC09; rates estimated from both methods differ by 32 to 77% (Table B3.5). Comparison of whole core net sedimentation rate using CRS and CIC methods resulted in similar values only for cores CWP and IGC13. None of the Chicago and IGC cores had significantly large ^{137}Cs peaks to enable confirmation of peak/onset deposition dates. Therefore, net sedimentation (deposition minus any resuspension) was calculated from the top five segments in all cases. Reported net sedimentation rate, shown in Table 3.3, were corrected for estimated minimal focus factors using the method described in Zhu and Hites (2005).⁽⁵⁰⁾ This was done because fully supported ^{210}Pb may not have been reached in all cores.⁽⁵⁰⁾ Comparison of the whole-core CIC and CRS methods to the net sedimentation rate estimated from the top five sediment segments resulted in a difference of 0.4 to 36% in all cores (Table B3.5).

In Table 3.3, the surface net deposition (as estimated from the top five sediment segments and focus factor corrected) and core inventories of BC, PBDEs, and PCBs from the metropolitan Chicago cores were compared to data from southern AR cores near the PBDE production area. The estimated net sedimentation rate from the top five sediment segments for core CBC was $1.40 \text{ g/cm}^2/\text{yr}$; substantially higher than the other cores which ranged from 0.06 to $0.30 \text{ g/cm}^2/\text{yr}$. This result is consistent with known high loadings from high volume RAPS CSO releases. Core CWP has net deposition rate of $0.08 \text{ g/cm}^2/\text{yr}$, similar to core AMW with net deposition rate of $0.06 \text{ g/cm}^2/\text{yr}$; CWP and AMW had the lowest net deposition rate in the Chicago and IGC cores and in the AR cores, respectively. Cores CLC and IGC13 had net deposition rates of 0.30 and $0.15 \text{ g/cm}^2/\text{yr}$, respectively, similar to cores AED and ACL with net deposition rates of 0.12 and $0.12 \text{ g/cm}^2/\text{yr}$, respectively.

BC can be viewed as a proxy measurement for industrial and/or transportation activities. Although BC levels were lower in CBC than in CWP, net BC deposition were higher in cores CBC and

CLC, exceeding $10 \text{ mg/cm}^2/\text{yr}$. This clearly indicates that these cores were highly affected by industrial and/or transportation activities. For perspective, BC deposition in the Great Lakes ranged only from 0.02 to $0.89 \text{ mg/cm}^2/\text{yr}$.⁽⁴⁶⁾ Net BC deposition in CWP and IGC13 cores were lower (even though CWP had higher BC concentrations), but typical for an urban air shed. For comparison, net BC deposition in southern AR (cores AED, AMW, and ACL) was less than $0.5 \text{ mg/cm}^2/\text{yr}$, as expected from the non-urban AR locations which is synonymous with a less industrial and/or transportation-related activities.

Core AED located closest to the PBDE manufacturing facilities in southern AR has the highest $\Sigma_{48}\text{PBDEs}$ and BDE-209 deposition rates.⁽¹⁵¹⁾ In the absence of industrial and or transportation activity (implied from the low BC deposition), the high $\Sigma_{48}\text{PBDEs}$ and BDE-209 deposition rates were likely due to large PBDE manufacturing facilities.⁽¹⁵¹⁾ $\Sigma_{48}\text{PBDEs}$ and BDE-209 deposition rates in cores AMW and ACL were also high and suspected to be influenced by the two PBDE manufacturing facilities.⁽¹⁵¹⁾ $\Sigma_{48}\text{PBDEs}$ and BDE-209 deposition in cores AMW and ACL were in the same magnitude as in cores CBC and IGC13. Although urban Chicago is lacking in PBDE point sources of the same magnitude as in AR, both CBC and IGC13 were highly impacted by industrial activities as indicated by the high BC deposition rate. Therefore, the high $\Sigma_{48}\text{PBDEs}$ and BDE-209 deposition rates observed in CBC and IGC13 are possibly from industrial origins. If that is the case, the similarity in PBDE deposition rate suggests that post-manufacture industrial discharges can be a large contributor towards PBDE contamination in the metropolitan Chicago area.

BDE-209 and $\Sigma_{48}\text{PBDEs}$ net deposition rates in AR cores from PBDE production area were >100 times higher than core CWP (urban site with primarily airborne deposition). This pronounced difference is consistent with the recorded BDE-209 industrial releases reported to Toxic Release Inventory (TRI) system. For example, in 2011, reported BDE-209 released from the two PBDE manufacturing facilities in AR were >11000 kg; three orders of magnitude higher than reported BDE-209 releases in IL. Additionally, BDE-209 was released from industrial facilities at distal locations from the sampling sites in metropolitan Chicago cores. Overall, BDE-209 deposition rates were 10 to 40 times higher than

Σ_{48} PBDEs net deposition rates in all the sediment cores. This could be due to the dominant usage of Saytex 102E TM relative to the other two PBDE TMs in Chicago.

Σ_{132} PCBs net deposition rates in cores CBC and IGC13 were much higher than the other sites. This is consistent with discharges of an industrial origin into CSOs and other discharges into the industrial waterways. Generally, Σ_{132} PCBs net deposition rates were substantially higher for urban Chicago and IGC cores compared to AR cores. This is expected as PCBs historical usage is largely associated with industrial applications. The large discrepancy in Σ_{132} PCBs net deposition rates between Chicago and IGC cores to AR cores are consistent with TRI data of PCB discharges. Total release for IL was 70 kg whereas AR had no reported industrial related PCB emissions in 2008.

In AR sediment cores, the PBDE/PCB net deposition ratios were at least two orders of magnitude higher than the urban Chicago and IGC cores. These were driven by the substantially higher Σ_{49} PBDEs net deposition in the PBDE production area, coupled with the lack of PCB deposition in AR sediments. Comparison of PBDE/PCB net deposition ratios in Chicago and IGC cores revealed that core CWP had the highest ratio. Observation of the PBDE and PCB concentration data with depth indicate that this trend emerged from the rapid increased in PBDE concentration rather than a substantial decline in PCB concentration (Figure 3.7a-b, panels d). This result demonstrates that prevention of release in the first place is the most effective remedial strategy. Four decades after the PCB ban, substantial amounts still enter the sediments.

In the metropolitan Chicago cores, Σ_{49} PBDEs and Σ_{132} PCBs inventories span two orders of magnitude and followed a similar decreasing trend of IGC13 > CBC > CLC > CWP. Maximum PCB and PBDE inventories were in core IGC13 with 14,700 ng/cm² and 130,800 ng/cm² for Σ_{49} PBDEs and Σ_{132} PCBs, respectively. Although the Σ_{49} PBDEs inventory in IGC13 was within the same order of magnitude to AMW and ACL, this was still one order of magnitude lower than core AED in the AR PBDE production area. Although there are no Σ_{132} PCBs inventory for AED and ACL (PCB concentrations were only analyzed at the surface due to low concentration), AR cores were expected to

have low Σ_{132} PCBs inventory compared to Chicago and IGC cores, as was observed in core AMW. Cores AED and ACL were expected to have high ratios of PBDE/PCB inventory as was observed in core AMW. The lowest PBDE inventory was in core CWP, the sole metropolitan Chicago core not influenced by any direct industrial or CSO discharges. As an interesting note, core CWP also had the lowest Σ_{132} PCBs inventory. Given the trend in increasing PBDE and declining PCB concentrations in recent years (Figure 3.7a-b, panels b), the PBDE/PCB ratios in core CWP are expected to increase in the future.

Table 3.3. Sedimentation and chemical loading for Chicago, IGC and Arkansas sample sites. Shown are net deposition rates of black carbon (BC), Σ_{49} PBDEs, and Σ_{132} PCBs in surface sediment, and inventories for core depth as shown.

Core	Core length (cm)	Net sedimentation rate ^a (g/cm ² /yr)	Focus factor ^b	Net surface deposition rate ^c				Σ_{49} PBDEs inventory (ng/cm ²)	Σ_{132} PCBs inventory (ng/cm ²)	PBDE/PCB Net deposition ratio	PBDE/PCB Inventory ratio
				BC (mg/cm ² /yr)	Σ_{48} PBDEs ^d (ng/cm ² /yr)	BDE 209 (ng/cm ² /yr)	Σ_{132} PCBs (ng/cm ² /yr)				
CWP	30	0.08	0.76	3.80	2.7	31.5	4.0	778	1540	8.1	0.51
CLC	34	0.30	0.86 ^b	15.4	9.6	21.5	84.3	2005	20200	0.4	0.10
CBC	35	1.40	1.40 ^b	22.4	40.4	235.0	740.1	9540	66200	0.8	0.14
IGC13	60	0.15	2.50	1.20	22.4	86.7	180.6	14700	130800	1.8	0.11
AED [151]	25	0.12	ND ^e	0.90	298.0	6690.0	0.1	289300	ND ^e	9300.0	ND ^e
AMW [151]	56	0.06	ND ^e	0.20	78.4	346.0	4.2	67200	4650	100.0	14.4
ACL [151]	45	0.12	ND ^e	0.20	13.2	298.2	0.4	10300	ND ^e	870.0	ND ^e

^a Calculated from top five segments in all cases. ^b Estimated minimum as full unsupported ²¹⁰Pb may not have been reached. ^c Focus factor corrected net deposition rate. ^d Sum of mono- through nona-BDEs. ^e ND = Not determined.

Comparison of PBDE and PCB concentrations. Surface PBDE concentrations in the Chicago and IGC cores were compared to other selected studies in the U.S. (Table 3.4). The highest surface PBDE concentration in the present study was observed in core IGC13; an order of magnitude higher than levels observed in the Great Lakes.^(45,49,47) PBDE concentrations in cores CBC, CLC, and CWP were higher than those observed in the Great Lakes with the exception of Lake Ontario.⁽⁴⁷⁾ The highest reported PBDE concentration in the U.S. was observed in core AED (6950 and 57193 ng/g at surface and peak concentrations, respectively).⁽¹⁵¹⁾ Cores AMW and ACL (located proximate to the two PBDE manufacturing facilities) have high PBDE concentrations as well; 35600 and 48481 ng/g for surface and peak concentrations in core AMW, and 2503 and 2580 ng/g for surface and peak concentrations in core ACL.⁽¹⁵¹⁾ While PBDE levels in the Chicago and IGC cores were higher than recent values reported in Lake Michigan,⁽⁵³⁾ Saginaw river watershed,⁽⁵¹⁾ and Hadley Lake, IN⁽⁵²⁾, the values observed in the current study were still one to two orders of magnitude lower than the AR cores proximate to the PBDE manufacturing facilities. In eastern and northern AR locations, PBDE concentrations were significantly lower. For example, total PBDE concentration in core AFR was less than 10 ng/g at all sediment depth; at least an order of magnitude lower than PBDE levels observed in the Chicago and IGC sites. This was expected as these northern AR sampling locations are less developed relative to the Chicago and IGC immediate surroundings (Figures 3.1 and A3.1) and outside the area of high atmospheric deposition near the PBDE source zone (i.e., at a location distal from the two PBDE manufacturing facilities). PCB levels in the Chicago and IGC cores were lower than the Great Lakes (Table 3.4).⁽⁵⁸⁾ In IGC13, surface Σ_{132} PCBs concentration was two orders of magnitude higher than total PCB concentrations in the Great Lakes⁽⁵⁸⁾ and much higher than the AR sediment cores. PCB concentrations in cores CBC, CWP, and CLC were one to two orders of magnitude lower than PCB levels from other industrialized areas such as the IHC⁽⁶⁰⁾ and the Houston Ship Channel.⁽⁶¹⁾ Although PCB concentration in IGC13 was comparable to these industrial areas, it was still an order of magnitude lower compared to PCB legacy sites such as Thompson Island Pool in the Hudson river, NY.⁽⁵⁾

Table 3.4. PBDE and PCB concentrations in selected recent studies of surface sediments in the U.S.

Contaminant	Area	Location	Sampling locations	Analyzed congeners	Concentration (ng/g d.w.)
PBDEs	Great Lakes	Lake Michigan ^(49,50)	3	10	47.9-97.3
			1	18	2.6
		Lake Huron ⁽⁴⁹⁾	3	10	23.2-37.9
		Lake Superior ⁽⁴⁵⁾	4	10	7.1-20.6
		Lake Erie ^(47,50)	2	10	52.0-57.4
			1	18	1.1
		Lake Ontario ⁽⁴⁷⁾	2	10	217.5-246.8
	Inland Lake Michigan	White Lake ⁽⁵³⁾	1	23	0.39-2.4
		Muskegon Lake ⁽⁵³⁾	1	23	0.98-3.9
	Saginaw River, Michigan	Shiawasse River ⁽⁵¹⁾	28	10	0.2-12.8
		Saginaw River ⁽⁵¹⁾	20	10	0.2-49.4
		Saginaw Bay ⁽⁵¹⁾	5	10	0.05-6.5
	Indiana	Hadley Lake, IN ⁽⁵²⁾	4	7	34-71
	Arkansas	Lake Calion (ACL) ⁽¹⁵¹⁾	1	49	2500
		Lake Jack Lee (AJL) ⁽¹⁵¹⁾	1	49	402
		West Lake of El Dorado (AED) ⁽¹⁵¹⁾	1	49	6950
		Magnolia WWTP Pond (AMW) ⁽¹⁵¹⁾	1	49	35,600
		Lake Old Town (AOT) ⁽¹⁵¹⁾	1	49	11.8
		Lake Frierson (AFR) ⁽¹⁵¹⁾	1	49	4.28
		Lake Michigan ⁽⁵⁸⁾	3	38	18.6-41.6
PCBs	Great Lakes	Lake Huron ⁽⁵⁸⁾	3	38	7.8-18.7
		Lake Superior ⁽⁵⁸⁾	4	19	3.4-27.5
		Lake Erie ⁽⁵⁸⁾	2	38	23-28.3
		Lake Ontario ⁽⁵⁸⁾	2	38	58.3-63.6
	Texas	Houston Ship Canal ⁽⁵⁸⁾	98	209	4 to 4601
	New York	Thompson Island Pool ⁽⁵⁾	1	28	20,140
	Indiana	Indiana Harbor and Canal ⁽⁶⁰⁾	2	209	1200

Airborne versus waterborne PBDE and PCB Exposure Pathways. Two modes of PBDE and PCB exposures were postulated for Chicago and IGC cores; 1) anthropogenic discharges including combined sewage outfall (CSO) and WWTP effluent and 2) atmospheric deposition. Cores CBC and IGC13 are riverine systems which are predominantly recharged by anthropogenic discharges. As previously discussed, site CBC is primarily fed by large volume CSO discharges from RAPS whereas site IGC13 originated primarily from HSD WWTP effluent, effluent from other WWTP and industries, as well as multiple CSO discharge points along its bank. Cores CBC and IGC13 are thus referred collectively as waterborne deposition-dominated cores.

Studies characterizing PBDE and PCB occurrences in WWTP effluent and CSOs are abundant; recent studies are summarized in Table A3.6. For example, discharges of up to 29 ng/L total PBDEs from a Palo Alto, CA WWTP facility was estimated to contribute 0.9 kg of PBDEs annually into the San Francisco estuary.⁽⁴⁰⁾ CSOs discharging into the Columbia River Basin and in Switzerland have documented PCB concentrations as high as 440 and 403 ng/L, respectively.^(184,185) Analysis of the scientific literature identified relatively few studies characterizing the level of PBDEs and PCBs in non-WWTP discharges. This limits the ability to compare PBDE and PCB levels in these non-WWTP discharges. In core CWP, the primary PBDE and PCB deposition pathways are via wet and dry atmospheric depositions as natural and anthropogenic hydrologic inflow are absent to site CWP.^(166,167) Core CWP is thus referred to as an airborne deposition-dominated. The documentation of PBDEs and PCBs in remote areas that is unlikely to be influenced by industrialization and urbanization (such as in Lake Siskiwit and the Arctic) are among the strongest evidence of long range atmospheric transport of PBDEs and PCBs.^(186,187,188,189) CLC has aspects of both types of sites; receiving waterborne runoff from Pullman creek, as well as a substantial airborne component due to its lacustrine environment and proximity to local airborne sources.

An interesting trend emerges when observing the Σ_{48} PBDEs, BDE-209, and Σ_{132} PCBs net surface deposition rates, Σ_{49} PBDEs and Σ_{132} PCBs inventories, and PBDE/PCB net deposition and inventory ratios

(Table 3.3). In urban waterborne deposition-dominated cores (CBC and IGC13), Σ_{48} PBDEs, BDE-209, and Σ_{132} PCBs net surface deposition rates were substantially higher compared to the atmospheric deposition-dominated core (CWP), which results in a relatively larger Σ_{49} PBDEs and Σ_{132} PCBs inventories in cores CBC and IGC13. All urban cores that receive some form of aqueous discharge have high Σ_{132} PCBs deposition rates. PBDE/PCB net deposition ratios in urban waterborne deposition-dominated cores were much lower compared to atmospheric deposition-dominated core. However, PBDE/PCB inventory ratio was much higher in the atmospheric deposition-dominated core. Overall, these observations suggest that urban aqueous discharges such as CSOs, stormwater discharges, and WWTP effluent can be a major of PBDEs and PCBs in the sediments of urban waterways. However, atmospheric loadings in such environments are still high compared to rural AR and the Great Lakes. For example, core CWP had high PBDE deposition (2.7 and 4.0 ng/cm²/yr for Σ_{48} PBDEs and BDE-209 net surface deposition rates, respectively) but much lower for PCBs (4.0 ng/cm²/yr Σ_{132} PCBs net surface deposition). This indicates that current atmospheric deposition of PCBs is not as high as in the past and is now greatly exceeded by PBDEs.

In AR sediment cores, Σ_{48} PBDEs and BDE-209 net surface deposition rates were one to three orders of magnitude larger than Σ_{132} PCBs net surface deposition. This results in a very high PBDE/PCB net deposition ratio. Interestingly, BDE-209 net surface deposition rates were similar in the AR and urban Chicago and IGC sediment cores. This may reflect the dominance of Saytex 102E in consumer products in metropolitan Chicago and/or a result from the differential transport of PBDE homologs. Driven by the large PBDE concentration, the Σ_{49} PBDEs inventories in AR sediments were one to three orders of magnitude larger than the Chicago and IGC sediment cores. In contrast to the case with PBDEs in riverine sediments, the Σ_{132} PCBs inventory in core AMW was similar to levels observed in core CWP, indicating that aqueous discharge is not a major contributor of PCBs to the sediment phase.

Radionuclide data enabled accurate sediment dating only for cores CWP and IGC13; thus the PBDE and PCB depositional trends in these cores were compared to core AMW to better understand

recent trends in atmospheric deposition. Core CWP, the only atmospheric deposition-dominated metropolitan Chicago core has increasing Σ_{49} PBDEs at a rate of $9.2 \pm 1.1\%$ per year since the 1980s (Figure 3.8a). Tracking of cumulative PBDE congeners in Saytex 102E, DE-71, and DE-79 TMs showed that all three TMs experienced increased deposition rates in recent year with the rates increasing in the order of DE-79 > DE-71 >> Saytex 102E (Figure 3.8d). In contrast, Σ_{49} PBDEs deposition has been increasing by only 1% per year at core IGC13 during this time (Figure 3.8b). The three PBDE TMs in core IGC13 also experienced an increase in deposition rates in similar order albeit at a less pronounced rate relative to core CWP (Figure 3.8e). In core IGC13, only DE-79 TM has a statistically significant regression. Over the same time, Σ_{132} PCBs deposition has declined by approximately 1% per year in cores CWP and IGC13 (the rate was only statistically significant at CWP at the 90% CI). Depositional trends for PCB Aroclors in recent years were not tracked because of the large number of congeners that overlap in the PCB Aroclor mixtures which makes reliable regression analysis difficult. The relatively slow decline in Σ_{132} PCBs deposition compare to the rapidly increasing rate of Σ_{49} PBDEs deposition provides further proof that the higher ratio of PBDE/PCB deposition in core CWP in recent years was driven primarily by the rapid increase in PBDE deposition rather than a decline in PCB deposition. PBDE deposition rate in the atmospheric deposition-dominated urban sediment was twice as high compared to the waterborne deposition-dominated urban sediments (CBC and IGC13). The increasing PBDE concentration and net deposition rate observed in core CWP does not match the fluctuating levels of atmospheric PBDE concentration in the Chicago area as recorded by the Integrated Atmospheric Deposition Network.⁽¹⁹⁰⁻¹⁹³⁾ However, it should be noted that air measurements respond much more quickly to changes than do integrated sediment core measurements over yearly to decadal time frames.

Sediment at site AMW provided an interesting point for comparison. While it received Magnolia WWTP effluent from 1952 to 1989 (i.e. waterborne-source dominated), and after the pond was no longer actively used for WWTP, PBDEs and PCBs would be expected to come primarily through airborne deposition. Core AMW had two dramatically different PBDE deposition regimes; this expectation is

consistent with observation. During the pond active use, PBDE deposition increased at a rate of 7.6% per year, and decreased by 4.9% per year since 1989 when the pond no longer received treated WWTP effluent from the Magnolia facility (Figure 3.8c). While Σ_{49} PBDEs net deposition rates were increasing, all three PBDE TMs also experienced an increase in deposition rate (Figure 3.8f). It is interesting to note that DE-79 increased at a faster rate compared to DE-71 in core AMW. Concomitant with the decline in Σ_{49} PBDEs net deposition rate, the decline in the net deposition rates of Saytex 102E and DE-79 were also observed. In contrast, there was no discernible trend in net deposition rate (either upward or downward) for DE-71. Since WWTP loading to site AMW ceased after 1989, core AMW has a similar Σ_{49} PBDEs deposition rate as core ACL, likely reflecting the predominance of PBDE atmospheric sources shared by these sediment columns (Table 3.3). Over both the pre- and post-1989 time periods, Σ_{132} PCBs declined at 7.6% per year; consistent with PCB usage decline since the U.S production ban took effect in the 1970s.

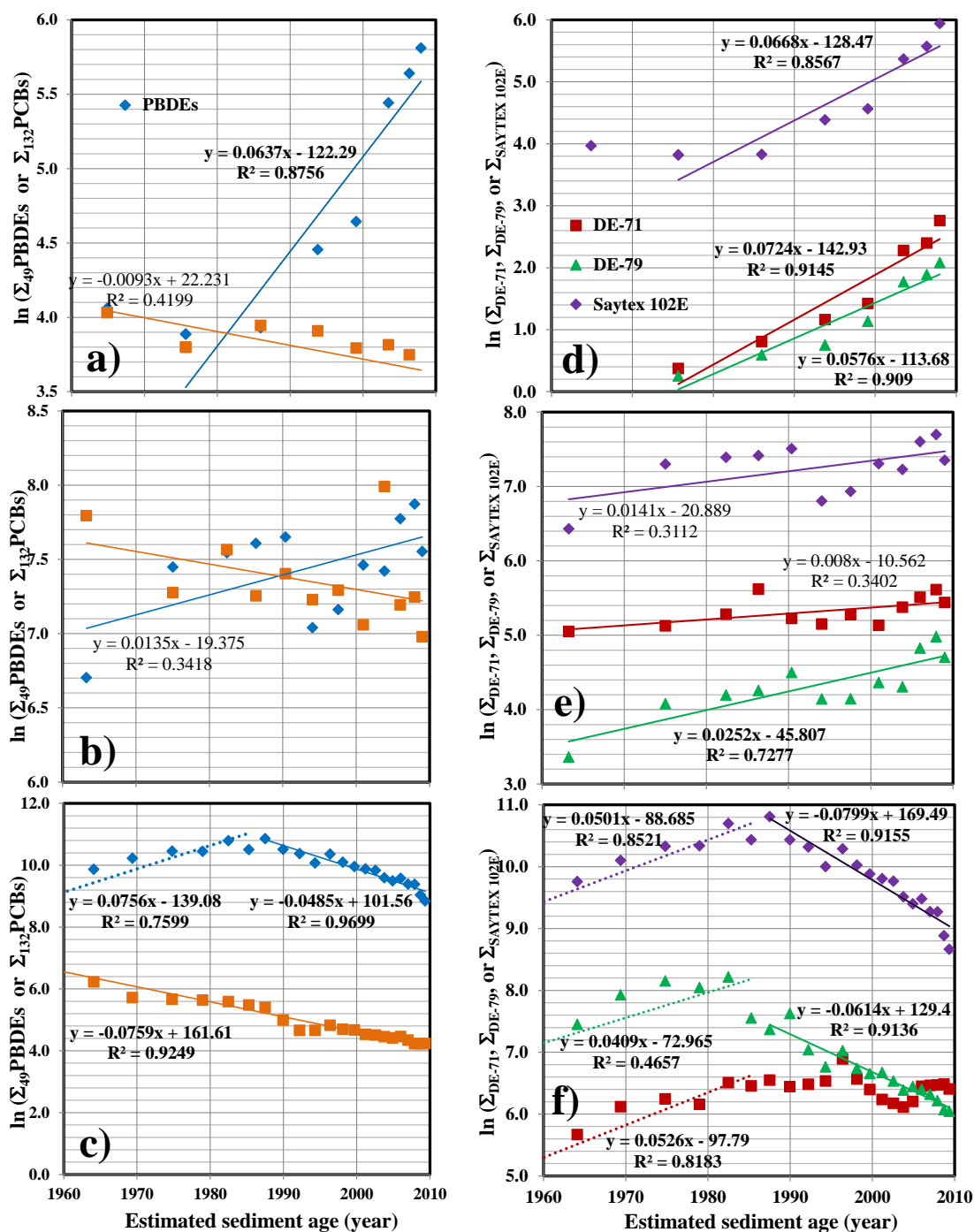


Figure 3.8: a-c) $\Sigma_{49}\text{PBDEs}$ and $\Sigma_{132}\text{PCBs}$ in 1960-2010 and d-f) Saytex 102E, DE-71, and DE-79 TMs in cores a,d) CWP, b,e) IGC13, and c,f) AMW. DE-71 TM contains congeners 17, 28/33, 47, 49, 66, 85, 99, 100, 126/155, 138, 139, and 154. DE-79 TM contains congeners 138, 153, 183, 196, 197, 201, 203, 207, and 208. Saytex 102E TM contains congeners 206 and 209. Statistically significant regressions at the 95% CI are in bold and 90% CI are non-bold. Regressions were split between periods of active pond use (pre-1989) and non-active use (post-1989) in AMW. Note the different scale on the y-axes in panels a-f.

A second major difference between waterborne- and atmospheric-sourced sites is the enrichment of LMW PBDE homologs in waterborne deposition-dominated cores. In the metropolitan Chicago cores, surface sediments in the waterborne deposition-dominated cores have higher tetra- and penta-PBDE homologs compared to surface sediment in atmospheric deposition-dominated core. For example, the tetra- and penta-BDE homologs have 4 to 5% composition in core CBC and 5 to 6% composition in core IGC13. In contrast, tetra- and penta-BDE homologs comprised only 1.8% each in core CWP (Figure 3.9). Core AMW had similar tetra- and penta-BDE compositions prior to 1989 as those observed in the waterborne deposition-dominated cores in metropolitan Chicago (4.7 and 3.4% tetra- and penta-BDE congeners, respectively). Previous study in the Great Lakes provide insight into the accumulation of LMW PBDE congeners observed in sediments influenced by waterborne deposition (the comparisons in this section only use Σ_{10} PBDEs and Σ_8 PCBs congeners measured in common between all studies). Lake Superior sediment cores from sites SU-08, SU-12, and SU-16 located towards the middle of the lake have lower surface fluxes of BDE homologs 1-9 (8 - 13 $\mu\text{g}/\text{cm}^2/\text{yr}$) whereas core SU-22 located comparatively close to the Duluth, MN metropolitan area had higher surface fluxes of BDE homologs 1-9 (31 $\mu\text{g}/\text{cm}^2/\text{yr}$);⁽⁴⁵⁾ possibly reflecting influence of waterborne sources. Anthropogenic discharges can carry a higher relative abundance of LMW PBDE congeners consistent with the increasing hydrophobicity and much lower aqueous solubility of the HMW PBDE congeners.⁽¹⁹⁾ For example, the dominant congeners in the DE-71 TM (BDE-47, 99, 100, 153, and 154) constituted 88% of the total PBDEs in a Palo Alto, CA WWTP effluent stream.⁽⁴⁰⁾ However, caution should be exercised in drawing too broad a conclusion without considering the impact of local PBDE sources. Marlowe Creek, NC, a site primarily fed by WWTP effluent that potentially treats wastewater originating from a plastic goods manufacturer,⁽¹⁹⁴⁾ has lower relative abundance of tetra- and penta-PBDE homologs (0.7 and 1.4% tetra- and penta-PBDE homologs, respectively). Additionally, hexa- and hepta-PBDE homologs were also absent in Marlowe Creek sediments;⁽¹⁹⁴⁾ indicating local sources of PBDEs unique to the site.

Cores CWP and northeastern AR (cores that were likely dominated by atmospheric-deposition) have similar homolog profiles to those observed in the Great Lakes. This similarity can arise due to

differential long distance PBDE atmospheric transport. In the Great Lakes region, detection of PBDEs in remote sediment cores at locations absent of anthropogenic contaminant sources demonstrates the substantial long-range transport potential of LMW and HMW PBDE congeners.^(26,45,47,49,186) The northeastern and southern AR sediment cores have distinctively different PBDE homolog profiles. In particular, LMW PBDE homologs were substantially lower in southern AR surface sediments near PBDE manufactures compared to northeastern AR surface sediments. The lack of LMW PBDE homologs in southern AR cores can be attributed to several factors: 1) low atmospheric concentrations of less brominated PBDE homologs stemming from voluntary industry bans on DE-71 and DE-79 TMs resulting in lower loadings of LMW PBDE to the sediment phase, 2) the short distance between the PBDE point source emissions and deposition sites resulting in little/no photolytic transformation from large to small BDE homologs prior to sedimentation, and 3) less partitioning to the sediment phase by LMW PBDE congeners such as BDE-47 and 99 relative to HMW PBDE congeners.⁽¹⁹⁰⁻¹⁹³⁾ This would result in greater mobility and thus dispersion of the lesser brominated congeners.

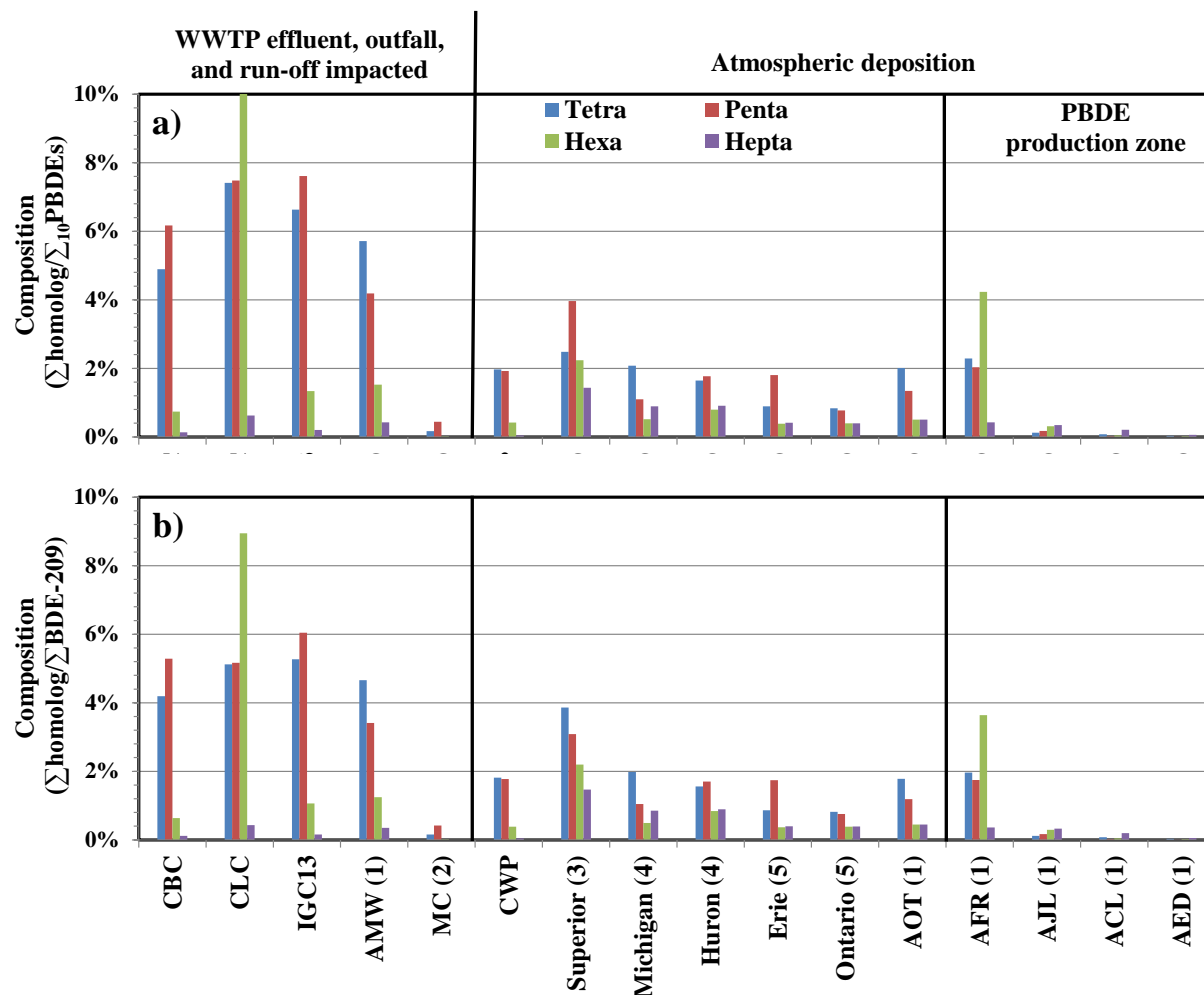


Figure 3.9: a) Compositions and b) BDE-209 normalized compositions of tetra-, penta-, hexa-, and hepta-PBDE homologs in Chicago, IGC, AR, MC, and Great Lakes surface sediments. In a) Σ_{10} PBDEs represent sum of commonly analyzed PBDE congeners in all the studies (BDE-28, 47, 66, 100, 99, 85, 154, 153, 183, and 209). In the Great Lakes, composition values shown represent average of all sampling sites within the lake. References: (1)⁽¹⁵¹⁾; (2)⁽¹⁹⁴⁾; (3)⁽⁴⁵⁾; (4)⁽⁴⁹⁾; and (5):⁽⁴⁷⁾.

It is also notable that cores from southern AR near the PBDE production areas (AED, AMW, and ACL) have Σ_{10} PBDEs/ Σ_8 PCBs ratios greater than 10:1; in contrast to the Great Lakes sites that have Σ_{10} PBDEs/ Σ_8 PCBs ratios less than unity (Figure 3.10). The Σ_{10} PBDEs/ Σ_8 PCBs ratios in the metropolitan Chicago cores were in between 1 and 10, but typically closer to the 1:1 line. The largest change in Σ_{10} PBDEs/ Σ_8 PCB ratio was observed in core CWP; the vertical series data point towards a clear temporal trend. Higher ratio on the y-axis corresponds to more recently deposited sediments.

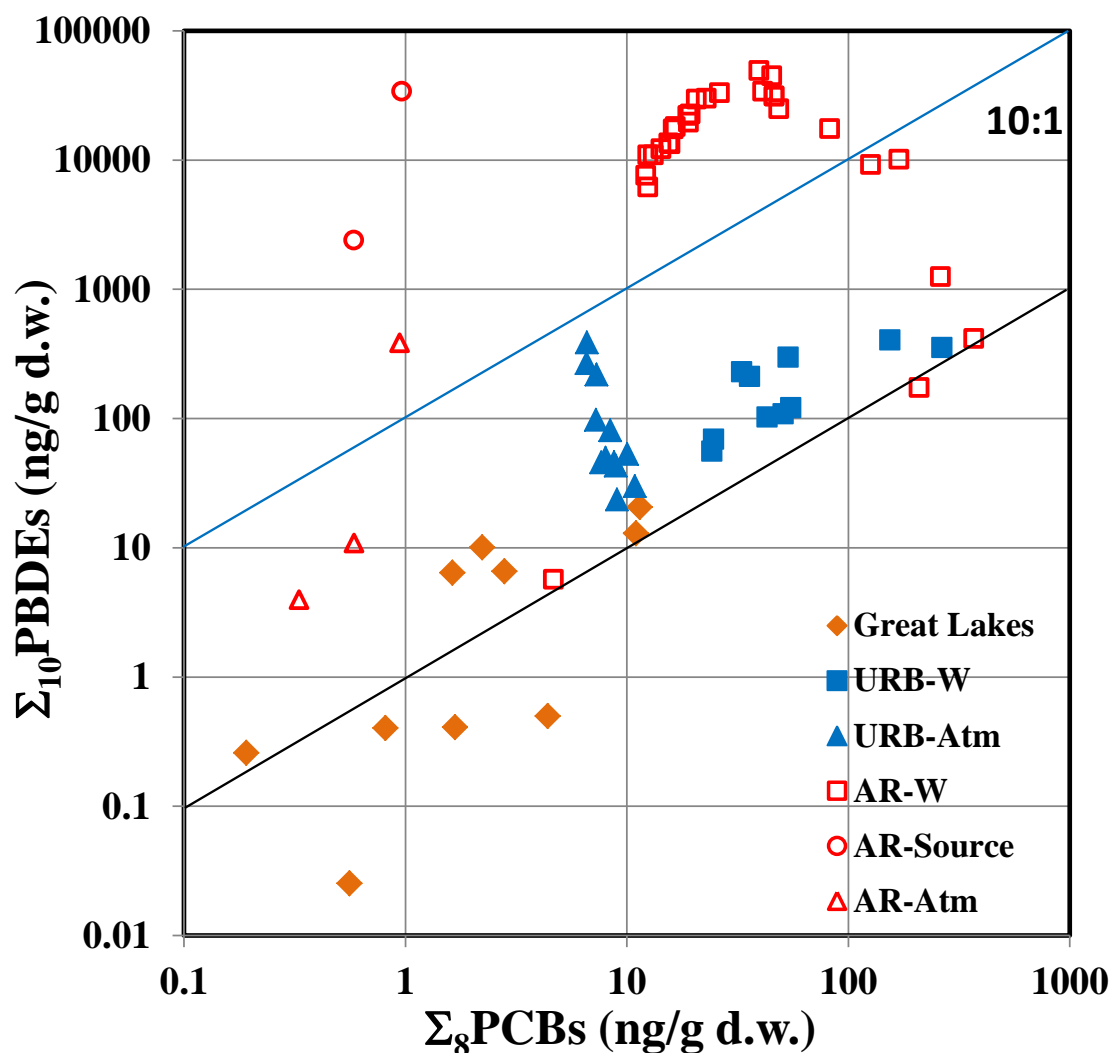


Figure 3.10: Ratio of Σ_{10} PBDEs and Σ_8 PCBs concentrations in sediments from the metropolitan Chicago, AR, and the Great Lakes. Σ_{10} PBDEs represent sum of commonly analyzed PBDE congeners in all the studies (BDE-28, 47, 66, 100, 99, 85, 154, 153, 183, and 209). URB-W are Chicago metropolitan waterborne deposition-dominated cores (CBC, CLC, and IGC13), URB-Atm is Chicago metropolitan atmospheric-deposition dominated core (CWP), AR-W is AR waterborne deposition-dominated cores (AMW), AR-Source are southern AR production area cores (AED and ACL), AR-Atm are northeastern AR atmospheric-deposition impacted cores (AJL, AOT, and AFR), and the Great Lakes. Lines represent 1:1 and 10:1 ratios of Σ_{10} PBDE: Σ_8 PCBs.

3.4.4. Evaluating evidence of *in-situ* degradation of PBDEs and PCBs

Enrichment of low molecular weight congener. Dehalogenation of PBDEs and PCBs over time would be expected to result in enrichment of LMW congeners that are observable in undisturbed cores. I investigated this possibility by analysis of the degree and type of halogen substitution. Such an approach was used in Lake Ontario, where increased in PCB homologs (Σ H1–3, Σ H4–6, and Σ H7–9) with increased sediment depth was interpreted as signs of *in-situ* PCB dehalogenation in Lake Ontario.⁽⁵⁸⁾ Using the same approach, PBDE degradation in core AMW was also suspected based on an apparent increased in the relative abundance of LMW PBDE homologs (Σ H1–4 and Σ H5–7) with increased sediment depth.⁽⁵⁸⁾

In the Chicago metropolitan sediment columns, there was no clear increase in Σ H1–4, Σ H5–7, and Σ H8–9 or clear decrease in H10 (BDE-209) with depth in cores CBC, CWP, and IGC13 (Figure 3.7a, panels f, g, and j). As a note, increased in H10 (BDE-209) composition in IGC13 sediment deeper than 25 cm stemmed from the low amount of BDE-209 rather than changes in the other PBDE homologs as was explained in Section 3.4.3. In core CLC, increased in Σ H1–4 and Σ H5–7 PBDE homologs and to some extent increased in Σ H8–9 PBDE homologs concomitant with a decrease in H10 (BDE-209) composition were observed towards the upper sediment segment; these trends in homologs distributions are similar to core AMW and can be an indication of *in-situ* PBDE dehalogenation in core CLC.

The composition of Σ H1–3, Σ H4–6, and Σ H7–9 PCBs were relatively constant with depth in core CWP and IGC13; more degree of fluctuations were observed in core IGC13 (Figures 3.7b, panels g and j). Increased in Σ H7–9 and decreased in Σ H4–6 were observed towards the upper sediment segments in core CBC (Figure 3.7, panel f). Generally, decrease in HMW homolog concomitant with increase in LMW homolog towards the upper sediment segment is observed under *in-situ* degradation, as was the case with PBDEs in core AMW and PCBs in Lake Ontario sediments;^(58,151) The increase in LMW homolog towards the surface sediment is attributed to degradation of the HMW congener. Given that in

core CBC, Σ H7–9 have a higher molecular weight than Σ H4–6, increased in Σ H7–9 and decreased in Σ H4–6 observed towards the surface sediment is not attributed to *in-situ* degradation and is more likely a response to PCB deposition at site CBC. In core CLC, increased in Σ H7–9 and Σ H4–6 towards the surface sediment were observed concomitant with decreased in Σ H1–3 (Figure 3.7b, panel h). The trends in homolog composition in core CLC can be interpreted as partial PCB dehalogenation of Σ H7–9 to Σ H4–6; although this is noted as not a strong indicator given the rapid decreased in Σ H1–3 concentration which could have influenced the homolog distribution in core CLC.

Comparison of PBDE TMs and PCB Aroclor mixtures to PBDE and PCB sediment profile. The increase in the relative abundance of LMW PBDE or PCB homologs concomitant with a decrease in HMW PBDE or PCB homologs towards the upper sediment segment should not be presented as a single indicator of *in-situ* dehalogenation; multiple lines of evidence are necessary to strengthen the argument in-favor *in-situ* dehalogenation. In an effort to better evaluate *in-situ* dehalogenation, the whole core mean PBDE and PCB congener profile in sediment was compared to PBDE TMs and PCB Aroclor mixtures profiles, respectively, using multiple least square regression (MLSR). The MLSR method was applied to previous studies to compare whole core mean PCB congener profile and a suite of PCB Aroclor mixtures to evaluate the contribution of PCB Aroclor mixtures to the observed PCB congener profile in the sediment.^(10, 16, 65) *In-situ* degradation can result in large MLSR residual between PBDE TMs and PCB Aroclor. However, it should be noted that discrepancy between PBDE TMs and PCB Aroclor mixtures to congener profile in sediment can be attributed to several other factors such as differential homolog transport rate and homolog transformation from source sites to receptor site, and homolog transport in the sediment column. In this study, MLSR analysis was applied to both PBDEs and PCBs. The DE-71, DE-79, and Saytex 102E were the model profiles for PBDEs, and Aroclor mixtures 1016, 1242, 1248, 1254, and 1260 were the model profiles for PCBs.

The weighted average of PBDE congener profile in Chicago and IGC13 cores are compared to PBDE TMs as shown in Figure 3.11. PBDE homologs 1 to 3 were observed in cores CBC, CWP, CLC, and IGC13; these LMW PBDE homologs were not present in the DE-71, DE-79, and Saytex 102E TMs. Although absent in the three PBDE TMs composition, BDE-49, 28/33, and 17 were consistently present in cores CBC, CWP, CLC, and IGC13. BDE-47, 100, and 99 which were the dominant congeners in the DE-71 TMs were present at much lower composition in the Chicago and IGC13 sediment cores. BDE-183 which is the most dominant congener in the DE-79 TM was only present in Chicago cores. The higher composition of PBDE congeners from the DE-71 TM relative to the DE-79 TM indicates that the PBDEs in the Chicago and IGC sediment cores were exposed to higher level of DE-71 compared to DE-79. Although the Saytex 102E was composed primarily of BDE-209 (> 96%), BDE-206 and BDE-207 were detected at ~2 % and ~0.02% , respectively. Interestingly, BDE-206 and BDE-207 compositions were higher in the Chicago and IGC13 cores compared to the compositions in the Saytex 102E TM.

MLSR residual, calculated as site average congener minus the sum of MLSR regression model represent the difference between the PBDE congener profile in sediment and the three PBDE TMs. The MLSR regression model assumes a linear mixing model (LMM). AMW MLSR residual provided an interesting comparison point as PBDE degradation is suspected in AMW. PBDE congeners absent in the three PBDE TMs but present in high compositions in the Chicago and IGC13 sediment cores such as BDE-49, 28/33, and 17 have high MLSR residual (Figure 3.12). Overall, the PBDE MLSR residuals were generally higher in the Chicago and IGC13 cores relative to AMW core. PBDE congeners that were present in the sediment cores at noticeable composition (Figures 3.11 a-d), but absent in the three PBDE TMs such as BDE-49, 28/33, and 17, have high MLSR residuals in the metropolitan Chicago and AMW cores. Dominant congeners in the DE-71 TM such as BDE-47 and BDE-99 have higher MLSR residuals than dominant congeners in the DE-79 TM such as BDE-183. Generally, nona-PBDE congeners (BDE-208, 207 and 206) have high MLSR residuals that increase in the order of BDE-206 < BDE-208 < BDE-207. Interestingly, BDE-209 MLSR residual in the Chicago metropolitan and AMW cores were negative. This trend would be consistent with a degradation of BDE-209 in the sediment phase.

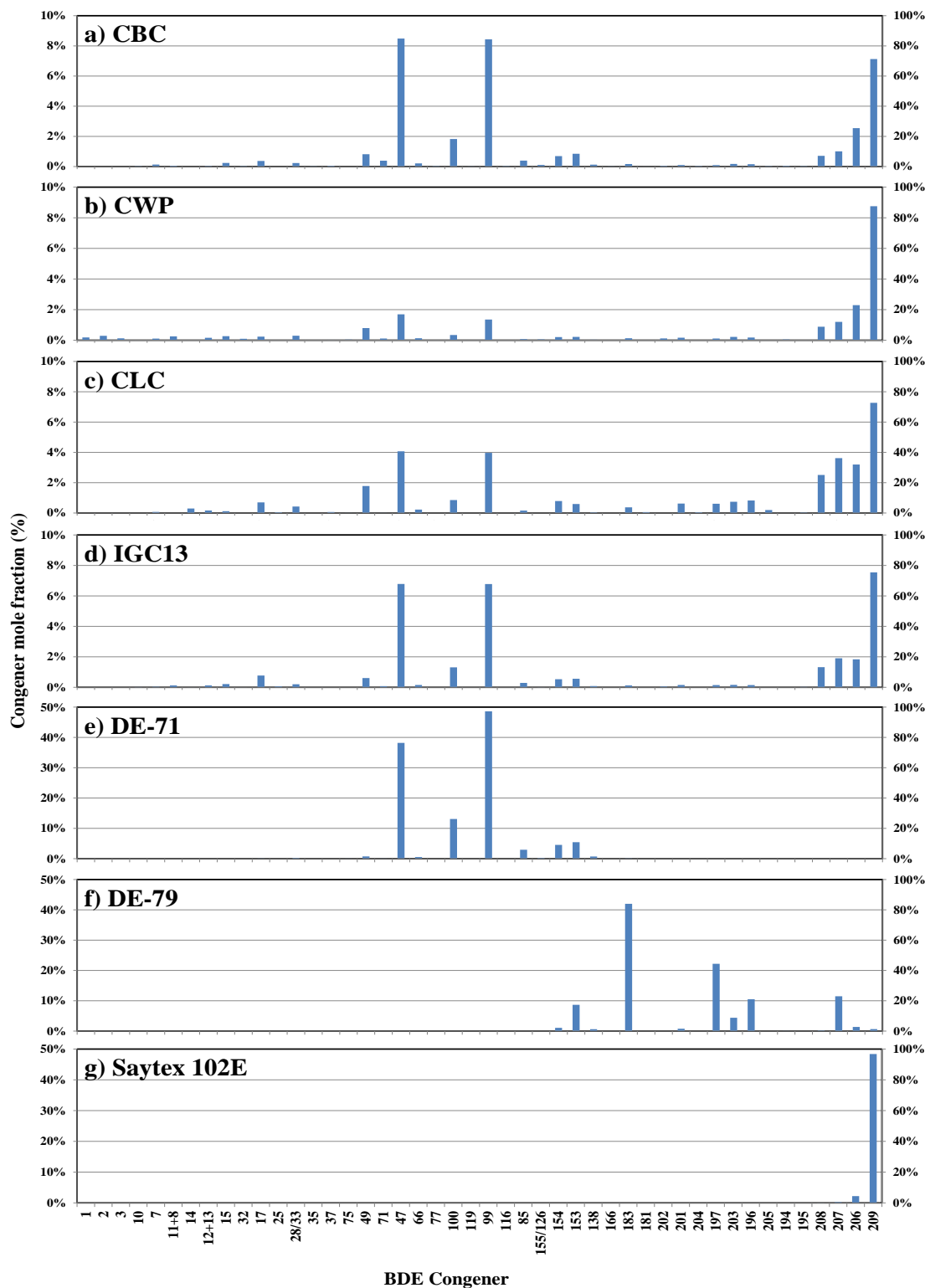


Figure 3.11: Weighted average PBDE congener mole fractions at a) CBC, b) CWP, c) CLC, and d) IGC13 compared to PBDE TMs congener mole fractions in e) DE-71, f) DE-79, and g) Saytex 102E. BDE-209 is shown on right y-axes; note different left y-axes for a) to d) and e) to g).

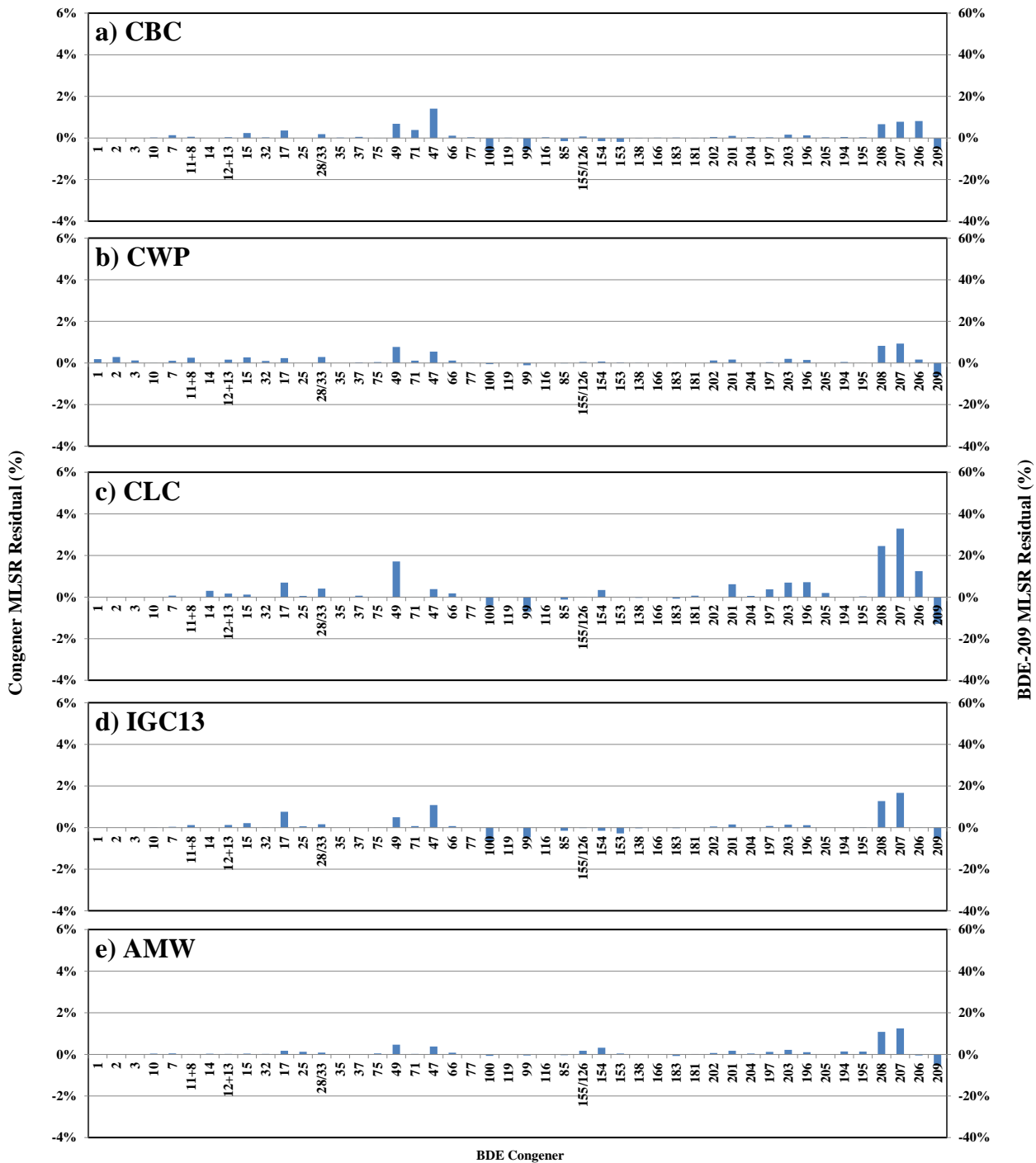


Figure 3.12: PBDE MLSR residuals calculated as site average congener mole fraction minus MLSR regression model assuming LMM in cores a) CBC, b) CWP, c) CLC, d) IGC13, and e) AMW. Note that BDE-209 is shown on the right y-axes at a 10x scale.

Comparison of the weighted average of PCB congener profile in sediment to four PCB Aroclor mixtures showed that both LMW and HMW PCB congeners were present in the Chicago and IGC13 cores (Figure 3.13 a-d). In contrast to the case of PBDEs, not one congener was highly dominant over the other in the sediment cores. Core CBC was enriched in HMW PCB; Generally, PCB congeners with six or more chlorine substitutions have high composition in core CBC. Medium PCB congeners (PCB congeners with four to six chlorine substitutions) were enriched in all the Chicago and IGC13 cores. LMW PCB congeners, in this case referring to PCB congeners with one to three chlorine substitutions were more enriched in cores CWP and CLC. PCB Aroclor mixtures also have a wide range of congeners; this is in contrast to PBDE TMs which are highly dominated by one to three congeners. Aroclor mixtures 1016 and 1242 have LMW PCB congeners, Aroclor mixtures 1248 has low to medium molecular weight PCB congeners, Aroclor mixture 1254 has medium molecular weight PCB congeners, and Aroclor mixture 1260 has HMW PCB congeners (Figure 3.13 e-i).

PCB MLSR residuals for the Chicago metropolitan and AMW cores are shown in Figure 3.14. HMW PCB congeners generally have positive residual values and were the highest residual in core CBC. Generally, most of the PCB congeners in core CWP have low MLSR residual relative to cores CBC, CLC, IGC13, and AMW. In core CLC, LMW PCB congeners (in this case referring to PCB congeners with one to three chlorine substitutions) have high MLSR residuals compared to medium and HMW PCB congeners (PCB congeners with four to six chlorine substitutions and six and more chlorine substitution, respectively). In cores IGC13 and AMW, LMW PCB congeners have high negative MLSR residual values whereas medium PCB congeners have high positive MLSR residual values. The trends in PCB MLSR residual values indicates that if *in-situ* PCB degradation is occurring, CBC has HMW PCB congeners degradation, CLC has LMW PCB congeners degradation, CWP is unlikely to have PCB degradation, and IGC13 and AMW has low and medium PCB congeners degradation.

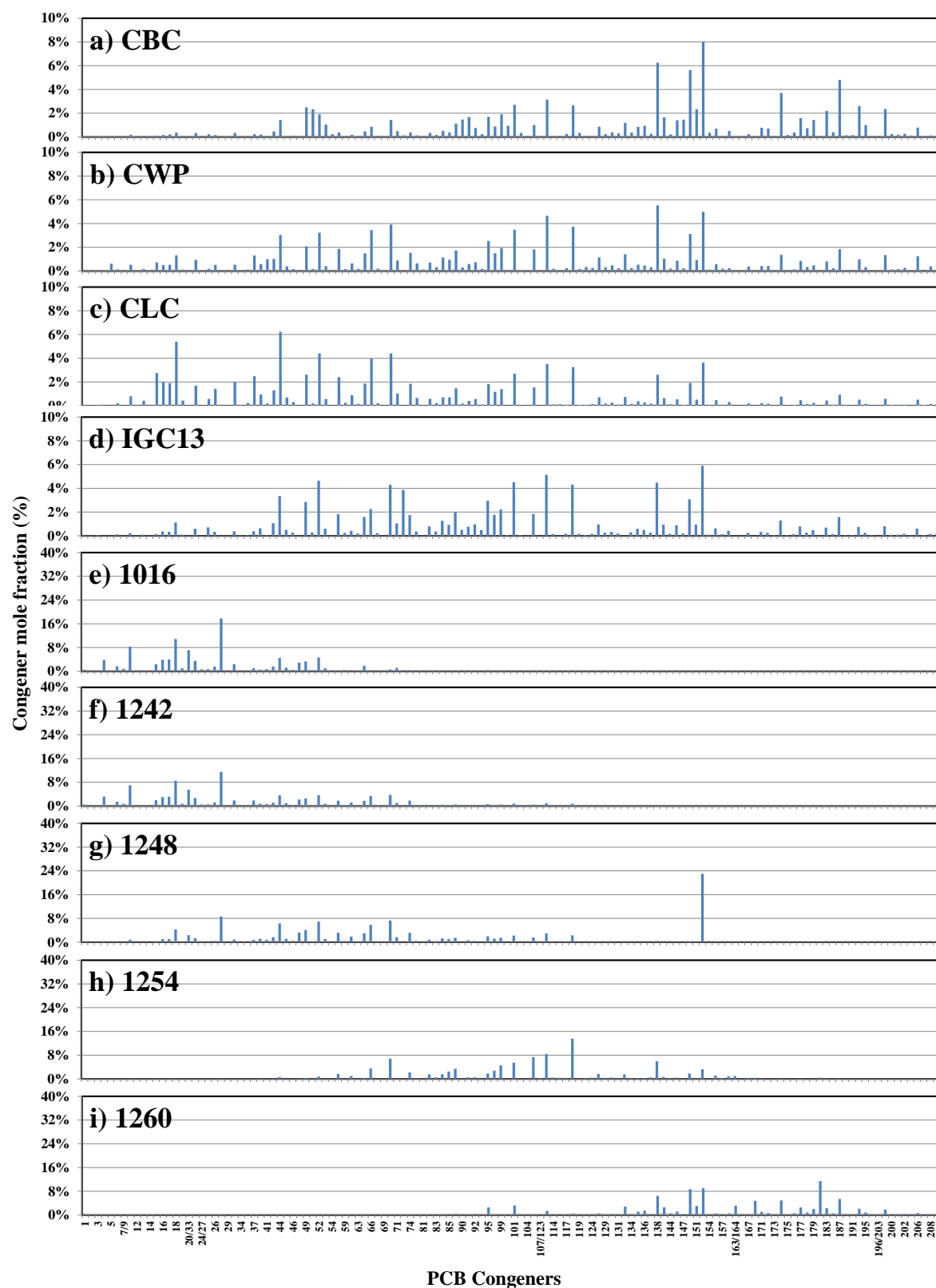


Figure 3.13: Weighted average PCB congener mole fractions at a) CBC, b) CWP, c) CLC, and d) IGC13 compared to PCB Aroclor mixtures congener mole fractions in e) Aroclor 1016, f) Aroclor 1242, g) Aroclor 1248, h) Aroclor 1254, and i) Aroclor 1260. Note the y-axis scale for a) to d) and e) to i).

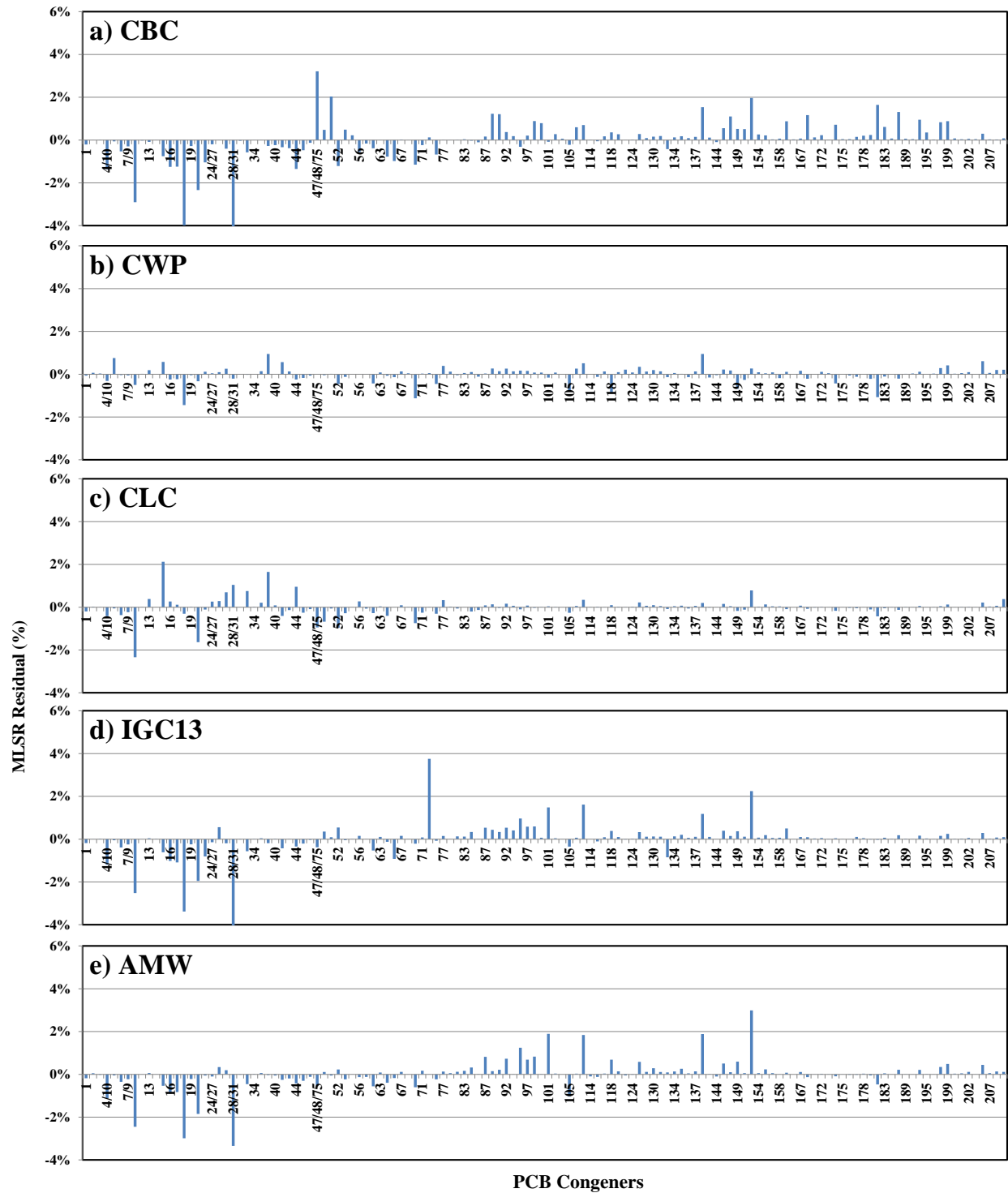


Figure 3.14: PCB MLSR residual values calculated as site average congener mole fraction minus MLSR regression model assuming LMM in cores a) CBC, b) CWP, c) CLC, d) IGC13, and e) AMW.

While the MLSR residual value represents the difference between PBDE or PCB sediment congener profile to PBDE TMs or PCB Aroclor mixtures congener profiles, the MLSR coefficient represent the loadings of model profiles into the sediment distribution. Cores CBC and IGC13, the two urban waterborne deposition-dominated cores had the highest DE-71 TM loading whereas core CWP, the urban atmospheric deposition-dominated core has the lowest DE-71 TM loading (Table 3.5). MLSR predicted low loadings of DE-79 TM in all sediment cores. AMW is the only core where DE-79 TM loading exceeded DE-71 TM loading; this is consistent with the higher deposition of DE-79 TM congeners relative to DE-71 TM especially during core AMW active use period (Figure 3.8c). Saytex 102E has the highest MLSR predicted loading consistent with the dominance of BDE-209 in all cores.

MLSR predicted loadings for PCB Aroclor mixture were more complex. Core CWP which is the only atmospheric deposition-dominated core has the lowest Aroclor 1016 predicted loading. Aroclor 1242 was not expected to contribute to PCB distributions in cores CBC, IGC13, and AMW whereas in cores CWP and CLC, predicted MLSR loadings were low ($< 1\%$). MLSR predicted Aroclor 1248 to be the dominant PCB contributors in all sediment cores except for CBC. MLSR predicted high loadings in cores CWP, IGC13, and AMW and low loadings in cores CBC and CLC for Aroclor 1254. Aroclor 1260 was predicted to have high loadings in all sediment cores and expected to be dominant in core CBC. The MLSR predicted loadings for PCB Aroclor mixtures highlights the complex nature of sediment deposited PCBs which can originate from many PCB Aroclor mixtures.

The highest PBDE MLSR residual values were observed in core CLC; a high residual would be consistent with dehalogenation activity producing congeners not found in PBDE TMs. On the other hand, the highest PCB MLSR residual values were observed in core CBC. Overall, the MLSR fit was better for PBDEs relative to PCBs (PBDE $R^2 = 0.776 - 0.974$; PCB $R^2 = 0.443 - 0.919$). Given that PCBs have 17 Aroclor mixtures, ⁽¹⁶⁾the relatively poor MLSR fit for PCBs could be due to other Aroclor mixtures not considered in this analysis.

Table 3.5. Multiple linear square regression (MLSR) predicted loading for PBDE TMs and PCB Aroclor mixtures, PBDE and PCB MLSR residuals and MLSR fit in Chicago metropolitan and AMW sediment cores.

Site	BDE TMs					Residual	R ²
	DE-71	DE-79	Saytex 102E				
CBC	0.173	0.003	0.736			0.088	0.974
CWP	0.028	0.003	0.904			0.065	0.776
CLC	0.082	0.009	0.751			0.158	0.863
IGC13	0.140	0.003	0.779			0.054	0.967
AMW	0.016	0.027	0.903			0.078	0.842
	PCB Aroclor Mixtures						
	1016	1242	1248	1254	1260		
CBC	0.248	0.000	0.189	0.072	0.327	0.165	0.443
CWP	0.059	0.005	0.383	0.197	0.262	0.094	0.919
CLC	0.271	0.002	0.480	0.091	0.133	0.025	0.895
IGC13	0.220	0.000	0.354	0.165	0.165	0.101	0.609
AMW	0.242	0.000	0.257	0.242	0.219	0.039	0.672

Ortho, meta, and para-substitution. Microbial reductive dehalogenation can favor *meta*- and *para*-halogens removal,^(62,67,102,103) a relative enrichment of *ortho*-halogens along with a lower degree of halogenation are expected if substantial reductive dehalogenation was occurring in these sediment cores.

In most cores, there were no observable temporal trends in *ortho*-substitution or average chlorination (Figure 3.15 a-e). Site CLC was an exception; decreased in degree of chlorination was observed along with increased in *ortho*-substitution and decreased in *meta*-substitution (Figure 3.14c). This could be the best evidence for microbial facilitated *in-situ* PCB dehalogenation.

No change in cores CBC and CWP degree of bromination or clear trends in *ortho*-, *meta*-, and *para*-substitutions (OMP-substitution) were observed in cores CBC and CWP (Figure 3.14 f-g). In core CLC, increase in degree of bromination with depth was observed (Figure 3.15h); this is possibly due to the increased composition of BDE-209 with depth (Figure 3.7h). Decreased in *para*-substituted congeners with sediment depth was observed along with increase in *meta*-substituted congeners; this trend does not

fit into the observation that microbial reductive dehalogenation favors *meta*- and *para*-halogens removal. While the decreased in *para*-substituted congeners could be facilitated by microbial reductive debromination, it could also be an artifact of change in PBDE congener deposition in core CLC. Overall, the potential for PBDE degradation in core CLC was inconclusive from the OMP-substitution pattern. In core IGC13, decreased in degree of debromination along with decreased in *meta*-substitution concomitant with increased in *para*-substitution was observed in the lower sediment segment (Figure 3.15 i). Although this trend is in favor of microbial facilitated PBDE degradation in the lower sediment segment, further observation into the PBDE concentration showed that the decreased in degree of bromination is attributed to the rapid decline of BDE-209 in the lower sediment segment (Figure 3.7a, panel j) rather than actual loss of halogen; at best, the potential for PBDE degradation in IGC13 based on trends in OMP-substitution is inconclusive. In core AMW, increased in degree of debromination was observed between 0 to 10 cm depth (Figure 3.15 j); this is consistent with increased of BDE-209 composition in the same region. ⁽¹⁵¹⁾ Increased in *meta*-substitution was observed along with decreased in *para*-substitution; while this observation contradicts expectation of microbial facilitated PBDE degradation, this does not suggest a lack of degradation either. The potential for PBDE degradation in core AMW was inconclusive from the OMP-substitution analysis as was the case with CLC.

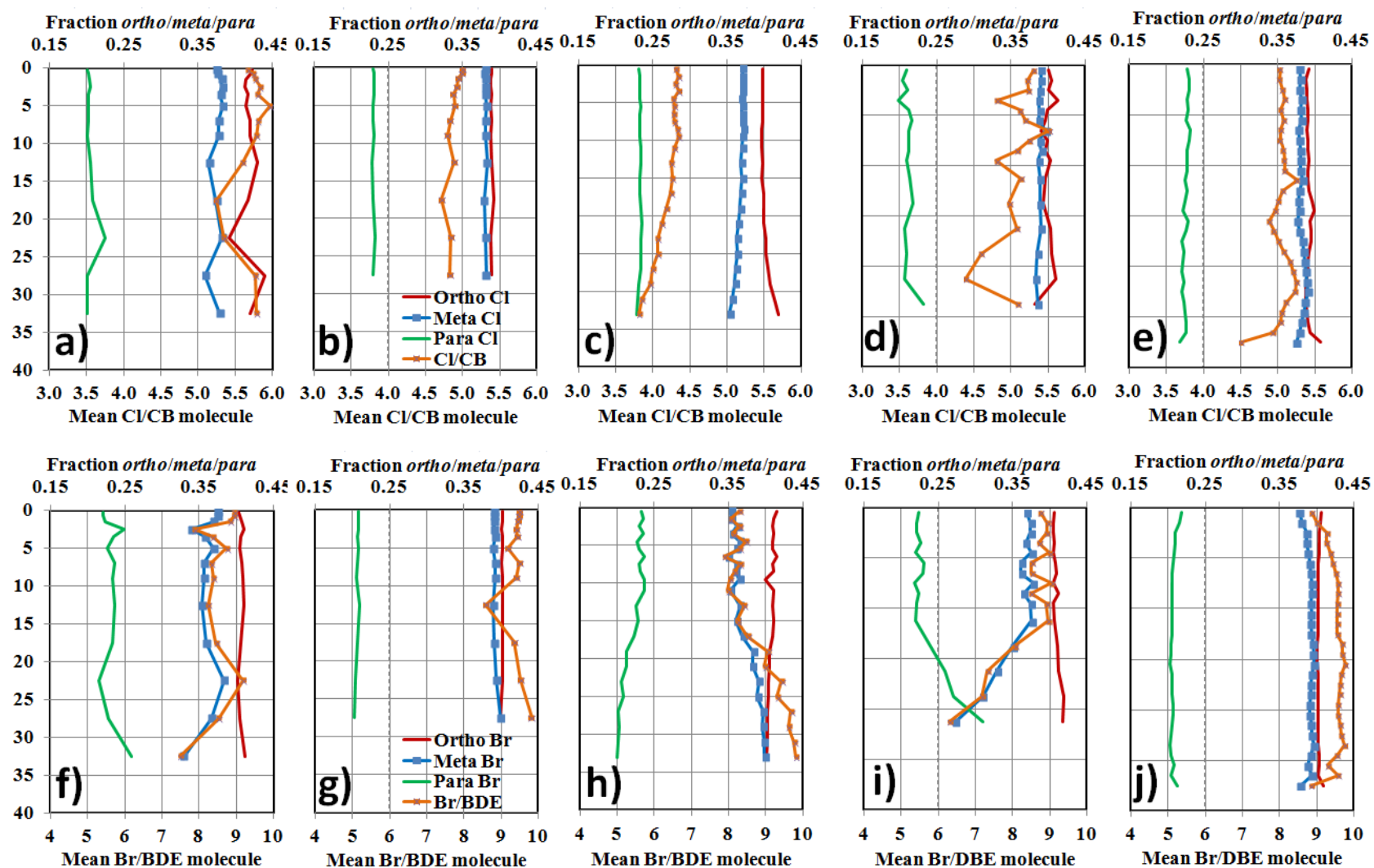


Figure 3.15: Concentration of *ortho*- (red), *meta*- (blue), and *para*- (green) chlorines (a-e) and bromines (f-j) in non-co-eluting PCB/PBDE congeners, as well as mean Cl/PCB or Br/PBDE molecule (yellow) as a function of depth in cores a, f) CBC, b, g) CWP, c, h) CLC, d,i) IGC13, and e, j) AMW. Co-eluting congeners are not included as their substitution pattern is not certain. Note the different scale on the x-axis for cores IGC13 and AMW.

3.5. Conclusion

PBDEs and PCBs concentrations in sediments from five urban waterways in the metropolitan Chicago areas were characterized. Out of these five cores obtained in this study, core IGC09 was found to have signs of severe sediment mixing and disturbance based on physical, chemical, and radionuclide profiles and was thus not discussed in detail. While criteria were defined to aid selection of the optimal study sites, confirmation of the suitability of each study site can only be evaluated a posteriori.

This study showed that PBDE and PCB contamination in the metropolitan Chicago area sediments are ubiquitous. High levels of PBDEs and PCBs were found in all the characterized sediment cores. Although PBDE concentrations in the Chicago and IGC cores were not as high as southern AR cores proximate to the PBDE manufacturing facilities,⁽¹⁵¹⁾ these concentrations were higher compared to other areas in the U.S. reported in previous studies.⁽⁵¹⁻⁵³⁾ PCB concentrations in Chicago and IGC cores were generally higher relative to AR cores. Comparison showed that PCB contamination in the Chicago and IGC cores are comparable to other industrial areas, such as the IHC and the Houston Ship Channel.^(58,60) However, PCB concentrations observed in the metropolitan Chicago cores were lower than known legacy PCB contaminated sites such as the Thompson Island Pool in the Hudson River.⁽⁵⁾ Generally, sediment phase PBDE concentrations have been gradually increasing following the widespread utilization of PBDEs in various consumer products starting in the early 1970s. Given that PBDEs are still actively produced and utilized, PBDE concentrations are expected to keep increasing in the near future. In contrast, a reverse trend was observed for PCBs. This would indicate that the ban on PCB manufacture starting in the 1970s has resulted in gradually decreasing PCB concentrations. Although the PCB manufacture was over four decades ago, PCBs can still be detected at high concentration in the sediment phase reflecting the highly persistent nature of PCBs.

Two routes of PBDE and PCB deposition to aquatic sediments were ascertained from this study; waterborne deposition-dominated in cores CBC and IGC13 which are riverine sites with substantial

contribution of anthropogenic hydraulic discharges, and atmospheric deposition-dominated core CWP which has no natural inflows and outflows. Core CLC was likely influenced by both deposition pathways. Waterborne deposition-dominated cores have higher PBDE and PCB net surface deposition rates and inventories, indicating urban anthropogenic discharges are a major contributor to PBDE and PCB dissemination in the aquatic environment. It is interesting to note that waterborne deposition resulted in a higher percentage of tetra- and penta-PBDE congeners (which are more toxic) compared to air deposition. From a risk perspective, the higher loadings of smaller, more toxic, and more labile PBDE congeners, coupled with study sites located in the midst of highly populated areas may translate into higher exposure risk. Although PBDE net surface deposition and inventory in atmospheric deposition-dominated core CWP was relatively lower than waterborne deposition-dominated cores, a sharp increase in PBDE depositions was observed in recent years. Given continuous usage of PBDEs, PBDE atmospheric deposition rate is likely to increase. Overall, PCB loadings for waterborne-deposition sites substantially exceeded PCB loadings observed in atmospheric deposition-dominated sites, indicating that hydraulic discharges are a major source of urban sediment phase PCB contamination.

Several analyses were provided to evaluate the potential for *in-situ* PBDE and PCB transformations in the Chicago metropolitan cores; these analyses were summarized in Table 3.6. All the sediment cores have quantifiable MLSR residual values. High PBDE and PCB MLSR residuals can be indicative of *in-situ* transformation; however, other factors including differential transport rates and transformation between source sites to receptor sites of PBDE or PCB homologs, as well as PBDE or PCB in-column mass transport could also contribute towards high MLSR value. Therefore, MLSR residual should not be directly interpreted as signs of *in-situ* dehalogenation and should be interpreted in light of other indicators. *In-situ* PBDE or PCB dehalogenation is suspected to form LMW PBDE or PCB congener and show a decrease in HMW PBDE or PCB. This was observed only in CLC and AMW sediment columns for PBDEs and only in CLC sediment column for PCBs. PBDE OMP-substitution in CLC and AMW sediment columns showed decreased in *para*-substitution, consistent with microbial facilitated PBDE dehalogenation; however, the increased in *meta*-substitution was not consistent with

reported microbial preferences for *meta*-halogen removal. PCB OMP-substitution in core CLC showed decreased in *meta*-substitution concomitant with increased in *ortho*-substitution; this was among the strongest support of microbial facilitated PCB dehalogenation.

Table 3.6. Indicators of PBDE and PCB *in-situ* transformation.

Site	PBDEs			PCBs		
	Δ Hom ⁽¹⁾	MLSR Residual ⁽²⁾	OMP ⁽³⁾	Δ Hom ⁽¹⁾	MLSR Residual ⁽²⁾	OMP ⁽³⁾
CBC		0.088			0.165	
CLC	√	0.158	○	√	0.025	√
CWP		0.065			0.099	
IGC13		0.054	○		0.101	
AMW	√	0.078	○		0.439	

(1) Check indicates enrichment of LMW PBDE or PCB homologs concomitant with decrease in HMW PBDE or PCB homologs in the sediment column.

(2) MLSR residual quantifying differences between PBDE and PCB congener profile in sediment to PBDE TMs and PCB Aroclor mixtures.

(3) Check indicates that OMP-substitution patterns support PBDE or PCB *in-situ* transformation and decrease in PBDE or PCB degree of halogenation. Hollow circle indicates that OMP-substitution patterns provide inconclusive support of PBDE or PCB *in-situ* transformation.

Multiple lines of evidence provided by PBDE and PCB homolog distribution, MLSR analysis, and OMP-substitution pattern, are consistent with PBDE and PCB *in-situ* transformation in cores CLC and AMW, and CLC, respectively. It is acknowledge that the MLSR analysis performed only confirmed the differences between PBDE TMs or PCB Aroclor mixtures to PBDE or PCB congener profile in sediment and does not distinguished between contributing factors such as *in-situ* PBDE and PCB microbial dehalogenation. In addition to consistency with *in-situ* transformation, OMP-substitution patterns consistent with microbial dehalogenation were observed especially for PCB in core CLC. In the next chapter, microbial community structure in these PBDE- and PCB-impacted sediments will be characterize to shed further light into the role of indigenous microbial community in facilitating *in-situ* transformation.

CHAPTER 4. INDIGINEOUS MICROBIAL COMMUNITY IN PBDE AND PCB IMPACTED SEDIMENTS IN METROPOLITAN CHICAGO AND ARKANSAS

4.0. Abstract

Microbial degradation of polybrominated diphenyl ethers (PBDEs) and polychlorinated biphenyls (PCBs) has an important impact on their environmental fate. Data is, however, lacking on the composition of the indigenous microbial community in PBDE- and PCB-impacted sediments. In this study, DNA was extracted from eleven surface sediments: six cores from AR in varying distance from the only two PBDE manufacturers in North America, five cores from the highly urbanized Chicago metropolitan area, as well as ten sediment segments from a core in a former municipal wastewater treatment plant (WWTP) in Magnolia, AR. These DNA extracts were subjected to high yield pyrosequencing in an effort to characterize the indigenous microbial community composition in sediments impacted with varying levels of contamination from 4 to 60000 ng/g PBDEs and 1 to 1980 ng/g PCBs. The overall objective was to evaluate the presence of microbes capable of PBDE and PCB degradation based on chemical and physical indicators of dehalogenation activity.

Although potential PBDE and PCB degraders were identified in varying amounts in all surface sediments (10 to 28% and 10 to 27% of potential PBDE and PCB, respectively), only sites AMW and CLC displayed strong evidence for PBDE and PCB degradation such as increased in low molecular weight (LMW) homolog composition concomitant with decreased in high molecular weight (HMW) homolog composition, increased *meta* or *para*-substitution concomitant with decreased *ortho*-substitution, and decreased in mean halogenation degree. This study illustrates the importance of interpreting multiple lines of evidence to accurately evaluate the possibility of *in-situ* degradation in organic-rich sediments.

4.1. Introduction

Laboratory scale bioaugmentation and biostimulation studies have provided ample demonstration of microbial dehalogenation of polybrominated diphenyl ethers (PBDEs) and polychlorinated biphenyls (PCBs); ^(79,102,103,108,195-198) however, the feasibility of *in-situ* microbial facilitated PBDE and PCB degradation is not fully understood, partially stemming from existing data gap on the indigenous microbial community composition in PBDE- and PCB-impacted sediments.

Investigation of microbial community composition using conventional DNA sequencing methods (such as the Sanger's method) can be time consuming and cost prohibitive. The advent of high throughput DNA sequencing technology such as 454-pyrosequencing enables a faster and more comprehensive snapshot of the *in-situ* microbial community. Additionally, the availability of powerful bioinformatics programs has removed the expensive computational cost associated with analyzing the large volumes of nucleotide data generated from metagenomics analysis.

There are few, if any, reported studies on the indigenous microbial community composition in PBDE and PCB contaminated sediments. In this study, the microbial communities in eleven surface sediments from AR and Metropolitan Chicago area with varying levels of contamination (4 to 60000 ng/g PBDEs, and 1 to 1980 ng/g of PCBs) were characterized to provide a better understanding of the microbial community in these sediments. In addition, microbial communities in ten sediment segments at approximately five year time interval from site AMW, a former wastewater treatment plant (WWTP) lagoon in Magnolia, AR with PBDE and PCB concentrations ranging from 1400 to 51000 ng/g and 4 to 1000 ng/g, respectively were characterized to provide a temporal record of the microbial community structure in a sediment column with expected active PBDE dehalogenation. The focus of this chapter was to characterize the microbial community composition and to quantify known PBDE and PCB potential degraders to evaluate the feasibility of *in-situ* dehalogenation in light of other indicators of *in-situ*

dehalogenation including PBDE and PCB concentrations, homolog compositions, congener substitutions, and physico-chemical properties.

4.2. Objectives and Hypotheses

The overall objective of this study was to address the data gap on the *in-situ* microbial community composition in PBDE and PCB-impacted sediments. This study was divided into two parts; 1) evaluation of the microbial community in eleven surface sediments aimed at understanding the spatial variation in microbial community composition driven by physico-chemical and spatial differences, and 2) evaluation of the microbial community composition in AMW sediment segments with depth aimed to understand the temporal variation in microbial community composition driven by physico-chemical differences. Specific objectives and hypotheses for this study were as follows:

- Detailed characterization of the microbial community in all the sediment samples impacted by varying levels of PBDE and PCB contamination. Sediment samples selected in this study have PBDE and PCB concentrations ranging from 4 to 60000 ng/g and 1 to 1980 ng/g, respectively in the eleven surface sediments. AMW sediment segments have PBDE and PCB concentrations ranging from 1400 to 51000 ng/g and 4 to 1000 ng/g, respectively. High total PBDE (\sum_{49} PBDEs) and PCB (\sum_{132} PCBs) concentrations were hypothesized to impact the *in-situ* microbial diversity. This hypothesis was derived from a study showing impaired and irreversibly transformed microbial community composition of a pristine mountain soil after elongated exposure to different levels of BDE209 and BDE15 concentrations.⁽¹⁹⁹⁾
- Identify and quantify potential PBDE and PCB degraders abundance in the sediments. PBDE and PCB degraders were hypothesized to be common in all the sediment segments. A previous study

showed that sediments collected from three different geographical regions in East Asia, Southeast Asia, and North America demonstrated extensive hexa- to octa-PBDE degradation after two months incubation period. In addition, the abundance of potential PBDE and PCB degrading communities were also hypothesized to correlate with \sum_{49} PBDEs and \sum_{132} PCBs concentrations. The feasibility of *in-situ* microbial degradation will be assessed based upon trends in microbial community composition in light of other physico-chemical dehalogenation indicators.

- Evaluate the changes in the microbial community composition in AMW sediment segments in response to changes in physico-chemical properties to understand the temporal microbial evolution in core AMW spanning over 40 years. It was hypothesized that microbial diversity decreases with increasing sediment depth as electron donors and high energy electron acceptors were expected to decrease in deeper sediment. A gradual change in microbial community with depth was also expected. Initial physical characterization in core AMW suggested PBDE degradation in the upper five cm sediment segments. These sediment segments were hypothesized to have higher abundance of microbes capable of PBDE degradation.

4.3. Experimental Method

Sediment samples: Selected sediment segments for this study and their associated physico-chemical properties are summarized in Table 4.1. AMW sediment segments selected were at approximately five years interval.

Table 4.1. Physicochemical properties of sediment segments selected for DNA extractions.

Sample	Sediment age ⁽¹⁾	$\Sigma_{49}\text{PBDEs}$ (⁽²⁾)	$\Sigma_{132}\text{PCBs}$ (⁽³⁾)	Organic carbon (OC)	Organic matter (OM)	Black Carbon (BC)
		(ng/g)			(mg/g)	
AED0-1cm	2009	35635	4	52	81	4
AMW0-2cm	2009	6950	69	312	474	3
AMW8-10cm	2005	14440	87	284	439	2
AMW18-20cm	2000	21050	107	204	388	2
AMW24-26cm	1995	23745	106	178	349	2
AMW30-32cm	1990	51785	222	176	314	3
AMW34-36cm	1985	48643	267	206	349	3
AMW 38-40cm	1981	34622	288	204	329	3
AMW42-44cm	1974	19352	506	204	346	3
AMW46-48cm	1969	11058	998	241	436	3
AMW48-50cm	1965	1427	1517	262	421	3
ACL0-1cm	2008	2503	3	8	18	5
AJL 0-1cm	2009	402	5	22	32	2
AOT 0-1cm	2010	12	3	74	141	2
AFR0-1cm	2009	4	1	52	80	9
CBC 0-1cm	2009	313	403	25	40	22
CLC 0-1cm	2009	90	236	99	176	41
CWP0-1cm	2008	404	43	89	141	40
IGC09 0-1cm	2010	3461	4979	142	245	16
IGC13 0-1cm	2010	1908	1075	140	234	20

⁽¹⁾: Sediment age for AMW sediment segments as determined by single and multi-slope CIC and CRS models. Details were previously provided in Wei et al. (2012) [151]

⁽²⁾: Total concentration of 49 PBDE congeners

⁽³⁾: Total concentration of 132 PCB congeners

DNA isolation: The Mobio PowerSoil® DNA isolation kit was used to extract nucleic acids following the manufacturer's instruction (Mo Bio Laboratories, Carlsbad, CA). Sediment samples kept at -40°C was homogenized and 0.25 g was used for extraction, the maximum sediment mass suggested by the manufacturer. Approximately 0.25 mL of homogenized sediment sample was added to Power Bead extraction tubes with buffer solution to disperse the soil particles, dissolve humic acids, and protect the

nucleic acids from degradation. Sediment samples in the Power Bead tubes were subjected to gentle vortexing after addition of 60 μ L of lysis solution (solution C1) containing sodium dodecyl sulfate followed by 20 minutes of vortexing at high rate. Following centrifugation at 10000 x for one minute, supernatant was transferred to clean 2 mL collection tube before addition of 250 μ L lysing solution containing proprietary Inhibitor Removal Technology® (Mo Bio Laboratories, Carlsbad, CA). Centrifugation followed by addition of lysing solutions C3 and C4 at 200 and 1200 μ L, respectively. After centrifugation at 10000 x for one minute, the supernatant was loaded into the spin filter in increments of 675 μ L each for three consecutive times. 500 μ L of solution C5 was added to the spin filter followed by 30 seconds of centrifugation at 10000 x. Filtrate from the spin filters was discarded and the filter was placed in a clean 2 mL collection tube and was centrifuged for 30 seconds at 10000 x with addition of the final C6 DNA coeluting solution of 50 μ L of sterile solution buffer. DNA concentrations were determined using the nanodrop 2000 spectrophotometer (Thermo Scientific, Waltham, MA) and quality was checked using the optical density ratio OD_{260}/OD_{280} . Only DNA extractions with OD_{260}/OD_{280} between 1.7 and 1.9 were selected to ensure high quality DNA extracts. DNA extracts were stored at -20 °C until further analysis.

16s rRNA gene tag sequencing and data analysis: DNA extracts were sent to the Research and Testing Laboratory (Lubbock, TX, USA) for bacterial tag-encoded FLX454 pyrosequencing (bTEFAP) and data processing on Roche 454 FLX platform (Roche, Indianapolis, IN). Procedures were described previously.^(200,201) Titanium reagents were applied to amplicon sequencing to accommodate longer generation of average read lengths. Amplification targeted the variable V1 to V3 regions in relation to the 16s *Escheria coli* gene⁽²⁰²⁾ with the primers Gray28F and Gray519R (Table 4.2) optimized for bacterial amplification. Each amplification was performed using a 35 cycle single PCR step with Qiagen HotStar Master Mix with addition of 0.5 μ L of Hot Star HiFidelity Polymerase (Qiagen Inc., Valencia, CA).

Table 4.2. Barcode sequences for primers Gray28f and Gray519R used in Roche 454 pyrosequencing.

		Primer	Annealing Temperature
Primer	Sequence (5'-3')	Location	(°C)
Gray28F	GAGTTTGATCNTGGCTCAG	9-27	60
Gray519R	GTNTTACNGCGGCKGCTG	536-519	60

Estimates of Microbial Diversity: Sequences obtained from the tag-encoded Roche 454 pyrosequencing were submitted to the MGRAST pipeline at Argonne National Laboratory.⁽²⁰³⁾ Low quality sequences and tags were removed. To ensure enough discriminating data from the variable V1-V3 regions, sequences shorter than 300 bp after trimming were removed from further analysis.

Pyrosequencing nucleotide data were initially identified using four RNA databases (SSU, RDP, m5RNA, and Greengenes) at 1×10^5 maximum cutoff, 60% minimum identity cutoff, and 15% minimum alignment length cutoff. Overall, 2 to 37% percent of the submitted sequences were unclassified and/or unassigned. Unclassified and unassigned percentage in the selected sediment samples are shown in Figure 4.1. Comparison to the RDP database consistently resulted in the smallest percentage of unassigned and unclassified sequences in all the sediment samples. Additionally, sequence identification based on RDP database also resulted in the lowest unclassified *Bacteria* percentage compared to the other three databases.

In this chapter, sequences identified from the RDP database were used for microbial characterization purposes. In the RDP database, phylogenetic alignment of bacterial 16s rRNA gene sequences used the Bayesian rRNA classifier with 80% bootstrap cutoff.⁽²⁰⁴⁾ Sequences were compared using the complete-linkage clustering (also known as the farthest neighbor linkage) and similar sequences were assigned to the same phylotype clusters at a 3% cutoff level.

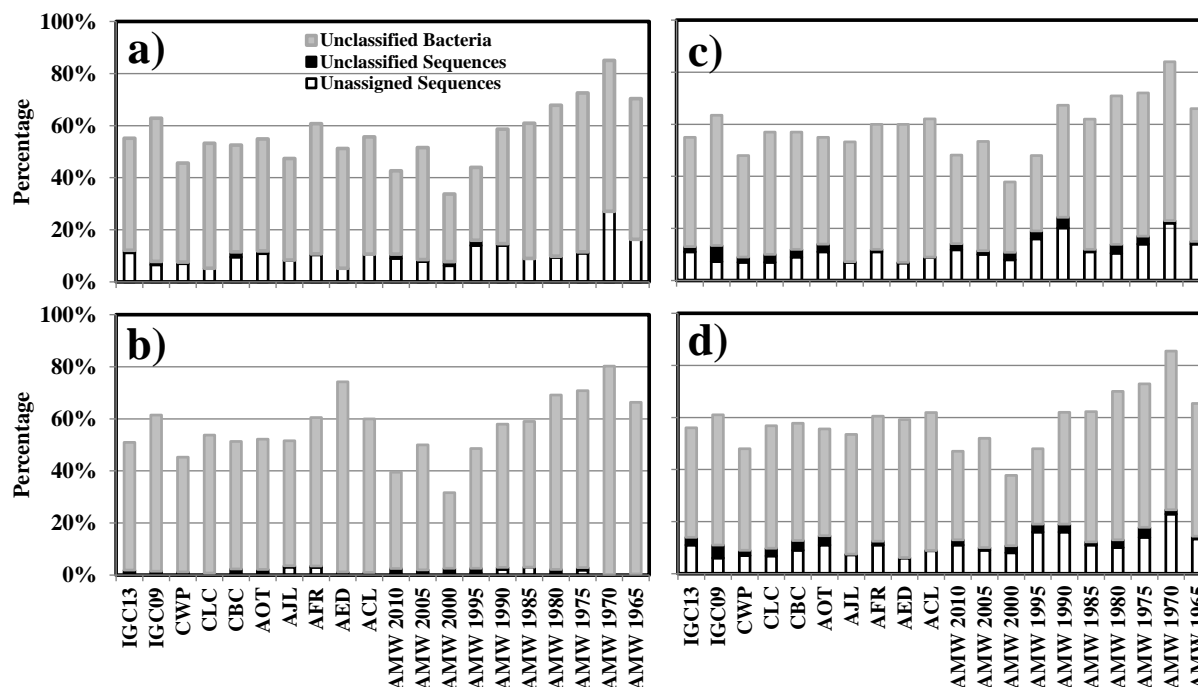


Figure 4.1: Distribution of unassigned and unclassified sequences, and unclassified *Bacteria* in selected sediment samples as identified by a) SSU, b) RDP, c) m5RNA, and d) Greengenes databases in MGRAST.

4.4. Results and Discussion

4.4.1. Indigenous Microbial Community In Surface Sediments

4.4.1.1. General Sequence Statistics In Surface Sediments

Pyrosequencing data submitted to MGRAST were subjected to stringent quality control to ensure high quality data classification. Table 4.3 is a summary of pre- and post-quality control sequence statistics for microbial community in the surface sediments. During quality control, sequence lengths that deviate by greater than two times the standard deviation of the average length were discarded. In all surface sediments, $\geq 95\%$ of the total sequence submitted to MGRAST passed quality control (only CBC had $< 95\%$).

Table 4.3. Pre- and post-quality control sequence statistics for surface sediments.

Pre-quality Control					Post-quality Control			
Site	bp ⁽¹⁾	Sequence	Length	GC (%) ⁽²⁾	bp ⁽¹⁾	Sequence	Length	GC (%) ⁽²⁾
ACL	3161214	7469	423 ± 67	57 ± 2	3093175	7141	433 ± 54	57 ± 2
AED	2905639	6921	419 ± 69	56 ± 2	2838957	6582	431 ± 2	56 ± 2
AFR	1350204	3165	426 ± 70	56 ± 2	1311237	2998	437 ± 53	56 ± 2
AJL	1853398	4385	422 ± 68	56 ± 2	1802860	4150	434 ± 49	56 ± 2
AMW	1407698	3339	421 ± 74	55 ± 2	1375415	3184	431 ± 60	56 ± 3
AOT	2432288	5617	433 ± 79	56 ± 3	2368481	5322	445 ± 60	57 ± 3
CBC	1195435	2813	434 ± 90	54 ± 2	1159489	2617	443 ± 61	54 ± 2
CLC	1677997	3953	424 ± 69	55 ± 3	1636509	3767	434 ± 55	55 ± 3
CWP	1426842	3357	425 ± 76	55 ± 3	1390768	3177	437 ± 58	55 ± 3
IGC09	1493375	3581	417 ± 76	55 ± 2	1455669	3395	428 ± 62	55 ± 3
IGC13	1152621	2808	410 ± 82	54 ± 3	1125304	2663	422 ± 66	54 ± 3

⁽¹⁾ Basepairs

⁽²⁾ Guanine and cytosine nucleic acids

4.4.1.2. Species Richness and Abundance In Surface Sediments

A rarefaction curve which plots the number of microbial taxa as a function of sequence count provides a graphical overview of the species richness in a sample. The rarefaction curves for the microbial community in the surface sediments are provided in Figure 4.2. Rarefaction curves for ACL, AED, and AOT surface sediments almost reached the plateau point indicating that most bacterial species were sampled by the pyrosequencing cycle. In all other surface sediments, the slopes of the rarefaction curves indicate that the species diversity was not yet completely sampled during the pyrosequencing cycle; however, they were sufficient for characterization purposes.

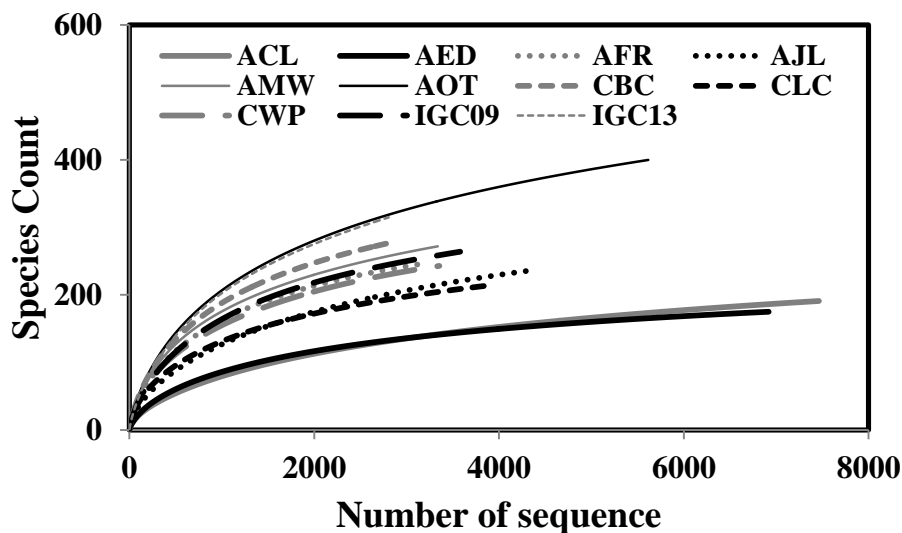


Figure 4.2: Rarefaction curves measuring microbial species richness in all surface sediments.

The alpha diversity is a quantitative measure of microbial species diversity; microbial alpha diversity for the surface sediments is shown in Figure 4.3. The alpha diversity values increased in the order of AED (7.6) < ACL (9.8) < IGC09 (20.5) < AJL (24.0) < CLC (24.3) < AFR (27.0) < AMW (41.1) < CBC (41.2) < AOT (44.9). In general, the microbial diversity was typically higher in Chicago metropolitan surface sediments compared to AR surface sediments.

With the exception of core AMW and AOT, microbial diversity generally increased with increasing average distance from the southern AR PBDE manufacturing facilities (Figure 4.3a) and consequently with decreasing $\sum_{49}\text{PBDEs}$ surface concentrations. Correlations between alpha diversity to $\sum_{49}\text{PBDEs}$ surface concentrations and average distance from the southern AR PBDE manufacturing facilities have R^2 values of 0.85 and 0.83. This trend suggests that PBDEs may influence the microbial community distribution. This may be particularly the case in the AR sediment cores with very high PBDE levels, which may provide a niche environment for the microorganisms. Core AMW was not included in the distance–concentration and distance–bacterial diversity analyses as it is a sediment column with unique physical properties stemming from the its origin as a treated WWTP effluent. A detailed description of core AMW as a WWTP effluent lagoon was discussed previously in Chapter 3. Core AMW

was characterized with high OM and OC content, as well as having an ORP level consistent with facultative metabolism. The OM-enriched environment in the AMW sediment column was a likely contributor towards the high alpha diversity observed in these samples (Figure 4.3a). Although \sum_{49} PBDEs surface concentrations in core AOT conformed to the distance-concentration correlation,⁽¹⁵¹⁾ the microbial diversity and indigenous microbial community composition were clearly impacted by factors other than PBDE concentration(Figure 4.3a). More detailed investigation of the microbial community composition in AOT surface sediment discussed in the later sections will further highlight the unique microbial community in this surface sediment. Microbial diversity is a complex function of many factors including physicochemical properties and bioavailability of nutrients and substrates.

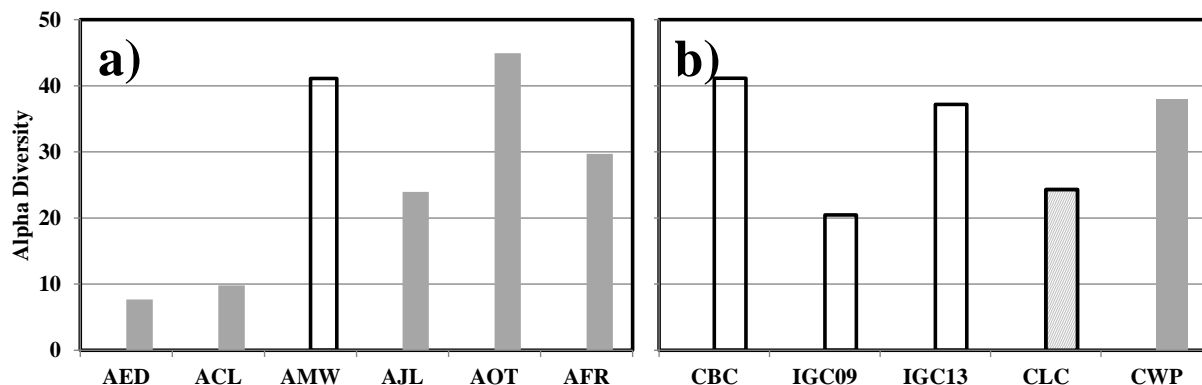


Figure 4.3: Microbial species diversity, as alpha diversity based on RDP database classification⁽²⁰⁴⁾ in a) AR and b) Chicago metropolitan surface sediments. Grey bar indicates primarily atmospheric- deposition-dominated cores, hollow bar indicates primarily hydraulic-deposition-dominated cores, and patterned bar indicates likely mixed exposure pathways. AR sites are in order of increasing distance from PBDE source zone.

As discussed in Chapter 3, sources of PBDEs and PCBs to the sediment likely came from two exposure modes. Waterborne deposition-dominated sediment columns are water bodies impacted by anthropogenic aqueous discharges such as treated WWTP effluent, stormwater, and combined sewage outflows(CSO). Atmospheric deposition-dominated sediments were not primarily impacted by

anthropogenic aqueous discharges, but rather through wet and dry depositions. There does not appear to be a dependence of microbial diversity to PBDE and PCB exposure pathways (Figure 4.3 a-b). Additionally, no trend was observed between microbial diversity in all surface sediments to other physical parameters such as ORP, carbon content (OC, OM, and BC), and bulk sediment column properties (wet and dry densities, moisture and solid contents, porosity, and particle density) (data not shown).

4.4.1.3. Dominant Microbial Community Distribution In Surface Sediments

This section provides an overview of the microbial community composition in the surface sediments. The microbial community composition in the surface sediments is shown in Figure 4.6a-k and the complete microbial community distribution in the surface sediments is provided in Table C4.1 in the appendix. For clarity, only the dominant phyla (ad-hoc defined as having phylum abundance >1% of the total bacteria) are further discussed in this chapter.

ACL: Ten phyla were identified in core ACL with four phyla having >1% of the total distribution (Figure 4.6a). Dominant phyla increased in the order of *Firmicutes* < *Acidobacteria* < *Bacteroidetes* < *Proteobacteria*. The *Proteobacteria* phylum was further classified into four phyla which increased in the order of unclassified *Proteobacteria* < *Deltaproteobacteria* < *Alphaproteobacteria* < *Gammaproteobacteria* < *Betaproteobacteria*. The *Bacteroidetes* phylum was composed of one class, the *Sphingobacteriia*. Additionally, all the *Bacteroidetes* sequences were from the order *Sphingobacteriales*. The phylum *Acidobacteria* was composed of two classes which increased in the order of *Solibacteres* <<< *Acidobacteriia*. Further classification indicates the *Acidobacteriia* and *Solibacteres* were composed of the order *Acidobacteriales* and *Solibacterales*, respectively. In the *Firmicutes* phylum, the order *Clostridiales* which made up all of the *Clostridia* class was much larger than *Thermoanaerobacterales* and *Natranaerobiales* microbial orders.

AED: Of the 14 identified bacterial phyla, only five has >1% dominance (Figure 4.6b). Dominant phyla increased in the order of *Bacteroidetes* < *Firmicutes* < *Nitrospirae* < *Acidobacteria* < *Proteobacteria*. The *Proteobacteria* phylum consisted of four microbial classes which increased in the order of *Alphaproteobacteria* < *Gammaproteobacteria* < *Deltaproteobacteria* < *Betaproteobacteria*. The *Acidobacteria* phylum was dominated by the *Acidobacteriia* and *Solibacteres* microbial classes. The *Nitrospirae* phylum was composed only of the *Nitrospira* class. The *Firmicutes* phylum constituted of *Clostridia* < *Bacilli* < *Negativicutes* in increasing microbial class order. In the *Bacteroidetes* phylum, class dominance increased in the order of *Flavobacteria* < *Cytophagia* < *Bacteroidia* < *Sphingobacteriia*.

AFR: The dominant phylum in AFR surface sediment increased in the order of *Aquificae* < *Cyanobacteria* < *Bacteroidetes* < *Firmicutes* < *Actinobacteria* < *Acidobacteria* < *Verrucomicrobia* < *Nitrospirae* < *Proteobacteria*; an overview of the microbial community composition is provided in Figure 4.6c. The *Aquificae* and *Cyanobacteria* phyla were not further classified into microbial order. The *Bacteroidetes* phylum was composed of the *Flavobacteriia* < *Bacteroidia* < *Sphingobacteriia* < *Cytophagia* microbial classes. The *Firmicutes* phylum was composed of *Negativicutes* < *Bacilli* < *Clostridia*. The *Actinobacteria* phylum was composed of the *Actinobacteria* class which included *Bifidobacteriales* < *Coriobacteriales* < *Actinomycetales* families. The *Acidobacteria* phylum was composed of *Acidobacteriia* < *Solibacteres* < unclassified *Acidobacteria* microbial classes. The *Verrucomicrobia* was composed primarily of the *Opitutae* class.

AJL: Only four phyla were dominant in AJL surface sediment (Figure 4.6d). Phylum dominance increased in the order of *Bacteroidetes* < *Acidobacteria* < *Firmicutes* < *Proteobacteria*. In the *Proteobacteria* phylum, class dominance increased in the order of *Epsilonproteobacteria* < unclassified *Proteobacteria* < *Gammaproteobacteria* < *Deltaproteobacteria* < *Alphaproteobacteria* < *Betaproteobacteria*. The *Firmicutes* phylum was composed of increasing order of *Negativicutes* < *Erysipelotrichi* < *Clostridia* < *Bacilli*. Microbial classes increased in the order of unclassified *Acidobacteria* < *Solibacteres* < *Acidobacteriia* in the *Acidobacteria* phylum. In the *Bacteroidetes*

phylum, class increased in the order of unclassified *Bacteroidetes* < *Cytophagia* < *Flavobacteriia* < *Bacteroidia* < *Sphingobacteriia*.

AMW: In the AMW surface sediment, phylum dominance increased in the order of *Cyanobacteria* < *Planctomycetes* < *Actinobacteria* < *Verrucomicrobia* < *Firmicutes* < *Bacteroidetes* < *Proteobacteria* (Figure 4.6e). Class in the *Proteobacteria* phylum increased in the order of unclassified *Proteobacteria* < *Epsilonproteobacteria* < *Alphaproteobacteria* < *Gammaproteobacteria* < *Deltaproteobacteria* < *Betaproteobacteria*. The phylum *Bacteroidetes* was composed of unclassified *Bacteroidetes* < *Bacteroidia* < *Cytophagia* < *Sphingobacteriia* in increased order. *Firmicutes* was composed of *Erysipelotrichi* < *Negativicutes* < *Bacilli* < *Clostridia* in increased order. Class dominance in the *Verrucomicrobia* phylum increased in the order of *Verrucomicrobiae* < *Opitutae*. The *Actinobacteria* and *Planctomycetes* phyla were not assigned to microbial class.

AOT: The dominant phylum in core AOT increased in the order of *Planctomycetes* < *Nitrospirae* < *Actinobacteria* < *Cyanobacteria* < *Firmicutes* < *Bacteroidetes* < *Proteobacteria* (Figure 4.6f). The *Proteobacteria* phylum increased in the order of unclassified *Proteobacteria* < *Epsilonproteobacteria* < *Betaproteobacteria* = *Alphaproteobacteria* < *Gammaproteobacteria* < *Deltaproteobacteria*. In the *Bacteroidetes* phylum, class dominance increased in the order of unclassified *Bacteroidetes* < *Bacteroidia* < *Sphingobacteriia* < *Flavobacteriia* < *Cytophagia*. *Firmicutes* was composed of *Negativicutes* < *Erysipelotrichi* < *Bacilli* < *Clostridia* classes. The *Actinobacteria* and *Cyanobacteria* phyla were not identified by microbial class. The *Nitrospirae* and *Planctomycetes* phyla were composed entirely off the *Nitrospira* and *Planctomycetia* class, respectively.

CBC: Microbial community distribution for CBC surface sediment is shown in Figure 4.6g. In CBC surface sediment, phylum dominance increased in the order of *Aquificae* < *Spirochaetes* < *Actinobacteria* < *Cyanobacteria* < *Firmicutes* < *Bacteroidetes* < *Proteobacteria*. Microbial classes in the *Proteobacteria* phylum increased in the order of *Epsilonproteobacteria* < unclassified *Proteobacteria* <

Alphaproteobacteria < *Gammaproteobacteria* < *Deltaproteobacteria* < *Betaproteobacteria*. Microbial classes increased in the order of unclassified *Bacteroidetes* < *Cytophagia* < *Bacteroidia* < *Sphingobacteria* < *Flavobacteriia* in the *Bacteroidetes* phylum. The *Firmicutes* phylum consisted of the class *Negativicutes* < *Erysipelotrichi* < *Bacilli* < *Clostridia* in increased dominance. The phyla *Cyanobacteria*, *Actinobacteria*, and *Spirochaetes* were not further classified into microbial class.

CLC: Of the 12 phyla, four phyla were dominant which increased in the order of *Firmicutes* < *Nitrospirae* < *Bacteroidetes* < *Proteobacteria* (Figure 4.6h). The *Proteobacteria* phylum consisted of five classes (excluding unclassified *Proteobacteria*) which increased in the order of *Epsilonproteobacteria* < *Alphaproteobacteria* < *Gammaproteobacteria* < *Deltaproteobacteria* < *Betaproteobacteria*. The phylum *Bacteroidetes* has a high abundance in CLC surface sediment; the phylum *Bacteroidetes* consisted of *Bacteroidia* < unclassified *Bacteroidetes* < *Sphingobacteriia* < *Flavobacteria* < *Cytophagia* in increasing order. The phylum *Nitrospirae* was not further classified into microbial class. The phylum *Firmicutes* consisted only of the *Clostridia* class.

CWP: In CWP surface sediment, phylum dominance increased in the order of *Nitrospirae* < *Firmicutes* < *Bacteroidetes* < *Proteobacteria* (Figure 4.6i). The phylum *Proteobacteria* consisted of five microbial classes (excluding unclassified *Proteobacteria*) which increased in the order of *Epsilonproteobacteria* = *Gammaproteobacteria* < *Deltaproteobacteria* < *Betaproteobacteria* < *Alphaproteobacteria*. Classes in the *Bacteroidetes* phylum increased in the order of *Flavobacteriia* < *Sphingobacteriia* < *Bacteroidia* < *Cytophagia*. The class *Clostridia* was highly dominant over the class *Bacilli* in the *Firmicutes* phylum. The *Nitrospirae* phylum consisted entirely of the class *Nitrospira*.

IGC09: Of the 14 phyla in IGC09 surface sediments, only three had >1% abundance (Figure 4.6j). These dominant phylum increased in the order of *Firmicutes* < *Bacteroidetes* < *Proteobacteria*. Microbial classes in the *Proteobacteria* phylum increased in the order of unclassified *Proteobacteria* = *Alphaproteobacteria* < *Epsilonproteobacteria* < *Gammaproteobacteria* < *Deltaproteobacteria* <

Betaproteobacteria. The *Bacteroidetes* phylum consisted of four classes which increased in the order of *Cytophagia* < *Sphingobacteriia* < *Bacteroidia* < *Flavobacteriia*. Microbial classes dominance in the *Firmicutes* phylum increased in the order *Negativicutes* < *Bacilli* < *Erysipelotrichi* < *Clostridia*.

IGC13: Five phyla were dominant in core IGC13 (Figure 4.6k); these phyla increased in the order of *Spirochaetes* < *Actinobacteria* < *Firmicutes* < *Bacteroidetes* < *Proteobacteria*. In the *Proteobacteria* phylum, microbial classes increased in the order of unclassified *Proteobacteria* < *Epsilonproteobacteria* < *Alphaproteobacteria* < *Gammaproteobacteria* < *Deltaproteobacteria* < *Betaproteobacteria*. Classes in the *Bacteroidetes* phylum increased in the order of unclassified *Bacteroidetes* < *Cytophagia* < *Sphingobacteriia* < *Bacteroidia*. The *Firmicutes* phylum was composed of *Negativicutes* < *Erysipelotrichi* < *Bacilli* < *Clostridia* microbial classes. The *Actinobacteria* phylum was not further classified into microbial class. The *Spirochaetes* phylum was composed entirely of the *Spirochaetia* class.

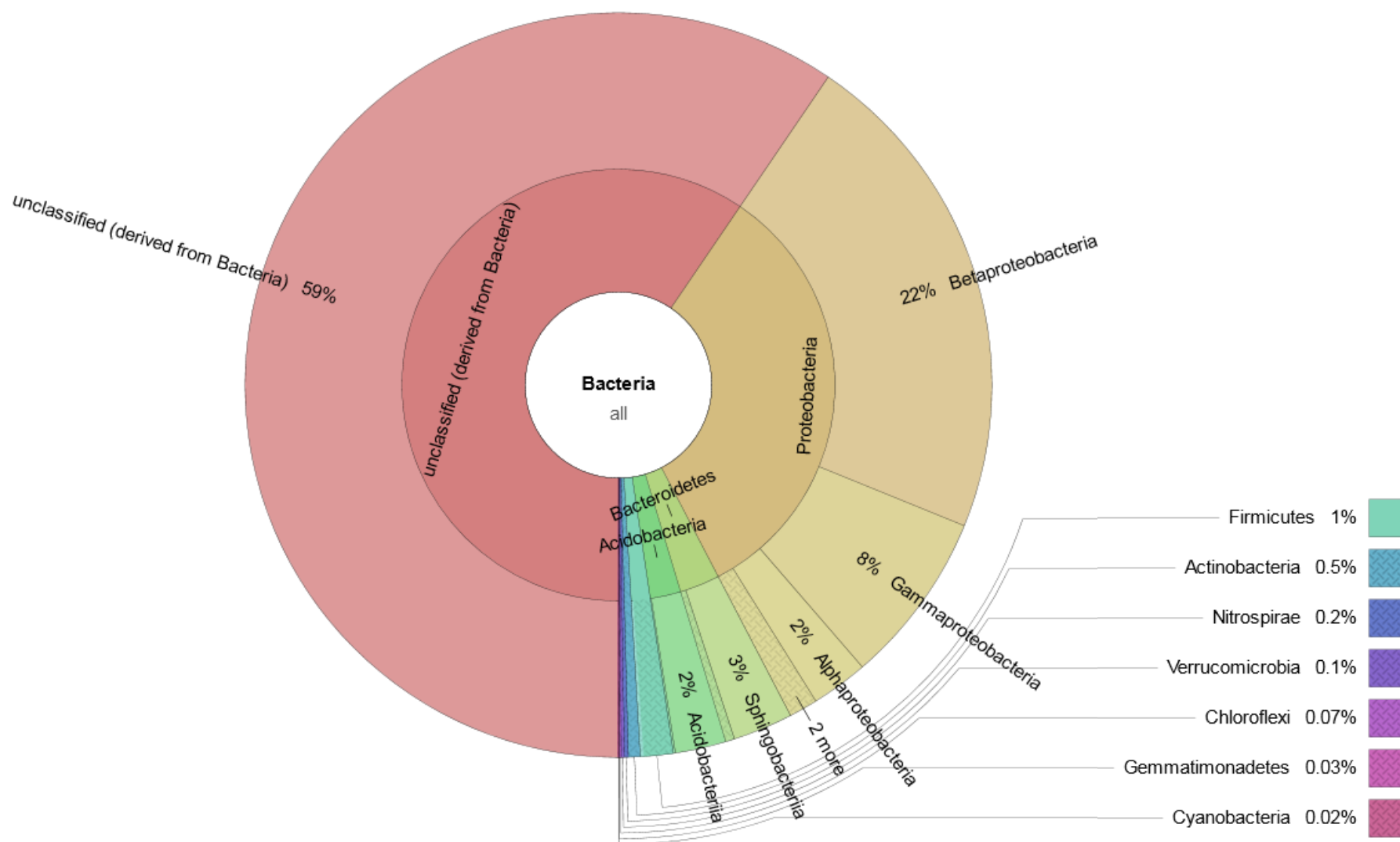


Figure 4.6a: Overview of the microbial community in ACL surface sediment as characterized by the RDP database⁽²⁰⁴⁾. Visualization was generated in Krona.⁽²⁰⁵⁾

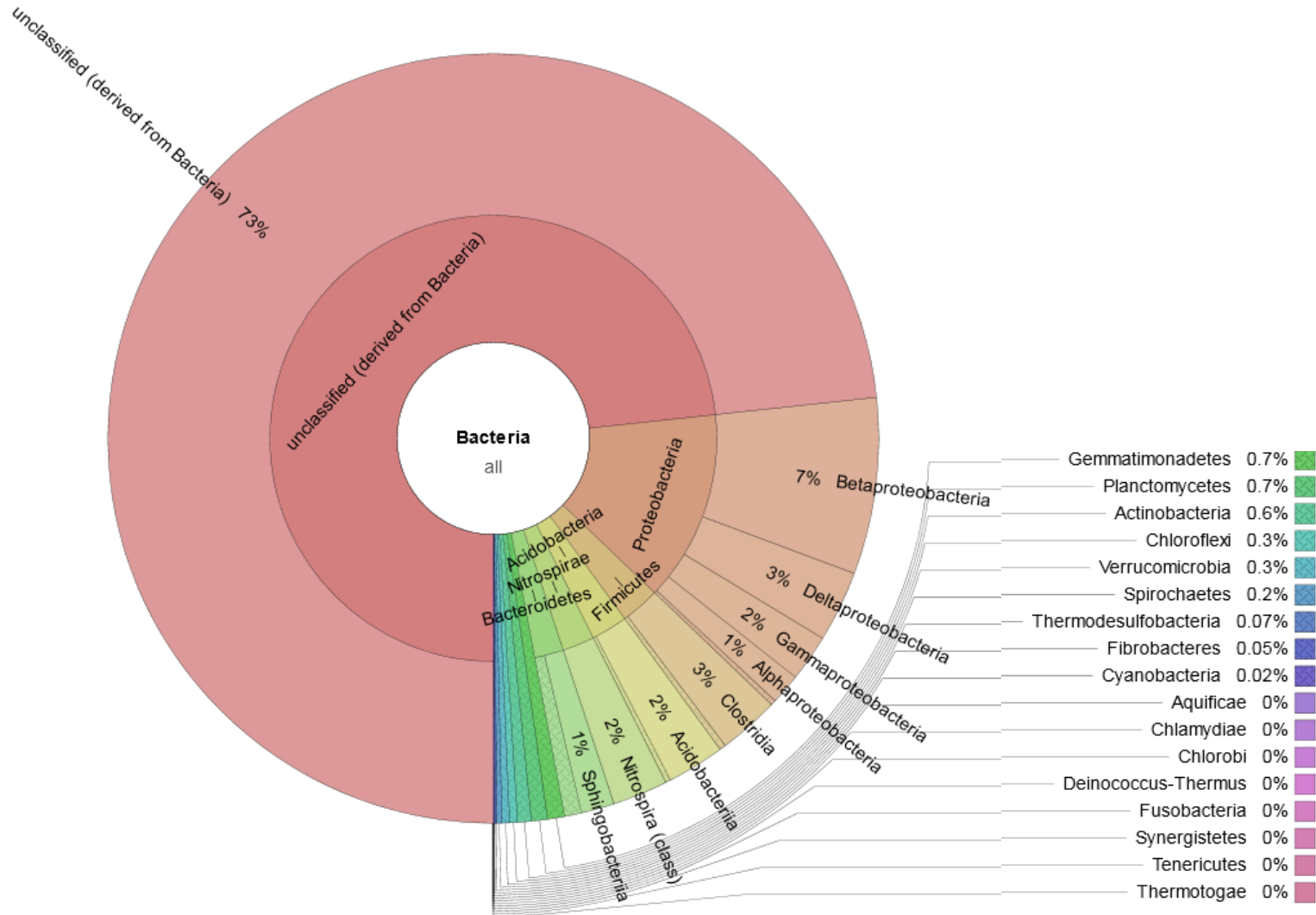


Figure 4.6b: Overview of the microbial community in AED surface sediment as characterized by the RDP database⁽²⁰⁴⁾. Visualization was generated in Krona.⁽²⁰⁵⁾

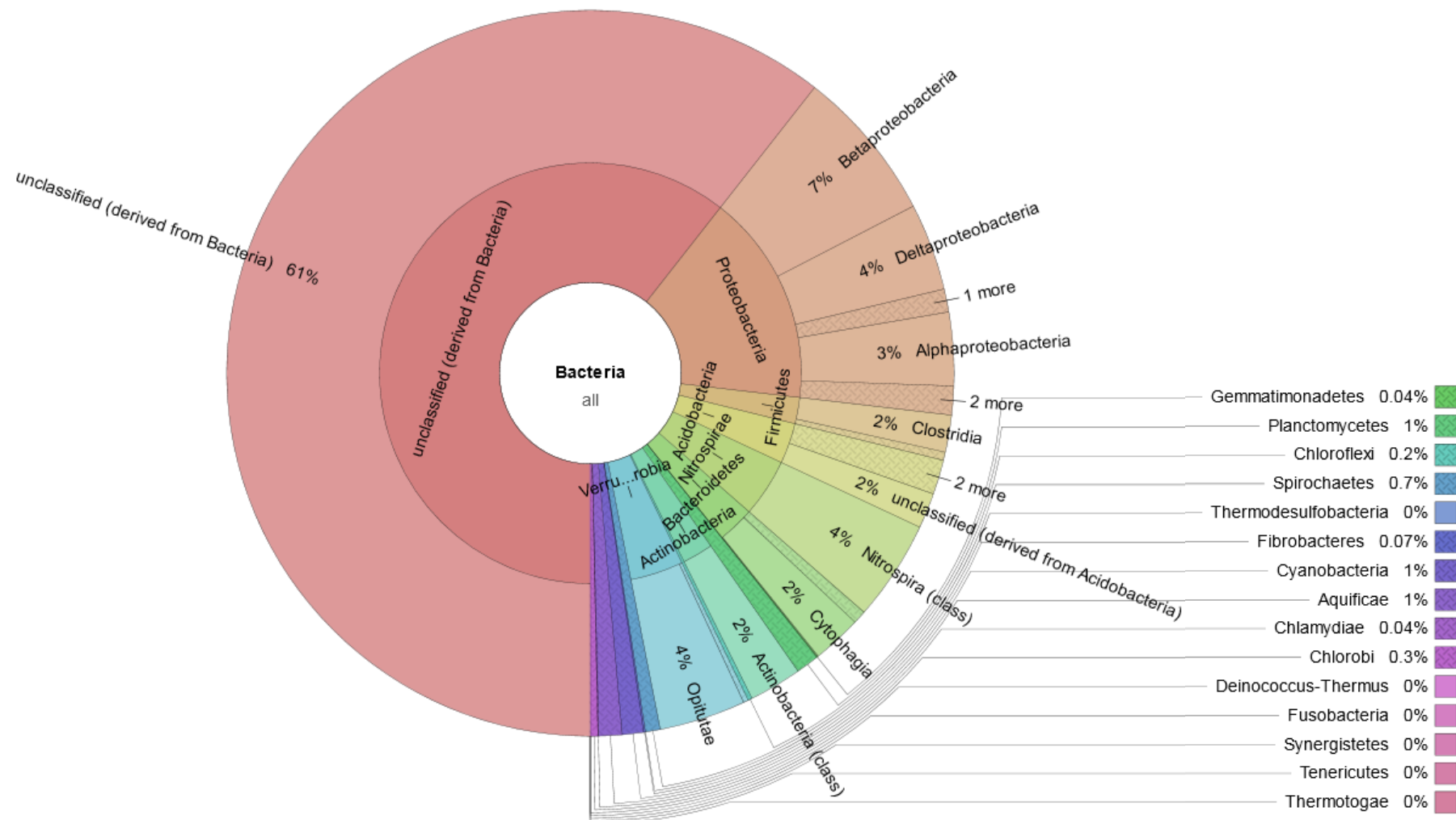


Figure 4.6c: Overview of the microbial community in AFR surface sediment as characterized by the RDP database.⁽²⁰⁴⁾ Visualization was generated in Krona.⁽²⁰⁵⁾

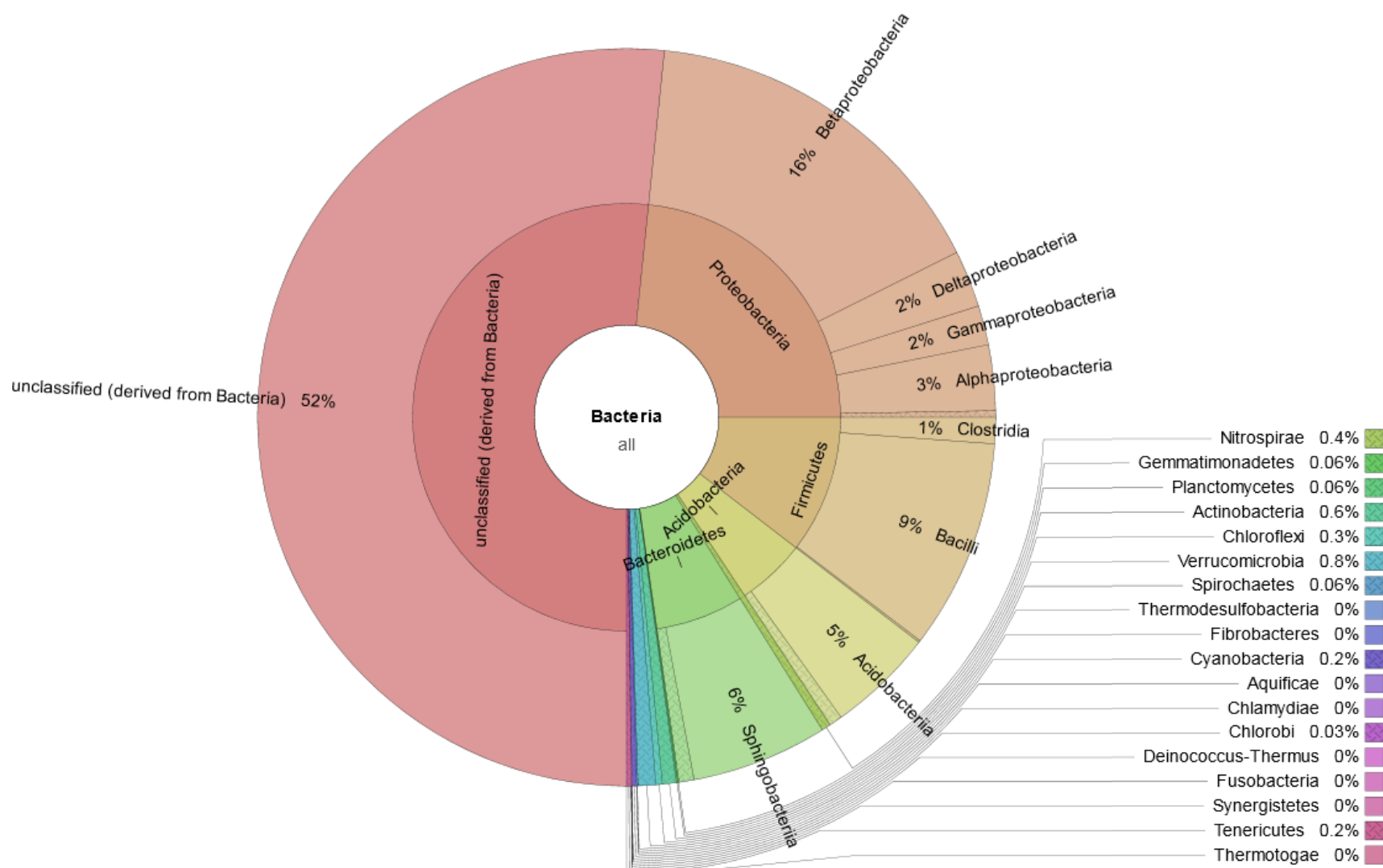


Figure 4.6d: Overview of the microbial community in AJL surface sediment as characterized by the RDP database.⁽²⁰⁴⁾ Visualization was generated in Krona.⁽²⁰⁵⁾

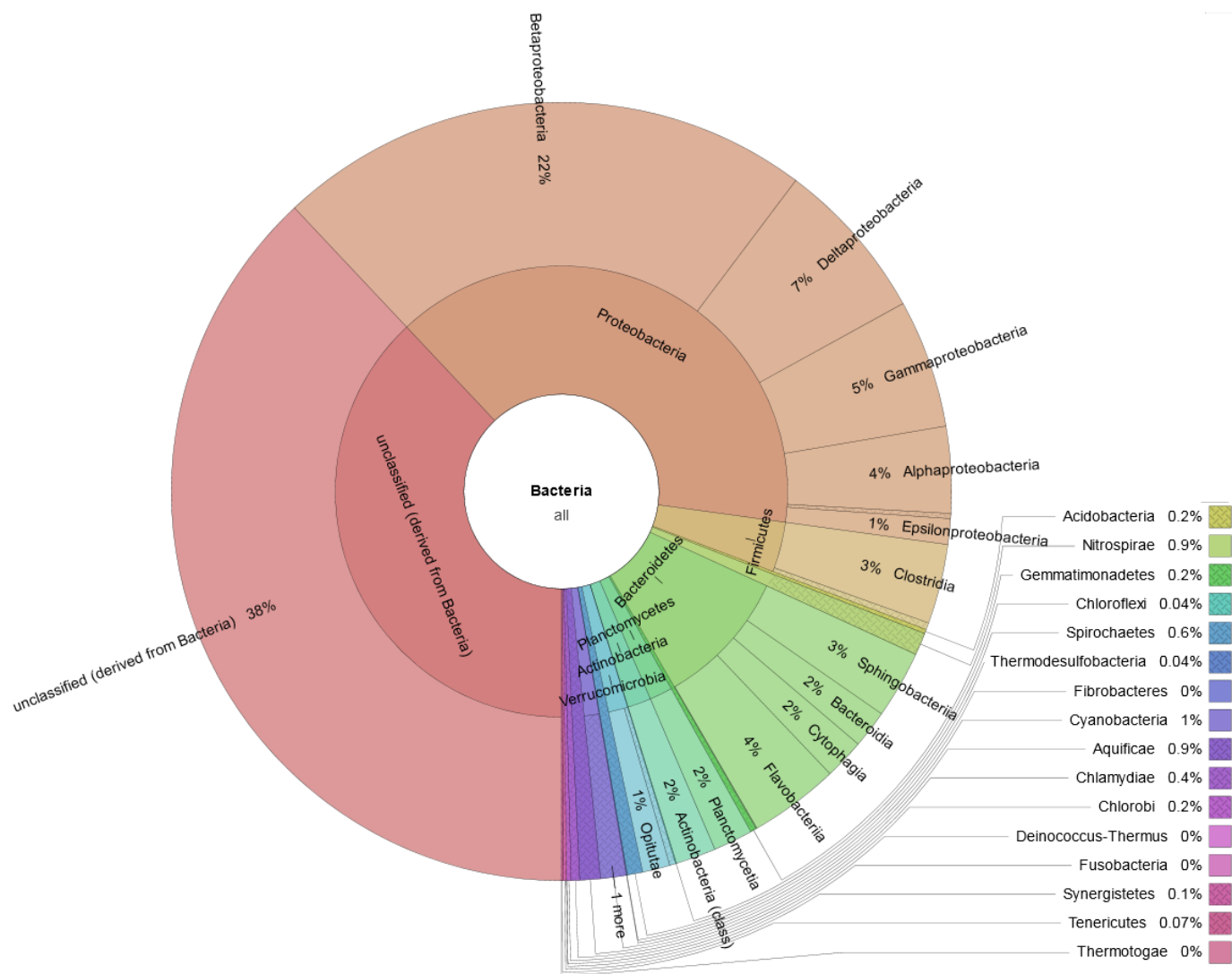


Figure 4.6e: Overview of the microbial community in AMW surface sediment as characterized by the RDP database. ⁽²⁰⁴⁾ Visualization was generated in Krona. ⁽²⁰⁵⁾

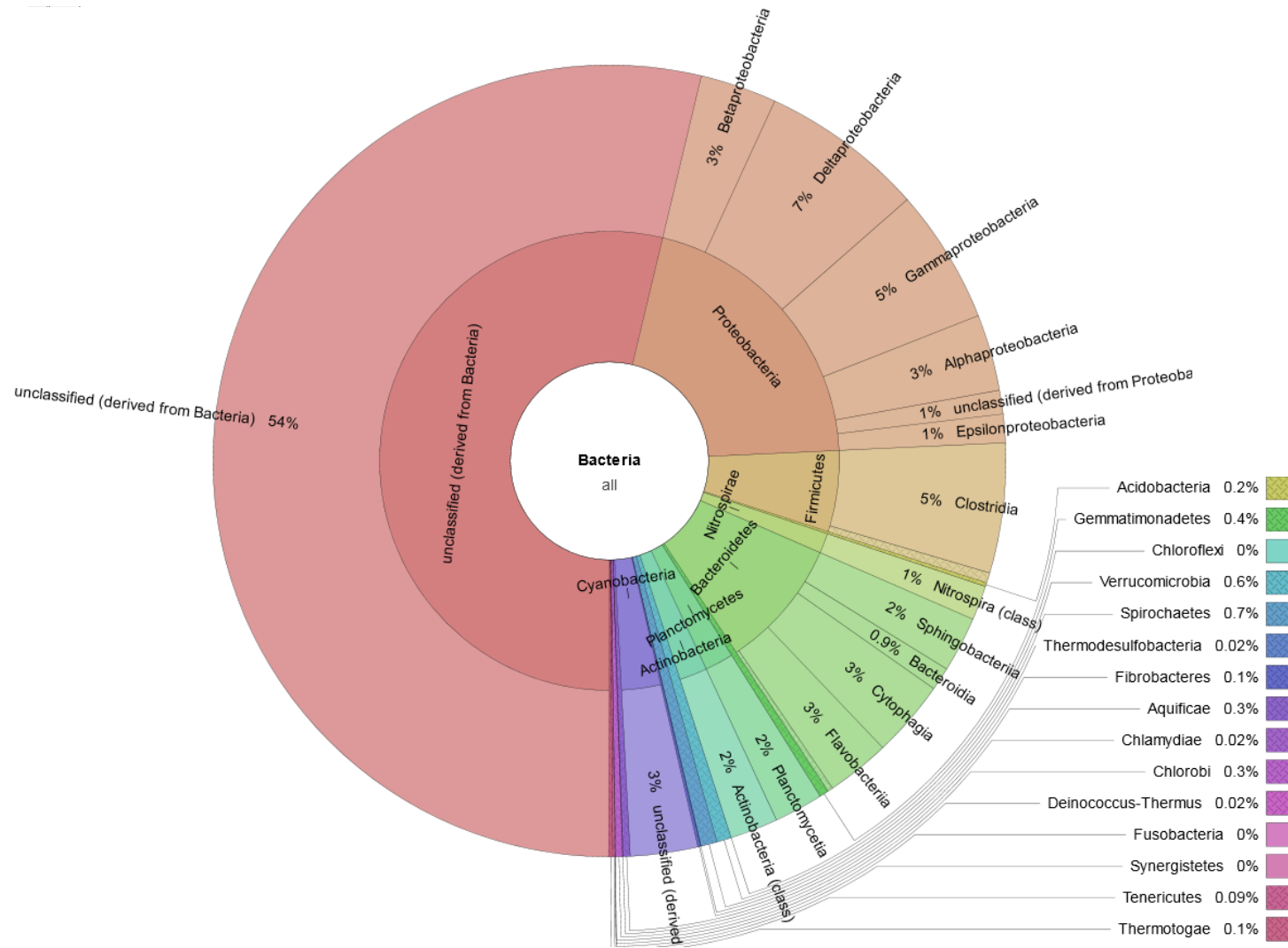


Figure 4.6f: Overview of the microbial community in AOT surface sediment as characterized by the RDP database.⁽²⁰⁴⁾ Visualization was generated in Krona.⁽²⁰⁵⁾

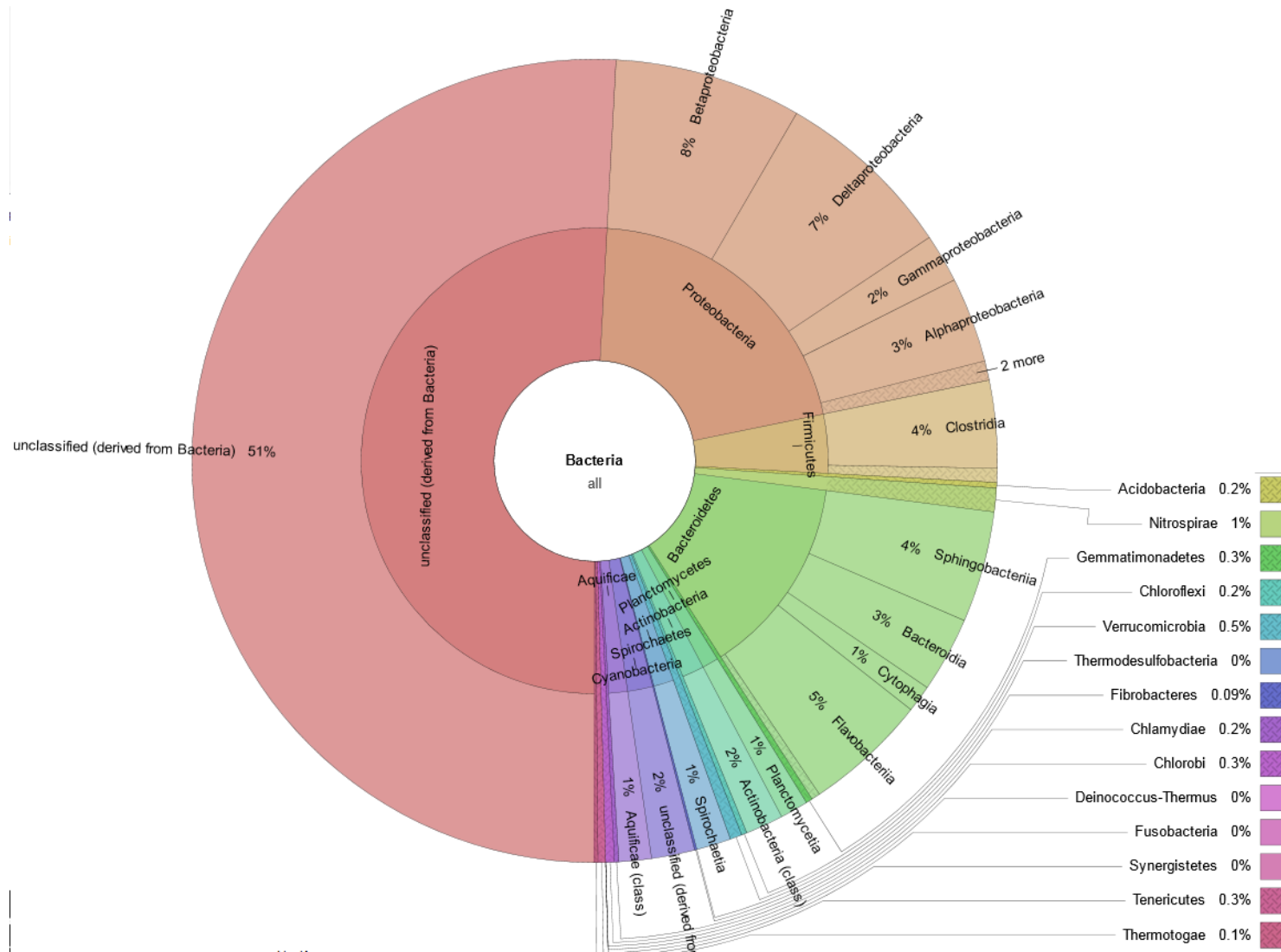


Figure 4.6g: Overview of the microbial community in CBC surface sediment as characterized by the RDP database.⁽²⁰⁴⁾ Visualization was generated in Krona.⁽²⁰⁵⁾

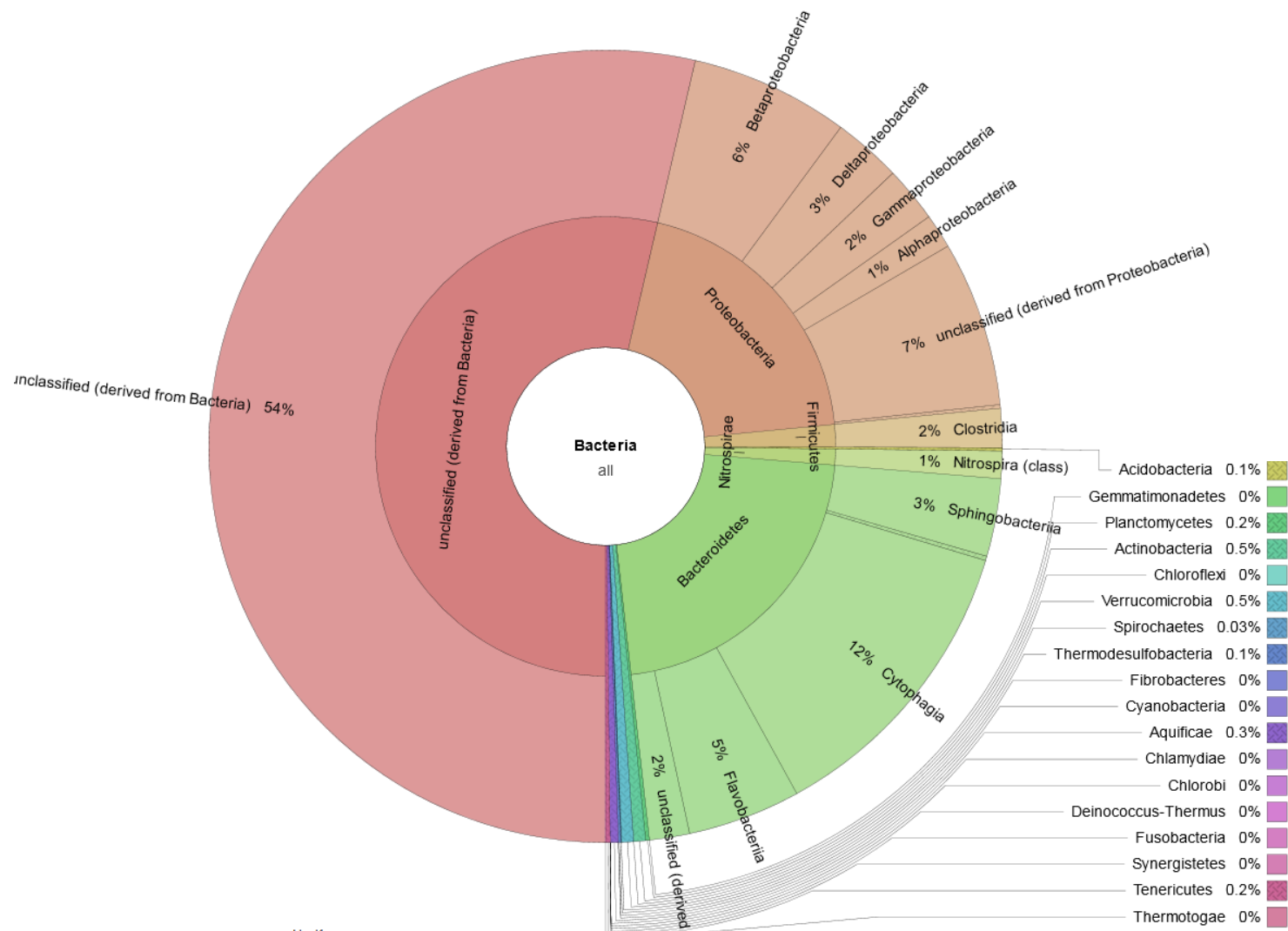


Figure 4.6h: Overview of the microbial community in CLC surface sediment as characterized by the RDP database.⁽²⁰⁴⁾ Visualization was generated in Krona.⁽²⁰⁵⁾



Figure 4.6i: Overview of the microbial community in CWP surface sediment as characterized by the RDP database.⁽²⁰⁴⁾ Visualization was generated in Krona.⁽²⁰⁵⁾

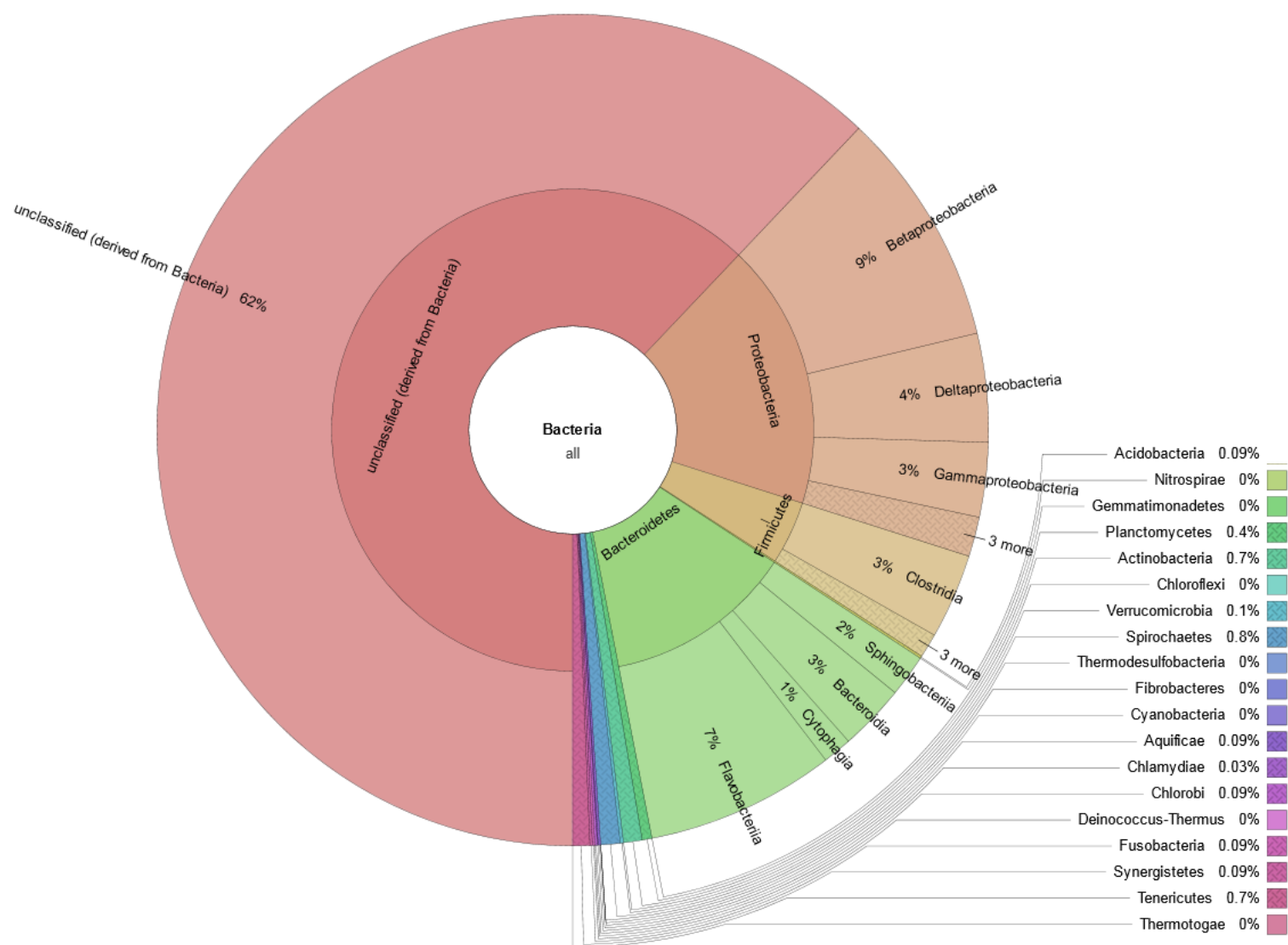


Figure 4.6j: Overview of the microbial community in IGC09 surface sediment as characterized by the RDP database.⁽²⁰⁴⁾ Visualization was generated in Krona.⁽²⁰⁵⁾

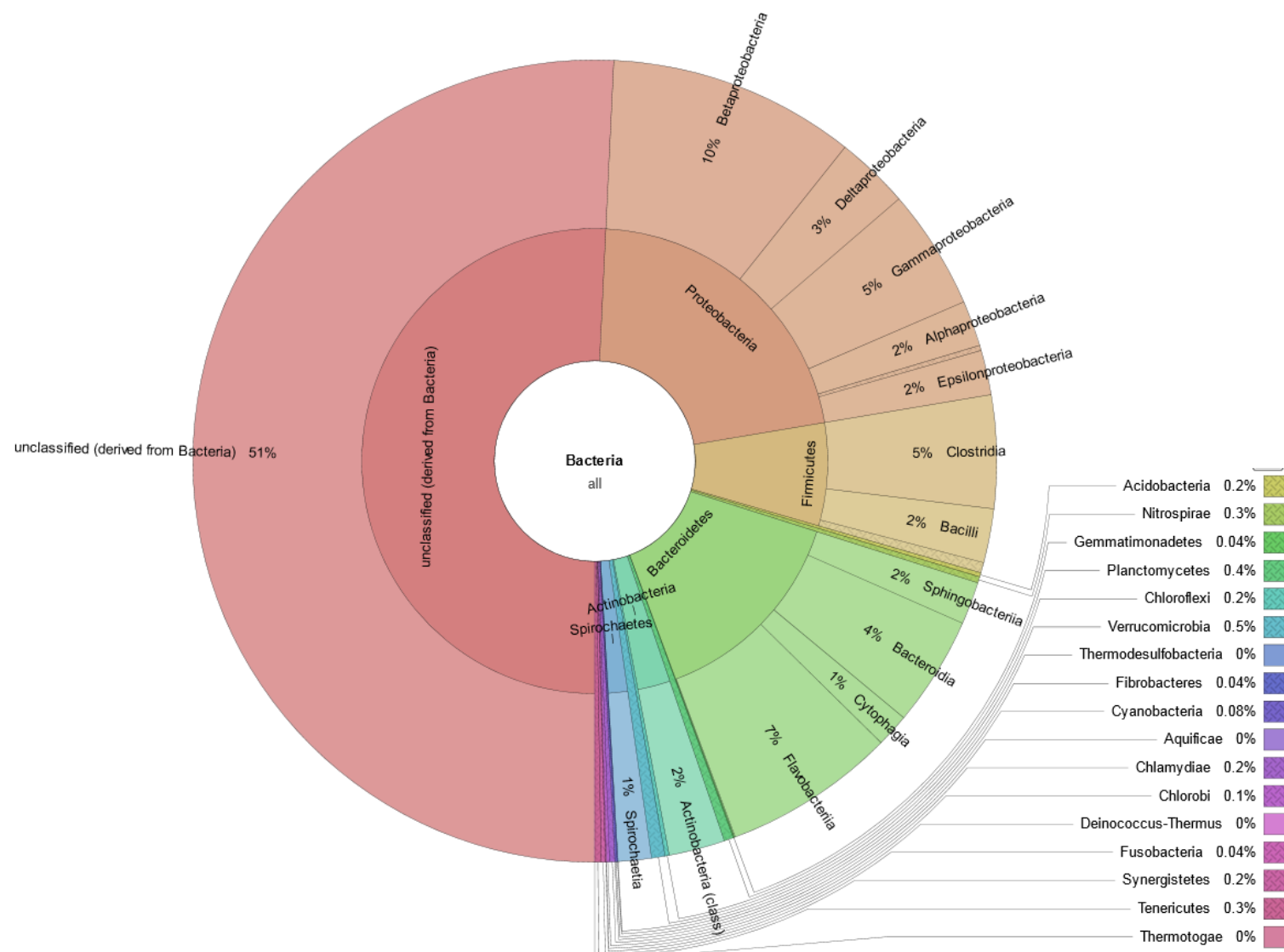


Figure 4.6k: Overview of the microbial community in IGC13 surface sediment as characterized by the RDP database.⁽²⁰⁴⁾ Visualization was generated in Krona.⁽²⁰⁵⁾

The dominant microbial phylum distribution in all the surface sediments is compared in Figure 4.7. One of the most striking features of the microbial phylum distribution was the high abundance of unclassified *Bacteria* in the surface sediments. This was also previously highlighted in section 4.2 where sequences identified from four different RNA databases all resulted in high abundance of unclassified *Bacteria*. The RDP database identified 39 to 74% unclassified *Bacteria* in the sediment samples. A detailed discussion of the distribution of unclassified *Bacteria* in AR, Chicago, and IGC surface sediments is given in Chapter 4.4.1.4.

The *Proteobacteria*, *Firmicutes*, and *Bacteroidetes* phyla were consistently the dominant identified phyla in all the sediment samples. Eilers et al. (2000), Spain et al. (2000), and Fierer et al. (2007) have argued that the *Proteobacteria* phylum is consistently the most abundant microbial taxa in soil and sediment samples.⁽²⁰⁶⁻²⁰⁸⁾ Although the *Proteobacteria* phylum was consistently dominant in all the sediment samples, the microbial class distribution varied substantially in the surface sediments (Figure 4.7a-k). In AED, AFR, AMW, CBC, CLC, IGC09, and IGC13 surface sediments, the microbial classes dominance increased in the order of *Gammaproteobacteria* < *Deltaproteobacteria* < *Betaproteobacteria*. In the ACL, AJL, AOT, and CWP surface sediments, microbial classes in the *Proteobacteria* phylum increased in the order of *Alphaproteobacteria* < *Gammaproteobacteria* < *Betaproteobacteria*, *Gammaproteobacteria* < *Deltaproteobacteria* < *Alphaproteobacteria*, *Alphaproteobacteria* = *Betaproteobacteria* < *Gammaproteobacteria* < *Deltaproteobacteria*, and *Deltaproteobacteria* < *Betaproteobacteria* < *Alphaproteobacteria*.

As was the case with the *Proteobacteria* phylum, the dominant microbial classes in the *Bacteroidetes* phylum also varied from core to core. The *Sphingobacteriia* class was the most dominant in the *Bacteroidetes* phylum in all AR surface sediments except for AOT. In AOT, CLC, and CWP surface sediments, *Clostridia* was the most dominant class in the *Bacteroidetes* phylum. The *Flavobacteriia* phylum was the most dominant class in CBC and IGC09 surface sediments. The *Bacteroidia* class was the most dominant class in the *Bacteroidetes* phylum in IGC13.

The *Firmicutes* phylum was primarily dominated by the *Clostridia* class in most of the surface sediments (ACL, AFR, AMW, AOT, CBC, CLC, CWP, and IGC09). In AED, AJL, and IGC13 surface sediments, the most dominant microbial class in the *Firmicutes* phylum was the *Negativicutes* and *Bacilli*.

The high abundance of unclassified *Bacteria* combined with observations of the microbial taxa constituents in the sediment samples painted a very diverse picture of the microbial community structure in the AR, Chicago, and IGC surface sediments. These observations are consistent with those in other studies which also found highly diverse microbial communities in soil and sediment.⁽²⁰⁹⁻²¹¹⁾ Overall, the microbial community structure in these sediments likely result from the varying physico-chemical attributes of the sediment samples.

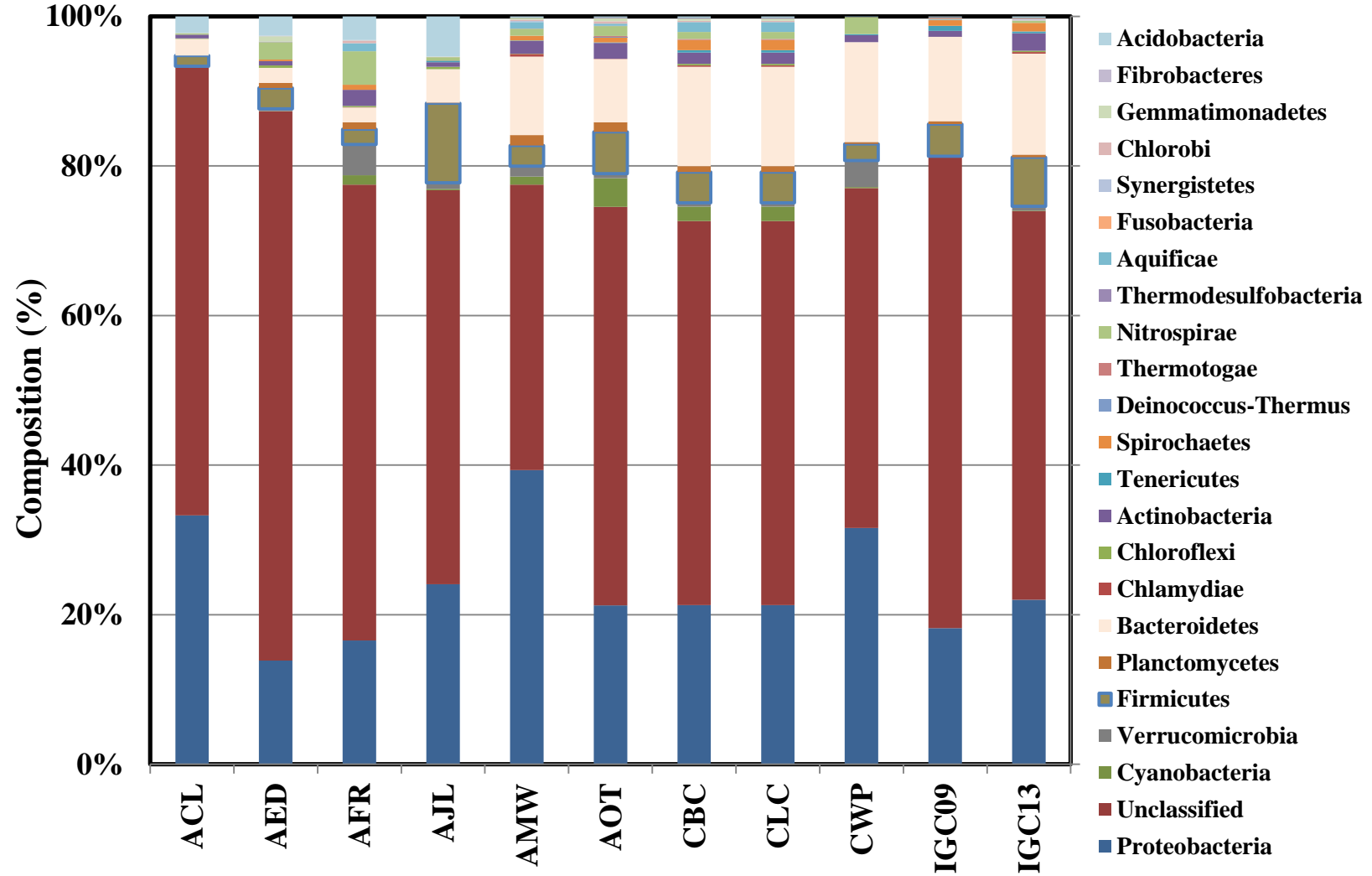


Figure 4.7: Visual comparison of the microbial phylum composition in all surface sediments as classified by the RDP database ⁽²⁰⁴⁾ through MGRAST interface. ⁽²⁰³⁾ The unclassified notation in the legend refers to unclassified sequences of the *Bacteria* origin.

4.4.1.4. Similarity In Microbial Community Composition In Surface Sediments

A hierarchical cluster map was generated to facilitate characterization and comprehension of the microbial community distribution in the surface sediments. The results are shown in Figure 4.8. Grouping and distance were measured using the Manhattan method.⁽²⁰³⁾ Results from the hierarchical analysis were interpreted along with principal component analysis (PCA) results which are shown in Figure 4.9.

The hierarchical cluster analysis resulted in two main groups. The first group consisted of AED, ACL, AJL, and AFR surface sediments. The surface sediments grouping in this particular cluster corresponded to increased average distance from the two PBDE manufacturing facilities and consequently, decreased \sum_{49} PBDEs concentrations.⁽¹⁵¹⁾ The PCA results reflected the same trend with a decreased in factor one and an increased in factor two observed with increased average distance from the PBDE point sources. This trend is noted with an arrow in Figure 4.9. The high correlation between microbial diversity and \sum_{49} PBDEs concentrations, and grouping by hierarchical cluster map and PCA provided collective support indicating that PBDEs impact the microbial community composition in these four surface sediments (ACL, AED, AFR, AJL). It is important to note that although lines of evidence point towards PBDE influencing the microbial community composition in these surface sediments, other factors not considered here can also play a role.

The second group in Figure 4.8 was composed of the remaining six cores. One hierarchical branch grouped the microbial community in AOT to CWP and CLC. In Chapter 3, two PBDE and PCB exposure pathways for the sediments were postulated based on PBDE homolog distributions. These exposure pathways were anthropogenic hydraulic deposition primarily impacted by WWTP effluent, stormwater discharges, and CSOs; and atmospheric deposition-dominated sources via wet and dry deposition. CWP is an urban Chicago site with no anthropogenic and natural hydraulic inflow and outflow, and was thus postulated as an atmospheric deposition-dominated site (detailed description on site CWP provided in Chapter 3.3.1.). The site history at CLC suggests a mixed atmospheric and hydraulic

exposure pathways (Chapter 3.3.1). However, the observed PBDE and PCB homolog distributions in the CLC sediment core were more reflective of a hydraulic deposition-dominated site (Chapter 3.4.4.). In contrast, the microbial community composition in CLC surface sediment bore closer resemblance to the urban, atmospheric deposition surface sediment, CWP. Site AOT was postulated to be atmospheric deposition-dominated; similar to sites AED, ACL, AJL, and AFR. Additionally, \sum_{49} PBDEs surface concentrations in AOT fit into the distance-concentration correlation along with sites AED, ACL, AJL, and AFR. Despite the similarity between site AOT to sites AED, ACL, AJL, and AFR, the microbial community composition in AOT surface sediment bore closer resemblance to CWP, the urban atmospheric deposition-dominated surface sediment and CLC, the urban mixed influenced surface sediment. This deviation from the expected trend highlights the complexity of microbial community structure in these diverse sediment samples.

Another branch in the second cluster consisted of the AMW, CBC, IGC09, and IGC13 surface sediments. This grouping is also reflected in the PCA analysis (Figure 4.9). Sites AMW, CBC, IGC09, and IGC13 are all anthropogenic hydraulic deposition-dominated. Site AMW had previously received WWTP effluent from the Magnolia WWTP, site CBC received large volume discharges from the Racine Avenue Pumping Station (RAPS), and sites IGC09 and IGC13 located on the West Branch of the Grand Calumet River (WBGCR) which is primarily fed by Hammond Sanitary District (HSD) WWTP effluent. Details on the site history and characteristics of these anthropogenic hydraulic discharges are provided in Chapter 3.3.1. The hierarchical cluster analysis indicated that microbial community composition in AMW was more similar to CBC, while the microbial community composition in IGC09 was more similar to IGC13, reflecting the origin from the anthropogenic hydraulic discharges. AMW and CBC received municipal WWTP and stormwater discharges, respectively whereas IGC09 and IGC13 received HSD WWTP effluent with municipal and industrial origin. The hierarchical cluster map and PCA results showed that the microbial composition clustering in these surface sediments is a reflection of a shared origin and similar niche environment provided by the different waste discharges.

Generally, the overall microbial community composition gradually change with increased average distance from the two PBDE manufacturing facilities, and thus with decreased \sum_{49} PBDEs concentrations in AR surface sediments (AED, ACL, AJL, and AOT surface sediments). The microbial community in Chicago surface sediments showed no correlation to \sum_{49} PBDEs concentration. In general, the hierarchical cluster and PCA differentiate the microbial community composition in Chicago sediments by exposure mode. These trends suggest that \sum_{49} PBDEs concentration can influence the microbial community composition in AR surface sediments, while mode of exposure pathway is a driver affecting the microbial community composition in Chicago surface sediments.

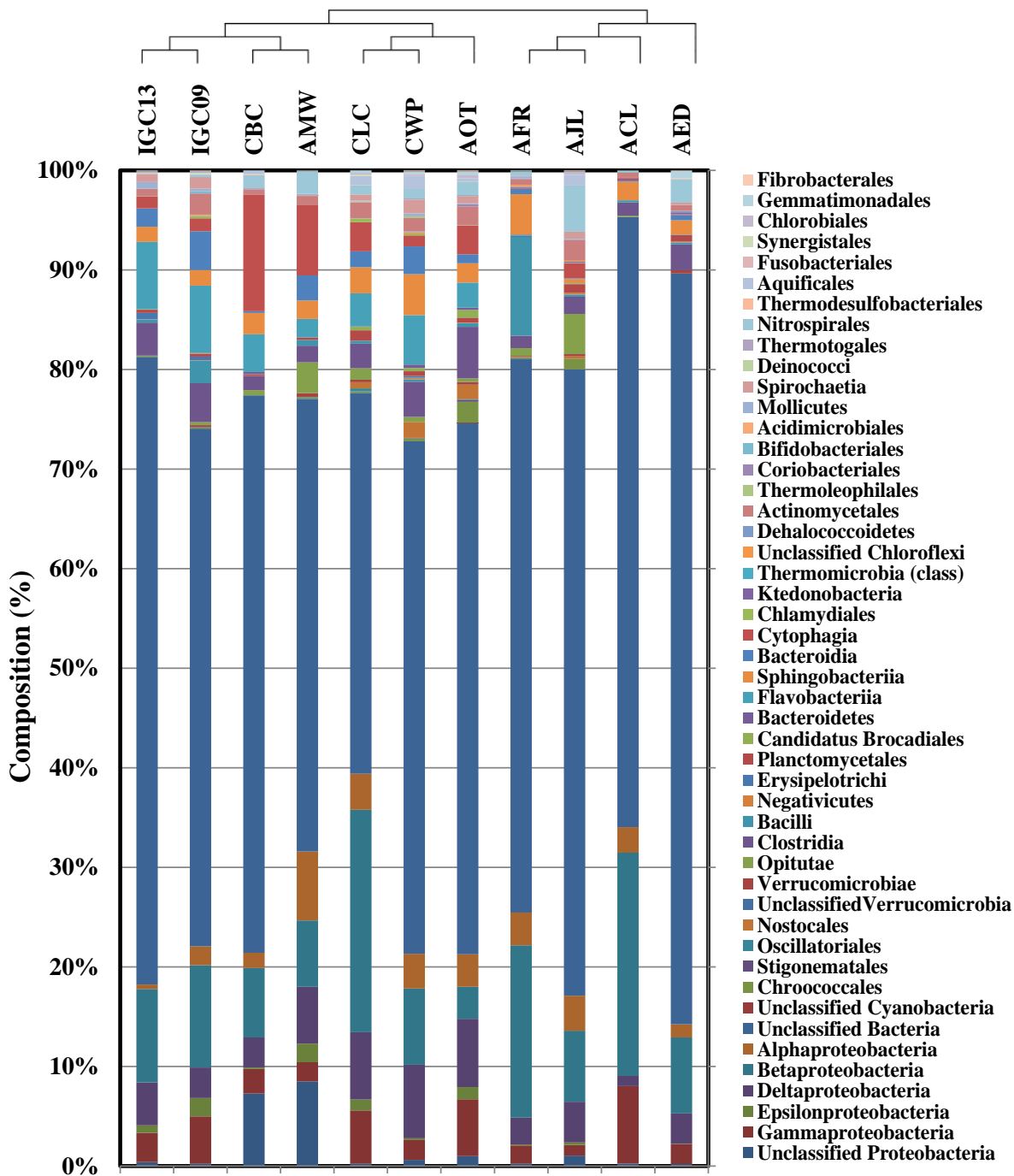


Figure 4.8: Hierarchical cluster map analysis performed in MGRAST⁽²⁰³⁾ and microbial community composition at the class operational taxonomic unit (OTU) level for all surface sediments. The hierarchical cluster map used the Manhattan method to cluster and measure distance or similarity in the microbial community composition in the surface sediments.

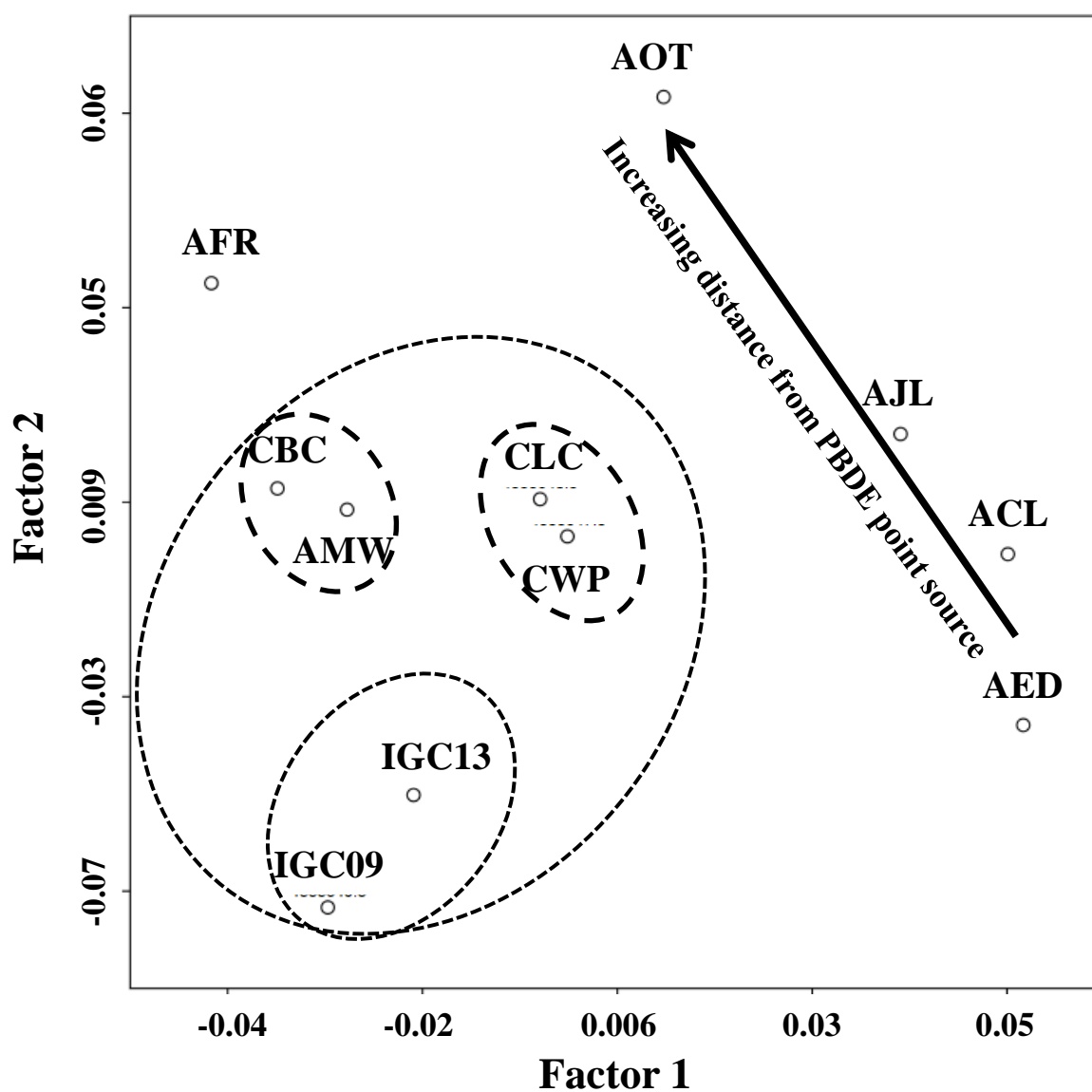


Figure 4.9: Result of principal component analysis (PCA) of microbial community distribution performed in MGRAST.⁽²⁰³⁾ Arrow points in the direction of average increased distance between four AR sites to two PBDE manufacturing facilities. Dotted lines reflect surface sediment grouping in the hierarchical cluster map shown in Figure 4.8.

4.4.1.5. Microorganisms With Confirmed PBDE and PCB Degradation Capability

Table 4.4 is a summary of microbial species present in the sediment samples with confirmed PBDE degradation capability. To date, microbial species from five phyla were identified as confirmed PBDE degraders. In the *Proteobacteria* phylum, all the *Sphingomonas* sp. identified have demonstrated low molecular weight (LMW) PBDE congeners degradation capability (<5 bromines) and diphenyl ether degradation capability (i.e., the non-brominated form of PBDE).^(107, 212, 213) Similarly, *Burkholderia xenovorans* LB400 have confirmed LMW PBDE congeners degradation capability as well (<6 bromines).⁽¹⁰⁸⁾ In the *Proteobacteria* phylum, *Sulfurospirillum multivorans* from the *Epsilonproteobacteria* order demonstrated high molecular weight (HMW) PBDE congeners degradation capability (6 to 10 bromine substitutions).⁽¹⁰²⁾ *Rhodococcus jostii* RHA1, *Rhodococcus* sp RR1, and *Pseudonocardia dioxanivorans* CB1190 were capable of degrading mono- to hexa-, mono- to di-, and mono- to di-BDE congeners, respectively.⁽¹⁰⁸⁾ *Lysinibacillus fusiformis* strain DB-1 was isolated from PBDE-contaminated sediments in China and was able to degrade the deca-BDE congener (BDE-209) provided with the carbon sources lactate, acetate, and pyruvate.⁽¹⁰⁹⁾ Microbial species from the *Firmicutes* and *Chloroflexi* phyla have confirmed capability to dehalogenate HMW PBDE congeners.^(102,103) A detailed review on microbial facilitated PBDE degradation is provided in Chapter 2.5.

Table 4.4. A summary of reported microorganisms and the associated microbial taxa with confirmed PBDE degradation capability under laboratory simulations.

Microbial Strain	Taxa (Phylum/Class/Order/Family)
<i>Sphingomonas</i> sp. strain SS3 ⁽¹⁰⁷⁾ , <i>Sphingomonas</i> sp. strain SS33 ⁽²¹³⁾ , <i>Sphingomonas</i> sp. PH-07 ⁽²¹²⁾	<i>Proteobacteria</i> / <i>Alphaproteobacteria</i> / <i>Sphingomonadales</i> / <i>Sphingomonadaceae</i>
<i>Sulfurospirillum multivorans</i> ⁽¹⁰²⁾	<i>Proteobacteria</i> / <i>Epsilonproteobacteria</i> / <i>Campylobacteriales</i> / <i>Campylobacteraceae</i>
<i>Burkholderia xenovorans</i> LB400 ⁽¹⁰⁸⁾	<i>Proteobacteria</i> / <i>Betaproteobacteria</i> / <i>Burkholderiales</i> / <i>Burkholderiaceae</i> ,
<i>Rhodococcus jostii</i> RHA1 ⁽¹⁰⁸⁾ , <i>Rhodococcus</i> sp RR1 ⁽¹⁰⁸⁾	<i>Actinobacteria</i> /- / <i>Actinomycetales</i> (<i>Corynebacterineae</i>) / <i>Nocardiaceae</i>
<i>Pseudonocardia dioxanivorans</i> CB1190 ⁽¹⁰⁸⁾	<i>Actinobacteria</i> / - / <i>Actinomycetales</i> / <i>Pseudonocardiaceae</i>
<i>Lysinibacillus fusiformis</i> strain DB-1 ⁽¹⁰⁹⁾	<i>Firmicutes</i> / <i>Bacilli</i> / <i>Bacillales</i> / <i>Bacillaceae</i>
<i>Desulfitobacterium chlororespirans</i> Co23 ⁽¹⁰³⁾ , <i>Desulfitobacterium dehalogenans</i> JW/IU- DC1) ⁽¹⁰²⁾ , <i>Dehalobacter restrictus</i> PER-K23 ⁽¹⁰³⁾ , <i>Desulfitobacterium hafniense</i> strain PCP-1 ⁽¹⁰²⁾	<i>Firmicutes</i> / <i>Clostridia</i> / <i>Clostridiales</i> / <i>Peptococcaceae</i>
<i>Dehalococcoides ethenogenes</i> 195 ⁽¹⁰²⁾ , <i>Dehalococcoides</i> sp. strain BAV1) ⁽¹⁰²⁾	<i>Chloroflexi</i> / <i>Dehalococcoidetes</i> / <i>Dehalococcoidetes</i> / <i>Dehalococcoidetes</i>

Decades of research on PCB degradation have resulted in the identification of more microbial species with confirmed PCB degradation capability. In general, microbial species with confirmed PCB degradation capability were from the *Proteobacteria*, *Actinobacteria*, *Chloroflexi* and *Firmicutes* phyla. ⁽¹⁹⁸⁾ A sample subset of these microorganisms and their associated microbial taxa are summarized in Table 4.5. Several of the identified PCB degraders traced their phylogenic root to the *Proteobacteria* phylum, which is the dominant phylum in many sediment and soil samples, ⁽²⁰⁶⁻²⁰⁸⁾ as in the present study (Figure 4.7a-k). With the exception of *Dehalococcoides* spp. and *Desulfobivrio* spp., ^(96, 97) most of the microorganisms identified in Table 4.5 have confirmed LMW PCB congener (< 6 chlorines) degradation

capability under biostimulation or bioaugmentation laboratory scale experiments.^(69,75,77,79,81,214-216) A detail review of the literature on PCB biodegradation is provided in Chapter 2.5.

Microorganisms with confirmed PBDE and PCB degradation capability were observed to share common phylogenic roots. To illustrate, microbial species from the *Proteobacteria*, *Firmicutes*, and *Chloroflexi* phyla have confirmed PBDE and PCB degradation capability. Although common phylogenic roots were observed, these identified microorganism species can differ in the smaller operational taxonomic unit (OTU) classification. For example, microbial species with confirmed PBDE degradation capability from the *Proteobacteria* phylum were classified into the *Alphaproteobacteria*, *Epsilonproteobacteria*, and *Betaproteobacteria* class, whereas microbial species with confirmed PCB degradation capability from the *Proteobacteria* phylum were in the *Betaproteobacteria*, *Gammaproteobacteria*, and *Deltaproteobacteria* classes. Additionally, confirmed dehalogenation capability is not equal within the same phylum. To illustrate, the *Lysinibacillus fusiformis* strain DB-1 from the *Bacilli* order has confirmed HMW PBDE congener (>6 bromines) degradation capability.⁽¹⁰⁹⁾ On the other hand, the *Bacillus brevis* strain B-257, also from the *Bacilli* order, has confirmed LMW PCB congener (<6 chlorines) degradation capability.⁽²¹⁶⁾

Table 4.5. A summary of reported microorganisms and the associated microbial taxa with confirmed PCB degradation capability under laboratory conditions

Microorganism Strain	Taxa (Phylum/Class/Order/Family)
<i>Burkholderia cepacia</i> ⁽²¹⁴⁾	<i>Proteobacteria/Betaproteobacteria/Burkholderiales/Burkholderiaceae/</i>
<i>Ralstonia</i> spp. strain SA-3 and <i>Ralstonia</i> spp. strain SA-4 ⁽⁸¹⁾	<i>Proteobacteria/Betaproteobacteria/Burkholderiales/Ralstoniaceae</i>
<i>Comamonas testosteroni</i> ⁽⁶⁹⁾	<i>Proteobacteria/Betaproteobacteria/Burkholderiales/Comamonadaceae</i>
<i>Achromobacter</i> sp. ⁽²¹⁵⁾	<i>Proteobacteria/Betaproteobacteria/Burkholderiales/Alcaligenaceae</i>
<i>Alcaligenes</i> sp. strain Y42 ⁽⁷⁵⁾	<i>Proteobacteria/Betaproteobacteria/Burkholderiales/Alcaligenaceae</i>
<i>Desulfovibrio</i> spp. ⁽⁹⁷⁾	<i>Proteobacteria/Deltaproteobacteria/Desulfovibrionales/Desulfovibrionaceae</i>
<i>Acinetobacter</i> sp. strain P6 ⁽⁷⁵⁾	<i>Proteobacteria/Gammaproteobacteria/Pseudomonadales/Moraxellaceae</i>
<i>Pseudomonas aeruginosa</i> ⁽⁷⁷⁾ , <i>Pseudomonas putida</i> ⁽⁶⁹⁾ , <i>Pseudomonas</i> sp. 7509 ⁽⁶⁹⁾ , <i>Pseudomonas</i> strain LB400 ⁽⁷⁹⁾	<i>Proteobacteria/ Gammaproteobacteria / Pseudomonadales / Pseudomonadaceae /</i>
<i>Rhodococcus erythropolis</i> & <i>Rhodococcus ruber</i> ⁽⁸³⁾ , <i>Rhodococcus rhodochrous</i> ⁽⁶⁹⁾	<i>Actinobacteria/- /Actinomycetales (Corynebacterineae) / Nocardiaceae</i>
<i>Bacillus brevis</i> strain B-257 ⁽²¹⁶⁾	<i>Firmicutes/Bacilli/Bacillales/Bacillaceae</i>
<i>Dehalococcoides</i> spp. ⁽⁹⁶⁾	<i>Chloroflexi / Dehalococcoidetes / Dehalococcoidetes / Dehalococcoidetes</i>

4.4.1.6. Composition of PBDE and PCB Potential Degraders In Surface Sediments

To evaluate the potential for in-situ PBDE and PCB degradation, the presence of known PBDE and PCB potential degraders in the surface sediments were evaluated. The class OTU was chosen because it provides a high level overview of the potential for PBDE and PCB degradation in the surface sediments. As demonstrated by Tables 4.4 and 4.5, several microbial species with confirmed PBDE or PCB degradation capability could exist within the same phylogenic root. This is consistent with the fact that phylogenically close microorganisms can share the same dehalogenase enzyme that enables PBDE and PCB dehalorespiration.^(217,218) Decreasing the analysis resolution by looking at higher OTU (i.e., phylum and class) provides results that are too generic for interpretation. On the other hand, increasing the analysis resolution by looking at smaller OTU (i.e., family, species, and genus) could result in dismissal of some microorganisms capable of PBDE and PCB degradation.

The distribution of potential PBDE and PCB degraders in the surface sediments are shown in Figure 4.10a and 4.12a, respectively. As it was desired to capture as many potential PBDE and PCB degraders, the distribution of the unclassified microbial class of constituent with confirmed PBDE and PCB degradation capability was also included. For example, these OTUs include unclassified *Betaproteobacteria*, unclassified *Epsilonproteobacteria*, and unclassified *Chloroflexi*. It is noted that this grouping likely overestimate the actual PBDE and PCB degraders abundance. Since the objective of this study is to provide new in-sight into *in-situ* microbial facilitated PBDE and PCB degradation in the sediment phase and not to quantify *in-situ* degradation rates, interpretation was based upon observed trends and not a quantitative relationship. The abundance of PBDE or PCB degraders was compared to $\sum_{49}\text{PBDEs}$ or $\sum_{132}\text{PCBs}$ concentrations (panel b) and to the residual values of multiple linear square regression (MLSR) analysis (panel c); MLSR analysis is discussed in section 3.4.4. and 5.6. The MLSR analysis quantifies the difference between model profiles to sediment profile; large residual value indicates a large difference between model and sediment profile and vice-versa for smaller residual value.

Three PBDE TMs (DE-71, DE-79, and Saytex 102E TMs) and four PCB Aroclors (Aroclors 1016, 1248, 1254, and 1260) were used in the MLSR analysis for PBDEs and PCBs, respectively.

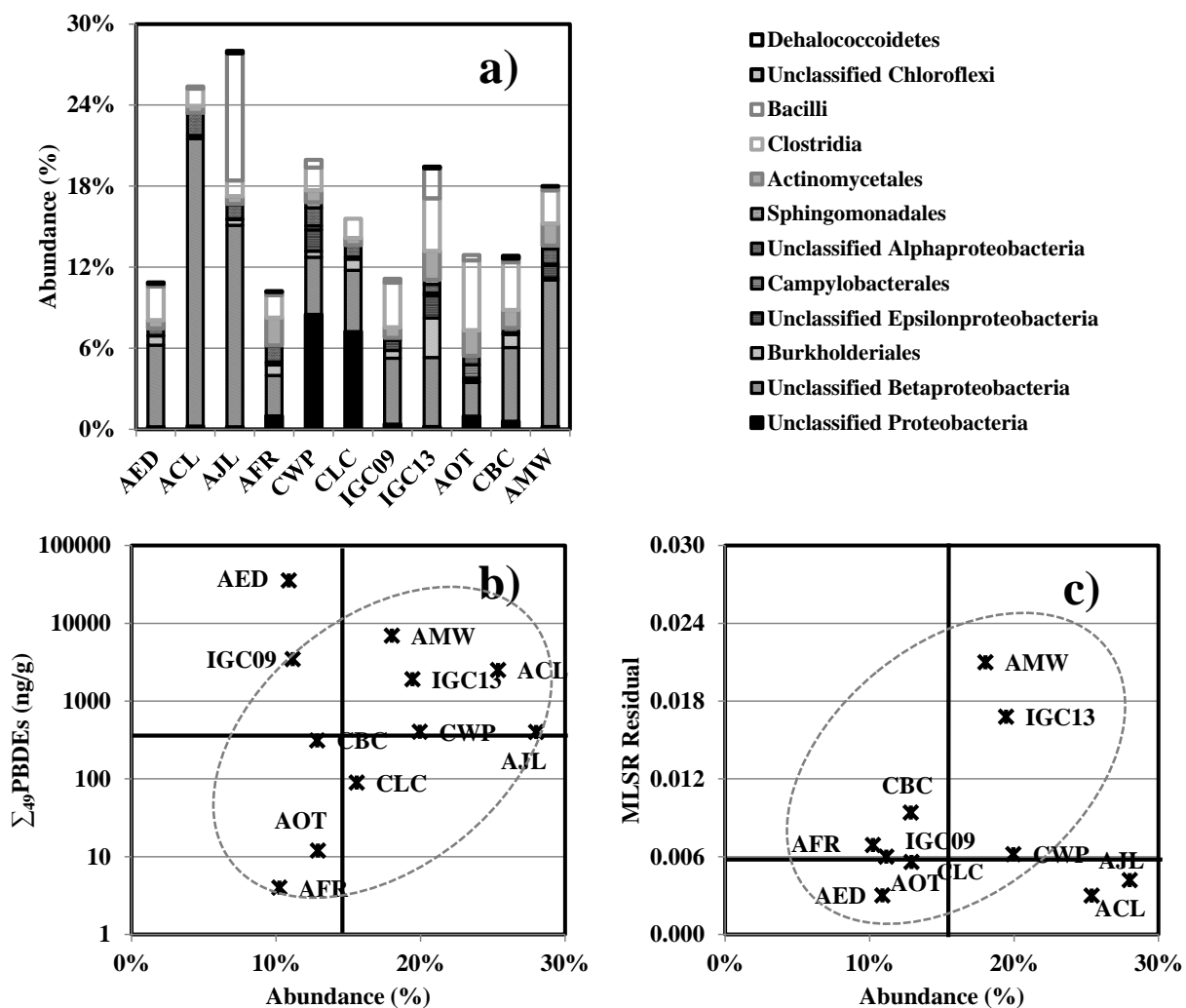


Figure 4.10: a) Abundance of potential PBDE degraders by the microbial class operational taxonomic unit (OTU) level, b) Σ_{49} PBDEs concentration and total abundance of potential PBDE degraders, and c) residual value of multiple linear square regression (MLSR) between three PBDE technical mixtures (DE-71, DE-79, and Saytex 102E TMs) versus total abundance of potential PBDE degraders in surface sediments. Note that the surface sediments in the x-axis of panel a) are arranged by hierarchical cluster map in Figure 4.7. In b) and c), vertical bold lines represent the 50th percentile value of the abundance of potential PBDE degraders and horizontal lines represent the 50th percentile value for Σ_{49} PBDEs concentration and PBDE MLSR residual value, respectively, in all surface sediments.

The fraction of all microbial class OTUs that are potential PBDE degraders in the surface sediment ranged from 10 to 28% and increased in the order of AFR (10%) < AED (11%) < IGC09 (11%) < CBC (13%) < AOT (13%) < CLC (16%) < AMW (18%) < IGC13 (20%) < CWP (20%) < ACL (26%) < AJL (28%) (Figure 4.10a). The unclassified *Betaproteobacteria* constituted 20 to 84% of the microbial class OTUs designated as PBDE degraders and was the most dominant OTU in all the surface sediment samples. There was a general trend of increased abundance of potential PBDE degraders with increased \sum_{49} PBDEs concentrations as observed within the dotted gray oval in Figure 4.10b (Spearman coefficients between abundance of potential PBDE degraders and \sum_{49} PBDEs are -0.3, 0.1, and 0.22 for all surface sediments, respectively).

For the purpose of discussion, high \sum_{49} PBDEs concentrations was ad-hoc defined as having \sum_{49} PBDEs concentration $\geq 50^{\text{th}}$ percentile value, high abundance ad-hoc was defined as having abundance $\geq 50^{\text{th}}$ percentile value, and high MLSR residual was ad-hoc defined as having $\geq 50^{\text{th}}$ percentile value; low \sum_{49} PBDEs, abundance, and MLSR residual were ad-hoc defined as having $< 50^{\text{th}}$ percentile value of the respective parameters. AED and IGC09 have high \sum_{49} PBDEs concentrations; however, potential PBDE degraders abundance was small. In contrast, AMW, IGC13, ACL, and CWP have high \sum_{49} PBDEs concentrations and high abundance of potential PBDE degraders in the surface sediments. Generally, surface sediments with low \sum_{49} PBDEs concentrations such as AOT, AFR, and CLC have low abundance of potential PBDE degraders. In Figure 4.10c, a general trend of increased MLSR residual value with increased potential PBDE degraders abundance was observed (Spearman coefficients between MLSR residual value and abundance of potential PBDE degraders are -0.06, 0.05, 0.07, and 0.34 for all surface sediments, excluding ACL, excluding AJL, and excluding ACL and AJL, respectively). CBC, IGC09, CLC, and AFR surface sediments have low abundance of potential PBDE degraders and high MLSR residual values whereas AED and AOT surface sediments also with low abundance of potential PBDE degraders have low MLSR residual values. In surface sediments with high abundance of potential PBDE degraders, AMW, IGC13, and CWP surface sediments have high MLSR residual values whereas AJL and

ALC surface sediments have low MLSR residual values. The trend in Figure 4.10b suggests that higher \sum_{49} PBDEs concentrations may enrich for the presence of potential PBDE degraders. Additionally, Figure 4.10c suggests that the increased residual values between the three PBDE TMs to the PBDE congener distribution in the sediment profiles are correlated with increased abundance of potential PBDE degraders.

Comparison of the PBDE degradation ability by pure cultures to mixed enrichment cultures often revealed that mixed cultures have a wider range of PBDE degradation capability.[102] This suggests that microorganisms with confirmed PBDE degradation capability generally can only degrade PBDEs within a specific range of bromine substitution. For example, the *Dehalococcoides* spp. ANAS culture which contained multiple *Dehalococcoides* strains produced a diverse range of debromination products from octa-PBDE. In contrast to pure cultures of *Dehalococcoides ethenogenes*, *Dehalococcoides* spp. strain BAV1, and *Dehalococcoides* sp. strain CBDB1 produced only a limited number of debromination products.⁽¹⁰²⁾

The potential PBDE degraders abundance was divided into OTUs capable of LMW PBDE (1-6 bromines) and HMW PBDE (>6 bromines) degradation (Figure 4.11); these classifications were noted as \sum_{LMW} PBDE potential degraders and \sum_{HMW} PBDE potential degraders, respectively. Unclassified *Protoebacteria* were not included in this analysis because microorganisms with confirmed PBDE degradation capability from the *Proteobacteria* phylum showed a wide range of degradation capability. For example, *Alphaproteobacteria* and *Betaproteobacteria* classes are capable of LMW PBDE dehalogenation whereas microorganisms with confirmed PBDE degradation capability from the *Epsilonproteobacteria* class are capable of HMW PBDE dehalogenation.^(102,107,213)

Overall, abundance of \sum_{LMW} PBDE potential degraders ranged from 5 to 24% and abundance of \sum_{HMW} PBDE potential degraders ranged from 1 to 10% (Figure 4.11a). The abundance of \sum_{LMW} PBDE potential degraders to abundance \sum_{HMW} PBDE potential degraders ($\sum_{LMW/HMW}$ PBDE potential degraders

ratio) ranged from 0.75 to 16 (Figure 4.11b). Only AOT surface sediment has $\sum_{\text{LMW/HMW}}\text{PBDE}$ potential degraders <1 . No observable trend was discerned between $\sum_{\text{LMW/HMW}}\text{PBDE}$ potential degraders ratio in relation to microbial community clustering (Figure 4.11b).

With the exception of ACL surface sediment, $\sum_{\text{LMW/HMW}}\text{PBDE}$ potential degraders ratio did not vary significantly with concentration and MLSR residual value (Figure 4.11c, e, and f) (Spearman coefficients between $\sum_{\text{LMW/HMW}}\text{PBDE}$ potential degraders ratio to $\sum_{\text{LMW/HMW}}\text{PBDE}$ potential degraders ratio and MLSR residual values are -0.05 and 0.10 for all surface sediments and excluding ACL, respectively), nor with homolog 1 to 6 composition ($\sum_{\text{H1-6Br}}\text{PBDEs}$) (Figure 4.11d) (Spearman coefficients between $\sum_{\text{LMW/HMW}}\text{PBDE}$ potential degraders ratio to $\sum_{\text{H1-6Br}}\text{PBDEs}$ are of -0.06 and 0.15 for all surface sediments and excluding ACL, respectively). The trends observed in Figure 4.11c and f suggest that the higher abundance of $\sum_{\text{LMW}}\text{PBDE}$ potential degraders does not correlate to decreasing $\sum_{\text{H1-6Br}}\text{PBDEs}$ debromination. Further, the lack of correlation between PBDE MLSR residual values and $\sum_{\text{LMW/HMW}}\text{PBDE}$ potential degraders suggests that increased abundance of $\sum_{\text{LMW}}\text{PBDE}$ potential degraders does not enhance the dehalogenation of LMW PBDE congeners in any observable way. This is in contrast to expectation from laboratory scale experiments.^(102,103,108) While *in-situ* microbial facilitated PBDE degradation is possible in the surface sediments, it does not appear to favor the formation of LMW PBDE congeners. This unexpected trend could arise from several reasons; the possibility may be low concentrations of PBDE congeners amenable to dehalogenation, and low bioavailability due to solid phase binding, and/or sediment column properties that do not support degradation such as lack of electron donors.

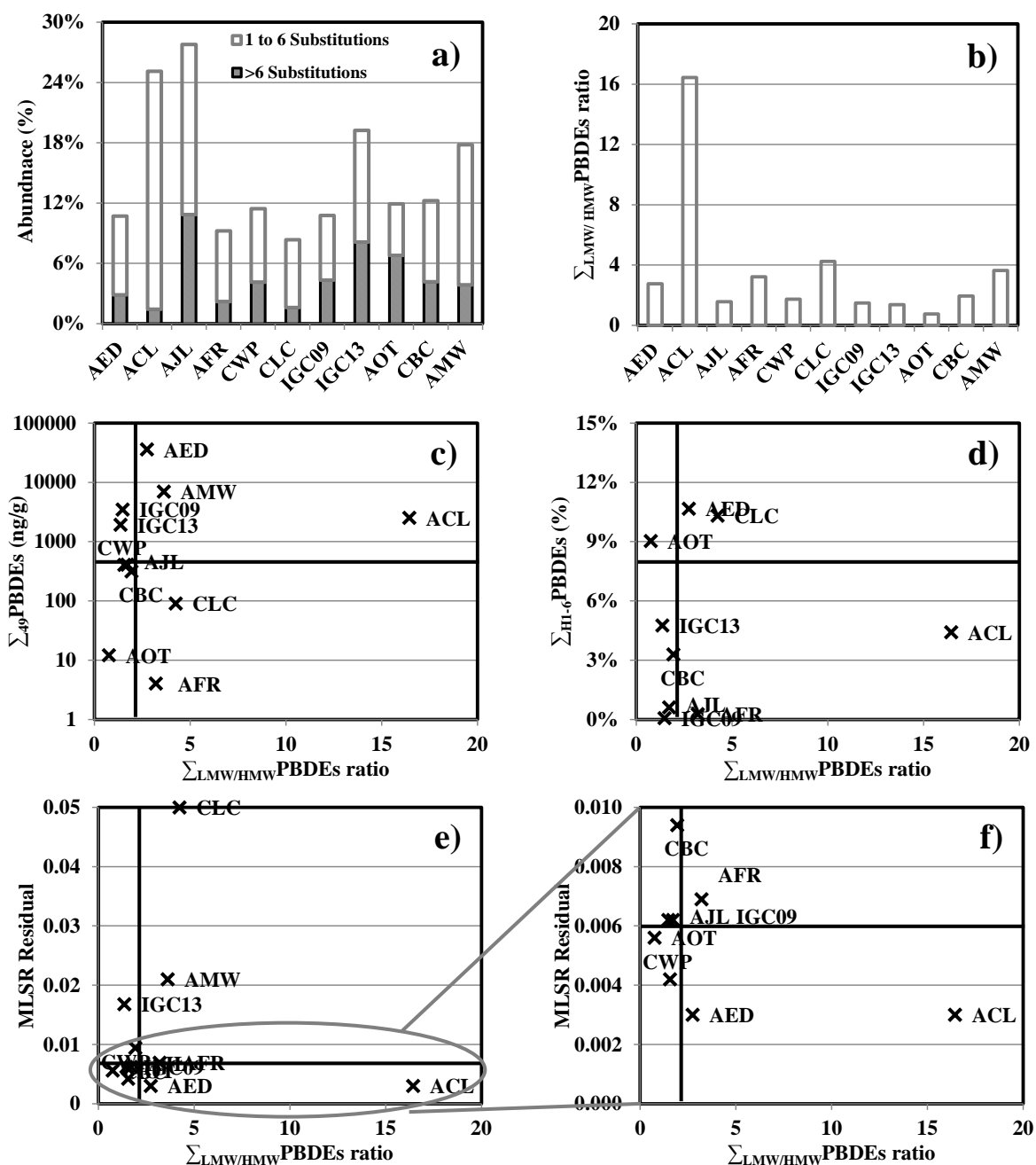


Figure 4.11: a) Abundance of \sum_{LMW} PBDE and \sum_{HMW} PBDE potential degraders, b) \sum_{LMW}/\sum_{HMW} PBDE potential degraders ratio, c) \sum_{49} PBDEs concentration versus \sum_{LMW}/\sum_{HMW} PBDE potential degraders, d) \sum_{H1-6} PBDEs versus \sum_{LMW}/\sum_{HMW} PBDE potential degraders, e) MLSR residual value versus \sum_{LMW}/\sum_{HMW} PBDE potential degraders, and f) a scale-up of the region surrounded by bold grey oval in e) in all surface sediments. In c) through f), vertical bold lines represent the 50th percentile value of ratio of \sum_{1-6Br} PBDE potential degraders over $\sum_{>6Br}$ PBDE potential degraders and horizontal lines represent the 50th percentile value of \sum_{LMW}/\sum_{HMW} PBDE potential degraders ratio, \sum_{H1-6} PBDEs composition, and MLSR residual value (e-f). Note the different scales on the x and y-axes.

Abundance of microbial class OTUs capable of PCB degradation ranged from ~10 to 27% and increased in the order of AMW (10%) < IGC09 (10%) < ACL (10%) < AED (13%) < AFR (13%) < AOT (16%) < AJL (17%) < CWP (20%) < CBC (21%) < CLC (21%) < IGC13 (2 %) (Figure 4.12a). With the exception of IGC09 surface sediment, Chicago and IGC13 surface sediments have much higher abundances of potential PCB degraders relative to AR surface sediments suggesting that PCB degraders are enriched in the Chicago metropolitan sediments due to the higher \sum_{132} PCBs concentrations. Similar to the case with PBDEs, there was a general trend of increasing abundance of potential PCB degraders with increased \sum_{132} PCBs concentrations and MLSR residual values (Spearman coefficients for \sum_{132} PCBs and abundance of potential PCB degraders are -0.2 and 0.33 for all surface sediments and excluding IGC09; Spearman coefficients for PCB MLSR residual and abundance of potential PCB degraders are -0.14, 0.08, and 0.23 for all surface sediments, excluding AOT, and excluding AOT and CLC, respectively). This trend is denoted by the grey dotted oval in Figure 4.12b and c.

Most microbial PCB degradation studies in the literature focused on degradation of LMW PCB homologs.^(73-75,77-79,82,83,89-91) In contrast, relatively little information is available on the degradation of HMW PCB congeners; therefore, abundance of potential PCB degraders was not further evaluated by chlorine substitution degradation capability.

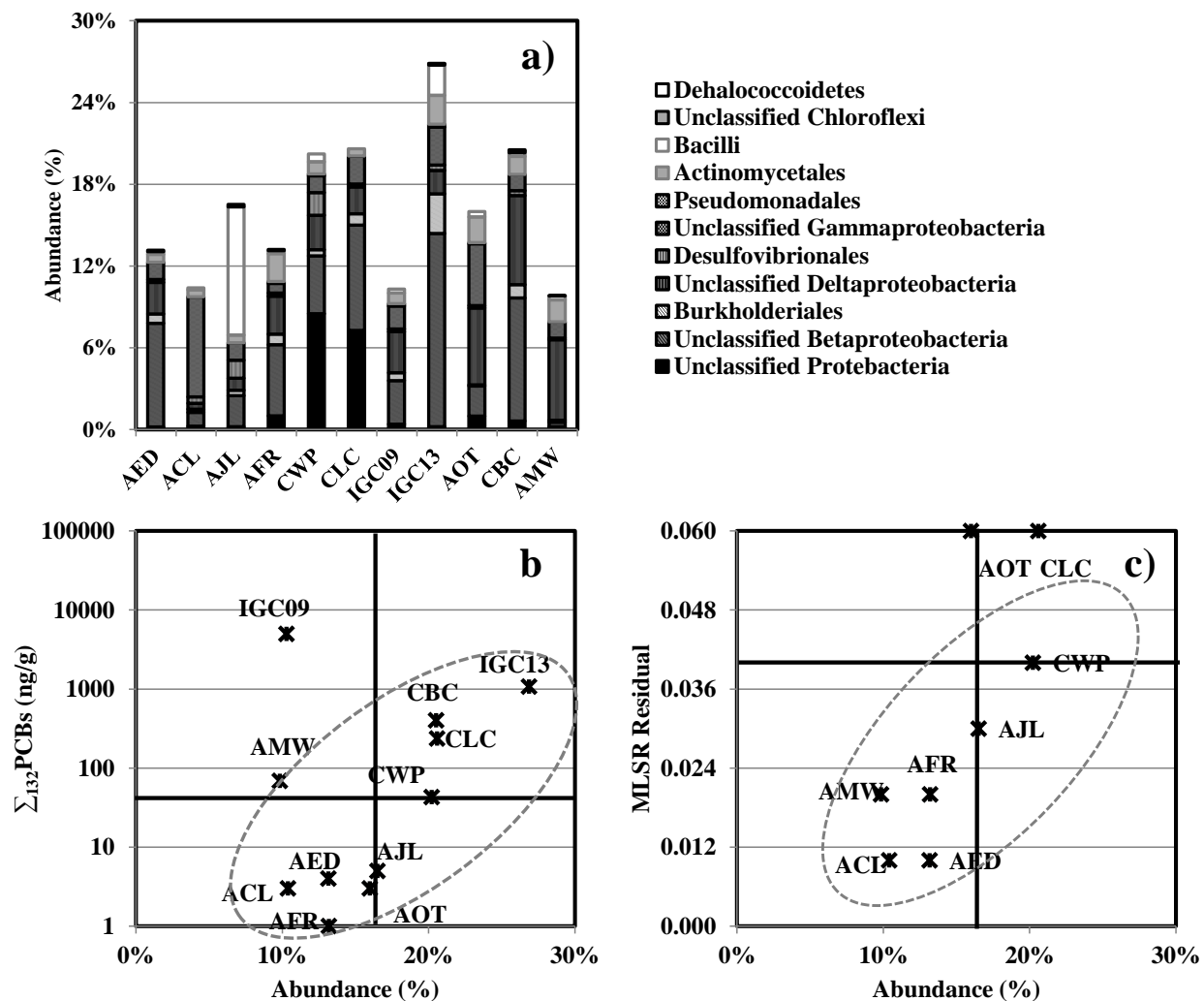


Figure 4.12: a) Abundance of potential PCB degraders by the microbial class operational taxonomic unit (OTU) level, b) Σ_{132} PCBs concentration and abundance of potential PCB degraders, and c) PCB MLSR residual value and abundance of potential PCB degraders in all surface sediments. Note that surface sediments in a) were arranged by hierarchical cluster map in Figure 4.7. In b) and c), vertical bold lines represent the 50th percentile value of PBDE potential degraders abundance and horizontal lines represent the 50th percentile value for Σ_{132} PBDEs concentrations and MLSR residual values, respectively, in all surface sediments.

In Figure 4.13, the abundance of both potential PBDE and PCB degraders in the surface sediments were compared. Generally, the surface sediments have roughly equal ratio of potential PBDE

degraders to potential PCB degraders. ACL and AJL surface sediments have lower than a 2:1 ratio while AMW surface sediment has a slightly higher than 2:1 ratio.

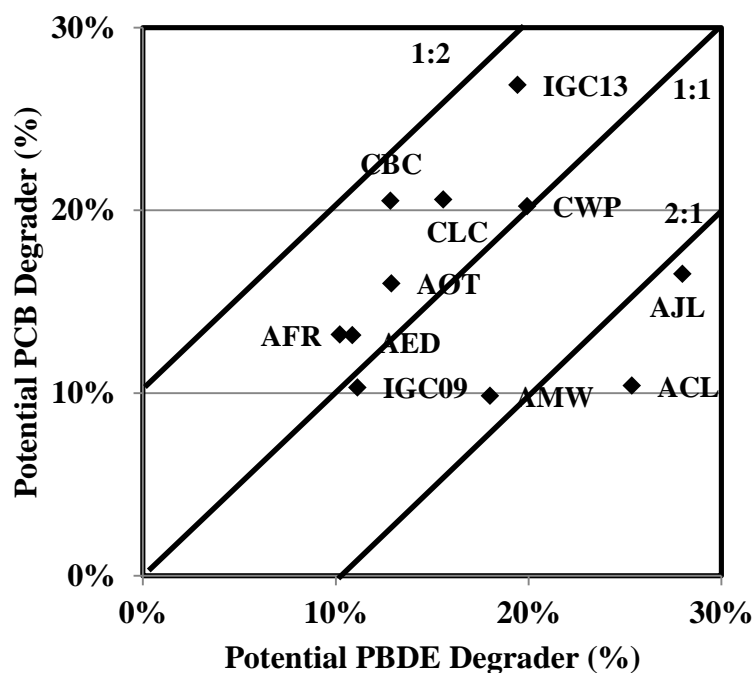


Figure 4.13: Abundance of potential PBDE and PCB degraders OTUs in all surface sediments. Also shown are the 1:2, 1:1 and 2:1 slopes as bold lines.

4.4.1.7. Composition of Unclassified *Bacteria* In Surface Sediments

Among the most striking features observed in the microbial community structure of the surface sediments was the large abundance of unclassified *Bacteria*. Figure 4.14a shows the distribution of unclassified *Bacteria* in all surface sediments. Overall, the unclassified *Bacteria* ranged from 34 to 5% in increased order of AMW (38%) < CWP (39%) < AOT (41%) < IGC13 (42%) < CBC (45%) < AJL (46%) < CLC (47%) < AFR (48%) < IGC09 (50%) < (AED 53%) < ACL (53%). A very interesting trend is the increased in abundance of unclassified *Bacteria* with decreased alpha diversity (Figure 4.14b). Although some surface sediments such as AED and ACL have low microbial diversity (Figures 4.2 and

4.3), a large fraction of the total bacterial community is not yet identified suggesting that the microbial diversity in these surface sediments could be largely underestimated. While increased in the unclassified *Bacteria* abundance was observed along with increasing \sum_{49} PBDEs concentration, the opposite was true for \sum_{132} PCBs concentration (Spearman coefficients between abundance and \sum_{49} PBDEs are -0.03 and 0.37 for all surface sediments and excluding AMW, respectively; Spearman coefficients between abundance and \sum_{132} PCBs are -0.07 and 0.29 for all surface sediments and excluding IGC09, respectively). These trends were noted by the bold dotted grey oval in Figure 4.14a and c. Generally, increased in the unclassified *Bacteria* abundance corresponded with a decrease in the PBDE MLSR residual values (Figure 4.14e), whereas no trend was apparent between unclassified *Bacteria* abundance and PCB MLSR residual values (Spearman coefficient between abundance to PBDE and PCB residual values are -0.02 and 0.41, respectively) (Figure 4.14f). The increased in unclassified *Bacteria* abundance with increased \sum_{49} PBDEs concentrations suggest that high PBDE levels may select for these unclassified *Bacteria*; however, given that the unclassified *Bacteria* abundance decreased with increased PBDE MLSR residual value suggests that these unclassified *Bacteria* are not active PBDE dehalorespirers. The decrease in unclassified *Bacteria* abundance with increasing \sum_{132} PCBs levels was unexpected. As previously shown in Tables 4.4 and 4.5, PBDE and PCB degraders generally share the same phylogenetic root, suggesting that phylogenetically close microorganisms can adapt to both PBDEs and PCBs. Therefore, if the PBDE contamination provided a niche environment for the enrichment of these unclassified *Bacteria*, PCBs also would be expected to have the same effect on the unclassified *Bacteria*, which does not appear to be the case.

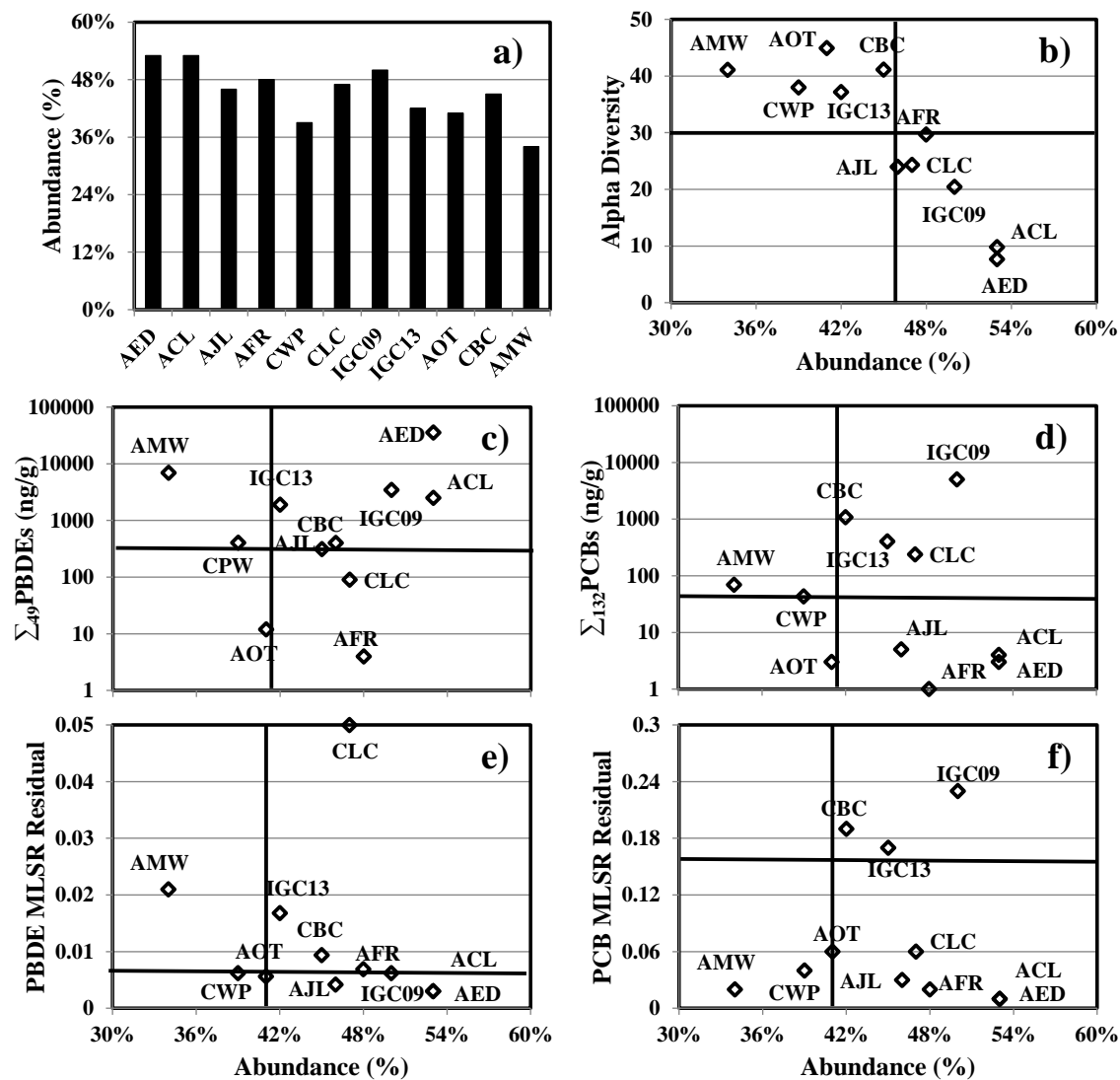


Figure 4.14: a) Abundance of unclassified *Bacteria*, b) microbial alpha diversity as a function of unclassified *Bacteria* abundance, c) Σ_{49} PBDEs concentration as a function of unclassified *Bacteria* abundance d) Σ_{132} PCBs concentration as a function of unclassified *Bacteria* abundance, e) PBDE MLRS residual value versus unclassified *Bacteria* abundance, and f) PCB MLRS residual value versus unclassified *Bacteria* abundance in all surface sediment samples. Y-axes on c) and d) are in log scale. Note the different scale of the x and y-axes.

4.4.2. Indigenous Microbial Community In AMW Sediment Segments

4.4.2.1. General Sequence Statistics

Pyrosequencing data from the AMW sediment segments submitted to MGRAST were also subjected to similar quality control as the pyrosequencing data from the surface sediments. Quality control details were previously provided in Chapter 4.4.1.1. Table 4.6 is a summary of pre- and post-quality control sequence statistics for microbial community in AMW sediment segments. In all AMW sediment segments, $\geq 96\%$ of the total sequence submitted to MGRAST passed quality control.

Table 4.6: Sequence statistic for AMW sediment segments.

Site	bp ⁽¹⁾	Pre-quality Control			bp ⁽¹⁾	Post-quality Control		
		Sequence	Length	GC(%) ⁽²⁾		Sequence	Length	GC(%) ⁽²⁾
AMW 2010	1407698	3339	421 \pm 74	55 \pm 2	1375415	3184	431 \pm 60	56 \pm 3
AMW 2005	1266461	2983	424 \pm 69	56 \pm 2	1228057	2822	435 \pm 52	56 \pm 3
AMW 2000	1806166	4612	391 \pm 46	56 \pm 2	1686827	4317	390 \pm 44	56 \pm 3
AMW 1995	1730652	4174	414 \pm 71	56 \pm 2	1691845	3987	424 \pm 61	56 \pm 3
AMW 1990	1840200	4404	417 \pm 67	56 \pm 2	1800550	4211	427 \pm 54	56 \pm 2
AMW 1985	1296905	3105	417 \pm 75	56 \pm 2	1264292	2936	430 \pm 57	56 \pm 2
AMW 1980	1380473	3429	402 \pm 84	55 \pm 2	1336033	3175	420 \pm 63	56 \pm 2
AMW 1975	3925355	9852	398 \pm 86	55 \pm 2	3786252	9049	418 \pm 64	55 \pm 2
AMW 1970	2417370	5998	403 \pm 65	55 \pm 2	2362540	5712	413 \pm 2	55 \pm 2
AMW 1965	1508169	3687	409 \pm 81	54 \pm 2	1461597	3426	426 \pm 30	54 \pm 3

⁽¹⁾ Basepairs

⁽²⁾ Guanine and cytosine nucleic acid composition

4.4.2.2. Microbial Species Richness and Abundance In AMW Sediment Segments

The AMW sediment segments were divided into two categories that spanned a 15 and 25 year period. The upper sediment segments consisted of AMW 2010 to AMW 1995, and the lower sediment segments consisted of AMW 1990 to AMW 1965. The rarefaction curves for the microbial community in the AMW sediment segments are shown in Figure 4.15a-b. Generally, the upper sediment segments did not reach a plateau. More sequences were sampled in the lower sediment segments allowing the rarefaction curve to approach the plateau. The rarefaction curves shown in Figure 4.15a-b indicate that substantial microbial species richness has not yet been sampled in the upper AMW sediment segments, whereas the microbial species richness was relatively better captured in the lower AMW sediment segments.

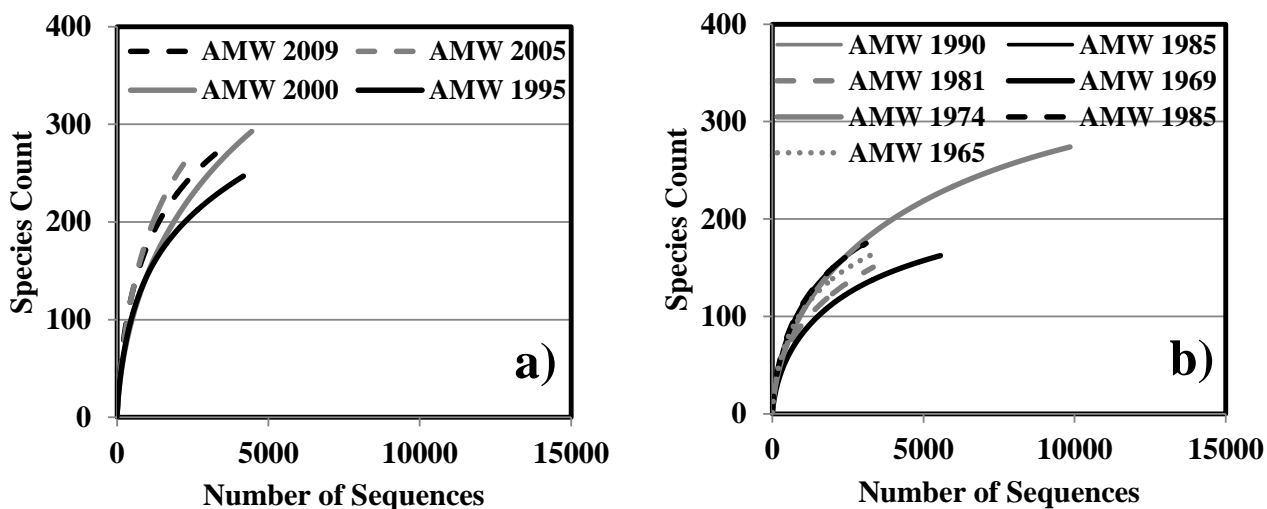


Figure 4.15: Rarefaction curves for a) the upper AMW sediment segments with sediment age of 2010 to 1995, and b) the lower AMW sediment segments with sediment age of 1990 to 1965.

The microbial species abundance as defined by the alpha diversity for the AMW sediment segments is shown in Figure 4.16. Generally, microbial diversity decreased with increased sediment

depth and age in the AMW sediment segment ($R^2=0.84$). This is consistent with the trend in rarefaction curves in Figure 4.15a-b which indicated that lower sediment segments better capture the microbial species richness relative to the upper sediment segments; fewer species in the lower sediment segments resulted in better capture of species richness. Other studies characterizing soil and sediment microbial community composition also reported decreased microbial diversity with increasing sediment depth and age.⁽²¹⁹⁻²²¹⁾

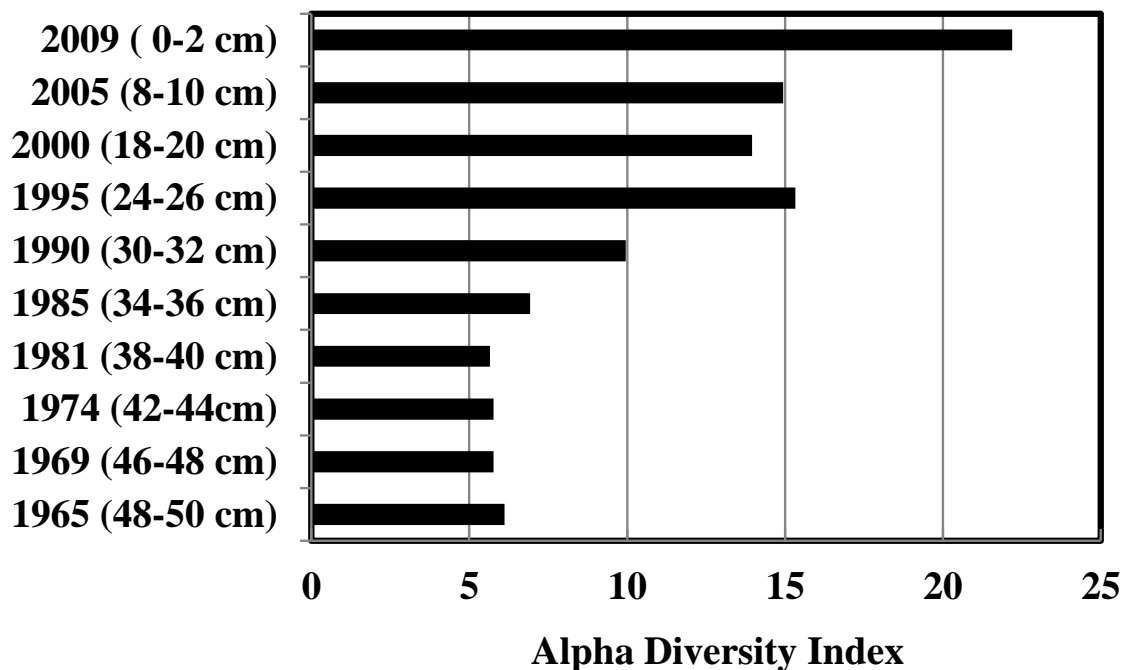


Figure 4.15: Microbial species diversity as measured by the alpha diversity index for the AMW sediment segments.

4.4.2.3. Dominant Microbial Community Composition In AMW Sediment Segments

Similar definition of dominant microbial phyla was used as described previously as having >1% of the total bacterial abundance. The dominant microbial phyla in AMW 2010 (0-2cm) was previously detailed in section 4.4.1.3.1. Figure 4.16a-i provides an overview of the microbial community in AMW

sediment segments. The complete microbial distributions in all AMW sediment segments are shown in Table C4.2 in the appendix.

AMW 2005 (8-10cm): The RDP databases identified 18 phyla (excluding unclassified bacteria) in AMW 2005 sediment; among these phyla, six were dominant. Phylum dominance increased in the order of *Cyanobacteria* < *Actinobacteria* < *Spirochaetes* < *Firmicutes* < *Bacteroidetes* < *Proteobacteria*. In the *Proteobacteria* phylum, class increased in the order of unclassified *Proteobacteria* < *Gammaproteobacteria* < *Alphaproteobacteria*=*Epsilonproteobacteria* < *Deltaproteobacteria* < *Betaproteobacteria*. Microbial classes in the *Bacteroidetes* phylum increased in the order of *Cytophagia* < unclassified *Bacteroidetes* < *Sphingobacteriia* < *Flavobacteriia*. Microbial classes increased in the order of *Negativicutes* < *Erysipelotrichi* < *Bacilli* < *Clostridia* in the *Firmicutes* phylum. The *Spirochaetes* phylum was composed entirely of *Spirochaetia* class whereas the *Actinobacteria* and *Cyanobacteria* phyla were not further classified into smaller microbial taxa.

AMW 2000 (18-20cm): Excluding unclassified *Bacteria*, phylum dominance in the AMW 2000 sediment segment increased in the order of *Spirochaetes* < *Firmicutes* < *Bacteroidetes* < *Proteobacteria*. Microbial classes abundance in the *Proteobacteria* phylum increased in the order of unclassified *Proteobacteria* < *Alphaproteobacteria* < *Epsilonproteobacteria* < *Gammaproteobacteria* < *Betaproteobacteria*. The *Bacteroidetes* phylum was composed of *Cytophagia* < unclassified *Bacteroidetes* < *Sphingobacteriia* < *Flavobacteriia* < *Bacteroidia* class in increased order. Microbial classes abundance in the *Firmicutes* phylum increased in the order of *Negativicutes* < *Erysipelotrichi* < *Bacilli* < *Clostridia*.

AMW 1995 (24-26 cm): Phylum dominance increased in the order of *Actinobacteria* < *Bacteroidetes* < *Firmicutes* < *Proteobacteria*. In the *Proteobacteria* phylum, microbial classes abundance increased in the order of unclassified *Proteobacteria* < *Epsilonproteobacteria* < *Alphaproteobacteria* < *Gammaproteobacteria* < *Betaproteobacteria*. Microbial classes abundance increased in the order of

Spingobacteria < *Cytophagia* < *Bacteroidia* < *Flavobacteriia*. The *Clostridia* class in the *Firmicutes* phylum was substantially larger than the *Bacilli*, *Negativicutes*, and *Erysipelotrichi*. The *Spirochaetes* phylum was composed entirely of the *Spirochaetia* class. The *Actinobacteria* phylum was not further classified into microbial classes.

AMW 1990 (30-32 cm): Phylum abundance increased in the order *Actinobacteria* < *Firmicutes* < *Verrucomicrobia* < *Bacteroidetes* < *Proteobacteria* in AMW 1990 sediment segment. In the *Proteobacteria* phylum, microbial classes abundance increased in the order of unclassified *Proteobacteria* < *Epsilonproteobacteria* < *Alphaproteobacteria* < *Gammaproteobacteria* < *Deltaproteobacteria* < *Betaproteobacteria*. In the *Bacteroidetes* phylum, microbial classes increased in the order of unclassified *Bacteroidetes* < *Cytophagia* < *Flavobacteriia* < *Bacteroidia* < *Sphingobacteriia*. The *Opitutae* microbial class was highly dominant over the *Verrucomicrobiae* microbial class in the *Verrucomicrobia* phylum. The *Firmicutes* phylum consisted only of the *Clostridia* class. The phylum *Actinobacteria* was not classified into microbial class but consisted of sequences from the *Actinomycetales* order which was highly dominant over the *Bifidobacteriales* order.

AMW 1985 (34-36 cm): Excluding unclassified *Bacteria*, there were 14 phyla in the AMW 1985 (34-36cm) sediment segment. Of these, five phyla were dominant. Phylum dominance increased in the order of *Spirochaetes* < *Actinobacteria* < *Firmicutes* < *Bacteroidetes* < *Proteobacteria*. The *Spirochaetes* phylum consisted entirely of the microbial class *Spirochaetia*. The microbial class in the *Actinobacteria* phylum consisted of the *Actinomycetales* order which was further classified into *Dermatophilaceae* = *Corynebacteriaceae* < *Segniliparaceae* < *Nocardiaceae* < *Frankiaceae* < *Intrasporangiaceae* < *Nocardiopsaceae* < *Streptomycetaceae* microbial classes. Microbial classes abundance in the *Bacteroidetes* phylum increased in the order of *Cytophagia* < *Flavobacteriia* < *Bacteroidia* < *Sphingobacteriia*. The *Proteobacteria* phylum consisted of the *Epsilonproteobacteria* < *Deltaproteobacteria* < *Alphaproteobacteria* < *Gammaproteobacteria* < *Betaproteobacteria*.

AMW 1980 (38-40 cm): Excluding unclassified *Bacteria*, five of the twelve microbial phyla were dominant in the AMW 1980 sediment segment. Dominant phylum increased in the order of *Firmicutes* < *Nitrospirae* < *Bacteroidetes* < *Proteobacteria*. The *Clostridia* microbial class was more dominant than the *Bacilli* microbial class in the *Firmicutes* phylum. The *Nitrospirae* phylum consisted of *Nitrospira* class only. The microbial classes in the *Bacteroidetes* phylum increased in the order of *Cytophagia* < *Flavobacteriia* < *Bacteroidia* < *Sphingobacteriia*. In the *Proteobacteria* phylum, microbial classes abundance increased in the order of unclassified *Proteobacteria* < *Alphaproteobacteria* < *Epsilonproteobacteria* = *Deltaproteobacteria* < *Gammaproteobacteria* < *Betaproteobacteria*.

AMW 1975 (42-44 cm): Dominant phylum increased in the order of *Firmicutes* < *Bacteroidetes* < *Proteobacteria*. The *Proteobacteria* phylum consisted of six microbial classes which increased in the order of unclassified *Proteobacteria* < *Deltaproteobacteria* < *Alphaproteobacteria* < *Gammaproteobacteria* < *Epsilonproteobacteria* < *Betaproteobacteria*. Microbial classes in the *Bacteroidetes* phylum increased in the order of unclassified *Bacteroidetes* < *Cytophagia* < *Bacteroidia* < *Flavobacteria* < *Sphingobacteriia*. The microbial classes increased in the order of *Negativicutes* < *Bacilli* < *Clostridia* in the *Firmicutes* phylum.

AMW 1970 (46-48 cm): Dominant phylum increased in the order of *Bacteroidetes* < *Firmicutes* < *Proteobacteria*. The *Proteobacteria* phylum consisted of microbial classes that increased in the order of *Alphaproteobacteria* < unclassified *Proteobacteria* < *Deltaproteobacteria* < *Gammaproteobacteria* < *Epsilonproteobacteria* < *Betaproteobacteria*. Microbial classes in the *Firmicutes* phylum increased in the order of *Negativicutes* < *Bacilli* < *Clostridia*. The *Bacteroidetes* phylum consisted of microbial classes with increasing abundance in the order of *Cytophagia* < unclassified *Bacteroidetes* < *Bacteroidia* < *Sphingobacteriia* < *Flavobacteriia*.

AMW 1965 (48-50 cm): Dominant phylum in the AMW 1965 sediment segment increased in the order of *Spirochaetes* < *Bacteroidetes* < *Firmicutes* < *Proteobacteria*. The *Proteobacteria* phylum consisted of

unclassified *Proteobacteria* < *Deltaproteobacteria* < *Gammaproteobacteria* < *Alphaproteobacteria* < *Betaproteobacteria* < *Epsilonproteobacteria*. Microbial classes abundance in the *Firmicutes* phylum increased in the order of *Negativicutes* < *Bacilli* < *Clostridia*. The *Bacteroidetes* consisted of unclassified *Bacteroidetes* < *Cytophagia* < *Bacteroidia* < *Sphingobacteriia* in increasing order of microbial class. The *Spiricohaetes* phylum consisted entirely of the *Spirochaetia* microbial class.

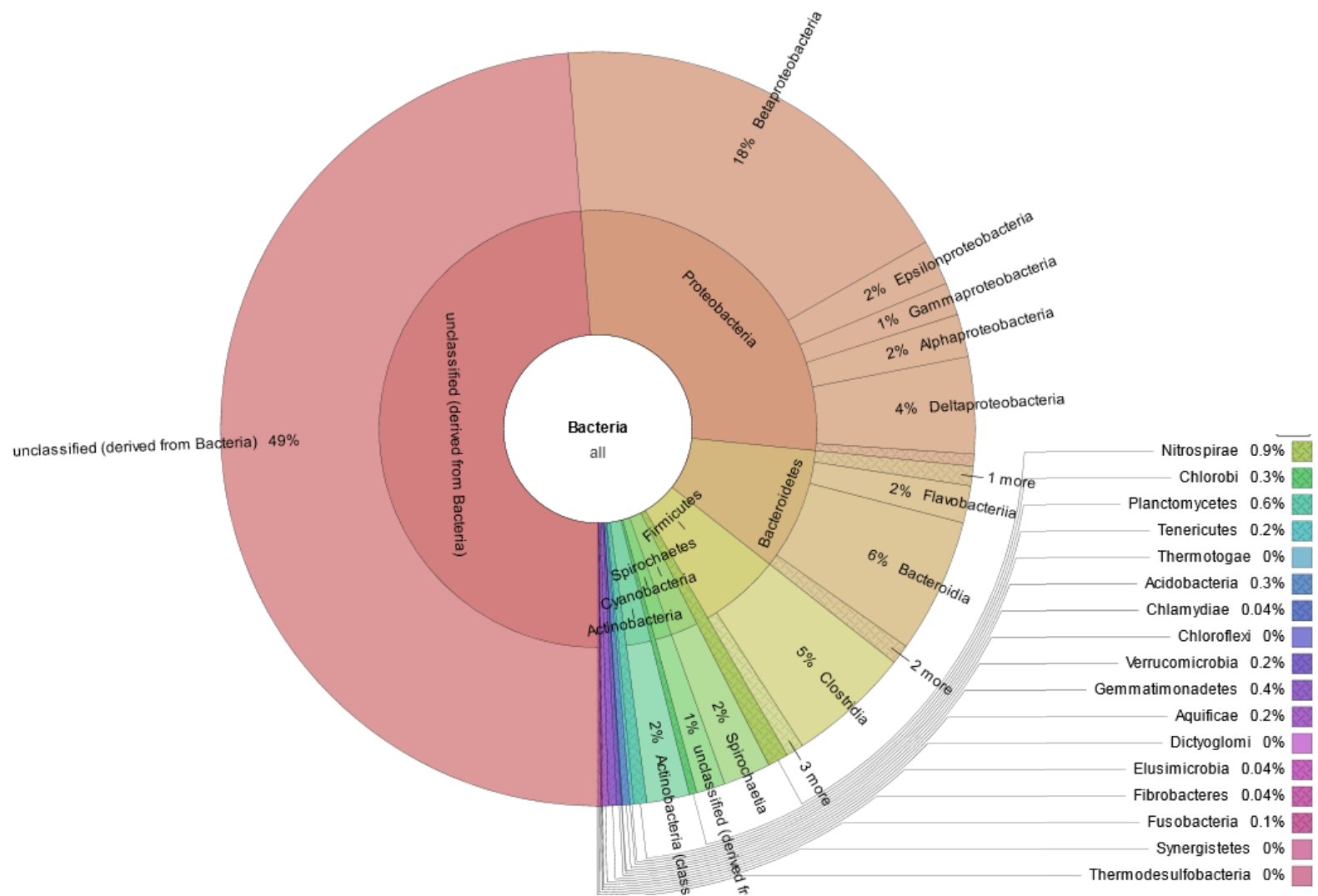


Figure 4.16a: Overview of the microbial community in AMW 2005(8-10cm) sediment segments as identified by the RDP database.⁽²⁰⁴⁾ Visualization was generated in Krona.⁽²⁰⁵⁾

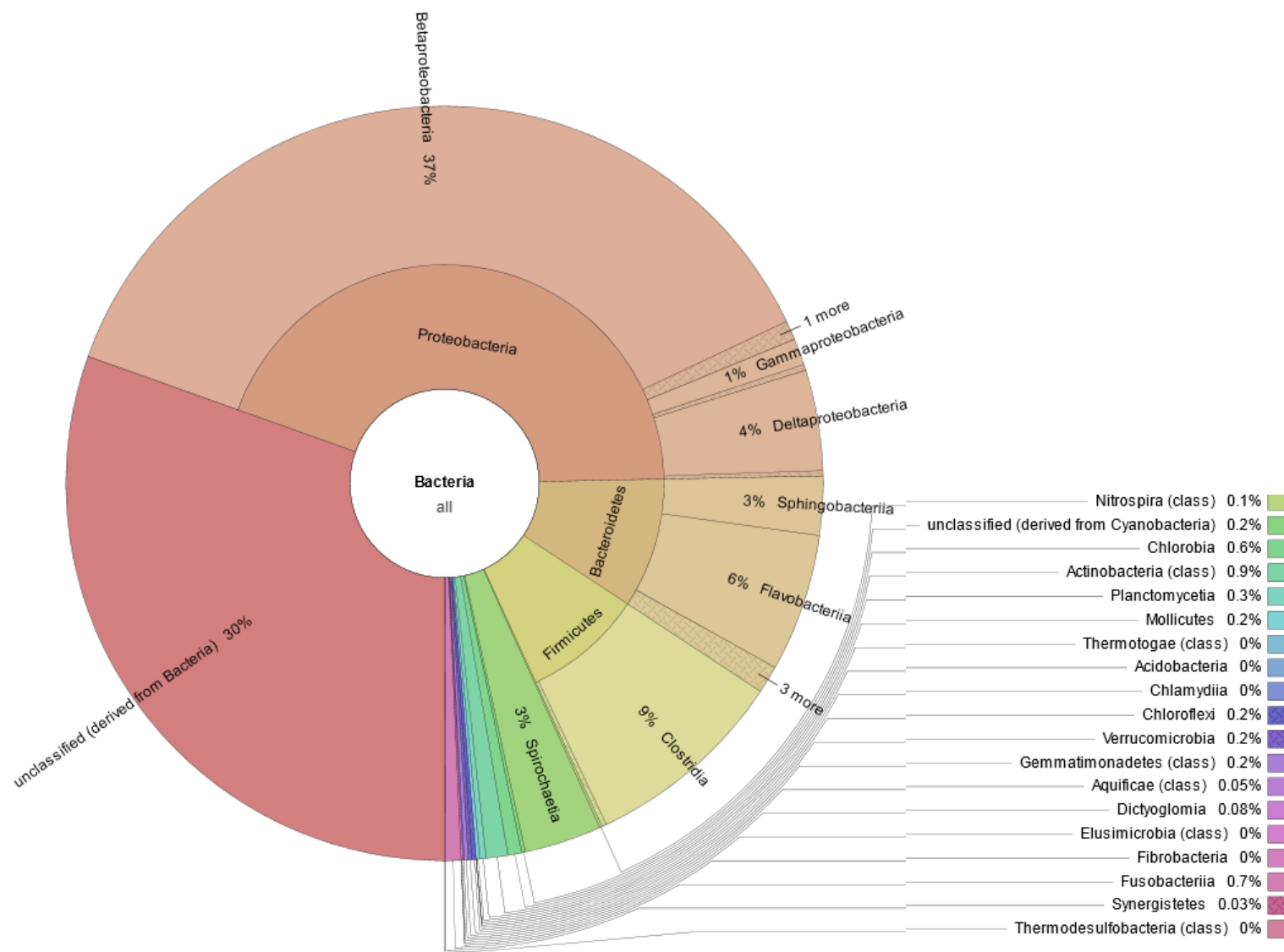


Figure 4.16b: Overview of the microbial community in AMW 2000 (18-20cm) sediment segments as identified by the RDP database.⁽²⁰⁴⁾
Visualization was generated in Krona.⁽²⁰⁵⁾

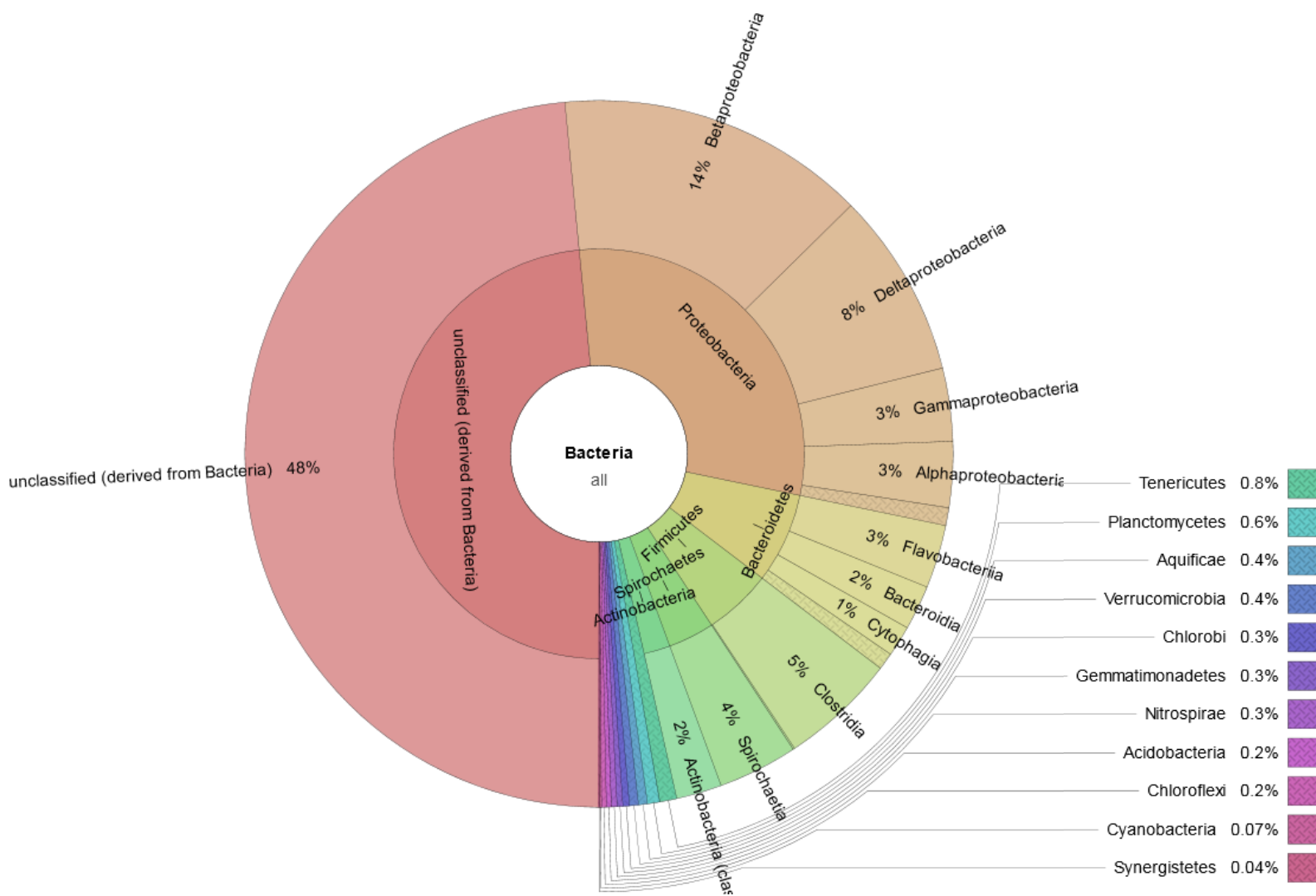


Figure 4.16c: Overview of the microbial community in AMW 1995 (24-26cm) sediment segments as identified by the RDP database.⁽²⁰⁴⁾ Visualization was generated in Krona.⁽²⁰⁵⁾

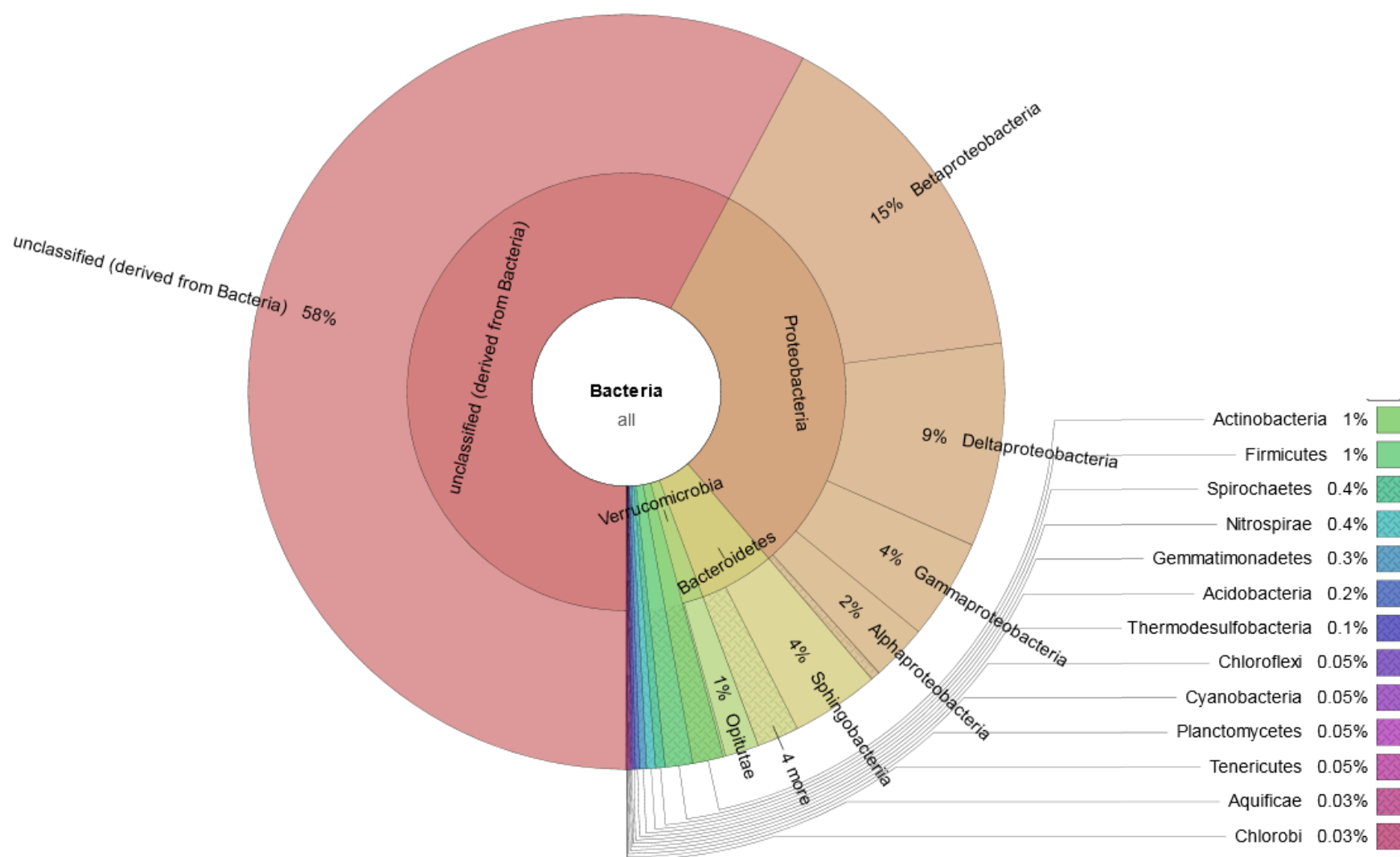


Figure 4.16d: Overview of the microbial community in AMW 1990 (30-32cm) sediment segments as identified by the RDP database.⁽²⁰⁴⁾ Visualization was generated in Krona.⁽²⁰⁵⁾

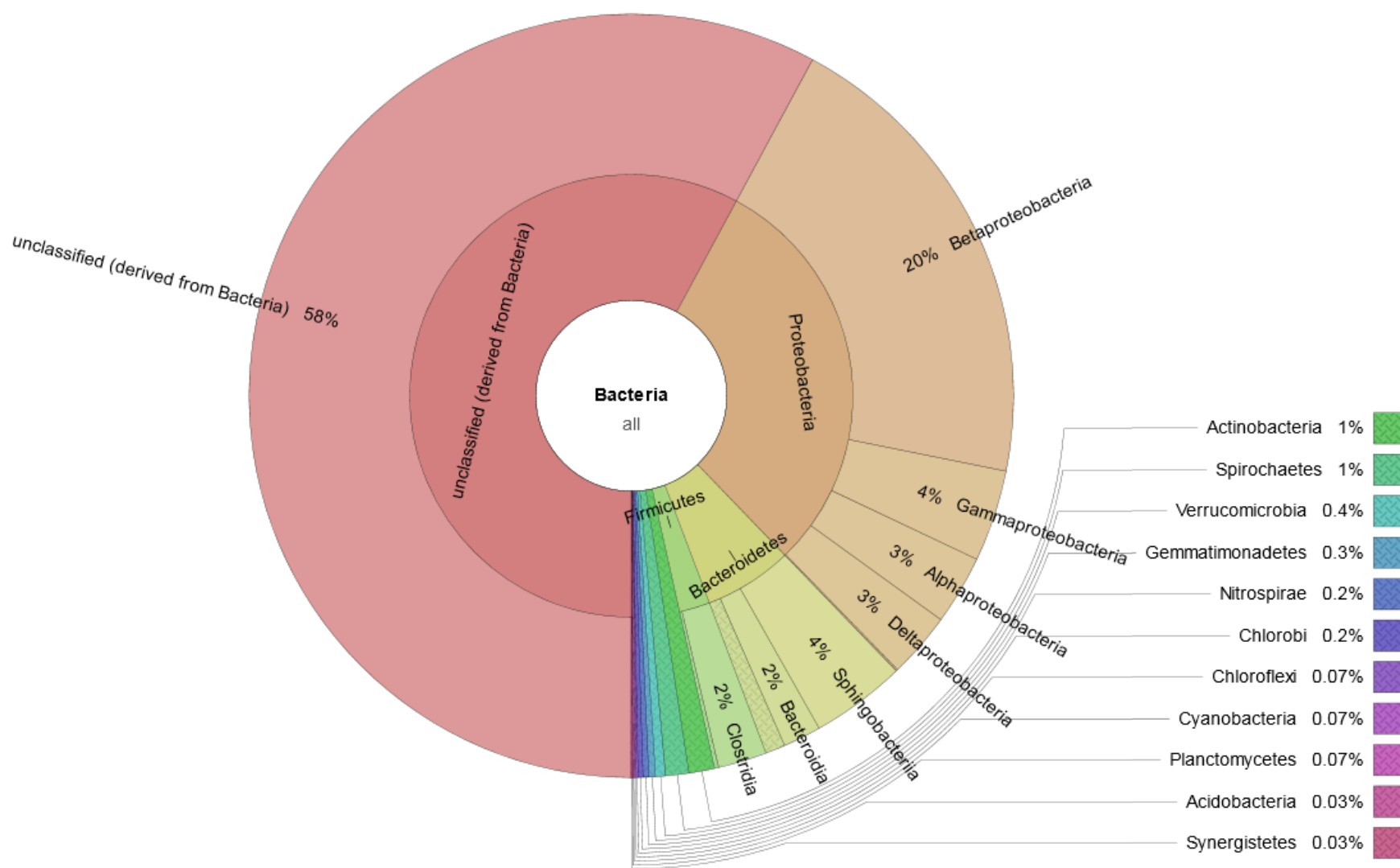


Figure 4.16e: Overview of the microbial community in AMW 1985 (34-36cm) sediment segments as identified by the RDP database. ⁽²⁰⁴⁾
 Visualization was generated in Krona. ⁽²⁰⁵⁾

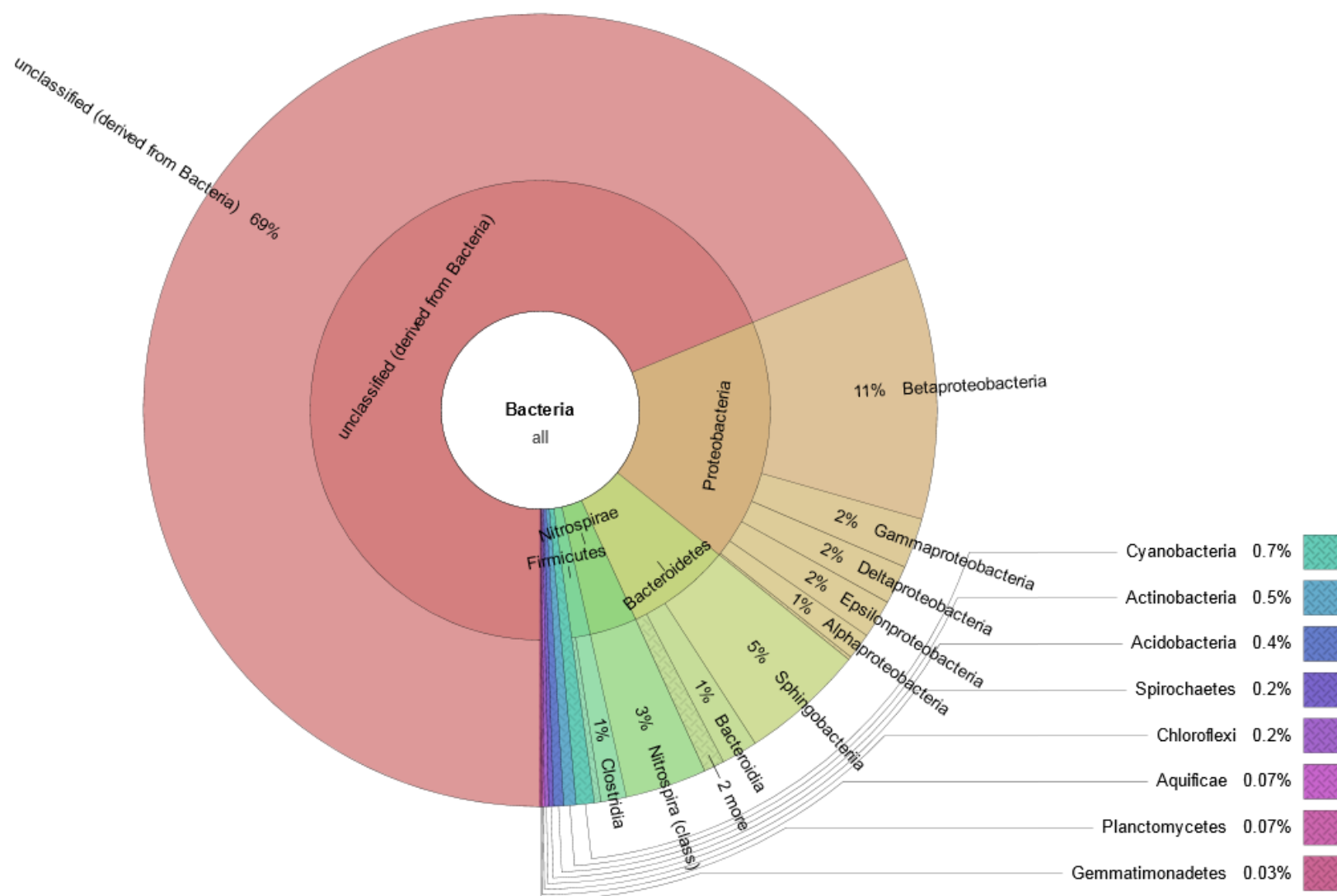


Figure 4.16f: Overview of the microbial community in AMW 1980 (38-40cm) sediment segments as identified by the RDP database. ⁽²⁰⁴⁾
 Visualization was generated in Krona. ⁽²⁰⁵⁾

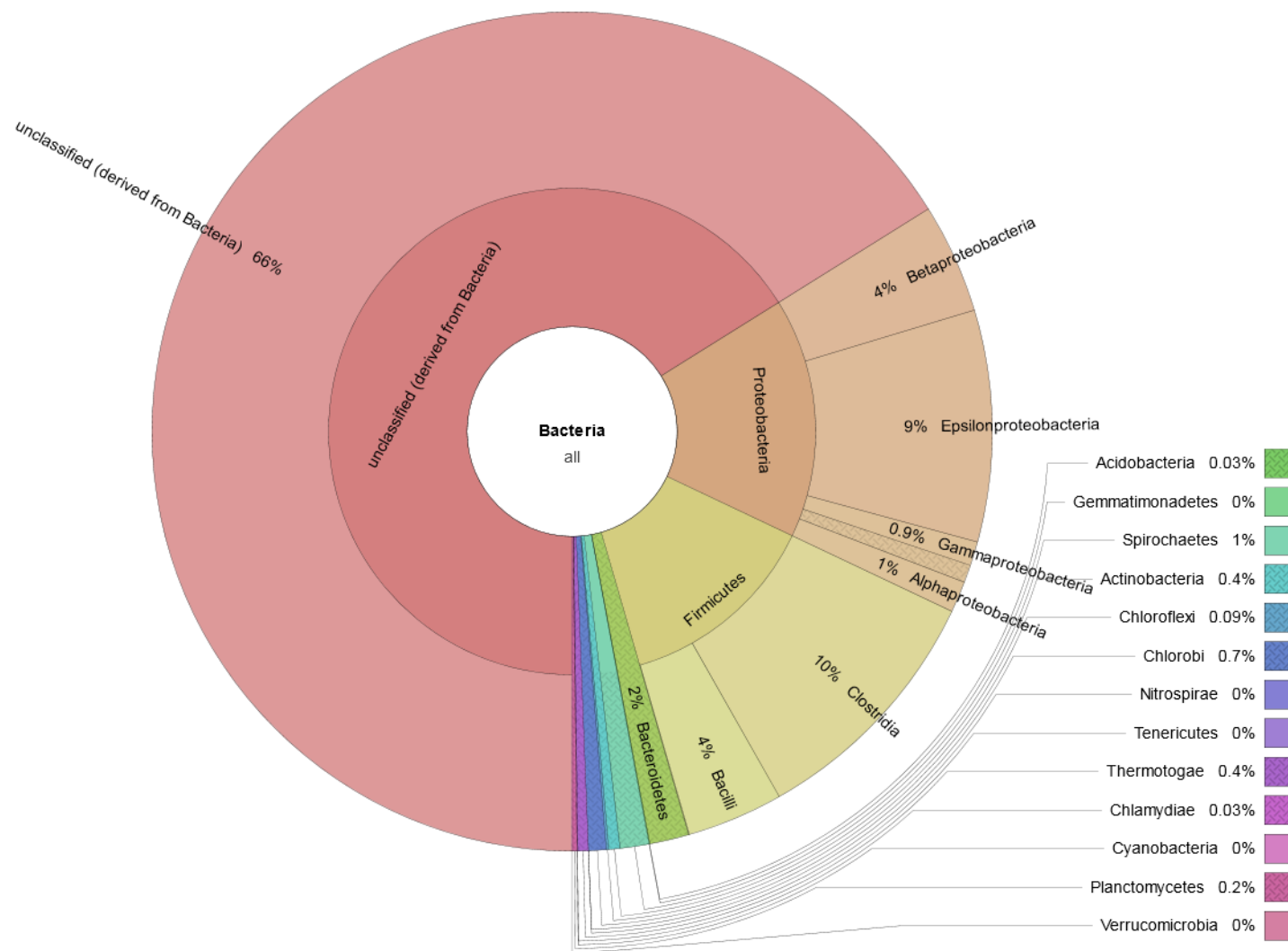


Figure 4.16g: Overview of the microbial community in AMW 1975 (42-44cm) sediment segments as identified by the RDP database. ⁽²⁰⁴⁾
Visualization was generated in Krona. ⁽²⁰⁵⁾

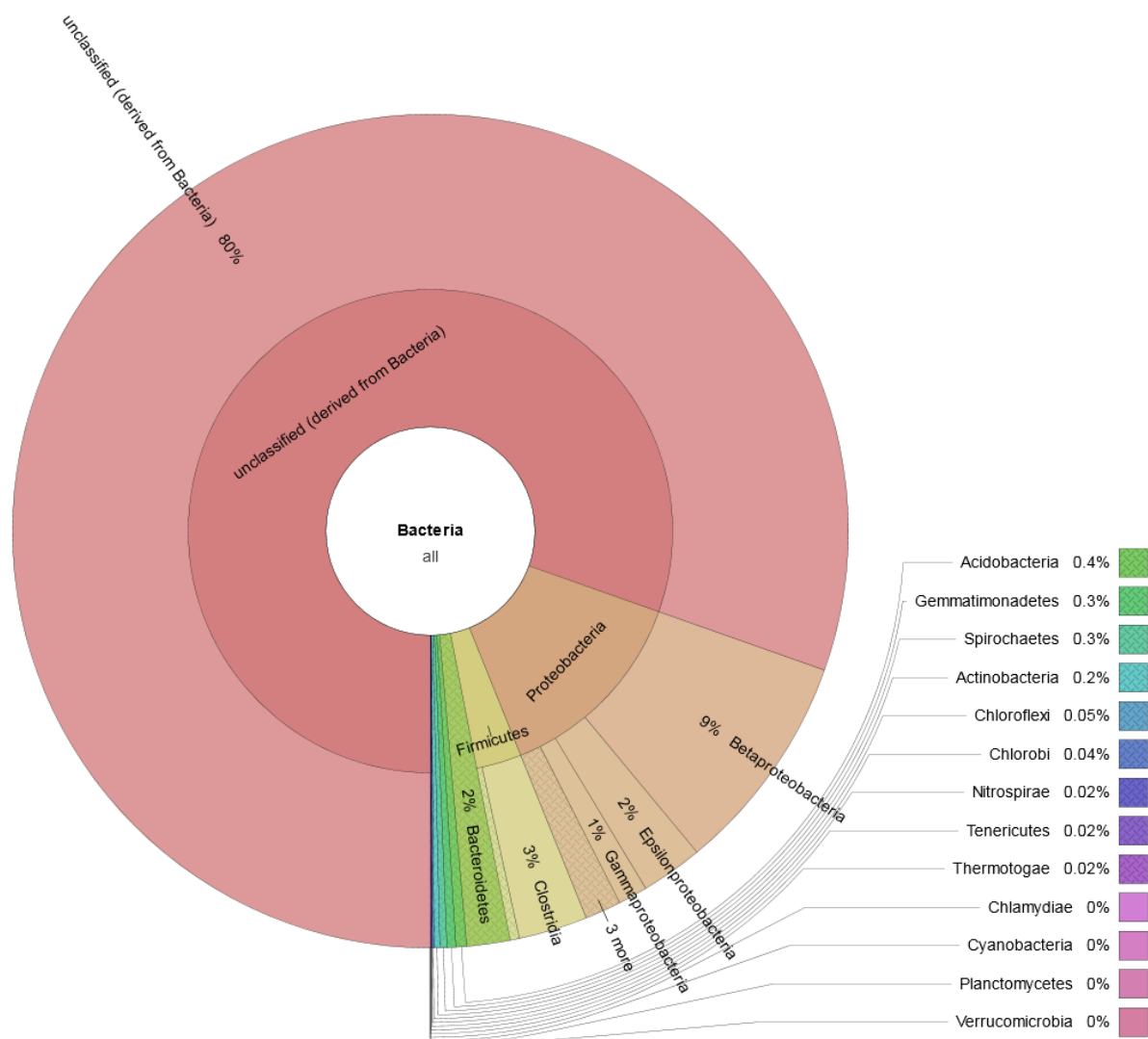


Figure 4.16h: Overview of the microbial community in AMW 1970 (46-48cm) sediment segments as identified by the RDP database. ⁽²⁰⁴⁾
Visualization was generated in Krona. ⁽²⁰⁵⁾

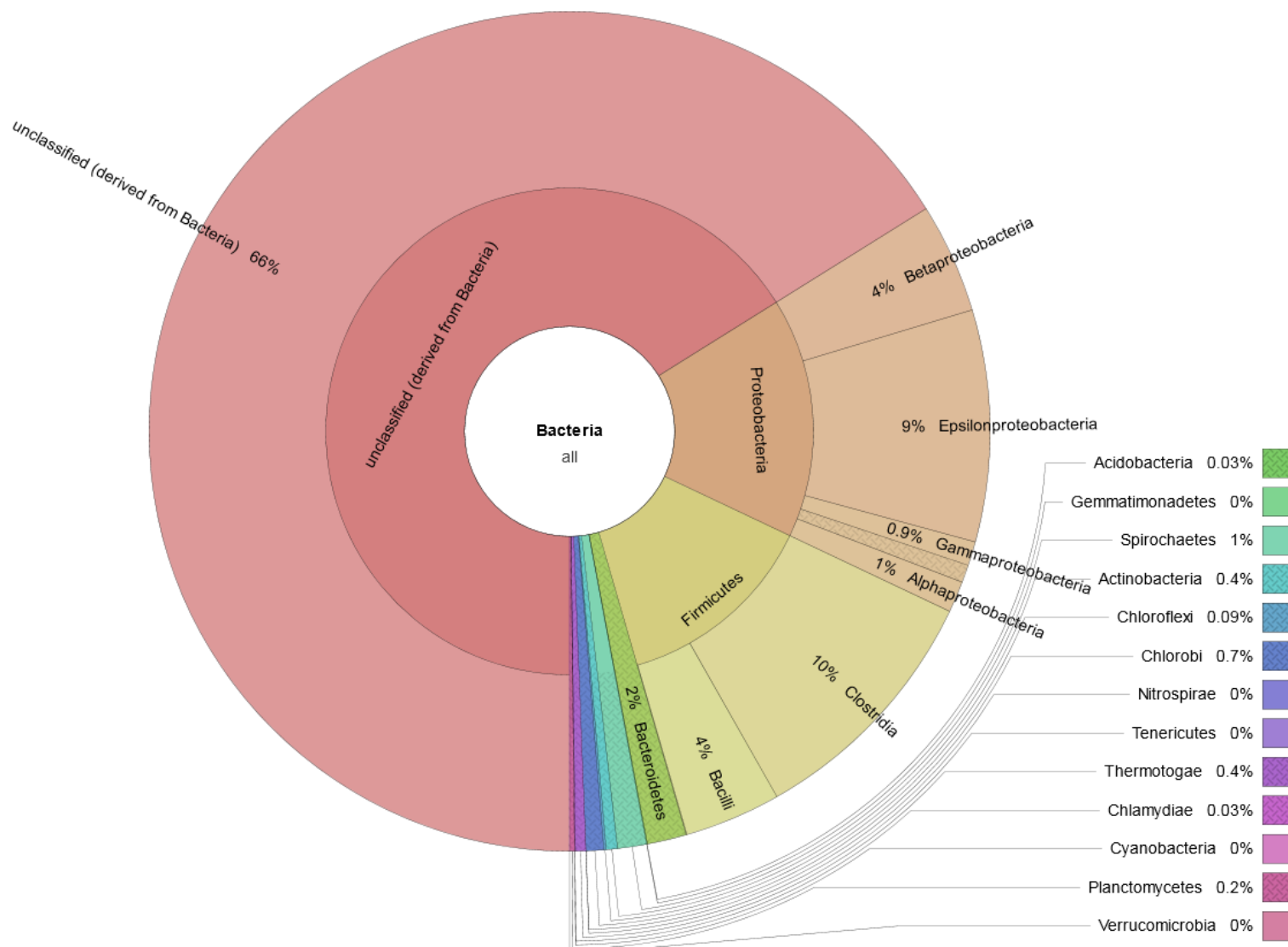


Figure 4.16i: Overview of the microbial community in AMW 1965 (48-50cm) sediment segments as identified by the RDP database. ⁽²⁰⁴⁾
 Visualization was generated in Krona. ⁽²⁰⁵⁾

4.4.2.4. Similarity in Microbial Community Composition In AMW Sediment Segments

A hierarchical cluster map measuring the similarity in AMW sediment segments is shown in Figure 4.17. The Manhattan method was used to predict clustering and calculate clustering distance. The PCA of the microbial community structure is also included in Figure 4.18. The hierarchical analysis grouped the AMW sediment segments into two main clusters; the first group included AMW 2010 to AMW 1995 sediment segments and the second group included the remaining AMW sediment segments.

The grouping of microbial community composition by sediment depth or age observed in the hierarchical cluster map in Figure 4.17 was also reflected in the PCA results (Figure 4.18). Generally, upper sediment segments (AMW 2010 to AMW 1995) were low in factors one and two while deeper sediment segments (AMW 1990 to AMW 1965) were higher in factors one and two. Within each group cluster (i.e, grouping of AMW 2010 to AMW 1995 and AMW 1990 to AMW 1965), factor one values increased with increased sediment depth and age. The inverse trend was observed for factor two. Although both hierarchical cluster map and PCA were performed independent of sediment age and depth, both resulted in similar microbial community grouping based on sediment age or depth. This provided strong support for the hypothesis of gradual changes in microbial community composition with sediment age or depth in AMW sediment segments

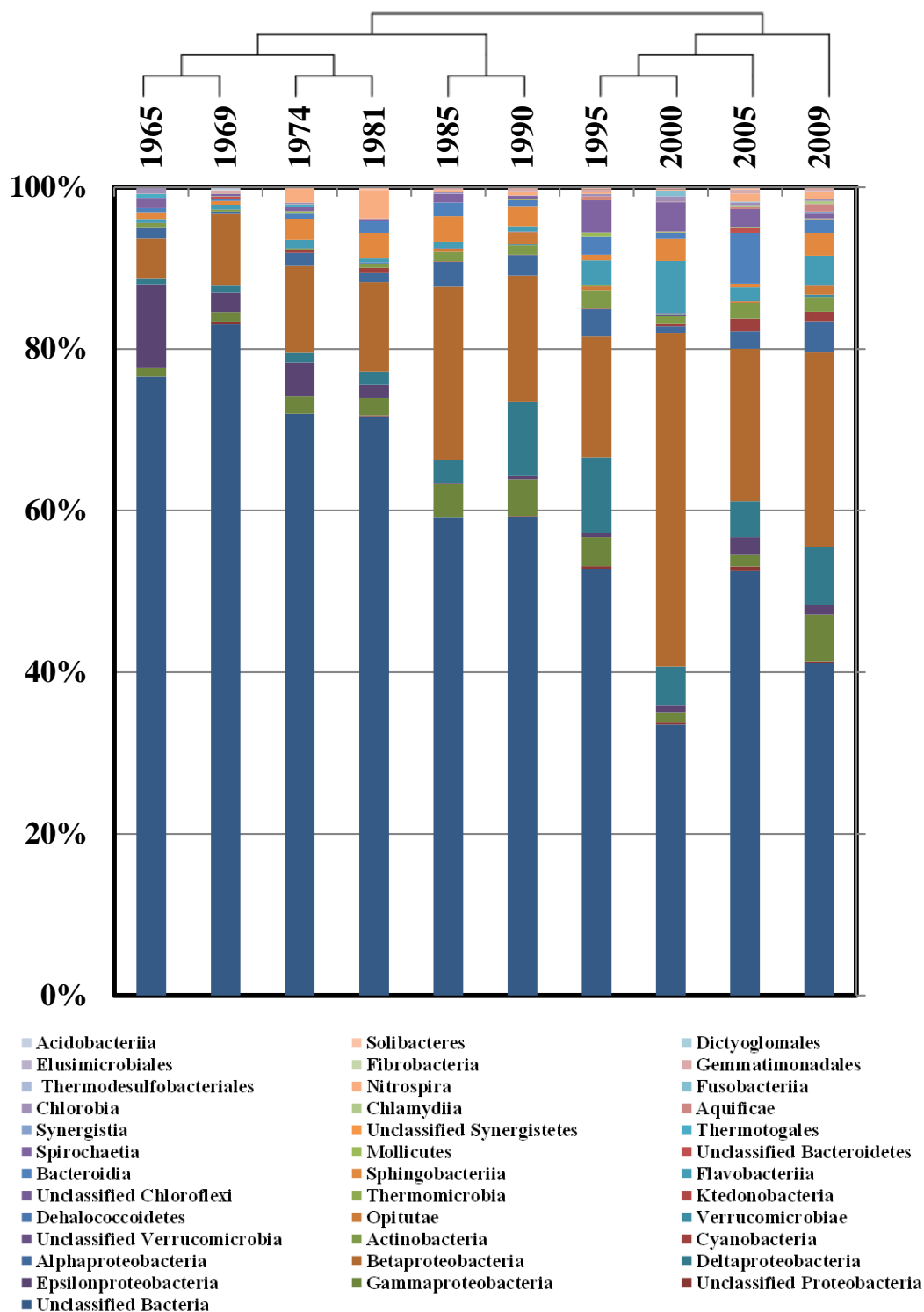


Figure 4.17: Hierarchical cluster map analysis performed in MGRAST⁽²⁰³⁾ and microbial community structure at the class operational taxonomic unit (OTU) level for AMW sediment segments. The hierarchical cluster map used the Manhattan method to cluster and measure distance or similarity in the microbial community structure in the surface sediments.

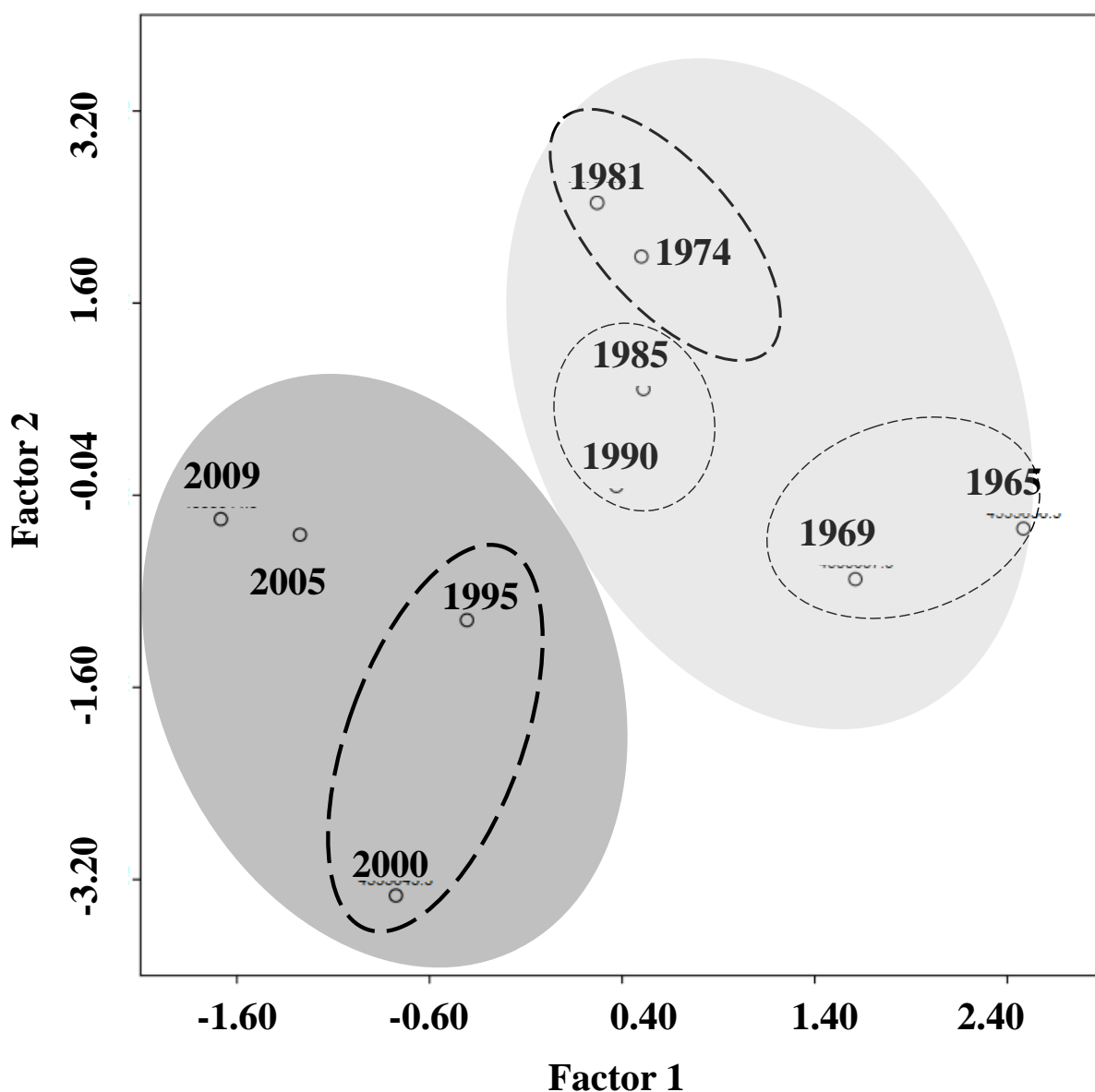


Figure 4.18: Principal component analysis (PCA) of the microbial community structure in AMW sediment segments. Dotted hollow spheres reflect the grouping based on microbial community clustering (Figure 4.17). Dark grey shaded area represents the upper sediment segments (AMW 2010 to AMW 1995) and light grey shaded area represents the lower sediment segments (AMW 1990 to AMW 1965).

Temporal Changes In The Microbial Community Composition Of AMW Sediment Columns.

Gradual changes in microbial community composition with increased sediment depth or age was observed in the AMW sediment segments. Similar to the case of the surface sediments, unclassified

Bacteria in the AMW sediment segment was present in high abundance ranging from 30 to 80% and generally increased with increased sediment depth and age. More detailed discussion on the unclassified *Bacteria* distribution is provided in Chapter 4.4.2.6. The *Proteobacteria* phylum abundance ranged from 13 to ~45%. Unlike unclassified *Bacteria*, the *Proteobacteria* phylum decreased with increased sediment age or depth. Within the *Proteobacteria* phylum, the *Gammaproteobacteria* and *Deltaproteobacteria* microbial classes increased with sediment age or depth, whereas the inverse trend was observed for *Epsilonproteobacteria*. Other bacterial phyla that decreased with increasing sediment depth or age were the *Actinobacteria*, *Planctomycetia*, *Bacteroidetes*, and *Aquificae*. No observable trend was observed with *Acidobacteria*, *Cyanobacteria*, *Tenericutes*, *Synergistetes*, *Chlamydia*, *Chlorobia*, *Thermodesulfobacteria*, and *Gemmatimonadales* phyla. The *Spirochaetia* and *Verrucomicrobia* phyla were only enriched in the upper sediment segments and generally not present in the lower sediment segments. On the other hand, the *Thermotogales* and *Nitrospira* phyla were only enriched in the three lowest sediment segments (AMW 1975, AMW 1970, and AMW 1965). Interestingly, *Cyanobacteria* phylum (phylum including photosynthetic bacteria) were found below sunlight penetration depth.

Previously, physico-chemical characterization in Chapter 3 revealed that the AMW sediment column generally has oxidation-reduction potential (ORP) levels consistent with a facultative metabolism (-20 to -80 mv) (Figure B3.3b). These sediments also have low sulfide concentrations in the surface sediments (~10 ppm) and relatively constant sulfide concentration between 2.5 to 11 cm and in deeper sediment segment (~25 and ~100 ppm, respectively) (Figure B3.4b). They also have a relatively constant wet and dry density (ρ_w and ρ_D of ~1 and 0.05 g/mL, respectively) with depth (Figure B3.5b) and high water content in all the sediment segments (>98%) (Figure B3.6b). The AMW sediment column also has high organic matter (OM) and organic carbon (OC) level that gradually decrease with increased sediment depth (160 to 320 mg/g and 240 to 480 mg/g for OC and OM, respectively) (Figure B3.7b), relatively low and constant BC concentration (<5 mg/g in all AMW sediment column) (Figure B3.8b), and homogenous grading of particle size distribution (PSD) with increased sediment depth (Figure B3.9b). They also have

increased BDE-209 concentrations (5666 and 48181 ng/g at the surface sediment and peak concentration, respectively) and increased composition of PBDE homologs 1-4, 5-7, and 8-9 concomitant with decreased composition of BDE-209 with depth,⁽¹⁵¹⁾ and decreased \sum_{132} PCBs concentrations with depth. It is possible that the adaptations of the *Spirochaetia* and *Verrucomicrobia* phyla, and the *Thermotogales* and *Nitrospira* phyla in the upper and lower AMW sediment segments, respectively were a response to changes in OM, OC, \sum_{49} PBDEs, or \sum_{132} PCBs. While no observable trend was observed in the *Chloroflexi* phylum, it was present in all AMW sediment segments and abundance reached up to 0.23%. The *Firmicutes* phylum abundance ranged from 1 to 10% and was present in all sediment segments.

4.4.2.5. Potential PBDE and PCB Degraders In AMW Sediment Segments

The abundance of microbial taxa with potential PBDE and PCB degradation capabilities (capabilities were inferred from demonstrated PBDE and PCB degradation under laboratory scale studies) was monitored to better understand the potential for microbial facilitated *in-situ* PBDE and PCB degradation. Abundance was also similarly evaluated at the microbial class OTU as was previously done in section 4.4.1.6.

Abundance of potential PBDE degraders in the AMW sediment segments ranged from 6 to 31%; the highest abundance was observed in AMW 2000 and the lowest abundance was observed in AMW 1990 (Figure 4.19a). The most dominant OTU was the unclassified *Betaproteobacteria* (Figure 4.10a). Unclassified *Betaproteobacteria* constituted 11 to 61% of the total potential PBDE degraders abundance in AMW sediment segment. The highest abundance of unclassified *Betaproteobacteria* was observed in AMW 2000. Additionally, *Burkholderiales*, *Campylobacterales*, *Clostridia*, and unclassified *Chloroflexi* OTUs were also present at the highest levels in segment AMW. Unclassified *Epsilonproteobacteria* and unclassified *Actinobacteria* phyla abundance decreased with increasing sediment depth and age. This is

consistent with the general trend of total *Epsilonproteobacteria* and total *Actinobacteria* phyla described previously in Section 4.4.2.4. The *Campylobacteriales* order was only enriched in the upper sediment segments (AMW 2009 to AMW 1990). No trend was observed in the distribution of unclassified *Alphaproteobacteria*, *Sphingomonadales*, and *Clostridia*. The *Bacilli* microbial order abundance was <1 % in all AMW sediment segments except in AMW 1965, where the abundance was ~4%. The unclassified *Proteobacteria*, unclassified *Actinobacteria*, and unclassified *Chloroflexi* phyla were only found in AMW 2005, AMW 1965, and AMW 2000 and AMW 1990, respectively. The *Dehalococcoidetes* microbial order was present in low amounts (<1%) in all AMW sediment segments except AMW 2005 and AMW 1990. Further observation indicated that the sequences in the *Dehalococcoidetes* class were not resolved at the smaller OTU (i.e., at the order, family, genus, and species level).

In contrast to the surface sediments, a general trend of decreasing abundance of potential PBDE degraders with increased \sum_{49} PBDEs concentration was observed (Spearman coefficients between abundance and \sum_{49} PBDEs are -0.3 and -0.44 for all AMW sediment segments and excluding AMW2000, respectively) (Figure 4.19b). AMW 2009, AMW 2000, and AMW 1965 have high abundance of potential PBDE degraders and low \sum_{49} PBDEs concentrations. AMW 2005, AMW 1974, and AMW 1969 have high potential PBDE degraders compositions and low \sum_{49} PBDEs concentrations. AMW 1995, AMW 1990, AMW 1985, and AMW 1981 have high potential PBDE degraders compositions and low \sum_{49} PBDEs concentrations. No AMW sediment segment has high potential PBDE degraders abundance and high \sum_{49} PBDEs concentration.

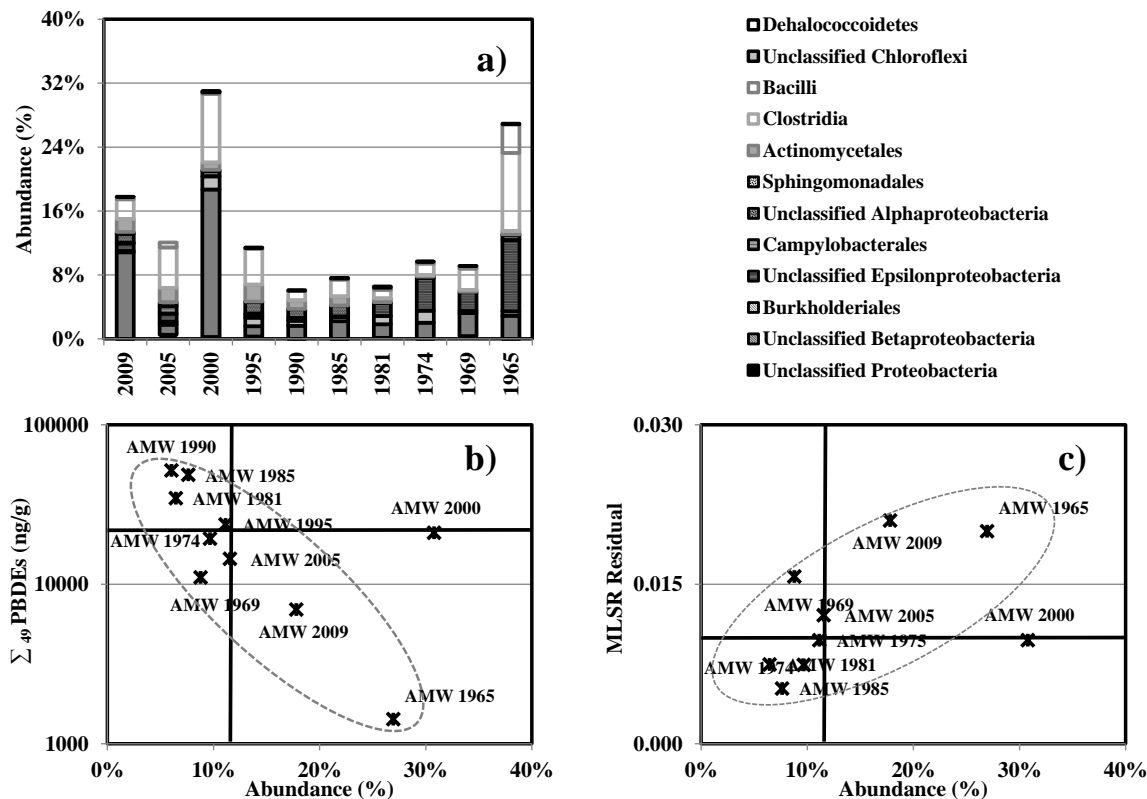


Figure 4.19: a) Abundance of potential PBDE degraders at the class operational taxonomic unit (OTU) level, b) Σ_{49} PBDEs concentration and total abundance of potential PBDE degraders, and c) PBDE MLSR residual value versus total abundance of potential PBDE potential degraders in AMW sediment segments. In b) and c), vertical bold lines represent the 50th percentile value of the potential PBDE degraders abundance and horizontal lines represent the 50th percentile value for Σ_{49} PBDEs concentration and MLSR residual value, respectively, in all AMW sediment segments.

In general, increased potential PBDE degraders abundance coincided with increased PBDE MLSR residual value (Spearman coefficient between abundance and PBDE MLSR is 0.39 for all AMW sediment segments) (Figure 4.19c). No AMW sediment segments have high abundance of potential PBDE degraders and low PBDE MLSR residual value. AMW 1995, AMW 1985, AMW 1981, and AMW 1974 have low abundance of potential PBDE degraders and low PBDE MLSR residual values. AMW 2005 and AMW 1969 have low abundance of potential PBDE degraders and high PBDE MLSR residual values. AMW 2009, AMW 2000, and AMW 1965 have high abundance of potential PBDE degraders and high PBDE MLSR residual values. The trend between PBDE MLSR residual value and potential PBDE degraders abundance observed in Figure 4.19c would be consistent with *in-situ* microbial facilitated

PBDE degradation. This trend suggest that the increased in PBDE MLSR residual values which indicated larger disparity between the three PBDE TMs to the sediment profile can be attributed to the increased PBDE dehalogenation by indigenous sediment microorganisms.

Abundance of \sum_{LMW} PBDE and \sum_{HMW} PBDE potential degraders are shown in Figure 4.20. Composition of \sum_{LMW} PBDE potential degraders ranged from 3 to 21%. The highest abundance was observed in AMW 2000 and the lowest in AMW 1981. Abundance of \sum_{HMW} PBDE potential degraders ranged from 2 to 22%; the highest abundance was observed in AMW 1965 and the lowest abundance was observed in AMW 1990. No observable trend in abundance of either \sum_{LMW} PBDE and \sum_{HMW} PBDE potential degraders were found with depth. Ratio of $\sum_{\text{LMW/HMW}}$ PBDE potential degraders ranged from 0.2 to 14.3%- the highest ratio was observed in AMW 2009 (surface sediment) and the lowest was observed in AMW 1965 (bottom sediment) (Figure 4.19b); in AMW 2005 to AMW 1985, the ratio increased with increasing sediment depth and age, whereas the ratio in AMW 1985 to AMW 1965 decreased with increasing sediment depth and age. In contrast to the surface sediments which have ratios of $\sum_{\text{LMW/HMW}}$ PBDE potential degraders >1 (except AOT), many AMW sediment segments have ratios <1, especially towards the bottom.

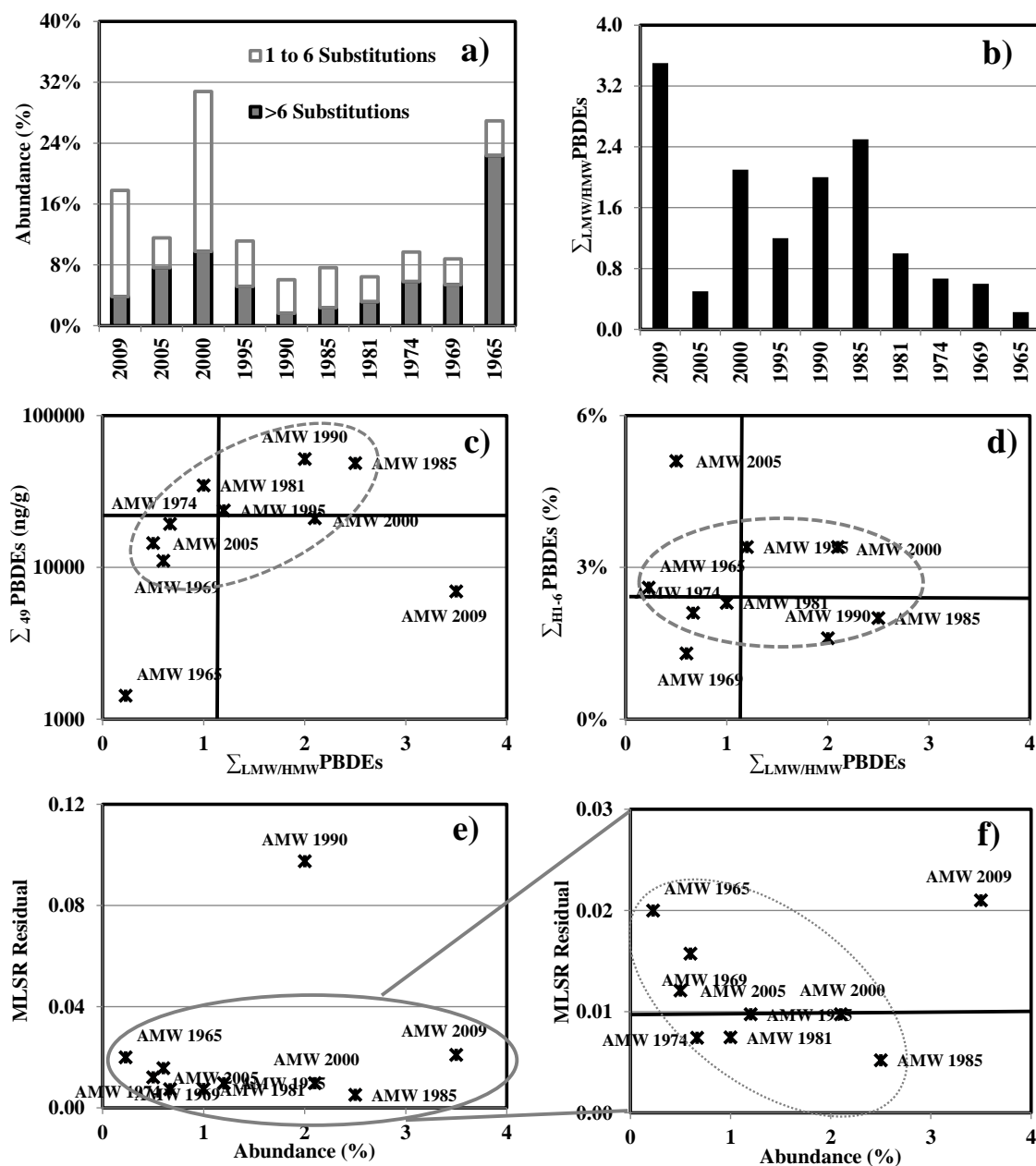


Figure 4.20: a) Abundance of \sum_{LMW} PBDE and \sum_{HMW} PBDE potential degraders, b) ratio of \sum_{LMW}/\sum_{HMW} PBDE potential degraders, c) \sum_{49} PBDEs concentration versus ratio of \sum_{LMW}/\sum_{HMW} PBDE potential degraders, d) \sum_{HI-6} PBDEs composition versus ratio of \sum_{LMW}/\sum_{HMW} PBDE potential degraders, e) PBDE MLSR residual value versus ratio of \sum_{LMW}/\sum_{HMW} PBDE potential degraders, and f) a scale-up of the region surrounded by bold grey oval in e) for all AMW sediment segments. In c) through f), vertical bold lines represent the 50th percentile value of ratio of \sum_{LMW}/\sum_{HMW} PBDE potential degraders and horizontal lines represent the 50th percentile value for \sum_{49} PBDEs concentration (c), \sum_{HI-6} PBDEs composition (d), and MLSR residual value (e-f). Y-axes in c) is in the log scale. Note the different scales on the x and y-axes in c) through f).

With the exception of AMW 2009 and AMW 1965, increased in $\sum_{49}\text{PBDEs}$ concentration corresponded with increased in the ratio of $\sum_{\text{LMW/HMW}}\text{PBDE}$ potential degraders (Spearman coefficients between $\sum_{49}\text{PBDEs}$ and $\sum_{\text{LMW/HMW}}\text{PBDE}$ are -0.001, 0.11, and 0.37 for all AMW sediment segments, excluding AMW 1965, and excluding AMW 1965 and AMW 2000, respectively) (Figure 4.19c). A trend of decreasing abundance of $\sum_{\text{H1-6}}\text{PBDEs}$ with increasing ratio of $\sum_{\text{LMW/HMW}}\text{PBDE}$ potential degraders was observed (Spearman coefficient between $\sum_{\text{H1-6}}\text{PBDEs}$ and $\sum_{\text{LMW/HMW}}\text{PBDE}$ is 0.21 for all AMW sediment segments)(Figure 4.19d). A lower $\sum_{\text{H1-6}}\text{PBDEs}$ abundance would be expected due to degradation of PBDE with 1 to 6 bromine substitutions by LMW PBDE degraders. With some exception (AMW 2009 and AMW 1990), increased ratio of $\sum_{\text{LMW/HMW}}\text{PBDE}$ potential degraders corresponded to decreased MLSR residual value (Spearman coefficients between $\sum_{\text{LMW/HMW}}\text{PBDE}$ and MLSR residual values are -0.04, 0.19, and 0.28 for all AMW sediment segments, excluding AMW 1990, and excluding AMW 1990 and AMW 2000, respectively) (Figure 4.19 e and f). Generally the $\sum_{\text{LMW}}\text{PBDE}$ potential degraders abundance increased between AMW 2005 to AMW 1985, whereas the $\sum_{\text{HMW}}\text{PBDE}$ potential degraders abundance increased between AMW1985 to AMW1965. Although the potential PBDE degraders abundance had an inverse relationship to $\sum_{49}\text{PBDEs}$ concentration, taken together these results suggest the possibility of *in-situ* microbial dehalogenation of PBDEs in AMW sediment segments.

Abundance of potential PCB degraders in AMW sediment segments ranged from 6 to 26% as shown in Figure 4.21a. The highest potential PCB degraders abundance was observed in AMW 2000 with unclassified *Betaproteobacteria* as the dominant OTU contributing ~10 to 72% of the total. Both of these observations were consistent with trends observed for PBDEs. No trend with increased sediment depth or age was apparent in unclassified *Proteobacteria*, unclassified *Betaproteobacteria*, *Burkholderiales*, and unclassified *Gammaproteobacteria*. The unclassified *Deltaproteobacteria*, *Pseudomonadales*, and *Actinomycetales* all decreased with increased sediment depth and age. The *Desulfovibrionales* microbial class was generally present in all AMW sediment segments in very low amounts (<1%), except in AMW 1995 and AMW 1990 where abundance were ~5% and ~4%, respectively. The unclassified

Actinobacteria OTU was only present in low abundance (<1%) in AMW 1969 (bottom sediment). The microbial class *Bacilli* was present in all AMW sediment segments in low amounts (<1%), except in AMW 1969 (bottom sediment) where the composition was ~4%.

Increased in \sum_{132} PCBs concentration corresponded to decreased in potential PCB degraders abundance (Spearman coefficient of -0.01, -0.17, and -0.23 for all AMW sediment segments, excluding AMW 1969, and excluding AMW 2000, respectively) (Figure 4.21b); however, this inverse trend is likely due to the effect of high \sum_{49} PBDEs concentration on the microbial community given the phylogenetic root shared by many of the potential PBDE and PCB degraders (for example, unclassified *Chloroflexi*, *Dehalococcoidetes*, unclassified *Betaproteobacteria*). The \sum_{132} PCBs concentrations in AMW sediment segments were one to three orders of magnitude lower than \sum_{49} PBDEs concentrations and thus, PBDEs would likely have a greater impact on the microbial community. Increased in MLSR residual value coincided with decreased potential PCB degraders abundance (Spearman coefficient of -0.02 and -0.27 for all AMW sediment segments and excluding AMW 1965, respectively) (Figure 4.21c). This was in contrast to the trend observed between PBDE MLSR residual value and potential PBDE degraders abundance (Figure 4.19c). The trend in Figure 4.21c suggests that the deviation between PCB Aroclor profile (Aroclors 1016, 1248, 1254, and 1260) and PCB sediment congener profile may not be due to dechlorination by a PCB degrading community.

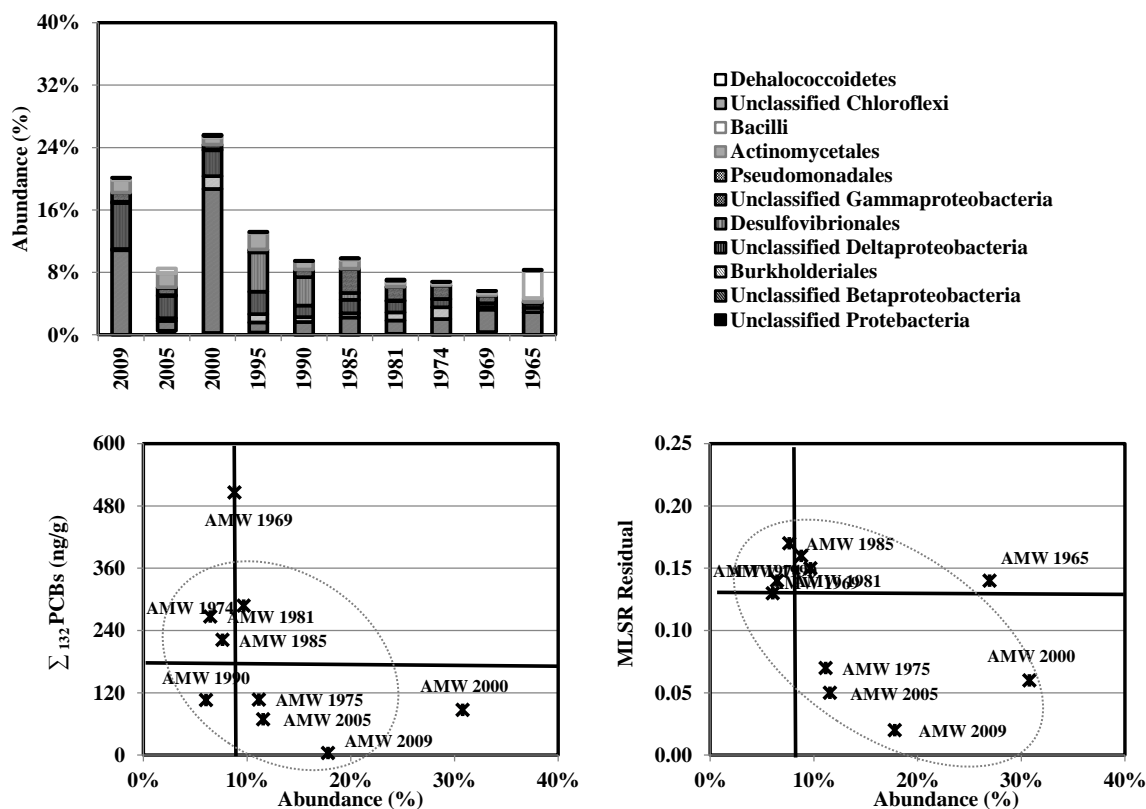


Figure 4.21: a) Abundance of potential PCB degraders by the microbial class operational taxonomic unit (OTU) level, b) \sum_{132} PCBs concentrations and total abundance of potential PCB degraders, and c) PCB MLRSR residual value versus total abundance of potential PCB degraders in all surface sediments. In b) and c), vertical bold lines represent the 50th percentile value of the potential PCB degraders abundance and horizontal bold lines represent the 50th percentile value for \sum_{132} PBDEs concentration and MLRSR residual value, respectively, in all AMW sediment segments.

In Figure 4.22, the abundance of potential PBDE and PCB degraders in the AMW sediment segment were compared. Generally, the abundance of both PBDE and PCB degraders in the AMW sediment segments were clustered around the 1:1 line except for AMW 1965 which had twice the abundance of potential PCB degraders compared to potential PBDE degraders.

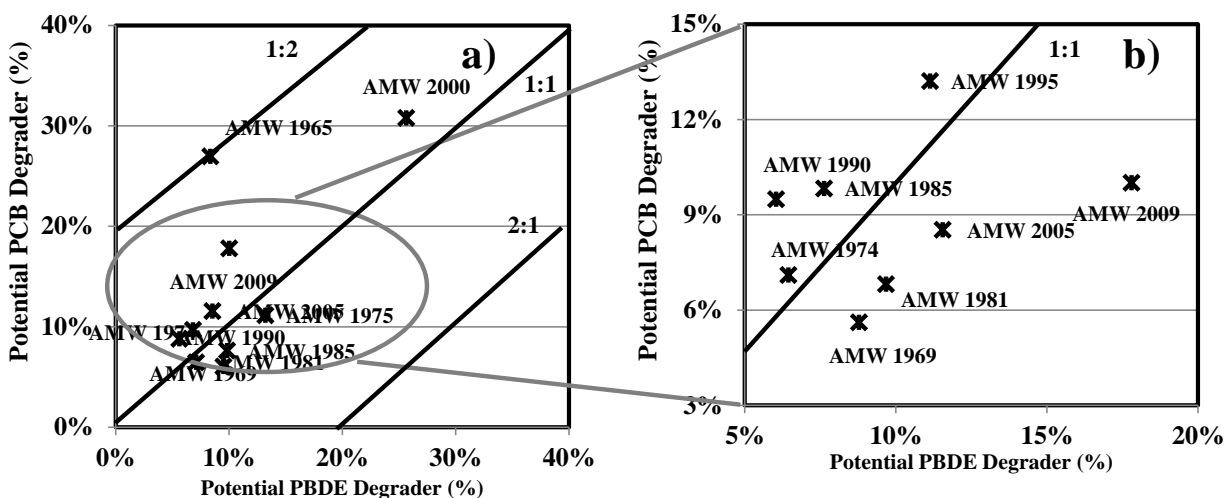


Figure 4.22: a) Abundance of PBDE and PCB potential degraders in all surface sediments, and b) a scale up of the area bounded by the bold grey oval in a). Also shown are the 1:2, 1:1 and 2:1 slopes in bold lines. Note the different scale in x- and y-axes in a) and b).

4.4.2.6. Unclassified *Bacteria* Composition In AMW Sediment Segments

The unclassified *Bacteria* OTU was highly abundant in the AMW sediment segments as shown in Figure 4.23a. Overall, unclassified *Bacteria* abundance ranged from 30 to 76%. Generally, unclassified *Bacteria* abundance increased with increasing sediment depth and age ($R^2=0.81$). This trend was also observed in other studies characterizing soil and sediment microbial community population with depth. (219-221) Increased alpha diversity also corresponded with decreasing unclassified *Bacteria* abundance (Spearman coefficient of 0.33) (Figure 4.23b). Given that microbial diversity decreased with increased sediment depth, the trend in Figure 4.23b suggests that the microbial diversity in the lower sediment segments could be largely underestimated. Increased \sum_{49} PBDEs concentration corresponded with decreased unclassified *Bacteria* abundance whereas increased \sum_{132} PCBs levels corresponded with increased unclassified *Bacteria* abundance (Figure 4.23 c and d). Increased PBDE MLSR residual value corresponded with decreased unclassified *Bacteria* abundance; the inverse trend was observed for PCBs. The trends in Figures 4.23c and e suggest that the high \sum_{49} PBDEs concentrations in AMW do not enrich for the microorganisms represented by the unclassified *Bacteria* OTU and that the greater residual values

between the three PBDE TM profiles (DE-71, DE-79, and Saytex 102E TMs) and PBDE congener distribution in AMW sediment segments were not due to activity by unclassified *Bacteria*. Given these observation, it would not appear that the unclassified *Bacteria* are active dehalorespirers of PBDEs in AMW sediment. On the other hand, the increased in unclassified *Bacteria* abundance with increased \sum_{132} PCBs concentration and increased PCB MLSR residual value, would be consistent with PCB dehalogenation.

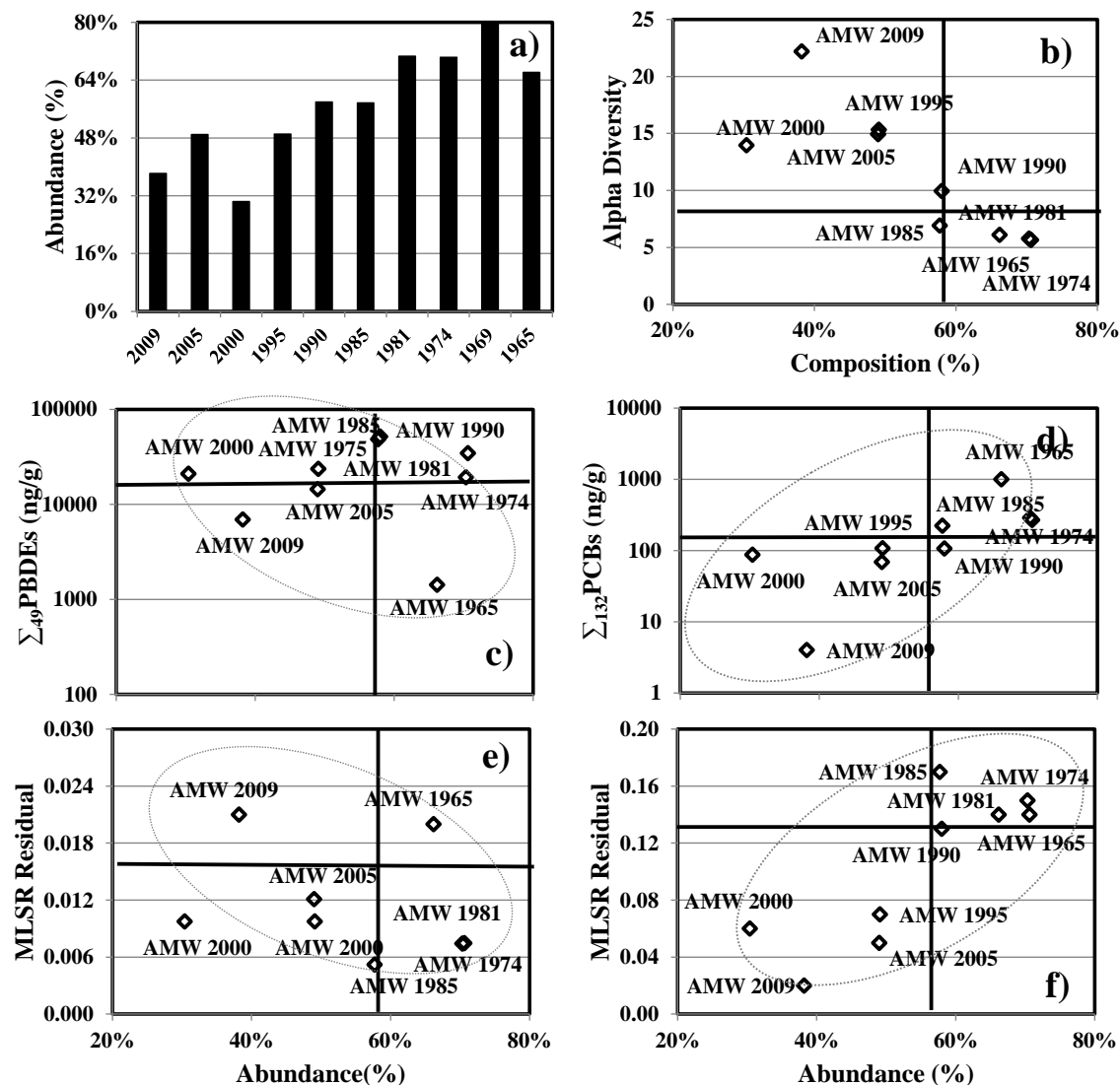


Figure 4.23: a) Abundance of unclassified *Bacteria*, b) alpha diversity as a function of unclassified *Bacteria* abundance, c) Σ_{49} PBDEs concentration as a function of unclassified *Bacteria* abundance, d) Σ_{132} PCBs concentration as a function of unclassified *Bacteria* abundance, e) PBDE MLSR residual value versus unclassified *Bacteria* abundance, and f) PCB MLSR residual value versus unclassified *Bacteria* abundance in AMW sediment segments. Y-axes on c) and d) are in log scale. Note that the y-axes in e) and f) and x-axes on c) and d) are not in the same scale.

4.5. Conclusion

MLSR analysis comparing PBDE TMs and PCB Aroclors to PBDE and PCB sediment profiles in conjunction with observations of changes in PBDE and PCB homolog and congener substitution patterns can be used to provide multiple lines of evidence to evaluate the possibility of *in-situ* microbial PBDE or PCB dehalogenation. Throughout this chapter, the indigenous microbial community composition in all the surface sediments and at 5-years interval in AMW sediment column were characterized to better understand the presence of microbial class OTUs capable of *in-situ* dehalogenation. These observations together with other indicators of dehalogenation help further our understanding on *in-situ* microbial facilitated PBDE and PCB transformation processes.

Utilization of high yield pyrosequencing analysis resulted in high quality sequences with a majority exceeding the stringent quality control parameters. As expected, the geospatial differences and variant physico-chemical properties resulted in a very diverse microbial community structure in each of the surface sediments. The low microbial diversity and high abundance of unclassified *Bacteria* in AED and ACL surface sediments suggest that the microbial diversity and in general, the representative microbial community structure in these PBDE rich surface sediments was under predicted and not adequately understood.

In the AR surface sediments, high levels of PBDEs can be an important driver in influencing the microbial community composition. The microbial diversity in AED, ACL, AJL, and AFR in general increased with increased average distance from the two PBDE manufacturing facilities, and consequently with decreased \sum_{49} PBDEs concentration. Microbial community composition hierarchical cluster analysis and PCA grouped these surface sediments in order of increased average distance from the PBDE manufacturing facilities even though these analyses were performed independent of distance or \sum_{49} PBDEs concentrations.

Microbial community composition in the surface sediments also showed similarity based on the contaminant source pathway. IGC09 and IGC13 located proximate to each other (~400 m) on the WBGCR that is fed predominantly by treated effluent from the HSD WWTP are similar in the microbial community structure as shown by hierarchical cluster analysis and PCA. The microbial community composition in AMW and CBC that are both exposed to anthropogenic hydraulic discharges also bore close resemblance. The hierarchical cluster analysis and PCA also highlighted the unique microbial community composition in AOT surface sediments. Although AOT is located in AR, the microbial community composition resembled the urban CWP and CLC microbial community compositions.

Microorganisms capability for PBDE and PCB degradations were inferred from laboratory scale studies. Overall, potential PBDE and PCB degraders OTUs were present in varying abundance in all the surface sediments. Generally, increasing potential PBDE degraders abundance coincided with increasing \sum_{49} PBDEs concentration and increasing PBDE MLSR residual value. These results are consistent with *in-situ* PBDE dehalogenation. A similar trend was observed for PCBs with increasing \sum_{132} PCBs concentration and PCB MLSR residual value corresponding to increasing potential PCB degraders abundance.

The presence of the potential PBDE and PCB degraders should not be misinterpreted as active microbial facilitated PBDE and PCB dehalogenation. PBDE and PCB microbial facilitated degradation is a complex process that is dependent upon factors such as bioavailability, substrate and nutrient availability, and presence/absence of inhibitor. Most of these factors cannot be evaluated given the data resolution of this study. It is therefore important to interpret the microbial community results in light of other indicators.

Table 4.7a: Overview of potential PBDE and PCB degraders in all surface sediments in relations to other *in-situ* microbial facilitated dehalogenation indicators.

Sample	Potential degraders (%)		Physico-chemical properties and analysis								Sediment column indicators			
	PBDEs	PCBs	$\Sigma_{49}\text{PBDEs}$ (ng/g)	$\Sigma_{132}\text{PCBs}$ (ng/g)	PBDE MLSR Residual	PCB MLSR Residual	ORP (mV) ⁽¹⁾	OC (mg/g) ⁽²⁾	OM (mg/g) ⁽³⁾	BC (mg/g) ⁽⁴⁾	ΔHom ⁽⁵⁾	<i>OMP</i> ⁽⁶⁾	ΔHom ⁽⁵⁾	<i>OMP</i> ⁽⁶⁾
AED	11%	13%	35635	4	0.003	0.010	-80.7	52	81	4				
ACL	25%	10%	2503	3	0.003	0.010	-100.1	8	18	5				
AJL	28%	17%	402	5	0.004	0.030	-34.4	22	32	2				
AFR	10%	13%	4	1	0.007	0.020	-84.6	52	80	9				
CWP	20%	20%	404	43	0.006	0.040	-84.4	89	141	40				
CLC	16%	21%	90	236	0.050	0.060	-77.8	99	176	41	√	√	√	√
IGC09	11%	10%	3461	4979	0.006	0.230	NA	142	245	16				
IGC13	19%	27%	1908	1075	0.017	0.190	NA	140	234	20				
AOT	13%	16%	12	3	0.006	0.060	-73.3	74	141	2				
CBC	13%	21%	313	403	0.009	0.170	-59.5	25	40	22				
AMW	18%	10%	6950	69	0.021	0.020	-22.5	312	474	3	√	√		
⁽¹⁾ Oxidation reduction potential ⁽²⁾ Organic carbon ⁽³⁾ Organic matter ⁽⁴⁾ Black Carbon ⁽⁵⁾ Change in small (homologs 1-4 and homologs 5-7 for PBDEs and homologs 1-3 and homologs 4-6 in PCBs) and large (homologs 8-9 and homolog 10 in PBDEs, and homologs 7-9 and homolog 10 in PCBs) PBDE or PCB composition with increased sediment depth. Check mark indicates observed increased in small PBDE or PCB homologs concomitant with decreased in large PBDE or PCB homologs with increased sediment depth. ⁽⁶⁾ Composition of <i>ortho</i> , <i>meta</i> , and <i>para</i> -substituted PBDE or PCB congeners. Check mark indicates observed increased in <i>meta</i> and <i>ortho</i> -substituted PBDE or PCB congener substitution concomitant with decreased in <i>para</i> -substituted PBDE or PCB congener substitution.														

Previously, *in-situ* PBDE and PCB degradations were evaluated based upon increasing composition of LMW PBDE and PCB homologs concomitant with decreasing HMW PBDE and PCB homologs (Figure 3.7a-b).⁽¹⁵¹⁾ This trend was only observed in AMW sediment column for PBDEs and CLC sediment column for PBDEs and PCBs. Although potential PBDE and PCB degraders were present in all surface sediments, active/ongoing microbial facilitated PBDE dehalogenation does not appear to be occurring at observable rates in the other nine surface sediments given the absence of increased LMW PBDE and PCB homolog that should manifest from microbial facilitated degradation of large PBDE and PCB homologs. The lack of dehalogenation activity despite high abundance of potential PBDE and PCB degraders in some surface sediments such as AED could be attributed to many factors including low bioavailability, lack of suitable electron donors, presence of dehalorespiration inhibitors in the sediment, or competition with other high energy electron acceptors.

In the AMW sediment column, *para*-substituted PBDE congeners decreased concomitant with increased *meta*-substituted PBDE congeners (Figure 3.14j) in the top 10 cm sediment segment. The decrease in *para*-substituted PBDE congeners is consistent with microbial facilitated PBDE dehalogenation; however, the increase in *meta*-substituted PBDE congeners contradicts expectation of microbial PBDE dehalogenation which was reported to favor *para*- and *meta*-bromine removal.^(102,103,108) AMW sediment segments generally have high PBDE MLSR residual values. Physico-chemical properties in AMW surface sediments such as ORP values consistent with facultative metabolism, high OM and OC, and high \sum_{49} PBDEs concentrations may also favor of *in-situ* PBDE dehalogenation. Taken together, the possibility of *in-situ* microbial facilitated PBDE dehalogenation at site AMW is likely.

In the CLC sediment column, decreased in *para*-substituted PBDE congeners concomitant with increased in *meta*-substituted PBDE congeners with sediment depth were observed (Figure 3.14h). As was discussed for the AMW sediment column, the decrease in *para*-substituted PBDE congeners is consistent with microbial facilitated PBDE dehalogenation whereas the increase in *meta*-substituted PBDE congeners contradicts expectation of microbial PBDE dehalogenation. This trend, however, was

accompanied by increased in mean degree of bromination which was attributed to the rapidly increasing BDE-209 concentration and abundance with depth as previously discussed in Chapter 3.4.4. Observation of the PCB OMP-substitution pattern shed some light on PBDEs. Increased in *ortho*-substituted PCB congeners concomitant with decreased in *meta*-substituted PCB congeners with increased sediment depth was observed in CLC sediment column (Figure 3.14c). This phenomenon was accompanied by an observable decreased in mean degree of chlorination with sediment depth (Figure 3.14c). These are among the best evidence of microbial facilitated PCB dehalogenation. In the CLC surface sediment, potential PCB degraders abundance exceeded that of PBDEs. Additionally, \sum_{132} PCBs concentrations were four times higher than \sum_{49} PBDEs concentrations. Given these trends, microbial facilitated PCB degradation may be more likely than microbial facilitated PBDE degradation in the CLC surface sediment. While some of the constituents comprised by the potential PBDE and PCB degraders are the same (for example, *Dehalococcoidetes* and unclassified *Chloroflexi*), these microorganisms may exhibit preferential PCB dehalogenation given the potentially greater PCB bioavailability.

Through multiple lines of evidence, *in-situ* microbial facilitated PBDE degradation in AMW surface sediment seems likely. Further observation of the microbial community composition in AMW sediment segments can provide a temporal snapshot and a visualization of the microbial community evolution in a sediment column that demonstrates active PBDE degradation. The microbial species richness in the AMW upper sediment segments was not entirely captured by the pyrosequencing analysis. In contrast, the rarefaction curves for the lower sediment segments in AMW approached a plateau indicating most species richness was captured. Microbial diversity decreased with increased sediment depth in the AMW sediment column consistent with other published studies of the microbial community in soil and sediment with depth.⁽²¹⁹⁻²²¹⁾ Hierarchical cluster analysis and PCA performed independent from sediment depth and age showed microbial community grouping based on depth confirming the hypothesis of gradual changes in the microbial community structure in response to changes in the AMW sediment column.

Potential PBDE and PCB degraders were present in all AMW sediment segments (Table 4.7b summarizes the potential PBDE and PCB degraders in relation to other microbial facilitated dehalogenation indicators). As can be observed in Table 4.7b, potential PBDE degraders abundance generally decreased with depth. In the AMW sediment segments, increased in \sum_{49} PBDEs concentration and PBDE MLSR residual value corresponded to increased potential PBDE degraders abundance consistent with the hypothesis of *in-situ* PBDE dehalogenation in the AMW sediment column. In the AMW sediment column, composition of homologs 1 to 4 and homologs 5-7 decreased with increasing sediment depth up to ~30 cm,⁽¹⁵¹⁾ consistent with the expectation of dehalogenation of LMW PBDE congeners(1 to 6 bromine substitutions) in AMW upper sediment segments. The decreased in LMW PBDE congeners with depth correlated with increased in \sum_{LMW} PBDE potential degraders abundance. In AMW sediment depth >30cm, the small decreased in BDE-209 composition corresponded with increased composition of homologs 8-9 and to some extent, increased composition of homologs 5-7.⁽¹⁵¹⁾ It is possible that this trend was facilitated by the increased abundance of \sum_{HMW} PBDE potential degraders in the lower sediment segments.

Although the abundance of potential PCB degraders exceeded those of PBDEs in the lower sediment segments, indicators of *in-situ* microbial facilitated PCB dehalogenation such as increased LMW PCB concomitant with decreased HMW PCB, decreased in average degree of chlorination, or decreased in *meta* and *para*-substituted congener concomitant with increased in *ortho*-substituted congener was not observed in the lower AMW sediment segments. Given the lack of supportive indicators, *in-situ* microbial facilitated PCB degradation does not seem likely in the AMW sediment column.

Table 4.7b: Overview of potential PBDE and PCB degraders in AMW sediment segments in relations to other in-situ microbial facilitated dehalogenation indicators.

Sample	Potential degraders (%)		Physico-chemical properties and analysis								Sediment column indicators			
	PBDEs	PCBs	Σ_{49} PBDEs (ng/g)	Σ_{132} PCBs (ng/g)	PBDE MLSR Residual	PCB MLSR Residual	ORP (mV) ⁽¹⁾	OC (mg/g) ⁽²⁾	OM (mg/g) ⁽³⁾	BC (mg/g) ⁽⁴⁾	Δ Hom ₍₅₎	OMP ₍₆₎	Δ Hom ₍₅₎	OMP ₍₆₎
2009	18%	10%	6950	4	0.021	0.020	-22.5	312	474	3				
2005	12%	9%	14440	69	0.012	0.050	-22.0	284	439	2				
2000	31%	26%	21050	87	0.010	0.060	-34.9	204	388	2				
1995	11%	13%	23745	107	0.010	0.070	-47.8	178	349	2				
1990	6%	9%	51785	106	0.098	0.130	-52.3	176	314	3	√	√	√	√
1985	8%	10%	48643	222	0.005	0.170	-50.1	206	349	3				
1981	6%	7%	34622	267	0.007	0.140	-48.7	204	329	3				
1974	10%	7%	19352	288	0.007	0.150	-45.5	204	346	3				
1969	9%	6%	11058	506	0.016	0.160	-41.9	241	436	3				
1965	27%	8%	1427	998	0.020	0.140	-54.1	262	421	3				

⁽¹⁾ Oxidation reduction potential

⁽²⁾ Organic carbon

⁽³⁾ Organic matter

⁽⁴⁾ Black Carbon

⁽⁵⁾ Change in small (homologs 1-4 and homologs 5-7 for PBDEs and homologs 1-3 and homologs 4-6 in PCBs) and large (homologs 8-9 and homolog 10 in PBDEs, and homologs 7-9 and homolog 10 in PCBs) PBDE or PCB composition with increased sediment depth. Check mark indicates observed increased in small PBDE or PCB homologs concomitant with decreased in large PBDE or PCB homologs with increased sediment depth.

⁽⁶⁾ Composition of *ortho*, *meta*, and *para*-substituted PBDE or PCB congeners. Check mark indicates observed increased in *meta* and *ortho*-substituted PBDE or PCB congener substitution concomitant with decreased in *para*-substituted PBDE or PCB congener substitution.

Overall, characterization of the microbial community composition in the surface sediments and in AMW sediment segments have provided insight into the role indigenous microorganisms may play in sediment phase transformation of PBDEs and PCBs. Potential PBDE and PCB degraders were present in all surface sediments and in all AMW sediment segments indicating that microorganisms capable of PBDE and PCB dehalogenation may be common in the sediment environment. While the occurrences of these class OTUs are common, active PBDE and PCB dehalogenation were not as common. It is important to note that presence of microorganisms capable of PBDE and PCB degradations does not equal active degradation. Other indicators, such as high MLSR residual value, increase composition of LMW PBDE or PCB concomitant with decrease composition of HMW PBDE or PCB, decrease composition of *meta* and *para*-substitution concomitant with increase composition of *para*-substitution should be provided in order to provide strong support for *in-situ* microbial facilitated PBDE or PCB degradation. Future studies should focus on identifying trace indicators of microbial facilitated PBDE and PCB degradation to enable better prediction of PBDE and PCB fate in environmental fate modeling.

CHAPTER 5. MODELLING POLYBROMINATED DIPHENYL ETHER (PBDE) AND POLYCHLORINATED BIPHENYL (PCB) *IN-SITU* MASS TRANSPORT IN NATURAL SEDIMENT COLUMNS

5.0. Abstract

The mass transport of PBDEs and PCBs in eleven sediment columns under diffusion and advection-diffusion conditions with organic carbon (OC) and organic carbon and black carbon (OCBC) co-sorption was modeled using known transport equations. The sediment columns modeled in this study exhibited a wide range of physical properties. A Monte Carlo approach was taken to address existing chemical data gaps. In an effort to provide a conservative estimate, the modeling approach simulated the most mobile contaminant transport conditions.

Overall, PBDE homologs have lower mobility potential compared to equivalent PCB homologs. The reduced mobility potential of PBDE homologs can be attributed to high molecular weight (HMW) and higher hydrophobicity which increased solid phase partitioning and reduce aqueous phase mobility. Consideration of OCBC co-sorption substantially reduced the mobility of PBDE and PCB homologs especially in urban sediment columns with high BC fraction. The highest contaminant mobility scenario was achieved under advection-diffusion condition with OC only sorption (A(OC)). The low aqueous saturation concentration for hydrophobic contaminants was identified as a major transport limitation especially in high molecular weight PBDE and PCB homologs. Hydraulic conductivity (K_H) and organic carbon fraction (f_{OC}) were major drivers for PBDE and PCB transport under the A(OC) transport scenario. Under the 40 year model simulation, fraction of mass loss through A(OC) transport was very small for PBDE and PCB homologs 1 and 2, and was negligible for HMW homologs. Superimposition of the mass simulation results on sediment PBDE and PCB concentrations demonstrate that *in-situ* mass transport does not shift the deposited PBDE and PCB sediment profiles even under highly optimum transport conditions.

5.1. Introduction

Sediment can frequently serve as the final sink for hydrophobic organic contaminants (HOCs) such as polybrominated diphenyl ethers (PBDEs) and polychlorinated biphenyls (PCBs) in the aquatic environment. Although the use of mixing models for source apportionment is commonly employed, there are typically disparities between PBDE and PCB source profiles of technical mixtures (TMs) and Aroclor mixtures and the distribution of congeners in the sediment. Such disparity (or residual between the model prediction and values) can either result from pre-deposition differential transport or transformation, or post-depositional transport and/or transformation.

Pre-depositional transport processes may include differential transport rate and potential transformation occurring between the source and receptor sites. In the Lake Superior atmosphere, >95% of BDE209 can be removed from the atmospheric phase via wet and dry deposition.⁽¹⁸⁶⁾ This rate is much larger than the atmospheric removal rate of the smaller BDE-47 congener.⁽¹⁸⁶⁾ Further, it is likely that differences in volatility and air/solid partitioning (K_{OA}) would result in differences in congener pattern during transport to the receptor. Photolytic transformations of PBDE and PCB congeners during atmospheric transport have been studied extensively.^(154,186) Post-depositional transport and transformation processes in sediment include in-situ mass transport (advection or diffusion) and microbial facilitated transformation. Contaminants deposited in sediments are susceptible to transport processes induced by concentration gradient (diffusion) and bulk porewater movement (advection).^(119,121,141,222) Additionally, substantial microbial facilitated PBDE and PCB transformations have been demonstrated in bio-enriched (biostimulation and bioaugmentation) PBDE and PCB laboratory scale studies.^(68,91,102,103,223) Post-depositional transport processes are expected to have comparatively longer time frames relative to pre-depositional transport processes. Therefore, pre-depositional transport processes, if substantial, should have relatively rapid kinetics.

Previously in Chapter III, indicators of PBDE and PCB transformations suggested by multivariate least square regression (MLSR) analysis, changes in homolog distribution, and differences in *ortho*-, *meta*-, and *para*- (OMP) substitution patterns were observed in cores AMW and CLC. While these analyses provide evidence in support of PBDE and PCB environmental transformations, these results alone cannot differentiate and quantify the contribution of pre- and post-depositional transport processes to the observed sediment phase PBDE and PCB concentrations and distributions. The focus of this chapter is on modeling the in-situ PBDE and PCB mass transport equations together with a stochastic parameterization in natural aquatic sediments by applying known diffusion and advection-diffusion mass transport principals to evaluate the contribution and role of in-situ mass transport on the observed PBDE and PCB congener profiles in the sediment columns.

5.2. Objective and Hypotheses

In this chapter, the magnitude of sediment phase PBDE and PCB in-situ mass transport in natural aquatic sediment columns was evaluated through application of known mass transport equations. The predicted mass transport of PBDE and PCB homologs was used to assess the contribution of in-situ mass transport in influencing the observed PBDE and PCB sediment profiles. Specific objectives and hypotheses are listed below.

- Investigate the difference in transport mobility between low molecular weight (LMW) and high molecular weight (HMW) PBDE and PCB homologs under diffusion and advection-diffusion conditions. As HMW can result in decreased mass transport rate, it was hypothesized that LMW PBDE and PCB homologs have a larger potential for mass transport relative to HMW homologs. Additionally, as HMW PBDE homologs are more hydrophobic than their respective HMW PCB homologs, PCBs were expected to show higher overall mass transport mobility. Advection-diffusion transport process is generally of much greater magnitude than diffusion alone; hence,

advection-diffusion transport process was hypothesized to be the major driver for in-situ PBDE and PCB mass transport in natural aquatic sediments.

- Evaluate the effect of PBDE and PCB adsorption to black carbon (BC) on the diffusion and advection-diffusion transport processes. Typically, only absorption to organic carbon (OC) is considered. As PBDEs and PCBs are highly hydrophobic compounds, adsorption to BC were expected to increase PBDE and PCB solid phase partitioning substantially and thus reduce aqueous phase mobility. This will reduce the magnitude of PBDE and PCB in-situ mass transport. PBDE and PCB mass transport in urban Chicago and IGC sediment cores with higher BC levels were hypothesized to be much less than AR sediments.
- Investigate the effect of varying sorbent properties including octanol-water partition coefficient (K_{OW}) and initial sediment starting concentration, and sorbate properties including porosity (ϕ), bulk and particle densities (ρ_{WBD} and ρ_{PD} , respectively), composition of OC and BC (f_{OC} and f_{BC}), and hydraulic conductivity (K_h) on the magnitude of PBDE and PCB in-situ mass transport in natural aquatic sediments. Increasing K_{OW} values with increasing PBDE and PCB molecular weight were hypothesized to reduce in-situ mass transport. Higher initial sediment starting concentration was expected to increase PBDE and PCB mass transport. Sediment cores with high ϕ and K_h , as well as low ρ_{PD} , f_{OC} , and f_{BC} were hypothesized to have more mobile PBDE and PCB mass transport. In-situ mass transport of LMW PBDE and PCB congeners were expected to substantially change PBDE and PCB sediment profiles given their high mass transport likelihood.

5.3. Materials and Methods

5.3.1. Overview

PBDE and PCB vertical migration in 0.02 m sediment segments in eleven sediment cores (six from AR and five from metropolitan Chicago) were modeled under diffusion and advection-diffusion

conditions. Sampling sites, field sampling methodologies, and sample characterization were discussed in detailed in Chapter 3.3. Each model simulation separately considers sorption only to organic carbon (OC), and sorption to both OC and BC (OCBC) components measured in the sediment. The mass transport modeling effort presented in this chapter assumed a sediment segment in a vertical sediment column contaminated with a homogenous fixed mass of PBDEs or PCBs. Flux occurred by diffusion or advection-diffusion in both directions (upwards and downwards) across the sediment segment into neighboring sediment segments. Figure 5.1 is a schematic of the modeled mass transport processes. The quantitative prediction derived from this modeling effort is for the most mobile case possible where the maximum concentration gradient exists between the contaminated sediment segment and neighboring “clean” sediment segments. In other words, the predicted PBDE and PCB mass fluxes are the maximum amount of PBDEs and PCBs that are expected to migrate in a natural sediment column. In actual sediment, adjacent sediment segment will likely have contaminants present and thus the concentration gradient would be less than maximal. Therefore, the model results here would be a “worst case” of maximal mobility.

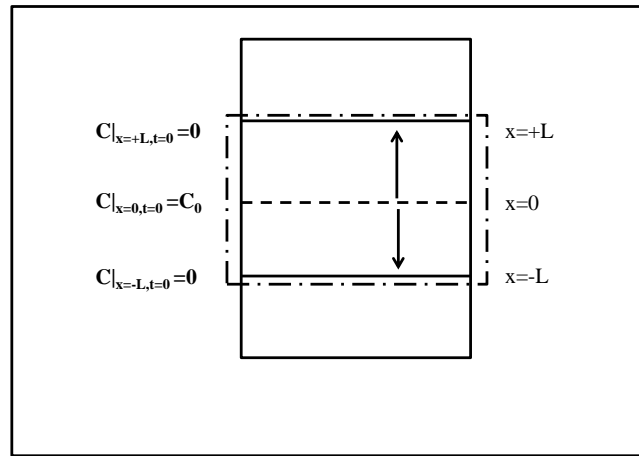


Figure 5.1: Schematic showing the hypothetical scenario used to model PBDE and PCB mass transport through diffusion and advection-diffusion transport in natural sediment column provided with the most mobile mass transport conditions. Boundary conditions are shown on the left and segment boundary layers are bounded by the box with dotted lines. It is assumed that contaminants move equally in both upward and downward directions.

Monte Carlo simulation was required to address the gaps in data and variability in PBDE and PCB physico-chemical properties, as well as to address variability within individual sediment columns. Relevant sorbate (PBDEs and PCBs) and sorbent (eleven sediment columns) parameters were subjected to 50,000 random Monte Carlo samplings each to obtain a probabilistic distribution function (PDF). Monte Carlo simulation was guided by experimental and literature values. Application of Monte Carlo simulation to diffusion and advection-diffusion transport processes was performed in Matlab version R2012b. Statistical analysis was performed in Systat version 13.

5.3.2. Mathematical Model Development

Diffusion and advection-diffusion can be mathematically described by Fick's law (Equation 2.9) and the expanded form of Ficks' first law (Equation 2.16), respectively.^(133,134) Provided initial condition of $c(x,0) = c(\infty,t) = 0$ and $c(0,t) = C_0$, closed form analytical solutions for Equation 2.9 and 2.16 are shown in Equations 5.1 and 5.2, respectively. Expanded solutions for Equations 5.1 and 5.2 are provided in Equations 2.15 and 2.19, respectively.

$$\frac{C}{C_0} = \text{erfc}\left(\frac{x}{\sqrt{4D_{obs}t}}\right) \quad (5.1)$$

$$\frac{C}{C_0} = \frac{1}{2} \left(\text{erfc}\left(\frac{x-vt}{\sqrt{4D_{obs}t}}\right) + \exp\left(\frac{vx}{D_{obs}}\right) \text{erfc}\left(\frac{x+vt}{\sqrt{4D_{obs}t}}\right) \right) \quad (5.2)$$

In Equations 5.1 and 5.2, x is the length of migration. D_{obs} is the observed diffusivity (m^2/year) expressed as a function of molecular diffusivity (D_{mol}), tortuosity (τ), and retardation factor (R); D_{obs} expressions are included in Equations 2.11 through 2.14. The advective velocity term, v (m/year) was previously defined in Equation 2.17 as a function of hydraulic gradient (dh/dx), hydraulic conductivity (K_h), and porosity (ϕ) of the sediment with a retardation factor (R). C/C_0 is the aqueous phase breakthrough concentration, defined as the ratio of concentration in the aqueous phase at length $x=\pm L$,

where L is diffusion or advection-diffusion transport length, over the initial concentration in the aqueous phase at $x=0$ and $t=0$. Under local equilibrium assumption (LEA), C_o is the initial concentration in the aqueous phase that depends on the homogenous concentration of contaminant in the sediment phase. C_o at a given time t ($C_{aq}|_{x=0,t}$) can be described using Equation 5.3.

$$C_{aq}|_{x=0m,t} = \frac{C_{sed}|_{x=0m,t}}{K_d} \quad (5.3)$$

In Equation 5.3, K_d (L/kg) is the sediment-porewater partition coefficient as defined in Equation 2.7 for absorption to OC and can be expanded to Equation 2.23 to include OCBC co-sorption. In this chapter, C_{aq} at a specific time is referred to as $C_{aq}|_{x=0m,t=n}$, where n is the transport time in years.

The aqueous concentration predicted by the LEA is used to determine the aqueous concentration leaving the boundary layer at length $\pm L$ after a period of a given time ($C_{aq}|_{x=L,t=n}$), using Equation 5.4 for diffusion and Equation 5.5 for diffusion-advection. The modeling effort in this chapter specifically looks at a transport length (i.e., sectional sediment segment length) equal to 0.02 m, therefore $C_{aq}|_{x=\pm L,t=n}$ is represented as $C_{aq}|_{x=0.02m,t=n}$.

$$C_{aq}|_{x=0.02m,t=n} = C_{aq}|_{x=0m,t=n} * \operatorname{erfc}\left(\frac{x}{\sqrt{4D_{obs}t}}\right) \quad (5.4)$$

$$C_{aq}|_{x=0.02m,t=n} = C_{aq}|_{x=0m,t=n} * \left[\frac{1}{2} \left(\operatorname{erfc}\left(\frac{x-vt}{\sqrt{4D_{obs}t}}\right) + \exp\left(\frac{vx}{D_{obs}t}\right) \operatorname{erfc}\left(\frac{x-vt}{\sqrt{4D_{obs}t}}\right) \right) \right] \quad (5.5)$$

The mass flux leaving the defined boundary layer in the aqueous phase ($M_{t_{x=\pm L,t=n}}$) can be derived from the predicted $C_{aq}|_{x=\pm L,t=n}$. For diffusion only transport, a closed form solution adapted from Crank (1976), was used to estimate mass flux leaving the boundary layer under diffusion only condition (Equation 5.6).⁽¹³³⁾ For advection-diffusion, mass breakthrough was estimated from the porewater Darcy velocity as shown in Equation 5.7.^(119,141) Given the fixed sediment segment used in this chapter, $C_{aq}|_{x=\pm L,t=n}$ is represented as $C_{aq}|_{x=0.02m,t=n}$ and $M_{t_{x=\pm L,t=n}}$ as $M_{t_{x=0.02m,t=n}}$.

$$\Delta M_{t_{x=0.02m,t=n}} = 2 * (C_{aq}|_{x=0.02m,t=n}) * (D_{obs}\Delta t/\pi)^{1/2} \quad (5.6)$$

$$M_{t_{x=0.02m,t=n}} = \phi * \left(\frac{dh}{dx}\right) * \left(\frac{K_h}{\phi R}\right) * (C_{aq}|_{x=0.02m,t=n}) * t \quad (5.7)$$

In Equations 5.6 and 5.7, $M_{aq_{x=0.02m,t=n}}$ is the predicted mass flux moving out of the boundary layer via the aqueous phase, D_{obs} is the observed molecular diffusivity ($m^2/year$), dh/dx is the hydraulic gradient across the sediment layer (m/m), and K_h is the sediment column hydraulic conductivity (m/year). In Equation 5.6, $\Delta M_{t_{x=0.02m,t=n}}$ is the mass flux leaving the boundary layer between $t=n$ to $t=n+1$. The cumulative mass flux can be obtained by summing up the $\Delta M_{t_{x=0.02m,t=n}}$ over the time period of interest. Equation 5.7 is thus an expression of the cumulative mass flux leaving the boundary layer over a period of defined time.

The mass leaving the boundary layer in the aqueous phase reduced the equilibrium contaminant concentration in the sediment phase with increasing transport time. The new contaminant concentration in the sediment phase ($C_{sed}|_{x=0m,t=n+1}$) can be derived from mass balance. The resulting equation is shown below.

$$C_{sed}|_{x=0m,t=n+1} = \frac{C_{sed}|_{x=0m,t=0} * M_{sed} - M_{aq_{x=0.02m,t=n}} * A}{M_{sed}} \quad (5.8)$$

In Equation 5.8, M_{sed} is mass of sediment which can be calculated from wet bulk density (ρ_{WD}) multiplied by a fixed volume, and A is the cross sectional area ($Length^2$). The new adjusted $C_{sed}|_{x=0m,t=n+1}$ is substituted into Equation 5.3 in finite difference form to determine the adjusted $C_{aq}|_{x=0m,t=n+1}$. The process is repeated at fixed time interval between $n=0$ to the desired time length to obtain a time dependent profile of sediment and aqueous phase contaminant concentration. Figure 5.2 illustrates the application of Equations 5.1 to 5.8 to evaluate PBDE and PCB in-situ mass transport in natural sediment columns.

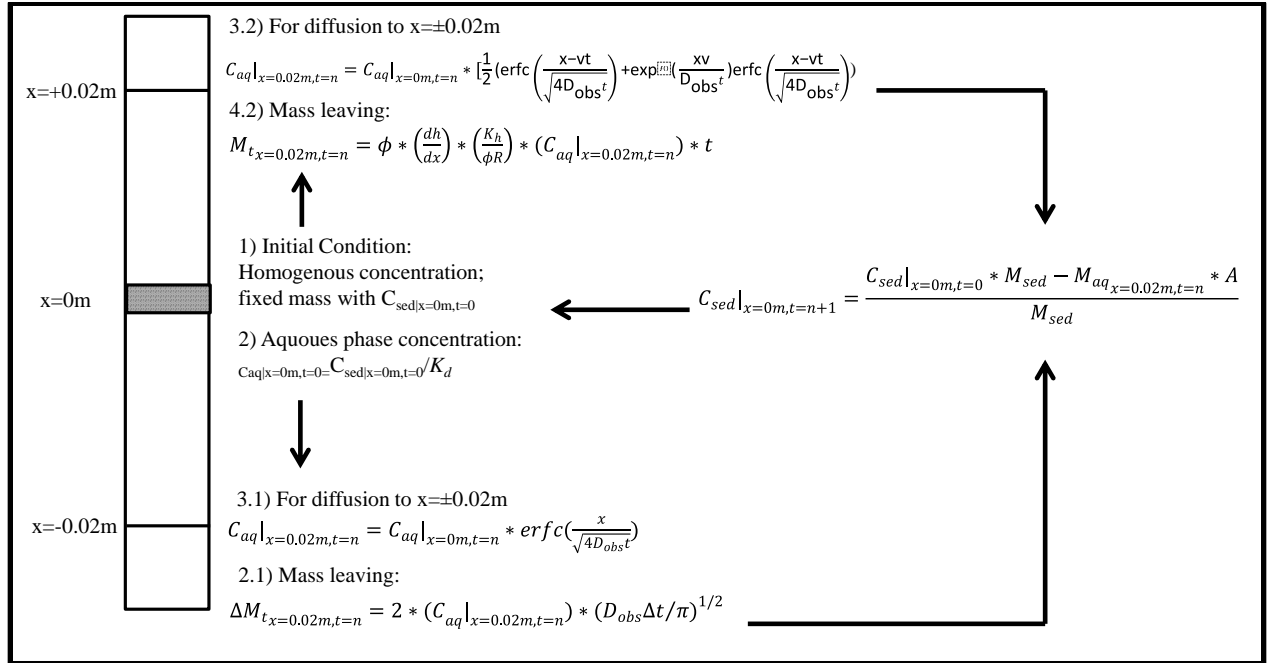


Figure 5.2: Application of known transport processes equations to evaluate PBDE and PCB in-situ mass transport in natural sediment columns. Note that diffusion and advection-diffusion can occur in both upward and downward directions.

5.3.3. Model Parameterization

For modeling purposes, the area and volume of the boundary layer were kept constant to enable equivalent concentration and mass flux comparison between different sediment columns. A is chosen as the area of the cylindrical polycarbonate tube used for sampling (I.D. 0.066 cm, Chapter 3.3.1). The transport length is 0.02m rendering the volume of the layer at $5.6 \times 10^{-5} \text{m}^3$.

5.3.3.1. Sorbate Properties

Sorbate properties that affect diffusion and advection-diffusion mass transport are organic carbon partition coefficient (K_{OC}) and molecular diffusivities (D_{mol}). When sorption to BC is considered, black carbon partitioning coefficient (K_{BC}) is also important. K_{OC} , K_{BC} , and D_{mol} are independent of the sediment

column properties and are the same across the eleven sediment columns. It was assumed that congeners from the same homolog share roughly similar properties (i.e., variability within the homolog is exceeded by parameter uncertainty) and consequently, exhibit the same transport behavior. Synergistic or antagonistic effects between PBDE and PCB homologs currently are not known. Therefore an additional assumption posited is that the in-situ mass transport of one homolog does not affect the other homologs.

K_{OC} was estimated from the octanol water partition coefficient (K_{OW}). Quantitative structure property relationships (QSPRs) shown in Equations 2.1 through 2.4 were used to estimate PBDE and PCB log K_{OW} values. Literature values and estimates from the USEPA EPI suite v4.11 were also obtained. These values were previously summarized in Table A2.5 and A2.6. Overall, 90 and 221 log K_{OW} values were obtained for PBDEs and PCBs, respectively. These K_{OW} values were subjected to regression analysis and the results are shown in Figure D5.1. Only K_{OW} values within the lower 5% confidence interval (CI) and upper 95% CI were used to guide the Monte Carlo simulations. Following regression analysis, 79 and 111 discrete K_{OW} values for PBDEs and PCBs were used to guide the Monte Carlo simulations and these values are summarized in Table 5.1.

Table 5.1. Summary of 79 and 111 discrete log K_{OW} values for PBDEs and PCBs used to guide Monte Carlo simulations for mass transport modeling.

Homolog	PBDE				PCB			
	Minimum	Maximum	Average	Std. Dev	Minimum	Maximum	Average	Std. Dev
1	4.59	5.00	4.80	0.15	3.75	4.81	4.52	0.25
2	5.03	5.72	5.44	0.12	3.55	5.58	5.09	0.31
3	5.41	6.60	6.04	0.29	4.34	6.22	5.61	0.28
4	5.87	7.49	6.70	0.46	5.08	7.12	6.12	0.25
5	6.3	8.38	7.33	0.65	5.37	7.64	6.61	0.31
6	6.39	9.27	7.96	0.86	6.11	8.35	7.15	0.36
7	7.14	10.20	8.62	1.06	7.05	8.27	7.62	0.47
8	5.5	10.88	9.06	1.48	7.10	9.77	8.08	0.65
9	8.22	11.77	9.9	1.46	7.21	9.14	8.28	0.54
10	7.37	12.66	10.57	2.10	8.20	11.19	8.95	0.96

The log K_{OW} PDFs generated from the Monte Carlo simulation were used to derive log K_{OC} PDFs. Empirical correlations relating K_{OW} to K_{OC} were available for PCBs.⁽¹²⁴⁾ However, as yet there are no similar correlations for PBDEs. To generate K_{OC} distributions for PBDE and PCB homologs, empirical correlations for other compounds that share similarities to PBDEs (e.g., aromaticity, halogenation, and degree of hydrophobicity) were used. These compounds included organopesticides, polyaromatic hydrocarbons (PAHs), and halogenated benzenes.^(123-126,128-130,132) A summary of the empirical correlations relating log K_{OW} to log K_{OC} is included in Table 2.6. Expressing the empirical correlations as $A \cdot \log K_{OW} + B$, where the A value ranged from 0.63 to 1 (average \pm sd) (0.96 ± 0.60) and the b value ranged from -0.81 to 1.38 (0.22 ± 0.58). The log K_{OC} distribution generated from the Monte Carlo simulations and fraction organic carbon (f_{OC}) were used to estimate sediment water partitioning coefficient (K_d) as shown in Equation 2.7.

While it is common to express K_d as a function of K_{OC} and f_{OC} , adsorption of sorbates (PBDEs and PCBs) to BC was also considered. This can be achieved by expanding Equation 2.7 to include BC adsorption component as shown in Equation 2.24. The porewater-BC partitioning coefficient (K_{BC}) was defined in Equation 2.20. Adsorption to BC is expected to behave as a Freundlich isotherm; empirical correlations to predict the Freundlich constant for PBDE and PCB adsorption to BC are shown in Equations 2.22 to 2.23. A more detailed explanation of the PBDE and PCB BC adsorption was included in Chapter 2.6.4.

For diffusion and advection-diffusion modeling purposes, the dissolved aqueous phase concentration (C_w) was set to saturation concentration (C_{sat}). As the goal of this study is to predict the most mobile PBDE and PCB diffusion and advection-diffusion transport processes, C_w were approximated as C_{sat} . Increased C_w values ensure higher mass flux out of the boundary layer from the aqueous phase therefore inducing the most mobile contaminant migration scenario from the standpoint of the aqueous phase mobility.

C_{sat} values were estimated in USEPA EPI v4.1 program via two methodologies (WSKOW estimates C_{sat} concentration from K_{OW} values and WATERNT estimates C_{sat} concentration from bond

contribution method).⁽²⁵⁾ The predicted values for each PBDE and PCB congeners are shown in Table A2.5 and A2.6. For model simplification, Monte Carlo simulation used the same value for congeners from the same homolog. USEPA EPI predicted C_{sat} values for PCB homologs were generally close to literature values; these values are summarized in Table 5.2.

Table 5.2: C_{Sat} values (ug/L) predicted by USEPA EPI v4.11 software. Comparison to literature values is included when available.

Homolog	PBDE			PCB		
	Avg	Sd	Literature values	Avg	Sd	Literature values ⁽¹⁾
H1	2238	826		3454	1850	1269-5860
H2	386	196		961	384	60-2089
H3	68	56	70-130	220	116	15-414
H4	13	12	60-150	48	37	1-103
H5	2.5	2.5	40-94	12	15	5-20
H6	0.6	1.2	0.9	2.7	2.1	0.2-5
H7	0.09	0.09	1.5	1.1	2.1	0.3-2
H8	0.02	0.02		0.13	0.11	0.3-2
H9	0.003	0.003		0.04	0.05	0.02-1
H10	0.001	0.001		0.04	0.03	0.001

References:

⁽¹⁾: From ⁽¹⁸⁾

Absorption of PBDEs and PCBs to OC was expected to be linear. However, PBDE and PCB adsorption to BC was expected to better fit a Freundlich isotherm.^(27,224) The NF term in Equation 2.20 reflects the adsorption degree. In sludge, NF values for PBDEs ranged from 0.2 to 0.6.⁽²⁷⁾ It is also observed that the NF values for individual congeners were larger than congeners mixed in TMs,⁽²⁷⁾ indicating that PBDE homolog partitioning can be a synergistic process. To the best of my knowledge, there are not yet literature reports of NF values for PCBs. Literature values for NF for phenanthrene adsorbed to lacustrine sediments and soils, spiked sediments or soils, soot (pure and isolated), and charcoal have variability between 0.24 to 0.79.^(137,138,225) Given that the PBDE NF values were similar to reported NF values for other organic compounds, it is assumed that PCB NF values are also within a

similar range. The structural similarities between PBDEs and PCBs provide support for the posited assumption that PCB NF values ranged from 0.2 to 0.8, similar to PBDEs. The uncertainties in NF were addressed via Monte Carlo simulation.

D_{mol} is another sorbent parameter that is specific to each PBDE and PCB homolog. D_{mol} can be estimated using the Hayduk-Laudie method shown in Equation 5.9.⁽²²⁶⁾

$$D_{mol} = \frac{13.26 \times 10^{-5}}{\mu^{1.14} V^{0.589}} \quad (5.9)$$

In Equation 5.9, D_{mol} is molecular diffusivity in water (m²/year), μ is viscosity (g/m/second), and V is the molar volume (m³/mol). The calculated D_{mol} at 25°C is summarized in Table 5.3; overall the D_{mol} values for PCBs calculated using the Hayduk-Laudie method (Equation 5.9) were close to those reported in the literature⁽²²⁷⁾ and were larger at higher temperature as expected. Overall, PBDE D_{mol} values were smaller than PCB D_{mol} values for the same homolog. This is consistent with expectation given that PBDEs have a larger molecular weight than PCBs. PBDE and PCB homologs 1 have similar D_{mol} values to tetrachlorobiphenyl (D_{mol} =0.0138 m²/yr), PBDE and PCB homologs 4 and 5 have similar D_{mol} values to dodecane and tetradecane (D_{mol} =0.0161 m²/yr and D_{mol} =0.0161 m²/yr for dodecane and tetradecane, respectively), and PBDE and PCB homologs 8 and 9 have similar D_{mol} values to phenanthrene and pyrene (D_{mol} =0.0139 m²/yr and D_{mol} =0.0142 m²/yr for phenanthrene and pyrene, respectively).^(120,121,222) A comparison of the D_{mol} values is shown in Figure 5.3.

Table 5.3. Predicted D_{mol} ($m^2/year$) at 25°C for PBDE and PCB homologs as calculated by the Hayduk-Laudie method. When available, predicted values were compared to literature value.

Homolog	PBDE		PCB Literature Values ⁽¹⁾
	Calculated	Calculated	
1	0.0190	0.0191	
2	0.0180	0.0182	0.0152
3	0.0171	0.0174	0.0144
4	0.0163	0.0167	0.0137
5	0.0156	0.0160	0.0131
6	0.0150	0.0154	0.0126
7	0.0145	0.0149	0.0121
8	0.0140	0.0144	0.0116
9	0.0135	0.0139	
10	0.0131	0.0135	

Reference:

⁽¹⁾ Reference [227]

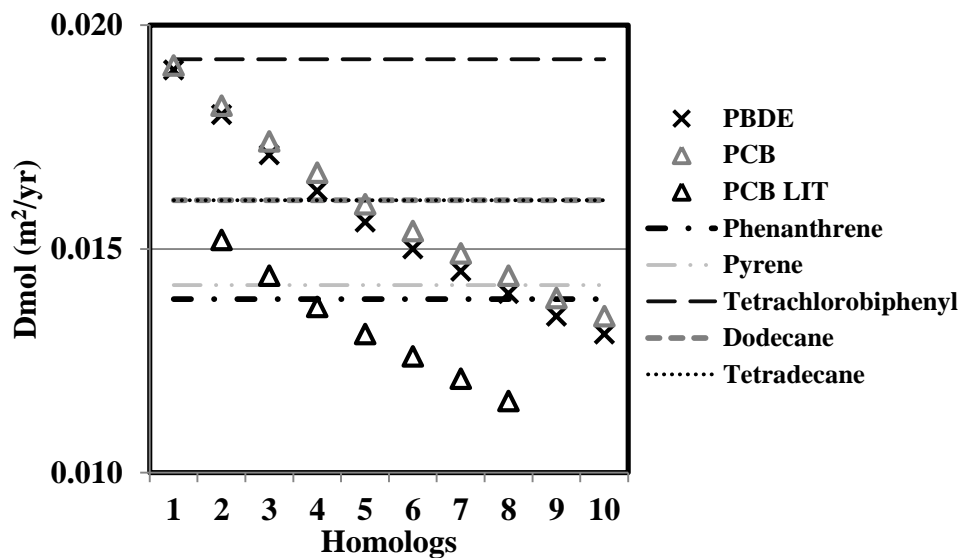


Figure 5.3: Molecular diffusivities (D_{mol}) at 25°C for PBDE and PCB homologs as predicted by Hayduk-Laudie method compared to literature PCB molecular diffusivities at 15°C.⁽²²⁷⁾ Molecular diffusivities (D_{mol}) values for phenanthrene, pyrene, tetrachlorobiphenyl, dodecane, and tetradecane were indicated by horizontal lines.^(120, 121, 222)

5.3.3.2. Sorbent Properties

The sediment columns have variable values of f_{OC} , f_{BC} , ϕ , ρ_{PD} , and K_h . Monte Carlo simulations were applied to these sorbent parameters to address the variability by producing PDFs that are expected to mirror the actual distribution in a particular sediment column. Table 5.4 is a summary of the sediment column properties used to guide the Monte Carlo simulations.

Table 5.4. Sediment column properties used to guide the Monte Carlo simulations.

Column	f_{OC}		f_{BC}		ρ_{PD} (kg/L)		ϕ	
	Avg ⁽¹⁾	SD ⁽²⁾	Avg ⁽¹⁾	SD ⁽²⁾	Avg ⁽¹⁾	SD ⁽²⁾	Avg ⁽¹⁾	SD ⁽²⁾
ACL	0.041	0.011	0.003	0.001	2.523	0.037	84.68	15.38
AED	0.033	0.017	0.002	0.001	2.553	0.047	83.69	10.94
AJL	0.047	0.029	0.002	0.001	2.500	0.082	76.62	11.27
AFR	0.016	0.002	0.002	0.001	2.602	0.005	80.13	11.35
AMW	0.211	0.067	0.003	0.001	2.124	0.144	95.67	6.83
AOT	0.032	0.008	0.005	0.003	2.556	0.025	92.28	3.67
CBC	0.037	0.028	0.018	0.003	2.550	0.058	57.76	10.04
CWP	0.074	0.014	0.038	0.002	2.442	0.041	83.44	7.04
CLC	0.061	0.002	0.035	0.003	2.486	0.009	63.87	1.5
IGC09	0.122	0.016	0.012	0.003	2.314	0.043	87.49	4.67
IGC13	0.128	0.023	0.022	0.005	2.300	0.057	85.72	6.51

⁽¹⁾ Average

⁽²⁾ Standard deviation

K_h measures the upward porewater movement and submarine downward advective water movement in the sediment column. K_h depends partially on the particle size.⁽¹¹⁸⁾ The eleven sediment columns modeled contain agglomerate particle size in the silt to sand size ranges (very fine sand to very coarse sand) range using the USDA size definition. Particle size characterization results were previously summarized in Figure A3.9. Review shows that silt- and sand-sized particles have a wide range of reported K_h values. These reported values were used to estimate the sediment column K_h values. Silt has

K_h values ranging from 1×10^{-7} to 1×10^{-2} cm/sec and sand (very fine sand to very rough sand, clean and mixed) has K_h values ranging from 1×10^{-5} to 1 cm/sec.^(118,228,229) It is assumed that K_h values are proportional to the composition of silt and sand in the sediment columns. The composition of silt and sand in the sediment columns, and the predicted range of K_h values for the sediment columns in this study are shown in Table 5.5. Monte Carlo analysis was applied to generate a cumulative K_h PDF for each sediment core.

Table 5.5. Range of silt and sand composition in the sediment columns (as determined by agglomerate particle size distribution analysis and USDA particle size classification) and predicted range of K_h values (assuming linear proportionality to agglomerate particle size).

Column	Silt composition (min-max)	Sand composition (min-max)⁽¹⁾	K_h(m/yr) (min-max)
ACL	90-100	0.01	0.037-994.00
AED	41-100	0.00-58.56	0.037-750.00
AFR	80-99	1.25-20.19	0.77-211.00
AJL	85-100	0.00-14.83	0.037-151.00
AMW	21-38	61.56-79.36	0.23-800.00
AOT	92-100	0.00-8.48	0.03-80.90
CBC	4-45	54.56-95.90	20.10-960.00
CLC	97-97	1.39-3.13	0.77-41.00
CWP	67-95	4.86-32.56	1.86-331.00
IGC09	50-98	2.10-49.95	1.13-501.00
IGC13	9-92	8.19-90.72	3.32-910.00

⁽¹⁾ Includes very fine sand to very rough sand as classified by the USDA

Hydraulic head gradient, dh/dx results in the movement of porewater induced by differential surface elevation or pressure.⁽²³⁰⁾ In a previous modeling effort by Viana et al. (2011), dh/dx was given a fixed value of 0.005 and 0.05 m/m⁻¹ which was assumed to cover the range of typical hydraulic gradients for North America near shore areas.⁽¹¹⁹⁾ In this study, Monte Carlo analysis was applied to generate a PDF composed of 50,000 dh/dx values between the specified dh/dx interval.

5.3.3.3. Initial Sediment Concentration

In an effort to provide a more realistic simulation condition, initial sediment concentration ($C_{sed}|_{x=0m,t=0}$) was defined from the range of \sum_{49} PBDEs and \sum_{132} PCBs concentration in the sediment columns. A detailed description of the PBDE and PCB distributions was included in Chapter 3. PBDEs have a wider concentration range relative to PCBs. Both contaminants have a left-skewed distribution; however, PCB distribution was extremely left-skewed. Distribution of the \sum_{49} BDEs and \sum_{132} PCB concentrations in the sediment columns is summarized in Table 5.6.

Table 5.6. Distribution of \sum_{49} PBDEs and \sum_{132} PCBs concentrations (ng/g) in the sediment samples at specific percentile.

Percentile	\sum_{49} PBDEs	\sum_{132} PCBs
0.05	1.52E-01	0.00E+00
0.25	9.63E+00	0.00E+00
0.5	6.01E+01	1.91E+01
0.75	1.74E+03	2.62E+02
0.95	3.61E+04	1.64E+03

5.4. Results and Discussion

5.4.1. Sorbate Properties

Site independent PBDE and PCB properties which included K_{OW} , K_{OC} , and K_{FBC} partitioning coefficients are discussed in the following sections in this chapter.

Octanol Water (K_{OW}) and Organic Carbon (K_{OC}) Partitioning Coefficient: Monte Carlo simulation generated 50,000 discreet log K_{OW} values per PBDE and PCB homolog. A summary of the distribution is included in Table D5.1. Log K_{OW} values predicted by Monte Carlo simulation, empirical correlations

(Equations 2.1 and 2.2 for PBDEs and Equations 2.3 to 2.4 for PCBs), and USEPA EPI program are shown in Figure 5.4a-b. Overall, the USEPA EPI v4.11 $\log K_{OW}$ predicted values were higher than the Monte Carlo predicted values at the 95th percentile. Empirical correlation predicted $\log K_{OW}$ values (Equations 2.1 to 2.2 for PBDEs and Equations 2.3 to 2.4 for PCBs) generally were within the Monte Carlo 25th and 5th percentile predicted values. When available, comparison to average literature $\log K_{OW}$ values was also included. Generally the literature $\log K_{OW}$ values were lower or close to the Monte Carlo 5th percentile predicted values.

50,000 discrete $\log K_{OC}$ values were generated per each PBDE and PCB homolog by Monte Carlo simulation. A summary is provided in Table D5.2. PBDE and PCB $\log K_{OC}$ values predicted by Monte Carlo and USEPA EPI v4.11 program are shown in Figure 5.4c-d. In the USEPA EPI v4.11 program, PBDE and PCB $\log K_{OC}$ values were predicted using two methods; the bond contribution method (MCI) and using built-in empirical correlations relating $\log K_{OW}$ to $\log K_{OC}$.⁽²⁵⁾ For both PBDEs and PCBs, the USEPA EPI predicted K_{OC} values were between the Monte Carlo 25th percentile and 5th percentile predicted values.

Application of Monte Carlo simulation resulted in a wider range of $\log K_{OW}$ and $\log K_{OC}$ PDFs with increasing PBDE and PCB homolog size. Overall, PBDE homologs have a wider range of PDFs compared to their counterpart PCB homologs. This is an artifact of the $\log K_{OW}$ values used to guide the Monte Carlo simulations (Table 5.1). The uncertainty as measured by standard deviation was larger for PBDE homologs compared to PCB homologs and increased with larger homologs.

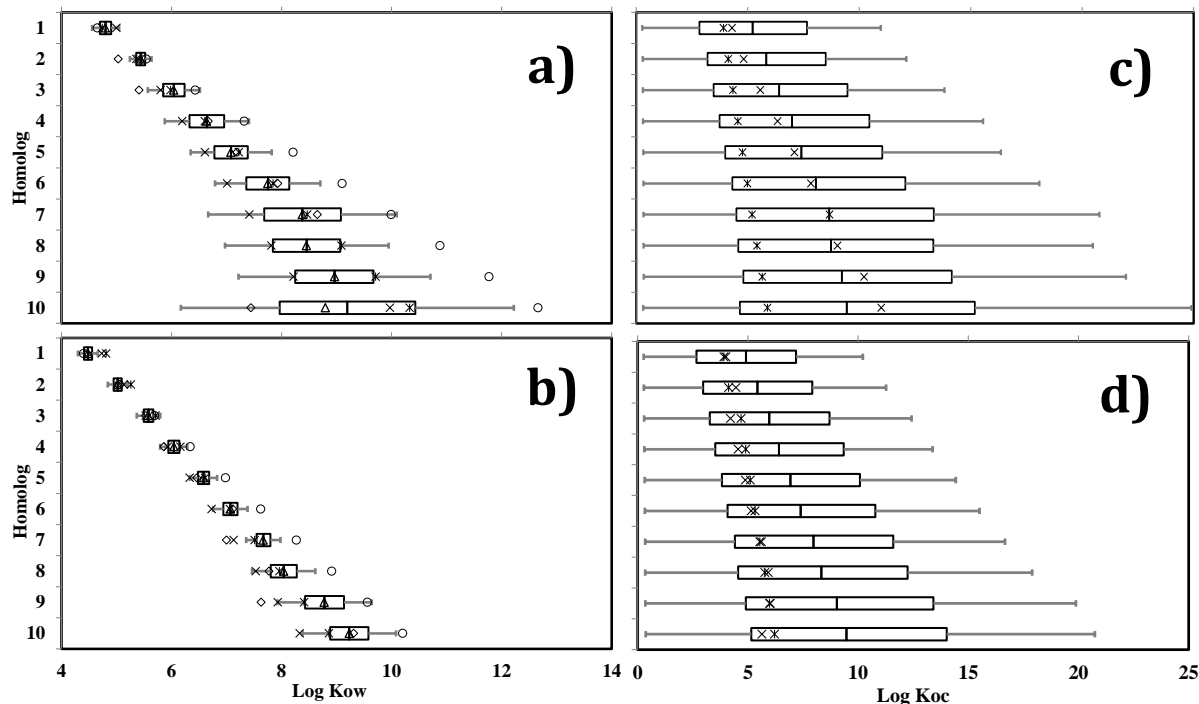


Figure 5.4: Distribution of log K_{OW} (a-b) and log K_{OC} (c-d) as predicted by 50,000 Monte Carlo simulations for PBDEs (a,c) and PCBs (b,d). The 5th and 95th percentiles are shown by the error bars, the box covers the 25th to 75th percentiles, and the middle vertical bar in the box is the 50th percentile. For log K_{OW} , average values used in Monte Carlo simulations are denoted by a hollow triangle. Log K_{OW} values predicted by empirical correlations are denoted by * and ^X (* is Equation 2.1 and ^X is Equation 2.2 for PBDEs; * is Equation 2.3 and ^X is Equation 2.4 for PCBs). USEPA EPI predicted log K_{OW} values are denoted by hollow sphere. Average literature log K_{OW} values are denoted by hollow diamond. For log K_{OC} , ^X are values predicted by EPI MCI method and * are values predicted by EPI KOW method.

Black Carbon Freundlich Adsorption Partitioning Coefficient (K_{FBC}): The porous nature of BC promotes solid phase partitioning of HOCs, such as PBDEs and PCBs. Increased solid phase sorption can effectively retard aqueous phase migration. K_{FBC} was predicted from Equations 2.21 to 2.22 for PBDEs and PCBs, respectively.⁽¹³⁹⁾ Application of the Monte Carlo simulation resulted in the distribution shown in Figure 5.5. A summary of PBDE and PCB K_{FBC} distributions are also included in Table D5.3. The Monte Carlo predicted distribution range was wider for larger PBDE and PCB homologs, and was consistently larger for PBDE homologs relative to PCB homologs. The similarity in K_{FBC} distribution to K_{OW} distribution is an artifact of the dependence of K_{FBC} on K_{OW} .

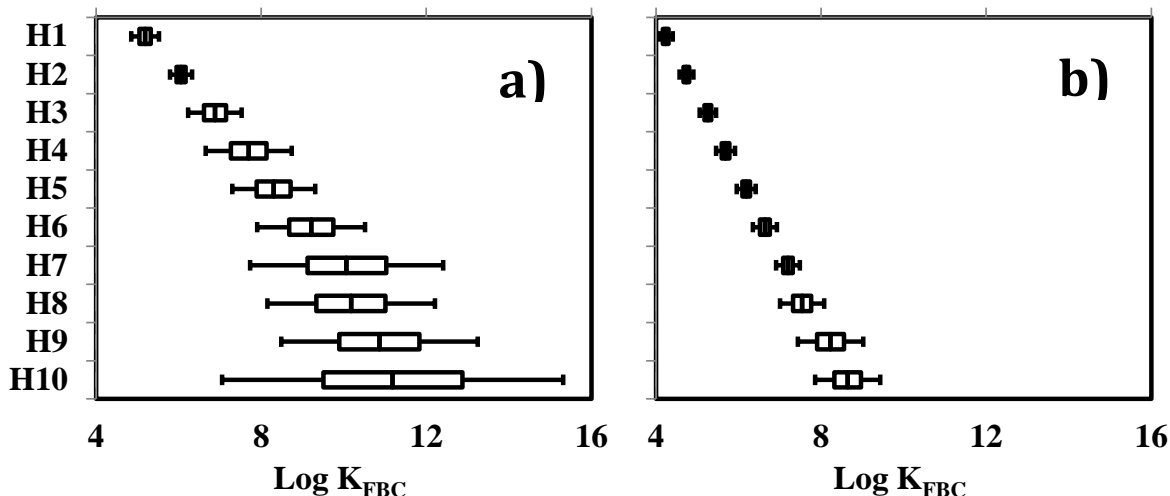


Figure 5.5: Black carbon Freundlich adsorption constant (K_{FBC}) for PBDE (a) and PCB (b) homologs as predicted from literature empirical correlations.⁽¹³⁹⁾

5.4.2. Sorbent Properties

Monte Carlo simulations were used to address the parameter variability within a particular sediment column to generate a representative PDF for each parameter. Among the sorbent properties that affect PBDE and PCB in-situ mass transport are f_{OC} , f_{BC} , ϕ , ρ_{PD} , and K_h . The following sections in this chapter detail the results from the Monte Carlo simulation for these site specific parameters. A summary of the distribution of these site specific properties is included in Table D5.4.

Fraction Organic Carbon (f_{OC}) and Fraction Black Carbon (f_{BC}): Previous physical characterization detailed in Chapter 3.4.1 showed that the sediment columns have a wide range of f_{OC} and f_{BC} values. Additionally, large variation of f_{OC} and f_{BC} values can exist within a particular sediment column. Monte Carlo analysis was used to provide PDFs that reflect the actual distribution in the sediment columns. Results for the Monte Carlo analysis for f_{OC} and f_{BC} are shown in Figure 5.6 (f_{OC} and f_{BC} in panel a and b, respectively). The highest 95th percentile Monte Carlo predicted f_{OC} values were observed in column AMW, followed by IGC13 and IGC09. This is consistent with the physical characterization results (Table 5.4) which indicated that AMW, IGC13, and IGC09 have among the highest f_{OC} values. Monte Carlo

simulation resulted in substantially higher f_{BC} values at the 95th percentile for urban Chicago and IGC sediment columns compared to AR cores, consistent with the higher f_{BC} in Chicago and IGC sediment columns.

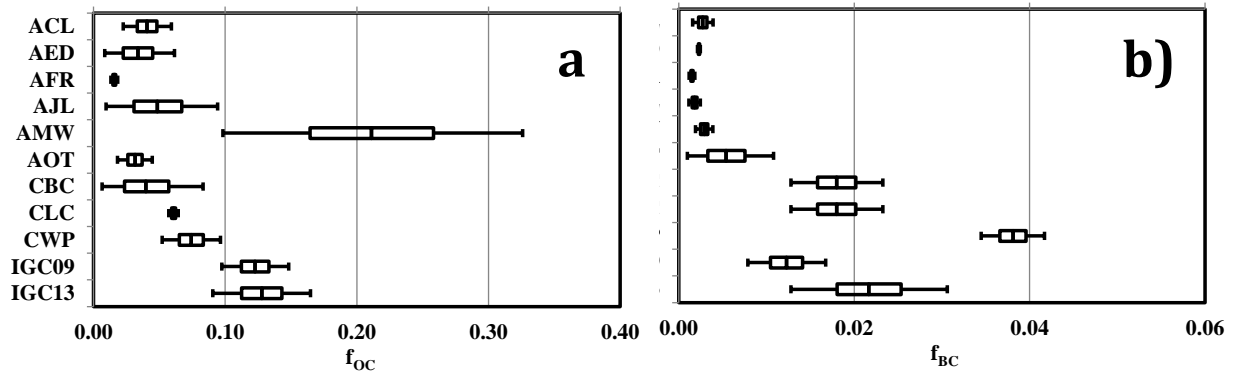


Figure 5.6: Distribution range of fraction organic carbon (f_{OC}) (a) and fraction black carbon (f_{BC}) (b) in the sediment columns as predicted by 50,000 Monte Carlo simulations.

Porosity (ϕ) and Particle Density (ρ_{PD}): ϕ and ρ_{PD} affect mass transport processes by controlling transport length or route. The distribution of ϕ and ρ_{PD} generated from Monte Carlo analysis is shown in Figure 5.7 (ϕ and ρ_{PD} in panel a and b, respectively). The low ϕ in columns CBC and CLC resulted from the particle size distribution in these columns composed primarily of sand particles. Other sediment columns have comparable ϕ values. AMW has the lowest ρ_{PD} while other rural AR sediment columns have ρ_{PD} values comparable to urban (Chicago and IGC) sediment columns.

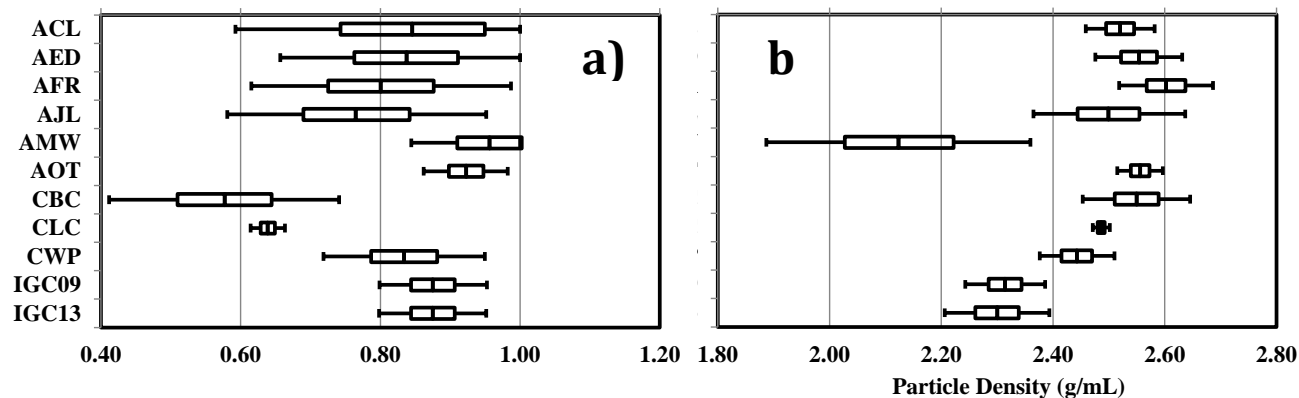


Figure 5.7: Porosity (a) and particle density (b) distribution range in the sediment columns as predicted by 50,000 Monte Carlo simulations.

Hydraulic Conductivity (K_h): Literature review indicates that sand and silt has a wide range of K_h values; Monte Carlo analysis was applied to obtain a representative K_h PDF for each sediment column assuming linear proportionality to agglomerate particle size. K_h distributions are shown in Figure 5.8. Generally, sediment columns with higher silt composition have a lower 95th percentile predicted Monte Carlo K_h values as silt tends to reduce fluid conductivity. Cores that have highly graded PSDs such as CBC, ACL, and AED have a wider range of predicted Monte Carlo K_h values and cores with homogenous PSDs such as CLC, CWP, and AOT have a narrower range of predicted Monte Carlo K_h values. Monte Carlo predicted K_h values at the 95th percentile for the sediment columns in this study were generally larger than saturated material such as organoclay ($K_h = 10 \pm 207$ m/yr), apatite ($K_h = 22 \pm 25$ m/yr), and granular activated carbon ($K_h = 60 \pm 25$ m/yr).⁽¹¹⁹⁻¹²¹⁾

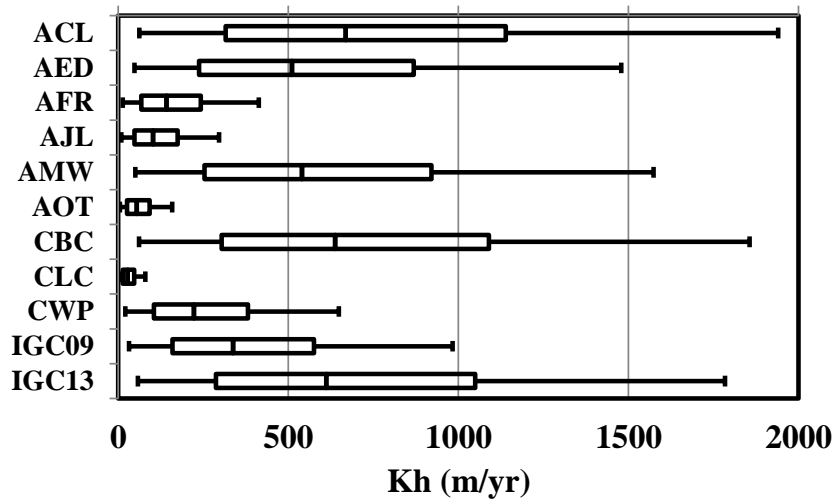


Figure 5.8: Hydraulic conductivity (K_h) distributions in the sediment columns as predicted by 50,000 Monte Carlo simulation.

5.4.3. Sediment Porewater Partitioning Coefficient (K_d)

PBDE and PCB K_d PDFs considering only OC sorption (K_d (OC)) and under OCBC co-sorption (K_d (OCBC)) was predicted via Monte Carlo simulation guided by Equation 2.7 and 2.27, respectively. Monte Carlo predicted $\log K_d$ (OC) and $\log K_d$ (OCBC) values at the 25th, 50th, 75th, and 95th percentile are summarized in Table D5.5a-d (PBDEs: a-b; PCBs:c-d; OC sorption: a,d ; OCBC co-sorption: b,d) and distributions are included in Figure D5.2a-h (PBDEs: a-d; PCBs: e-h; OC sorption: a-b and e-f; OCBC co-sorption: c-d and g-h). PBDE and PCB Monte Carlo predicted $\log K_d$ (OC) and $\log K_d$ (OCBC) values at the 95th percentile are summarized in Figure 5.9a-d (PBDEs:a-b, PCBs:c-d) and Table 5.7a-b.

Table 5.7a (Cont.): PBDE and PCB Monte Carlo predicted log K_d values at the 95th percentile for organic carbon (OC) only sorption, and organic carbon and black carbon (OCBC) sorption.

PBDE log K_d values for OC only sorption										
Site	H1	H2	H3	H4	H5	H6	H7	H8	H9	H10
ACL	3.82	4.41	5.29	6.18	6.59	7.48	8.2	8.86	9.48	10.99
AED	3.84	4.43	5.3	6.19	6.61	7.49	8.22	8.88	9.5	11.01
AFR	3.31	3.9	4.78	5.67	6.08	6.97	7.7	8.36	8.97	10.49
AJL	4.02	4.61	5.49	6.38	6.79	7.68	8.4	9.07	9.68	11.2
AMW	4.56	5.15	6.03	6.92	7.33	8.22	8.94	9.61	10.22	11.73
AOT	3.7	4.29	5.16	6.05	6.47	7.35	8.08	8.74	9.36	10.87
CBC	3.97	4.56	5.44	6.33	6.74	7.63	8.35	9.01	9.63	11.14
CLC	3.86	4.45	5.32	6.22	6.63	7.51	8.24	8.9	9.52	11.03
CWP	4.03	4.62	5.5	6.39	6.8	7.69	8.41	9.08	9.69	11.21
IGC09	4.22	4.81	5.69	6.58	6.99	7.88	8.6	9.26	9.88	11.39
IGC13	4.26	4.85	5.73	6.62	7.04	7.92	8.65	9.31	9.92	11.44
PBDE log K_d values for OCBC co-sorption										
Site	H1	H2	H3	H4	H5	H6	H7	H8	H9	H10
ACL	6.6	8.07	10.23	12.4	13.45	15.61	17.4	19.07	20.57	24.2
AED	6.42	7.89	10.04	12.22	13.27	15.43	17.22	18.88	20.39	24.02
AFR	5.76	7.23	9.39	11.57	12.62	14.77	16.56	18.23	19.74	23.37
AJL	6.6	8.07	10.23	12.4	13.45	15.61	17.4	19.07	20.57	24.2
AMW	7.34	8.81	10.96	13.14	14.19	16.35	18.14	19.81	21.31	24.94
AOT	6.92	8.39	10.55	12.72	13.77	15.93	17.72	19.39	20.89	24.52
CBC	7.52	8.99	11.15	13.33	14.38	16.53	18.32	19.99	21.5	25.12
CLC	7.41	8.88	11.04	13.22	14.26	16.42	18.21	19.88	21.38	25.01
CWP	7.84	9.31	11.47	13.64	14.69	16.85	18.64	20.31	21.81	25.44
IGC09	7.63	9.1	11.26	13.43	14.48	16.64	18.43	20.1	21.6	25.23
IGC13	7.94	9.41	11.57	13.74	14.79	16.95	18.74	20.41	21.91	25.54

Table 5.7a (Cont.): PBDE and PCB Monte Carlo predicted log K_d values at the 95th percentile for organic carbon (OC) only sorption, and organic carbon and black carbon (OCBC) sorption.

PCB log K _d values for OC only sorption										
Site	H1	H2	H3	H4	H5	H6	H7	H8	H9	H10
ACL	3.09	3.63	4.19	4.65	5.19	5.68	6.28	6.65	7.39	7.84
AED	3.01	3.55	4.11	4.57	5.11	5.6	6.2	6.57	7.31	7.76
AFR	2.68	3.22	3.78	4.24	4.78	5.27	5.87	6.24	6.98	7.43
AJL	3.17	3.71	4.27	4.73	5.27	5.75	6.36	6.72	7.47	7.91
AMW	3.81	4.34	4.9	5.36	5.91	6.39	6.99	7.36	8.1	8.55
AOT	2.98	3.52	4.08	4.54	5.08	5.57	6.17	6.54	7.28	7.73
CBC	3.08	3.62	4.18	4.64	5.18	5.67	6.27	6.64	7.38	7.83
CLC	3.26	3.8	4.36	4.82	5.36	5.85	6.45	6.82	7.56	8.01
CWP	3.35	3.89	4.45	4.91	5.45	5.94	6.54	6.91	7.65	8.1
IGC09	3.57	4.11	4.67	5.13	5.67	6.16	6.76	7.13	7.87	8.32
IGC13	3.59	4.13	4.69	5.15	5.69	6.18	6.78	7.15	7.89	8.33
PCB log K _d values for OCBC co-sorption										
Site	H1	H2	H3	H4	H5	H6	H7	H8	H9	H10
ACL	3.09	4.31	5.71	6.93	8.27	9.55	10.9	12.07	13.75	14.6
AED	3.01	4.16	5.56	6.77	8.12	9.39	10.74	11.92	13.59	14.44
AFR	2.68	3.64	5.04	6.26	7.6	8.88	10.22	11.4	13.08	13.93
AJL	3.17	4.21	5.61	6.83	8.17	9.44	10.79	11.97	13.64	14.5
AMW	3.81	5.05	6.45	7.67	9.01	10.29	11.64	12.81	14.49	15.34
AOT	3.18	4.5	5.9	7.11	8.46	9.73	11.08	12.26	13.93	14.79
CBC	3.81	5.12	6.52	7.74	9.08	10.36	11.71	12.88	14.56	15.41
CLC	3.99	5.31	6.71	7.92	9.27	10.54	11.89	13.07	14.74	15.59
CWP	4.4	5.72	7.12	8.34	9.68	10.95	12.3	13.48	15.15	16.01
IGC09	4.13	5.45	6.85	8.06	9.41	10.68	12.03	13.21	14.88	15.73

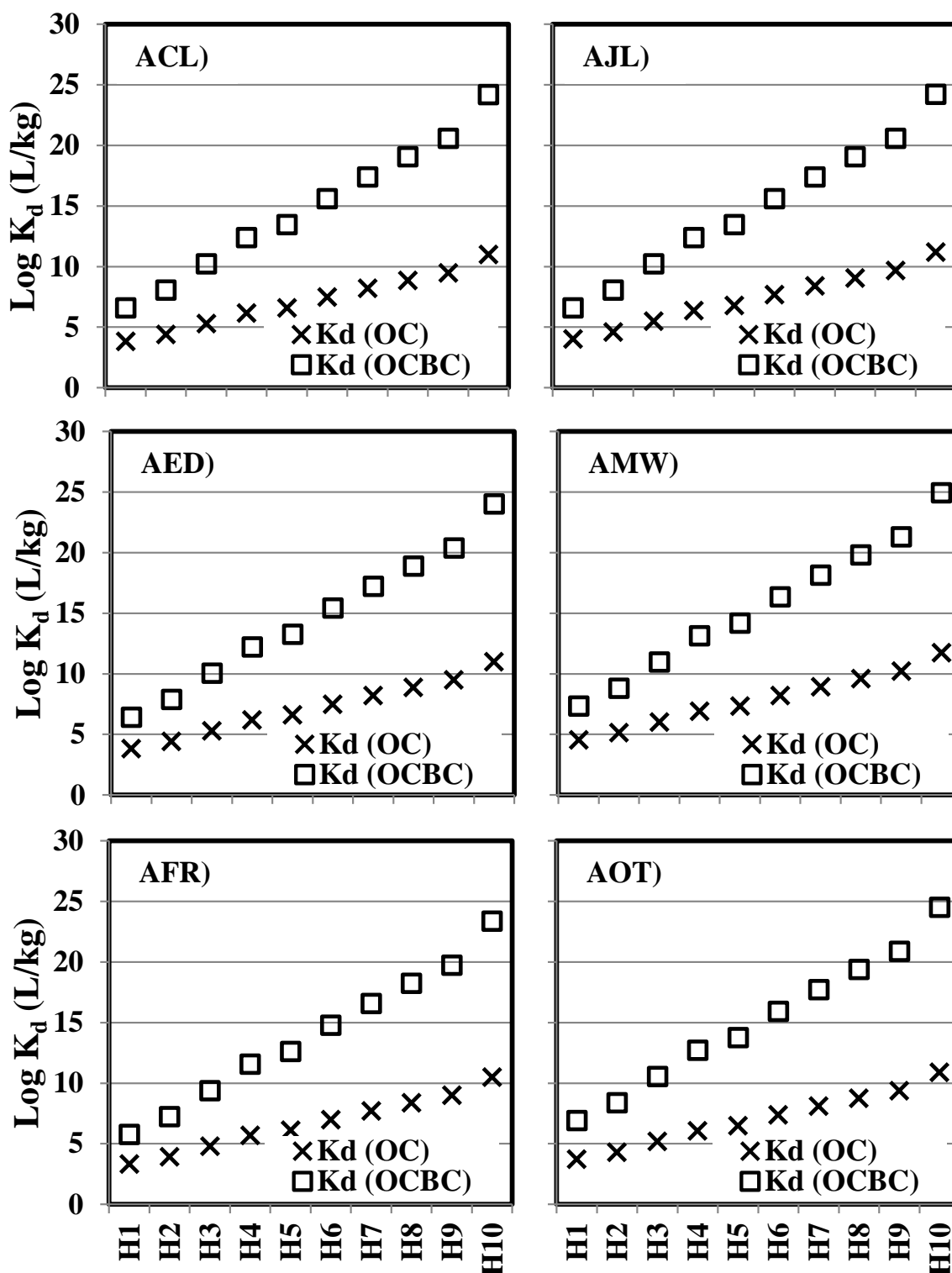


Figure 5.9a: The 95th percentile PBDE log K_d values as predicted by 50,000 Monte Carlo simulations for organic carbon only sorption (K_d (OC)) and organic carbon and black carbon co-sorption (K_d (OCBC)) in AR sediment columns. Y-axes are homologs 1 through 10 (H1-H10).

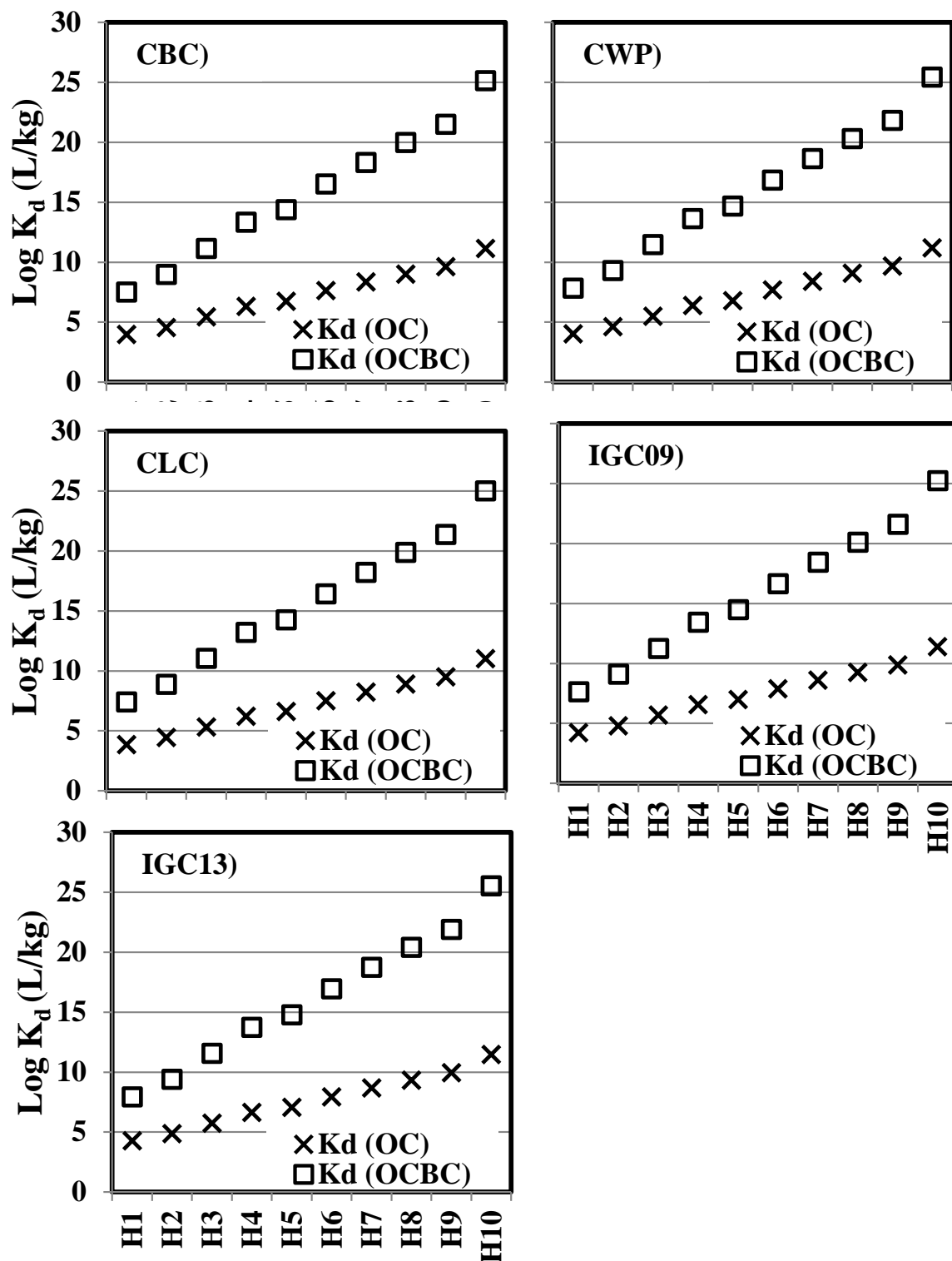


Figure 5.9b: The 95th percentile PBDE log K_d values as predicted by 50,000 Monte Carlo simulations for organic carbon only sorption (K_d (OC)) and organic carbon and black carbon co-sorption (K_d (OCBC)) in Chicago and IGC sediment columns. Y-axes are homologs 1 through 10 (H1-H10).

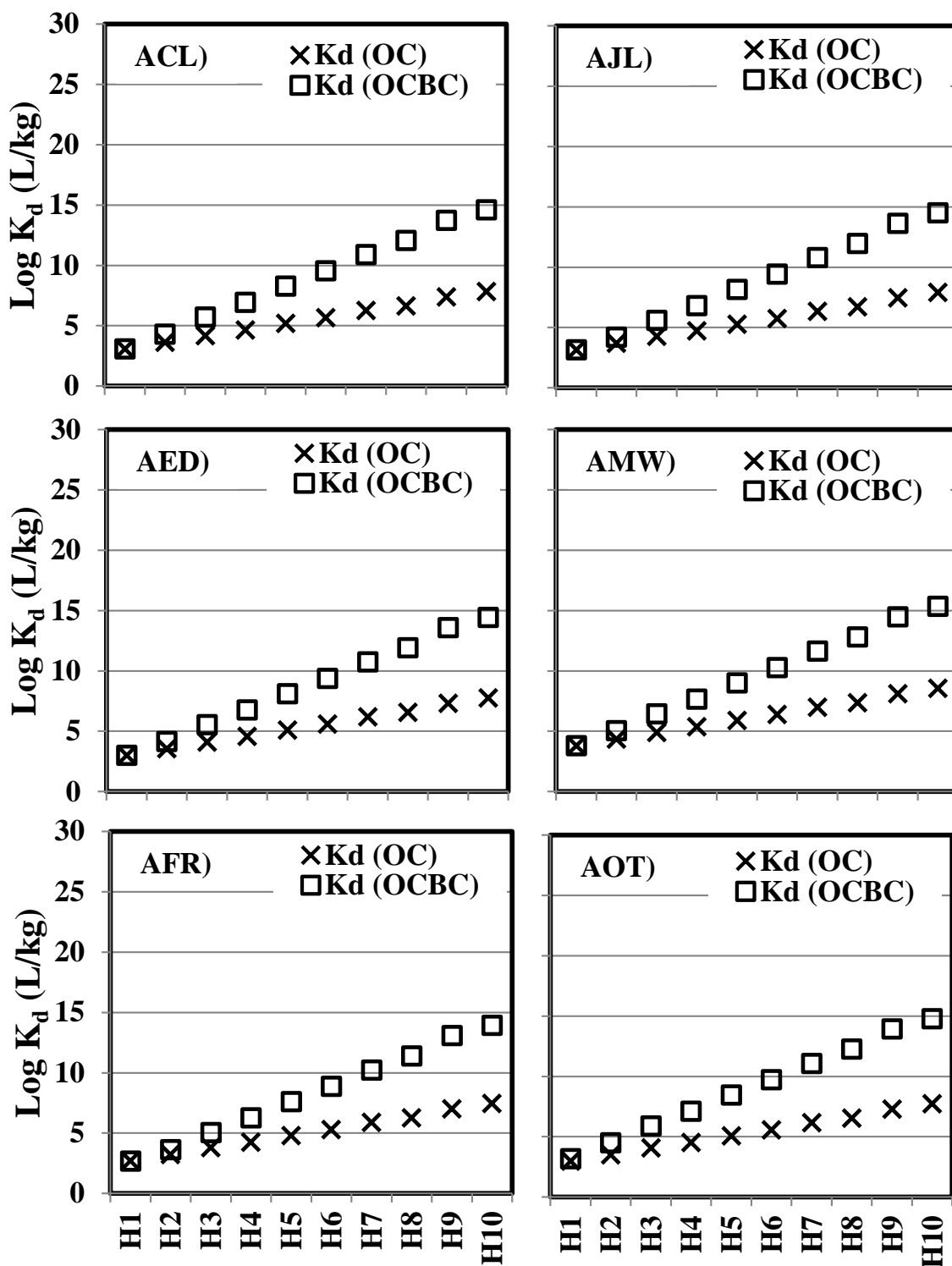


Figure 5.9c: The 95th percentile PCB log K_d values as predicted by 50,000 Monte Carlo simulations for organic carbon only sorption (K_d (OC)) and organic carbon and black carbon co-sorption (K_d (OCBC)) in AR sediment columns. Y-axes are homologs 1 through 10 (H1-H10).

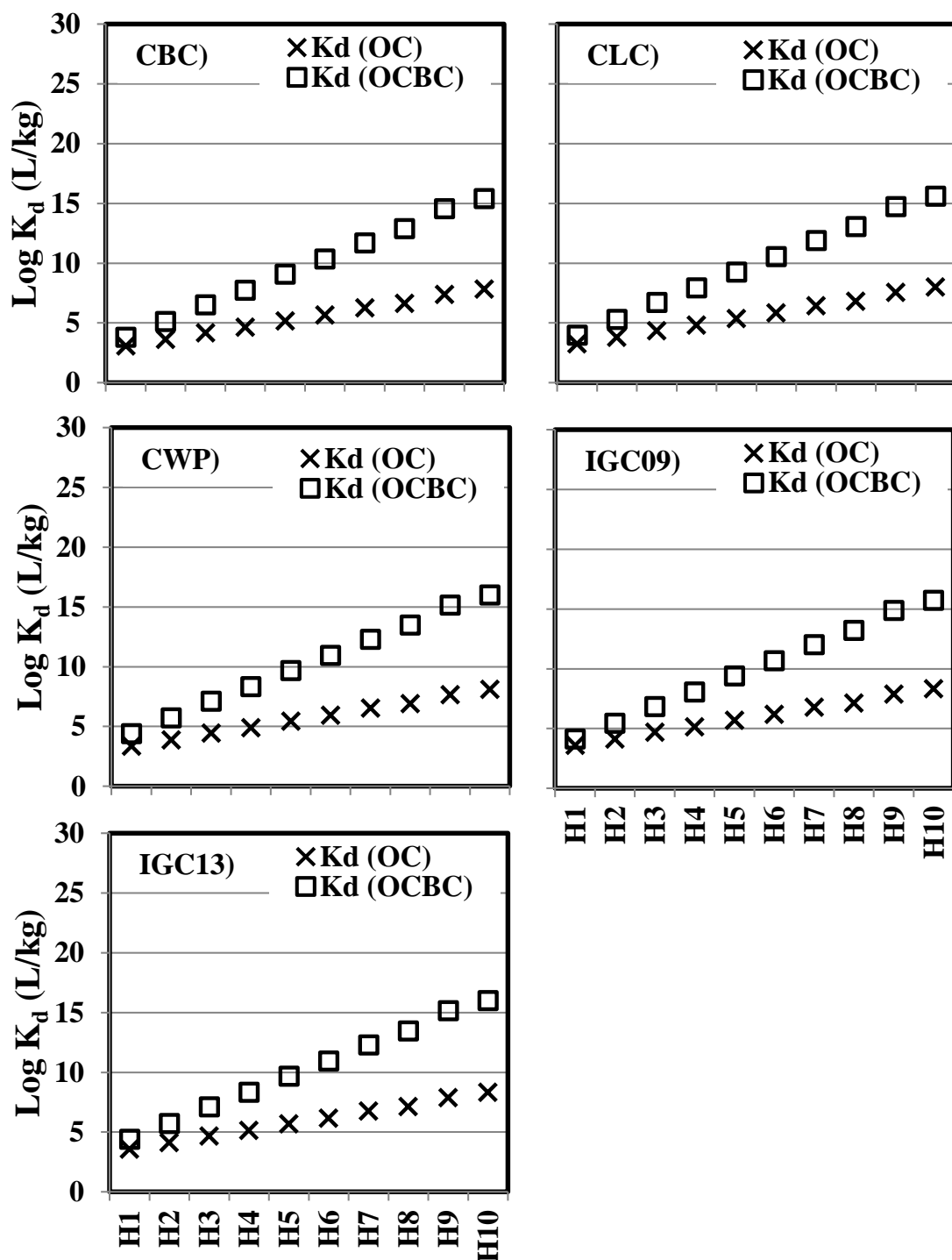


Figure 5.9d: The 95th percentile PCB log K_d values as predicted by 50,000 Monte Carlo simulations for organic carbon only sorption (K_d (OC)) and organic carbon and black carbon co-sorption (K_d (OCBC)) in Chicago and IGC sediment columns. Y-axes are homologs 1 through 10 (H1-H10).

Overall, Monte Carlo predicted $\log K_d$ (OC) and $\log K_d$ (OCBC) values for PBDE homologs were larger than the respective PCB homologs. $\log K_d$ (OC) and $\log K_d$ (OCBC) values increased with increasing PBDE and PCB homologs. This is expected as $\log K_d$ (OC) and $\log K_d$ (OCBC) values are a function of $\log K_{OW}$. Due to their lower hydrophobicity, small PBDE and PCB homologs can partition better into the aqueous phase reflected by their smaller $\log K_d$ (OC) and $\log K_d$ (OCBC) values, whereas large PBDE and PCB homologs tend to partition into the solid phase as shown by their large $\log K_d$ (OC) and $\log K_d$ (OCBC) values.

PBDE and PCB Monte Carlo predicted $\log K_d$ (OC) values for the sediment cores increased in the order of AFR < AOT < AED < CBC < ACL < CLC < AJL < CWP < IGC09 < IGC13 < AMW. This is consistent with the increased order of f_{OC} . The globular, porous structure of BC increases the sorption of hydrophobic organic contaminant to the solid phase which results in larger $\log K_d$ (OCBC) values relative to $\log K_d$ (OC) values. For PBDE and PCB OCBC co-sorption, $\log K_d$ (OCBC) values increased in the order of AFR < AED < AJL < ACL < AOT < AMW < CBC < CLC < IGC09 < IGC13 < CWP which closely resembled the increasing order of f_{BC} which is AFR < AED=AJL < ACL < AOT < AMW < CBC < CLC < IGC09 < IGC13 < CWP. The increased order of f_{BC} did not mirror that of $\log K_d$ (OCBC) because $\log K_d$ (OCBC) is not just a function of f_{BC} , but also of f_{OC} and other sediment properties (Equation 2.27).

The ratios of PBDE and PCB $\log K_d$ (OCBC) to $\log K_d$ (OC) are shown in Figure 5.10a-b. $\log K_d$ (OCBC) values were determined by expanding the $\log K_d$ (OC) expression to include the BC adsorption component ($\log K_{BC}$) which can be mathematically expressed as $f_{BC} * K_{FBC} * C_w^{NF-1}$ (Equation 2.20). The 95th percentile Monte Carlo predicted $\log K_{BC}$ values are summarized in Figure 5.11a-d (PBDEs:a-b; PCBs:c-d) and Table 5.8; the complete distributional values are provided in Table D5.6a-b (PBDEs:a; PCBs:b). $\log K_{BC}$ values for small PBDE and PCB homologs were smaller in rural AR compared to urban Chicago and IGC sites. For example, PBDE homolog 1 in AR, Chicago, and IGC sediment cores have $\log K_{BC}$ values ranging from 0.69 to 1.24, 1.77 to 2.09, and 1.60 to 1.85, respectively whereas PCB homolog 1 in AR, Chicago, and IGC sediment cores have $\log K_{BC}$ values ranging from 0 to

0.20, 0.72 to 1.05, and 0.56 to 0.80, respectively. In large homologs such as homolog 10, only a small disparity in $\log K_{BC}$ values exist between rural AR to urban Chicago and IGC sites. For example, PBDE homolog 10 in AR, Chicago, and IGC sediment cores have $\log K_{BC}$ values ranging from 9.86 to 10.42, 10.94 to 11.27, and 10.77 to 11.02, respectively whereas PCB homolog 10 in AR, Chicago, and IGC sediment cores have $\log K_{BC}$ values ranging from 6.50 to 7.06, 7.58 to 7.91, and 7.42 to 7.66, respectively.

Given the more hydrophobic nature of PBDEs, the $\log K_{BC}$ values for PBDEs were larger than PCBs. $\log K_d(\text{OCBC})$ values of small PBDE and PCB homologs (H1 to ~H3) were only slightly larger or overlap with $\log K_d(\text{OC})$ values; however the disparity between $\log K_d(\text{OCBC})$ values and $\log K_d(\text{OC})$ values increased with increasing PBDE and PCB homologs. This trend is driven by the K_{FBC} and C_w values. Large PBDE and PCB homologs have large $\log K_{FBC}$ values as can be observed in Figure 5.5 which resulted in large $\log K_{BC}$ values and consequently large $\log K_d(\text{OCBC})$ values. Additionally, the C_w values which were approximated as C_{sat} values were small for HMW PBDE and PCB homologs. This resulted in large C_w^{NF-1} values. In LMW PBDE and PCB homologs, the small $\log K_{FBC}$ values led to small $\log K_{BC}$ values and consequently small $\log K_d(\text{OCBC})$ values. Additionally, the higher C_{sat} in LMW PBDE and PCB homologs resulted in small C_w^{NF-1} and in some cases, negligible $\log K_{BC}$ values for small PBDE and PCB homologs. The combination of these two factors resulted in lower ratios of $\log K_d(\text{OC})$ to $\log K_d(\text{OCBC})$ for small PBDE and PCB homologs and higher ratio of $\log K_d(\text{OC})$ to $\log K_d(\text{OCBC})$ in large PBDE and PCB homologs. This observation indicates that mass transport processes of small PBDE and PCB homologs are primarily driven by the OC component whereas the presence of BC can be a control mechanism for the transport processes of large PBDE and PCB homologs.

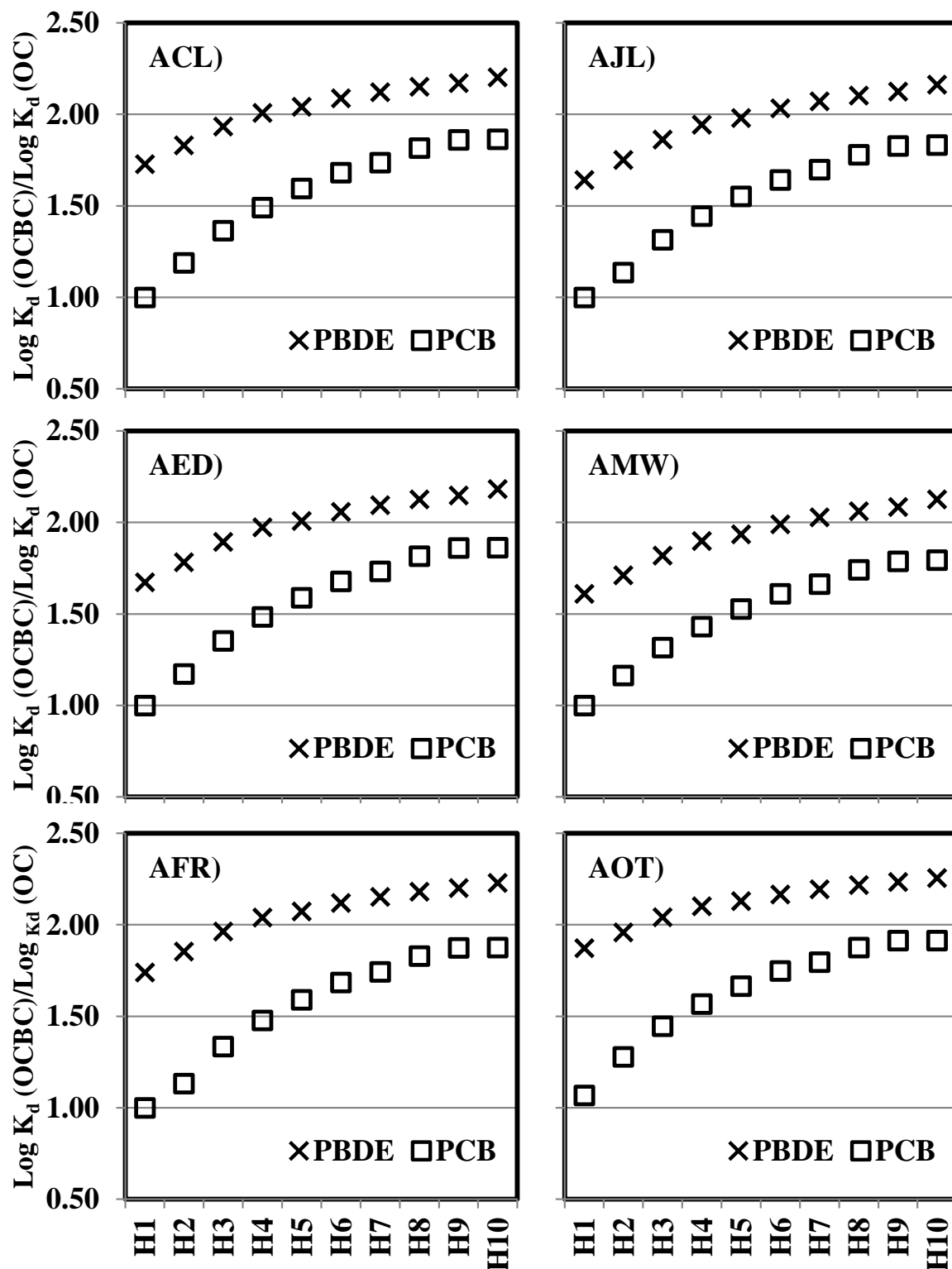


Figure 5.10a: Ratios of PBDE and PCB sediment porewater partitioning coefficient under sorption to organic carbon only and organic carbon and black carbon co-sorption ($\log K_d (\text{OCBC})/\log K_d (\text{OC})$) in AR sediment cores.

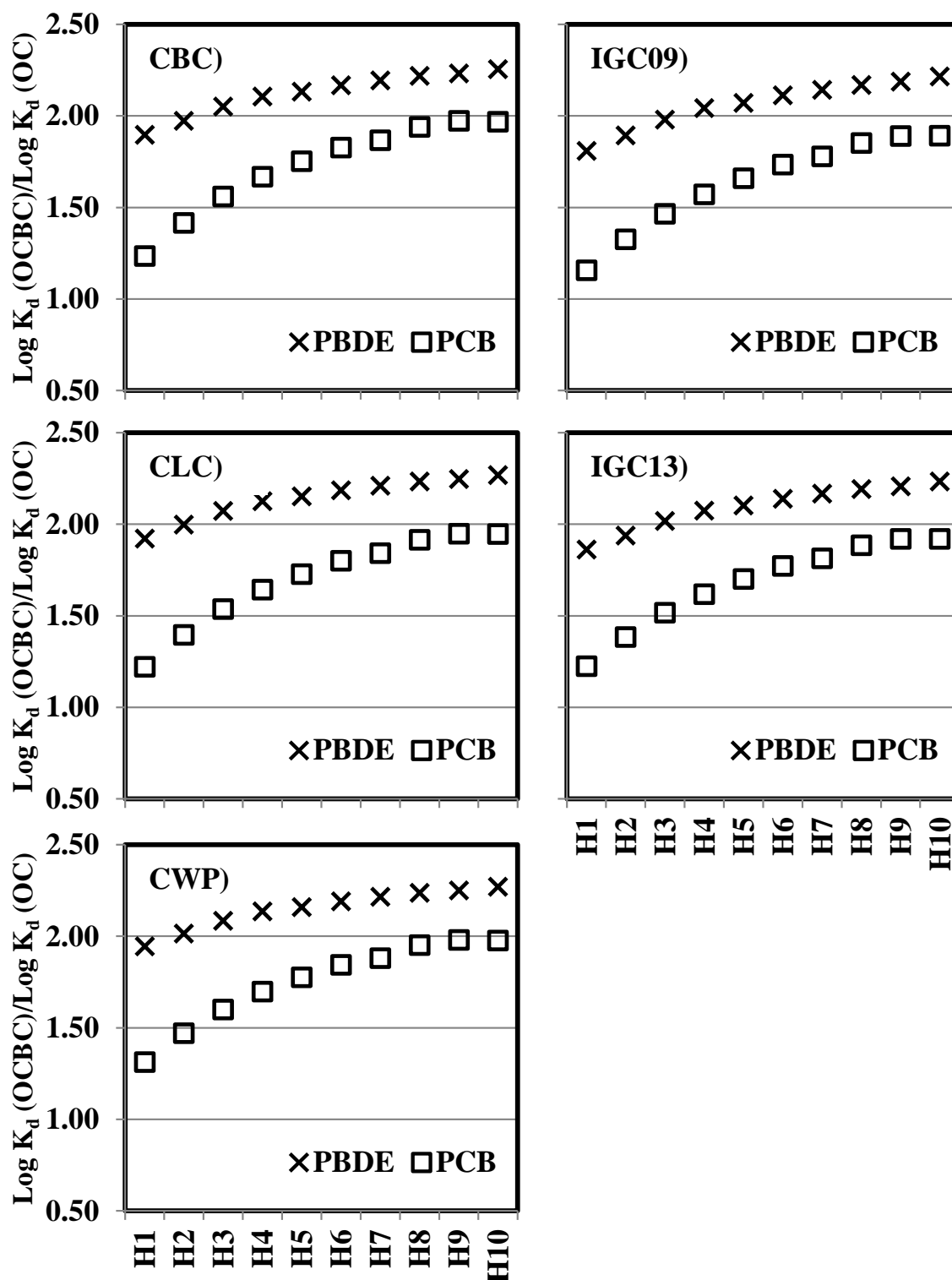


Figure 5.10b: Ratios of PBDE and PCB sediment porewater partitioning coefficient under sorption to organic carbon only and organic carbon and black carbon co-sorption ($\log K_d(\text{OCBC})/\log K_d(\text{OC})$) in Chicago and IGC sediment cores.

Table 5.8. Monte Carlo predicted PBDE and PCB log K_{BC} values at the 95th percentile in all sediment cores.

PBDE log K_{BC} values										
Site	H1	H2	H3	H4	H5	H6	H7	H8	H9	H10
ACL	2.78	3.66	4.94	6.22	6.86	8.13	9.20	10.20	11.09	13.21
AED	2.58	3.46	4.74	6.03	6.66	7.93	9.00	10.00	10.89	13.01
AFR	2.45	3.33	4.61	5.90	6.53	7.80	8.87	9.87	10.76	12.88
AJL	2.58	3.46	4.74	6.02	6.66	7.93	9.00	10.00	10.89	13.01
AMW	2.78	3.66	4.94	6.22	6.86	8.13	9.20	10.20	11.09	13.21
AOT	3.22	4.10	5.38	6.67	7.30	8.57	9.64	10.64	11.54	13.65
CBC	3.56	4.44	5.71	7.00	7.64	8.91	9.97	10.98	11.87	13.98
CLC	3.56	4.44	5.71	7.00	7.64	8.91	9.97	10.98	11.87	13.98
CWP	3.81	4.69	5.97	7.25	7.89	9.16	10.23	11.23	12.12	14.24
IGC09	3.41	4.29	5.57	6.86	7.49	8.76	9.83	10.83	11.73	13.84
IGC13	3.67	4.56	5.83	7.12	7.75	9.03	10.09	11.10	11.99	14.10
PCB log K_{BC} values										
Site	H1	H2	H3	H4	H5	H6	H7	H8	H9	H10
ACL	1.64	2.20	2.81	3.34	3.90	4.48	5.07	5.75	6.75	7.16
AED	1.44	2.00	2.61	3.14	3.70	4.28	4.88	5.56	6.55	6.96
AFR	1.31	1.87	2.48	3.01	3.57	4.15	4.75	5.43	6.42	6.83
AJL	1.44	2.00	2.61	3.13	3.70	4.28	4.87	5.55	6.55	6.96
AMW	1.64	2.20	2.81	3.33	3.90	4.48	5.07	5.75	6.75	7.16
AOT	2.08	2.64	3.26	3.78	4.34	4.92	5.52	6.20	7.19	7.61
CBC	2.42	2.98	3.59	4.11	4.68	5.26	5.85	6.53	7.53	7.94
CLC	2.42	2.98	3.59	4.11	4.68	5.26	5.85	6.53	7.53	7.94
CWP	2.67	3.23	3.84	4.36	4.93	5.51	6.10	6.78	7.78	8.19
IGC09	2.27	2.83	3.45	3.97	4.53	5.11	5.71	6.39	7.39	7.80
IGC13	2.54	3.10	3.71	4.23	4.79	5.38	5.97	6.65	7.65	8.06

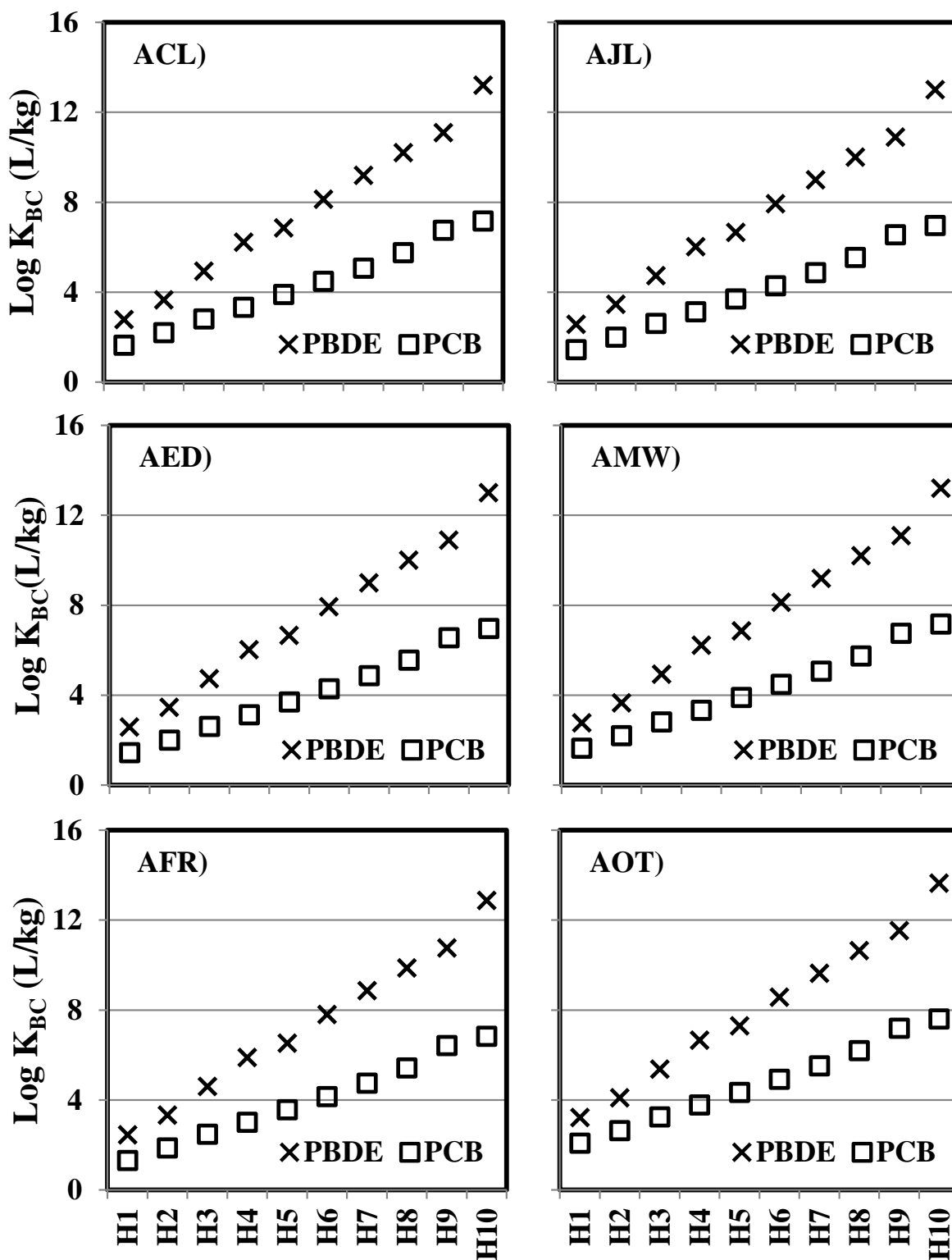


Figure 5.11a: The 95th percentile PBDE and PCB black carbon-porewater partitioning coefficient (log K_{BC}) as predicted by Monte Carlo simulation in AR sediment cores.

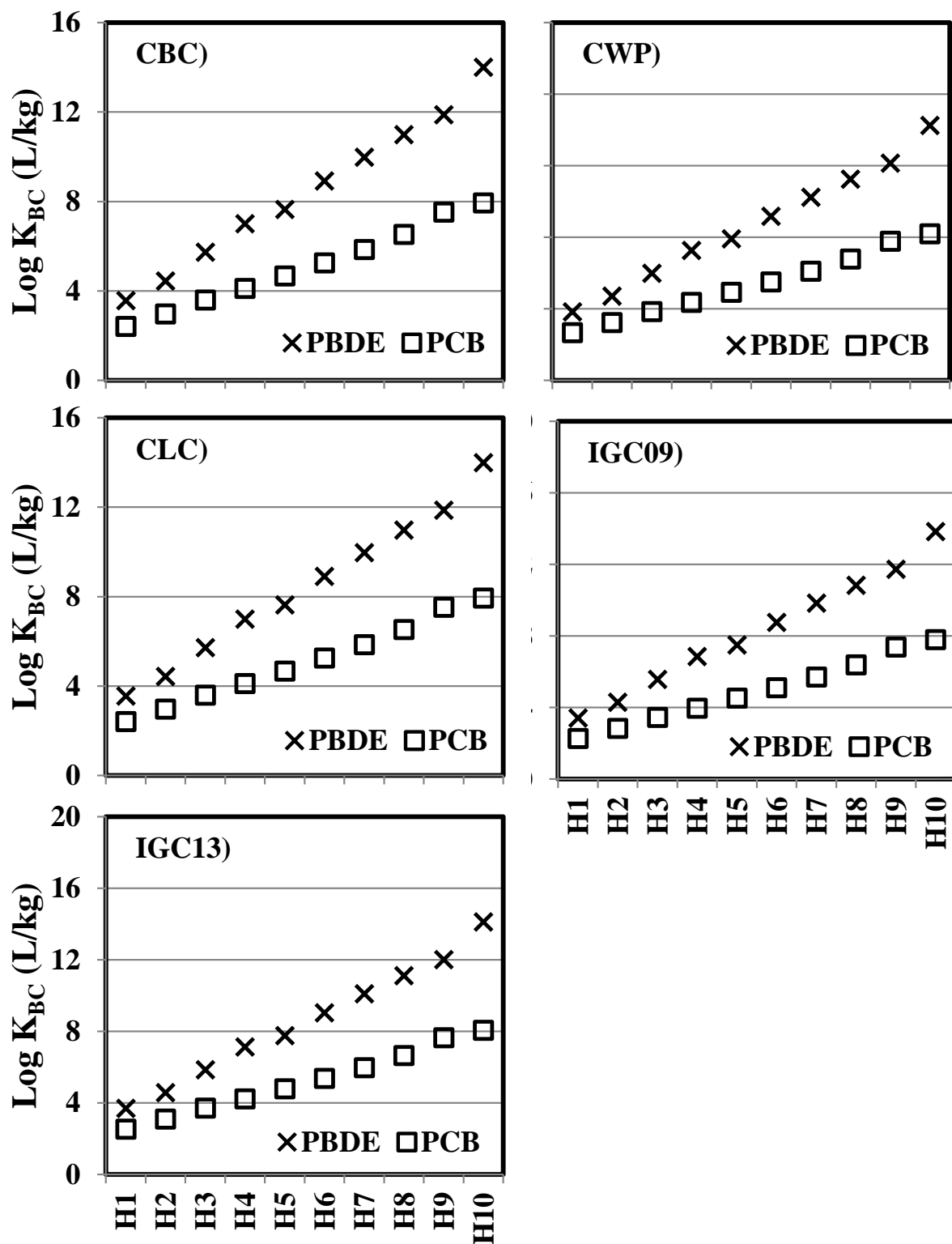


Figure 5.11b: The 95th percentile PBDE and PCB black carbon-porewater partitioning coefficient (log K_{BC}) as predicted by Monte Carlo simulation in Chicago and IGC sediment cores.

5.4.4. PBDE and PCB Diffusion And Advection-Diffusion Transport Processes

5.4.4.1. Observed Diffusivities (D_{obs})

D_{obs} quantifies the aqueous phase mobility of the contaminant driven by the concentration gradient. D_{obs} values were calculated from predicted K_d (OC) and K_d (OCBC) values. The Monte Carlo predicted D_{obs} distributions under OC only sorption (D_{obs} (OC)) and under OCBC co-sorption (D_{obs} (OCBC)) are included in Table D5.7a-d (PBDEs: a-b ; PCBs:c-d; OC sorption: a,c ; OCBC co-sorption: b,d), distributions of the D_{obs} (OC) and D_{obs} (OCBC) values are included in Figure D5.3 a-h (PBDEs: a-d; PCBs: e-h; OC sorption: a-b, e-f; OCBC co-sorption: b-d, g-h). A summary of the D_{obs} (OC) and D_{obs} (OCBC) values at the 95th percentile is provided in Figure 5.12a-d (PBDEs:a-b, PCBs:c-d) and Table 5.9.

Overall, PBDE D_{obs} (OC) and D_{obs} (OCBC) values were smaller than PCBs. The relatively HMW of PBDEs can retard diffusion process. With increasing PBDE and PCB homologs, D_{obs} (OC) and D_{obs} (OCBC) values decreased as expected. In the eleven sediment cores, PBDE and PCB D_{obs} (OC) and D_{obs} (OCBC) values can span >5 and >10 orders of magnitude, respectively. Generally, PBDE and PCB D_{obs} (OC) values increased in the order of CLC < IGC09 < IGC13 < AMW < CWP < ACL < CBC < AFR < AJL < AOT < AED; however, PBDE and PCB D_{obs} (OCBC) values increased in the order of CWP < CLC < IGC13 < IGC09 < CBC < AMW < ACL < AFR < AED < AJL < AOT. BC inclusion substantially reduced the magnitude of PBDE and PCB mass transport via diffusion as evidenced by the much smaller Chicago and IGC D_{obs} (OCBC) values relative to AR sediment cores.

As was previously discussed, BC inclusion can more than double the log K_d (OCBC) relative to log K_d (OC) values in large PBDE and PCB homologs. This effect was also observed in D_{obs} (OC) and D_{obs} (OCBC). Large log K_d (OCBC) and log K_d (OC) values corresponded to small D_{obs} (OC) and D_{obs} (OCBC) values, respectively; therefore D_{obs} (OC) and D_{obs} (OCBC) values decreased with increasing

PBDE and PCB homologs in addition to decreased ratio of D_{obs} (OCBC) to D_{obs} (OC) with increasing PBDE and PCB homologs (Figure 5.13a-d).

Table 5.9 (Cont.): The 95th percentile Monte Carlo predicted PBDE and PCB observe diffusivity (D_{obs}) values for organic carbon only sorption (OC), and organic carbon and black carbon co-sorption (OCBC).

PBDE D_{obs} values for OC only sorption										
Site	H1	H2	H3	H4	H5	H6	H7	H8	H9	H10
ACL	2.81E-06	5.49E-07	2.47E-07	1.16E-07	3.73E-08	1.70E-08	1.25E-08	7.94E-09	4.35E-09	2.36E-09
AED	9.46E-06	1.85E-06	8.30E-07	3.89E-07	1.26E-07	5.74E-08	4.21E-08	2.67E-08	1.47E-08	7.95E-09
AFR	5.14E-06	1.00E-06	4.51E-07	2.11E-07	6.82E-08	3.12E-08	2.28E-08	1.45E-08	7.96E-09	4.32E-09
AJL	6.57E-06	1.28E-06	5.77E-07	2.70E-07	8.72E-08	3.98E-08	2.92E-08	1.86E-08	1.02E-08	5.52E-09
AMW	1.92E-06	3.76E-07	1.69E-07	7.91E-08	2.55E-08	1.17E-08	8.55E-09	5.43E-09	2.98E-09	1.62E-09
AOT	8.15E-06	1.59E-06	7.15E-07	3.35E-07	1.08E-07	4.94E-08	3.62E-08	2.30E-08	1.26E-08	6.85E-09
CBC	4.24E-06	8.27E-07	3.72E-07	1.74E-07	5.62E-08	2.57E-08	1.88E-08	1.20E-08	6.56E-09	3.56E-09
CLC	1.20E-06	2.35E-07	1.05E-07	4.95E-08	1.59E-08	7.29E-09	5.34E-09	3.40E-09	1.86E-09	1.01E-09
CWP	1.98E-06	3.86E-07	1.74E-07	8.14E-08	2.62E-08	1.20E-08	8.79E-09	5.59E-09	3.06E-09	1.66E-09
IGC09	1.44E-06	2.80E-07	1.26E-07	5.90E-08	1.90E-08	8.70E-09	6.38E-09	4.05E-09	2.22E-09	1.21E-09
IGC13	1.56E-06	3.05E-07	1.37E-07	6.43E-08	2.07E-08	9.47E-09	6.95E-09	4.42E-09	2.42E-09	1.31E-09
PBDE D_{obs} values for OCBC co-sorption										
Site	H1	H2	H3	H4	H5	H6	H7	H8	H9	H10
ACL	2.81E-06	1.21E-07	4.07E-09	1.64E-10	2.73E-12	1.25E-13	1.25E-14	5.67E-16	4.86E-17	3.53E-17
AED	9.46E-06	2.99E-07	1.01E-08	4.04E-10	6.75E-12	3.09E-13	3.10E-14	1.40E-15	1.20E-16	8.73E-17
AFR	5.14E-06	2.96E-07	9.99E-09	4.01E-10	6.69E-12	3.06E-13	3.07E-14	1.39E-15	1.19E-16	8.65E-17
AJL	6.57E-06	3.89E-07	1.31E-08	5.27E-10	8.79E-12	4.02E-13	4.03E-14	1.82E-15	1.56E-16	1.14E-16
AMW	1.92E-06	6.80E-08	2.29E-09	9.21E-11	1.54E-12	7.03E-14	7.05E-15	3.19E-16	2.74E-17	1.99E-17
AOT	8.15E-06	5.65E-07	1.91E-08	7.65E-10	1.28E-11	5.84E-13	5.86E-14	2.65E-15	2.27E-16	1.65E-16
CBC	4.24E-06	2.23E-08	7.53E-10	3.02E-11	5.05E-13	2.31E-14	2.32E-15	1.05E-16	8.99E-18	6.53E-18
CLC	1.20E-06	6.34E-09	2.14E-10	8.58E-12	1.43E-13	6.56E-15	6.57E-16	2.97E-17	2.55E-18	1.85E-18
CWP	8.34E-07	3.87E-09	1.30E-10	5.23E-12	8.73E-14	4.00E-15	4.01E-16	1.81E-17	1.56E-18	1.13E-18
IGC09	1.44E-06	1.23E-08	4.15E-10	1.67E-11	2.78E-13	1.27E-14	1.28E-15	5.77E-17	4.95E-18	3.59E-18
IGC13	1.56E-06	8.24E-09	2.78E-10	1.11E-11	1.86E-13	8.52E-15	8.54E-16	3.86E-17	3.31E-18	2.41E-18

Table 5.9 (Cont.): The 95th percentile Monte Carlo predicted PBDE and PCB observe diffusivity (D_{obs}) values for organic carbon only sorption (OC), and organic carbon and black carbon co-sorption (OCBC).

PCB D_{obs} values for OC only sorption										
Site	H1	H2	H3	H4	H5	H6	H7	H8	H9	H10
ACL	5.10E-06	1.40E-06	3.98E-07	1.43E-07	3.93E-08	2.89E-08	1.39E-08	1.32E-08	4.39E-09	3.05E-09
AED	1.72E-05	4.71E-06	1.34E-06	4.81E-07	1.32E-07	9.72E-08	4.69E-08	4.46E-08	1.48E-08	1.03E-08
AFR	9.37E-06	2.58E-06	7.28E-07	2.61E-07	7.19E-08	5.28E-08	2.55E-08	2.42E-08	8.03E-09	5.58E-09
AJL	1.19E-05	3.27E-06	9.31E-07	3.34E-07	9.19E-08	6.75E-08	3.26E-08	3.10E-08	1.03E-08	7.13E-09
AMW	3.49E-06	9.57E-07	2.73E-07	9.77E-08	2.69E-08	1.98E-08	9.53E-09	9.06E-09	3.00E-09	2.09E-09
AOT	1.48E-05	4.06E-06	1.16E-06	4.14E-07	1.14E-07	8.38E-08	4.04E-08	3.84E-08	1.27E-08	8.84E-09
CBC	7.68E-06	2.11E-06	6.00E-07	2.15E-07	5.92E-08	4.35E-08	2.10E-08	1.99E-08	6.62E-09	4.60E-09
CLC	2.18E-06	5.98E-07	1.70E-07	6.10E-08	1.68E-08	1.24E-08	5.95E-09	5.66E-09	1.88E-09	1.30E-09
CWP	3.59E-06	9.84E-07	2.80E-07	1.00E-07	2.77E-08	2.03E-08	9.80E-09	9.32E-09	3.09E-09	2.15E-09
IGC09	2.60E-06	7.14E-07	2.03E-07	7.29E-08	2.01E-08	1.47E-08	7.11E-09	6.76E-09	2.24E-09	1.56E-09
IGC13	2.84E-06	7.78E-07	2.22E-07	7.94E-08	2.19E-08	1.61E-08	7.74E-09	7.36E-09	2.44E-09	1.70E-09
PCB D_{obs} values for OCBC co-sorption										
Site	H1	H2	H3	H4	H5	H6	H7	H8	H9	H10
ACL	5.10E-06	1.40E-06	2.84E-07	1.04E-08	2.58E-10	1.96E-11	1.18E-12	1.30E-13	6.93E-15	2.12E-16
AED	1.72E-05	4.71E-06	7.03E-07	2.56E-08	6.38E-10	4.84E-11	2.91E-12	3.21E-13	1.71E-14	5.24E-16
AFR	9.37E-06	2.58E-06	6.97E-07	2.54E-08	6.32E-10	4.80E-11	2.89E-12	3.18E-13	1.70E-14	5.20E-16
AJL	1.19E-05	3.27E-06	9.15E-07	3.34E-08	8.31E-10	6.30E-11	3.79E-12	4.18E-13	2.23E-14	6.83E-16
AMW	3.49E-06	9.57E-07	1.60E-07	5.84E-09	1.45E-10	1.10E-11	6.63E-13	7.30E-14	3.90E-15	1.19E-16
AOT	1.48E-05	4.06E-06	1.16E-06	4.85E-08	1.21E-09	9.15E-11	5.51E-12	6.07E-13	3.24E-14	9.91E-16
CBC	7.68E-06	2.11E-06	5.26E-08	1.92E-09	4.77E-11	3.62E-12	2.18E-13	2.40E-14	1.28E-15	3.92E-17
CLC	2.18E-06	5.98E-07	1.49E-08	5.44E-10	1.35E-11	1.03E-12	6.18E-14	6.81E-15	3.64E-16	1.11E-17
CWP	3.59E-06	3.71E-07	9.10E-09	3.32E-10	8.26E-12	6.26E-13	3.77E-14	4.15E-15	2.22E-16	6.79E-18
IGC09	2.60E-06	7.14E-07	2.89E-08	1.06E-09	2.63E-11	1.99E-12	1.20E-13	1.32E-14	7.06E-16	2.16E-17
IGC13	2.84E-06	7.78E-07	1.94E-08	7.07E-10	1.76E-11	1.33E-12	8.03E-14	8.84E-15	4.73E-16	1.45E-17

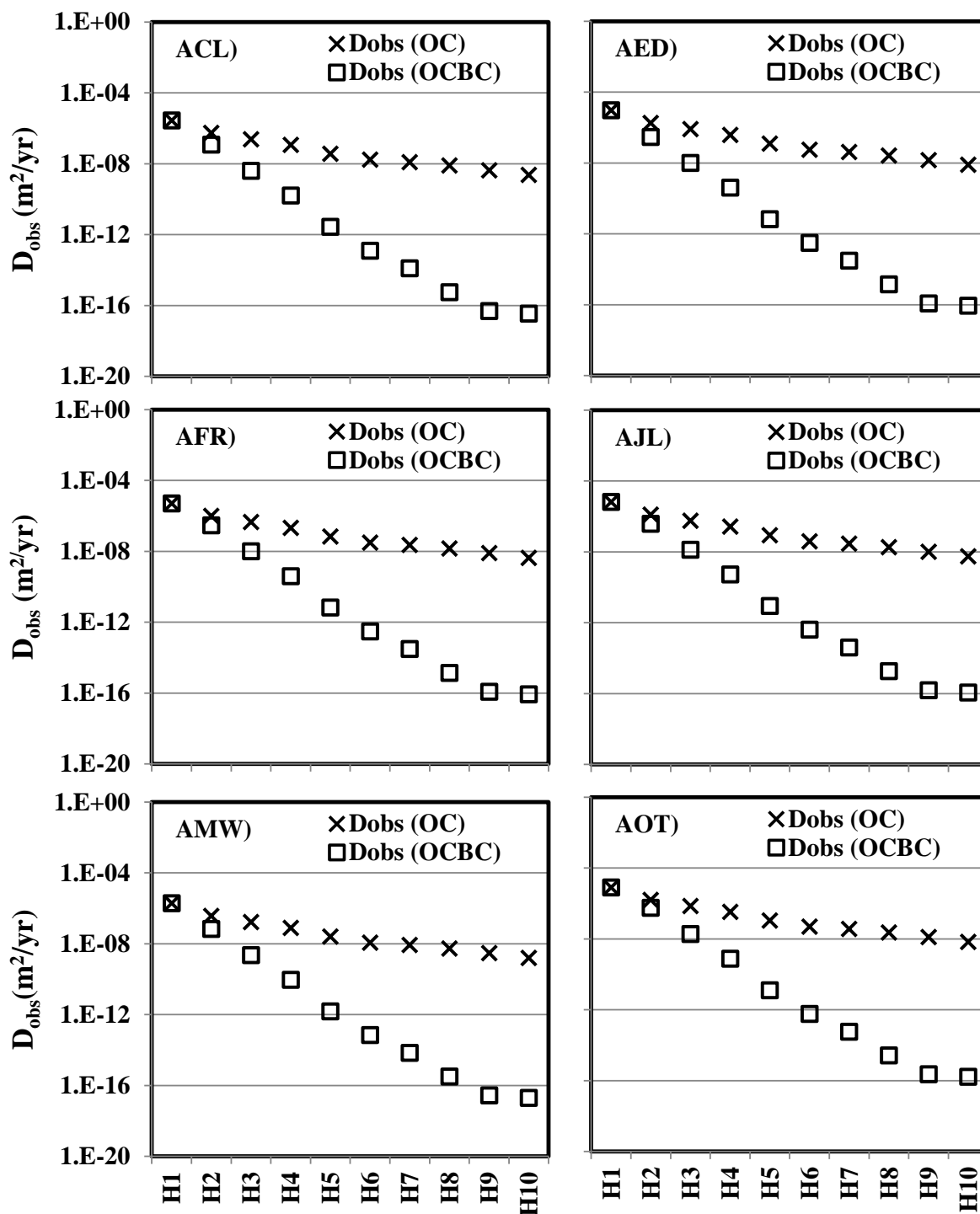


Figure 5.12a: The Monte Carlo 95th percentile predicted PBDE D_{obs} (m²/yr) values for organic carbon only sorption (D_{obs} (OC)), and organic carbon and black carbon co-sorption (D_{obs} (OCBC)) in AR sediment columns.

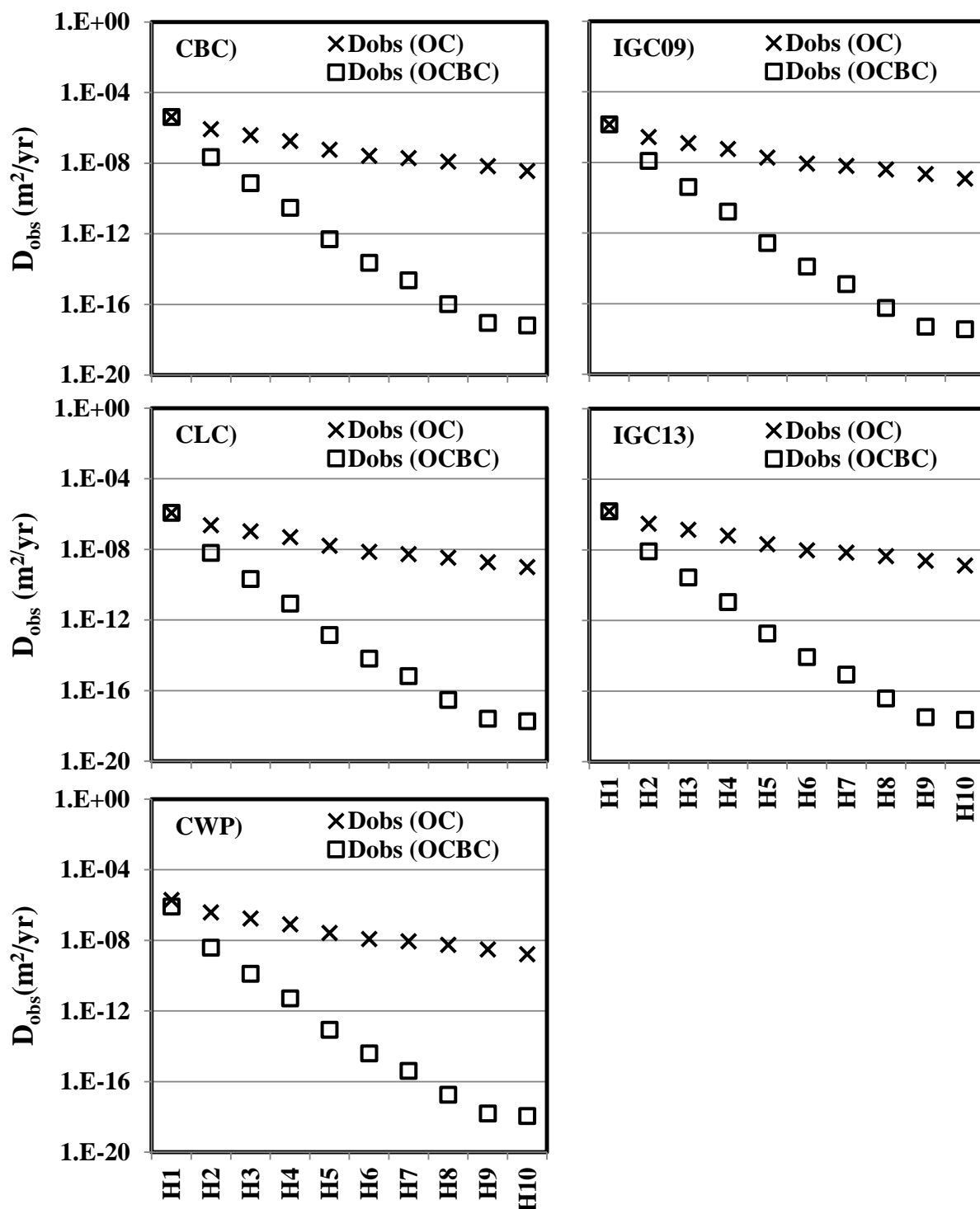


Figure 5.12b: The Monte Carlo 95th percentile predicted PBDE D_{obs} (m²/yr) values for organic carbon only sorption (D_{obs} (OC)), and organic carbon and black carbon co-sorption (D_{obs} (OCBC)) in Chicago and IGC sediment columns.

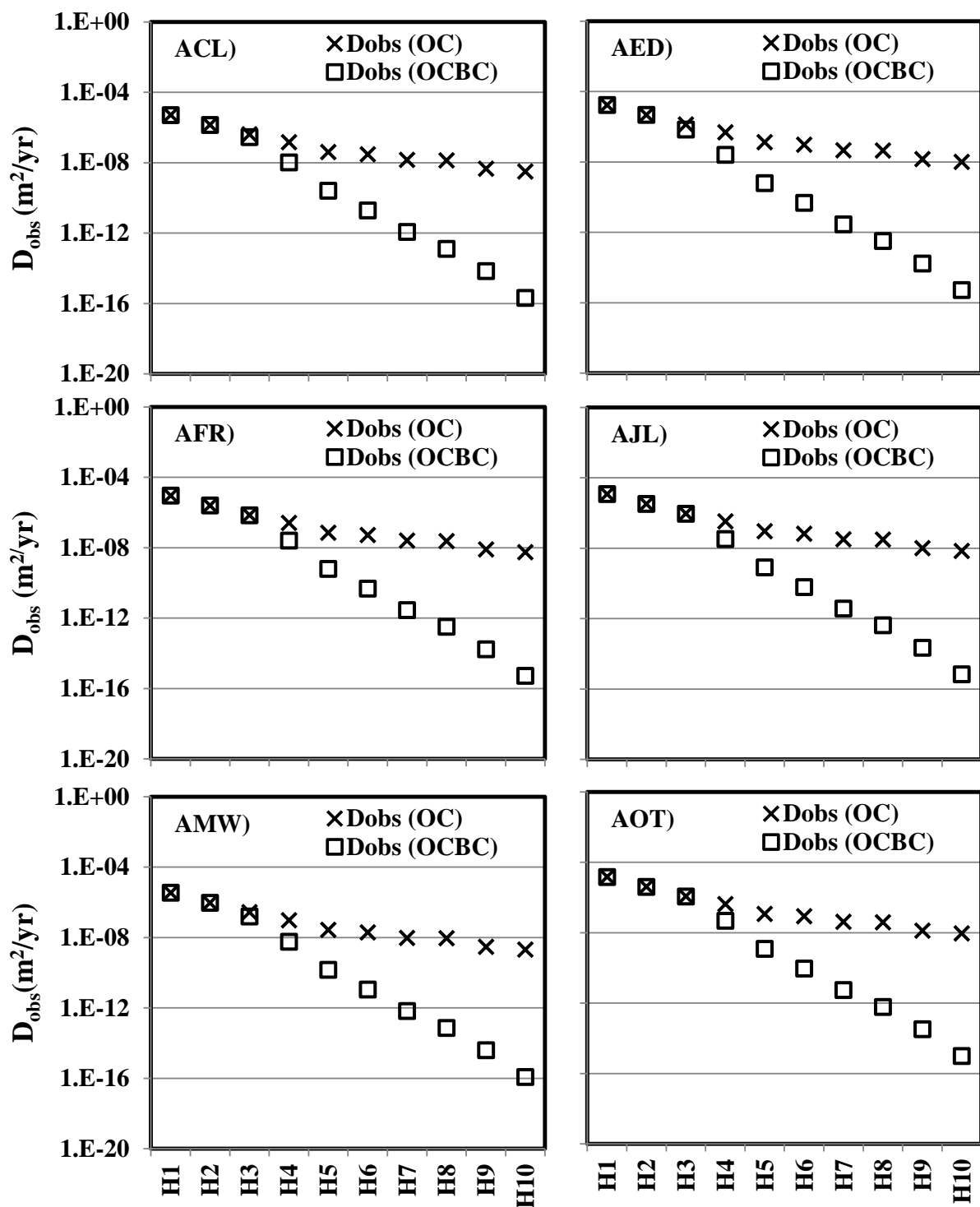


Figure 5.12c: The Monte Carlo 95th percentile predicted PCB D_{obs} (m²/yr) values for organic carbon only sorption (D_{obs} (OC)), and organic carbon and black carbon co-sorption (D_{obs} (OCBC)) in AR sediment columns.

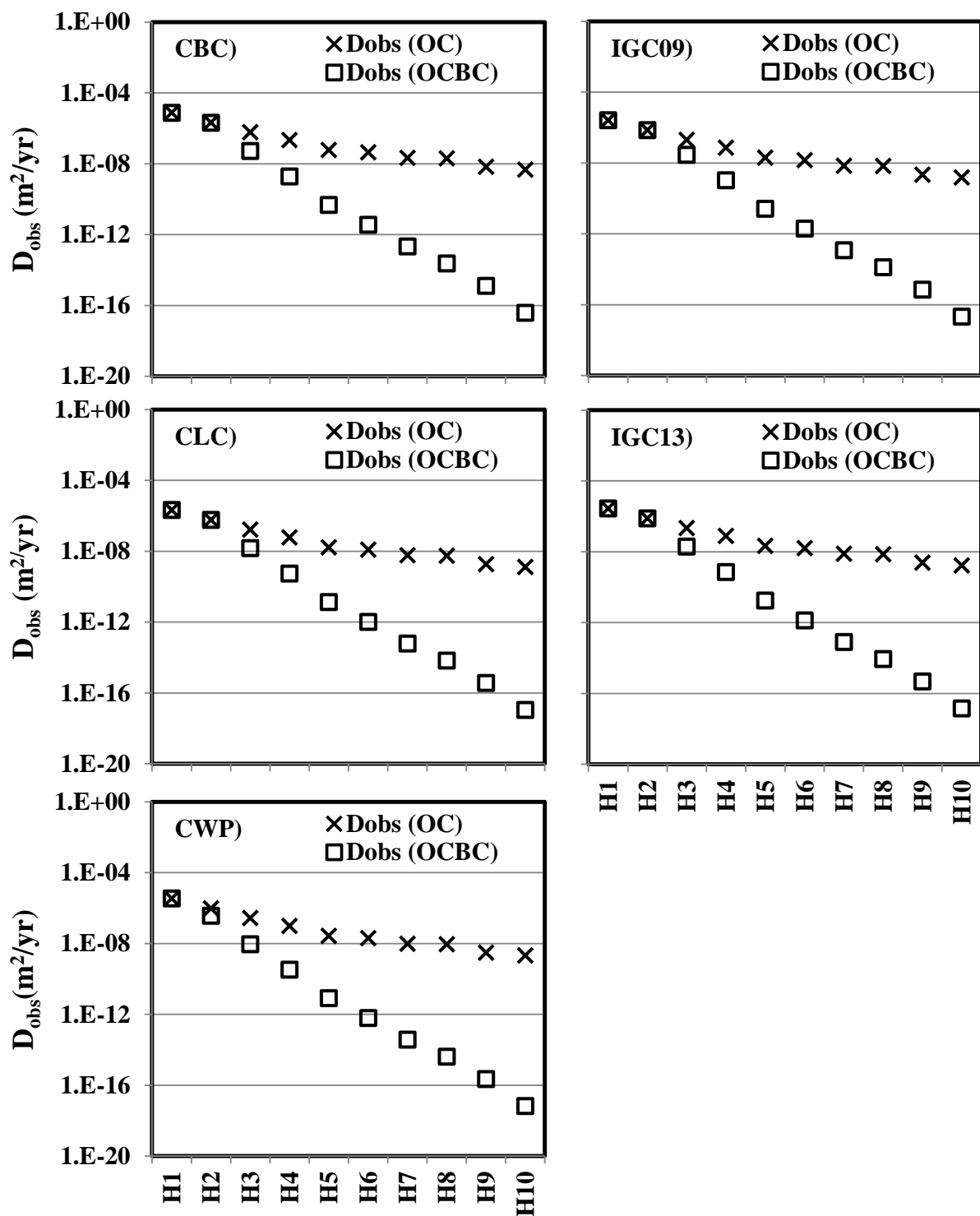


Figure 5.12d: The Monte Carlo 95th percentile predicted PCB D_{obs} (m²/yr) values for organic carbon only sorption (D_{obs} (OC)), and organic carbon and black carbon co-sorption (D_{obs} (OCBC)) in Chicago and IGC sediment columns.

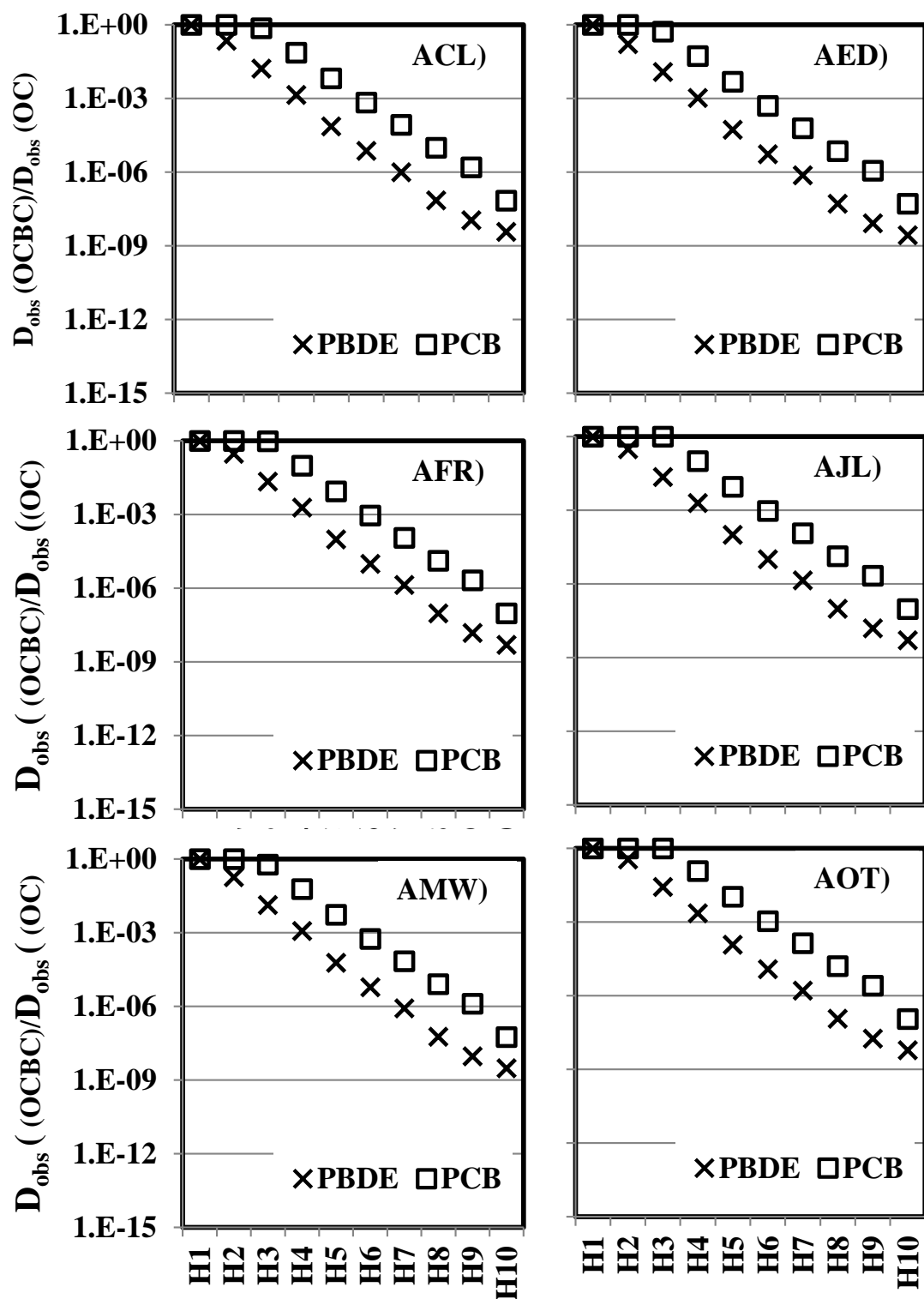


Figure 5.13a: Ratios of observed diffusivity under organic carbon and black carbon co-sorption ($D_{obs}((OCBC))$) to observed diffusivity under organic carbon only sorption ($D_{obs}(OC)$) for PBDE and PCB homologs in AR sediment columns.

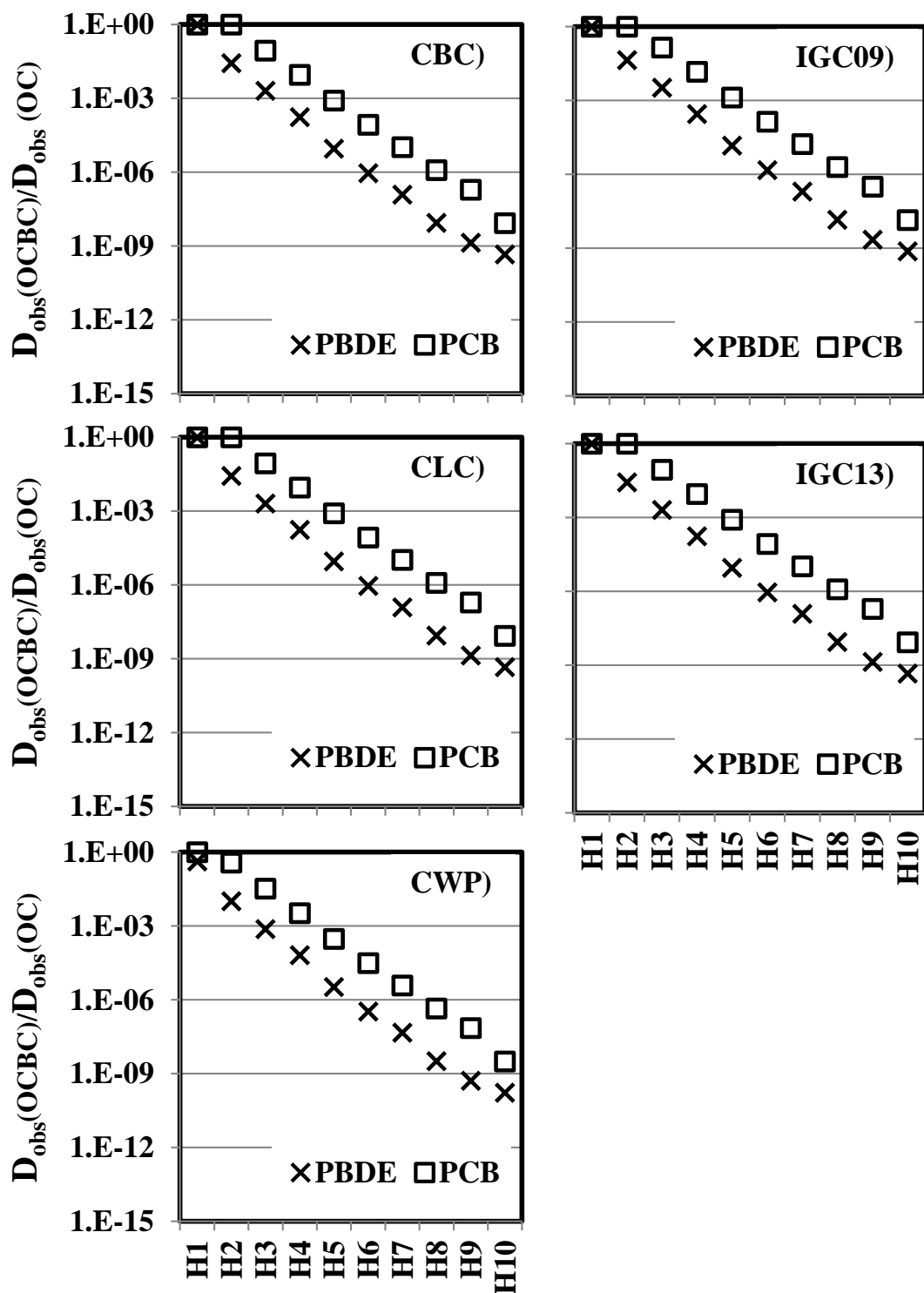


Figure 5.13b: Ratios of observed diffusivity under organic carbon and black carbon co-sorption ($D_{obs}(OCBC)$) to observed diffusivity under organic carbon only sorption ($D_{obs}(OC)$) for PBDE and PCB homologs in Chicago and IGC sediment columns.

5.4.4.2. Advective Velocity (v)

Advective velocity, v , quantifies the bulk porewater movement in the sediment column and is an important parameter in advection-diffusion transport process. v is influenced by R values which are different for OC only sorption ($v(OC)$) and OCBC co-sorption ($v(OCBC)$). Complete $v(OC)$ and $v(OCBC)$ distributions, as predicted by 50,000 Monte Carlo samplings are included in Table D5.8a-d (PBDEs: a-b; PCBs:c-d; OC sorption: a, c; OCBC co-sorption: b,d) and Figure D5.4 a-h (PBDEs: a-d; PCBs: e-h; OC sorption: a-b, e-f; OCBC co-sorption: b-d, g-h). A summary of the Monte Carlo predicted $v(OC)$ and $v(OCBC)$ values at the 95th percentile is provided in Figure 5.14a-d (PBDEs:a-b, PCBs:c-d) and in Table 5.10.

PBDE $v(OC)$ and $v(OCBC)$ values were smaller compared to PCBs. As PBDEs are more hydrophobic than PCBs, their mass transport via porewater advection is much less compared to PCBs advection. $v(OC)$ and $v(OCBC)$ values decreased with increasing PBDE and PCB homologs. The HMW of large PBDE and PCB homologs retard the advective transport process. For PBDE and PCB homologs 1 to 10, $v(OC)$ and $v(OCBC)$ values span >4 and >12 orders of magnitude, respectively.

PBDE and PCB $v(OC)$ values increased in the order of CLC < AJL < AOT < CWP < IGC09 < AMW < IGC13 < CBC < AFR < AED < ACL. PBDE and PCB $v(OCBC)$ values increased in the order CLC < CWP < IGC13 < IGC09 < AOT < CBC < AJL < AMW < AFR < AED < ACL. $v(OCBC)$ values were smaller than $v(OC)$ values, reflecting the role of BC in increasing contaminants adsorption to the solid phase and thus effectively reducing the magnitude of transport via aqueous phase. In PBDEs and PCBs, ratio of $v(OCBC)$ to $v(OC)$ decreased with increasing homologs as shown in Figure 5.15a-b. This effect was similarly realized in $D_{obs}(OCBC)$ and $D_{obs}(OC)$.

Table 5.10 (Cont): Monte Carlo predicted PBDE and PCB ν values at the 95th percentile for organic carbon only sorption (OC), and organic carbon and black carbon (OCBC) co-sorption.

PBDE ν values for OC only sorption.										
Site	H1	H2	H3	H4	H5	H6	H7	H8	H9	H10
ACL	2.80E-03	6.40E-04	1.60E-04	2.89E-05	1.01E-05	2.63E-06	7.43E-07	5.99E-07	1.92E-07	1.13E-07
AED	1.79E-03	4.09E-04	1.02E-04	1.85E-05	6.93E-06	1.71E-06	4.74E-07	3.92E-07	1.22E-07	7.21E-08
AFR	9.49E-04	2.17E-04	5.43E-05	1.37E-05	4.98E-06	8.02E-07	1.65E-07	1.40E-07	4.63E-08	3.83E-08
AJL	2.11E-04	4.83E-05	1.21E-05	2.31E-06	8.17E-07	2.04E-07	5.60E-08	4.63E-08	1.45E-08	8.51E-09
AMW	4.72E-04	1.08E-04	2.70E-05	4.79E-06	1.68E-06	4.42E-07	1.25E-07	1.04E-07	3.24E-08	1.91E-08
AOT	2.47E-04	5.65E-05	1.41E-05	2.59E-06	1.00E-06	2.19E-07	6.55E-08	4.38E-08	1.69E-08	9.96E-09
CBC	8.96E-04	2.05E-04	5.13E-05	1.02E-05	3.57E-06	8.62E-07	2.38E-07	1.97E-07	6.14E-08	3.62E-08
CLC	3.15E-05	7.21E-06	1.80E-06	4.25E-07	1.64E-07	2.43E-08	7.40E-09	4.23E-09	2.08E-09	1.27E-09
CWP	3.66E-04	8.37E-05	2.09E-05	4.74E-06	1.83E-06	2.90E-07	9.46E-08	4.82E-08	2.51E-08	1.48E-08
IGC09	3.91E-04	8.93E-05	2.23E-05	4.95E-06	1.91E-06	3.10E-07	1.01E-07	5.07E-08	2.68E-08	1.58E-08
IGC13	6.82E-04	1.56E-04	3.90E-05	8.04E-06	3.10E-06	5.64E-07	1.81E-07	9.87E-08	4.68E-08	2.75E-08
PBDE ν values for OCBC co-sorption										
Site	H1	H2	H3	H4	H5	H6	H7	H8	H9	H10
ACL	1.56E-04	4.00E-06	6.31E-08	1.06E-09	4.26E-11	5.39E-13	7.37E-15	1.49E-15	5.19E-17	8.55E-18
AED	1.36E-04	3.03E-06	4.79E-08	8.03E-10	3.23E-11	4.09E-13	5.59E-15	1.13E-15	3.93E-17	6.48E-18
AFR	6.03E-05	1.29E-06	3.90E-08	6.55E-10	2.63E-11	3.33E-13	4.55E-15	9.19E-16	3.21E-17	5.29E-18
AJL	1.95E-05	4.59E-07	7.24E-09	1.22E-10	4.89E-12	6.18E-14	8.45E-16	1.70E-16	5.95E-18	9.81E-19
AMW	2.71E-05	6.36E-07	1.00E-08	1.69E-10	6.78E-12	8.58E-14	1.17E-15	2.37E-16	8.26E-18	1.36E-18
AOT	1.14E-05	1.79E-07	2.83E-09	4.74E-11	1.91E-12	2.41E-14	3.30E-16	6.65E-17	2.32E-18	3.83E-19
CBC	1.53E-05	1.94E-07	3.07E-09	5.15E-11	2.07E-12	2.62E-14	3.58E-16	7.22E-17	2.52E-18	4.15E-19
CLC	5.39E-07	5.32E-09	1.08E-10	1.81E-12	7.29E-14	9.22E-16	1.26E-17	2.54E-18	8.87E-20	1.46E-20
CWP	2.96E-06	2.52E-08	5.92E-10	9.93E-12	3.99E-13	5.05E-15	6.90E-17	1.39E-17	4.86E-19	8.01E-20
IGC09	9.79E-06	1.19E-07	1.96E-09	3.29E-11	1.32E-12	1.67E-14	2.28E-16	4.61E-17	1.61E-18	2.65E-19
IGC13	9.70E-06	1.23E-07	1.94E-09	3.26E-11	1.31E-12	1.66E-14	2.26E-16	4.57E-17	1.59E-18	2.63E-19

Table 5.10 (Cont): Monte Carlo predicted PBDE and PCB ν values at the 95th percentile for organic carbon only sorption (OC), and organic carbon and black carbon (OCBC) co-sorption.

PCB ν values for OC only sorption										
Site	H1	H2	H3	H4	H5	H6	H7	H8	H9	H10
ACL	5.83E-03	1.68E-03	4.64E-04	1.61E-04	4.63E-05	1.50E-05	3.77E-06	1.55E-06	2.27E-07	7.98E-08
AED	3.72E-03	1.07E-03	2.96E-04	1.03E-04	2.96E-05	9.60E-06	2.41E-06	1.03E-06	1.46E-07	5.12E-08
AFR	1.98E-03	5.71E-04	1.57E-04	5.45E-05	1.57E-05	5.10E-06	1.28E-06	5.47E-07	9.41E-08	3.38E-08
AJL	4.39E-04	1.27E-04	3.50E-05	1.21E-05	3.49E-06	1.13E-06	2.85E-07	1.22E-07	1.82E-08	6.40E-09
AMW	9.84E-04	2.84E-04	7.83E-05	2.71E-05	7.81E-06	2.54E-06	6.37E-07	2.49E-07	3.77E-08	1.32E-08
AOT	5.14E-04	1.48E-04	4.09E-05	1.42E-05	4.08E-06	1.33E-06	3.33E-07	1.42E-07	1.87E-08	6.55E-09
CBC	1.87E-03	5.39E-04	1.49E-04	5.15E-05	1.48E-05	4.82E-06	1.21E-06	5.17E-07	8.01E-08	2.81E-08
CLC	6.57E-05	1.90E-05	5.23E-06	1.81E-06	5.22E-07	1.69E-07	4.25E-08	1.82E-08	2.50E-09	8.99E-10
CWP	7.62E-04	2.20E-04	6.07E-05	2.10E-05	6.05E-06	1.97E-06	4.93E-07	2.11E-07	2.79E-08	1.00E-08
IGC09	8.13E-04	2.35E-04	6.48E-05	2.24E-05	6.46E-06	2.10E-06	5.27E-07	2.25E-07	2.92E-08	1.05E-08
IGC13	1.42E-03	4.11E-04	1.13E-04	3.92E-05	1.13E-05	3.67E-06	9.20E-07	3.93E-07	4.81E-08	1.70E-08
PCB ν values for OCBC co-sorption										
Site	H1	H2	H3	H4	H5	H6	H7	H8	H9	H10
ACL	1.79E-03	1.11E-04	1.39E-05	6.56E-07	2.58E-08	1.65E-09	6.78E-11	4.75E-12	8.84E-14	1.24E-14
AED	1.53E-03	1.00E-04	1.05E-05	4.20E-07	2.33E-08	1.18E-09	6.36E-11	3.10E-12	7.99E-14	1.12E-14
AFR	5.91E-04	9.83E-05	4.96E-06	3.83E-07	1.67E-08	1.19E-09	5.63E-11	3.73E-12	5.53E-14	7.60E-15
AJL	1.91E-04	1.34E-05	1.59E-06	9.65E-08	3.12E-09	2.00E-10	7.98E-12	5.59E-13	1.47E-14	2.06E-15
AMW	3.02E-04	1.87E-05	2.21E-06	9.36E-08	4.35E-09	2.75E-10	1.02E-11	7.12E-13	1.49E-14	2.09E-15
AOT	7.19E-05	5.93E-06	6.22E-07	3.76E-08	1.71E-09	7.91E-11	3.57E-12	2.24E-13	5.74E-15	8.03E-16
CBC	1.66E-04	1.69E-05	6.76E-07	4.09E-08	1.35E-09	8.64E-11	3.41E-12	2.38E-13	6.23E-15	8.72E-16
CLC	3.87E-06	4.96E-07	1.29E-08	9.35E-10	5.33E-11	2.48E-12	1.56E-13	7.79E-15	1.76E-16	2.42E-17
CWP	2.25E-05	2.39E-06	7.04E-08	5.43E-09	2.75E-10	1.54E-11	8.54E-13	4.84E-14	9.08E-16	1.25E-16
IGC09	6.64E-05	6.80E-06	2.88E-07	1.60E-08	9.57E-10	4.59E-11	2.58E-12	1.26E-13	3.28E-15	4.61E-16
IGC13	6.29E-05	1.07E-05	3.48E-07	1.52E-08	9.07E-10	4.84E-11	2.29E-12	1.25E-13	3.10E-15	4.36E-16

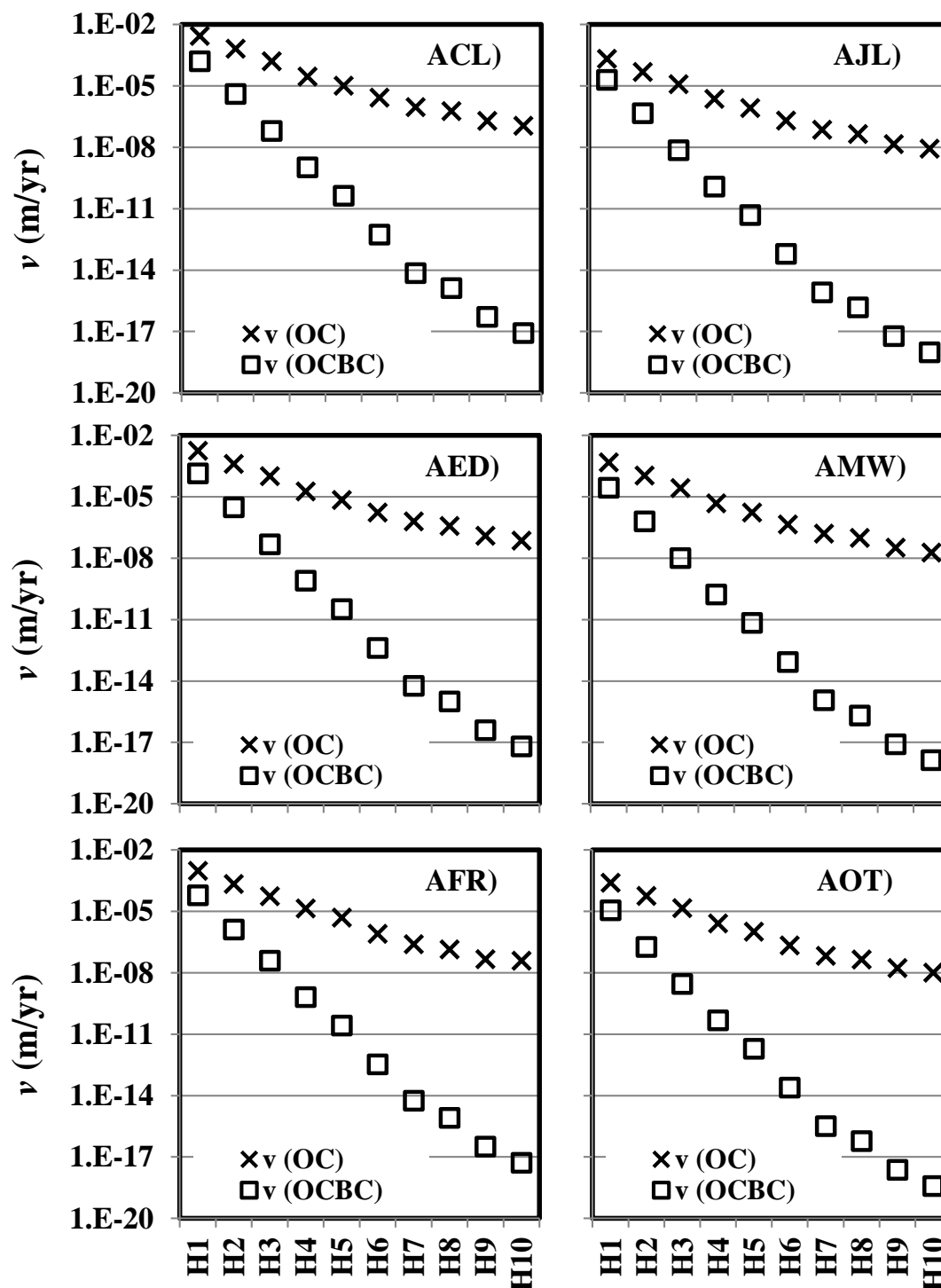


Figure 5.14a: Monte Carlo predicted 95th percentile PBDE ν values for organic carbon only sorption (ν (OC)), and organic carbon and black carbon co-sorption (ν (OCBC)) in AR sediment columns.

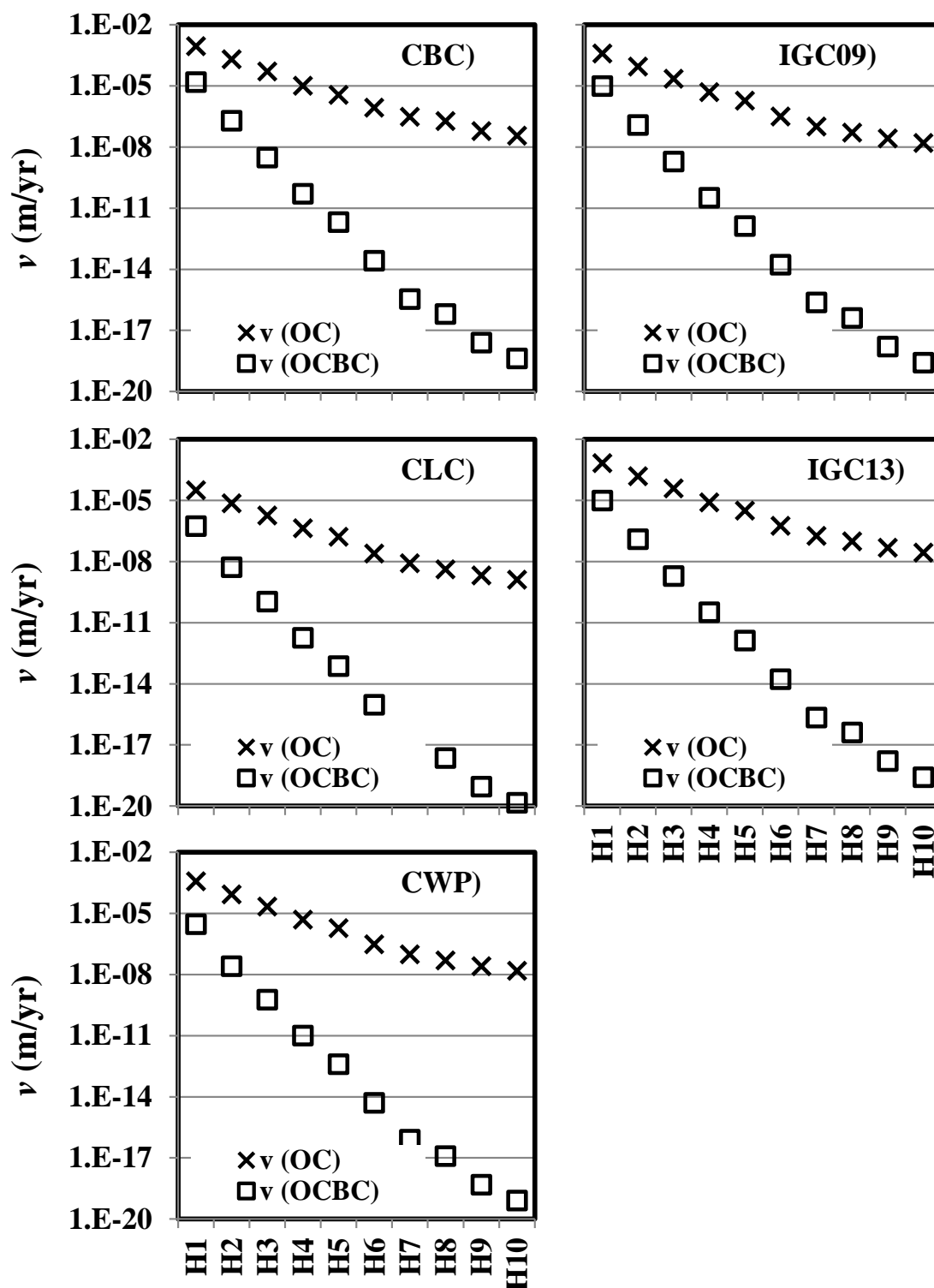


Figure 5.14b: Monte Carlo predicted 95th percentile PBDE ν values for organic carbon only sorption (ν (OC)), and organic carbon and black carbon co-sorption (ν (OCBC)) in Chicago and IGC sediment columns.

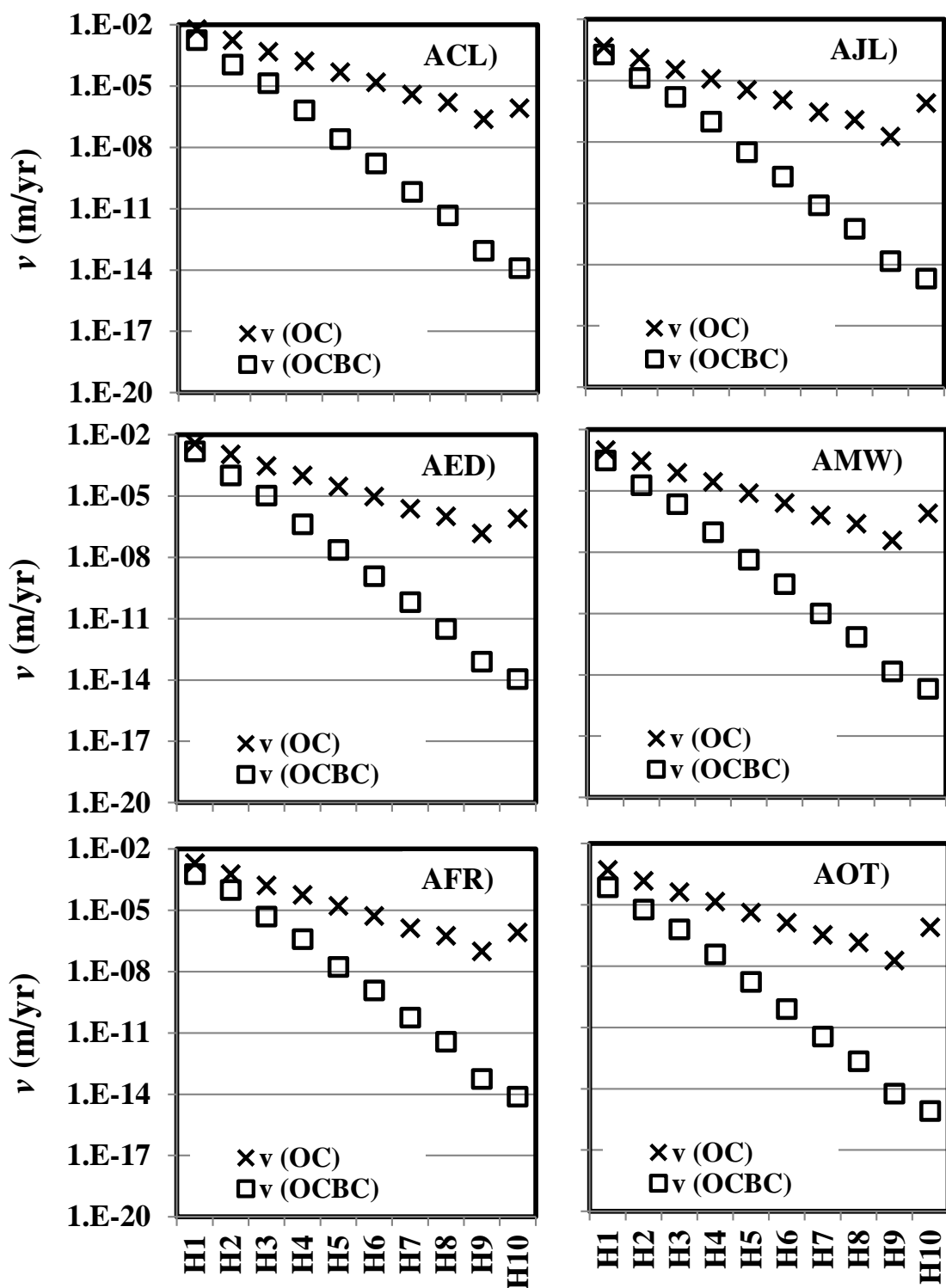


Figure 5.14c: Monte Carlo predicted 95th percentile PCB ν values for organic carbon only sorption (ν (OC)), and organic carbon and black carbon co-sorption (ν (OCBC)) in AR sediment columns.

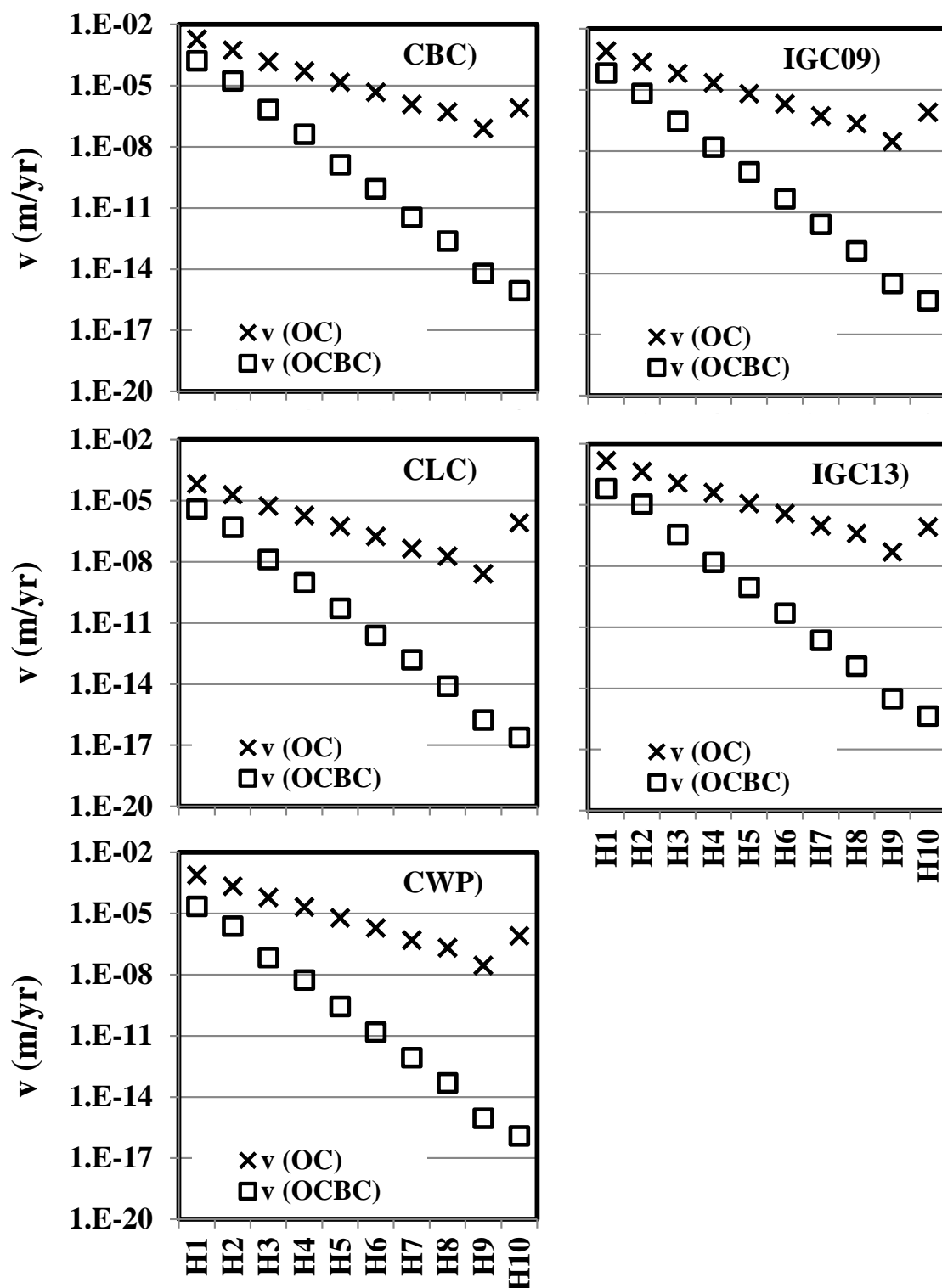


Figure 5.14d: Monte Carlo predicted 95th percentile PCB v values for organic carbon only sorption ($v(OC)$), and organic carbon and black carbon co-sorption ($v(OCBC)$) in Chicago and IGC sediment columns.

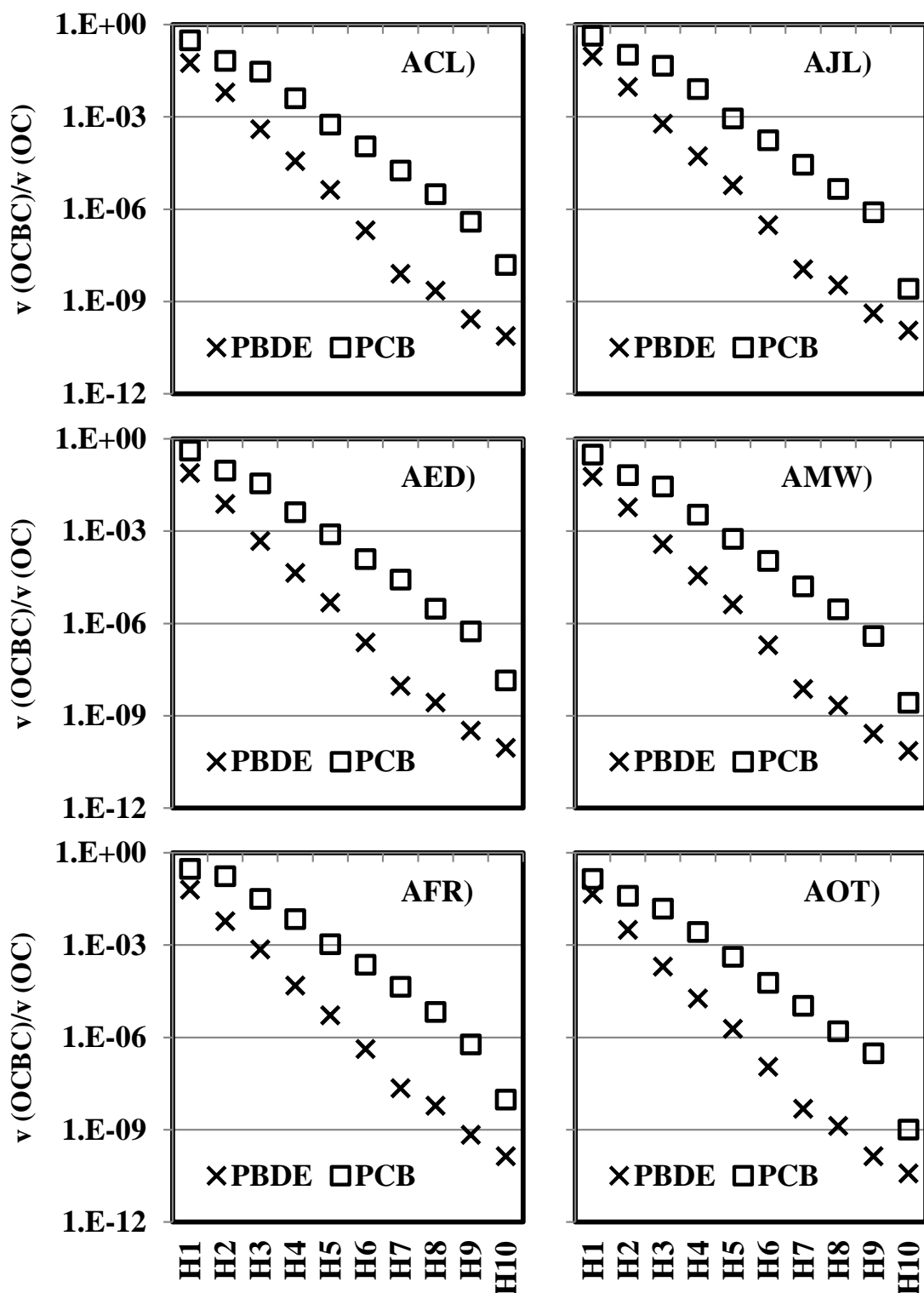


Figure 5.15a: Ratio of advective velocity under organic carbon and black carbon co-sorption ($v(OCBC)$) to advective velocity under organic carbon sorption ($v(OC)$) for PBDE and PCB homologs in AR sediment columns.

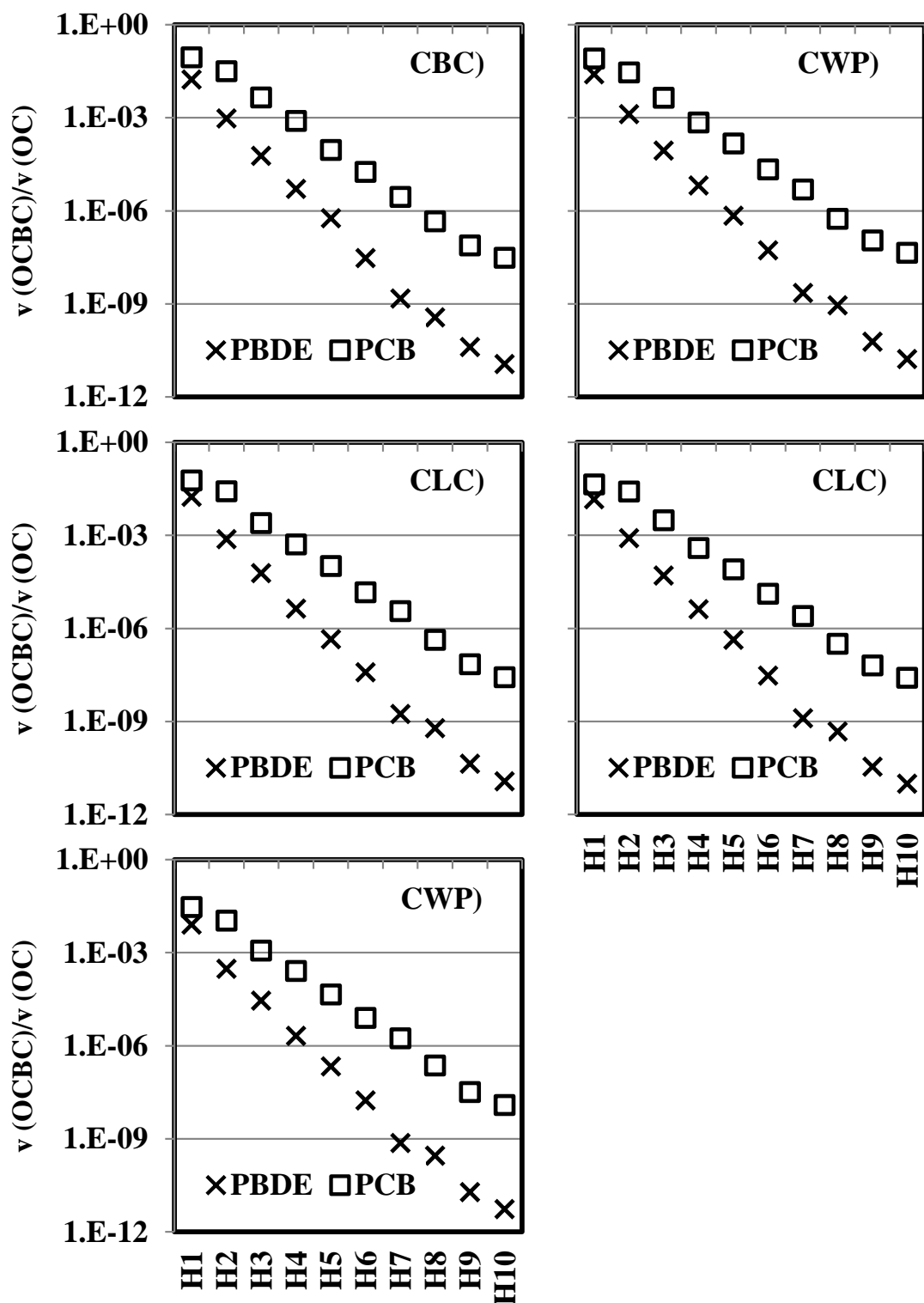


Figure 5.15b: Ratios of advective velocity under organic carbon and black carbon co-sorption ($v(OCBC)/v(OC)$) to advective velocity under organic carbon sorption ($v(OC)$) for PBDE and PCB homologs in Chicago and IGC sediment columns.

5.4.4.3. Drivers Of Diffusion And Advection-Diffusion Transport Processes.

A principal component analysis (PCA) was applied to the D_{mol} , ϕ , K_{OW} , f_{OC} , K_d , and K_h to evaluate the drivers behind the magnitude of the diffusion and advection-diffusion flux. Three factors PCA analysis explained 45.35, 24.07, and 16.24% of the variances. Component loadings for factors 1, 2, and 3 are shown in Figure 5.16 and 5.17.

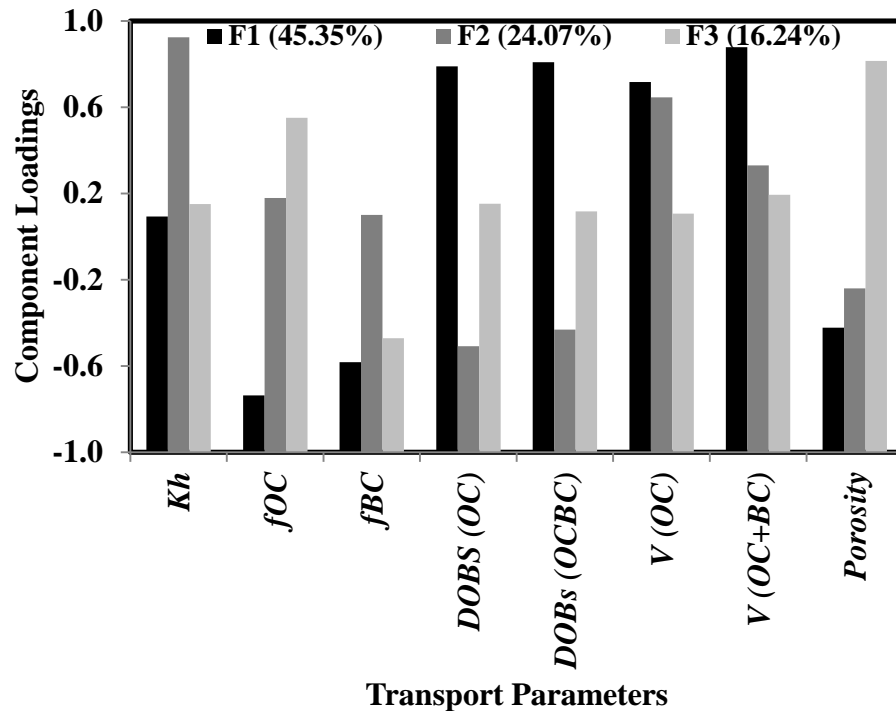


Figure 5.16: Transport parameter component loadings in factors 1, 2, and 3 (F1, F2, and F3) which explained 45.35, 24.07, and 16.24% of the variance, respectively. Negative component loading indicates an inverse relationship between the transport parameter and factor.

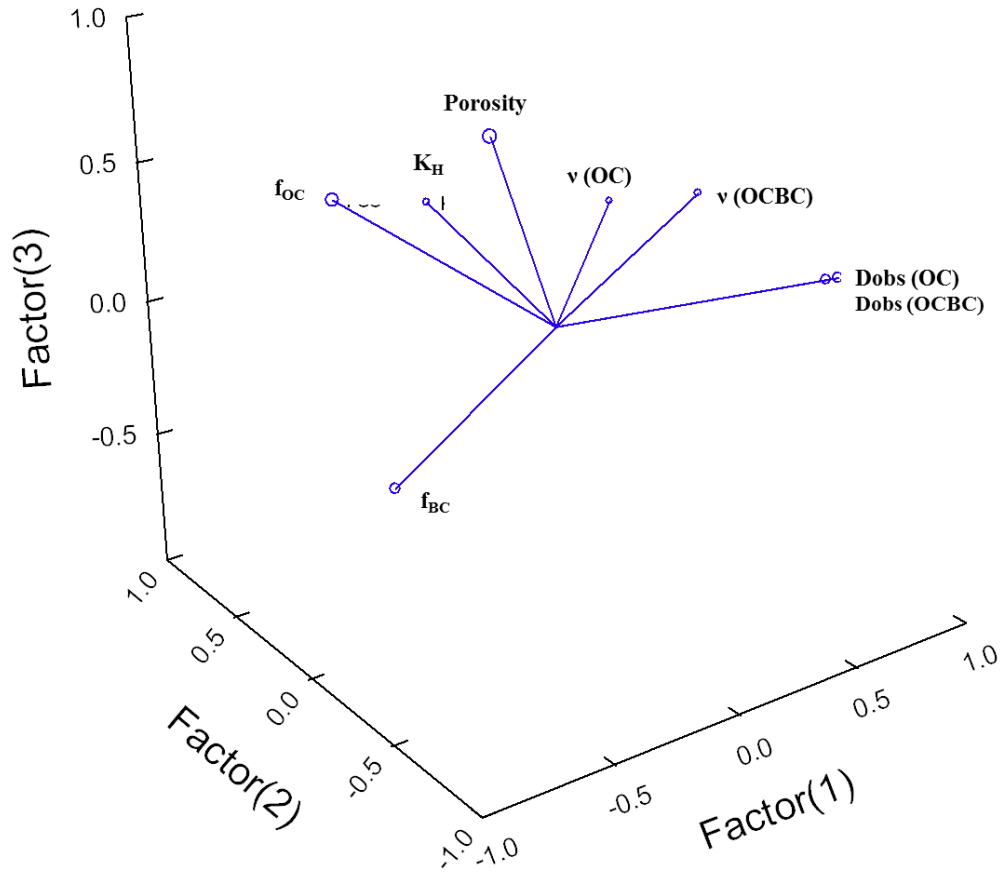


Figure 5.17: Factor loadings plot for the transport parameters as generated in SYSTAT version 13.

Factor 1 which explained the largest amount of variance, has f_{OC} and f_{BC} loadings of -0.74 and -0.58, respectively, indicating that f_{OC} and f_{BC} can be an important driver to predict the magnitude of D_{obs} (OC), D_{obs} (OCBC), v (OC), and v (OCBC). The increasing order of D_{obs} (OC) (CLC < IGC09 < IGC13 < AMW < CWP < ACL < CBC < AFR < AJL < AOT < AED) and D_{obs} (OCBC) (CWP < CLC < IGC13 < IGC09 < CBC < AMW < ACL < AFR < AED < AJL < AOT) shared some cluster resemblances to the increasing order of f_{OC} (AJL < AOT < AED < CBC < ACL < AFR < CWP < CLC < IGC09 < IGC13 < AMW) and f_{BC} (AED < AFR < AJL < ACL < AMW < AOT < IGC09 < CBC < IGC13 < CWP < CLC).

Factor 2 which explained 24.07% of the variance has high K_h loadings (0.93). However observation of the increasing order in K_h values showed a large disparity when compared to the relative

increasing order of ν (OC) and ν (OCBC) (K_h : ACL < AED < AFR < AJL < AMW < AOT < CBC < CLC < CWP < IGC09 < IGC13; ν (OC): CLC < AJL < AOT < CWP < IGC09 < AMW < IGC13 < CBC < AFR < AED < ACL; ν (OCBC): CBC < AFR < ACL < AED < AMW < IGC13 < CWP < IGC09 < AOT < AJL < CLC). This suggests that K_h alone cannot be a sole predictor to assess ν (OC) and ν (OCBC) magnitudes.

Overall, the PCA results suggest that f_{OC} , f_{BC} , and K_h can be strong predictors of mass transport parameters such as D_{obs} (OC), D_{obs} (OCBC), ν (OC), and ν (OCBC); however it should be noted that the most reliable prediction of the relative magnitude of mass transport occurring in a sediment column comes from collectively evaluating all sorbent and sorbate parameters that can affect the mass transport processes.

5.4.4.4. PBDE and PCB Aqueous Phase Breakthrough Under Diffusion and Advection-Diffusion Conditions

Using D_{obs} (OC), D_{obs} (OCBC), ν (OC), and ν (OCBC) distributions generated in Monte Carlo simulations (Table D5.7a-d and Table D5.8a-d), aqueous phase breakthrough (C/C_o) was predicted using Equations 5.1 and 5.2 for diffusion and advection-diffusion mass transport processes, respectively. In this context, C/C_o indicates the fraction of aqueous phase contaminant leaving the sediment boundary layer at a distance of $x=\pm L$ relative to the initial LEA aqueous phase contaminant concentration. Diffusion and advection-diffusion mass transport under OC only sorption and OCBC co-sorption are denoted as D(OC), D(OCBC), A(OC), and A(OCBC), respectively throughout the remaining of this chapter. Note that A(OC) and A(OCBC) constitutes both advection and diffusion mass transport processes.

The predicted PBDE and PCB C/C_o breakthrough profiles at the 95th percentile values for D(OC), D(OCBC), A(OC), and A(OCBC) mass transport in the eleven sediment columns are shown in

Figure 5.18a-v (PBDEs:a-k; PCBs:l-v; ACL:a, l; AED:b,m; AFR:c, n; AJL:d, o ; AMW:e, p; AOT:f ,q ; CBC: g,r; CLC:h ,s; CWP:i ,t; IGC09:j,u; IGC13:k, v).

Generally, PBDE and PCB homologs 1 to 4 were predicted to achieve 10% C/C_o breakthrough under D(OC) and A(OC) conditions in 1000 years. BC inclusion which increases solid phase absorption resulted in PBDE and PCB homologs 3 and 4 to achieve only 1% or less C/C_o breakthrough under D(OCBC) and A(OCBC) conditions in 1000 years. PBDE and PCB homolog 5 were predicted to achieve C/C_o breakthrough between 1 to 10% in 1000 years under D(OC) and A(OC) simulations. Under similar conditions, PBDE and PCB homologs 7 to 10 were predicted to achieve less than 1% C/C_o breakthrough in 1000 years. An ad-hoc value of 1E-18% is deemed as negligible in the C/C_o breakthrough figures and thus simulations resulting in C/C_o breakthrough below 1E-18 % are not shown in Figure 5.17a-v. Inclusion of BC generally resulted in negligible C/C_o breakthrough for PBDE and PCB homologs 5 to 10 under D(OCBC) and A(OCBC) in 1000 years. Table 5.11 summarizes the PBDE and PCB homologs achieving 1 to 10% breakthrough in the eleven sediment cores studied in this chapter.

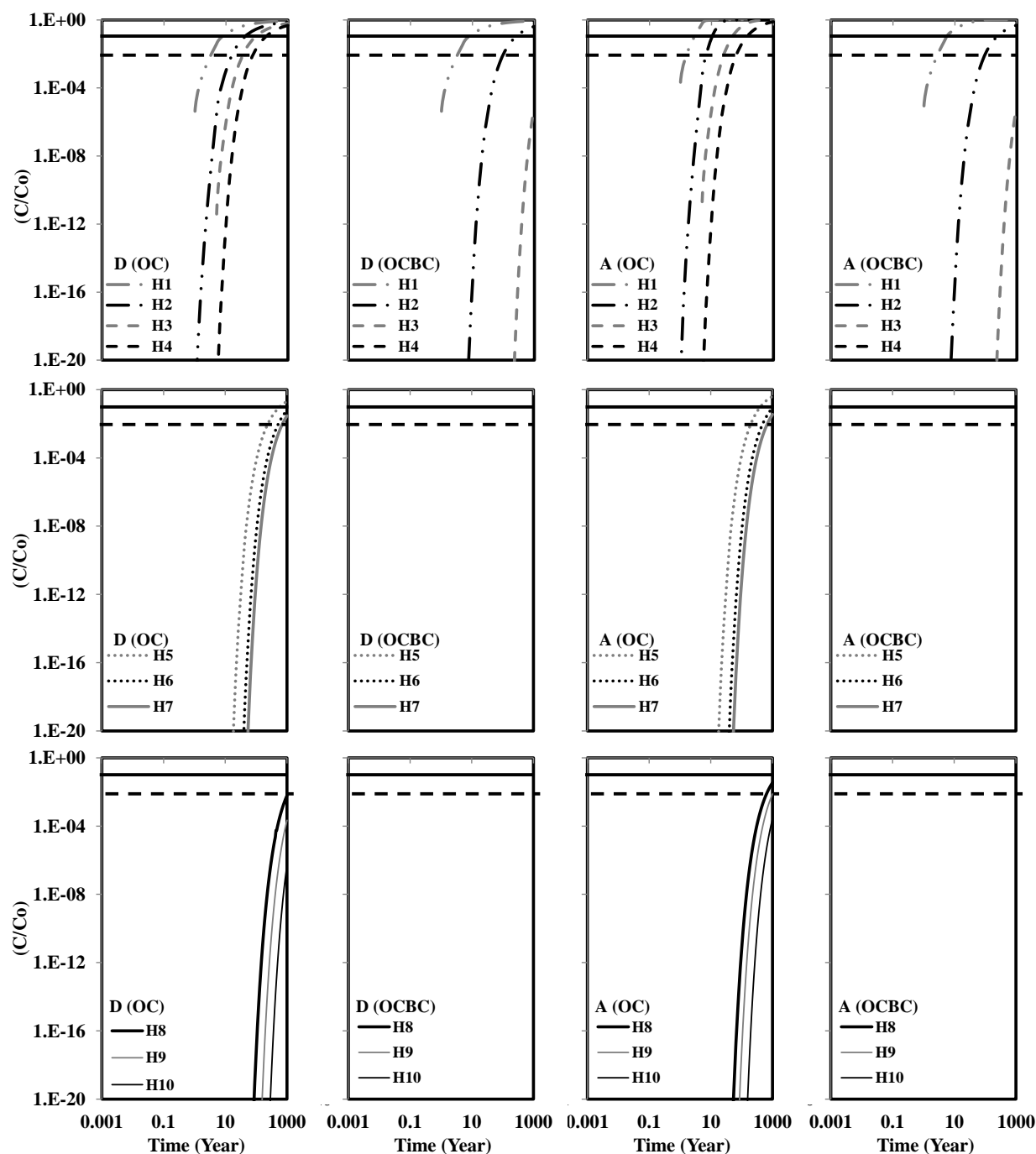


Figure 5.18a: PBDE breakthrough (C/C_o) in core ACL under the 95th percentile transport parameter values for diffusion with organic carbon only sorption (D(OC)), and organic carbon and black carbon co-sorption (D(OCBC)) and under advection-diffusion with organic carbon only sorption (A(OC)), and organic carbon and black carbon co-sorption (A(OCBC)). Horizontal bold line marks the 10% C/C_o breakthrough and horizontal dotted line marks the 1% C/C_o breakthrough. Data not shown indicates that C/C_o breakthrough is below $1E-18\%$.

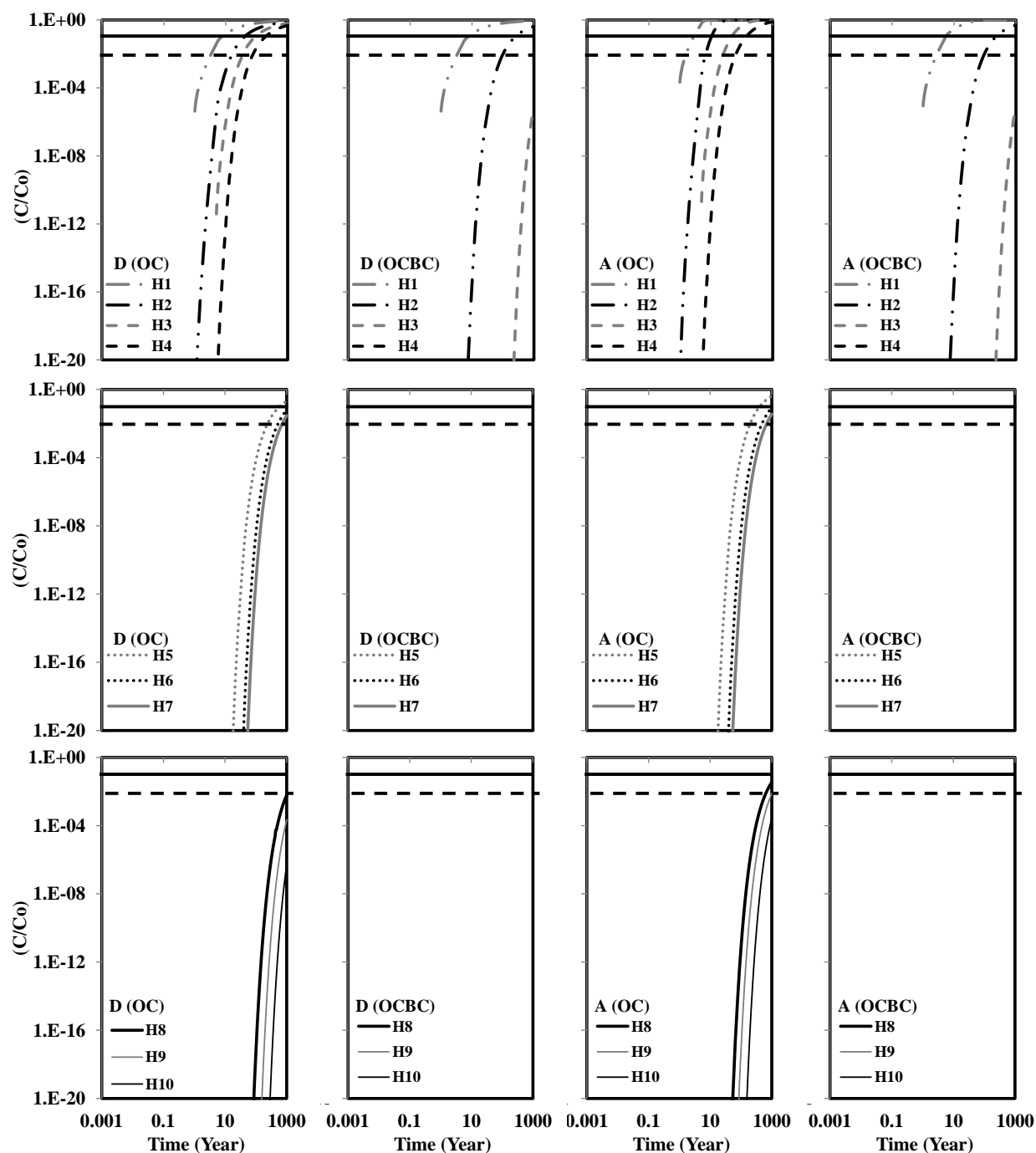


Figure 5.18b: PBDE breakthrough (C/C_o) in core AED under the 95th percentile transport parameter values for diffusion with organic carbon only sorption (D(OC)), and organic carbon and black carbon co-sorption (D(OCBC)) and under advection-diffusion with organic carbon only sorption (A(OC)), and organic carbon and black carbon co-sorption (A(OCBC)). Horizontal bold line marks the 10% C/C_o breakthrough and horizontal dotted line marks the 1% C/C_o breakthrough. Data not shown indicates that C/C_o breakthrough is below 1E-18%.

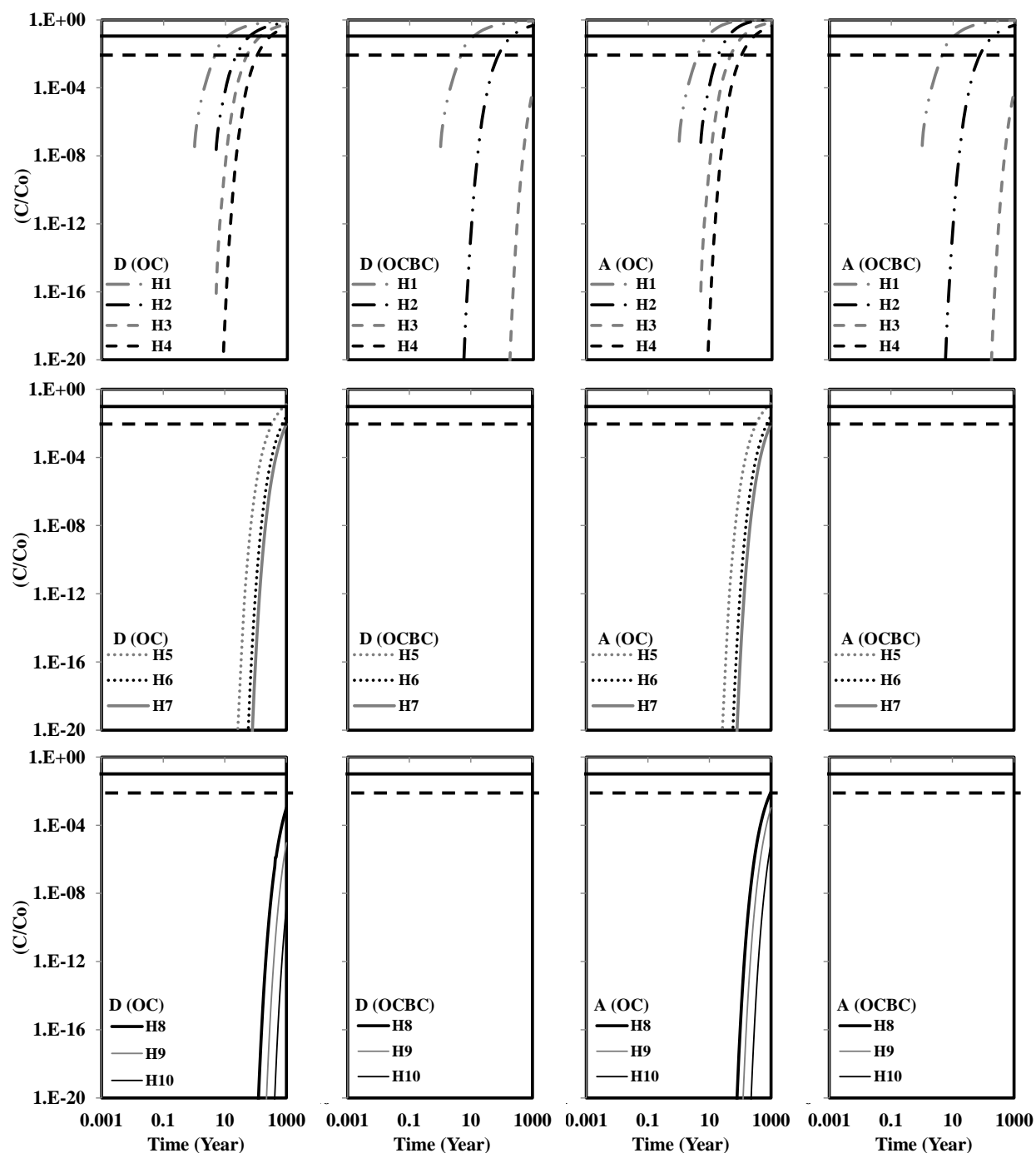


Figure 5.18c: PBDE breakthrough (C/C_0) in core AFR under the 95th percentile transport parameter values for diffusion with organic carbon only sorption (D(OC)), and organic carbon and black carbon co-sorption (D(OCBC)) and under advection-diffusion with organic carbon only sorption (A(OC)), and organic carbon and black carbon co-sorption (A(OCBC)). Horizontal bold line marks the 10% C/C_0 breakthrough and horizontal dotted line marks the 1% C/C_0 breakthrough. Data not shown indicates that C/C_0 breakthrough is below $1E-18\%$.

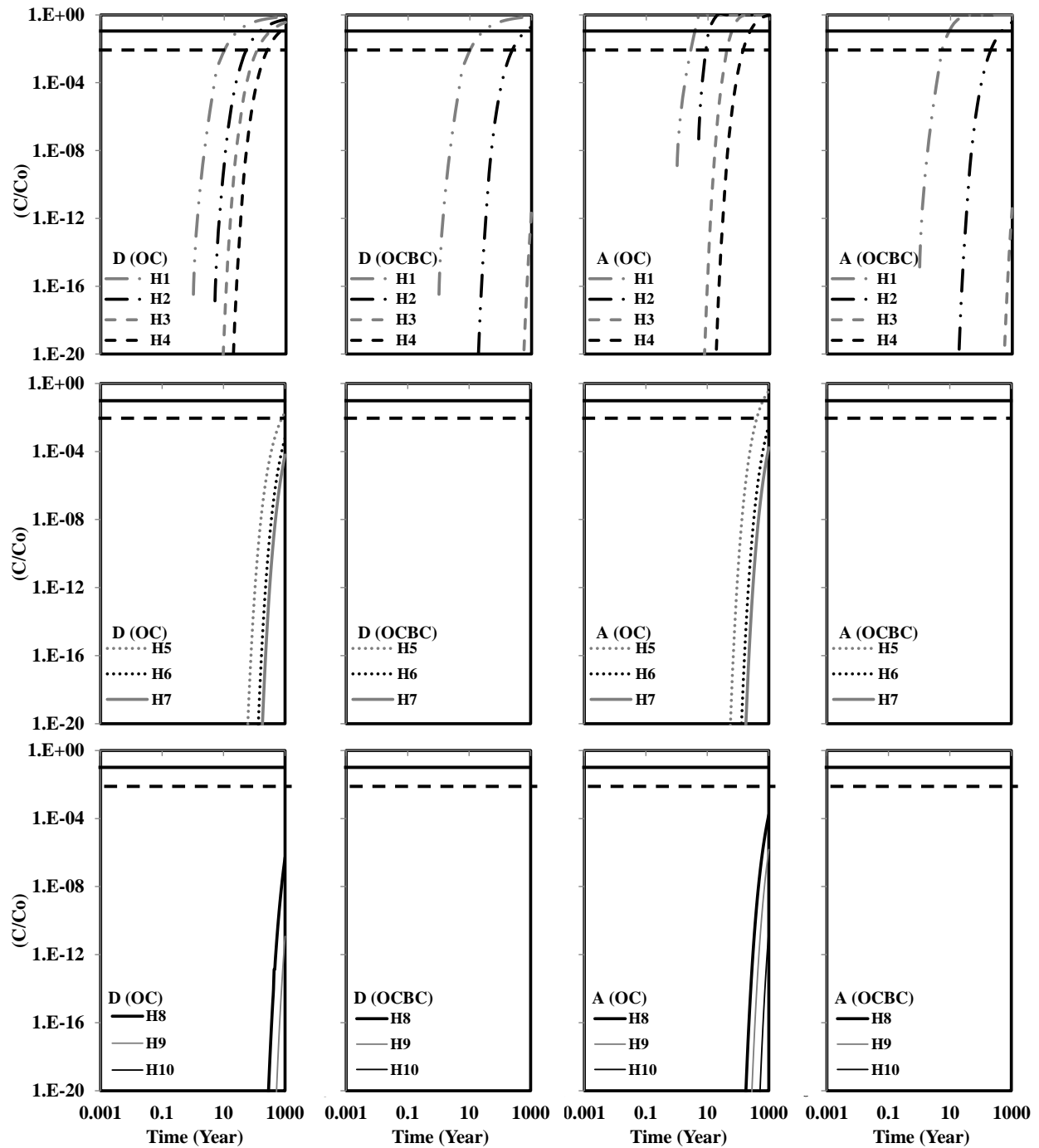


Figure 5.18d: PBDE breakthrough (C/C_o) in core AJL under the 95th percentile transport parameter values for diffusion with organic carbon only sorption (D(OC)), and organic carbon and black carbon co-sorption (D(OCBC)) and under advection-diffusion with organic carbon only sorption (A(OC)), and organic carbon and black carbon co-sorption (A(OCBC)). Horizontal bold line marks the 10% C/C_o breakthrough and horizontal dotted line marks the 1% C/C_o breakthrough. Data not shown indicates that C/C_o breakthrough is below $1.E-18\%$.

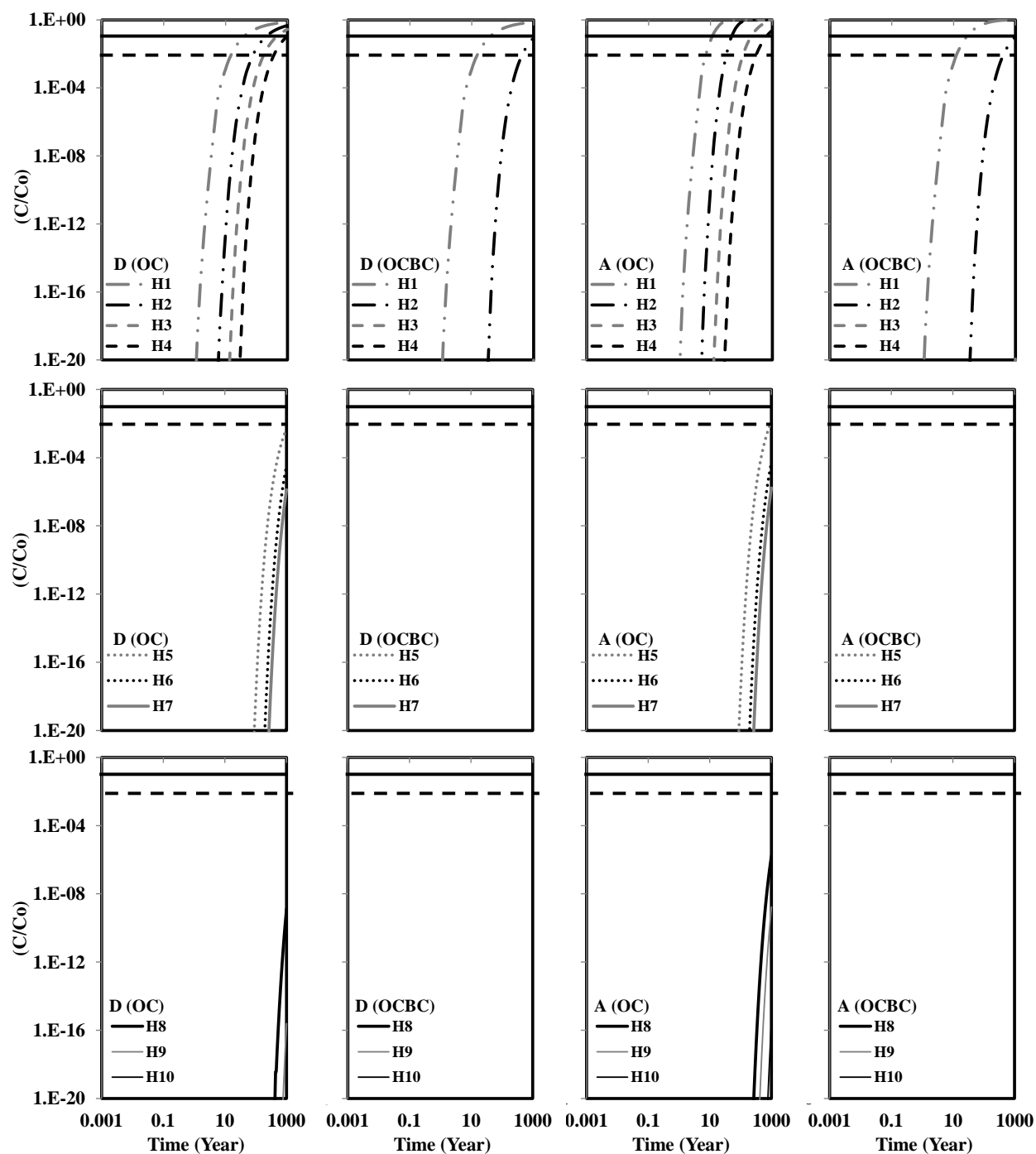


Figure 5.17e: PBDE breakthrough (C/C_o) in core AMW under the 95th percentile transport parameter values for diffusion with organic carbon only sorption (D(OC)), and organic carbon and black carbon co-sorption (D(OCBC)) and under advection-diffusion with organic carbon only sorption (A(OC)), and organic carbon and black carbon co-sorption (A(OCBC)). Horizontal bold line marks the 10% C/C_o breakthrough and horizontal dotted line marks the 1% C/C_o breakthrough. Data not shown indicates that C/C_o breakthrough is below $1E-18\%$.

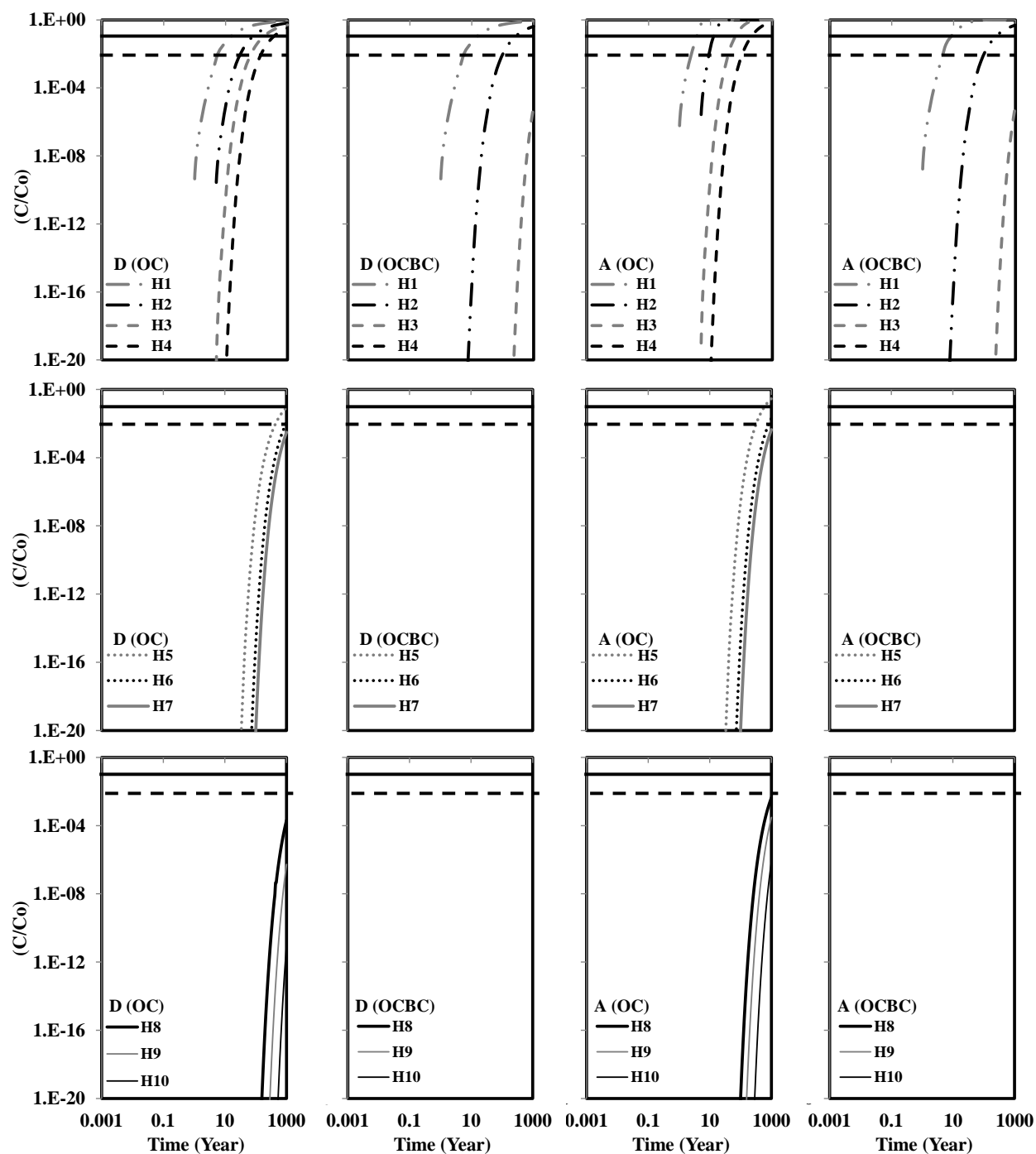


Figure 5.18f: PBDE breakthrough (C/C_o) in core AOT under the 95th percentile transport parameter values for diffusion with organic carbon only sorption (D(OC)), and organic carbon and black carbon co-sorption (D(OCBC)) and under advection-diffusion with organic carbon only sorption (A(OC)), and organic carbon and black carbon co-sorption (A(OCBC)). Horizontal bold line marks the 10% C/C_o breakthrough and horizontal dotted line marks the 1% C/C_o breakthrough. Data not shown indicates that C/C_o breakthrough is below $1E-18\%$.

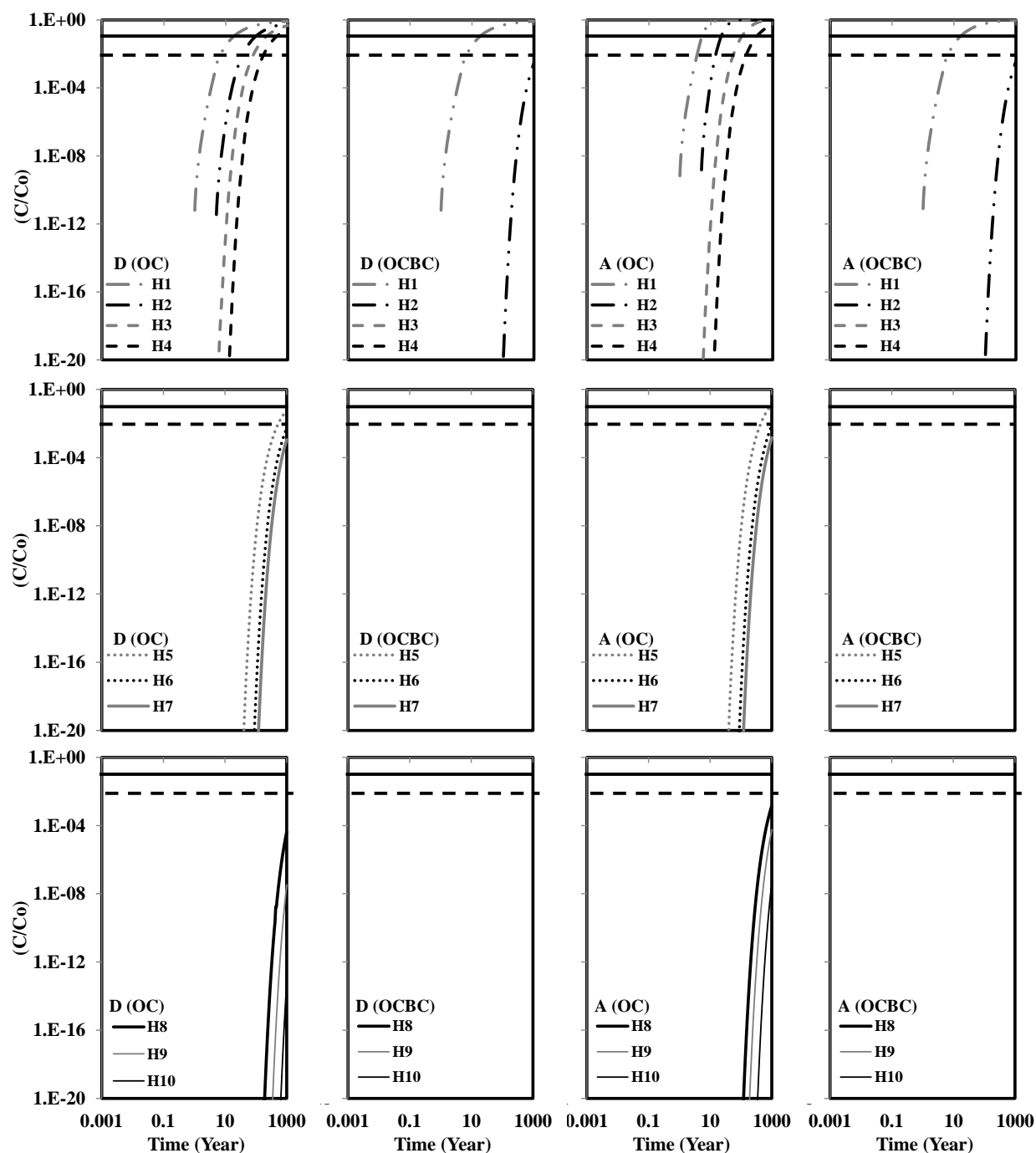


Figure 5.18g: PBDE breakthrough (C/C_0) in core CBC under the 95th percentile transport parameter values for diffusion with organic carbon only sorption (D(OC)), and organic carbon and black carbon co-sorption (D(OCBC)) and under advection-diffusion with organic carbon only sorption (A(OC)), and organic carbon and black carbon co-sorption (A(OCBC)). Horizontal bold line marks the 10% C/C_0 breakthrough and horizontal dotted line marks the 1% C/C_0 breakthrough. Data not shown indicates that C/C_0 breakthrough is below $1E-18\%$.

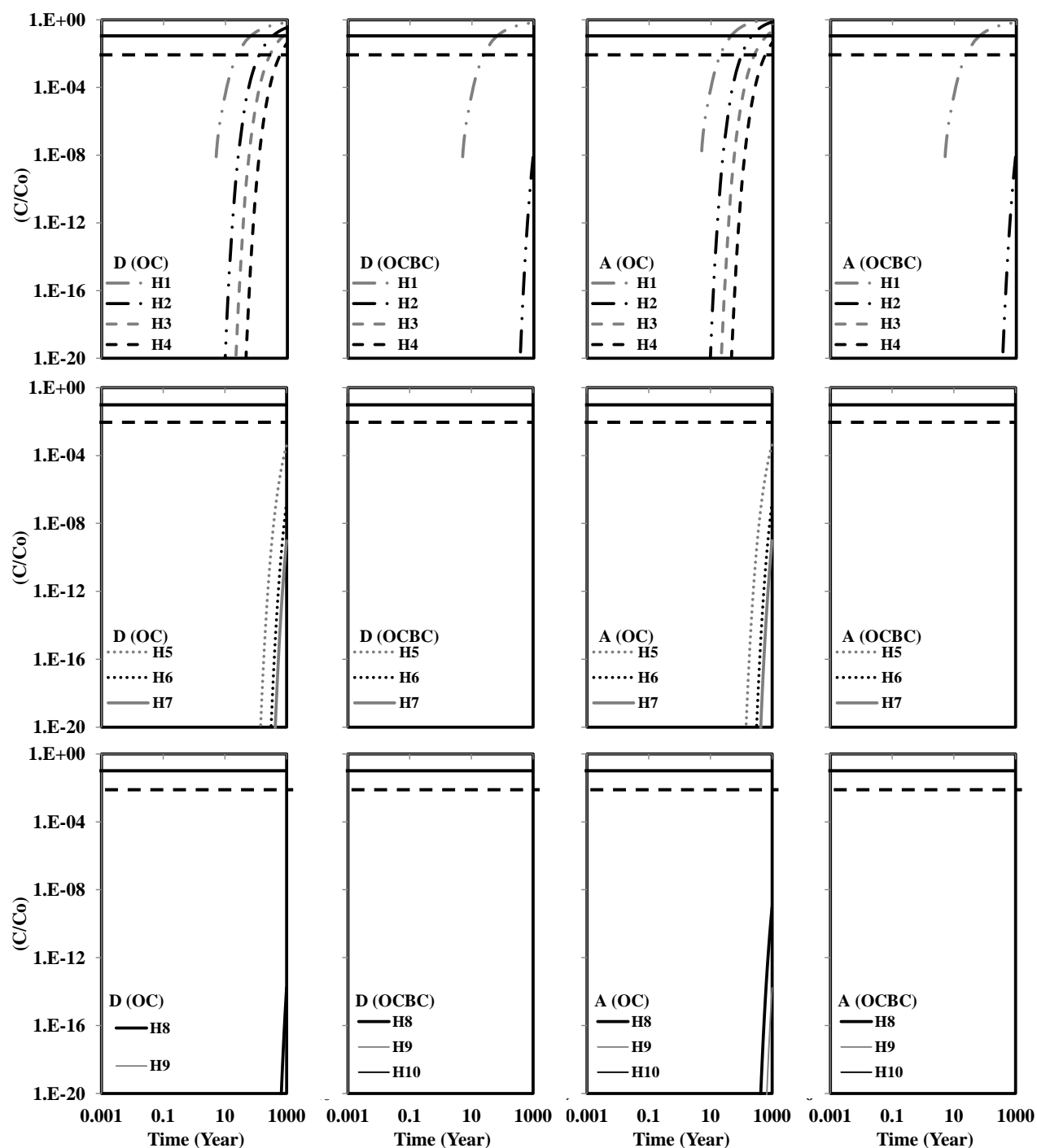


Figure 5.18h: PBDE breakthrough (C/C_0) in core CLC under the 95th percentile transport parameter values for diffusion with organic carbon only sorption (D(OC)), and organic carbon and black carbon co-sorption (D(OCBC)) and under advection-diffusion with organic carbon only sorption (A(OC)), and organic carbon and black carbon co-sorption (A(OCBC)). Horizontal bold line marks the 10% C/C_0 breakthrough and horizontal dotted line marks the 1% C/C_0 breakthrough. Data not shown indicates that C/C_0 breakthrough is below $1E-18\%$.

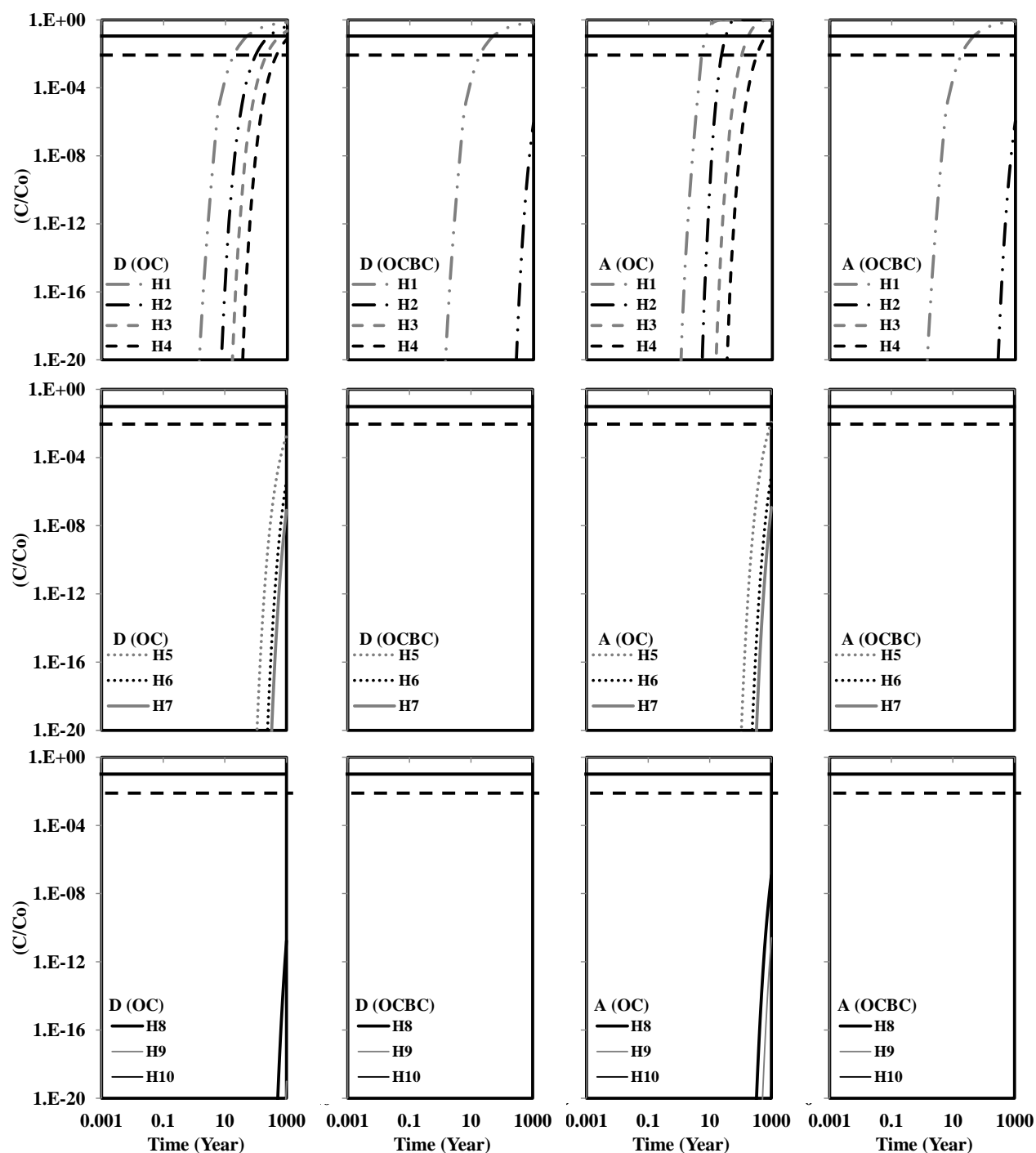


Figure 5.18i: PBDE breakthrough (C/C_0) in core CWP under the 95th percentile transport parameter values for diffusion with organic carbon only sorption (D(OC)), and organic carbon and black carbon co-sorption (D(OCBC)) and under advection-diffusion with organic carbon only sorption (A(OC)), and organic carbon and black carbon co-sorption (A(OCBC)). Horizontal bold line marks the 10% C/C_0 breakthrough and horizontal dotted line marks the 1% C/C_0 breakthrough. Data not shown indicates that C/C_0 breakthrough is below $1E-18\%$.

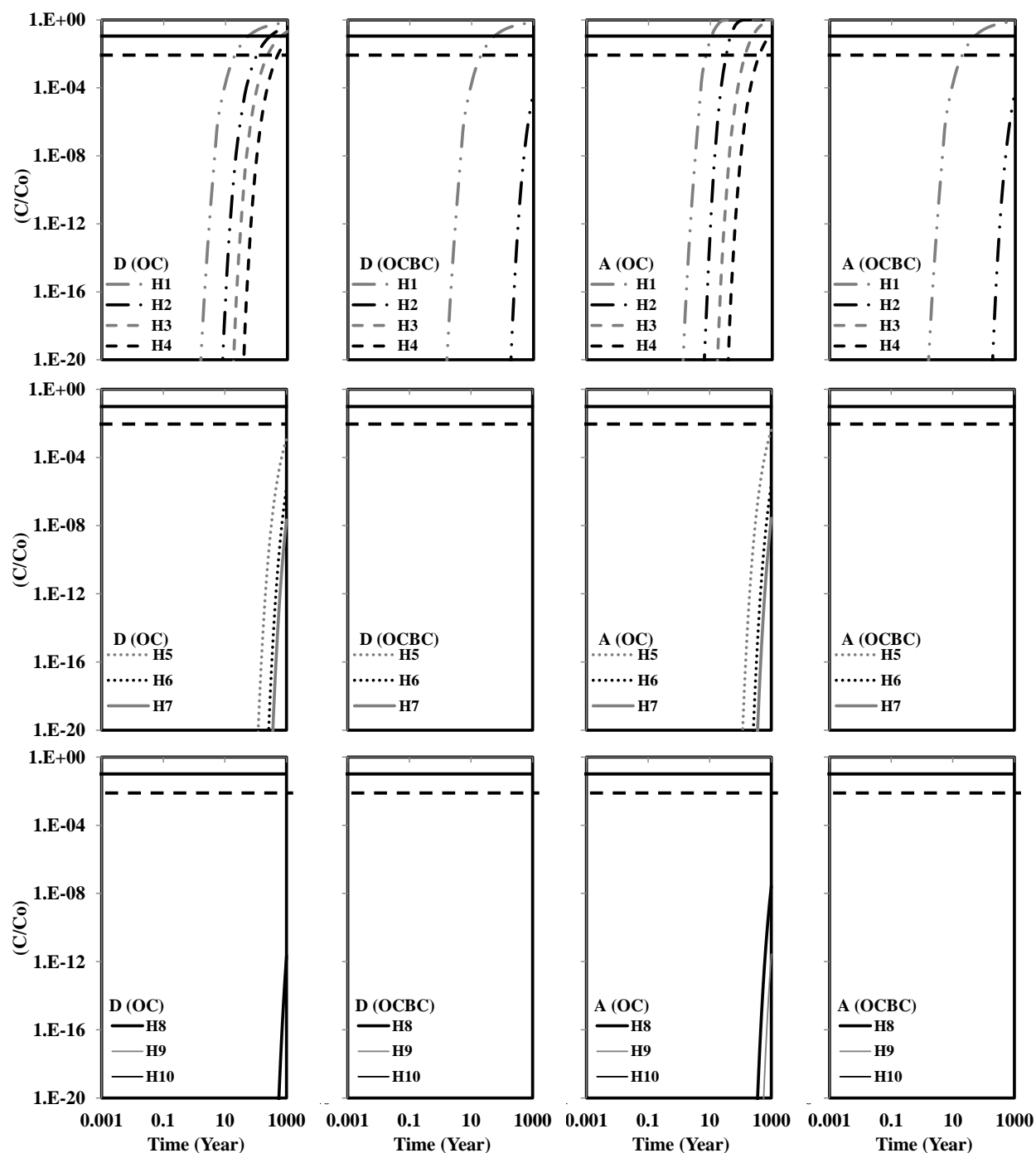


Figure 5.18j: PBDE breakthrough (C/C_0) in core IGC09 under the 95th percentile transport parameter values for diffusion with organic carbon only sorption (D(OC)), and organic carbon and black carbon co-sorption (D(OCBC)) and under advection-diffusion with organic carbon only sorption (A(OC)), and organic carbon and black carbon co-sorption (A(OCBC)). Horizontal bold line marks the 10% C/C_0 breakthrough and horizontal dotted line marks the 1% C/C_0 breakthrough. Data not shown indicates that C/C_0 breakthrough is below 1E-18%.

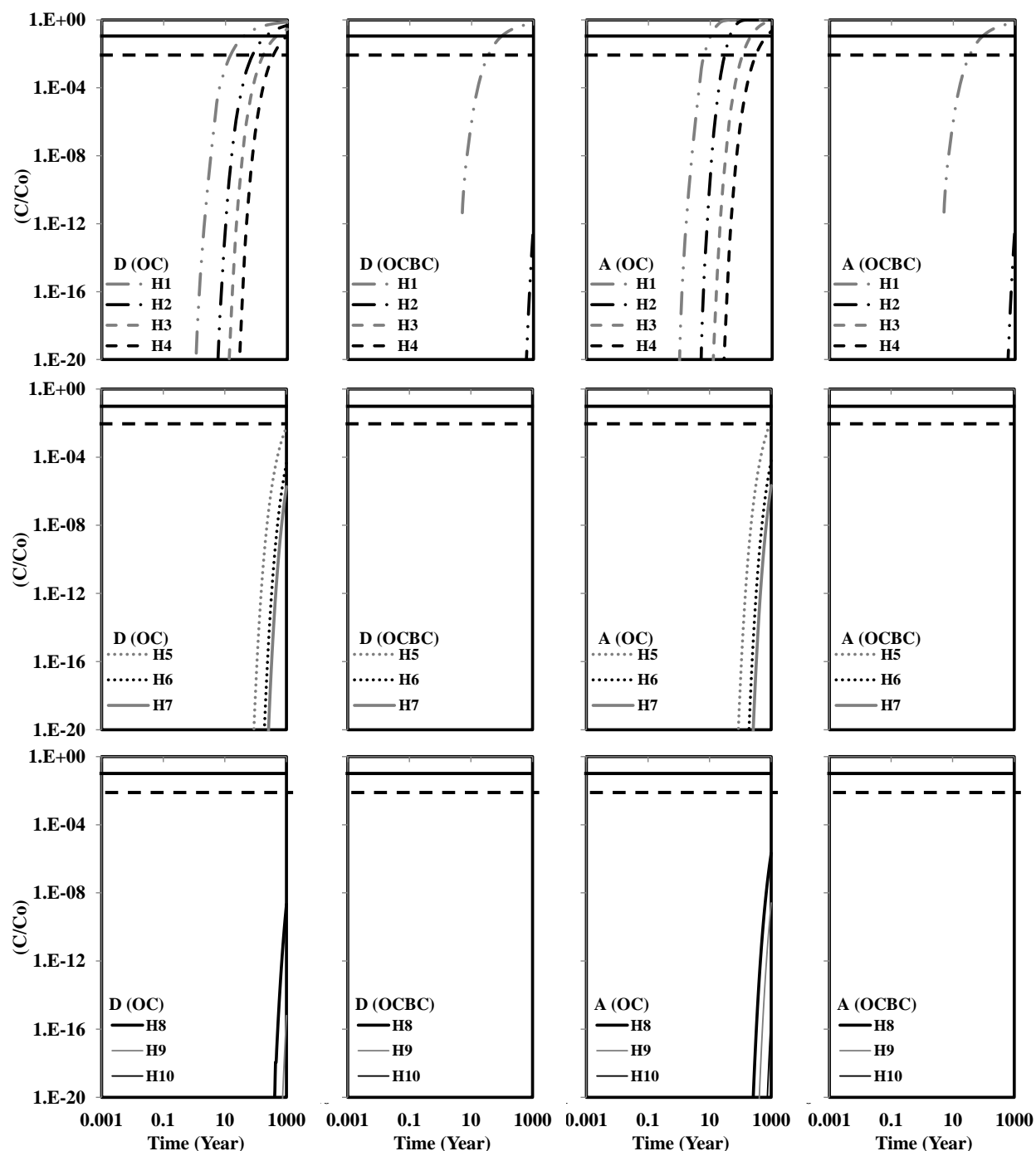


Figure 5.18k: PBDE breakthrough (C/C_0) in core IGC13 under the 95th percentile transport parameter values for diffusion with organic carbon only sorption (D(OC)), and organic carbon and black carbon co-sorption (D(OCBC)) and under advection-diffusion with organic carbon only sorption (A(OC)), and organic carbon and black carbon co-sorption (A(OCBC)). Horizontal bold line marks the 10% C/C_0 breakthrough and horizontal dotted line marks the 1% C/C_0 breakthrough. Data not shown indicates that C/C_0 breakthrough is below 1E-18%.

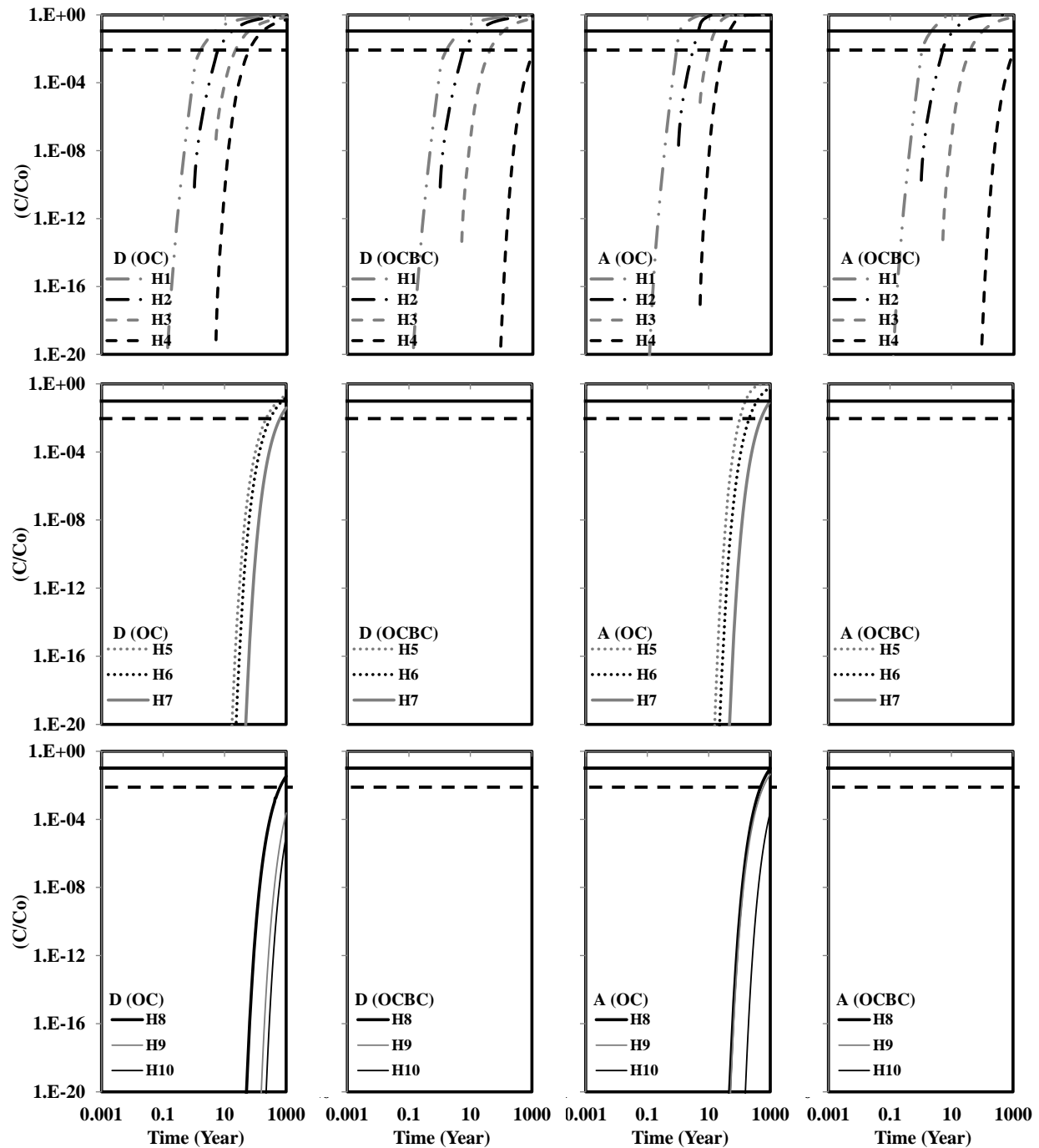


Figure 5.18l: PCB breakthrough (C/C_o) in core ACL under the 95th percentile transport parameter values for diffusion with organic carbon only sorption (D(OC)), and organic carbon and black carbon co-sorption (D(OCBC)) and under advection-diffusion with organic carbon only sorption (A(OC)), and organic carbon and black carbon co-sorption (A(OCBC)). Horizontal bold line marks the 10% C/C_o breakthrough and horizontal dotted line marks the 1% C/C_o breakthrough. Data not shown indicates that C/C_o breakthrough is below 1E-18%.

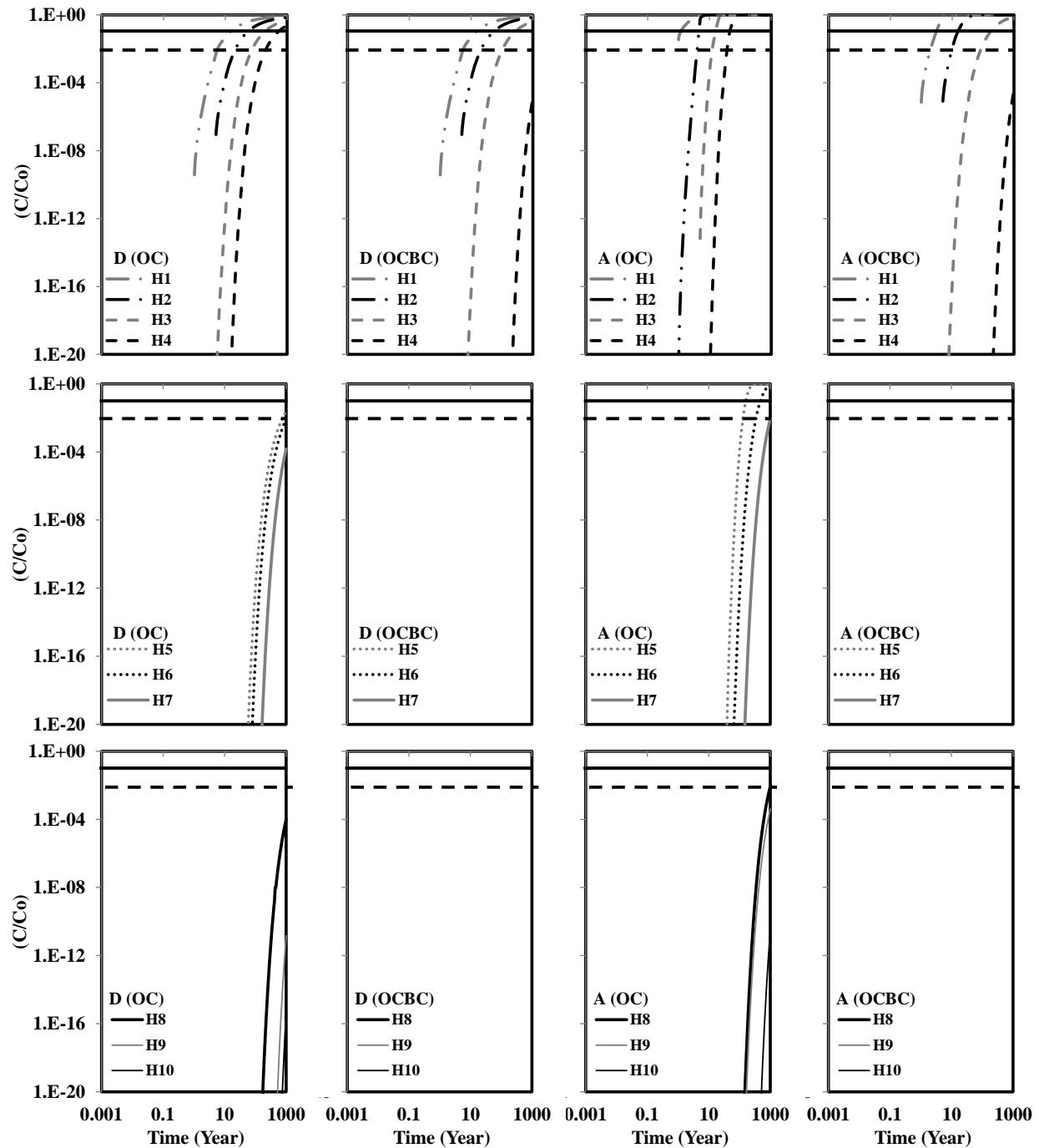


Figure 5.18m: PCB breakthrough (C/C_0) in core AED under the 95th percentile transport parameter values for diffusion with organic carbon only sorption (D(OC)), and organic carbon and black carbon co-sorption (D(OCBC)) and under advection-diffusion with organic carbon only sorption (A(OC)), and organic carbon and black carbon co-sorption (A(OCBC)). Horizontal bold line marks the 10% C/C_0 breakthrough and horizontal dotted line marks the 1% C/C_0 breakthrough. Data not shown indicates that C/C_0 breakthrough is below $1E-18$.

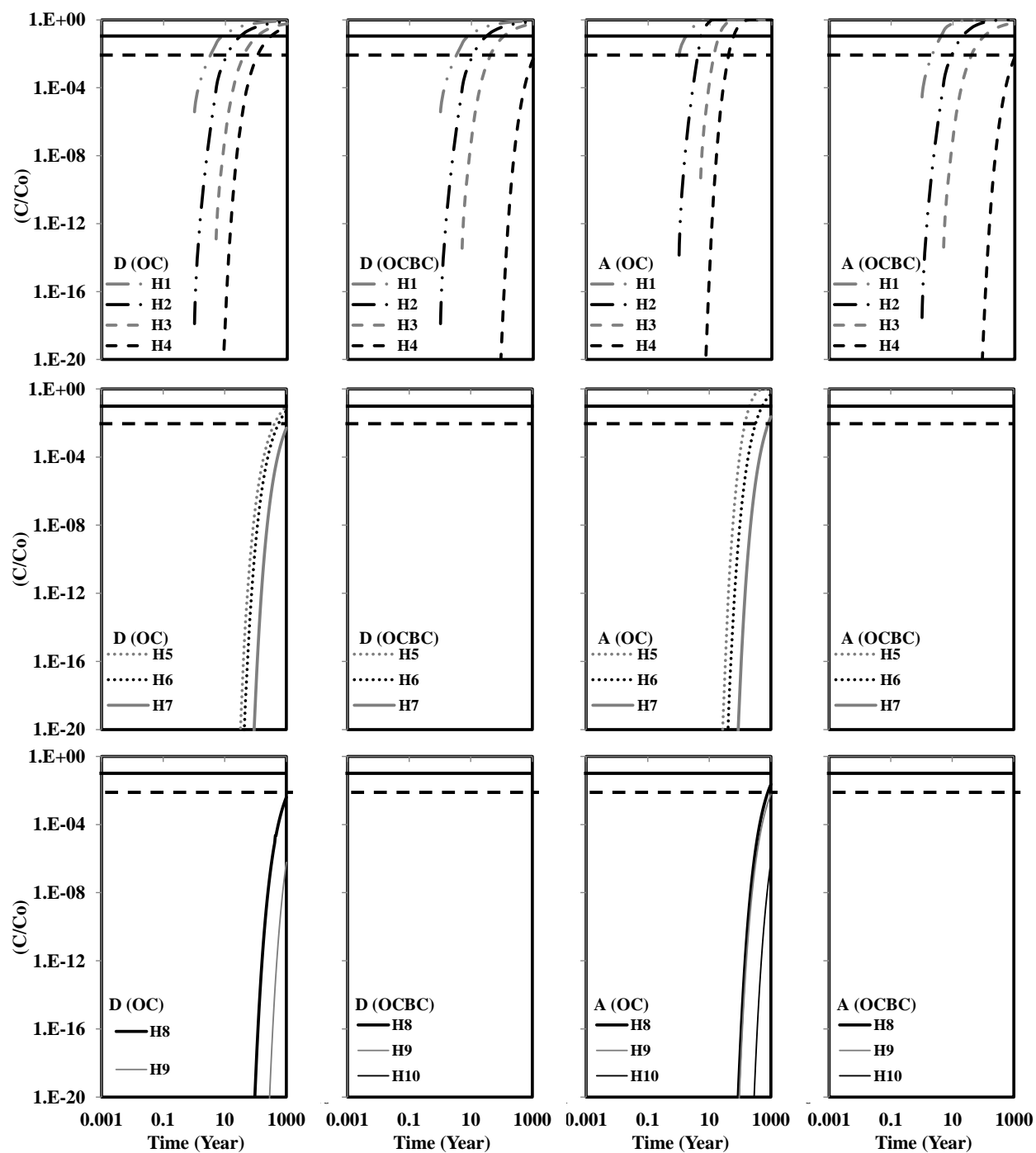


Figure 5.18n: PCB breakthrough (C/C_o) in core AFR under the 95th percentile transport parameter values for diffusion with organic carbon only sorption (D(OC)), and organic carbon and black carbon co-sorption (D(OCBC)) and under advection-diffusion with organic carbon only sorption (A(OC)), and organic carbon and black carbon co-sorption (A(OCBC)). Horizontal bold line marks the 10% C/C_o breakthrough and horizontal dotted line marks the 1% C/C_o breakthrough. Data not shown indicates that C/C_o breakthrough is below $1E-18$.

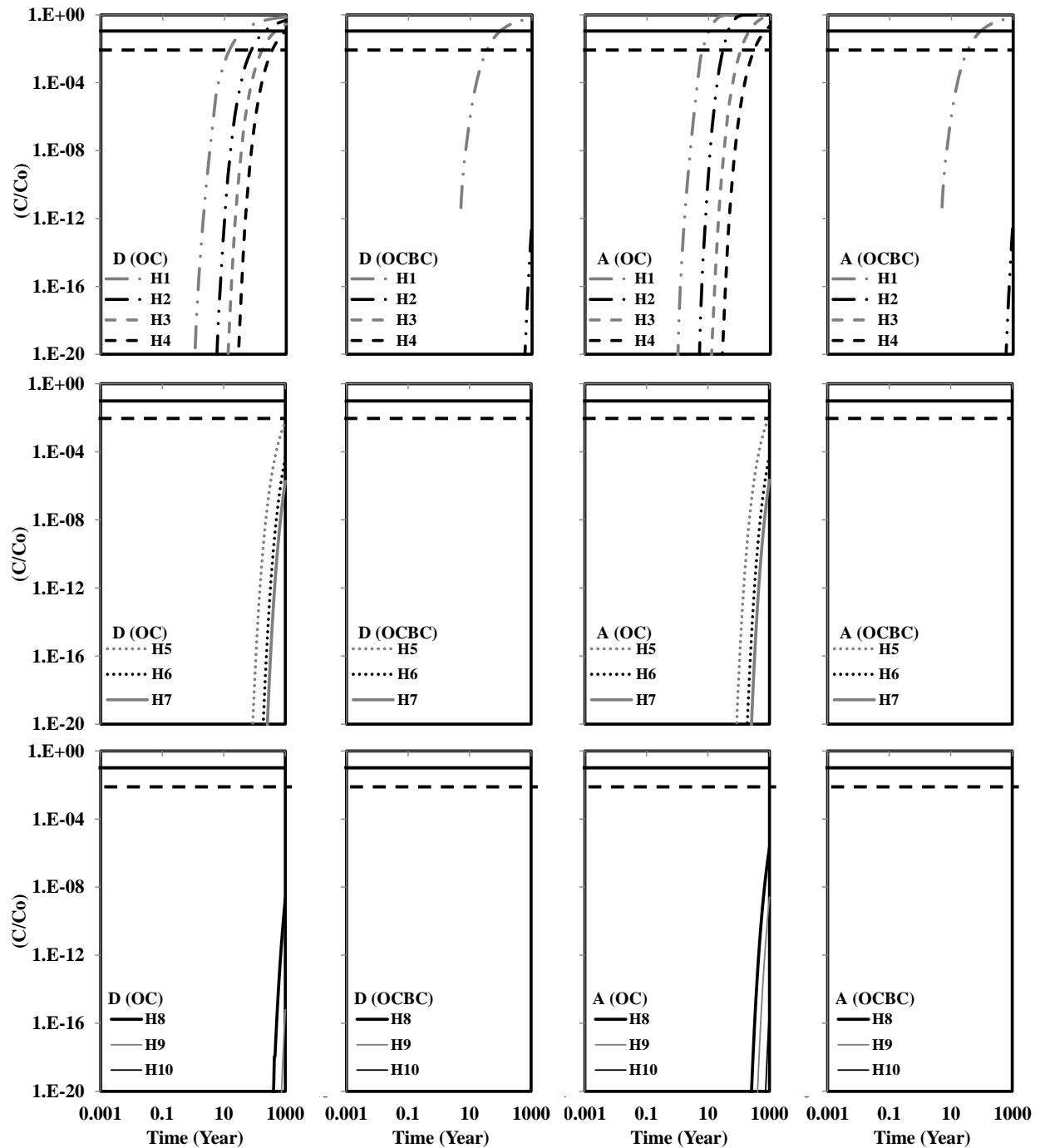


Figure 5.18o: PCB breakthrough (C/C_0) in core AJL under the 95th percentile transport parameter values for diffusion with organic carbon only sorption (D(OC)), and organic carbon and black carbon co-sorption (D(OCBC)) and under advection-diffusion with organic carbon only sorption (A(OC)), and organic carbon and black carbon co-sorption (A(OCBC)). Horizontal bold line marks the 10% C/C_0 breakthrough and horizontal dotted line marks the 1% C/C_0 breakthrough. Data not shown indicates that C/C_0 breakthrough is below $1.E-18$.

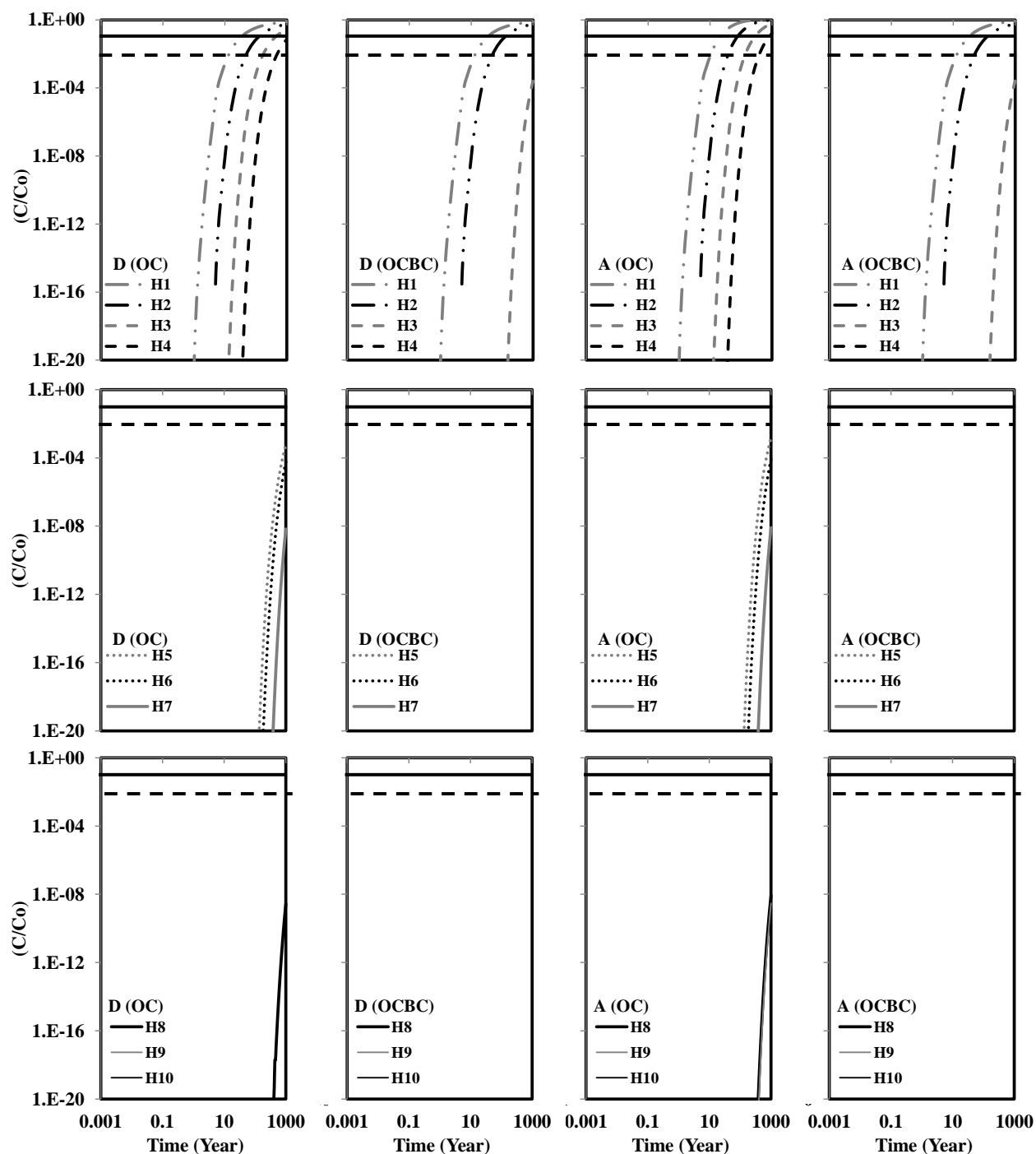


Figure 5.18p: PCB breakthrough (C/C_o) in core AMW under the 95th percentile transport parameter values for diffusion with organic carbon only sorption (D(OC)), and organic carbon and black carbon co-sorption (D(OCBC)) and under advection-diffusion with organic carbon only sorption (A(OC)), and organic carbon and black carbon co-sorption (A(OCBC)). Horizontal bold line marks the 10% C/C_o breakthrough and horizontal dotted line marks the 1% C/C_o breakthrough. Data not shown indicates that C/C_o breakthrough is below $1E-18\%$.

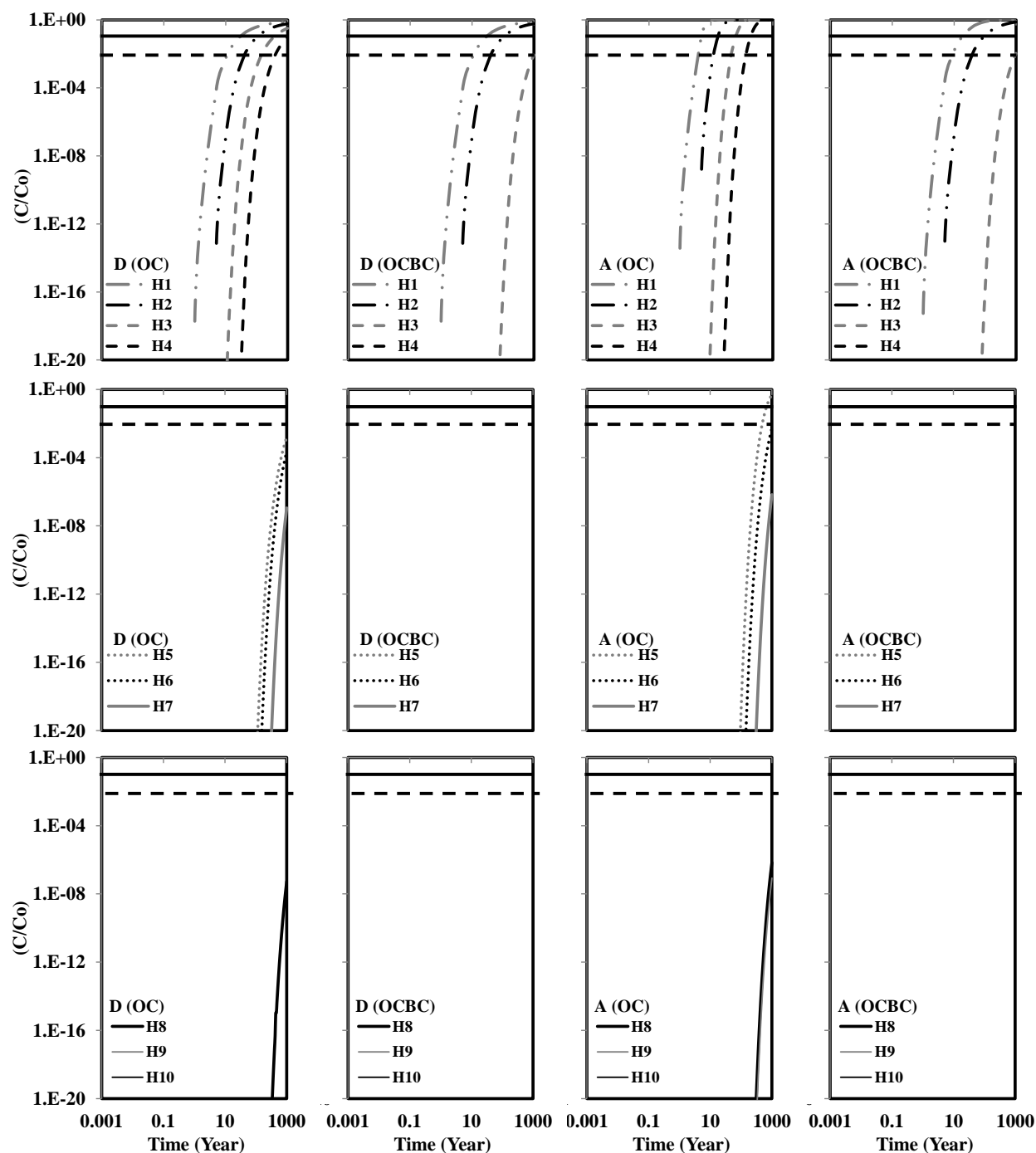


Figure 5.18q: PCB breakthrough (C/C_0) in core AOT under the 95th percentile transport parameter values for diffusion with organic carbon only sorption (D(OC)), and organic carbon and black carbon co-sorption (D(OCBC)) and under advection-diffusion with organic carbon only sorption (A(OC)), and organic carbon and black carbon co-sorption (A(OCBC)). Horizontal bold line marks the 10% C/C_0 breakthrough and horizontal dotted line marks the 1% C/C_0 breakthrough. Data not shown indicates that C/C_0 breakthrough is below $1E-18$.

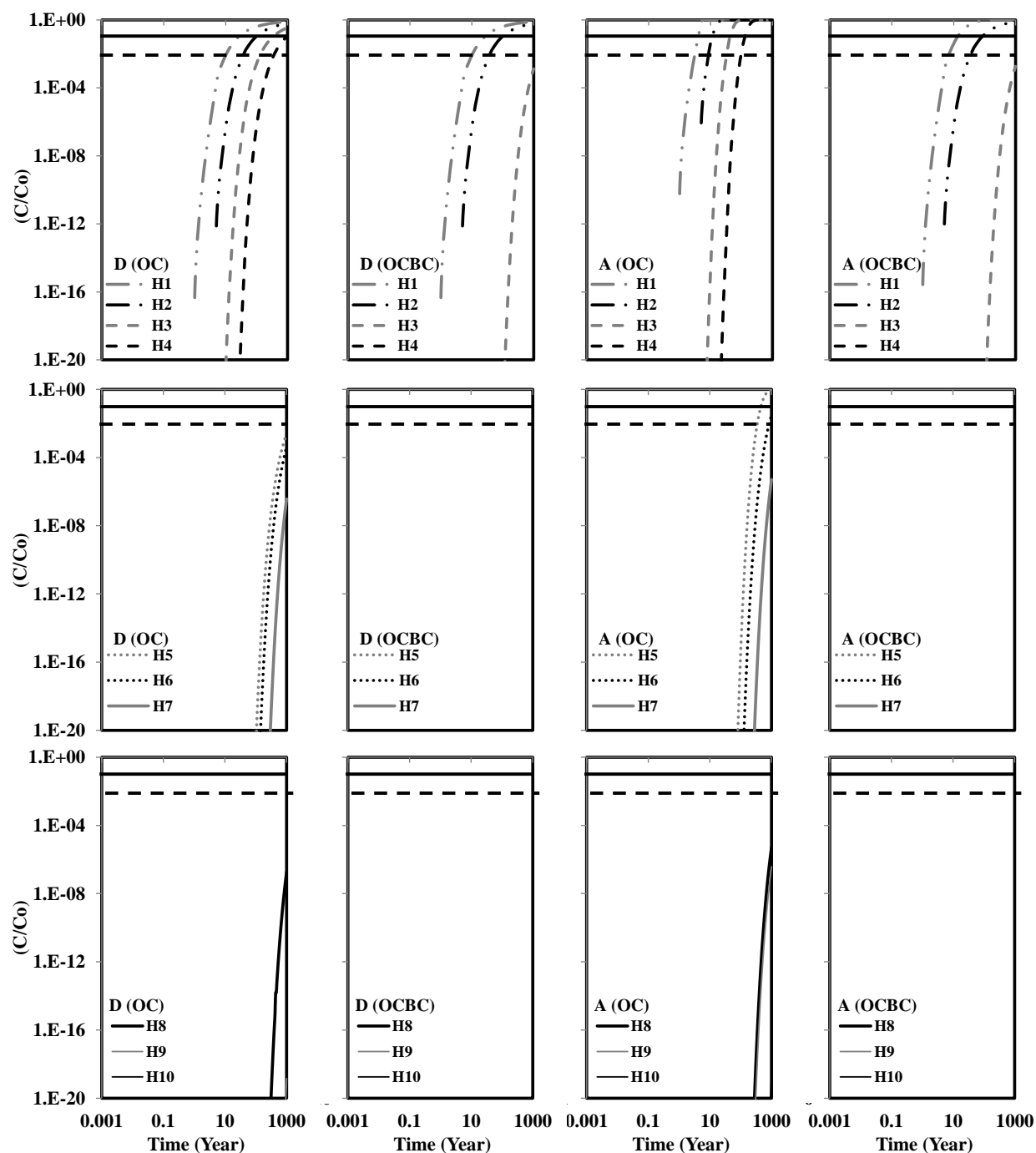


Figure 5.18r: PCB breakthrough (C/C_o) in core CBC under the 95th percentile transport parameter values for diffusion with organic carbon only sorption (D(OC)), and organic carbon and black carbon co-sorption (D(OCBC)) and under advection-diffusion with organic carbon only sorption (A(OC)), and organic carbon and black carbon co-sorption (A(OCBC)). Horizontal bold line marks the 10% C/C_o breakthrough and horizontal dotted line marks the 1% C/C_o breakthrough. Data not shown indicates that C/C_o breakthrough is below $1.E-18$.

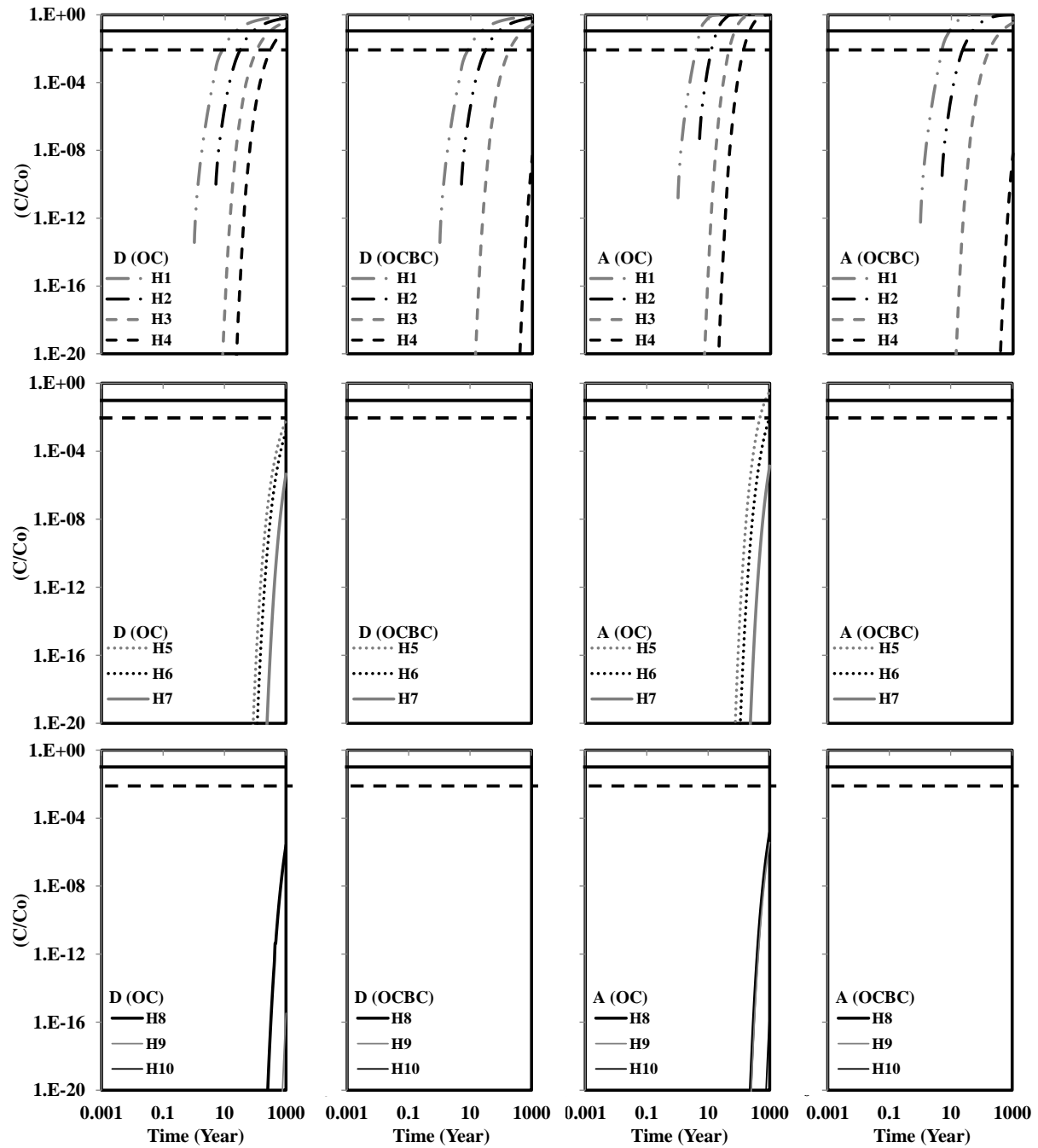


Figure 5.18s: PCB breakthrough (C/C_o) in core CLC under the 95th percentile transport parameter values for diffusion with organic carbon only sorption (D(OC)), and organic carbon and black carbon co-sorption (D(OCBC)) and under advection-diffusion with organic carbon only sorption (A(OC)), and organic carbon and black carbon co-sorption (A(OCBC)). Horizontal bold line marks the 10% C/C_o breakthrough and horizontal dotted line marks the 1% C/C_o breakthrough. Data not shown indicates that C/C_o breakthrough is below 10^{-18} .

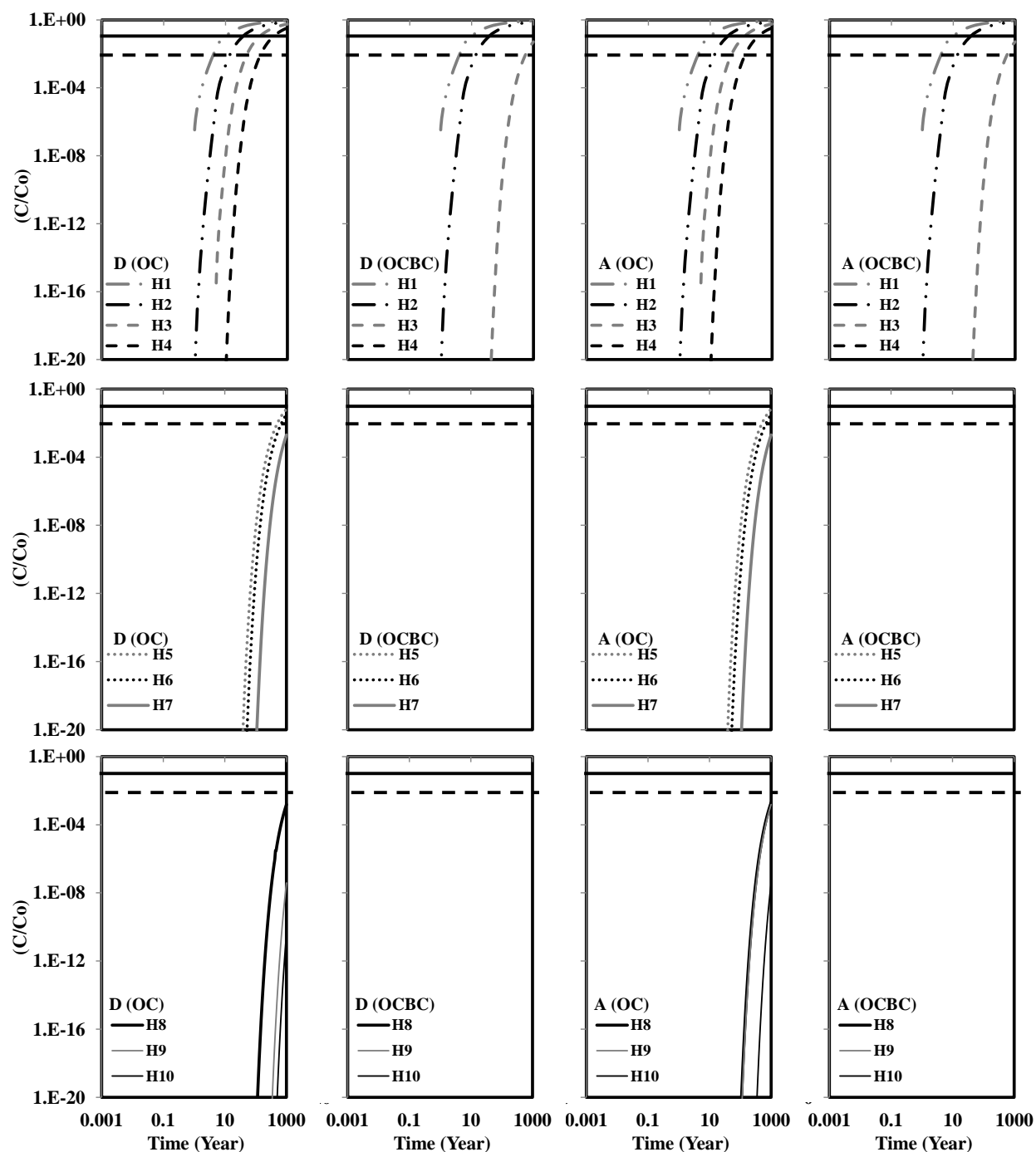


Figure 5.18t: PCB breakthrough (C/C_0) in core CWP under the 95th percentile transport parameter values for diffusion with organic carbon only sorption (D(OC)), and organic carbon and black carbon co-sorption (D(OCBC)) and under advection-diffusion with organic carbon only sorption (A(OC)), and organic carbon and black carbon co-sorption (A(OCBC)). Horizontal bold line marks the 10% C/C_0 breakthrough and horizontal dotted line marks the 1% C/C_0 breakthrough. Data not shown indicates that C/C_0 breakthrough is below $1E-18\%$.

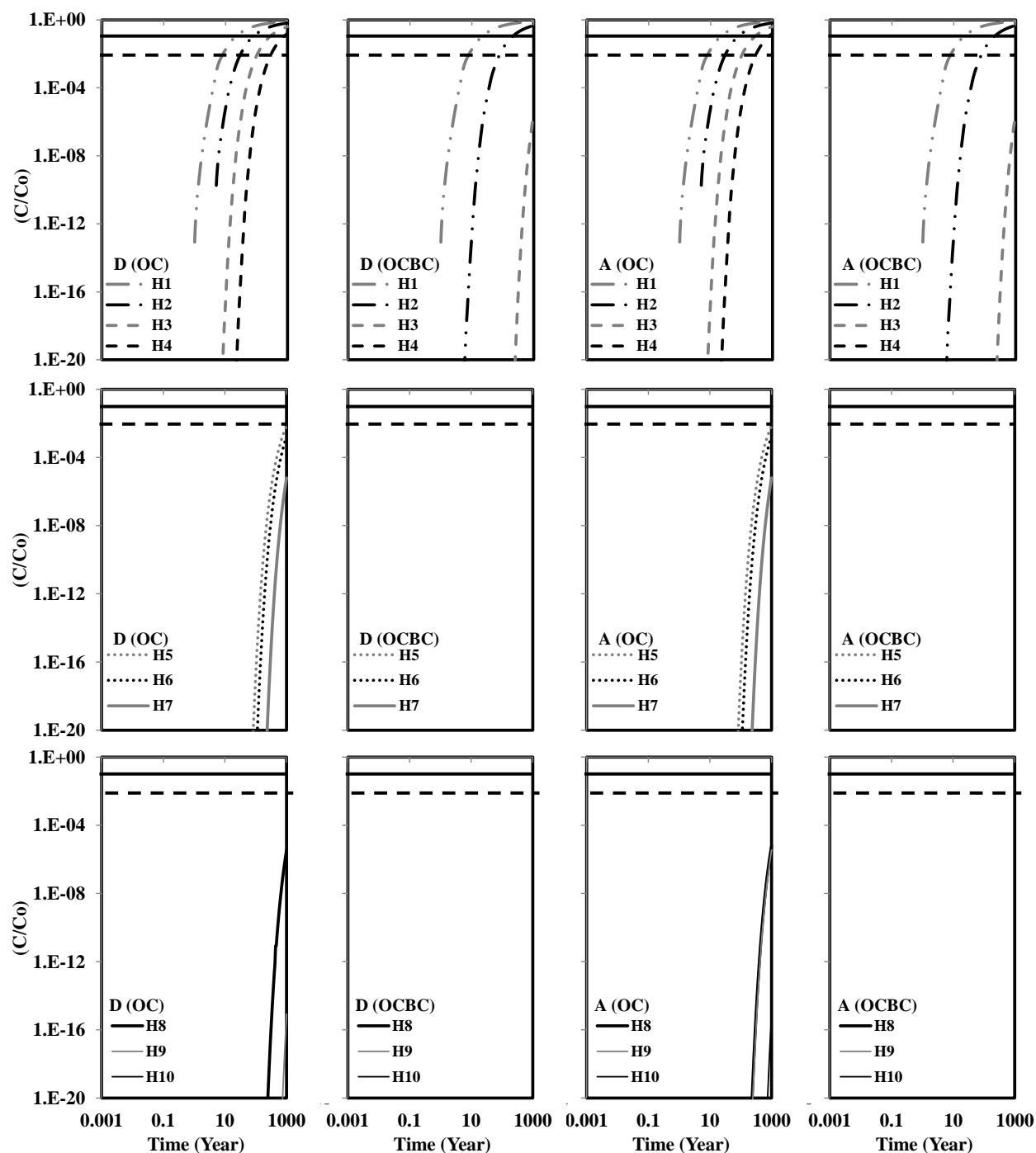


Figure 5.18u: PCB breakthrough (C/C_o) in core IGC09 under the 95th percentile transport parameter values for diffusion with organic carbon only sorption (D(OC)), and organic carbon and black carbon co-sorption (D(OCBC)) and under advection-diffusion with organic carbon only sorption (A(OC)), and organic carbon and black carbon co-sorption (A(OCBC)). Horizontal bold line marks the 10% C/C_o breakthrough and horizontal dotted line marks the 1% C/C_o breakthrough. Data not shown indicates that C/C_o breakthrough is below $1E-18\%$.

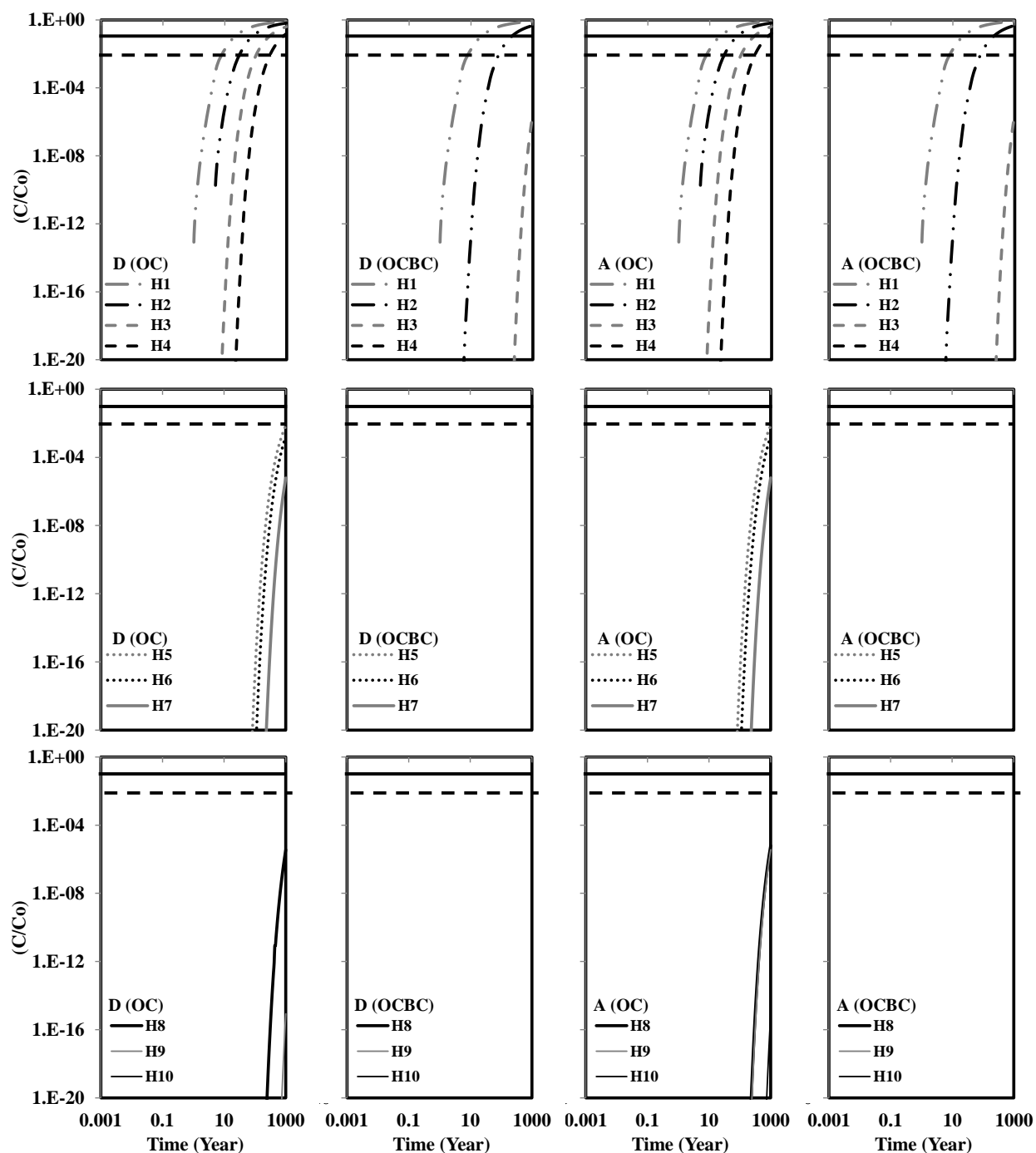


Figure 5.18v: PCB breakthrough (C/C_0) in core IGC13 under the 95th percentile transport parameter values for diffusion with organic carbon only sorption (D(OC)), and organic carbon and black carbon co-sorption (D(OCBC)) and under advection-diffusion with organic carbon only sorption (A(OC)), and organic carbon and black carbon co-sorption (A(OCBC)). Horizontal bold line marks the 10% C/C_0 breakthrough and horizontal dotted line marks the 1% C/C_0 breakthrough. Data not shown indicates that C/C_0 breakthrough is below $1.E-18$.

Table 5.13. PBDE and PCB homologs that reached 10% (non-underlined) and 1% (underlined) *C/Co* breakthrough under diffusion with organic carbon only sorption (D(OC)) (black), diffusion with organic carbon and black carbon co-sorption (D(OCBC)) (charcoal), advection-diffusion with organic carbon only sorption (A(OC)) (dark grey), and advection-diffusion with organic carbon and black carbon co-sorption (A(OCBC)) (light grey).

Core	Transport Process	Homologs									
		H1	H2	H3	H4	H5	H6	H7	H8	H9	H10
ACL	PBDE	√ √ √ √	√ √ √ √	√ √	√ √	√ √	<u>√</u> <u>√</u>	<u>√</u> <u>√</u>	<u>√</u> <u>√</u>		
	PCB	√ √ √ √	√ √ √ √	√ √ √ √	√ <u>√</u> <u>√</u> <u>√</u>	√ √	√ √	<u>√</u> √	<u>√</u> <u>√</u>		
AED	PBDE	√ √ √ √	√ √ √ √	√ √	√ √	√ √	<u>√</u> <u>√</u>	<u>√</u> <u>√</u>	<u>√</u> <u>√</u>		
	PCB	√ √ √ √	√ √ √ √	√ √ √ √	√ √	√ √	<u>√</u> √	<u>√</u> <u>√</u>	<u>√</u> <u>√</u>		
AFR	PBDE	√ √ √ √	√ √ √ √	√ √	√ √	√ √	<u>√</u> <u>√</u>	<u>√</u> <u>√</u>	<u>√</u>		
	PCB	√ √ √ √	√ √ √ √	√ √ √ √	√ √	√ √	<u>√</u> √	<u>√</u> <u>√</u>	<u>√</u> <u>√</u>		
AJL	PBDE	√ √ √ √	√ √ √ √	√ √	√ √	<u>√</u> √					
	PCB	√ √ √ √	√ √ √ √	√ √	√ √	<u>√</u> √					
AMW	PBDE	√ √ √ √	√ √ √ √	√ √	√ √	<u>√</u>					
	PCB	√ √ √ √	√ √ √ √	√ √	√ √						
AOT	PBDE	√ √ √ √	√ √ √ √	√ √	√ √	<u>√</u> √					
	PCB	√ √ √ √	√ √ √ √	√ <u>√</u> <u>√</u> <u>√</u>	√ √	<u>√</u> √					
CBC	PBDE	√ √ √ √	√ <u>√</u> <u>√</u> <u>√</u>	√ √	√ √	<u>√</u> √					
	PCB	√ √ √ √	√ √ √ √	√ <u>√</u> <u>√</u> <u>√</u>	√ √	<u>√</u> √					
CLC	PBDE	√ √ √ √	√ <u>√</u>								
	PCB	√ √ √ √	√ √ √ √	√ <u>√</u> <u>√</u> <u>√</u>	√ √						
CWP	PBDE	√ √ √ √	√ √	<u>√</u> <u>√</u>	<u>√</u> <u>√</u>						
	PCB	√ √ √ √	√ √ √ √	√ √	<u>√</u> <u>√</u>	<u>√</u> <u>√</u>					
IGC09	PBDE	√ √ √ √	√ √								
	PCB	√ √ √ √	√ √ √ √	√ √	√ √						
IGC13	PBDE	√ √ √ √	√ √	√ √	√ √	<u>√</u> <u>√</u>					
	PCB	√ √ √ √	√ √ √ √	√ √	√ √	<u>√</u> <u>√</u>					

In Figure 5.19a-h, C/C_o for PBDE and PCB homologs predicted from the 95th percentile transport parameter values for D(OC), D(OCBC), A(OC), and A(OCBC) in-situ sediment transport processes in all the sediment columns at 40, 100, and 1000 years are compared (PBDE: a-d; PCB: e-h). Several trends that can be discerned from Figure 5.18 and Table 5.11 are highlighted in Figure 5.19a-h. First, PBDE homologs have smaller C/C_o relative to PCB homologs under the same transport condition (i.e., in the same core under the same mass transport processes); second, small PBDE and PCB homologs have larger C/C_o relative to large PBDE and PCB homologs under the same transport condition, and finally, inclusion of the BC component has a retardation effect on PBDE and PCB homolog transport with the effect more pronounced in urban Chicago and IGC sediment cores.

The cumulative C/C_o values, defined as sum C/C_o for PBDE or PCB homologs 1 through 10, for transport time of 1000 years under D(OC), D(OCBC), A(OC), and A(OCBC) transport conditions are summarized in Figure 5.20 to provide a quick overview of the relative magnitude of these transport processes in the sediment cores. Under D(OC), mass transport magnitude increased in the order of CLC < IGC09 < IGC13 < AMW < CWP < ACL < CBC < AFR < AJL < AOT < AED which was the same increased order for D_{obs} (OC); this was expected as D_{obs} (OC) is the control parameter for D(OC) transport process. Similarly, for D(OCBC) transport process, C/C_o for PBDE or PCB homologs increased in the same order of D_{obs} (OCBC) which is CWP < CLC < IGC09 < IGC13 < CBC < AMW < ACL < AFR < AED < AJL < AOT. C/C_o for PBDE and PCB homologs under A(OC) transport increased in the order of CLC < IGC09 < CWP < AMW < IGC13 < AJL < AOT < CBC < AFR < AED < ACL which showed slight variation from the increased order of ν (OC) which was CLC < AJL < AOT < CWP < IGC09 < AMW < IGC13 < CBC < AFR < AED < ACL. For PBDE and PCB homologs under A (OCBC) transport condition, C/C_o increased in the order of CWP < CLC < IGC09 < IGC13 < AJL < AOT < CBC < AFR < ACL < AED which also showed slight variation from the increased order of ν (OCBC) which was CLC < CWP < IGC13 < IGC09 < AOT < CBC < AJL < AMW < AFR < AED < ACL. While D_{obs} (OC) and D_{obs} (OCBC) can predict the magnitude of C/C_o reliably under D(OC) and D(OCBC) mass

transport conditions, v (OC) and v (OCBC) were less reliable predictors of the magnitude of C/Co under A(OC) and A(OCBC) mass transport conditions simulation in sediment columns. Under diffusion only condition, D_{obs} is the only control parameter that can be observed in Equations 5.1 and 5.4. The C/Co under advection-diffusion condition is a function of D_{obs} as well as v . Advection-diffusion is a complex mass transport process governed by various parameters which rendered the prediction of C/Co based on a single v parameter less reliable.

As was expected from Table 5.11, cumulative and individual (i.e., by homolog) magnitude of C/Co is the highest under A(OC) > D(OC) > A(OCBC) > D(OCBC) transport processes. It is interesting to note that although C/Co increased with time, the rate of C/Co ($\Delta (C/Co)$) decreased with time (Figure 5.19a-h, panels d-f). This is due to the contaminant mass leaving the sediment boundary layer via the aqueous phase; mass conservation dictates that C_{sed} will gradually decrease over time resulting in gradual decrease of the rate of $\Delta (C/Co)$ over time as the concentration gradient decreases.

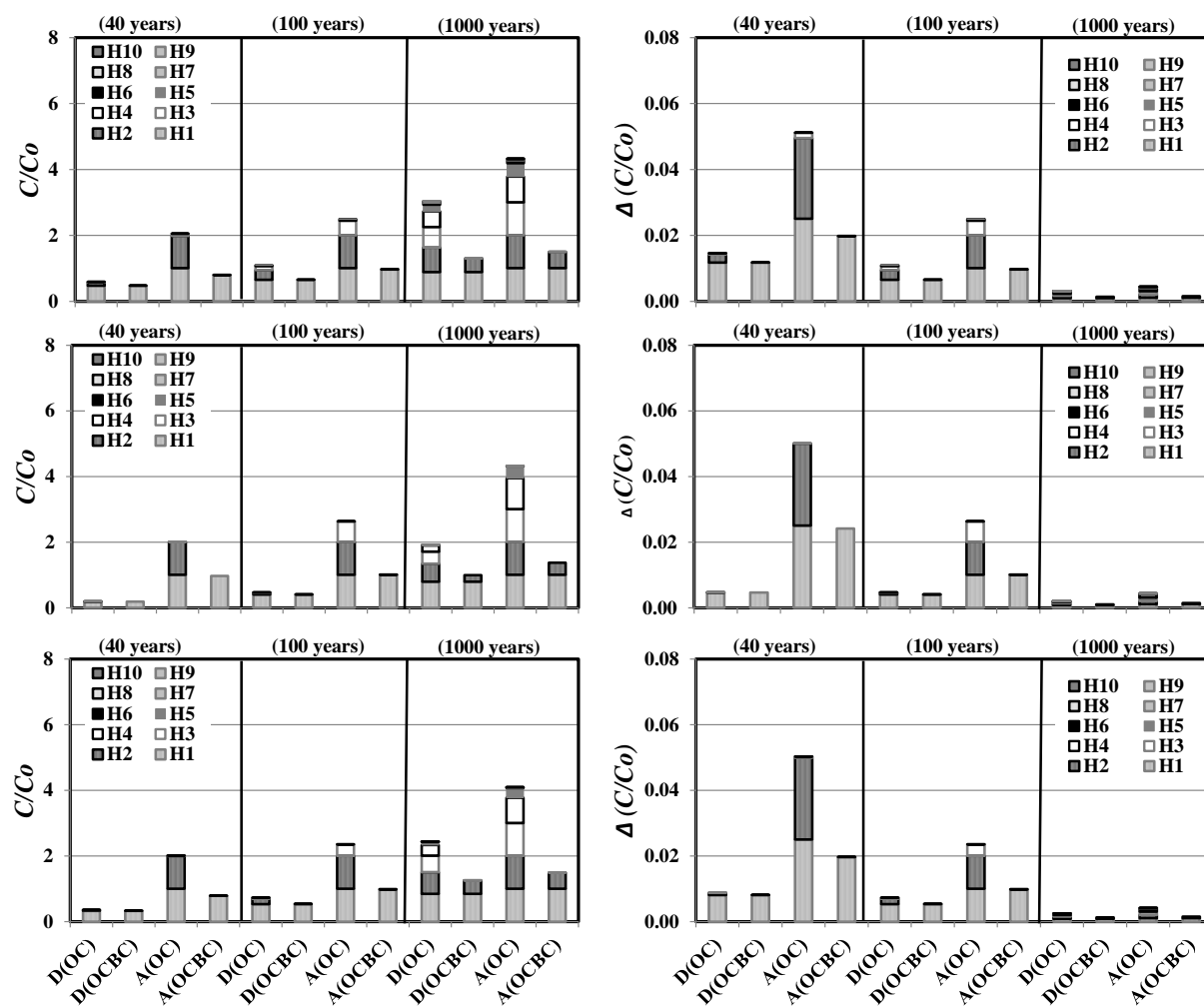


Figure 5.19a: PBDE breakthrough (C/C_o) (a-c) and change of breakthrough rate ($\Delta(C/C_o)$) (d-f) at $x=0.02\text{m}$ in cores ACL (a,d), AED (b,e), and AFR (c,f) predicted from the Monte Carlo 95th percentile transport parameter values for diffusion with organic carbon only sorption (D(OC)), diffusion with organic carbon and black carbon co-sorption (D(OCBC)), advection-diffusion with organic carbon only sorption (A(OC)), and advection-diffusion with organic carbon and black carbon co-sorption (A(OCBC)).

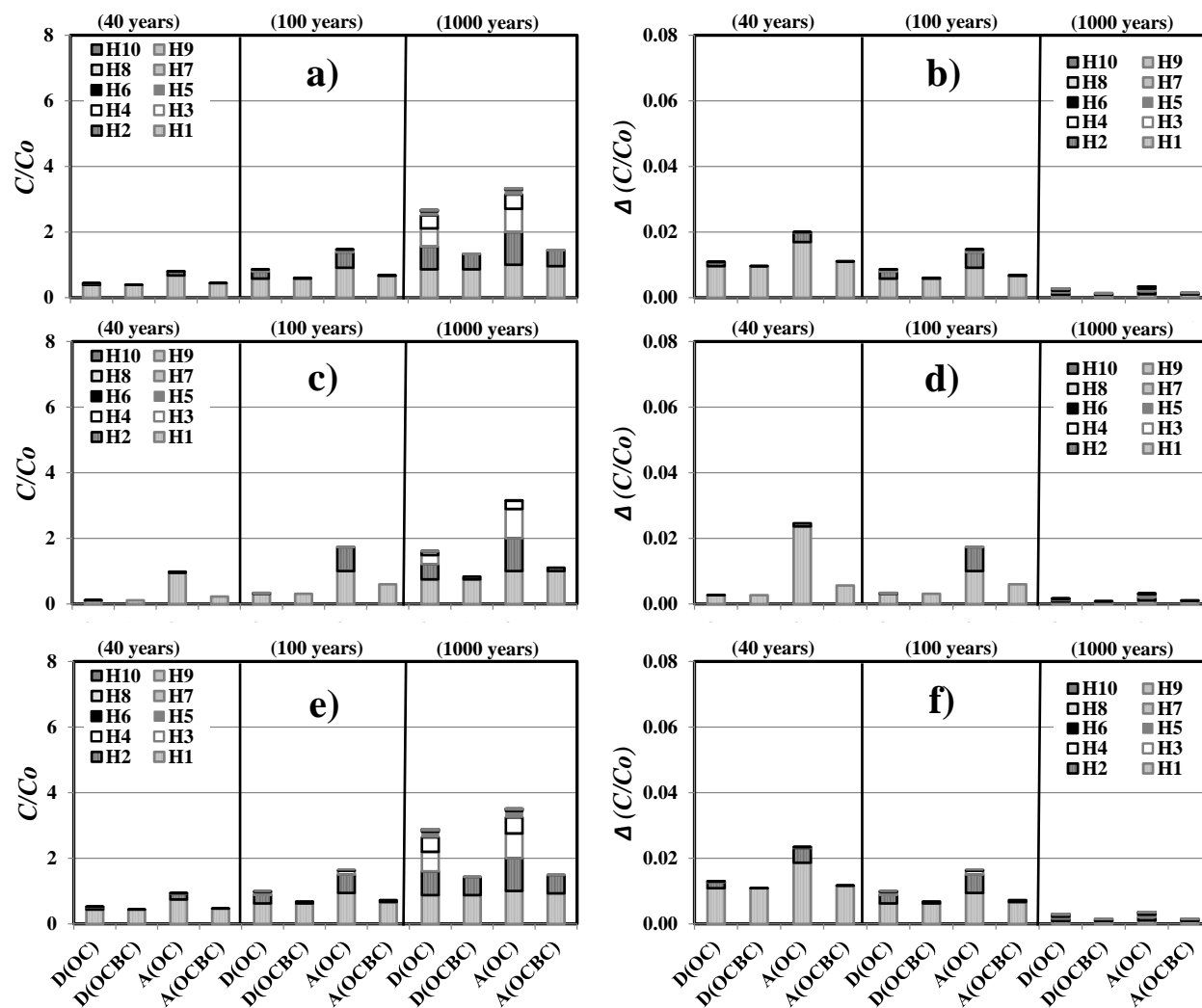


Figure 5.19b: PBDE breakthrough (C/C_o) (a-c) and change of breakthrough rate ($\Delta(C/C_o)$) (d-f) at $x=0.02\text{m}$ in cores AJL (a,d), AMW (b,e), and AOT (c,f) predicted from the Monte Carlo 95th percentile transport parameter values for diffusion with organic carbon only sorption (D(OC)), diffusion with organic carbon and black carbon co-sorption (D(OCBC)), advection-diffusion with organic carbon only sorption (A(OC)), and advection-diffusion with organic carbon and black carbon co-sorption (A(OCBC)).

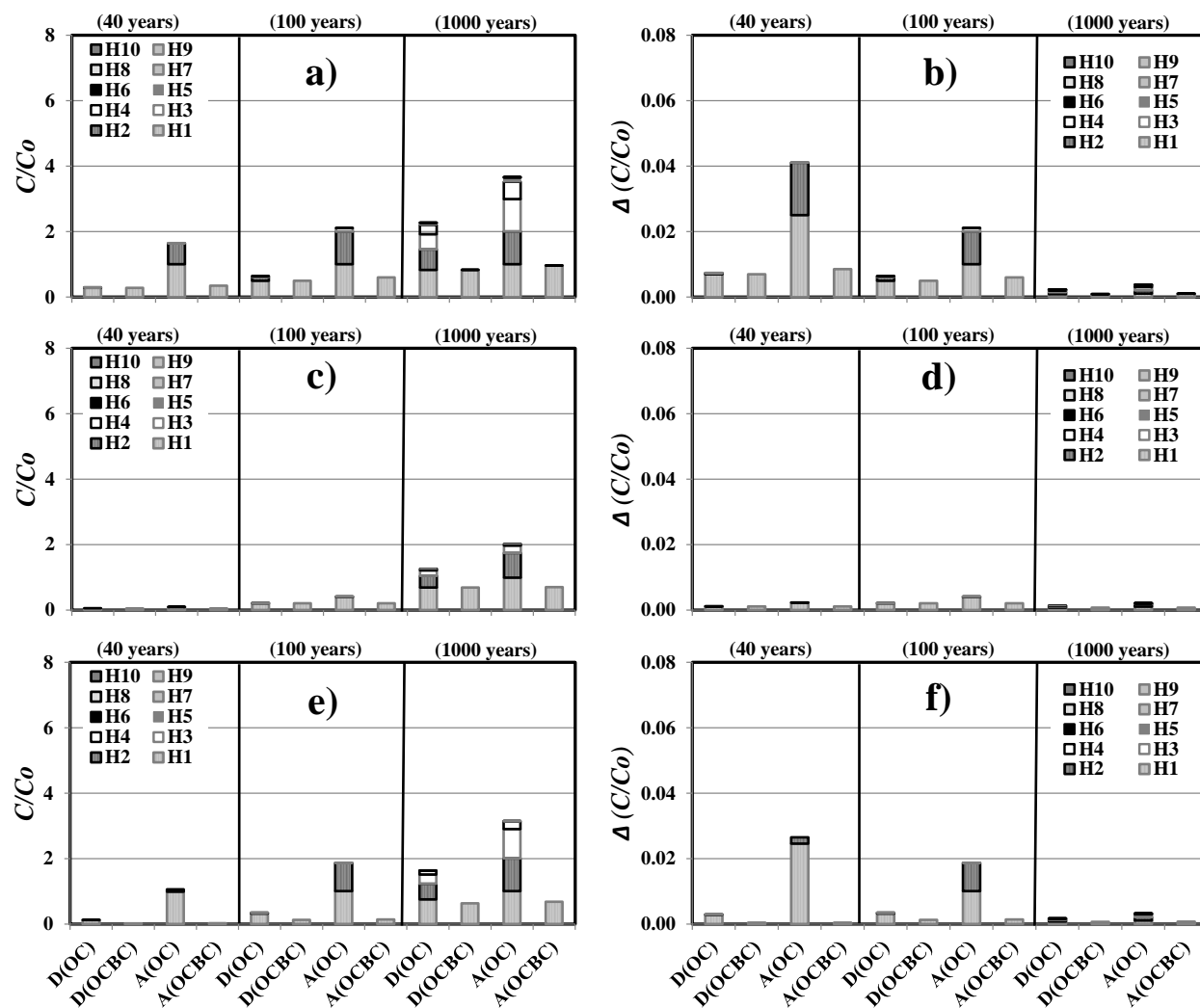


Figure 5.19c: PBDE breakthrough (C/C_o) (a-c) and change of breakthrough rate ($\Delta(C/C_o)$) (d-f) at $x=0.02\text{m}$ in cores CBC (a,d), CLC (b,e), and CWP (c,f) predicted from the Monte Carlo 95th percentile transport parameter values for diffusion with organic carbon only sorption (D(OC)), diffusion with organic carbon and black carbon co-sorption (D(OCBC)), advection-diffusion with organic carbon only sorption (A(OC)), and advection-diffusion with organic carbon and black carbon co-sorption (A(OCBC)).

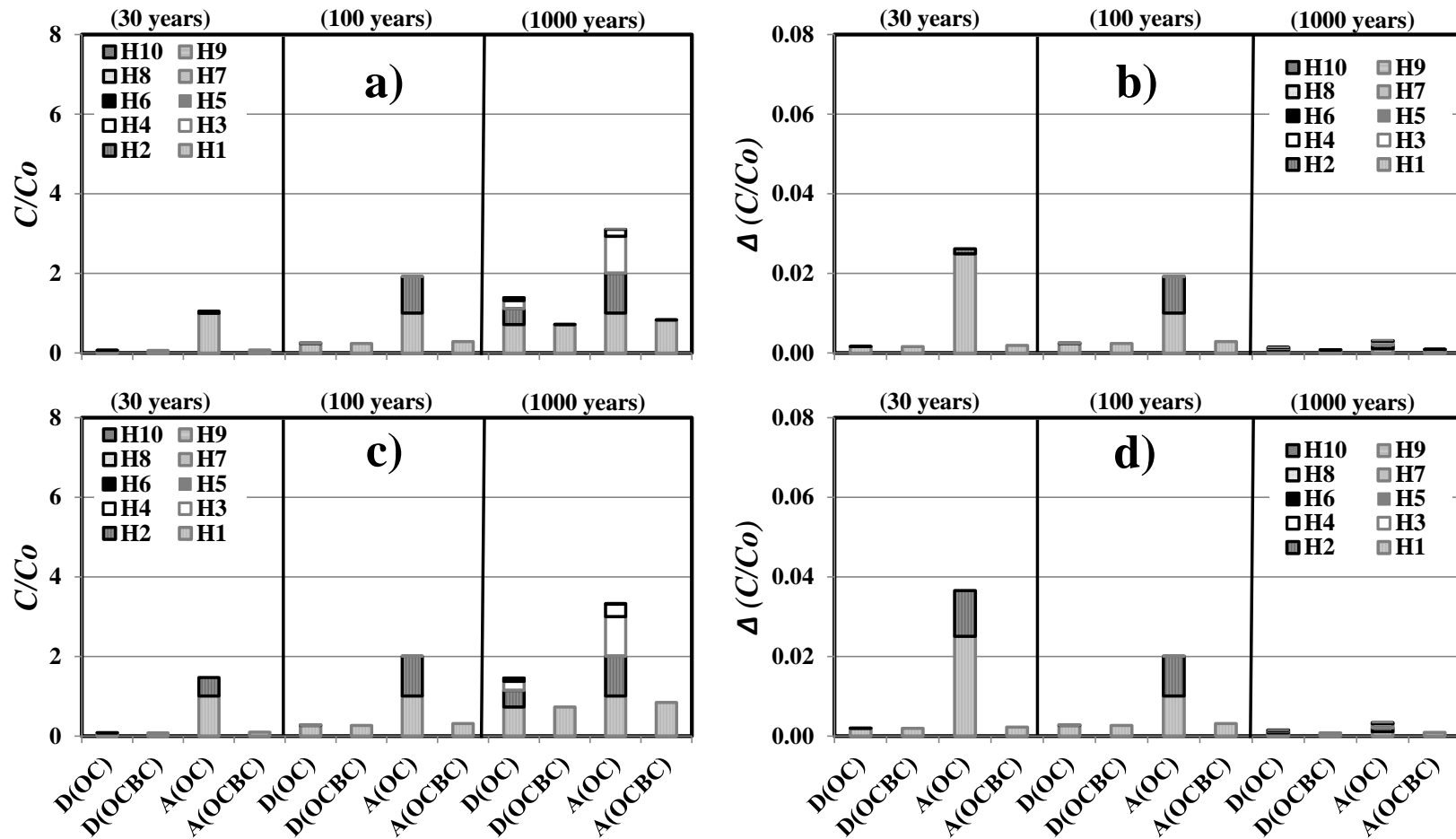


Figure 5.19d: PBDE breakthrough (C/C_o) (a-b) (left panels) and change of breakthrough rate ($\Delta(C/C_o)$) (c-d) at $x=0.02\text{m}$ in cores IGC09 (a,c) and IGC13 (b,d) predicted from the Monte Carlo 95th percentile transport parameter values for diffusion with organic carbon only sorption (D(OC)), diffusion with organic carbon and black carbon co-sorption (D(OCBC)), advection-diffusion with organic carbon only sorption (A(OC)), and advection-diffusion with organic carbon and black carbon co-sorption (A(OCBC)).

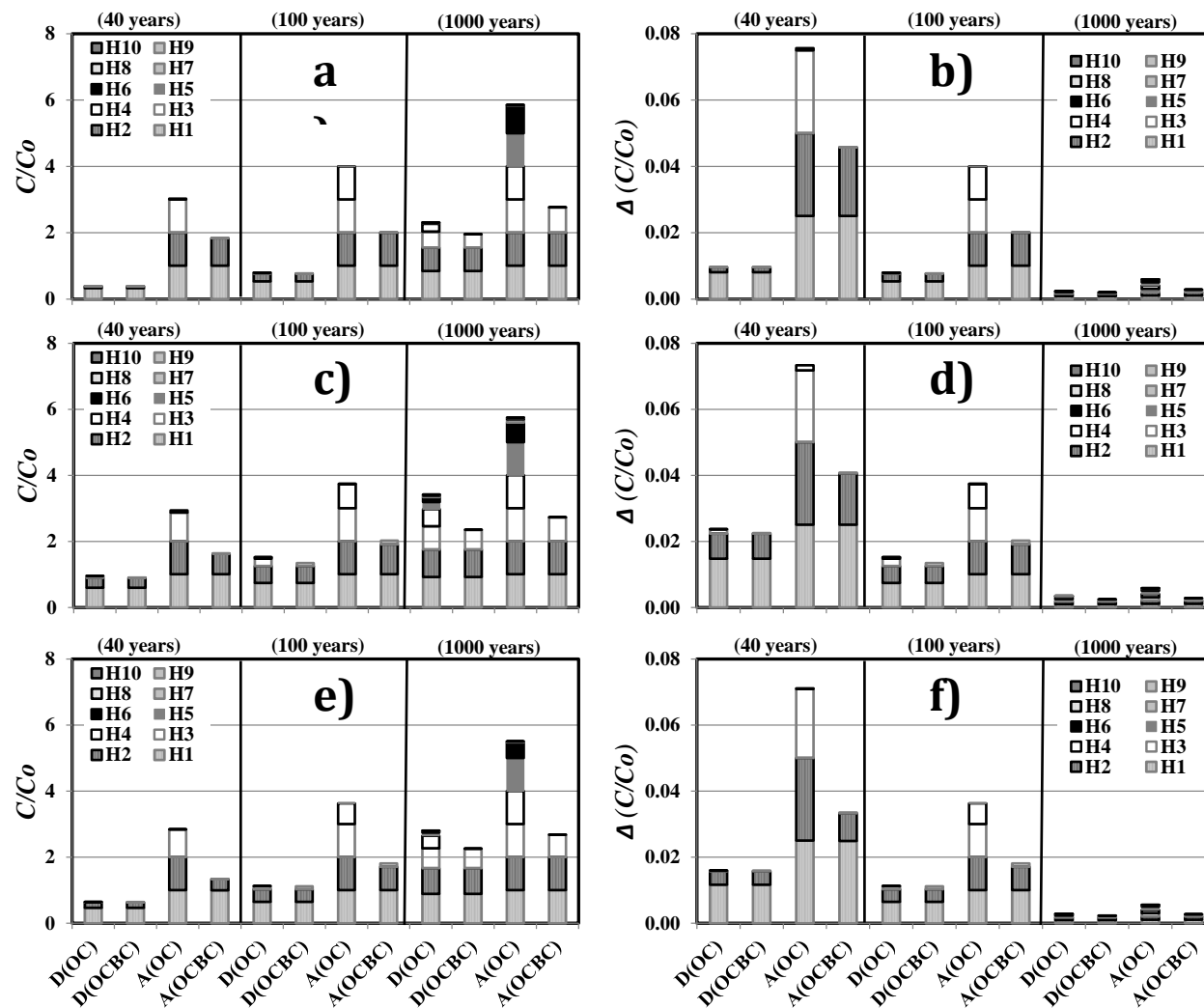


Figure 5.19e: PCB breakthrough (C/C_o) (a-c) and change of breakthrough rate ($\Delta(C/C_o)$) (d-f) at $x=0.02\text{m}$ in cores ACL (a,c), AED (b,e), and AFR (c,f) predicted from the Monte Carlo 95th percentile transport parameter values for diffusion with organic carbon only sorption (D(OC)), diffusion with organic carbon and black carbon co-sorption (D(OCBC)), advection-diffusion with organic carbon only sorption (A(OC)), and advection-diffusion with organic carbon and black carbon co-sorption (A(OCBC)).

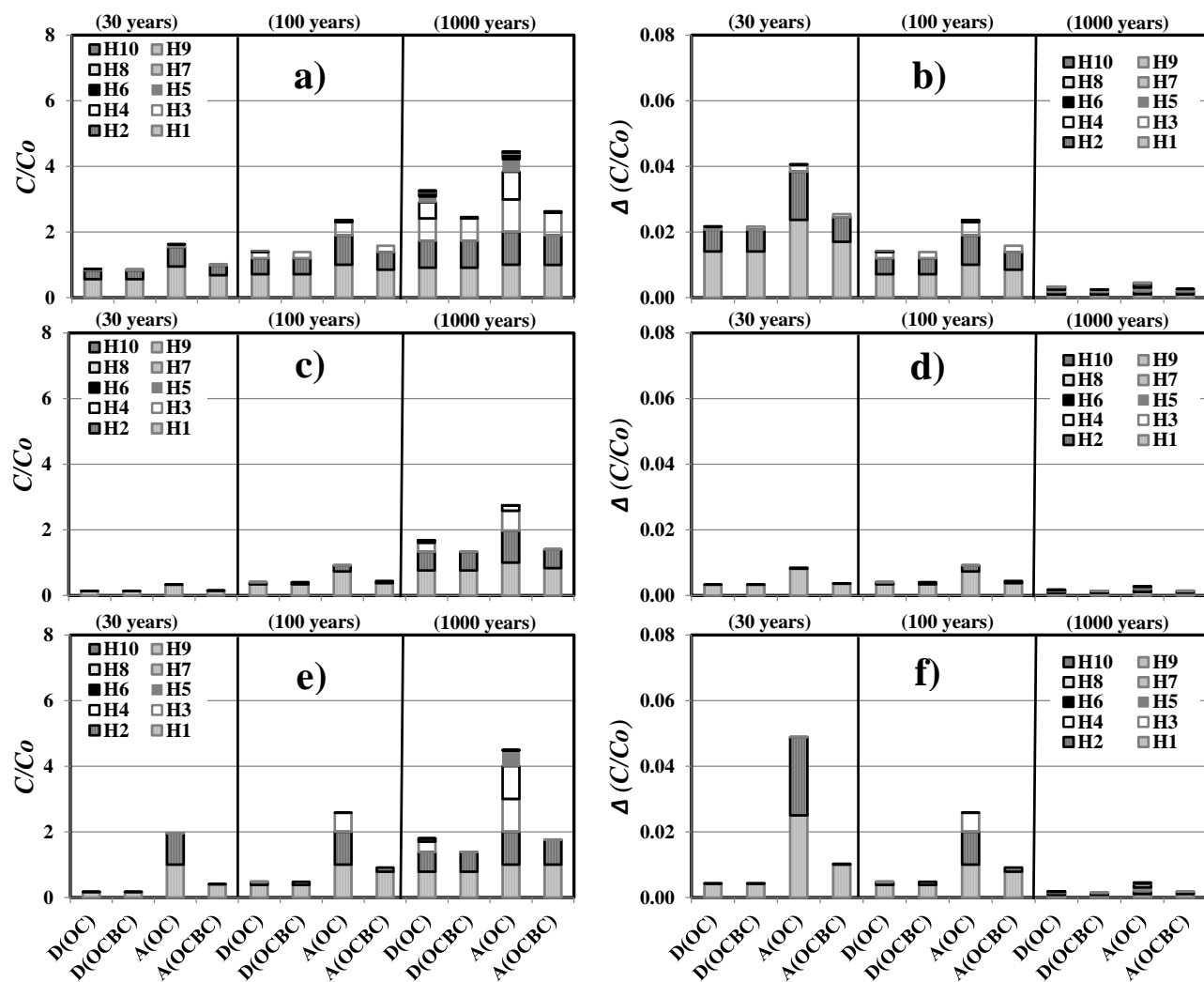


Figure 5.19f: PCB breakthrough (C/C_o) (a-c) and change of breakthrough rate ($\Delta(C/C_o)$) (d-f) at $x=0.02\text{m}$ in cores AJL (a,c), AMW (b,e), and AOT (c,f) predicted from the Monte Carlo 95th percentile transport parameter values for diffusion with organic carbon only sorption (D(OC)), diffusion with organic carbon and black carbon co-sorption (D(OCBC)), advection-diffusion with organic carbon only sorption (A(OC)), and advection-diffusion with organic carbon and black carbon co-sorption (A(OCBC)).

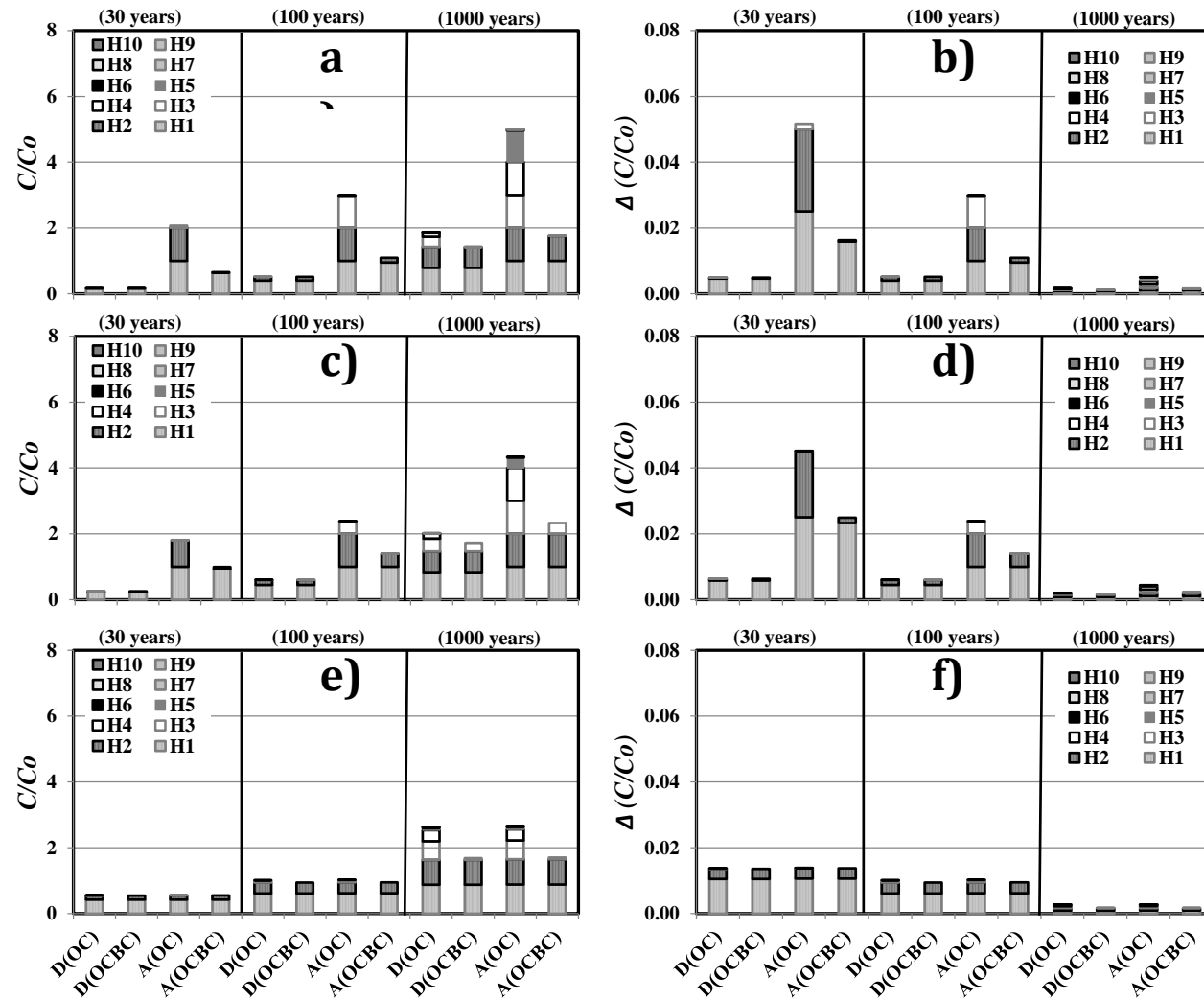


Figure 5.19g: PCB breakthrough (C/C_o) (a-c) and change of breakthrough rate ($\Delta(C/C_o)$) (d-f) at $x=0.02\text{m}$ in cores CBC (a,d), CLC (c,e), and CWP (b,f) predicted from the Monte Carlo 95th percentile transport parameter values for diffusion with organic carbon only sorption (D(OC)), diffusion with organic carbon and black carbon co-sorption (D(OCBC)), advection-diffusion with organic carbon only sorption (A(OC)), and advection-diffusion with organic carbon and black carbon co-sorption (A(OCBC)).

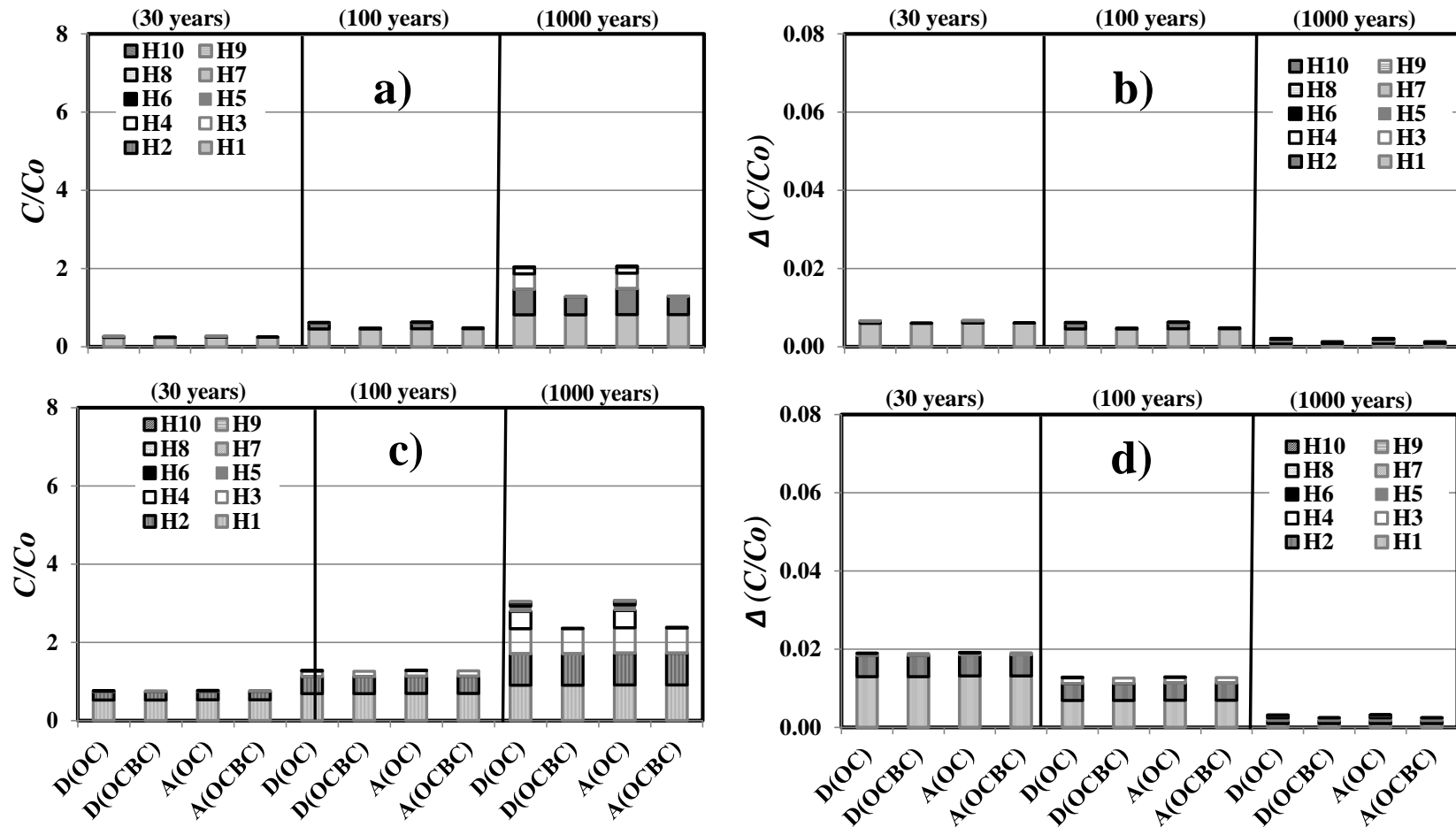


Figure 5.19h: PCB breakthrough (C/Co) (a-b) and change of breakthrough rate ($\Delta(C/Co)$) (c-d) at $x=0.02\text{m}$ in cores IGC09 (a,c) and IGC13 (b,d) predicted from the Monte Carlo 95th percentile transport parameter values for diffusion with organic carbon only sorption (D(OC)), diffusion with organic carbon and black carbon co-sorption (D(OCBC)), advection-diffusion with organic carbon only sorption (A(OC)), and advection-diffusion with organic carbon and black carbon co-sorption (A(OCBC)).

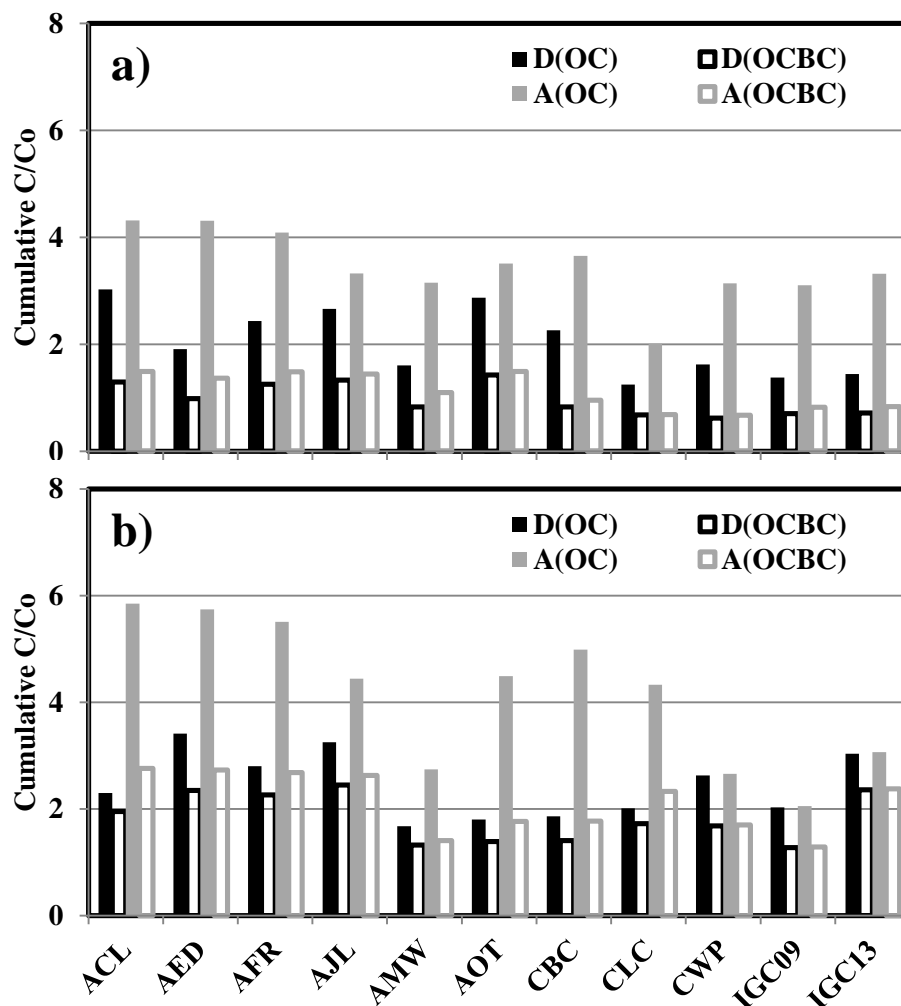


Figure 5.20: Cumulative C/C_o under diffusion with organic carbon sorption (D(OC)), diffusion with organic carbon and black carbon co-sorption (D(OCBC)), advection-diffusion with organic carbon sorption (A(OC)), and advection-diffusion with organic carbon and black carbon co-sorption (A(OCBC)) in all sediment cores as predicted from the Monte Carlo 95th percentile transport parameter values for 1000 years simulation period.

Peclet Number. The Peclet number is a dimensionless number that represent the ratio of advection over diffusion.⁽¹³⁴⁾ The Peclet number can be mathematically expressed as Equation 5.10 below.

$$Peclet\ number = \frac{xv}{D_{obs}} \quad (5.10)$$

The Peclet number for PBDE and PCB homologs under A(OC) and A(OCBC) assuming a 95th percentile transport parameter values are shown in Figure 5.21. Under advection-diffusion transport, the

Peclet number represents the magnitude of advection relative to diffusion. Peclet number >1 signifies advection as the more dominant mass transport process and Peclet number <1 signifies diffusion as the more dominant transport process. Overall, the cumulative Peclet number, defined as the sum of Peclet number for PBDE or PCB homologs 1 through 10, shows that for PBDE homologs, the Peclet numbers were 6 to 20 times larger than the counterpart PCB homolog Peclet numbers in the same core. The xv term in Equation 5.10 is equal for the same PBDE and PCB homologs from the same core, therefore the differences arised from the relatively small D_{obs} values of PBDEs compared to PCBs. From a mass transport perspective, it is expected that PBDE mass transport is dominated more by advection compared to diffusion as the relatively HMW of PBDE homologs compared to their counterpart PCB homologs can retard the diffusion process (previously discussed in Chapter 5.4.4.1.). Under the A(OCBC) transport conditions, the cumulative Peclet numbers were only >2 times larger compared to A(OC) transport conditions. This is also an artifact of the smaller D_{obs} (OCBC) values relative to D_{obs} (OC), resulting in increased solid phase partitioning with the inclusion of BC component. Figure 5.21 also highlights the importance of K_h as the key parameter in advection mass transport process. Generally, with decreased K_h values, the cumulative Peclet number decreased. The order of decrease in K_h values closely resembles the order of decrease in Peclet numbers. This is due to the fact that advection-diffusion mass transport is also influenced by other parameters such as f_{OC} , ϕ , and ρ_{PD} .

Peclet number decreased with increasing PBDE and PCB homologs. Generally, LMW PBDE and PCB homologs have Peclet numbers >1 , whereas HMW PBDE and PCB homologs have Peclet number <1 . This suggests that in-situ mass transport of LMW PBDE and PCB homologs occurs primarily through advection, whereas in-situ sediment transport of HMW PBDE and PCB homologs occurred primarily through diffusion. The increasing hydrophobicity of HMW PBDE and PCB homologs increased the resistance for aqueous phase advective transport. Table 5.12 provides an overview of the dominance of diffusion or advection-diffusion in PBDE and PCB homologs in the natural sediment columns.

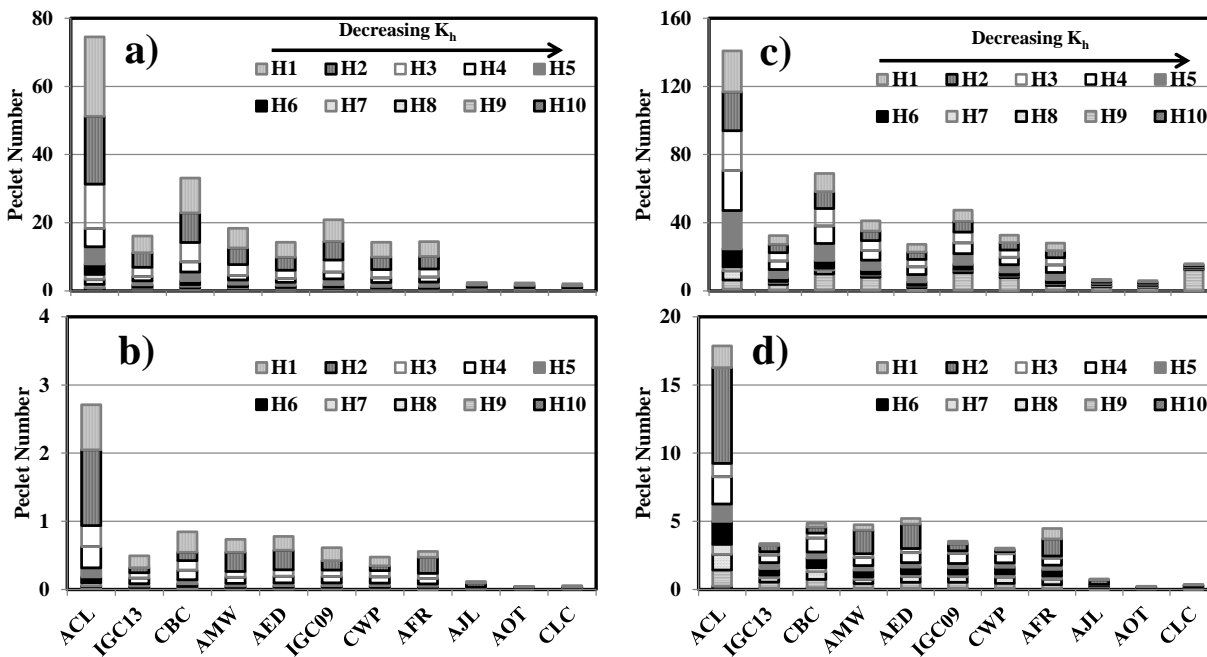


Figure 5.21: Cumulative Peclet number in all sediment cores under advection-diffusion with organic carbon only sorption (A(OC)) (a,c) and organic carbon and black carbon co-sorption (A(OCBC)) (b,d) predicted by the Monte Carlo 95th percentile transport parameter values for PBDE (a,b) and PCB (c,d) homologs.

Table 5.12: Summary of PBDE and PCB transport process dominance as predicted by the Monte Carlo 95th percentile transport parameter values. The black dots indicate advection dominance and hollow dots indicate diffusion dominance. Organic carbon only sorption processes are signified by no line whereas organic carbon and black carbon co-sorption is signified by an underline below the dots.

PBDE										
Site	H1	H2	H3	H4	H5	H6	H7	H8	H9	H10
ACL	● <u>○</u>	● <u>○</u>	● <u>○</u>	● <u>○</u>	● <u>○</u>	● <u>○</u>	● <u>○</u>	● <u>○</u>	○ <u>○</u>	○ <u>○</u>
IGC13	● <u>○</u>	● <u>○</u>	● <u>○</u>	● <u>○</u>	● <u>○</u>	○ <u>○</u>	○ <u>○</u>	○ <u>○</u>	○ <u>○</u>	○ <u>○</u>
CBC	● <u>○</u>	● <u>○</u>	● <u>○</u>	● <u>○</u>	● <u>○</u>	● <u>○</u>	○ <u>○</u>	○ <u>○</u>	○ <u>○</u>	○ <u>○</u>
AMW	● <u>○</u>	● <u>○</u>	● <u>○</u>	● <u>○</u>	● <u>○</u>	○ <u>○</u>	○ <u>○</u>	○ <u>○</u>	○ <u>○</u>	○ <u>○</u>
AED	● <u>○</u>	● <u>○</u>	● <u>○</u>	● <u>○</u>	○ <u>○</u>	○ <u>○</u>	○ <u>○</u>	○ <u>○</u>	○ <u>○</u>	○ <u>○</u>
IGC09	● <u>○</u>	● <u>○</u>	● <u>○</u>	● <u>○</u>	● <u>○</u>	○ <u>○</u>	○ <u>○</u>	○ <u>○</u>	○ <u>○</u>	○ <u>○</u>
CWP	● <u>○</u>	● <u>○</u>	● <u>○</u>	● <u>○</u>	● <u>○</u>	○ <u>○</u>	○ <u>○</u>	○ <u>○</u>	○ <u>○</u>	○ <u>○</u>
AFR	● <u>○</u>	● <u>○</u>	● <u>○</u>	● <u>○</u>	● <u>○</u>	○ <u>○</u>	○ <u>○</u>	○ <u>○</u>	○ <u>○</u>	○ <u>○</u>
AJL	○ <u>○</u>	○ <u>○</u>	○ <u>○</u>	○ <u>○</u>	○ <u>○</u>	○ <u>○</u>	○ <u>○</u>	○ <u>○</u>	○ <u>○</u>	○ <u>○</u>
AOT	○ <u>○</u>	○ <u>○</u>	○ <u>○</u>	○ <u>○</u>	○ <u>○</u>	○ <u>○</u>	○ <u>○</u>	○ <u>○</u>	○ <u>○</u>	○ <u>○</u>
CLC	○ <u>○</u>	○ <u>○</u>	○ <u>○</u>	○ <u>○</u>	○ <u>○</u>	○ <u>○</u>	○ <u>○</u>	○ <u>○</u>	○ <u>○</u>	○ <u>○</u>
PCB										
Site	H1	H2	H3	H4	H5	H6	H7	H8	H9	H10
ACL	●● <u>○</u>	●● <u>○</u>	● <u>○</u>	● <u>○</u>	● <u>○</u>	● <u>○</u>	● <u>○</u>	● <u>○</u>	● <u>○</u>	○ <u>○</u>
IGC13	● <u>○</u>	● <u>○</u>	● <u>○</u>	● <u>○</u>	● <u>○</u>	● <u>○</u>	○ <u>○</u>	○ <u>○</u>	○ <u>○</u>	○ <u>○</u>
CBC	● <u>○</u>	● <u>○</u>	● <u>○</u>	● <u>○</u>	● <u>○</u>	● <u>○</u>	● <u>○</u>	○ <u>○</u>	○ <u>○</u>	○ <u>○</u>
AMW	● <u>○</u>	● <u>○</u>	● <u>○</u>	● <u>○</u>	● <u>○</u>	● <u>○</u>	○ <u>○</u>	○ <u>○</u>	○ <u>○</u>	○ <u>○</u>
AED	● <u>○</u>	● <u>○</u>	● <u>○</u>	● <u>○</u>	● <u>○</u>	○ <u>○</u>	○ <u>○</u>	○ <u>○</u>	○ <u>○</u>	○ <u>○</u>
IGC09	● <u>○</u>	● <u>○</u>	● <u>○</u>	● <u>○</u>	● <u>○</u>	● <u>○</u>	○ <u>○</u>	○ <u>○</u>	○ <u>○</u>	○ <u>○</u>
CWP	● <u>○</u>	● <u>○</u>	● <u>○</u>	● <u>○</u>	● <u>○</u>	● <u>○</u>	○ <u>○</u>	○ <u>○</u>	○ <u>○</u>	○ <u>○</u>
AFR	● <u>○</u>	● <u>○</u>	● <u>○</u>	● <u>○</u>	● <u>○</u>	● <u>○</u>	○ <u>○</u>	○ <u>○</u>	○ <u>○</u>	○ <u>○</u>
AJL	● <u>○</u>	○ <u>○</u>	○ <u>○</u>	○ <u>○</u>	○ <u>○</u>	○ <u>○</u>	○ <u>○</u>	○ <u>○</u>	○ <u>○</u>	○ <u>○</u>
AOT	● <u>○</u>	○ <u>○</u>	○ <u>○</u>	○ <u>○</u>	○ <u>○</u>	○ <u>○</u>	○ <u>○</u>	○ <u>○</u>	○ <u>○</u>	○ <u>○</u>
CLC	● <u>○</u>	○ <u>○</u>	○ <u>○</u>	○ <u>○</u>	○ <u>○</u>	○ <u>○</u>	○ <u>○</u>	○ <u>○</u>	○ <u>○</u>	○ <u>○</u>

5.5. PBDE and PCB Mass Removal From The Sediment Columns

In the previous Section 5.4., it was established that LMW PBDE and PCB homologs (PBDE homolog ≤ 5 , and PCB homologs ≤ 6) can have significant breakthrough (C/C_o), particularly under the A(OC) transport condition. Transport simulations shown in Chapter 5.3.2. were used to predict the amount of PBDE and PCB mass leaving the sediment segment boundary layer under the A(OC) condition. The A(OC) condition was chosen as it was proven to result in the most mobile *in-situ* PBDE and PCB mass transport scenarios in all the sediment columns and thus provide an upper bound to the mass flux. Initial concentrations were selected from measured PBDE and PCB levels shown in Table 5.6. PBDE homolog concentrations for the initial conditions were assumed to be at the 95th, 50th, and 5th percentile concentrations (36100, 60, and 0.2 ng/g, respectively). Due to the extreme left skewing in PCB concentrations, PCB homolog initial sediment concentrations were assumed to be at the 95th, 75th, and 50th percentile concentrations (1640, 262, and 19 ng/g, respectively).

The following is a summary of the flux form of the model; LEA was assumed and $C_{aq}|_{x=0m,t=0 \text{ year}}$ was calculated using Equation 5.3, which is then used to predict $C_{aq}|_{x=0.02m,t=0+n \text{ year}}$ leaving the sediment boundary layer as shown in Equation 5.5 for A(OC) transport (n is transport time in years). For A(OC), the mass leaving the boundary layer, $M_{t|t=0+n \text{ year}}$, was calculated using Equation 5.7 assuming the 5th, 50th, and 95th percentile transport parameter values to provide the most mobile PBDE and PCB mass transport range in the sediment columns. The $C_{aq}|_{x=0.02m,t=0+n \text{ year}}$ (aqueous phase concentration leaving the sediment layer), $C_{aq}|_{x=0.02m,t=0+n \text{ year}}/C_o|_{x=0m,t=0 \text{ year}}$ (aqueous phase breakthrough), and $M_{t|t=0+n \text{ year}}$ (mass leaving the sediment segment via the aqueous phase) for PBDE and PCB homologs as a function of time are shown in Figure D5.5a-bn (PBDEs: a-ag; PCBs: ah-bn ; ACL:a-c,ah-aj ; AED:d-f,ak-am ; AFR:g-i,an-ap ; AJL:j-l, aq-as ; AMW:m-o,at-av ; AOT:p-r, aw-ay ; CBC:s-u,az-bb ; CLC:v-x, bc-be ; CWP:y-aa, bf-bh ; IGC09:ab-ad,bi-bk ; IGC13:ae-ag,bl-bn). A summary of $C_{aq}|_{x=0.02m,t}$, $C_{aq}|_{x=0.02m,t}/C_o|_{x=0m,t}$, $M_{t|t}$, and $M_{t|t}/M_{sed|t=0}$ (mass fraction leaving the boundary layer relative to initial mass) at 40, 100, and 1000 years

as predicted by the 95th, 50th, and 5th percentile transport parameters values are shown in Figure 5.22a-v (PBDEs:a-k ; PCBs:l-v ; ACL:a,l; AED:b,m, ; AFR:c,n ; AJL:d,o ; AMW:e,p ; AOT:f,q ; CBC: g,r ; CLC:h,s ; CWP: i,t : IGC09:j,u ; IGC13:k,v).

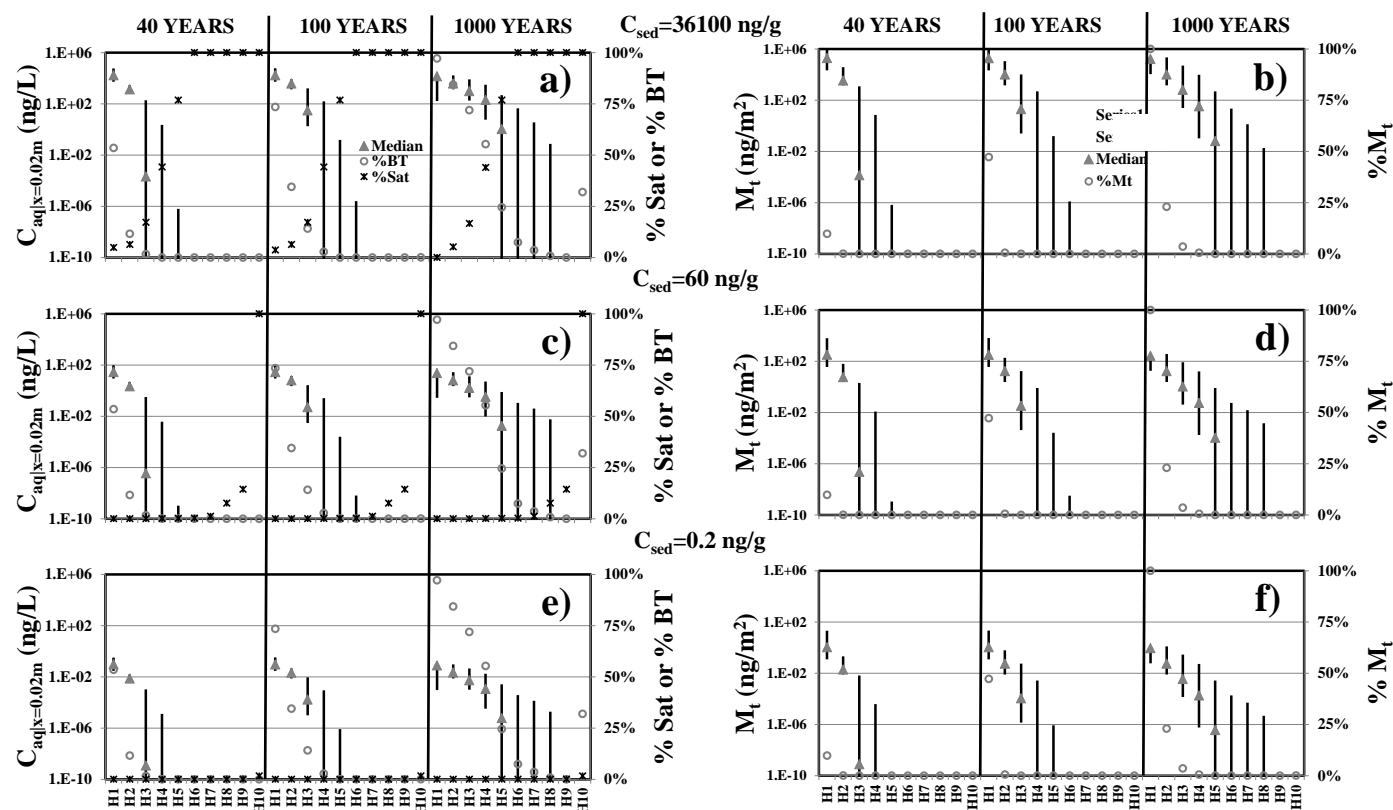


Figure 5.22a: Predicted flux of PBDE homologs in core ACL under advection-diffusion with organic carbon only sorption (A(OC)) conditions for initial sediment concentration of 36100, 60, and 0.2 ng/g at 40, 100, and 1000 years. Panels a,c, and e show aqueous phase concentration leaving the sediment boundary layer ($C_{aq|x=0.02m,t}$), aqueous phase breakthrough percentage ($C_{aq|x=0.02m,t}/C_{aq|x=0m,t=0year}$) (%BT), and ratio of aqueous phase concentration under local equilibrium assumption to saturation concentration ($C_{aq|x=0m,t}/C_{sat}$) (%Sat) represented as grey triangle with vertical lines, hollow sphere, and star, respectively. Panels b,d, and f show mass leaving the sediment boundary layer at specific time ($M_{t|t}$) and ratio of mass leaving the sediment boundary layer to initial starting mass ($M_{t|t}/M_{sed|t=0year}$) represented as grey triangle with vertical lines and hollow sphere, respectively. For $C_{aq|x=0.02m,t}$ and $M_{t|t}$, median values as predicted by the 50th percentile transport parameters values are represented by the grey triangle while upper and lower boundaries as predicted by the 95th and 5th percentile transport parameters values are indicated by the vertical lines. Lines that did not appear in figure are below the minimum y-axes values. X-axes are homologs 1 to 10 (H1 to H10).

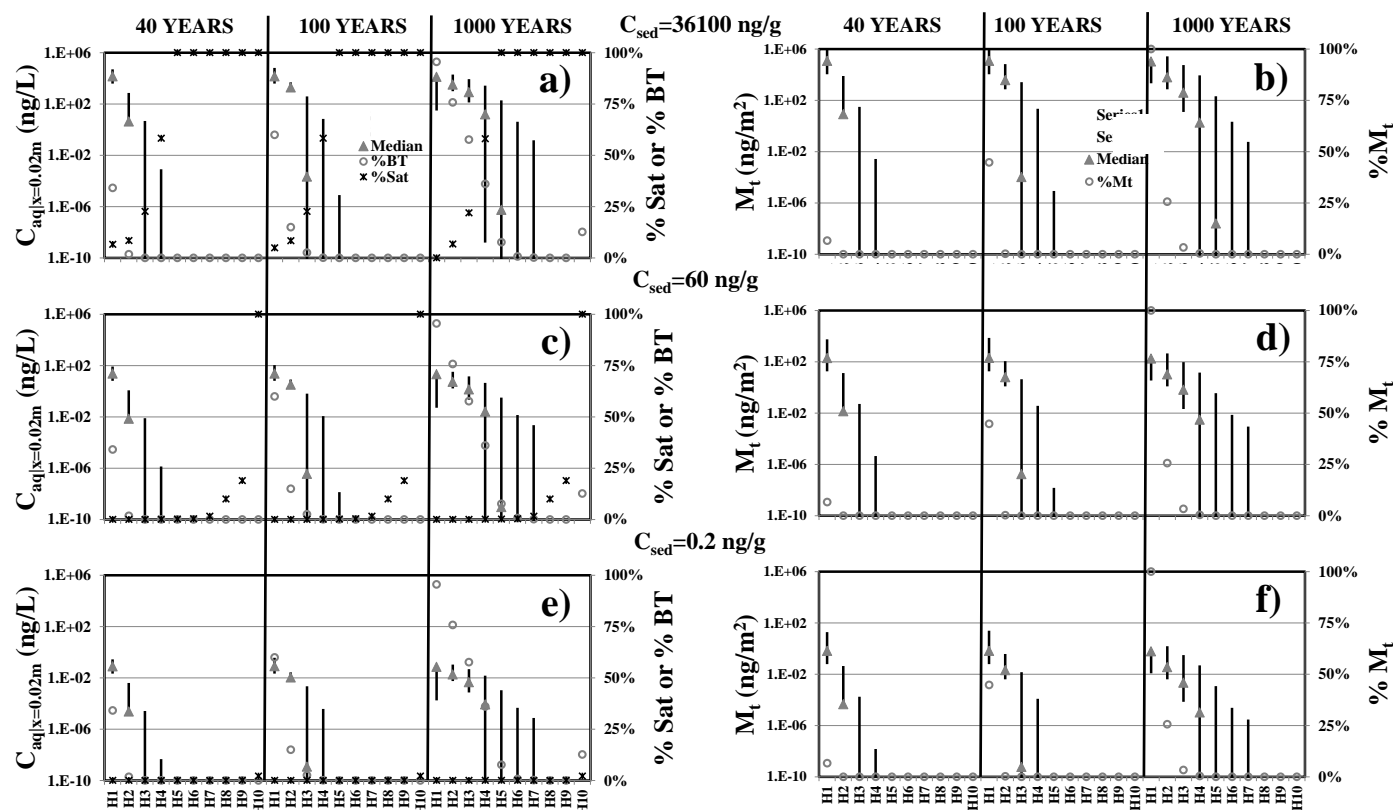


Figure 5.22b: Predicted flux of PBDE homologs in core AED under advection-diffusion with organic carbon only sorption (A(OC)) conditions for initial sediment concentration of 36100, 60, and 0.2 ng/g at 40, 100, and 1000 years. Panels a,c, and e show aqueous phase concentration leaving the sediment boundary layer ($C_{aq|x=0.02m,t}$), aqueous phase breakthrough percentage ($C_{aq|x=0.02m,t}/C_{aq|x=0m,t=0year}$) (%BT), and ratio of aqueous phase concentration under local equilibrium assumption to saturation concentration ($C_{aq|x=0m,t}/C_{sat}$) (%Sat) represented as grey triangle with vertical lines, hollow sphere, and star, respectively. Panels b,d, and f show mass leaving the sediment boundary layer at specific time ($M_{t|t}$) and ratio of mass leaving the sediment boundary layer to initial starting mass ($M_{t|t}/M_{sed|t=0year}$) represented as grey triangle with vertical lines and hollow sphere, respectively. For $C_{aq|x=0.02m,t}$ and $M_{t|t}$, median values as predicted by the 50th percentile transport parameters values are represented by the grey triangle while upper and lower boundaries as predicted by the 95th and 5th percentile transport parameters values are indicated by the vertical lines. Lines that did not appear in figure are below the minimum y-axes values. X-axes are homologs 1 to 10 (H1 to H10).

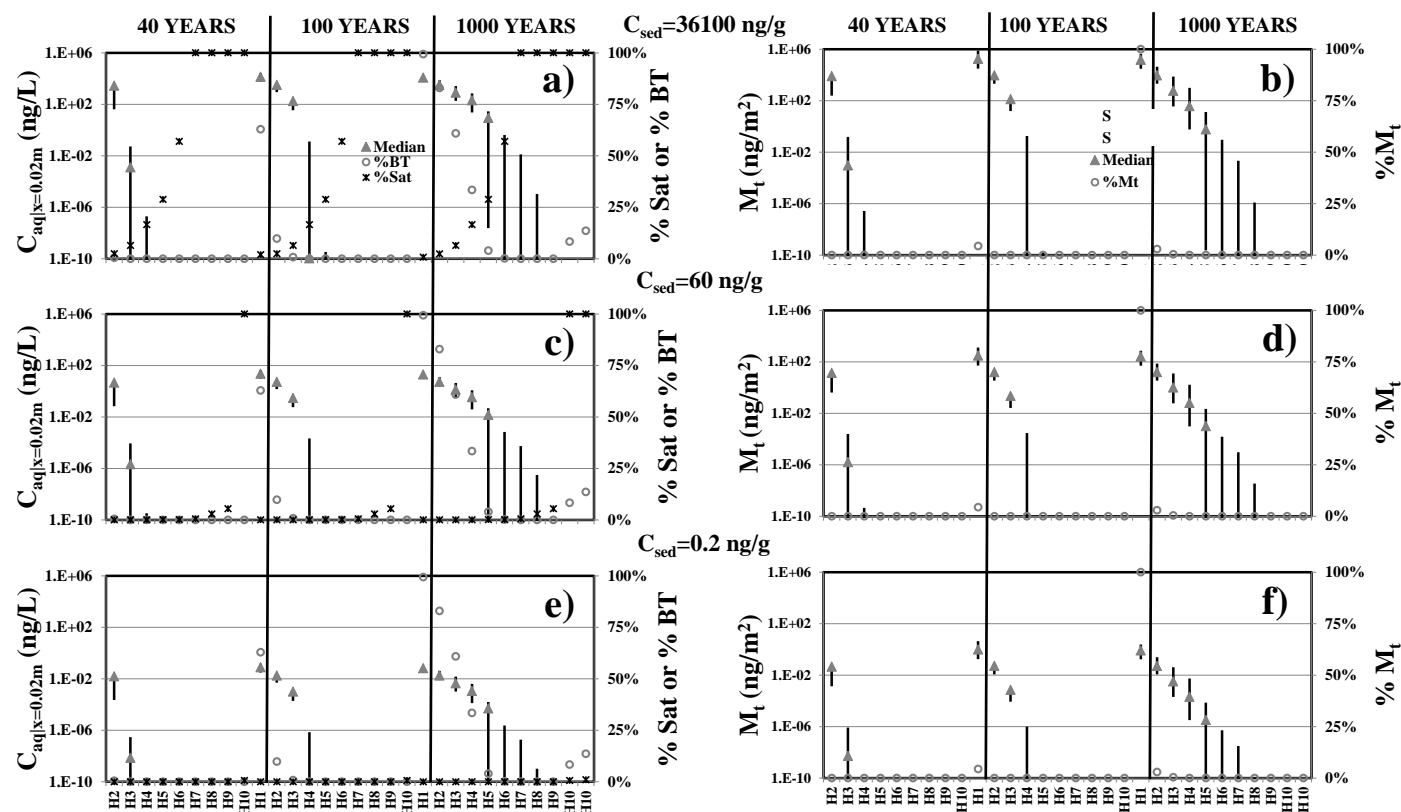


Figure 5.22c: Predicted flux of PBDE homologs in core AFR under advection-diffusion with organic carbon only sorption (A(OC)) conditions for initial sediment concentration of 36100, 60, and 0.2 ng/g at 40, 100, and 1000 years. Panels a,c, and e show aqueous phase concentration leaving the sediment boundary layer ($C_{aq|x=0.02m,t}$), aqueous phase breakthrough percentage ($C_{aq|x=0.02m,t}/C_{aq|x=0m,t=0year}$) (%BT), and ratio of aqueous phase concentration under local equilibrium assumption to saturation concentration ($C_{aq|x=0m,t}/C_{sat}$) (%Sat) represented as grey triangle with vertical lines, hollow sphere, and star, respectively. Panels b,d, and f show mass leaving the sediment boundary layer at specific time ($M_{t|t}$) and ratio of mass leaving the sediment boundary layer to initial starting mass ($M_{t|t}/M_{sed|t=0year}$) represented as grey triangle with vertical lines and hollow sphere, respectively. For $C_{aq|x=0.02m,t}$ and $M_{t|t}$, median values as predicted by the 50th percentile transport parameters values are represented by the grey triangle while upper and lower boundaries as predicted by the 95th and 5th percentile transport parameters values are indicated by the vertical lines. Lines that did not appear in figure are below the minimum y-axes values. X-axes are homologs 1 to 10 (H1 to H10).

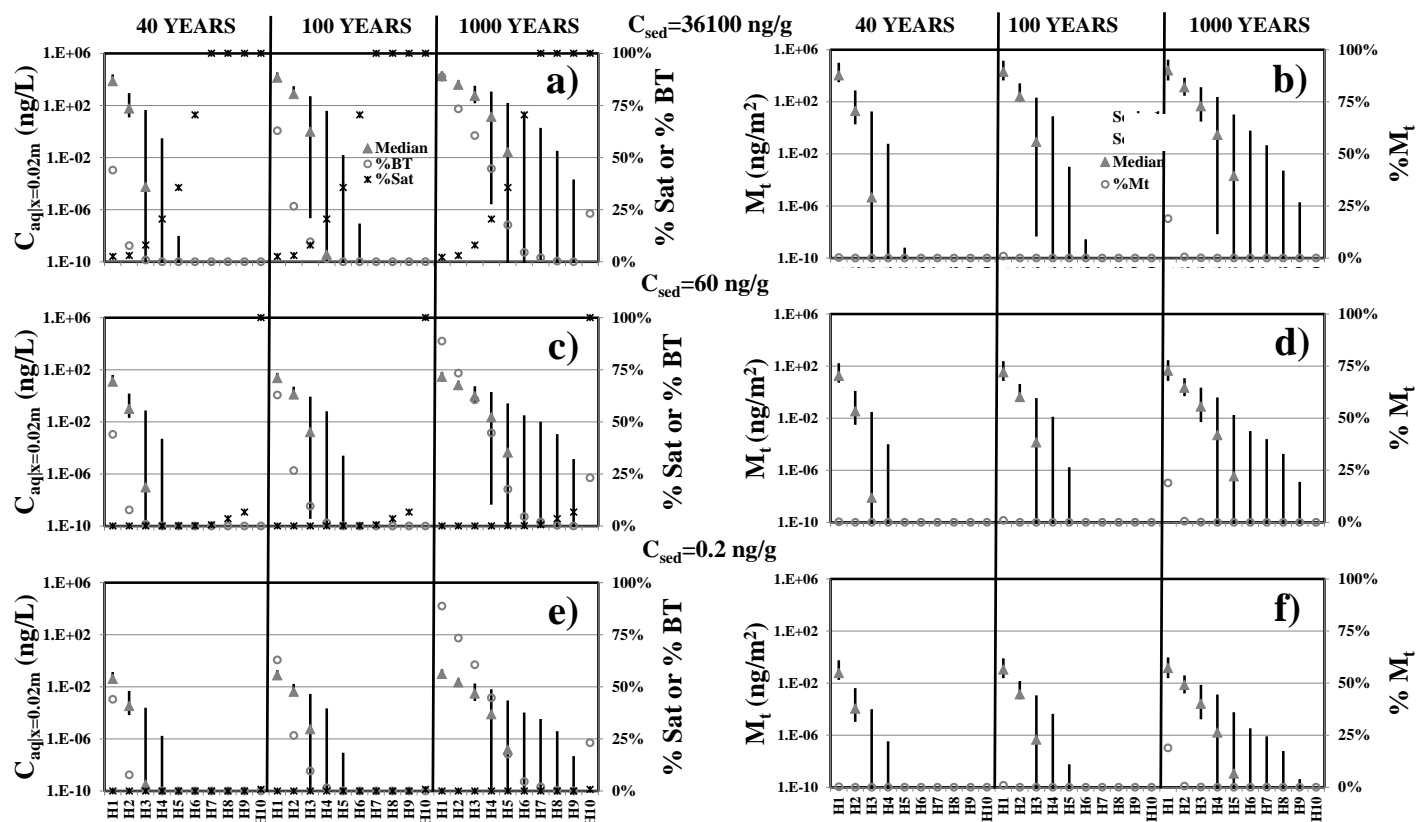


Figure 5.22d: Predicted flux of PBDE homologs in core AJL under advection-diffusion with organic carbon only sorption (A(OC)) conditions for initial sediment concentration of 36100, 60, and 0.2 ng/g at 40, 100, and 1000 years. Panels a,c, and e show aqueous phase concentration leaving the sediment boundary layer ($C_{aq|x=0.02m,t}$), aqueous phase breakthrough percentage ($C_{aq|x=0.02m,t}/C_{aq|x=0m,t=0year}$) (%BT), and ratio of aqueous phase concentration under local equilibrium assumption to saturation concentration ($C_{aq|x=0m,t}/C_{sat}$) (%Sat) represented as grey triangle with vertical lines, hollow sphere, and star, respectively. Panels b,d, and f show mass leaving the sediment boundary layer at specific time ($M_{t|t}$) and ratio of mass leaving the sediment boundary layer to initial starting mass ($M_{t|t}/M_{sed|t=0year}$) represented as grey triangle with vertical lines and hollow sphere, respectively. For $C_{aq|x=0.02m,t}$ and $M_{t|t}$, median values as predicted by the 50th percentile transport parameters values are represented by the grey triangle while upper and lower boundaries as predicted by the 95th and 5th percentile transport parameters values are indicated by the vertical lines. Lines that did not appear in figure are below the minimum y-axes values. X-axes are homologs 1 to 10 (H1 to H10).

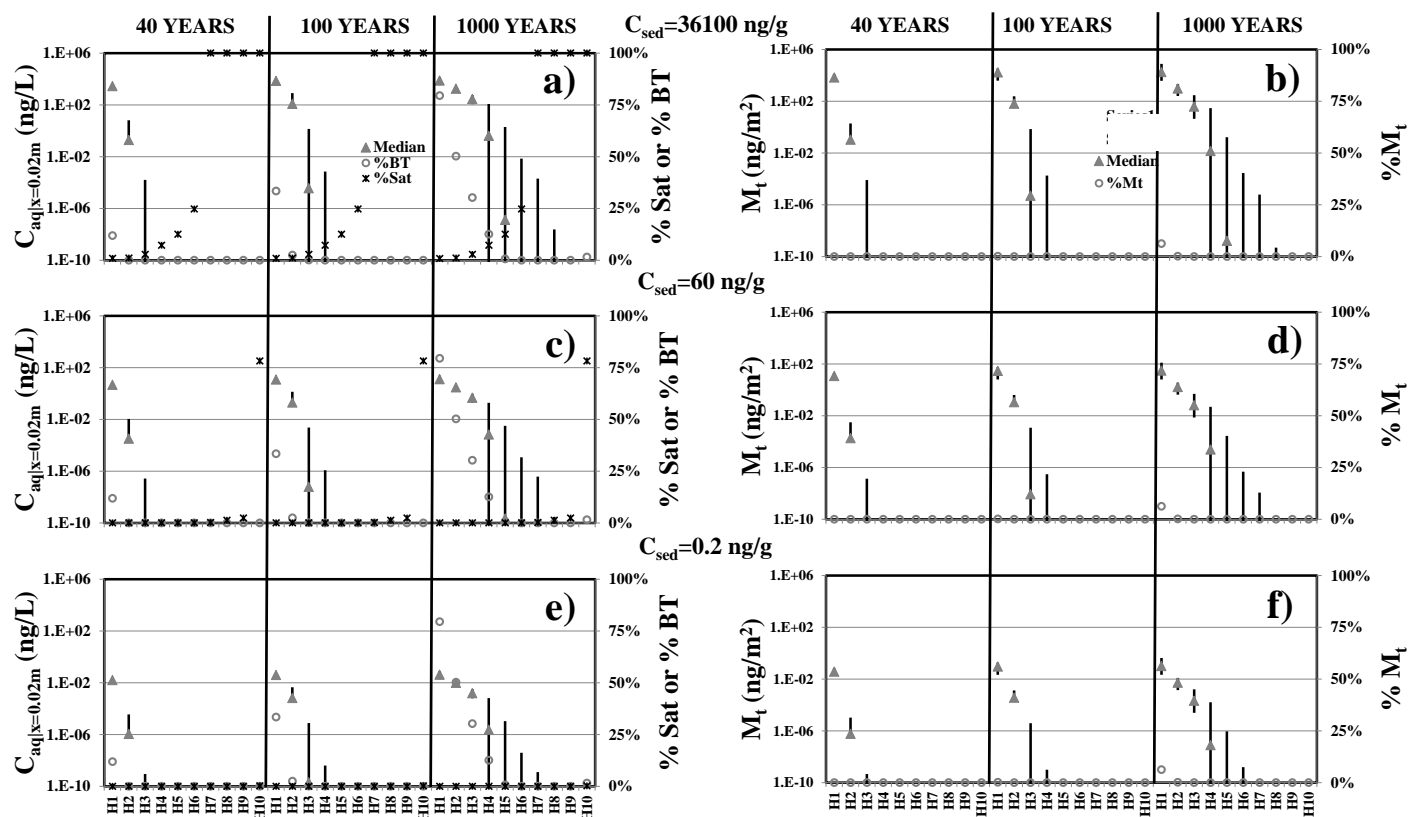


Figure 5.22e: Predicted flux of PBDE homologs in core AMW under advection-diffusion with organic carbon only sorption (A(OC)) conditions for initial sediment concentration of 36100, 60, and 0.2 ng/g at 40, 100, and 1000 years. Panels a,c, and e show aqueous phase concentration leaving the sediment boundary layer ($C_{aq|x=0.02m,t}$), aqueous phase breakthrough percentage ($C_{aq|x=0.02m,t}/C_{aq|x=0m,t=0year}$) (%BT), and ratio of aqueous phase concentration under local equilibrium assumption to saturation concentration ($C_{aq|x=0m,t}/C_{sat}$) (%Sat) represented as grey triangle with vertical lines, hollow sphere, and star, respectively. Panels b,d, and f show mass leaving the sediment boundary layer at specific time ($M_{t|t}$) and ratio of mass leaving the sediment boundary layer to initial starting mass ($M_{t|t}/M_{sed|t=0year}$) represented as grey triangle with vertical lines and hollow sphere, respectively. For $C_{aq|x=0.02m,t}$ and $M_{t|t}$, median values as predicted by the 50th percentile transport parameters values are represented by the grey triangle while upper and lower boundaries as predicted by the 95th and 5th percentile transport parameters values are indicated by the vertical lines. Lines that did not appear in figure are below the minimum y-axes values. X-axes are homologs 1 to 10 (H1 to H10).

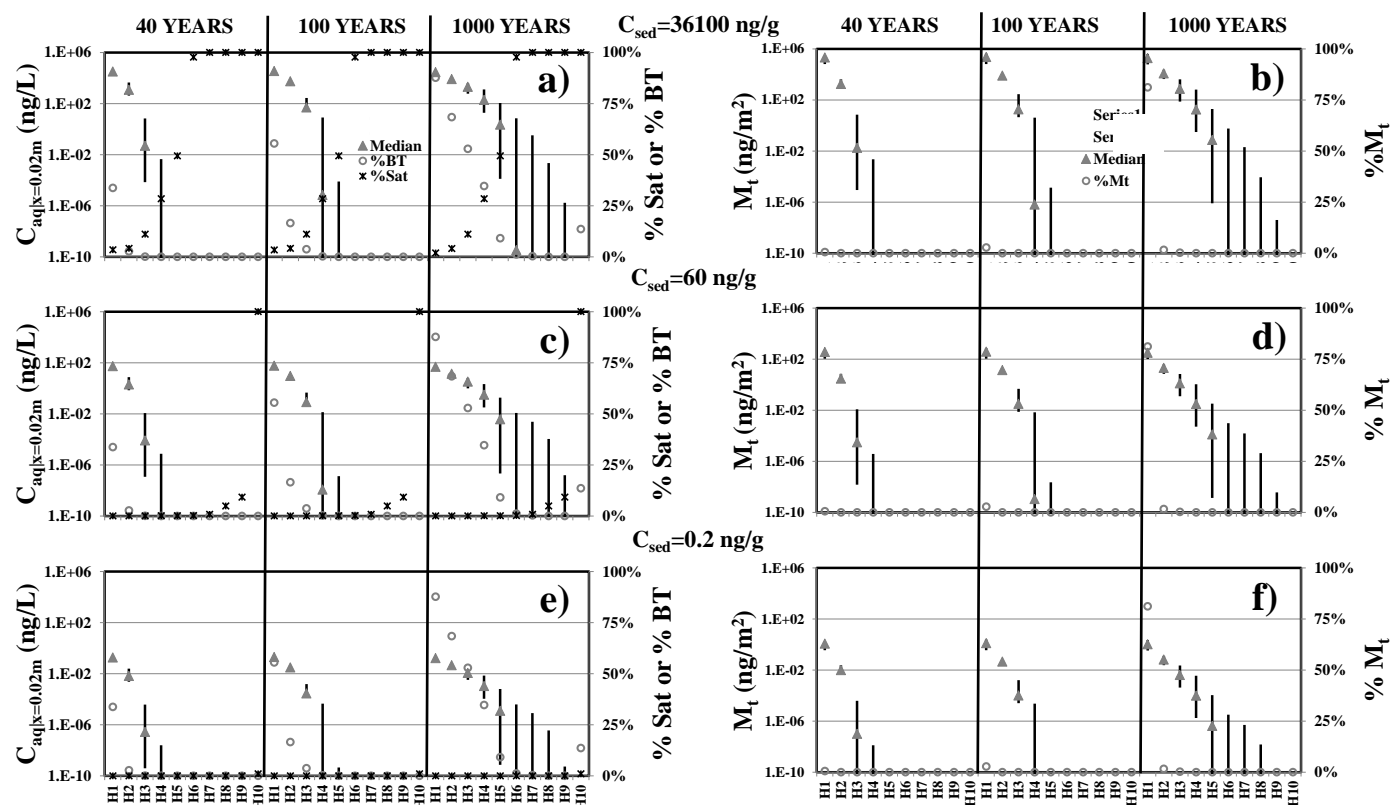


Figure 5.22f: Predicted flux of PBDE homologs in core AOT under advection-diffusion with organic carbon only sorption (A(OC)) conditions for initial sediment concentration of 36100, 60, and 0.2 ng/g at 40, 100, and 1000 years. Panels a,c, and e show aqueous phase concentration leaving the sediment boundary layer ($C_{aq|x=0.02m,t}$), aqueous phase breakthrough percentage ($C_{aq|x=0.02m,t}/C_{aq|x=0m,t=0year}$) (%BT), and ratio of aqueous phase concentration under local equilibrium assumption to saturation concentration ($C_{aq|x=0m,t}/C_{sat}$) (%Sat) represented as grey triangle with vertical lines, hollow sphere, and star, respectively. Panels b,d, and f show mass leaving the sediment boundary layer at specific time ($M_{t|t}$) and ratio of mass leaving the sediment boundary layer to initial starting mass ($M_{t|t}/M_{sed|t=0year}$) represented as grey triangle with vertical lines and hollow sphere, respectively. For $C_{aq|x=0.02m,t}$ and $M_{t|t}$, median values as predicted by the 50th percentile transport parameters values are represented by the grey triangle while upper and lower boundaries as predicted by the 95th and 5th percentile transport parameters values are indicated by the vertical lines. Lines that did not appear in figure are below the minimum y-axes values. X-axes are homologs 1 to 10 (H1 to H10).

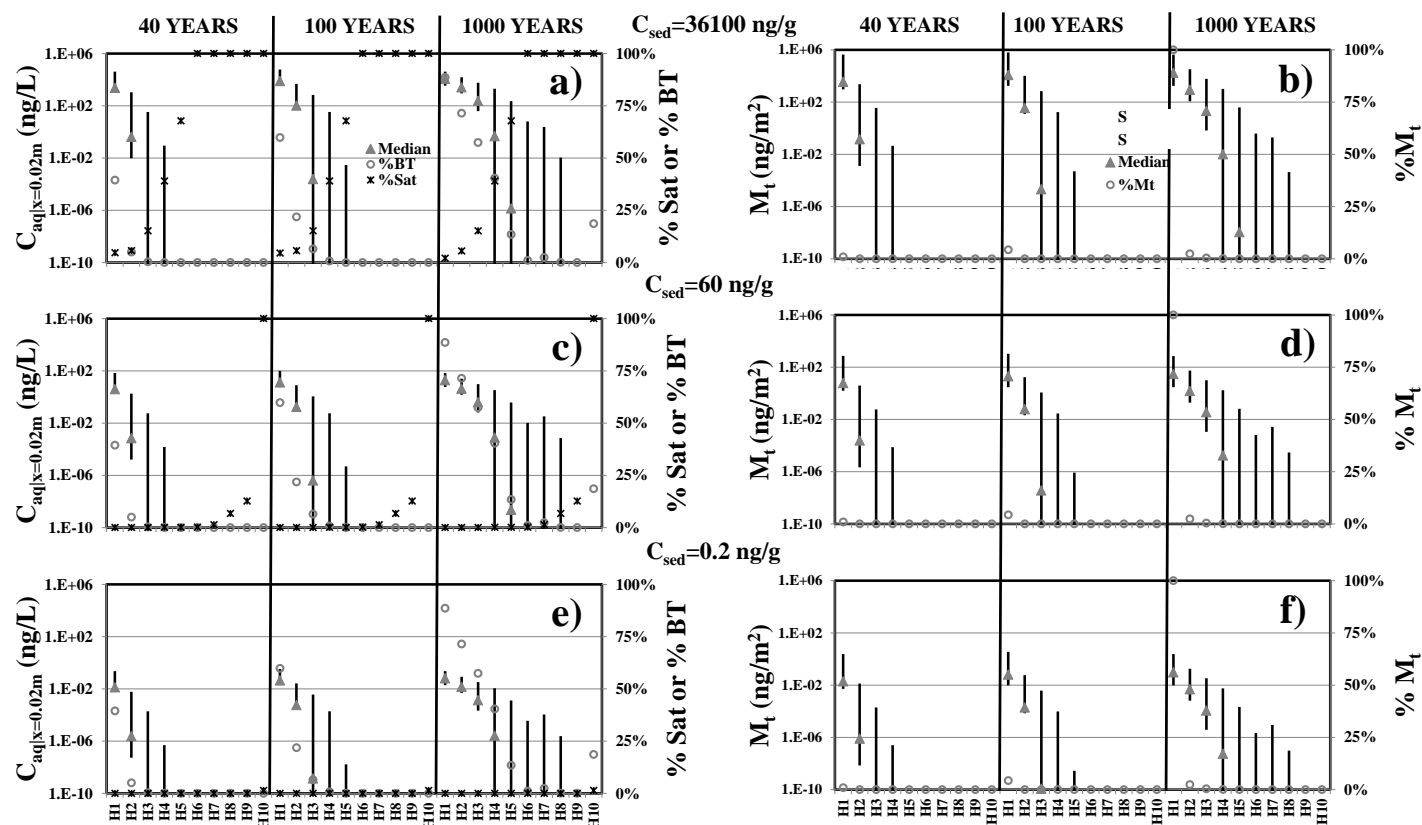


Figure 5.22g: Predicted flux of PBDE homologs in core CBC under advection-diffusion with organic carbon only sorption (A(OC)) conditions for initial sediment concentration of 36100, 60, and 0.2 ng/g at 40, 100, and 1000 years. Panels a,c, and e show aqueous phase concentration leaving the sediment boundary layer ($C_{aq|x=0.02m,t}$), aqueous phase breakthrough percentage ($C_{aq|x=0.02m,t}/C_{aq|x=0m,t=0year}$) (%BT), and ratio of aqueous phase concentration under local equilibrium assumption to saturation concentration ($C_{aq|x=0m,t}/C_{sat}$) (%Sat) represented as grey triangle with vertical lines, hollow sphere, and star, respectively. Panels b,d, and f show mass leaving the sediment boundary layer at specific time ($M_{t|t}$) and ratio of mass leaving the sediment boundary layer to initial starting mass ($M_{t|t}/M_{sed|t=0year}$) represented as grey triangle with vertical lines and hollow sphere, respectively. For $C_{aq|x=0.02m,t}$ and $M_{t|t}$, median values as predicted by the 50th percentile transport parameters values are represented by the grey triangle while upper and lower boundaries as predicted by the 95th and 5th percentile transport parameters values are indicated by the vertical lines. Lines that did not appear in figure are below the minimum y-axes values. X-axes are homologs 1 to 10 (H1 to H10).

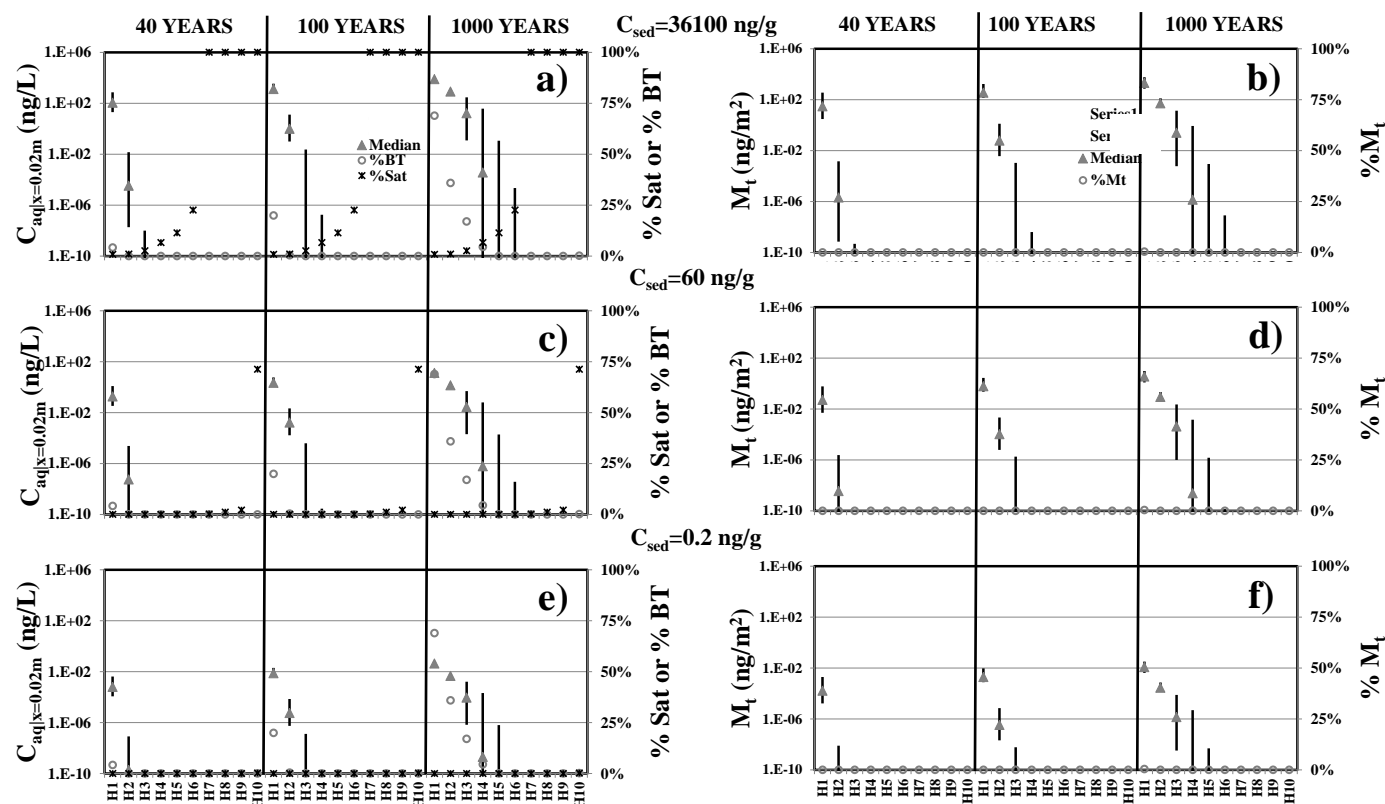


Figure 5.22h: Predicted flux of PBDE homologs in core CLC under advection-diffusion with organic carbon only sorption (A(OC)) conditions for initial sediment concentration of 36100, 60, and 0.2 ng/g at 40, 100, and 1000 years. Panels a,c, and e show aqueous phase concentration leaving the sediment boundary layer ($C_{aq|x=0.02m,t}$), aqueous phase breakthrough percentage ($C_{aq|x=0.02m,t}/C_{aq|x=0m,t=0year}$) (%BT), and ratio of aqueous phase concentration under local equilibrium assumption to saturation concentration ($C_{aq|x=0m,t}/C_{sat}$) (%Sat) represented as grey triangle with vertical lines, hollow sphere, and star, respectively. Panels b,d, and f show mass leaving the sediment boundary layer at specific time ($M_{t|t}$) and ratio of mass leaving the sediment boundary layer to initial starting mass ($M_{t|t}/M_{sed|t=0year}$) represented as grey triangle with vertical lines and hollow sphere, respectively. For $C_{aq|x=0.02m,t}$ and $M_{t|t}$, median values as predicted by the 50th percentile transport parameters values are represented by the grey triangle while upper and lower boundaries as predicted by the 95th and 5th percentile transport parameters values are indicated by the vertical lines. Lines that did not appear in figure are below the minimum y-axes values. X-axes are homologs 1 to 10 (H1 to H10).

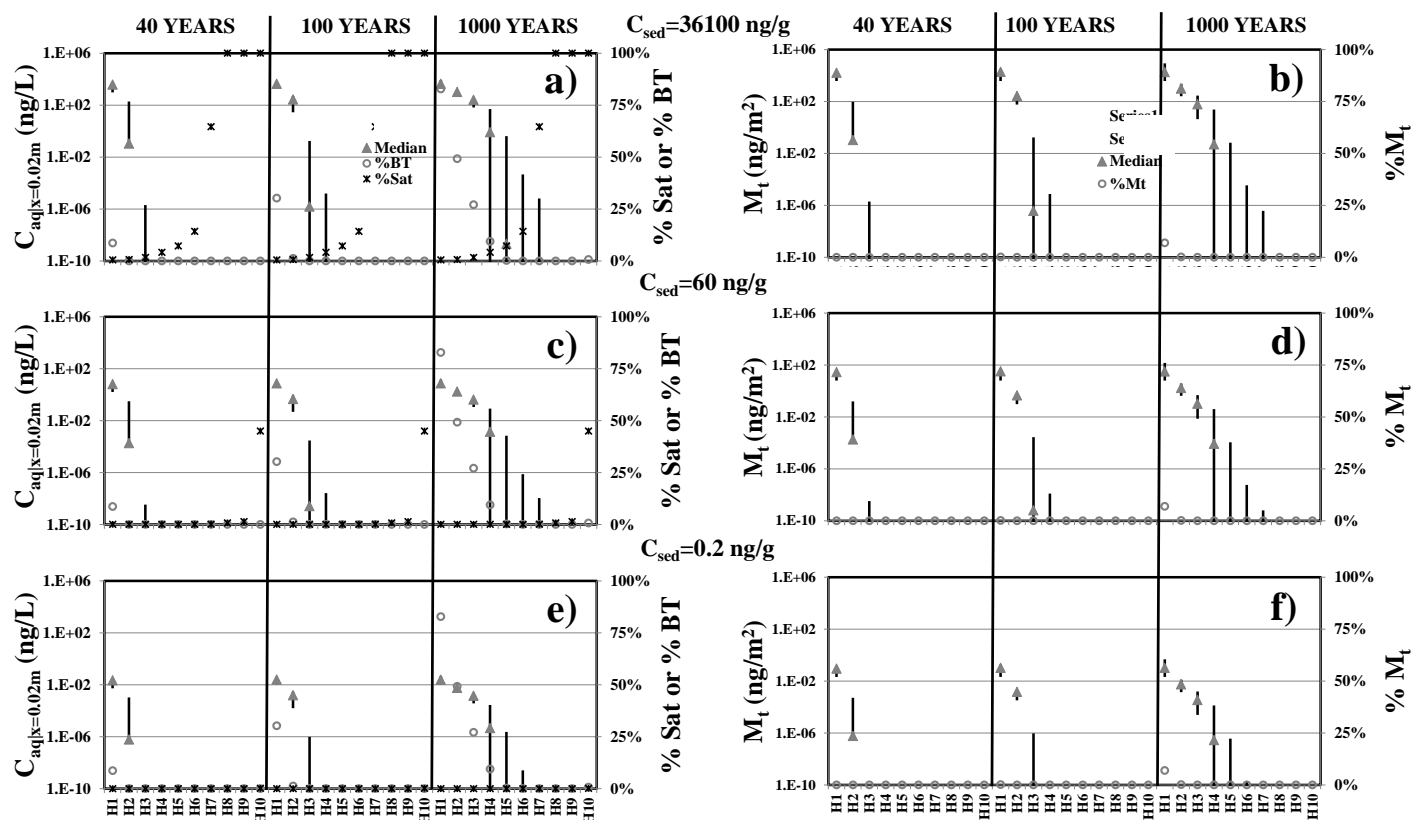


Figure 5.22i: Predicted flux of PBDE homologs in core CWP under advection-diffusion with organic carbon only sorption (A(OC)) conditions for initial sediment concentration of 36100, 60, and 0.2 ng/g at 40, 100, and 1000 years. Panels a,c, and e show aqueous phase concentration leaving the sediment boundary layer ($C_{aq|x=0.02m,t}$), aqueous phase breakthrough percentage ($C_{aq|x=0.02m,t}/C_{aq|x=0m,t=0year}$) (%BT), and ratio of aqueous phase concentration under local equilibrium assumption to saturation concentration ($C_{aq|x=0m,t}/C_{sat}$) (%Sat) represented as grey triangle with vertical lines, hollow sphere, and star, respectively. Panels b,d, and f show mass leaving the sediment boundary layer at specific time ($M_{t|t}$) and ratio of mass leaving the sediment boundary layer to initial starting mass ($M_{t|t}/M_{sed|t=0year}$) represented as grey triangle with vertical lines and hollow sphere, respectively. For $C_{aq|x=0.02m,t}$ and $M_{t|t}$, median values as predicted by the 50th percentile transport parameters values are represented by the grey triangle while upper and lower boundaries as predicted by the 95th and 5th percentile transport parameters values are indicated by the vertical lines. Lines that did not appear in figure are below the minimum y-axes values. X-axes are homologs 1 to 10 (H1 to H10).

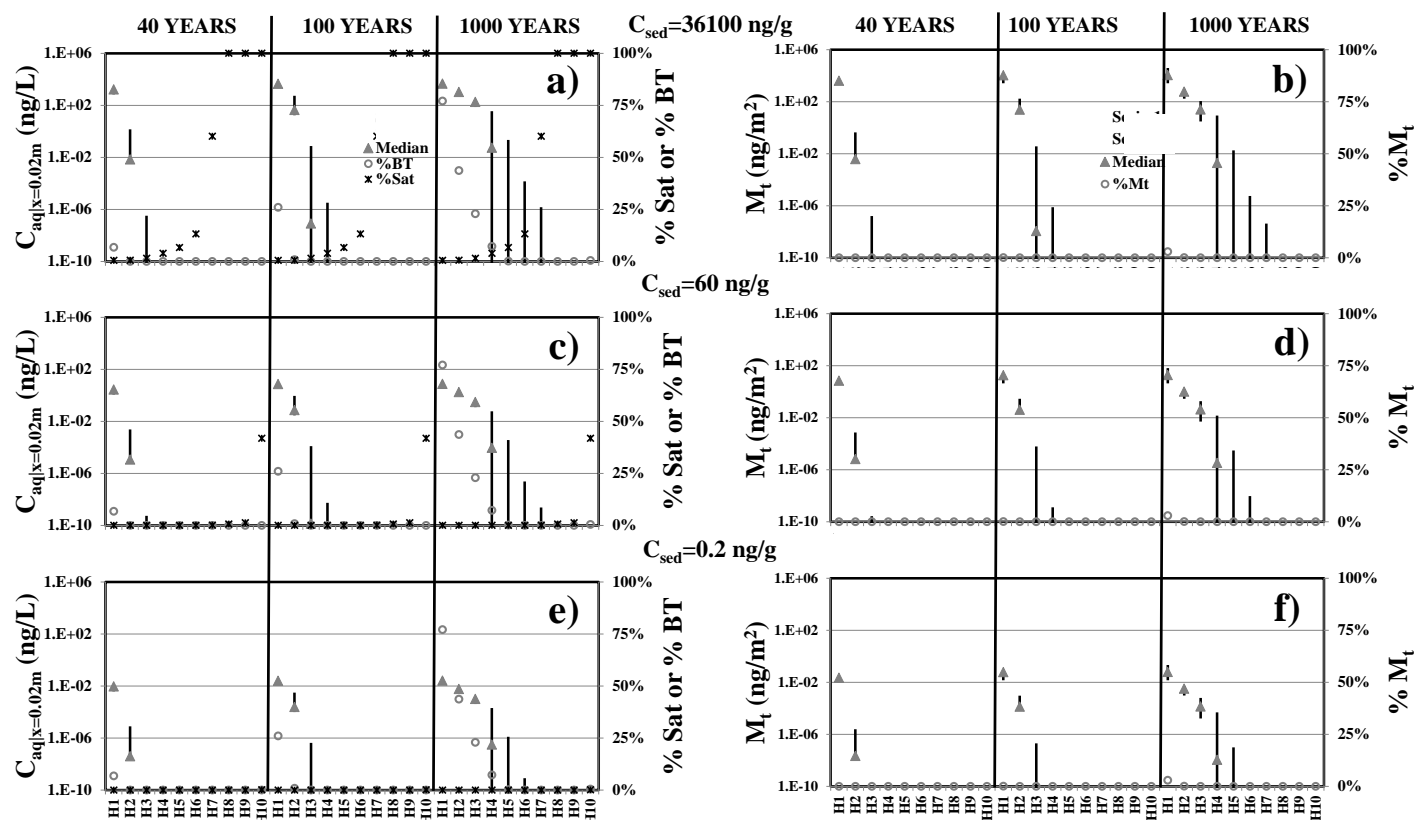


Figure 5.22j: Predicted flux of PBDE homologs in core IGC09 under advection-diffusion with organic carbon only sorption (A(OC)) conditions for initial sediment concentration of 36100, 60, and 0.2 ng/g at 40, 100, and 1000 years. Panels a,c, and e show aqueous phase concentration leaving the sediment boundary layer ($C_{aq|x=0.02m,t}$), aqueous phase breakthrough percentage ($C_{aq|x=0.02m,t}/C_{aq|x=0m,t=0year}$) (%BT), and ratio of aqueous phase concentration under local equilibrium assumption to saturation concentration ($C_{aq|x=0m,t}/C_{sat}$) (%Sat) represented as grey triangle with vertical lines, hollow sphere, and star, respectively. Panels b,d, and f show mass leaving the sediment boundary layer at specific time ($M_{t|t}$) and ratio of mass leaving the sediment boundary layer to initial starting mass ($M_{t|t}/M_{sed|t=0year}$) represented as grey triangle with vertical lines and hollow sphere, respectively. For $C_{aq|x=0.02m,t}$ and $M_{t|t}$, median values as predicted by the 50th percentile transport parameters values are represented by the grey triangle while upper and lower boundaries as predicted by the 95th and 5th percentile transport parameters values are indicated by the vertical lines. Lines that did not appear in figure are below the minimum y-axes values. X-axes are homologs 1 to 10 (H1 to H10).

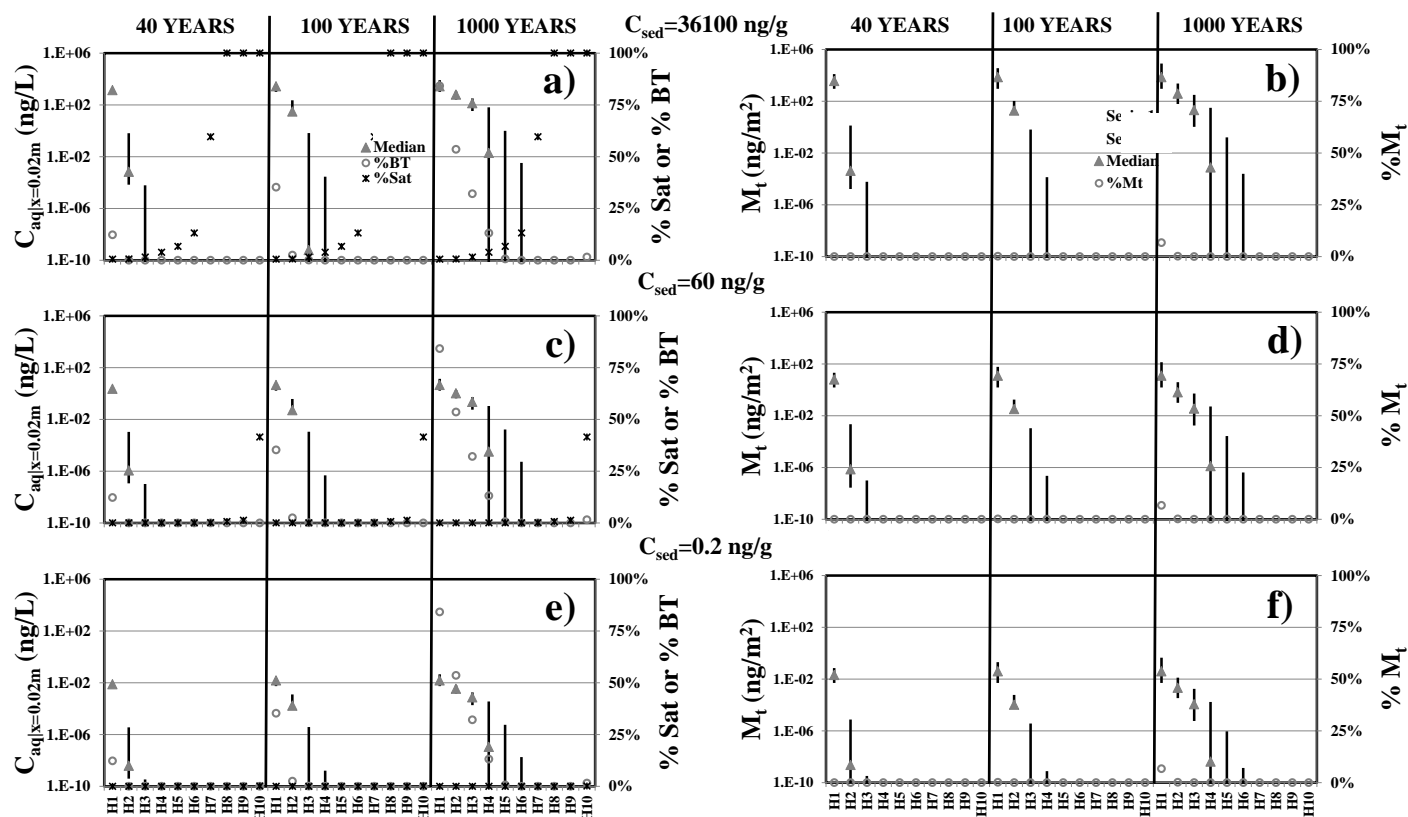


Figure 5.22k: Predicted flux of PBDE homologs in core IGC13 under advection-diffusion with organic carbon only sorption (A(OC)) conditions for initial sediment concentration of 36100, 60, and 0.2 ng/g at 40, 100, and 1000 years. Panels a,c, and e show aqueous phase concentration leaving the sediment boundary layer ($C_{aq|x=0.02m,t}$), aqueous phase breakthrough percentage ($C_{aq|x=0.02m,t}/C_{aq|x=0m,t=0year}$) (%BT), and ratio of aqueous phase concentration under local equilibrium assumption to saturation concentration ($C_{aq|x=0m,t}/C_{sat}$) (%Sat) represented as grey triangle with vertical lines, hollow sphere, and star, respectively. Panels b,d, and f show mass leaving the sediment boundary layer at specific time ($M_{t|t}$) and ratio of mass leaving the sediment boundary layer to initial starting mass ($M_{t|t}/M_{sed|t=0year}$) represented as grey triangle with vertical lines and hollow sphere, respectively. For $C_{aq|x=0.02m,t}$ and $M_{t|t}$, median values as predicted by the 50th percentile transport parameters values are represented by the grey triangle while upper and lower boundaries as predicted by the 95th and 5th percentile transport parameters values are indicated by the vertical lines. Lines that did not appear in figure are below the minimum y-axes values. X-axes are homologs 1 to 10 (H1 to H10).

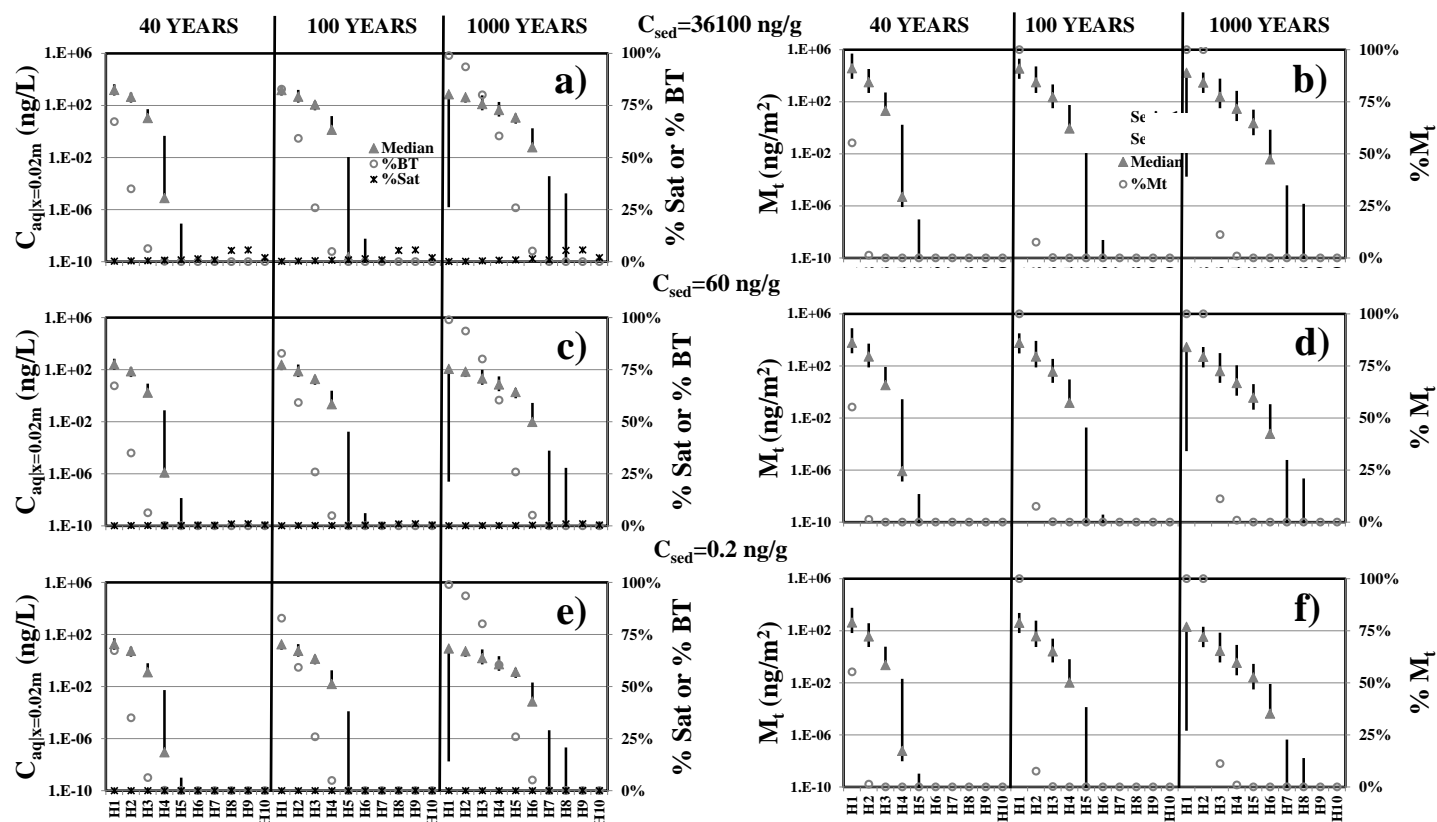


Figure 5.22l: Predicted flux of PCB homologs in core ACL under advection-diffusion with organic carbon only sorption (A(OC)) conditions for initial sediment concentration of 1640, 262, and 19 ng/g at 40, 100, and 1000 years. Panels a,c, and e show aqueous phase concentration leaving the sediment boundary layer ($C_{aq|x=0.02m,t}$), aqueous phase breakthrough percentage ($C_{aq|x=0.02m,t}/C_{aq|x=0m,t=0year}$) (%BT), and ratio of aqueous phase concentration under local equilibrium assumption to saturation concentration ($C_{aq|x=0m,t}/C_{sat}$) (%Sat) represented as grey triangle with vertical lines, hollow sphere, and star, respectively. Panels b,d, and f show mass leaving the sediment boundary layer at specific time ($M_{t|t}$) and ratio of mass leaving the sediment boundary layer to initial starting mass ($M_{t|t}/M_{sed|t=0year}$) represented as grey triangle with vertical lines and hollow sphere, respectively. For $C_{aq|x=0.02m,t}$ and $M_{t|t}$, median values as predicted by the 50th percentile transport parameters values are represented by the grey triangle while upper and lower boundaries as predicted by the 95th and 5th percentile transport parameters values are indicated by the vertical lines. Lines that did not appear in figure are below the minimum y-axes values. X-axes are homologs 1 to 10 (H1 to H10).

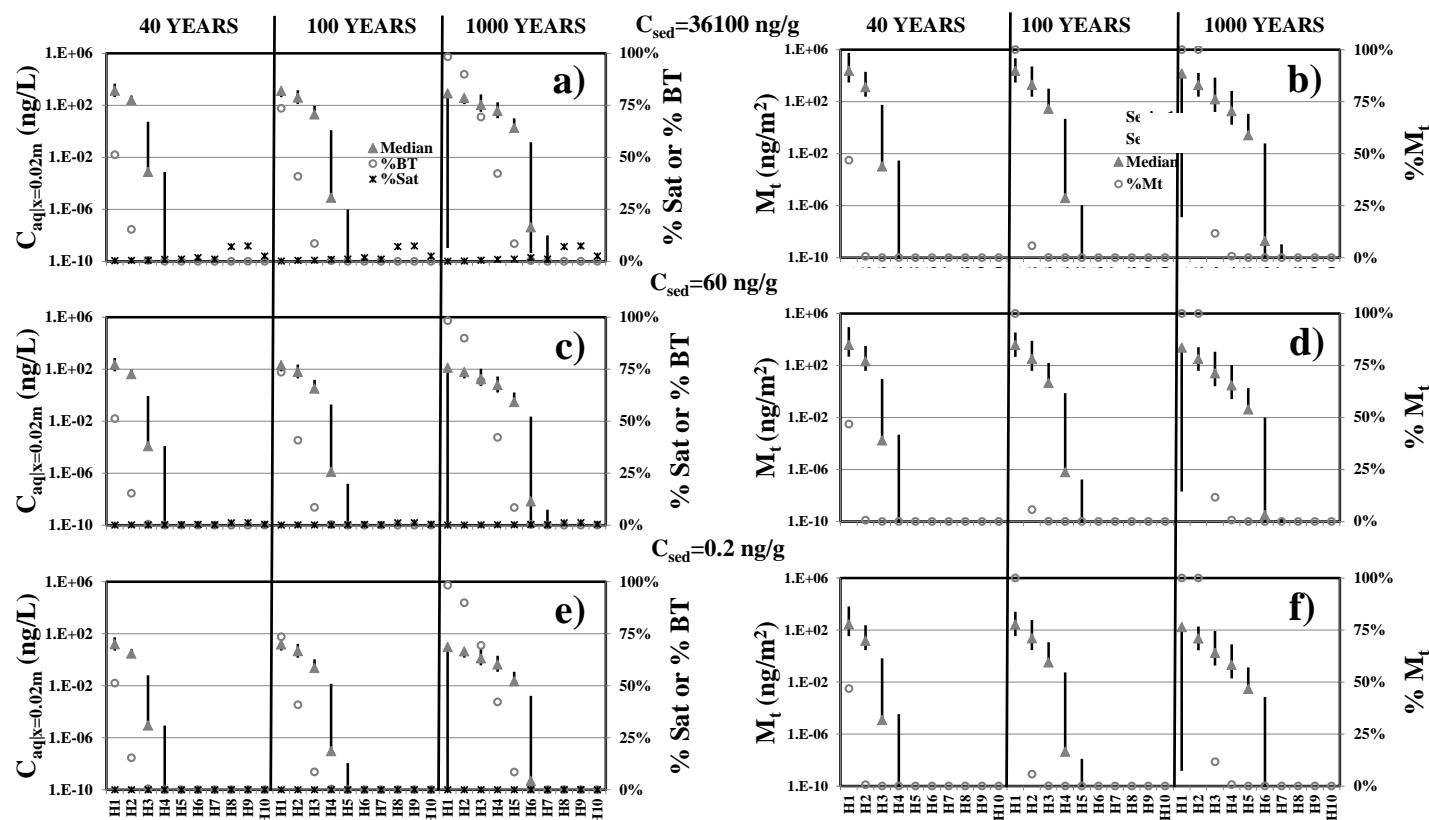


Figure 5.22m: Predicted flux of PCB homologs in core AED under advection-diffusion with organic carbon only sorption (A(OC)) conditions for initial sediment concentration of 1640, 262, and 19 ng/g at 40, 100, and 1000 years. Panels a,c, and e show aqueous phase concentration leaving the sediment boundary layer ($C_{aq|x=0.02m,t}$), aqueous phase breakthrough percentage ($C_{aq|x=0.02m,t}/C_{aq|x=0m,t=0year}$) (%BT), and ratio of aqueous phase concentration under local equilibrium assumption to saturation concentration ($C_{aq|x=0m,t}/C_{sat}$) (%Sat) represented as grey triangle with vertical lines, hollow sphere, and star, respectively. Panels b,d, and f show mass leaving the sediment boundary layer at specific time ($M_{t|t}$) and ratio of mass leaving the sediment boundary layer to initial starting mass ($M_{t|t}/M_{sed|t=0year}$) represented as grey triangle with vertical lines and hollow sphere, respectively. For $C_{aq|x=0.02m,t}$ and $M_{t|t}$, median values as predicted by the 50th percentile transport parameters values are represented by the grey triangle while upper and lower boundaries as predicted by the 95th and 5th percentile transport parameters values are indicated by the vertical lines. Lines that did not appear in figure are below the minimum y-axes values. X-axes are homologs 1 to 10 (H1 to H10).

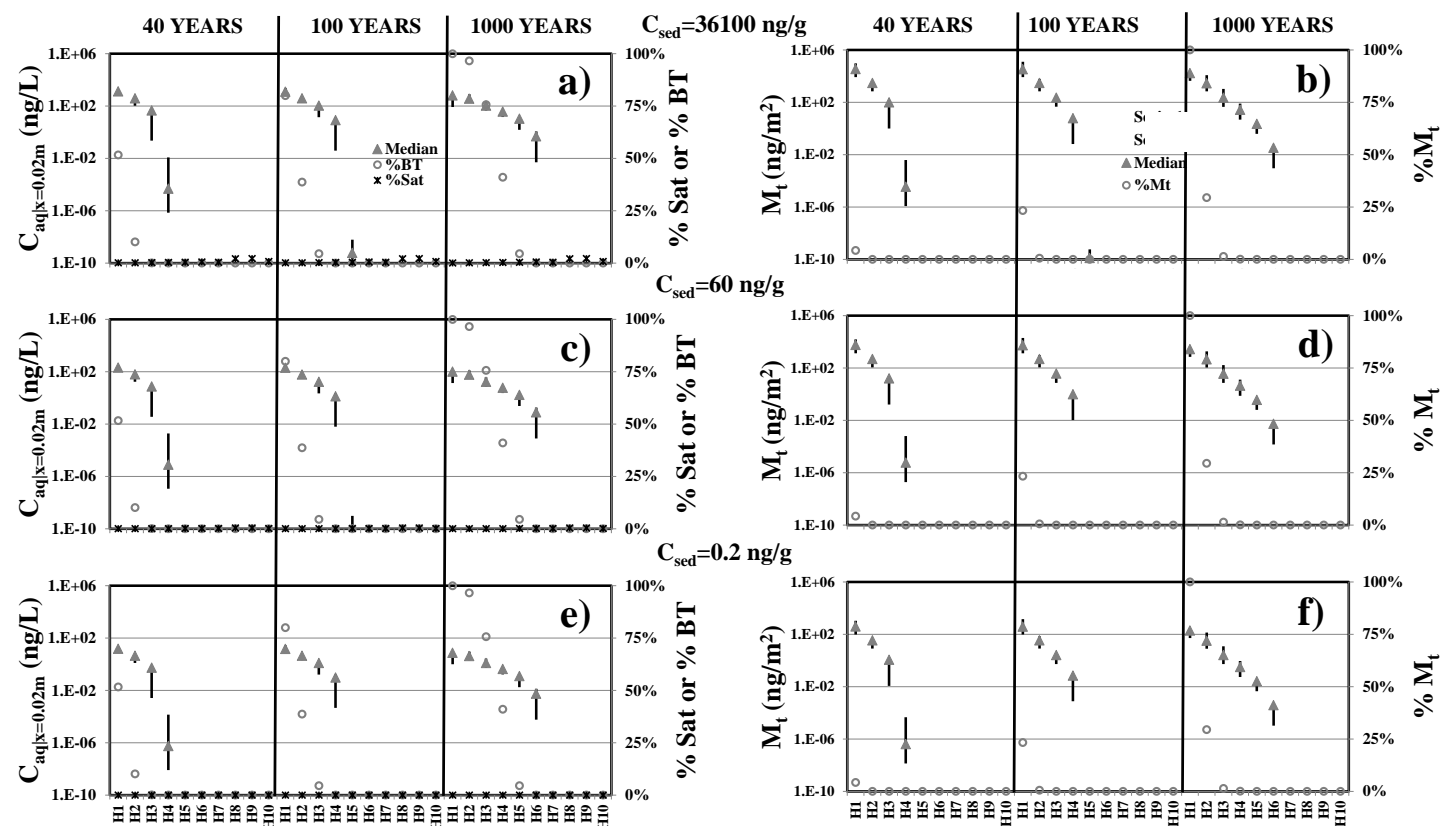


Figure 5.22n: Predicted flux of PCB homologs in core AFR under advection-diffusion with organic carbon only sorption (A(OC)) conditions for initial sediment concentration of 1640, 262, and 19 ng/g at 40, 100, and 1000 years. Panels a,c, and e show aqueous phase concentration leaving the sediment boundary layer ($C_{aq|x=0.02m,t}$), aqueous phase breakthrough percentage ($C_{aq|x=0.02m,t}/C_{aq|x=0m,t=0year}$) (%BT), and ratio of aqueous phase concentration under local equilibrium assumption to saturation concentration ($C_{aq|x=0m,t}/C_{sat}$) (%Sat) represented as grey triangle with vertical lines, hollow sphere, and star, respectively. Panels b,d, and f show mass leaving the sediment boundary layer at specific time ($M_{t|t}$) and ratio of mass leaving the sediment boundary layer to initial starting mass ($M_{t|t}/M_{sed|t=0year}$) represented as grey triangle with vertical lines and hollow sphere, respectively. For $C_{aq|x=0.02m,t}$ and $M_{t|t}$, median values as predicted by the 50th percentile transport parameters values are represented by the grey triangle while upper and lower boundaries as predicted by the 95th and 5th percentile transport parameters values are indicated by the vertical lines. Lines that did not appear in figure are below the minimum y-axes values. X-axes are homologs 1 to 10 (H1 to H10).

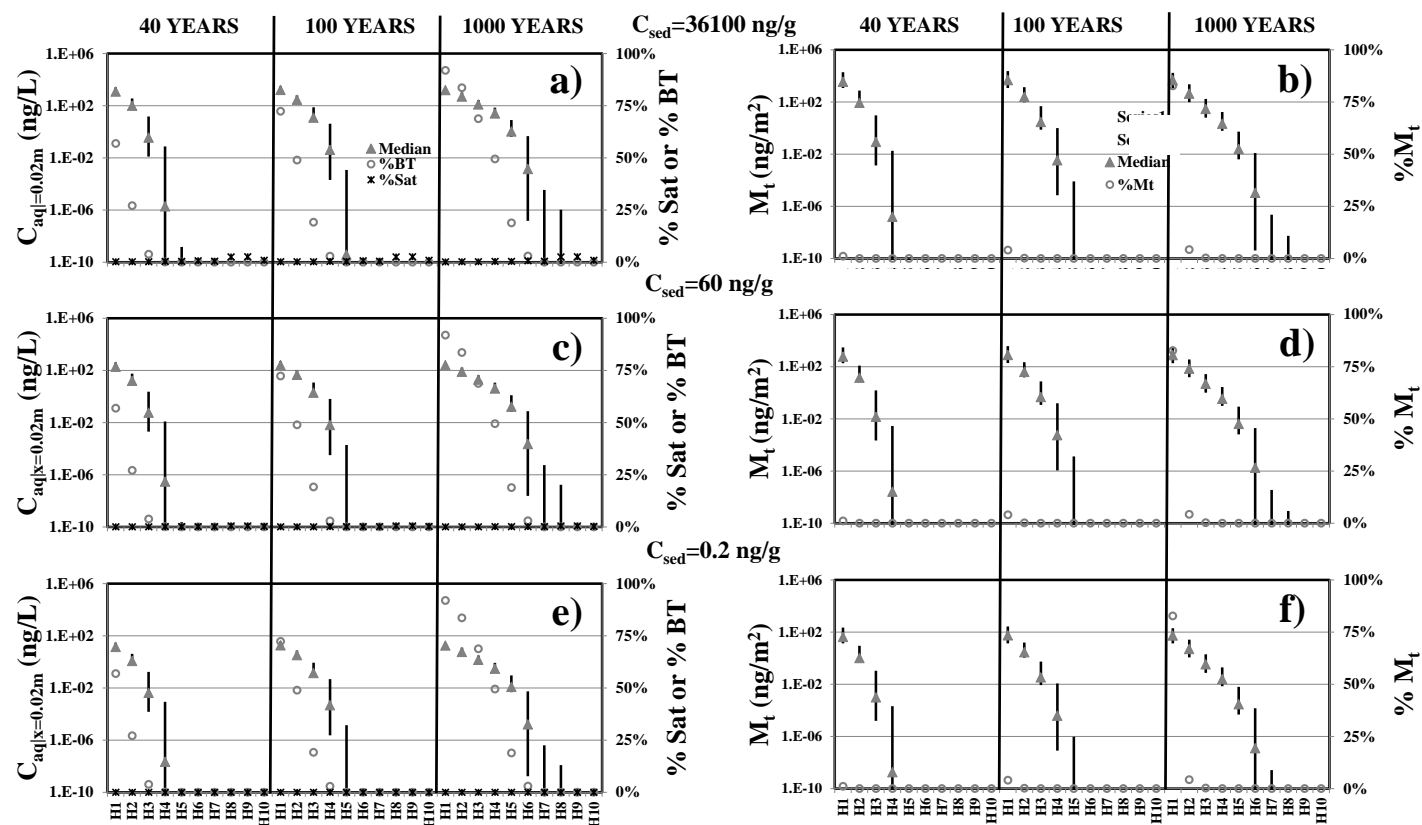


Figure 5.22o: Predicted flux of PCB homologs in core AJL under advection-diffusion with organic carbon only sorption (A(OC)) conditions for initial sediment concentration of 1640, 262, and 19 ng/g at 40, 100, and 1000 years. Panels a,c, and e show aqueous phase concentration leaving the sediment boundary layer ($C_{aq|x=0.02m,t}$), aqueous phase breakthrough percentage ($C_{aq|x=0.02m,t}/C_{aq|x=0m,t=0year}$) (%BT), and ratio of aqueous phase concentration under local equilibrium assumption to saturation concentration ($C_{aq|x=0m,t}/C_{sat}$) (%Sat) represented as grey triangle with vertical lines, hollow sphere, and star, respectively. Panels b,d, and f show mass leaving the sediment boundary layer at specific time ($M_{t|t}$) and ratio of mass leaving the sediment boundary layer to initial starting mass ($M_{t|t}/M_{sed|t=0year}$) represented as grey triangle with vertical lines and hollow sphere, respectively. For $C_{aq|x=0.02m,t}$ and $M_{t|t}$, median values as predicted by the 50th percentile transport parameters values are represented by the grey triangle while upper and lower boundaries as predicted by the 95th and 5th percentile transport parameters values are indicated by the vertical lines. Lines that did not appear in figure are below the minimum y-axes values. X-axes are homologs 1 to 10 (H1 to H10).

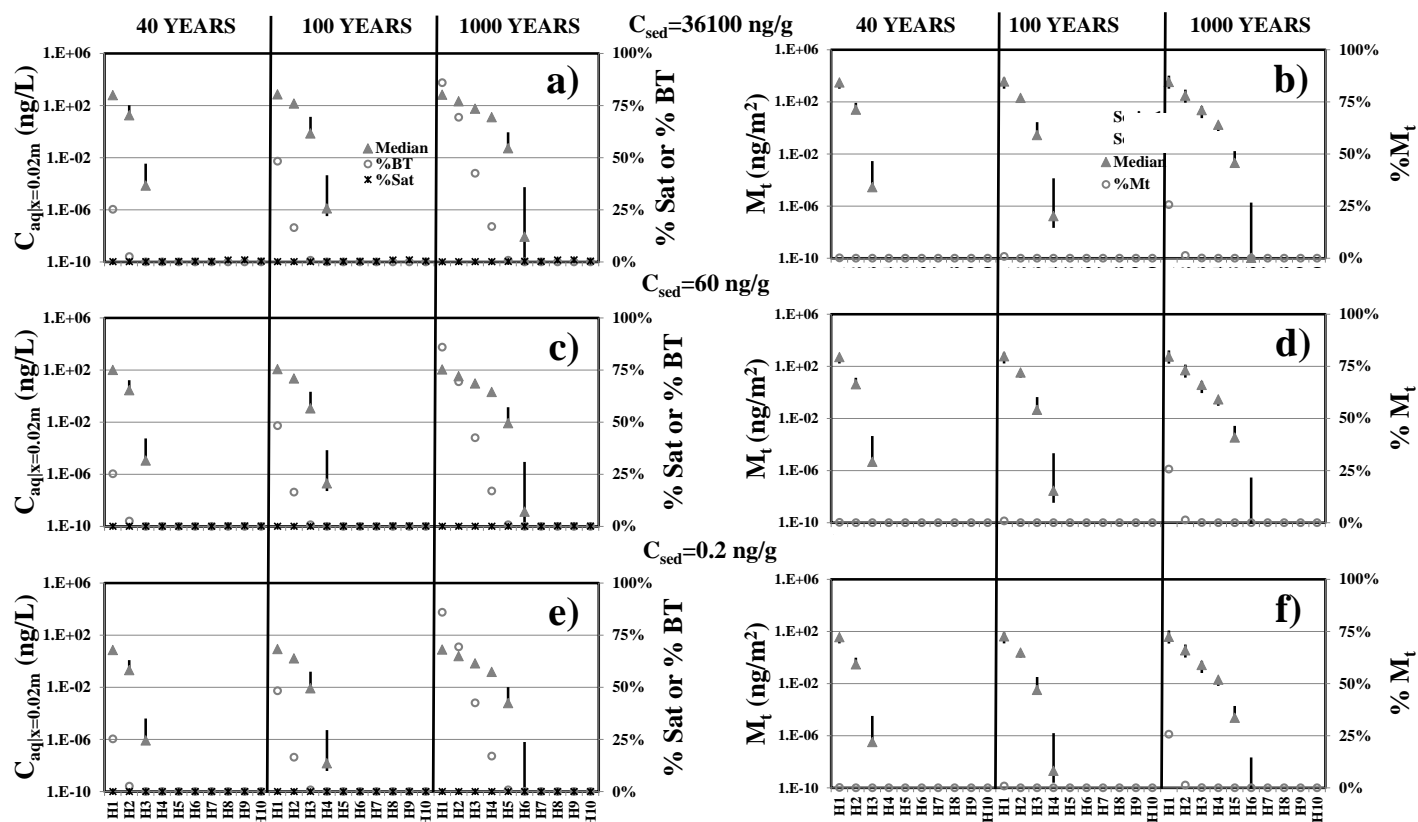


Figure 5.22p: Predicted flux of PCB homologs in core AMW under advection-diffusion with organic carbon only sorption (A(OC)) conditions for initial sediment concentration of 1640, 262, and 19 ng/g at 40, 100, and 1000 years. Panels a,c, and e show aqueous phase concentration leaving the sediment boundary layer ($C_{aq|x=0.02m,t}$), aqueous phase breakthrough percentage ($C_{aq|x=0.02m,t}/C_{aq|x=0m,t=0year}$) (%BT), and ratio of aqueous phase concentration under local equilibrium assumption to saturation concentration ($C_{aq|x=0m,t}/C_{sat}$) (%Sat) represented as grey triangle with vertical lines, hollow sphere, and star, respectively. Panels b,d, and f show mass leaving the sediment boundary layer at specific time ($M_{t|t}$) and ratio of mass leaving the sediment boundary layer to initial starting mass ($M_{t|t}/M_{sed|t=0year}$) represented as grey triangle with vertical lines and hollow sphere, respectively. For $C_{aq|x=0.02m,t}$ and $M_{t|t}$, median values as predicted by the 50th percentile transport parameters values are represented by the grey triangle while upper and lower boundaries as predicted by the 95th and 5th percentile transport parameters values are indicated by the vertical lines. Lines that did not appear in figure are below the minimum y-axes values. X-axes are homologs 1 to 10 (H1 to H10).

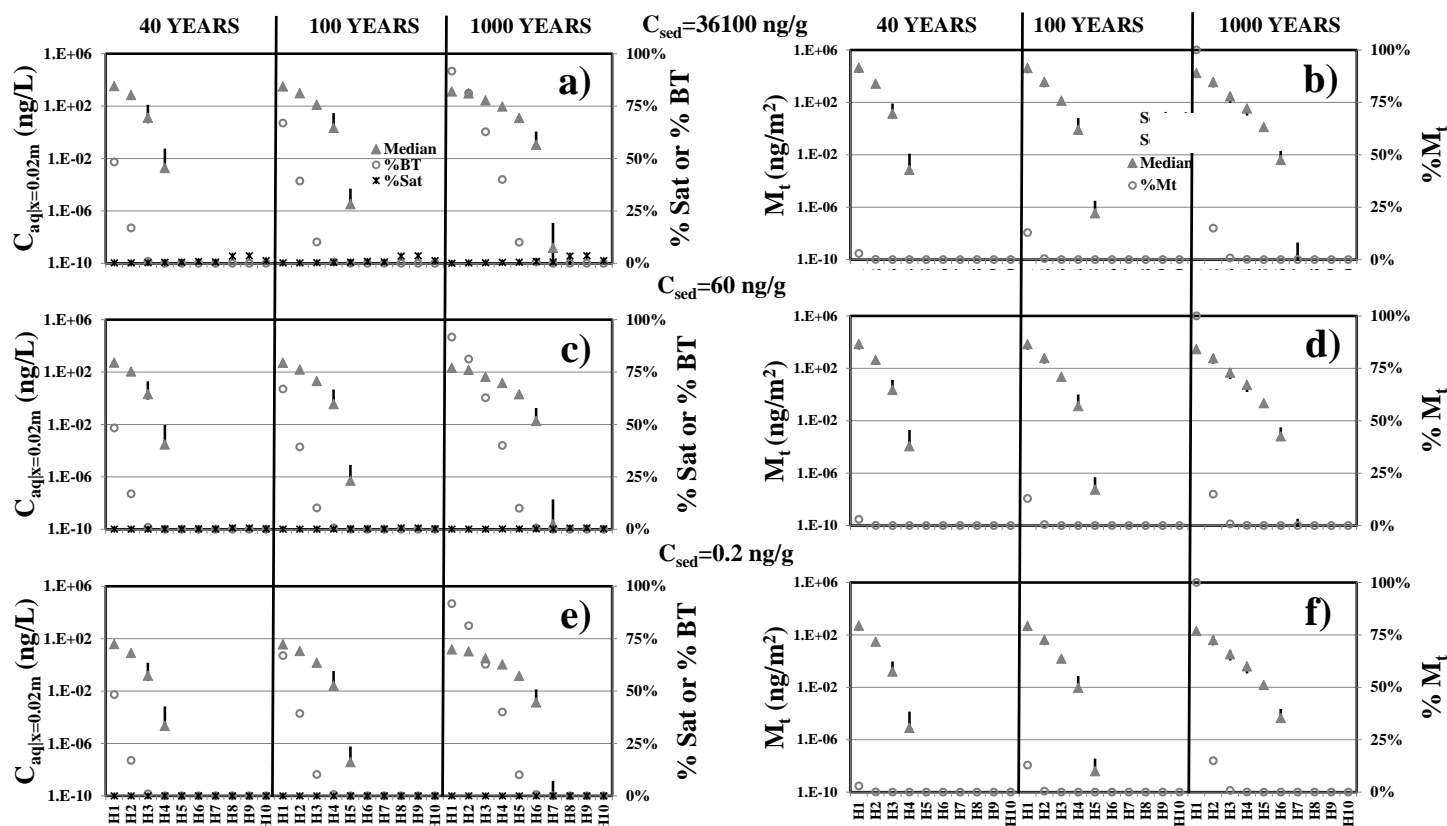


Figure 5.22q: Predicted flux of PCB homologs in core AOT under advection-diffusion with organic carbon only sorption (A(OC)) conditions for initial sediment concentration of 1640, 262, and 19 ng/g at 40, 100, and 1000 years. Panels a,c, and e show aqueous phase concentration leaving the sediment boundary layer ($C_{aq|x=0.02m,t}$), aqueous phase breakthrough percentage ($C_{aq|x=0.02m,t}/C_{aq|x=0m,t=0year}$) (%BT), and ratio of aqueous phase concentration under local equilibrium assumption to saturation concentration ($C_{aq|x=0m,t}/C_{sat}$) (%Sat) represented as grey triangle with vertical lines, hollow sphere, and star, respectively. Panels b,d, and f show mass leaving the sediment boundary layer at specific time ($M_{t|t}$) and ratio of mass leaving the sediment boundary layer to initial starting mass ($M_{t|t}/M_{sed|t=0year}$) represented as grey triangle with vertical lines and hollow sphere, respectively. For $C_{aq|x=0.02m,t}$ and $M_{t|t}$, median values as predicted by the 50th percentile transport parameters values are represented by the grey triangle while upper and lower boundaries as predicted by the 95th and 5th percentile transport parameters values are indicated by the vertical lines. Lines that did not appear in figure are below the minimum y-axes values. X-axes are homologs 1 to 10 (H1 to H10).

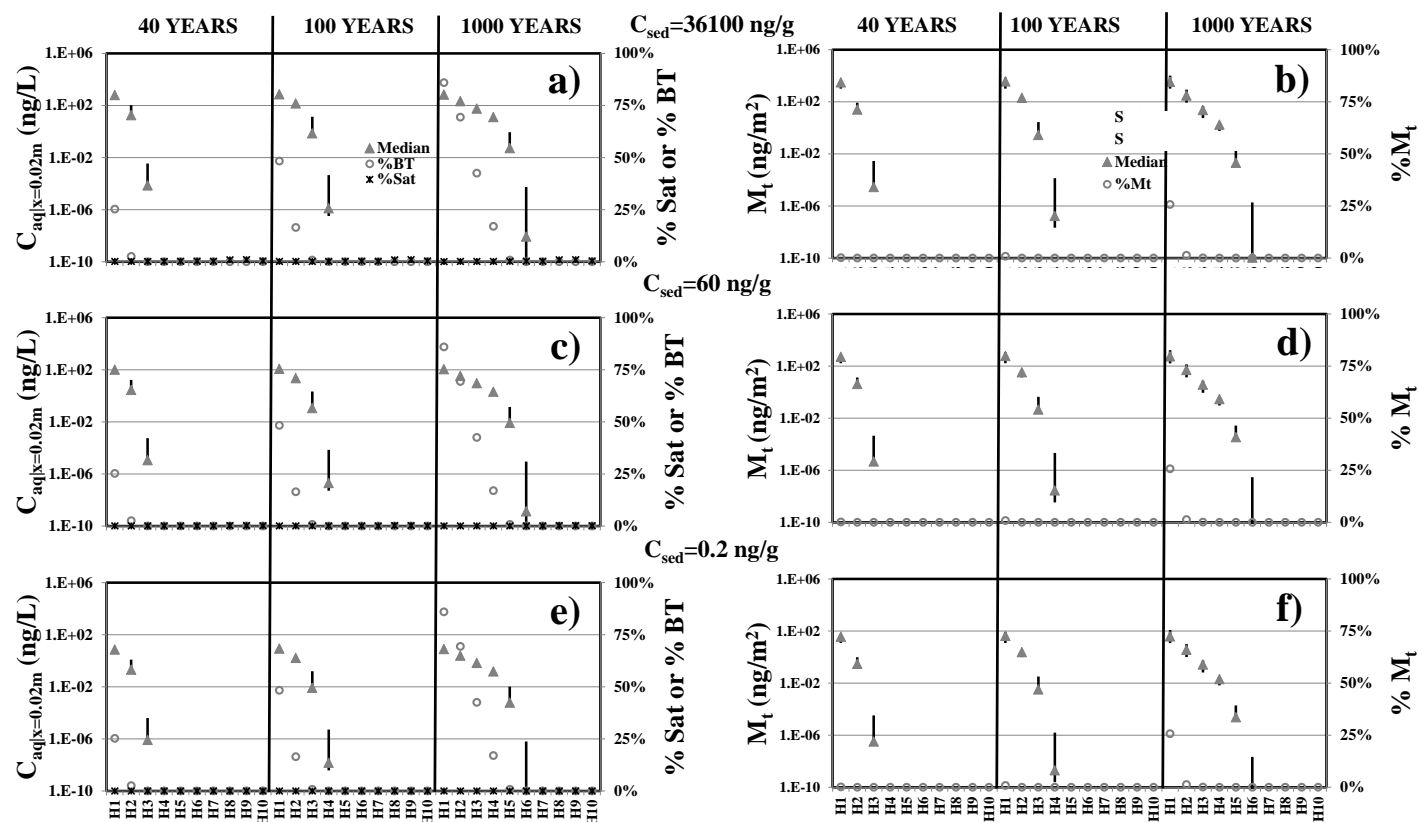


Figure 5.22r: Predicted flux of PCB homologs in core AMW under advection-diffusion with organic carbon only sorption (A(OC)) conditions for initial sediment concentration of 1640, 262, and 19 ng/g at 40, 100, and 1000 years. Panels a,c, and e show aqueous phase concentration leaving the sediment boundary layer ($C_{aq|x=0.02m,t}$), aqueous phase breakthrough percentage ($C_{aq|x=0.02m,t}/C_{aq|x=0m,t=0year}$) (%BT), and ratio of aqueous phase concentration under local equilibrium assumption to saturation concentration ($C_{aq|x=0m,t}/C_{sat}$) (%Sat) represented as grey triangle with vertical lines, hollow sphere, and star, respectively. Panels b,d, and f show mass leaving the sediment boundary layer at specific time ($M_{t|t}$) and ratio of mass leaving the sediment boundary layer to initial starting mass ($M_{t|t}/M_{sed|t=0year}$) represented as grey triangle with vertical lines and hollow sphere, respectively. For $C_{aq|x=0.02m,t}$ and $M_{t|t}$, median values as predicted by the 50th percentile transport parameters values are represented by the grey triangle while upper and lower boundaries as predicted by the 95th and 5th percentile transport parameters values are indicated by the vertical lines. Lines that did not appear in figure are below the minimum y-axes values. X-axes are homologs 1 to 10 (H1 to H10).

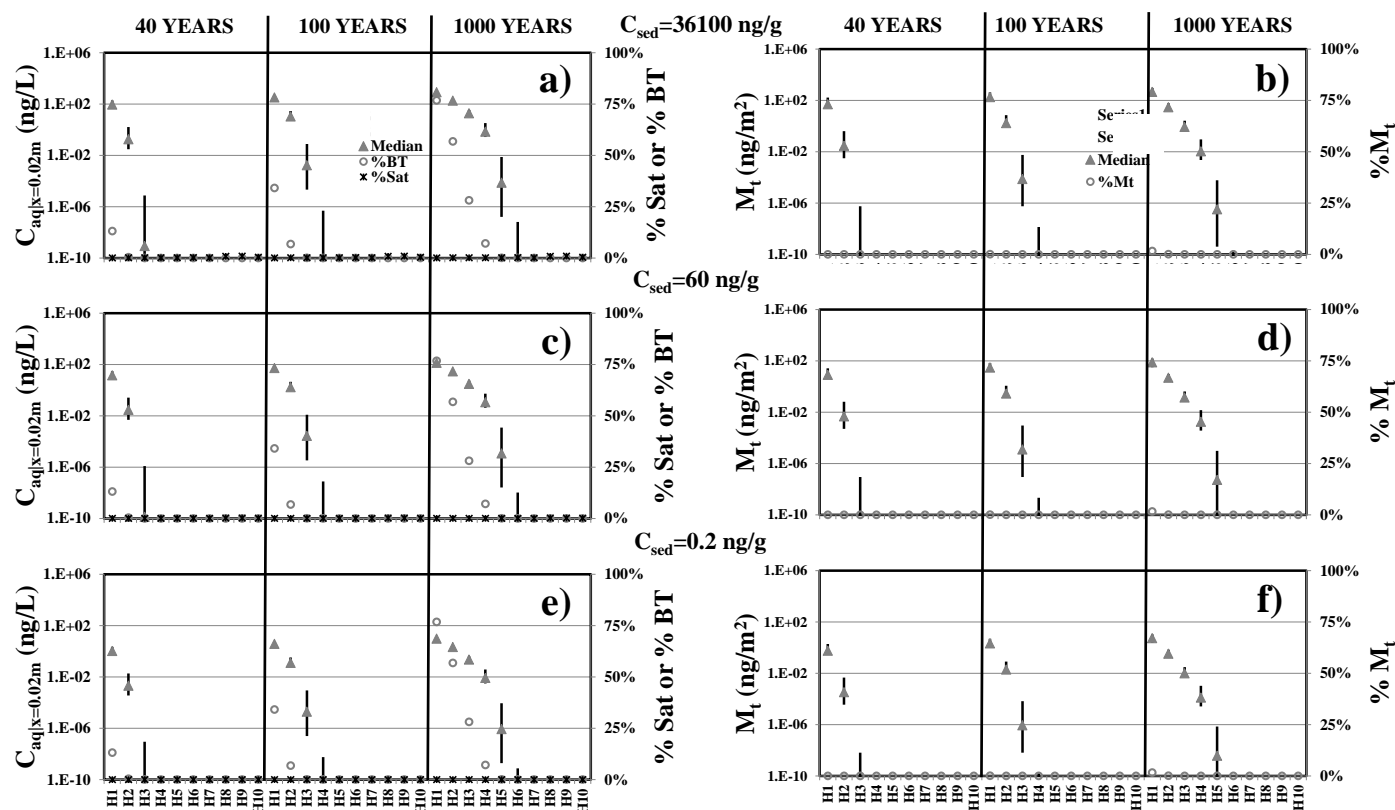


Figure 5.22s: Predicted flux of PCB homologs in core CBC under advection-diffusion with organic carbon only sorption (A(OC)) conditions for initial sediment concentration of 1640, 262, and 19 ng/g at 40, 100, and 1000 years. Panels a,c, and e show aqueous phase concentration leaving the sediment boundary layer ($C_{aq|x=0.02m,t}$), aqueous phase breakthrough percentage ($C_{aq|x=0.02m,t}/C_{aq|x=0m,t=0year}$) (%BT), and ratio of aqueous phase concentration under local equilibrium assumption to saturation concentration ($C_{aq|x=0m,t}/C_{sat}$) (%Sat) represented as grey triangle with vertical lines, hollow sphere, and star, respectively. Panels b,d, and f show mass leaving the sediment boundary layer at specific time ($M_{t|t}$) and ratio of mass leaving the sediment boundary layer to initial starting mass ($M_{t|t}/M_{sed|t=0year}$) represented as grey triangle with vertical lines and hollow sphere, respectively. For $C_{aq|x=0.02m,t}$ and $M_{t|t}$, median values as predicted by the 50th percentile transport parameters values are represented by the grey triangle while upper and lower boundaries as predicted by the 95th and 5th percentile transport parameters values are indicated by the vertical lines. Lines that did not appear in figure are below the minimum y-axes values. X-axes are homologs 1 to 10 (H1 to H10).

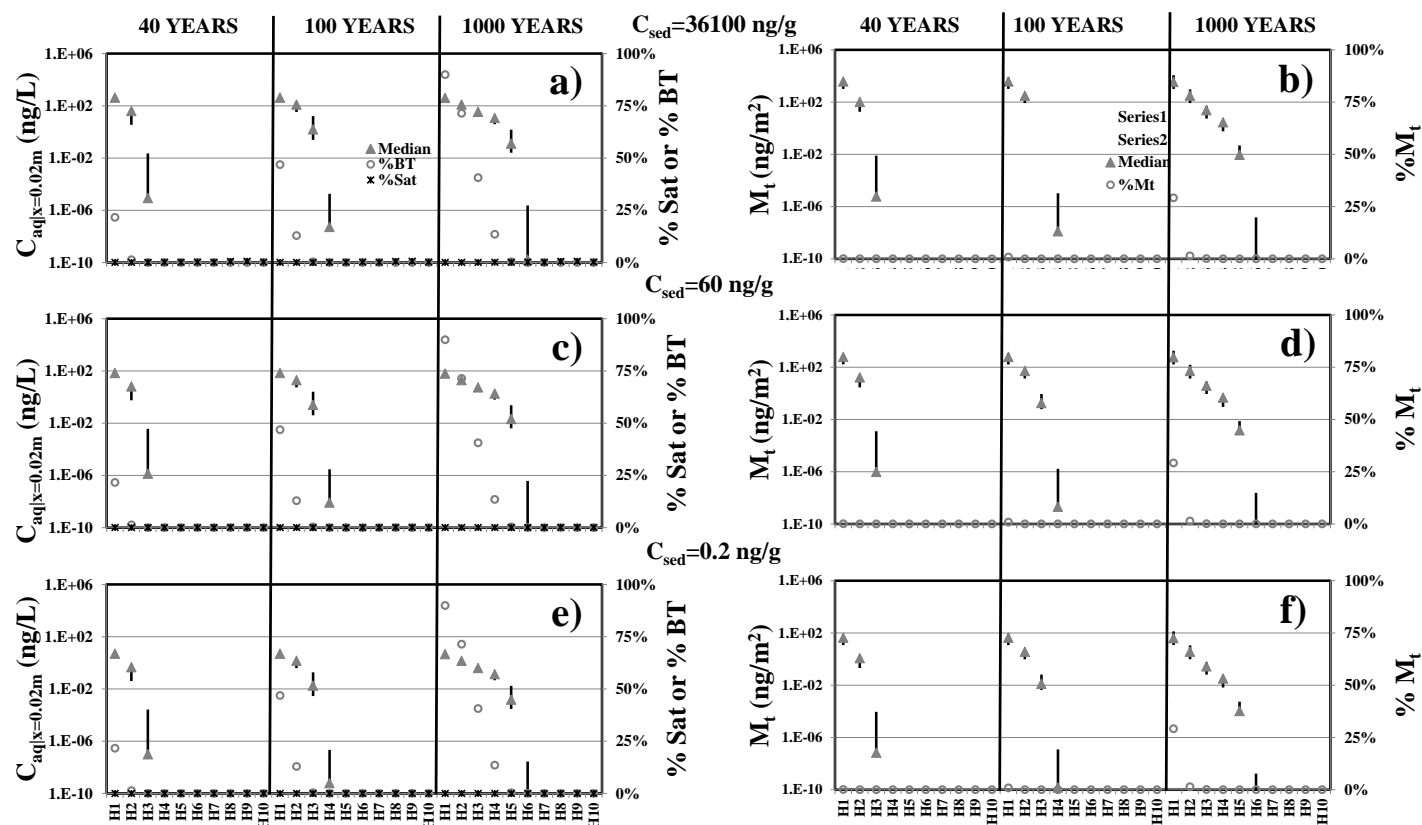


Figure 5.22t: Predicted flux of PCB homologs in core CWP under advection-diffusion with organic carbon only sorption (A(OC)) conditions for initial sediment concentration of 1640, 262, and 19 ng/g at 40, 100, and 1000 years. Panels a,c, and e show aqueous phase concentration leaving the sediment boundary layer ($C_{aq|x=0.02m,t}$), aqueous phase breakthrough percentage ($C_{aq|x=0.02m,t}/C_{aq|x=0m,t=0year}$) (%BT), and ratio of aqueous phase concentration under local equilibrium assumption to saturation concentration ($C_{aq|x=0m,t}/C_{sat}$) (%Sat) represented as grey triangle with vertical lines, hollow sphere, and star, respectively. Panels b,d, and f show mass leaving the sediment boundary layer at specific time ($M_{t|t}$) and ratio of mass leaving the sediment boundary layer to initial starting mass ($M_{t|t}/M_{sed|t=0year}$) represented as grey triangle with vertical lines and hollow sphere, respectively. For $C_{aq|x=0.02m,t}$ and $M_{t|t}$, median values as predicted by the 50th percentile transport parameters values are represented by the grey triangle while upper and lower boundaries as predicted by the 95th and 5th percentile transport parameters values are indicated by the vertical lines. Lines that did not appear in figure are below the minimum y-axes values. X-axes are homologs 1 to 10 (H1 to H10).

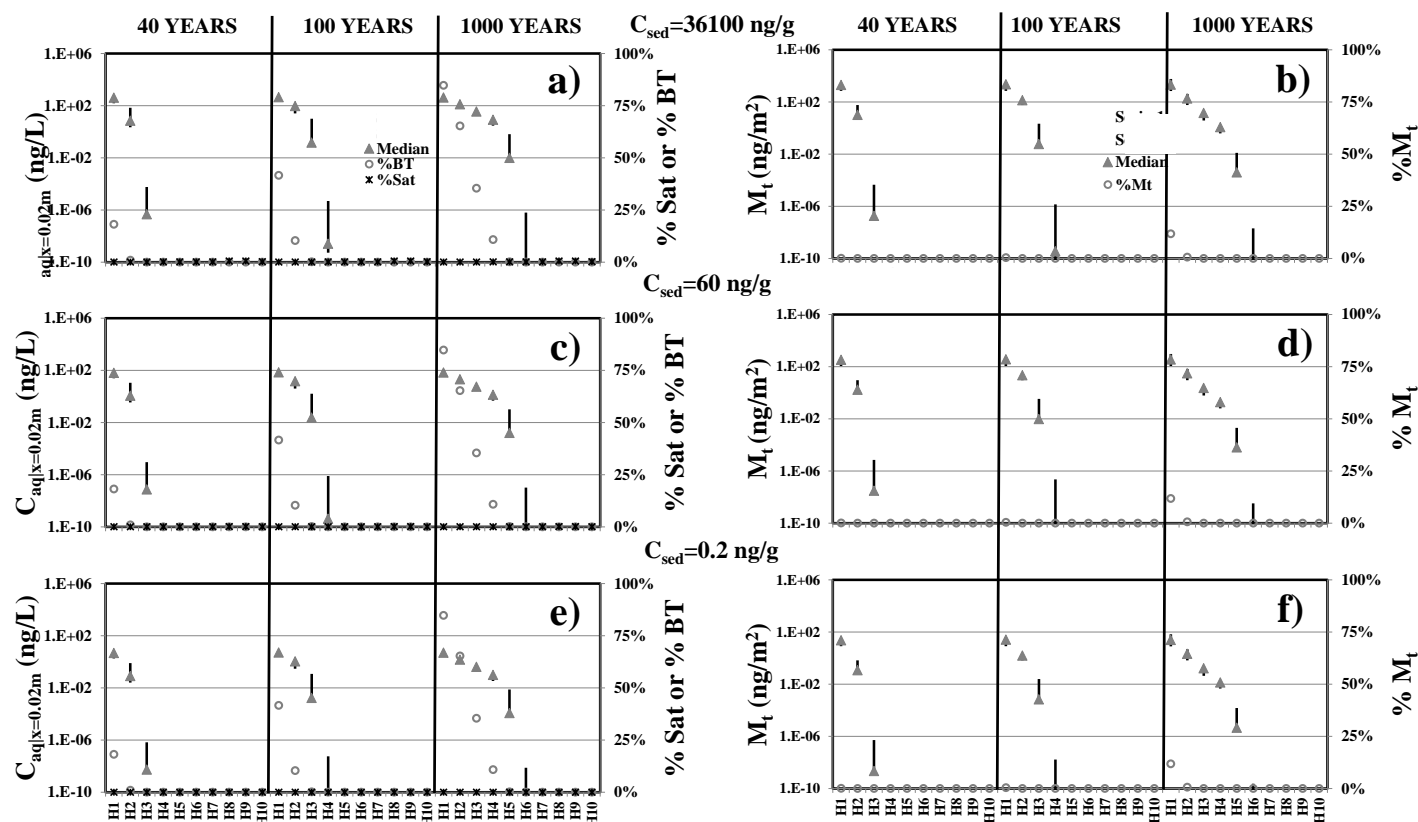


Figure 5.22u: Predicted flux of PCB homologs in core IGC09 under advection-diffusion with organic carbon only sorption (A(OC)) conditions for initial sediment concentration of 1640, 262, and 19 ng/g at 40, 100, and 1000 years. Panels a,c, and e show aqueous phase concentration leaving the sediment boundary layer ($C_{aq|x=0.02m,t}$), aqueous phase breakthrough percentage ($C_{aq|x=0.02m,t}/C_{aq|x=0m,t=0year}$) (%BT), and ratio of aqueous phase concentration under local equilibrium assumption to saturation concentration ($C_{aq|x=0m,t}/C_{sat}$) (%Sat) represented as grey triangle with vertical lines, hollow sphere, and star, respectively. Panels b,d, and f show mass leaving the sediment boundary layer at specific time (M_t) and ratio of mass leaving the sediment boundary layer to initial starting mass ($M_t/M_{sed|t=0year}$) represented as grey triangle with vertical lines and hollow sphere, respectively. For $C_{aq|x=0.02m,t}$ and M_t , median values as predicted by the 50th percentile transport parameters values are represented by the grey triangle while upper and lower boundaries as predicted by the 95th and 5th percentile transport parameters values are indicated by the vertical lines. Lines that did not appear in figure are below the minimum y-axes values. X-axes are homologs 1 to 10 (H1 to H10).

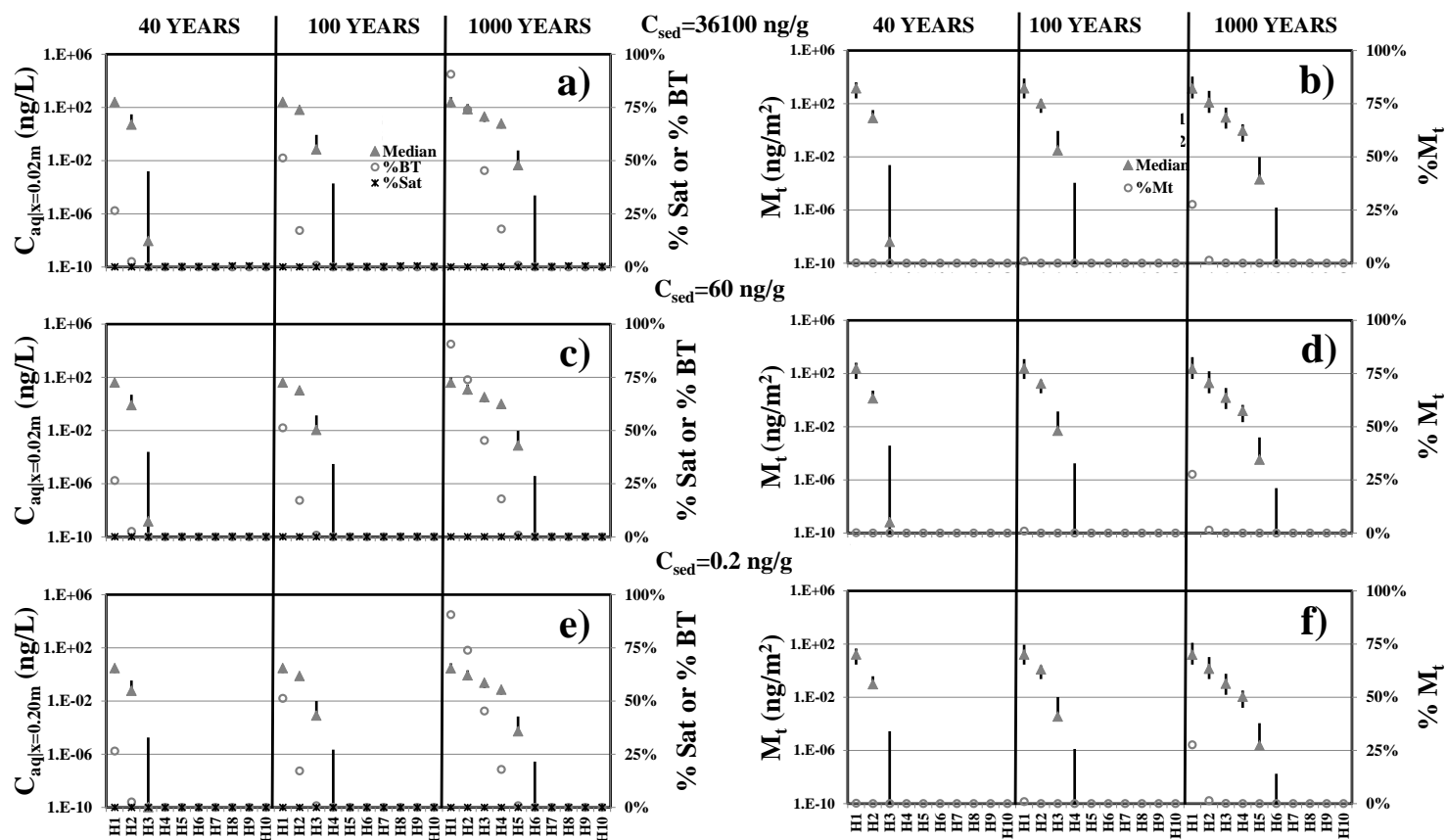


Figure 5.22v: Predicted flux of PCB homologs in core IGC13 under advection-diffusion with organic carbon only sorption (A(OC)) conditions for initial sediment concentration of 1640, 262, and 19 ng/g at 40, 100, and 1000 years. Panels a,c, and e show aqueous phase concentration leaving the sediment boundary layer ($C_{aq|x=0.02m,t}$), aqueous phase breakthrough percentage ($C_{aq|x=0.02m,t}/C_{aq|x=0m,t=0year}$) (%BT), and ratio of aqueous phase concentration under local equilibrium assumption to saturation concentration ($C_{aq|x=0m,t}/C_{sat}$) (%Sat) represented as grey triangle with vertical lines, hollow sphere, and star, respectively. Panels b,d, and f show mass leaving the sediment boundary layer at specific time ($M_{t|t}$) and ratio of mass leaving the sediment boundary layer to initial starting mass ($M_{t|t}/M_{sed|t=0year}$) represented as grey triangle with vertical lines and hollow sphere, respectively. For $C_{aq|x=0.02m,t}$ and $M_{t|t}$, median values as predicted by the 50th percentile transport parameters values are represented by the grey triangle while upper and lower boundaries as predicted by the 95th and 5th percentile transport parameters values are indicated by the vertical lines. Lines that did not appear in figure are below the minimum y-axes values. X-axes are homologs 1 to 10 (H1 to H10).

Figures 5.22a-v provides an overall picture of the changes in the contaminant profile and flux with time under the A(OC) transport process. PBDE transport occurs at a higher magnitude than PCBs. Similarly, the variation from core to core resulted in largely similar behavior at different concentration magnitudes as well. Previously, the increasing order of C/Co magnitude under the 95th percentile transport parameter values for A(OC) transport process was detailed in Section 5.4. The order was CLC < IGC09 < CWP < AMW < IGC13 < AJL < AOT < CBC < AFR < AED < ACL. For illustration purposes, core ACL is used as an illustrative case to shed light on PBDE and PCB in-situ mass flux under A(OC) conditions (the most mobile simulation from transport perspective) with the understanding that similar behavior is observed in the other sediment cores.

In core ACL, PBDE and PCB log K_d values for homologs 1 to 10 were predicted to span over four orders of magnitude (Table 5.7, Figure 5.9a and c, and Table D5.5a-d), which resulted in a wide range of predicted $C_{aq|x=0m,t}$ values under the LEA. For example, under the 95th percentile transport parameter values (most mobile simulation), predicted $C_{aq|x=0m,t=0\text{year}}$ values for PBDE and PCB homologs 1 and 10 ranged from 44,500 to 1 ng/L and 3650 to 0.3 ng/L, respectively (Figure D5.5a-c and ah-aj). Note that the difference between PBDEs and PCBs of the same homolog was driven by the difference in initial sediment concentrations (95th percentile concentrations were 36100 and 1640 ng/g for PBDEs and PCBs, respectively). In both PBDEs and PCBs, HMW homologs have lower predicted $C_{aq|x=0m,t=0\text{ year}}$ due to their higher hydrophobicity. At lower initial sediment concentrations (50th and 5th percentile concentration for PBDEs, and 75th and 50th percentile concentration for PCBs), the predicted $C_{aq|x=0m,t=0\text{ year}}$ values were lower.

The $C_{aq|x=0.02m,t}$, predicted from the $C_{aq|x=0m,t}$ using Equation 5.3 for the A(OC) transport condition under the 5th, 50th, and 95th percentile transport parameter values at 40, 100, and 1000 years are shown in Figure 5.22a-v (panels a,c, and e). Predicted $C_{aq|x=0.02m,t}$ generally increased with increasing transport time. For the purpose of this study, an ad-hoc $C_{aq|x=0.02m,t}$ value <1E-10 ng/L was deemed negligible (i.e., does not result in noticeable PBDE and PCB mass transport). At t=40 years in core ACL, only PBDE

homologs 1 and 2, and PCB homologs 1 through 4 were predicted to show non-negligible $C_{aq}|_{x=0.02m,t}$ values under the 95th percentile initial sediment concentration and 95th percentile transport parameter values (high concentration gradient combined with high mobility conditions). In 100 and 1000 years, appreciable $C_{aq}|_{x=0.02m,t}$ values under the same conditions were predicted for PBDE and PCB homologs 1 to 3 and 1 to 5, respectively (Figure 5.22 a-v, panels a,c, and e). As expected, PCB flux under A(OC) condition was higher than PBDEs. Overall, PBDE and PCB predicted $C_{aq}|_{x=0.02m,t}$ values decreased with increasing homolog. With a lower initial sediment concentration, $C_{aq}|_{x=0.02m,t}$ values at the same transport time were predicted to be lower.

Increased predicted $C_{aq}|_{x=0.02m,t}$ values with time resulted in increased values of $C_{aq}|_{x=0.02m,t} / C_{aq}|_{x=0m,t=0year}$. LMW PBDE and PCB homolog aqueous phase breakthrough was predicted to be more rapid. For instance in core ACL, PBDE homolog 1 predicted $C_{aq}|_{x=0.02m,t} / C_{aq}|_{x=0m,t=0}$ values were 30, 63, and 99% at 40, 100, and 1000 years, respectively, whereas PBDE homolog 4 predicted $C_{aq}|_{x=0.02m,t} / C_{aq}|_{x=0m,t=0}$ values were 0, 0.01 and 33%, respectively. The increase in $C_{aq}|_{x=0.02m,t} / C_{aq}|_{x=0m,t=0}$ with time was more rapid for PCBs; PCB homologs 1 and 4 have predicted $C_{aq}|_{x=0.02m,t} / C_{aq}|_{x=0m,t=0}$ values of 52, 80, and 100% , and 0, 0.03, and 41%, respectively. With decreasing initial sediment concentrations, predicted $C_{aq}|_{x=0.02m,t} / C_{aq}|_{x=0m,t=0}$ values for the same transport time were similar as the aqueous phase breakthrough is a function of initial sediment concentration.

The increase in predicted $C_{aq}|_{x=0.02m,t}$ values resulted in an increase in the predicted $C_{aq}|_{x=0m,t} / C_{sat}$ values with time. As was previously discussed, lower initial PBDE and PCB sediment concentrations resulted in lower predicted $C_{aq}|_{x=0.02m,t}$. Therefore the predicted $C_{aq}|_{x=0m,t} / C_{sat}$ values were also lower for lower initial sediment concentrations. At the 95th percentile initial sediment concentration, PBDE homologs 6 and higher have predicted $C_{aq}|_{x=0m,t} / C_{sat}$ values of 100% at 40 years transport time. This trend was driven by two factors; the high predicted $C_{aq}|_{x=0.02m,t}$ values stemming from high initial sediment concentration and low C_{sat} with increasing homologs hydrophobicity. PCB homologs have lower

predicted $C_{aq|x=0m,t}/C_{sat}$ values stemming from the lower initial sediment concentrations and higher C_{sat} . Detailed discussion on the impact of C_{sat} on PBDE and PCB mass transport processes are provided later.

The $C_{aq|x=0.02m,t}$ was used to predict the mass flux, $M_{t/t}$ under the A(OC) transport condition using Equation 5.7. M_t values below the ad-hoc value of $1E-10$ ng/m² were deemed negligible because the contaminant mass leaving the sediment boundary layer was negligible compared to the starting mass. In core ACL, only LMW PBDE homologs 1 to 5, and PCB homologs 1 to 6 were predicted to have appreciable M_t values at 40, 100, and 1000 years. As the $M_{t/t}$ was determined by $C_{aq|x=0.02m,t}$, lower initial sediment concentrations resulted in lower predicted $M_{t/t}$ values. With increasing transport time, the predicted M_t values increased consistent with expectation of increased PBDE and PCB mass flux out of the sediment boundary layer over time.

Detailed inspection on the PBDE and PCB homolog behavior in core ACL showed that the percent mass loss ($M_{t/t}/M_{sed|t=0}$) in PBDE homolog 1 and PCB homologs 1 and 2 was substantial. For PBDE homolog 1, $M_{t/t}/M_{sed|t=0}$ reached 0.6, 4.4, and 100% for 40, 100, and 1000 years, respectively. For PCB homolog 1, $M_{t/t}/M_{sed|t=0}$ reached 4.3, 23.3, and 100% at 40, 100, and 1000 years, respectively. For PCB homolog 2, $M_{t/t}/M_{sed|t=0}$ reached 0.1, 0.6, and 30% for 40, 100, and 1000 years, respectively. Due to the substantial, and in some cases complete contaminant flux out of the sediment segment for these LMW PBDE and PCB homologs, gradual changes in the respective C_{sed} as a function of time are predicted to occur in core ACL. Predicted C_{sed} values over time are provided in Figure 5.23a-h (a-c panels) (PBDEs:a-d, PCBs:e-h). With $C_{sed|t}$ substantially reduced relative to $C_{sed|t=0}$, the porewater was predicted to be less saturated with PBDEs or PCBs as quantified by the gradually reducing $C_{aq|x=0m,t}/C_{sat}$ (Figure 5.23a-h, d-f panels). Other cores predicted to have substantial mass loss due to flux out of the core segment ($C_{sed|t=1000\text{ years}}/C_{sed|t=0\text{ years}} \geq 90\%$) of PBDE homolog 1 and PCB homologs 1 and 2 are AED, AJL, and CBC. In PBDE homologs 2 and larger, and PCB homologs 3 and larger, no substantial mass loss were predicted. Although there was appreciable $M_{t/t}$ (Figure 5.22a-v, panels b,d, and f), the $M_{t/t}/M_{sed|t=0\text{ year}}$ mass loss was small and negligible for these homologs.

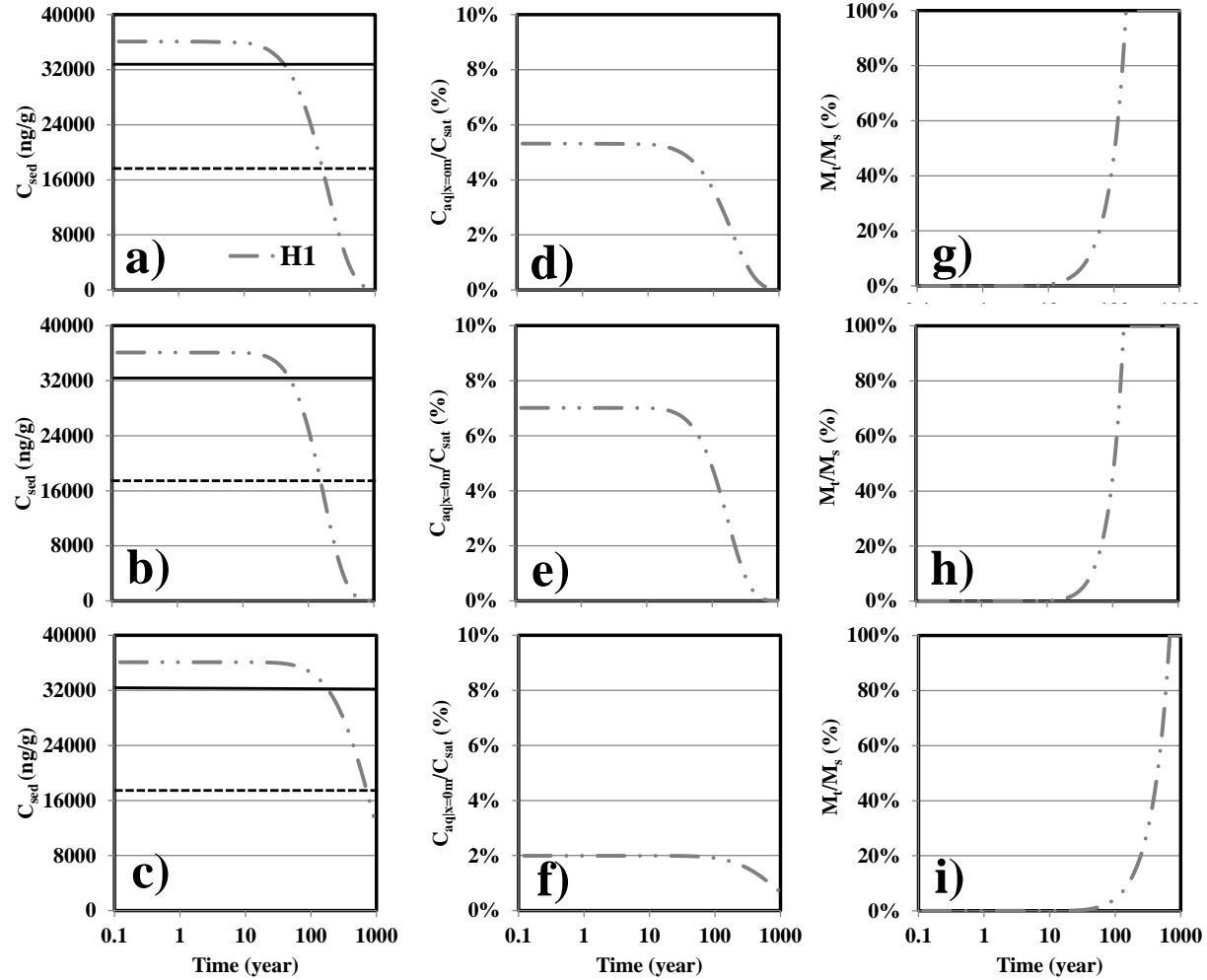


Figure 5.23a: PBDE homolog 1 sediment concentration (C_{sed}) (a-c), percent porewater saturation ($C_{aq|x=0m}/C_{sat}$) (d-f), and fraction of mass leaving the sediment boundary layer relative to initial starting mass (M_t/M_{sed}) (g-i) as a function of time in cores ACL (a,d,g), AED (b,e,h), and AFR (c,f,i) as predicted by the Monte Carlo 95th percentile transport parameters values under advection-diffusion with organic carbon only sorption (A(OC)) mass transport condition.

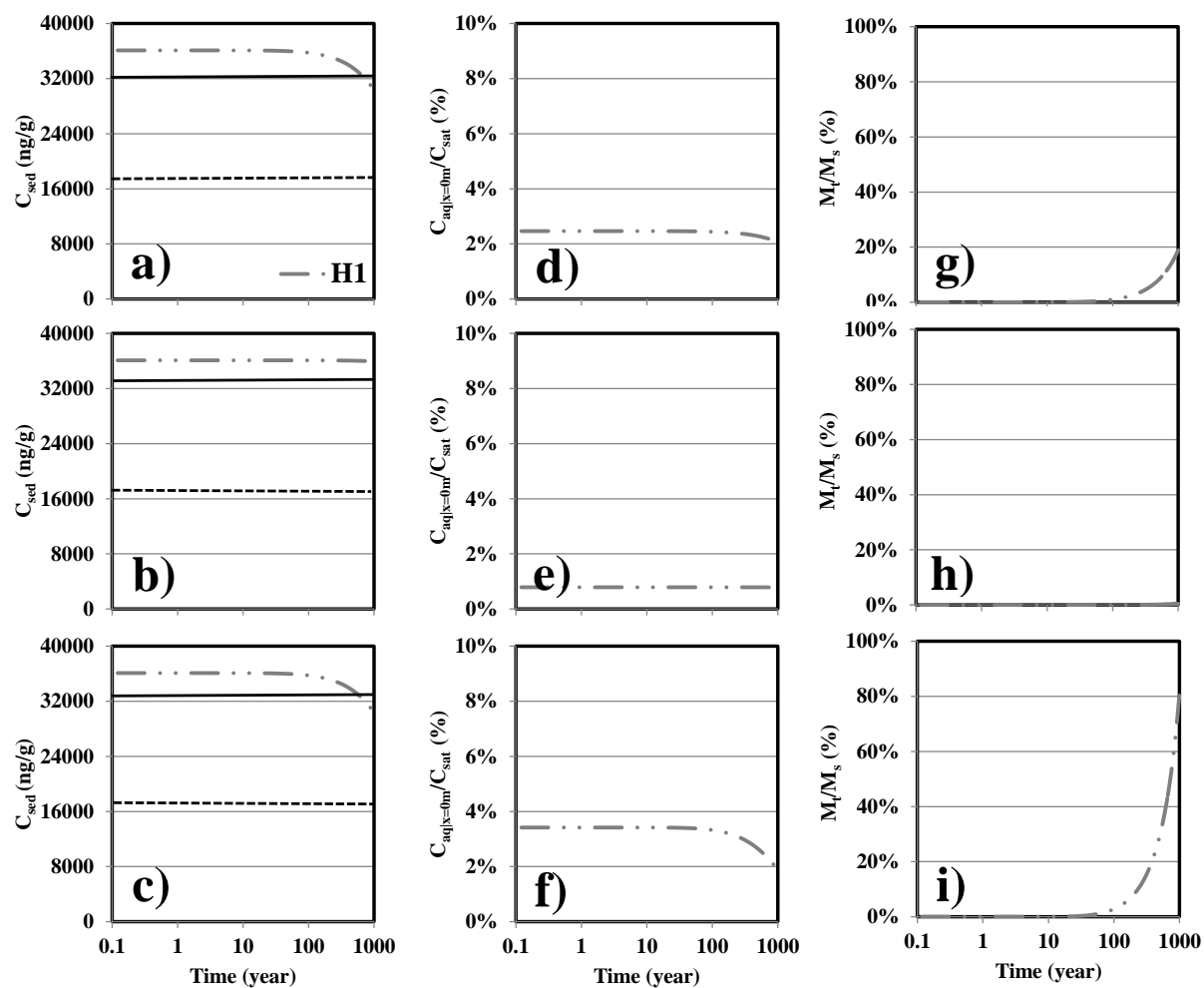


Figure 5.23b: PBDE homolog 1 sediment concentration (C_{sed}) (a-c), percent porewater saturation ($C_{aq|x=0m}/C_{sat}$) (d-f), and fraction of mass leaving the sediment boundary layer relative to initial starting mass (M_t/M_{sed}) (g-i) as a function of time in cores AJL (a,d,g), AMW (b,e,h), and AOT (c,f,i) as predicted by the Monte Carlo 95th percentile transport parameters values under advection-diffusion with organic carbon only sorption (A(OC)) mass transport condition.

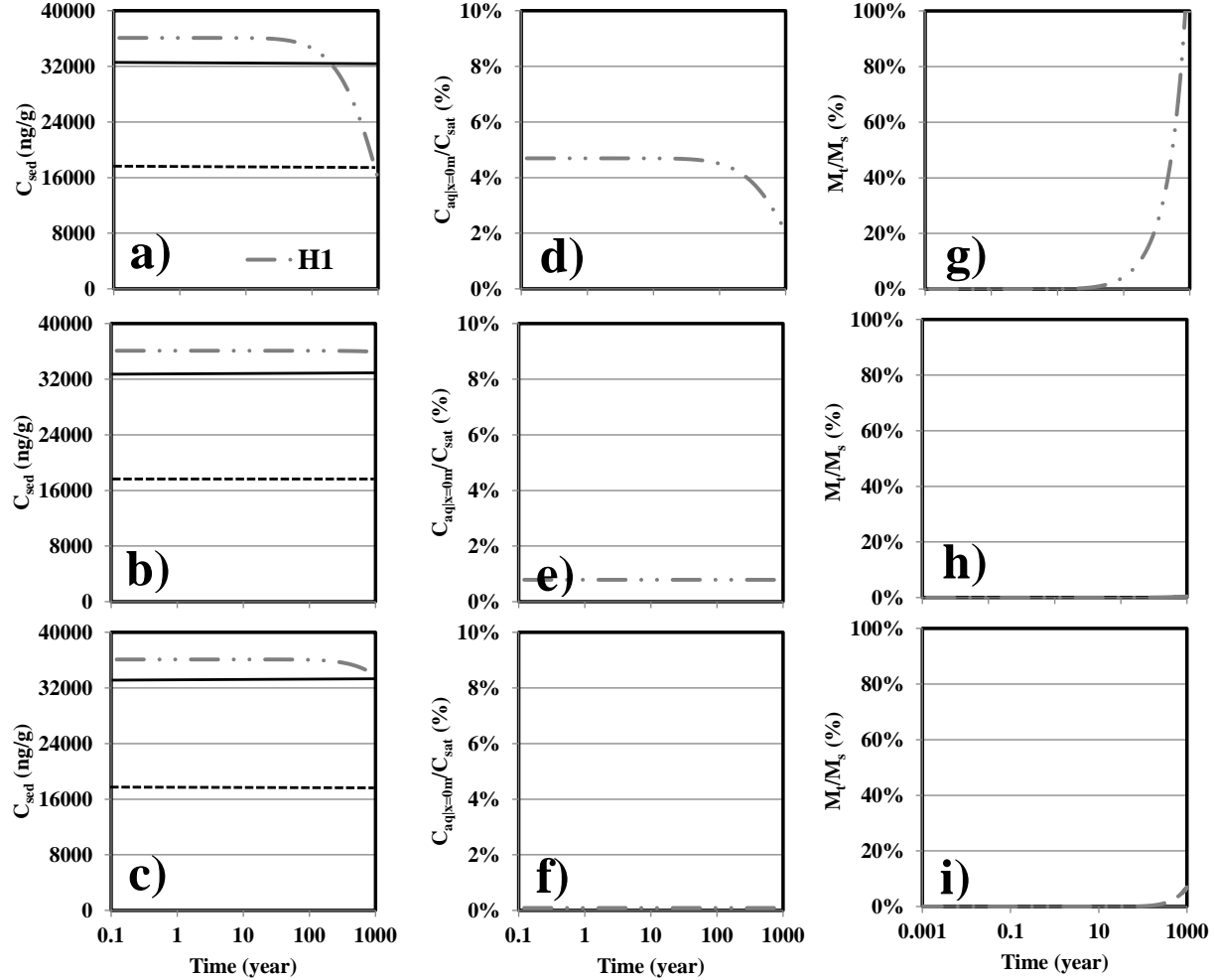


Figure 5.23c: PBDE homolog 1 sediment concentration (C_{sed}) (a-c), percent porewater saturation ($C_{aq|x=0m}/C_{sat}$) (d-f), and fraction of mass leaving the sediment boundary layer relative to initial starting mass (M_t/M_{sed}) (g-i) as a function of time in cores CBC (a,d,g), CLC (b,e,h), and CWP (c,f,i) as predicted by the Monte Carlo 95th percentile transport parameters values under advection-diffusion with organic carbon only sorption (A(OC)) mass transport condition.

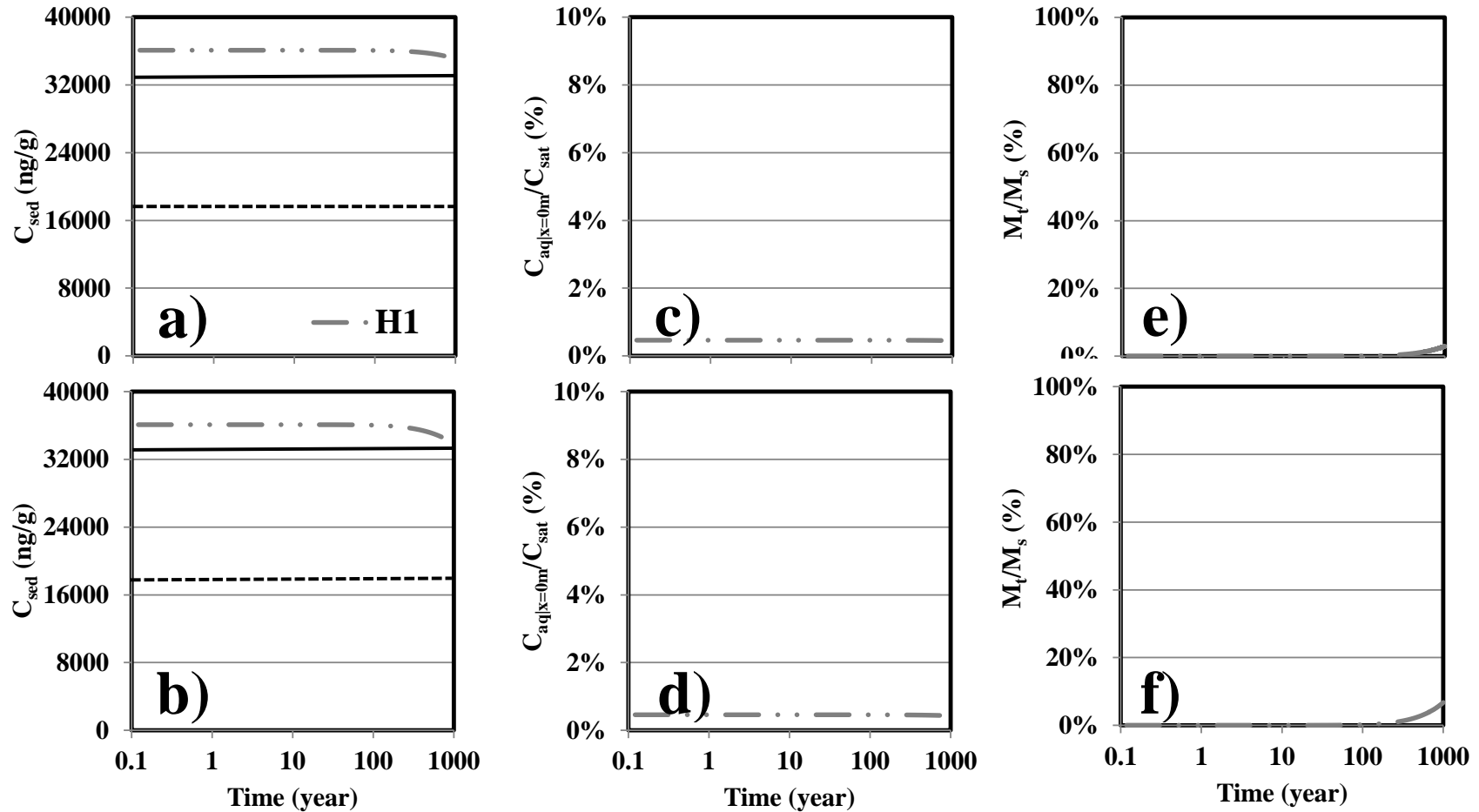


Figure 5.23d: PBDE homolog 1 concentration (C_{sed}) (a-c), percent porewater saturation ($C_{aq|x=0m}/C_{sat}$) (d-f), and fraction of mass leaving the sediment boundary layer relative to initial starting mass (M_t/M_{sed}) (g-i) as a function of time in cores IGC09 (a,c,e) and IGC13 (b,d,f), and CWP (c,f,i) as predicted by the Monte Carlo 95th percentile transport parameters values under advection-diffusion with organic carbon only sorption (A(OC)) mass transport condition.

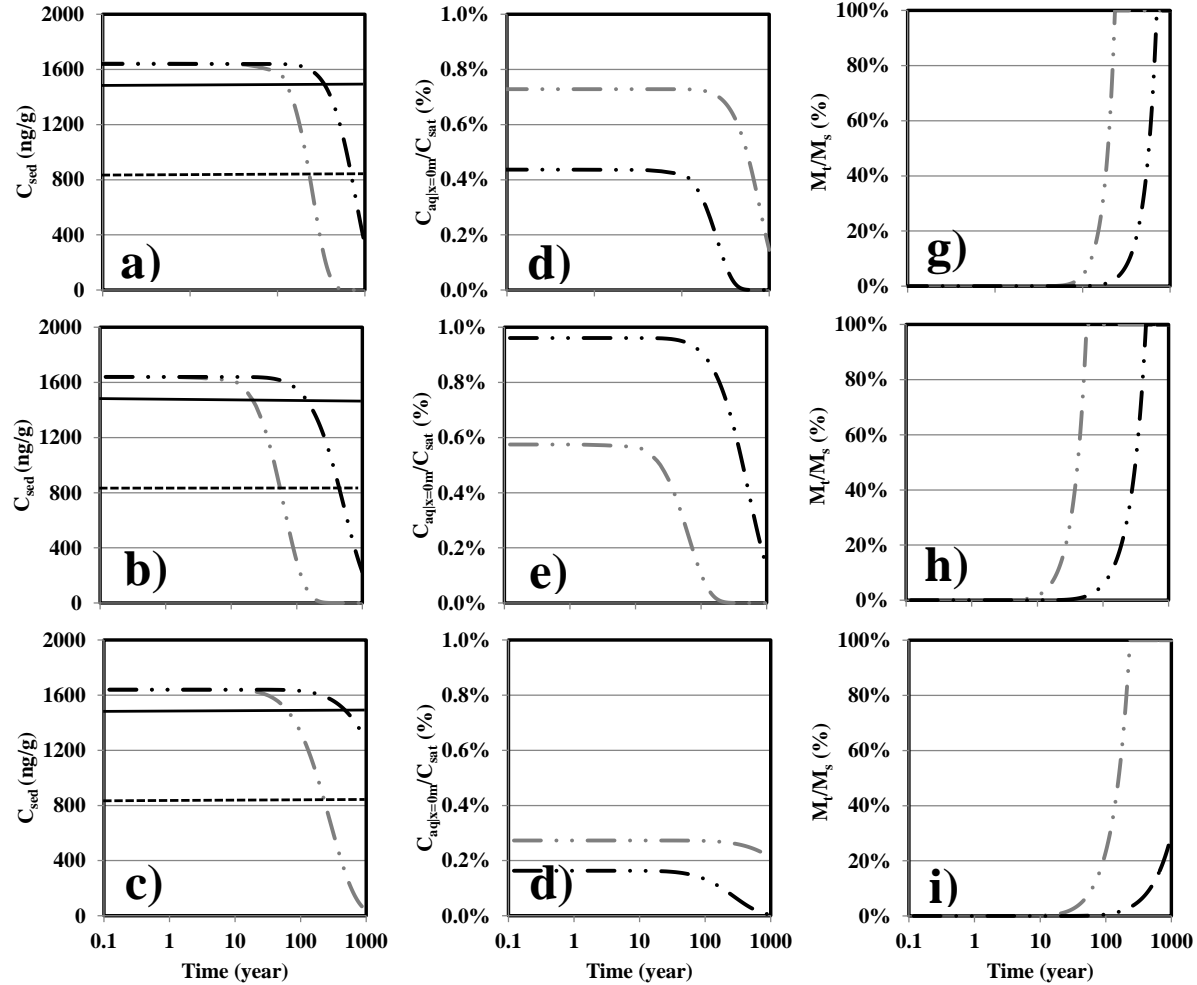


Figure 5.23e: PCB homologs 1 and 2 sediment concentration (C_{sed}) (a-c), percent porewater saturation ($C_{aq|x=0m}/C_{sat}$) (d-f), and fraction of mass leaving the sediment boundary layer relative to initial starting mass (M_t/M_{sed}) (g-i) as a function of time in cores ACL (a,d,g), AED (b,e,h), and AFR (c,f,i) as predicted by the Monte Carlo 95th percentile transport parameters values under advection-diffusion with organic carbon only sorption (A(OC)) mass transport condition.

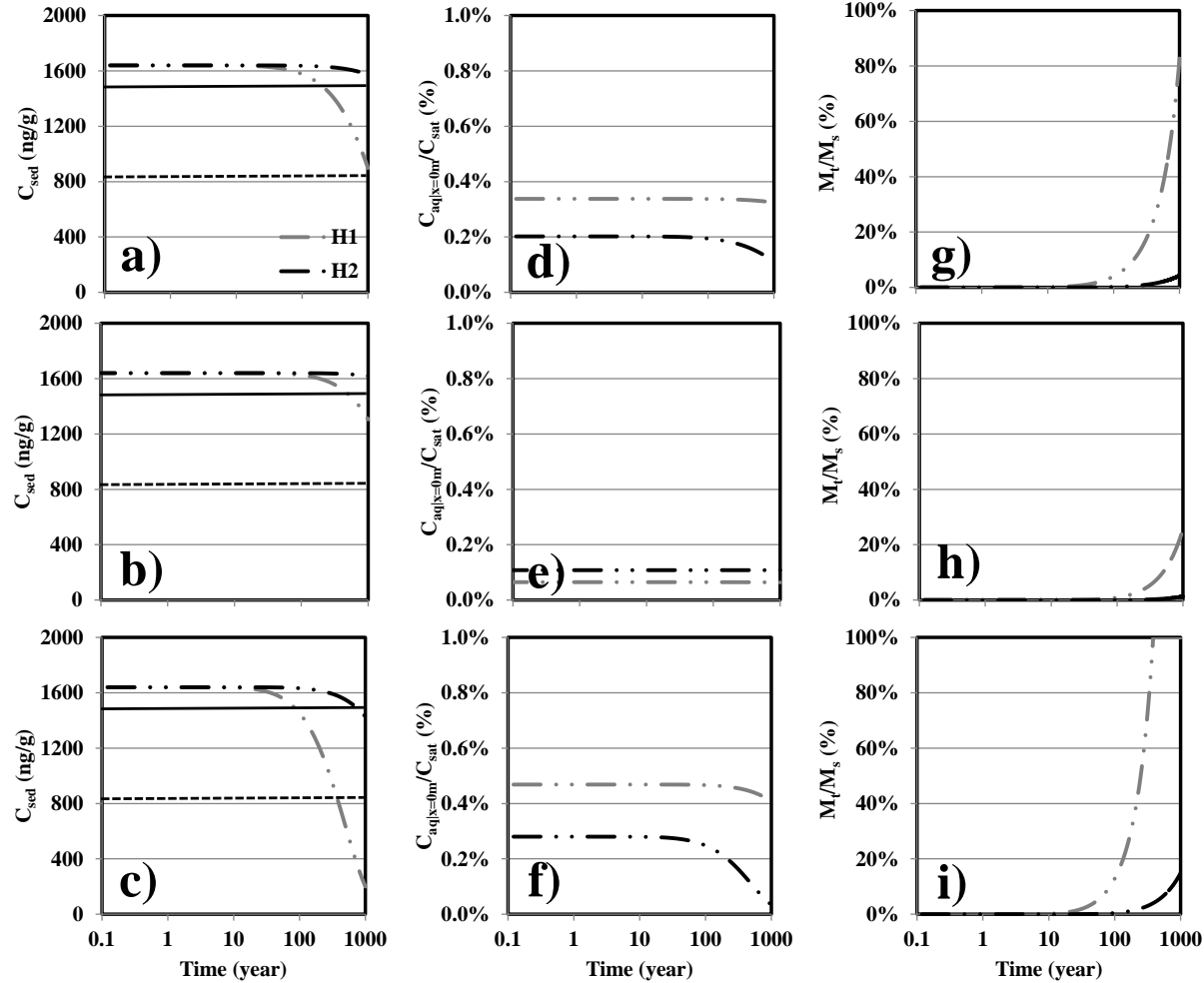


Figure 5.23f: PCB homologs 1 and 2 sediment concentration (C_{sed}) (a-c), percent porewater saturation ($C_{aq|x=0m}/C_{sat}$) (d-f), and fraction of mass leaving the sediment boundary layer relative to initial starting mass (M_t/M_{sed}) (g-i) as a function of time in cores AJL (a,d,g), AMW (b,e,h), and AOT (c,f,i) as predicted by the Monte Carlo 95th percentile transport parameters values under advection-diffusion with organic carbon only sorption (A(OC)) mass transport condition.

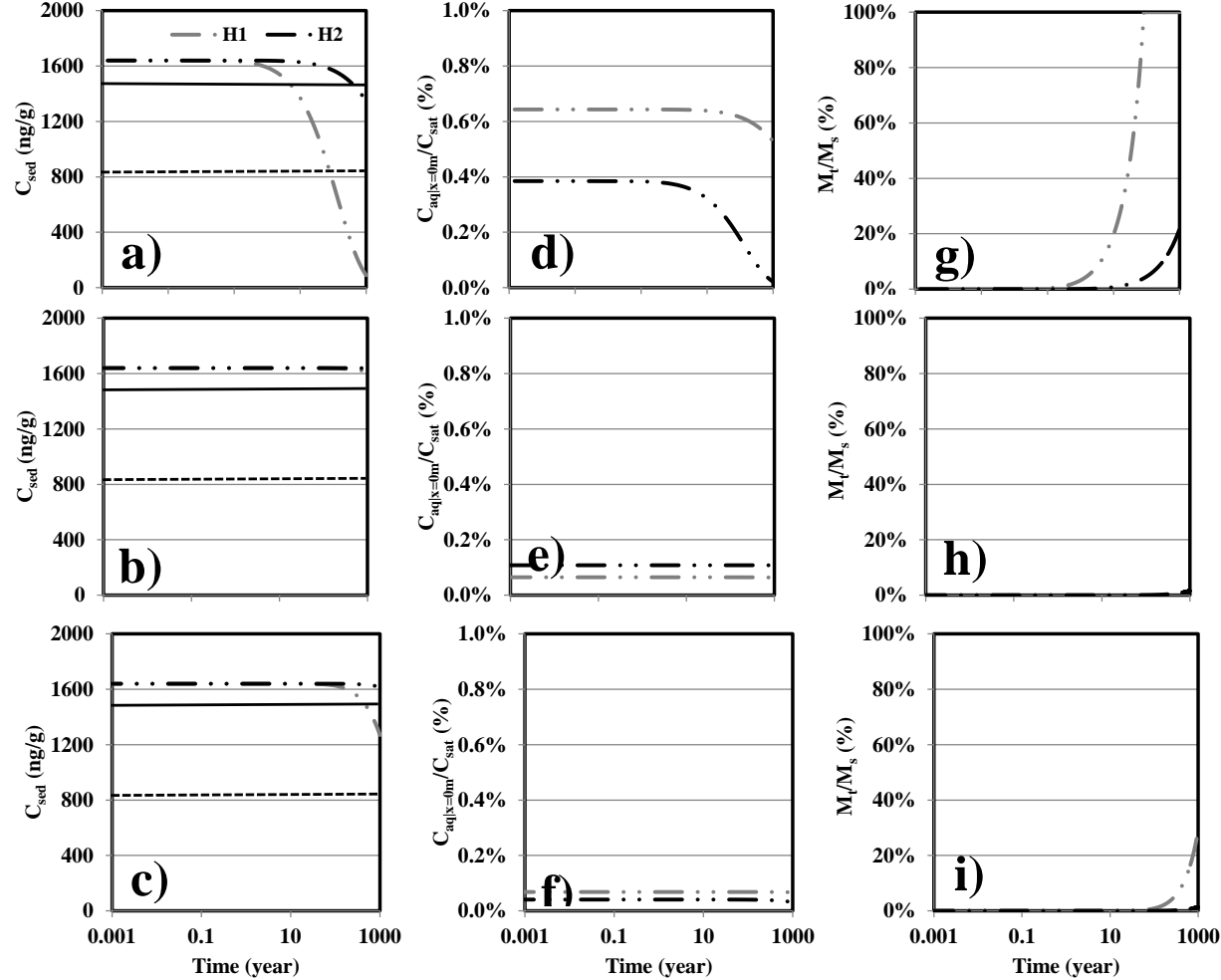


Figure 5.23g: PCB homologs 1 and 2 sediment concentration (C_{sed}) (a-c), percent porewater saturation ($C_{aq|x=0m}/C_{sat}$) (d-f), and fraction of mass leaving the sediment boundary layer relative to initial starting mass (M_t/M_{sed}) (g-i) as a function of time in cores CBC (a,d,g), CLC (b,e,h), and CWP (c,f,i) as predicted by the Monte Carlo 95th percentile transport parameters values under advection-diffusion with organic carbon only sorption (A(OC)) mass transport condition.

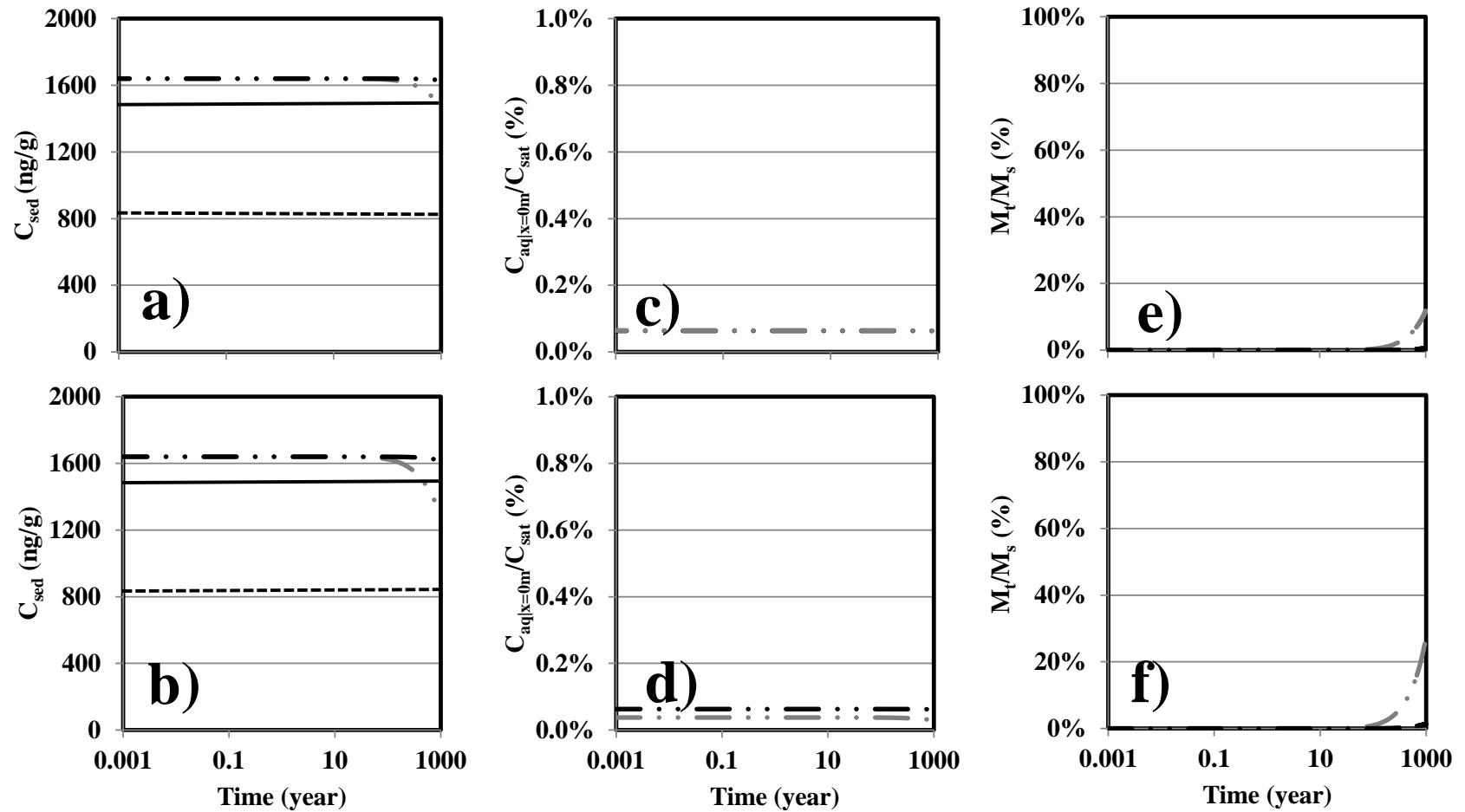


Figure 5.23h: PCB homologs 1 and 2 sediment concentration (C_{sed}) (a-c), percent porewater saturation ($C_{aq|x=0m}/C_{sat}$) (d-f), and fraction of mass leaving the sediment boundary layer relative to initial starting mass (M_t/M_{sed}) (g-i) as a function of time in cores IGC09 (a,c,e) and IGC13 (b,d,f), as predicted by the Monte Carlo 95th percentile transport parameters values under advection-diffusion with organic carbon only sorption (A(OC)) mass transport condition.

Transport limitation due to aqueous phase saturation. In core ACL, PBDE homologs 7 through 10 generally had no appreciable predicted $C_{aq|x=0.02m,t}$ values (i.e., predicted $C_{aq|x=0.02m,t} < 1\text{E-}10$ ng/L) at 40, 100, and 1000 years with PBDE 95th percentile initial sediment concentration. PBDE homologs 7 and 8 have upper end predicted $C_{aq|x=0.02m,t}$ of $>1\text{E-}2$ and $>1\text{E-}5$ ng/L at 1000 years. Although the predicted $C_{aq|x=0.02m,t}/C_{aq|x=0m,t=0}$ values at 1000 years transport time were less than 1% for PBDE homologs 7 through 10 in core ACL, the predicted $C_{aq|x=0m,t}/C_{sat}$ values were 100%. This is due to the fact that PBDE homologs 7 through 10 have very low C_{sat} and the high initial sediment in the core and simulation provided led to $C_{aq|x=0m,t} = C_{sat}$. Although the porewater was at saturation, the low rate of A(OC) transport, as inferred by low D_{obs} and v values for PBDE homologs 7 through 10 led to no appreciable difference in M_{it} for 40 and 100 years. At 1000 years, PBDE homologs 7 and 8 have M_{it} of $>2\text{E-}3$ and $>1\text{E-}6$ ng/m²; however, these values were less than 1% of the initial M_{sed} . Sediment phase contaminant concentration does play a role in PBDE and PCB in-situ mass flux as it dictates the LEA contaminant porewater concentration. Higher C_{sed} results in higher $C_{aq|x=0m,t}$ which can promote a higher cumulative M_i fluxes from the sediment segment via the aqueous phase. The upper limit of contaminant absorption to porewater is $C_{sat} \cdot C_{sed}$ which resulted in $C_{aq|x=0m,t} = C_{sat}$ at the 5th, 50th, and 95th percentile predicted by log K_d (OC) and log K_d (OCBC) values were back calculated and summarized in Figure 5.24a-e and Table D5.10. PBDE and PCB concentrations at or higher than the C_{sed} estimated in Figure 5.24a-e and Table D5.10 will not experience accelerated or enhanced in-situ sediment transport; rather the magnitude of the in-situ sediment transport is similar to the magnitude at $C_{aq|x=0m,t} = C_{sat}$ which is the maximum magnitude and rate of in-situ sediment transport. The modeling in this chapter ensures that $C_{aq|x=0m,t} \leq C_{sat}$ to respect PBDE and PCB mass transport limitations.

The increased solid phase partitioning under OCBC co-sorption consideration resulted in relatively lower log K_d (OCBC) values compared to log K_d (OC). Therefore C_{sed} values predicted to result in $C_{aq|x=0m,t} = C_{sat}$ under OCBC co-sorption were higher compared to OC only sorption. Overall, PCBs were predicted to require larger C_{sed} values relative to PBDEs in order to reach the $C_{aq|x=0m,t} = C_{sat}$ condition.

Although PCB C_{sat} values were larger than PBDE C_{sat} values, PBDEs are more hydrophobic than PCBs and thus, have an increased affinity for solid phase partitioning. With increasing PBDE and PCB homologs, the range of C_{sed} values as predicted from the 5th and 95th percentile $\log K_d$ values were larger reflecting the increased uncertainty of $\log K_{ow}$ values of large PBDE and PCB homologs (Table 5.1). The impact of uncertainty on mass flux predictions was very pronounced for HMW PBDE homologs, as these homologs carry larger associated uncertainty compared to their counterpart PCB homologs. Under OCBC co-sorption, PBDE and PCB C_{sed} values predicted to achieve the $C_{aq/x=0m}=C_{sat}$ condition shared a similar trend of increasing C_{sed} values with increasing PBDE and PCB homologs. This trend was also observed in LMW PBDE and PCB homologs; however, PBDE and PCB C_{sed} values predicted to achieve the $C_{aq/x=0m}=C_{sat}$ condition decreased for HMW PBDE and PCB homologs. The predicted C_{sed} values were a function of C_{sat} and K_d . Under OCBC co-sorption, PBDE and PCB $\log K_d$ (OCBC) values consistently increased at a faster rate than C_{sat} decline. This is also true for small PBDE and PCB homologs under OC only sorption; however, in large PBDE and PCB homologs, the decline in C_{sat} values were occurring at a faster rate than the increase of $\log K_d$ (OC) values rendering lower predicted C_{sed} values.

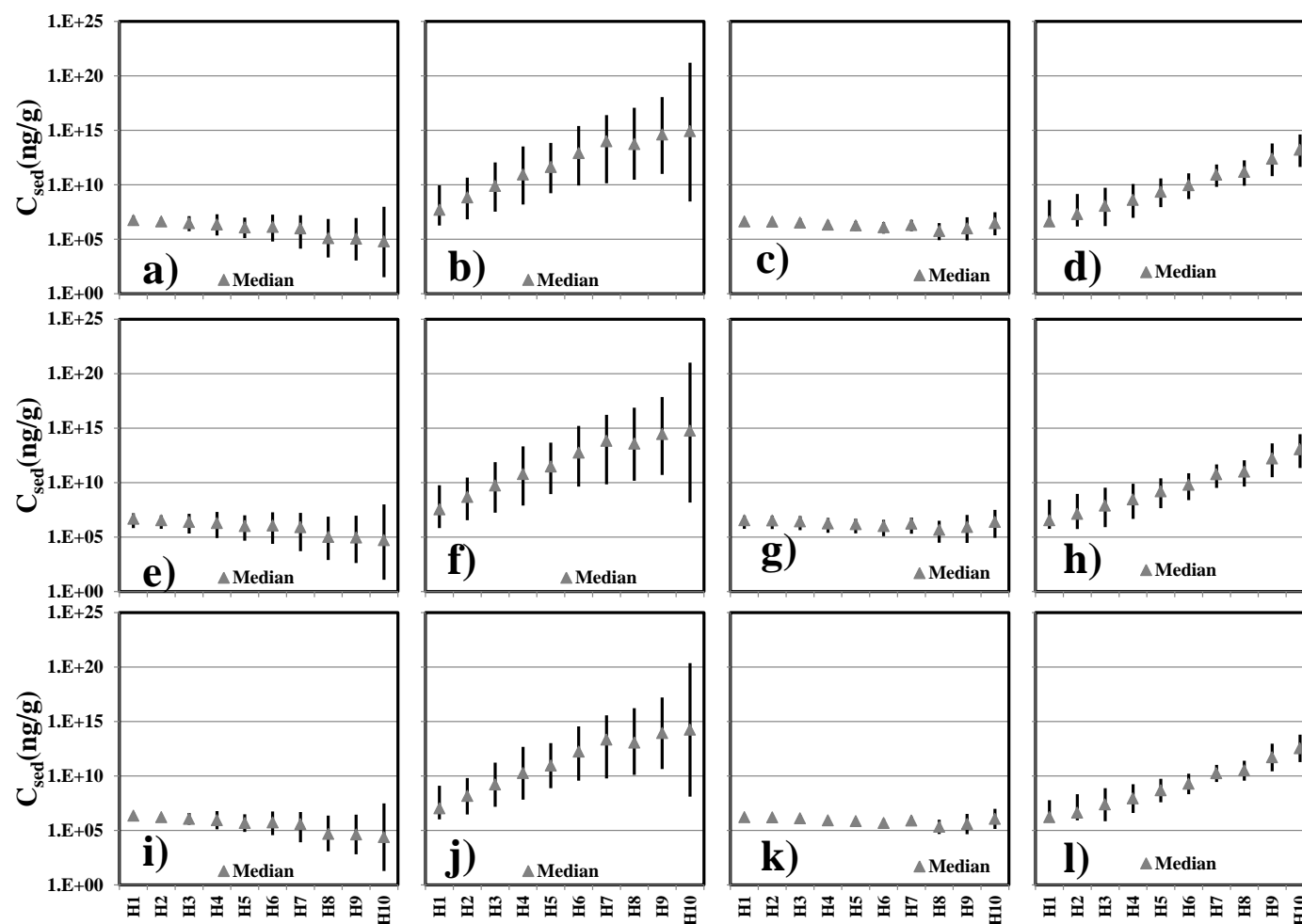


Figure 5.24a: Sediment phase concentrations (C_{sed}) of PBDE (a-b, e-f, i-j) and PCB (c-d, g-h, k-l) homologs that result in local equilibrium aqueous phase concentration equals to saturation concentration ($C_{aq|x=0m}=C_{sat}$) predicted from sediment-porewater partitioning coefficient for organic carbon only sorption ($K_d(OC)$) (PBDEs: a,e,i ; PCBs: c,g,k) and organic carbon and black carbon co-sorption ($K_d(OCBC)$) (PBDEs: b,f,j ; PCBs: d,h,l) at the 5th, 50th, and 95th percentile values in cores ACL(a-d), AED (e-h), and AFR (i-l). C_{sed} values predicted from the 50th percentile log K_d values are marked by the grey triangle and C_{sed} values predicted from the 5th and 95th percentile are shown as the bold vertical lines.

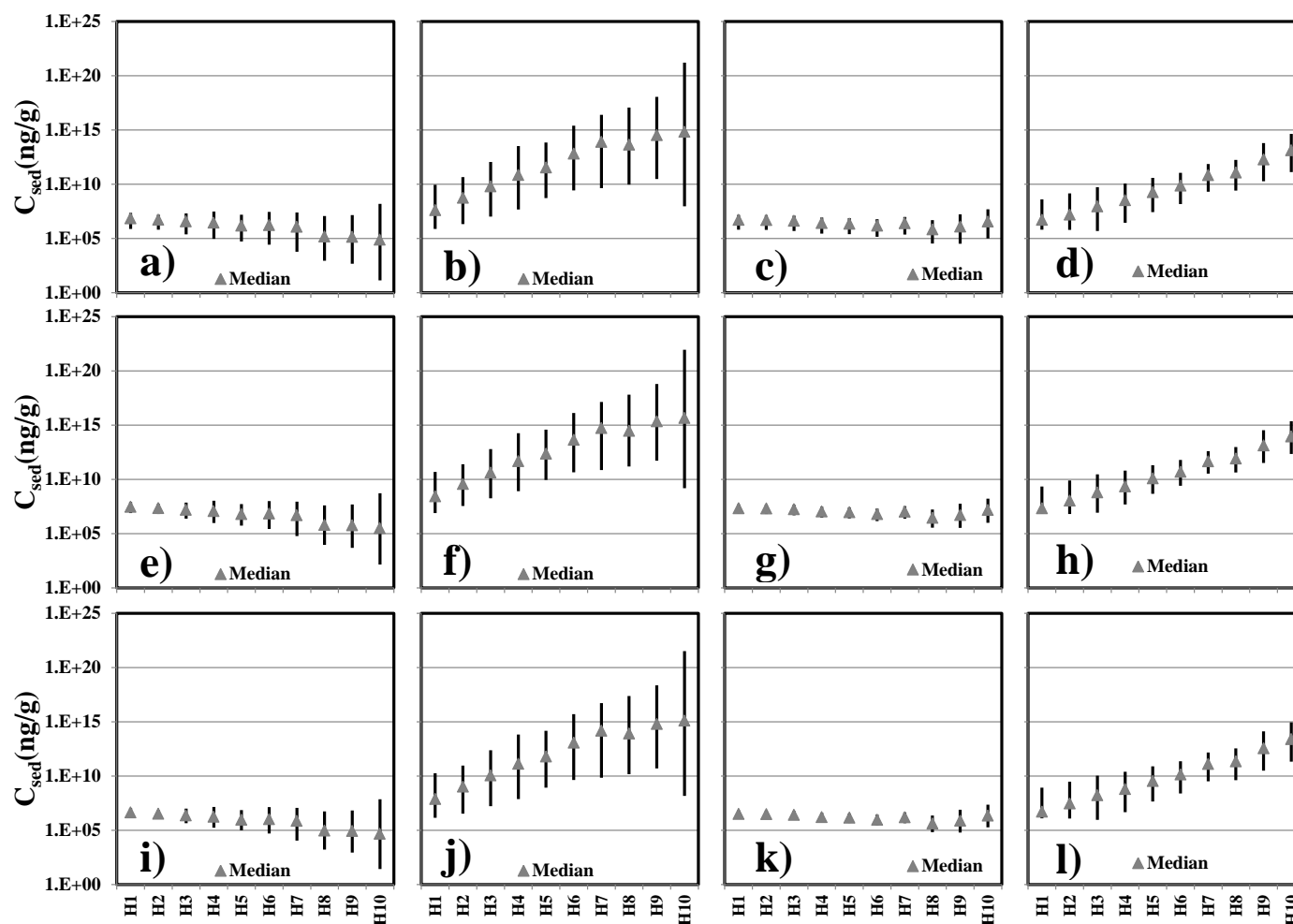


Figure 5.24b: Sediment phase concentrations (C_{sed}) of PBDE (a-b, e-f, i-j) and PCB (c-d, g-h, k-l) homologs that result in local equilibrium aqueous phase concentration equals to saturation concentration ($C_{aq|x=0m}=C_{sat}$) predicted from sediment-porewater partitioning coefficient for organic carbon only sorption ($K_d(OC)$) (PBDEs: a,e,i ; PCBs: c,g,k) and organic carbon and black carbon co-sorption ($K_d(OCBC)$) (PBDEs: b,f,j ; PCBs: d,h,l) at the 5th, 50th, and 95th percentile values in cores AJL(a-d), AMW (e-h), and AOT (i-l). C_{sed} values predicted from the 50th percentile log K_d values are marked by the grey triangle and C_{sed} values predicted from the 5th and 95th percentile are shown as the bold vertical lines.

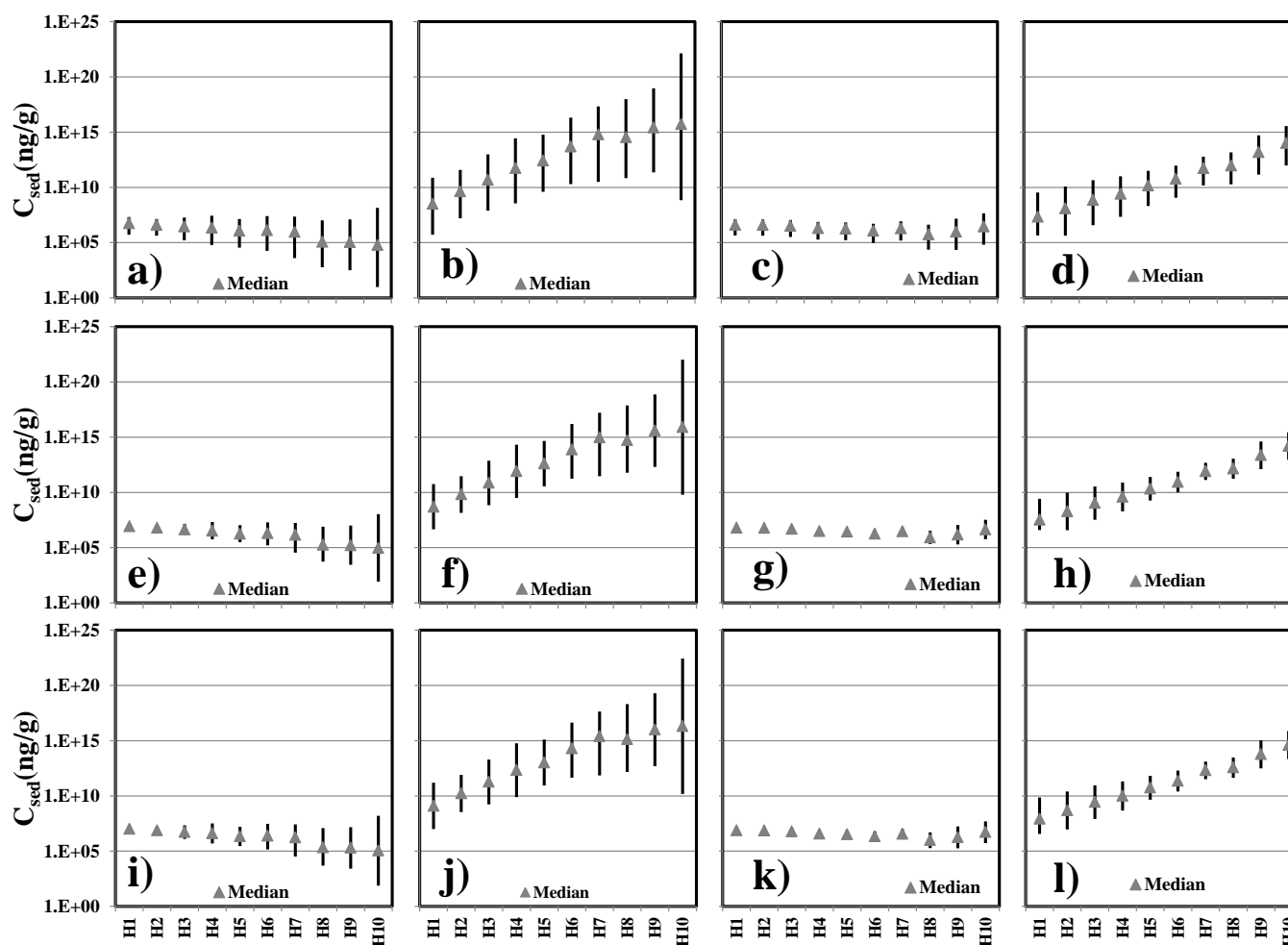


Figure 5.24c: Sediment phase concentrations (C_{sed}) of PBDE (a-b, e-f, i-j) and PCB (c-d, g-h, k-l) homologs that result in local equilibrium aqueous phase concentration equals to saturation concentration ($C_{aq|x=0m}=C_{sat}$) predicted from sediment-porewater partitioning coefficient for organic carbon only sorption ($K_d(OC)$) (PBDEs: a,e,i ; PCBs: c,g,k) and organic carbon and black carbon co-sorption ($K_d(OCBC)$) (PBDEs: b,f,j ; PCBs: d,h,l) at the 5th, 50th, and 95th percentile values in cores CBC(a-d), CLC (e-h), and CWP (i-l). C_{sed} values predicted from the 50th percentile log K_d values are marked by the grey triangle and C_{sed} values predicted from the 5th and 95th percentile are shown as the bold vertical lines.

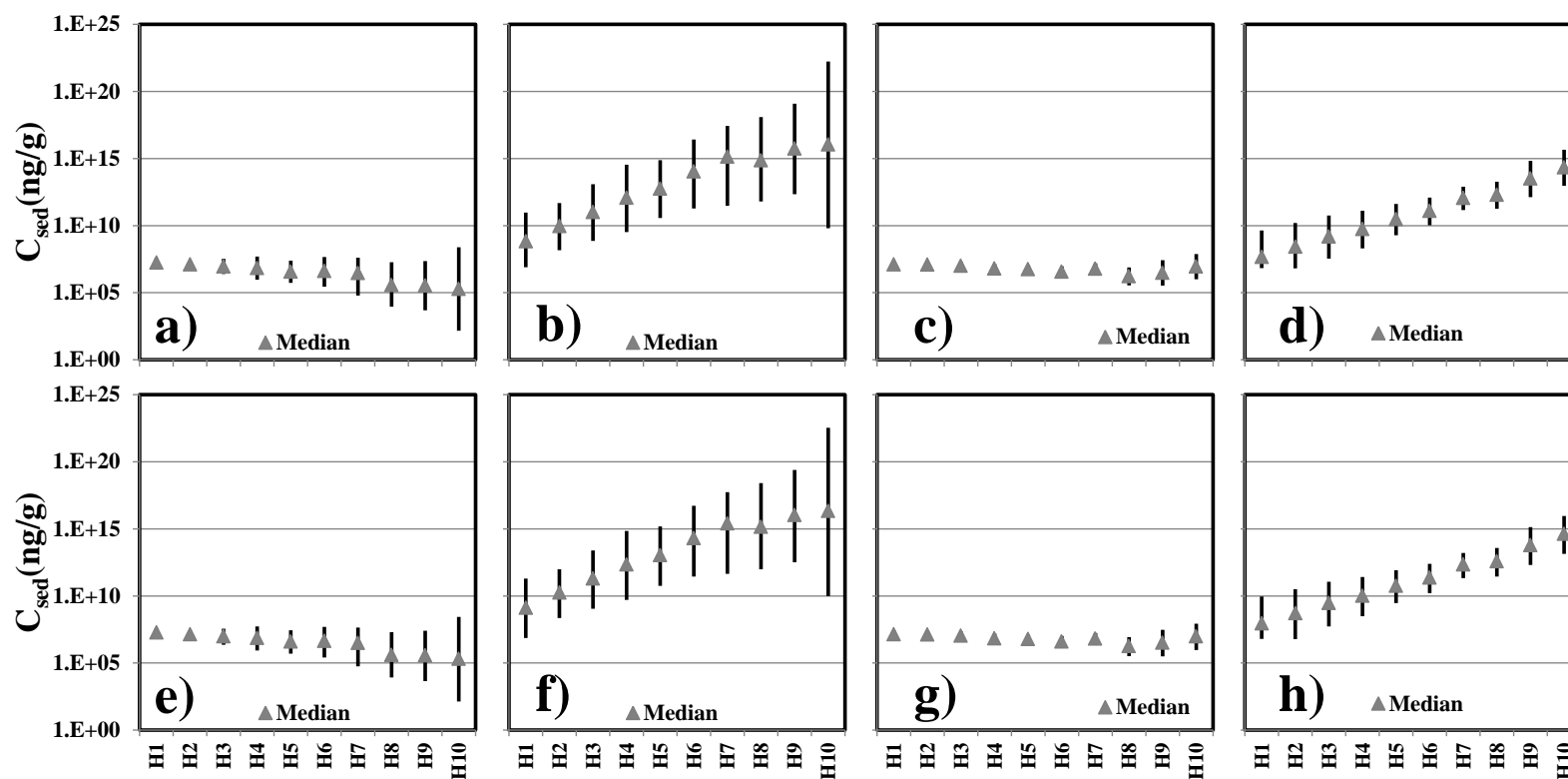


Figure 5.24d: Sediment phase concentrations (C_{sed}) of PBDE (a-b, e-f, i-j) and PCB (c-d, g-h, k-l) homologs that result in local equilibrium aqueous phase concentration equals to saturation concentration ($C_{aq|x=0m}=C_{sat}$) predicted from sediment-porewater partitioning coefficient for organic carbon only sorption ($K_d(OC)$) (PBDEs:a,e,i ; PCBs: c,g,k) and organic carbon and black carbon co-sorption ($K_d(OCBC)$) (PBDEs:b,f,j ; PCBs: d,h,l) at the 5th, 50th, and 95th percentile values in cores IGC09(a-d) and IGC13 CLC (e-h). C_{sed} values predicted from the 50th percentile log K_d values are marked by the grey triangle and C_{sed} values predicted from the 5th and 95th percentile are shown as the bold vertical lines.

Drivers of PBDE and PCB Mass Flux. Overall, the results of PBDE and PCB homolog mass flux simulations shown in Figure 5.22a-l followed trend in predicted C/C_o under A(OC) mass transport, where the magnitude increased in the order of CLC < IGC09 < CWP < AMW < IGC13 < AJL < AOT < CBC < AFR < AED < ACL. PCA analysis suggested that although f_{OC} , f_{BC} , and K_h cannot entirely predict the magnitude of PBDE and PCB mass flux in the sediment columns, these parameters are important drivers in D(OC), D(OCBC), A(OC), and A(OCBC). In the case of A(OC) mass simulations as shown in Chapter 5.5, f_{OC} and K_h are the important drivers. In Figure 5.25, the magnitude of PBDE homolog 1 and PCB homologs 1 and 2 under A(OC) transport process at 40, 100, and 1000 years are shown to have substantial mass removal over a period of 1000 years (>20%, ad-hoc value). Overall, the mass flux magnitude increased in the order of PCB homolog 2 < PBDE homolog 1 < PCB homolog 1. From Figure 5.25, it can be seen that a combination of high K_h and high f_{OC} as seen in cores ACL and AED resulted in high amounts of PBDE homolog 1 and PCB homologs 1 and 2 removal. In general, f_{OC} values >0.1 substantially retard the A(OC) mass flux. Figure 5.25 showed M_{it}/M_{sed} values decreased at a faster rate with increased f_{OC} values compared to decreased K_h values indicating that PBDE and PCB mass transport in sediment columns are more sensitive to variation in f_{OC} values.

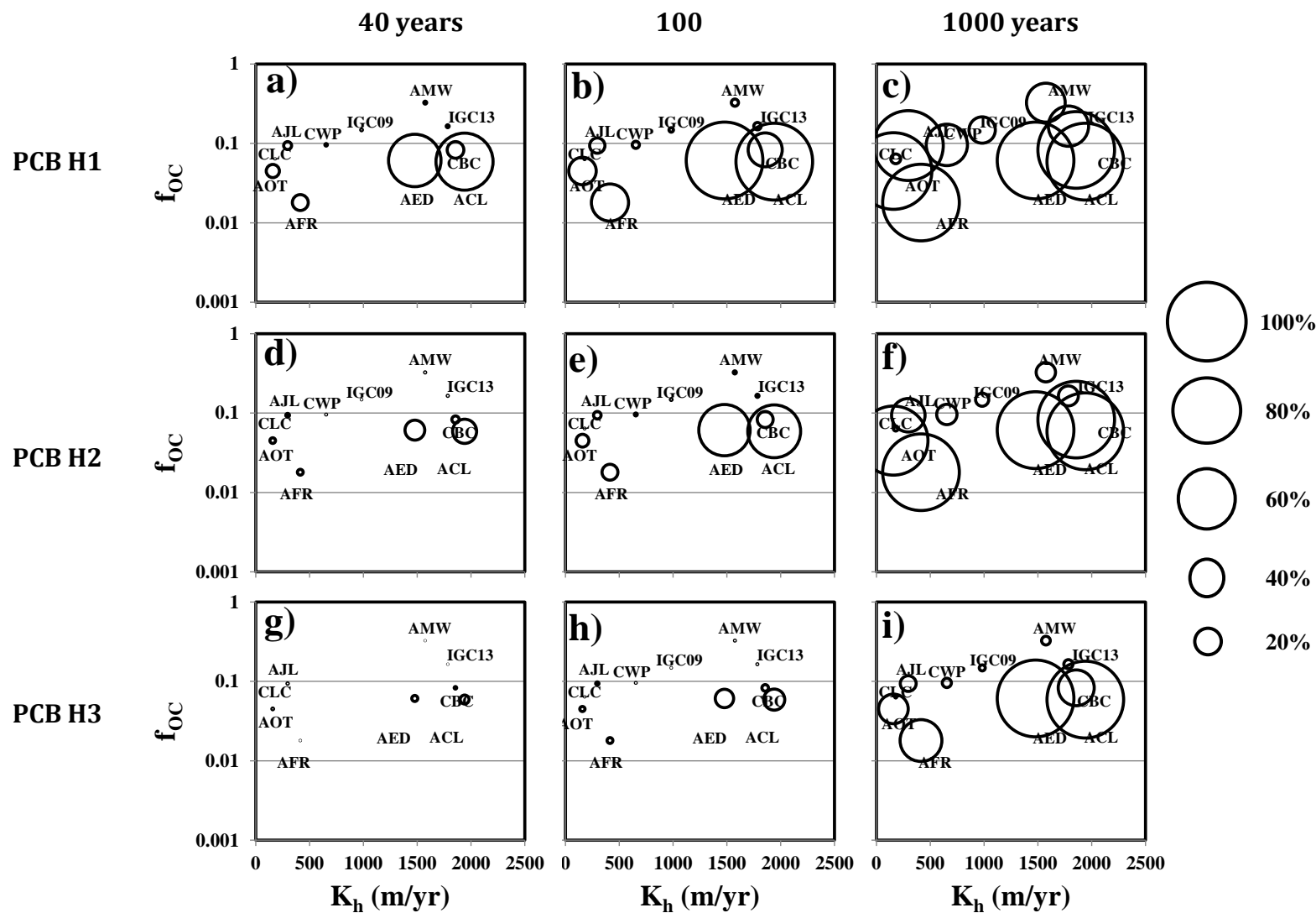


Figure 5.25: The fraction of PCB homolog 1 (a-c), PBDE homolog 1 (d-f), and PCB homolog 2 (g-i) leaving the sediment segment relative to initial sediment concentration at the 95th percentile concentration (1640 and 36100 ng/g for PCB homologs 1 and 2, and PBDE homolog 1, respectively) ($M_t/M_{sed|t=0year}$) in all sediment cores at 40 (a,d,g), 100 (b,e,h) and 1000 (c,f,i) years. Size of the hollow circle represent the % $M_t/M_{sed|t=0year}$.

5.6. The Impact of PBDE and PCB In-Situ Mass Flux On Sediment Contaminant Profile

Thus far, the modeling effort presented in this chapter indicated that PBDE homolog 1 and PCB homologs 1 and 2 in cores ACL, AED, AFR, AJL, and CBC can exhibit substantial in-situ mass flux under the A(OC) mass transport process ($>20\% \ M_{i|t} / M_{sed|t=0 \text{ year}}$) at 1000 years simulation condition period. Previously, in Section 5.4, the A(OC) was determined to simulate the most mobile mass transport scenario. It is of interest to evaluate if the *in-situ* mass transport of PBDE and PCB homologs under the most mobile conditions is sufficient to shift the distribution of the actual sediment concentration profile towards the observed sediment profiles. In this analysis, PBDE transport simulations were limited to cores ACL, AED, AMW, CBC, CLC, CWP, and IGC13 as radionuclide dating data were only available for these eight cores. PCB transport simulations were limited to core AMW, CBC, CLC, CWP, and IGC13 only as PCB concentration with depth data are only characterized for these six cores.

In order to understand how something has changed temporally, we need a point of reference for comparison of sufficiently long duration to result in possibly significant transport. This objective was achieved by fitting the observed PBDE and PCB congener data to a linear mixing model (LMM) using PBDE TMs and PCB Aroclors. Initially, the difference in sediment contaminant profile in the selected cores from PBDE TMs and PCB Aroclors were quantified by employing MLSR analysis. For PBDEs, the sediment contaminant profile (in molar composition) at each sediment depth was regressed simultaneously against DE-71, DE-79, and Saytex 102E. For PCBs, simultaneous regression was performed against Aroclors 1016, 1248, 1254 and 1260. Previously, whole core average MLSR against five Aroclors (Aroclors 1016, 1242, 1248, 1254, and 1260) indicated that Aroclor 1242 did not have significant contribution in any of the five selected cores and was therefore excluded from the depth specific MLSR analysis (Table 3.5). In the MLSR analysis, the coefficients represent the fraction of TMs or Aroclors that contributed towards the sediment contaminant profile and the residuals quantify the

difference between the sediment contaminant profile and the LMM mixed TM or Aroclor profiles. The TM or Aroclor coefficients and residuals, as predicted by MLSR analysis are shown in Figure 5.25a-c.

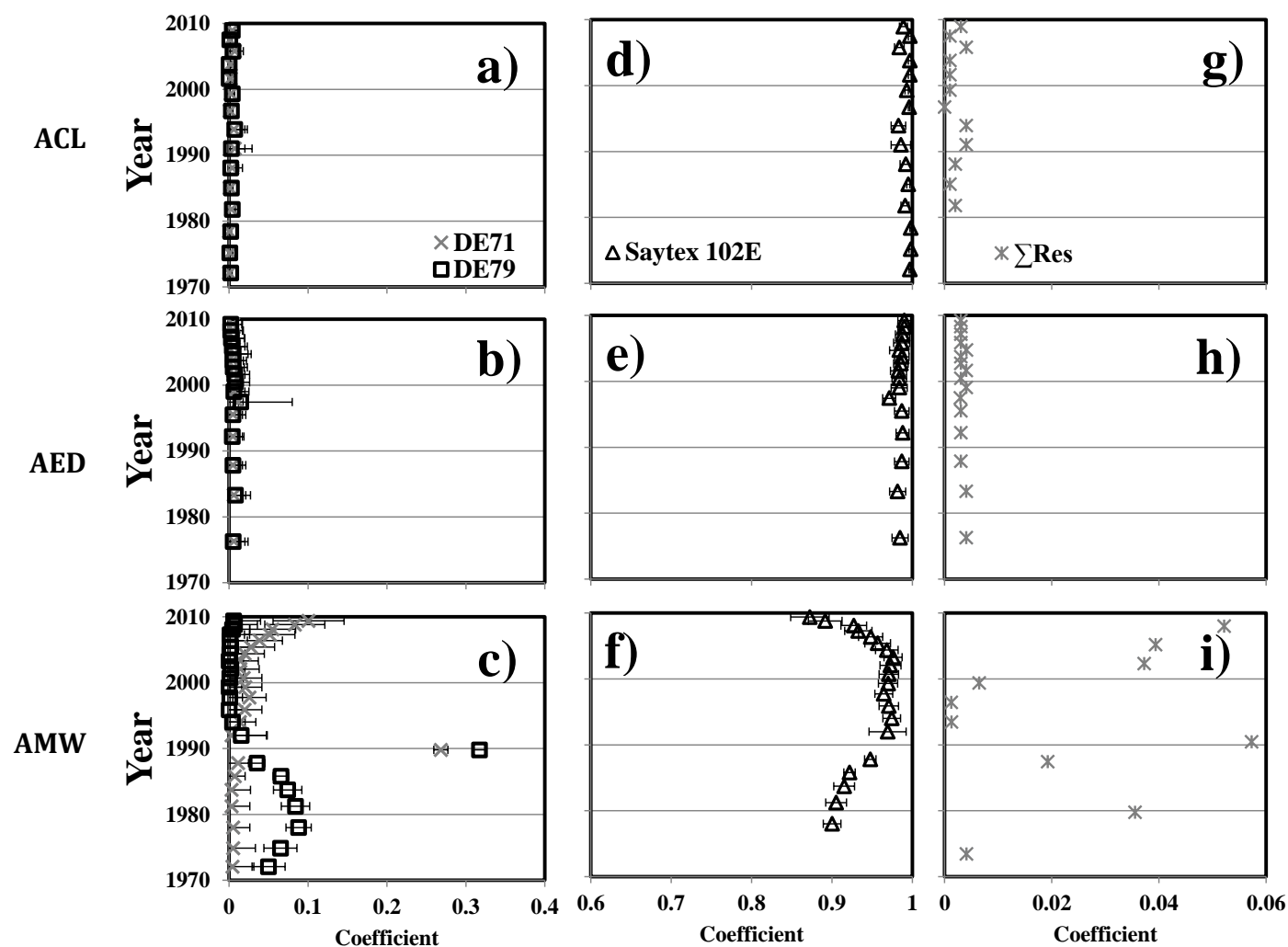


Figure 5.25a: DE-71 and DE-79 (a-c), and Saytex 102E (d-f) coefficients and residual (ΣRes) (g-i) as determined by multivariate least square regression analysis for cores ACL (a,d,g), AED (b,e,h), and AMW (c,f,i).

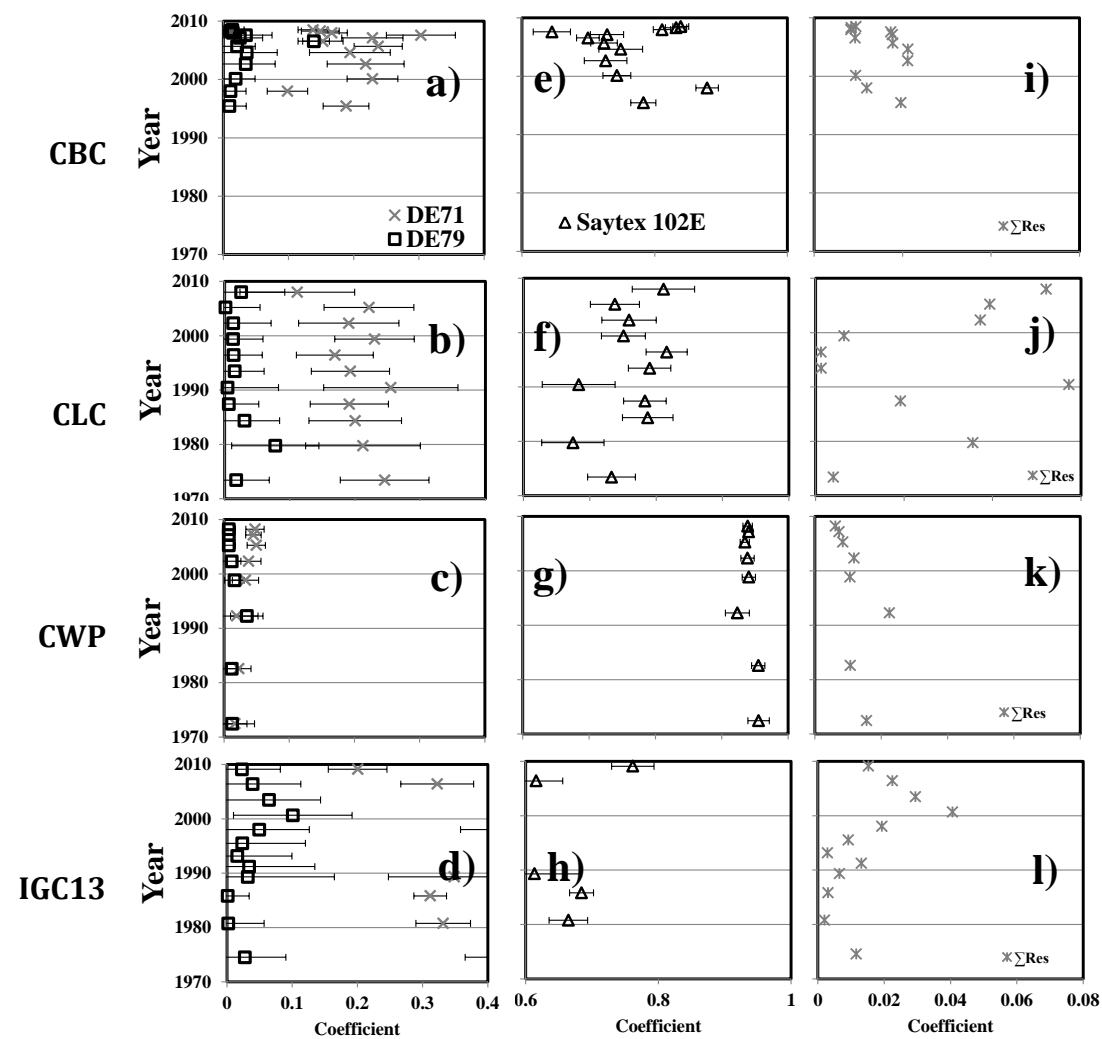


Figure 5.25b: DE-71 and DE-79 (a-h), and Saytex 102E (e-h) coefficients and residuals (ΣRes) (i-l) as determined by multivariate least square regression analysis for cores CBC (a,e,i), CLC (b,f,j), CWP (c,g,k) and IGC13 (d,h,l).

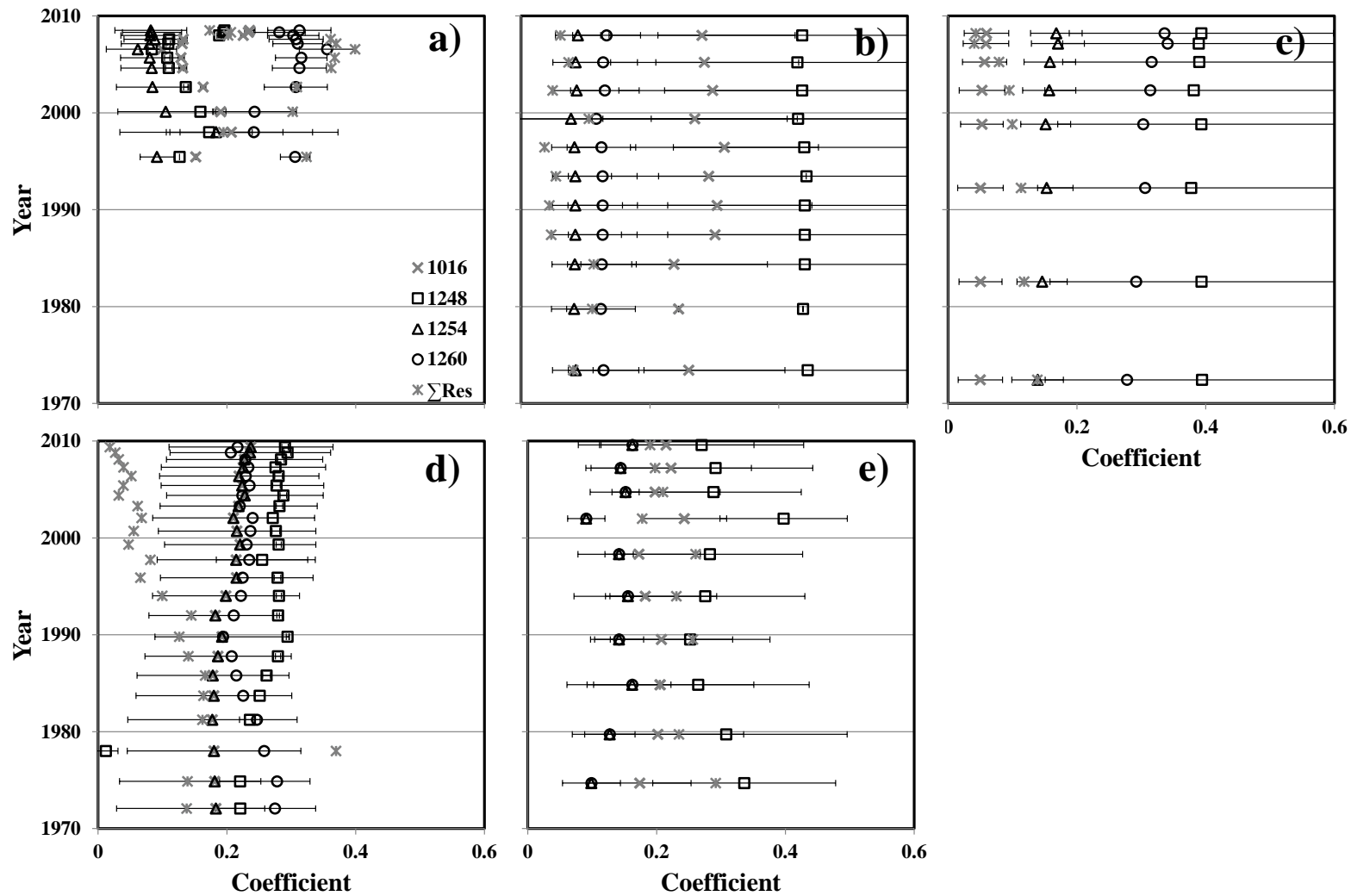


Figure 5.25c: Aroclors 1016, 1248, 1254, and 1260 coefficients and residuals (Σ Res) (g-i) as determined by multivariate least square regression analysis for cores a)CBC, b) CLC, c) CWP,d) AMW , and e)IGC13.

Sediment characterization described in Chapter 3 showed that the \sum_{49} PBDEs compositions in all the sediment cores were dominated by H10 (BDE-209). The MLSR analysis showed that Saytex 102E TM composed primarily of BDE-209 had a much higher contribution relative to DE-71 and DE-79 TMs at all sites and core depths (Figure 5.25a-b). In Table 5.13, whole core MLSR analysis results are compared to multivariate least median square (MLMS). With the MLMS method, the median of squared residuals are minimized to estimate the regression coefficients rendering it more robust against outlier in the dependent and independent variables. Analysis compared homolog composition and z-transformed homolog composition. With the z-transformation, the homolog composition is normalized with respect to homolog 10 (BDE-209) composition to reduce the weighting of BDE-209 on the regression analysis. Generally, the more robust regression analysis increased the Saytex102E TM contributions only slightly. There were also increased in DE-71 TM contribution in the sediment cores, albeit not substantial (<5%). The more robust regression analyses under-predicted the contribution of DE-79 TM. The predicted contributions of DE-71 and DE-79 TMs from homolog composition MLSR do not vary substantially from the predicted contributions of DE-71 and DE-79 TMs from homolog composition MLMS and z-transformed homolog composition of MLSR and MLMS analyses. Additionally, the contributions of Saytex 102E were more closely predicted by the homolog composition MLSR. Overall, the more robust regression analyses do not appear to perform better relative to the homolog composition MLSR. This suggests that the small coefficients for DE-71 and DE-79 TMs predicted by the homolog composition MLSR is not an artifact of the large dominance of H10 (BDE-209) in the sediment cores, but rather a reflection of the quantified difference between PBDE TMs and sediment profile.

Table 5.13. Multivariate least square regression (MLSR) and multivariate least median square regression (MLMS) analyses for PBDE homolog and z-transformed composition in select sediment cores.

		PBDE		Z-transformed homolog composition	
Core	TMs	Homolog Composition			
		MLSR	MLMR	MLSR	MLMR
	DE-71	0.173	0.182	0.183	0.167
	DE-79	0.003	-0.018	-0.015	-0.008
CBC	Saytex 102E	0.736	1.226	1.007	1.97
	DE-71	0.028	0.081	0.02	0.068
	DE-79	0.003	-0.016	-0.01	-0.011
CWP	Saytex 102E	0.904	1.627	1	1.008
	DE-71	0.082	0.156	0.104	0.144
	DE-79	0.009	-0.012	0.002	-0.01
CLC	Saytex 102E	0.751	3.313	1.005	1.038
	DE-71	0.057	0.221	0.044	0.005
	DE-79	0.008	0.052	0.004	0.001
ACL	Saytex 102E	0.949	2.976	1.007	1.198
	DE-71	0.016	0.025	0.017	0.057
	DE-79	0.027	0.058	0.013	0.033
AMW	Saytex 102E	0.903	1.788	1.005	1.948
	DE-71	0.009	0.001	-0.005	0.001
	DE-79	0.004	0.214	0.003	0.002
AED	Saytex 102E	0.968	0.971	0.999	2.141
	DE-71	0.165	0.142	0.173	0.149
	DE-79	0.025	-0.03	-0.02	-0.024
IGC13	Saytex 102E	0.798	1.443	1.006	2.08

The PBDE sediment profiles in cores ACL, AED, and AMW (Figure 5.25a) showed little resemblance to the DE-71 and DE-79 TMs as evidenced by the small associated coefficient values (<0.1). In contrast, Saytex 102E contributions (Figure 5.25a, panels d-f) were very large in these three cores, resulting in a relatively small overall residual. This is thought to be an artifact of the core proximity to two large PBDE point sources (two PBDE manufacturing facilities) which according to the USEPA TRI, largely emit only the BDE-209 congener. Previous temporal PBDE congener analysis in core AMW indicated that there are two deposition regimes marked by the change in AMW utilization from a pond actively receiving treated WWTP effluent between 1952 through 1989 to a dormant WWTP effluent

lagoon from 1989 onwards (Figure 3.11c). During periods of active use, Saytex 102E, DE-79, and DE-71 deposition increased. This trend was reversed after ~1990. Additionally, core AMW was the only core where DE-79 loading exceeded DE-71 loading. This trend was more obvious during the period of active pond use. The depth specific MLSR analysis performed in this chapter highlights this trend. During 1952 to 1989, Saytex 102E, DE-79, and DE-71 contributions increased. During this particular time period, DE-79 contribution exceeded DE-71 contribution. The agreement between these two independent assessment methods (temporal congener loading analysis (Figure 3.11c) and MLSR analysis (Figure 5.25a, panels c,f, and i)) provided support for to the validity of the interpretation of these analyses.

While MLSR analysis for AR cores located proximate to PBDE large point sources in El Dorado, AR, suggested dominance of Saytex 102E as a single source for PBDE loading, results for Chicago and IGC cores showed a relatively higher contribution of the DE-71 and DE-79 TMs. Although Saytex 102E was still the dominant contributor on a mass basis, the contribution to total PBDE load was relatively less in the Chicago and IGC cores compared to the AR cores. DE-71, DE-79, and Saytex 102E contributions with depth in core CBC are consistent with sediment mixing; in agreement with our interpretation of the radionuclide dating, sediment PSD data, and sediment contaminant profile. Core CWP which received contaminants only through airborne deposition showed few variations in DE-71, DE-79, and Saytex 102E contributions with depth. Saytex 102E was the dominant contributor and only small or negligible variance was observed for DE-71 and DE-79 contributions with depth to the bottom of the core. Previously, whole core average MLSR analysis indicated that core CLC has the highest residual (Table 3.5). This was also true for depth specific MLSR (Figure 5.25b, panels b, f, and g). Depth specific MLSR results match that of whole core MLSR results for core IGC13.

For the four PCB Aroclors considered, not one Aroclor was found to be highly dominant over the others. In core CBC, Aroclors contributions with depth suggested sediment mixing, consistent with PBDE MLSR, radionuclide dating, PSD data, and PBDE and PCB contaminant profiles. Whole core average MLSR indicated that PCB Aroclor contributions increase in the order of $1254 < 1248 < 1016 < 1260$ in

core CBC. This trend was also observed for depth specific MLSR (Figure 5.25c, panel a). In core CLC, depth specific MLSR analysis showed increased in PCB Aroclor contributions in the order of 1254 < 1260 < 1016 < 1248 consistent with whole core average MLSR prediction. Whole core average MLSR results predicted the highest residual value in core CWP. This was also observed in the depth specific MLSR as expected. In core AMW, the PCB depth specific MLSR also reflected the known change in pond utilization. Prior to 1989, core AMW was dominated by Aroclor 1260, followed by 1248. After 1989, the contribution of Aroclor 1248 exceeded that of Aroclor 1260. This suggests that Aroclor 1260 has a higher loading from the aqueous phase (i.e., the treated WWTP effluent) relative to the atmospheric deposition. Overall, the depth specific MLSR results for PBDEs and PCBs agreed with the whole core average MLSR (Table 3.5).

Assuming LMM, PBDE TMs and PCB Aroclor fluxes and flux contributions were determined (Figure 5.26a-e). Measured depositional flux was calculated as sedimentation rate (Mass/Length²/Time) multiplied by measured concentration (Mass/Mass). For Chicago and IGC cores, sedimentation rates were estimated from the top five sediment segments and were focus factor corrected (Details and values were previously provided in Section 3.4.3 and in Table 3.3). With the LMM, PBDE TMs and PCB Aroclor contributions were assumed to be linear, therefore total LMM flux can be described as Equation 5.11.

$$Flux_{SLMM} = m^1 * Flux_{measured} + m^2 * Flux_{measured} + m^3 * Flux_{measured} \quad (5.11)$$

In Equation 5.11, m^1 , m^2 , and m^3 are contributions of specific PBDE TMs or PCB Aroclors determined through depth specific MLSR analysis. For PCB Aroclors, an additional m^4 term is introduced to reflect the four Aroclor mixtures considered in the MLSR analysis.

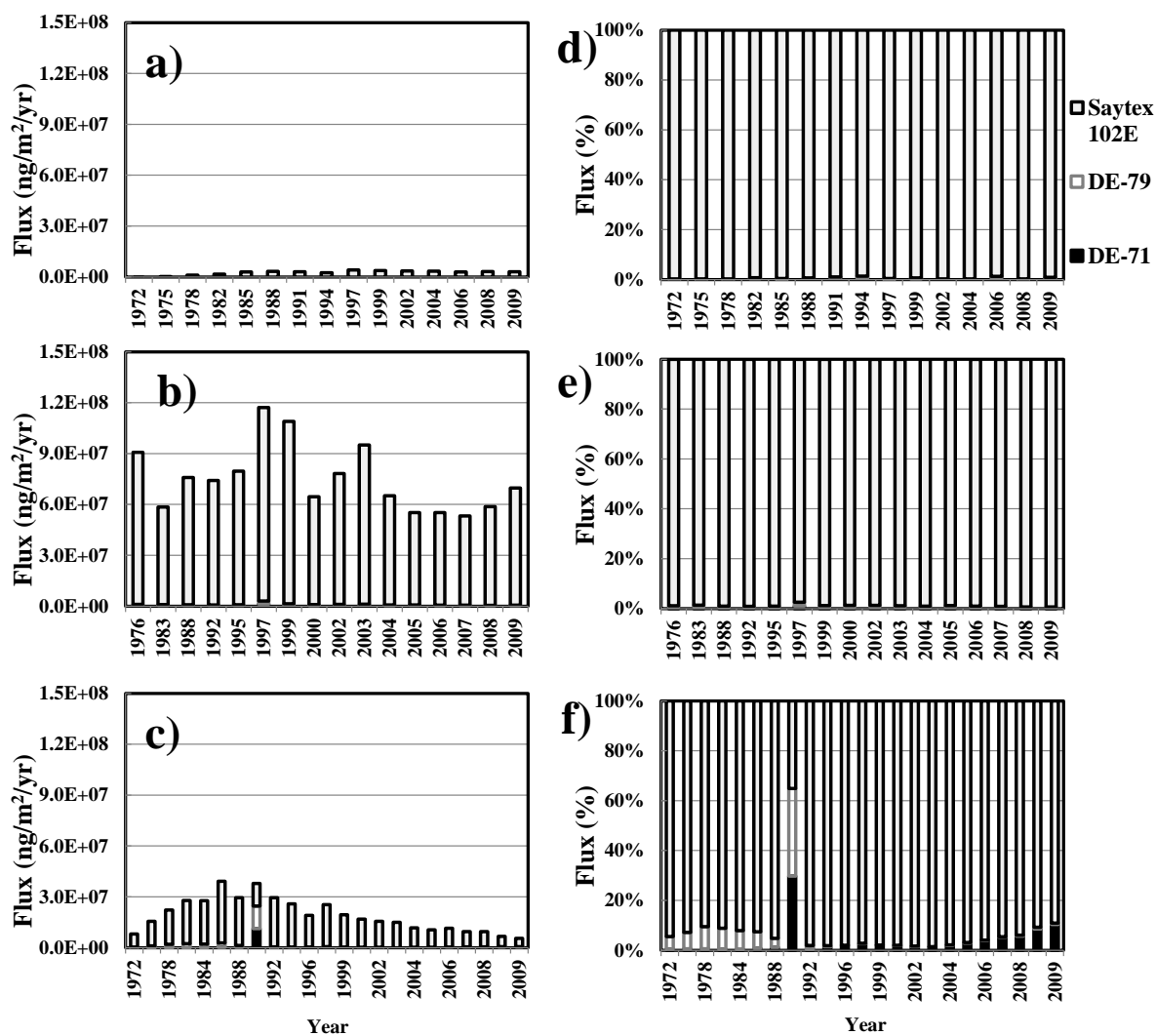


Figure 5.26a: Flux (a-c) and flux contribution (d-f) of DE-71, DE-79, and Saytex 102E PBDE technical mixtures as predicted by the linear mixing model for cores ACL (a,d), AED (b,e), and AMW (c,f).

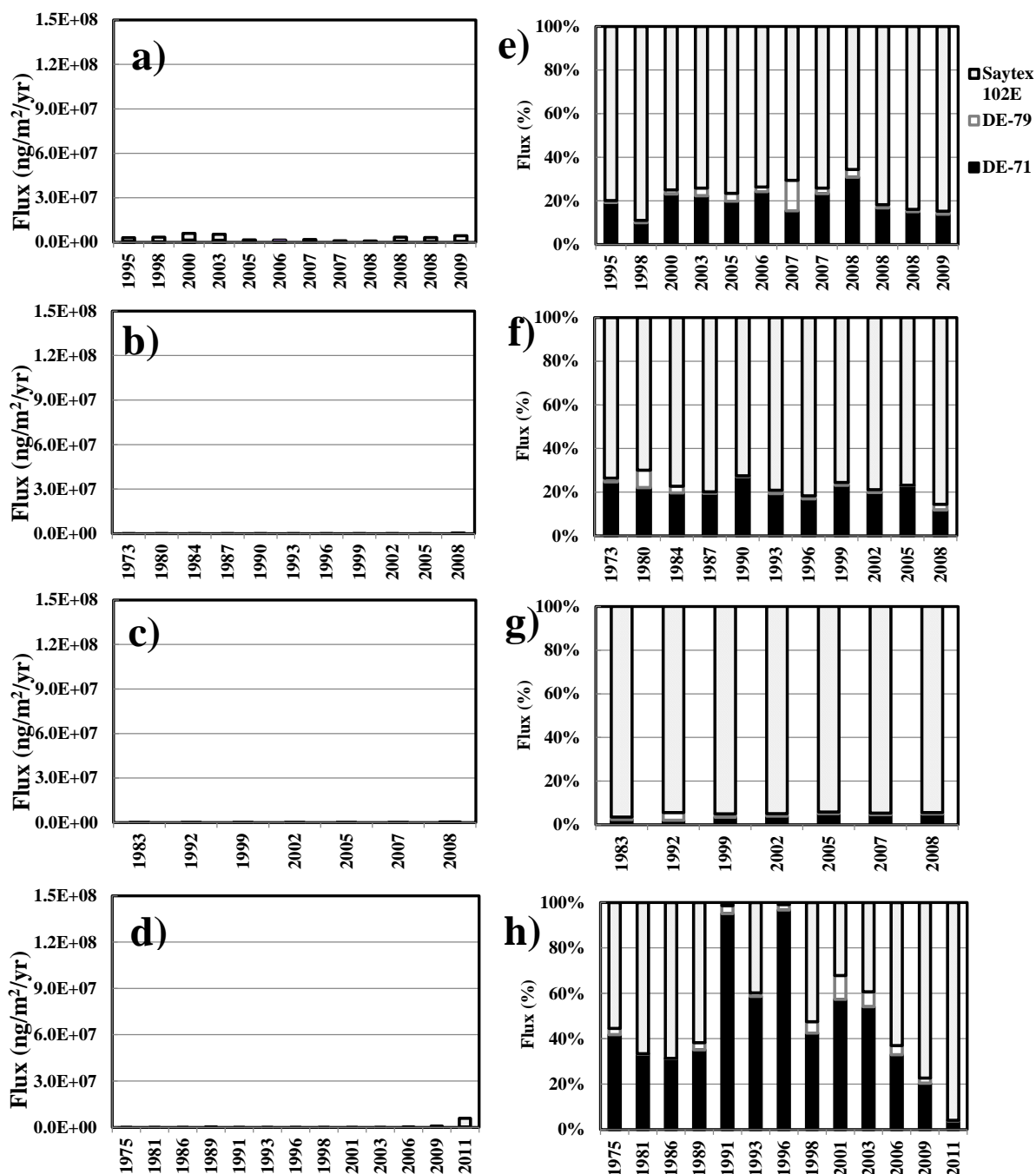


Figure 5.26b: Flux (a-d) and flux contribution (d-f) of DE-71, DE-79, and Saytex 102E predicted by the linear mixing model for cores CBC (a,e), CLC (b,f), CWP (c,g), and IGC13(d,h).

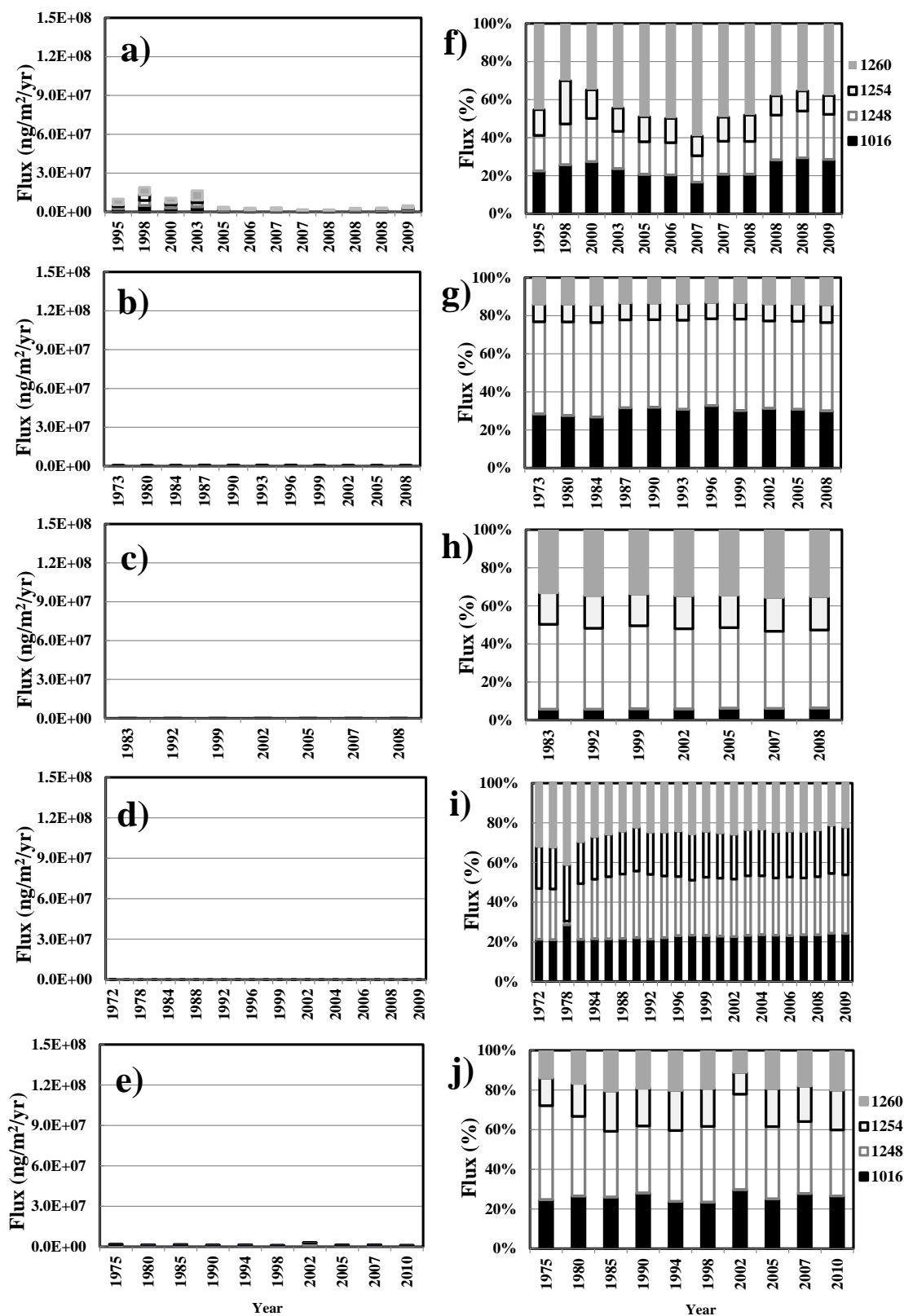


Figure 5.26c: Flux (a-e) and flux contribution (f-j) of Aroclors 1016, 1248, 1254, and 1260 predicted by the linear mixing model for cores a,f) CBC, b,g) CLC, c,h) CWP, d,i) AMW, and e,j) IGC13.

Cores ACL, AED, and AMW have substantially higher fluxes of DE-71, DE-79, and Saytex 102E TMs compared to Chicago and IGC cores. As the sedimentation rates for cores ACL, AED, and AMW cores were smaller than cores Chicago and IGC, the higher flux rates were driven by the high PBDE concentrations in these cores due to site proximity to the PBDE manufacturing facilities. In accordance with the depth specific MLSR results, flux contributions by Saytex 102E were higher than DE-71 and DE-79 in all the sediment cores and were more pronounced in the AR cores relative to the Chicago and IGC cores. In core CBC, PCB fluxes were higher than PBDE fluxes due to the higher PCB concentration. In cores CLC, CWP, and AMW, PBDE fluxes were larger than PCB fluxes; however, PBDE and PCB fluxes were within the same magnitude for core IGC13. PCB flux contributions also reflected the contributions of the four Aroclor mixtures. The LMM accounted for >90 % of the measured PBDE flux; however LMM on average only accounted for 65% of the measured PCB fluxes. In Figure 5.27a-d, measured PBDE and PCB homolog concentrations were compared to LMM predicted homolog concentrations to evaluate the origin of discrepancy between measured PBDE and PCB fluxes to LMM predicted fluxes.

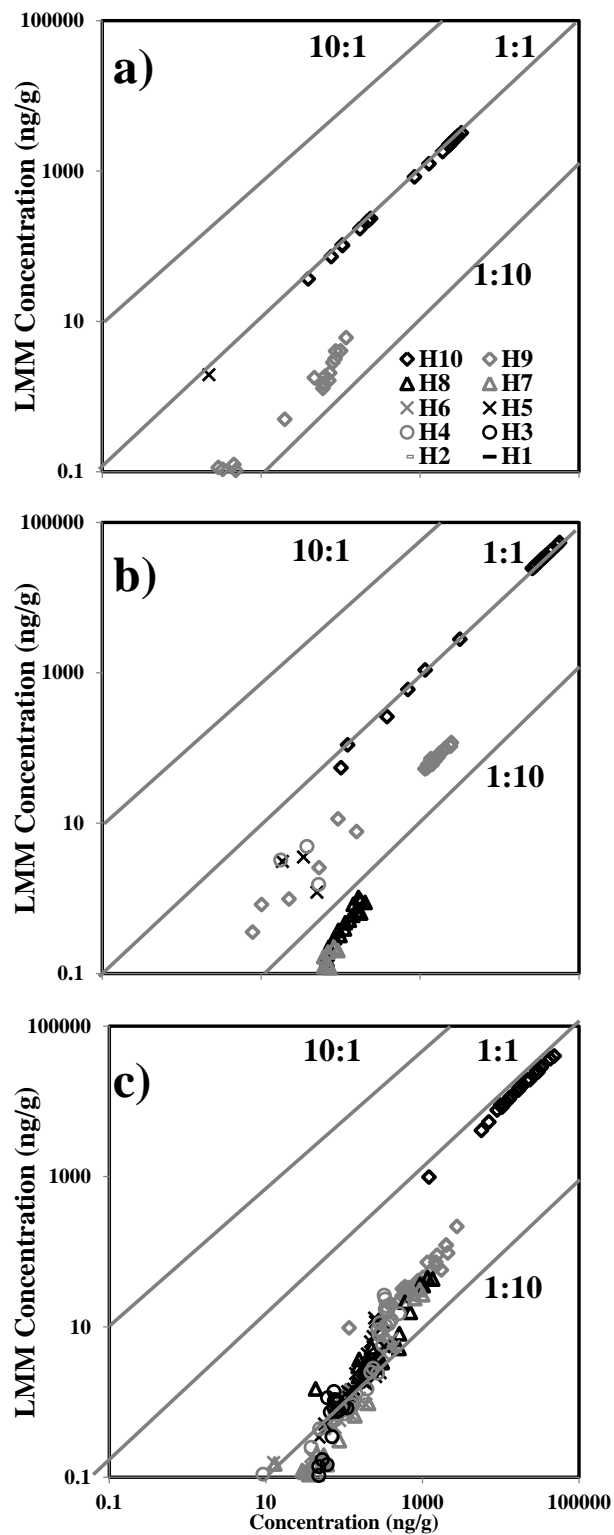


Figure 5.27a: Comparison of measured PBDE homolog concentrations to the linear mixing model predicted concentrations in cores ACL (a), AED (b), and AMW (c). Also shown are the 1:1, 10:1, and 1:10 lines. Note log scale on axes.

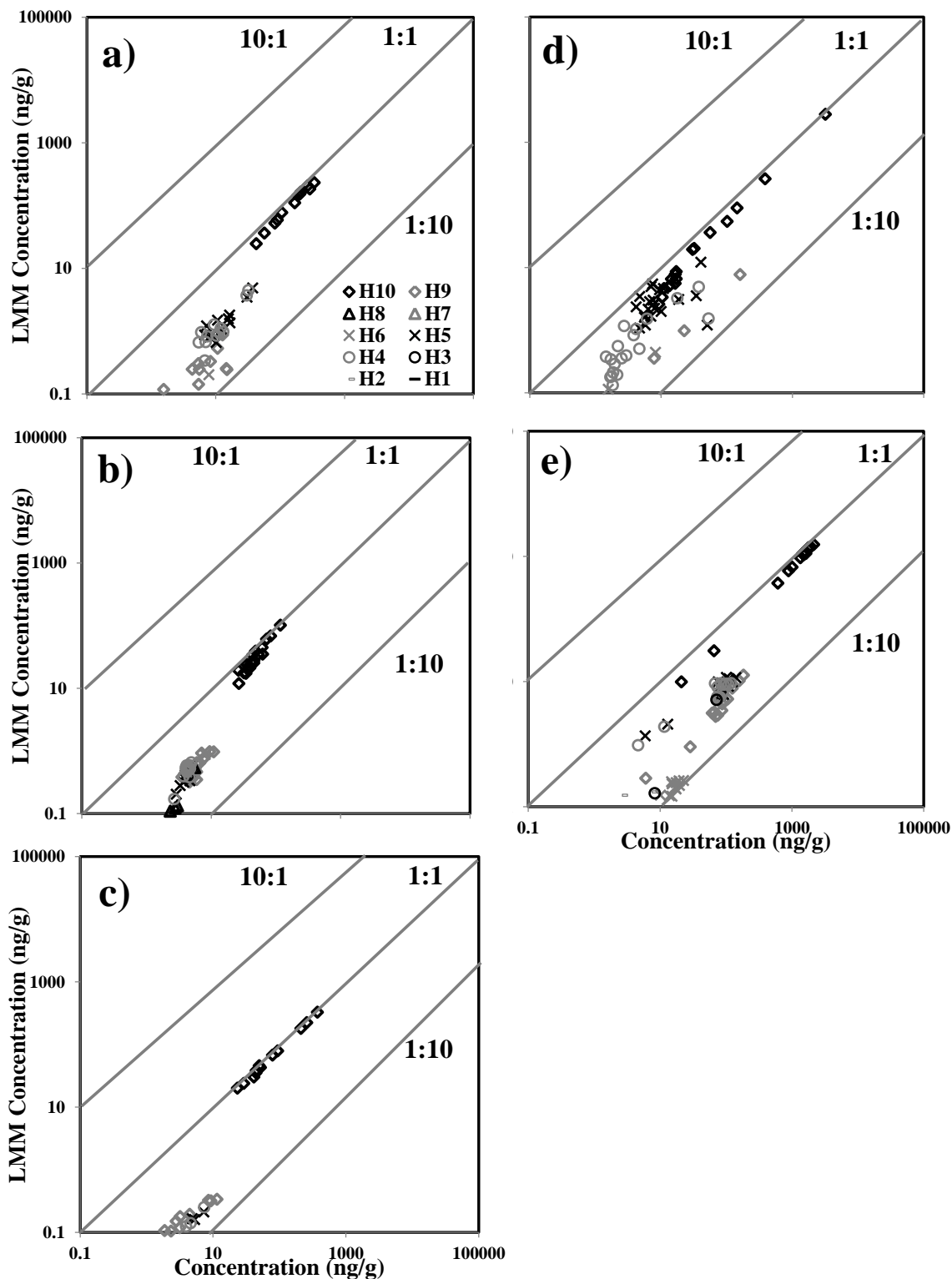


Figure 5.27b: Comparison of measured PBDE homolog concentrations to the linear mixing model predicted concentrations in cores CBC (a), CLC (b), CWP (c), AMW (d), and IGC13(e). Also shown are the 1:1, 10:1, and 1:10 lines. Note log scale on axes.

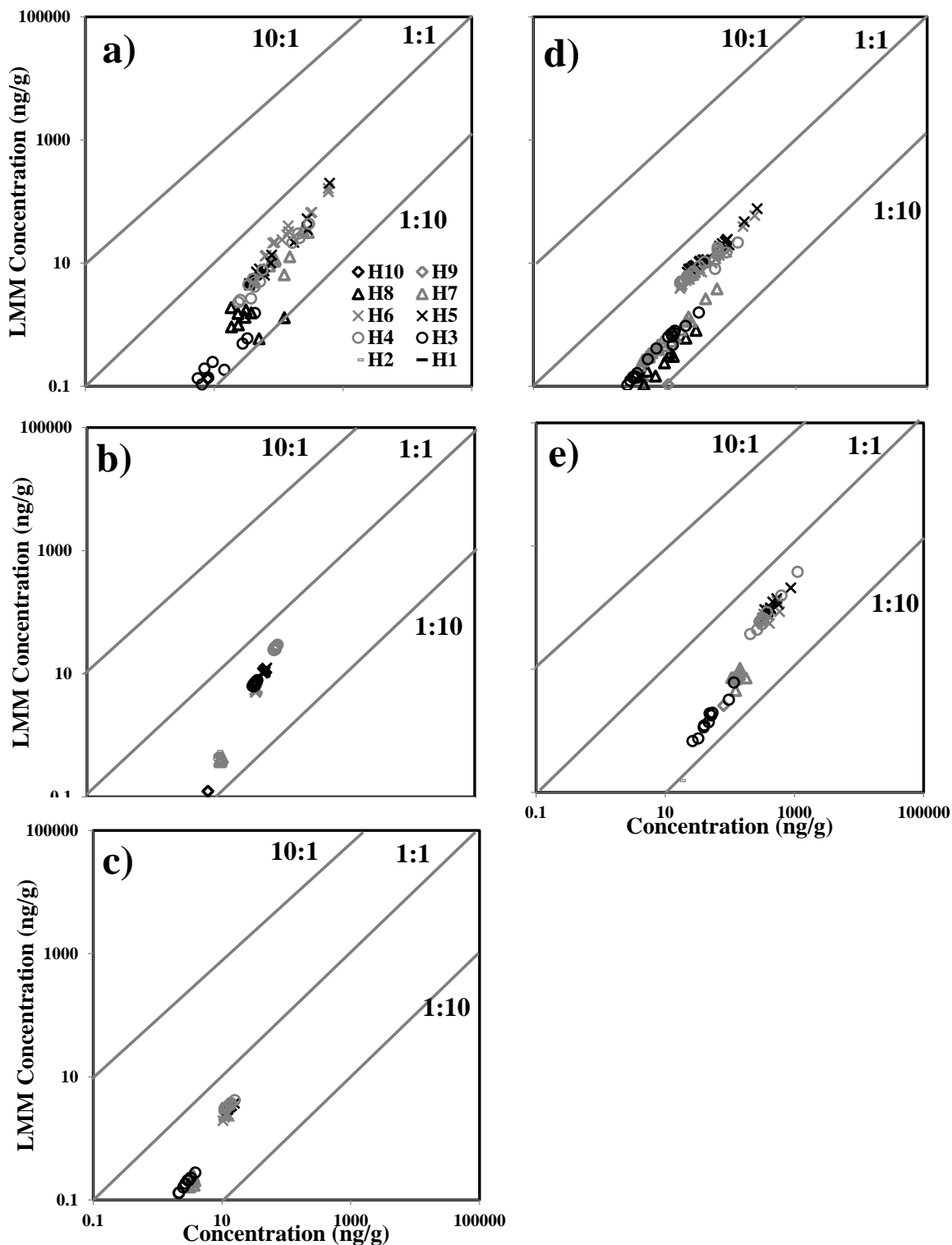


Figure 5.27c: Comparison of measured PCB homolog concentrations to the linear mixing model predicted concentrations in cores CBC (a), CLC (b), CWP (c), AMW(d), IGC09 (e), and IGC13(f). Also shown are the 1:1, 10:1, and 1:10 lines. Note log scale on axes.

For PBDEs, the TMs LMM predicted concentration accounted for more than >95% of the measured concentration for homolog 10. This was evidenced by the similarity between the measured versus the predicted data of homolog 10. In contrast, the LMM typically underestimated the concentration of PBDE homologs 9 and smaller as shown by the measured versus predicted results within the 1:1 and 1:10 lines. For PCBs, the LMM underestimated the PCB concentrations across the PCB homologs spectrum. Several reasons could have resulted in this including PCBs in the sediment originating from other Aroclor mixtures not considered in the depth specific MLSR (there are 17 different PCB Aroclors and some sediment cores have high depth specific MLSR residuals), and transformation of PCBs during pre- and post-depositional stages.

In relations to PBDE and PCB in-situ mass transport, it is of interest to evaluate if the difference in LMM predicted concentrations and measured concentrations are influenced and/or affected by PBDE and PCB in-situ mass transport processes. PBDE and PCB LMM predicted concentrations and measured concentrations with depth are shown in Figure 5.28a-n.

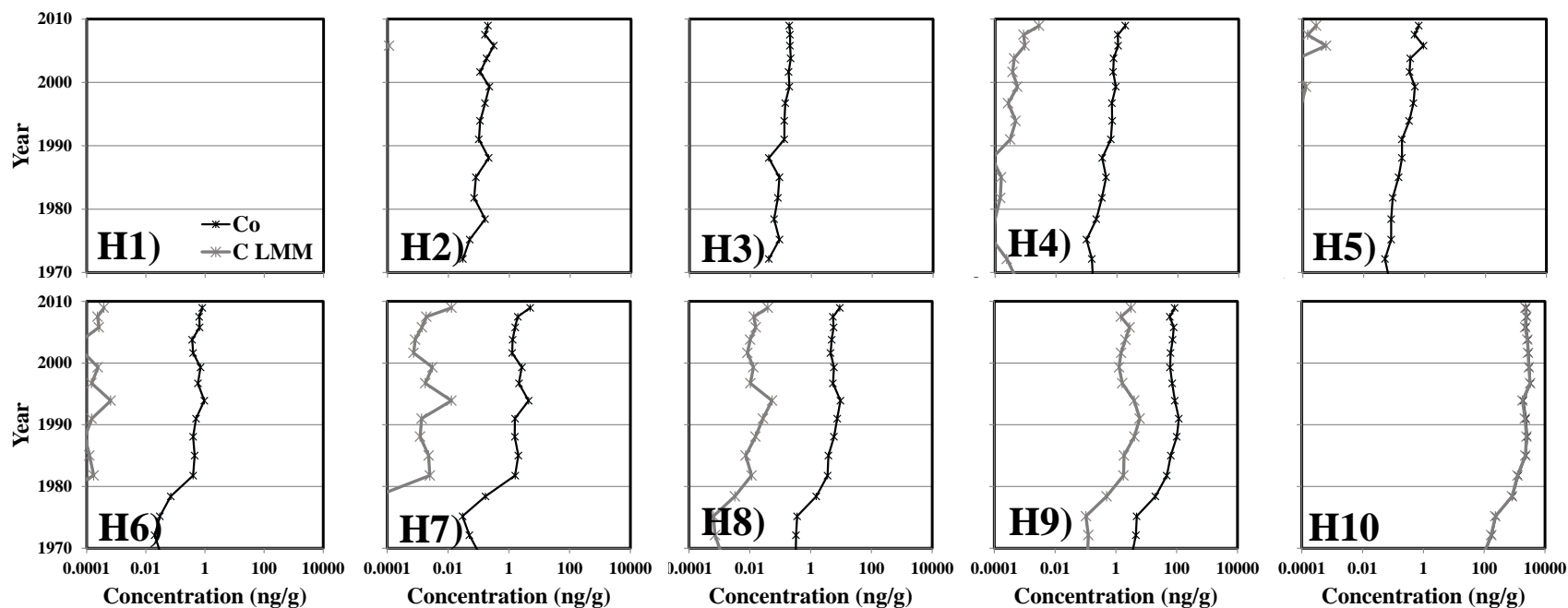


Figure 5.28a: LMM predicted and measured PBDE homologs (H1-H10: homolog 1 to homolog 10) concentrations in core ACL. Lines that do not show up are below the minimum concentration level. Error bars, representing the maximum amount of mass percentage moving out of the sediment boundary layer relative to initial sediment mass at 40 years ($M_{t=40 \text{ years}}/M_{\text{sed}|t=0 \text{ year}}$) under advection with organic carbon only sorption (A(OC)) were added to the measured PBDE homologs. Note that error bars are at a 10x scale. In most cases, predicted $M_{t=40 \text{ years}}/M_{\text{sed}|t=0 \text{ year}}$ were very low and error bars are not visible. X-axes are in the log scale.

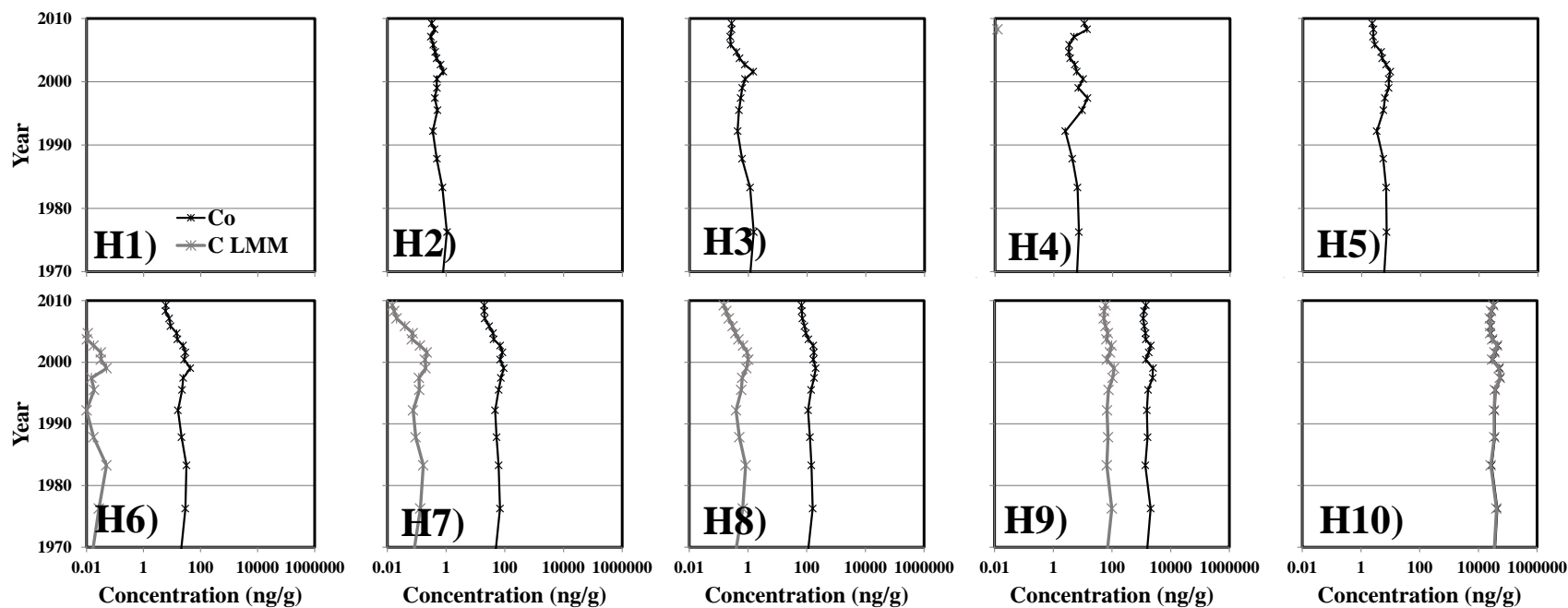


Figure 5.28b: LMM predicted and measured PBDE homologs (H1-H10: homolog 1 to homolog 10) concentrations in core AED. Lines that do not show up are below the minimum concentration level. Error bars, representing the maximum amount of mass percentage moving out of the sediment boundary layer relative to initial sediment mass at 40 years ($M_{t=40 \text{ years}}/M_{\text{sed}|t=0 \text{ year}}$) under advection with organic carbon only sorption (A(OC)) were added to the measured PBDE homologs. Note that error bars are at a 10x scale. In most cases, predicted $M_{t=40 \text{ years}}/M_{\text{sed}|t=0 \text{ year}}$ were very low and error bars are not visible. X-axes are in the log scale.

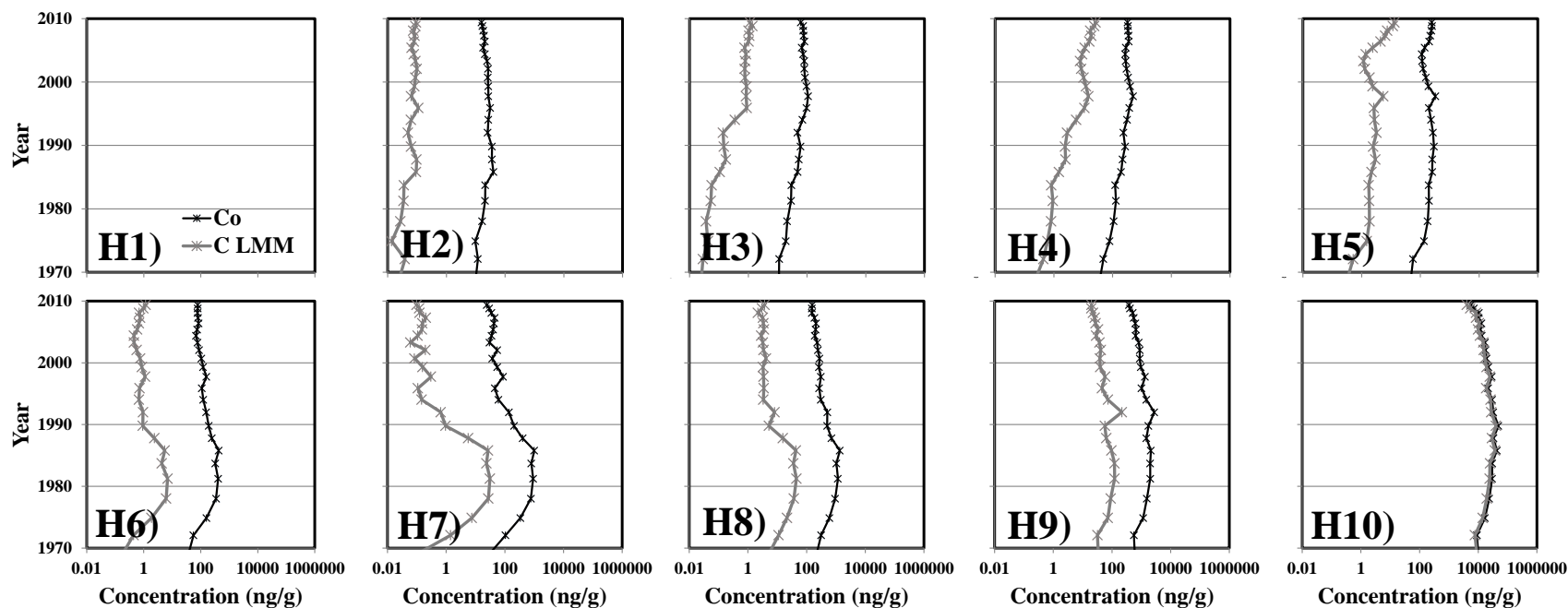


Figure 5.28c: LMM predicted and measured PBDE homologs (H1-H10: homolog 1 to homolog 10) concentrations in core AMW. Lines that do not show up are below the minimum concentration level. Error bars, representing the maximum amount of mass percentage moving out of the sediment boundary layer relative to initial sediment mass at 40 years ($M_{t=40 \text{ years}}/M_{\text{sed}|t=0 \text{ year}}$) under advection with organic carbon only sorption (A(OC)) were added to the measured PBDE homologs. Note that error bars are at a 10x scale. In most cases, predicted $M_{t=40 \text{ years}}/M_{\text{sed}|t=0 \text{ year}}$ were very low and error bars are not visible. X-axes are in the log scale.

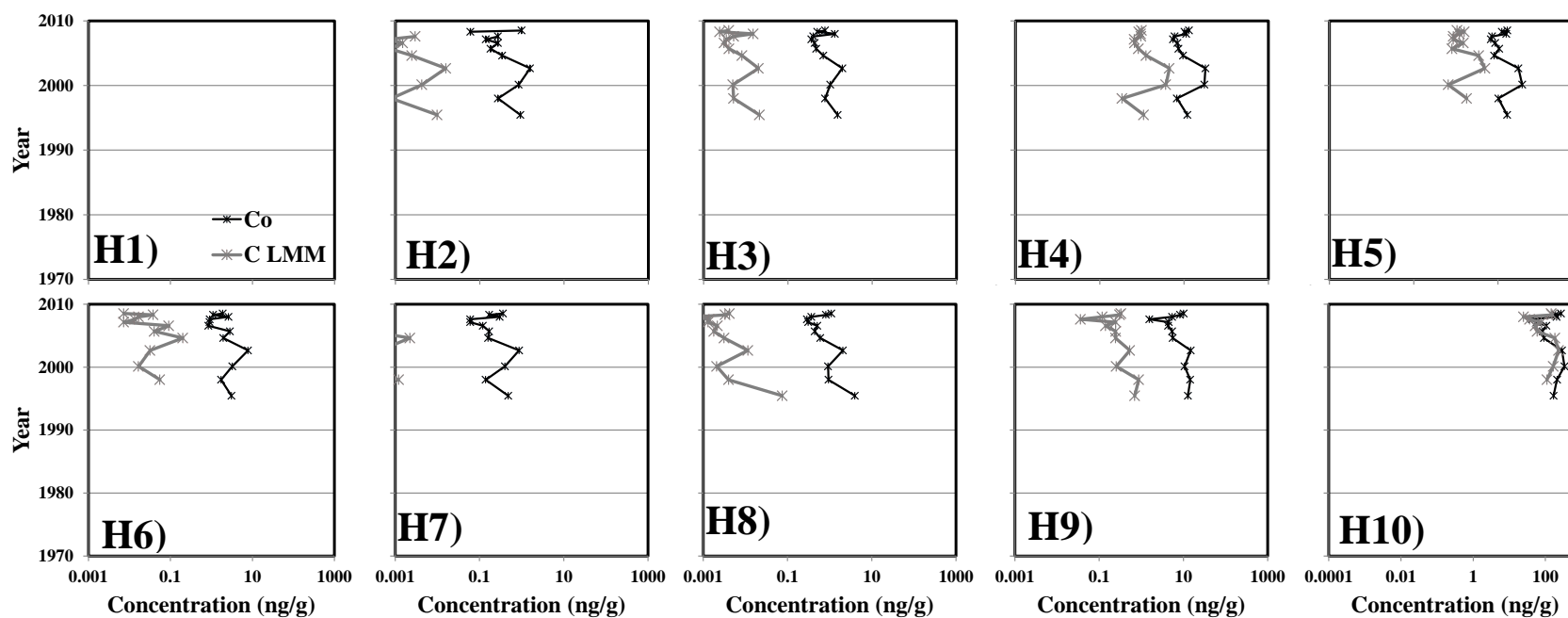


Figure 5.28d: LMM predicted and measured PBDE homologs (H1-H10: homolog 1 to homolog 10) concentrations in core CBC. Lines that do not show up are below the minimum concentration level. Error bars, representing the maximum amount of mass percentage moving out of the sediment boundary layer relative to initial sediment mass at 40 years ($M_{t|t=40 \text{ years}}|M_{\text{sed}|t=0 \text{ year}}$) under advection with organic carbon only sorption (A(OC)) were added to the measured PBDE homologs. Note that error bars are at a 10x scale. In most cases, predicted $M_{t|t=40 \text{ years}}|M_{\text{sed}|t=0 \text{ year}}$ were very low and error bars are not visible. X-axes are in the log scale.

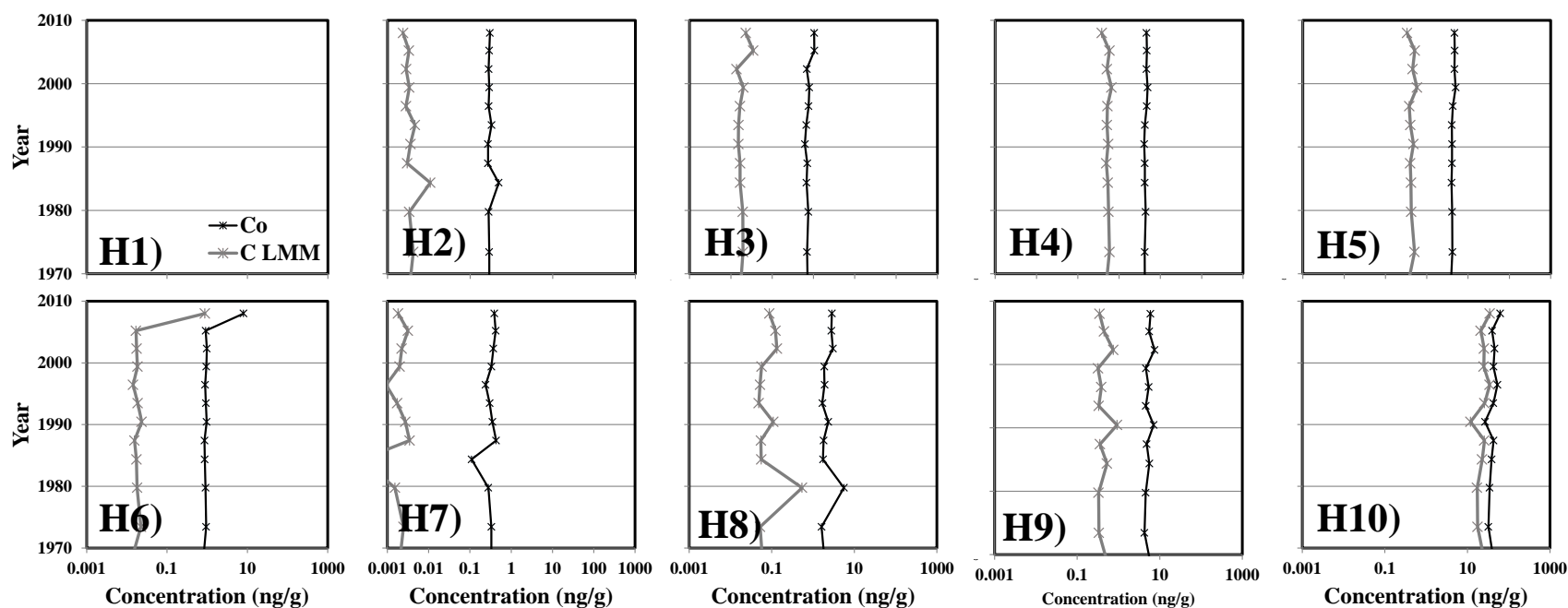


Figure 5.28e: LMM predicted and measured PBDE homologs (H1-H10: homolog 1 to homolog 10) concentrations in core CLC. Lines that do not show up are below the minimum concentration level. Error bars, representing the maximum amount of mass percentage moving out of the sediment boundary layer relative to initial sediment mass at 40 years ($M_{t=40 \text{ years}}/M_{\text{sed}|t=0 \text{ year}}$) under advection with organic carbon only sorption (A(OC)) were added to the measured PBDE homologs. Note that error bars are at a 10x scale. In most cases, predicted $M_{t=40 \text{ years}}/M_{\text{sed}|t=0 \text{ year}}$ were very low and error bars are not visible. X-axes are in the log scale.

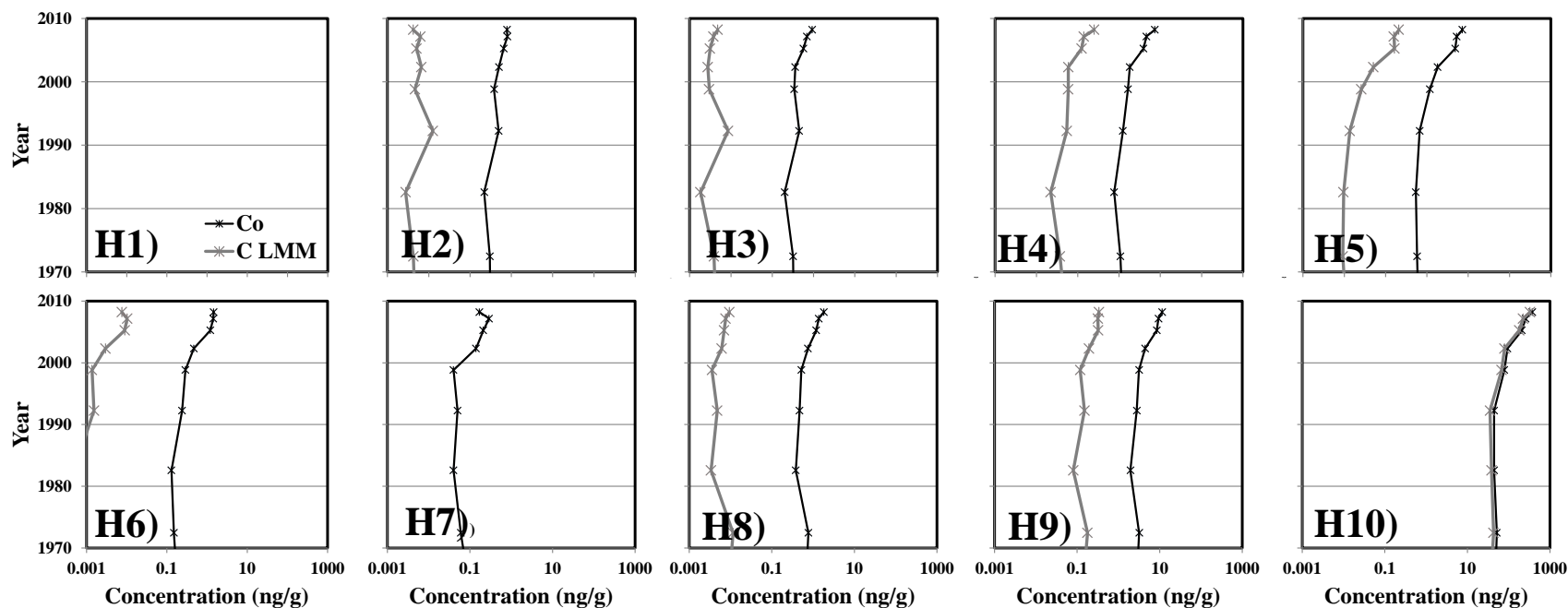


Figure 5.28f: LMM predicted and measured PBDE homologs (H1-H10: homolog 1 to homolog 10) concentrations in core CWP. Lines that do not show up are below the minimum concentration level. Error bars, representing the maximum amount of mass percentage moving out of the sediment boundary layer relative to initial sediment mass at 40 years ($M_{t=40 \text{ years}}|M_{\text{sed}}|_{t=0 \text{ year}}$) under advection with organic carbon only sorption (A(OC)) were added to the measured PBDE homologs. Note that error bars are at a 10x scale. In most cases, predicted $M_{t=40 \text{ years}}|M_{\text{sed}}|_{t=0 \text{ year}}$ were very low and error bars are not visible. X-axes are in the log scale.

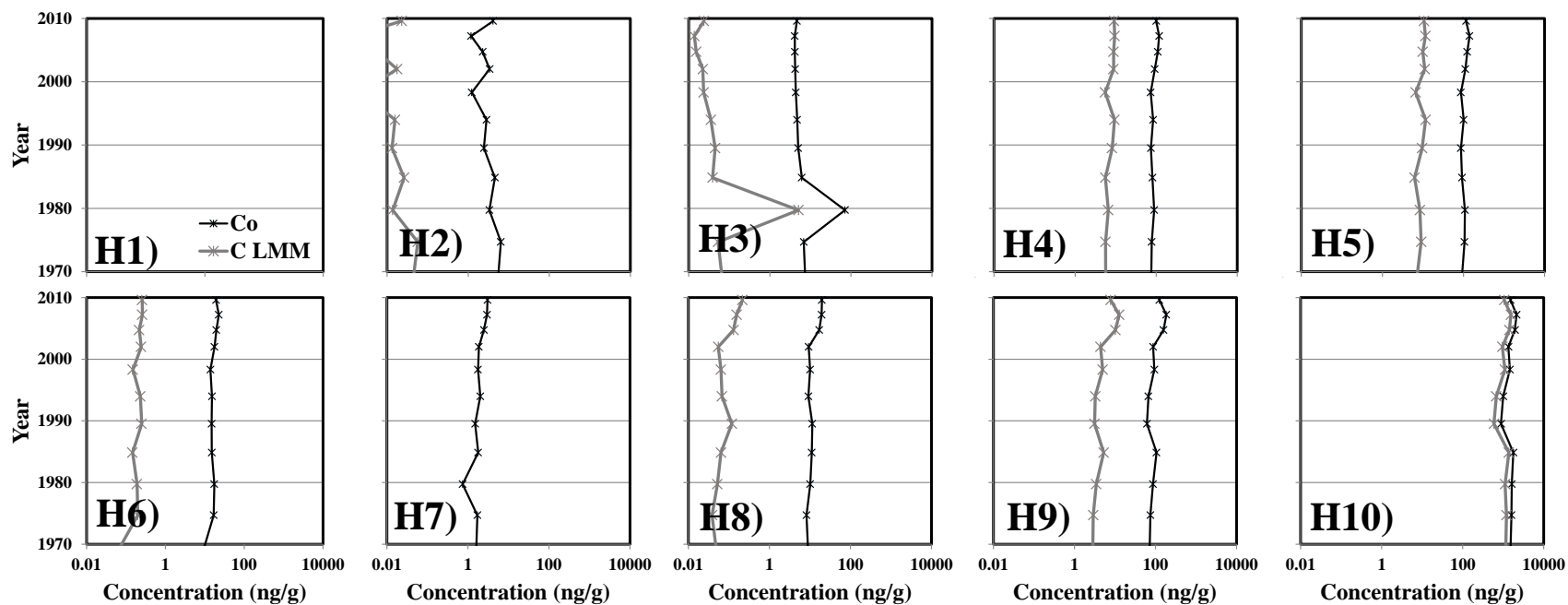


Figure 5.28g: LMM predicted and measured PBDE homologs (H1-H10: homolog 1 to homolog 10) concentrations in core IGC13. Lines that do not show up are below the minimum concentration level. Error bars, representing the maximum amount of mass percentage moving out of the sediment boundary layer relative to initial sediment mass at 40 years ($M_{t|t=40 \text{ years}}|M_{\text{sed}|t=0 \text{ year}}$) under advection with organic carbon only sorption (A(OC)) were added to the measured PBDE homologs. Note that error bars are at a 10x scale. In most cases, predicted $M_{t|t=40 \text{ years}}|M_{\text{sed}|t=0 \text{ year}}$ were very low and error bars are not visible. X-axes are in the log scale.

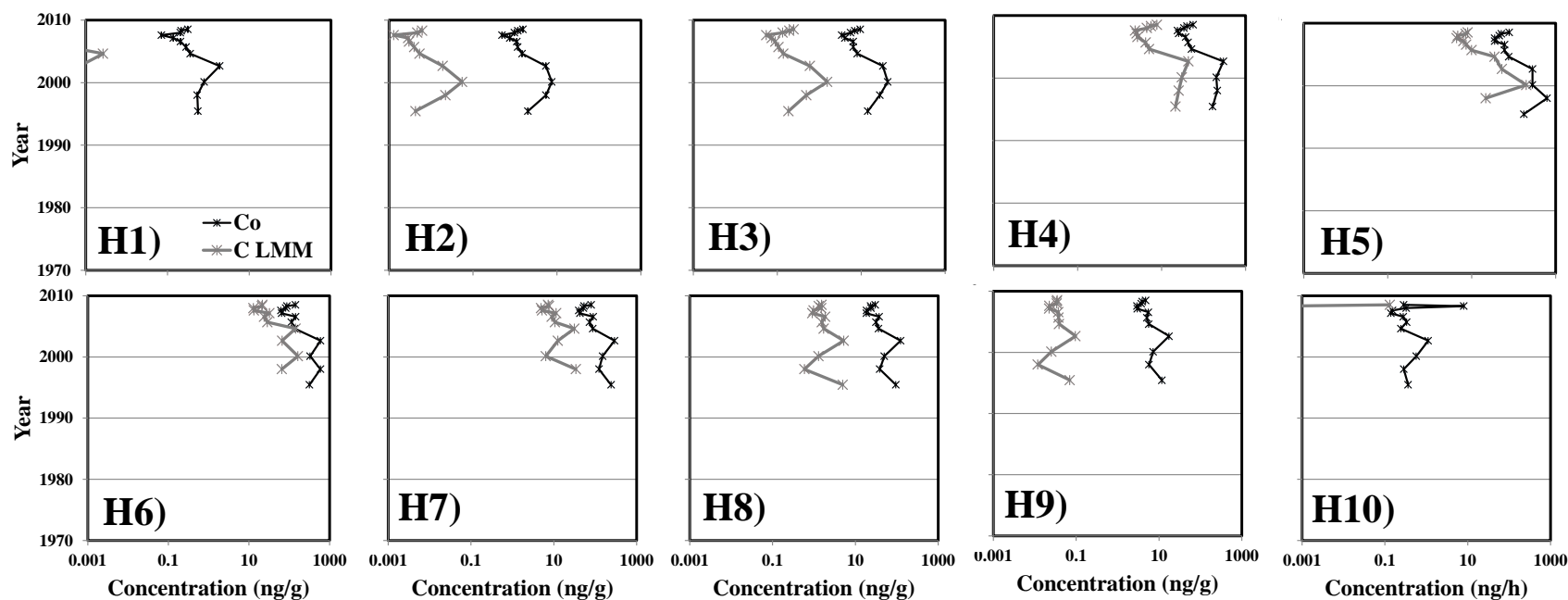


Figure 5.28h: LMM predicted and measured PBDE homologs (H1-H10: homolog 1 to homolog 10) concentrations in core CBC. Lines that do not show up are below the minimum concentration level. Error bars, representing the maximum amount of mass percentage moving out of the sediment boundary layer relative to initial sediment mass at 40 years ($M_{t=40 \text{ years}}/M_{\text{sed}|t=0 \text{ year}}$) under advection with organic carbon only sorption (A(OC)) were added to the measured PBDE homologs. Note that error bars are at a 10x scale. In most cases, predicted $M_{t=40 \text{ years}}/M_{\text{sed}|t=0 \text{ year}}$ were very low and error bars are not visible. X-axes are in the log scale.

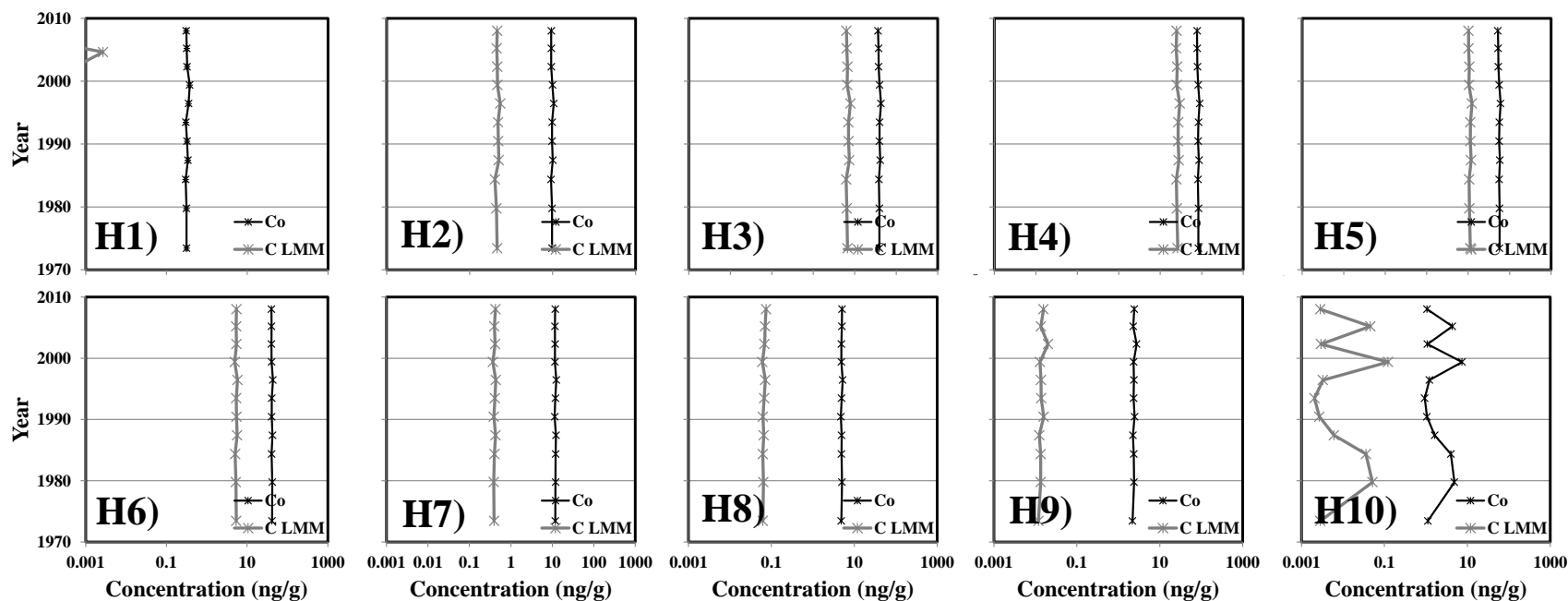


Figure 5.28i: LMM predicted and measured PBDE homologs (H1-H10: homolog 1 to homolog 10) concentrations in core CLC. Lines that do not show up are below the minimum concentration level. Error bars, representing the maximum amount of mass percentage moving out of the sediment boundary layer relative to initial sediment mass at 40 years ($M_{t=40 \text{ years}}/M_{\text{sed}|t=0 \text{ year}}$) under advection with organic carbon only sorption (A(OC)) were added to the measured PBDE homologs. Note that error bars are at a 10x scale. In most cases, predicted $M_{t=40 \text{ years}}/M_{\text{sed}|t=0 \text{ year}}$ were very low and error bars are not visible. X-axes are in the log scale.

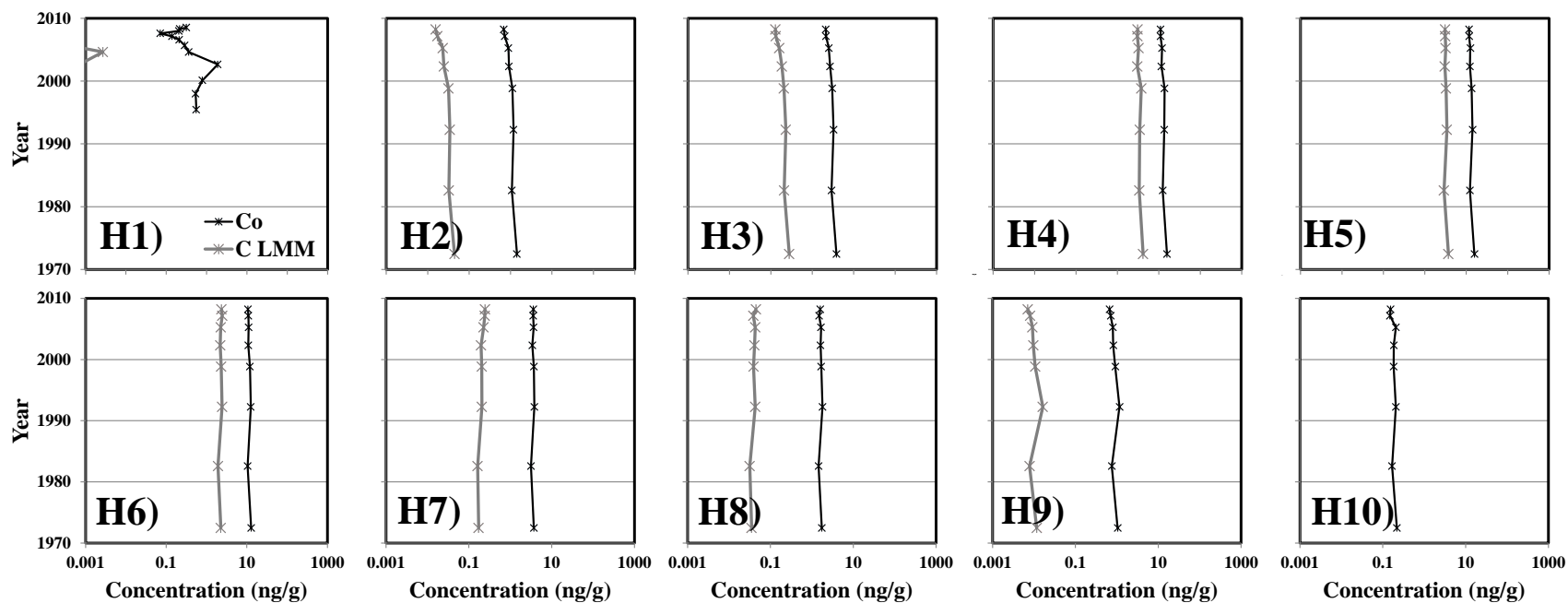


Figure 5.28j: LMM predicted and measured PBDE homologs (H1-H10: homolog 1 to homolog 10) concentrations in core CWP. Lines that do not show up are below the minimum concentration level. Error bars, representing the maximum amount of mass percentage moving out of the sediment boundary layer relative to initial sediment mass at 40 years ($M_{t|t=40 \text{ years}}|M_{\text{sed}|t=0 \text{ year}}$) under advection with organic carbon only sorption (A(OC)) were added to the measured PBDE homologs. Note that error bars are at a 10x scale. In most cases, predicted $M_{t|t=40 \text{ years}}|M_{\text{sed}|t=0 \text{ year}}$ were very low and error bars are not visible. X-axes are in the log scale.

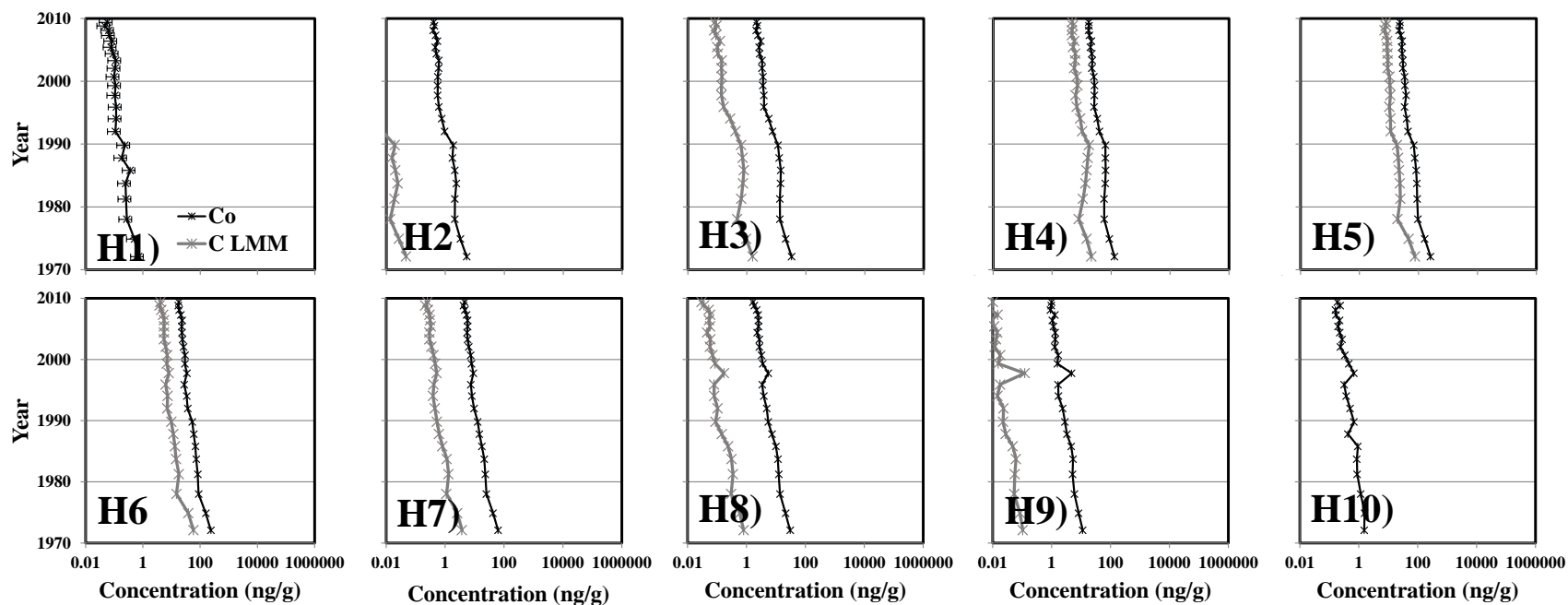


Figure 5.28k: LMM predicted and measured PBDE homologs (H1-H10: homolog 1 to homolog 10) concentrations in core AMW. Lines that do not show up are below the minimum concentration level. Error bars, representing the maximum amount of mass percentage moving out of the sediment boundary layer relative to initial sediment mass at 40 years ($M_{t=40 \text{ years}}|M_{\text{sed}|t=0 \text{ year}}$) under advection with organic carbon only sorption (A(OC)) were added to the measured PBDE homologs. Note that error bars are at a 10x scale. In most cases, predicted $M_{t=40 \text{ years}}|M_{\text{sed}|t=0 \text{ year}}$ were very low and error bars are not visible. X-axes are in the log scale.

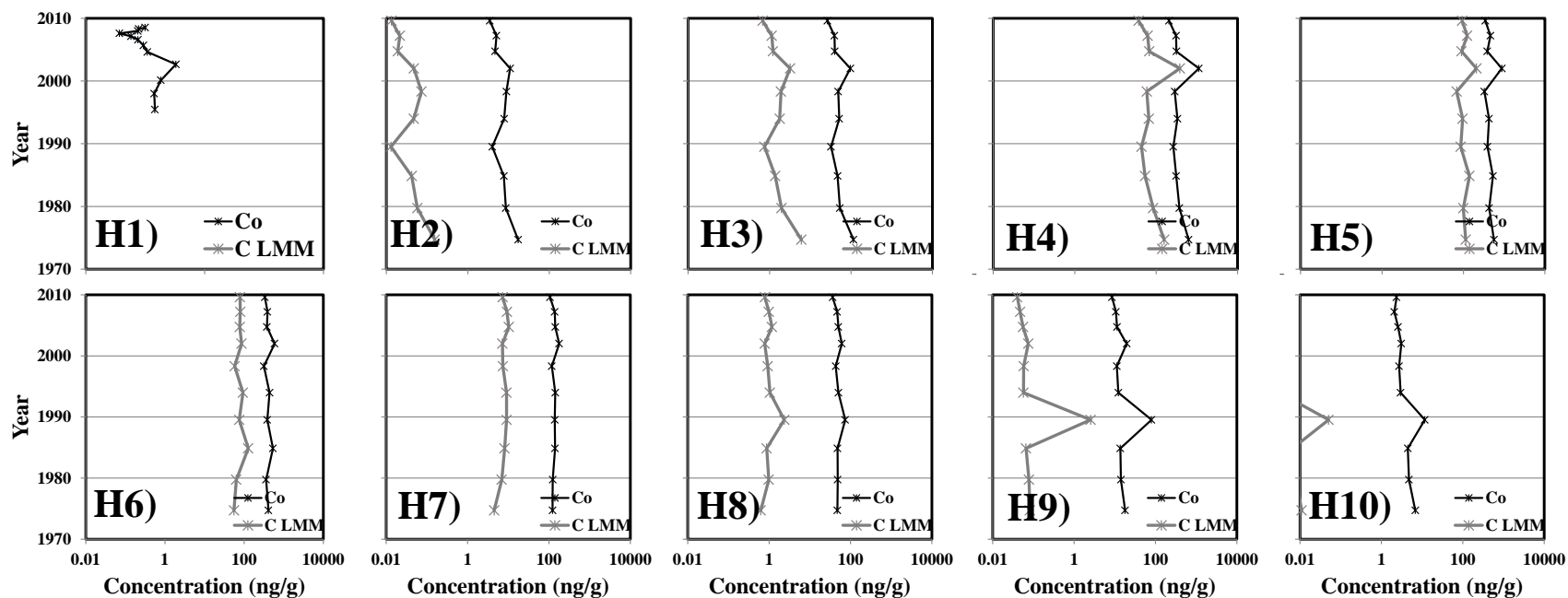


Figure 5.28l: LMM predicted and measured PBDE homologs (H1-H10: homolog 1 to homolog 10) concentrations in core IGC13. Lines that do not show up are below the minimum concentration level. Error bars, representing the maximum amount of mass percentage moving out of the sediment boundary layer relative to initial sediment mass at 40 years ($M_{t=40 \text{ years}}/M_{\text{sed}|t=0 \text{ year}}$) under advection with organic carbon only sorption (A(OC)) were added to the measured PBDE homologs. Note that error bars are at a 10x scale. In most cases, predicted $M_{t=40 \text{ years}}/M_{\text{sed}|t=0 \text{ year}}$ were very low and error bars are not visible. X-axes are in the log scale.

The discrepancy between measured and LMM-predicted homolog concentrations varied substantially by homolog for PBDEs (Figure 5.27). The dominance of Saytex 102E in the sediment cores resulted in the LMM performing well for PBDE homolog 10 (Figure 5.28a-g, panels H10, Figure 5.27a-b). In Figure 5.27a-b, it was shown that the LMM underestimated PBDE homologs 1 through 9, which is manifested as large gaps between LMM predicted and measured concentrations observed in Figure 5.28a-g (panels H1 to H9). As the LMM under-predicts the measured concentrations in all homologs (Figure 5.27c), noticeable gaps reflecting the difference between LMM-predicted and measured concentrations were also observed for PCBs homologs 1 through 10 (Figure 5.28i-l).

Error bars were added to the measured concentrations in Figure 5.28a-n; these error bars represent the largest amount of PBDE or PCB homologs that were predicted to leave the sediment boundary layer (± 0.02 m) within a 40 years time period ($M_{t|t=40 \text{ years}}$) used in the transport simulations, and also representing the approximate time frame of the deeper cores. Previously, in Section 5.4, it was established that the A(OC) transport process simulated the most mobile conditions for PBDEs and PCBs mass flux in sediment segment. Additionally in Section 5.5, it was shown that given the 1000 year simulation period, only PBDE homolog 1 and PCB homologs 1 and 2 were predicted to have substantial contaminant mass removal via the A(OC) transport process (substantial defined $M_{t|t} / M_{sed|t=0 \text{ year}}$ as $\geq 20\%$). The sediment cores studied in this chapter were estimated to span 40 years between the 1970s to 2010. Given a relevant time frame of only 40 years, the predicted $M_{t|t=40 \text{ years}} / M_{sed|t=0 \text{ years}}$ values were very small, if not negligible. To provide a quick recap of the magnitude, Table 5.14 summarized the $M_{t|t=40 \text{ years}} / M_{sed|t=0 \text{ years}}$ values in PBDE homolog 1 and PCB homologs 1 and 2 after a 40 year transport period.

Table 5.14: Summary of the fraction of mass leaving the sediment boundary layer relative to initial mass in the sediment phase under advection-diffusion with organic carbon only sorption for transport time of 40 years.

Core	$M_{t t=40 \text{ years}} / M_{sed t=0 \text{ years}} (\%)$		
	PBDE homolog 1	PCB homolog 1	PCB homolog 2
ACL	9.8	NA ⁽¹⁾	NA ⁽¹⁾
AED	6.7	NA ⁽¹⁾	NA ⁽¹⁾
AMW	0.9	4.7	0.1
CBC	0	0.1	0
CLC	0.2	1.1	0
CWP	0	0.1	0
IGC09	0	0	0
IGC13	0	0	0

(1): Not applicable

Although in cores ACL and AED, $M_{t|t=40 \text{ years}} / M_{sed|t=0 \text{ years}}$ values for PBDE homolog 1 were predicted to be substantial during the relevant 40 years period, generally the sediment cores studied in this chapter typically do not have measureable levels of PBDE homolog 1. In PBDE homologs 2 and larger, the predicted $M_{t|t=40 \text{ years}} / M_{sed|t=0 \text{ years}}$ values were negligible. After 1000 years transport period, predicted $M_{t|t=1000 \text{ years}} / M_{sed|t=0 \text{ years}}$ values in cores AED and ACL were <25% and were <5% in the other sediment cores reflecting the substantially slow mass transfer rate and magnitude of PBDE homolog 2 even under the most mobile mass transport simulation. PCB homolog 1 in core AMW have a $M_{t|t=40 \text{ years}} / M_{sed|t=0 \text{ years}}$ value of 4.7%; however when plotted even at a 10X scale, the error bars were barely visible (Figure 5.26I, panel H1) due to the small concentration of PCB homolog 1 (<1 ng/g), which renders the value of 4.7% not visible in Figure 5.26I, panel H1. Superimposing the results from PBDE and PCB in-situ mass flux modeling under the most mobile condition from the perspective of aqueous phase on depth specific LMM predicted concentrations provides a graphical illustration of the fact that in-situ PBDE and PCB mass transport in natural sediment columns do not occur at a high enough magnitude to explain the discrepancy between PBDE TMs or PCB Aroclors to PBDE or PCB sediment profiles. Thus, we must conclude that PBDE and PCB in-situ transport processes under the 40 years relevant sediment age results in negligible mass removal. Further, under the 1000 years simulation period, only LMW PBDE and PCB homologs

(specifically, PBDE homolog 1 and PCB homologs 1 and 2) showed substantial mass flux rates (>20% mass removal). In HMW PBDE and PCB homologs (specifically, PBDE homologs 2 and larger, and PCB homologs 3 and larger), no substantial mass transport rates were predicted even after a 1000 years simulation period (<20% mass removal). The overall conclusion is that the small magnitude of PBDE and PCB transport over the 40 years relevant sediment age does not explain the discrepancy between PBDE and PCB sediment profiles to PBDE TMs and PCB Aroclors, respectively. Previously, it was noted that the discrepancy between PBDE TMs or PCB Aroclors to PBDE and PCB sediment profiles could arise from either pre-depositional transport and/or transformation which includes differential transport rates for different homologs and transformation from source locations to receptor site, or from post-depositional transport or transformation which includes in-situ sediment transport and microbial facilitated transformation. Through mass transport modeling enhanced with a robust Monte Carlo simulation to capture parameter uncertainty in natural sediments, the modeling effort in this chapter showed that *in-situ* sediment transport cannot appreciably affect the congener profiles in any the studied sediment columns. Thus, it can be concluded that in-situ sediment transport can be excluded from any future studies as the cause for discrepancy between PBDE TMs and PCB Aroclors to PBDE or PCB sediment profiles.

5.7. Conclusion

In this chapter, mass transport of PBDEs and PCBs was modeled in eleven natural sediment cores to investigate the magnitude of *in-situ* sediment transports. Monte Carlo simulation was applied to generate realistic PDFs of parameters and to control for gaps in the data. The original hypotheses postulated for this phase of the study can now be assessed.

- As postulated, LMW PBDE and PCB homologs have greater mass transport potential than HMW PBDE and PCB homologs under diffusion and advection-diffusion mass transport conditions.

Modeling results predicted that only PBDE homolog 1 and PCB homologs 1 and 2 can exhibit substantial mass transport under the relevant 40 year time frame (>1% mass removal for 40 years mass transport simulation). HMW PBDE and PCB homologs generally showed no appreciable mass loss even under a 1000 years simulation time frame (<5% mass removal for 1000 years mass transport simulation). Overall, PBDE homologs consistently have larger K_d , K_{FBC} and smaller D_{obs} and ν values relative to their counterpart PCB homologs. This confirmed the hypothesis that PBDE *in-situ* mobility is substantially less than PCBs. In all the sediment cores, the magnitude of PBDE and PCB homologs sediment transport increase in the order (D(OCBC) < (A(OCBC)) < (D(OC)) < (A(OC))). Advection-diffusion is a complex process and calculated Peclet number which quantified the relative magnitude of advection to diffusion indicated that LMW PBDE and PCB homologs mass transport is driven by advection, whereas HMW PBDE and PCB homologs mass transport is driven by diffusion. This suggests that while advection can accelerate and increase the mobility of LMW PBDE and PCB homologs, it have little effect on HMW homologs given their increased hydrophobicity.

- BC levels in the urban sediments are sufficient to greatly retard the mobility of PBDEs and PCBs compared to prediction based solely on OC. As predicted by K_{BC} , PBDE adsorption to BC was stronger than PCBs reflective off the more hydrophobic nature of PBDEs. The predicted K_{BC} values increased with increasing PBDE and PCB homolog. In urban Chicago and IGC sediments that have higher f_{BC} , the effect of BC inclusion was more pronounced especially in the HMW PBDE and PCB homolog. Inclusion of the BC component more than doubled the predicted effective K_d values and in some cases, more than halved the predicted D_{obs} . This suggests that exclusion of the BC component in urban sediments can lead to gross over prediction of the magnitude of HMW PBDE and PCB homologs mobility.
- In this chapter, mass transport of PBDE and PCB homologs provided with initial sediment concentration at the 5th, 50th, and 95th percentile concentration values under A(OC) conditions were simulated. The A(OC) sorption case was shown to consistently result in the highest mobility

of PBDEs and PCBs. Overall, the magnitude of PBDE and PCB homolog mass transport under A(OC) condition increased in the order of CLC < IGC09 < CWP < AMW < IGC13 < AJL < AOT < CBC < AFR < AED < ACL. K_h and f_{OC} were determined to be important drivers for PBDE and PCB mass transport under the A(OC) condition. Core ACL with high K_h and low f_{OC} had the greatest PBDE and PCB mobility and thus the highest PBDE and PCB mass removal. Core CLC with low K_h and high f_{OC} resulted in low, if not negligible, PBDE and PCB homolog mass removal. Observation of mass simulation results suggests that PBDE and PCB mass transport were more sensitive to the variations in f_{OC} relative to K_h (i.e., decreased in f_{OC} resulted in larger increased in mass removal relative to similar increased in K_h). Higher initial sediment concentration increased the concentration gradient resulting in larger predicted $C_{aq|x=0.02m,t}$ leaving the sediment boundary layer; consequently, the predicted $M_{t/t}$ leaving the sediment boundary layer was also higher. Given the low transport rates, $C_{aq|x=0.02m,t}$ and $M_{t/t}$ of HMW PBDE and PCB homologs were predicted to be lower than LMW PBDE and PCB homologs. The sediment cores in this study had time spans of approximately forty years (estimated from radionuclide data between 1970s to 2010). Under the 40 years model simulation, the predicted fraction of $M_{t/t}/M_{sed|t=0 \text{ year}}$ values for PBDE homolog 1, and PCB homologs 1 and 2, were very small (<10%), whereas for PBDE homologs 2 and larger, and PCB homologs 3 and larger, the $M_{t/t}/M_{sed|t=0 \text{ year}}$ values were negligible. For HMW PBDE and PCB homologs, the $M_{t/t}/M_{sed|t=0 \text{ year}}$ values were negligible even after a 1000 year simulation period. Superimposition of the mass simulation results on measured PBDE and PCB homologs concentrations showed that in-situ mass transport of PBDE and PCB homologs cannot explain the disparity between PBDE and PCB TMs or PCB Aroclors and measured PBDE or PCB sediment profiles.

Sorbate parameters such as low hydrophobicity and LMW, as well certain sorbent parameters such as high K_h and low f_{OC} promote the mass transport of PBDE and PCB homologs in natural aquatic

sediments. The mass transport modeling effort in this chapter simulated the most mobile transport conditions by providing the highest concentration gradient achieved through a hypothetical non-contaminated neighboring sediment segments assumption and high initial sediment concentrations. Even under conditions of optimal mobility, the predicted PBDE and PCB mass transports in the relevant time frame of 40 years was negligible. Thus, it is concluded that the observed disparity between PBDE TMs or PCB Aroclors to PBDE or PCB sediment profile is not a result of *in-situ* sediment transport, but rather it is a result of either pre-depositional processes including differential transport rates of different homologs, and transformation of congeners between the source sites to receptor sites, or post-depositional transformation including microbial facilitated PBDE and PCB transformations. Future analysis to evaluate *in-situ* PBDE and PCB transformations should exclude *in-situ* sediment transport as a contributing factor to congener profile shape and focus on better understanding the contribution of other pre-depositional and post-depositional transport and transformation to heighten the scientific understanding on the fate of PBDEs and PCBs in the environment.

CHAPTER 6. CONCLUSION

Polybrominated diphenyl ethers (PBDEs) and polychlorinated biphenyls (PCBs) are persistent organic contaminants that are ubiquitous in the environment. The Chicago metropolitan sediments are also no exception to PBDE and PCB contamination. PBDE concentration in the five urban metropolitan Chicago cores in this study were lower compared to sediment cores from Arkansas near the PBDE manufacturing facilities⁽¹⁵¹⁾ but higher than reported values for the Great Lakes and in other areas in the U.S.^(45,47,49,50,51,53) The PCB concentration observed in this study was comparable to other industrialized areas such as the Houston Ship Channel⁽⁶¹⁾ and Indiana Harbor Canal.⁽⁶⁰⁾ It is worth noting the PCB concentrations were lower than PCB-historically contaminated sites such as the Thompson Island Pool, NY.⁽⁵⁾ In recent years, PBDE deposition rapidly increased whereas PCB deposition slowly declined.

Two routes of PBDE and PCB depositions to the Chicago sediments were ascertained; hydraulic deposition-dominated sediment cores are heavily impacted by anthropogenic hydraulic discharges such as wastewater treatment plant effluents, stormwater discharges, and combined sewage outfalls and atmospheric deposition-dominated sediment core which is primarily exposed to PBDE and PCB via wet and dry depositions. Hydraulic deposition-dominated cores have higher PBDE and PCB net surface deposition rates compared to atmospheric deposition-dominated cores. Another striking difference between hydraulic and atmospheric deposition-dominated cores was the enrichment of tetra- and penta-PBDE in hydraulic deposition dominated cores.

A multivariate least square regression (MLSR) analysis showed that disparity exist between PBDE and PCB congener profiles in sediment to PBDE technical mixtures (TMs) and PCB Aroclor mixtures. This disparity can be due to several reasons including pre-depositional transformation induced by differential transport rates for different PBDE and PCB homologs and transformation between source sites to receptor sites, and post-depositional transformation including microbial facilitated dehalogenation and *in-situ* contaminant transport in the sediment column. It is important to note while MLSR analysis

confirmed the disparity between sediment profiles to source profiles, this analysis cannot distinguish the source of the disparity.

In this study, several analyses were performed to evaluate the potential of PBDE and PCB degradation in the sediment. Increased in low molecular weight (LMW) homolog concomitant with decreased in high molecular weight homolog (HMW) was observed in core AMW for PBDEs and core CLC for PBDEs and PCBs. Additionally, in these two cores, *ortho*-, *meta*-, and *para*-congener substitution pattern were consistent with microbial facilitated dehalogenation which was reported to preferentially favor *meta*- and *para*-removal. Coupled with high MLSR residuals, *in-situ* dehalogenation in these sediment columns are possible.

Using high-yield pyrosequencing technology, the microbial community structure in the surface sediments and in AMW sediment segment at five years interval were characterized. Overall, the microbial community structure in the surface sediments and in AMW sediment segment were very diverse. Hierarchical analysis and PCA generally grouped the microbial structure in AR surface sediments by increased average distance to PBDE manufacturing facilities and consequently, by decreased PBDE concentrations. Additionally, microbial diversity also increased with increasing distance from the PBDE manufacturing facilities for the AR sediment cores. The high PBDE concentration could be important in influencing the microbial community structure. In the Chicago cores, microbial community was grouped based on exposure pathways. Interestingly, the microbial community structure in AMW was grouped based on depth despite depth-independent hierarchical and PCA analysis; this confirmed the hypothesis of gradual changes in AMW microbial community structure in response to physico-chemical changes in the AMW column. A very striking feature in the surface sediments and in-depth AMW sediment segments are the high abundance of unclassified *Bacteria*. This highlights the diversity of the sediment microbial community structure which up to present day, is still not adequately characterized and understood. The abundance of the unclassified *Bacteria* did not correlate to PBDE and PCB concentrations, or to PBDE

and PCB MLSR residuals. It is thus concluded that the unclassified *Bacteria* is unlikely to play a role in active PBDE and PCB dehalogenation.

Potential PBDE and PCB degrading class OTUs were found in all surface sediments and in in-depth AMW sediment segments. The “super-bug” *Dehalococcoides* spp. was found in only 3 surface sediments; however, in AMW in-depth sediment, *Dehalococcoides* spp. was found in almost all sediment segments and appeared to be better enriched in the lower sediment segment. It should be noted that the occurrences of potential PDBE and PCB degrading class OTUs should not be interpreted as active dehalogenation. In evaluating the potential for microbial PBDE and PCB degradation, it is necessary to look at other dehalogenation indicators as well. In core AMW, the occurrences of the potential PBDE degrader coincided with increased LMW PBDE homologs concomitant with decreased HMW PBDE homologs, increased *para*-substituted congeners, and beneficial sediment column properties for microbial PBDE dehalogenation such as ORP consistent with facultative metabolism, high organic matter and organic carbon concentrations, and high PBDE concentrations.

Collectively evaluating the abundance of potential PBDE and PCB degrading class OTUs in core CLC provided beneficial insight into the role of indigenous microorganisms in PBDE and PCB transformation. Increased LMW PBDE homologs concomitant with decreased HMW PBDE homologs, as well as decreased *para*-substitution was observed; however, increased mean degree of bromination was also observed. Increased LMW PCB homologs concomitant with a decreased HMW PCB homologs was also observed. In addition to decreased degree of chlorination, decreased in *meta*-substituted PCB congeners concomitant with increased in *ortho*-substituted PCB congeners provided among the best indicators of microbial facilitated PCB degradation. PCB concentrations were approximately three times higher than PBDE concentration in core CLC. Additionally, abundance of potential PCB degrader far exceeded that of PBDEs. Taken collectively, it is concluded that microbial facilitated PCB degradation in core CLC was more likely than PBDE degradation.

This study also evaluated PBDE and PCB *in-situ* mass transport in natural sediment columns. Overall, PBDE homologs have higher mobility than PCB homologs; this was expected as PBDEs have HMW and higher hydrophobicity which increase solid phase partitioning and decrease aqueous mobility. HMW PBDE and PCB homologs have restricted mobility. Peclet numbers suggest that mass transport of LMW PBDE and PCB homologs were driven by diffusion whereas mass transport of HMW PBDE and PCB homologs were driven by advection. Consideration of organic carbon and black carbon (OCBC) co-sorption showed that PBDE and PCB mobility, especially HMW congeners, were highly restricted relative to organic carbon only sorption. Exclusion of the BC sorption component, especially in urban sediments with high BC fraction, can result in gross over-prediction of the magnitude of PBDE and PCB vertical mass transport in the sediment column. The highest PBDE and PCB mobility scenario was provided by advection-diffusion mass transport with organic carbon (OC) only sorption. Mass simulation performed at 40, 100, and 1000 years showed that overall, PBDE and PCB mass transport if occurring, is only at a negligible rate. For PBDE and PCB homolog 1, mass simulation under 1000 year simulation period only predicted less than 25% mass loss. At a 40 year simulation period, PBDE and PCB breakthrough even under highly optimum mobility condition were negligible. With the exception of PBDE H10 (BDE-209), linear mixing model (LMM) underpredicted the measured PBDE and PCB concentrations significantly. Addition of error bars representing maximum mass loss of PBDE and PCB to measured PBDE and PCB concentrations were far from overlapping with LMM predicted PBDE and PCB concentrations; this suggest that *in-situ* mass transport of PBDE and PCB homologs in the sediment column is not sufficient to substantially shift the deposited PBDE and PCB profiles. Overall, it was concluded that PBDE and PCB mass transport, although occurring, is occurring at very slow rate and cannot account for the disparity observed between PBDE and PCB congener profiles in sediment and PBDE TMs and PCB Aroclor mixtures.

This research has elucidated upon the recent trend and extends of PBDE and PCB contamination in the metropolitan Chicago area. The microbial community characterization provided beneficial insight

into the role of microorganisms in influencing PBDE and PCB fate. Rigorous mass simulation predicted that *in-situ* PBDE and PCB mass transport, even under highly optimum conditions for mobility, are occurring at a very low rate and will not affect observed PBDE and PCB distribution in the sediment phase. Future studies should focus on finding trace indicators in support of *in-situ* microbial facilitated PBDE and PCB degradation. Multiple lines of evidence provided in this research including observation of homolog changes, OMP-substitution pattern, and MLSR analysis, as well as physical properties beneficial for degradation, can only act as indicators that need to be evaluated collectively to provide supportive evidence in support of dehalogenation, but is not a direct indicator of dehalogenation. To better understand the fate of sediment phase PBDEs and PCBs, it is necessary to understand other factors that can affect *in-situ* degradation. The rigorous mass simulation showed that PBDE and PCB mass transport simulated under conditions optimum for mobility, has no observable effect on the PBDE and PCB sediment profile. Future studies should focus on understanding other factors that contribute towards the disparity between PBDE TMs and PCB Aroclor mixtures to PBDE and PCB sediment profile including pre-depositional process such as differential transport rate and transformation between source sites to receptor sites, and other post-depositional process such as microbial facilitated dehalogenation. Overall, this research has helped provide better understanding on the indigenous microbial community structure in PBDE- and PCB-impacted sediments, and has confirmed *in-situ* mass transport as a negligible factor influencing the fate of environmental deposited PBDEs and PCBs.

Cited Literature

1. Imm, P., et al., *Household exposures to polybrominated diphenyl ethers (PBDEs) in a Wisconsin cohort*. Environmental health perspectives, 2009. **117**(12): p. 1890.
2. Betts, K.S., *New thinking on flame retardants*. Environmental Health Perspectives, 2008. **116**(5): p. A210.
3. Shaw, S., *Halogenated flame retardants: do the fire safety benefits justify the risks?* Reviews on environmental health, 2010. **25**(4): p. 261-306.
4. Shiu, W.Y. and D. Mackay, *A critical review of aqueous solubilities, vapor pressures, Henry's law constants, and octanol-water partition coefficients of the polychlorinated biphenyls*. 1986: American Chemical Society and the American Institute of Physics for the National Bureau of Standards.
5. Butcher, J.B. and E.A. Garvey, *PCB loading from sediment in the Hudson River: Congener signature analysis of pathways*. Environmental science & technology, 2004. **38**(12): p. 3232-3238.
6. Troitzsch, J., *Flame Retardants*. Kunststoffe-German Plastics, 1990. **80**(3): p. 434-435.
7. Alaei, M., et al., *An overview of commercially used brominated flame retardants, their applications, their use patterns in different countries/regions and possible modes of release*. Environment International, 2003. **29**(6): p. 683-689.
8. Birnbaum, L.S. and D.F. Staskal, *Brominated flame retardants: Cause for concern?* Environmental Health Perspectives, 2004. **112**(1): p. 9-17.
9. de Wit, C.A., *An overview of brominated flame retardants in the environment*. Chemosphere, 2002. **46**(5): p. 583-624.
10. La Guardia, M.J., R.C. Hale, and E. Harvey, *Detailed polybrominated diphenyl ether (PBDE) congener composition of the widely used penta-, octa-, and deca-PBDE technical flame-retardant mixtures*. Environmental science & technology, 2006. **40**(20): p. 6247-6254.
11. Hale, R.C., et al., *Polybrominated diphenyl ether flame retardants in the North American environment*. Environment International, 2003. **29**(6): p. 771.
12. Birnbaum, L.S. and E.A.C. Hubal, *Polybrominated diphenyl ethers: a case study for using biomonitoring data to address risk assessment questions*. Environmental health perspectives, 2006. **114**(11): p. 1770.
13. Institute, E.P.R., *The PCB Information Manual: Volume 1: Production, Uses, Characteristics, and Toxicity of PCBs*.
14. BIPHENYLS, P., *TOXICOLOGICAL PROFILE FOR POLYCHLORINATED BIPHENYLS (PCBs)*. 2000.
15. Ballschmiter, K. and M. Zell, *Analysis of polychlorinated biphenyls (PCB) by glass capillary gas chromatography*. Fresenius' Journal of Analytical Chemistry, 1980. **302**(1): p. 20-31.
16. Frame, G.M., J.W. Cochran, and S.S. Bøwadt, *Complete PCB congener distributions for 17 aroclor mixtures determined by 3 HRGC systems optimized for comprehensive, quantitative, congener-specific analysis*. Journal of High Resolution Chromatography, 2005. **19**(12): p. 657-668.
17. Bolton, E.E., et al., *PubChem: integrated platform of small molecules and biological activities*. Annual reports in computational chemistry, 2008. **4**: p. 217-241.
18. Tittlemier, S.A., et al., *Vapor pressures, aqueous solubilities, and Henry's law constants of some brominated flame retardants*. Environmental Toxicology and Chemistry, 2002. **21**(9): p. 1804-1810.
19. Braekvelt, E., S.A. Tittlemier, and G.T. Tomy, *Direct measurement of octanol-water partition coefficients of some environmentally relevant brominated diphenyl ether congeners*. Chemosphere, 2003. **51**(7): p. 563-567.

20. Kuramochi, H., et al., *Determination of physicochemical properties of tetrabromobisphenol A*. Environmental Toxicology and Chemistry, 2008. **27**(12): p. 2413-2418.
21. Hayward, S.J., Y.D. Lei, and F. Wania, *Comparative evaluation of three high-performance liquid chromatography-based Kow estimation methods for highly hydrophobic organic compounds: Polybrominated diphenyl ethers and hexabromocyclododecane*. Environmental toxicology and chemistry, 2006. **25**(8): p. 2018-2027.
22. Kuramochi, H. and S.-i. Sakai, *Measurement of vapor pressures of some PBDEs and HBCD diastereoisomers*.
23. Wania, F. and C.B. Dugani, *Assessing the long-range transport potential of polybrominated diphenyl ethers: A comparison of four multimedia models*. Environmental Toxicology and Chemistry, 2009. **22**(6): p. 1252-1261.
24. De Bruijn, J., et al., *Determination of octanol/water partition coefficients for hydrophobic organic chemicals with the "slow-stirring" method*. Environmental Toxicology and Chemistry, 1989. **8**(6): p. 499-512.
25. EPA, U., *Estimation Program Interface (EPI) Suite, version 4.10*. Office of Pollution Prevention & Toxics (OPPT) and Syracuse Research Corporation (SRC), Washington, DC, USA, 2003.
26. Ying, G.-G., X.-Y. Yu, and R.S. Kookana, *Biological degradation of triclocarban and triclosan in a soil under aerobic and anaerobic conditions and comparison with environmental fate modelling*. Environmental Pollution, 2007. **150**(3): p. 300-305.
27. Langford, K.H., et al., *The partitioning of alkylphenolic surfactants and polybrominated diphenyl ether flame retardants in activated sludge batch tests*. Chemosphere, 2005. **61**(9): p. 1221-1230.
28. Weininger, D., *SMILES, a chemical language and information system. 1. Introduction to methodology and encoding rules*. Journal of chemical information and computer sciences, 1988. **28**(1): p. 31-36.
29. Allchin, C., R. Law, and S. Morris, *Polybrominated diphenylethers in sediments and biota downstream of potential sources in the UK*. Environmental Pollution, 1999. **105**(2): p. 197-207.
30. Watanabe, I. and S. Sakai, *Environmental release and behavior of brominated flame retardants*. Environment International, 2003. **29**(6): p. 665-682.
31. Alcock, R.E., et al., *Understanding levels and trends of BDE-47 in the UK and North America: an assessment of principal reservoirs and source inputs*. Environment international, 2003. **29**(6): p. 691-698.
32. Rahman, F., et al., *Polybrominated diphenyl ether (PBDE) flame retardants*. Science of the Total Environment, 2001. **275**(1): p. 1-17.
33. Sellström, U., et al., *Polybrominated diphenyl ethers and hexabromocyclododecane in sediment and fish from a Swedish river*. Environmental Toxicology and Chemistry, 2009. **17**(6): p. 1065-1072.
34. Butt, C.M., et al., *Spatial distribution of polybrominated diphenyl ethers in southern Ontario as measured in indoor and outdoor window organic films*. Environmental science & technology, 2004. **38**(3): p. 724-731.
35. Jones-Otazo, H.A., et al., *Is house dust the missing exposure pathway for PBDEs? An analysis of the urban fate and human exposure to PBDEs*. Environmental science & technology, 2005. **39**(14): p. 5121-5130.
36. Zota, A.R., et al., *Elevated house dust and serum concentrations of PBDEs in California: unintended consequences of furniture flammability standards?* Environmental science & technology, 2008. **42**(21): p. 8158-8164.
37. Rudel, R.A., et al., *Phthalates, alkylphenols, pesticides, polybrominated diphenyl ethers, and other endocrine-disrupting compounds in indoor air and dust*. Environmental science & technology, 2003. **37**(20): p. 4543-4553.
38. Harrad, S., et al., *Polybrominated diphenyl ethers in domestic indoor dust from Canada, New Zealand, United Kingdom and United States*. Environment International, 2008. **34**(2): p. 232-238.

39. Davis, E.F., S.L. Klosterhaus, and H.M. Stapleton, *Measurement of flame retardants and triclosan in municipal sewage sludge and biosolids*. Environment international, 2012. **40**: p. 1-7.
40. North, K.D., *Tracking polybrominated diphenyl ether releases in a wastewater treatment plant effluent, Palo Alto, California*. Environmental science & technology, 2004. **38**(17): p. 4484.
41. La Guardia, M.J., et al., *Organic contaminants of emerging concern in land-applied sewage sludge (biosolids)*. J Residuals Sci Technol, 2004. **1**(2): p. 105-116.
42. de Boer, J., et al., *Polybrominated diphenyl ethers in influents, suspended particulate matter, sediments, sewage treatment plant and effluents and biota from the Netherlands*. Environmental Pollution, 2003. **122**(1): p. 63-74.
43. Oros, D.R., et al., *Levels and distribution of polybrominated diphenyl ethers in water, surface sediments, and bivalves from the San Francisco Estuary*. Environmental science & technology, 2005. **39**(1): p. 33-41.
44. Breivik, K., et al., *Towards a global historical emission inventory for selected PCB congeners—a mass balance approach: 2. Emissions*. Science of the Total Environment, 2002. **290**(1): p. 199-224.
45. Song, W.L., et al., *Polybrominated Diphenyl Ethers in the Sediment of the Great Lakes. 1 - Lake Superior*. Environmental Science and Technology, 2004. **38**(12): p. 38(12):3286-3293.
46. Buckley, D.R., et al., *Soot deposition in the Great Lakes: implications for semi-volatile hydrophobic organic pollutant deposition*. Environ Sci Technol, 2004. **38**(6): p. 1732-9.
47. Song, W., et al., *Polybrominated diphenyl ethers in the sediments of the Great Lakes. 3. Lakes Ontario and Erie*. Environ Sci Technol, 2005. **39**(15): p. 5600-5.
48. Samara, F., C.W. Tsai, and D.S. Aga, *Determination of potential sources of PCBs and PBDEs in sediments of the Niagara River*. Environmental pollution (Barking, Essex: 1987), 2006. **139**(3): p. 489.
49. Song, W., et al., *Polybrominated diphenyl ethers in the sediments of the Great Lakes. 2. Lakes Michigan and Huron*. Environ Sci Technol, 2005. **39**(10): p. 3474-9.
50. Zhu, L.Y. and R.A. Hites, *Brominated flame retardants in sediment cores from Lakes Michigan and Erie*. Environmental science & technology, 2005. **39**(10): p. 3488-3494.
51. Yun, S.H., et al., *Polybrominated diphenyl ethers and polybrominated biphenyls in sediment and floodplain soils of the Saginaw River watershed, Michigan, USA*. Archives of environmental contamination and toxicology, 2008. **55**(1): p. 1-10.
52. Dodder, N.G., B. Strandberg, and R.A. Hites, *Concentrations and spatial variations of polybrominated diphenyl ethers and several organochlorine compounds in fishes from the northeastern United States*. Environmental science & technology, 2002. **36**(2): p. 146-151.
53. Bradley, P.W., et al., *PBDEs and methoxylated analogues in sediment cores from two Michigan, USA, inland lakes*. Environmental Toxicology and Chemistry, 2011. **30**(6): p. 1236-1242.
54. Frank, R., et al., *Organochlorine insecticides and PCB in surficial sediments (1968) and sediment cores (1976) from Lake Ontario*. Journal of Great Lakes Research, 1979. **5**(1): p. 18-27.
55. Frank, R., et al., *Organochlorine insecticides and PCB in the surficial sediments of Lake Superior (1973)*. Journal of Great Lakes Research, 1980. **6**(2): p. 113-120.
56. Frank, R., et al., *Organochlorine insecticides and PCB in surficial sediments of Lake Michigan (1975)*. Journal of Great Lakes Research, 1981. **7**(1): p. 42-50.
57. Frank, R., et al., *Organochlorine insecticides and PCB in the sediments of Lake Huron (1969) and Georgian Bay and North Channel (1973)*. Science of the Total Environment, 1979. **13**(2): p. 101-117.
58. Li, A., et al., *PCBs in sediments of the Great Lakes—Distribution and trends, homolog and chlorine patterns, and in situ degradation*. Environmental Pollution, 2009. **157**(1): p. 141-147.
59. Jeremiason, J.D., K.C. Hornbuckle, and S.J. Eisenreich, *PCBs in Lake Superior, 1978-1992: decreases in water concentrations reflect loss by volatilization*. Environmental science & technology, 1994. **28**(5): p. 903-914.

60. Martinez, A. and K.C. Hornbuckle, *Record of PCB congeners, sorbents and potential toxicity in core samples in Indiana Harbor and Ship Canal*. Chemosphere, 2011. **85**(3): p. 542-547.
61. Howell, N.L., et al., *Concentrations of polychlorinated biphenyls (PCBs) in water, sediment, and aquatic biota in the Houston Ship Channel, Texas*. Chemosphere, 2008. **70**(4): p. 593-606.
62. Bedard, D.L., *Polychlorinated biphenyls in aquatic sediments: environmental fate and outlook for biological treatment*, in *Dehalogenation*. 2004, Springer. p. 443-465.
63. Magar, V.S., et al., *Long-term recovery of PCB-contaminated sediments at the Lake Hartwell superfund site: PCB dechlorination. 1. End-member characterization*. Environmental science & technology, 2005. **39**(10): p. 3538-3547.
64. Bedard, D.L. and R.J. May, *Characterization of the polychlorinated biphenyls in the sediments of Woods Pond: evidence for microbial dechlorination of Aroclor 1260 in situ*. Environmental science & technology, 1995. **30**(1): p. 237-245.
65. Soonthornnonda, P., et al., *PCBs in Great Lakes sediments, determined by positive matrix factorization*. Journal of Great Lakes Research, 2011. **37**(1): p. 54-63.
66. Abramowicz, D.A., *Aerobic and anaerobic biodegradation of PCBs: a review*. Critical Reviews in Biotechnology, 1990. **10**(3): p. 241-251.
67. Abramowicz, D.A., *Aerobic and anaerobic PCB biodegradation in the environment*. Environmental health perspectives, 1995. **103**(Suppl 5): p. 97.
68. Bedard, D.L., et al., *Extensive degradation of Aroclors and environmentally transformed polychlorinated biphenyls by *Alcaligenes eutrophus* H850*. Applied and environmental microbiology, 1987. **53**(5): p. 1094-1102.
69. Boyle, A.W., et al., *Bacterial PCB biodegradation*. Biodegradation, 1992. **3**(2-3): p. 285-298.
70. Flanagan, W.P. and R.J. May, *Metabolite detection as evidence for naturally occurring aerobic PCB biodegradation in Hudson River sediments*. Environmental science & technology, 1993. **27**(10): p. 2207-2212.
71. Abramowicz, D.A. and D.R. Olson, *Accelerated biodegradation of PCBs*. Chemtech, 1995. **25**(7).
72. Goris, J., et al., *Classification of the biphenyl-and polychlorinated biphenyl-degrading strain LB400T and relatives as *Burkholderia xenovorans* sp. nov.* International journal of systematic and evolutionary microbiology, 2004. **54**(5): p. 1677-1681.
73. Rodrigues, J.L., et al., *Degradation of Aroclor 1242 dechlorination products in sediments by *Burkholderia xenovorans* LB400 (ohb) and *Rhodococcus* sp. strain RHA1 (fcb)*. Applied and environmental microbiology, 2006. **72**(4): p. 2476-2482.
74. Rehmann, L. and A.J. Daugulis, *Enhancement of PCB degradation by *Burkholderia xenovorans* LB400 in biphasic systems by manipulating culture conditions*. Biotechnology and bioengineering, 2008. **99**(3): p. 521-528.
75. Furukawa, K., N. Tomizuka, and A. Kamibayashi, *Metabolic breakdown of Kaneclors (polychlorobiphenyls) and their products by *Acinetobacter* sp.* Applied and environmental microbiology, 1983. **46**(1): p. 140-145.
76. Furukawa, K., N. Tomizuka, and A. Kamibayashi, *Effect of chlorine substitution on the bacterial metabolism of various polychlorinated biphenyls*. Applied and environmental microbiology, 1979. **38**(2): p. 301-310.
77. Hatamian-Zarmi, A., et al., *Extensive biodegradation of highly chlorinated biphenyl and Aroclor 1242 by *Pseudomonas aeruginosa* TMU56 isolated from contaminated soils*. International Biodeterioration & Biodegradation, 2009. **63**(6): p. 788-794.
78. Gibson, D.T., et al., *Oxidation of polychlorinated biphenyls by *Pseudomonas* sp. strain LB400 and *Pseudomonas pseudoalcaligenes* KF707*. Journal of bacteriology, 1993. **175**(14): p. 4561-4564.
79. Bopp, L.H., *Degradation of highly chlorinated PCBs by *Pseudomonas* strain LB400*. Journal of Industrial Microbiology & Biotechnology, 1986. **1**(1): p. 23-29.

80. Billingsley, K., et al., *Remediation of PCBs in soil by surfactant washing and biodegradation in the wash by Pseudomonas sp. LB400*. Biotechnology letters, 2002. **24**(21): p. 1827-1832.
81. Adebuseye, S.A., et al., *Metabolism of chlorinated biphenyls: Use of 3, 3'-and 3, 5-dichlorobiphenyl as sole sources of carbon by natural species of *Ralstonia* and *Pseudomonas**. Chemosphere, 2008. **70**(4): p. 656-663.
82. Seto, M., et al., *A novel transformation of polychlorinated biphenyls by Rhodococcus sp. strain RHA1*. Applied and environmental microbiology, 1995. **61**(9): p. 3353-3358.
83. Begonja Kolar, A., et al., *PCB-degrading potential of aerobic bacteria enriched from marine sediments*. International biodeterioration & biodegradation, 2007. **60**(1): p. 16-24.
84. Seto, M., et al., *Multiple Polychlorinated Biphenyl Transformation Systems in the Gram-Positive Bacterium Rhodococcus sp. Strain RHA1*. Applied and environmental microbiology, 1995. **61**(12): p. 4510-4513.
85. Bell, K., et al., *The genus Rhodococcus*. Journal of Applied Microbiology, 1998. **85**(2): p. 195-210.
86. Madigan, M.T., et al., *Biology of microorganisms*. Vol. 985. 1997: prentice hall Upper Saddle River, NJ.
87. Nies, L. and T.M. Vogel, *Effects of organic substrates on dechlorination of Aroclor 1242 in anaerobic sediments*. Applied and environmental microbiology, 1990. **56**(9): p. 2612-2617.
88. Borja, J., et al., *Polychlorinated biphenyls and their biodegradation*. Process Biochemistry, 2005. **40**(6): p. 1999-2013.
89. Cutter, L., K.R. Sowers, and H.D. May, *Microbial dechlorination of 2, 3, 5, 6-tetrachlorobiphenyl under anaerobic conditions in the absence of soil or sediment*. Applied and environmental microbiology, 1998. **64**(8): p. 2966-2969.
90. Berkaw, M., K.R. Sowers, and H.D. May, *Anaerobic ortho Dechlorination of Polychlorinated Biphenyls by Estuarine Sediments from Baltimore Harbor*. Applied and Environmental Microbiology, 1996. **62**(7): p. 2534-2539.
91. Van Dort, H.M. and D.L. Bedard, *Reductive ortho and meta dechlorination of a polychlorinated biphenyl congener by anaerobic microorganisms*. Applied and environmental microbiology, 1991. **57**(5): p. 1576-1578.
92. Bedard, D.L., K.M. Ritalahti, and F.E. Löffler, *The Dehalococcoides population in sediment-free mixed cultures metabolically dechlorinates the commercial polychlorinated biphenyl mixture Aroclor 1260*. Applied and environmental microbiology, 2007. **73**(8): p. 2513-2521.
93. Quensen, J.F., J.M. Tiedje, and S.A. Boyd, *Reductive dechlorination of polychlorinated biphenyls by anaerobic microorganisms from sediments*. Science, 1988. **242**(4879): p. 752-754.
94. Adrian, L., et al., *"Dehalococcoides" sp. strain CBDB1 extensively dechlorinates the commercial polychlorinated biphenyl mixture Aroclor 1260*. Applied and environmental microbiology, 2009. **75**(13): p. 4516-4524.
95. Kjellerup, B.V., et al., *Site-specific microbial communities in three PCB-impacted sediments are associated with different in situ dechlorinating activities*. Environmental Microbiology, 2008. **10**(5): p. 1296-1309.
96. Yan, T., T.M. LaPara, and P.J. Novak, *The reductive dechlorination of 2, 3, 4, 5-tetrachlorobiphenyl in three different sediment cultures: evidence for the involvement of phylogenetically similar Dehalococcoides-like bacterial populations*. FEMS microbiology ecology, 2006. **55**(2): p. 248-261.
97. May, H.D., et al., *Dehalorespiration with polychlorinated biphenyls by an anaerobic ultramicrobacterium*. Applied and environmental microbiology, 2008. **74**(7): p. 2089-2094.
98. Scholz-Muramatsu, H., et al., *Isolation and characterization of Dehalospirillum multivorans gen. nov., sp. nov., a tetrachloroethene-utilizing, strictly anaerobic bacterium*. Archives of Microbiology, 1995. **163**(1): p. 48-56.

99. Richardson, R.E., et al., *Phylogenetic characterization of microbial communities that reductively dechlorinate TCE based upon a combination of molecular techniques*. Environmental science & technology, 2002. **36**(12): p. 2652-2662.
100. Fennell, D.E., et al., *Dehalococcoides ethenogenes strain 195 reductively dechlorinates diverse chlorinated aromatic pollutants*. Environmental science & technology, 2004. **38**(7): p. 2075-2081.
101. Maymo-Gatell, X., et al., *Isolation of a bacterium that reductively dechlorinates tetrachloroethene to ethene*. Science, 1997. **276**(5318): p. 1568-1571.
102. He, J., K.R. Robrock, and L. Alvarez-Cohen, *Microbial reductive debromination of polybrominated diphenyl ethers (PBDEs)*. Environmental Science & Technology, 2006. **40**(14): p. 4429-4434.
103. Robrock, K.R., P. Korytár, and L. Alvarez-Cohen, *Pathways for the anaerobic microbial debromination of polybrominated diphenyl ethers*. Environmental science & technology, 2008. **42**(8): p. 2845-2852.
104. Bedard, D.L. and H.M. Van Dort, *Complete reductive dehalogenation of brominated biphenyls by anaerobic microorganisms in sediment*. Applied and environmental microbiology, 1998. **64**(3): p. 940-947.
105. Wiegel, J. and Q. Wu, *Microbial reductive dehalogenation of polychlorinated biphenyls*. FEMS microbiology ecology, 2006. **32**(1): p. 1-15.
106. Sanford, R.A., et al., *Characterization of Desulfitobacterium chlororespirans sp. nov., which grows by coupling the oxidation of lactate to the reductive dechlorination of 3-chloro-4-hydroxybenzoate*. Applied and environmental microbiology, 1996. **62**(10): p. 3800-3808.
107. Schmidt, S., et al., *Biodegradation of diphenyl ether and its monohalogenated derivatives by Sphingomonas sp. strain SS3*. Applied and environmental microbiology, 1992. **58**(9): p. 2744-2750.
108. Robrock, K.R., et al., *Aerobic biotransformation of polybrominated diphenyl ethers (PBDEs) by bacterial isolates*. Environmental science & technology, 2009. **43**(15): p. 5705-5711.
109. Deng, D., et al., *Aerobic debromination of deca-BDE: Isolation and characterization of an indigenous isolate from a PBDE contaminated sediment*. International Biodeterioration & Biodegradation, 2011. **65**(3): p. 465-469.
110. Rockne, K.J. and S.E. Strand, *Biodegradation of bicyclic and polycyclic aromatic hydrocarbons in anaerobic enrichments*. Environmental science & technology, 1998. **32**(24): p. 3962-3967.
111. Rockne, K.J., et al., *Anaerobic naphthalene degradation by microbial pure cultures under nitrate-reducing conditions*. Applied and Environmental Microbiology, 2000. **66**(4): p. 1595-1601.
112. Rockne, K.J. and S.E. Strand, *Anaerobic biodegradation of naphthalene, phenanthrene, and biphenyl by a denitrifying enrichment culture*. Water research, 2001. **35**(1): p. 291-299.
113. Bouwer, E.J. and P.L. McCarty, *Removal of trace chlorinated organic compounds by activated carbon and fixed-film bacteria*. Environmental Science & Technology, 1982. **16**(12): p. 836-843.
114. Rayne, S., M.G. Ikonomou, and M.M.D. Whale, *Anaerobic microbial and photochemical degradation of 4, 4'-dibromodiphenyl ether*. Water Research, 2003. **37**(3): p. 551-560.
115. Gerecke, A.C., et al., *Anaerobic degradation of decabromodiphenyl ether*. Environmental science & technology, 2005. **39**(4): p. 1078-1083.
116. Lee, L.K. and J. He, *Reductive debromination of polybrominated diphenyl ethers by anaerobic bacteria from soils and sediments*. Applied and environmental microbiology, 2010. **76**(3): p. 794-802.
117. Shendure, J. and H. Ji, *Next-generation DNA sequencing*. Nature biotechnology, 2008. **26**(10): p. 1135-1145.
118. Hemond, H.F. and E.J. Fechner-Levy, *Chemical fate and transport in the environment*. 2000: Academic Press.

119. Viana, P.Z., K. Yin, and K.J. Rockne, *Modeling active capping efficacy. 1. Metal and organometal contaminated sediment remediation*. Environ Sci Technol, 2008. **42**(23): p. 8922-9.
120. Yin, K., P.Z. Viana, and K.J. Rockne. *Verification of active cap contaminant breakthrough simulations via laboratory column studies*. in *Fifth International Conference on Remediation of Contaminated Sediments*. 2009. Jacksonville, FL.
121. Yin, K., et al. *A Monte Carlo simulation approach for active caps in mixed contaminant environments; Paper D-018*. in *Proceedings of the Fourth International Conference on Remediation of Contaminated Sediments*. 2007. Columbus, OH: Battele Press.
122. EPI, U. *Estimation Program Interface (EPI)*. Available from: <http://www.epa.gov/opptintr/exposure/pubs/episuite.htm>.
123. Seth, R., D. Mackay, and J. Muncke, *Estimating the organic carbon partition coefficient and its variability for hydrophobic chemicals*. Environmental Science & Technology, 1999. **33**(14): p. 2390-2394.
124. Baker, J.R., et al., *Evaluation of estimation methods for organic carbon normalized sorption coefficients*. Water environment research, 1997: p. 136-145.
125. Gerstl, Z., *Estimation of organic chemical sorption by soils*. Journal of contaminant hydrology, 1990. **6**(4): p. 357-375.
126. Kenaga, E. and C. Goring, *Relationship between water solubility, soil sorption, octanol-water partitioning, and concentration of chemicals in biota*. Aquatic toxicology. American Society for Testing and Materials, Philadelphia, Pennsylvania, 1980: p. 78-115.
127. Sabljic, A., et al., *QSAR modelling of soil sorption. Improvements and systematics of log K_{OC} vs. log K_{OW} correlations*. Chemosphere, 1995. **31**(11): p. 4489-4514.
128. Chiou, C.T., D.W. Schmedding, and M. Manes, *Partitioning of organic compounds in octanol-water systems*. Environmental Science & Technology, 1982. **16**(1): p. 4-10.
129. Karickhoff, S.W., D.S. Brown, and T.A. Scott, *Sorption of hydrophobic pollutants on natural sediments*. Water research, 1979. **13**(3): p. 241-248.
130. Dai, J., et al., *QSAR for polychlorinated organic compounds (PCOCs). I. Prediction of partition properties for PCOCs using quantum chemical parameters*. Bulletin of environmental contamination and toxicology, 1999. **62**(5): p. 530-538.
131. Karickhoff, S.W., *Semi-empirical estimation of sorption of hydrophobic pollutants on natural sediments and soils*. Chemosphere, 1981. **10**(8): p. 833-846.
132. Schwarzenbach, R.P. and J. Westall, *Transport of nonpolar organic compounds from surface water to groundwater. Laboratory sorption studies*. Environmental Science & Technology, 1981. **15**(11): p. 1360-1367.
133. Crank, J., *The mathematics of diffusion*. 1979: Oxford university press.
134. Bird, R.B., W.E. Stewart, and E.N. Lightfoot, *Transport phenomena*. 2006: Wiley.
135. Weber, W.J., *Environmental systems and processes: Principles, modeling, and design*. 2001: Wiley-Interscience.
136. Rockne, K.J., G.L. Taghon, and D.S. Kosson, *Pore structure of soot deposits from several combustion sources*. Chemosphere, 2000. **41**(8): p. 1125-1135.
137. Lohmann, R., J. MacFarlane, and P. Gschwend, *Importance of black carbon to sorption of native PAHs, PCBs, and PCDDs in Boston and New York harbor sediments*. Environmental science & technology, 2005. **39**(1): p. 141-148.
138. Accardi-Dey, A. and P.M. Gschwend, *Assessing the combined roles of natural organic matter and black carbon as sorbents in sediments*. Environmental science & technology, 2002. **36**(1): p. 21-29.
139. Di Paolo, C., et al., *Black carbon inclusive multichemical modeling of PBDE and PCB biomagnification and-transformation in estuarine food webs*. Environmental science & technology, 2010. **44**(19): p. 7548-7554.

140. Alvarez, P.J. and W.A. Illman, *Bioremediation and natural attenuation: process fundamentals and mathematical models*. Vol. 27. 2005: John Wiley & Sons.
141. Viana, P.Z., K. Yin, and K.J. Rockne, *Field Measurements and Modeling of Ebullition-Facilitated Flux of Heavy Metals and Polycyclic Aromatic Hydrocarbons from Sediments to the Water Column*. Environmental Science & Technology, 2012. **46**(21): p. 12046-12054.
142. Fu, J., et al., *Persistent organic pollutants in environment of the Pearl River Delta, China: an overview*. Chemosphere, 2003. **52**(9): p. 1411-1422.
143. Mai, B., et al., *Distribution of polybrominated diphenyl ethers in sediments of the Pearl River Delta and adjacent South China Sea*. Environmental science & technology, 2005. **39**(10): p. 3521-3527.
144. Cheung, K., et al., *Assessment of metal and nutrient concentrations in river water and sediment collected from the cities in the Pearl River Delta, South China*. Chemosphere, 2003. **52**(9): p. 1431-1440.
145. Pouyat, R. and M. McDonnell, *Heavy metal accumulations in forest soils along an urban-rural gradient in southeastern New York, USA*. Water, Air, and Soil Pollution, 1991. **57**(1): p. 797-807.
146. Motelay-Massei, A., et al., *Using passive air samplers to assess urban-rural trends for persistent organic pollutants and polycyclic aromatic hydrocarbons. 2. Seasonal trends for PAHs, PCBs, and organochlorine pesticides*. Environmental science & technology, 2005. **39**(15): p. 5763-5773.
147. Chen, T., et al., *Assessment of trace metal distribution and contamination in surface soils of Hong Kong*. Environmental pollution, 1997. **96**(1): p. 61-68.
148. Wilcke, W., et al., *Urban soil contamination in Bangkok: heavy metal and aluminium partitioning in topsoils*. Geoderma, 1998. **86**(3): p. 211-228.
149. Minh, N., et al., *Contamination by persistent organic pollutants in dumping sites of Asian developing countries: implication of emerging pollution sources*. Archives of Environmental Contamination and Toxicology, 2006. **50**(4): p. 474-481.
150. Mukherjee, A., et al., *Arsenic contamination in groundwater: a global perspective with emphasis on the Asian scenario*. Journal of Health, Population and Nutrition, 2006. **24**(2): p. 142-163.
151. Wei, H., et al., *Polybromodiphenyl ethers and decabromodiphenyl ethane in aquatic sediments from southern and eastern Arkansas, United States*. Environ Sci Technol, 2012. **46**(15): p. 8017-24.
152. McDonald, T.A., *A perspective on the potential health risks of PBDEs*. Chemosphere, 2002. **46**(5): p. 745-755.
153. Darnerud, P.O., *Toxic effects of brominated flame retardants in man and in wildlife*. Environment International, 2003. **29**(6): p. 841.
154. Wei, H., et al., *Photolytic debromination pathway of polybrominated diphenyl ethers in hexane by sunlight*. Environ Pollut, 2012. **174C**: p. 194-200.
155. Söderström, G., et al., *Photolytic debromination of decabromodiphenyl ether (BDE 209)*. Environmental Science & Technology, 2004. **38**(1): p. 127-132.
156. Ahn, M.Y., et al., *Photodegradation of decabromodiphenyl ether adsorbed onto clay minerals, metal oxides, and sediment*. Environmental Science & Technology, 2006. **40**(1): p. 215-220.
157. Buehler, S.S., I. Basu, and R.A. Hites, *A comparison of PAH, PCB, and pesticide concentrations in air at two rural sites on Lake Superior*. Environmental science & technology, 2001. **35**(12): p. 2417-2422.
158. Buehler, S.S., I. Basu, and R.A. Hites, *Causes of variability in pesticide and PCB concentrations in air near the Great Lakes*. Environmental science & technology, 2004. **38**(2): p. 414-422.
159. Hung, H., et al., *Are PCBs in the Canadian Arctic atmosphere declining? Evidence from 5 years of monitoring*. Environmental science & technology, 2001. **35**(7): p. 1303-1311.
160. Meijer, S.N., et al., *Global distribution and budget of PCBs and HCB in background surface soils: implications for sources and environmental processes*. Environmental science & technology, 2003. **37**(4): p. 667-672.

161. Jaward, F.M., et al., *Passive air sampling of PCBs, PBDEs, and organochlorine pesticides across Europe*. Environmental science & technology, 2004. **38**(1): p. 34-41.
162. Jaward, F.M., et al., *Passive air sampling of polychlorinated biphenyls, organochlorine compounds, and polybrominated diphenyl ethers across Asia*. Environmental science & technology, 2005. **39**(22): p. 8638-8645.
163. Schneider, A.R., et al., *Recent declines in PAH, PCB, and toxaphene levels in the northern Great Lakes as determined from high resolution sediment cores*. Environmental science & technology, 2001. **35**(19): p. 3809-3815.
164. Viana, P., et al., *Active sediment capping for pollutant mixtures: Control of biogenic gas production under highly intermittent flows*. Land Contamination and Reclamation, 2007. **15**(4): p. 413.
165. Rockne, K.J., P. Viana, K. Yin, *Sediment Gas Ebullition and Flux Studies: Bubbly Creek, South Fork South Branch, Chicago River. Volume 1 of 2: Report and Appendices A-D*. 2010, United States Army Corps of Engineers Chicago District: United States Army Corps of Engineers Chicago District. p. 96 pp.
166. Li, A., J.K. Jang, and P.A. Scheff, *Application of EPA CMB8. 2 model for source apportionment of sediment PAHs in Lake Calumet, Chicago*. Environmental science & technology, 2003. **37**(13): p. 2958-2965.
167. Jang, J.K. and A. Li, *Temporal and Spatial Distributions of PAHs and PCBs in Lake Calumet Area, Chicago*. INTERNATIONAL JOURNAL OF SEDIMENT RESEARCH, 2003. **18**(2): p. 239-247.
168. CHICAGO, M.W.R.D.O.G. *Calumet WRP*. [cited 2013 05/21/2013]; Available from: <https://www.mwrd.org/irj/portal/anonymous/calumet>.
169. Rockne, K.J., R. Kaliappan, and G. Bourgon, *Sediment Gas Ebullition Study, Grand Calumet River, Western Branch, Reaches 1 and 2*. 2011, University of Illinois at Chicago: USACE-Chicago District. p. 234 pp.
170. Cahill, R. and M. Unger, *Evaluation of the extent of contaminated sediments in the West Branch of the Grand Calumet River, Indiana-Illinois, USA*. Water Science & Technology, 1993. **28**(8-9): p. 53-58.
171. Unger, M.T. and R. Sutton, *EAST Process Increases Capacity and Performance at the Sanitary District of Hammond*. Proceedings of the Water Environment Federation, 2003. **2003**(5): p. 137-143.
172. Hinchey, E.K. and L.C. Schaffner, *An evaluation of electrode insertion techniques for measurement of redox potential in estuarine sediments*. Chemosphere, 2005. **59**(5): p. 703-710.
173. Hargrave, B., M. Holmer, and C. Newcombe, *Towards a classification of organic enrichment in marine sediments based on biogeochemical indicators*. Marine pollution bulletin, 2008. **56**(5): p. 810-824.
174. Rockne, K.J., et al., *Distributed Sequestration and Release of PAHs in Weathered Sediment: The Role of Sediment Structure and Organic Carbon Properties*. Environmental Science & Technology, 2002. **36**(12): p. 2636-2644.
175. Li, A., et al., *Polybrominated diphenyl ethers in the sediments of the Great Lakes. 4. Influencing factors, trends, and implications*. Environ Sci Technol, 2006. **40**(24): p. 7528-34.
176. Gustafsson, Ö., et al., *Quantification of the dilute sedimentary soot phase: Implications for PAH speciation and bioavailability*. Environmental Science & Technology, 1996. **31**(1): p. 203-209.
177. Gustafsson, Ö. and P.M. Gschwend, *The flux of black carbon to surface sediments on the New England continental shelf*. Geochimica et Cosmochimica Acta, 1998. **62**(3): p. 465-472.
178. Appleby, P., *Chronostratigraphic techniques in recent sediments*. Tracking environmental change using lake sediments, 2002: p. 171-203.
179. Reddy, K.R. and R.D. DeLaune, *Biogeochemistry of wetlands: science and applications*. 2008: CRC.

180. Kannan, K., K.A. Maruya, and S. Tanabe, *Distribution and characterization of polychlorinated biphenyl congeners in soil and sediments from a superfund site contaminated with Aroclor 1268*. Environmental science & technology, 1997. **31**(5): p. 1483-1488.
181. Rowe, A.A., et al., *Air-water exchange of polychlorinated biphenyls in the Delaware River*. Environmental science & technology, 2007. **41**(4): p. 1152-1158.
182. Hu, D. and K.C. Hornbuckle, *Inadvertent Polychlorinated Biphenyls in Commercial Paint Pigments†*. Environmental science & technology, 2009. **44**(8): p. 2822-2827.
183. Eljarrat, E., S. Lacorte, and D. Barceló, *Optimization of congener-specific analysis of 40 polybrominated diphenyl ethers by gas chromatography/mass spectrometry*. Journal of mass spectrometry, 2001. **37**(1): p. 76-84.
184. Morace, J.L., *Reconnaissance of Contaminants in Selected Wastewater-Treatment-Plant Effluent and Stormwater Runoff Entering the Columbia River, Columbia River Basin, Washington and Oregon, 2008–10*.
185. Rossi, L., et al., *Urban stormwater contamination by polychlorinated biphenyls (PCBs) and its importance for urban water systems in Switzerland*. Science of the total environment, 2004. **322**(1): p. 179-189.
186. Raff, J.D. and R.A. Hites, *Deposition versus photochemical removal of PBDEs from Lake Superior air*. Environmental science & technology, 2007. **41**(19): p. 6725-6731.
187. Ter Schure, A.F.H., et al., *Atmospheric transport of polybrominated diphenyl ethers and polychlorinated biphenyls to the Baltic Sea*. Environmental science & technology, 2004. **38**(5): p. 1282-1287.
188. Halsall, C.J., et al., *Modelling the behaviour of PAHs during atmospheric transport from the UK to the Arctic*. Atmospheric environment, 2001. **35**(2): p. 255-267.
189. Li, H., et al., *Short-range transport of contaminants released from e-waste recycling site in South China*. Journal of Environmental Monitoring, 2011. **13**(4): p. 836-843.
190. Strandberg, B., et al., *Concentrations and spatial variations of polybrominated diphenyl ethers and other organohalogen compounds in Great Lakes air*. Environmental science & technology, 2001. **35**(6): p. 1078-1083.
191. Hoh, E. and R.A. Hites, *Brominated flame retardants in the atmosphere of the east-central United States*. Environmental science & technology, 2005. **39**(20): p. 7794-7802.
192. Venier, M. and R.A. Hites, *Flame retardants in the atmosphere near the Great Lakes*. Environmental science & technology, 2008. **42**(13): p. 4745-4751.
193. Salamova, A. and R.A. Hites, *Discontinued and alternative brominated flame retardants in the atmosphere and precipitation from the Great Lakes basin*. Environmental science & technology, 2011. **45**(20): p. 8698-8706.
194. La Guardia, M.J., R.C. Hale, and E. Harvey, *Evidence of debromination of decabromodiphenyl ether (BDE-209) in biota from a wastewater receiving stream*. Environmental science & technology, 2007. **41**(19): p. 6663-6670.
195. Tiedje, J.M., et al., *Microbial reductive dechlorination of PCBs*. Biodegradation, 1993. **4**(4): p. 231-240.
196. Fava, F., S. Gentilucci, and G. Zanaroli, *Anaerobic biodegradation of weathered polychlorinated biphenyls (PCBs) in contaminated sediments of Porto Marghera (Venice Lagoon, Italy)*. Chemosphere, 2003. **53**(2): p. 101-109.
197. Brown, J., *Determination of PCB metabolic, excretion, and accumulation rates for use as indicators of biological response and relative risk*. Environmental science & technology, 1994. **28**(13): p. 2295-2305.
198. Futagami, T., M. Goto, and K. Furukawa, *Genetic System of Organohalide-Respiring Bacteria, in Biodegradative Bacteria*. 2014, Springer. p. 59-81.
199. Zhu, W., et al., *Effect of decabromodiphenyl ether (BDE 209) on soil microbial activity and bacterial community composition*. World Journal of Microbiology and Biotechnology, 2010. **26**(10): p. 1891-1899.

200. Dowd, S., et al., *Survey of bacterial diversity in chronic wounds using pyrosequencing, DGGE, and full ribosome shotgun sequencing*. BMC microbiology, 2008. **8**(1): p. 43.
201. Kostka, J.E., et al., *Hydrocarbon-degrading bacteria and the bacterial community response in Gulf of Mexico beach sands impacted by the Deepwater Horizon oil spill*. Applied and environmental microbiology, 2011. **77**(22): p. 7962-7974.
202. Ishak, H.D., et al., *Bacterial diversity in Solenopsis invicta and Solenopsis geminata ant colonies characterized by 16S amplicon 454 pyrosequencing*. Microbial ecology, 2011. **61**(4): p. 821-831.
203. Meyer, F., et al., *The metagenomics RAST server—a public resource for the automatic phylogenetic and functional analysis of metagenomes*. BMC bioinformatics, 2008. **9**(1): p. 386.
204. Wang, Q., et al., *Naive Bayesian classifier for rapid assignment of rRNA sequences into the new bacterial taxonomy*. Applied and environmental microbiology, 2007. **73**(16): p. 5261-5267.
205. Ondov, B., N. Bergman, and A. Phillippy, *Interactive metagenomic visualization in a Web browser*. BMC bioinformatics, 2011. **12**(1): p. 385.
206. Eilers, H., et al., *Culturability and in situ abundance of pelagic bacteria from the North Sea*. Applied and Environmental Microbiology, 2000. **66**(7): p. 3044-3051.
207. Spain, A.M., L.R. Krumholz, and M.S. Elshahed, *Abundance, composition, diversity and novelty of soil Proteobacteria*. The ISME journal, 2009. **3**(8): p. 992-1000.
208. Fierer, N., M.A. Bradford, and R.B. Jackson, *Toward an ecological classification of soil bacteria*. Ecology, 2007. **88**(6): p. 1354-1364.
209. Torsvik, V., J. Goksøyr, and F.L. Daae, *High diversity in DNA of soil bacteria*. Applied and environmental microbiology, 1990. **56**(3): p. 782-787.
210. Gans, J., M. Wolinsky, and J. Dunbar, *Computational improvements reveal great bacterial diversity and high metal toxicity in soil*. Science, 2005. **309**(5739): p. 1387-1390.
211. Torsvik, V., et al., *Comparison of phenotypic diversity and DNA heterogeneity in a population of soil bacteria*. Applied and Environmental Microbiology, 1990. **56**(3): p. 776-781.
212. Kim, Y.-M., et al., *Biodegradation of diphenyl ether and transformation of selected brominated congeners by Sphingomonas sp. PH-07*. Applied microbiology and biotechnology, 2007. **77**(1): p. 187-194.
213. Schmidt, S., P. Fortnagel, and R. Wittich, *Biodegradation and transformation of 4, 4'-and 2, 4-dihalodiphenyl ethers by Sphingomonas sp. strain SS33*. Applied and environmental microbiology, 1993. **59**(11): p. 3931-3933.
214. Field, J.A. and R. Sierra-Alvarez, *Microbial transformation and degradation of polychlorinated biphenyls*. Environmental Pollution, 2008. **155**(1): p. 1-12.
215. Ahmed, M. and D. Focht, *Degradation of polychlorinated biphenyls by two species of Achromobacter*. Canadian Journal of Microbiology, 1973. **19**(1): p. 47-52.
216. Massé, R., et al., *Microbial biodegradation of 4-chlorobiphenyl, a model compound of chlorinated biphenyls*. Applied and environmental microbiology, 1984. **47**(5): p. 947-951.
217. Cheng, D. and J. He, *Isolation and characterization of "Dehalococcoides" sp. strain MB, which dechlorinates tetrachloroethene to trans-1, 2-dichloroethene*. Applied and environmental microbiology, 2009. **75**(18): p. 5910-5918.
218. Lee, L.K., et al., *Complete debromination of tetra-and penta-brominated diphenyl ethers by a coculture consisting of Dehalococcoides and Desulfovibrio species*. Environmental science & technology, 2011. **45**(19): p. 8475-8482.
219. Fierer, N., J.P. Schimel, and P.A. Holden, *Variations in microbial community composition through two soil depth profiles*. Soil Biology and Biochemistry, 2003. **35**(1): p. 167-176.
220. Koizumi, Y., H. Kojima, and M. Fukui, *Characterization of depth-related microbial community structure in lake sediment by denaturing gradient gel electrophoresis of amplified 16S rDNA and reversely transcribed 16S rRNA fragments*. FEMS microbiology ecology, 2003. **46**(2): p. 147-157.
221. Blume, E., et al., *Surface and subsurface microbial biomass, community structure and metabolic activity as a function of soil depth and season*. Applied Soil Ecology, 2002. **20**(3): p. 171-181.

222. Yin, K., et al., *Characterization, performance modeling, and design of an active capping remediation project in a heavily polluted urban channel*. Science of the Total Environment, 2010. **408**(16): p. 3454-3463.
223. Tokarz Iii, J.A., et al., *Reductive debromination of polybrominated diphenyl ethers in anaerobic sediment and a biomimetic system*. Environmental science & technology, 2008. **42**(4): p. 1157-1164.
224. Koelmans, A.A., et al., *Estimation of in situ sediment-to-water fluxes of polycyclic aromatic hydrocarbons, polychlorobiphenyls and polybrominated diphenylethers*. Environmental science & technology, 2010. **44**(8): p. 3014-3020.
225. Cornelissen, G., et al., *Extensive sorption of organic compounds to black carbon, coal, and kerogen in sediments and soils: Mechanisms and consequences for distribution, bioaccumulation, and biodegradation*. Environmental Science & Technology, 2005. **39**(18): p. 6881-6895.
226. Schwarzenbach, R.P., P.M. Gschwend, and D.M. Imboden, *Environmental organic chemistry*. 2002: Wiley-Interscience.
227. Hornbuckle, K.C., et al., *Seasonal variations in air-water exchange of polychlorinated biphenyls in Lake Superior*. Environmental science & technology, 1994. **28**(8): p. 1491-1501.
228. Charbeneau, R.J. and R. Charbeneau, *Groundwater hydraulics and pollutant transport*. 2000: Prentice Hall Upper Saddle River, NJ.
229. Daniel, D.E. and S.J. Trautwein, *Hydraulic conductivity and waste contaminant transport in soil*. Vol. 1142. 1994: Astm International.
230. Mott, R.L., *Applied fluid mechanics*. Vol. 4. 2000: Prentice Hall.

Appendix A

Table A2.1. Detailed congener composition (w/w %) in PBDE technical mixture (DE-71, DE-79, and Saytex102E) as reported in La Guardia et al. (2006). {La Guardia, 2006 #6}

Congener	DE-71	DE-79	Saytex 102E	Congener	DE-71	DE-79	Saytex 102E
		(w/w %)				(w / w %)	
17	0.07	nd	nd	139	0.8	nd	nd
28/33	0.25	nd	nd	140	0.17	<0.02	nd
Tetra	<0.02	nd	nd	138	0.73	0.62	nd
75	<0.02	nd	nd	184	<0.02	<0.02	nd
51	<0.02	nd	nd	Hepta	nd	<0.02	nd
49	0.74	nd	nd	175/183	0.1	42	nd
48/71	<0.02	nd	nd	191	nd	<0.02	nd
47/74	38.2	nd	nd	180	nd	1.7	nd
66/42	0.53	nd	nd	171	nd	1.81	nd
Penta	0.05	nd	nd	201	nd	0.78	nd
102	0.15	nd	nd	197	nd	22.2	nd
100	13.1	nd	nd	203	nd	4.4	nd
99	48.6	nd	nd	196	nd	10.5	nd
97/118	<0.02	nd	nd	194	nd	<0.02	nd
85	2.96	nd	nd	Octa	nd	<0.02	nd
126/155	0.21	nd	nd	208	nd	0.19	0.06
154	4.54	1.07	nd	207	nd	11.5	0.24
144	nd	0.1	nd	206	nd	1.38	2.19
Hexa	nd	<0.02	nd	209	nd	1.31	96.8
153	5.44	8.66	Nd				

nd: Non-detect

Table A2.2 (Cont.). Detailed congener composition (w/w %) in eight PCB Aroclors as reported in Frame et al. (2005) {Frame, 2005 #99}

Homolog	Congener	1221	1232	1016	1242	1248	1254	1260	1282
		(w/w %)							
1	1	35.8	15.21	0.52	0.51	0.05	0.02	0.03	0.02
1	2	3.81	1.98	0.02	0.02				
1	3	20.44	10.36	0.15	0.15	0.01			
2	4	6.19	5.32	3.62	3.11	0.32	0.02	0.03	0.07
2	5	0.74	0.49	0.17	0.13				
2	6	3.82	3.02	1.64	1.42	0.13	0	0.01	0.03
2	7	1.7	1.12	0.29	0.26	0.02			
2	8	12.34	10.71	8.29	6.99	0.81	0.05	0.06	0.15
2	9	1.74	1.25	0.58	0.5	0.04			
2	10	0.8	0.6	0.23	0.2				
2	11	0.16	0						
2	12	0.59	0.35	0.07	0.06				
2	13	1.1	0.73	0.24	0.2	0.02			
2	14		0						
2	15	4.18	3.24	2.4	1.98	0.22	0.01		0.03
3	16	0.31	1.79	3.88	3.03	1.04	0.02	0.02	0.07
3	17	0.34	1.83	3.98	3.14	1.05	0.02	0.02	0.07
3	18	0.78	4.89	10.86	8.53	4.29	0.08	0.07	0.19
3	19	0.08	0.46	0.99	0.79	0.22			0.02
3	20	0.07	0.42	0.88	0.68	0.14			
3	21								
3	22	0.26	1.62	3.5	2.71	1.33	0.02	0.02	0.06
3	23			0.01	0.01				
3	24	0.02	0.08	0.16	0.13				
3	25	0.09	0.37	0.72	0.57	0.11			
3	26	0.13	0.75	1.57	1.21	0.4			0.03
3	27	0.05	0.12	0.51	0.4	0.12			
3	28	0.62	3.92	8.5	6.68	3.59	0.06	0.05	0.15
3	29	0.01	0.05	0.1	0.08				
3	30	0	0						
3	31	0.6	4.17	9.32	7.18	5.07	0.11	0.06	0.16
3	32	0.17	1.08	2.37	1.85	0.88	0.01	0.01	0.05
3	33	0.48	2.84	6.21	4.85	2.23	0.05	0.04	0.13
3	34	0	0.01	0.03	0.02				
3	35	0	0.06	0.05	0.07				
3	36	0							
3	37	0.19	1.15	1.02	1.86	0.79	0.01	0.01	0.04
3	38	0							

Table A2.2 (Cont.). Detailed congener composition (w/w %) in eight PCB Aroclors as reported in Frame et al. (2005) {Frame, 2005 #99}

Homolog	Congener	1221	1232	1016	1242	1248	1254	1260	1282
		(w/w %)							
3	39								
4	40	0.04	0.4	0.58	0.77	1.13	0.15		
4	41	0.03	0.36	0.76	0.69	0.77	0.02		
4	42	0.09	0.66	1.59	1.13	1.67	0.09		0.03
4	43		0.12	0.28	0.18	0.3			
4	44	0.21	1.81	4.47	3.6	6.31	0.67	0.04	0.1
4	45	0.04	0.47	1.23	0.93	1.09	0.02		
4	46	0.02	0.19	0.49	0.37	0.47			
4	47	0.05	0.49	1.26	0.97	1.49	0.07		0.01
4	48	0.06	0.61	1.61	1.18	1.66	0.05		0.01
4	49	0.15	1.37	3.35	2.59	4.12	0.26	0.01	0.07
4	50			0.01					
4	51		0.12	0.32	0.25	0.3			
4	52	0.22	1.83	4.63	3.64	6.93	0.83	0.27	0.17
4	53	0.04	0.37	0.95	0.75	1.05	0.04		
4	54			0.01					
4	55		0.05		0.09	0.06			
4	56	0.12	0.93	0.07	1.8	3.16	1.7	0.02	0.04
4	57			0.01	0.02	0.02			
4	58								
4	59	0.01	0.2	0.41	0.37	0.37			
4	60	0.07	0.61	0.04	1.17	1.85	0.95	0.04	0.02
4	61								
4	62								
4	63			0.06	0.13	0.17	0.07		
4	64	0.1	0.1	1.87	1.76	3.01	0.36	0.01	0.04
4	65		0.87						
4	66	0.21	1.74	0.39	3.38	5.84	3.56	0.03	0.08
4	67		0.09	0.06	0.15	0.13			
4	68								
4	69								
4	70	0.24	1.9	0.59	3.76	7.28	6.83	0.04	0.12
4	71	0.06	0.54	1.16	1.04	1.67	0.11		
4	72				0.01	0.02			
4	73								
4	74	0.12	0.92	0.33	1.83	3.14	2.19	0.05	
4	75		0.02	0.06	0.05	0.08			
4	76				0.08	0.13	0.03		

Table A2.2 (Cont.). Detailed congener composition (w/w %) in eight PCB Aroclors as reported in Frame et al. (2005) {Frame, 2005 #99}

Homolog	Congener	1221	1232	1016	1242	1248	1254	1260	1282
					(w/w %)				
4	77	0.01	0.17		0.27	0.41	0.2		
4	78								
4	79								
4	80								
4	81					0.01			
5	82		0.12		0.29	0.81	1.53		
5	83		0.05		0.12	0.26	0.56		
5	84	0.02	0.2	0.05	0.46	1.26	1.58	0.11	0.05
5	85	0.03	0.17		0.36	0.98	2.49		0.03
5	86		0.01		0.03	0.11	0.1		
5	87	0.04	0.22		0.52	1.45	3.41	0.44	0.11
5	88					0.02			
5	89		0.05		0.1	0.2	0.11		
5	90	0.02							
5	91		0.1	0.06	0.24	0.63	0.53		0.01
5	92		0.05		0.06	0.38	0.57	0.34	0.07
5	93					0.04			
5	94					0.03			
5	95	0.05	0.3	0.31	0.68	1.96	1.84	2.56	0.87
5	96		0.01	0.04	0.03	0.08	0.01		
5	97	0.03	0.18		0.43	1.22	2.78	0.1	0.06
5	98								
5	99	0.04	0.21	0.01	0.53	1.47	4.53	0.03	0.06
5	100								
5	101	0.07	0.33	0.04	0.78	2.22	5.49	3.23	1.03
5	102			0.04	0.08	0.19	0.09		
5	103					0.02			
5	104								
5	105	0.05	0.22		0.52	1.6	7.37	0.22	0.18
5	106								
5	107								
5	108								
5	109		0.03		0.08	0.18	0.78		
5	110	0.05	0.38		0.94	2.97	8.42	1.38	0.36
5	111								
5	112								
5	113						0.01		
5	114		0.02		0.05	0.12	0.5		

Table A2.2 (Cont.). Detailed congener composition (w/w %) in eight PCB Aroclors as reported in Frame et al. (2005) {Frame, 2005 #99}

Homolog	Congener	1221	1232	1016	1242	1248	1254	1260	1282
					(w/w %)				
5	115		0.01		0.04	0.11	0.37		
5	116								
5	117		0.01		0.03	0.19	0.19		
5	118	0.08	0.29		0.78	2.29	13.59	0.51	0.17
5	119					0.06	0.12		
5	120								
5	121								
5	122				0.01	0.06	0.25		
5	123				0.03	0.07	0.32		
5	124				0.03	0.1	0.47		
5	125				0.02	0.04	0.03		
5	126						0.02		
5	127								
6	128				0.04	0.12	1.71	0.56	0.17
6	129					0.02	0.39	0.15	0.03
6	130					0.04	0.5	0.23	0.03
6	131						0.14	0.08	
6	132		0.02		0.05	0.15	1.5	2.84	1.07
6	133							0.08	0.03
6	134						0.2	0.36	0.11
6	135					0.04	0.28	1.14	0.67
6	136					0.05	0.24	1.48	1.02
6	137					0.03	0.52	0.02	0.01
6	138		0.06		0.16	0.38	5.95	6.47	2.33
6	139						0.14		
6	140								
6	141				0.01	0.07	0.69	2.62	1.63
6	142								
6	143								
6	144						0.12	0.61	0.41
6	145								
6	146					0.04	0.45	1.17	0.57
6	147						0.02		
6	148								
6	149		0.05		0.07	0.24	1.82	8.74	6.36
6	150								
6	151		0.01			0.04	0.22	3.04	3.14
6	152								

Table A2.2 (Cont.). Detailed congener composition (w/w %) in eight PCB Aroclors as reported in Frame et al. (2005) {Frame, 2005 #99}

Homolog	Congener	1221	1232	1016	1242 (w/w %)	1248	1254	1260	1282
6	153		0.05		0.09	23	3.29	9.09	6.78
6	154						0.02		
6	155								
6	156				0.02	0.06	1.13	0.53	0.14
6	157						0.3	0.02	
6	158				0.02	0.04	0.9	0.57	0.18
6	159								
6	160								
6	161								
6	162								
6	163		0.02			0.06	0.7	2.41	1.5
6	164					0.02	0.31	0.72	0.23
6	165								
6	166						0.05		
6	167						0.35	0.2	0.02
6	168								
6	169								
7	170						0.35	3.97	3.05
7	171						0.08	1.09	0.85
7	172						0.03	0.71	0.63
7	173							0.11	0.03
7	174						0.14	4.92	6.56
7	175							0.18	0.19
7	176							0.59	0.73
7	177						0.08	2.54	2.82
7	178							0.86	1.31
7	179						0.02	2.05	3.64
7	180		0.02			0.02	0.42	10.9	13.72
7	181								
7	182								
7	183						0.09	2.33	2.89
7	184								
7	185							0.56	0.93
7	186								
7	187		0.01				0.09	5.44	9.55
7	188								
7	189							0.08	0.03
7	190						0.05	0.82	0.74

Table A2.2 (Cont.). Detailed congener composition (w/w %) in eight PCB Aroclors as reported in Frame et al. (2005) {Frame, 2005 #99}

Homolog	Congener	1221	1232	1016	1242	1248	1254	1260	1282
		(w/w %)							
7	191							0.16	0.13
7	192								
7	193							0.54	0.67
8	194							2.11	3.79
8	195							0.86	1.39
8	196							1.02	2.41
8	197							0.07	0.14
8	198							0.1	0.24
8	199							1.87	4.91
8	200							0.26	0.69
8	201							0.25	0.66
8	202							0.36	1.2
8	203							1.5	4.11
8	204								
8	205							0.1	0.16
9	206						0.03	0.66	1.19
9	207							0.05	0.17
9	208						0.01	0.16	0.29
10	209								

References: {Frame, 2005 #99}

*Congeners with no reported value are either below detection limit, not measured, and/or not reported.

Table A2.3 (Cont.): Selected PBDE chemical properties estimated by EPI suite V4.11.

Congener ⁽¹⁾	Log K _{ow} ⁽²⁾		SW ₂₅ ⁽⁵⁾ (mg/L)			Log K _{oc} ⁽⁶⁾			Half life (hours) ⁽⁷⁾				Log K _{OA25C} ⁽⁸⁾	
	Est ⁽³⁾	Db ⁽⁴⁾	WSKOW	Db ⁽⁴⁾	WATERNT	Db ⁽⁴⁾	MCI	KOW	Air	Water	Soil	Sediment	Est ⁽³⁾	Db ⁽⁴⁾
1	4.65	4.59	3.52E+00		2.56E+00		3.92	3.98	74	900	1.80E+03	8.10E+03	6.77	
2	4.65	4.85	2.11E+00		2.56E+00		3.92	4.21	56	900	1.80E+03	8.10E+03	7.02	
3	4.65	4.96	1.70E+00	0.653	2.56E+00		3.92	4.30	74	900	1.80E+03	8.10E+03	7.13	
4	5.54		1.95E-01		5.81E-01		4.14	4.81	166	1440	2.88E+03	1.30E+03	8.11	
5	5.54		1.95E-01		5.81E-01		4.14	4.81	107	900	1.80E+03	8.10E+03	8.11	
6	5.54		1.95E-01		5.81E-01		4.13	4.81	110	1440	2.88E+03	1.30E+03	8.11	
7	5.54		1.95E-01		5.81E-01		4.13	4.81	110	900	1.80E+03	8.10E+03	8.11	
8	5.54		1.95E-01		5.81E-01		4.13	4.81	166	1440	2.88E+03	1.30E+03	8.11	
9	5.54		1.95E-01		5.81E-01		4.13	4.81	107	900	1.80E+03	8.10E+03	8.11	
10	5.54		1.95E-01		5.81E-01		4.14	4.81	110	900	1.80E+03	8.10E+03	8.11	
11	5.54		1.95E-01		5.81E-01		4.12	4.81	82	1440	2.88E+03	1.30E+03	8.11	
12	5.54		1.95E-01		5.81E-01		4.13	4.81	107	900	1.80E+03	8.10E+03	8.11	
13	5.54		1.95E-01		5.81E-01		4.12	4.81	110	1440	2.88E+03	1.30E+03	8.11	
14	5.54		1.95E-01		5.81E-01		4.12	4.81	82	900	1.80E+03	8.10E+03	8.11	
15	5.54	5.72	1.36E-01		5.81E-01		4.12	4.96	166	1440	2.88E+03	1.30E+03	8.29	
16	6.43		1.13E-02		1.24E-01		4.35	5.58	265	1440	2.88E+03	1.30E+03	9.40	
17	6.43		1.13E-02		1.24E-01		4.34	5.58	256	1440	2.88E+03	1.30E+03	9.40	
18	6.43		1.13E-02		1.24E-01		4.35	5.58	265	1440	2.88E+03	1.30E+03	9.40	
19	6.43		1.13E-02		1.24E-01		4.34	5.58	256	1440	2.88E+03	1.30E+03	9.40	
20	6.43		1.13E-02		1.24E-01		4.34	5.58	164	1440	2.88E+03	1.30E+03	9.40	
21	6.43		1.13E-02		1.24E-01		4.35	5.58	209	1440	2.88E+03	1.30E+03	9.40	
22	6.43		1.13E-02		1.24E-01		4.34	5.58	265	1440	2.88E+03	1.30E+03	9.40	
23	6.43		1.13E-02		1.24E-01		4.34	5.58	179	1440	2.88E+03	1.30E+03	9.40	
24	6.43		1.13E-02		1.24E-01		4.35	5.58	209	1440	2.88E+03	1.30E+03	9.40	
25	6.43		1.13E-02		1.24E-01		4.34	5.58	160	1440	2.88E+03	1.30E+03	9.40	
26	6.43		1.13E-02		1.24E-01		4.34	5.58	164	1440	2.88E+03	1.30E+03	9.40	
27	6.43		1.13E-02		1.24E-01		4.34	5.58	160	1440	2.88E+03	1.30E+03	9.40	

Table A2.3 (Cont.): Selected PBDE chemical properties estimated by EPI suite V4.11.

Congener ⁽¹⁾	Log K _{ow} ⁽²⁾		SW ₂₅ ⁽⁵⁾ (mg/L)			Log K _{oc} ⁽⁶⁾			Half life (hours) ⁽⁷⁾				Log K _{OA25C} ⁽⁸⁾	
	Est ⁽³⁾	Db ⁽⁴⁾	WSKOW	Db ⁽⁴⁾	WATERNT	Db ⁽⁴⁾	MCI	KOW	Air	Water	Soil	Sediment	Est ⁽³⁾	Db ⁽⁴⁾
28	6.43		1.13E-02		1.24E-01		4.34	5.58	256	1440	2.88E+03	1.30E+03	9.40	
29	6.43		1.13E-02		1.24E-01		4.34	5.23	209	1440	2.88E+03	1.30E+03	9.40	
30	6.43	6.03	1.13E-02		1.24E-01		4.34	5.58	183	1440	2.88E+03	1.30E+03	9.00	
31	6.43		1.13E-02		1.24E-01		4.34	5.58	265	1440	2.88E+03	1.30E+03	9.40	
32	6.43		1.13E-02		1.24E-01		4.34	5.58	256	1440	2.88E+03	1.30E+03	9.40	
33	6.43		1.13E-02		1.24E-01		4.34	5.58	265	1440	2.88E+03	1.30E+03	9.40	
34	6.43		1.13E-02		1.24E-01		4.34	5.58	170	1440	2.88E+03	1.30E+03	9.40	
35	6.43		1.13E-02		1.24E-01		4.34	5.58	164	1440	2.88E+03	1.30E+03	9.40	
36	6.43		1.13E-02		1.24E-01		4.33	5.58	122	1440	2.88E+03	1.30E+03	9.40	
37	6.43		1.13E-02		1.24E-01		4.34	5.58	265	1440	2.88E+03	1.30E+03	9.40	
38	6.43		1.13E-02		1.24E-01		4.34	5.58	179	1440	2.88E+03	1.30E+03	9.40	
39	6.43		1.13E-02		1.24E-01		4.33	5.58	170	1440	2.88E+03	1.30E+03	9.40	
40	7.32		6.30E-04		2.52E-02		4.57	6.35	400	4320	8.64E+03	3.89E+04	10.69	
41	7.32		6.30E-04		2.52E-02		4.57	6.35	517	4320	8.64E+03	3.89E+04	10.69	
42	7.32		6.30E-04		2.52E-02		4.59	6.35	397	4320	8.64E+03	3.89E+04	10.69	
43	7.32		6.30E-04		2.52E-02		4.59	6.35	401	4320	8.64E+03	3.89E+04	10.69	
44	7.32		6.30E-04		2.52E-02		4.56	6.35	400	4320	8.64E+03	3.89E+04	10.69	
45	7.32		6.30E-04		2.52E-02		4.57	6.35	517	4320	8.64E+03	3.89E+04	10.69	
46	7.32		6.30E-04		2.52E-02		4.57	6.35	397	4320	8.64E+03	3.89E+04	10.69	
47	7.32		6.30E-04		2.52E-02		4.55	6.35	394	4320	8.64E+03	3.89E+04	10.69	
48	7.32		6.30E-04		2.52E-02		4.59	6.35	517	4320	8.64E+03	3.89E+04	10.69	
49	7.32		6.30E-04		2.52E-02		4.55	6.35	397	4320	8.64E+03	3.89E+04	10.69	
50	7.32		6.30E-04		2.52E-02		4.59	6.35	387	4320	8.64E+03	3.89E+04	10.69	
51	7.32		6.30E-04		2.52E-02		4.59	6.35	394	4320	8.64E+03	3.89E+04	10.69	
52	7.32		6.30E-04		2.52E-02		4.55	6.35	400	4320	8.64E+03	3.89E+04	10.69	
53	7.32		6.30E-04		2.52E-02		4.59	6.35	397	4320	8.64E+03	3.89E+04	10.69	
54	7.32	6.5	3.14E-03		2.52E-02		4.57	5.64	394	4320	8.64E+03	3.89E+04	9.87	

Table A2.3 (Cont.): Selected PBDE chemical properties estimated by EPI suite V4.11.

Congener ⁽¹⁾	Log K _{ow} ⁽²⁾		SW ₂₅ ⁽⁵⁾ (mg/L)			Log K _{oc} ⁽⁶⁾			Half life (hours) ⁽⁷⁾				Log K _{OA25C} ⁽⁸⁾	
	Est ⁽³⁾	Db ⁽⁴⁾	WSKOW	Db ⁽⁴⁾	WATERNT	Db ⁽⁴⁾	MCI	KOW	Air	Water	Soil	Sediment	Est ⁽³⁾	Db ⁽⁴⁾
55	7.32		6.30E-04		2.52E-02		4.56	6.35	320	4320	8.64E+03	3.89E+04	10.69	
56	7.32		6.30E-04		2.52E-02		4.56	6.35	400	4320	8.64E+03	3.89E+04	10.69	
57	7.32		6.30E-04		2.52E-02		4.55	6.35	271	4320	8.64E+03	3.89E+04	10.69	
58	7.32		6.30E-04		2.52E-02		4.55	6.35	250	4320	8.64E+03	3.89E+04	10.69	
59	7.32		6.30E-04		2.52E-02		4.56	6.35	320	4320	8.64E+03	3.89E+04	10.69	
60	7.32		6.30E-04		2.52E-02		4.56	6.35	517	4320	8.64E+03	3.89E+04	10.69	
61	7.32		6.30E-04		2.52E-02		4.57	6.35	332	4320	8.64E+03	3.89E+04	10.69	
62	7.32		6.30E-04		2.52E-02		4.57	6.35	337	4320	8.64E+03	3.89E+04	10.69	
63	7.32		6.30E-04		2.52E-02		4.55	6.35	401	4320	8.64E+03	3.89E+04	10.69	
64	7.32		6.30E-04		2.52E-02		4.56	6.35	517	4320	8.64E+03	3.89E+04	10.69	
65	7.32		6.30E-04		2.52E-02		4.57	6.35	332	4320	8.64E+03	3.89E+04	10.69	
66	7.32		6.30E-04		2.52E-02		4.55	6.35	397	4320	8.64E+03	3.89E+04	10.69	
67	7.32		6.30E-04		2.52E-02		4.55	6.35	320	4320	8.64E+03	3.89E+04	10.69	
68	7.32		6.30E-04		2.52E-02		4.54	6.35	249	4320	8.64E+03	3.89E+04	10.69	
69	7.32		6.30E-04		2.52E-02		4.55	6.35	265	4320	8.64E+03	3.89E+04	10.69	
70	7.32		6.30E-04		2.52E-02		4.55	6.35	400	4320	8.64E+03	3.89E+04	10.69	
71	7.32		6.30E-04		2.52E-02		4.56	6.35	397	4320	8.64E+03	3.89E+04	10.69	
72	7.32		6.30E-04		2.52E-02		4.54	6.35	250	4320	8.64E+03	3.89E+04	10.69	
73	7.32		6.30E-04		2.52E-02		4.55	6.35	249	4320	8.64E+03	3.89E+04	10.69	
74	7.32		6.30E-04		2.52E-02		4.55	6.35	517	4320	8.64E+03	3.89E+04	10.69	
75	7.32		6.30E-04		2.52E-02		4.55	6.35	387	4320	8.64E+03	3.89E+04	10.69	
76	7.32		6.30E-04		2.52E-02		4.56	6.35	401	4320	8.64E+03	3.89E+04	10.69	
77	7.32		6.30E-04		2.52E-02		4.55	6.35	400	4320	8.64E+03	3.89E+04	10.69	
78	7.32		6.30E-04		2.52E-02		4.55	6.35	271	4320	8.64E+03	3.89E+04	10.69	
79	7.32		6.30E-04		2.52E-02		4.54	6.35	250	4320	8.64E+03	3.89E+04	10.69	
80	7.32		6.30E-04		2.52E-02		4.53	6.35	182	4320	8.64E+03	3.89E+04	10.69	
81	7.32		6.30E-04		2.52E-02		4.55	6.35	401	4320	8.64E+03	3.89E+04	10.69	

Table A2.3 (Cont.): Selected PBDE chemical properties estimated by EPI suite V4.11.

Congener ⁽¹⁾	Log K _{ow} ⁽²⁾		SW ₂₅ ⁽⁵⁾ (mg/L)			Log K _{oc} ⁽⁶⁾			Half life (hours) ⁽⁷⁾				Log K _{OA25C} ⁽⁸⁾	
	Est ⁽³⁾	Db ⁽⁴⁾	WSKOW	Db ⁽⁴⁾	WATERNT	Db ⁽⁴⁾	MCI	KOW	Air	Water	Soil	Sediment	Est ⁽³⁾	Db ⁽⁴⁾
82	8.21		3.41E-05		5.00E-03		4.78	7.13	907	4320	8.64E+03	3.89E+04	11.98	
83	8.21		3.41E-05		5.00E-03		4.77	7.13	655	4320	8.64E+03	3.89E+04	11.98	
84	8.21		3.41E-05		5.00E-03		4.78	7.13	907	4320	8.64E+03	3.89E+04	11.98	
85	8.21		3.41E-05		5.00E-03		4.77	7.13	807	4320	8.64E+03	3.89E+04	11.98	
86	8.21		3.41E-05		5.00E-03		4.78	7.13	747	4320	8.64E+03	3.89E+04	11.98	
87	8.21		3.41E-05		5.00E-03		4.77	7.13	907	4320	8.64E+03	3.89E+04	11.98	
88	8.21		3.41E-05		5.00E-03		4.78	7.13	733	4320	8.64E+03	3.89E+04	11.98	
89	8.21		3.41E-05		5.00E-03		4.78	7.13	807	4320	8.64E+03	3.89E+04	11.98	
90	8.21		3.41E-05		5.00E-03		4.76	7.13	601	4320	8.64E+03	3.89E+04	11.98	
91	8.21		3.41E-05		5.00E-03		4.77	7.13	807	4320	8.64E+03	3.89E+04	11.98	
92	8.21		3.41E-05		5.00E-03		4.76	7.13	655	4320	8.64E+03	3.89E+04	11.98	
93	8.21		3.41E-05		5.00E-03		4.78	7.13	7	4320	8.64E+03	3.89E+04	11.98	
94	8.21		3.41E-05		5.00E-03		4.77	7.13	601	4320	8.64E+03	3.89E+04	11.98	
95	8.21		3.41E-05		5.00E-03		4.77	7.13	907	4320	8.64E+03	3.89E+04	11.98	
96	8.21		3.41E-05		5.00E-03		4.78	7.13	807	4320	8.64E+03	3.89E+04	11.98	
97	8.21		3.41E-05		5.00E-03		4.77	7.13	907	4320	8.64E+03	3.89E+04	11.98	
98	8.21		3.41E-05		5.00E-03		4.77	7.13	650	4320	8.64E+03	3.89E+04	11.98	
99	8.21		3.41E-05		5.00E-03		4.76	7.13	807	4320	8.64E+03	3.89E+04	11.98	
100	8.21		3.41E-05		5.00E-03		4.76	7.13	597	4320	8.64E+03	3.89E+04	11.98	
101	8.21	7.1	3.00E-04	0.00103	5.00E-03		4.76	6.16	907	4320	8.64E+03	3.89E+04	10.87	
102	8.21		3.41E-05		5.00E-03		4.77	7.13	807	4320	8.64E+03	3.89E+04	11.98	
103	8.21		3.41E-05		5.00E-03		4.76	7.13	650	4320	8.64E+03	3.89E+04	11.98	
104	8.21		3.41E-05		5.00E-03		4.77	7.13	597	4320	8.64E+03	3.89E+04	11.98	
105	8.21		3.41E-05		5.00E-03		4.77	7.13	907	4320	8.64E+03	3.89E+04	11.98	
106	8.21		3.41E-05		5.00E-03		4.77	7.13	515	4320	8.64E+03	3.89E+04	11.98	
107	8.21		3.41E-05		5.00E-03		4.76	7.13	655	4320	8.64E+03	3.89E+04	11.98	
108	8.21		3.41E-05		5.00E-03		4.76	7.13	503	4320	8.64E+03	3.89E+04	11.98	

Table A2.3 (Cont.): Selected PBDE chemical properties estimated by EPI suite V4.11.

Congener ⁽¹⁾	Log K _{ow} ⁽²⁾		SW ₂₅ ⁽⁵⁾ (mg/L)			Log K _{oc} ⁽⁶⁾			Half life (hours) ⁽⁷⁾				Log K _{OA25C} ⁽⁸⁾	
	Est ⁽³⁾	Db ⁽⁴⁾	WSKOW	Db ⁽⁴⁾	WATERNT	Db ⁽⁴⁾	MCI	KOW	Air	Water	Soil	Sediment	Est ⁽³⁾	Db ⁽⁴⁾
109	8.21		3.41E-05		5.00E-03		4.77	7.13	509	4320	8.64E+03	3.89E+04	11.98	
110	8.21		3.41E-05		5.00E-03		4.77	7.13	907	4320	8.64E+03	3.89E+04	11.98	
111	8.21		3.41E-05		5.00E-03		4.75	7.13	415	4320	8.64E+03	3.89E+04	11.98	
112	8.21		3.41E-05		5.00E-03		4.77	7.13	515	4320	8.64E+03	3.89E+04	11.98	
113	8.21		3.41E-05		5.00E-03		4.76	7.13	503	4320	8.64E+03	3.89E+04	11.98	
114	8.21		3.41E-05		5.00E-03		4.77	7.13	747	4320	8.64E+03	3.89E+04	11.98	
115	8.21		3.41E-05		5.00E-03		4.77	7.13	773	4320	8.64E+03	3.89E+04	11.98	
116	8.21		3.41E-05		5.00E-03		4.79	7.13	496	4320	8.64E+03	3.89E+04	11.98	
117	8.21		3.41E-05		5.00E-03		4.79	7.13	747	4320	8.64E+03	3.89E+04	11.98	
118	8.21		3.41E-05		5.00E-03		4.76	7.13	907	4320	8.64E+03	3.89E+04	11.98	
119	8.21		3.41E-05		5.00E-03		4.76	7.13	650	4320	8.64E+03	3.89E+04	11.98	
120	8.21		3.41E-05		5.00E-03		4.75	7.13	503	4320	8.64E+03	3.89E+04	11.98	
121	8.21		3.41E-05		5.00E-03		4.75	7.13	413	4320	8.64E+03	3.89E+04	11.98	
122	8.21		3.41E-05		5.00E-03		4.77	7.13	655	4320	8.64E+03	3.89E+04	11.98	
123	8.21		3.41E-05		5.00E-03		4.76	7.13	601	4320	8.64E+03	3.89E+04	11.98	
124	8.21		3.41E-05		5.00E-03		4.76	7.13	655	4320	8.64E+03	3.89E+04	11.98	
125	8.21		3.41E-05		5.00E-03		4.77	7.13	601	4320	8.64E+03	3.89E+04	11.98	
126	8.21		3.41E-05		5.00E-03		4.77	7.13	601	4320	8.64E+03	3.89E+04	11.98	
127	8.21		3.41E-05		5.00E-03		4.75	7.13	415	4320	8.64E+03	3.89E+04	11.98	
128	9.1		1.80E-06		9.70E-04		5.00	7.90	1990	4320	8.64E+03	3.89E+04	13.27	
129	9.1		1.80E-06		9.70E-04		5.00	7.90	1450	4320	8.64E+03	3.89E+04	13.27	
130	9.1		1.80E-06		9.70E-04		4.99	7.90	1400	4320	8.64E+03	3.89E+04	13.27	
131	9.1		1.80E-06		9.70E-04		5.00	7.90	1440	4320	8.64E+03	3.89E+04	13.27	
132	9.1		1.80E-06		9.70E-04		5.00	7.90	1990	4320	8.64E+03	3.89E+04	13.27	
133	9.1		1.80E-06		9.70E-04		4.98	7.90	1070	4320	8.64E+03	3.89E+04	13.27	
134	9.1		1.80E-06		9.70E-04		5.00	7.90	1450	4320	8.64E+03	3.89E+04	13.27	
135	9.1		1.80E-06		9.70E-04		4.99	7.90	1400	4320	8.64E+03	3.89E+04	13.27	

Table A2.3 (Cont.): Selected PBDE chemical properties estimated by EPI suite V4.11.

Congener ⁽¹⁾	Log K _{ow} ⁽²⁾		SW ₂₅ ⁽⁵⁾ (mg/L)			Log K _{oc} ⁽⁶⁾			Half life (hours) ⁽⁷⁾				Log K _{OA25C} ⁽⁸⁾	
	Est ⁽³⁾	Db ⁽⁴⁾	WSKOW	Db ⁽⁴⁾	WATERNT	Db ⁽⁴⁾	MCI	KOW	Air	Water	Soil	Sediment	Est ⁽³⁾	Db ⁽⁴⁾
136	9.1		1.80E-06		9.70E-04		5.00	7.90	1990	4320	8.64E+03	3.89E+04	13.27	
137	9.1		1.80E-06		9.70E-04		4.99	7.90	1150	4320	8.64E+03	3.89E+04	13.27	
138	9.1		1.80E-06		9.70E-04		4.99	7.90	1990	4320	8.64E+03	3.89E+04	13.27	
139	9.1		1.80E-06		9.70E-04		4.99	7.90	1150	4320	8.64E+03	3.89E+04	13.27	
140	9.1		1.80E-06		9.70E-04		4.99	7.90	1250	4320	8.64E+03	3.89E+04	13.27	
141	9.1		1.80E-06		9.70E-04		4.99	7.90	1450	4320	8.64E+03	3.89E+04	13.27	
142	9.1		1.80E-06		9.70E-04		5.00	7.90	1180	4320	8.64E+03	3.89E+04	13.27	
143	9.1		1.80E-06		9.70E-04		5.00	7.90	1150	4320	8.64E+03	3.89E+04	13.27	
144	9.1		1.80E-06		9.70E-04		4.99	7.90	1440	4320	8.64E+03	3.89E+04	13.27	
145	9.1		1.80E-06		9.70E-04		5.00	7.90	1150	4320	8.64E+03	3.89E+04	13.27	
146	9.1		1.80E-06		9.70E-04		4.98	7.90	1400	4320	8.64E+03	3.89E+04	13.27	
147	9.1		1.80E-06		9.70E-04		4.99	7.90	1150	4320	8.64E+03	3.89E+04	13.27	
148	9.1		1.80E-06		9.70E-04		4.98	7.90	983	4320	8.64E+03	3.89E+04	13.27	
149	9.1		1.80E-06		9.70E-04		4.99	7.90	1990	4320	8.64E+03	3.89E+04	13.27	
150	9.1		1.80E-06		9.70E-04		4.99	7.90	1250	4320	8.64E+03	3.89E+04	13.27	
151	9.1		1.80E-06		9.70E-04		4.99	7.90	1450	4320	8.64E+03	3.89E+04	13.27	
152	9.1		1.80E-06		9.70E-04		5.00	7.90	1150	4320	8.64E+03	3.89E+04	13.27	
153	9.1		1.80E-06		9.70E-04		4.98	7.90	1990	4320	8.64E+03	3.89E+04	13.27	
154	9.1		1.80E-06		9.70E-04		4.98	7.90	1250	4320	8.64E+03	3.89E+04	13.27	
155	9.1	6.39	3.70E-04	0.011	9.70E-04		4.98	5.55	906	4320	8.64E+03	3.89E+04	10.15	
156	9.1		1.80E-06		9.70E-04		4.99	7.90	1450	4320	8.64E+03	3.89E+04	13.27	
157	9.1		1.80E-06		9.70E-04		4.99	7.90	1400	4320	8.64E+03	3.89E+04	13.27	
158	9.1		1.80E-06		9.70E-04		4.99	7.90	1440	4320	8.64E+03	3.89E+04	13.27	
159	9.1		1.80E-06		9.70E-04		4.98	7.90	802	4320	8.64E+03	3.89E+04	13.27	
160	9.1		1.80E-06		9.70E-04		5.00	7.90	775	4320	8.64E+03	3.89E+04	13.27	
161	9.1		1.80E-06		9.70E-04		4.98	7.90	799	4320	8.64E+03	3.89E+04	13.27	
162	9.1		1.80E-06		9.70E-04		4.98	7.90	1070	4320	8.64E+03	3.89E+04	13.27	

Table A2.3 (Cont.): Selected PBDE chemical properties estimated by EPI suite V4.11.

Congener ⁽¹⁾	Log K _{ow} ⁽²⁾		SW ₂₅ ⁽⁵⁾ (mg/L)			Log K _{oc} ⁽⁶⁾			Half life (hours) ⁽⁷⁾				Log K _{OA25C} ⁽⁸⁾	
	Est ⁽³⁾	Db ⁽⁴⁾	WSKOW	Db ⁽⁴⁾	WATERNT	Db ⁽⁴⁾	MCI	KOW	Air	Water	Soil	Sediment	Est ⁽³⁾	Db ⁽⁴⁾
163	9.1		1.80E-06		9.70E-04		4.99	7.90	1450	4320	8.64E+03	3.89E+04	13.27	
164	9.1		1.80E-06		9.70E-04		4.99	7.90	1400	4320	8.64E+03	3.89E+04	13.27	
165	9.1		1.80E-06		9.70E-04		4.98	7.90	802	4320	8.64E+03	3.89E+04	13.27	
166	9.1		1.80E-06		9.70E-04		5.00	7.90	1180	4320	8.64E+03	3.89E+04	13.27	
167	9.1		1.80E-06		9.70E-04		4.98	7.90	1400	4320	8.64E+03	3.89E+04	13.27	
168	9.1		1.80E-06		9.70E-04		4.98	7.90	983	4320	8.64E+03	3.89E+04	13.27	
169	9.1		1.80E-06		9.70E-04		4.98	7.90	1070	4320	8.64E+03	3.89E+04	13.27	
170	9.99		9.40E-08		1.85E-04		5.21	8.67	3150	4320	8.64E+03	3.89E+04	14.56	
171	9.99		9.40E-08		1.85E-04		5.21	8.67	2920	4320	8.64E+03	3.89E+04	14.56	
172	9.99		9.40E-08		1.85E-04		5.20	8.67	2350	4320	8.64E+03	3.89E+04	14.56	
173	9.99		9.40E-08		1.85E-04		5.22	8.67	2460	4320	8.64E+03	3.89E+04	14.56	
174	9.99		9.40E-08		1.85E-04		5.21	8.67	3150	4320	8.64E+03	3.89E+04	14.56	
175	9.99		9.40E-08		1.85E-04		5.20	8.67	2200	4320	8.64E+03	3.89E+04	14.56	
176	9.99		9.40E-08		1.85E-04		5.21	8.67	2920	4320	8.64E+03	3.89E+04	14.56	
177	9.99		9.40E-08		1.85E-04		5.21	8.67	3150	4320	8.64E+03	3.89E+04	14.56	
178	9.99		9.40E-08		1.85E-04		5.20	8.67	2350	4320	8.64E+03	3.89E+04	14.56	
179	9.99		9.40E-08		1.85E-04		5.21	8.67	3150	4320	8.64E+03	3.89E+04	14.56	
180	9.99		9.40E-08		1.85E-04		5.20	8.67	3150	4320	8.64E+03	3.89E+04	14.56	
181	9.99		9.40E-08		1.85E-04		5.21	8.67	1860	4320	8.64E+03	3.89E+04	14.56	
182	9.99		9.40E-08		1.85E-04		5.20	8.67	1860	4320	8.64E+03	3.89E+04	14.56	
183	9.99		9.40E-08		1.85E-04		5.20	8.67	2920	4320	8.64E+03	3.89E+04	14.56	
184	9.99		9.40E-08		1.85E-04		5.20	8.67	1780	4320	8.64E+03	3.89E+04	14.56	
185	9.99		9.40E-08		1.85E-04		5.21	8.67	2460	4320	8.64E+03	3.89E+04	14.56	
186	9.99		9.40E-08		1.85E-04		5.22	8.67	1860	4320	8.64E+03	3.89E+04	14.56	
187	9.99		9.40E-08		1.85E-04		5.20	8.67	3150	4320	8.64E+03	3.89E+04	14.56	
188	9.99		9.40E-08		1.85E-04		5.20	8.67	1860	4320	8.64E+03	3.89E+04	14.56	
189	9.99		9.40E-08		1.85E-04		5.20	8.67	2350	4320	8.64E+03	3.89E+04	14.56	

Table A2.3 (Cont.): Selected PBDE chemical properties estimated by EPI suite V4.11.

Congener ⁽¹⁾	Log K _{ow} ⁽²⁾		SW ₂₅ ⁽⁵⁾ (mg/L)			Log K _{oc} ⁽⁶⁾			Half life (hours) ⁽⁷⁾				Log K _{OA25C} ⁽⁸⁾	
	Est ⁽³⁾	Db ⁽⁴⁾	WSKOW	Db ⁽⁴⁾	WATERNT	Db ⁽⁴⁾	MCI	KOW	Air	Water	Soil	Sediment	Est ⁽³⁾	Db ⁽⁴⁾
190	9.99		9.40E-08		1.85E-04		5.21	8.67	2460	4320	8.64E+03	3.89E+04	14.56	
191	9.99		9.40E-08		1.85E-04		5.20	8.67	2220	4320	8.64E+03	3.89E+04	14.56	
192	9.99		9.40E-08		1.85E-04		5.20	8.67	1220	4320	8.64E+03	3.89E+04	14.56	
193	9.99		9.40E-08		1.85E-04		5.20	8.67	2350	4320	8.64E+03	3.89E+04	14.56	
194	10.88		4.84E-09		3.50E-05		5.42	9.42	5950	4320	8.64E+03	3.89E+04	15.85	
195	10.88		4.84E-09		3.50E-05		5.42	9.42	5530	4320	8.64E+03	3.89E+04	15.85	
196	10.88		4.84E-09		3.50E-05		5.42	9.42	5000	4320	8.64E+03	3.89E+04	15.85	
197	10.88		4.84E-09		3.50E-05		5.42	9.42	4310	4320	8.64E+03	3.89E+04	15.85	
198	10.88		4.84E-09		3.50E-05		5.42	9.42	3840	4320	8.64E+03	3.89E+04	15.85	
199	10.88		4.84E-09		3.50E-05		5.42	9.42	5950	4320	8.64E+03	3.89E+04	15.85	
200	10.88		4.84E-09		3.50E-05		5.42	9.42	5530	4320	8.64E+03	3.89E+04	15.85	
201	10.88		4.84E-09		3.50E-05		5.42	9.42	5000	4320	8.64E+03	3.89E+04	15.85	
202	10.88	5.5	4.84E-09		3.50E-05		5.42	4.77	5950	4320	8.64E+03	3.89E+04	10.47	
203	10.88		4.84E-09		3.50E-05		5.42	9.42	5530	4320	8.64E+03	3.89E+04	15.85	
204	10.88		4.84E-09		3.50E-05		5.42	9.42	2920	4320	8.64E+03	3.89E+04	15.85	
205	10.88		4.84E-09		3.50E-05		5.42	9.42	3840	4320	8.64E+03	3.89E+04	15.85	
206	11.77		2.46E-10		6.54E-06		5.65	10.22	1050	4320	8.64E+03	3.89E+04	17.14	
207	11.77		2.46E-10		6.54E-06		5.65	10.22	8430	4320	8.64E+03	3.89E+04	17.14	
208	11.77		2.46E-10		6.54E-06		5.65	10.22	1050	4320	8.64E+03	3.89E+04	17.14	
209	12.66		1.25E-11		1.21E-06		5.87	10.99	2050	4320	8.64E+03	3.89E+04	18.43	

Table A2.3 (Cont.): Selected PBDE chemical properties estimated by EPI suite V4.11.

Congener ⁽¹⁾	Log K _{ow} ⁽²⁾		SW ₂₅ ⁽⁵⁾ (mg/L)				Log K _{oc} ⁽⁶⁾			Half life (hours) ⁽⁷⁾			Log K _{OA25C} ⁽⁸⁾	
	Est ⁽³⁾	Db ⁽⁴⁾	WSKOW	Db ⁽⁴⁾	WATERNT	Db ⁽⁴⁾	MCI	KOW	Air	Water	Soil	Sediment	Est ⁽³⁾	Db ⁽⁴⁾

(1): Congener number as designated by IUPAC .

(2): Log K_{OW} was estimated from fragment constant method.

(3): Est: Estimate

(4): Db=Database. Values were used as comparison.

(5): SW₂₅ is estimated from Log K_{OW} (WSKOW) and from bond contribution method (WATERNT).

(6): Log K_{OC} is estimated from molecular connectivity indices (MCI) and through QSPR regression that uses log KOW as input (WSKOW).

(7): Half life is estimated from biodegradation expert survey model of the BIOWIN program in the EPI suite V4.11.

(8):Log K_{OA} is estimated from log K_{OW} and Henry's law constant.

Table A2.4 (Cont.): Selected PCB chemical properties estimated by EPI suite V4.11.

# ⁽¹⁾	Log K _{ow} ⁽²⁾		SW ₂₅ ⁽⁵⁾ (mg/L)			Log K _{oc} ⁽⁶⁾		Half life (hours) ⁽⁷⁾				Log K _{OA25C} ⁽⁸⁾	
	Est ⁽³⁾	Db ⁽⁴⁾	WSKOW	Db ⁽⁴⁾	WATERNT	Est ⁽³⁾	Db ⁽⁴⁾	WSKOW	Db ⁽⁴⁾	WATERNT		Est ⁽³⁾	Db ⁽⁴⁾
1	4.4	4.53	5.34E+00	1.45E+00	2.48E+00	3.92	4.04	91	900	1.80E+03	8.10E+03	6.17	
2	4.4	4.58	6.12E+00	3.63E+00	2.48E+00	3.92	3.98	49	900	1.80E+03	8.10E+03	6.18	6.82
3	4.4	4.61	5.77E+00	1.34E+00	2.48E+00	3.92	4.00	67	900	1.80E+03	8.10E+03	6.24	6.80
4	5.05	4.97	1.78E+00	1.85E+00	5.96E-01	4.14	4.34	128	900	1.80E+03	8.10E+03	7.03	7.18
5	5.05	5.02	1.71E+00	9.97E-01	5.96E-01	4.14	4.36	104	900	1.80E+03	8.10E+03	7.05	
6	5.05	5.02	1.71E+00	5.80E-01	5.96E-01	4.13	4.36	98	900	1.80E+03	8.10E+03	7.01	
7	5.05	5.16	1.30E+00	1.15E+00	5.96E-01	4.13	4.48	99	900	1.80E+03	8.10E+03	7.10	
8	5.05	5.09	1.49E+00	1.17E+00	5.96E-01	4.13	4.42	149	900	1.80E+03	8.10E+03	7.11	7.40
9	5.05	5.1	1.46E+00	1.12E+00	5.96E-01	4.13	4.43	104	900	1.80E+03	8.10E+03	7.04	
10	5.05	4.98	1.85E+00	2.41E+00	5.96E-01	4.14	4.32	104	900	1.80E+03	8.10E+03	7.01	4.98
11	5.05	5.27	1.05E+00	3.55E-01	5.96E-01	4.12	4.57	63	900	1.80E+03	8.10E+03	7.29	
12	5.05	5.29	1.01E+00	9.09E-02	5.96E-01	4.13	4.59	104	900	1.80E+03	8.10E+03	7.53	
13	5.05	5.15	1.33E+00	8.80E-02	5.96E-01	4.12	4.47	98	900	1.80E+03	8.10E+03	7.18	
14	5.05	5.41	7.95E-01		5.96E-01	4.12	4.70	61	900	1.80E+03	8.10E+03	7.46	
15	5.05	5.23	1.13E+00	6.20E-02	5.96E-01	4.12	4.54	128	900	1.80E+03	8.10E+03	7.32	7.68
16	5.69	5.34	6.27E-01	2.93E-01	1.40E-01	4.70	4.01	235	1440	2.88E+03	1.30E+04	7.40	
17	5.69	5.76	2.59E-01	8.33E-02	1.40E-01	4.69	4.26	217	1440	2.88E+03	1.30E+04	7.92	
18	5.69	5.48	3.91E-01	4.00E-01	1.40E-01	4.69	4.14	235	1440	2.88E+03	1.30E+04	7.54	7.60
19	5.69	5.48	4.49E-01	3.24E-01	1.40E-01	4.70	4.10	217	1440	2.88E+03	1.30E+04	7.51	
20	5.69	5.57	3.76E-01		1.40E-01	4.69	4.15	146	1440	2.88E+03	1.30E+04	7.75	
21	5.69	5.86	2.13E-01	1.70E-01	1.40E-01	4.70	4.31	205	1440	2.88E+03	1.30E+04	8.02	
22	5.69	5.42	5.05E-01	1.42E-01	1.40E-01	4.69	4.07	235	1440	2.88E+03	1.30E+04	7.66	
23	5.69		2.97E-01		1.40E-01	4.69	4.22	167	1440	2.88E+03	1.30E+04	7.85	
24	5.69	5.67	3.09E-01	8.33E-02	1.40E-01	4.70	4.21	205	1440	2.88E+03	1.30E+04	7.72	
25	5.69		2.97E-01		1.40E-01	4.68	4.22	138	1440	2.88E+03	1.30E+04	7.85	
26	5.69	5.76	2.59E-01	2.53E-01	1.40E-01	4.68	4.26	146	1440	2.88E+03	1.30E+04	7.85	

Table A2.4 (Cont.): Selected PCB chemical properties estimated by EPI suite V4.11.

# ⁽¹⁾	Log K _{ow} ⁽²⁾		SW ₂₅ ⁽⁵⁾ (mg/L)			Log K _{oc} ⁽⁶⁾		Half life (hours) ⁽⁷⁾			Log K _{OA25C} ⁽⁸⁾	
	Est ⁽³⁾	Db ⁽⁴⁾	WSKOW	Db ⁽⁴⁾	WATERNT	Est ⁽³⁾	Db ⁽⁴⁾	WSKOW	Db ⁽⁴⁾	WATERNT	Est ⁽³⁾	Db ⁽⁴⁾
27	5.69		2.97E-01	3.86E-02	1.40E-01	4.69	4.22	138	1440	2.88E+03 1.30E+04	7.85	
28	5.69	5.62	3.41E-01	4.20E-01	1.40E-01	4.68	4.18	233	1440	2.88E+03 1.30E+04	7.71	
29	5.69	5.81	2.35E-01	1.63E-01	1.40E-01	4.69	4.28	197	1440	2.88E+03 1.30E+04	7.90	8.00
30	5.69	5.47	4.58E-01	2.51E-01	1.40E-01	4.69	4.10	167	1440	2.88E+03 1.30E+04	6.88	
31	5.69	5.69	2.97E-01	1.43E-01	1.40E-01	4.70	4.22	214	1440	2.88E+03 1.30E+04	7.80	7.92
32	5.69	5.75	2.64E-01	1.59E-01	1.40E-01	4.69	4.25	217	1440	2.88E+03 1.30E+04	7.84	7.72
33	5.69	5.87	2.08E-01	1.33E-01	1.40E-01	4.69	4.32	257	1440	2.88E+03 1.30E+04	8.05	
34	5.69		2.97E-01	1.29E-01	1.40E-01	4.68	4.22	142	1440	2.88E+03 1.30E+04	7.78	
35	5.69		2.97E-01		1.40E-01	4.68	4.22	146	1440	2.88E+03 1.30E+04	7.85	
36	5.69		2.35E-01		1.40E-01	4.67	4.28	103	1440	2.88E+03 1.30E+04	7.97	
37	5.69	5.9	1.97E-01	7.19E-02	1.40E-01	4.68	4.33	235	1440	2.88E+03 1.30E+04	8.29	
38	5.69		2.97E-01		1.40E-01	4.69	4.22	167	1440	2.88E+03 1.30E+04	7.85	
39	5.69		2.97E-01		1.40E-01	4.67	4.22	142	1440	2.88E+03 1.30E+04	7.85	
40	6.34	6.18	7.21E-02	1.56E-02	3.22E-02	4.91	4.49	352	4320	8.64E+03 3.89E+04	8.57	
41	6.34	6.11	8.74E-02	4.32E-02	3.22E-02	4.91	4.45	445	4320	8.64E+03 3.89E+04	8.35	
42	6.34		5.32E-02	6.08E-02	3.22E-02	4.90	4.58	333	4320	8.64E+03 3.89E+04	8.58	
43	6.34		5.32E-02	1.72E-01	3.22E-02	4.90	4.58	338	4320	8.64E+03 3.89E+04	8.63	
44	6.34	5.81	1.49E-01	1.00E-01	3.22E-02	4.90	4.28	321	4320	8.64E+03 3.89E+04	8.05	8.36
45	6.34		5.32E-02	1.46E-01	3.22E-02	4.91	4.58	445	4320	8.64E+03 3.89E+04	8.63	
46	6.34		5.32E-02	1.46E-01	3.22E-02	4.91	4.58	333	4320	8.64E+03 3.89E+04	8.63	
47	6.34	7.1	5.81E-02	2.77E-01	3.22E-02	4.89	4.55	257	4320	8.64E+03 3.89E+04	8.40	
48	6.34		5.32E-02	1.64E-02	3.22E-02	4.90	4.58	445	4320	8.64E+03 3.89E+04	8.63	
49	6.34	6.22	6.67E-02	7.81E-02	3.22E-02	4.89	4.51	333	4320	8.64E+03 3.89E+04	8.29	8.39
50	6.34		5.32E-02	6.54E-02	3.22E-02	4.90	4.58	311	4320	8.64E+03 3.89E+04	8.63	
51	6.34		5.32E-02	6.54E-02	3.22E-02	4.90	4.58	316	4320	8.64E+03 3.89E+04	8.58	
52	6.34	6.09	8.61E-02	1.53E-02	3.22E-02	4.89	4.44	352	4320	8.64E+03 3.89E+04	8.18	8.47

Table A2.4 (Cont.): Selected PCB chemical properties estimated by EPI suite V4.11.

# ⁽¹⁾	Log K _{ow} ⁽²⁾		SW ₂₅ ⁽⁵⁾ (mg/L)			Log K _{oc} ⁽⁶⁾		Half life (hours) ⁽⁷⁾				Log K _{OA25C} ⁽⁸⁾	
	Est ⁽³⁾	Db ⁽⁴⁾	WSKOW	Db ⁽⁴⁾	WATERNT	Est ⁽³⁾	Db ⁽⁴⁾	WSKOW	Db ⁽⁴⁾	WATERNT		Est ⁽³⁾	Db ⁽⁴⁾
53	6.34		5.32E-02	4.76E-02	3.22E-02	4.90	4.58	333	4320	8.64E+03	3.89E+04	8.47	8.45
54	6.34	5.94	1.16E-01	1.19E-02	3.22E-02	4.91	4.36	316	4320	8.64E+03	3.89E+04	8.03	
55	6.34		5.32E-02	4.96E-02	3.22E-02	4.90	4.58	280	4320	8.64E+03	3.89E+04	8.63	
56	6.34		5.32E-02		3.22E-02	4.90	4.58	352	4320	8.64E+03	3.89E+04	8.63	
57	6.34		5.32E-02		3.22E-02	4.89	4.58	233	4320	8.64E+03	3.89E+04	8.63	
58	6.34	6.17	7.35E-02		3.22E-02	4.89	4.48	206	4320	8.64E+03	3.89E+04	8.46	
59	6.34		5.32E-02		3.22E-02	4.90	4.58	280	4320	8.64E+03	3.89E+04	8.63	
60	6.34	5.84	1.41E-01	3.89E-02	3.22E-02	4.90	4.30	445	4320	8.64E+03	3.89E+04	8.13	
61	6.34	6.41	4.59E-02	1.40E-02	3.22E-02	4.91	4.62	319	4320	8.64E+03	3.89E+04	7.79	8.74
62	6.34		5.32E-02		3.22E-02	4.91	4.58	319	4320	8.64E+03	3.89E+04	8.41	
63	6.34		5.32E-02	4.96E-02	3.22E-02	4.89	4.58	338	4320	8.64E+03	3.89E+04	8.63	
64	6.34		5.32E-02		3.22E-02	4.90	4.58	445	4320	8.64E+03	3.89E+04	8.58	8.41
65	6.34		5.32E-02	1.64E-02	3.22E-02	4.91	4.58	319	4320	8.64E+03	3.89E+04	8.38	
66	6.34	6.31	5.58E-03		3.22E-02	4.89	4.58	323	4320	8.64E+03	3.89E+04	8.44	9.02
67	6.34	6.31	5.32E-02	3.68E-02	3.22E-02	4.89	4.56	333	4320	8.64E+03	3.89E+04	8.62	
68	6.34		6.93E-02	2.17E-02	3.22E-02	4.88	4.58	280	4320	8.64E+03	3.89E+04	8.73	
69	6.34	6.2	5.32E-02	1.00E-01	3.22E-02	4.89	4.50	200	4320	8.64E+03	3.89E+04	7.95	
70	6.34		5.32E-02	2.05E-02	3.22E-02	4.90	4.58	220	4320	8.64E+03	3.89E+04	8.41	
71	6.34		5.32E-02	2.79E-02	3.22E-02	4.88	4.58	333	4320	8.64E+03	3.89E+04	8.63	
72	6.34		5.32E-02		3.22E-02	4.89	4.58	206	4320	8.64E+03	3.89E+04	8.63	
73	6.34		5.32E-02		3.22E-02	4.89	4.58	200	4320	8.64E+03	3.89E+04	8.63	
74	6.34	6.67	2.75E-02	4.96E-03	3.22E-02	4.89	4.76	445	4320	8.64E+03	3.89E+04	9.06	
75	6.34	6.67	2.75E-02	4.96E-03	3.22E-02	4.90	4.76	445	4320	8.64E+03	3.89E+04	9.06	
76	6.34		5.32E-02		3.22E-02	4.89	4.58	338	4320	8.64E+03	3.89E+04	8.63	
77	6.34	6.63	2.98E-02	5.69E-04	3.22E-02	4.89	4.74	352	4320	8.64E+03	3.89E+04	10.05	9.70
78	6.34		5.32E-02		3.22E-02	4.88	4.58	233	4320	8.64E+03	3.89E+04	8.63	

Table A2.4 (Cont.): Selected PCB chemical properties estimated by EPI suite V4.11.

# ⁽¹⁾	Log K _{ow} ⁽²⁾		SW ₂₅ ⁽⁵⁾ (mg/L)			Log K _{oc} ⁽⁶⁾		Half life (hours) ⁽⁷⁾				Log K _{OA25C} ⁽⁸⁾	
	Est ⁽³⁾	Db ⁽⁴⁾	WSKOW	Db ⁽⁴⁾	WATERNT	Est ⁽³⁾	Db ⁽⁴⁾	WSKOW	Db ⁽⁴⁾	WATERNT		Est ⁽³⁾	Db ⁽⁴⁾
79	6.34		5.32E-02		3.22E-02	4.88	4.58	206	4320	8.64E+03	3.89E+04	8.77	
80	6.34	6.6	3.16E-02	1.23E-03	3.22E-02	4.88	4.72	146	4320	8.64E+03	3.89E+04	8.89	
81	6.34		5.32E-02		3.22E-02	4.89	4.58	338	4320	8.64E+03	3.89E+04	8.63	
82	6.98		9.39E-03	2.91E-02	7.33E-03	5.12	4.93	767	4320	8.64E+03	3.89E+04	9.40	
83	6.98		9.39E-03		7.33E-03	5.12	4.93	543	4320	8.64E+03	3.89E+04	9.40	
84	6.98	6.04	9.39E-03	5.42E-02	7.33E-03	5.12	4.41	767	4320	8.64E+03	3.89E+04	8.46	8.80
85	6.98	6.61	1.94E-02	7.83E-03	7.33E-03	5.12	4.73	642	4320	8.64E+03	3.89E+04	9.18	
86	6.98		9.39E-03	9.80E-03	7.33E-03	5.12	4.93	644	4320	8.64E+03	3.89E+04	7.88	
87	6.98	6.85	1.21E-02	2.94E-02	7.33E-03	5.12	4.86	767	4320	8.64E+03	3.89E+04	9.37	
88	6.98		9.39E-03	1.20E-02	7.33E-03	5.12	4.93	614	4320	8.64E+03	3.89E+04	9.40	
89	6.98		9.39E-03	5.42E-02	7.33E-03	5.12	4.93	642	4320	8.64E+03	3.89E+04	9.40	
90	6.98		9.39E-03	4.94E-03	7.33E-03	5.11	4.93	477	4320	8.64E+03	3.89E+04	9.41	
91	6.98		9.39E-03	2.21E-02	7.33E-03	5.12	4.93	642	4320	8.64E+03	3.89E+04	9.40	
92	6.98	6.79	1.36E-02	4.94E-03	7.33E-03	5.11	4.83	543	4320	8.64E+03	3.89E+04	9.21	
93	6.98		9.39E-03	1.30E-02	7.33E-03	5.12	4.93	644	4320	8.64E+03	3.89E+04	9.40	
94	6.98		9.39E-03		7.33E-03	5.12	4.93	477	4320	8.64E+03	3.89E+04	9.40	
95	6.98	6.55	2.19E-02	2.10E-02	7.33E-03	5.12	4.93	477	4320	8.64E+03	3.89E+04	9.40	
96	6.98		9.39E-03		7.33E-03	5.12	4.93	642	4320	8.64E+03	3.89E+04	9.40	
97	6.98	6.67	1.73E-02	2.84E-02	7.33E-03	5.12	4.76	767	4320	8.64E+03	3.89E+04	9.19	
98	6.98		9.39E-03	1.30E-02	7.33E-03	5.12	4.93	511	4320	8.64E+03	3.89E+04	9.40	
99	6.98	7.21	5.97E-03	3.66E-03	7.33E-03	5.11	5.06	642	4320	8.64E+03	3.89E+04	9.71	
100	6.98		9.39E-03	7.14E-03	7.33E-03	5.11	4.93	453	4320	8.64E+03	3.89E+04	9.40	
101	6.98	5.68	1.34E-02	1.54E-02	7.33E-03	5.11	4.83	767	4320	8.64E+03	3.89E+04	9.23	
102	6.98		9.39E-03		7.33E-03	5.12	4.93	642	4320	8.64E+03	3.89E+04	9.40	
103	6.98		9.39E-03	1.11E-02	7.33E-03	5.11	4.93	511	4320	8.64E+03	3.89E+04	9.40	
104	6.98		9.39E-03	1.58E-02	7.33E-03	5.12	4.93	453	4320	8.64E+03	3.89E+04	9.40	

Table A2.4 (Cont.): Selected PCB chemical properties estimated by EPI suite V4.11.

# ⁽¹⁾	Log K _{ow} ⁽²⁾		SW ₂₅ ⁽⁵⁾ (mg/L)			Log K _{oc} ⁽⁶⁾		Half life (hours) ⁽⁷⁾			Log K _{OA25C} ⁽⁸⁾	
	Est ⁽³⁾	Db ⁽⁴⁾	WSKOW	Db ⁽⁴⁾	WATERNT	Est ⁽³⁾	Db ⁽⁴⁾	WSKOW	Db ⁽⁴⁾	WATERNT	Est ⁽³⁾	Db ⁽⁴⁾
105	6.98	6.5	1.36E-01	3.40E-03	7.33E-03	5.12	4.83	767	4320	8.64E+03 3.89E+04	8.73	
106	6.98		9.39E-03		7.33E-03	5.12	4.93	450	4320	8.64E+03 3.89E+04	9.40	
107	6.98		9.39E-03		7.33E-03	5.11	4.93	543	4320	8.64E+03 3.89E+04	9.40	
108	6.98		9.39E-03		7.33E-03	5.11	4.93	402	4320	8.64E+03 3.89E+04	9.40	
109	6.98		9.39E-03		7.33E-03	5.12	4.93	435	4320	8.64E+03 3.89E+04	9.40	
110	6.98	6.22	4.18E-02	7.31E-03	7.33E-03	5.12	4.51	428	4320	8.64E+03 3.89E+04	8.64	9.06
111	6.98		9.39E-03		7.33E-03	5.10	4.93	330	4320	8.64E+03 3.89E+04	9.40	
112	6.98		9.39E-03	5.67E-03	7.33E-03	5.12	4.93	450	4320	8.64E+03 3.89E+04	9.40	
113	6.98		9.39E-03	3.66E-03	7.33E-03	5.11	4.93	402	4320	8.64E+03 3.89E+04	9.40	
114	6.98		9.39E-03	1.60E-02	7.33E-03	5.12	4.93	644	4320	8.64E+03 3.89E+04	9.40	
115	6.98		9.39E-03	3.66E-03	7.33E-03	5.12	4.93	614	4320	8.64E+03 3.89E+04	9.40	
116	6.98	6.75	1.48E-02	4.01E-03	7.33E-03	5.13	4.80	285	4320	8.64E+03 3.89E+04	9.17	
117	6.98		9.39E-03	4.30E-03	7.33E-03	5.12	4.93	644	4320	8.64E+03 3.89E+04	9.40	
118	6.98	7.12	7.13E-02	1.34E-02	7.33E-03	5.11	5.01	767	4320	8.64E+03 3.89E+04	9.05	9.82
119	6.98		9.39E-03	4.02E-03	7.33E-03	5.11	4.93	511	4320	8.64E+03 3.89E+04	9.50	
120	6.98		9.39E-03	1.11E-02	7.33E-03	5.10	4.93	402	4320	8.64E+03 3.89E+04	9.62	
121	6.98		9.39E-03	3.93E-03	7.33E-03	5.10	4.93	318	4320	8.64E+03 3.89E+04	9.40	
122	6.98		9.39E-03	1.28E-02	7.33E-03	5.12	4.93	543	4320	8.64E+03 3.89E+04	9.40	
123	6.98		9.39E-03		7.33E-03	5.11	4.93	477	4320	8.64E+03 3.89E+04	9.40	
124	6.98		9.39E-03	1.28E-02	7.33E-03	5.11	4.93	543	4320	8.64E+03 3.89E+04	9.40	
125	6.98		9.39E-03		7.33E-03	5.12	4.93	477	4320	8.64E+03 3.89E+04	9.40	
126	6.98		9.39E-03		7.33E-03	5.11	4.93	543	4320	8.64E+03 3.89E+04	9.40	10.35
127	6.98		9.39E-03		7.33E-03	5.10	4.93	330	4320	8.64E+03 3.89E+04	9.40	
128	7.62	7.31	3.04E-03	3.50E-04	1.65E-03	5.34	5.11	1570	4320	8.64E+03 3.89E+04	10.59	
129	7.62	7.31	2.98E-03	1.37E-03	1.65E-03	5.34	5.12	1220	4320	8.64E+03 3.89E+04	10.25	
130	7.62	7.39	2.60E-03		1.65E-03	5.33	5.16	1100	4320	8.64E+03 3.89E+04	10.21	

Table A2.4 (Cont.): Selected PCB chemical properties estimated by EPI suite V4.11.

# ⁽¹⁾	Log K _{ow} ⁽²⁾		SW ₂₅ ⁽⁵⁾ (mg/L)			Log K _{oc} ⁽⁶⁾		Half life (hours) ⁽⁷⁾				Log K _{OA25C} ⁽⁸⁾	
	Est ⁽³⁾	Db ⁽⁴⁾	WSKOW	Db ⁽⁴⁾	WATERNT	Est ⁽³⁾	Db ⁽⁴⁾	WSKOW	Db ⁽⁴⁾	WATERNT		Est ⁽³⁾	Db ⁽⁴⁾
131	7.62	7.25	3.43E-03	1.20E-03	1.65E-03	5.34	5.08	1170	4320	8.64E+03	3.89E+04	10.05	
132	7.62	7.04	5.18E-03	8.08E-03	1.65E-03	5.34	4.96	1570	4320	8.64E+03	3.89E+04	9.79	
133	7.62	7.07	4.88E-03		1.65E-03	5.32	4.98	845	4320	8.64E+03	3.89E+04	9.62	
134	7.62	7.25	3.43E-03	8.99E-05	1.65E-03	5.34	5.08	1220	4320	8.64E+03	3.89E+04	9.95	
135	7.62	7.15	4.17E-03	5.44E-03	1.65E-03	5.33	5.02	1100	4320	8.64E+03	3.89E+04	9.79	
136	7.62	7.12	4.42E-03	4.51E-03	1.65E-03	5.34	5.01	1570	4320	8.64E+03	3.89E+04	9.56	
137	7.62	7.44	2.36E-03	1.09E-03	1.65E-03	5.33	5.19	913	4320	8.64E+03	3.89E+04	9.99	
138	7.62	7.44	2.36E-03	1.50E-03	1.65E-03	5.33	5.19	1570	4320	8.64E+03	3.89E+04	10.51	9.51
139	7.62		1.64E-03	1.22E-02	1.65E-03	5.33	5.28	886	4320	8.64E+03	3.89E+04	10.17	
140	7.62	7.25	3.43E-03	2.08E-03	1.65E-03	5.33	5.08	918	4320	8.64E+03	3.89E+04	9.80	
141	7.62	7.19	3.85E-03	7.55E-03	1.65E-03	5.33	5.05	1220	4320	8.64E+03	3.89E+04	10.22	
142	7.62		1.64E-03		1.65E-03	5.35	5.28	1020	4320	8.64E+03	3.89E+04	10.17	
143	7.62		1.64E-03	2.68E-03	1.65E-03	5.34	5.28	913	4320	8.64E+03	3.89E+04	10.42	
144	7.62		1.64E-03	3.53E-03	1.65E-03	5.33	5.28	1170	4320	8.64E+03	3.89E+04	10.17	
145	7.62		1.64E-03		1.65E-03	5.34	5.28	886	4320	8.64E+03	3.89E+04	10.17	
146	7.62	7.12	4.42E-03	9.49E-04	1.65E-03	5.32	5.01	1100	4320	8.64E+03	3.89E+04	10.11	
147	7.62		1.64E-03		1.65E-03	5.33	5.28	913	4320	8.64E+03	3.89E+04	10.30	
148	7.62	6.87	7.23E-03		1.65E-03	5.32	4.87	734	4320	8.64E+03	3.89E+04	9.42	
149	7.62	7.28	3.23E-03	4.24E-03	1.65E-03	5.33	5.07	1570	4320	8.64E+03	3.89E+04	8.53	9.27
150	7.62	6.75	9.16E-03		1.65E-03	5.33	4.80	918	4320	8.64E+03	3.89E+04	9.30	
151	7.62		1.64E-03	1.36E-02	1.65E-03	5.33	5.28	1220	4320	8.64E+03	3.89E+04	10.24	
152	7.62		1.64E-03		1.65E-03	5.34	5.28	913	4320	8.64E+03	3.89E+04	10.17	
153	7.62	6.34	1.28E-03	9.50E-04	1.65E-03	5.32	5.36	1570	4320	8.64E+03	3.89E+04	10.78	9.73
154	7.62		1.64E-03	2.74E-03	1.65E-03	5.32	5.28	918	4320	8.64E+03	3.89E+04		
155	7.62	7.55	1.90E-03	4.08E-03	1.65E-03	5.32	5.25	650	4320	8.64E+03	3.89E+04	10.17	8.99
156	7.62	7.6	1.72E-03	5.33E-03	1.65E-03	5.33	5.27	1220	4320	8.64E+03	3.89E+04	8.54	

Table A2.4 (Cont.): Selected PCB chemical properties estimated by EPI suite V4.11.

# ⁽¹⁾	Log K _{ow} ⁽²⁾		SW ₂₅ ⁽⁵⁾ (mg/L)			Log K _{oc} ⁽⁶⁾		Half life (hours) ⁽⁷⁾				Log K _{OA25C} ⁽⁸⁾	
	Est ⁽³⁾	Db ⁽⁴⁾	WSKOW	Db ⁽⁴⁾	WATERNT	Est ⁽³⁾	Db ⁽⁴⁾	WSKOW	Db ⁽⁴⁾	WATERNT		Est ⁽³⁾	Db ⁽⁴⁾
157	7.62	7.6	1.72E-03		1.65E-03	5.33	5.27	1100	4320	8.64E+03	3.89E+04	9.83	
158	7.62		1.64E-03	8.07E-03	1.65E-03	5.33	5.28	1170	4320	8.64E+03	3.89E+04	10.15	
159	7.62	7.43	2.40E-03		1.65E-03	5.32	5.18	637	4320	8.64E+03	3.89E+04	10.17	
160	7.62	7.3	3.10E-03		1.65E-03	5.34	5.11	678	4320	8.64E+03	3.89E+04	10.52	
161	7.62	7.1	4.60E-03		1.65E-03	5.32	5.00	624	4320	8.64E+03	3.89E+04	10.39	
162	7.62	7.47	2.22E-03		1.65E-03	5.32	5.20	845	4320	8.64E+03	3.89E+04	9.65	
163	7.62	7.2	3.78E-03	1.20E-03	1.65E-03	5.33	5.05	1220	4320	8.64E+03	3.89E+04	10.02	
164	7.62		1.64E-03	1.94E-03	1.65E-03	5.33	5.28	1100	4320	8.64E+03	3.89E+04	10.41	
165	7.62	7.31	3.04E-03		1.65E-03	5.34	5.11	1020	4320	8.64E+03	3.89E+04	10.17	
166	7.62	7.31	3.04E-03		1.65E-03	5.34	5.11	1020	4320	8.64E+03	3.89E+04	9.63	
167	7.62	7.5	2.10E-03	2.23E-03	1.65E-03	5.32	5.22	1100	4320	8.64E+03	3.89E+04	9.63	
168	7.62	7.25	3.43E-03		1.65E-03	5.32	5.08	734	4320	8.64E+03	3.89E+04	10.05	
169	7.62	7.41	2.50E-03	5.10E-04	1.65E-03	5.32	5.17	845	4320	8.64E+03	3.89E+04	9.80	
170	8.27		2.84E-04	3.47E-03	3.67E-04	5.55	5.64	2450	4320	8.64E+03	3.89E+04	9.96	
171	8.27		2.84E-04	3.47E-03	3.67E-04	5.55	5.64	2180	4320	8.64E+03	3.89E+04	11.70	10.24
172	8.27		2.84E-04	2.17E-03	3.67E-04	5.54	5.64	1830	4320	8.64E+03	3.89E+04	10.13	
173	8.27		2.84E-04		3.67E-04	5.56	5.64	2070	4320	8.64E+03	3.89E+04	12.55	
174	8.27		2.84E-04	1.02E-03	3.67E-04	5.55	5.64	2450	4320	8.64E+03	3.89E+04	11.51	
175	8.27		2.84E-04	8.26E-04	3.67E-04	5.54	5.64	1670	4320	8.64E+03	3.89E+04	11.51	
176	8.27		2.84E-04	2.80E-03	3.67E-04	5.55	5.64	2180	4320	8.64E+03	3.89E+04	10.95	
177	8.27		2.84E-04	1.50E-03	3.67E-04	5.55	5.64	2450	4320	8.64E+03	3.89E+04	10.95	
178	8.27		2.84E-04	1.02E-03	3.67E-04	5.54	5.64	1830	4320	8.64E+03	3.89E+04	11.30	
179	8.27		2.84E-04	4.54E-03	3.67E-04	5.55	5.64	2450	4320	8.64E+03	3.89E+04	11.28	
180	8.27		2.84E-04	3.85E-03	3.67E-04	5.54	5.64	2450	4320	8.64E+03	3.89E+04	11.66	9.88
181	8.27		2.84E-04	4.23E-04	3.67E-04	5.55	5.64	1460	4320	8.64E+03	3.89E+04	10.95	10.51
182	8.27		2.84E-04	8.26E-04	3.67E-04	5.54	5.64	1350	4320	8.64E+03	3.89E+04	10.95	

Table A2.4 (Cont.): Selected PCB chemical properties estimated by EPI suite V4.11.

# ⁽¹⁾	Log K _{ow} ⁽²⁾		SW ₂₅ ⁽⁵⁾ (mg/L)			Log K _{oc} ⁽⁶⁾		Half life (hours) ⁽⁷⁾			Log K _{OA25C} ⁽⁸⁾	
	Est ⁽³⁾	Db ⁽⁴⁾	WSKOW	Db ⁽⁴⁾	WATERNT	Est ⁽³⁾	Db ⁽⁴⁾	WSKOW	Db ⁽⁴⁾	WATERNT	Est ⁽³⁾	Db ⁽⁴⁾
183	8.27		2.84E-04	4.90E-03	3.67E-04	5.54	5.64	2180	4320	8.64E+03 3.89E+04	10.95	
184	8.27	7.55	1.17E-03	1.44E-02	3.67E-04	5.54	5.25	1270	4320	8.64E+03 3.89E+04	9.41	
185	8.27	7.93	5.53E-04	5.46E-03	3.67E-04	5.55	5.46	2070	4320	8.64E+03 3.89E+04	11.11	
186	8.27		2.84E-04		3.67E-04	5.56	5.64	1460	4320	8.64E+03 3.89E+04	10.95	
187	8.27		2.84E-04	4.51E-03	3.67E-04	5.54	5.64	2450	4320	8.64E+03 3.89E+04	10.95	9.87
188	8.27		2.84E-04	1.28E-03	3.67E-04	5.54	5.64	1350	4320	8.64E+03 3.89E+04	10.95	
189	8.27		2.84E-04	7.53E-04	3.67E-04	5.54	5.64	1830	4320	8.64E+03 3.89E+04	10.95	
190	8.27		2.84E-04		3.67E-04	5.55	5.64	2070	4320	8.64E+03 3.89E+04	10.95	
191	8.27		2.84E-04	3.10E-04	3.67E-04	5.54	5.64	1670	4320	8.64E+03 3.89E+04	10.95	
192	8.27		2.84E-04	3.10E-04	3.67E-04	5.54	5.64	968	4320	8.64E+03 3.89E+04	10.95	
193	8.27		2.84E-04	3.10E-04	3.67E-04	5.54	5.64	1830	4320	8.64E+03 3.89E+04	10.95	
194	8.91	8.68	7.72E-05	2.72E-04	8.10E-05	5.77	5.87	4590	4320	8.64E+03 3.89E+04	12.07	
195	8.91		4.88E-05	2.20E-04	8.10E-05	5.78	6.00	4200	4320	8.64E+03 3.89E+04	12.26	
196	8.91		4.88E-05	1.63E-04	8.10E-05	5.77	6.00	3650	4320	8.64E+03 3.89E+04	12.30	
197	8.91		4.88E-05	3.41E-04	8.10E-05	5.77	6.00	3030	4320	8.64E+03 3.89E+04	11.72	
198	8.91		4.88E-05	1.63E-04	8.10E-05	5.77	6.00	2950	4320	8.64E+03 3.89E+04	12.15	
199	8.91		4.88E-05	2.20E-04	8.10E-05	5.77	6.00	4590	4320	8.64E+03 3.89E+04	12.30	
200	8.91		4.88E-05	3.41E-04	8.10E-05	5.78	6.00	4200	4320	8.64E+03 3.89E+04	11.72	
201	8.91		4.88E-05	2.71E-04	8.10E-05	5.77	6.00	3650	4320	8.64E+03 3.89E+04	12.07	
202	8.91	7.73	5.00E-04	1.47E-04	8.10E-05	5.77	5.35	4590	4320	8.64E+03 3.89E+04	10.86	
203	8.91		4.88E-05	1.36E-04	8.10E-05	5.77	6.00	4200	4320	8.64E+03 3.89E+04	11.72	
204	8.91		4.88E-05	1.42E-04	8.10E-05	5.77	6.00	2080	4320	8.64E+03 3.89E+04	11.72	
205	8.91		4.88E-05	8.58E-05	8.10E-05	5.77	6.00	2950	4320	8.64E+03 3.89E+04	11.72	
206	8.91	9.14	1.89E-05	2.50E-05	1.78E-05	5.99	6.12	7800	4320	8.64E+03 3.89E+04	12.08	
207	8.91		8.34E-06	8.34E-06	1.78E-05	5.99	6.36	5900	4320	8.64E+03 3.89E+04	12.50	
208	8.91	8.16	1.30E-04	1.30E-04	1.78E-05	5.99	5.58	7800	4320	8.64E+03 3.89E+04	11.10	

Table A2.4 (Cont.): Selected PCB chemical properties estimated by EPI suite V4.11.

# ⁽¹⁾	Log K _{ow} ⁽²⁾		SW ₂₅ ⁽⁵⁾ (mg/L)			Log K _{oc} ⁽⁶⁾		Half life (hours) ⁽⁷⁾			Log K _{OA25C} ⁽⁸⁾	
	Est ⁽³⁾	Db ⁽⁴⁾	WSKOW	Db ⁽⁴⁾	WATERNT	Est ⁽³⁾	Db ⁽⁴⁾	WSKOW	Db ⁽⁴⁾	WATERNT	Est ⁽³⁾	Db ⁽⁴⁾
209	8.91	8.27	6.32E-05	6.32E-05	3.89E-06	6.21	5.64	14100	4320	8.64E+03	3.89E+04	8.69

(1): Congener number as designated by IUPAC .

(2): Log K_{OW} was estimated from fragment constant method.

(3): Est: Estimate

(4): Db=Database. Values were used as comparison.

(5): SW₂₅ is estimated from Log K_{OW} (WSKOW) and from bond contribution method (WATERNT).

(6): Log K_{OC} is estimated from molecular connectivity indices (MCI) and through QSPR regression that uses log KOW as input (WSKOW).

(7): Half life is estimated from biodegradation expert survey model of the BIOWIN program in the EPI suite V4.11.

(8):Log K_{OA} is estimated from log K_{OW} and Henry's law constant.

Appendix B

Table B3.1: Target PBDE analytes in this study.

Congener	Homolog	Structure	Molecular weight (g/mol)	Congener	Homolog	Structure	Molecular weight (g/mol)
1	1	2,	248.904	99	5	2,2',4,4',5	564.52
2	1	3,	248.904	116	5	2,3,4,5,6	564.52
3	1	4,	248.904	85	5	2,2',3,4,4',	564.52
10	2	2,6,	327.808	126	5	3,3',4,4',5	564.52
7	2	2,4,	327.808	155	6	2,2',4,4',6,6'	643.424
11	2	3,3'	327.808	154	6	2,2',4,4',5,6'	643.424
8	2	2,4'	327.808	153	6	2,2',4,4',5,5',	643.424
12	2	3,4	327.808	138	6	2,2',3,4,4',5,	643.424
13	2	3,4'	327.808	166	6	2,3,4,4',5,6,	643.424
15	2	4,4',	327.808	183	7	2,2',3,4,4',5',6,	722.328
32	3	2,4',6'	406.712	181	7	2,2',3,4,4',5,6,	722.328
17	3	2,2',4,	406.712	202	8	2,2',3,3',5,5',6,6',	801.232
25	3	2,3',4,	406.712	201	8	2,2',3,3',4,5',6,6',	801.232
28	3	2,4,4'	406.712	204	8	2,2',3,4,4',5,6,6',	801.232
33	3	2,3',4'	406.712	197	8	2,2',3,3',4,4',6,6',	801.232
35	3	3,3',4,	406.712	203	8	2,2',3,4,4',5,5',6,	801.232
37	3	3,4,4'	406.712	196	8	2,2',3,3',4,4',5,6,	801.232
75	4	2,4,4',6,	485.616	205	8	2,3,3',4,4',5,5',6,	801.232
49	4	2,2',4,5',	485.616	194	8	2,2',3,3',4,4',5,5'	801.232
71	4	2,3',4',6,	485.616	195	8	2,2',3,3',4,4',5,6,	801.232
47	4	2,2',4,4',	485.616	208	9	2,2',3,3',4,5,5',6,6',	880.136
66	4	2,3',4,4',	485.616	207	9	2,2',3,3',4,4',5,6,6',	880.136
77	4	3,3',4,4',	485.616	206	9	2,2',3,3',4,4',5,5',6,	880.136
100	5	2,2',4,4',6,	564.52	209	10	2,2',3,3',4,4',5,5',6,6',	959.04
119	5	2,3',4,4',6,	564.52				

Table B3.2 (Cont.): Target PCB analytes in this study.

Congener	Homolog	Structure	Molecular weight (g/mol)	Congener	Homolog	Structure	Molecular weight (g/mol)
1	1	2	198.66	103	5	2,2',4,5',6-	336.46
2	1	3	198.66	104	5	2,2',4,6,6'-	336.46
3	1	4	198.66	105	5	2,3,3',4,4'-	336.46
5	2	2,3	233.11	110	5	2,3,3',4',6	336.46
6	2	2, 3'	233.11	114	5	2,3,4,4',5-	336.46
8	2	2,4'	233.11	115	5	2,3,4,4',6-	336.46
12	2	3,4	233.11	117	5	2,3,4',5,6-	336.46
13	2	3,4'	233.11	118	5	2,3',4,4',5-	336.46
14	2	3,5	233.11	119	5	2,3',4,4',6	336.46
15	2	4,4'-	233.11	122	5	2,3,3',4',5'	336.46
16	3	2,2',3-	267.56	124	5	2,3',4',5,5'	336.46
17	3	2,2',4	267.56	128	6	2,2',3,3',4,4'-	370.91
18	3	2,2',5-	267.56	129	6	2,2',3,3',4,5-	370.91
19	3	2,2',6	267.56	130	6	2,2',3,3',4,5'-	370.91
22	3	2,3,4'	267.56	131	6	2,2',3,3',4,6-	370.91
25	3	2,3',4	267.56	132	6	2,2',3,3',4,6'-	370.91
26	3	2,3',5-	267.56	134	6	2,2',3,3',5,6-	370.91
29	3	2,4,5	267.56	135	6	2,2',3,3',5,6'-	370.91
32	3	2,4',6-	267.56	136	6	2,2',3,3',6,6'-	370.91
34	3	2,3',5	267.56	137	6	2,2',3,4,4',5-	370.91
35	3	3,3',4-	267.56	138	6	2,2',3,4,4',5'-	370.91
37	3	3,4,4'	267.56	141	6	2,2',3,4,5,5'-	370.91
40	4	2,2',3,3'	302.01	144	6	2,2',3,4,5',6-	370.91
41	4	2,2',3,4	302.01	146	6	2,2',3,4',5,5'-	370.91
42	4	2,2',3,4'-	302.01	147	6	2,2',3,4',5,6-	370.91
44	4	2,2',3,5'-	302.01	149	6	2,2',3,4',5',6-	370.91
45	4	2,2',3,6-	302.01	151	6	2,2',3,5,5',6-	370.91
46	4	2,2',3,6'-	302.01	153	6	2,2',4,4',5,5'-	370.91
49	4	2,2',4,5'-	302.01	154	6	2,2',4,4',5,6'-	370.91
51	4	2,2',4,6'	302.01	156	6	2,3,3',4,4',5-	370.91
52	4	2,2',5,5'	302.01	157	6	2,3,3',4,4',5'-	370.91
53	4	2,2',5,6'-T	302.01	158	6	2,3,3',4,4',6-	370.91
54	4	2,2',6,6'	302.01	165	6	2,3,3',5,5',6-	370.91
56	4	2,3,3',4'-	302.01	167	6	2,3',4,4',5,5'-	370.91
59	4	2,3,3',6-	302.01	171	7	2,2',3,3',4,4',6-	405.36
60	4	2,3,4,4'-	302.01	172	7	2,2',3,3',4,5,5'-	405.36
63	4	2,3,4',5-	302.01	173	7	2,2',3,3',4,5,6-	405.36
64	4	2,3,4',6-	302.01	174	7	2,2',3,3',4,5,6'-	405.36

Table B3.2 (Cont.): Target PCB analytes in this study.

Congener	Homolog	Structure	Molecular weight (g/mol)	Congener	Homolog	Structure	Molecular weight (g/mol)
66	4	2,3',4,4'-	302.01	175	7	2,2',3,3',4,5',6-	405.36
67	4	2,3',4,5	302.01	176	7	2,2',3,3',4,6,6'-	405.36
69	4	2,3',4,6-T	302.01	177	7	2,2',3,3',4,5',6'-	405.36
70	4	2,3',4',5	302.01	178	7	2,2',3,3',5,5',6-	405.36
71	4	2,3',4',6-	302.01	179	7	2,2',3,3',5,6,6'-	405.36
73	4	2,3',5',6-	302.01	183	7	2,2',3,4,4',5',6-	405.36
74	4	2,4,4',5-	302.01	185	7	2,2',3,4,5,5',6-H	405.36
77	4	3,3',4,4'	302.01	187	7	2,2',3,4',5,5',6-	405.36
81	4	3,4,4',5	302.01	189	7	2,3,3',4,4',5,5'-	405.36
82	5	2,2',3,3',4-	336.46	191	7	2,3,3',4,4',5',6-	405.36
83	5	2,2',3,3',5	336.46	194	8	2,2',3,3',4,4',5,5'-	439.81
84	5	2,2',3,3',6-	336.46	195	8	2,2',3,3',4,4',5,6-	439.81
85	5	2,2',3,4,4'-	336.46	197	8	2,2',3,3',4,4',6,6'-	439.81
87	5	2,2',3,4,5'-P	336.46	199	8	2,2',3,3',4,5,5',6'	439.81
90	5	2,2',3,4',5	336.46	200	8	2,2',3,3',4,5,6,6'-	439.81
91	5	2,2',3,4',6	336.46	201	8	2,2',3,3',4,5',6,6'-	439.81
92	5	2,2',3,5,5'	336.46	202	8	2,2',3,3',5,5',6,6'-	439.81
93	5	2,2',3,5,6	336.46	205	8	2,3,3',4,4',5,5',6-	439.81
95	5	2,2',3,5',6	336.46	206	9	2,2',3,3',4,4',5,5',6	474.26
97	5	2,2',3,4',5'	336.46	207	9	2,2',3,3',4,4',5,6,6'	474.26
99	5	2,2',4,4',5-	336.46	208	9	2,2',3,3',4,5,5',6,6'-	474.26
100	5	2,2',4,4',6	336.46	209	10	2,2',3,3',4,4',5,5',6,6'-	508.71
101	5	2,2',4,5,5'-	336.46				

Table B3.3 (Cont.): Summary of oxidation reduction potential (ORP) and sulfide measurement in metropolitan Chicago sediment cores.

Core	Depth (cm)	ORP (mV)	Depth (cm)	Sulfide (ppm)
CBC	0.0	-59.5	1.3	17.9
	0.6	-58.8	2.5	105.0
	1.3	-59.6	5.1	125.0
	1.9	-61.1	7.6	318.0
	2.5	-61.4	10.2	250.0
	3.2	-62.7	12.7	240.0
	3.8	-61.9	15.2	187.0
	4.4	-62.8	17.8	115.0
	5.1	-73.0	20.3	113.0
	5.7	-72.2	22.9	97.0
	6.4	-97.2	25.4	64.9
	7.0	-84.0	34.3	87.0
	7.6	-84.8	43.2	88.0
	8.3	-84.9		
	8.9	-86.0		
	9.5	-90.8		
	10.2	-90.1		
	12.7	-107.6		
	15.2	-146.4		
	17.8	-146.1		
	20.3	-159.9		
	22.9	-158.8		
	25.4	-158.0		
	27.9	-159.1		
	30.5	-147.9		
	31.8	-145.5		
	Average	-99.2		139.1
	Standard deviation	38.7		85.0
CWP	0.0	-77.8	0.0	49.5
	0.5	-78.1	0.5	59.7
	1.0	-79.6	1.0	63.8
	1.5	-84.4	2.0	98.0
	2.0	-88.2	3.0	114.0
	3.0	-104.0	4.0	104.0
	5.0	-99.2	6.0	98.6
	6.0	-106.4	8.0	90.8
	7.0	-108.9	10.0	89.1

Table B3.3 (Cont.): Summary of oxidation reduction potential (ORP) and sulfide measurement in metropolitan Chicago sediment cores.

Core	Depth (cm)	ORP (mV)	Depth (cm)	Sulfide (ppm)
	8.0	-113.5	15.0	97.3
	9.0	-117.8	20.0	96.7
	10.0	-120.3	25.0	93.4
	12.0	-120.6	30.0	86.2
	14.0	-123.4	35.0	85.2
	16.0	-126.0	45.0	87.3
	18.0	-129.4		
	20.0	-130.9		
	25.0	-133.6		
	30.0	-140.6		
	35.0	-143.7		
	38.0	-142.4		
	Average	-112.8		87.6
	Standard deviation	21.6		17.4
	0.5	-64.3	0.5	4.1
	1.5	-61.2	1.5	56.0
	2.5	-77.4	2.5	115.0
	3.5	-60.3	3.5	97.5
	4.5	-70.8	4.5	161.0
	5.5	-40.4	5.5	91.9
	6.5	-61.2	6.5	93.2
	7.5	-66.8	7.5	123.0
	8.5	-63.7	8.5	87.2
	9.5	-75.5	9.5	144.0
	11.0	-87.3	11.0	92.1
	13.0	-60.8	13.0	111.0
	15.0	-95.4	15.0	214.0
	17.0	-80.3	17.0	176.0
	19.0	-128.9	19.0	282.0
	21.0	-90.5	21.0	98.1
	23.0	-135.6	23.0	114.0
	25.0	-252.3	25.0	193.0
	27.0	-155.6	27.0	526.0
	29.0	-149.3	29.0	193.0
	31.0	-153.0	31.0	106.0
CLC	33.0	-145.8	33.0	86.7
	Average	-98.9		143.9
	Standard deviation	49.6		103.9
IGC09	NA	NA	1.0	17.4

Table B3.3 (Cont.): Summary of oxidation reduction potential (ORP) and sulfide measurement in metropolitan Chicago sediment cores.

Core	Depth (cm)	ORP (mV)	Depth (cm)	Sulfide (ppm)
			3.0	16.5
			5.0	14.3
			7.0	19.1
			9.0	17.5
			11.0	13.5
			13.0	19.5
			15.0	24.5
			17.0	21.6
			19.0	19.8
			22.5	19.3
			27.5	18.4
			32.5	16.4
			37.5	17.4
			42.5	19.3
			47.5	21.9
			52.5	23.4
			57.5	24.8
	Average			19.1
	Standard deviation			3.2
			1.0	28.4
			3.0	24.8
			5.0	39.2
			7.0	21.9
			9.0	36.5
			11.0	27.0
			13.0	34.3
			15.0	25.9
			17.0	28.4
			19.0	21.9
			22.5	23.2
			27.5	26.7
			32.5	27.3
			37.5	28.4
			42.5	26.9
			47.5	25.4
			52.5	26.3
IGC13	NA	NA	57.5	27.4
	Average			27.8
	Standard deviation			4.6

Table B3.4 (Cont.): Summary of physical characterization results in the metropolitan Chicago cores.

Site	Avg Depth (cm)	Wet Bulk Density (g/mL)	Dry Bulk Density (g/mL)	Particle Density (g/mL)	AverageOC (mg/g)	SC (mg/g)	NonSC (mg/g)	OM(mg/g)	Avg% Moisture	Average % solid	Porosity
CBC	0.5	1.56	0.93	2.58	25.46	21.77	3.69	40.26	40.55	59.45	63.98
CBC	1.5	1.38	1.01	2.58	24.80	20.20	4.60	37.94	27.32	72.68	61.00
CBC	2.5	1.04	0.75	2.56	28.53	20.43	8.10	49.71	27.51	72.49	70.55
CBC	3.5	1.51	1.33	2.58	22.86	19.68	3.18	35.48	11.96	88.04	48.55
CBC	5.0	0.72	0.63	2.57	31.95	21.54	10.41	46.69	12.75	87.25	75.42
CBC	7.0	1.54	1.35	2.57	26.40	13.03	13.37	41.66	11.95	88.05	47.43
CBC	9.0	1.57	1.07	2.57	31.08	16.21	14.87	46.53	32.36	67.64	58.48
CBC	12.5	2.55	1.36	2.37	122.34	12.76	109.59	166.32	46.83	53.17	42.77
CBC	17.5	1.26	0.95	2.56	32.67	18.92	13.75	49.25	24.94	75.06	63.00
CBC	22.5	1.20	0.97	2.53	40.07	14.38	25.69	66.43	19.13	80.87	61.55
CBC	27.5	1.56	1.34	2.56	31.52	17.49	14.04	49.70	14.16	85.84	47.80
CBC	32.5	1.39	1.22	2.58	20.98	19.49	1.49	39.87	11.89	88.11	52.55
CWP	0.25	1.05	0.17	2.36	99.23	40.99	58.23	175.74	84.32	15.68	92.98
CWP	0.75	1.11	0.20	2.39	93.66	34.36	59.30	155.83	81.89	18.11	91.56
CWP	1.50	1.18	0.23	2.41	89.10	40.10	49.00	141.50	80.78	19.22	90.55
CWP	2.50	1.23	0.28	2.45	82.93	39.33	43.60	114.04	77.49	22.51	88.69
CWP	3.50	1.31	0.33	2.43	72.58	35.81	36.76	129.74	75.20	24.80	86.57
CWP	5.00	1.38	0.40	2.45	70.64	37.51	33.12	115.29	70.63	29.37	83.50
CWP	7.00	1.47	0.43	2.47	65.34	37.29	28.05	101.92	70.71	29.29	82.57
CWP	9.00	1.56	0.44	2.45	65.05	36.21	28.85	115.57	71.69	28.31	81.93
CWP	12.50	1.63	0.46	2.47	68.11	36.84	31.28	100.85	72.05	27.95	81.57
CWP	17.50	1.68	0.58	2.48	60.84	39.34	21.50	96.93	65.80	34.20	76.76
CWP	22.50	1.73	0.71	2.48	61.14	38.37	22.76	98.15	59.27	40.73	71.50
CWP	27.50	1.65	0.67	2.48	61.91	41.34	20.57	95.68	59.61	40.39	73.13
CLC	0.5	1.46	0.79	2.47	65.77	44.59	21.18	103.56	45.71	54.29	67.80
CLC	1.5	1.55	0.86	2.47	62.67	37.00	25.68	103.32	44.72	55.28	65.30
CLC	2.5	1.50	0.86	2.50	60.31	37.43	22.88	86.31	42.70	57.30	65.68
CLC	3.5	1.49	0.87	2.48	64.10	36.61	27.50	95.10	41.72	58.28	65.03
CLC	4.5	1.47	0.87	2.48	61.59	33.34	28.25	93.99	40.86	59.14	64.90
CLC	5.5	1.51	0.89	2.49	60.91	35.84	25.06	90.77	41.07	58.93	64.27
CLC	6.5	1.53	0.89	2.49	61.63	35.58	26.05	88.71	41.67	58.33	64.30
CLC	7.5	1.54	0.90	2.49	61.58	35.88	25.70	89.76	41.68	58.32	63.89
CLC	8.5	1.54	0.91	2.49	61.20	32.48	28.72	91.87	41.18	58.82	63.61
CLC	9.5	1.47	0.91	2.49	61.10	35.00	26.10	90.91	38.15	61.85	63.53
CLC	11	1.60	0.96	2.49	61.76	35.52	26.25	89.81	39.94	60.06	61.46
CLC	13	1.57	0.97	2.49	61.34	35.20	26.13	91.80	38.45	61.55	61.04
CLC	15	1.57	0.96	2.50	61.38	34.77	26.61	86.04	38.43	61.57	61.41
CLC	17	1.50	0.91	2.49	61.33	33.74	27.58	92.93	39.41	60.59	63.36
CLC	19	1.53	0.92	2.48	60.24	34.18	26.06	95.14	40.08	59.92	63.06
CLC	21	1.51	0.90	2.48	59.40	30.50	28.90	96.76	40.34	59.66	63.57
CLC	23	1.53	0.91	2.49	59.41	33.69	25.73	92.83	40.81	59.19	63.58
CLC	25	1.53	0.89	2.50	59.43	32.93	26.51	86.16	41.64	58.36	64.24
CLC	27	1.56	0.90	2.50	58.85	33.36	25.49	83.17	42.49	57.51	64.19

Table B3.4 (Cont.): Summary of physical characterization results in the metropolitan Chicago cores.

Site	Avg Depth (cm)	Wet Bulk Density (g/mL)	Dry Bulk Density (g/mL)	Particle Density (g/mL)	AverageOC (mg/g)	SC (mg/g)	NonSC (mg/g)	OM(mg/g)	Avg% Moisture	Average % solid	Porosity
CLC	29	1.54	0.90	2.48	58.46	33.77	24.70	99.41	41.48	58.52	63.57
CLC	31	1.53	0.90	2.47	54.91	31.91	23.00	100.76	40.76	59.24	63.45
IGC09	1	1.08	0.11	2.26	142.07	16.43	125.64	244.65	89.56	10.44	95.01
IGC09	3	1.14	0.27	2.32	123.53	12.14	111.39	202.53	75.07	24.93	88.15
IGC09	5	1.21	0.36	2.35	113.07	11.14	101.94	181.45	70.51	29.49	84.86
IGC09	7	1.13	0.33	2.34	110.45	10.18	100.27	186.95	70.90	29.10	85.98
IGC09	9	1.15	0.33	2.33	113.58	10.58	102.99	194.61	71.33	28.67	85.82
IGC09	11	1.15	0.28	2.33	122.83	10.27	112.56	196.35	73.14	26.86	87.78
IGC09	13	1.18	0.30	2.35	114.72	14.23	100.49	183.27	74.26	25.74	87.08
IGC09	15	1.14	0.24	2.33	115.21	16.44	98.77	192.11	78.44	21.56	89.50
IGC09	17	1.10	0.21	2.32	117.31	16.68	100.63	198.87	81.16	18.84	91.07
IGC09	19	1.14	0.23	2.33	117.86	17.17	100.69	193.34	79.40	20.60	89.94
IGC09	22.5	1.11	0.23	2.28	126.88	12.77	114.11	225.57	79.06	20.94	89.80
IGC09	27.5	1.12	0.24	2.21	158.68	11.72	146.96	282.73	78.63	21.37	89.19
IGC09	32.5	1.12	0.53	2.21	163.22	11.70	151.51	278.24	52.89	47.11	76.12
IGC09	37.5	1.21	0.52	2.29	129.87	13.20	116.67	221.72	54.93	45.07	77.49
IGC09	42.5	1.17	0.33	2.36	108.26	9.29	98.97	171.94	72.13	27.87	86.18
IGC09	47.5	1.16	0.12	2.31	126.44	13.69	112.75	206.62	89.56	10.44	94.76
IGC09	52.5	1.14	0.18	2.34	115.44	9.15	106.29	189.76	84.25	15.75	92.31
IGC09	57.5	1.17	0.35	2.34	112.65	9.20	103.45	185.01	69.79	30.21	84.93
IGC09	62.5	2.30	0.30	2.33	116.19	9.52	106.67	190.54	74.38	25.62	87.17
IGC09	67.5	2.32	0.31	2.36	107.00	9.71	97.29	174.07	73.80	26.20	86.74
IGC13	1	1.06	0.14	2.27	140.01	20.16	119.85	233.84	93.35	6.65	93.79
IGC13	3	1.09	0.17	2.22	155.58	22.70	132.89	275.22	84.37	15.63	92.33
IGC13	5	1.08	0.16	2.20	160.49	22.81	137.67	288.71	85.60	14.40	92.95
IGC13	7	1.10	0.20	2.24	155.03	20.48	134.55	255.55	81.61	18.39	90.97
IGC13	9	1.13	0.28	2.35	103.74	21.75	81.99	178.62	75.21	24.79	88.13
IGC13	11	1.13	0.29	2.37	100.60	20.85	79.75	167.04	74.58	25.42	87.83
IGC13	13	1.15	0.29	2.30	125.33	22.62	102.71	211.76	74.30	25.70	87.20
IGC13	15	1.15	0.32	2.28	131.45	20.79	110.66	227.87	72.50	27.50	86.13
IGC13	17	1.18	0.35	2.32	114.91	22.69	92.21	202.06	69.99	30.01	84.73
IGC13	19	1.00	0.30	2.31	124.72	26.68	98.03	208.93	69.68	30.32	86.80
IGC13	22.5	1.17	0.37	2.35	110.19	28.53	81.67	179.60	68.61	31.39	84.35
IGC13	27.5	1.11	0.42	2.27	137.01	33.59	103.42	236.89	67.43	32.57	81.67
IGC13	32.5	1.33	0.68	2.33	120.29	22.49	97.79	194.28	48.75	51.25	70.68
IGC13	37.5	1.39	0.66	2.33	118.64	12.07	106.57	196.89	49.77	50.23	71.45
IGC13	42.5	1.08	0.46	2.30	126.22	15.77	110.45	211.79	57.15	42.85	79.90
IGC13	47.5	1.10	0.27	2.25	155.42	10.13	145.29	252.25	75.07	24.93	87.80
IGC13	52.5	1.10	0.20	2.27	146.51	22.16	124.35	232.75	81.92	18.08	91.28
IGC13	57.5	1.24	0.37	2.43	74.59	24.38	50.21	125.35	70.36	29.64	84.96

Table B3.5: Estimated whole core net sedimentation rate using constant initial rate (CIC) and constant rate of sedimentation (CRS).

Cores	Net sedimentation rate (g/cm ² /yr)	
	CIC	CRS
CBC	1.53	2.26
CWP	0.07	0.08
CLC	0.11	0.30
IGC09	0.06	0.27
IGC13	0.17	0.13

Table B3.6: Selected recent reports of PBDE and PCB concentrations in outfall discharges.

Contaminant	Discharge Type	Location	Analyzed Congeners	Concentration Range (ng/L)
PBDEs	WWTP Effluent	Zandvliet, Cape Town, South Africa ⁷⁹	8	16-1240
		Australia ⁸⁰	37	0.1-0.5
		Columbia River Basin, Oregon ⁶⁴	9	0.4-6
		Palo Alto, CA ⁶³	41	29000
		Columbia River Basin, Oregon ⁶⁴	9	BDL-53
PCBs	WWTP Effluent	Columbia River Basin, Oregon ⁶⁴	18	BDL-0.07
	CSO	Columbia River Basin, Oregon ⁶⁴	18	BDL-440
		New York/New Jersey ⁸¹	71	10 to 60
	Stormwater runoff	Switzerland ⁶⁵	12	BDL-403

WWTP= Wastewater treatment plant, CSO=Combined sewage outfall, BDL= Below detection limit.

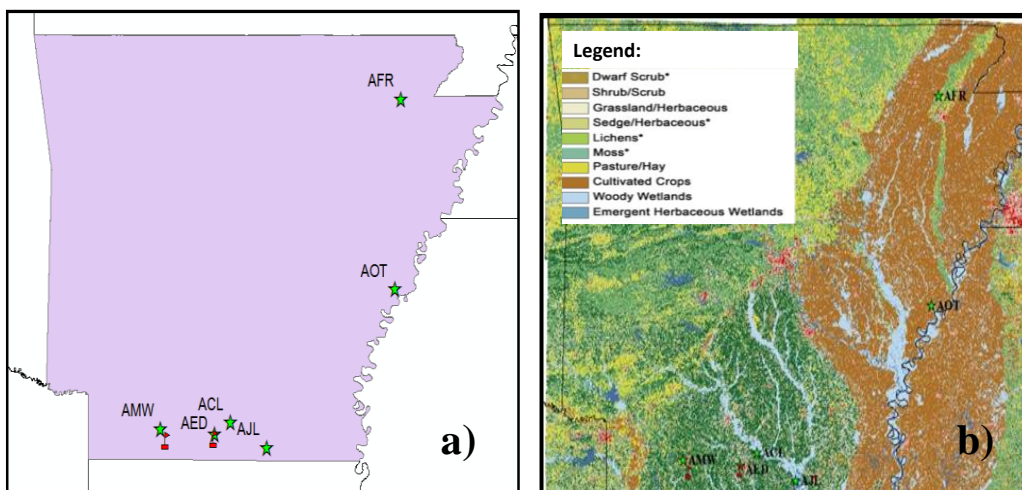


Figure B3.1: Location of AR sampling sites as reported in a previous study by Wei et al.(2012){Wei, 2012 #291}showing a) general location and b) land categorized by the United States Geological Services 2006 National Land Cover Database for the AR area. AR is less developed compared to Chicago.

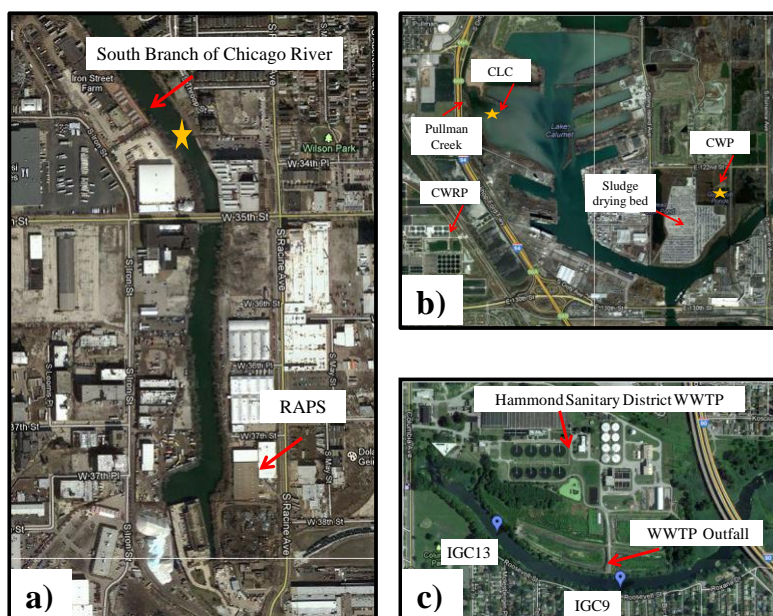


Figure B3.2: Detailed maps of sampling locations at a) CBC, b) CLC, and CWP, and c) IGC09 and IGC13. Golden stars marked approximate locations where sediment cores were collected.

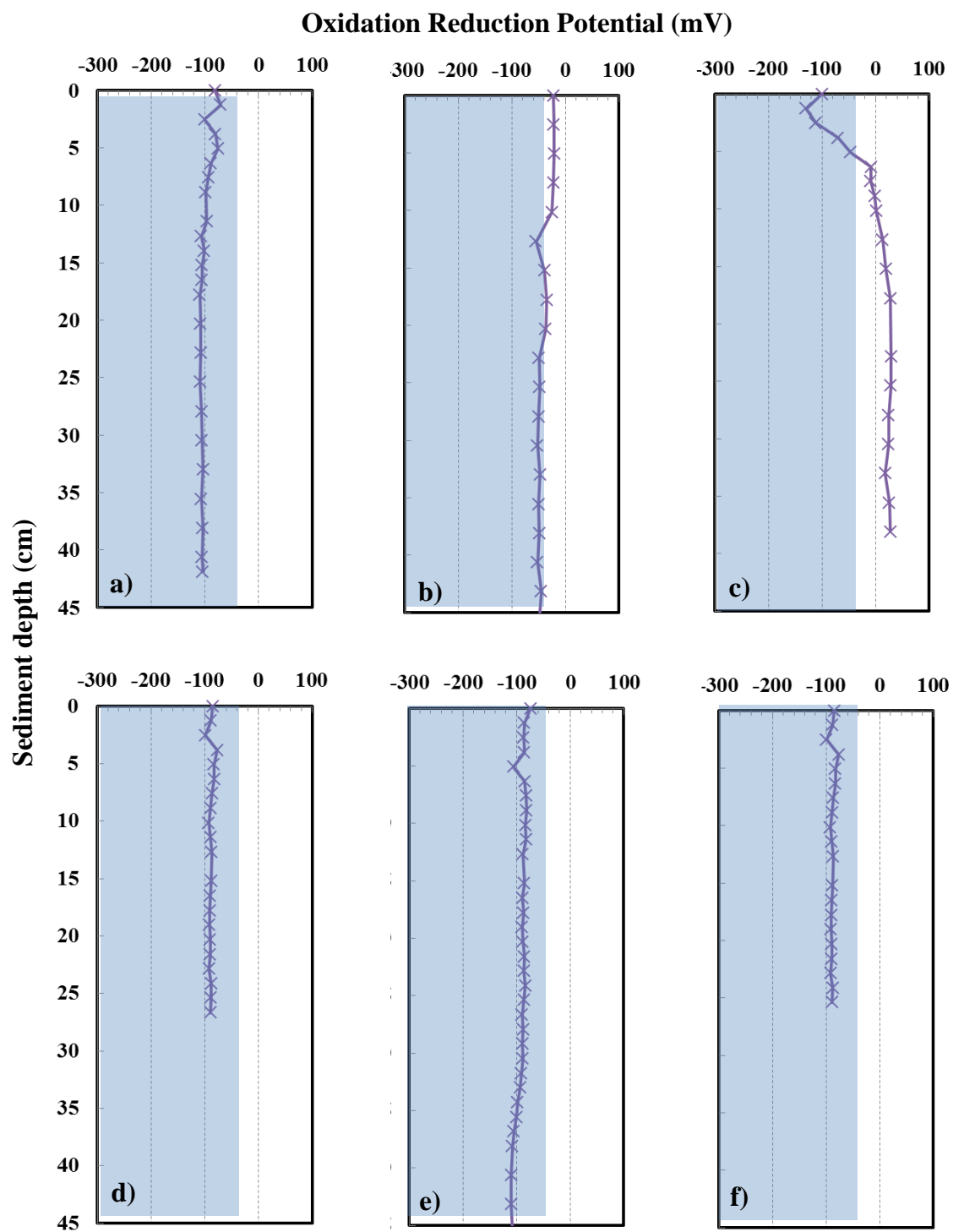


Figure B3.3: Oxidation reduction potential (ORP) measurement in a) AED, b) AMW, c) ACL, d) AJL, e) AOT, and f) AFR. Shaded areas represent anaerobic region.

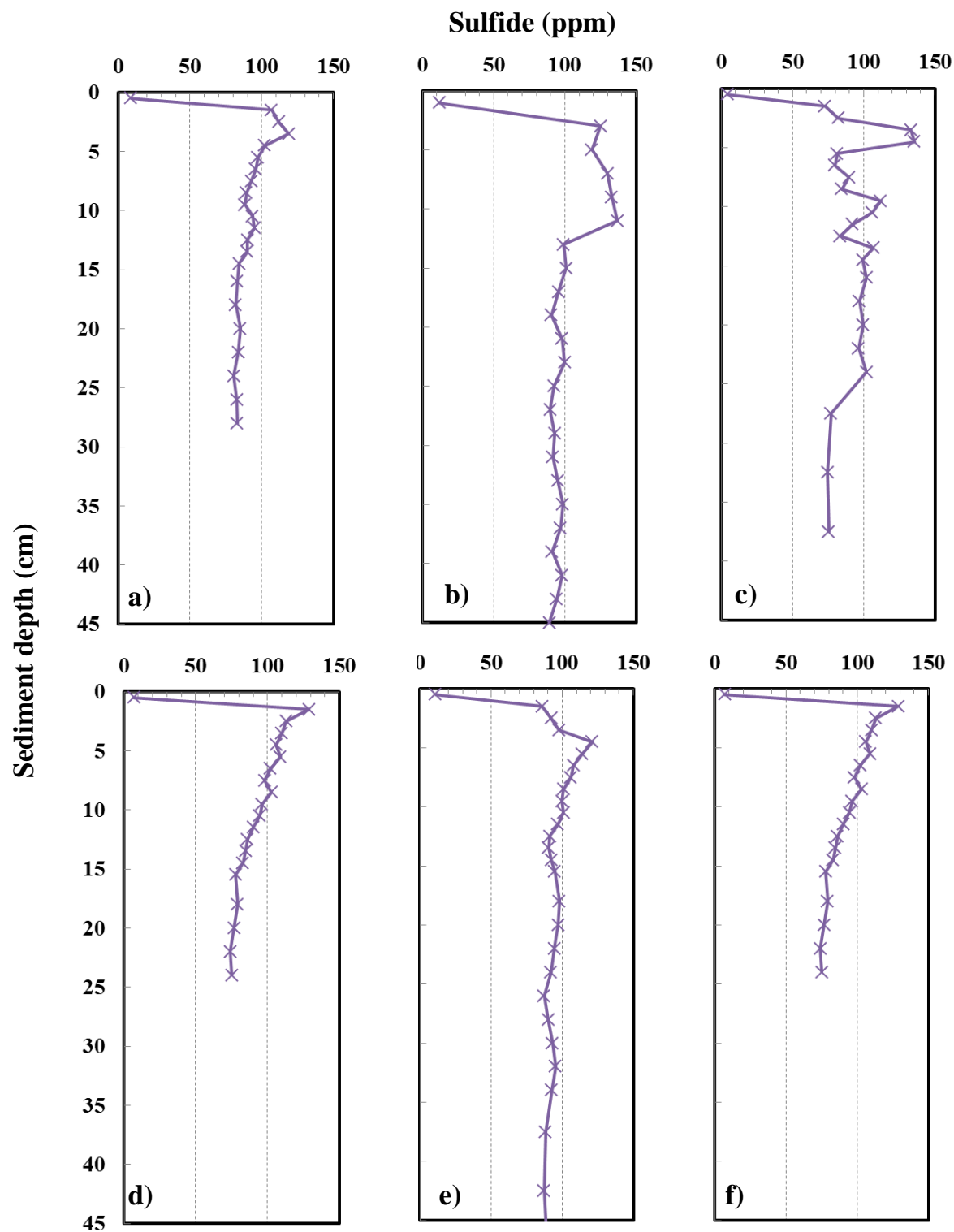


Figure B3.4: Sulfide measurement in a) AED, b) AMW, c) ACL, d) AJL, e) AOT, and f) AFR.

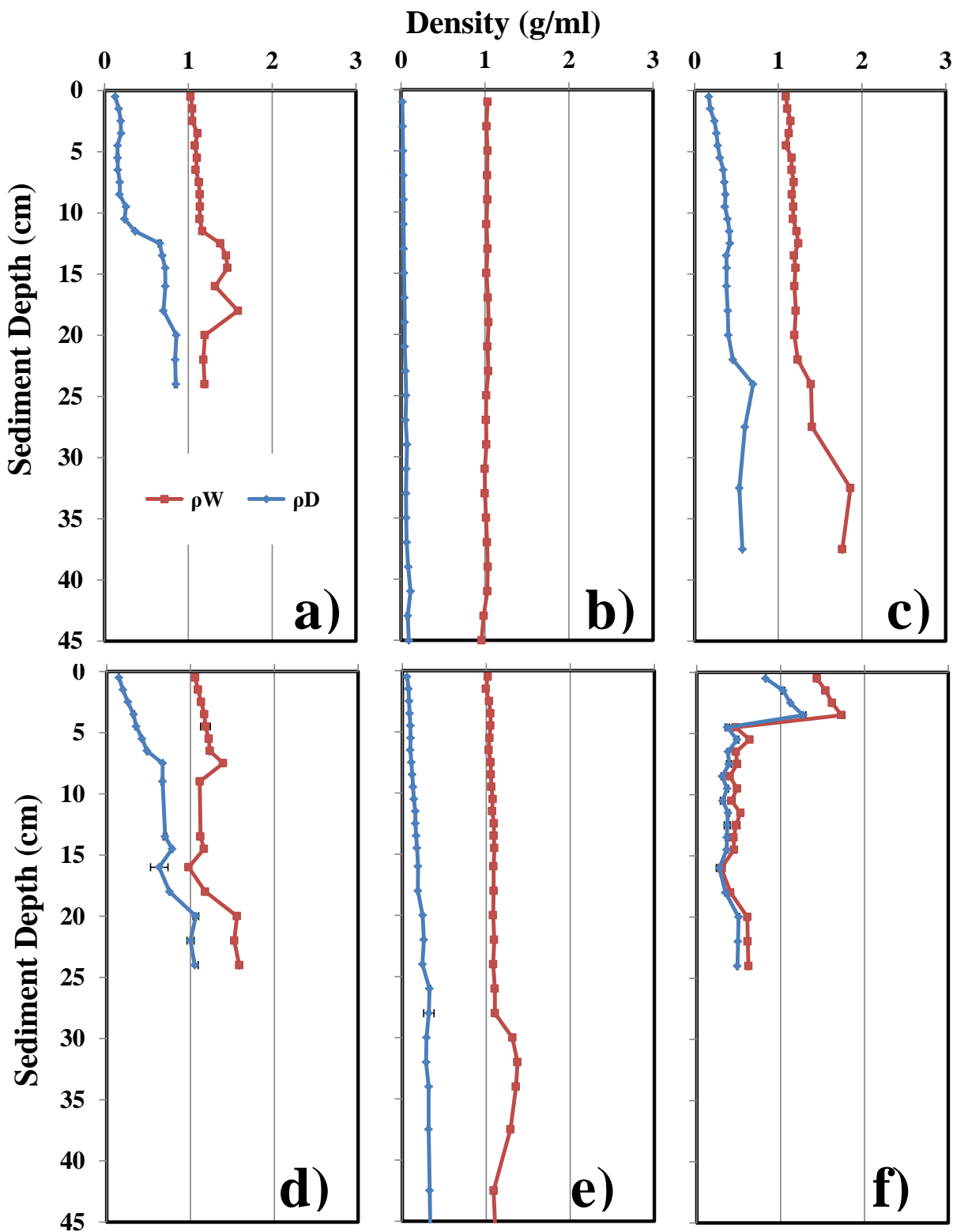


Figure B3.5: Wet and dry densities (ρ_W and ρ_D , respectively) in cores a) AED, b) AMW, c) ACL, d) AJL, e) AOT, and f) AFR. Error bars represent the standard deviation of triplicate measurements. These were typically smaller than the data symbol.

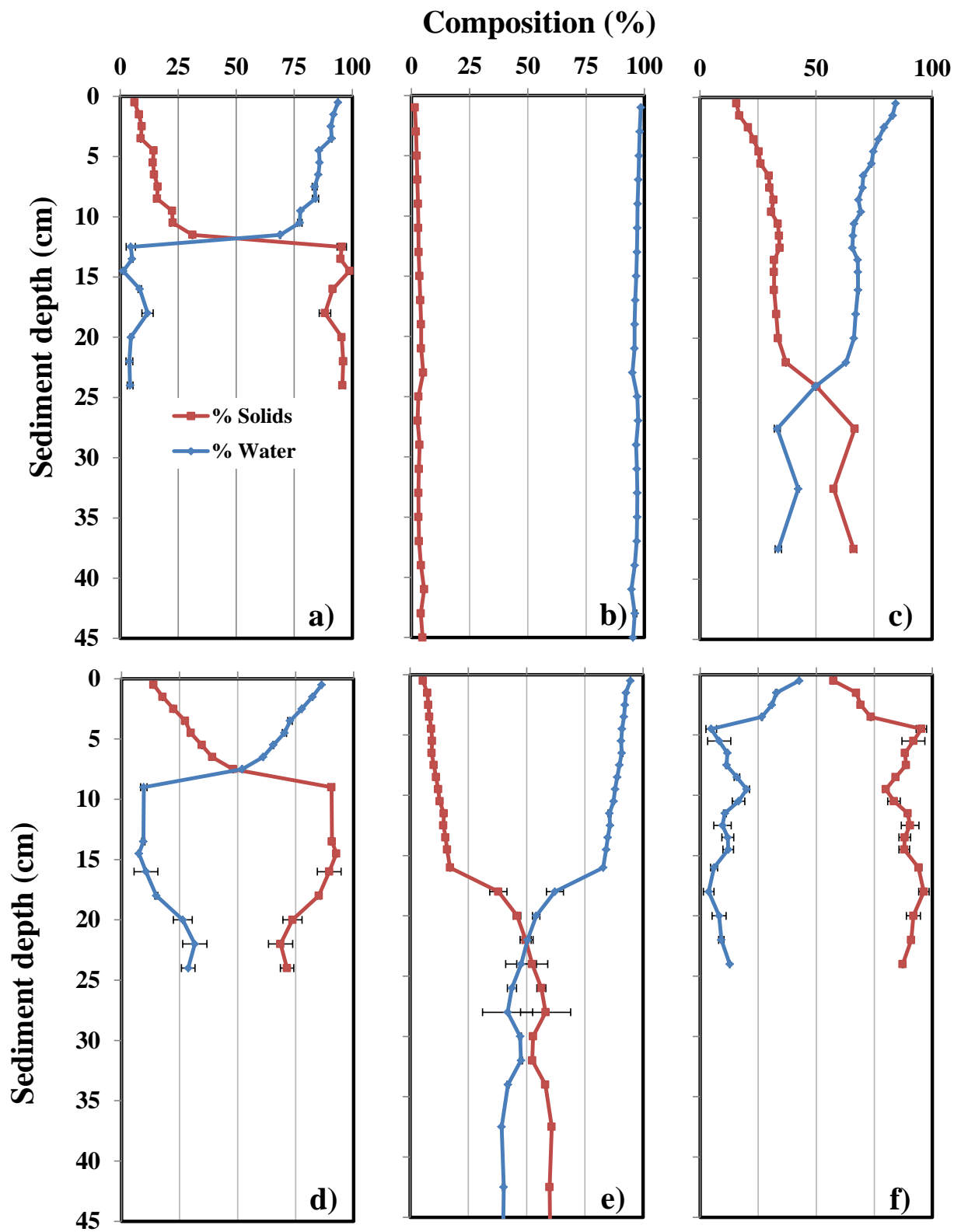


Figure B3.6: Solids and water compositions in cores a) AED, b) AMW, c) ACL, d) AJL, e) AOT, and f) AFR.

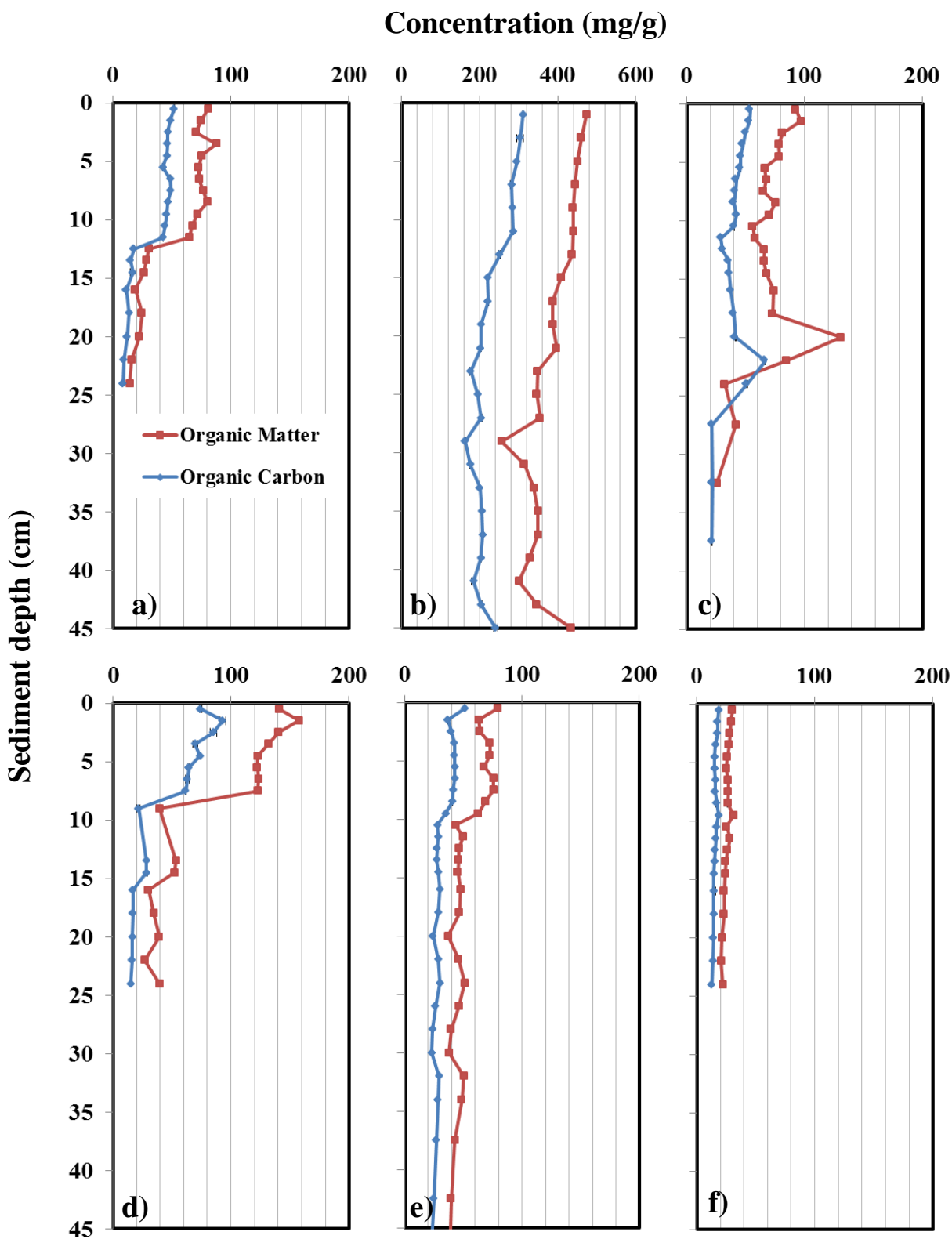


Figure B3.7: Carbon and organic matter concentrations in a) AED, b) AMW, c) ACL, d) AJL, e) AOT, and f) AFR. Note the different x-axis on panel b.

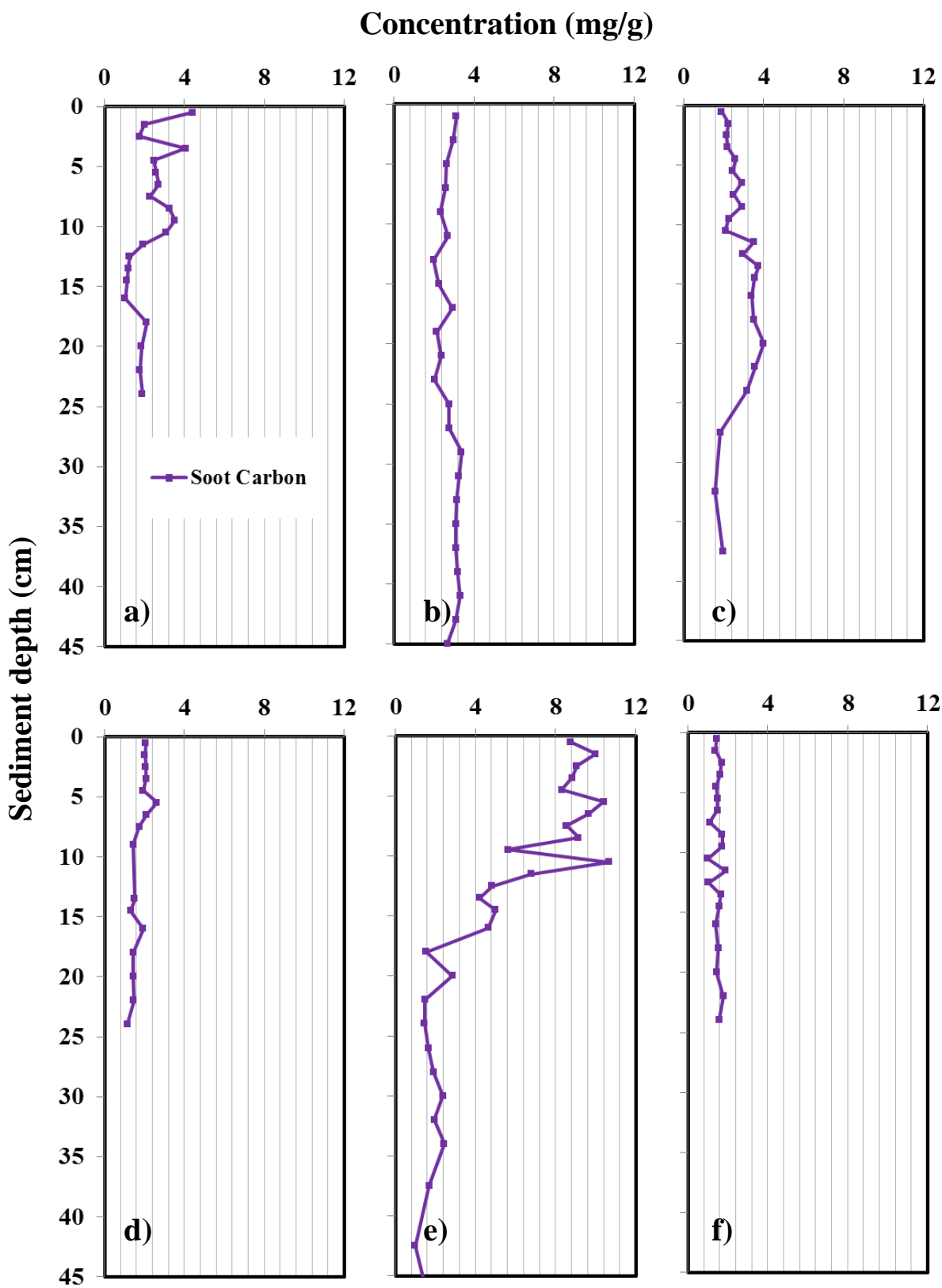


Figure B3.8: Black carbon concentration in a) AED, b) AMW, c) ACL, d) AJL, e) AOT, and f) AFR.

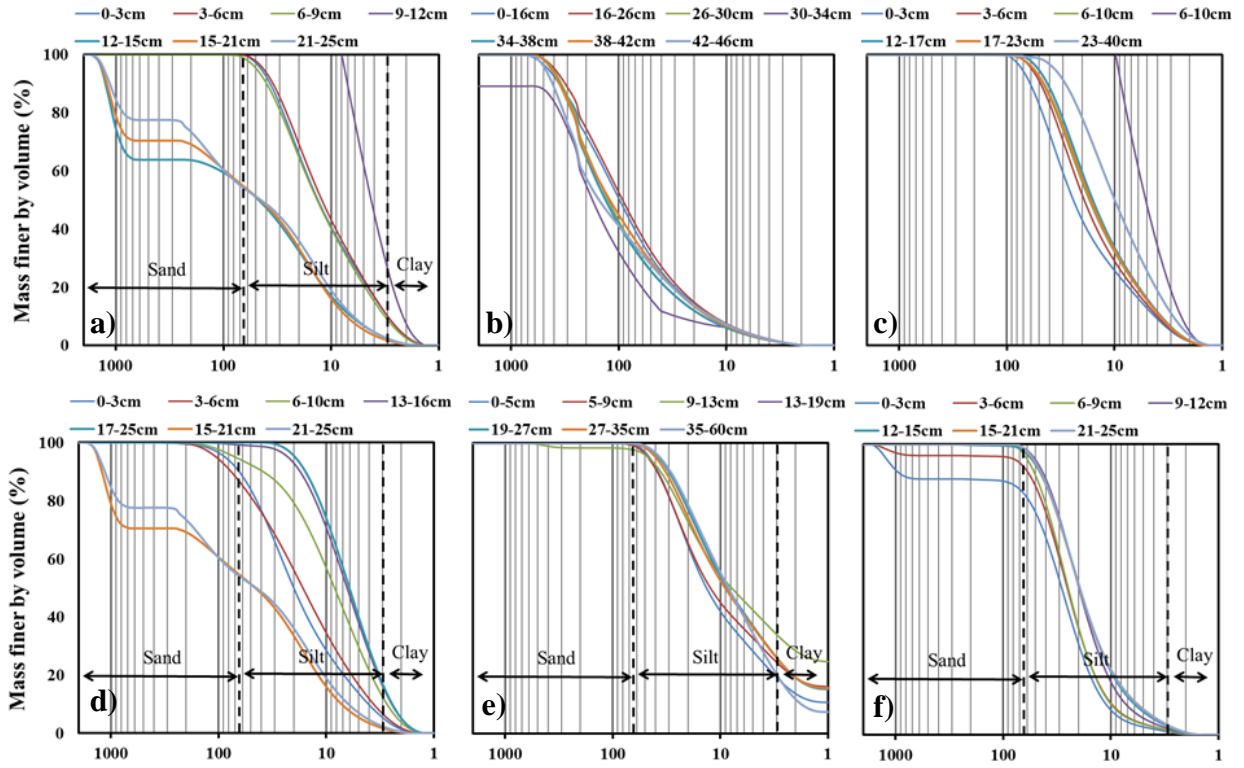


Figure B3.9: Particle size distribution in a) AED, b) AMW, c) ACL, d) AJL, e) AOT, and f) AFR.

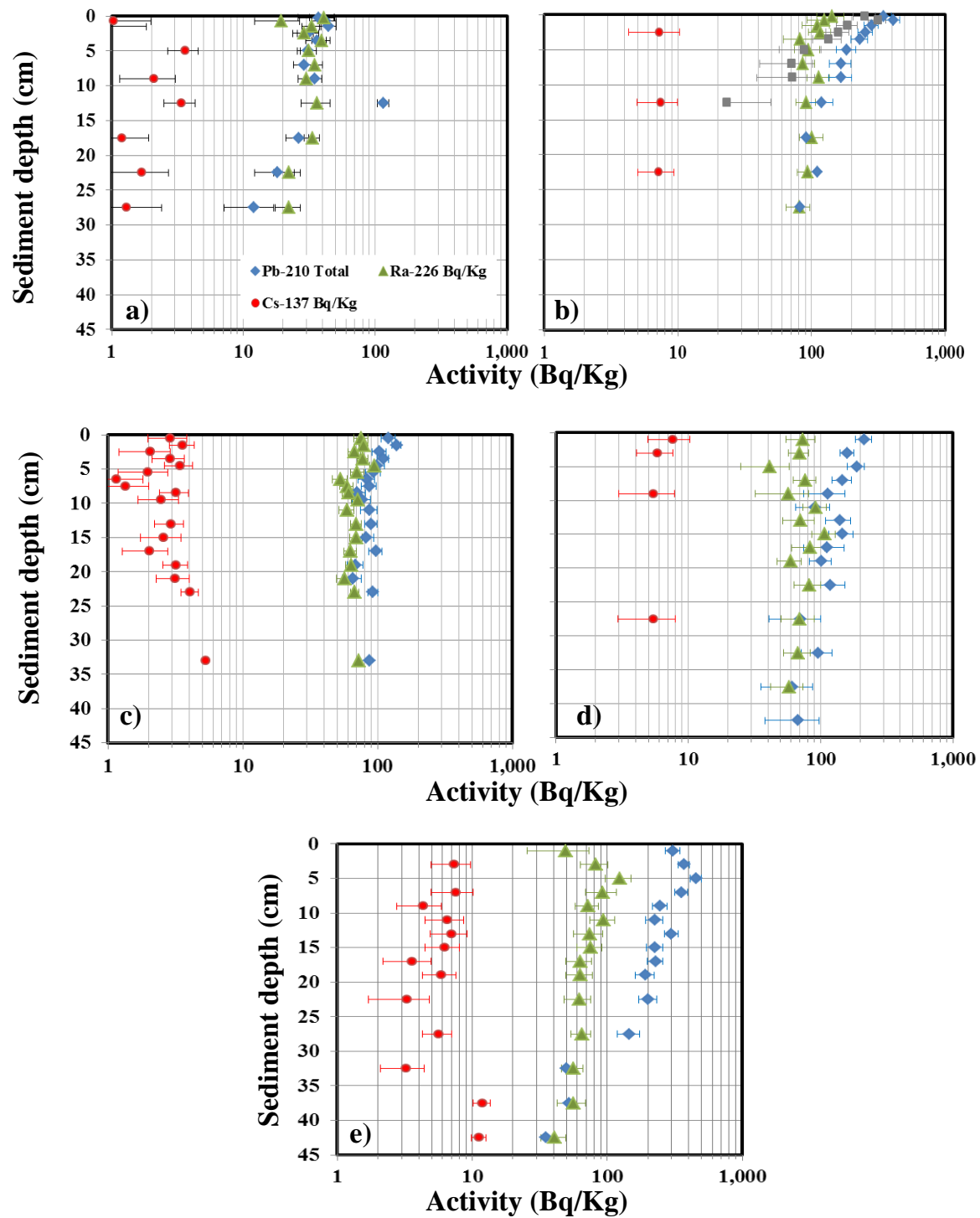


Figure B3.10: ^{210}Pb , ^{226}Ra , and ^{137}Cs activities in cores a) CBC, b) CWP, c) CLC, d) IGC09, and e) IGC13.

Appendix C

Table C4.1. Number of sequences and abundance of microbial community phylum in surface sediments. Abundance is shown in parentheses.

Name	IGC13	IGC09	CWP	CLC	CBC	AOT	AMW	AJL	AFR	AED	ACL
<i>Proteobacteria</i>	513 (22.02%)	567 (18.21%)	925 (31.59%)	776 (21.38%)	482 (21.29%)	927 (21.24%)	1099 (39.33%)	822 (24.10%)	446 (16.57%)	579 (13.87%)	2016 (33.29%)
<i>Unclassified Bacteria</i>	1210 (51.93%)	1961 (62.99%)	1331 (45.46%)	2030 (55.92%)	1163 (51.37%)	2326 (53.29%)	1067 (38.19%)	1796 (52.65%)	1640 (60.92%)	3065 (73.45%)	3628 (59.91%)
<i>Cyanobacteria</i>	2 (0.09%)	0 (0%)	4 (0.14%)	0 (0%)	44 (1.94%)	167 (3.83%)	30 (1.07%)	7 (0.21%)	34 (1.26%)	1 (0.02%)	1 (0.02%)
<i>Verrucomicrobia</i>	13 (0.56%)	4 (0.13%)	103 (3.52%)	19 (0.52%)	11 (0.49%)	27 (0.62%)	39 (1.40%)	27 (0.79%)	111 (4.12%)	13 (0.31%)	8 (0.13%)
<i>Firmicutes</i>	153 (6.57%)	133 (4.27%)	66 (2.25%)	52 (1.43%)	93 (4.11%)	245 (5.61%)	77 (2.76%)	364 (10.67%)	55 (2.04%)	116 (2.78%)	87 (1.44%)
<i>Planctomycetes</i>	8 (0.34%)	12 (0.39%)	7 (0.24%)	6 (0.17%)	18 (0.80%)	55 (1.26%)	39 (1.40%)	2 (0.06%)	25 (0.93%)	28 (0.67%)	0 (0%)
<i>Bacteroidetes</i>	315 (13.52%)	351 (11.28%)	391 (13.35%)	654 (18.02%)	301 (13.30%)	370 (8.48%)	293 (10.49%)	153 (4.49%)	53 (1.97%)	84 (2.01%)	133 (2.20%)
<i>Chlamydiae</i>	5 (0.21%)	1 (0.03%)	0 (0%)	0 (0%)	4 (0.18%)	1 (0.02%)	10 (0.36%)	0 (0%)	1 (0.04%)	0 (0%)	0 (0%)
<i>Chloroflexi</i>	4 (0.17%)	0 (0%)	0 (0%)	0 (0%)	5 (0.22%)	0 (0%)	1 (0.04%)	10 (0.29%)	5 (0.19%)	14 (0.34%)	4 (0.07%)
<i>Actinobacteria</i>	54 (2.32%)	24 (0.77%)	27 (0.92%)	19 (0.52%)	34 (1.50%)	92 (2.11%)	47 (1.68%)	21 (0.62%)	58 (2.15%)	24 (0.58%)	31 (0.51%)
<i>Tenericutes</i>	6 (0.26%)	21 (0.67%)	5 (0.17%)	7 (0.19%)	7 (0.31%)	4 (0.09%)	2 (0.07%)	7 (0.21%)	0 (0%)	0 (0%)	0 (0%)
<i>Spirochaetes</i>	27 (1.16%)	24 (0.77%)	0 (0%)	1 (0.03%)	31 (1.37%)	30 (0.69%)	18 (0.64%)	2 (0.06%)	18 (0.67%)	9 (0.22%)	0 (0%)

Table C4.1. Number of sequences and abundance of microbial community phylum in surface sediments. Abundance is shown in parentheses.

Name	IGC13	IGC09	CWP	CLC	CBC	AOT	AMW	AJL	AFR	AED	ACL
<i>Deinococcus-Thermus</i>	0 (0%)	0 (0%)	0 (0%)	0 (0%)	0 (0%)	1 (0.02%)	0 (0%)	0 (0%)	0 (0%)	0 (0%)	0 (0%)
<i>Thermotogae</i>	0 (0%)	0 (0%)	0 (0%)	0 (0%)	3 (0.13%)	6 (0.14%)	0 (0%)	0 (0%)	0 (0%)	0 (0%)	0 (0%)
<i>Nitrospirae</i>	6 (0.26%)	0 (0%)	67 (2.29%)	44 (1.21%)	21 (0.93%)	58 (1.33%)	26 (0.93%)	14 (0.41%)	121 (4.49%)	97 (2.32%)	11 (0.18%)
<i>Thermodesulfobacteria</i>	0 (0%)	0 (0%)	1 (0.03%)	4 (0.11%)	0 (0%)	1 (0.02%)	1 (0.04%)	0 (0%)	0 (0%)	3 (0.07%)	0 (0%)
<i>Aquificae</i>	0 (0%)	3 (0.10%)	1 (0.03%)	13 (0.36%)	30 (1.33%)	13 (0.30%)	24 (0.86%)	0 (0%)	28 (1.04%)	0 (0%)	0 (0%)
<i>Fusobacteria</i>	1 (0.04%)	3 (0.10%)	0 (0%)	0 (0%)	0 (0%)	0 (0%)	0 (0%)	0 (0%)	0 (0%)	0 (0%)	0 (0%)
<i>Synergistetes</i>	4 (0.17%)	3 (0.10%)	0 (0%)	0 (0%)	0 (0%)	0 (0%)	4 (0.14%)	0 (0%)	0 (0%)	0 (0%)	0 (0%)
<i>Chlorobi</i>	3 (0.13%)	3 (0.10%)	0 (0%)	0 (0%)	4 (0.18%)	13 (0.30%)	5 (0.18%)	1 (0.03%)	9 (0.33%)	0 (0%)	0 (0%)
<i>Gemmatimonadetes</i>	1 (0.04%)	0 (0%)	0 (0%)	0 (0%)	6 (0.27%)	17 (0.39%)	7 (0.25%)	2 (0.06%)	1 (0.04%)	30 (0.72%)	2 (0.03%)
<i>Fibrobacteres</i>	1 (0.04%)	0 (0%)	0 (0%)	0 (0%)	2 (0.09%)	5 (0.11%)	0 (0%)	0 (0%)	2 (0.07%)	2 (0.05%)	0 (0%)
<i>Acidobacteria</i>	4 (0.17%)	3 (0.10%)	0 (0%)	5 (0.14%)	5 (0.22%)	7 (0.16%)	5 (0.18%)	183 (5.36%)	85 (3.16%)	108 (2.59%)	135 (2.23%)

Table C4.2. Number of sequences and abundance of microbial community phylum in AMW sediment segments.
Abundance is shown in parantheses.

Name	2009	2005	2000	1995	1990	1985	1981	1974	1969	1965
Unclassified <i>Bacteria</i>	1067 (38.19%)	1214 (48.99%)	1182 (30.39%)	1301 (49.09%)	2085 (57.98%)	1597 (57.70%)	2050 (70.62%)	5746 (70.32%)	4470 (80.34%)	2142 (66.17%)
<i>Proteobacteria</i>	1099 (39.33%)	685 (27.64%)	1737 (44.66%)	790 (29.81%)	1139 (31.67%)	852 (30.78%)	507 (17.46%)	1587 (19.42%)	751 (13.50%)	517 (15.97%)
<i>Cyanobacteria</i>	30 (1.07%)	37 (1.49%)	9 (0.23%)	2 (0.08%)	2 (0.06%)	2 (0.07%)	19 (0.65%)	25 (0.31%)	0 (0%)	0 (0%)
<i>Actinobacteria</i>	47 (1.68%)	44 (1.78%)	36 (0.93%)	56 (2.11%)	40 (1.11%)	31 (1.12%)	15 (0.52%)	16 (0.20%)	12 (0.22%)	14 (0.43%)
<i>Verrucomicrobia</i>	39 (1.40%)	5 (0.20%)	5 (0.13%)	11 (0.42%)	58 (1.61%)	12 (0.43%)	0 (0%)	3 (0.04%)	0 (0%)	0 (0%)
<i>Chloroflexi</i>	1 (0.04%)	0 (0%)	7 (0.18%)	6 (0.23%)	2 (0.06%)	2 (0.07%)	5 (0.17%)	3 (0.04%)	3 (0.05%)	3 (0.09%)
<i>Planctomycetes</i>	39 (1.40%)	13 (0.52%)	10 (0.26%)	15 (0.57%)	2 (0.06%)	2 (0.07%)	2 (0.07%)	13 (0.16%)	0 (0%)	6 (0.19%)
<i>Firmicutes</i>	77 (2.76%)	144 (5.81%)	342 (8.79%)	121 (4.57%)	44 (1.22%)	62 (2.24%)	39 (1.34%)	144 (1.76%)	168 (3.02%)	433 (13.38%)
<i>Bacteroidetes</i>	293 (10.49%)	219 (8.84%)	363 (9.33%)	197 (7.43%)	169 (4.70%)	157 (5.67%)	147 (5.06%)	380 (4.65%)	98 (1.76%)	49 (1.51%)
<i>Tenericutes</i>	2 (0.07%)	3 (0.12%)	4 (0.10%)	13 (0.49%)	2 (0.06%)	0 (0%)	0 (0%)	16 (0.20%)	1 (0.02%)	0 (0%)
<i>Spirochaetes</i>	18 (0.64%)	51 (2.06%)	128 (3.29%)	98 (3.70%)	15 (0.42%)	28 (1.01%)	6 (0.21%)	47 (0.58%)	15 (0.27%)	36 (1.11%)
<i>Thermotogae</i>	0 (0%)	0 (0%)	0 (0%)	0 (0%)	0 (0%)	0 (0%)	0 (0%)	16 (0.20%)	1 (0.02%)	13 (0.40%)
<i>Synergistetes</i>	4 (0.14%)	0 (0%)	1 (0.03%)	1 (0.04%)	0 (0%)	1 (0.04%)	0 (0%)	0 (0%)	0 (0%)	0 (0%)

Table C4.2. Number of sequences and abundance of microbial community phylum in AMW sediment segments.
Abundance is shown in parantheses.

Name	2009	2005	2000	1995	1990	1985	1981	1974	1969	1965
<i>Aquificae</i>	24 (0.86%)	6 (0.24%)	2 (0.05%)	11 (0.42%)	1 (0.03%)	0 (0%)	2 (0.07%)	0 (0%)	0 (0%)	0 (0%)
<i>Chlamydiae</i>	10 (0.36%)	5 (0.20%)	0 (0%)	0 (0%)	0 (0%)	0 (0%)	0 (0%)	5 (0.06%)	0 (0%)	1 (0.03%)
<i>Chlorobi</i>	5 (0.18%)	8 (0.32%)	23 (0.59%)	8 (0.30%)	1 (0.03%)	6 (0.22%)	0 (0%)	19 (0.23%)	2 (0.04%)	22 (0.68%)
<i>Fusobacteria</i>	0 (0%)	3 (0.12%)	26 (0.67%)	0 (0%)	0 (0%)	0 (0%)	0 (0%)	0 (0%)	0 (0%)	0 (0%)
<i>Nitrospirae</i>	26 (0.93%)	22 (0.89%)	4 (0.10%)	7 (0.26%)	14 (0.39%)	7 (0.25%)	98 (3.38%)	134 (1.64%)	1 (0.02%)	0 (0%)
<i>Thermodesulfobacteria</i>	1 (0.04%)	0 (0%)	0 (0%)	0 (0%)	4 (0.11%)	0 (0%)	0 (0%)	0 (0%)	0 (0%)	0 (0%)
<i>Gemmatimonadetes</i>	7 (0.25%)	9 (0.36%)	7 (0.18%)	7 (0.26%)	11 (0.31%)	8 (0.29%)	1 (0.03%)	2 (0.02%)	19 (0.34%)	0 (0%)
<i>Fibrobacteres</i>	0 (0%)	1 (0.04%)	0 (0%)	0 (0%)	0 (0%)	0 (0%)	0 (0%)	0 (0%)	0 (0%)	0 (0%)
<i>Elusimicrobia</i>	0 (0%)	1 (0.04%)	0 (0%)	0 (0%)	0 (0%)	0 (0%)	0 (0%)	0 (0%)	0 (0%)	0 (0%)
<i>Dictyoglomi</i>	0 (0%)	0 (0%)	3 (0.08%)	0 (0%)	0 (0%)	0 (0%)	0 (0%)	0 (0%)	0 (0%)	0 (0%)
<i>Acidobacteria</i>	5 (0.18%)	8 (0.32%)	0 (0%)	6 (0.23%)	7 (0.19%)	1 (0.04%)	12 (0.41%)	15 (0.18%)	23 (0.41%)	1 (0.03%)

Appendix D

Table D5.1: Distribution of log K_{OW} values for PBDE and PCB homologs as predicted from Monte Carlo simulation.

Percentile	PBDE log K_{OW}									
	H1	H2	H3	H4	H5	H6	H7	H8	H9	H10
0.05	4.55	5.24	5.57	5.87	6.35	6.79	6.67	6.97	7.22	6.17
0.25	4.7	5.36	5.85	6.32	6.78	7.36	7.68	7.84	8.25	7.96
0.5	4.8	5.44	6.04	6.64	7.08	7.75	8.38	8.46	8.96	9.19
0.75	4.9	5.52	6.24	6.96	7.38	8.14	9.08	9.07	9.67	10.43
0.95	5.05	5.64	6.52	7.41	7.82	8.71	10.09	9.94	10.71	12.22

Percentile	PCB log K_{OW}									
	H1	H2	H3	H4	H5	H6	H7	H8	H9	H10
0.05	4.3	4.84	5.37	5.79	6.33	6.75	7.36	7.46	7.93	8.38
0.25	4.41	4.95	5.49	5.94	6.48	6.94	7.54	7.8	8.43	8.88
0.5	4.48	5.02	5.58	6.04	6.58	7.07	7.67	8.04	8.78	9.23
0.75	4.55	5.09	5.67	6.14	6.68	7.2	7.8	8.28	9.13	9.58
0.95	4.66	5.2	5.79	6.29	6.83	7.38	7.98	8.61	9.64	10.08

Table D5.2: Distribution of log K_{oc} values for PBDE and PCB homologs as predicted from Monte Carlo simulation.

Percentile	PBDE log K_{oc}									
	H1	H2	H3	H4	H5	H6	H7	H8	H9	H10
0.05	0.27	0.29	0.3	0.3	0.31	0.32	0.32	0.33	0.33	0.31
0.25	2.83	3.2	3.47	3.74	3.99	4.31	4.49	4.58	4.8	4.65
0.5	5.22	5.83	6.41	6.99	7.41	8.05	8.65	8.73	9.22	9.44
0.75	7.66	8.5	9.47	10.45	11.04	12.07	13.34	13.33	14.15	15.18
0.95	10.97	12.12	13.82	15.55	16.36	18.08	20.77	20.48	21.96	24.9

Percentile	PCB log K_{oc}									
	H1	H2	H3	H4	H5	H6	H7	H8	H9	H10
0.05	0.27	0.28	0.29	0.3	0.31	0.32	0.34	0.34	0.35	0.36
0.25	2.67	2.97	3.27	3.52	3.82	4.08	4.41	4.56	4.91	5.16
0.5	4.91	5.43	5.97	6.41	6.93	7.4	7.98	8.33	9.04	9.47
0.75	7.19	7.92	8.7	9.35	10.08	10.78	11.6	12.25	13.42	14.02
0.95	10.22	11.27	12.42	13.38	14.43	15.51	16.67	17.9	19.88	20.75

Table D5.3: Distribution of black carbon Freundlich adsorption constant (K_{FBC}) values for PBDE and PCB homologs as predicted from Monte Carlo simulation.

PBDE log K_{FBC}										
Percentile	H1	H2	H3	H4	H5	H6	H7	H8	H9	H10
0.05	4.85	5.79	6.23	6.65	7.30	7.90	7.73	8.15	8.49	7.05
0.25	0.20	0.16	0.38	0.61	0.59	0.78	1.39	1.19	1.41	2.45
0.50	0.14	0.11	0.27	0.43	0.41	0.54	0.94	0.84	0.98	1.68
0.75	0.14	0.11	0.26	0.43	0.41	0.53	0.96	0.83	0.97	1.69
0.95	0.20	0.16	0.38	0.62	0.59	0.77	1.38	1.20	1.41	2.44
PCB log K_{FBC}										
Percentile	H1	H2	H3	H4	H5	H6	H7	H8	H9	H10
0.05	4.07	4.57	5.06	5.46	5.96	6.35	6.91	7.00	7.44	7.86
0.25	0.10	0.10	0.12	0.14	0.14	0.17	0.17	0.32	0.46	0.47
0.50	0.07	0.07	0.08	0.09	0.09	0.12	0.12	0.22	0.33	0.32
0.75	0.07	0.07	0.08	0.09	0.09	0.12	0.12	0.22	0.33	0.33
0.95	0.10	0.10	0.12	0.13	0.13	0.17	0.17	0.31	0.47	0.47

Table D5.4 (Cont.): Distribution of fraction organic carbon (f_{OC}), fraction black carbon (f_{BC}), porosity (ϕ), particle density (ρ_{PD}), and hydraulic conductivity (K_h) in all sediment cores as predicted by Monte Carlo simulation.

f_{OC}											
Percentile	ACL	AED	AFR	AJL	AMW	AOT	CBC	CLC	CWP	IGC09	IGC13
0.05	0.0226	0.0085	0.0132	0.0096	0.0982	0.0183	0.0064	0.0571	0.0521	0.0974	0.091
0.25	0.0107	0.0140	0.0016	0.0211	0.0663	0.0078	0.0171	0.0021	0.0130	0.0150	0.022
0.50	0.0074	0.0112	0.0011	0.0178	0.0466	0.0055	0.0163	0.0015	0.0091	0.0104	0.015
0.75	0.0074	0.0113	0.0011	0.0185	0.0471	0.0054	0.0174	0.0015	0.0092	0.0104	0.015
0.95	0.0111	0.0165	0.0016	0.0274	0.0677	0.0077	0.0260	0.0021	0.0131	0.0151	0.022
f_{BC}											
Percentile	ACL	AED	AFR	AJL	AMW	AOT	CBC	CLC	CWP	IGC09	IGC13
0.05	0.0016	0.0021	0.0012	0.0011	0.0019	0.0010	0.0128	0.0128	0.0345	0.0079	0.0128
0.25	0.0007	0.0001	0.0002	0.0004	0.0006	0.0023	0.0030	0.0030	0.0021	0.0026	0.0053
0.50	0.0005	0.0001	0.0001	0.0003	0.0004	0.0021	0.0022	0.0022	0.0015	0.0018	0.0036
0.75	0.0005	0.0001	0.0001	0.0003	0.0004	0.0022	0.0022	0.0022	0.0015	0.0018	0.0037
0.95	0.0007	0.0001	0.0002	0.0004	0.0006	0.0033	0.0031	0.0031	0.0021	0.0026	0.0053
ϕ											
Percentile	ACL	AED	AFR	AJL	AMW	AOT	CBC	CLC	CWP	IGC09	IGC13
0.05	0.5925	0.6566	0.6153	0.5809	0.8441	0.8620	0.4115	0.6143	0.7185	0.7990	0.7980
0.25	0.1504	0.1063	0.1100	0.1090	0.0661	0.0360	0.0982	0.0144	0.0683	0.0449	0.0460
0.50	0.1028	0.0747	0.0751	0.0749	0.0461	0.0247	0.0675	0.0101	0.0472	0.0312	0.0310
0.75	0.1039	0.0736	0.0759	0.0770	0.0460	0.0248	0.0671	0.0102	0.0475	0.0314	0.0313
0.95	0.1507	0.1053	0.1109	0.1097	0.0665	0.0351	0.0967	0.0145	0.0679	0.0460	0.0454
ρ_{PD} (g/mL)											
Percentile	ACL	AED	AFR	AJL	AMW	AOT	CBC	CLC	CWP	IGC09	IGC13
0.05	2.4584	2.4758	2.5184	2.3650	1.8870	2.5149	2.4534	2.4711	2.3762	2.2428	2.2060
0.25	0.0365	0.0457	0.0493	0.0791	0.1402	0.0242	0.0570	0.0089	0.0391	0.0418	0.0551
0.50	0.0251	0.0323	0.0348	0.0552	0.0961	0.0167	0.0395	0.0063	0.0274	0.0296	0.0391
0.75	0.0253	0.0322	0.0347	0.0552	0.0986	0.0168	0.0392	0.0062	0.0272	0.0296	0.0385
0.95	0.0364	0.0454	0.0493	0.0821	0.1377	0.0237	0.0566	0.0090	0.0399	0.0420	0.0545

Table D5.4 (Cont.): Distribution of fraction organic carbon (f_{OC}), fraction black carbon (f_{BC}), porosity (ϕ), particle density (ρ_{PD}), and

Percentile	K_h (m/yr)										
	ACL	AED	AFR	AJL	AMW	AOT	CBC	CLC	CWP	IGC09	IGC13
0.05	62.3098	47.5545	13.3661	9.4246	50.6244	5.0645	61.5815	2.5672	21.0164	32.1659	58.0398
0.25	253.5861	190.2544	54.2918	38.5890	203.3548	20.5402	242.8451	10.3671	84.2616	127.2085	229.4927
0.50	353.1756	273.2315	74.5612	54.0266	286.1936	28.8593	332.8978	14.3197	117.0790	178.6593	323.6648
0.75	469.9290	357.4104	100.3353	72.3265	380.6013	38.2208	452.4981	19.3183	159.2704	237.3156	438.0986
0.95	801.4415	610.0208	171.0769	121.7732	652.8351	65.6066	766.5368	32.7330	267.2526	408.0191	734.7028

Table 5.5a (Cont.): Distribution of sediment-porewater partitioning coefficient for organic carbon only sorption ($\log K_d$ (OC)) for PBDE homologs as predicted by Monte Carlo simulation in all sediment cores.

ACL										
Percentile	H1	H2	H3	H4	H5	H6	H7	H8	H9	H10
0.05	2.91	3.59	3.92	4.23	4.70	5.14	5.02	5.33	5.57	4.52
0.25	3.22	3.88	4.37	4.85	5.30	5.88	6.21	6.36	6.77	6.49
0.50	3.41	4.05	4.65	5.25	5.69	6.36	6.98	7.07	7.57	7.80
0.75	3.58	4.20	4.92	5.64	6.07	6.82	7.76	7.75	8.35	9.11
0.95	3.82	4.41	5.29	6.18	6.59	7.48	8.86	8.72	9.48	10.99
AED										
Percentile	H1	H2	H3	H4	H5	H6	H7	H8	H9	H10
0.05	2.48	3.17	3.49	3.80	4.27	4.72	4.59	4.90	5.14	4.10
0.25	3.05	3.71	4.20	4.68	5.13	5.71	6.04	6.19	6.60	6.32
0.50	3.33	3.97	4.57	5.17	5.61	6.28	6.90	6.99	7.49	7.72
0.75	3.55	4.17	4.89	5.61	6.04	6.79	7.73	7.72	8.32	9.08
0.95	3.84	4.43	5.30	6.19	6.61	7.49	8.88	8.73	9.50	11.01
AFR										
Percentile	H1	H2	H3	H4	H5	H6	H7	H8	H9	H10
0.05	2.67	3.36	3.69	3.99	4.47	4.91	4.79	5.09	5.34	4.29
0.25	2.87	3.53	4.01	4.49	4.95	5.53	5.85	6.01	6.41	6.13
0.50	3.00	3.64	4.24	4.84	5.28	5.95	6.57	6.66	7.16	7.39
0.75	3.13	3.75	4.46	5.18	5.61	6.37	7.31	7.29	7.90	8.66
0.95	3.31	3.90	4.78	5.67	6.08	6.97	8.36	8.21	8.97	10.49
AJL										
Percentile	H1	H2	H3	H4	H5	H6	H7	H8	H9	H10
0.05	2.54	3.22	3.55	3.86	4.33	4.77	4.65	4.95	5.20	4.15
0.25	3.18	3.85	4.33	4.81	5.27	5.85	6.17	6.33	6.73	6.45
0.50	3.49	4.13	4.73	5.33	5.77	6.44	7.06	7.14	7.65	7.88
0.75	3.73	4.35	5.06	5.78	6.21	6.97	7.91	7.89	8.50	9.26
0.95	4.02	4.61	5.49	6.38	6.79	7.68	9.07	8.92	9.68	11.20
AMW										
Percentile	H1	H2	H3	H4	H5	H6	H7	H8	H9	H10
0.05	3.55	4.23	4.56	4.87	5.34	5.78	5.66	5.96	6.21	5.16
0.25	3.91	4.57	5.06	5.54	6.00	6.58	6.90	7.06	7.46	7.18
0.50	4.12	4.76	5.37	5.97	6.40	7.08	7.70	7.78	8.29	8.52
0.75	4.31	4.93	5.65	6.37	6.80	7.55	8.49	8.48	9.08	9.84
0.95	4.56	5.15	6.03	6.92	7.33	8.22	9.61	9.46	10.22	11.73

Table 5.5a (Cont.): Distribution of sediment-porewater partitioning coefficient for organic carbon only sorption ($\log K_d$ (OC)) for PBDE homologs as predicted by Monte Carlo simulation in all sediment cores.

AOT										
Percentile	H1	H2	H3	H4	H5	H6	H7	H8	H9	H10
0.05	2.82	3.50	3.83	4.14	4.61	5.05	4.93	5.23	5.48	4.43
0.25	3.11	3.77	4.26	4.74	5.19	5.77	6.10	6.26	6.66	6.38
0.50	3.30	3.94	4.54	5.14	5.58	6.25	6.87	6.96	7.46	7.69
0.75	3.47	4.09	4.80	5.52	5.95	6.71	7.65	7.63	8.24	9.00
0.95	3.70	4.29	5.16	6.05	6.47	7.35	8.74	8.59	9.36	10.87
CBC										
Percentile	H1	H2	H3	H4	H5	H6	H7	H8	H9	H10
0.05	2.36	3.05	3.37	3.68	4.15	4.60	4.47	4.78	5.02	3.98
0.25	3.07	3.73	4.22	4.69	5.15	5.73	6.06	6.21	6.62	6.34
0.50	3.40	4.04	4.64	5.24	5.68	6.35	6.98	7.06	7.56	7.79
0.75	3.66	4.28	4.99	5.71	6.14	6.90	7.84	7.82	8.43	9.19
0.95	3.97	4.56	5.44	6.33	6.74	7.63	9.01	8.86	9.63	11.14
CLC										
Percentile	H1	H2	H3	H4	H5	H6	H7	H8	H9	H10
0.05	3.31	4.00	4.32	4.63	5.10	5.55	5.42	5.73	5.97	4.93
0.25	3.47	4.13	4.62	5.10	5.55	6.13	6.46	6.61	7.02	6.74
0.50	3.58	4.22	4.83	5.42	5.86	6.54	7.16	7.24	7.75	7.98
0.75	3.69	4.31	5.03	5.75	6.18	6.93	7.87	7.86	8.47	9.23
0.95	3.86	4.45	5.32	6.22	6.63	7.51	8.90	8.75	9.52	11.03
CWP										
Percentile	H1	H2	H3	H4	H5	H6	H7	H8	H9	H10
0.05	3.27	3.96	4.28	4.59	5.06	5.51	5.38	5.69	5.93	4.88
0.25	3.51	4.17	4.66	5.14	5.59	6.17	6.50	6.66	7.06	6.78
0.50	3.67	4.31	4.91	5.51	5.95	6.62	7.25	7.33	7.83	8.06
0.75	3.82	4.44	5.16	5.88	6.30	7.06	8.00	7.99	8.59	9.35
0.95	4.03	4.62	5.50	6.39	6.80	7.69	9.08	8.93	9.69	11.21
IGC09										
Percentile	H1	H2	H3	H4	H5	H6	H7	H8	H9	H10
0.05	3.54	4.23	4.55	4.86	5.34	5.78	5.65	5.96	6.21	5.16
0.25	3.75	4.41	4.90	5.37	5.83	6.41	6.74	6.89	7.30	7.02
0.50	3.89	4.53	5.13	5.73	6.17	6.84	7.46	7.55	8.05	8.28
0.75	4.02	4.64	5.36	6.08	6.51	7.26	8.20	8.19	8.80	9.56
0.95	4.22	4.81	5.69	6.58	6.99	7.88	9.26	9.11	9.88	11.39

Table 5.5a (Cont.): Distribution of sediment-porewater partitioning coefficient for organic carbon only sorption ($\log K_d$ (OC)) for PBDE homologs as predicted by Monte Carlo simulation in all sediment cores.

Percentile	IGC13									
	H1	H2	H3	H4	H5	H6	H7	H8	H9	H10
0.05	3.51	4.20	4.52	4.83	5.30	5.75	5.62	5.93	6.17	5.13
0.25	3.75	4.41	4.90	5.38	5.83	6.41	6.74	6.89	7.30	7.02
0.50	3.91	4.55	5.15	5.75	6.19	6.86	7.48	7.56	8.07	8.30
0.75	4.06	4.68	5.39	6.11	6.54	7.30	8.23	8.22	8.83	9.59
0.95	4.26	4.85	5.73	6.62	7.04	7.92	9.31	9.16	9.92	11.44

Table 5.5b (Cont.): Distribution of sediment-porewater partitioning coefficient for organic carbon and black carbon sorption ($\log K_d$ (OCBC)) for PBDE homologs as predicted by Monte Carlo simulation in all sediment cores.

Percentile	ACL									
	H1	H2	H3	H4	H5	H6	H7	H8	H9	H10
0.05	2.91	4.25	5.70	7.08	8.84	10.44	10.85	12.47	13.52	11.47
0.25	3.28	5.37	7.06	8.69	10.26	12.07	13.38	14.46	15.78	15.45
0.50	4.36	6.25	8.06	9.83	11.23	13.12	14.99	15.68	17.14	17.92
0.75	5.41	7.10	9.02	10.94	12.17	14.14	16.60	16.87	18.45	20.39
0.95	6.60	8.07	10.23	12.40	13.45	15.61	18.97	18.72	20.57	24.20
Percentile	AED									
	H1	H2	H3	H4	H5	H6	H7	H8	H9	H10
0.05	2.48	3.96	5.41	6.79	8.54	10.15	10.56	12.18	13.23	11.18
0.25	3.10	5.20	6.88	8.51	10.09	11.89	13.21	14.28	15.61	15.27
0.50	4.20	6.10	7.90	9.67	11.07	12.97	14.83	15.53	16.98	17.77
0.75	5.25	6.94	8.86	10.78	12.01	13.98	16.44	16.71	18.29	20.23
0.95	6.42	7.89	10.04	12.22	13.27	15.43	18.78	18.53	20.39	24.02
Percentile	AFR									
	H1	H2	H3	H4	H5	H6	H7	H8	H9	H10
0.05	2.67	3.89	5.34	6.72	8.47	10.08	10.49	12.11	13.16	11.11
0.25	2.87	4.80	6.49	8.12	9.69	11.50	12.81	13.88	15.21	14.87
0.50	3.69	5.58	7.38	9.16	10.55	12.45	14.32	15.01	16.47	17.25
0.75	4.66	6.35	8.27	10.19	11.42	13.39	15.85	16.12	17.70	19.65
0.95	5.76	7.23	9.39	11.57	12.62	14.77	18.13	17.88	19.74	23.37

Table 5.5b (Cont.): Distribution of sediment-porewater partitioning coefficient for organic carbon and black carbon sorption ($\log K_d$ (OCBC)) for PBDE homologs as predicted by Monte Carlo simulation in all sediment cores.

AJL										
Percentile	H1	H2	H3	H4	H5	H6	H7	H8	H9	H10
0.05	2.54	3.74	5.19	6.57	8.33	9.93	10.34	11.96	13.01	10.96
0.25	3.18	5.17	6.85	8.49	10.06	11.87	13.18	14.25	15.58	15.24
0.50	4.25	6.15	7.95	9.72	11.12	13.02	14.88	15.58	17.03	17.82
0.75	5.36	7.06	8.97	10.89	12.12	14.09	16.55	16.82	18.41	20.35
0.95	6.60	8.07	10.23	12.40	13.45	15.61	18.97	18.72	20.57	24.20
AMW										
Percentile	H1	H2	H3	H4	H5	H6	H7	H8	H9	H10
0.05	3.55	4.98	6.43	7.80	9.56	11.17	11.57	13.19	14.25	12.20
0.25	4.01	6.11	7.79	9.43	11.00	12.81	14.12	15.19	16.52	16.18
0.50	5.10	6.99	8.80	10.57	11.97	13.86	15.73	16.42	17.88	18.66
0.75	6.15	7.85	9.76	11.68	12.91	14.88	17.34	17.61	19.19	21.14
0.95	7.34	8.81	10.96	13.14	14.19	16.35	19.71	19.45	21.31	24.94
AOT										
Percentile	H1	H2	H3	H4	H5	H6	H7	H8	H9	H10
0.05	2.82	3.95	5.40	6.78	8.54	10.14	10.55	12.17	13.22	11.17
0.25	3.34	5.43	7.12	8.75	10.32	12.13	13.44	14.52	15.84	15.51
0.50	4.54	6.44	8.24	10.01	11.41	13.31	15.17	15.87	17.32	18.11
0.75	5.66	7.36	9.28	11.20	12.42	14.40	16.85	17.12	18.71	20.65
0.95	6.92	8.39	10.55	12.72	13.77	15.93	19.29	19.04	20.89	24.52
CBC										
Percentile	H1	H2	H3	H4	H5	H6	H7	H8	H9	H10
0.05	2.36	4.62	6.07	7.44	9.20	10.81	11.21	12.84	13.89	11.84
0.25	3.97	6.07	7.75	9.38	10.96	12.76	14.08	15.15	16.47	16.14
0.50	5.17	7.06	8.87	10.64	12.04	13.93	15.80	16.49	17.95	18.73
0.75	6.28	7.98	9.90	11.81	13.04	15.02	17.47	17.74	19.33	21.27
0.95	7.52	8.99	11.15	13.33	14.38	16.53	19.89	19.64	21.50	25.12
CLC										
Percentile	H1	H2	H3	H4	H5	H6	H7	H8	H9	H10
0.05	3.31	5.57	7.02	8.39	10.15	11.76	12.16	13.79	14.84	12.79
0.25	4.37	6.47	8.15	9.79	11.36	13.17	14.48	15.55	16.88	16.54
0.50	5.35	7.25	9.05	10.82	12.22	14.12	15.98	16.68	18.13	18.92
0.75	6.32	8.01	9.93	11.85	13.08	15.05	17.51	17.78	19.36	21.31
0.95	7.41	8.88	11.04	13.22	14.26	16.42	19.78	19.53	21.38	25.01

Table 5.5b (Cont.): Distribution of sediment-porewater partitioning coefficient for organic carbon and black carbon sorption ($\log K_d$ (OCBC)) for PBDE homologs as predicted by Monte Carlo simulation in all sediment cores.

CWP										
Percentile	H1	H2	H3	H4	H5	H6	H7	H8	H9	H10
0.05	3.65	5.96	7.41	8.78	10.54	12.15	12.55	14.18	15.23	13.18
0.25	4.78	6.88	8.56	10.19	11.77	13.57	14.89	15.96	17.28	16.95
0.50	5.76	7.66	9.46	11.24	12.63	14.53	16.39	17.09	18.55	19.33
0.75	6.74	8.43	10.35	12.27	13.50	15.47	17.93	18.20	19.78	21.72
0.95	7.84	9.31	11.47	13.64	14.69	16.85	20.21	19.96	21.81	25.44
IGC09										
Percentile	H1	H2	H3	H4	H5	H6	H7	H8	H9	H10
0.05	3.54	5.59	7.04	8.41	10.17	11.78	12.18	13.81	14.86	12.81
0.25	4.47	6.57	8.25	9.88	11.46	13.26	14.58	15.65	16.97	16.64
0.50	5.49	7.39	9.19	10.96	12.36	14.26	16.12	16.82	18.27	19.06
0.75	6.49	8.19	10.11	12.03	13.25	15.23	17.68	17.95	19.54	21.48
0.95	7.63	9.10	11.26	13.43	14.48	16.64	20.00	19.75	21.60	25.23
IGC13										
Percentile	H1	H2	H3	H4	H5	H6	H7	H8	H9	H10
0.05	3.51	5.77	7.22	8.59	10.35	11.96	12.36	13.99	15.04	12.99
0.25	4.71	6.81	8.49	10.12	11.70	13.50	14.82	15.89	17.21	16.88
0.50	5.75	7.65	9.45	11.23	12.62	14.52	16.38	17.08	18.54	19.32
0.75	6.78	8.47	10.39	12.31	13.54	15.51	17.97	18.24	19.82	21.77
0.95	7.94	9.41	11.57	13.74	14.79	16.95	20.31	20.06	21.91	25.54

Table 5.5c (Cont.): Distribution of sediment-porewater partitioning coefficient for organic carbon only sorption ($\log K_d$ (OC)) for PCB homologs as predicted by Monte Carlo simulation in all sediment cores.

Percentile	ACL									
	H1	H2	H3	H4	H5	H6	H7	H8	H9	H10
0.05	2.65	3.19	3.72	4.15	4.69	5.11	5.71	5.81	6.28	6.73
0.25	2.93	3.47	4.01	4.46	5.00	5.46	6.07	6.33	6.95	7.40
0.50	3.09	3.63	4.19	4.65	5.19	5.68	6.28	6.65	7.39	7.84
0.75	3.24	3.78	4.35	4.82	5.36	5.88	6.48	6.96	7.82	8.26
0.95	3.43	3.97	4.57	5.06	5.60	6.16	6.75	7.39	8.41	8.85

Percentile	AED									
	H1	H2	H3	H4	H5	H6	H7	H8	H9	H10
0.05	2.23	2.77	3.29	3.72	4.26	4.68	5.28	5.39	5.86	6.31
0.25	2.76	3.30	3.84	4.29	4.83	5.29	5.90	6.16	6.78	7.23
0.50	3.01	3.55	4.11	4.57	5.11	5.60	6.20	6.57	7.31	7.76
0.75	3.21	3.75	4.32	4.79	5.34	5.85	6.45	6.93	7.79	8.23
0.95	3.45	3.99	4.58	5.07	5.62	6.17	6.77	7.40	8.42	8.87

Percentile	AFR									
	H1	H2	H3	H4	H5	H6	H7	H8	H9	H10
0.05	2.42	2.96	3.48	3.91	4.45	4.87	5.48	5.58	6.05	6.50
0.25	2.57	3.11	3.66	4.11	4.65	5.11	5.71	5.97	6.60	7.05
0.50	2.68	3.22	3.78	4.24	4.78	5.27	5.87	6.24	6.98	7.43
0.75	2.78	3.32	3.89	4.37	4.91	5.43	6.02	6.50	7.36	7.81
0.95	2.93	3.47	4.06	4.55	5.09	5.65	6.25	6.88	7.90	8.35

Percentile	AJL									
	H1	H2	H3	H4	H5	H6	H7	H8	H9	H10
0.05	2.28	2.82	3.35	3.77	4.32	4.73	5.34	5.44	5.91	6.36
0.25	2.89	3.43	3.98	4.43	4.97	5.43	6.03	6.29	6.91	7.37
0.50	3.17	3.71	4.27	4.73	5.27	5.75	6.36	6.72	7.47	7.91
0.75	3.38	3.92	4.49	4.97	5.51	6.02	6.62	7.10	7.96	8.40
0.95	3.63	4.18	4.77	5.26	5.80	6.36	6.96	7.59	8.61	9.06

Percentile	AMW									
	H1	H2	H3	H4	H5	H6	H7	H8	H9	H10
0.05	3.29	3.83	4.36	4.79	5.33	5.75	6.35	6.45	6.92	7.37
0.25	3.62	4.16	4.71	5.16	5.70	6.16	6.76	7.02	7.64	8.10
0.50	3.81	4.34	4.90	5.36	5.91	6.39	6.99	7.36	8.10	8.55
0.75	3.97	4.51	5.08	5.55	6.09	6.61	7.21	7.69	8.55	8.99
0.95	4.17	4.72	5.31	5.80	6.34	6.90	7.49	8.13	9.15	9.59

Table 5.5c (Cont.): Distribution of sediment-porewater partitioning coefficient for organic carbon only sorption ($\log K_d$ (OC)) for PCB homologs as predicted by Monte Carlo simulation in all sediment cores.

AOT										
Percentile	H1	H2	H3	H4	H5	H6	H7	H8	H9	H10
0.05	2.56	3.10	3.63	4.05	4.60	5.01	5.62	5.72	6.19	6.64
0.25	2.82	3.36	3.91	4.35	4.90	5.36	5.96	6.22	6.84	7.30
0.50	2.98	3.52	4.08	4.54	5.08	5.57	6.17	6.54	7.28	7.73
0.75	3.12	3.66	4.23	4.71	5.25	5.77	6.36	6.84	7.70	8.15
0.95	3.31	3.85	4.44	4.93	5.48	6.03	6.63	7.26	8.29	8.73
CBC										
Percentile	H1	H2	H3	H4	H5	H6	H7	H8	H9	H10
0.05	2.11	2.65	3.17	3.60	4.14	4.56	5.16	5.27	5.73	6.19
0.25	2.78	3.32	3.86	4.31	4.85	5.31	5.91	6.17	6.80	7.25
0.50	3.08	3.62	4.18	4.64	5.18	5.67	6.27	6.64	7.38	7.83
0.75	3.31	3.85	4.43	4.90	5.44	5.96	6.55	7.03	7.89	8.34
0.95	3.58	4.12	4.71	5.21	5.75	6.30	6.90	7.53	8.56	9.00
CLC										
Percentile	H1	H2	H3	H4	H5	H6	H7	H8	H9	H10
0.05	3.06	3.60	4.12	4.55	5.09	5.51	6.11	6.22	6.68	7.14
0.25	3.18	3.72	4.27	4.71	5.25	5.71	6.32	6.58	7.20	7.66
0.50	3.26	3.80	4.36	4.82	5.36	5.85	6.45	6.82	7.56	8.01
0.75	3.35	3.89	4.46	4.94	5.48	5.99	6.59	7.07	7.93	8.37
0.95	3.47	4.01	4.60	5.09	5.64	6.19	6.79	7.42	8.45	8.89
CWP										
Percentile	H1	H2	H3	H4	H5	H6	H7	H8	H9	H10
0.05	3.02	3.56	4.08	4.51	5.05	5.47	6.07	6.18	6.64	7.10
0.25	3.22	3.76	4.31	4.75	5.29	5.75	6.36	6.62	7.24	7.70
0.50	3.35	3.89	4.45	4.91	5.45	5.94	6.54	6.91	7.65	8.10
0.75	3.48	4.02	4.59	5.06	5.60	6.12	6.72	7.20	8.05	8.50
0.95	3.64	4.19	4.78	5.27	5.81	6.37	6.97	7.60	8.62	9.07
IGC09										
Percentile	H1	H2	H3	H4	H5	H6	H7	H8	H9	H10
0.05	3.29	3.83	4.35	4.78	5.32	5.74	6.35	6.45	6.92	7.37
0.25	3.46	4.00	4.54	4.99	5.53	5.99	6.59	6.85	7.48	7.93
0.50	3.57	4.11	4.67	5.13	5.67	6.16	6.76	7.13	7.87	8.32
0.75	3.68	4.22	4.79	5.27	5.81	6.32	6.92	7.40	8.26	8.70
0.95	3.83	4.37	4.97	5.46	6.00	6.55	7.15	7.78	8.81	9.25

Table 5.5c (Cont.): Distribution of sediment-porewater partitioning coefficient for organic carbon only sorption ($\log K_d$ (OC)) for PCB homologs as predicted by Monte Carlo simulation in all sediment cores.

Percentile	IGC13									
	H1	H2	H3	H4	H5	H6	H7	H8	H9	H10
0.05	3.26	3.80	4.32	4.75	5.29	5.71	6.31	6.42	6.89	7.34
0.25	3.46	4.00	4.54	4.99	5.53	5.99	6.59	6.85	7.48	7.93
0.50	3.59	4.13	4.69	5.15	5.69	6.18	6.78	7.15	7.89	8.33
0.75	3.71	4.25	4.82	5.30	5.84	6.35	6.95	7.43	8.29	8.73
0.95	3.88	4.42	5.01	5.50	6.05	6.60	7.20	7.83	8.85	9.30

Table 5.5d (Cont.): Distribution of sediment-porewater partitioning coefficient for organic carbon and black carbon sorption ($\log K_d$ (OCBC)) for PCB homologs as predicted by Monte Carlo simulation in all sediment cores.

Percentile	ACL									
	H1	H2	H3	H4	H5	H6	H7	H8	H9	H10
0.05	2.65	3.19	3.87	5.29	6.87	8.28	9.78	10.82	12.16	13.02
0.25	2.93	3.47	4.90	6.23	7.69	9.04	10.48	11.63	13.18	14.04
0.50	3.09	4.31	5.71	6.93	8.27	9.55	10.90	12.07	13.75	14.60
0.75	3.99	5.20	6.49	7.61	8.83	10.02	11.29	12.49	14.30	15.15
0.95	5.07	6.17	7.38	8.39	9.50	10.64	11.83	13.14	15.16	16.02
Percentile	AED									
	H1	H2	H3	H4	H5	H6	H7	H8	H9	H10
0.05	2.23	2.77	3.57	4.99	6.58	7.98	9.49	10.53	11.87	12.73
0.25	2.76	3.30	4.73	6.05	7.52	8.87	10.30	11.46	13.00	13.86
0.50	3.01	4.16	5.56	6.77	8.12	9.39	10.74	11.92	13.59	14.44
0.75	3.83	5.03	6.33	7.44	8.67	9.86	11.13	12.33	14.13	14.99
0.95	4.89	5.99	7.20	8.21	9.32	10.45	11.65	12.96	14.98	15.83
Percentile	AFR									
	H1	H2	H3	H4	H5	H6	H7	H8	H9	H10
0.05	2.42	2.96	3.50	4.92	6.51	7.91	9.42	10.46	11.80	12.66
0.25	2.57	3.11	4.33	5.66	7.12	8.47	9.90	11.06	12.60	13.46
0.50	2.68	3.64	5.04	6.26	7.60	8.88	10.22	11.40	13.08	13.93
0.75	3.24	4.45	5.74	6.86	8.08	9.27	10.54	11.75	13.55	14.40
0.95	4.24	5.34	6.54	7.56	8.66	9.80	10.99	12.30	14.32	15.18

Table 5.5d (Cont.): Distribution of sediment-porewater partitioning coefficient for organic carbon and black carbon sorption ($\log K_d$ (OCBC)) for PCB homologs as predicted by Monte Carlo simulation in all sediment cores.

AJL										
Percentile	H1	H2	H3	H4	H5	H6	H7	H8	H9	H10
0.05	2.28	2.82	3.35	4.77	6.36	7.76	9.27	10.31	11.65	12.51
0.25	2.89	3.43	4.70	6.03	7.49	8.84	10.27	11.43	12.97	13.83
0.50	3.17	4.21	5.61	6.83	8.17	9.44	10.79	11.97	13.64	14.50
0.75	3.94	5.15	6.45	7.56	8.78	9.98	11.24	12.45	14.25	15.10
0.95	5.08	6.18	7.38	8.39	9.50	10.64	11.83	13.14	15.16	16.02
AMW										
Percentile	H1	H2	H3	H4	H5	H6	H7	H8	H9	H10
0.05	3.29	3.83	4.59	6.01	7.59	9.00	10.51	11.55	12.89	13.74
0.25	3.62	4.16	5.64	6.97	8.43	9.78	11.21	12.37	13.91	14.77
0.50	3.81	5.05	6.45	7.67	9.01	10.29	11.64	12.81	14.49	15.34
0.75	4.73	5.94	7.24	8.35	9.57	10.77	12.03	13.24	15.04	15.89
0.95	5.81	6.91	8.12	9.13	10.24	11.38	12.57	13.88	15.90	16.75
AOT										
Percentile	H1	H2	H3	H4	H5	H6	H7	H8	H9	H10
0.05	2.56	3.10	3.63	4.99	6.57	7.98	9.48	10.52	11.86	12.72
0.25	2.82	3.46	4.96	6.29	7.75	9.10	10.53	11.69	13.23	14.10
0.50	3.18	4.50	5.90	7.11	8.46	9.73	11.08	12.26	13.93	14.79
0.75	4.24	5.45	6.75	7.86	9.09	10.28	11.55	12.75	14.55	15.40
0.95	5.39	6.49	7.70	8.71	9.82	10.96	12.15	13.46	15.48	16.34
CBC										
Percentile	H1	H2	H3	H4	H5	H6	H7	H8	H9	H10
0.05	2.11	2.65	4.23	5.65	7.24	8.64	10.15	11.19	12.53	13.38
0.25	2.78	4.10	5.60	6.92	8.39	9.74	11.17	12.33	13.87	14.73
0.50	3.81	5.12	6.52	7.74	9.08	10.36	11.71	12.88	14.56	15.41
0.75	4.86	6.07	7.37	8.48	9.70	10.90	12.17	13.37	15.17	16.02
0.95	6.00	7.10	8.30	9.32	10.42	11.56	12.75	14.06	16.08	16.94
CLC										
Percentile	H1	H2	H3	H4	H5	H6	H7	H8	H9	H10
0.05	3.06	3.60	5.18	6.60	8.19	9.59	11.10	12.14	13.48	14.33
0.25	3.18	4.50	6.00	7.33	8.79	10.14	11.57	12.73	14.27	15.13
0.50	3.99	5.31	6.71	7.92	9.27	10.54	11.89	13.07	14.74	15.59
0.75	4.90	6.11	7.40	8.52	9.74	10.93	12.20	13.40	15.21	16.06
0.95	5.89	6.99	8.19	9.21	10.31	11.45	12.64	13.95	15.97	16.83

Table 5.5d (Cont.): Distribution of sediment-porewater partitioning coefficient for organic carbon and black carbon sorption ($\log K_d$ (OCBC)) for PCB homologs as predicted by Monte Carlo simulation in all sediment cores.

CWP										
Percentile	H1	H2	H3	H4	H5	H6	H7	H8	H9	H10
0.05	3.02	3.98	5.57	6.99	8.58	9.98	11.49	12.53	13.87	14.72
0.25	3.48	4.90	6.41	7.73	9.20	10.55	11.98	13.13	14.68	15.54
0.50	4.40	5.72	7.12	8.34	9.68	10.95	12.30	13.48	15.15	16.01
0.75	5.32	6.53	7.82	8.94	10.16	11.35	12.62	13.82	15.63	16.48
0.95	6.32	7.42	8.62	9.63	10.74	11.88	13.07	14.38	16.40	17.26
IGC09										
Percentile	H1	H2	H3	H4	H5	H6	H7	H8	H9	H10
0.05	3.29	3.83	5.20	6.62	8.21	9.61	11.12	12.16	13.50	14.35
0.25	3.46	4.60	6.10	7.42	8.89	10.24	11.67	12.82	14.37	15.23
0.50	4.13	5.45	6.85	8.06	9.41	10.68	12.03	13.21	14.88	15.73
0.75	5.07	6.28	7.58	8.69	9.91	11.11	12.38	13.58	15.38	16.23
0.95	6.11	7.21	8.41	9.43	10.53	11.67	12.86	14.17	16.19	17.05
IGC13										
Percentile	H1	H2	H3	H4	H5	H6	H7	H8	H9	H10
0.05	3.26	3.80	5.38	6.80	8.39	9.79	11.30	12.34	13.68	14.53
0.25	3.46	4.84	6.34	7.66	9.13	10.48	11.91	13.06	14.61	15.47
0.50	4.39	5.71	7.11	8.33	9.67	10.94	12.29	13.47	15.14	16.00
0.75	5.36	6.57	7.86	8.98	10.20	11.39	12.66	13.86	15.67	16.52
0.95	6.41	7.51	8.72	9.73	10.84	11.98	13.17	14.48	16.50	17.36

Table 5.6a (Cont.): Distribution of black carbon-porewater partitioning ($\log K_{BC}$) for PBDE homologs as predicted by Monte Carlo simulation in all sediment cores.

Percentile	ACL									
	H1	H2	H3	H4	H5	H6	H7	H8	H9	H10
0.05	0.00	0.66	1.78	2.85	4.14	5.30	5.83	7.15	7.95	6.95
0.25	0.06	1.49	2.69	3.84	4.96	6.19	7.18	8.09	9.01	8.96
0.50	0.95	2.20	3.40	4.58	5.54	6.76	8.00	8.62	9.57	10.12
0.75	1.83	2.90	4.10	5.30	6.10	7.32	8.84	9.12	10.10	11.28
0.95	2.78	3.66	4.94	6.22	6.86	8.13	10.10	10.00	11.09	13.21
Percentile	AED									
	H1	H2	H3	H4	H5	H6	H7	H8	H9	H10
0.05	0.00	0.79	1.92	2.98	4.27	5.43	5.96	7.28	8.09	7.08
0.25	0.05	1.49	2.68	3.84	4.96	6.18	7.17	8.09	9.01	8.96
0.50	0.87	2.13	3.33	4.51	5.46	6.69	7.93	8.54	9.49	10.05
0.75	1.69	2.77	3.97	5.17	5.97	7.19	8.70	8.99	9.97	11.15
0.95	2.58	3.46	4.74	6.03	6.66	7.93	9.90	9.80	10.89	13.01
Percentile	AFR									
	H1	H2	H3	H4	H5	H6	H7	H8	H9	H10
0.05	0.00	0.53	1.65	2.72	4.01	5.17	5.70	7.02	7.82	6.82
0.25	0.00	1.27	2.47	3.63	4.75	5.97	6.96	7.87	8.79	8.74
0.50	0.69	1.94	3.14	4.32	5.28	6.50	7.74	8.36	9.31	9.86
0.75	1.53	2.61	3.81	5.01	5.81	7.03	8.54	8.82	9.81	10.99
0.95	2.45	3.33	4.61	5.90	6.53	7.80	9.77	9.67	10.76	12.88
Percentile	AJL									
	H1	H2	H3	H4	H5	H6	H7	H8	H9	H10
0.05	0.00	0.52	1.64	2.71	4.00	5.16	5.69	7.01	7.81	6.81
0.25	0.00	1.33	2.52	3.68	4.80	6.02	7.01	7.92	8.84	8.79
0.50	0.77	2.02	3.22	4.40	5.35	6.58	7.82	8.43	9.39	9.94
0.75	1.63	2.71	3.91	5.11	5.91	7.13	8.64	8.93	9.91	11.09
0.95	2.58	3.46	4.74	6.02	6.66	7.93	9.90	9.80	10.89	13.01
Percentile	AMW									
	H1	H2	H3	H4	H5	H6	H7	H8	H9	H10
0.05	0.00	0.74	1.87	2.93	4.22	5.38	5.91	7.23	8.04	7.04
0.25	0.10	1.54	2.73	3.89	5.01	6.23	7.22	8.14	9.05	9.00
0.50	0.97	2.23	3.43	4.61	5.56	6.79	8.03	8.64	9.59	10.15
0.75	1.84	2.91	4.12	5.32	6.11	7.33	8.85	9.13	10.11	11.29
0.95	2.78	3.66	4.94	6.22	6.86	8.13	10.10	10.00	11.09	13.21

Table 5.6a (Cont.): Distribution of black carbon-porewater partitioning ($\log K_{BC}$) for PBDE homologs as predicted by Monte Carlo simulation in all sediment cores.

AOT										
Percentile	H1	H2	H3	H4	H5	H6	H7	H8	H9	H10
0.05	0.00	0.45	1.57	2.64	3.93	5.09	5.62	6.94	7.74	6.74
0.25	0.22	1.66	2.85	4.01	5.13	6.35	7.34	8.26	9.18	9.13
0.50	1.24	2.50	3.70	4.88	5.83	7.06	8.30	8.91	9.86	10.42
0.75	2.20	3.27	4.48	5.67	6.47	7.69	9.21	9.49	10.47	11.65
0.95	3.22	4.10	5.38	6.67	7.30	8.57	10.54	10.44	11.54	13.65
CBC										
Percentile	H1	H2	H3	H4	H5	H6	H7	H8	H9	H10
0.05	0.00	1.57	2.69	3.76	5.05	6.21	6.74	8.06	8.86	7.86
0.25	0.90	2.34	3.53	4.69	5.81	7.03	8.02	8.94	9.86	9.81
0.50	1.77	3.02	4.22	5.40	6.36	7.58	8.82	9.44	10.39	10.94
0.75	2.62	3.70	4.90	6.10	6.90	8.12	9.63	9.92	10.90	12.08
0.95	3.56	4.44	5.71	7.00	7.64	8.91	10.88	10.78	11.87	13.98
CLC										
Percentile	H1	H2	H3	H4	H5	H6	H7	H8	H9	H10
0.05	0.00	1.57	2.69	3.76	5.05	6.21	6.74	8.06	8.86	7.86
0.25	0.90	2.34	3.53	4.69	5.81	7.03	8.02	8.94	9.86	9.81
0.50	1.77	3.02	4.22	5.40	6.36	7.58	8.82	9.44	10.39	10.94
0.75	2.62	3.70	4.90	6.10	6.90	8.12	9.63	9.92	10.90	12.08
0.95	3.56	4.44	5.71	7.00	7.64	8.91	10.88	10.78	11.87	13.98
CWP										
Percentile	H1	H2	H3	H4	H5	H6	H7	H8	H9	H10
0.05	0.38	2.00	3.12	4.19	5.48	6.64	7.17	8.49	9.29	8.29
0.25	1.27	2.70	3.90	5.05	6.17	7.40	8.39	9.30	10.22	10.17
0.50	2.09	3.35	4.55	5.73	6.68	7.91	9.15	9.76	10.71	11.27
0.75	2.92	3.99	5.20	6.39	7.19	8.41	9.93	10.21	11.19	12.37
0.95	3.81	4.69	5.97	7.25	7.89	9.16	11.13	11.03	12.12	14.24
IGC09										
Percentile	H1	H2	H3	H4	H5	H6	H7	H8	H9	H10
0.05	0.00	1.36	2.48	3.55	4.84	6.00	6.53	7.85	8.65	7.65
0.25	0.72	2.16	3.35	4.51	5.63	6.85	7.84	8.76	9.68	9.63
0.50	1.60	2.86	4.06	5.23	6.19	7.42	8.66	9.27	10.22	10.77
0.75	2.47	3.54	4.75	5.95	6.74	7.96	9.48	9.76	10.74	11.92
0.95	3.41	4.29	5.57	6.86	7.49	8.76	10.73	10.63	11.73	13.84

Table 5.6a (Cont.): Distribution of black carbon-porewater partitioning ($\log K_{BC}$) for PBDE homologs as predicted by Monte Carlo simulation in all sediment cores.

Percentile	IGC13									
	H1	H2	H3	H4	H5	H6	H7	H8	H9	H10
0.05	0.00	1.57	2.69	3.76	5.05	6.21	6.74	8.06	8.86	7.86
0.25	0.96	2.40	3.59	4.75	5.87	7.09	8.08	9.00	9.91	9.86
0.50	1.85	3.10	4.30	5.48	6.44	7.66	8.90	9.52	10.47	11.02
0.75	2.72	3.80	5.00	6.20	7.00	8.22	9.73	10.02	11.00	12.18
0.95	3.67	4.56	5.83	7.12	7.75	9.03	11.00	10.89	11.99	14.10

Table 5.6b (Cont.): Distribution of black carbon-porewater partitioning ($\log K_{BC}$) for PCB homologs as predicted by Monte Carlo simulation in all sediment cores.

Percentile	ACL									
	H1	H2	H3	H4	H5	H6	H7	H8	H9	H10
0.05	0.00	0.00	0.15	1.14	2.18	3.17	4.07	5.01	5.88	6.28
0.25	0.00	0.00	0.89	1.77	2.69	3.58	4.41	5.30	6.23	6.63
0.50	0.00	0.68	1.52	2.28	3.08	3.87	4.62	5.43	6.36	6.76
0.75	0.75	1.42	2.14	2.78	3.46	4.14	4.81	5.54	6.48	6.89
0.95	1.64	2.20	2.81	3.34	3.90	4.48	5.07	5.75	6.75	7.16

Percentile	AED									
	H1	H2	H3	H4	H5	H6	H7	H8	H9	H10
0.05	0.00	0.00	0.28	1.27	2.32	3.30	4.21	5.14	6.01	6.42
0.25	0.00	0.00	0.89	1.76	2.69	3.58	4.41	5.30	6.22	6.63
0.50	0.00	0.61	1.45	2.21	3.01	3.79	4.54	5.35	6.28	6.69
0.75	0.62	1.29	2.01	2.65	3.33	4.01	4.68	5.40	6.35	6.75
0.95	1.44	2.00	2.61	3.14	3.70	4.28	4.88	5.56	6.55	6.96

Percentile	AFR									
	H1	H2	H3	H4	H5	H6	H7	H8	H9	H10
0.05	0.00	0.00	0.02	1.01	2.06	3.04	3.95	4.88	5.75	6.16
0.25	0.00	0.00	0.67	1.55	2.47	3.36	4.19	5.09	6.01	6.41
0.50	0.00	0.42	1.26	2.02	2.82	3.61	4.36	5.17	6.10	6.50
0.75	0.46	1.13	1.85	2.49	3.17	3.85	4.52	5.24	6.19	6.59
0.95	1.31	1.87	2.48	3.01	3.57	4.15	4.75	5.43	6.42	6.83

Table 5.6b (Cont.): Distribution of black carbon-porewater partitioning ($\log K_{BC}$) for PCB homologs as predicted by Monte Carlo simulation in all sediment cores.

AJL										
Percentile	H1	H2	H3	H4	H5	H6	H7	H8	H9	H10
0.05	0.00	0.00	0.01	1.00	2.04	3.03	3.93	4.87	5.74	6.14
0.25	0.00	0.00	0.72	1.60	2.52	3.41	4.24	5.14	6.06	6.46
0.50	0.00	0.50	1.34	2.10	2.90	3.69	4.44	5.24	6.18	6.58
0.75	0.56	1.23	1.95	2.59	3.27	3.95	4.62	5.35	6.29	6.69
0.95	1.44	2.00	2.61	3.13	3.70	4.28	4.87	5.55	6.55	6.96
AMW										
Percentile	H1	H2	H3	H4	H5	H6	H7	H8	H9	H10
0.05	0.00	0.00	0.23	1.22	2.27	3.25	4.16	5.09	5.97	6.37
0.25	0.00	0.00	0.93	1.81	2.73	3.63	4.45	5.35	6.27	6.68
0.50	0.00	0.71	1.55	2.31	3.11	3.89	4.64	5.45	6.38	6.79
0.75	0.76	1.43	2.16	2.79	3.48	4.15	4.82	5.55	6.49	6.90
0.95	1.64	2.20	2.81	3.33	3.90	4.48	5.07	5.75	6.75	7.16
AOT										
Percentile	H1	H2	H3	H4	H5	H6	H7	H8	H9	H10
0.05	0.00	0.00	0.00	0.93	1.98	2.96	3.86	4.80	5.67	6.08
0.25	0.00	0.10	1.06	1.93	2.86	3.75	4.58	5.47	6.39	6.80
0.50	0.20	0.98	1.82	2.58	3.38	4.16	4.91	5.72	6.65	7.06
0.75	1.12	1.79	2.51	3.15	3.84	4.51	5.18	5.91	6.85	7.26
0.95	2.08	2.64	3.26	3.78	4.34	4.92	5.52	6.20	7.19	7.61
CBC										
Percentile	H1	H2	H3	H4	H5	H6	H7	H8	H9	H10
0.05	0.00	0.00	1.06	2.05	3.09	4.08	4.98	5.92	6.79	7.19
0.25	0.00	0.78	1.74	2.61	3.54	4.43	5.26	6.15	7.07	7.48
0.50	0.72	1.50	2.34	3.10	3.90	4.69	5.44	6.25	7.18	7.58
0.75	1.55	2.22	2.94	3.58	4.26	4.94	5.61	6.33	7.28	7.68
0.95	2.42	2.98	3.59	4.11	4.68	5.26	5.85	6.53	7.53	7.94
CLC										
Percentile	H1	H2	H3	H4	H5	H6	H7	H8	H9	H10
0.05	0.00	0.00	1.06	2.05	3.09	4.08	4.98	5.92	6.79	7.19
0.25	0.00	0.78	1.74	2.61	3.54	4.43	5.26	6.15	7.07	7.48
0.50	0.72	1.50	2.34	3.10	3.90	4.69	5.44	6.25	7.18	7.58
0.75	1.55	2.22	2.94	3.58	4.26	4.94	5.61	6.33	7.28	7.68
0.95	2.42	2.98	3.59	4.11	4.68	5.26	5.85	6.53	7.53	7.94

Table 5.6b (Cont.): Distribution of black carbon-porewater partitioning ($\log K_{BC}$) for PCB homologs as predicted by Monte Carlo simulation in all sediment cores.

CWP										
Percentile	H1	H2	H3	H4	H5	H6	H7	H8	H9	H10
0.05	0.00	0.42	1.49	2.48	3.53	4.51	5.41	6.35	7.22	7.62
0.25	0.26	1.15	2.10	2.98	3.90	4.79	5.62	6.51	7.44	7.84
0.50	1.05	1.83	2.67	3.43	4.23	5.01	5.76	6.57	7.50	7.91
0.75	1.84	2.51	3.23	3.87	4.56	5.23	5.90	6.63	7.57	7.98
0.95	2.67	3.23	3.84	4.36	4.93	5.51	6.10	6.78	7.78	8.19
IGC09										
Percentile	H1	H2	H3	H4	H5	H6	H7	H8	H9	H10
0.05	0.00	0.00	0.85	1.84	2.88	3.87	4.77	5.71	6.58	6.98
0.25	0.00	0.60	1.56	2.43	3.36	4.25	5.08	5.97	6.89	7.30
0.50	0.56	1.34	2.18	2.93	3.74	4.52	5.27	6.08	7.01	7.42
0.75	1.39	2.06	2.79	3.42	4.11	4.79	5.46	6.18	7.12	7.53
0.95	2.27	2.83	3.45	3.97	4.53	5.11	5.71	6.39	7.39	7.80
IGC13										
Percentile	H1	H2	H3	H4	H5	H6	H7	H8	H9	H10
0.05	0.00	0.00	1.06	2.05	3.09	4.08	4.98	5.92	6.79	7.19
0.25	0.00	0.84	1.79	2.67	3.60	4.49	5.31	6.21	7.13	7.54
0.50	0.80	1.58	2.42	3.18	3.98	4.77	5.52	6.33	7.26	7.66
0.75	1.65	2.32	3.04	3.68	4.36	5.04	5.71	6.43	7.38	7.78
0.95	2.54	3.10	3.71	4.23	4.79	5.38	5.97	6.65	7.65	8.06

Table 5.7a: Distribution of observed diffusivity for organic carbon only sorption (D_{obs} (OC)) (m^2/yr) values as predicted by Monte Carlo simulation for PBDE homologs in all sediment cores.

ACL										
Percentile	H1	H2	H3	H4	H5	H6	H7	H8	H9	H10
0.05	1.40E-06	3.40E-07	4.27E-08	5.24E-09	1.94E-09	2.42E-10	9.60E-12	1.30E-11	2.17E-12	6.45E-14
0.25	1.73E-06	3.94E-07	7.20E-08	1.31E-08	4.67E-09	7.86E-10	8.74E-11	8.69E-11	2.09E-11	3.51E-12
0.50	1.99E-06	4.32E-07	1.03E-07	2.46E-08	8.57E-09	1.76E-09	4.04E-10	3.22E-10	9.70E-11	5.54E-11
0.75	2.29E-06	4.75E-07	1.46E-07	4.65E-08	1.56E-08	3.95E-09	1.81E-09	1.21E-09	4.61E-10	8.56E-10
0.95	2.81E-06	5.49E-07	2.47E-07	1.16E-07	3.73E-08	1.29E-08	1.66E-08	7.94E-09	4.35E-09	4.72E-08
AED										
Percentile	H1	H2	H3	H4	H5	H6	H7	H8	H9	H10
0.05	1.10E-06	2.67E-07	3.35E-08	4.11E-09	1.52E-09	1.90E-10	7.53E-12	1.02E-11	1.70E-12	5.06E-14
0.25	1.65E-06	3.76E-07	6.88E-08	1.25E-08	4.46E-09	7.51E-10	8.36E-11	8.31E-11	1.99E-11	3.35E-12
0.50	2.32E-06	5.03E-07	1.19E-07	2.87E-08	9.98E-09	2.04E-09	4.70E-10	3.75E-10	1.13E-10	6.45E-11
0.75	3.57E-06	7.39E-07	2.28E-07	7.25E-08	2.43E-08	6.15E-09	2.81E-09	1.89E-09	7.17E-10	1.33E-09
0.95	9.46E-06	1.85E-06	8.30E-07	3.89E-07	1.26E-07	4.34E-08	5.60E-08	2.67E-08	1.47E-08	1.59E-07
AFR										
Percentile	H1	H2	H3	H4	H5	H6	H7	H8	H9	H10
0.05	3.35E-06	8.15E-07	1.02E-07	1.26E-08	4.64E-09	5.79E-10	2.30E-11	3.12E-11	5.20E-12	1.54E-13
0.25	3.95E-06	8.98E-07	1.64E-07	2.98E-08	1.07E-08	1.79E-09	2.00E-10	1.98E-10	4.76E-11	8.01E-12
0.50	4.36E-06	9.45E-07	2.25E-07	5.39E-08	1.88E-08	3.85E-09	8.84E-10	7.06E-10	2.12E-10	1.21E-10
0.75	4.76E-06	9.86E-07	3.04E-07	9.67E-08	3.24E-08	8.21E-09	3.75E-09	2.52E-09	9.57E-10	1.78E-09
0.95	5.14E-06	1.00E-06	4.51E-07	2.11E-07	6.82E-08	2.36E-08	3.04E-08	1.45E-08	7.96E-09	8.64E-08
AJL										
Percentile	H1	H2	H3	H4	H5	H6	H7	H8	H9	H10
0.05	6.11E-07	1.49E-07	1.87E-08	2.29E-09	8.47E-10	1.06E-10	4.20E-12	5.70E-12	9.50E-13	2.82E-14
0.25	9.35E-07	2.13E-07	3.89E-08	7.06E-09	2.52E-09	4.25E-10	4.72E-11	4.70E-11	1.13E-11	1.90E-12
0.50	1.33E-06	2.88E-07	6.85E-08	1.65E-08	5.73E-09	1.17E-09	2.70E-10	2.15E-10	6.48E-11	3.70E-11
0.75	2.14E-06	4.42E-07	1.36E-07	4.34E-08	1.45E-08	3.68E-09	1.68E-09	1.13E-09	4.29E-10	7.98E-10
0.95	6.57E-06	1.28E-06	5.77E-07	2.70E-07	8.72E-08	3.02E-08	3.89E-08	1.86E-08	1.02E-08	1.10E-07

Table 5.7a: Distribution of observed diffusivity for organic carbon only sorption (D_{obs} (OC)) (m^2/yr) values as predicted by Monte Carlo simulation for PBDE homologs in all sediment cores.

AMW										
Percentile	H1	H2	H3	H4	H5	H6	H7	H8	H9	H10
0.05	2.59E-07	6.31E-08	7.91E-09	9.72E-10	3.59E-10	4.48E-11	1.78E-12	2.42E-12	4.03E-13	1.20E-14
0.25	4.19E-07	9.52E-08	1.74E-08	3.16E-09	1.13E-09	1.90E-10	2.12E-11	2.10E-11	5.05E-12	8.50E-13
0.50	6.06E-07	1.31E-07	3.12E-08	7.49E-09	2.61E-09	5.34E-10	1.23E-10	9.81E-11	2.95E-11	1.69E-11
0.75	9.16E-07	1.90E-07	5.86E-08	1.86E-08	6.24E-09	1.58E-09	7.22E-10	4.85E-10	1.84E-10	3.42E-10
0.95	1.92E-06	3.76E-07	1.69E-07	7.91E-08	2.55E-08	8.82E-09	1.14E-08	5.43E-09	2.98E-09	3.23E-08
AOT										
Percentile	H1	H2	H3	H4	H5	H6	H7	H8	H9	H10
0.05	1.42E-06	3.45E-07	4.32E-08	5.31E-09	1.96E-09	2.45E-10	9.73E-12	1.32E-11	2.20E-12	6.53E-14
0.25	2.22E-06	5.05E-07	9.24E-08	1.68E-08	6.00E-09	1.01E-09	1.12E-10	1.12E-10	2.68E-11	4.51E-12
0.50	3.10E-06	6.73E-07	1.60E-07	3.84E-08	1.34E-08	2.74E-09	6.29E-10	5.02E-10	1.51E-10	8.64E-11
0.75	4.48E-06	9.28E-07	2.86E-07	9.10E-08	3.05E-08	7.73E-09	3.53E-09	2.37E-09	9.01E-10	1.67E-09
0.95	8.15E-06	1.59E-06	7.15E-07	3.35E-07	1.08E-07	3.74E-08	4.82E-08	2.30E-08	1.26E-08	1.37E-07
CBC										
Percentile	H1	H2	H3	H4	H5	H6	H7	H8	H9	H10
0.05	3.85E-07	9.38E-08	1.18E-08	1.44E-09	5.34E-10	6.66E-11	2.65E-12	3.59E-12	5.99E-13	1.78E-14
0.25	5.78E-07	1.32E-07	2.41E-08	4.37E-09	1.56E-09	2.63E-10	2.92E-11	2.91E-11	6.97E-12	1.17E-12
0.50	8.24E-07	1.79E-07	4.24E-08	1.02E-08	3.55E-09	7.26E-10	1.67E-10	1.33E-10	4.01E-11	2.29E-11
0.75	1.34E-06	2.77E-07	8.56E-08	2.72E-08	9.13E-09	2.31E-09	1.06E-09	7.09E-10	2.69E-10	5.00E-10
0.95	4.24E-06	8.27E-07	3.72E-07	1.74E-07	5.62E-08	1.94E-08	2.50E-08	1.20E-08	6.56E-09	7.12E-08
CLC										
Percentile	H1	H2	H3	H4	H5	H6	H7	H8	H9	H10
0.05	4.06E-07	9.91E-08	1.24E-08	1.52E-09	5.63E-10	7.03E-11	2.79E-12	3.79E-12	6.32E-13	1.88E-14
0.25	5.61E-07	1.28E-07	2.34E-08	4.24E-09	1.51E-09	2.55E-10	2.84E-11	2.82E-11	6.76E-12	1.14E-12
0.50	7.01E-07	1.52E-07	3.61E-08	8.67E-09	3.02E-09	6.18E-10	1.42E-10	1.13E-10	3.42E-11	1.95E-11
0.75	8.76E-07	1.81E-07	5.60E-08	1.78E-08	5.97E-09	1.51E-09	6.90E-10	4.64E-10	1.76E-10	3.27E-10
0.95	1.20E-06	2.35E-07	1.05E-07	4.95E-08	1.59E-08	5.52E-09	7.11E-09	3.40E-09	1.86E-09	2.02E-08

Table 5.7a: Distribution of observed diffusivity for organic carbon only sorption (D_{obs} (OC)) (m^2/yr) values as predicted by Monte Carlo simulation for PBDE homologs in all sediment cores.

CWP										
Percentile	H1	H2	H3	H4	H5	H6	H7	H8	H9	H10
0.05	6.24E-07	1.52E-07	1.91E-08	2.34E-09	8.65E-10	1.08E-10	4.29E-12	5.83E-12	9.71E-13	2.88E-14
0.25	8.65E-07	1.97E-07	3.60E-08	6.54E-09	2.33E-09	3.93E-10	4.37E-11	4.34E-11	1.04E-11	1.75E-12
0.50	1.09E-06	2.36E-07	5.61E-08	1.35E-08	4.69E-09	9.61E-10	2.21E-10	1.76E-10	5.31E-11	3.03E-11
0.75	1.38E-06	2.87E-07	8.84E-08	2.81E-08	9.43E-09	2.39E-09	1.09E-09	7.32E-10	2.78E-10	5.17E-10
0.95	1.98E-06	3.86E-07	1.74E-07	8.14E-08	2.62E-08	9.07E-09	1.17E-08	5.59E-09	3.06E-09	3.32E-08
IGC09										
Percentile	H1	H2	H3	H4	H5	H6	H7	H8	H9	H10
0.05	4.31E-07	1.05E-07	1.32E-08	1.62E-09	5.97E-10	7.45E-11	2.96E-12	4.02E-12	6.70E-13	1.99E-14
0.25	6.09E-07	1.38E-07	2.53E-08	4.60E-09	1.64E-09	2.77E-10	3.08E-11	3.06E-11	7.34E-12	1.24E-12
0.50	7.78E-07	1.69E-07	4.00E-08	9.62E-09	3.35E-09	6.86E-10	1.58E-10	1.26E-10	3.79E-11	2.16E-11
0.75	9.98E-07	2.07E-07	6.38E-08	2.03E-08	6.80E-09	1.72E-09	7.86E-10	5.28E-10	2.01E-10	3.73E-10
0.95	1.44E-06	2.80E-07	1.26E-07	5.90E-08	1.90E-08	6.58E-09	8.49E-09	4.05E-09	2.22E-09	2.41E-08
IGC13										
Percentile	H1	H2	H3	H4	H5	H6	H7	H8	H9	H10
0.05	3.85E-07	9.39E-08	1.18E-08	1.44E-09	5.34E-10	6.66E-11	2.65E-12	3.60E-12	5.99E-13	1.78E-14
0.25	5.68E-07	1.29E-07	2.36E-08	4.29E-09	1.53E-09	2.58E-10	2.87E-11	2.85E-11	6.84E-12	1.15E-12
0.50	7.51E-07	1.63E-07	3.87E-08	9.29E-09	3.23E-09	6.62E-10	1.52E-10	1.22E-10	3.66E-11	2.09E-11
0.75	1.01E-06	2.09E-07	6.44E-08	2.05E-08	6.86E-09	1.74E-09	7.94E-10	5.33E-10	2.02E-10	3.76E-10
0.95	1.56E-06	3.05E-07	1.37E-07	6.43E-08	2.07E-08	7.17E-09	9.24E-09	4.42E-09	2.42E-09	2.63E-08

Table 5.7b (Cont.): Distribution of observed diffusivity for organic carbon and black carbon sorptions (D_{obs} (OCBC)) (m^2/yr) values as predicted by Monte Carlo simulation for PBDE homologs in all sediment cores.

ACL										
Percentile	H1	H2	H3	H4	H5	H6	H7	H8	H9	H10
0.05	2.32E-09	7.42E-11	4.93E-13	3.12E-15	2.67E-16	1.78E-18	7.59E-22	1.30E-21	1.75E-23	3.99E-27
0.25	2.58E-08	4.94E-10	5.66E-12	6.51E-14	3.70E-15	3.76E-17	1.28E-19	6.62E-20	1.66E-21	1.84E-23
0.50	2.25E-07	2.70E-09	4.04E-11	6.47E-13	2.49E-14	3.03E-16	4.00E-18	7.79E-19	2.62E-20	4.19E-21
0.75	2.01E-06	1.53E-08	3.00E-10	6.69E-12	1.70E-13	2.56E-15	1.20E-16	9.81E-18	4.50E-19	9.39E-19
0.95	2.81E-06	1.21E-07	4.07E-09	1.64E-10	2.73E-12	6.47E-14	2.46E-14	5.67E-16	4.86E-17	5.29E-15
AED										
Percentile	H1	H2	H3	H4	H5	H6	H7	H8	H9	H10
0.05	2.88E-09	9.22E-11	6.12E-13	3.88E-15	3.32E-16	2.21E-18	9.42E-22	1.62E-21	2.18E-23	4.96E-27
0.25	3.35E-08	6.41E-10	7.34E-12	8.44E-14	4.80E-15	4.88E-17	1.66E-19	8.59E-20	2.15E-21	2.38E-23
0.50	3.11E-07	3.73E-09	5.59E-11	8.95E-13	3.44E-14	4.19E-16	5.53E-18	1.08E-18	3.63E-20	5.80E-21
0.75	3.16E-06	2.40E-08	4.72E-10	1.05E-11	2.67E-13	4.03E-15	1.89E-16	1.54E-17	7.06E-19	1.48E-18
0.95	9.46E-06	2.99E-07	1.01E-08	4.04E-10	6.75E-12	1.60E-13	6.08E-14	1.40E-15	1.20E-16	1.31E-14
AFR										
Percentile	H1	H2	H3	H4	H5	H6	H7	H8	H9	H10
0.05	1.18E-08	3.79E-10	2.52E-12	1.60E-14	1.37E-15	9.11E-18	3.88E-21	6.67E-21	8.96E-23	2.04E-26
0.25	1.16E-07	2.22E-09	2.54E-11	2.92E-13	1.66E-14	1.69E-16	5.73E-19	2.97E-19	7.43E-21	8.24E-23
0.50	8.96E-07	1.08E-08	1.61E-10	2.58E-12	9.94E-14	1.21E-15	1.60E-17	3.11E-18	1.05E-19	1.67E-20
0.75	4.76E-06	5.23E-08	1.03E-09	2.29E-11	5.83E-13	8.79E-15	4.12E-16	3.36E-17	1.54E-18	3.22E-18
0.95	5.14E-06	2.96E-07	9.99E-09	4.01E-10	6.69E-12	1.59E-13	6.03E-14	1.39E-15	1.19E-16	1.30E-14
AJL										
Percentile	H1	H2	H3	H4	H5	H6	H7	H8	H9	H10
0.05	1.61E-09	5.16E-11	3.42E-13	2.17E-15	1.86E-16	1.24E-18	5.27E-22	9.07E-22	1.22E-23	2.78E-27
0.25	2.17E-08	4.15E-10	4.75E-12	5.46E-14	3.11E-15	3.16E-17	1.07E-19	5.56E-20	1.39E-21	1.54E-23
0.50	2.28E-07	2.74E-09	4.11E-11	6.57E-13	2.53E-14	3.08E-16	4.07E-18	7.92E-19	2.67E-20	4.26E-21
0.75	2.14E-06	2.09E-08	4.11E-10	9.16E-12	2.33E-13	3.51E-15	1.65E-16	1.34E-17	6.16E-19	1.29E-18
0.95	6.57E-06	3.89E-07	1.31E-08	5.27E-10	8.79E-12	2.08E-13	7.92E-14	1.82E-15	1.56E-16	1.70E-14

Table 5.7b (Cont.): Distribution of observed diffusivity for organic carbon and black carbon sorptions (D_{obs} (OCBC)) (m^2/yr) values as predicted by Monte Carlo simulation for PBDE homologs in all sediment cores.

AMW										
Percentile	H1	H2	H3	H4	H5	H6	H7	H8	H9	H10
0.05	4.32E-10	1.38E-11	9.18E-14	5.82E-16	4.98E-17	3.32E-19	1.41E-22	2.43E-22	3.27E-24	7.45E-28
0.25	6.08E-09	1.16E-10	1.33E-12	1.53E-14	8.71E-16	8.85E-18	3.01E-20	1.56E-20	3.90E-22	4.32E-24
0.50	6.45E-08	7.74E-10	1.16E-11	1.86E-13	7.15E-15	8.70E-17	1.15E-18	2.24E-19	7.53E-21	1.20E-21
0.75	7.28E-07	5.52E-09	1.09E-10	2.42E-12	6.15E-14	9.28E-16	4.34E-17	3.55E-18	1.63E-19	3.40E-19
0.95	1.92E-06	6.80E-08	2.29E-09	9.21E-11	1.54E-12	3.64E-14	1.39E-14	3.19E-16	2.74E-17	2.98E-15
AOT										
Percentile	H1	H2	H3	H4	H5	H6	H7	H8	H9	H10
0.05	8.48E-10	2.72E-11	1.80E-13	1.14E-15	9.78E-17	6.52E-19	2.78E-22	4.77E-22	6.41E-24	1.46E-27
0.25	1.41E-08	2.70E-10	3.09E-12	3.55E-14	2.02E-15	2.05E-17	6.97E-20	3.62E-20	9.05E-22	1.00E-23
0.50	1.78E-07	2.13E-09	3.20E-11	5.12E-13	1.97E-14	2.40E-16	3.16E-18	6.17E-19	2.08E-20	3.32E-21
0.75	1.78E-07	2.13E-09	3.20E-11	5.12E-13	1.97E-14	2.40E-16	3.16E-18	6.17E-19	2.08E-20	3.32E-21
0.95	2.69E-06	2.04E-08	4.01E-10	8.92E-12	2.27E-13	3.42E-15	1.60E-16	1.31E-17	6.00E-19	1.25E-18
CBC										
Percentile	H1	H2	H3	H4	H5	H6	H7	H8	H9	H10
0.05	1.07E-10	3.43E-12	2.28E-14	1.44E-16	1.23E-17	8.24E-20	3.51E-23	6.03E-23	8.10E-25	1.85E-28
0.25	1.37E-09	2.63E-11	3.01E-13	3.46E-15	1.97E-16	2.00E-18	6.79E-21	3.52E-21	8.81E-23	9.77E-25
0.50	1.41E-08	1.69E-10	2.54E-12	4.06E-14	1.56E-15	1.90E-17	2.51E-19	4.89E-20	1.65E-21	2.63E-22
0.75	1.68E-07	1.27E-09	2.50E-11	5.57E-13	1.42E-14	2.13E-16	1.00E-17	8.17E-19	3.74E-20	7.82E-20
0.95	4.24E-06	2.23E-08	7.53E-10	3.02E-11	5.05E-13	1.20E-14	4.55E-15	1.05E-16	8.99E-18	9.79E-16
CLC										
Percentile	H1	H2	H3	H4	H5	H6	H7	H8	H9	H10
0.05	1.13E-10	3.62E-12	2.40E-14	1.52E-16	1.30E-17	8.70E-20	3.70E-23	6.36E-23	8.55E-25	1.95E-28
0.25	1.33E-09	2.55E-11	2.92E-13	3.36E-15	1.91E-16	1.94E-18	6.59E-21	3.42E-21	8.55E-23	9.49E-25
0.50	1.20E-08	1.44E-10	2.16E-12	3.45E-14	1.33E-15	1.62E-17	2.14E-19	4.16E-20	1.40E-21	2.24E-22
0.75	1.10E-07	8.32E-10	1.63E-11	3.64E-13	9.26E-15	1.40E-16	6.54E-18	5.34E-19	2.45E-20	5.12E-20
0.95	1.20E-06	6.34E-09	2.14E-10	8.58E-12	1.43E-13	3.39E-15	1.29E-15	2.97E-17	2.55E-18	2.78E-16

Table 5.7b (Cont.): Distribution of observed diffusivity for organic carbon and black carbon sorptions (D_{obs} (OCBC)) (m^2/yr) values as predicted by Monte Carlo simulation for PBDE homologs in all sediment cores.

CWP										
Percentile	H1	H2	H3	H4	H5	H6	H7	H8	H9	H10
0.05	9.69E-11	3.10E-12	2.06E-14	1.31E-16	1.12E-17	7.45E-20	3.17E-23	5.45E-23	7.33E-25	1.67E-28
0.25	1.05E-09	2.00E-11	2.29E-13	2.64E-15	1.50E-16	1.53E-18	5.18E-21	2.69E-21	6.72E-23	7.45E-25
0.50	8.81E-09	1.06E-10	1.59E-12	2.54E-14	9.77E-16	1.19E-17	1.57E-19	3.06E-20	1.03E-21	1.65E-22
0.75	7.48E-08	5.68E-10	1.12E-11	2.49E-13	6.32E-15	9.53E-17	4.46E-18	3.65E-19	1.67E-20	3.49E-20
0.95	8.34E-07	3.87E-09	1.30E-10	5.23E-12	8.73E-14	2.07E-15	7.88E-16	1.81E-17	1.56E-18	1.69E-16
IGC09										
Percentile	H1	H2	H3	H4	H5	H6	H7	H8	H9	H10
0.05	1.67E-10	5.33E-12	3.54E-14	2.24E-16	1.92E-17	1.28E-19	5.45E-23	9.37E-23	1.26E-24	2.87E-28
0.25	2.07E-09	3.96E-11	4.53E-13	5.21E-15	2.96E-16	3.01E-18	1.02E-20	5.31E-21	1.33E-22	1.47E-24
0.50	1.95E-08	2.34E-10	3.51E-12	5.61E-14	2.16E-15	2.63E-17	3.47E-19	6.76E-20	2.28E-21	3.64E-22
0.75	1.89E-07	1.43E-09	2.82E-11	6.28E-13	1.60E-14	2.41E-16	1.13E-17	9.21E-19	4.22E-20	8.82E-20
0.95	1.44E-06	1.23E-08	4.15E-10	1.67E-11	2.78E-13	6.59E-15	2.51E-15	5.77E-17	4.95E-18	5.39E-16
IGC13										
Percentile	H1	H2	H3	H4	H5	H6	H7	H8	H9	H10
0.05	8.15E-11	2.61E-12	1.73E-14	1.10E-16	9.39E-18	6.27E-20	2.67E-23	4.59E-23	6.16E-25	1.40E-28
0.25	1.07E-09	2.06E-11	2.35E-13	2.71E-15	1.54E-16	1.56E-18	5.31E-21	2.76E-21	6.89E-23	7.64E-25
0.50	1.07E-08	1.28E-10	1.92E-12	3.08E-14	1.18E-15	1.44E-17	1.90E-19	3.71E-20	1.25E-21	2.00E-22
0.75	1.10E-07	8.38E-10	1.65E-11	3.67E-13	9.33E-15	1.41E-16	6.59E-18	5.38E-19	2.47E-20	5.15E-20
0.95	1.56E-06	8.24E-09	2.78E-10	1.11E-11	1.86E-13	4.41E-15	1.68E-15	3.86E-17	3.31E-18	3.61E-16

Table 5.7c (Cont.): Distribution of observed diffusivity for organic carbon only sorption (D_{obs} (OC)) (m^2/yr) values as predicted by Monte Carlo simulation for PCB homologs in all sediment cores.

ACL										
Percentile	H1	H2	H3	H4	H5	H6	H7	H8	H9	H10
0.05	3.40E-06	9.25E-07	2.25E-07	6.92E-08	1.90E-08	5.08E-09	1.24E-09	2.79E-10	2.55E-11	8.90E-12
0.25	3.84E-06	1.05E-06	2.66E-07	8.52E-08	2.35E-08	6.88E-09	1.67E-09	5.37E-10	7.18E-11	2.50E-11
0.50	4.15E-06	1.14E-06	2.97E-07	9.81E-08	2.71E-08	8.45E-09	2.05E-09	8.46E-10	1.48E-10	5.11E-11
0.75	4.49E-06	1.23E-06	3.31E-07	1.13E-07	3.11E-08	1.04E-08	2.50E-09	1.33E-09	3.03E-10	1.03E-10
0.95	5.07E-06	1.38E-06	3.91E-07	1.39E-07	3.83E-08	1.41E-08	3.39E-09	2.57E-09	8.47E-10	2.89E-10
AED										
Percentile	H1	H2	H3	H4	H5	H6	H7	H8	H9	H10
0.05	2.67E-06	7.26E-07	1.76E-07	5.43E-08	1.49E-08	3.99E-09	9.72E-10	2.19E-10	2.00E-11	6.98E-12
0.25	3.67E-06	1.00E-06	2.54E-07	8.14E-08	2.24E-08	6.57E-09	1.60E-09	5.13E-10	6.86E-11	2.39E-11
0.50	4.83E-06	1.32E-06	3.46E-07	1.14E-07	3.15E-08	9.84E-09	2.39E-09	9.85E-10	1.72E-10	5.95E-11
0.75	6.99E-06	1.91E-06	5.16E-07	1.76E-07	4.84E-08	1.62E-08	3.89E-09	2.06E-09	4.72E-10	1.61E-10
0.95	1.71E-05	4.66E-06	1.32E-06	4.69E-07	1.29E-07	4.74E-08	1.14E-08	8.67E-09	2.85E-09	9.75E-10
AFR										
Percentile	H1	H2	H3	H4	H5	H6	H7	H8	H9	H10
0.05	8.15E-06	2.22E-06	5.39E-07	1.66E-07	4.54E-08	1.22E-08	2.97E-09	6.69E-10	6.12E-11	2.13E-11
0.25	8.75E-06	2.39E-06	6.08E-07	1.94E-07	5.35E-08	1.57E-08	3.82E-09	1.23E-09	1.64E-10	5.71E-11
0.50	9.08E-06	2.49E-06	6.51E-07	2.15E-07	5.93E-08	1.85E-08	4.49E-09	1.85E-09	3.24E-10	1.12E-10
0.75	9.32E-06	2.55E-06	6.88E-07	2.35E-07	6.45E-08	2.16E-08	5.19E-09	2.75E-09	6.30E-10	2.15E-10
0.95	9.27E-06	2.53E-06	7.16E-07	2.55E-07	7.01E-08	2.57E-08	6.19E-09	4.71E-09	1.55E-09	5.29E-10
AJL										
Percentile	H1	H2	H3	H4	H5	H6	H7	H8	H9	H10
0.05	1.49E-06	4.05E-07	9.84E-08	3.03E-08	8.30E-09	2.22E-09	5.42E-10	1.22E-10	1.12E-11	3.89E-12
0.25	2.07E-06	5.67E-07	1.44E-07	4.60E-08	1.27E-08	3.71E-09	9.05E-10	2.90E-10	3.88E-11	1.35E-11
0.50	2.77E-06	7.59E-07	1.99E-07	6.56E-08	1.81E-08	5.65E-09	1.37E-09	5.65E-10	9.88E-11	3.42E-11
0.75	4.18E-06	1.14E-06	3.09E-07	1.05E-07	2.89E-08	9.67E-09	2.33E-09	1.23E-09	2.83E-10	9.64E-11
0.95	1.19E-05	3.23E-06	9.15E-07	3.26E-07	8.96E-08	3.29E-08	7.92E-09	6.02E-09	1.98E-09	6.77E-10

Table 5.7c (Cont.): Distribution of observed diffusivity for organic carbon only sorption (D_{obs} (OC)) (m^2/yr) values as predicted by Monte Carlo simulation for PCB homologs in all sediment cores.

AMW										
Percentile	H1	H2	H3	H4	H5	H6	H7	H8	H9	H10
0.05	6.31E-07	1.72E-07	4.17E-08	1.28E-08	3.52E-09	9.42E-10	2.30E-10	5.18E-11	4.74E-12	1.65E-12
0.25	9.29E-07	2.54E-07	6.44E-08	2.06E-08	5.67E-09	1.66E-09	4.05E-10	1.30E-10	1.74E-11	6.05E-12
0.50	1.26E-06	3.45E-07	9.04E-08	2.99E-08	8.23E-09	2.57E-09	6.24E-10	2.57E-10	4.50E-11	1.56E-11
0.75	1.80E-06	4.91E-07	1.33E-07	4.51E-08	1.24E-08	4.15E-09	9.98E-10	5.30E-10	1.21E-10	4.13E-11
0.95	3.47E-06	9.47E-07	2.68E-07	9.53E-08	2.62E-08	9.62E-09	2.32E-09	1.76E-09	5.80E-10	1.98E-10
AOT										
Percentile	H1	H2	H3	H4	H5	H6	H7	H8	H9	H10
0.05	3.45E-06	9.38E-07	2.28E-07	7.01E-08	1.92E-08	5.15E-09	1.26E-09	2.83E-10	2.59E-11	9.02E-12
0.25	4.93E-06	1.35E-06	3.42E-07	1.09E-07	3.01E-08	8.83E-09	2.15E-09	6.90E-10	9.22E-11	3.21E-11
0.50	6.46E-06	1.77E-06	4.63E-07	1.53E-07	4.22E-08	1.32E-08	3.19E-09	1.32E-09	2.31E-10	7.97E-11
0.75	8.78E-06	2.40E-06	6.48E-07	2.21E-07	6.07E-08	2.03E-08	4.88E-09	2.59E-09	5.93E-10	2.02E-10
0.95	1.47E-05	4.01E-06	1.14E-06	4.04E-07	1.11E-07	4.08E-08	9.82E-09	7.47E-09	2.46E-09	8.40E-10
CBC										
Percentile	H1	H2	H3	H4	H5	H6	H7	H8	H9	H10
0.05	9.38E-07	2.55E-07	6.20E-08	1.91E-08	5.23E-09	1.40E-09	3.42E-10	7.69E-11	7.04E-12	2.45E-12
0.25	1.28E-06	3.51E-07	8.90E-08	2.85E-08	7.84E-09	2.30E-09	5.60E-10	1.80E-10	2.40E-11	8.36E-12
0.50	1.72E-06	4.70E-07	1.23E-07	4.06E-08	1.12E-08	3.50E-09	8.48E-10	3.50E-10	6.12E-11	2.12E-11
0.75	2.62E-06	7.18E-07	1.94E-07	6.60E-08	1.82E-08	6.07E-09	1.46E-09	7.74E-10	1.77E-10	6.04E-11
0.95	7.64E-06	2.08E-06	5.90E-07	2.10E-07	5.77E-08	2.12E-08	5.10E-09	3.88E-09	1.28E-09	4.36E-10
CLC										
Percentile	H1	H2	H3	H4	H5	H6	H7	H8	H9	H10
0.05	9.90E-07	2.69E-07	6.54E-08	2.01E-08	5.52E-09	1.48E-09	3.61E-10	8.12E-11	7.43E-12	2.59E-12
0.25	1.25E-06	3.40E-07	8.64E-08	2.76E-08	7.61E-09	2.23E-09	5.43E-10	1.74E-10	2.33E-11	8.11E-12
0.50	1.46E-06	4.00E-07	1.05E-07	3.45E-08	9.53E-09	2.98E-09	7.22E-10	2.98E-10	5.21E-11	1.80E-11
0.75	1.72E-06	4.70E-07	1.27E-07	4.32E-08	1.19E-08	3.97E-09	9.55E-10	5.07E-10	1.16E-10	3.95E-11
0.95	2.17E-06	5.92E-07	1.67E-07	5.96E-08	1.64E-08	6.02E-09	1.45E-09	1.10E-09	3.62E-10	1.24E-10

Table 5.7c (Cont.): Distribution of observed diffusivity for organic carbon only sorption (D_{obs} (OC)) (m^2/yr) values as predicted by Monte Carlo simulation for PCB homologs in all sediment cores.

CWP										
Percentile	H1	H2	H3	H4	H5	H6	H7	H8	H9	H10
0.05	1.52E-06	4.13E-07	1.00E-07	3.09E-08	8.48E-09	2.27E-09	5.54E-10	1.25E-10	1.14E-11	3.98E-12
0.25	1.92E-06	5.24E-07	1.33E-07	4.26E-08	1.17E-08	3.44E-09	8.37E-10	2.69E-10	3.59E-11	1.25E-11
0.50	2.27E-06	6.21E-07	1.63E-07	5.37E-08	1.48E-08	4.62E-09	1.12E-09	4.63E-10	8.09E-11	2.80E-11
0.75	2.71E-06	7.41E-07	2.00E-07	6.82E-08	1.88E-08	6.27E-09	1.51E-09	8.00E-10	1.83E-10	6.24E-11
0.95	3.57E-06	9.74E-07	2.75E-07	9.80E-08	2.70E-08	9.90E-09	2.38E-09	1.81E-09	5.96E-10	2.04E-10
IGC09										
Percentile	H1	H2	H3	H4	H5	H6	H7	H8	H9	H10
0.05	1.05E-06	2.85E-07	6.93E-08	2.13E-08	5.85E-09	1.57E-09	3.82E-10	8.61E-11	7.88E-12	2.74E-12
0.25	1.35E-06	3.69E-07	9.37E-08	3.00E-08	8.25E-09	2.42E-09	5.89E-10	1.89E-10	2.53E-11	8.80E-12
0.50	1.62E-06	4.43E-07	1.16E-07	3.83E-08	1.06E-08	3.30E-09	8.00E-10	3.30E-10	5.78E-11	2.00E-11
0.75	1.95E-06	5.35E-07	1.44E-07	4.92E-08	1.35E-08	4.52E-09	1.09E-09	5.77E-10	1.32E-10	4.50E-11
0.95	2.59E-06	7.07E-07	2.00E-07	7.11E-08	1.96E-08	7.18E-09	1.73E-09	1.31E-09	4.32E-10	1.48E-10
IGC13										
Percentile	H1	H2	H3	H4	H5	H6	H7	H8	H9	H10
0.05	9.38E-07	2.55E-07	6.20E-08	1.91E-08	5.23E-09	1.40E-09	3.42E-10	7.70E-11	7.04E-12	2.45E-12
0.25	1.26E-06	3.44E-07	8.74E-08	2.79E-08	7.69E-09	2.26E-09	5.49E-10	1.76E-10	2.36E-11	8.20E-12
0.50	1.56E-06	4.28E-07	1.12E-07	3.70E-08	1.02E-08	3.19E-09	7.73E-10	3.19E-10	5.58E-11	1.93E-11
0.75	1.97E-06	5.40E-07	1.46E-07	4.96E-08	1.37E-08	4.56E-09	1.10E-09	5.83E-10	1.33E-10	4.55E-11
0.95	2.82E-06	7.70E-07	2.18E-07	7.75E-08	2.13E-08	7.82E-09	1.88E-09	1.43E-09	4.71E-10	1.61E-10

Table 5.7d(Cont.): Distribution of observed diffusivity for organic carbon and black carbon sorption (D_{obs} (OCBC)) (m^2/yr) values as predicted by Monte Carlo simulation for PCB homologs in all sediment cores.

ACL										
Percentile	H1	H2	H3	H4	H5	H6	H7	H8	H9	H10
0.05	7.76E-08	5.83E-09	3.45E-10	3.19E-11	2.39E-12	1.68E-13	1.04E-14	4.91E-16	4.52E-18	6.11E-19
0.25	6.80E-07	3.99E-08	1.91E-09	1.41E-10	8.04E-12	4.95E-13	2.58E-14	1.56E-15	2.38E-17	3.25E-18
0.50	4.15E-06	2.35E-07	8.90E-09	5.13E-10	2.23E-11	1.14E-12	4.95E-14	3.17E-15	6.48E-17	8.81E-18
0.75	4.49E-06	1.23E-06	4.27E-08	1.93E-09	6.32E-11	2.72E-12	9.72E-14	6.58E-15	1.81E-16	2.41E-17
0.95	5.07E-06	1.38E-06	2.79E-07	1.01E-08	2.51E-10	9.53E-12	2.87E-13	2.52E-14	1.11E-15	1.51E-16
AED										
Percentile	H1	H2	H3	H4	H5	H6	H7	H8	H9	H10
0.05	9.64E-08	7.24E-09	4.28E-10	3.96E-11	2.97E-12	2.08E-13	1.30E-14	6.10E-16	5.61E-18	7.59E-19
0.25	8.81E-07	5.17E-08	2.48E-09	1.82E-10	1.04E-11	6.42E-13	3.34E-14	2.02E-15	3.09E-17	4.21E-18
0.50	4.83E-06	3.25E-07	1.23E-08	7.10E-10	3.09E-11	1.58E-12	6.85E-14	4.39E-15	8.97E-17	1.22E-17
0.75	6.99E-06	1.91E-06	6.71E-08	3.03E-09	9.93E-11	4.27E-12	1.53E-13	1.03E-14	2.84E-16	3.79E-17
0.95	1.71E-05	4.66E-06	6.91E-07	2.50E-08	6.22E-10	2.36E-11	7.09E-13	6.24E-14	2.76E-15	3.73E-16
AFR										
Percentile	H1	H2	H3	H4	H5	H6	H7	H8	H9	H10
0.05	3.97E-07	2.98E-08	1.76E-09	1.63E-10	1.22E-11	8.57E-13	5.33E-14	2.51E-15	2.31E-17	3.12E-18
0.25	3.05E-06	1.79E-07	8.58E-09	6.31E-10	3.61E-11	2.22E-12	1.16E-13	7.00E-15	1.07E-16	1.46E-17
0.50	9.08E-06	9.38E-07	3.55E-08	2.05E-09	8.90E-11	4.56E-12	1.97E-13	1.27E-14	2.59E-16	3.51E-17
0.75	9.27E-06	2.55E-06	1.46E-07	6.61E-09	2.17E-10	9.31E-12	3.33E-13	2.25E-14	6.19E-16	8.27E-17
0.95	9.32E-06	2.53E-06	6.85E-07	2.48E-08	6.17E-10	2.34E-11	7.03E-13	6.19E-14	2.73E-15	3.70E-16
AJL										
Percentile	H1	H2	H3	H4	H5	H6	H7	H8	H9	H10
0.05	5.39E-08	4.05E-09	2.40E-10	2.22E-11	1.66E-12	1.17E-13	7.25E-15	3.41E-16	3.14E-18	4.25E-19
0.25	5.71E-07	3.35E-08	1.61E-09	1.18E-10	6.75E-12	4.16E-13	2.16E-14	1.31E-15	2.00E-17	2.73E-18
0.50	2.77E-06	2.39E-07	9.05E-09	5.22E-10	2.27E-11	1.16E-12	5.03E-14	3.22E-15	6.59E-17	8.95E-18
0.75	4.18E-06	1.14E-06	5.85E-08	2.64E-09	8.66E-11	3.72E-12	1.33E-13	9.01E-15	2.48E-16	3.30E-17
0.95	1.19E-05	3.23E-06	8.99E-07	3.26E-08	8.10E-10	3.07E-11	9.23E-13	8.12E-14	3.59E-15	4.86E-16

Table 5.7d(Cont.): Distribution of observed diffusivity for organic carbon and black carbon sorption (D_{obs} (OCBC)) (m^2/yr) values as predicted by Monte Carlo simulation for PCB homologs in all sediment cores.

AMW										
Percentile	H1	H2	H3	H4	H5	H6	H7	H8	H9	H10
0.05	1.45E-08	1.09E-09	6.44E-11	5.95E-12	4.45E-13	3.13E-14	1.95E-15	9.16E-17	8.42E-19	1.14E-19
0.25	1.60E-07	9.39E-09	4.50E-10	3.31E-11	1.89E-12	1.17E-13	6.07E-15	3.67E-16	5.60E-18	7.65E-19
0.50	1.26E-06	6.75E-08	2.56E-09	1.47E-10	6.40E-12	3.28E-13	1.42E-14	9.10E-16	1.86E-17	2.53E-18
0.75	1.80E-06	4.91E-07	1.54E-08	6.98E-10	2.29E-11	9.83E-13	3.52E-14	2.38E-15	6.54E-17	8.72E-18
0.95	3.47E-06	9.47E-07	1.57E-07	5.70E-09	1.42E-10	5.37E-12	1.61E-13	1.42E-14	6.27E-16	8.50E-17
AOT										
Percentile	H1	H2	H3	H4	H5	H6	H7	H8	H9	H10
0.05	2.84E-08	2.13E-09	1.26E-10	1.17E-11	8.74E-13	6.14E-14	3.82E-15	1.80E-16	1.65E-18	2.24E-19
0.25	3.71E-07	2.18E-08	1.04E-09	7.68E-11	4.39E-12	2.70E-13	1.41E-14	8.52E-16	1.30E-17	1.77E-18
0.50	4.08E-06	1.86E-07	7.05E-09	4.06E-10	1.77E-11	9.04E-13	3.92E-14	2.51E-15	5.13E-17	6.97E-18
0.75	8.78E-06	1.91E-06	5.70E-08	2.58E-09	8.44E-11	3.63E-12	1.30E-13	8.78E-15	2.41E-16	3.22E-17
0.95	1.47E-05	4.01E-06	1.14E-06	4.73E-08	1.18E-09	4.46E-11	1.34E-12	1.18E-13	5.21E-15	7.06E-16
CBC										
Percentile	H1	H2	H3	H4	H5	H6	H7	H8	H9	H10
0.05	3.59E-09	2.69E-10	1.60E-11	1.47E-12	1.10E-13	7.75E-15	4.82E-16	2.27E-17	2.09E-19	2.83E-20
0.25	3.62E-08	2.12E-09	1.02E-10	7.48E-12	4.28E-13	2.63E-14	1.37E-15	8.31E-17	1.27E-18	1.73E-19
0.50	3.24E-07	1.48E-08	5.59E-10	3.22E-11	1.40E-12	7.17E-14	3.11E-15	1.99E-16	4.07E-18	5.53E-19
0.75	2.62E-06	1.19E-07	3.55E-09	1.61E-10	5.26E-12	2.26E-13	8.09E-15	5.47E-16	1.50E-17	2.01E-18
0.95	7.64E-06	2.08E-06	5.17E-08	1.87E-09	4.65E-11	1.76E-12	5.30E-14	4.67E-15	2.06E-16	2.79E-17
CLC										
Percentile	H1	H2	H3	H4	H5	H6	H7	H8	H9	H10
0.05	3.79E-09	2.84E-10	1.68E-11	1.56E-12	1.17E-13	8.18E-15	5.09E-16	2.40E-17	2.20E-19	2.98E-20
0.25	3.51E-08	2.06E-09	9.88E-11	7.26E-12	4.15E-13	2.56E-14	1.33E-15	8.06E-17	1.23E-18	1.68E-19
0.50	2.76E-07	1.26E-08	4.76E-10	2.74E-11	1.19E-12	6.10E-14	2.64E-15	1.69E-16	3.46E-18	4.70E-19
0.75	1.72E-06	7.78E-08	2.33E-09	1.05E-10	3.44E-12	1.48E-13	5.29E-15	3.58E-16	9.84E-18	1.31E-18
0.95	2.17E-06	5.92E-07	1.47E-08	5.31E-10	1.32E-11	5.00E-13	1.50E-14	1.32E-15	5.85E-17	7.92E-18

Table 5.7d(Cont.): Distribution of observed diffusivity for organic carbon and black carbon sorption (D_{obs} (OCBC)) (m^2/yr) values as predicted by Monte Carlo simulation for PCB homologs in all sediment cores.

CWP										
Percentile	H1	H2	H3	H4	H5	H6	H7	H8	H9	H10
0.05	3.24E-09	2.44E-10	1.44E-11	1.33E-12	9.98E-14	7.01E-15	4.36E-16	2.05E-17	1.89E-19	2.56E-20
0.25	2.76E-08	1.62E-09	7.76E-11	5.70E-12	3.26E-13	2.01E-14	1.05E-15	6.33E-17	9.66E-19	1.32E-19
0.50	2.02E-07	9.23E-09	3.49E-10	2.01E-11	8.75E-13	4.48E-14	1.94E-15	1.24E-16	2.54E-18	3.45E-19
0.75	1.51E-06	5.31E-08	1.59E-09	7.17E-11	2.35E-12	1.01E-13	3.61E-15	2.44E-16	6.72E-18	8.96E-19
0.95	3.57E-06	3.67E-07	8.94E-09	3.24E-10	8.05E-12	3.05E-13	9.18E-15	8.08E-16	3.57E-17	4.83E-18
IGC09										
Percentile	H1	H2	H3	H4	H5	H6	H7	H8	H9	H10
0.05	5.58E-09	4.19E-10	2.48E-11	2.29E-12	1.72E-13	1.20E-14	7.50E-16	3.53E-17	3.24E-19	4.39E-20
0.25	5.44E-08	3.20E-09	1.53E-10	1.13E-11	6.44E-13	3.97E-14	2.06E-15	1.25E-16	1.91E-18	2.60E-19
0.50	4.48E-07	2.04E-08	7.73E-10	4.46E-11	1.94E-12	9.91E-14	4.29E-15	2.75E-16	5.63E-18	7.64E-19
0.75	1.95E-06	1.34E-07	4.01E-09	1.81E-10	5.93E-12	2.55E-13	9.12E-15	6.17E-16	1.70E-17	2.26E-18
0.95	2.59E-06	7.07E-07	2.84E-08	1.03E-09	2.56E-11	9.71E-13	2.92E-14	2.57E-15	1.14E-16	1.54E-17
IGC13										
Percentile	H1	H2	H3	H4	H5	H6	H7	H8	H9	H10
0.05	2.73E-09	2.05E-10	1.21E-11	1.12E-12	8.40E-14	5.89E-15	3.67E-16	1.73E-17	1.59E-19	2.15E-20
0.25	2.83E-08	1.66E-09	7.96E-11	5.85E-12	3.34E-13	2.06E-14	1.07E-15	6.49E-17	9.90E-19	1.35E-19
0.50	2.45E-07	1.12E-08	4.24E-10	2.44E-11	1.06E-12	5.43E-14	2.35E-15	1.51E-16	3.08E-18	4.19E-19
0.75	1.97E-06	7.83E-08	2.34E-09	1.06E-10	3.47E-12	1.49E-13	5.33E-15	3.61E-16	9.91E-18	1.32E-18
0.95	2.82E-06	7.70E-07	1.90E-08	6.90E-10	1.71E-11	6.50E-13	1.95E-14	1.72E-15	7.60E-17	1.03E-17

Table 5.8a(Cont.): Distribution of advective velocity for organic carbon only sorption (v (OC)) (m/yr) values as predicted by Monte Carlo simulation for PBDE homologs in all sediment cores.

ACL										
Percentile	H1	H2	H3	H4	H5	H6	H7	H8	H9	H10
0.05	1.56E-04	3.22E-05	1.52E-05	7.49E-06	2.52E-06	9.08E-07	5.14E-08	7.23E-08	1.25E-08	3.82E-10
0.25	1.22E-03	2.67E-04	8.66E-05	2.49E-05	9.63E-06	1.25E-06	3.02E-07	3.11E-07	7.74E-08	1.34E-08
0.50	2.80E-03	6.40E-04	1.60E-04	2.89E-05	1.01E-05	2.63E-06	7.43E-07	5.99E-07	1.92E-07	1.13E-07
0.75	4.57E-03	1.10E-03	1.94E-04	4.02E-05	1.47E-05	2.66E-06	1.21E-06	6.15E-07	3.40E-07	6.61E-07
0.95	5.71E-03	1.47E-03	2.11E-04	4.04E-05	1.50E-05	3.13E-06	1.26E-06	8.76E-07	3.45E-07	3.81E-06
AED										
Percentile	H1	H2	H3	H4	H5	H6	H7	H8	H9	H10
0.05	1.36E-04	2.81E-05	1.33E-05	6.53E-06	2.20E-06	7.92E-07	3.70E-08	5.20E-08	8.98E-09	2.75E-10
0.25	7.82E-04	1.71E-04	5.55E-05	1.79E-05	6.49E-06	8.99E-07	2.01E-07	2.07E-07	5.16E-08	8.95E-09
0.50	1.79E-03	4.09E-04	1.02E-04	1.85E-05	6.93E-06	1.71E-06	4.74E-07	3.92E-07	1.22E-07	7.21E-08
0.75	3.04E-03	7.30E-04	1.39E-04	2.57E-05	9.36E-06	1.75E-06	8.07E-07	5.22E-07	2.21E-07	4.24E-07
0.95	4.10E-03	1.06E-03	1.41E-04	2.68E-05	1.00E-05	2.00E-06	1.06E-06	5.62E-07	2.97E-07	3.32E-06
AFR										
Percentile	H1	H2	H3	H4	H5	H6	H7	H8	H9	H10
0.05	2.13E-05	4.38E-06	2.07E-06	1.02E-06	3.44E-07	1.24E-07	3.29E-08	4.63E-08	8.01E-09	2.45E-10
0.25	3.02E-04	6.60E-05	2.14E-05	7.15E-06	2.50E-06	6.60E-07	1.36E-07	8.15E-08	3.48E-08	6.05E-09
0.50	9.49E-04	2.17E-04	5.43E-05	1.37E-05	4.98E-06	8.02E-07	1.65E-07	1.40E-07	4.63E-08	3.83E-08
0.75	2.05E-03	4.93E-04	9.50E-05	1.60E-05	6.17E-06	1.06E-06	2.52E-07	2.09E-07	6.51E-08	1.63E-07
0.95	3.66E-03	9.41E-04	1.24E-04	1.81E-05	6.75E-06	1.18E-06	3.12E-07	2.17E-07	8.54E-08	5.18E-07
AJL										
Percentile	H1	H2	H3	H4	H5	H6	H7	H8	H9	H10
0.05	1.95E-05	4.03E-06	1.90E-06	9.37E-07	3.16E-07	1.06E-07	4.36E-09	6.13E-09	1.06E-09	3.24E-11
0.25	9.77E-05	2.14E-05	6.94E-06	2.12E-06	8.11E-07	1.14E-07	2.35E-08	2.42E-08	6.01E-09	1.04E-09
0.50	2.11E-04	4.83E-05	1.21E-05	2.31E-06	8.17E-07	2.04E-07	5.60E-08	4.63E-08	1.45E-08	8.51E-09
0.75	3.54E-04	8.51E-05	1.64E-05	3.04E-06	1.11E-06	2.14E-07	1.01E-07	7.02E-08	2.76E-08	5.29E-08
0.95	4.84E-04	1.25E-04	1.64E-05	3.12E-06	1.16E-06	2.36E-07	1.51E-07	7.49E-08	4.26E-08	4.76E-07

Table 5.8a(Cont.): Distribution of advective velocity for organic carbon only sorption (v (OC)) (m/yr) values as predicted by Monte Carlo simulation for PBDE homologs in all sediment cores.

Percentile	AMW									
	H1	H2	H3	H4	H5	H6	H7	H8	H9	H10
0.05	2.71E-05	5.59E-06	2.64E-06	1.30E-06	4.38E-07	1.58E-07	8.27E-09	1.16E-08	2.01E-09	6.15E-11
0.25	2.02E-04	4.42E-05	1.44E-05	4.02E-06	1.55E-06	2.01E-07	5.24E-08	5.39E-08	1.34E-08	2.33E-09
0.50	4.72E-04	1.08E-04	2.70E-05	4.79E-06	1.68E-06	4.42E-07	1.25E-07	1.04E-07	3.24E-08	1.91E-08
0.75	7.91E-04	1.90E-04	3.12E-05	6.81E-06	2.47E-06	4.55E-07	2.09E-07	1.04E-07	5.72E-08	1.10E-07
0.95	9.19E-04	2.36E-04	3.66E-05	6.97E-06	2.60E-06	5.27E-07	2.10E-07	1.45E-07	5.91E-08	6.61E-07
Percentile	AOT									
	H1	H2	H3	H4	H5	H6	H7	H8	H9	H10
0.05	1.14E-05	2.35E-06	1.11E-06	5.47E-07	1.84E-07	6.63E-08	5.34E-09	7.52E-09	1.30E-09	3.97E-11
0.25	1.00E-04	2.19E-05	7.11E-06	2.37E-06	8.31E-07	1.30E-07	2.85E-08	2.93E-08	7.30E-09	1.27E-09
0.50	2.47E-04	5.65E-05	1.41E-05	2.59E-06	1.00E-06	2.19E-07	6.55E-08	4.38E-08	1.69E-08	9.96E-09
0.75	4.30E-04	1.03E-04	1.99E-05	3.56E-06	1.29E-06	2.48E-07	8.84E-08	5.42E-08	2.49E-08	5.42E-08
0.95	5.93E-04	1.53E-04	2.01E-05	3.79E-06	1.41E-06	2.76E-07	1.03E-07	7.19E-08	2.83E-08	2.78E-07
Percentile	CBC									
	H1	H2	H3	H4	H5	H6	H7	H8	H9	H10
0.05	9.23E-05	1.90E-05	9.00E-06	4.42E-06	1.49E-06	4.55E-07	1.87E-08	2.63E-08	4.55E-09	1.39E-10
0.25	4.30E-04	9.40E-05	3.05E-05	9.09E-06	3.51E-06	5.36E-07	9.92E-08	1.02E-07	2.54E-08	4.41E-09
0.50	8.96E-04	2.05E-04	5.13E-05	1.02E-05	3.57E-06	8.62E-07	2.38E-07	1.97E-07	6.14E-08	3.62E-08
0.75	1.50E-03	3.60E-04	6.92E-05	1.29E-05	4.70E-06	9.39E-07	4.44E-07	3.09E-07	1.22E-07	2.33E-07
0.95	2.08E-03	5.35E-04	7.05E-05	1.32E-05	4.92E-06	1.00E-06	7.15E-07	3.54E-07	2.01E-07	2.25E-06
Percentile	CLC									
	H1	H2	H3	H4	H5	H6	H7	H8	H9	H10
0.05	9.56E-07	1.97E-07	9.31E-08	4.58E-08	1.54E-08	5.55E-09	8.76E-10	1.23E-09	2.13E-10	6.51E-12
0.25	1.11E-05	2.44E-06	7.91E-07	2.64E-07	9.25E-08	2.13E-08	4.10E-09	3.66E-09	1.05E-09	1.82E-10
0.50	3.15E-05	7.21E-06	1.80E-06	4.25E-07	1.64E-07	2.43E-08	7.40E-09	4.23E-09	2.08E-09	1.27E-09
0.75	6.20E-05	1.49E-05	2.87E-06	4.54E-07	1.65E-07	3.52E-08	8.37E-09	6.92E-09	2.16E-09	6.04E-09
0.95	9.73E-05	2.50E-05	3.30E-06	5.46E-07	2.04E-07	3.57E-08	1.15E-08	8.00E-09	3.15E-09	2.33E-08

Table 5.8a(Cont.): Distribution of advective velocity for organic carbon only sorption (v (OC)) (m/yr) values as predicted by Monte Carlo simulation for PBDE homologs in all sediment cores.

CWP										
Percentile	H1	H2	H3	H4	H5	H6	H7	H8	H9	H10
0.05	1.22E-05	2.52E-06	1.19E-06	5.86E-07	1.97E-07	7.10E-08	9.77E-09	1.37E-08	2.37E-09	7.26E-11
0.25	1.33E-04	2.90E-05	9.44E-06	3.15E-06	1.10E-06	2.38E-07	4.68E-08	4.68E-08	1.20E-08	2.08E-09
0.50	3.66E-04	8.37E-05	2.09E-05	4.74E-06	1.83E-06	2.90E-07	9.46E-08	4.82E-08	2.51E-08	1.48E-08
0.75	7.07E-04	1.70E-04	3.27E-05	5.27E-06	1.92E-06	4.07E-07	9.71E-08	8.03E-08	2.66E-08	7.20E-08
0.95	1.08E-03	2.79E-04	3.68E-05	6.22E-06	2.32E-06	4.09E-07	1.37E-07	9.54E-08	3.76E-08	2.98E-07
IGC09										
Percentile	H1	H2	H3	H4	H5	H6	H7	H8	H9	H10
0.05	1.31E-05	2.70E-06	1.28E-06	6.28E-07	2.12E-07	7.61E-08	1.02E-08	1.44E-08	2.48E-09	7.58E-11
0.25	1.42E-04	3.10E-05	1.01E-05	3.35E-06	1.18E-06	2.48E-07	4.92E-08	5.02E-08	1.26E-08	2.19E-09
0.50	3.91E-04	8.93E-05	2.23E-05	4.95E-06	1.91E-06	3.10E-07	1.01E-07	5.07E-08	2.68E-08	1.58E-08
0.75	7.43E-04	1.78E-04	3.43E-05	5.63E-06	2.05E-06	4.28E-07	1.04E-07	8.58E-08	2.85E-08	7.67E-08
0.95	1.13E-03	2.91E-04	3.84E-05	6.54E-06	2.44E-06	4.36E-07	1.46E-07	1.02E-07	4.01E-08	3.19E-07
IGC13										
Percentile	H1	H2	H3	H4	H5	H6	H7	H8	H9	H10
0.05	2.58E-05	5.31E-06	2.51E-06	1.23E-06	4.16E-07	1.50E-07	1.66E-08	2.33E-08	4.02E-09	1.23E-10
0.25	2.58E-04	5.64E-05	1.83E-05	6.11E-06	2.14E-06	4.03E-07	8.37E-08	8.62E-08	2.14E-08	3.72E-09
0.50	6.82E-04	1.56E-04	3.90E-05	8.04E-06	3.10E-06	5.64E-07	1.81E-07	9.87E-08	4.68E-08	2.75E-08
0.75	1.26E-03	3.03E-04	5.84E-05	9.83E-06	3.58E-06	7.27E-07	1.99E-07	1.50E-07	5.61E-08	1.40E-07
0.95	1.84E-03	4.73E-04	6.24E-05	1.11E-05	4.15E-06	7.62E-07	2.66E-07	1.85E-07	7.30E-08	6.27E-07

Table 5.8b(Cont.): Distribution of advective velocity for organic carbon and black carbon sorptions (v (OCBC)) (m/yr) values as predicted by Monte Carlo simulation for PBDE homologs in all sediment cores.

ACL										
Percentile	H1	H2	H3	H4	H5	H6	H7	H8	H9	H10
0.05	9.47E-06	3.20E-07	2.24E-09	1.49E-11	1.33E-12	9.23E-15	4.06E-18	7.23E-18	1.01E-19	2.37E-23
0.25	6.81E-05	1.38E-06	1.66E-08	2.00E-10	1.19E-11	1.26E-13	4.41E-16	2.37E-16	6.15E-18	7.03E-20
0.50	1.56E-04	4.00E-06	6.31E-08	1.06E-09	4.26E-11	5.39E-13	7.37E-15	1.49E-15	5.19E-17	8.55E-18
0.75	3.16E-04	7.09E-06	1.78E-07	4.15E-09	1.10E-10	1.73E-12	8.37E-14	7.08E-15	3.37E-16	7.25E-16
0.95	1.07E-03	8.58E-06	2.52E-07	1.06E-08	1.85E-10	4.55E-12	1.79E-12	4.28E-14	3.80E-15	4.27E-13
AED										
Percentile	H1	H2	H3	H4	H5	H6	H7	H8	H9	H10
0.05	1.08E-05	3.64E-07	2.54E-09	1.69E-11	1.51E-12	1.05E-14	4.62E-18	8.23E-18	1.15E-19	2.69E-23
0.25	6.16E-05	1.24E-06	1.50E-08	1.81E-10	1.07E-11	1.14E-13	3.99E-16	2.14E-16	5.56E-18	6.35E-20
0.50	1.36E-04	3.03E-06	4.79E-08	8.03E-10	3.23E-11	4.09E-13	5.59E-15	1.13E-15	3.93E-17	6.48E-18
0.75	2.39E-04	4.54E-06	1.15E-07	2.68E-09	7.13E-11	1.12E-12	5.42E-14	4.58E-15	2.18E-16	4.69E-16
0.95	6.93E-04	5.55E-06	1.61E-07	6.79E-09	1.18E-10	2.92E-12	1.15E-12	2.74E-14	2.44E-15	2.73E-13
AFR										
Percentile	H1	H2	H3	H4	H5	H6	H7	H8	H9	H10
0.05	1.30E-05	4.38E-07	3.06E-09	2.03E-11	1.82E-12	1.26E-14	5.55E-18	9.89E-18	1.38E-19	3.24E-23
0.25	2.13E-05	1.22E-06	1.47E-08	1.77E-10	1.05E-11	1.11E-13	3.91E-16	2.10E-16	5.44E-18	6.22E-20
0.50	6.03E-05	1.29E-06	3.90E-08	6.55E-10	2.63E-11	3.33E-13	4.55E-15	9.19E-16	3.21E-17	5.29E-18
0.75	1.95E-04	2.47E-06	4.59E-08	1.69E-09	3.37E-11	7.06E-13	3.42E-14	2.89E-15	1.38E-16	2.96E-16
0.95	3.02E-04	3.50E-06	7.25E-08	1.93E-09	4.50E-11	8.31E-13	3.27E-13	7.80E-15	6.94E-16	7.79E-14
AJL										
Percentile	H1	H2	H3	H4	H5	H6	H7	H8	H9	H10
0.05	1.28E-06	4.32E-08	3.01E-10	2.01E-12	1.79E-13	1.24E-15	5.47E-19	9.75E-19	1.36E-20	3.19E-24
0.25	8.22E-06	1.66E-07	2.00E-09	2.41E-11	1.43E-12	1.52E-14	5.33E-17	2.86E-17	7.42E-19	8.48E-21
0.50	1.95E-05	4.59E-07	7.24E-09	1.22E-10	4.89E-12	6.18E-14	8.45E-16	1.70E-16	5.95E-18	9.81E-19
0.75	3.62E-05	1.01E-06	2.09E-08	4.89E-10	1.30E-11	2.04E-13	9.87E-15	8.35E-16	3.97E-17	8.54E-17
0.95	9.77E-05	1.22E-06	4.33E-08	1.82E-09	3.18E-11	7.84E-13	3.09E-13	7.36E-15	6.55E-16	7.35E-14

Table 5.8b(Cont.): Distribution of advective velocity for organic carbon and black carbon sorptions (v (OCBC)) (m/yr) values as predicted by Monte Carlo simulation for PBDE homologs in all sediment cores.

Percentile	AMW									
	H1	H2	H3	H4	H5	H6	H7	H8	H9	H10
0.05	1.53E-06	5.18E-08	3.62E-10	2.41E-12	2.15E-13	1.49E-15	6.57E-19	1.17E-18	1.63E-20	3.83E-24
0.25	1.15E-05	2.32E-07	2.79E-09	3.37E-11	2.00E-12	2.12E-14	7.44E-17	4.00E-17	1.04E-18	1.18E-20
0.50	2.71E-05	6.36E-07	1.00E-08	1.69E-10	6.78E-12	8.58E-14	1.17E-15	2.37E-16	8.26E-18	1.36E-18
0.75	5.02E-05	1.01E-06	2.66E-08	6.22E-10	1.65E-11	2.59E-13	1.26E-14	1.06E-15	5.05E-17	1.09E-16
0.95	1.61E-04	1.29E-06	3.59E-08	1.51E-09	2.64E-11	6.50E-13	2.56E-13	6.10E-15	5.43E-16	6.09E-14
Percentile	AOT									
	H1	H2	H3	H4	H5	H6	H7	H8	H9	H10
0.05	3.55E-07	1.20E-08	8.39E-11	5.58E-13	4.99E-14	3.46E-16	1.52E-19	2.71E-19	3.78E-21	8.88E-25
0.25	2.73E-06	5.52E-08	6.65E-10	8.02E-12	4.77E-13	5.04E-15	1.77E-17	9.51E-18	2.47E-19	2.82E-21
0.50	1.14E-05	1.79E-07	2.83E-09	4.74E-11	1.91E-12	2.41E-14	3.30E-16	6.65E-17	2.32E-18	3.83E-19
0.75	1.41E-05	4.81E-07	9.95E-09	2.32E-10	6.18E-12	9.69E-14	4.69E-15	3.97E-16	1.89E-17	4.06E-17
0.95	6.00E-05	8.35E-07	2.96E-08	1.25E-09	2.18E-11	5.36E-13	2.11E-13	5.04E-15	4.48E-16	5.03E-14
Percentile	CBC									
	H1	H2	H3	H4	H5	H6	H7	H8	H9	H10
0.05	5.78E-07	1.95E-08	1.37E-10	9.08E-13	8.12E-14	5.63E-16	2.48E-19	4.42E-19	6.16E-21	1.45E-24
0.25	3.56E-06	7.19E-08	8.66E-10	1.05E-11	6.21E-13	6.56E-15	2.31E-17	1.24E-17	3.21E-19	3.67E-21
0.50	1.53E-05	1.94E-07	3.07E-09	5.15E-11	2.07E-12	2.62E-14	3.58E-16	7.22E-17	2.52E-18	4.15E-19
0.75	5.38E-05	4.31E-07	8.91E-09	2.08E-10	5.53E-12	8.68E-14	4.20E-15	3.56E-16	1.69E-17	3.64E-17
0.95	9.23E-05	5.14E-07	1.82E-08	7.68E-10	1.34E-11	3.30E-13	1.30E-13	3.10E-15	2.76E-16	3.09E-14
Percentile	CLC									
	H1	H2	H3	H4	H5	H6	H7	H8	H9	H10
0.05	2.71E-08	9.15E-10	6.39E-12	4.25E-14	3.80E-15	2.64E-17	1.16E-20	2.07E-20	2.88E-22	6.76E-26
0.25	1.47E-07	2.97E-09	3.58E-11	4.32E-13	2.57E-14	2.72E-16	9.54E-19	5.12E-19	1.33E-20	1.52E-22
0.50	5.39E-07	5.32E-09	1.08E-10	1.81E-12	7.29E-14	9.22E-16	1.26E-17	2.54E-18	8.87E-20	1.46E-20
0.75	9.56E-07	6.84E-09	1.89E-10	5.40E-12	1.39E-13	2.25E-15	1.09E-16	9.22E-18	4.38E-19	9.44E-19
0.95	1.39E-06	1.12E-08	2.31E-10	7.95E-12	1.43E-13	3.42E-15	1.35E-15	3.21E-17	2.85E-18	3.20E-16

Table 5.8b(Cont.): Distribution of advective velocity for organic carbon and black carbon sorptions (v (OCBC)) (m/yr) values as predicted by Monte Carlo simulation for PBDE homologs in all sediment cores.

CWP										
Percentile	H1	H2	H3	H4	H5	H6	H7	H8	H9	H10
0.05	1.68E-07	5.69E-09	3.97E-11	2.64E-13	2.36E-14	1.64E-16	7.22E-20	1.29E-19	1.79E-21	4.21E-25
0.25	8.56E-07	1.73E-08	2.08E-10	2.51E-12	1.49E-13	1.58E-15	5.54E-18	2.98E-18	7.73E-20	8.83E-22
0.50	2.96E-06	2.52E-08	5.92E-10	9.93E-12	3.99E-13	5.05E-15	6.90E-17	1.39E-17	4.86E-19	8.01E-20
0.75	5.15E-06	3.75E-08	8.95E-10	2.78E-11	6.57E-13	1.16E-14	5.62E-16	4.75E-17	2.26E-18	4.86E-18
0.95	7.19E-06	5.75E-08	1.19E-09	3.77E-11	7.39E-13	1.62E-14	6.37E-15	1.52E-16	1.35E-17	1.52E-15
IGC09										
Percentile	H1	H2	H3	H4	H5	H6	H7	H8	H9	H10
0.05	4.38E-07	1.48E-08	1.03E-10	6.88E-13	6.15E-14	4.27E-16	1.88E-19	3.34E-19	4.66E-21	1.09E-24
0.25	2.53E-06	5.10E-08	6.14E-10	7.42E-12	4.40E-13	4.66E-15	1.64E-17	8.79E-18	2.28E-19	2.60E-21
0.50	9.79E-06	1.19E-07	1.96E-09	3.29E-11	1.32E-12	1.67E-14	2.28E-16	4.61E-17	1.61E-18	2.65E-19
0.75	1.31E-05	1.24E-07	4.21E-09	1.04E-10	2.76E-12	4.33E-14	2.10E-15	1.77E-16	8.43E-18	1.82E-17
0.95	2.68E-05	2.15E-07	4.45E-09	1.77E-10	3.09E-12	7.61E-14	3.00E-14	7.14E-16	6.36E-17	7.13E-15
IGC13										
Percentile	H1	H2	H3	H4	H5	H6	H7	H8	H9	H10
0.05	3.89E-07	1.31E-08	9.18E-11	6.11E-13	5.46E-14	3.79E-16	1.67E-19	2.97E-19	4.14E-21	9.72E-25
0.25	2.39E-06	4.83E-08	5.82E-10	7.02E-12	4.17E-13	4.41E-15	1.55E-17	8.32E-18	2.16E-19	2.47E-21
0.50	9.70E-06	1.23E-07	1.94E-09	3.26E-11	1.31E-12	1.66E-14	2.26E-16	4.57E-17	1.59E-18	2.63E-19
0.75	2.58E-05	1.43E-07	4.69E-09	1.10E-10	2.91E-12	4.57E-14	2.21E-15	1.87E-16	8.89E-18	1.92E-17
0.95	2.83E-05	2.27E-07	5.08E-09	2.14E-10	3.73E-12	9.20E-14	3.62E-14	8.63E-16	7.68E-17	8.62E-15

Table 5.8c (Cont.): Distribution of advective velocity for organic carbon only sorption (v (OC)) (m/yr) values as predicted by Monte Carlo simulation for PCB homologs in all sediment cores.

ACL										
Percentile	H1	H2	H3	H4	H5	H6	H7	H8	H9	H10
0.05	2.82E-04	8.12E-05	2.42E-05	9.03E-06	2.59E-06	9.90E-07	2.47E-07	1.94E-07	6.63E-08	2.33E-08
0.25	2.39E-03	6.90E-04	1.96E-04	7.01E-05	2.01E-05	7.00E-06	1.74E-06	9.57E-07	1.47E-07	5.27E-08
0.50	5.83E-03	1.68E-03	4.64E-04	1.61E-04	4.63E-05	1.50E-05	3.77E-06	1.55E-06	2.27E-07	7.98E-08
0.75	1.01E-02	2.92E-03	7.81E-04	2.62E-04	7.53E-05	2.30E-05	5.79E-06	1.61E-06	2.67E-07	9.57E-08
0.95	1.39E-02	3.99E-03	1.02E-03	3.29E-04	9.44E-05	2.63E-05	6.63E-06	1.92E-06	2.93E-07	1.04E-07
AED										
Percentile	H1	H2	H3	H4	H5	H6	H7	H8	H9	H10
0.05	2.46E-04	7.08E-05	2.11E-05	7.87E-06	2.26E-06	8.64E-07	2.15E-07	1.69E-07	5.78E-08	2.04E-08
0.25	1.53E-03	4.42E-04	1.26E-04	4.49E-05	1.29E-05	4.49E-06	1.12E-06	6.14E-07	1.06E-07	3.79E-08
0.50	3.72E-03	1.07E-03	2.96E-04	1.03E-04	2.96E-05	9.60E-06	2.41E-06	1.03E-06	1.46E-07	5.12E-08
0.75	6.74E-03	1.95E-03	5.20E-04	1.74E-04	5.02E-05	1.53E-05	3.86E-06	1.11E-06	1.78E-07	6.37E-08
0.95	1.00E-02	2.87E-03	7.34E-04	2.37E-04	6.79E-05	1.89E-05	4.77E-06	1.28E-06	1.87E-07	6.65E-08
AFR										
Percentile	H1	H2	H3	H4	H5	H6	H7	H8	H9	H10
0.05	3.84E-05	1.10E-05	3.29E-06	1.23E-06	3.53E-07	1.35E-07	3.36E-08	2.64E-08	9.02E-09	3.18E-09
0.25	5.91E-04	1.71E-04	4.85E-05	1.73E-05	4.98E-06	1.73E-06	4.31E-07	2.37E-07	5.62E-08	1.98E-08
0.50	1.98E-03	5.71E-04	1.57E-04	5.45E-05	1.57E-05	5.10E-06	1.28E-06	5.47E-07	9.41E-08	3.38E-08
0.75	4.55E-03	1.31E-03	3.51E-04	1.18E-04	3.39E-05	1.03E-05	2.60E-06	8.66E-07	9.93E-08	3.54E-08
0.95	8.91E-03	2.56E-03	6.54E-04	2.11E-04	6.05E-05	1.69E-05	4.25E-06	9.92E-07	1.20E-07	4.31E-08
AJL										
Percentile	H1	H2	H3	H4	H5	H6	H7	H8	H9	H10
0.05	3.52E-05	1.01E-05	3.02E-06	1.13E-06	3.24E-07	1.24E-07	3.08E-08	2.43E-08	8.29E-09	2.92E-09
0.25	1.91E-04	5.53E-05	1.57E-05	5.61E-06	1.61E-06	5.61E-07	1.40E-07	7.67E-08	1.25E-08	4.47E-09
0.50	4.39E-04	1.27E-04	3.50E-05	1.21E-05	3.49E-06	1.13E-06	2.85E-07	1.22E-07	1.82E-08	6.40E-09
0.75	7.86E-04	2.27E-04	6.06E-05	2.03E-05	5.85E-06	1.78E-06	4.49E-07	1.31E-07	2.07E-08	7.43E-09
0.95	1.18E-03	3.38E-04	8.66E-05	2.79E-05	8.01E-06	2.23E-06	5.63E-07	1.49E-07	2.21E-08	7.86E-09

Table 5.8c (Cont.): Distribution of advective velocity for organic carbon only sorption (v (OC)) (m/yr) values as predicted by Monte Carlo simulation for PCB homologs in all sediment cores.

AMW										
Percentile	H1	H2	H3	H4	H5	H6	H7	H8	H9	H10
0.05	4.89E-05	1.41E-05	4.19E-06	1.57E-06	4.50E-07	1.72E-07	4.28E-08	3.37E-08	1.15E-08	4.05E-09
0.25	3.96E-04	1.14E-04	3.25E-05	1.16E-05	3.34E-06	1.16E-06	2.89E-07	1.59E-07	2.36E-08	8.49E-09
0.50	9.84E-04	2.84E-04	7.83E-05	2.71E-05	7.81E-06	2.54E-06	6.37E-07	2.49E-07	3.77E-08	1.32E-08
0.75	1.75E-03	5.06E-04	1.35E-04	4.54E-05	1.31E-05	3.98E-06	1.00E-06	2.72E-07	4.62E-08	1.66E-08
0.95	2.24E-03	6.42E-04	1.64E-04	5.30E-05	1.52E-05	4.23E-06	1.07E-06	3.33E-07	4.94E-08	1.76E-08
AOT										
Percentile	H1	H2	H3	H4	H5	H6	H7	H8	H9	H10
0.05	2.06E-05	5.93E-06	1.77E-06	6.60E-07	1.90E-07	7.24E-08	1.80E-08	1.42E-08	4.84E-09	1.71E-09
0.25	1.96E-04	5.66E-05	1.61E-05	5.75E-06	1.65E-06	5.75E-07	1.43E-07	7.86E-08	1.53E-08	5.48E-09
0.50	5.14E-04	1.48E-04	4.09E-05	1.42E-05	4.08E-06	1.33E-06	3.33E-07	1.42E-07	1.87E-08	6.55E-09
0.75	9.54E-04	2.75E-04	7.36E-05	2.47E-05	7.10E-06	2.17E-06	5.46E-07	1.61E-07	2.51E-08	9.02E-09
0.95	1.44E-03	4.15E-04	1.06E-04	3.42E-05	9.81E-06	2.73E-06	6.90E-07	1.81E-07	2.58E-08	9.19E-09
CBC										
Percentile	H1	H2	H3	H4	H5	H6	H7	H8	H9	H10
0.05	1.66E-04	4.79E-05	1.43E-05	5.33E-06	1.53E-06	5.85E-07	1.46E-07	1.15E-07	3.91E-08	1.38E-08
0.25	8.42E-04	2.43E-04	6.91E-05	2.47E-05	7.10E-06	2.47E-06	6.14E-07	3.37E-07	5.35E-08	1.92E-08
0.50	1.87E-03	5.39E-04	1.49E-04	5.15E-05	1.48E-05	4.82E-06	1.21E-06	5.17E-07	8.01E-08	2.81E-08
0.75	3.32E-03	9.58E-04	2.56E-04	8.59E-05	2.47E-05	7.54E-06	1.90E-06	5.64E-07	8.75E-08	3.14E-08
0.95	5.06E-03	1.45E-03	3.72E-04	1.20E-04	3.44E-05	9.58E-06	2.42E-06	6.31E-07	9.37E-08	3.34E-08
CLC										
Percentile	H1	H2	H3	H4	H5	H6	H7	H8	H9	H10
0.05	1.72E-06	4.96E-07	1.48E-07	5.52E-08	1.59E-08	6.06E-09	1.51E-09	1.19E-09	4.05E-10	1.43E-10
0.25	2.18E-05	6.30E-06	1.79E-06	6.40E-07	1.84E-07	6.39E-08	1.59E-08	8.74E-09	2.08E-09	7.29E-10
0.50	6.57E-05	1.90E-05	5.23E-06	1.81E-06	5.22E-07	1.69E-07	4.25E-08	1.82E-08	2.50E-09	8.99E-10
0.75	1.37E-04	3.96E-05	1.06E-05	3.56E-06	1.02E-06	3.12E-07	7.86E-08	2.61E-08	3.30E-09	1.17E-09
0.95	2.37E-04	6.80E-05	1.74E-05	5.61E-06	1.61E-06	4.48E-07	1.13E-07	2.64E-08	3.62E-09	1.30E-09

Table 5.8c (Cont.): Distribution of advective velocity for organic carbon only sorption (v (OC)) (m/yr) values as predicted by Monte Carlo simulation for PCB homologs in all sediment cores.

CWP										
Percentile	H1	H2	H3	H4	H5	H6	H7	H8	H9	H10
0.05	2.20E-05	6.35E-06	1.89E-06	7.06E-07	2.03E-07	7.74E-08	1.93E-08	1.52E-08	5.18E-09	1.82E-09
0.25	2.60E-04	7.52E-05	2.14E-05	7.63E-06	2.19E-06	7.62E-07	1.90E-07	1.04E-07	2.48E-08	8.70E-09
0.50	7.62E-04	2.20E-04	6.07E-05	2.10E-05	6.05E-06	1.97E-06	4.93E-07	2.11E-07	2.79E-08	1.00E-08
0.75	1.57E-03	4.52E-04	1.21E-04	4.05E-05	1.17E-05	3.56E-06	8.96E-07	2.94E-07	3.82E-08	1.36E-08
0.95	2.64E-03	7.58E-04	1.94E-04	6.26E-05	1.79E-05	5.00E-06	1.26E-06	2.98E-07	4.13E-08	1.48E-08
IGC09										
Percentile	H1	H2	H3	H4	H5	H6	H7	H8	H9	H10
0.05	2.36E-05	6.80E-06	2.03E-06	7.56E-07	2.17E-07	8.30E-08	2.07E-08	1.63E-08	5.55E-09	1.96E-09
0.25	2.78E-04	8.01E-05	2.28E-05	8.14E-06	2.34E-06	8.13E-07	2.02E-07	1.11E-07	2.64E-08	9.27E-09
0.50	8.13E-04	2.35E-04	6.48E-05	2.24E-05	6.46E-06	2.10E-06	5.27E-07	2.25E-07	2.92E-08	1.05E-08
0.75	1.65E-03	4.75E-04	1.27E-04	4.26E-05	1.23E-05	3.74E-06	9.42E-07	3.07E-07	4.08E-08	1.45E-08
0.95	2.76E-03	7.92E-04	2.03E-04	6.54E-05	1.87E-05	5.22E-06	1.32E-06	3.13E-07	4.34E-08	1.56E-08
IGC13										
Percentile	H1	H2	H3	H4	H5	H6	H7	H8	H9	H10
0.05	4.65E-05	1.34E-05	3.98E-06	1.49E-06	4.27E-07	1.63E-07	4.06E-08	3.20E-08	1.09E-08	3.84E-09
0.25	5.06E-04	1.46E-04	4.15E-05	1.48E-05	4.26E-06	1.48E-06	3.69E-07	2.03E-07	4.73E-08	1.69E-08
0.50	1.42E-03	4.11E-04	1.13E-04	3.92E-05	1.13E-05	3.67E-06	9.20E-07	3.93E-07	4.81E-08	1.70E-08
0.75	2.80E-03	8.08E-04	2.16E-04	7.25E-05	2.09E-05	6.36E-06	1.60E-06	4.99E-07	7.13E-08	2.54E-08
0.95	4.48E-03	1.29E-03	3.29E-04	1.06E-04	3.04E-05	8.47E-06	2.14E-06	5.33E-07	7.38E-08	2.65E-08

Table 5.8d(Cont.): Distribution of advective velocity for organic carbon and black carbon sorption (v (OCBC)) (m/yr) values as predicted by Monte Carlo simulation for PCB homologs in all sediment cores.

ACL										
Percentile	H1	H2	H3	H4	H5	H6	H7	H8	H9	H10
0.05	2.82E-04	2.51E-05	1.57E-06	1.52E-07	1.19E-08	6.71E-10	2.09E-11	1.90E-12	2.60E-14	3.62E-15
0.25	3.17E-04	8.12E-05	5.61E-06	4.32E-07	1.70E-08	8.68E-10	5.59E-11	2.72E-12	8.72E-14	1.22E-14
0.50	1.79E-03	1.11E-04	1.39E-05	6.56E-07	2.58E-08	1.65E-09	6.78E-11	4.75E-12	8.84E-14	1.24E-14
0.75	2.39E-03	3.49E-04	1.73E-05	8.41E-07	3.82E-08	1.83E-09	8.91E-11	5.59E-12	1.28E-13	1.80E-14
0.95	5.83E-03	6.90E-04	2.52E-05	1.20E-06	4.10E-08	2.03E-09	9.11E-11	6.05E-12	1.35E-13	1.86E-14
AED										
Percentile	H1	H2	H3	H4	H5	H6	H7	H8	H9	H10
0.05	2.46E-04	2.86E-05	1.78E-06	1.73E-07	1.09E-08	4.30E-10	1.34E-11	1.22E-12	2.96E-14	4.12E-15
0.25	3.61E-04	7.08E-05	5.07E-06	3.91E-07	1.35E-08	9.87E-10	4.39E-11	3.07E-12	5.58E-14	7.79E-15
0.50	1.53E-03	1.00E-04	1.05E-05	4.20E-07	2.33E-08	1.18E-09	6.36E-11	3.10E-12	7.99E-14	1.12E-14
0.75	1.62E-03	2.65E-04	1.10E-05	6.38E-07	2.65E-08	1.49E-09	6.91E-11	4.59E-12	8.76E-14	1.20E-14
0.95	3.72E-03	4.42E-04	1.63E-05	7.74E-07	2.90E-08	1.54E-09	8.05E-11	5.05E-12	9.73E-14	1.36E-14
AFR										
Percentile	H1	H2	H3	H4	H5	H6	H7	H8	H9	H10
0.05	3.84E-05	1.10E-05	2.14E-06	1.20E-07	3.11E-09	1.22E-10	3.81E-12	3.47E-13	1.59E-14	2.22E-15
0.25	4.34E-04	3.44E-05	3.15E-06	2.08E-07	1.63E-08	7.48E-10	2.77E-11	1.94E-12	3.55E-14	4.95E-15
0.50	5.91E-04	9.83E-05	4.96E-06	3.83E-07	1.67E-08	1.19E-09	5.63E-11	3.73E-12	5.53E-14	7.60E-15
0.75	1.59E-03	1.71E-04	8.60E-06	4.89E-07	2.29E-08	1.26E-09	7.64E-11	3.74E-12	7.82E-14	1.10E-14
0.95	1.98E-03	2.16E-04	1.03E-05	5.20E-07	2.36E-08	1.46E-09	7.88E-11	4.94E-12	7.93E-14	1.11E-14
AJL										
Percentile	H1	H2	H3	H4	H5	H6	H7	H8	H9	H10
0.05	3.52E-05	3.39E-06	2.11E-07	2.05E-08	1.60E-09	1.16E-10	3.60E-12	3.28E-13	3.50E-15	4.88E-16
0.25	4.27E-05	1.01E-05	6.77E-07	5.22E-08	2.93E-09	1.17E-10	7.53E-12	3.67E-13	1.07E-14	1.50E-15
0.50	1.91E-04	1.34E-05	1.59E-06	9.65E-08	3.12E-09	2.00E-10	7.98E-12	5.59E-13	1.47E-14	2.06E-15
0.75	2.16E-04	4.00E-05	2.97E-06	1.13E-07	4.38E-09	2.16E-10	1.05E-11	6.74E-13	1.50E-14	2.10E-15
0.95	4.39E-04	5.53E-05	2.97E-06	1.41E-07	4.83E-09	2.33E-10	1.07E-11	6.94E-13	1.59E-14	2.19E-15

Table 5.8d(Cont.): Distribution of advective velocity for organic carbon and black carbon sorption (v (OCBC)) (m/yr) values as predicted by Monte Carlo simulation for PCB homologs in all sediment cores.

AMW										
Percentile	H1	H2	H3	H4	H5	H6	H7	H8	H9	H10
0.05	4.89E-05	4.07E-06	2.54E-07	2.46E-08	1.92E-09	9.58E-11	2.98E-12	2.72E-13	4.20E-15	5.86E-16
0.25	5.13E-05	1.41E-05	9.45E-07	7.29E-08	2.43E-09	1.40E-10	9.04E-12	4.41E-13	1.24E-14	1.74E-15
0.50	3.02E-04	1.87E-05	2.21E-06	9.36E-08	4.35E-09	2.75E-10	1.02E-11	7.12E-13	1.49E-14	2.09E-15
0.75	3.96E-04	5.55E-05	2.46E-06	1.34E-07	6.08E-09	2.79E-10	1.45E-11	9.42E-13	2.03E-14	2.79E-15
0.95	9.84E-04	1.14E-04	3.79E-06	1.80E-07	6.15E-09	3.24E-10	1.50E-11	9.62E-13	2.04E-14	2.86E-15
AOT										
Percentile	H1	H2	H3	H4	H5	H6	H7	H8	H9	H10
0.05	1.19E-05	9.43E-07	5.88E-08	5.70E-09	4.46E-10	3.26E-11	2.10E-12	1.02E-13	9.75E-16	1.36E-16
0.25	2.06E-05	4.45E-06	2.25E-07	1.73E-08	1.04E-09	6.63E-11	2.46E-12	2.24E-13	3.54E-15	4.98E-16
0.50	7.19E-05	5.93E-06	6.22E-07	3.76E-08	1.71E-09	7.91E-11	3.57E-12	2.24E-13	5.74E-15	8.03E-16
0.75	1.96E-04	1.56E-05	1.42E-06	6.71E-08	2.01E-09	9.10E-11	3.80E-12	2.66E-13	7.58E-15	1.04E-15
0.95	3.24E-04	4.50E-05	1.77E-06	7.73E-08	2.30E-09	1.03E-10	4.08E-12	2.71E-13	1.03E-14	1.43E-15
CBC										
Percentile	H1	H2	H3	H4	H5	H6	H7	H8	H9	H10
0.05	1.94E-05	1.54E-06	9.57E-08	9.28E-09	7.26E-10	4.86E-11	1.51E-12	1.38E-13	1.59E-15	2.21E-16
0.25	9.36E-05	5.80E-06	2.93E-07	2.26E-08	1.23E-09	5.30E-11	3.40E-12	1.66E-13	4.62E-15	6.49E-16
0.50	1.66E-04	1.69E-05	6.76E-07	4.09E-08	1.35E-09	8.64E-11	3.41E-12	2.38E-13	6.23E-15	8.72E-16
0.75	3.52E-04	4.03E-05	1.25E-06	4.75E-08	1.86E-09	9.19E-11	4.43E-12	2.92E-13	6.32E-15	8.82E-16
0.95	8.42E-04	4.79E-05	1.27E-06	6.01E-08	2.06E-09	9.88E-11	4.65E-12	2.94E-13	6.79E-15	9.34E-16
CLC										
Percentile	H1	H2	H3	H4	H5	H6	H7	H8	H9	H10
0.05	9.06E-07	7.19E-08	4.48E-09	4.34E-10	1.28E-11	5.04E-13	1.57E-14	1.43E-15	6.54E-17	9.13E-18
0.25	1.72E-06	2.40E-07	1.21E-08	4.92E-10	3.40E-11	2.38E-12	8.82E-14	6.18E-15	7.42E-17	1.04E-17
0.50	3.87E-06	4.96E-07	1.29E-08	9.35E-10	5.33E-11	2.48E-12	1.56E-13	7.79E-15	1.76E-16	2.42E-17
0.75	1.24E-05	5.96E-07	2.38E-08	1.44E-09	5.58E-11	3.48E-12	1.60E-13	1.03E-14	1.91E-16	2.69E-17
0.95	2.18E-05	1.04E-06	3.29E-08	1.56E-09	6.53E-11	3.57E-12	1.92E-13	1.21E-14	2.19E-16	3.07E-17

Table 5.8d(Cont.): Distribution of advective velocity for organic carbon and black carbon sorption (v (OCBC)) (m/yr) values as predicted by Monte Carlo simulation for PCB homologs in all sediment cores.

CWP										
Percentile	H1	H2	H3	H4	H5	H6	H7	H8	H9	H10
0.05	5.64E-06	4.47E-07	2.78E-08	2.33E-09	6.05E-11	2.39E-12	7.42E-14	6.77E-15	3.10E-16	4.33E-17
0.25	2.20E-05	1.40E-06	6.13E-08	2.70E-09	2.11E-10	1.23E-11	4.55E-13	3.19E-14	4.62E-16	6.44E-17
0.50	2.25E-05	2.39E-06	7.04E-08	5.43E-09	2.75E-10	1.54E-11	8.54E-13	4.84E-14	9.08E-16	1.25E-16
0.75	6.79E-05	3.27E-06	1.30E-07	7.88E-09	3.24E-10	1.91E-11	9.93E-13	5.67E-14	1.11E-15	1.56E-16
0.95	1.45E-04	5.38E-06	1.69E-07	8.03E-09	3.58E-10	2.08E-11	1.12E-12	7.02E-14	1.20E-15	1.68E-16
IGC09										
Percentile	H1	H2	H3	H4	H5	H6	H7	H8	H9	H10
0.05	1.47E-05	1.16E-06	7.24E-08	7.03E-09	2.85E-10	1.12E-11	3.49E-13	3.18E-14	1.20E-15	1.68E-16
0.25	2.36E-05	4.12E-06	2.08E-07	1.10E-08	5.50E-10	4.01E-11	1.70E-12	1.19E-13	1.46E-15	2.03E-16
0.50	6.64E-05	6.80E-06	2.88E-07	1.60E-08	9.57E-10	4.59E-11	2.58E-12	1.26E-13	3.28E-15	4.61E-16
0.75	2.25E-04	1.08E-05	4.31E-07	2.61E-08	1.03E-09	6.13E-11	2.83E-12	1.88E-13	3.39E-15	4.66E-16
0.95	2.78E-04	2.01E-05	6.32E-07	3.00E-08	1.18E-09	6.31E-11	3.30E-12	2.07E-13	3.98E-15	5.57E-16
IGC13										
Percentile	H1	H2	H3	H4	H5	H6	H7	H8	H9	H10
0.05	1.30E-05	1.03E-06	6.43E-08	6.24E-09	3.44E-10	1.36E-11	4.22E-13	3.84E-14	1.07E-15	1.49E-16
0.25	4.65E-05	3.90E-06	1.97E-07	1.32E-08	4.88E-10	3.56E-11	1.79E-12	1.12E-13	1.76E-15	2.46E-16
0.50	6.29E-05	1.07E-05	3.48E-07	1.52E-08	9.07E-10	4.84E-11	2.29E-12	1.25E-13	3.10E-15	4.36E-16
0.75	2.23E-04	1.34E-05	4.27E-07	2.59E-08	1.08E-09	5.80E-11	2.80E-12	1.86E-13	3.57E-15	4.91E-16
0.95	5.06E-04	2.12E-05	6.67E-07	3.16E-08	1.17E-09	6.25E-11	3.13E-12	1.96E-13	3.94E-15	5.52E-16

Table D5.9 (Cont.): Summary of $C_{aq|x=0.02m,t}$ (ng/L), $C_{aq|x=0.02m,t}/C_{aq|x=0m,t=0year}$ (%), $C_{aq|x=0m,t}/C_{sat}$ (%), $M_{t|t}$ (ng/m²), and $M_{t|t}/M_{sed}$ (%) in all the sediment cores at the 95th percentile initial sediment concentration (36100 and 1640 ng/g for PBDE and PCB homologs, respectively) as predicted from the 95th percentile transport parameters values under advection-diffusion with organic carbon only sorption (A(OC)) at 40,100, and 1000 years in all sediment cores.

PBDE										
ACL										
40 years										
Time	H1	H2	H3	H4	H5	H6	H7	H8	H9	H10
Homolog										
$C_{aq x=0.02m,t}$	5.82E+04	2.84E+03	1.92E+02	2.28E+00	6.36E-07	7.15E-18	1.34E-25	1.74E-41	1.29E-75	2.52E-08
$C_{aq x=0.02m,t}/C_{aq x=0m,t=0year}$	53.52%	11.61%	1.66%	0.04%	0.00%	0.00%	0.00%	0.00%	0.00%	0.00%
$C_{aq x=0m,t}/C_{sat}$	4.84%	6.36%	17.16%	44.16%	76.79%	100.00%	100.00%	100.00%	100.00%	100.00%
$M_{t t}$	3.75E+06	3.78E+04	1.21E+03	7.05E+00	6.63E-07	3.54E-18	5.05E-26	4.30E-42	1.81E-76	3.96E-08
$M_{t t}/M_{sed}$	9.82%	0.05%	0.00%	0.00%	0.00%	0.00%	0.00%	0.00%	0.00%	0.00%
100 years										
Time										
$C_{aq x=0.02m,t}$	5.97E+04	9.74E+03	2.16E+03	2.70E+02	6.91E-01	6.46E-05	5.18E-08	5.91E-14	1.40E-25	1.63E-03
$C_{aq x=0.02m,t}/C_{aq x=0m,t=0year}$	73.49%	40.05%	18.70%	4.74%	0.04%	0.00%	0.00%	0.00%	0.00%	0.16%
$C_{aq x=0m,t}/C_{sat}$	3.61%	6.31%	17.15%	44.16%	76.79%	100.00%	100.00%	100.00%	100.00%	100.00%
$M_{t t}$	3.85E+06	1.12E+05	1.03E+04	4.87E+02	1.57E-01	1.26E-06	2.43E-10	1.56E-17	8.10E-32	7.54E-04
$M_{t t}/M_{sed}$	47.24%	0.51%	0.03%	0.00%	0.00%	0.00%	0.00%	0.00%	0.00%	0.00%
1000 years										
Time										
$C_{aq x=0.02m,t}$	1.67E+02	1.68E+04	8.05E+03	3.14E+03	4.71E+02	4.44E+01	3.52E+00	7.57E-02	8.09E-04	3.20E-01
$C_{aq x=0.02m,t}/C_{aq x=0m,t=0year}$	97.17%	84.36%	71.96%	55.36%	24.51%	7.40%	3.52%	0.76%	0.03%	31.98%
$C_{aq x=0m,t}/C_{sat}$	0.01%	5.17%	16.57%	43.92%	76.77%	100.00%	100.00%	100.00%	100.00%	100.00%
$M_{t t}$	1.08E+04	2.24E+05	5.06E+04	9.70E+03	4.91E+02	2.20E+01	1.32E+00	1.87E-02	1.14E-04	5.03E-01
$M_{t t}/M_{sed}$	100.00%	23.01%	3.55%	0.55%	0.02%	0.00%	0.00%	0.00%	0.00%	0.00%

Table D5.9 (Cont.): Summary of $C_{aq|x=0.02m,t}$ (ng/L), $C_{aq|x=0.02m,t}/C_{aq|x=0m,t=0year}$ (%), $C_{aq|x=0m,t}/C_{sat}$ (%), $M_{t|t}$ (ng/m²), and $M_{t|t}/M_{sed}$ (%) in all the sediment cores at the 95th percentile initial sediment concentration (36100 and 1640 ng/g for PBDE and PCB homologs, respectively) as predicted from the 95th percentile transport parameters values under advection-diffusion with organic carbon only sorption (A(OC)) at 40,100, and 1000 years in all sediment cores.

		AED									
		40 years									
Time	Homolog	H1	H2	H3	H4	H5	H6	H7	H8	H9	H10
	$C_{aq x=0.02m,t}$	7.08E-17	5.03E+04	5.65E+02	4.74E+00	8.18E-04	1.29E-17	2.26E-41	1.34E-57	9.50E-92	3.27E-167
	$C_{aq x=0.02m,t}/C_{aq x=0m,t=0year}$	100.00%	34.10%	1.75%	0.03%	0.00%	0.00%	0.00%	0.00%	0.00%	0.00%
	$C_{aq x=0m,t}/C_{sat}$	0.00%	6.57%	8.39%	22.64%	58.26%	100.00%	100.00%	100.00%	100.00%	100.00%
	$M_{t t}$	7.08E-17	3.40E+06	7.88E+03	3.13E+01	2.65E-03	1.41E-17	1.17E-41	5.28E-58	2.46E-92	4.81E-168
	$M_{t t}/M_{sed}$	5.36%	6.67%	0.01%	0.00%	0.00%	0.00%	0.00%	0.00%	0.00%	0.00%
		100 years									
	$C_{aq x=0.02m,t}$	1.57E-07	6.50E+04	5.05E+03	4.31E+02	8.14E+00	1.35E-05	2.68E-15	4.10E-22	4.82E-36	9.58E-66
	$C_{aq x=0.02m,t}/C_{aq x=0m,t=0year}$	100.00%	60.69%	15.68%	2.82%	0.11%	0.00%	0.00%	0.00%	0.00%	0.00%
	$C_{aq x=0m,t}/C_{sat}$	0.00%	4.76%	8.37%	22.64%	58.26%	100.00%	100.00%	100.00%	100.00%	100.00%
	$M_{t t}$	1.57E-07	4.42E+06	6.73E+04	2.60E+03	2.20E+01	8.64E-06	4.40E-16	3.39E-23	1.08E-37	1.64E-68
	$M_{t t}/M_{sed}$	5.64%	44.75%	0.22%	0.01%	0.00%	0.00%	0.00%	0.00%	0.00%	0.00%
		1000 years									
	$C_{aq x=0.02m,t}$	1.27E-01	3.13E+01	1.95E+04	8.53E+03	2.70E+03	1.92E+02	4.13E+00	1.48E-01	5.82E-04	1.36E-07
	$C_{aq x=0.02m,t}/C_{aq x=0m,t=0year}$	100.00%	95.59%	75.76%	57.65%	36.05%	7.66%	0.69%	0.15%	0.01%	0.00%
	$C_{aq x=0m,t}/C_{sat}$	12.68%	0.00%	6.68%	21.92%	58.03%	100.00%	100.00%	100.00%	100.00%	100.00%
	$M_{t t}$	1.27E-01	2.12E+03	2.72E+05	5.62E+04	8.75E+03	2.09E+02	2.14E+00	5.82E-02	1.51E-04	2.01E-08
	$M_{t t}/M_{sed}$	6.95%	100.00%	25.59%	3.29%	0.39%	0.01%	0.00%	0.00%	0.00%	0.00%

Table D5.9 (Cont.): Summary of $C_{aq|x=0.02m,t}$ (ng/L), $C_{aq|x=0.02m,t}/C_{aq|x=0m,t=0year}$ (%), $C_{aq|x=0m,t}/C_{sat}$ (%), $M_{t|t}$ (ng/m²), and $M_{t|t}/M_{sed}$ (%) in all the sediment cores at the 95th percentile initial sediment concentration (36100 and 1640 ng/g for PBDE and PCB homologs, respectively) as predicted from the 95th percentile transport parameters values under advection-diffusion with organic carbon only sorption (A(OC)) at 40,100, and 1000 years in all sediment cores.

Time Homolog	AFR 40 years									
	H1	H2	H3	H4	H5	H6	H7	H8	H9	H10
$C_{aq x=0.02m,t}$	4.11E+04	1.08E+03	3.42E+01	8.88E-02	6.43E-11	3.78E-35	8.38E-28	1.70E-59	2.33E-108	1.78E-11
$C_{aq x=0.02m,t}/C_{aq x=0m,t=0year}$	39.46%	5.00%	0.33%	0.00%	0.00%	0.00%	0.00%	0.00%	0.00%	0.00%
$C_{aq x=0m,t}/C_{sat}$	4.65%	5.62%	15.15%	38.99%	67.80%	100.00%	100.00%	100.00%	100.00%	100.00%
$M_{t t}$	4.34E+05	2.35E+03	3.52E+01	4.50E-02	1.10E-11	2.32E-36	6.87E-29	6.88E-61	5.37E-110	4.58E-12
$M_{t t}/M_{sed}$	0.90%	0.00%	0.00%	0.00%	0.00%	0.00%	0.00%	0.00%	0.00%	0.00%
Time Homolog	100 years									
	H1	H2	H3	H4	H5	H6	H7	H8	H9	H10
$C_{aq x=0.02m,t}$	6.03E+04	7.25E+03	1.50E+03	1.67E+02	2.82E-01	8.58E-08	1.63E-06	2.97E-15	7.00E-28	8.31E-04
$C_{aq x=0.02m,t}/C_{aq x=0m,t=0year}$	59.85%	33.55%	14.69%	3.32%	0.02%	0.00%	0.00%	0.00%	0.00%	0.08%
$C_{aq x=0m,t}/C_{sat}$	4.50%	5.61%	15.15%	38.99%	67.80%	100.00%	100.00%	100.00%	100.00%	100.00%
$M_{t t}$	6.37E+05	1.03E+04	6.81E+02	1.72E+01	5.02E-04	1.46E-14	6.21E-12	1.31E-25	8.66E-46	5.60E-06
$M_{t t}/M_{sed}$	4.32%	0.04%	0.00%	0.00%	0.00%	0.00%	0.00%	0.00%	0.00%	0.00%
Time Homolog	1000 years									
	H1	H2	H3	H4	H5	H6	H7	H8	H9	H10
$C_{aq x=0.02m,t}$	4.06E+04	1.51E+04	5.85E+03	2.03E+03	2.28E+02	6.24E+00	2.42E+00	1.07E-02	2.91E-05	1.86E-01
$C_{aq x=0.02m,t}/C_{aq x=0m,t=0year}$	88.59%	71.45%	57.42%	40.33%	13.47%	1.04%	2.42%	0.11%	0.00%	18.61%
$C_{aq x=0m,t}/C_{sat}$	2.05%	5.48%	15.09%	38.97%	67.80%	100.00%	100.00%	100.00%	100.00%	100.00%
$M_{t t}$	4.29E+05	3.29E+04	6.03E+03	1.03E+03	3.90E+01	3.83E-01	1.98E-01	4.35E-04	6.69E-07	4.79E-02
$M_{t t}/M_{sed}$	100.00%	2.43%	0.37%	0.05%	0.00%	0.00%	0.00%	0.00%	0.00%	0.00%

Table D5.9 (Cont.): Summary of $C_{aq|x=0.02m,t}$ (ng/L), $C_{aq|x=0.02m,t}/C_{aq|x=0m,t=0year}$ (%), $C_{aq|x=0m,t}/C_{sat}$ (%), $M_{t|t}$ (ng/m²), and $M_{t|t}/M_{sed}$ (%) in all the sediment cores at the 95th percentile initial sediment concentration (36100 and 1640 ng/g for PBDE and PCB homologs, respectively) as predicted from the 95th percentile transport parameters values under advection-diffusion with organic carbon only sorption (A(OC)) at 40,100, and 1000 years in all sediment cores.

		AJL									
		40 years									
Time	Homolog	H1	H2	H3	H4	H5	H6	H7	H8	H9	H10
	$C_{aq x=0.02m,t}$	2.42E+04	8.80E+02	4.47E+01	3.02E-01	9.49E-09	3.56E-21	7.34E-30	3.92E-48	1.17E-87	1.55E-09
	$C_{aq x=0.02m,t}/C_{aq x=0m,t=0year}$	43.97%	7.75%	0.83%	0.01%	0.00%	0.00%	0.00%	0.00%	0.00%	0.00%
	$C_{aq x=0m,t}/C_{sat}$	2.46%	2.95%	7.95%	20.47%	35.60%	70.47%	100.00%	100.00%	100.00%	100.00%
	$M_{t t}$	1.00E+05	7.51E+02	1.80E+01	6.00E-02	6.35E-10	1.13E-22	1.77E-31	6.22E-50	1.06E-89	1.56E-10
	$M_{t t}/M_{sed}$	0.22%	0.00%	0.00%	0.00%	0.00%	0.00%	0.00%	0.00%	0.00%	0.00%
		100 years									
	$C_{aq x=0.02m,t}$	3.44E+04	4.97E+03	1.31E+03	2.32E+02	2.30E+00	3.43E-03	1.87E-05	6.24E-10	3.07E-18	7.46E-03
	$C_{aq x=0.02m,t}/C_{aq x=0m,t=0year}$	62.91%	43.79%	24.43%	8.79%	0.26%	0.00%	0.00%	0.00%	0.00%	0.75%
	$C_{aq x=0m,t}/C_{sat}$	2.44%	2.95%	7.95%	20.47%	35.60%	70.47%	100.00%	100.00%	100.00%	100.00%
	$M_{t t}$	1.42E+05	2.58E+03	2.08E+02	7.78E+00	1.03E-03	2.71E-09	2.66E-13	1.90E-21	6.80E-38	1.36E-05
	$M_{t t}/M_{sed}$	0.96%	0.01%	0.00%	0.00%	0.00%	0.00%	0.00%	0.00%	0.00%	0.00%
		1000 years									
	$C_{aq x=0.02m,t}$	4.12E+04	8.29E+03	3.25E+03	1.18E+03	1.57E+02	1.90E+01	1.91E+00	3.27E-02	2.10E-04	2.31E-01
	$C_{aq x=0.02m,t}/C_{aq x=0m,t=0year}$	88.75%	73.36%	60.62%	44.71%	17.68%	4.50%	1.91%	0.33%	0.01%	23.15%
	$C_{aq x=0m,t}/C_{sat}$	2.07%	2.93%	7.95%	20.47%	35.60%	70.47%	100.00%	100.00%	100.00%	100.00%
	$M_{t t}$	1.70E+05	7.07E+03	1.31E+03	2.34E+02	1.05E+01	6.05E-01	4.61E-02	5.19E-04	1.90E-06	2.33E-02
	$M_{t t}/M_{sed}$	18.91%	0.52%	0.08%	0.01%	0.00%	0.00%	0.00%	0.00%	0.00%	0.00%

Table D5.9 (Cont.): Summary of $C_{aq|x=0.02m,t}$ (ng/L), $C_{aq|x=0.02m,t}/C_{aq|x=0m,t=0year}$ (%), $C_{aq|x=0m,t}/C_{sat}$ (%), $M_{t|t}$ (ng/m²), and $M_{t|t}/M_{sed}$ (%) in all the sediment cores at the 95th percentile initial sediment concentration (36100 and 1640 ng/g for PBDE and PCB homologs, respectively) as predicted from the 95th percentile transport parameters values under advection-diffusion with organic carbon only sorption (A(OC)) at 40,100, and 1000 years in all sediment cores.

		AMW									
		40 years									
Time	Homolog	H1	H2	H3	H4	H5	H6	H7	H8	H9	H10
	$C_{aq x=0.02m,t}$	2.30E+03	1.36E+00	1.61E-04	4.50E-12	8.09E-41	1.64E-90	1.08E-123	1.41E-195	0.00E+00	1.49E-34
	$C_{aq x=0.02m,t}/C_{aq x=0m,t=0year}$	11.90%	0.03%	0.00%	0.00%	0.00%	0.00%	0.00%	0.00%	0.00%	0.00%
	$C_{aq x=0m,t}/C_{sat}$	0.86%	1.03%	2.79%	7.18%	12.48%	24.71%	100.00%	100.00%	100.00%	100.00%
	$M_{t t}$	1.21E+04	1.48E+00	8.22E-05	1.13E-12	6.86E-42	6.62E-92	3.30E-125	2.83E-197	0.00E+00	1.90E-35
	$M_{t t}/M_{sed}$	0.02%	0.00%	0.00%	0.00%	0.00%	0.00%	0.00%	0.00%	0.00%	0.00%
Time		100 years									
	$C_{aq x=0.02m,t}$	6.46E+03	6.89E+02	7.46E+01	2.31E+00	2.75E-05	3.37E-13	2.09E-18	3.46E-30	5.08E-55	2.06E-06
	$C_{aq x=0.02m,t}/C_{aq x=0m,t=0year}$	33.45%	17.30%	3.96%	0.25%	0.00%	0.00%	0.00%	0.00%	0.00%	0.00%
	$C_{aq x=0m,t}/C_{sat}$	0.86%	1.03%	2.79%	7.18%	12.48%	24.71%	100.00%	100.00%	100.00%	100.00%
	$M_{t t}$	3.39E+04	1.05E+02	7.08E-01	1.78E-04	7.23E-17	2.32E-37	6.79E-51	1.73E-80	1.81E-145	1.20E-15
	$M_{t t}/M_{sed}$	0.16%	0.00%	0.00%	0.00%	0.00%	0.00%	0.00%	0.00%	0.00%	0.00%
Time		1000 years									
	$C_{aq x=0.02m,t}$	1.45E+04	2.00E+03	5.70E+02	1.16E+02	1.94E+00	7.07E-03	2.00E-04	2.38E-08	2.10E-15	1.55E-02
	$C_{aq x=0.02m,t}/C_{aq x=0m,t=0year}$	79.51%	50.27%	30.28%	12.55%	0.62%	0.00%	0.00%	0.00%	0.00%	1.55%
	$C_{aq x=0m,t}/C_{sat}$	0.81%	1.03%	2.79%	7.18%	12.48%	24.71%	100.00%	100.00%	100.00%	100.00%
	$M_{t t}$	7.59E+04	2.16E+03	2.92E+02	2.93E+01	1.64E-01	2.85E-04	6.10E-06	4.80E-10	2.40E-17	1.98E-03
	$M_{t t}/M_{sed}$	6.29%	0.12%	0.01%	0.00%	0.00%	0.00%	0.00%	0.00%	0.00%	0.00%

Table D5.9 (Cont.): Summary of $C_{aq|x=0.02m,t}$ (ng/L), $C_{aq|x=0.02m,t}/C_{aq|x=0m,t=0year}$ (%), $C_{aq|x=0m,t}/C_{sat}$ (%), $M_{t|t}$ (ng/m²), and $M_{t|t}/M_{sed}$ (%) in all the sediment cores at the 95th percentile initial sediment concentration (36100 and 1640 ng/g for PBDE and PCB homologs, respectively) as predicted from the 95th percentile transport parameters values under advection-diffusion with organic carbon only sorption (A(OC)) at 40,100, and 1000 years in all sediment cores.

AOT										
40 years										
Time	H1	H2	H3	H4	H5	H6	H7	H8	H9	H10
Homolog										
$C_{aq x=0.02m,t}$	2.57E+04	4.22E+02	6.78E+00	4.45E-03	1.44E-14	5.47E-34	1.69E-47	7.89E-76	4.04E-138	2.93E-14
$C_{aq x=0.02m,t}/C_{aq x=0m,t=0year}$	33.76%	2.68%	0.09%	0.00%	0.00%	0.00%	0.00%	0.00%	0.00%	0.00%
$C_{aq x=0m,t}/C_{sat}$	3.40%	4.09%	11.03%	28.40%	49.38%	97.74%	100.00%	100.00%	100.00%	100.00%
$M_{t t}$	2.75E+05	9.30E+02	7.07E+00	2.28E-03	2.48E-15	4.49E-35	1.05E-48	3.24E-77	9.42E-140	7.65E-15
$M_{t t}/M_{sed}$	0.53%	0.00%	0.00%	0.00%	0.00%	0.00%	0.00%	0.00%	0.00%	0.00%
100 years										
Time										
$C_{aq x=0.02m,t}$	4.13E+04	3.88E+03	6.02E+02	3.79E+01	7.15E-03	1.10E-08	4.33E-13	7.41E-22	7.18E-40	5.71E-05
$C_{aq x=0.02m,t}/C_{aq x=0m,t=0year}$	55.49%	24.67%	8.08%	1.03%	0.00%	0.00%	0.00%	0.00%	0.00%	0.01%
$C_{aq x=0m,t}/C_{sat}$	3.33%	4.09%	11.03%	28.40%	49.38%	97.74%	100.00%	100.00%	100.00%	100.00%
$M_{t t}$	4.42E+05	5.73E+03	2.86E+02	4.14E+00	1.37E-05	5.72E-14	5.42E-20	3.65E-32	1.03E-57	4.13E-07
$M_{t t}/M_{sed}$	2.78%	0.02%	0.00%	0.00%	0.00%	0.00%	0.00%	0.00%	0.00%	0.00%
1000 years										
Time										
$C_{aq x=0.02m,t}$	3.70E+04	1.06E+04	3.93E+03	1.27E+03	1.13E+02	6.97E+00	3.26E-01	2.18E-03	1.71E-06	1.36E-01
$C_{aq x=0.02m,t}/C_{aq x=0m,t=0year}$	87.65%	68.37%	52.87%	34.69%	9.13%	1.19%	0.33%	0.02%	0.00%	13.59%
$C_{aq x=0m,t}/C_{sat}$	1.89%	4.03%	11.01%	28.39%	49.38%	97.74%	100.00%	100.00%	100.00%	100.00%
$M_{t t}$	3.96E+05	2.34E+04	4.09E+03	6.51E+02	1.95E+01	5.72E-01	2.03E-02	8.95E-05	3.98E-08	3.54E-02
$M_{t t}/M_{sed}$	81.21%	1.64%	0.24%	0.03%	0.00%	0.00%	0.00%	0.00%	0.00%	0.00%

Table D5.9 (Cont.): Summary of $C_{aq|x=0.02m,t}$ (ng/L), $C_{aq|x=0.02m,t}/C_{aq|x=0m,t=0year}$ (%), $C_{aq|x=0m,t}/C_{sat}$ (%), $M_{t|t}$ (ng/m²), and $M_{t|t}/M_{sed}$ (%) in all the sediment cores at the 95th percentile initial sediment concentration (36100 and 1640 ng/g for PBDE and PCB homologs, respectively) as predicted from the 95th percentile transport parameters values under advection-diffusion with organic carbon only sorption (A(OC)) at 40,100, and 1000 years in all sediment cores.

Time Homolog	CBC 40 years									
	H1	H2	H3	H4	H5	H6	H7	H8	H9	H10
$C_{aq x=0.02m,t}$	1.33E+04	4.13E+01	5.33E-02	1.95E-07	7.21E-28	5.56E-63	9.22E-87	1.12E-137	4.31E-251	1.71E-24
$C_{aq x=0.02m,t}/C_{aq x=0m,t=0year}$	30.13%	0.45%	0.00%	0.00%	0.00%	0.00%	0.00%	0.00%	0.00%	0.00%
$C_{aq x=0m,t}/C_{sat}$	1.98%	2.38%	6.43%	16.54%	28.76%	56.94%	100.00%	100.00%	100.00%	100.00%
$M_{t t}$	3.85E+05	2.45E+02	1.50E-01	2.69E-07	3.36E-28	1.23E-63	1.55E-87	1.24E-138	2.70E-252	1.20E-24
$M_{t t}/M_{sed}$	0.60%	0.00%	0.00%	0.00%	0.00%	0.00%	0.00%	0.00%	0.00%	0.00%
Time	100 years									
	H1	H2	H3	H4	H5	H6	H7	H8	H9	H10
$C_{aq x=0.02m,t}$	2.69E+04	8.58E+02	3.17E+01	1.07E-01	1.93E-10	4.71E-25	4.15E-35	1.56E-56	3.34E-103	1.08E-10
$C_{aq x=0.02m,t}/C_{aq x=0m,t=0year}$	62.90%	9.35%	0.73%	0.01%	0.00%	0.00%	0.00%	0.00%	0.00%	0.00%
$C_{aq x=0m,t}/C_{sat}$	1.91%	2.38%	6.43%	16.54%	28.76%	56.94%	100.00%	100.00%	100.00%	100.00%
$M_{t t}$	7.75E+05	5.33E+03	9.74E+01	1.78E-01	1.57E-10	3.49E-25	3.61E-35	2.28E-56	2.31E-102	1.18E-10
$M_{t t}/M_{sed}$	4.37%	0.01%	0.00%	0.00%	0.00%	0.00%	0.00%	0.00%	0.00%	0.00%
Time	1000 years									
	H1	H2	H3	H4	H5	H6	H7	H8	H9	H10
$C_{aq x=0.02m,t}$	1.49E+04	7.40E+03	2.63E+03	7.13E+02	2.81E+01	4.14E-01	1.28E-02	1.09E-05	7.83E-11	8.36E-02
$C_{aq x=0.02m,t}/C_{aq x=0m,t=0year}$	99.39%	82.98%	60.86%	33.43%	3.91%	0.12%	0.01%	0.00%	0.00%	8.36%
$C_{aq x=0m,t}/C_{sat}$	0.67%	2.32%	6.40%	16.54%	28.76%	56.94%	100.00%	100.00%	100.00%	100.00%
$M_{t t}$	4.31E+05	4.40E+04	7.39E+03	9.86E+02	1.31E+01	9.16E-02	2.15E-03	1.20E-06	4.92E-12	5.87E-02
$M_{t t}/M_{sed}$	100.00%	2.92%	0.38%	0.04%	0.00%	0.00%	0.00%	0.00%	0.00%	0.00%

Table D5.9 (Cont.): Summary of $C_{aq|x=0.02m,t}$ (ng/L), $C_{aq|x=0.02m,t}/C_{aq|x=0m,t=0year}$ (%), $C_{aq|x=0m,t}/C_{sat}$ (%), $M_{t|t}$ (ng/m²), and $M_{t|t}/M_{sed}$ (%) in all the sediment cores at the 95th percentile initial sediment concentration (36100 and 1640 ng/g for PBDE and PCB homologs, respectively) as predicted from the 95th percentile transport parameters values under advection-diffusion with organic carbon only sorption (A(OC)) at 40,100, and 1000 years in all sediment cores.

CLC										
40 years										
Time	H1	H2	H3	H4	H5	H6	H7	H8	H9	H10
Homolog										
$C_{aq x=0.02m,t}$	7.37E+02	1.44E-02	1.00E-08	7.42E-21	1.08E-67	3.95E-149	1.58E-203	0.00E+00	0.00E+00	8.90E-56
$C_{aq x=0.02m,t}/C_{aq x=0m,t=0year}$	4.18%	0.00%	0.00%	0.00%	0.00%	0.00%	0.00%	0.00%	0.00%	0.00%
$C_{aq x=0m,t}/C_{sat}$	0.79%	0.94%	2.54%	6.54%	11.37%	22.51%	100.00%	100.00%	100.00%	100.00%
$M_{t t}$	3.54E+02	1.43E-03	4.68E-10	1.71E-22	8.41E-70	1.46E-151	4.42E-206	0.00E+00	0.00E+00	1.04E-57
$M_{t t}/M_{sed}$	0.00%	0.00%	0.00%	0.00%	0.00%	0.00%	0.00%	0.00%	0.00%	0.00%
100 years										
Time										
$C_{aq x=0.02m,t}$	3.50E+03	2.26E+02	9.19E+00	3.98E-02	2.17E-10	3.78E-24	3.13E-33	2.03E-53	2.79E-97	1.90E-10
$C_{aq x=0.02m,t}/C_{aq x=0m,t=0year}$	19.89%	6.22%	0.54%	0.00%	0.00%	0.00%	0.00%	0.00%	0.00%	0.00%
$C_{aq x=0m,t}/C_{sat}$	0.79%	0.94%	2.54%	6.54%	11.37%	22.51%	100.00%	100.00%	100.00%	100.00%
$M_{t t}$	1.68E+03	1.28E+00	1.08E-03	3.97E-09	9.27E-29	5.95E-62	5.98E-84	8.19E-132	3.84E-238	2.95E-25
$M_{t t}/M_{sed}$	0.01%	0.00%	0.00%	0.00%	0.00%	0.00%	0.00%	0.00%	0.00%	0.00%
1000 years										
Time										
$C_{aq x=0.02m,t}$	1.21E+04	1.30E+03	2.92E+02	3.77E+01	1.14E-01	2.20E-05	9.55E-08	1.69E-13	1.08E-24	1.67E-03
$C_{aq x=0.02m,t}/C_{aq x=0m,t=0year}$	68.89%	35.91%	17.00%	4.47%	0.04%	0.00%	0.00%	0.00%	0.00%	0.17%
$C_{aq x=0m,t}/C_{sat}$	0.78%	0.94%	2.54%	6.54%	11.37%	22.51%	100.00%	100.00%	100.00%	100.00%
$M_{t t}$	5.81E+03	1.29E+02	1.37E+01	8.70E-01	8.88E-04	8.11E-08	2.67E-10	3.11E-16	1.13E-27	1.95E-05
$M_{t t}/M_{sed}$	0.41%	0.01%	0.00%	0.00%	0.00%	0.00%	0.00%	0.00%	0.00%	0.00%

Table D5.9 (Cont.): Summary of $C_{aq|x=0.02m,t}$ (ng/L), $C_{aq|x=0.02m,t}/C_{aq|x=0m,t=0year}$ (%), $C_{aq|x=0m,t}/C_{sat}$ (%), $M_{t|t}$ (ng/m²), and $M_{t|t}/M_{sed}$ (%) in all the sediment cores at the 95th percentile initial sediment concentration (36100 and 1640 ng/g for PBDE and PCB homologs, respectively) as predicted from the 95th percentile transport parameters values under advection-diffusion with organic carbon only sorption (A(OC)) at 40,100, and 1000 years in all sediment cores.

CWP										
40 years										
Time	H1	H2	H3	H4	H5	H6	H7	H8	H9	H10
Homolog										
$C_{aq x=0.02m,t}$	2.30E+03	1.36E+00	1.61E-04	4.50E-12	8.09E-41	1.64E-90	1.08E-123	1.41E-195	0.00E+00	1.49E-34
$C_{aq x=0.02m,t}/C_{aq x=0m,t=0year}$	11.90%	0.03%	0.00%	0.00%	0.00%	0.00%	0.00%	0.00%	0.00%	0.00%
$C_{aq x=0m,t}/C_{sat}$	0.86%	1.03%	2.79%	7.18%	12.48%	24.71%	100.00%	100.00%	100.00%	100.00%
$M_{t t}$	1.21E+04	1.48E+00	8.22E-05	1.13E-12	6.86E-42	6.62E-92	3.30E-125	2.83E-197	0.00E+00	1.90E-35
$M_{t t}/M_{sed}$	0.02%	0.00%	0.00%	0.00%	0.00%	0.00%	0.00%	0.00%	0.00%	0.00%
100 years										
$C_{aq x=0.02m,t}$	6.46E+03	9.72E+01	1.38E+00	7.08E-04	8.53E-16	5.77E-36	2.22E-49	8.61E-79	1.58E-143	9.41E-15
$C_{aq x=0.02m,t}/C_{aq x=0m,t=0year}$	33.45%	2.44%	0.07%	0.00%	0.00%	0.00%	0.00%	0.00%	0.00%	0.00%
$C_{aq x=0m,t}/C_{sat}$	0.86%	1.03%	2.79%	7.18%	12.48%	24.71%	100.00%	100.00%	100.00%	100.00%
$M_{t t}$	3.39E+04	1.05E+02	7.08E-01	1.78E-04	7.23E-17	2.32E-37	6.79E-51	1.73E-80	1.81E-145	1.20E-15
$M_{t t}/M_{sed}$	0.16%	0.00%	0.00%	0.00%	0.00%	0.00%	0.00%	0.00%	0.00%	0.00%
1000 years										
$C_{aq x=0.02m,t}$	1.45E+04	2.00E+03	5.70E+02	1.16E+02	1.94E+00	7.07E-03	2.00E-04	2.38E-08	2.10E-15	1.55E-02
$C_{aq x=0.02m,t}/C_{aq x=0m,t=0year}$	79.51%	50.27%	30.28%	12.55%	0.62%	0.00%	0.00%	0.00%	0.00%	1.55%
$C_{aq x=0m,t}/C_{sat}$	0.81%	1.03%	2.79%	7.18%	12.48%	24.71%	100.00%	100.00%	100.00%	100.00%
$M_{t t}$	7.59E+04	2.16E+03	2.92E+02	2.93E+01	1.64E-01	2.85E-04	6.10E-06	4.80E-10	2.40E-17	1.98E-03
$M_{t t}/M_{sed}$	6.29%	0.12%	0.01%	0.00%	0.00%	0.00%	0.00%	0.00%	0.00%	0.00%

Table D5.9 (Cont.): Summary of $C_{aq|x=0.02m,t}$ (ng/L), $C_{aq|x=0.02m,t}/C_{aq|x=0m,t=0year}$ (%), $C_{aq|x=0m,t}/C_{sat}$ (%), $M_{t|t}$ (ng/m²), and $M_{t|t}/M_{sed}$ (%) in all the sediment cores at the 95th percentile initial sediment concentration (36100 and 1640 ng/g for PBDE and PCB homologs, respectively) as predicted from the 95th percentile transport parameters values under advection-diffusion with organic carbon only sorption (A(OC)) at 40,100, and 1000 years in all sediment cores.

IGC09										
40 years										
Time	H1	H2	H3	H4	H5	H6	H7	H8	H9	H10
Homolog										
$C_{aq x=0.02m,t}$	9.63E+02	1.41E-01	2.03E-06	7.50E-16	4.95E-52	8.99E-115	1.22E-156	4.12E-247	0.00E+00	3.31E-43
$C_{aq x=0.02m,t}/C_{aq x=0m,t=0year}$	8.68%	0.01%	0.00%	0.00%	0.00%	0.00%	0.00%	0.00%	0.00%	0.00%
$C_{aq x=0m,t}/C_{sat}$	0.50%	0.59%	1.60%	4.12%	7.17%	14.19%	64.59%	100.00%	100.00%	100.00%
$M_{t t}$	9.56E+03	2.89E-01	1.96E-06	3.57E-16	7.93E-53	6.84E-116	7.03E-158	1.57E-248	0.00E+00	7.99E-44
$M_{t t}/M_{sed}$	0.01%	0.00%	0.00%	0.00%	0.00%	0.00%	0.00%	0.00%	0.00%	0.00%
100 years										
Time										
$C_{aq x=0.02m,t}$	3.35E+03	3.87E+02	3.73E+01	9.05E-01	4.10E-06	9.25E-15	2.07E-20	4.64E-33	2.71E-60	7.39E-07
$C_{aq x=0.02m,t}/C_{aq x=0m,t=0year}$	30.26%	16.91%	3.45%	0.17%	0.00%	0.00%	0.00%	0.00%	0.00%	0.00%
$C_{aq x=0m,t}/C_{sat}$	0.50%	0.59%	1.60%	4.12%	7.17%	14.19%	64.59%	100.00%	100.00%	100.00%
$M_{t t}$	3.33E+04	5.82E+01	1.68E-01	7.49E-06	3.23E-21	6.27E-47	6.60E-64	8.08E-101	8.51E-183	8.03E-19
$M_{t t}/M_{sed}$	0.14%	0.00%	0.00%	0.00%	0.00%	0.00%	0.00%	0.00%	0.00%	0.00%
1000 years										
Time										
$C_{aq x=0.02m,t}$	8.60E+03	1.13E+03	2.93E+02	4.99E+01	4.15E-01	4.54E-04	6.46E-06	2.13E-10	3.74E-19	7.32E-03
$C_{aq x=0.02m,t}/C_{aq x=0m,t=0year}$	82.83%	49.25%	27.10%	9.39%	0.23%	0.00%	0.00%	0.00%	0.00%	0.73%
$C_{aq x=0m,t}/C_{sat}$	0.46%	0.59%	1.60%	4.12%	7.17%	14.19%	64.59%	100.00%	100.00%	100.00%
$M_{t t}$	8.53E+04	2.30E+03	2.83E+02	2.37E+01	6.65E-02	3.46E-05	3.73E-07	8.08E-12	8.09E-21	1.77E-03
$M_{t t}/M_{sed}$	6.96%	0.12%	0.01%	0.00%	0.00%	0.00%	0.00%	0.00%	0.00%	0.00%

Table D5.9 (Cont.): Summary of $C_{aq|x=0.02m,t}$ (ng/L), $C_{aq|x=0.02m,t}/C_{aq|x=0m,t=0year}$ (%), $C_{aq|x=0m,t}/C_{sat}$ (%), $M_{t|t}$ (ng/m²), and $M_{t|t}/M_{sed}$ (%) in all the sediment cores at the 95th percentile initial sediment concentration (36100 and 1640 ng/g for PBDE and PCB homologs, respectively) as predicted from the 95th percentile transport parameters values under advection-diffusion with organic carbon only sorption (A(OC)) at 40,100, and 1000 years in all sediment cores.

IGC13										
40 years										
Time	H1	H2	H3	H4	H5	H6	H7	H8	H9	H10
Homolog										
$C_{aq x=0.02m,t}$	1.26E+03	6.46E-01	6.09E-05	1.08E-12	3.09E-42	2.51E-93	2.15E-127	4.56E-201	0.00E+00	1.93E-35
$C_{aq x=0.02m,t}/C_{aq x=0m,t=0year}$	12.29%	0.03%	0.00%	0.00%	0.00%	0.00%	0.00%	0.00%	0.00%	0.00%
$C_{aq x=0m,t}/C_{sat}$	0.46%	0.55%	1.48%	3.81%	6.62%	13.10%	59.62%	100.00%	100.00%	100.00%
$M_{t t}$	1.26E+04	1.33E+00	5.93E-05	5.16E-13	4.99E-43	1.92E-94	1.25E-128	1.75E-202	0.00E+00	4.71E-36
$M_{t t}/M_{sed}$	0.02%	0.00%	0.00%	0.00%	0.00%	0.00%	0.00%	0.00%	0.00%	0.00%
100 years										
Time										
$C_{aq x=0.02m,t}$	3.61E+03	2.15E+02	1.27E+01	1.17E-01	1.17E-08	3.33E-20	8.56E-28	1.41E-44	3.05E-81	7.38E-09
$C_{aq x=0.02m,t}/C_{aq x=0m,t=0year}$	35.28%	10.19%	1.28%	0.02%	0.00%	0.00%	0.00%	0.00%	0.00%	0.00%
$C_{aq x=0m,t}/C_{sat}$	0.46%	0.55%	1.48%	3.81%	6.62%	13.10%	59.62%	100.00%	100.00%	100.00%
$M_{t t}$	3.61E+04	1.06E+02	6.53E-01	1.37E-04	2.68E-17	2.38E-38	3.31E-52	2.22E-82	3.49E-149	1.07E-15
$M_{t t}/M_{sed}$	0.17%	0.00%	0.00%	0.00%	0.00%	0.00%	0.00%	0.00%	0.00%	0.00%
1000 years										
Time										
$C_{aq x=0.02m,t}$	8.09E+03	1.13E+03	3.21E+02	6.45E+01	1.00E+00	3.23E-03	9.42E-05	1.57E-08	9.14E-16	1.57E-02
$C_{aq x=0.02m,t}/C_{aq x=0m,t=0year}$	84.23%	53.55%	32.13%	13.13%	0.61%	0.00%	0.00%	0.00%	0.00%	1.57%
$C_{aq x=0m,t}/C_{sat}$	0.43%	0.55%	1.48%	3.81%	6.62%	13.10%	59.62%	100.00%	100.00%	100.00%
$M_{t t}$	8.08E+04	2.32E+03	3.12E+02	3.09E+01	1.62E-01	2.47E-04	5.48E-06	6.02E-10	1.99E-17	3.82E-03
$M_{t t}/M_{sed}$	6.74%	0.13%	0.01%	0.00%	0.00%	0.00%	0.00%	0.00%	0.00%	0.00%

Table D5.9 (Cont.): Summary of $C_{aq|x=0.02m,t}$ (ng/L), $C_{aq|x=0.02m,t}/C_{aq|x=0m,t=0year}$ (%), $C_{aq|x=0m,t}/C_{sat}$ (%), $M_{t|t}$ (ng/m²), and $M_{t|t}/M_{sed}$ (%) in all the sediment cores at the 95th percentile initial sediment concentration (36100 and 1640 ng/g for PBDE and PCB homologs, respectively) as predicted from the 95th percentile transport parameters values under advection-diffusion with organic carbon only sorption (A(OC)) at 40,100, and 1000 years in all sediment cores.

PCB										
ACL										
40 years										
Time	H1	H2	H3	H4	H5	H6	H7	H8	H9	H10
Homolog										
C_{aq} (ng/L)	4.29E+03	9.69E+02	5.21E+01	4.61E-01	8.42E-08	1.48E-22	8.94E-94	4.41E-123	0.00E+00	0.00E+00
$(C_{aq x=0.02m}/C_{aq x=0m})$ (%)	67.19%	34.99%	6.24%	0.15%	0.00%	0.00%	0.00%	0.00%	0.00%	0.00%
C_{aq}/C_{sat} (%)	0.18%	0.29%	0.38%	0.65%	0.75%	1.32%	0.79%	5.32%	5.58%	1.87%
M_t (ng/m ²)	4.99E+05	3.25E+04	5.20E+02	1.72E+00	9.03E-08	6.07E-23	9.11E-95	3.54E-124	0.00E+00	0.00E+00
M_t/M_{sed} (%)	55.29%	1.35%	0.01%	0.00%	0.00%	0.00%	0.00%	0.00%	0.00%	0.00%
100 years										
Time										
Homolog										
C_{aq} (ng/L)	1.73E+03	1.50E+03	4.81E+02	9.84E+01	3.77E+00	2.14E-02	1.66E-11	4.48E-15	1.83E-44	6.96E-126
$(C_{aq x=0.02m}/C_{aq x=0m})$ (%)	82.85%	82.40%	58.90%	31.61%	4.21%	0.06%	0.00%	0.00%	0.00%	0.00%
C_{aq}/C_{sat} (%)	0.06%	0.19%	0.37%	0.65%	0.75%	1.32%	0.79%	5.32%	5.58%	1.87%
M_t (ng/m ²)	2.01E+05	5.18E+04	2.15E+03	5.65E+01	1.15E-02	2.37E-09	5.54E-39	6.63E-51	3.39E-150	0.00E+00
M_t/M_{sed} (%)	100.00%	7.55%	0.19%	0.00%	0.00%	0.00%	0.00%	0.00%	0.00%	0.00%
1000 years										
Time										
Homolog										
C_{aq} (ng/L)	1.52E-06	5.24E+02	6.02E+02	1.87E+02	2.31E+01	1.73E+00	3.69E-04	1.76E-05	5.51E-16	2.83E-44
$(C_{aq x=0.02m}/C_{aq x=0m})$ (%)	98.93%	93.57%	80.11%	60.36%	25.83%	5.07%	0.00%	0.00%	0.00%	0.00%
C_{aq}/C_{sat} (%)	0.00%	0.06%	0.34%	0.64%	0.75%	1.32%	0.79%	5.32%	5.58%	1.87%
M_t (ng/m ²)	1.77E-04	1.76E+04	6.01E+03	6.95E+02	2.48E+01	7.09E-01	3.76E-05	1.41E-06	1.51E-17	2.72E-46
M_t/M_{sed} (%)	100.00%	100.00%	11.18%	0.92%	0.02%	0.00%	0.00%	0.00%	0.00%	0.00%

Table D5.9 (Cont.): Summary of $C_{aq|x=0.02m,t}$ (ng/L), $C_{aq|x=0.02m,t}/C_{aq|x=0m,t=0year}$ (%), $C_{aq|x=0m,t}/C_{sat}$ (%), $M_{t|t}$ (ng/m²), and $M_{t|t}/M_{sed}$ (%) in all the sediment cores at the 95th percentile initial sediment concentration (36100 and 1640 ng/g for PBDE and PCB homologs, respectively) as predicted from the 95th percentile transport parameters values under advection-diffusion with organic carbon only sorption (A(OC)) at 40,100, and 1000 years in all sediment cores.

AED										
40 years										
Time	H1	H2	H3	H4	H5	H6	H7	H8	H9	H10
Homolog										
C_{aq} (ng/L)	4.57E+03	5.66E+02	5.43E+00	7.49E-04	6.13E-18	3.88E-50	3.66E-208	1.89E-273	0.00E+00	0.00E+00
$(C_{aq x=0.02m}/C_{aq x=0m})$ (%)	51.27%	15.39%	0.49%	0.00%	0.00%	0.00%	0.00%	0.00%	0.00%	0.00%
C_{aq}/C_{sat} (%)	0.25%	0.38%	0.50%	0.86%	0.99%	1.74%	1.04%	7.02%	7.37%	2.47%
M_t (ng/m ²)	5.57E+05	1.99E+04	5.68E+01	2.93E-03	6.88E-18	1.66E-50	3.91E-209	1.59E-274	0.00E+00	0.00E+00
M_t/M_{sed} (%)	46.86%	0.59%	0.00%	0.00%	0.00%	0.00%	0.00%	0.00%	0.00%	0.00%
100 years										
Time										
Homolog										
C_{aq} (ng/L)	1.78E+03	1.46E+03	5.18E+02	7.81E+01	9.22E-01	3.48E-04	4.16E-19	4.43E-25	1.01E-74	3.96E-213
$(C_{aq x=0.02m}/C_{aq x=0m})$ (%)	73.56%	78.14%	48.39%	18.99%	0.78%	0.00%	0.00%	0.00%	0.00%	0.00%
C_{aq}/C_{sat} (%)	0.07%	0.19%	0.49%	0.86%	0.99%	1.74%	1.04%	7.02%	7.37%	2.47%
M_t (ng/m ²)	2.17E+05	5.03E+04	9.86E+02	4.71E+00	1.07E-06	2.28E-20	1.01E-84	4.87E-111	0.00E+00	0.00E+00
M_t/M_{sed} (%)	100.00%	5.69%	0.06%	0.00%	0.00%	0.00%	0.00%	0.00%	0.00%	0.00%
1000 years										
Time										
Homolog										
C_{aq} (ng/L)	1.04E-09	4.56E+02	6.85E+02	1.72E+02	1.01E+01	1.43E-01	9.79E-09	1.69E-11	4.04E-34	1.68E-96
$(C_{aq x=0.02m}/C_{aq x=0m})$ (%)	98.35%	89.93%	69.39%	42.19%	8.50%	0.32%	0.00%	0.00%	0.00%	0.00%
C_{aq}/C_{sat} (%)	0.00%	0.05%	0.45%	0.85%	0.99%	1.74%	1.04%	7.02%	7.37%	2.47%
M_t (ng/m ²)	1.27E-07	1.60E+04	7.16E+03	6.73E+02	1.13E+01	6.13E-02	1.05E-09	1.42E-12	1.16E-35	1.70E-98
M_t/M_{sed} (%)	100.00%	100.00%	11.65%	0.71%	0.01%	0.00%	0.00%	0.00%	0.00%	0.00%

Table D5.9 (Cont.): Summary of $C_{aq|x=0.02m,t}$ (ng/L), $C_{aq|x=0.02m,t}/C_{aq|x=0m,t=0year}$ (%), $C_{aq|x=0m,t}/C_{sat}$ (%), $M_{t|t}$ (ng/m²), and $M_{t|t}/M_{sed}$ (%) in all the sediment cores at the 95th percentile initial sediment concentration (36100 and 1640 ng/g for PBDE and PCB homologs, respectively) as predicted from the 95th percentile transport parameters values under advection-diffusion with organic carbon only sorption (A(OC)) at 40,100, and 1000 years in all sediment cores.

AFR										
40 years										
Time	H1	H2	H3	H4	H5	H6	H7	H8	H9	H10
Homolog										
C_{aq} (ng/L)	4.38E+03	5.52E+02	1.56E+01	3.09E-02	1.34E-11	1.42E-32	9.96E-135	7.36E-177	0.00E+00	0.00E+00
$(C_{aq x=0.02m}/C_{aq x=0m})$ (%)	53.24%	22.31%	2.12%	0.01%	0.00%	0.00%	0.00%	0.00%	0.00%	0.00%
C_{aq}/C_{sat} (%)	0.24%	0.26%	0.34%	0.57%	0.66%	1.16%	0.70%	4.70%	4.93%	1.66%
M_t (ng/m ²)	8.35E+04	3.03E+03	2.55E+01	1.89E-02	2.35E-12	9.54E-34	1.66E-136	9.66E-179	0.00E+00	0.00E+00
M_t/M_{sed} (%)	4.74%	0.11%	0.00%	0.00%	0.00%	0.00%	0.00%	0.00%	0.00%	0.00%
100 years										
C_{aq} (ng/L)	5.06E+03	1.66E+03	3.44E+02	5.99E+01	1.39E+00	2.58E-03	8.23E-15	2.29E-19	4.68E-57	8.03E-162
$(C_{aq x=0.02m}/C_{aq x=0m})$ (%)	70.20%	71.02%	46.81%	21.76%	1.76%	0.01%	0.00%	0.00%	0.00%	0.00%
C_{aq}/C_{sat} (%)	0.21%	0.24%	0.33%	0.57%	0.66%	1.16%	0.70%	4.70%	4.93%	1.66%
M_t (ng/m ²)	9.64E+04	6.04E+03	1.78E+02	2.50E+00	4.45E-05	2.94E-14	2.88E-56	2.55E-73	8.84E-216	0.00E+00
M_t/M_{sed} (%)	19.68%	0.73%	0.01%	0.00%	0.00%	0.00%	0.00%	0.00%	0.00%	0.00%
1000 years										
C_{aq} (ng/L)	4.33E+02	1.68E+03	4.84E+02	1.25E+02	1.15E+01	4.68E-01	5.59E-06	8.12E-08	1.21E-22	4.40E-63
$(C_{aq x=0.02m}/C_{aq x=0m})$ (%)	92.15%	82.89%	66.38%	45.38%	14.52%	1.55%	0.00%	0.00%	0.00%	0.00%
C_{aq}/C_{sat} (%)	0.01%	0.21%	0.33%	0.57%	0.66%	1.16%	0.70%	4.70%	4.93%	1.66%
M_t (ng/m ²)	8.25E+03	9.25E+03	7.91E+02	7.62E+01	2.02E+00	3.14E-02	9.33E-08	1.07E-09	5.43E-25	6.94E-66
M_t/M_{sed} (%)	100.00%	21.86%	1.20%	0.09%	0.00%	0.00%	0.00%	0.00%	0.00%	0.00%

Table D5.9 (Cont.): Summary of $C_{aq|x=0.02m,t}$ (ng/L), $C_{aq|x=0.02m,t}/C_{aq|x=0m,t=0year}$ (%), $C_{aq|x=0m,t}/C_{sat}$ (%), $M_{t|t}$ (ng/m²), and $M_{t|t}/M_{sed}$ (%) in all the sediment cores at the 95th percentile initial sediment concentration (36100 and 1640 ng/g for PBDE and PCB homologs, respectively) as predicted from the 95th percentile transport parameters values under advection-diffusion with organic carbon only sorption (A(OC)) at 40,100, and 1000 years in all sediment cores.

AJL										
40 years										
Time	H1	H2	H3	H4	H5	H6	H7	H8	H9	H10
Homolog										
C_{aq} (ng/L)	2.54E+03	3.52E+02	1.47E+01	7.49E-02	1.49E-09	1.38E-26	3.94E-109	3.92E-143	0.00E+00	0.00E+00
$(C_{aq x=0.02m}/C_{aq x=0m})$ (%)	56.87%	27.08%	3.80%	0.05%	0.00%	0.00%	0.00%	0.00%	0.00%	0.00%
C_{aq}/C_{sat} (%)	0.13%	0.14%	0.18%	0.30%	0.35%	0.61%	0.37%	2.47%	2.59%	0.87%
M_t (ng/m ²)	1.90E+04	7.57E+02	9.43E+00	1.79E-02	1.02E-10	3.62E-28	2.58E-111	2.02E-145	0.00E+00	0.00E+00
M_t/M_{sed} (%)	1.07%	0.03%	0.00%	0.00%	0.00%	0.00%	0.00%	0.00%	0.00%	0.00%
100 years										
Time										
C_{aq} (ng/L)	3.14E+03	9.54E+02	2.06E+02	4.21E+01	1.78E+00	1.29E-02	3.47E-11	1.56E-14	4.87E-42	3.75E-118
$(C_{aq x=0.02m}/C_{aq x=0m})$ (%)	72.29%	74.41%	53.13%	29.09%	4.29%	0.08%	0.00%	0.00%	0.00%	0.00%
C_{aq}/C_{sat} (%)	0.13%	0.13%	0.18%	0.30%	0.35%	0.61%	0.37%	2.47%	2.59%	0.87%
M_t (ng/m ²)	2.35E+04	1.37E+03	4.74E+01	9.81E-01	8.15E-05	2.04E-12	1.40E-46	2.21E-60	1.78E-175	0.00E+00
M_t/M_{sed} (%)	4.00%	0.17%	0.00%	0.00%	0.00%	0.00%	0.00%	0.00%	0.00%	0.00%
1000 years										
Time										
C_{aq} (ng/L)	2.28E+03	1.04E+03	2.66E+02	7.15E+01	7.83E+00	4.66E-01	3.43E-05	1.06E-06	8.61E-19	1.57E-51
$(C_{aq x=0.02m}/C_{aq x=0m})$ (%)	91.95%	83.61%	68.76%	49.48%	18.84%	2.94%	0.00%	0.00%	0.00%	0.00%
C_{aq}/C_{sat} (%)	0.07%	0.13%	0.18%	0.30%	0.35%	0.61%	0.37%	2.47%	2.59%	0.87%
M_t (ng/m ²)	1.70E+04	2.24E+03	1.70E+02	1.71E+01	5.38E-01	1.22E-02	2.24E-07	5.43E-09	1.51E-21	9.73E-55
M_t/M_{sed} (%)	82.72%	4.27%	0.26%	0.02%	0.00%	0.00%	0.00%	0.00%	0.00%	0.00%

Table D5.9 (Cont.): Summary of $C_{aq|x=0.02m,t}$ (ng/L), $C_{aq|x=0.02m,t}/C_{aq|x=0m,t=0year}$ (%), $C_{aq|x=0m,t}/C_{sat}$ (%), $M_{t|t}$ (ng/m²), and $M_{t|t}/M_{sed}$ (%) in all the sediment cores at the 95th percentile initial sediment concentration (36100 and 1640 ng/g for PBDE and PCB homologs, respectively) as predicted from the 95th percentile transport parameters values under advection-diffusion with organic carbon only sorption (A(OC)) at 40,100, and 1000 years in all sediment cores.

AMW										
40 years										
Time	H1	H2	H3	H4	H5	H6	H7	H8	H9	H10
Homolog										
C_{aq} (ng/L)	4.00E+02	1.18E+01	3.49E-03	9.34E-11	5.15E-40	2.98E-108	0.00E+00	0.00E+00	0.00E+00	0.00E+00
$(C_{aq x=0.02m}/C_{aq x=0m})$ (%)	25.27%	2.58%	0.00%	0.00%	0.00%	0.00%	0.00%	0.00%	0.00%	0.00%
C_{aq}/C_{sat} (%)	0.05%	0.05%	0.06%	0.11%	0.12%	0.21%	0.13%	0.87%	0.91%	0.30%
M_t (ng/m ²)	3.79E+03	3.21E+01	2.83E-03	2.83E-11	4.49E-41	9.92E-110	0.00E+00	0.00E+00	0.00E+00	0.00E+00
M_t/M_{sed} (%)	0.14%	0.00%	0.00%	0.00%	0.00%	0.00%	0.00%	0.00%	0.00%	0.00%
100 years										
Time										
C_{aq} (ng/L)	7.59E+02	2.50E+02	3.27E+01	2.33E+00	1.80E-03	1.18E-09	2.99E-38	6.84E-50	3.33E-147	0.00E+00
$(C_{aq x=0.02m}/C_{aq x=0m})$ (%)	48.35%	55.14%	24.11%	4.61%	0.01%	0.00%	0.00%	0.00%	0.00%	0.00%
C_{aq}/C_{sat} (%)	0.05%	0.05%	0.06%	0.11%	0.12%	0.21%	0.13%	0.87%	0.91%	0.30%
M_t (ng/m ²)	7.19E+03	2.04E+02	8.90E-01	1.34E-04	2.51E-17	2.04E-45	1.64E-181	1.45E-237	0.00E+00	0.00E+00
M_t/M_{sed} (%)	0.89%	0.02%	0.00%	0.00%	0.00%	0.00%	0.00%	0.00%	0.00%	0.00%
1000 years										
Time										
C_{aq} (ng/L)	1.08E+03	3.12E+02	5.77E+01	8.60E+00	1.12E-01	5.48E-05	2.42E-19	4.41E-25	9.76E-73	1.51E-205
$(C_{aq x=0.02m}/C_{aq x=0m})$ (%)	86.00%	69.35%	42.54%	16.96%	0.77%	0.00%	0.00%	0.00%	0.00%	0.00%
C_{aq}/C_{sat} (%)	0.04%	0.05%	0.06%	0.11%	0.12%	0.21%	0.13%	0.87%	0.91%	0.30%
M_t (ng/m ²)	1.03E+04	8.51E+02	4.69E+01	2.61E+00	9.79E-03	1.82E-06	2.01E-21	2.88E-27	2.17E-75	1.19E-208
M_t/M_{sed} (%)	25.69%	1.30%	0.05%	0.00%	0.00%	0.00%	0.00%	0.00%	0.00%	0.00%

Table D5.9 (Cont.): Summary of $C_{aq|x=0.02m,t}$ (ng/L), $C_{aq|x=0.02m,t}/C_{aq|x=0m,t=0year}$ (%), $C_{aq|x=0m,t}/C_{sat}$ (%), $M_{t|t}$ (ng/m²), and $M_{t|t}/M_{sed}$ (%) in all the sediment cores at the 95th percentile initial sediment concentration (36100 and 1640 ng/g for PBDE and PCB homologs, respectively) as predicted from the 95th percentile transport parameters values under advection-diffusion with organic carbon only sorption (A(OC)) at 40,100, and 1000 years in all sediment cores.

AOT										
40 years										
Time	H1	H2	H3	H4	H5	H6	H7	H8	H9	H10
Homolog										
C_{aq} (ng/L)	2.94E+03	3.05E+02	4.94E+00	2.53E-03	4.51E-15	1.03E-41	4.54E-172	6.86E-226	0.00E+00	0.00E+00
$(C_{aq x=0.02m}/C_{aq x=0m})$ (%)	48.31%	16.92%	0.92%	0.00%	0.00%	0.00%	0.00%	0.00%	0.00%	0.00%
C_{aq}/C_{sat} (%)	0.18%	0.19%	0.24%	0.42%	0.48%	0.85%	0.51%	3.42%	3.59%	1.21%
M_t (ng/m ²)	5.68E+04	1.69E+03	8.17E+00	1.57E-03	8.01E-16	6.99E-43	7.67E-174	9.12E-228	0.00E+00	0.00E+00
M_t/M_{sed} (%)	2.96%	0.05%	0.00%	0.00%	0.00%	0.00%	0.00%	0.00%	0.00%	0.00%
100 years										
Time										
C_{aq} (ng/L)	3.72E+03	7.06E+02	5.48E+01	1.19E+00	8.06E-06	7.52E-17	1.55E-69	3.67E-91	1.66E-272	0.00E+00
$(C_{aq x=0.02m}/C_{aq x=0m})$ (%)	66.95%	39.30%	10.20%	0.59%	0.00%	0.00%	0.00%	0.00%	0.00%	0.00%
C_{aq}/C_{sat} (%)	0.16%	0.19%	0.24%	0.42%	0.48%	0.85%	0.51%	3.42%	3.59%	1.21%
M_t (ng/m ²)	7.18E+04	3.92E+03	9.06E+01	7.32E-01	1.43E-06	5.10E-18	2.62E-71	4.88E-93	7.51E-275	0.00E+00
M_t/M_{sed} (%)	12.90%	0.44%	0.01%	0.00%	0.00%	0.00%	0.00%	0.00%	0.00%	0.00%
1000 years										
Time										
C_{aq} (ng/L)	7.00E+02	1.27E+03	3.34E+02	8.01E+01	5.77E+00	1.37E-01	1.20E-07	5.94E-10	1.02E-28	3.13E-80
$(C_{aq x=0.02m}/C_{aq x=0m})$ (%)	91.67%	81.23%	62.72%	39.95%	10.01%	0.62%	0.00%	0.00%	0.00%	0.00%
C_{aq}/C_{sat} (%)	0.02%	0.16%	0.24%	0.42%	0.48%	0.85%	0.51%	3.42%	3.59%	1.21%
M_t (ng/m ²)	1.35E+04	7.08E+03	5.53E+02	4.95E+01	1.02E+00	9.29E-03	2.03E-09	7.90E-12	4.65E-31	5.00E-83
M_t/M_{sed} (%)	100.00%	14.95%	0.80%	0.05%	0.00%	0.00%	0.00%	0.00%	0.00%	0.00%

Table D5.9 (Cont.): Summary of $C_{aq|x=0.02m,t}$ (ng/L), $C_{aq|x=0.02m,t}/C_{aq|x=0m,t=0year}$ (%), $C_{aq|x=0m,t}/C_{sat}$ (%), $M_{t|t}$ (ng/m²), and $M_{t|t}/M_{sed}$ (%) in all the sediment cores at the 95th percentile initial sediment concentration (36100 and 1640 ng/g for PBDE and PCB homologs, respectively) as predicted from the 95th percentile transport parameters values under advection-diffusion with organic carbon only sorption (A(OC)) at 40,100, and 1000 years in all sediment cores.

CBC										
Time	40 years									
Homolog	H1	H2	H3	H4	H5	H6	H7	H8	H9	H10
C_{aq} (ng/L)	1.81E+03	1.06E+02	2.23E-01	7.05E-07	1.06E-27	6.56E-76	0.00E+00	0.00E+00	0.00E+00	0.00E+00
$(C_{aq x=0.02m}/C_{aq x=0m})$ (%)	51.64%	10.13%	0.07%	0.00%	0.00%	0.00%	0.00%	0.00%	0.00%	0.00%
C_{aq}/C_{sat} (%)	0.10%	0.11%	0.14%	0.24%	0.28%	0.49%	0.30%	1.99%	2.09%	0.70%
M_t (ng/m ²)	9.43E+04	1.59E+03	9.97E-01	1.17E-06	5.09E-28	1.20E-76	0.00E+00	0.00E+00	0.00E+00	0.00E+00
M_t/M_{sed} (%)	4.26%	0.04%	0.00%	0.00%	0.00%	0.00%	0.00%	0.00%	0.00%	0.00%
Time	100 years									
C_{aq} (ng/L)	2.37E+03	4.04E+02	1.40E+01	3.93E-02	6.29E-11	1.40E-30	3.25E-126	1.23E-165	0.00E+00	0.00E+00
$(C_{aq x=0.02m}/C_{aq x=0m})$ (%)	79.96%	38.67%	4.46%	0.03%	0.00%	0.00%	0.00%	0.00%	0.00%	0.00%
C_{aq}/C_{sat} (%)	0.09%	0.11%	0.14%	0.24%	0.28%	0.49%	0.30%	1.99%	2.09%	0.70%
M_t (ng/m ²)	1.24E+05	6.05E+03	6.22E+01	6.55E-02	3.01E-11	2.55E-31	1.48E-127	4.40E-167	0.00E+00	0.00E+00
M_t/M_{sed} (%)	0.2331	0.55%	0.00%	0.00%	0.00%	0.00%	0.00%	0.00%	0.00%	0.00%
Time	1000 years									
C_{aq} (ng/L)	8.48E+01	7.83E+02	2.33E+02	4.78E+01	1.51E+00	4.95E-03	2.20E-13	1.84E-17	3.33E-51	6.90E-145
$(C_{aq x=0.02m}/C_{aq x=0m})$ (%)	99.95%	96.53%	75.66%	40.99%	4.50%	0.04%	0.00%	0.00%	0.00%	0.00%
C_{aq}/C_{sat} (%)	0.00%	0.08%	0.14%	0.24%	0.28%	0.49%	0.30%	1.99%	2.09%	0.70%
M_t (ng/m ²)	4.41E+03	1.17E+04	1.04E+03	7.97E+01	7.24E-01	9.04E-04	1.00E-14	6.60E-19	4.07E-53	2.97E-147
M_t/M_{sed} (%)	100.00%	29.51%	1.37%	0.07%	0.00%	0.00%	0.00%	0.00%	0.00%	0.00%

Table D5.9 (Cont.): Summary of $C_{aq|x=0.02m,t}$ (ng/L), $C_{aq|x=0.02m,t}/C_{aq|x=0m,t=0year}$ (%), $C_{aq|x=0m,t}/C_{sat}$ (%), $M_{t|t}$ (ng/m²), and $M_{t|t}/M_{sed}$ (%) in all the sediment cores at the 95th percentile initial sediment concentration (36100 and 1640 ng/g for PBDE and PCB homologs, respectively) as predicted from the 95th percentile transport parameters values under advection-diffusion with organic carbon only sorption (A(OC)) at 40,100, and 1000 years in all sediment cores.

CLC										
40 years										
Time	H1	H2	H3	H4	H5	H6	H7	H8	H9	H10
Homolog										
C_{aq} (ng/L)	1.89E+02	1.61E+00	7.53E-06	6.66E-18	1.62E-65	2.26E-177	0.00E+00	0.00E+00	0.00E+00	0.00E+00
$(C_{aq x=0.02m}/C_{aq x=0m})$ (%)	13.11%	0.39%	0.00%	0.00%	0.00%	0.00%	0.00%	0.00%	0.00%	0.00%
C_{aq}/C_{sat} (%)	0.04%	0.04%	0.06%	0.10%	0.11%	0.19%	0.12%	0.79%	0.83%	0.28%
M_t (ng/m ²)	1.64E+02	4.02E-01	5.60E-07	1.85E-19	1.29E-67	6.88E-180	0.00E+00	0.00E+00	0.00E+00	0.00E+00
M_t/M_{sed} (%)	0.01%	0.00%	0.00%	0.00%	0.00%	0.00%	0.00%	0.00%	0.00%	0.00%
100 years										
Time										
C_{aq} (ng/L)	4.92E+02	1.66E+02	1.40E+01	3.70E-01	5.68E-06	3.64E-16	1.09E-64	1.37E-84	2.06E-251	0.00E+00
$(C_{aq x=0.02m}/C_{aq x=0m})$ (%)	34.10%	39.99%	11.30%	0.80%	0.00%	0.00%	0.00%	0.00%	0.00%	0.00%
C_{aq}/C_{sat} (%)	0.04%	0.04%	0.06%	0.10%	0.11%	0.19%	0.12%	0.79%	0.83%	0.28%
M_t (ng/m ²)	4.27E+02	7.06E+00	5.67E-03	1.35E-08	1.14E-28	3.29E-74	3.89E-297	0.00E+00	0.00E+00	0.00E+00
M_t/M_{sed} (%)	0.04%	0.00%	0.00%	0.00%	0.00%	0.00%	0.00%	0.00%	0.00%	0.00%
1000 years										
Time										
C_{aq} (ng/L)	1.09E+03	2.36E+02	3.48E+01	3.28E+00	7.54E-03	6.47E-08	5.85E-31	2.67E-40	3.00E-118	0.00E+00
$(C_{aq x=0.02m}/C_{aq x=0m})$ (%)	76.81%	56.79%	28.10%	7.09%	0.06%	0.00%	0.00%	0.00%	0.00%	0.00%
C_{aq}/C_{sat} (%)	0.04%	0.04%	0.06%	0.10%	0.11%	0.19%	0.12%	0.79%	0.83%	0.28%
M_t (ng/m ²)	9.46E+02	5.89E+01	2.58E+00	9.09E-02	6.01E-05	1.97E-10	4.44E-34	1.59E-43	6.11E-122	0.00E+00
M_t/M_{sed} (%)	1.63%	0.08%	0.00%	0.00%	0.00%	0.00%	0.00%	0.00%	0.00%	0.00%

Table D5.9 (Cont.): Summary of $C_{aq|x=0.02m,t}$ (ng/L), $C_{aq|x=0.02m,t}/C_{aq|x=0m,t=0year}$ (%), $C_{aq|x=0m,t}/C_{sat}$ (%), $M_{t|t}$ (ng/m²), and $M_{t|t}/M_{sed}$ (%) in all the sediment cores at the 95th percentile initial sediment concentration (36100 and 1640 ng/g for PBDE and PCB homologs, respectively) as predicted from the 95th percentile transport parameters values under advection-diffusion with organic carbon only sorption (A(OC)) at 40,100, and 1000 years in all sediment cores.

CWP										
40 years										
Time	H1	H2	H3	H4	H5	H6	H7	H8	H9	H10
Homolog										
C_{aq} (ng/L)	1.96E+02	3.49E+00	1.89E-04	7.30E-14	1.15E-50	7.82E-137	0.00E+00	0.00E+00	0.00E+00	0.00E+00
$(C_{aq x=0.02m}/C_{aq x=0m})$ (%)	21.61%	1.33%	0.00%	0.00%	0.00%	0.00%	0.00%	0.00%	0.00%	0.00%
C_{aq}/C_{sat} (%)	0.03%	0.03%	0.04%	0.06%	0.07%	0.12%	0.07%	0.50%	0.52%	0.18%
M_t (ng/m ²)	3.52E+03	1.80E+01	2.89E-04	4.18E-14	1.90E-51	4.91E-138	0.00E+00	0.00E+00	0.00E+00	0.00E+00
M_t/M_{sed} (%)	0.12%	0.00%	0.00%	0.00%	0.00%	0.00%	0.00%	0.00%	0.00%	0.00%
100 years										
Time										
Homolog										
C_{aq} (ng/L)	4.22E+02	1.48E+02	1.77E+01	1.01E+00	3.20E-04	2.55E-11	1.79E-44	5.31E-58	3.24E-171	0.00E+00
$(C_{aq x=0.02m}/C_{aq x=0m})$ (%)	46.83%	56.92%	22.73%	3.48%	0.00%	0.00%	0.00%	0.00%	0.00%	0.00%
C_{aq}/C_{sat} (%)	0.03%	0.03%	0.04%	0.06%	0.07%	0.12%	0.07%	0.50%	0.52%	0.18%
M_t (ng/m ²)	7.56E+03	1.74E+02	3.80E-01	1.04E-05	1.88E-21	1.03E-56	1.66E-228	2.34E-299	0.00E+00	0.00E+00
M_t/M_{sed} (%)	0.88%	0.01%	0.00%	0.00%	0.00%	0.00%	0.00%	0.00%	0.00%	0.00%
1000 years										
Time										
Homolog										
C_{aq} (ng/L)	6.34E+02	1.84E+02	3.16E+01	3.93E+00	2.53E-02	2.35E-06	2.79E-24	1.69E-31	1.32E-91	1.83E-259
$(C_{aq x=0.02m}/C_{aq x=0m})$ (%)	89.93%	71.36%	40.57%	13.50%	0.30%	0.00%	0.00%	0.00%	0.00%	0.00%
C_{aq}/C_{sat} (%)	0.02%	0.03%	0.04%	0.06%	0.07%	0.12%	0.07%	0.50%	0.52%	0.18%
M_t (ng/m ²)	1.13E+04	9.50E+02	4.85E+01	2.25E+00	4.16E-03	1.48E-07	4.38E-26	2.09E-33	5.55E-94	2.72E-262
M_t/M_{sed} (%)	29.16%	1.40%	0.05%	0.00%	0.00%	0.00%	0.00%	0.00%	0.00%	0.00%

Table D5.9 (Cont.): Summary of $C_{aq|x=0.02m,t}$ (ng/L), $C_{aq|x=0.02m,t}/C_{aq|x=0m,t=0year}$ (%), $C_{aq|x=0m,t}/C_{sat}$ (%), $M_{t|t}$ (ng/m²), and $M_{t|t}/M_{sed}$ (%) in all the sediment cores at the 95th percentile initial sediment concentration (36100 and 1640 ng/g for PBDE and PCB homologs, respectively) as predicted from the 95th percentile transport parameters values under advection-diffusion with organic carbon only sorption (A(OC)) at 40,100, and 1000 years in all sediment cores.

IGC09										
40 years										
Time	H1	H2	H3	H4	H5	H6	H7	H8	H9	H10
Homolog										
C_{aq} (ng/L)	1.54E+02	2.19E+00	5.70E-05	3.61E-15	3.50E-55	5.57E-149	0.00E+00	0.00E+00	0.00E+00	0.00E+00
$(C_{aq x=0.02m}/C_{aq x=0m})$ (%)	18.14%	0.90%	0.00%	0.00%	0.00%	0.00%	0.00%	0.00%	0.00%	0.00%
C_{aq}/C_{sat} (%)	0.02%	0.03%	0.03%	0.06%	0.06%	0.11%	0.07%	0.46%	0.49%	0.16%
M_t (ng/m ²)	1.39E+03	5.69E+00	4.42E-05	1.05E-15	2.91E-56	1.77E-150	0.00E+00	0.00E+00	0.00E+00	0.00E+00
M_t/M_{sed} (%)	0.05%	0.00%	0.00%	0.00%	0.00%	0.00%	0.00%	0.00%	0.00%	0.00%
100 years										
Time										
Homolog										
C_{aq} (ng/L)	3.51E+02	1.22E+02	1.32E+01	6.08E-01	8.38E-05	9.55E-13	4.34E-50	2.36E-65	3.53E-193	0.00E+00
$(C_{aq x=0.02m}/C_{aq x=0m})$ (%)	41.60%	50.23%	18.15%	2.24%	0.00%	0.00%	0.00%	0.00%	0.00%	0.00%
C_{aq}/C_{sat} (%)	0.02%	0.03%	0.03%	0.06%	0.06%	0.11%	0.07%	0.46%	0.49%	0.16%
M_t (ng/m ²)	3.17E+03	6.57E+01	1.06E-01	1.41E-06	1.31E-23	6.35E-62	6.65E-249	0.00E+00	0.00E+00	0.00E+00
M_t/M_{sed} (%)	0.36%	0.00%	0.00%	0.00%	0.00%	0.00%	0.00%	0.00%	0.00%	0.00%
1000 years										
Time										
Homolog										
C_{aq} (ng/L)	6.42E+02	1.58E+02	2.57E+01	2.93E+00	1.38E-02	6.34E-07	2.27E-26	3.21E-34	1.26E-99	2.15E-282
$(C_{aq x=0.02m}/C_{aq x=0m})$ (%)	84.71%	65.28%	35.41%	10.81%	0.18%	0.00%	0.00%	0.00%	0.00%	0.00%
C_{aq}/C_{sat} (%)	0.02%	0.03%	0.03%	0.06%	0.06%	0.11%	0.07%	0.46%	0.49%	0.16%
M_t (ng/m ²)	5.80E+03	4.12E+02	1.99E+01	8.48E-01	1.15E-03	2.01E-08	1.79E-28	2.00E-36	2.67E-102	1.61E-285
M_t/M_{sed} (%)	11.80%	0.59%	0.02%	0.00%	0.00%	0.00%	0.00%	0.00%	0.00%	0.00%

Table D5.9 (Cont.): Summary of $C_{aq|x=0.02m,t}$ (ng/L), $C_{aq|x=0.02m,t}/C_{aq|x=0m,t=0year}$ (%), $C_{aq|x=0m,t}/C_{sat}$ (%), $M_{t|t}$ (ng/m²), and $M_{t|t}/M_{sed}$ (%) in all the sediment cores at the 95th percentile initial sediment concentration (36100 and 1640 ng/g for PBDE and PCB homologs, respectively) as predicted from the 95th percentile transport parameters values under advection-diffusion with organic carbon only sorption (A(OC)) at 40,100, and 1000 years in all sediment cores.

IGC13										
Time	40 years									
Homolog	H1	H2	H3	H4	H5	H6	H7	H8	H9	H10
C_{aq} (ng/L)	3.55E+01	9.95E-01	2.47E-04	4.20E-12	3.61E-42	2.50E-112	0.00E+00	0.00E+00	0.00E+00	0.00E+00
$(C_{aq x=0.02m}/C_{aq x=0m})$ (%)	26.51%	2.58%	0.00%	0.00%	0.00%	0.00%	0.00%	0.00%	0.00%	0.00%
C_{aq}/C_{sat} (%)	0.00%	0.00%	0.01%	0.01%	0.01%	0.02%	0.01%	0.07%	0.08%	0.03%
M_t (ng/m ²)	6.40E+02	5.16E+00	3.81E-04	2.42E-12	5.98E-43	1.58E-113	0.00E+00	0.00E+00	0.00E+00	0.00E+00
M_t/M_{sed} (%)	0.15%	0.00%	0.00%	0.00%	0.00%	0.00%	0.00%	0.00%	0.00%	0.00%
Time	100 years									
C_{aq} (ng/L)	6.82E+01	6.61E+00	9.03E-02	3.04E-05	9.46E-18	3.43E-46	1.64E-185	4.78E-243	0.00E+00	0.00E+00
$(C_{aq x=0.02m}/C_{aq x=0m})$ (%)	51.28%	17.13%	0.79%	0.00%	0.00%	0.00%	0.00%	0.00%	0.00%	0.00%
C_{aq}/C_{sat} (%)	0.00%	0.00%	0.01%	0.01%	0.01%	0.02%	0.01%	0.07%	0.08%	0.03%
M_t (ng/m ²)	1.23E+03	3.43E+01	1.40E-01	1.75E-05	1.57E-18	2.17E-47	2.58E-187	5.93E-245	0.00E+00	0.00E+00
M_t/M_{sed} (%)	0.94%	0.02%	0.00%	0.00%	0.00%	0.00%	0.00%	0.00%	0.00%	0.00%
Time	1000 years									
C_{aq} (ng/L)	9.53E+01	2.81E+01	5.21E+00	7.65E-01	9.31E-03	3.82E-06	7.00E-21	8.87E-27	9.09E-76	2.45E-212
$(C_{aq x=0.02m}/C_{aq x=0m})$ (%)	90.64%	73.88%	45.33%	17.82%	0.75%	0.00%	0.00%	0.00%	0.00%	0.00%
C_{aq}/C_{sat} (%)	0.00%	0.00%	0.01%	0.01%	0.01%	0.02%	0.01%	0.07%	0.08%	0.03%
M_t (ng/m ²)	1.72E+03	1.46E+02	8.05E+00	4.41E-01	1.54E-03	2.41E-07	1.10E-22	1.10E-28	3.85E-78	3.65E-215
M_t/M_{sed} (%)	27.65%	1.40%	0.06%	0.00%	0.00%	0.00%	0.00%	0.00%	0.00%	0.00%

Table D5.10a (Cont.): PBDE sediment phase concentrations (C_{sed}) (ng/g) to yield aqueous phase concentration assuming local equilibrium assumption equals to saturation concentration ($C_{\text{aq}|x=0\text{m}}=C_{\text{sat}}$) as predicted from the 5th, 25th, 50th, 75th, and 95th percentile sediment-porewater partitioning coefficient values for organic carbon only sorption ($\log K_d$ (OC)).

Percentile	ACL									
	H1	H2	H3	H4	H5	H6	H7	H8	H9	H10
0.05	1.8E+06	1.5E+06	5.6E+05	2.2E+05	1.3E+05	6.3E+04	1.4E+04	2.1E+03	1.1E+03	3.3E+01
0.25	3.7E+06	2.9E+06	1.6E+06	9.1E+05	5.0E+05	4.6E+05	1.6E+05	2.3E+04	1.8E+04	3.1E+03
0.50	5.7E+06	4.3E+06	3.0E+06	2.3E+06	1.2E+06	1.4E+06	9.7E+05	1.2E+05	1.1E+05	6.3E+04
0.75	8.6E+06	6.1E+06	5.6E+06	5.6E+06	2.9E+06	4.0E+06	1.9E+06	5.8E+05	6.8E+05	1.3E+06
0.95	1.5E+07	9.9E+06	1.3E+07	1.9E+07	9.8E+06	1.8E+07	1.6E+07	7.3E+06	9.0E+06	9.8E+07
Percentile	AED									
	H1	H2	H3	H4	H5	H6	H7	H8	H9	H10
0.05	6.8E+05	5.7E+05	2.1E+05	8.2E+04	4.7E+04	2.4E+04	5.2E+03	7.9E+02	4.2E+02	1.2E+01
0.25	2.5E+06	2.0E+06	1.1E+06	6.1E+05	3.4E+05	3.1E+05	1.1E+05	1.6E+04	1.2E+04	2.1E+03
0.50	4.7E+06	3.6E+06	2.5E+06	1.9E+06	1.0E+06	1.1E+06	8.1E+05	1.0E+05	9.3E+04	5.3E+04
0.75	8.0E+06	5.7E+06	5.2E+06	5.2E+06	2.7E+06	3.7E+06	1.7E+06	5.4E+05	6.3E+05	1.2E+06
0.95	1.5E+07	1.0E+07	1.4E+07	2.0E+07	1.0E+07	1.9E+07	1.7E+07	7.6E+06	9.4E+06	1.0E+08
Percentile	AFR									
	H1	H2	H3	H4	H5	H6	H7	H8	H9	H10
0.05	1.1E+06	8.8E+05	3.3E+05	1.3E+05	7.3E+04	3.7E+04	8.1E+03	1.2E+03	6.5E+02	1.9E+01
0.25	1.6E+06	1.3E+06	7.0E+05	4.0E+05	2.2E+05	2.0E+05	7.0E+04	1.0E+04	7.8E+03	1.4E+03
0.50	2.2E+06	1.7E+06	1.2E+06	8.9E+05	4.7E+05	5.3E+05	3.8E+05	4.8E+04	4.4E+04	2.5E+04
0.75	3.0E+06	2.2E+06	2.0E+06	2.0E+06	1.0E+06	1.4E+06	6.6E+05	2.0E+05	2.4E+05	4.6E+05
0.95	4.6E+06	3.1E+06	4.1E+06	6.1E+06	3.0E+06	5.6E+06	5.0E+06	2.3E+06	2.8E+06	3.1E+07

Table D5.10a (Cont.): PBDE sediment phase concentrations (C_{sed}) (ng/g) to yield aqueous phase concentration assuming local equilibrium assumption equals to saturation concentration ($C_{\text{aq}|x=0\text{m}}=C_{\text{sat}}$) as predicted from the 5th, 25th, 50th, 75th, and 95th percentile sediment-porewater partitioning coefficient values for organic carbon only sorption ($\log K_d$ (OC)).

AJL										
Percentile	H1	H2	H3	H4	H5	H6	H7	H8	H9	H10
0.05	7.7E+05	6.4E+05	2.4E+05	9.3E+04	5.3E+04	2.7E+04	5.9E+03	9.0E+02	4.7E+02	1.4E+01
0.25	3.4E+06	2.7E+06	1.5E+06	8.3E+05	4.6E+05	4.2E+05	1.5E+05	2.1E+04	1.6E+04	2.8E+03
0.50	6.8E+06	5.1E+06	3.6E+06	2.7E+06	1.5E+06	1.6E+06	1.2E+06	1.5E+05	1.3E+05	7.6E+04
0.75	1.2E+07	8.5E+06	7.8E+06	7.8E+06	4.0E+06	5.6E+06	2.6E+06	8.0E+05	9.4E+05	1.8E+06
0.95	2.3E+07	1.6E+07	2.1E+07	3.1E+07	1.6E+07	2.9E+07	2.5E+07	1.2E+07	1.4E+07	1.6E+08
AMW										
Percentile	H1	H2	H3	H4	H5	H6	H7	H8	H9	H10
0.05	7.9E+06	6.6E+06	2.4E+06	9.5E+05	5.5E+05	2.8E+05	6.1E+04	9.2E+03	4.9E+03	1.4E+02
0.25	1.8E+07	1.4E+07	7.8E+06	4.5E+06	2.5E+06	2.3E+06	7.9E+05	1.1E+05	8.7E+04	1.5E+04
0.50	3.0E+07	2.2E+07	1.6E+07	1.2E+07	6.3E+06	7.1E+06	5.1E+06	6.4E+05	5.8E+05	3.3E+05
0.75	4.6E+07	3.3E+07	3.0E+07	3.0E+07	1.6E+07	2.1E+07	1.0E+07	3.1E+06	3.6E+06	7.0E+06
0.95	8.1E+07	5.4E+07	7.2E+07	1.1E+08	5.4E+07	9.9E+07	8.8E+07	4.0E+07	5.0E+07	5.4E+08
AOT										
Percentile	H1	H2	H3	H4	H5	H6	H7	H8	H9	H10
0.05	1.5E+06	1.2E+06	4.5E+05	1.8E+05	1.0E+05	5.1E+04	1.1E+04	1.7E+03	9.0E+02	2.7E+01
0.25	2.9E+06	2.3E+06	1.2E+06	7.1E+05	3.9E+05	3.6E+05	1.2E+05	1.8E+04	1.4E+04	2.4E+03
0.50	4.4E+06	3.3E+06	2.3E+06	1.8E+06	9.5E+05	1.1E+06	7.6E+05	9.5E+04	8.7E+04	4.9E+04
0.75	6.6E+06	4.7E+06	4.3E+06	4.3E+06	2.2E+06	3.1E+06	1.4E+06	4.4E+05	5.2E+05	1.0E+06
0.95	1.1E+07	7.4E+06	9.9E+06	1.5E+07	7.3E+06	1.4E+07	1.2E+07	5.5E+06	6.8E+06	7.4E+07
CBC										
Percentile	H1	H2	H3	H4	H5	H6	H7	H8	H9	H10
0.05	5.1E+05	4.3E+05	1.6E+05	6.2E+04	3.6E+04	1.8E+04	4.0E+03	6.0E+02	3.2E+02	9.5E+00
0.25	2.6E+06	2.1E+06	1.1E+06	6.4E+05	3.5E+05	3.2E+05	1.1E+05	1.6E+04	1.2E+04	2.2E+03
0.50	5.6E+06	4.2E+06	3.0E+06	2.2E+06	1.2E+06	1.3E+06	9.6E+05	1.2E+05	1.1E+05	6.2E+04
0.75	1.0E+07	7.3E+06	6.6E+06	6.7E+06	3.5E+06	4.7E+06	2.2E+06	6.9E+05	8.0E+05	1.5E+06
0.95	2.1E+07	1.4E+07	1.8E+07	2.7E+07	1.4E+07	2.5E+07	2.2E+07	1.0E+07	1.3E+07	1.4E+08

Table D5.10a (Cont.): PBDE sediment phase concentrations (C_{sed}) (ng/g) to yield aqueous phase concentration assuming local equilibrium assumption equals to saturation concentration ($C_{\text{aq}|x=0\text{m}}=C_{\text{sat}}$) as predicted from the 5th, 25th, 50th, 75th, and 95th percentile sediment-porewater partitioning coefficient values for organic carbon only sorption ($\log K_d$ (OC)).

Percentile	CLC									
	H1	H2	H3	H4	H5	H6	H7	H8	H9	H10
0.05	4.6E+06	3.8E+06	1.4E+06	5.5E+05	3.2E+05	1.6E+05	3.5E+04	5.4E+03	2.8E+03	8.4E+01
0.25	6.6E+06	5.2E+06	2.8E+06	1.6E+06	8.9E+05	8.1E+05	2.8E+05	4.1E+04	3.1E+04	5.5E+03
0.50	8.6E+06	6.4E+06	4.5E+06	3.4E+06	1.8E+06	2.1E+06	1.5E+06	1.8E+05	1.7E+05	9.5E+04
0.75	1.1E+07	7.9E+06	7.2E+06	7.3E+06	3.8E+06	5.2E+06	2.4E+06	7.5E+05	8.8E+05	1.7E+06
0.95	1.6E+07	1.1E+07	1.4E+07	2.1E+07	1.1E+07	2.0E+07	1.7E+07	8.0E+06	9.8E+06	1.1E+08
Percentile	CWP									
	H1	H2	H3	H4	H5	H6	H7	H8	H9	H10
0.05	4.2E+06	3.5E+06	1.3E+06	5.0E+05	2.9E+05	1.5E+05	3.2E+04	4.9E+03	2.6E+03	7.7E+01
0.25	7.3E+06	5.7E+06	3.1E+06	1.8E+06	9.8E+05	8.9E+05	3.1E+05	4.5E+04	3.4E+04	6.0E+03
0.50	1.0E+07	7.9E+06	5.5E+06	4.2E+06	2.2E+06	2.5E+06	1.8E+06	2.2E+05	2.0E+05	1.2E+05
0.75	1.5E+07	1.1E+07	9.7E+06	9.7E+06	5.0E+06	6.9E+06	3.2E+06	1.0E+06	1.2E+06	2.3E+06
0.95	2.4E+07	1.6E+07	2.1E+07	3.2E+07	1.6E+07	2.9E+07	2.6E+07	1.2E+07	1.5E+07	1.6E+08
Percentile	IGC09									
	H1	H2	H3	H4	H5	H6	H7	H8	H9	H10
0.05	7.8E+06	6.5E+06	2.4E+06	9.4E+05	5.4E+05	2.7E+05	6.0E+04	9.1E+03	4.8E+03	1.4E+02
0.25	1.3E+07	9.9E+06	5.3E+06	3.1E+06	1.7E+06	1.5E+06	5.4E+05	7.8E+04	5.9E+04	1.0E+04
0.50	1.7E+07	1.3E+07	9.1E+06	6.9E+06	3.7E+06	4.2E+06	2.9E+06	3.7E+05	3.4E+05	1.9E+05
0.75	2.4E+07	1.7E+07	1.5E+07	1.6E+07	8.1E+06	1.1E+07	5.2E+06	1.6E+06	1.9E+06	3.6E+06
0.95	3.7E+07	2.5E+07	3.3E+07	4.9E+07	2.4E+07	4.5E+07	4.0E+07	1.8E+07	2.3E+07	2.5E+08
Percentile	IGC13									
	H1	H2	H3	H4	H5	H6	H7	H8	H9	H10
0.05	7.3E+06	6.1E+06	2.3E+06	8.8E+05	5.0E+05	2.5E+05	5.6E+04	8.5E+03	4.5E+03	1.3E+02
0.25	1.3E+07	9.9E+06	5.3E+06	3.1E+06	1.7E+06	1.5E+06	5.4E+05	7.8E+04	6.0E+04	1.0E+04
0.50	1.8E+07	1.4E+07	9.5E+06	7.2E+06	3.8E+06	4.3E+06	3.1E+06	3.9E+05	3.5E+05	2.0E+05
0.75	2.5E+07	1.8E+07	1.7E+07	1.7E+07	8.6E+06	1.2E+07	5.6E+06	1.7E+06	2.0E+06	3.9E+06
0.95	4.1E+07	2.7E+07	3.7E+07	5.4E+07	2.7E+07	5.0E+07	4.4E+07	2.0E+07	2.5E+07	2.7E+08

Table D5.10b (Cont.): PBDE sediment phase concentrations (C_{sed}) (ng/g) to yield aqueous phase concentration assuming local equilibrium assumption equals to saturation concentration ($C_{\text{aq}|x=0\text{m}}=C_{\text{sat}}$) as predicted from the 5th, 25th, 50th, 75th, and 95th percentile sediment-porewater partitioning coefficient values for organic carbon and black carbon sorptions ($\log K_d$ (OCBC)).

Percentile	ACL									
	H1	H2	H3	H4	H5	H6	H7	H8	H9	H10
0.05	1.8E+06	6.9E+06	3.4E+07	1.5E+08	1.7E+09	8.6E+09	1.4E+10	3.0E+10	1.0E+11	3.0E+08
0.25	4.2E+06	9.1E+07	7.7E+08	6.3E+09	4.6E+10	7.0E+11	2.4E+12	2.8E+12	1.8E+13	2.8E+12
0.50	5.1E+07	6.9E+08	7.7E+09	8.7E+10	4.2E+11	8.0E+12	1.0E+14	5.4E+13	4.1E+14	8.4E+14
0.75	5.7E+08	4.9E+09	7.1E+10	1.1E+12	3.7E+12	8.3E+13	2.7E+14	7.9E+14	8.5E+15	2.5E+17
0.95	8.9E+09	4.5E+10	1.1E+12	3.3E+13	7.1E+13	2.4E+15	2.5E+16	1.2E+17	1.1E+18	1.6E+21
Percentile	AED									
	H1	H2	H3	H4	H5	H6	H7	H8	H9	H10
0.05	6.8E+05	3.5E+06	1.7E+07	7.9E+07	8.8E+08	4.4E+09	7.1E+09	1.5E+10	5.1E+10	1.5E+08
0.25	2.8E+06	6.1E+07	5.2E+08	4.2E+09	3.1E+10	4.7E+11	1.6E+12	1.9E+12	1.2E+13	1.9E+12
0.50	3.5E+07	4.8E+08	5.3E+09	6.1E+10	2.9E+11	5.6E+12	7.0E+13	3.8E+13	2.9E+14	5.8E+14
0.75	3.9E+08	3.4E+09	4.9E+10	7.8E+11	2.5E+12	5.7E+13	1.9E+14	5.4E+14	5.9E+15	1.7E+17
0.95	5.8E+09	3.0E+10	7.5E+11	2.1E+13	4.6E+13	1.6E+15	1.7E+16	7.7E+16	7.3E+17	1.0E+21
Percentile	AFR									
	H1	H2	H3	H4	H5	H6	H7	H8	H9	H10
0.05	1.1E+06	3.0E+06	1.5E+07	6.7E+07	7.5E+08	3.8E+09	6.0E+09	1.3E+10	4.3E+10	1.3E+08
0.25	1.6E+06	2.4E+07	2.1E+08	1.7E+09	1.2E+10	1.9E+11	6.3E+11	7.6E+11	4.8E+12	7.5E+11
0.50	1.1E+07	1.5E+08	1.6E+09	1.9E+10	9.0E+10	1.7E+12	2.1E+13	1.2E+13	8.8E+13	1.8E+14
0.75	1.0E+08	8.7E+08	1.3E+10	2.0E+11	6.5E+11	1.5E+13	4.9E+13	1.4E+14	1.5E+15	4.4E+16
0.95	1.3E+09	6.6E+09	1.7E+11	4.8E+12	1.0E+13	3.6E+14	3.7E+15	1.7E+16	1.6E+17	2.3E+20

Table D5.10b (Cont.): PBDE sediment phase concentrations (C_{sed}) (ng/g) to yield aqueous phase concentration assuming local equilibrium assumption equals to saturation concentration ($C_{\text{aq}|x=0\text{m}}=C_{\text{sat}}$) as predicted from the 5th, 25th, 50th, 75th, and 95th percentile sediment-porewater partitioning coefficient values for organic carbon and black carbon sorptions ($\log K_d$ (OCBC)).

AJL										
Percentile	H1	H2	H3	H4	H5	H6	H7	H8	H9	H10
0.05	7.7E+05	2.1E+06	1.0E+07	4.8E+07	5.3E+08	2.7E+09	4.3E+09	9.1E+09	3.1E+10	9.1E+07
0.25	3.4E+06	5.7E+07	4.8E+08	3.9E+09	2.9E+10	4.4E+11	1.5E+12	1.8E+12	1.1E+13	1.8E+12
0.50	4.0E+07	5.4E+08	6.0E+09	6.8E+10	3.3E+11	6.3E+12	7.8E+13	4.3E+13	3.3E+14	6.6E+14
0.75	5.1E+08	4.4E+09	6.4E+10	1.0E+12	3.3E+12	7.5E+13	2.5E+14	7.1E+14	7.6E+15	2.2E+17
0.95	8.9E+09	4.5E+10	1.1E+12	3.3E+13	7.1E+13	2.5E+15	2.5E+16	1.2E+17	1.1E+18	1.6E+21
AMW										
Percentile	H1	H2	H3	H4	H5	H6	H7	H8	H9	H10
0.05	7.9E+06	3.6E+07	1.8E+08	8.2E+08	9.1E+09	4.6E+10	7.3E+10	1.6E+11	5.3E+11	1.6E+09
0.25	2.3E+07	5.0E+08	4.2E+09	3.4E+10	2.5E+11	3.8E+12	1.3E+13	1.5E+13	9.9E+13	1.5E+13
0.50	2.8E+08	3.8E+09	4.2E+10	4.8E+11	2.3E+12	4.4E+13	5.5E+14	3.0E+14	2.3E+15	4.6E+15
0.75	3.2E+09	2.7E+10	3.9E+11	6.2E+12	2.0E+13	4.6E+14	1.5E+15	4.4E+15	4.7E+16	1.4E+18
0.95	4.9E+10	2.5E+11	6.2E+12	1.8E+14	3.9E+14	1.3E+16	1.4E+17	6.4E+17	6.1E+18	8.7E+21
AOT										
Percentile	H1	H2	H3	H4	H5	H6	H7	H8	H9	H10
0.05	1.5E+06	3.4E+06	1.7E+07	7.7E+07	8.6E+08	4.3E+09	7.0E+09	1.5E+10	5.0E+10	1.5E+08
0.25	4.8E+06	1.0E+08	8.8E+08	7.2E+09	5.3E+10	8.1E+11	2.7E+12	3.2E+12	2.1E+13	3.2E+12
0.50	7.8E+07	1.1E+09	1.2E+10	1.3E+11	6.4E+11	1.2E+13	1.5E+14	8.3E+13	6.3E+14	1.3E+15
0.75	1.0E+09	8.8E+09	1.3E+11	2.0E+12	6.6E+12	1.5E+14	5.0E+14	1.4E+15	1.5E+16	4.5E+17
0.95	1.9E+10	9.4E+10	2.4E+12	6.8E+13	1.5E+14	5.1E+15	5.2E+16	2.4E+17	2.3E+18	3.3E+21
CBC										
Percentile	H1	H2	H3	H4	H5	H6	H7	H8	H9	H10
0.05	5.1E+05	1.6E+07	7.9E+07	3.6E+08	4.0E+09	2.0E+10	3.2E+10	6.9E+10	2.3E+11	6.9E+08
0.25	2.1E+07	4.5E+08	3.8E+09	3.1E+10	2.3E+11	3.5E+12	1.2E+13	1.4E+13	8.9E+13	1.4E+13
0.50	3.3E+08	4.5E+09	4.9E+10	5.6E+11	2.7E+12	5.1E+13	6.4E+14	3.5E+14	2.7E+15	5.4E+15
0.75	4.3E+09	3.7E+10	5.3E+11	8.4E+12	2.7E+13	6.2E+14	2.1E+15	5.9E+15	6.4E+16	1.9E+18
0.95	7.5E+10	3.8E+11	9.5E+12	2.7E+14	5.9E+14	2.1E+16	2.1E+17	9.8E+17	9.4E+18	1.3E+22

Table D5.10b (Cont.): PBDE sediment phase concentrations (C_{sed}) (ng/g) to yield aqueous phase concentration assuming local equilibrium assumption equals to saturation concentration ($C_{\text{aq}|x=0\text{m}}=C_{\text{sat}}$) as predicted from the 5th, 25th, 50th, 75th, and 95th percentile sediment-porewater partitioning coefficient values for organic carbon and black carbon sorptions ($\log K_d$ (OCBC)).

Percentile	CLC									
	H1	H2	H3	H4	H5	H6	H7	H8	H9	H10
0.05	4.6E+06	1.4E+08	7.0E+08	3.2E+09	3.5E+10	1.8E+11	2.9E+11	6.1E+11	2.1E+12	6.1E+09
0.25	5.3E+07	1.1E+09	9.6E+09	7.9E+10	5.8E+11	8.8E+12	3.0E+13	3.5E+13	2.3E+14	3.5E+13
0.50	5.0E+08	6.8E+09	7.6E+10	8.6E+11	4.1E+12	7.9E+13	9.8E+14	5.4E+14	4.1E+15	8.3E+15
0.75	4.7E+09	4.0E+10	5.8E+11	9.2E+12	3.0E+13	6.8E+14	2.2E+15	6.4E+15	6.9E+16	2.0E+18
0.95	5.8E+10	2.9E+11	7.4E+12	2.1E+14	4.6E+14	1.6E+16	1.6E+17	7.6E+17	7.3E+18	1.0E+22
Percentile	CWP									
	H1	H2	H3	H4	H5	H6	H7	H8	H9	H10
0.05	9.9E+06	3.5E+08	1.7E+09	7.8E+09	8.7E+10	4.4E+11	7.0E+11	1.5E+12	5.1E+12	1.5E+10
0.25	1.3E+08	2.9E+09	2.4E+10	2.0E+11	1.5E+12	2.2E+13	7.5E+13	9.0E+13	5.7E+14	8.9E+13
0.50	1.3E+09	1.8E+10	2.0E+11	2.2E+12	1.1E+13	2.0E+14	2.5E+15	1.4E+15	1.1E+16	2.1E+16
0.75	1.2E+10	1.0E+11	1.5E+12	2.4E+13	7.8E+13	1.8E+15	5.9E+15	1.7E+16	1.8E+17	5.3E+18
0.95	1.5E+11	7.9E+11	2.0E+13	5.7E+14	1.2E+15	4.3E+16	4.4E+17	2.0E+18	2.0E+19	2.8E+22
Percentile	IGC09									
	H1	H2	H3	H4	H5	H6	H7	H8	H9	H10
0.05	7.8E+06	1.5E+08	7.3E+08	3.3E+09	3.7E+10	1.9E+11	3.0E+11	6.4E+11	2.2E+12	6.4E+09
0.25	6.6E+07	1.4E+09	1.2E+10	9.9E+10	7.2E+11	1.1E+13	3.7E+13	4.4E+13	2.8E+14	4.4E+13
0.50	6.9E+08	9.4E+09	1.0E+11	1.2E+12	5.7E+12	1.1E+14	1.4E+15	7.4E+14	5.6E+15	1.1E+16
0.75	7.0E+09	5.9E+10	8.6E+11	1.4E+13	4.5E+13	1.0E+15	3.3E+15	9.6E+15	1.0E+17	3.0E+18
0.95	9.6E+10	4.9E+11	1.2E+13	3.5E+14	7.6E+14	2.6E+16	2.7E+17	1.3E+18	1.2E+19	1.7E+22
Percentile	IGC13									
	H1	H2	H3	H4	H5	H6	H7	H8	H9	H10
0.05	7.3E+06	2.3E+08	1.1E+09	5.1E+09	5.6E+10	2.8E+11	4.5E+11	9.7E+11	3.3E+12	9.7E+09
0.25	1.1E+08	2.5E+09	2.1E+10	1.7E+11	1.2E+12	1.9E+13	6.4E+13	7.7E+13	4.9E+14	7.6E+13
0.50	1.3E+09	1.7E+10	1.9E+11	2.2E+12	1.0E+13	2.0E+14	2.5E+15	1.4E+15	1.0E+16	2.1E+16
0.75	1.3E+10	1.1E+11	1.7E+12	2.6E+13	8.6E+13	2.0E+15	6.5E+15	1.9E+16	2.0E+17	5.8E+18
0.95	1.9E+11	9.9E+11	2.5E+13	7.1E+14	1.5E+15	5.3E+16	5.5E+17	2.5E+18	2.4E+19	3.5E+22

Table D5.10c (Cont.): PCB sediment phase concentrations (C_{sed}) (ng/g) to yield aqueous phase concentration assuming local equilibrium assumption equals to saturation concentration ($C_{\text{aq}|x=0\text{m}}=C_{\text{sat}}$) as predicted from the 5th, 25th, 50th, 75th, and 95th percentile sediment-porewater partitioning coefficient values for organic carbon only sorption ($\log K_d$ (OCBC)).

Percentile	ACL									
	H1	H2	H3	H4	H5	H6	H7	H8	H9	H10
0.05	1.6E+06	1.5E+06	1.2E+06	6.7E+05	5.9E+05	3.3E+05	5.5E+05	8.2E+04	8.2E+04	2.2E+05
0.25	2.9E+06	2.8E+06	2.3E+06	1.4E+06	1.2E+06	7.5E+05	1.3E+06	2.7E+05	3.8E+05	1.0E+06
0.50	4.2E+06	4.1E+06	3.4E+06	2.1E+06	1.9E+06	1.2E+06	2.1E+06	5.6E+05	1.1E+06	2.8E+06
0.75	6.0E+06	5.7E+06	4.9E+06	3.2E+06	2.8E+06	2.0E+06	3.3E+06	1.1E+06	2.8E+06	7.5E+06
0.95	9.3E+06	9.1E+06	8.1E+06	5.5E+06	4.8E+06	3.7E+06	6.1E+06	3.1E+06	1.1E+07	2.9E+07
Percentile	AED									
	H1	H2	H3	H4	H5	H6	H7	H8	H9	H10
0.05	5.8E+05	5.6E+05	4.3E+05	2.5E+05	2.2E+05	1.2E+05	2.1E+05	3.1E+04	3.1E+04	8.3E+04
0.25	2.0E+06	1.9E+06	1.5E+06	9.4E+05	8.2E+05	5.1E+05	8.5E+05	1.8E+05	2.6E+05	7.0E+05
0.50	3.5E+06	3.4E+06	2.8E+06	1.8E+06	1.5E+06	1.0E+06	1.7E+06	4.6E+05	8.7E+05	2.3E+06
0.75	5.6E+06	5.4E+06	4.6E+06	3.0E+06	2.6E+06	1.8E+06	3.0E+06	1.1E+06	2.6E+06	7.0E+06
0.95	9.7E+06	9.4E+06	8.4E+06	5.7E+06	5.0E+06	3.9E+06	6.4E+06	3.2E+06	1.1E+07	3.0E+07
Percentile	AFR									
	H1	H2	H3	H4	H5	H6	H7	H8	H9	H10
0.05	9.0E+05	8.7E+05	6.7E+05	3.9E+05	3.4E+05	1.9E+05	3.2E+05	4.8E+04	4.8E+04	1.3E+05
0.25	1.3E+06	1.2E+06	1.0E+06	6.1E+05	5.3E+05	3.3E+05	5.6E+05	1.2E+05	1.7E+05	4.6E+05
0.50	1.7E+06	1.6E+06	1.3E+06	8.3E+05	7.2E+05	4.8E+05	8.0E+05	2.2E+05	4.1E+05	1.1E+06
0.75	2.1E+06	2.0E+06	1.7E+06	1.1E+06	9.7E+05	6.9E+05	1.1E+06	4.0E+05	9.9E+05	2.6E+06
0.95	2.9E+06	2.8E+06	2.5E+06	1.7E+06	1.5E+06	1.2E+06	1.9E+06	9.5E+05	3.4E+06	9.1E+06

Table D5.10c (Cont.): PCB sediment phase concentrations (C_{sed}) (ng/g) to yield aqueous phase concentration assuming local equilibrium assumption equals to saturation concentration ($C_{\text{aq}|x=0\text{m}}=C_{\text{sat}}$) as predicted from the 5th, 25th, 50th, 75th, and 95th percentile sediment-porewater partitioning coefficient values for organic carbon only sorption ($\log K_d$ (OCBC)).

AJL										
Percentile	H1	H2	H3	H4	H5	H6	H7	H8	H9	H10
0.05	6.6E+05	6.4E+05	4.9E+05	2.9E+05	2.5E+05	1.4E+05	2.4E+05	3.5E+04	3.5E+04	9.4E+04
0.25	2.7E+06	2.6E+06	2.1E+06	1.3E+06	1.1E+06	6.9E+05	1.2E+06	2.5E+05	3.5E+05	9.6E+05
0.50	5.1E+06	4.9E+06	4.1E+06	2.6E+06	2.2E+06	1.5E+06	2.4E+06	6.7E+05	1.3E+06	3.4E+06
0.75	8.3E+06	8.0E+06	6.8E+06	4.5E+06	3.9E+06	2.7E+06	4.5E+06	1.6E+06	3.9E+06	1.0E+07
0.95	1.5E+07	1.4E+07	1.3E+07	8.7E+06	7.6E+06	5.9E+06	9.8E+06	4.9E+06	1.8E+07	4.7E+07
AMW										
Percentile	H1	H2	H3	H4	H5	H6	H7	H8	H9	H10
0.05	6.7E+06	6.5E+06	5.0E+06	2.9E+06	2.5E+06	1.4E+06	2.4E+06	3.6E+05	3.6E+05	9.7E+05
0.25	1.4E+07	1.4E+07	1.1E+07	6.9E+06	6.0E+06	3.7E+06	6.2E+06	1.3E+06	1.9E+06	5.1E+06
0.50	2.2E+07	2.1E+07	1.8E+07	1.1E+07	9.6E+06	6.4E+06	1.1E+07	2.9E+06	5.5E+06	1.5E+07
0.75	3.2E+07	3.1E+07	2.6E+07	1.7E+07	1.5E+07	1.1E+07	1.7E+07	6.1E+06	1.5E+07	4.0E+07
0.95	5.1E+07	5.0E+07	4.5E+07	3.0E+07	2.6E+07	2.0E+07	3.4E+07	1.7E+07	6.1E+07	1.6E+08
AOT										
Percentile	H1	H2	H3	H4	H5	H6	H7	H8	H9	H10
0.05	1.3E+06	1.2E+06	9.3E+05	5.4E+05	4.7E+05	2.7E+05	4.5E+05	6.6E+04	6.6E+04	1.8E+05
0.25	2.3E+06	2.2E+06	1.8E+06	1.1E+06	9.4E+05	5.9E+05	9.8E+05	2.1E+05	3.0E+05	8.1E+05
0.50	3.3E+06	3.2E+06	2.6E+06	1.7E+06	1.4E+06	9.6E+05	1.6E+06	4.3E+05	8.2E+05	2.2E+06
0.75	4.6E+06	4.4E+06	3.8E+06	2.5E+06	2.1E+06	1.5E+06	2.5E+06	8.8E+05	2.2E+06	5.7E+06
0.95	7.0E+06	6.8E+06	6.1E+06	4.1E+06	3.6E+06	2.8E+06	4.6E+06	2.3E+06	8.3E+06	2.2E+07
CBC										
Percentile	H1	H2	H3	H4	H5	H6	H7	H8	H9	H10
0.05	4.4E+05	4.3E+05	3.3E+05	1.9E+05	1.7E+05	9.4E+04	1.6E+05	2.3E+04	2.3E+04	6.3E+04
0.25	2.1E+06	2.0E+06	1.6E+06	9.8E+05	8.5E+05	5.3E+05	8.9E+05	1.9E+05	2.7E+05	7.3E+05
0.50	4.2E+06	4.0E+06	3.3E+06	2.1E+06	1.8E+06	1.2E+06	2.0E+06	5.5E+05	1.0E+06	2.8E+06
0.75	7.1E+06	6.8E+06	5.9E+06	3.8E+06	3.3E+06	2.4E+06	3.9E+06	1.4E+06	3.4E+06	8.9E+06
0.95	1.3E+07	1.3E+07	1.1E+07	7.7E+06	6.7E+06	5.2E+06	8.6E+06	4.3E+06	1.5E+07	4.1E+07

Table D5.10c (Cont.): PCB sediment phase concentrations (C_{sed}) (ng/g) to yield aqueous phase concentration assuming local equilibrium assumption equals to saturation concentration ($C_{\text{aq}|x=0\text{m}}=C_{\text{sat}}$) as predicted from the 5th, 25th, 50th, 75th, and 95th percentile sediment-porewater partitioning coefficient values for organic carbon only sorption ($\log K_d$ (OCBC)).

Percentile	CLC									
	H1	H2	H3	H4	H5	H6	H7	H8	H9	H10
0.05	3.9E+06	3.8E+06	2.9E+06	1.7E+06	1.5E+06	8.4E+05	1.4E+06	2.1E+05	2.1E+05	5.6E+05
0.25	5.2E+06	5.0E+06	4.1E+06	2.5E+06	2.2E+06	1.3E+06	2.2E+06	4.8E+05	6.8E+05	1.9E+06
0.50	6.3E+06	6.1E+06	5.1E+06	3.2E+06	2.8E+06	1.9E+06	3.1E+06	8.4E+05	1.6E+06	4.2E+06
0.75	7.7E+06	7.4E+06	6.4E+06	4.1E+06	3.6E+06	2.6E+06	4.2E+06	1.5E+06	3.6E+06	9.7E+06
0.95	1.0E+07	9.9E+06	8.8E+06	6.0E+06	5.2E+06	4.0E+06	6.7E+06	3.3E+06	1.2E+07	3.2E+07
Percentile	CWP									
	H1	H2	H3	H4	H5	H6	H7	H8	H9	H10
0.05	3.6E+06	3.5E+06	2.7E+06	1.6E+06	1.4E+06	7.7E+05	1.3E+06	1.9E+05	1.9E+05	5.1E+05
0.25	5.7E+06	5.5E+06	4.4E+06	2.7E+06	2.4E+06	1.5E+06	2.5E+06	5.2E+05	7.5E+05	2.0E+06
0.50	7.7E+06	7.5E+06	6.2E+06	3.9E+06	3.4E+06	2.3E+06	3.7E+06	1.0E+06	1.9E+06	5.1E+06
0.75	1.0E+07	1.0E+07	8.5E+06	5.5E+06	4.8E+06	3.4E+06	5.6E+06	2.0E+06	4.9E+06	1.3E+07
0.95	1.5E+07	1.5E+07	1.3E+07	8.9E+06	7.8E+06	6.1E+06	1.0E+07	5.0E+06	1.8E+07	4.8E+07
Percentile	IGC09									
	H1	H2	H3	H4	H5	H6	H7	H8	H9	H10
0.05	6.7E+06	6.5E+06	5.0E+06	2.9E+06	2.5E+06	1.4E+06	2.4E+06	3.5E+05	3.5E+05	9.6E+05
0.25	9.9E+06	9.5E+06	7.7E+06	4.7E+06	4.1E+06	2.5E+06	4.2E+06	9.0E+05	1.3E+06	3.5E+06
0.50	1.3E+07	1.2E+07	1.0E+07	6.5E+06	5.6E+06	3.7E+06	6.2E+06	1.7E+06	3.2E+06	8.5E+06
0.75	1.6E+07	1.6E+07	1.4E+07	8.9E+06	7.7E+06	5.5E+06	9.0E+06	3.2E+06	7.8E+06	2.1E+07
0.95	2.3E+07	2.3E+07	2.0E+07	1.4E+07	1.2E+07	9.3E+06	1.5E+07	7.7E+06	2.8E+07	7.3E+07
Percentile	IGC13									
	H1	H2	H3	H4	H5	H6	H7	H8	H9	H10
0.05	6.2E+06	6.0E+06	4.6E+06	2.7E+06	2.4E+06	1.3E+06	2.2E+06	3.3E+05	3.3E+05	8.9E+05
0.25	9.9E+06	9.5E+06	7.7E+06	4.7E+06	4.1E+06	2.5E+06	4.2E+06	9.0E+05	1.3E+06	3.5E+06
0.50	1.3E+07	1.3E+07	1.1E+07	6.7E+06	5.8E+06	3.9E+06	6.4E+06	1.8E+06	3.3E+06	8.9E+06
0.75	1.8E+07	1.7E+07	1.5E+07	9.5E+06	8.3E+06	5.9E+06	9.7E+06	3.4E+06	8.4E+06	2.2E+07
0.95	2.6E+07	2.5E+07	2.3E+07	1.5E+07	1.3E+07	1.0E+07	1.7E+07	8.5E+06	3.1E+07	8.1E+07

Table D5.10d (Cont.): PCB sediment phase concentrations (C_{sed}) (ng/g) to yield aqueous phase concentration assuming local equilibrium assumption equals to saturation concentration ($C_{aq|x=0m}=C_{sat}$) as predicted from the 5th, 25th, 50th, 75th, and 95th percentile sediment-porewater partitioning coefficient values for organic carbon only sorption ($\log K_d$ (OCBC)).

ACL										
Percentile	H1	H2	H3	H4	H5	H6	H7	H8	H9	H10
	1.6E+	1.5E+	1.6E+	9.3E+	8.9E+	4.9E+	6.6E+	8.4E+	6.2E+	4.3E+
0.05	06	06	06	06	07	08	09	09	10	11
	2.9E+	2.8E+	1.8E+	8.1E+	5.9E+	2.9E+	3.2E+	5.4E+	6.4E+	4.5E+
0.25	06	06	07	07	08	09	10	10	11	12
	4.2E+	2.0E+	1.1E+	4.1E+	2.3E+	9.2E+	8.5E+	1.5E+	2.4E+	1.6E+
0.50	06	07	08	08	09	09	10	11	12	13
	3.4E+	1.5E+	6.8E+	1.9E+	8.1E+	2.7E+	2.1E+	3.9E+	8.5E+	5.8E+
0.75	07	08	08	09	09	10	11	11	12	13
	4.1E+	1.4E+	5.3E+	1.2E+	3.8E+	1.1E+	7.3E+	1.7E+	6.2E+	4.3E+
0.95	08	09	09	10	10	11	11	12	13	14
AED										
Percentile	H1	H2	H3	H4	H5	H6	H7	H8	H9	H10
	5.8E+	5.6E+	8.2E+	4.7E+	4.6E+	2.5E+	3.3E+	4.3E+	3.2E+	2.2E+
0.05	05	05	05	06	07	08	09	09	10	11
	2.0E+	1.9E+	1.2E+	5.4E+	4.0E+	1.9E+	2.2E+	3.6E+	4.3E+	3.0E+
0.25	06	06	07	07	08	09	10	10	11	12
	3.5E+	1.4E+	7.9E+	2.9E+	1.6E+	6.4E+	5.9E+	1.0E+	1.7E+	1.1E+
0.50	06	07	07	08	09	09	10	11	12	13
	2.3E+	1.0E+	4.7E+	1.3E+	5.6E+	1.9E+	1.5E+	2.7E+	5.9E+	4.0E+
0.75	07	08	08	09	09	10	11	11	12	13
	2.7E+	9.4E+	3.5E+	7.8E+	2.5E+	7.4E+	4.8E+	1.1E+	4.1E+	2.8E+
0.95	08	08	09	09	10	10	11	12	13	14
AFR										
Percentile	H1	H2	H3	H4	H5	H6	H7	H8	H9	H10
	9.0E+	8.7E+	7.0E+	4.0E+	3.9E+	2.1E+	2.8E+	3.6E+	2.7E+	1.9E+
0.05	05	05	05	06	07	08	09	09	10	11
	1.3E+	1.2E+	4.7E+	2.2E+	1.6E+	7.7E+	8.7E+	1.4E+	1.7E+	1.2E+
0.25	06	06	06	07	08	08	09	10	11	12
	1.7E+	4.2E+	2.4E+	8.7E+	4.8E+	2.0E+	1.8E+	3.2E+	5.1E+	3.5E+
0.50	06	06	07	07	08	09	10	10	11	12
	6.0E+	2.7E+	1.2E+	3.5E+	1.4E+	4.9E+	3.8E+	7.0E+	1.5E+	1.0E+
0.75	06	07	08	08	09	09	10	10	12	13
	6.0E+	2.1E+	7.7E+	1.7E+	5.5E+	1.6E+	1.1E+	2.5E+	9.1E+	6.2E+
0.95	07	08	08	09	09	10	11	11	12	13

Table D5.10d (Cont.): PCB sediment phase concentrations (C_{sed}) (ng/g) to yield aqueous phase concentration assuming local equilibrium assumption equals to saturation concentration ($C_{aq|x=0m}=C_{sat}$) as predicted from the 5th, 25th, 50th, 75th, and 95th percentile sediment-porewater

Percentile										
AJL										
le	H1	H2	H3	H4	H5	H6	H7	H8	H9	H10
0.05	6.6E+05	6.4E+05	5.0E+05	2.9E+06	2.8E+07	1.5E+08	2.0E+09	2.6E+09	1.9E+10	1.3E+11
0.25	2.7E+06	2.6E+06	1.1E+07	5.1E+07	3.7E+08	1.8E+09	2.0E+10	3.4E+10	4.0E+11	2.8E+12
0.50	5.1E+06	1.5E+07	8.9E+07	3.2E+08	1.8E+09	7.2E+09	6.7E+10	1.2E+11	1.9E+12	1.3E+13
0.75	3.0E+07	1.4E+08	6.1E+08	1.7E+09	7.3E+09	2.5E+10	1.9E+11	3.5E+11	7.6E+12	5.2E+13
0.95	4.1E+08	1.4E+09	5.3E+09	1.2E+10	3.8E+10	1.1E+11	7.3E+11	1.7E+12	6.2E+13	4.3E+14
AMW										
le	H1	H2	H3	H4	H5	H6	H7	H8	H9	H10
0.05	6.7E+06	6.5E+06	8.5E+06	4.9E+07	4.7E+08	2.6E+09	3.5E+10	4.4E+10	3.3E+11	2.3E+12
0.25	1.4E+07	1.4E+07	9.6E+07	4.4E+08	3.2E+09	1.6E+10	1.8E+11	2.9E+11	3.5E+12	2.4E+13
0.50	2.2E+07	1.1E+08	6.2E+08	2.3E+09	1.2E+10	5.0E+10	4.7E+11	8.2E+11	1.3E+13	9.0E+13
0.75	1.9E+08	8.3E+08	3.8E+09	1.1E+10	4.5E+10	1.5E+11	1.2E+12	2.2E+12	4.7E+13	3.2E+14
0.95	2.2E+09	7.9E+09	2.9E+10	6.5E+10	2.1E+11	6.2E+11	4.0E+12	9.5E+12	3.4E+14	2.3E+15
AOT										
le	H1	H2	H3	H4	H5	H6	H7	H8	H9	H10
0.05	1.3E+06	1.2E+06	9.3E+05	4.6E+06	4.5E+07	2.5E+08	3.3E+09	4.2E+09	3.1E+10	2.1E+11
0.25	2.3E+06	2.8E+06	2.0E+07	9.3E+07	6.8E+08	3.3E+09	3.7E+10	6.2E+10	7.4E+11	5.1E+12
0.50	5.2E+06	3.0E+07	1.7E+08	6.2E+08	3.4E+09	1.4E+10	1.3E+11	2.3E+11	3.7E+12	2.5E+13
0.75	6.1E+07	2.7E+08	1.2E+09	3.5E+09	1.5E+10	4.9E+10	3.8E+11	7.1E+11	1.5E+13	1.0E+14
0.95	8.5E+08	3.0E+09	1.1E+10	2.5E+10	7.9E+10	2.3E+11	1.5E+12	3.6E+12	1.3E+14	8.9E+14
CBC										
le	H1	H2	H3	H4	H5	H6	H7	H8	H9	H10
0.05	4.4E+05	4.3E+05	3.7E+06	2.1E+07	2.1E+08	1.1E+09	1.5E+10	1.9E+10	1.4E+11	9.9E+11
0.25	2.1E+06	1.2E+07	8.7E+07	4.0E+08	2.9E+09	1.4E+10	1.6E+11	2.7E+11	3.2E+12	2.2E+13
0.50	2.2E+07	1.3E+08	7.3E+08	2.6E+09	1.5E+10	5.9E+10	5.5E+11	9.6E+11	1.6E+13	1.1E+14
0.75	2.5E+08	1.1E+09	5.1E+09	1.4E+10	6.1E+10	2.1E+11	1.6E+12	2.9E+12	6.3E+13	4.3E+14

Table D5.10d (Cont.): PCB sediment phase concentrations (C_{sed}) (ng/g) to yield aqueous phase concentration assuming local equilibrium assumption equals to saturation concentration ($C_{aq|x=0m}=C_{sat}$) as predicted from the 5th, 25th, 50th, 75th, and 95th percentile sediment-porewater

	3.4E+09	1.2E+10	4.4E+10	1.0E+11	3.2E+11	9.5E+11	6.1E+12	1.5E+13	5.2E+14	3.6E+15
0.95	09	10	10	11	11	11	12	13	14	15
Percentile	CLC									
le	H1	H2	H3	H4	H5	H6	H7	H8	H9	H10
0.05	3.9E+06	3.8E+06	3.3E+07	1.9E+08	1.8E+09	1.0E+10	1.4E+11	1.7E+11	1.3E+12	8.8E+12
0.25	5.2E+06	3.0E+07	2.2E+08	1.0E+09	7.4E+09	3.6E+10	4.0E+11	6.7E+11	8.1E+12	5.6E+13
0.50	3.4E+07	1.9E+08	1.1E+09	4.0E+09	2.2E+10	9.0E+10	8.4E+11	1.5E+12	2.4E+13	1.6E+14
0.75	2.7E+08	1.2E+09	5.6E+09	1.6E+10	6.6E+10	2.2E+11	1.7E+12	3.2E+12	6.9E+13	4.7E+14
0.95	2.7E+09	9.3E+09	3.4E+10	7.7E+10	2.5E+11	7.3E+11	4.7E+12	1.1E+13	4.0E+14	2.8E+15
Percentile	CWP									
le	H1	H2	H3	H4	H5	H6	H7	H8	H9	H10
0.05	3.6E+06	9.2E+06	8.2E+07	4.7E+08	4.5E+09	2.5E+10	3.3E+11	4.3E+11	3.2E+12	2.2E+13
0.25	1.0E+07	7.7E+07	5.6E+08	2.6E+09	1.9E+10	9.1E+10	1.0E+12	1.7E+12	2.0E+13	1.4E+14
0.50	8.7E+07	5.0E+08	2.9E+09	1.0E+10	5.7E+10	2.3E+11	2.2E+12	3.8E+12	6.1E+13	4.2E+14
0.75	7.2E+08	3.2E+09	1.5E+10	4.1E+10	1.7E+11	5.9E+11	4.5E+12	8.4E+12	1.8E+14	1.2E+15
0.95	7.1E+09	2.5E+10	9.2E+10	2.1E+11	6.6E+11	2.0E+12	1.3E+13	3.0E+13	1.1E+15	7.4E+15
Percentile	IGC09									
le	H1	H2	H3	H4	H5	H6	H7	H8	H9	H10
0.05	6.7E+06	6.5E+06	3.5E+07	2.0E+08	1.9E+09	1.1E+10	1.4E+11	1.8E+11	1.4E+12	9.2E+12
0.25	9.9E+06	3.8E+07	2.8E+08	1.3E+09	9.3E+09	4.5E+10	5.1E+11	8.4E+11	1.0E+13	7.0E+13
0.50	4.6E+07	2.7E+08	1.5E+09	5.6E+09	3.1E+10	1.2E+11	1.2E+12	2.0E+12	3.3E+13	2.2E+14
0.75	4.1E+08	1.8E+09	8.3E+09	2.4E+10	9.9E+10	3.3E+11	2.6E+12	4.8E+12	1.0E+14	7.0E+14
0.95	4.4E+09	1.5E+10	5.7E+10	1.3E+11	4.1E+11	1.2E+12	7.8E+12	1.9E+13	6.7E+14	4.6E+15
Percentile	IGC13									
le	H1	H2	H3	H4	H5	H6	H7	H8	H9	H10
0.05	6.2E+06	6.0E+06	5.3E+07	3.0E+08	2.9E+09	1.6E+10	2.1E+11	2.7E+11	2.0E+12	1.4E+13
0.25	9.9E+06	6.6E+07	4.8E+08	2.2E+09	1.6E+10	7.8E+10	8.7E+11	1.5E+12	1.7E+13	1.2E+14
0.50	8.5E+07	4.9E+08	2.8E+09	1.0E+10	5.6E+10	2.3E+11	2.1E+12	3.7E+12	6.0E+13	4.1E+14

Table D5.10d (Cont.): PCB sediment phase concentrations (C_{sed}) (ng/g) to yield aqueous phase concentration assuming local equilibrium assumption equals to saturation concentration ($C_{aq|x=0m}=C_{sat}$) as predicted from the 5th, 25th, 50th, 75th, and 95th percentile sediment-porewater

	7.9E+	3.5E+	1.6E+	4.5E+	1.9E+	6.4E+	5.0E+	9.2E+	2.0E+	1.4E+
0.75	08	09	10	10	11	11	12	12	14	15
0.95	09	10	11	11	11	12	13	13	15	15

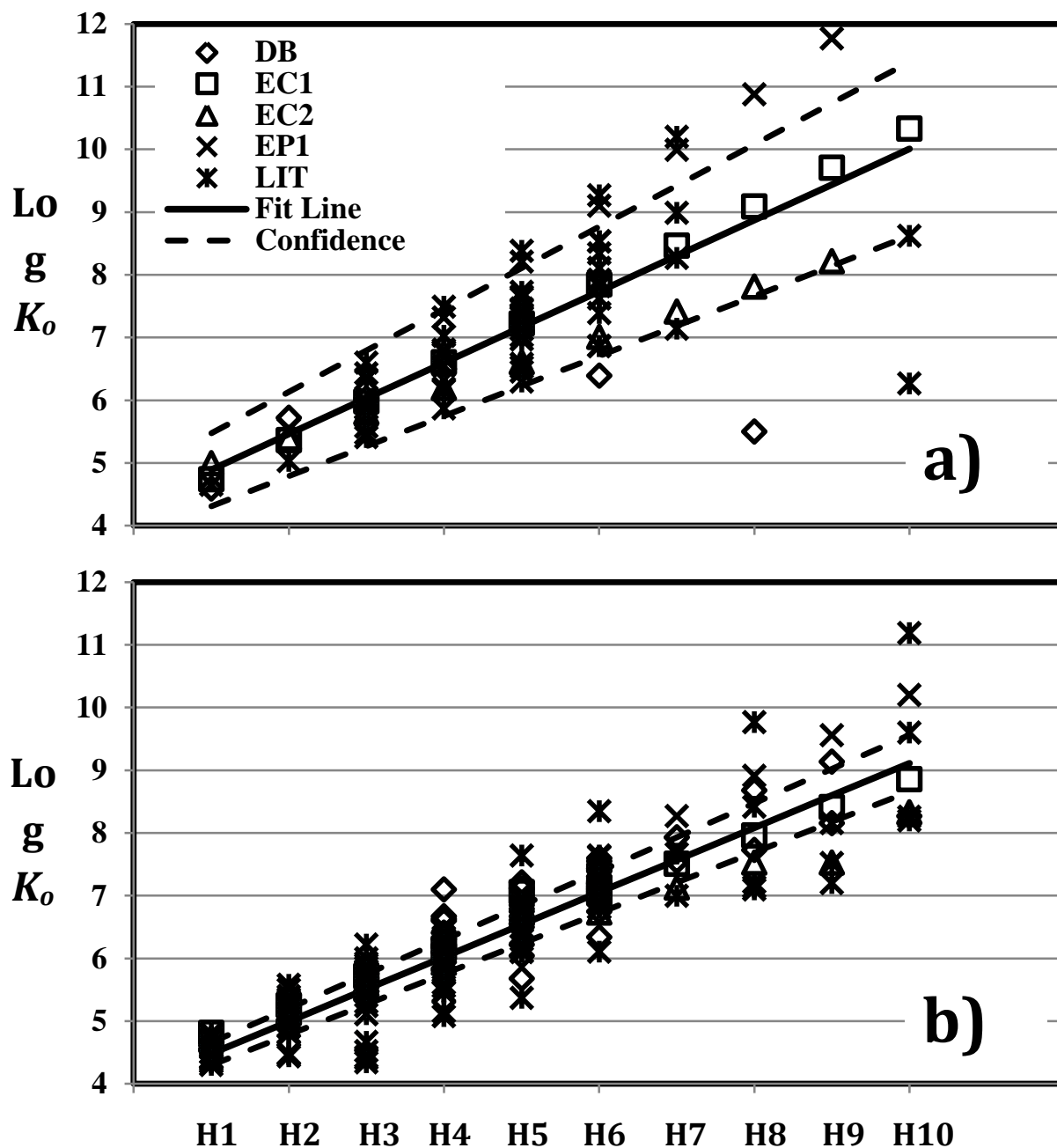


Figure D5.1: Regression analysis for 90 and 221 $\log K_{ow}$ values for a)PBDEs and b)PCBs predicted from empirical correlations (square and triangle, EC1 and EC2 are from Equations 2.1 and 2.2 for PBDEs, respectively, and Equations 2.3 and 2.4 for PCBs, respectively), USEPA EPI (EPI), EPI database (DB), and literature values (LIT). Straight line is best fit line and dotted lines are upper and lower 95% confidence interval obtained from regression analysis. X-axes are homologs 1 through 10 (H1 to H10).

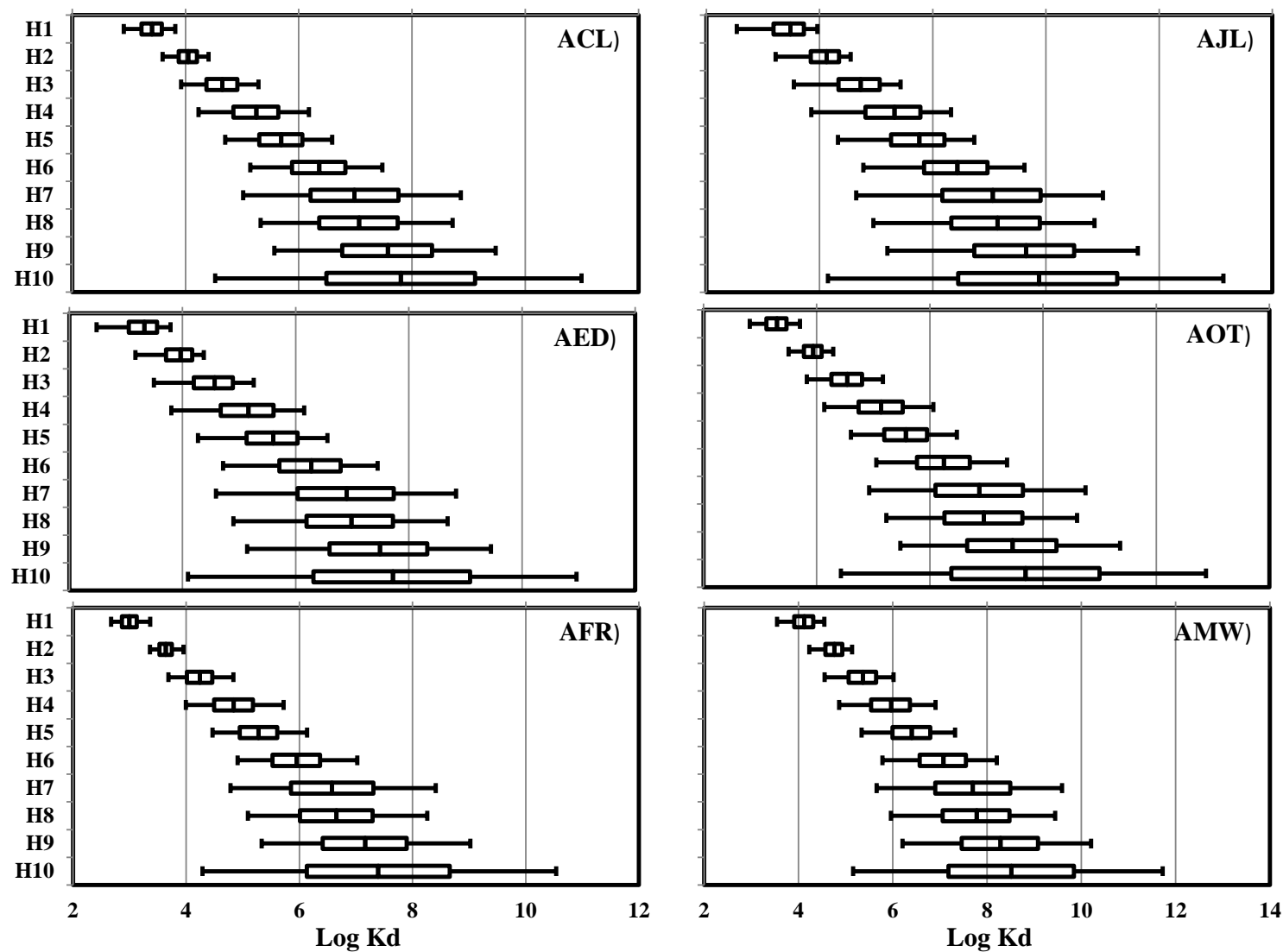


Figure D5.2a: Distribution of sediment porewater partitioning coefficient for organic carbon only sorption ($K_d(\text{OC})$) for PBDE absorption in AR sediment columns as predicted by Monte Carlo simulation. Y-axes are homologs 1 through 10 (H1 to H10).

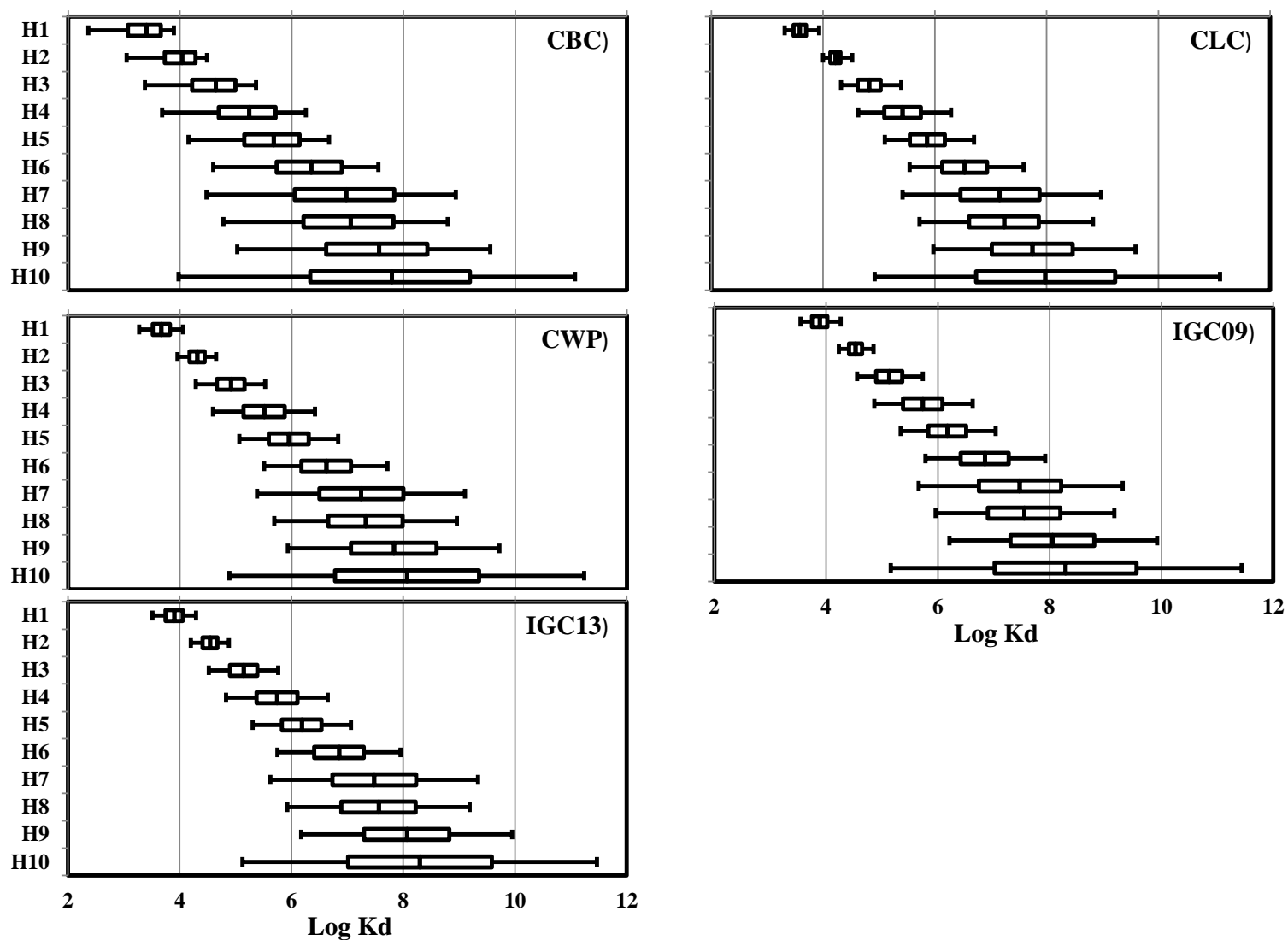


Figure D5.2b: Distribution of sediment porewater partitioning coefficient for organic carbon only sorption ($K_d(OC)$) for PBDE absorption in Chicago and IGC sediment columns as predicted by Monte Carlo simulation. Y-axes are homologs 1 through 10 (H1 to H10).

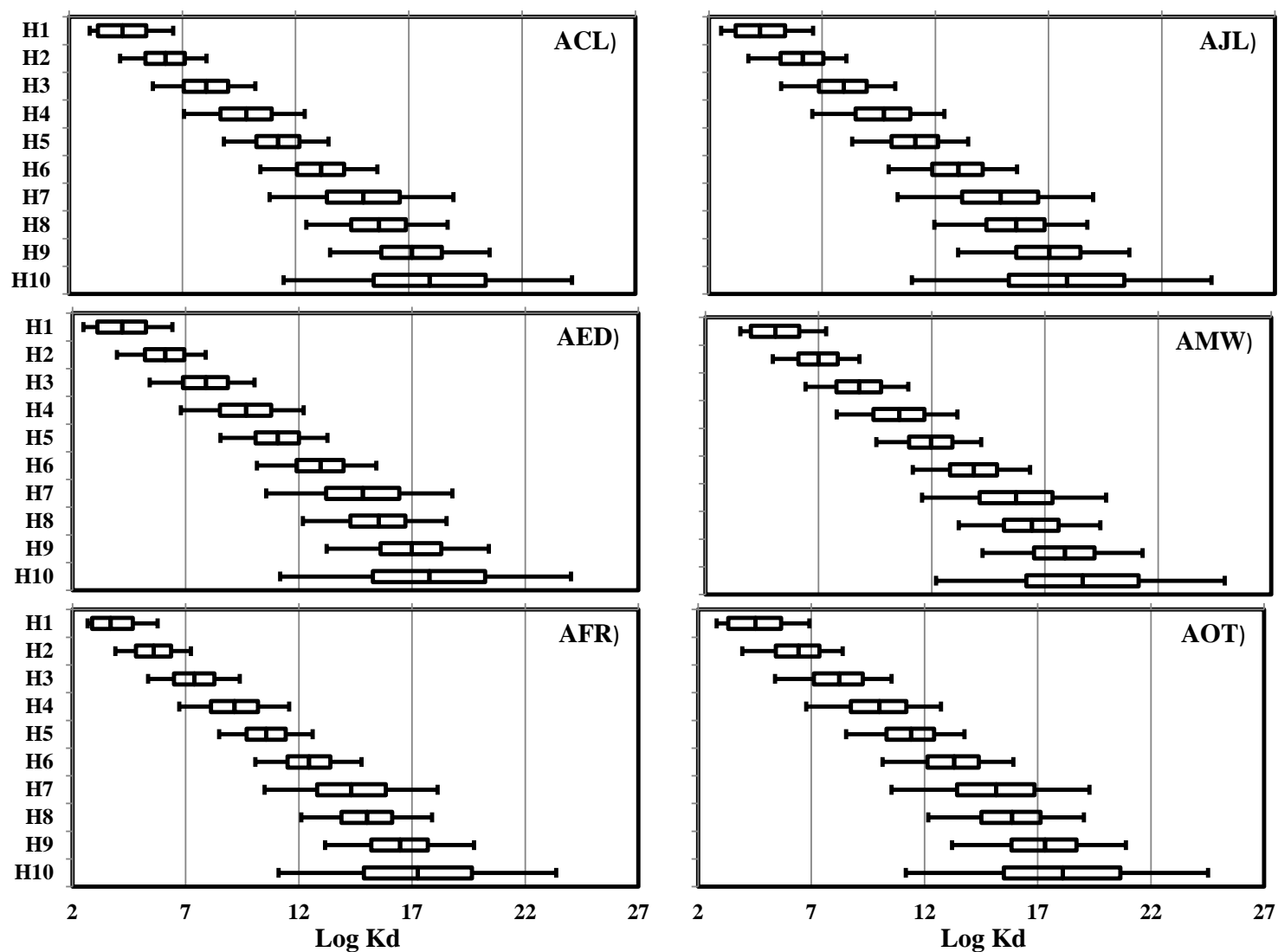


Figure D5.2c: Distribution of sediment porewater partitioning coefficient for organic carbon and black carbon sorptions (K_d (OCBC)) for PBDE absorption in AR sediment columns as predicted by Monte Carlo simulation. Y-axes are homologs 1 through 10 (H1 to H10).

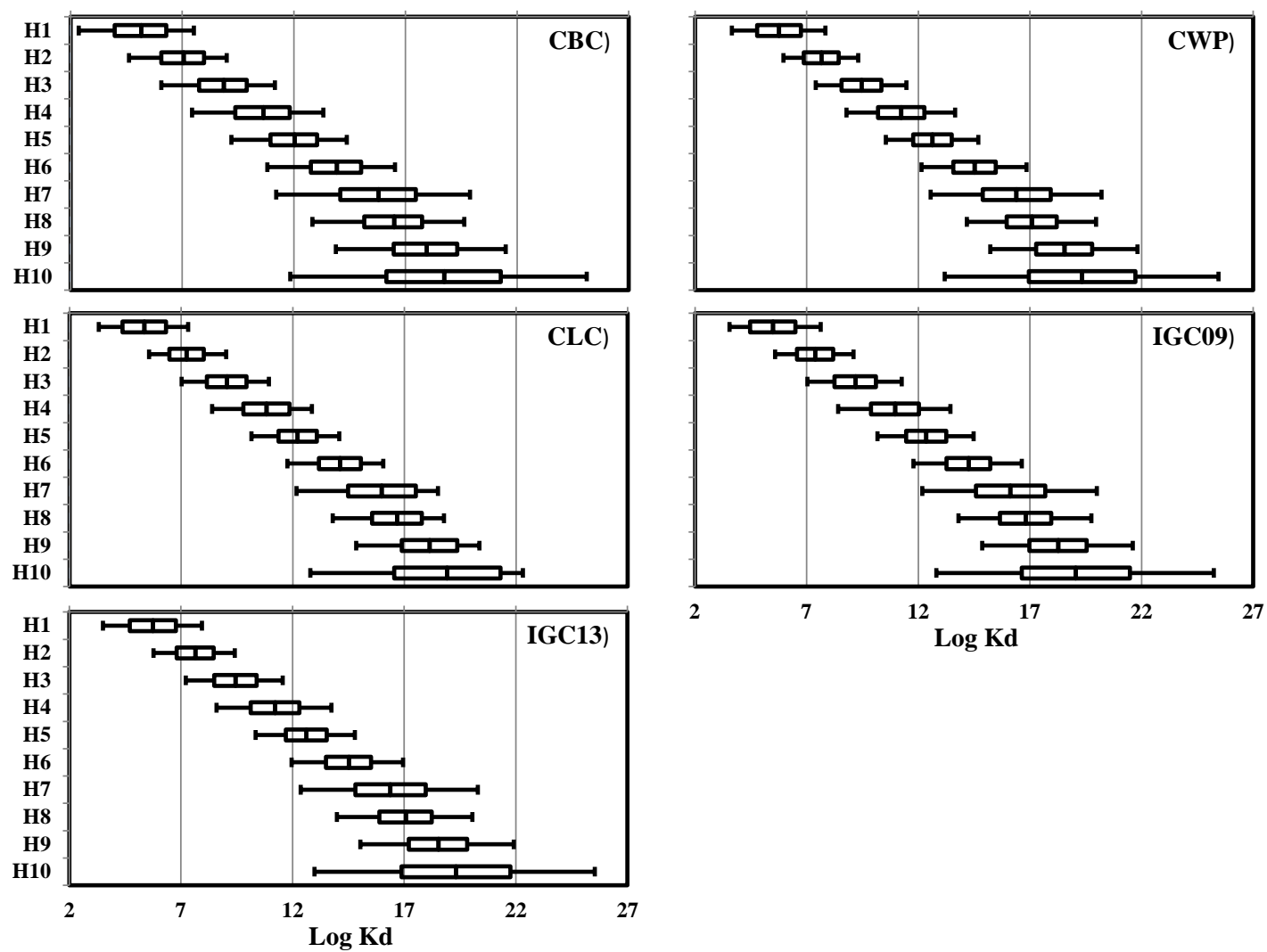


Figure D5.2d: Distribution of sediment porewater partitioning coefficient for organic carbon and black carbon sorptions (K_d (OCBC)) for PBDE absorption in Chicago and IGC sediment columns as predicted by Monte Carlo simulation. Y-axes are homologs 1 through 10 (H1 to H10).

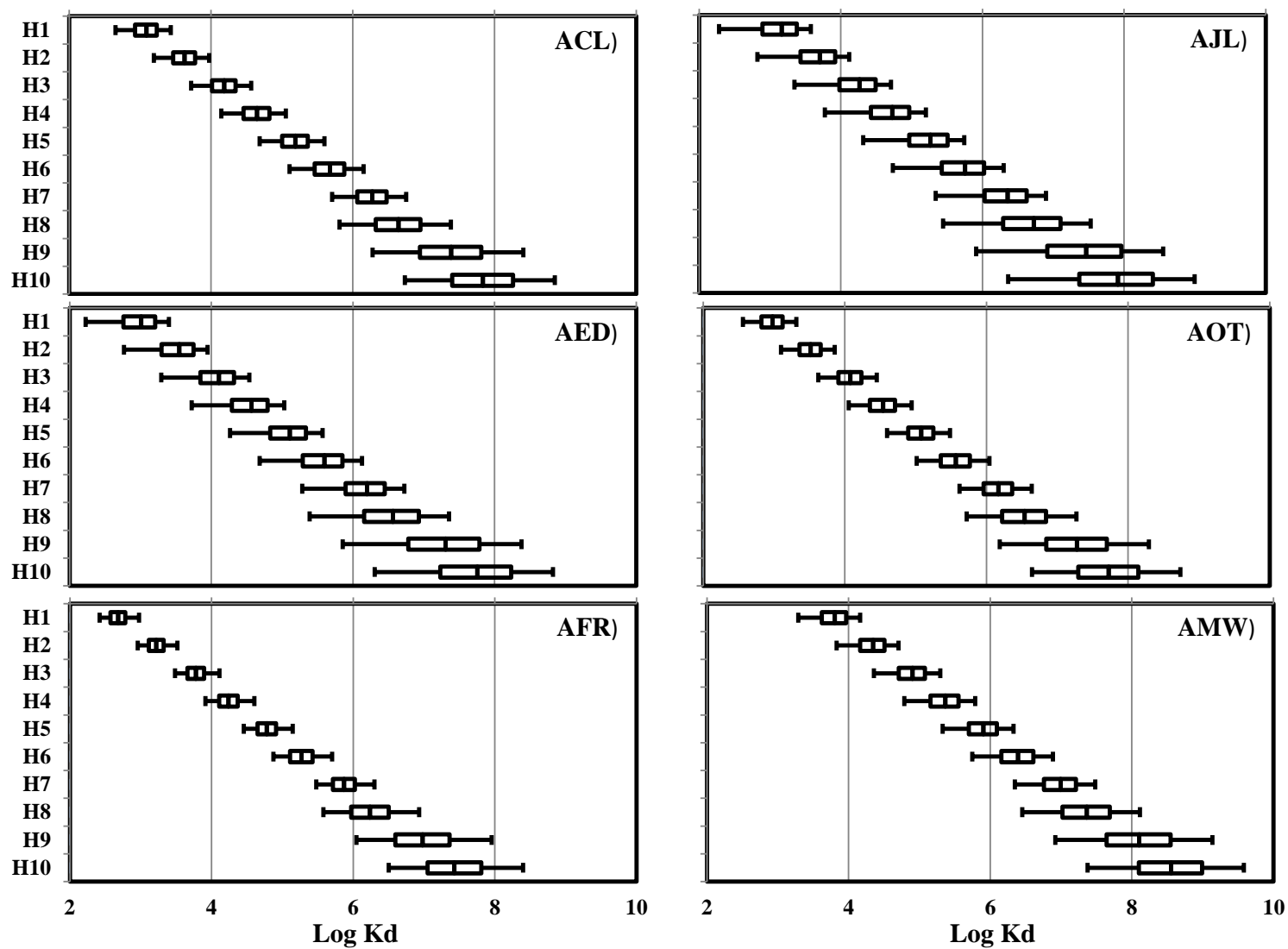


Figure D5.2e: Distribution of sediment porewater partitioning coefficient for organic carbon only sorption (K_d (OC)) for PCB absorption in AR sediment columns as predicted by Monte Carlo simulation. Y-axes are homologs 1 through 10 (H1 to H10).

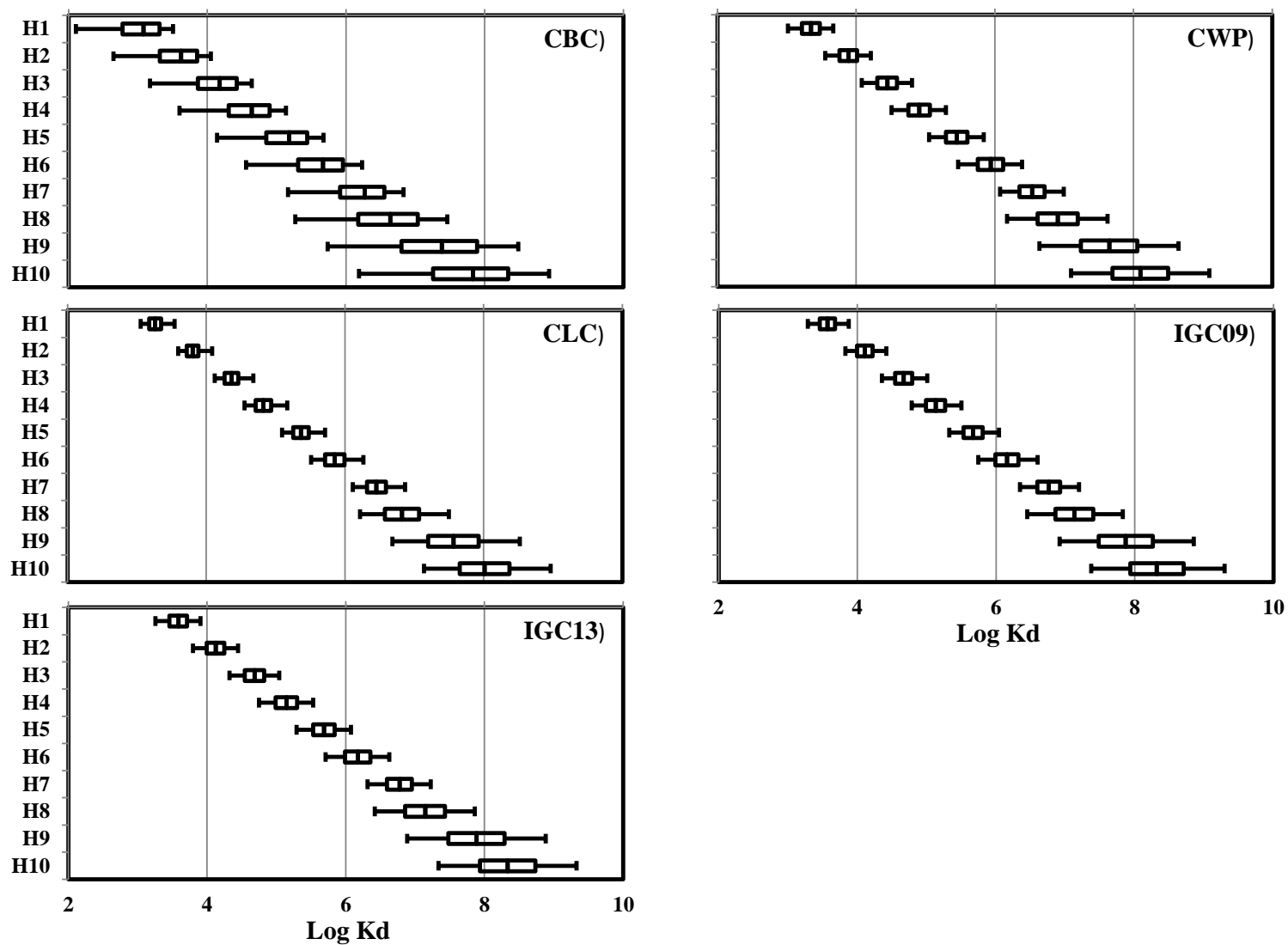


Figure D5.2f: Distribution of sediment porewater partitioning coefficient for organic carbon only sorption (K_d (OC)) for PCB absorption in Chicago and IGC sediment columns as predicted by Monte Carlo simulation. Y-axes are homologs 1 through 10 (H1 to H10).

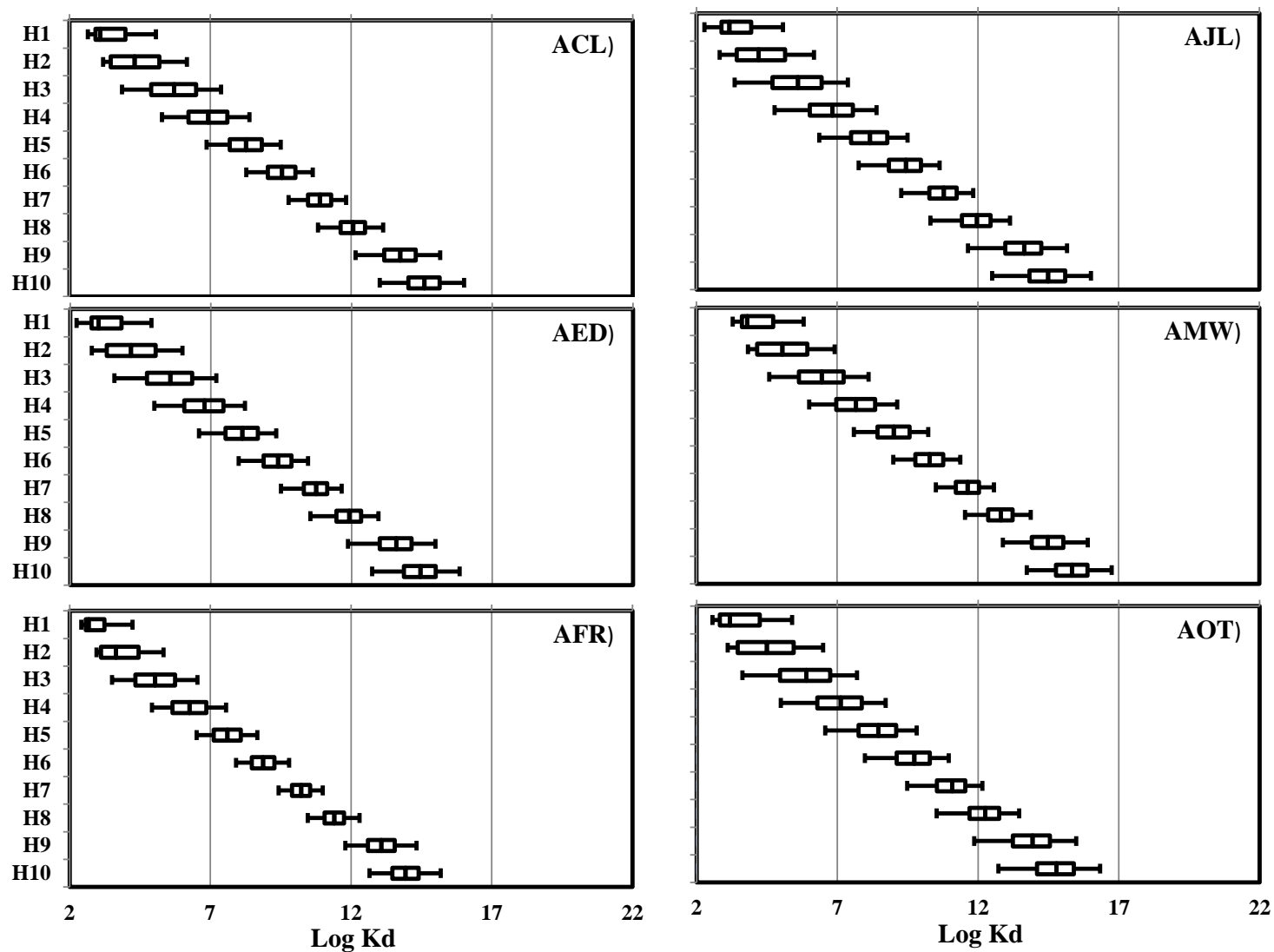


Figure D5.2g: Distribution of sediment porewater partitioning coefficient for organic carbon and black carbon sorptions (K_d (OCBC)) for PCB absorption in AR sediment columns as predicted by Monte Carlo simulation. Y-axes are homologs 1 through 10 (H1 to H10).

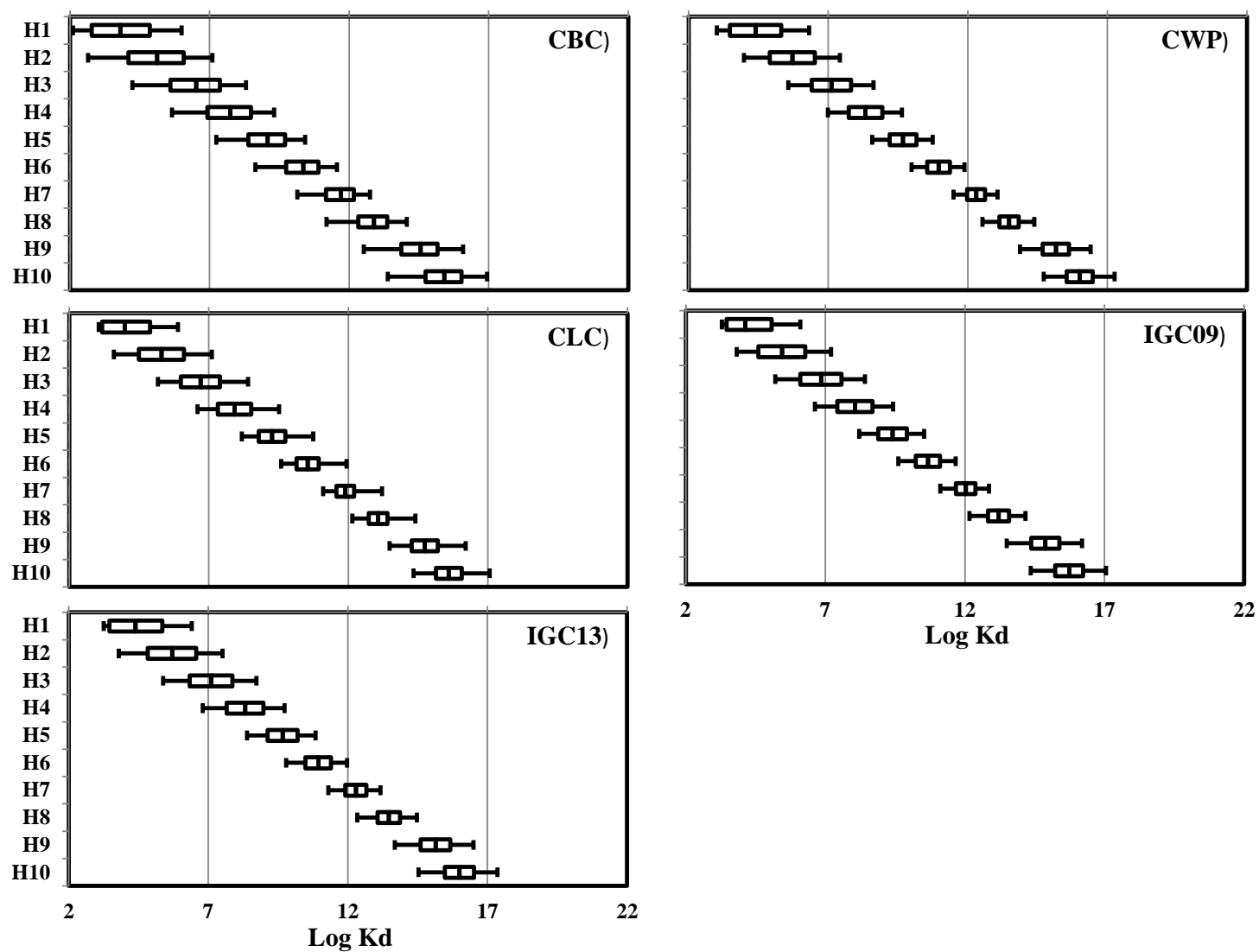


Figure D5.2g: Distribution of sediment porewater partitioning coefficient for organic carbon and black carbon sorptions (K_d (OCBC)) for PCB absorption in Chicago and IGC sediment columns as predicted by Monte Carlo simulation. Y-axes are homologs 1 through 10 (H1 to H10).

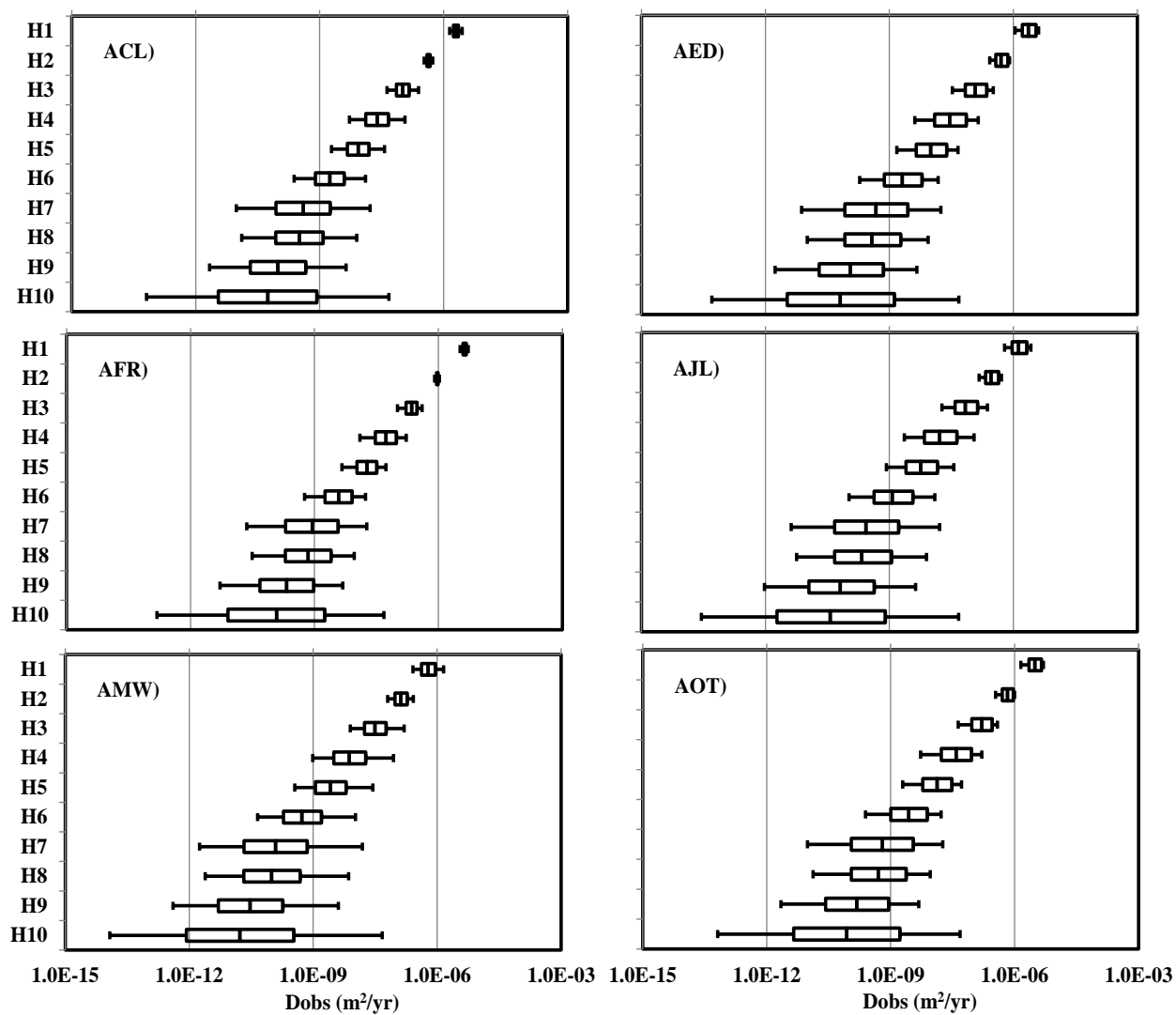


Figure D5.3a: Distribution of observed diffusivities values for organic carbon only sorption (D_{obs} (OC)) for PBDE homologs in AR sediment columns as predicted by Monte Carlo simulations. Y-axes are homologs 1 through 10 (H1 to H10).

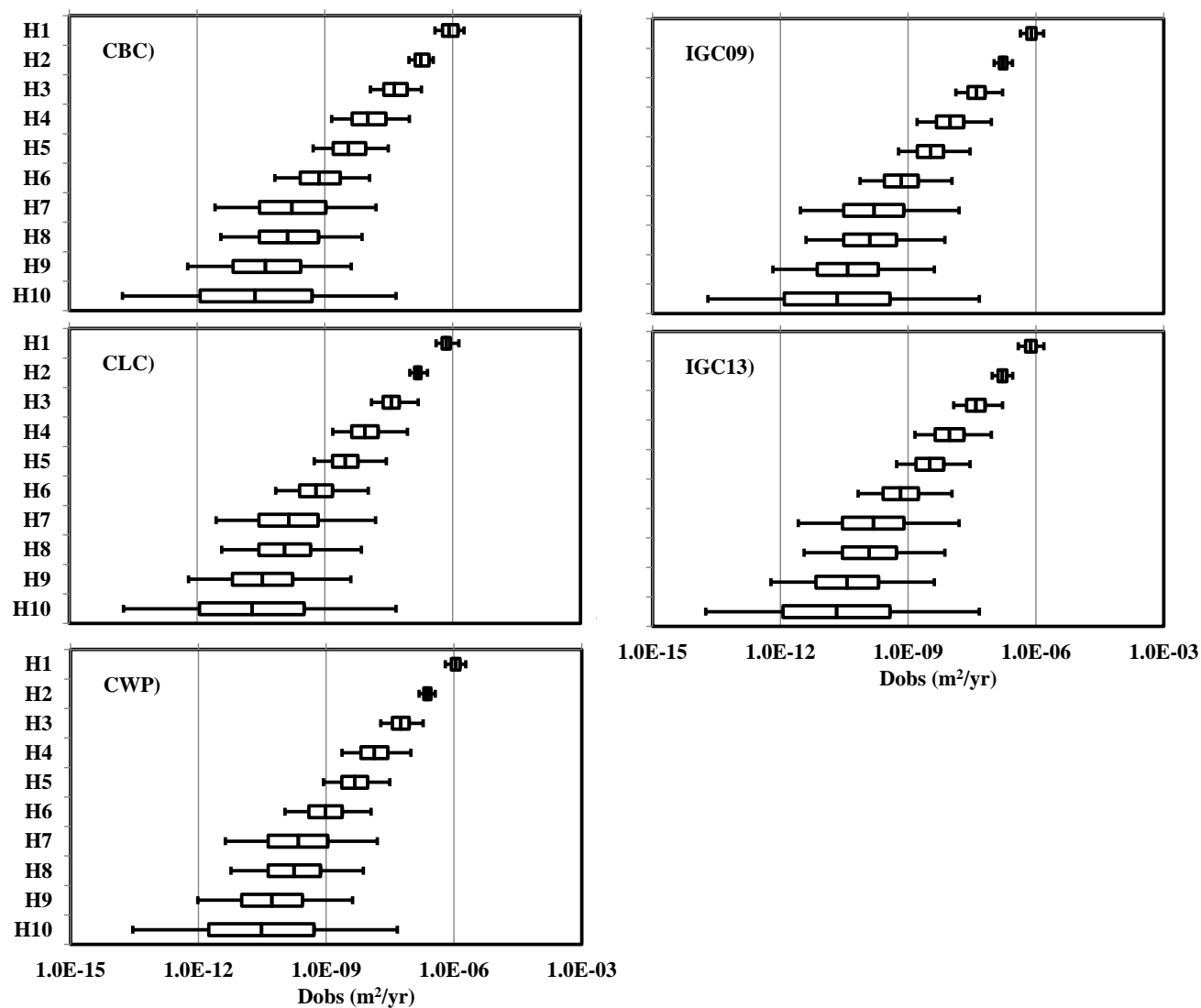


Figure D5.3b: Distribution of observed diffusivities values for organic carbon only sorption (D_{obs} (OC)) for PBDE homologs in Chicago and IGC sediment columns as predicted by Monte Carlo simulations. Y-axes are homologs 1 through 10 (H1 to H10).

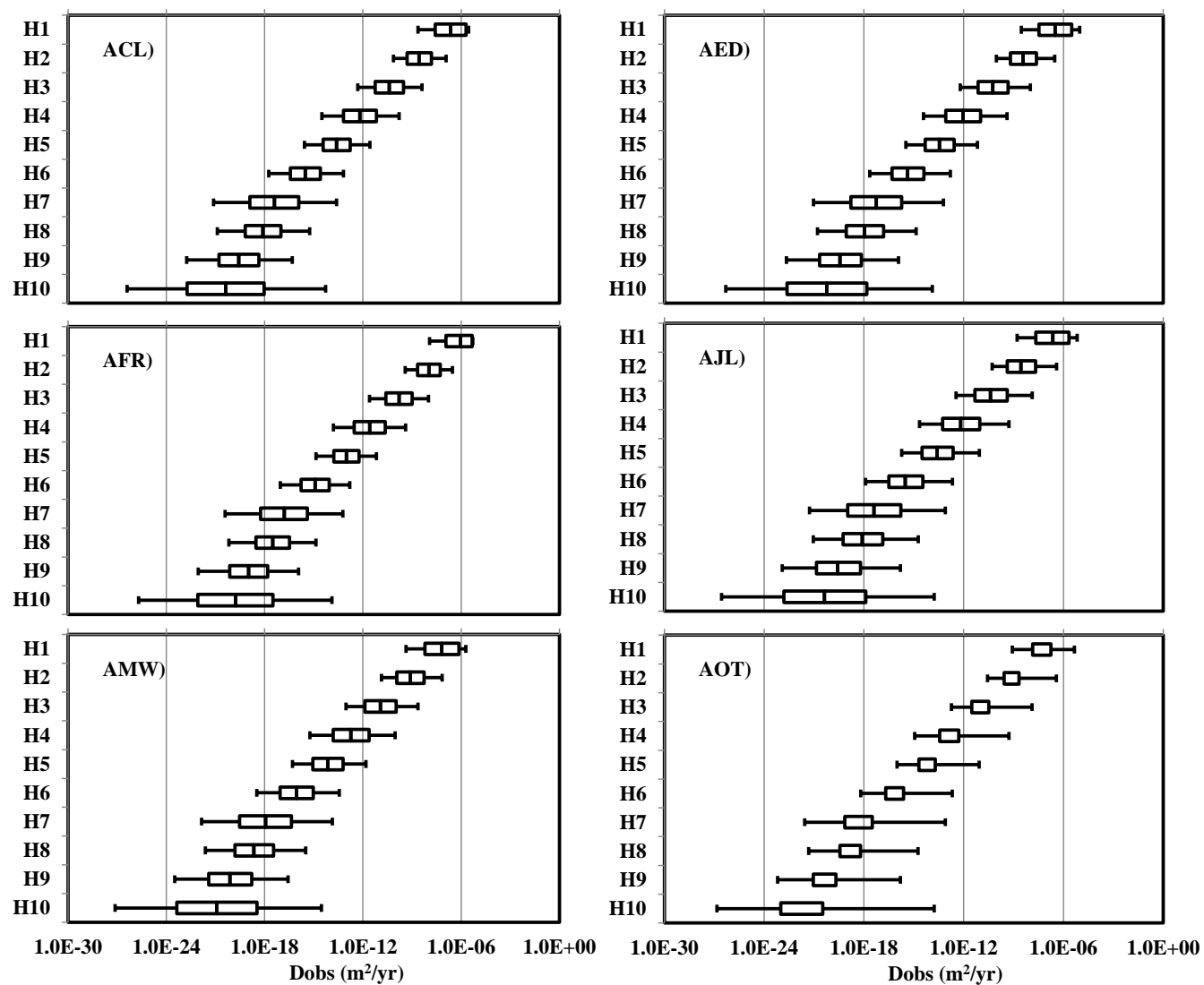


Figure D5.3c: Distribution of observed diffusivities values for organic carbon and black carbon sorptions (D_{obs} (OCBC)) for PBDE homologs in AR sediment columns as predicted by Monte Carlo simulations. Y-axes are homologs 1 through 10 (H1 to H10).

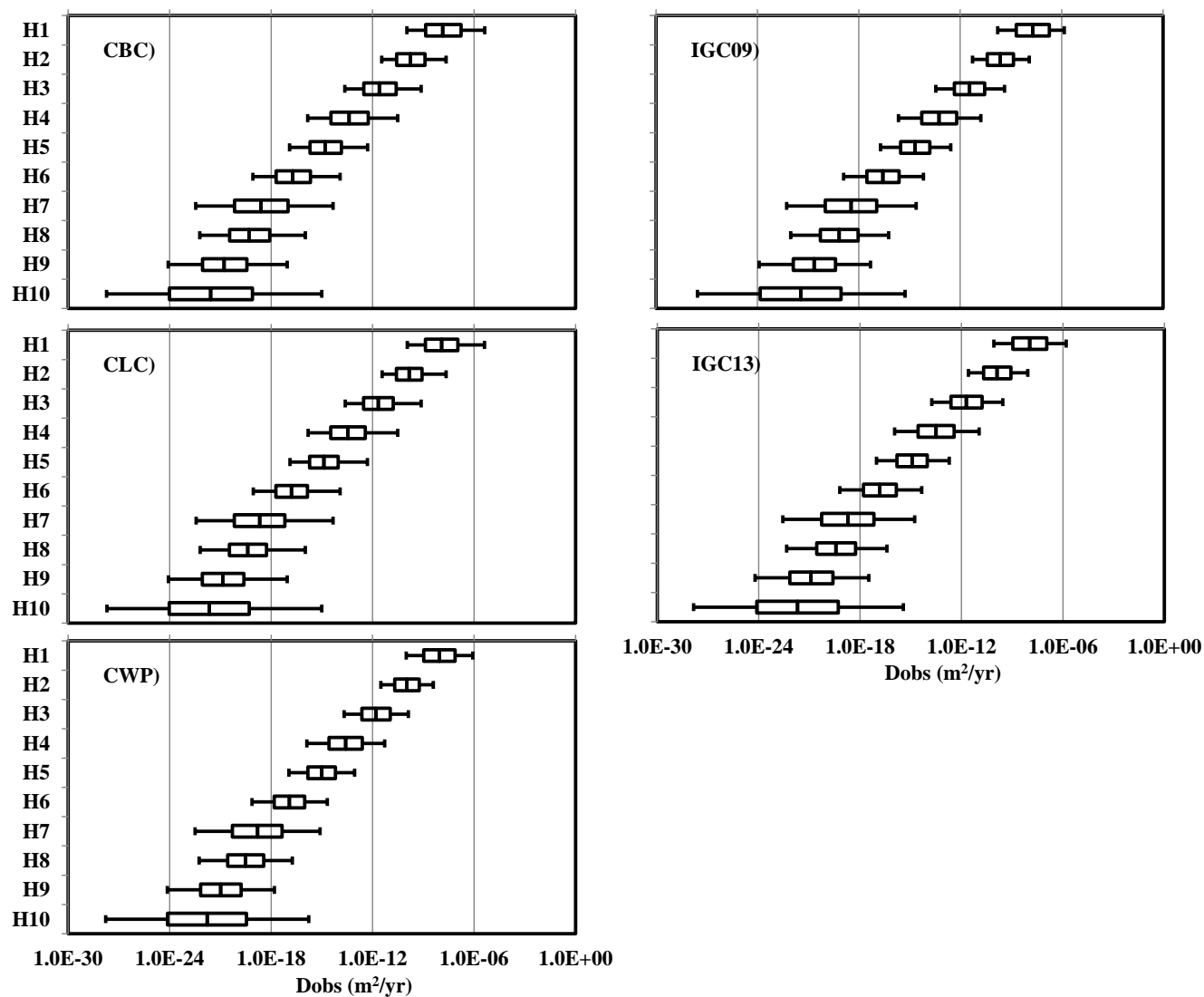


Figure D5.3d: Distribution of observed diffusivities values for organic carbon and black carbon sorptions (D_{obs} (OCBC)) for PBDE homologs in Chicago and IGC sediment columns as predicted by Monte Carlo simulations. Y-axes are homologs 1 through 10 (H1 to H10).

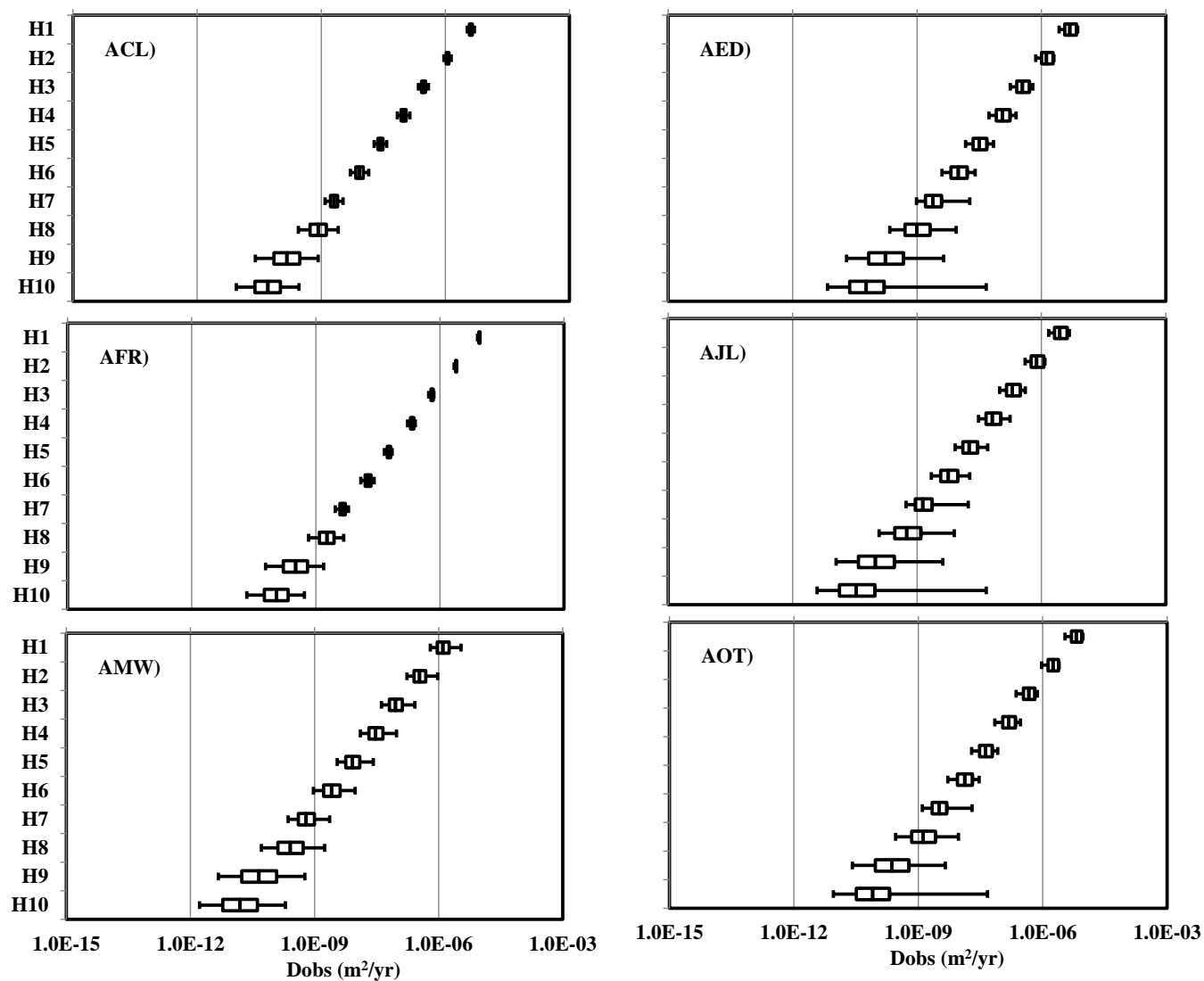


Figure D5.3e: Distribution of observed diffusivities values for organic carbon only sorption (D_{obs} (OC)) for PCB homologs in AR sediment columns as predicted by Monte Carlo simulations. Y-axes are homologs 1 through 10 (H1 to H10).

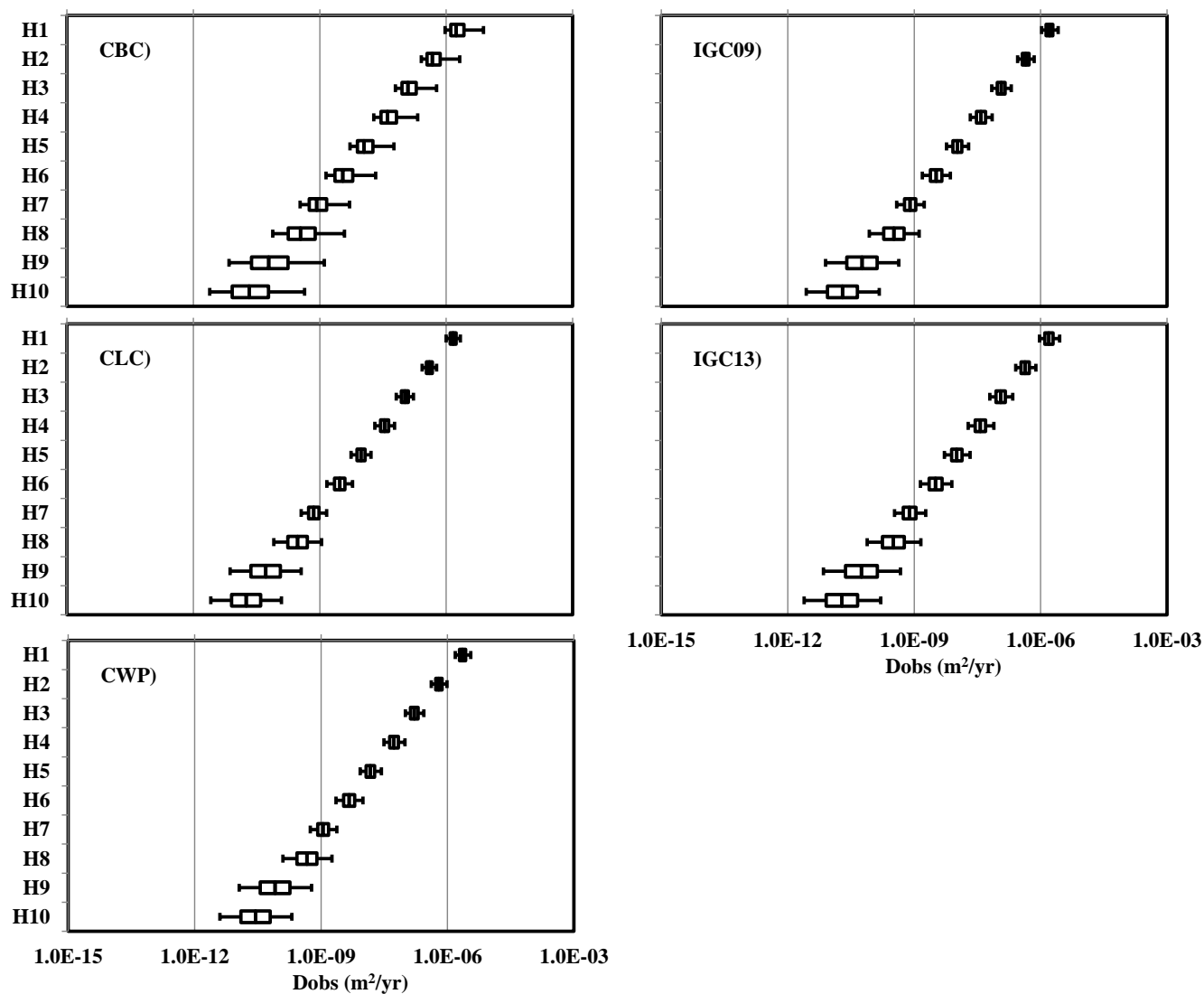


Figure D5.3f: Distribution of observed diffusivities values for organic carbon only sorption (D_{obs} (OC)) for PCB homologs in Chicago and IGC sediment columns as predicted by Monte Carlo simulations. Y-axes are homologs 1 through 10 (H1 to H10).

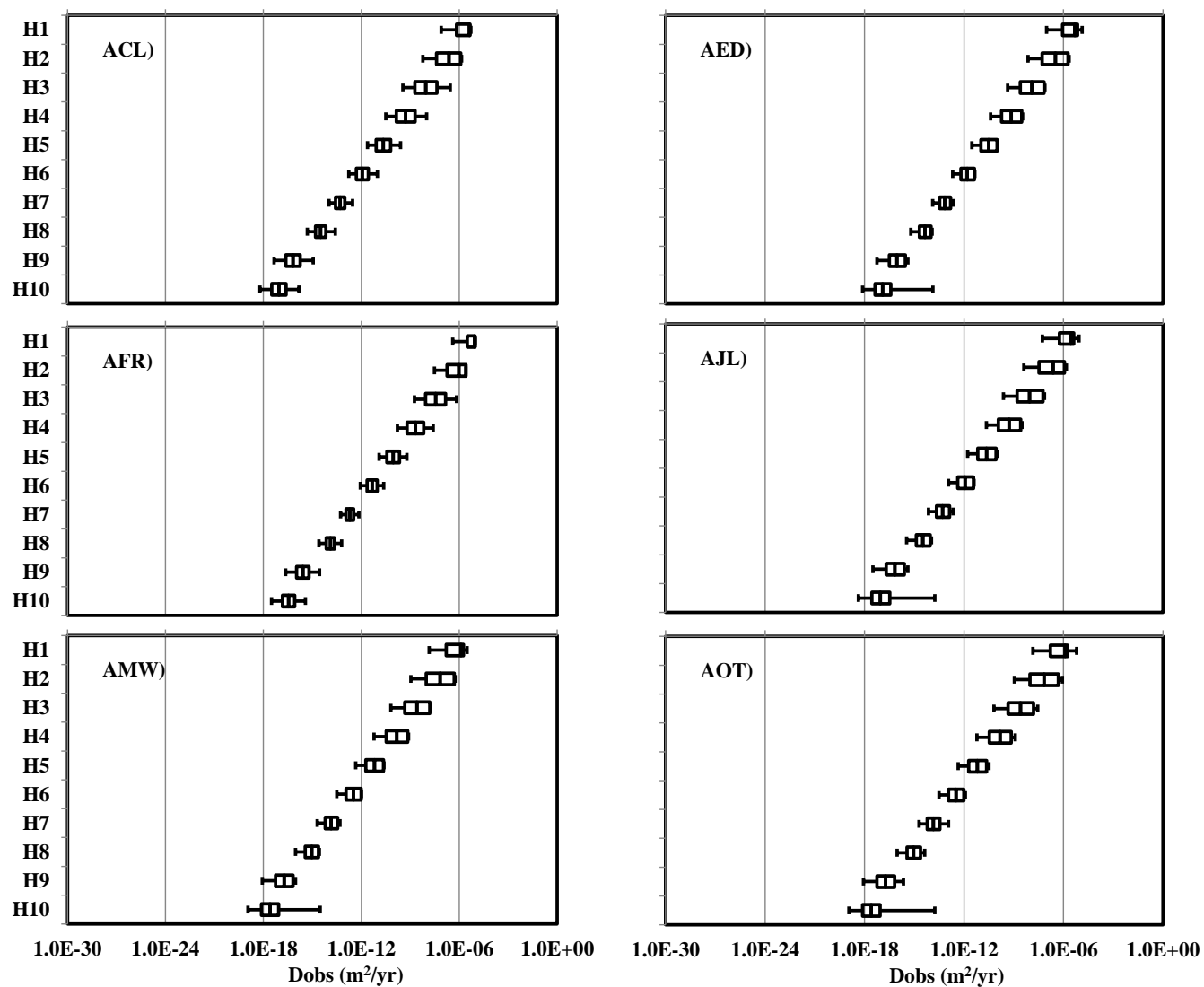


Figure D5.3g: Distribution of observed diffusivities values for organic carbon and black carbon sorptions (D_{obs} (OC)) for PCB homologs in AR sediment columns as predicted by Monte Carlo simulations. Y-axes are homologs 1 through 10 (H1 to H10).

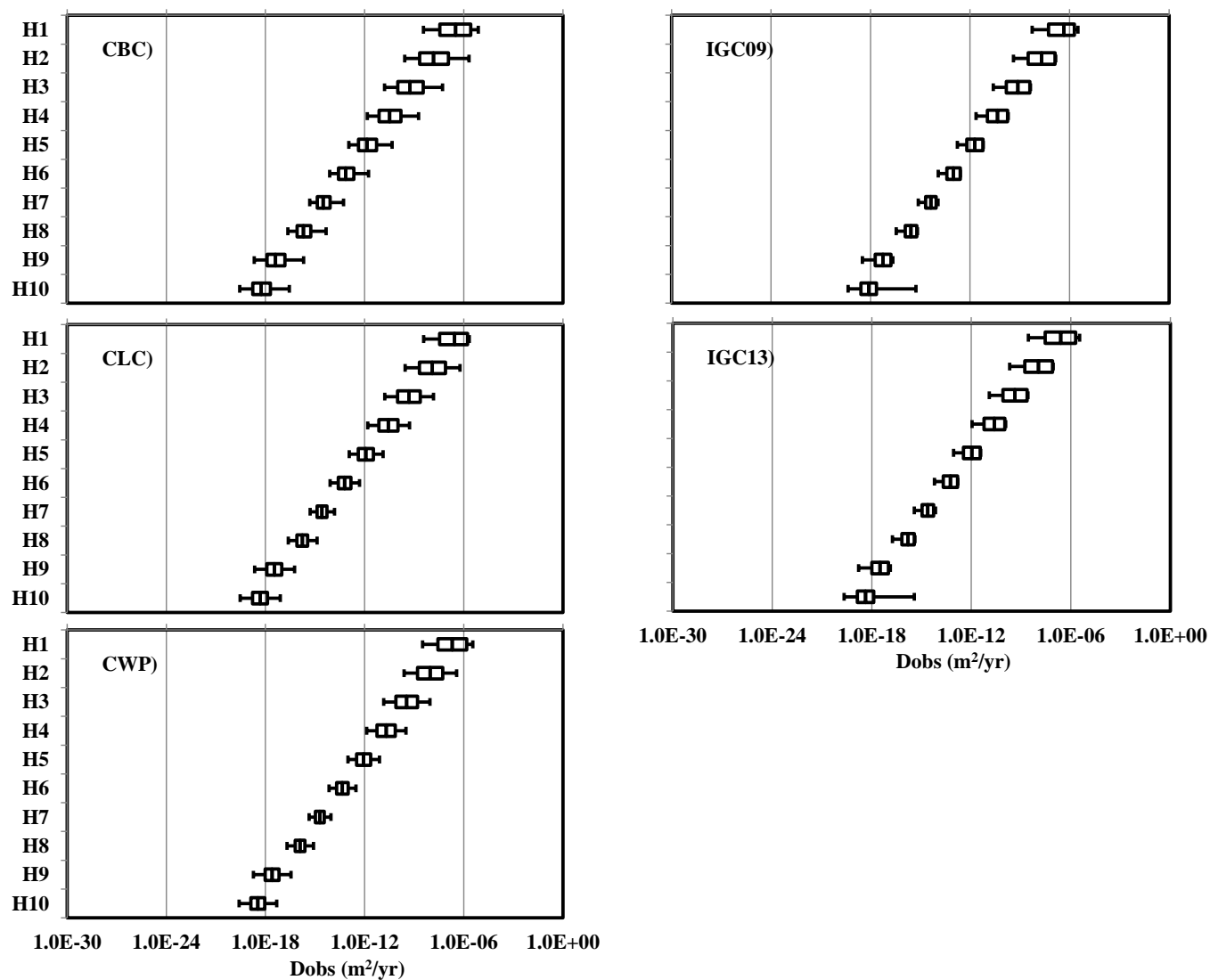


Figure D5.3h: Distribution of observed diffusivities values for organic carbon and black carbon sorptions (D_{obs} (OC)) for PCB homologs in Chicago and IGC sediment columns as predicted by Monte Carlo simulations. Y-axes are homologs 1 through 10 (H1 to H10).

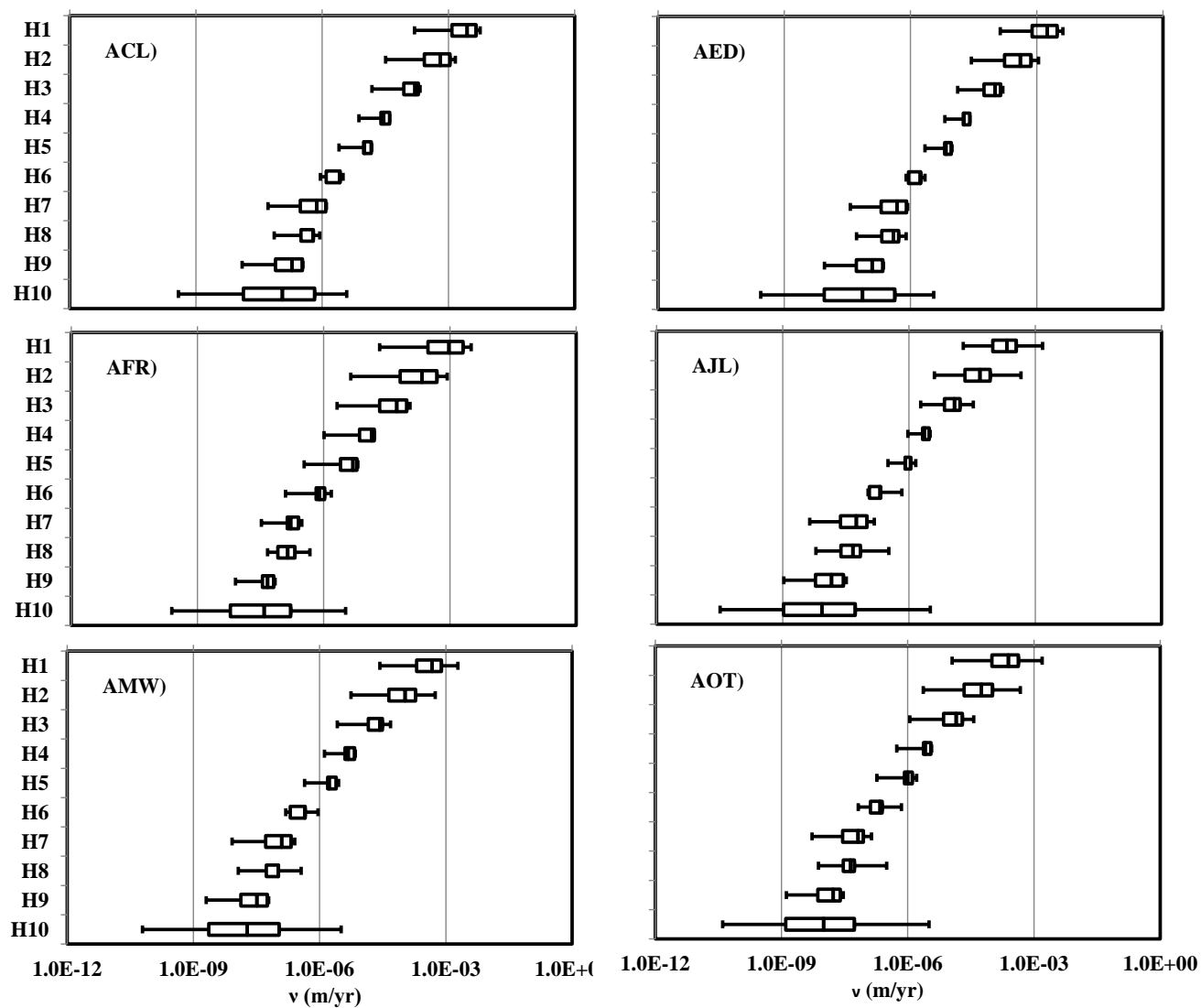


Figure D5.4a: Distribution of ν values for organic carbon sorption (ν (OC)) as predicted by Monte Carlo simulation for PBDE homologs in AR sediment columns. Y-axes are homologs 1 to 10 (H1-H10).

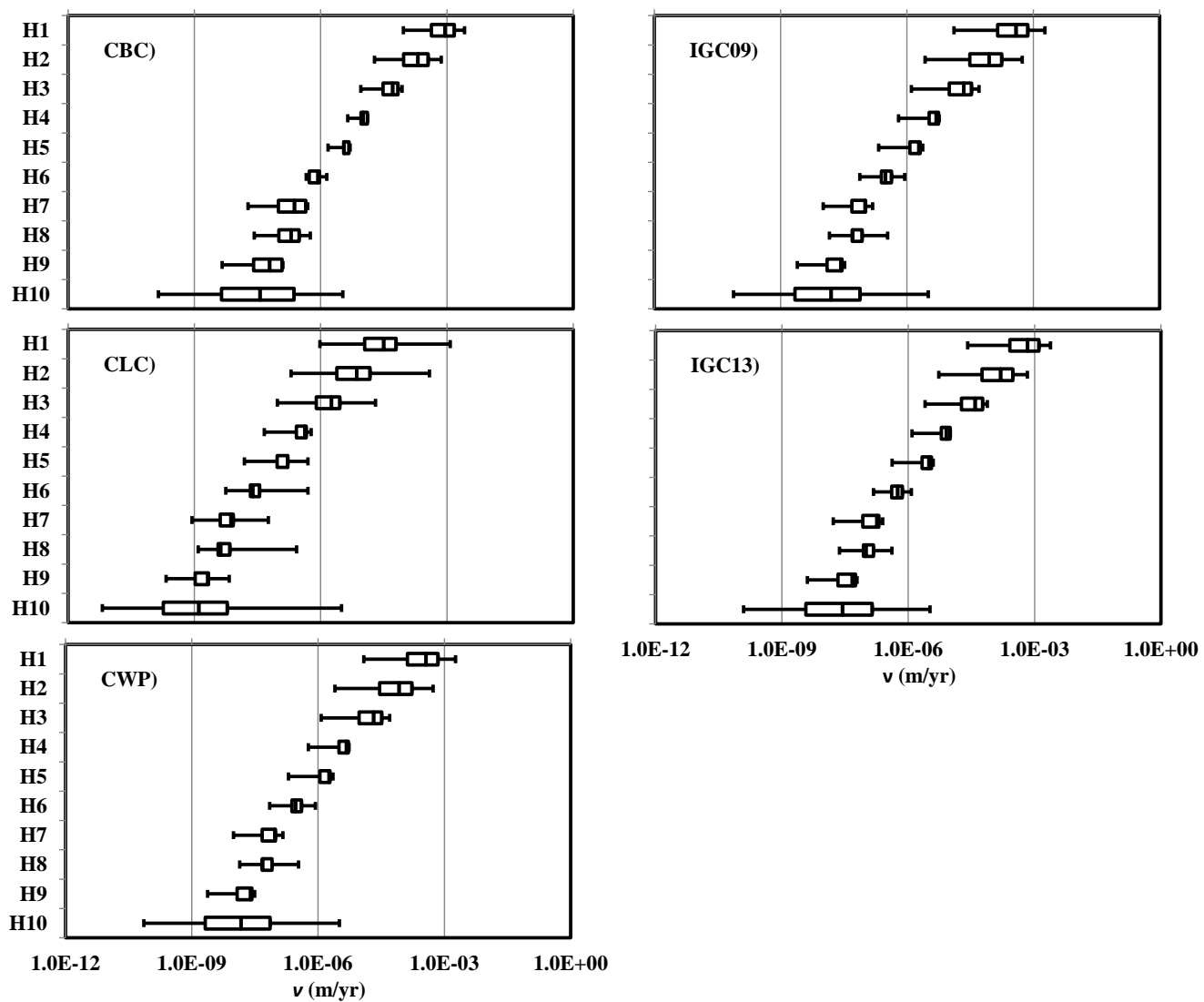


Figure D5.4b: Distribution of ν values for organic carbon sorption (ν (OC)) as predicted by Monte Carlo simulation for PBDE homologs in Chicago and IGC sediment columns. Y-axes are homologs 1 to 10 (H1-H10).

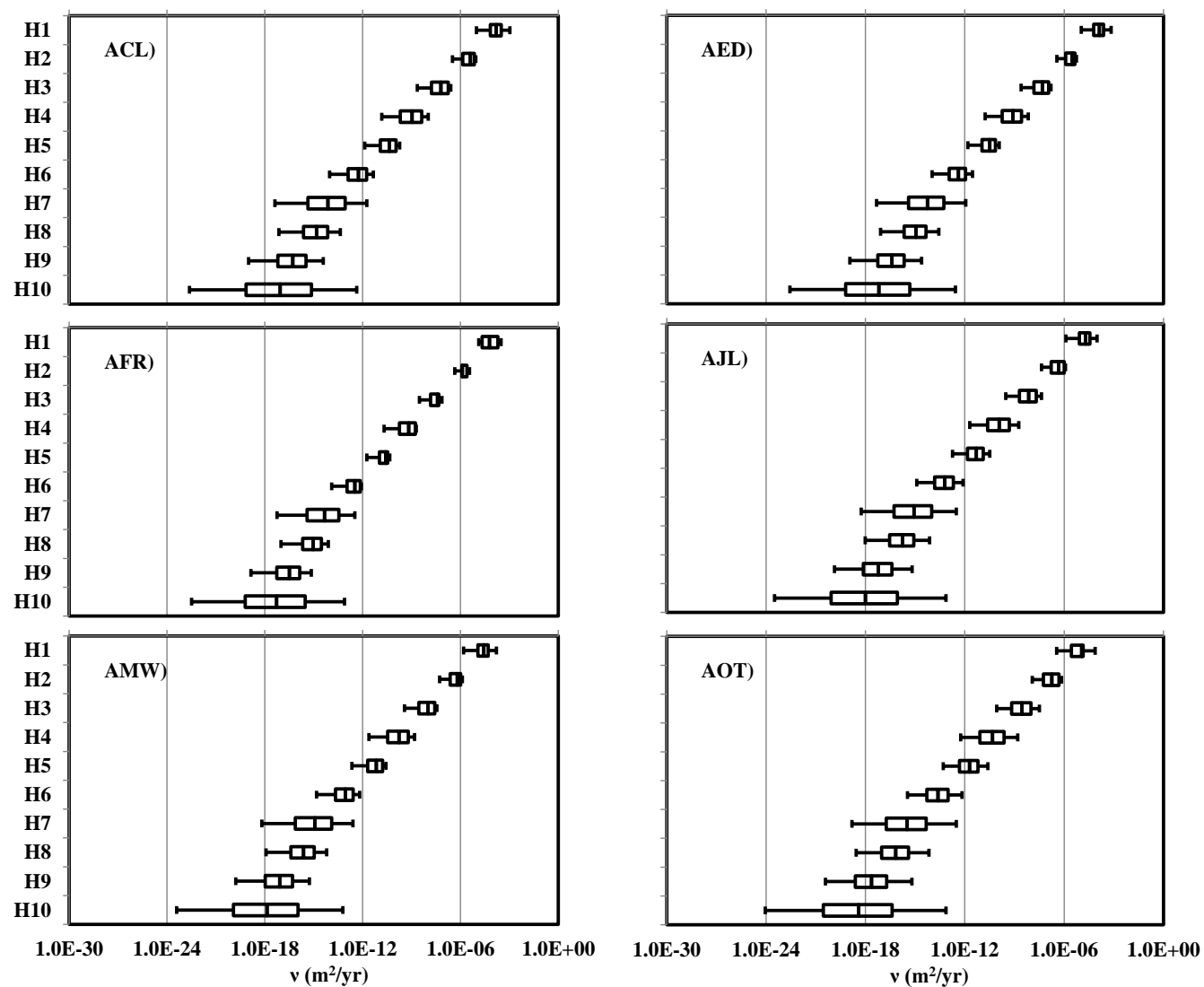


Figure D5.4c: Distribution of ν values for organic carbon and black carbon sorptions (ν (OCBC)) as predicted by Monte Carlo simulation for PBDE homologs in AR sediment columns. Y-axes are homologs 1 to 10 (H1-H10).

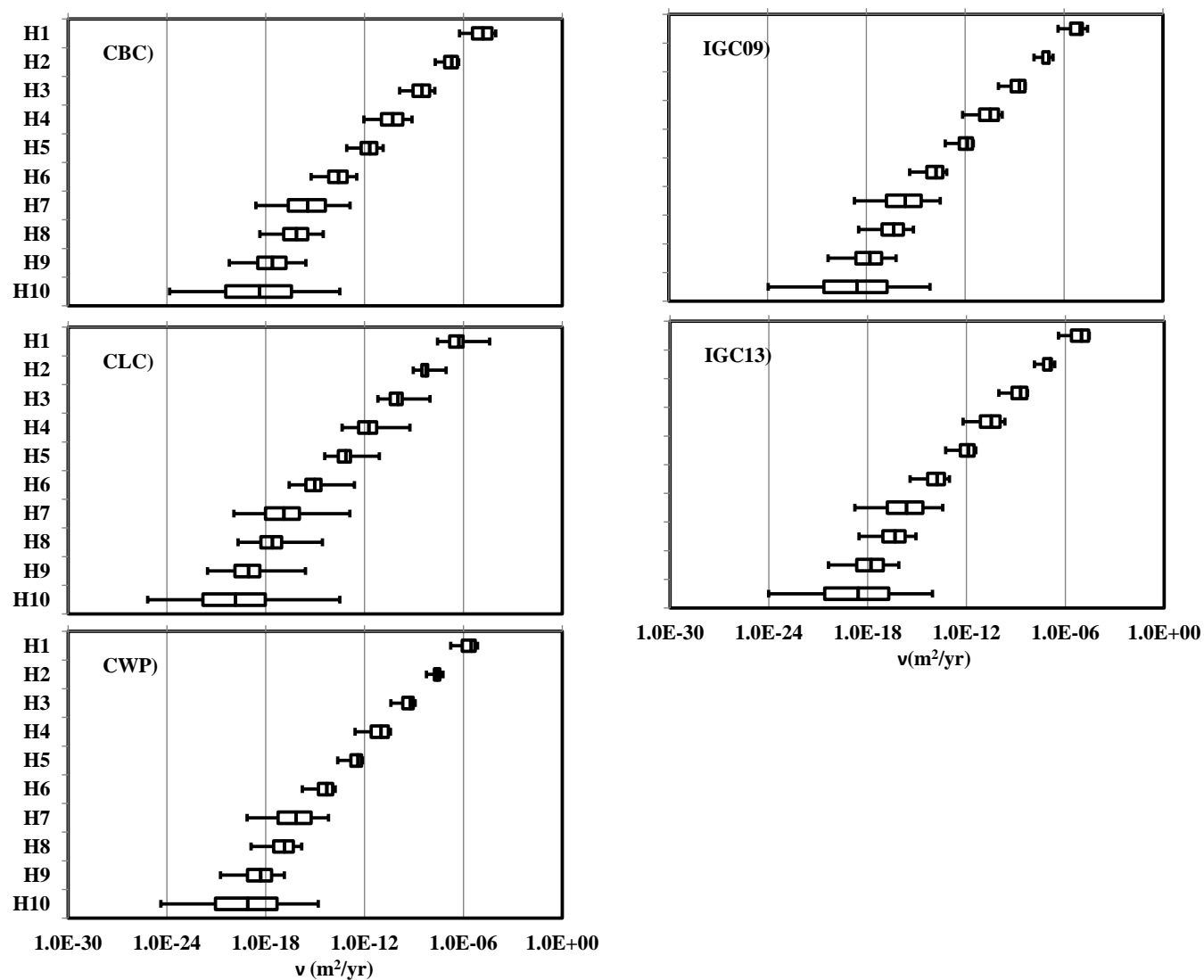


Figure D5.4d: Distribution of ν values for organic carbon and black carbon sorptions (ν (OCBC)) as predicted by Monte Carlo simulation for PBDE homologs in Chicago and IGC sediment columns. Y-axes are homologs 1 to 10 (H1-H10).

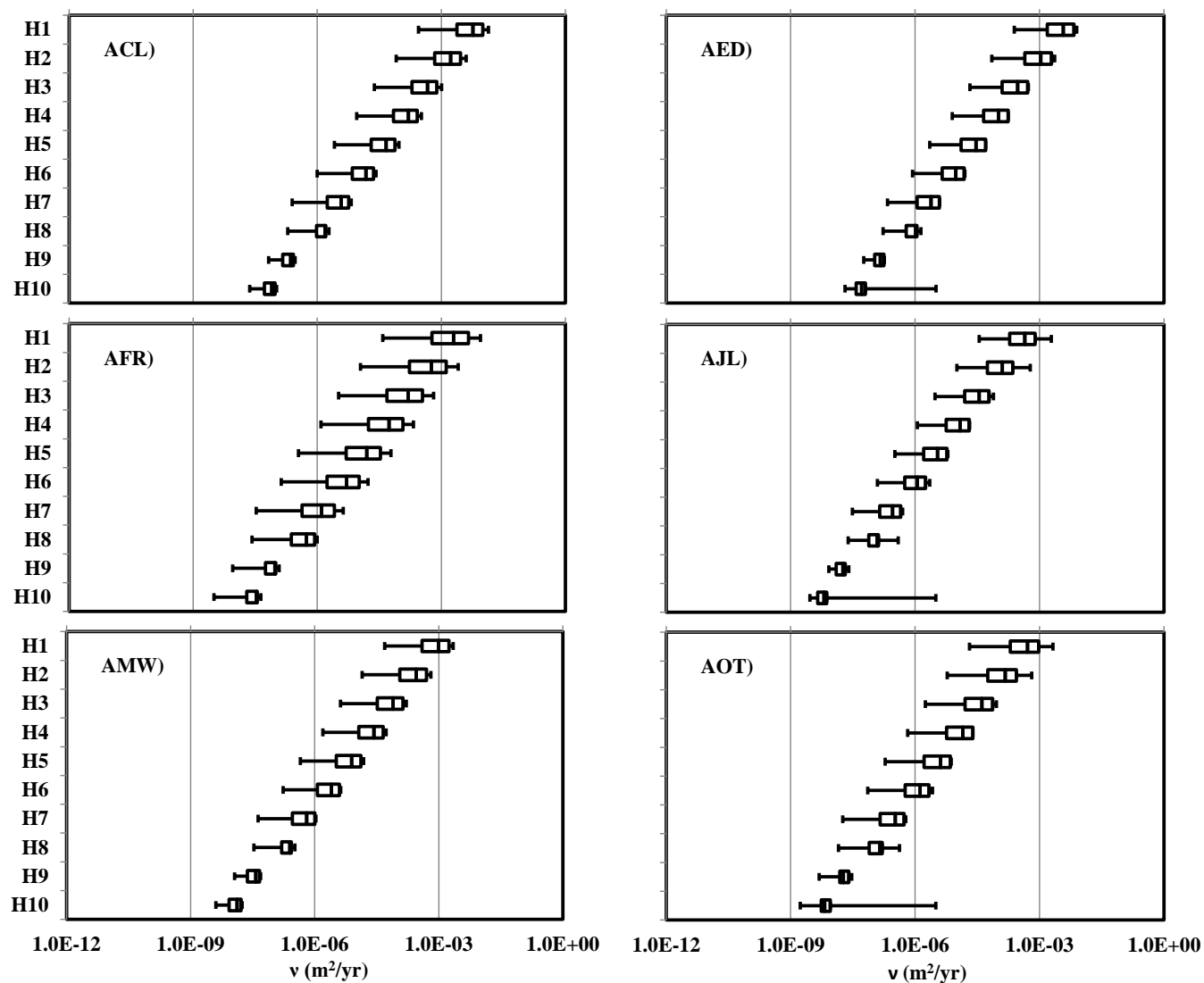


Figure D5.4e: Distribution of ν values for organic carbon sorption (ν (OC)) as predicted by Monte Carlo simulation for PCB homologs in AR sediment columns. Y-axes are homologs 1 to 10 (H1-H10).

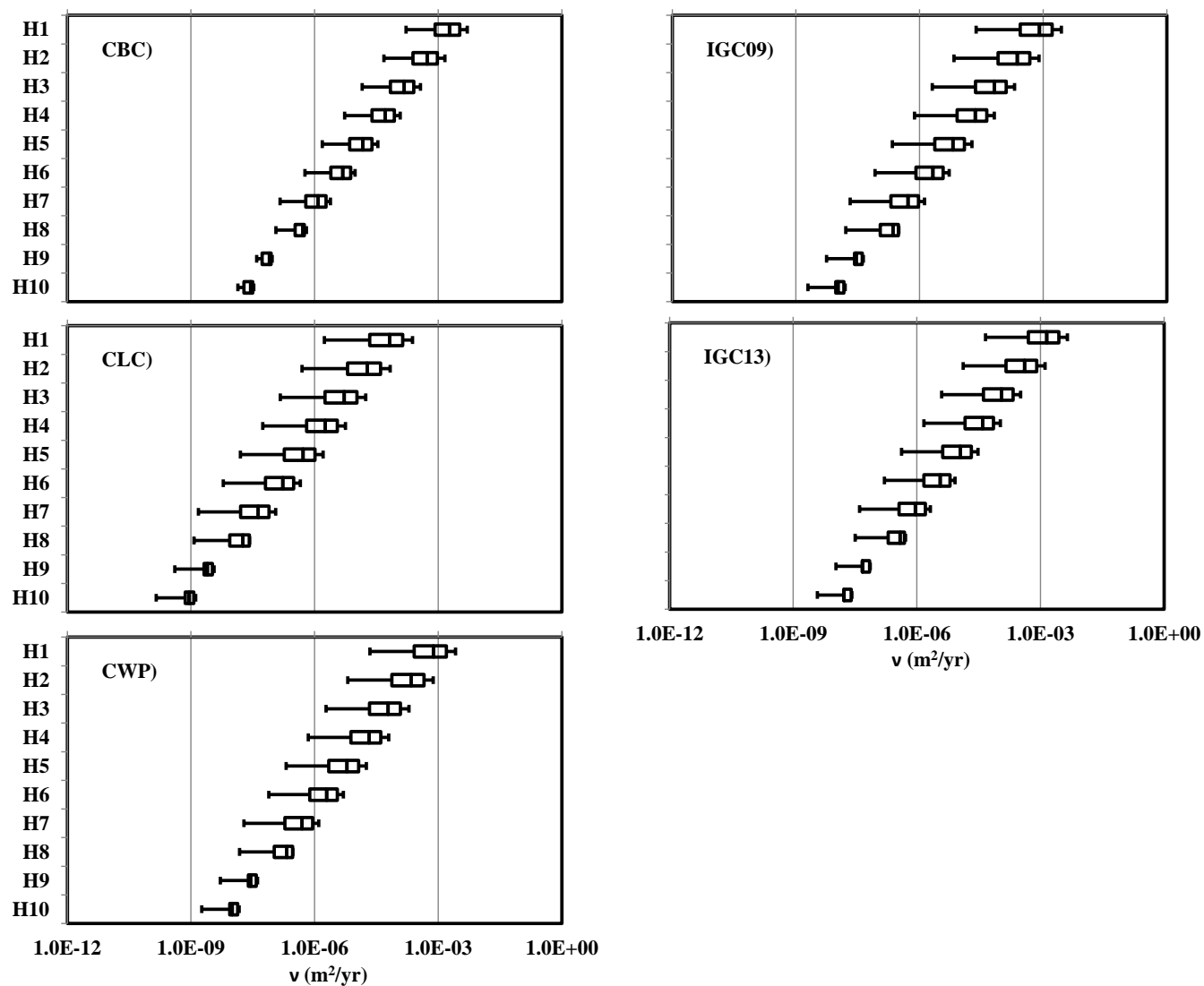


Figure D5.4f: Distribution of ν values for organic carbon sorption ($\nu(OC)$) as predicted by Monte Carlo simulation for PCB homologs in Chicago and IGC sediment columns. Y-axes are homologs 1 to 10 (H1-H10).

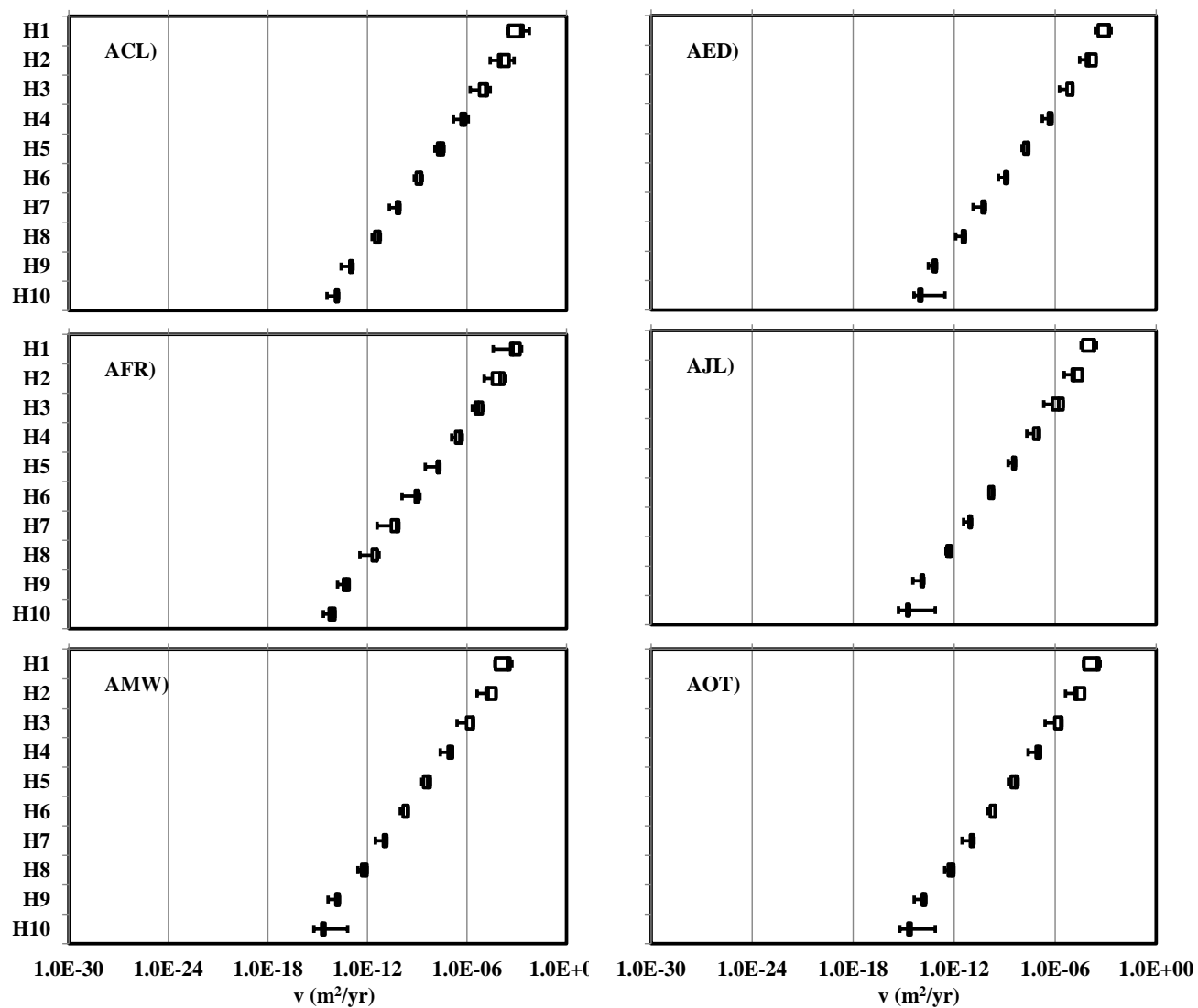


Figure D5.4g: Distribution of ν values for organic carbon and black carbon sorptions (ν (OCBC)) as predicted by Monte Carlo simulation for PCB homologs in AR sediment columns. Y-axes are homologs 1 to 10 (H1-H10).

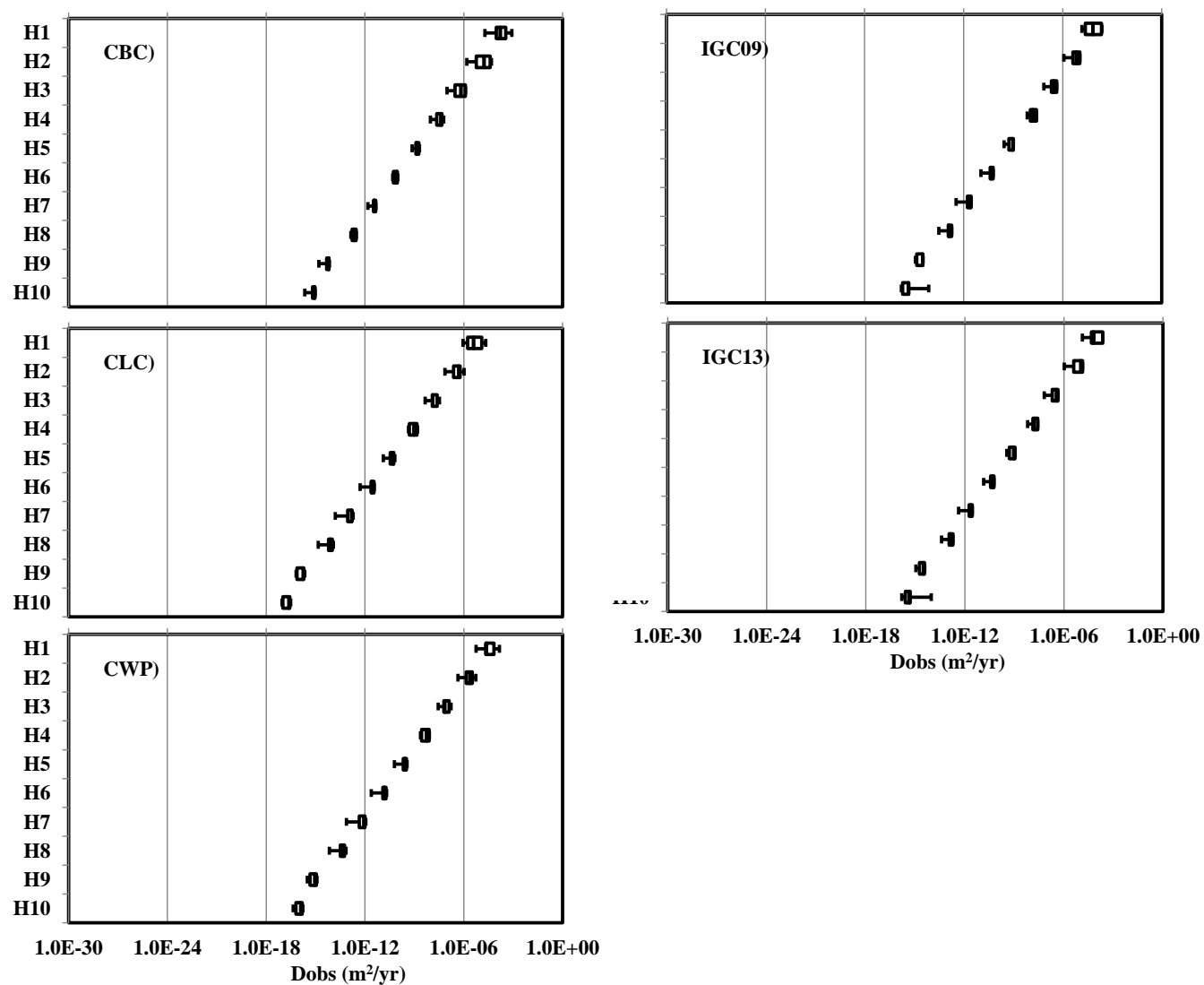


Figure D5.4h: Distribution of ν values for organic carbon and black carbon sorptions (ν (OCBC)) as predicted by Monte Carlo simulation for PCB homologs in Chicago and IGC sediment columns. Y-axes are homologs 1 to 10 (H1-H10).

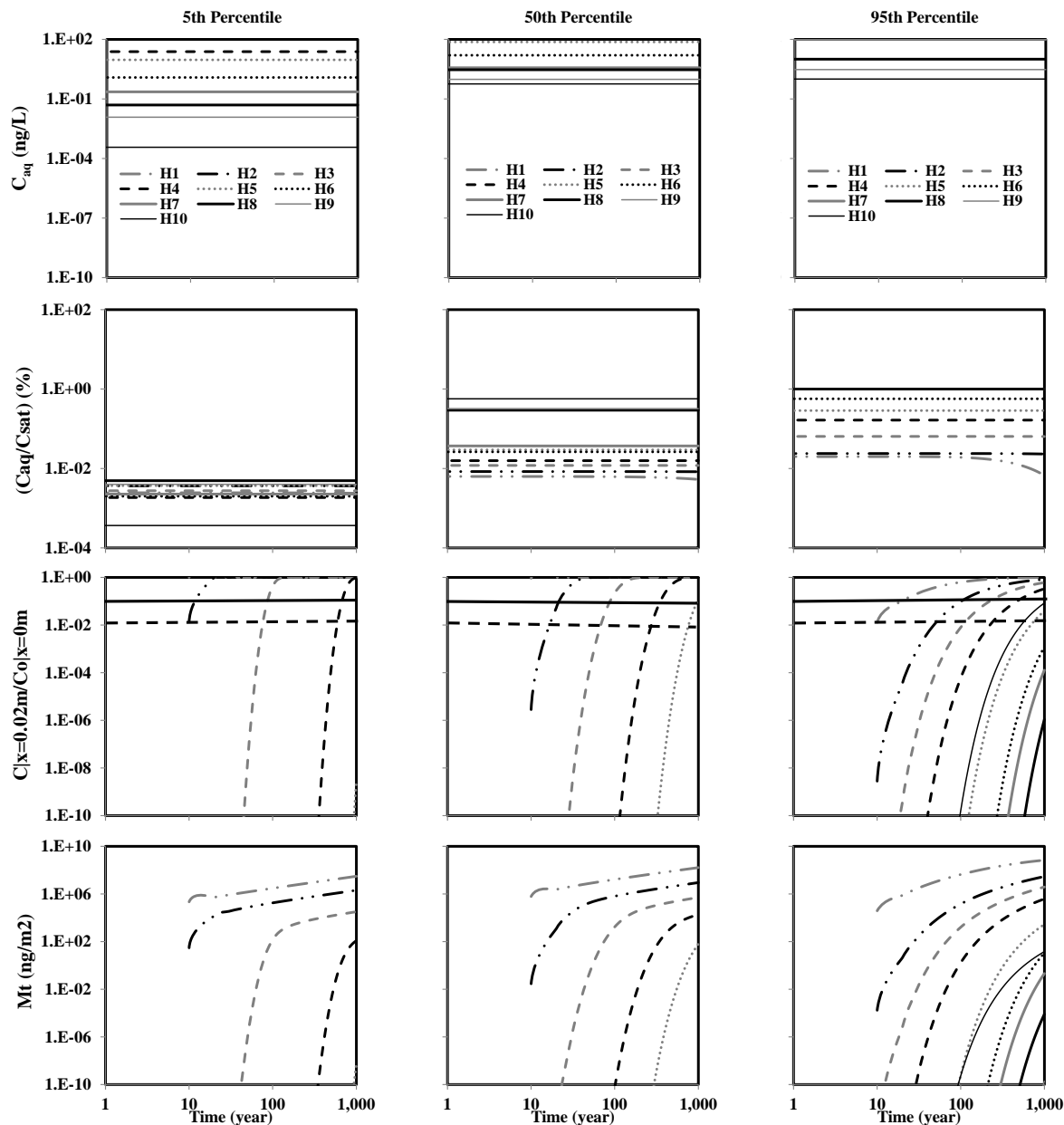


Figure D5.5a: Predicted PBDE aqueous phase concentration under local equilibrium assumption (C_{aq}), ratio of aqueous phase concentration to saturation concentration (C_{aq}/C_{sat}), ratio of aqueous phase concentration at sediment boundary layer to homogeneous aqueous phase concentration ($C|_{x=0.02m}/C|_{x=0m}$), and mass leaving the sediment boundary layer (M_t) under advection-diffusion with organic carbon only sorption ($A(OC)$) shown in row1 through 4, respectively as predicted by the 5th, 50th, and 95th percentile transport parameters values shown in column 1 through 3, respectively in core ACL for 95th percentile initial concentration values (36100 ng/g).

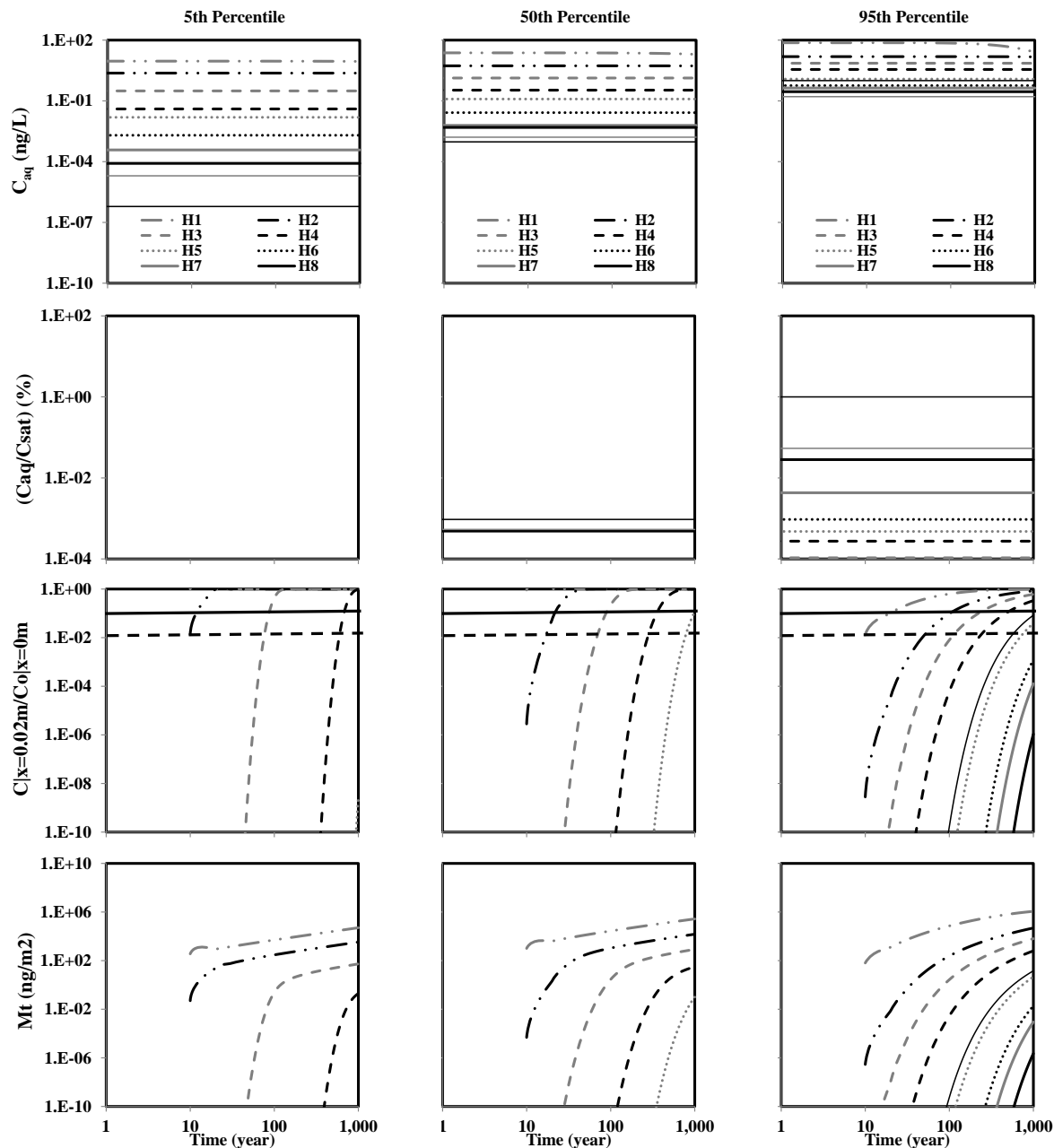


Figure D5.5b: Predicted PBDE aqueous phase concentration under local equilibrium assumption (C_{aq}), ratio of aqueous phase concentration to saturation concentration (C_{aq}/C_{sat}), ratio of aqueous phase concentration at sediment boundary layer to homogenous aqueous phase concentration ($C_{|x=0.02m}/C_{|x=0m}$), and mass leaving the sediment boundary layer (M_t) under advection-diffusion with organic carbon only sorption (A(OC)) shown in row1 through 4, respectively as predicted by the 5th, 50th, and 95th percentile transport parameters values shown in column 1 through 3, respectively in core ACL for 50th percentile initial concentration values (60 ng/g).

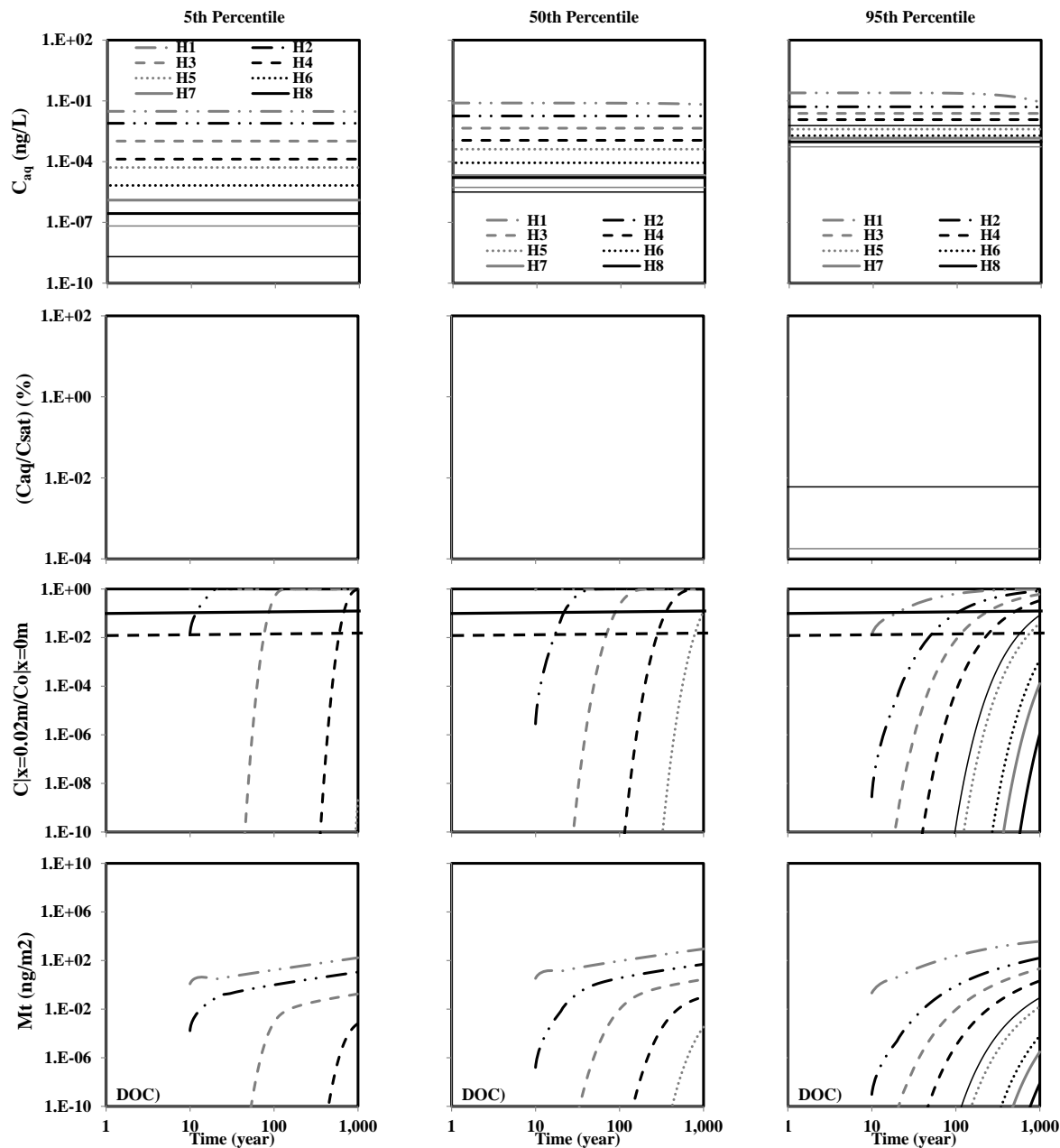


Figure D5.5c: Predicted PBDE aqueous phase concentration under local equilibrium assumption (C_{aq}), ratio of aqueous phase concentration to saturation concentration (C_{aq}/C_{sat}), ratio of aqueous phase concentration at sediment boundary layer to homogeneous aqueous phase concentration ($C_{|x=0.02m}/C_{|x=0m}$), and mass leaving the sediment boundary layer (M_t) under advection-diffusion with organic carbon only sorption (A(OC)) shown in row 1 through 4, respectively as predicted by the 5th, 50th, and 95th percentile transport parameters values shown in column 1 through 3, respectively in core ACL for 5th percentile initial concentration values (0.2 ng/g).

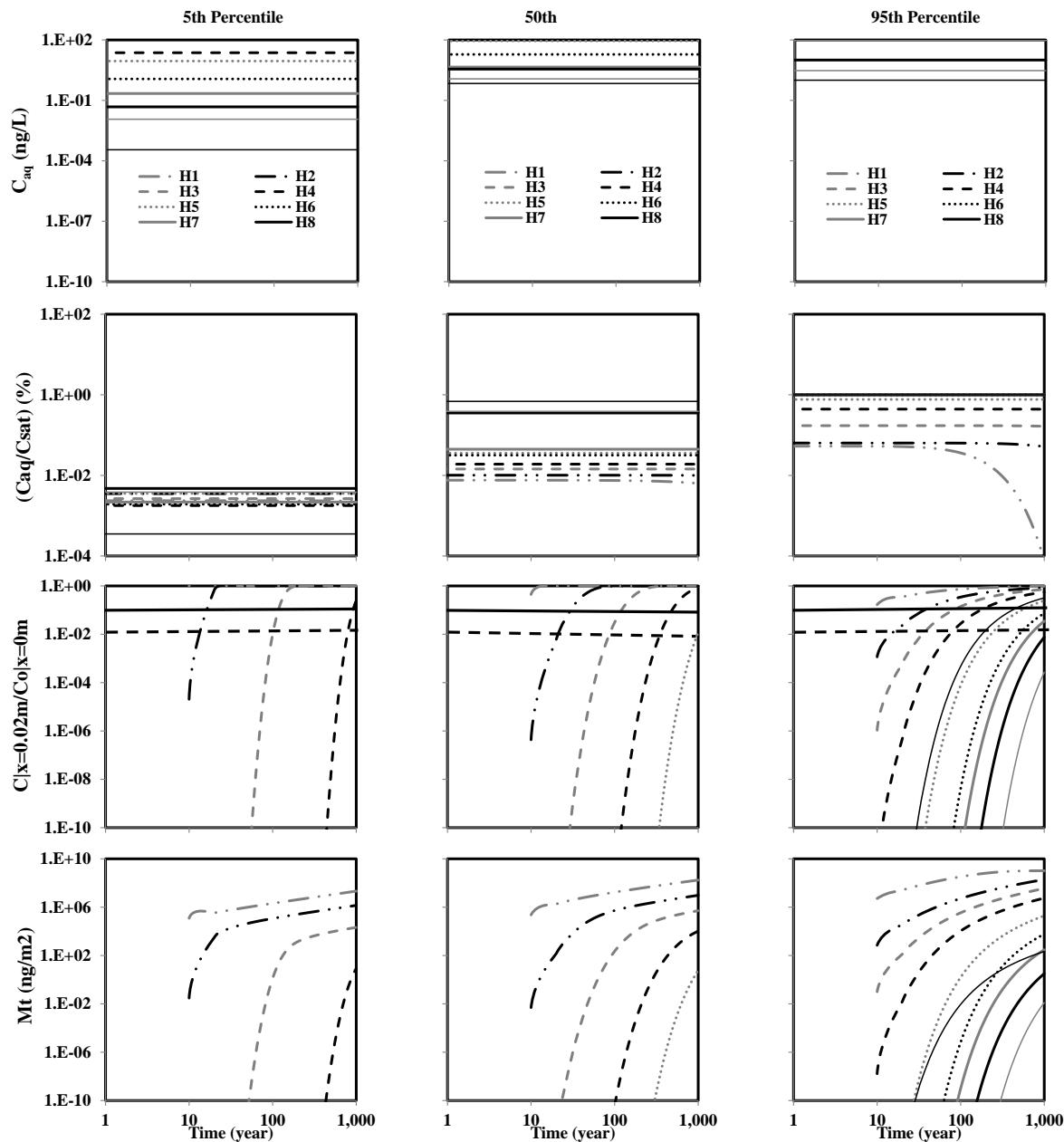


Figure D5.5d: Predicted PBDE aqueous phase concentration under local equilibrium assumption (C_{aq}), ratio of aqueous phase concentration to saturation concentration (C_{aq}/C_{sat}), ratio of aqueous phase concentration at sediment boundary layer to homogeneous aqueous phase concentration ($C_{|x=0.02m}/C_{|x=0m}$), and mass leaving the sediment boundary layer (M_t) under advection-diffusion with organic carbon only sorption (A(OC)) shown in row1 through 4, respectively as predicted by the 5th, 50th, and 95th percentile transport parameters values shown in column 1 through 3, respectively in core AED for 95th percentile initial concentration values (36100 ng/g).

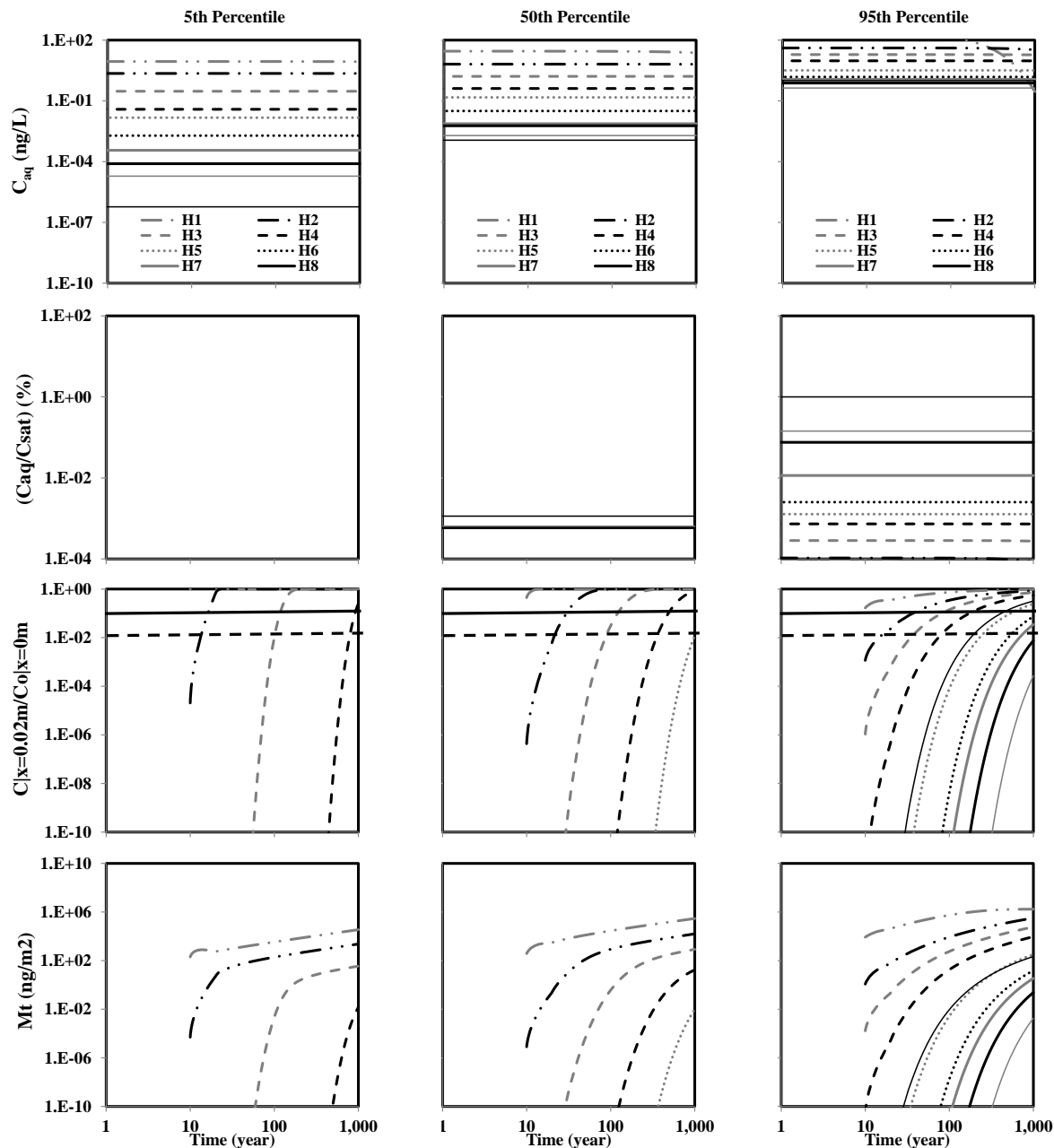


Figure D5.5e: Predicted PBDE aqueous phase concentration under local equilibrium assumption (C_{aq}), ratio of aqueous phase concentration to saturation concentration (C_{aq}/C_{sat}), ratio of aqueous phase concentration at sediment boundary layer to homogenous aqueous phase concentration ($C_{|x=0.02m}/C_{|x=0m}$), and mass leaving the sediment boundary layer (M_t) under advection-diffusion with organic carbon only sorption (A(OC)) shown in row1 through 4, respectively as predicted by the 5th, 50th, and 95th percentile transport parameters values shown in column 1 through 3, respectively in core AED for 50th percentile initial concentration values (60 ng/g).

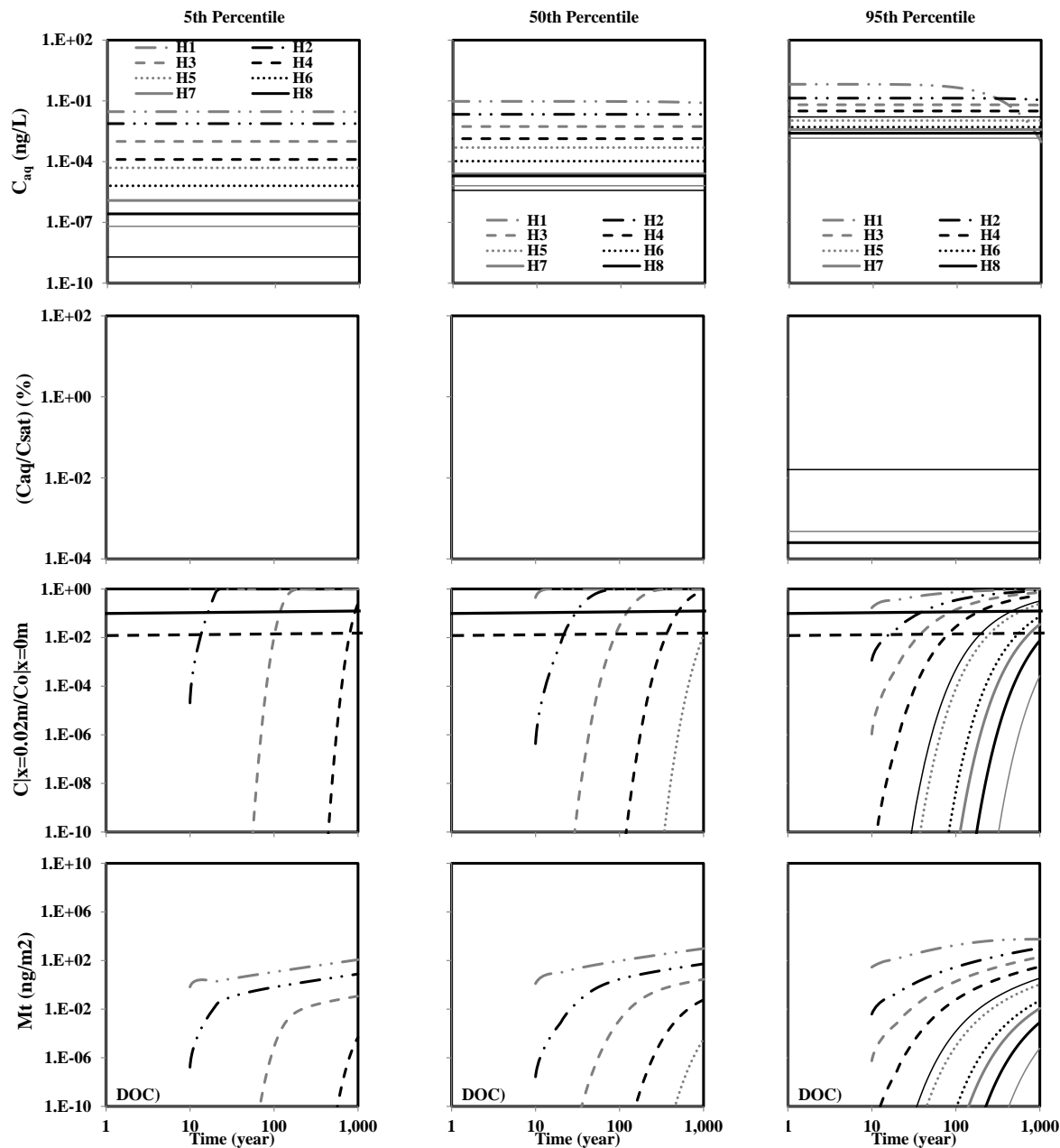


Figure D5.5f: Predicted PBDE aqueous phase concentration under local equilibrium assumption (C_{aq}), ratio of aqueous phase concentration to saturation concentration (C_{aq}/C_{sat}), ratio of aqueous phase concentration at sediment boundary layer to homogeneous aqueous phase concentration ($C_{|x=0.02m}/C_{|x=0m}$), and mass leaving the sediment boundary layer (M_t) under advection-diffusion with organic carbon only sorption (A(OC)) shown in row1 through 4, respectively as predicted by the 5th, 50th, and 95th percentile transport parameters values shown in column 1 through 3, respectively in core AED for 5th percentile initial concentration values (0.2 ng/g).

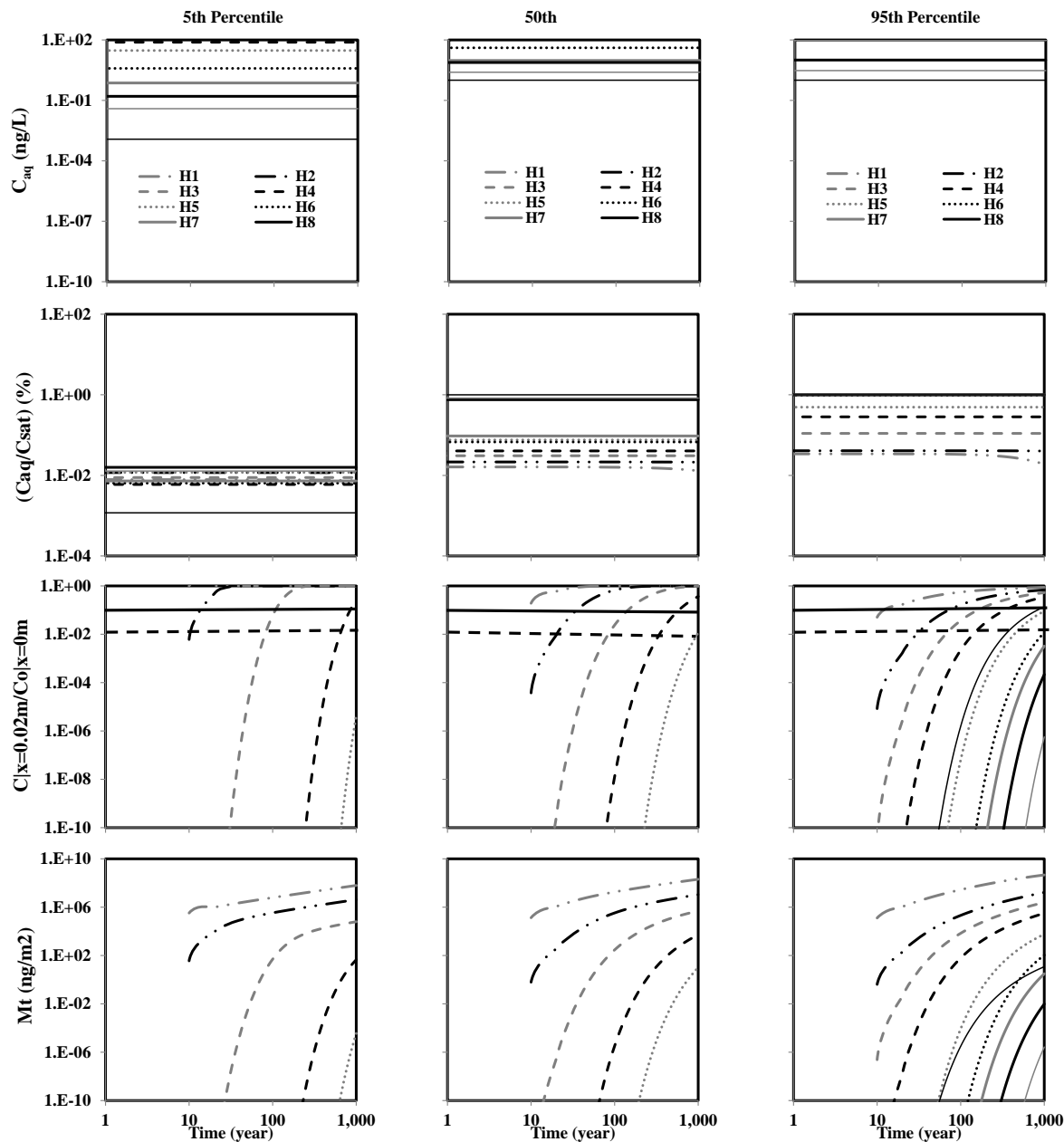


Figure D5.5g: Predicted PBDE aqueous phase concentration under local equilibrium assumption (C_{aq}), ratio of aqueous phase concentration to saturation concentration (C_{aq}/C_{sat}), ratio of aqueous phase concentration at sediment boundary layer to homogeneous aqueous phase concentration ($C_{|x=0.02m}/C_{|x=0m}$), and mass leaving the sediment boundary layer (M_t) under advection-diffusion with organic carbon only sorption (A(OC)) shown in row1 through 4, respectively as predicted by the 5th, 50th, and 95th percentile transport parameters values shown in column 1 through 3, respectively in core AFR for 95th percentile initial concentration values (36100 ng/g).

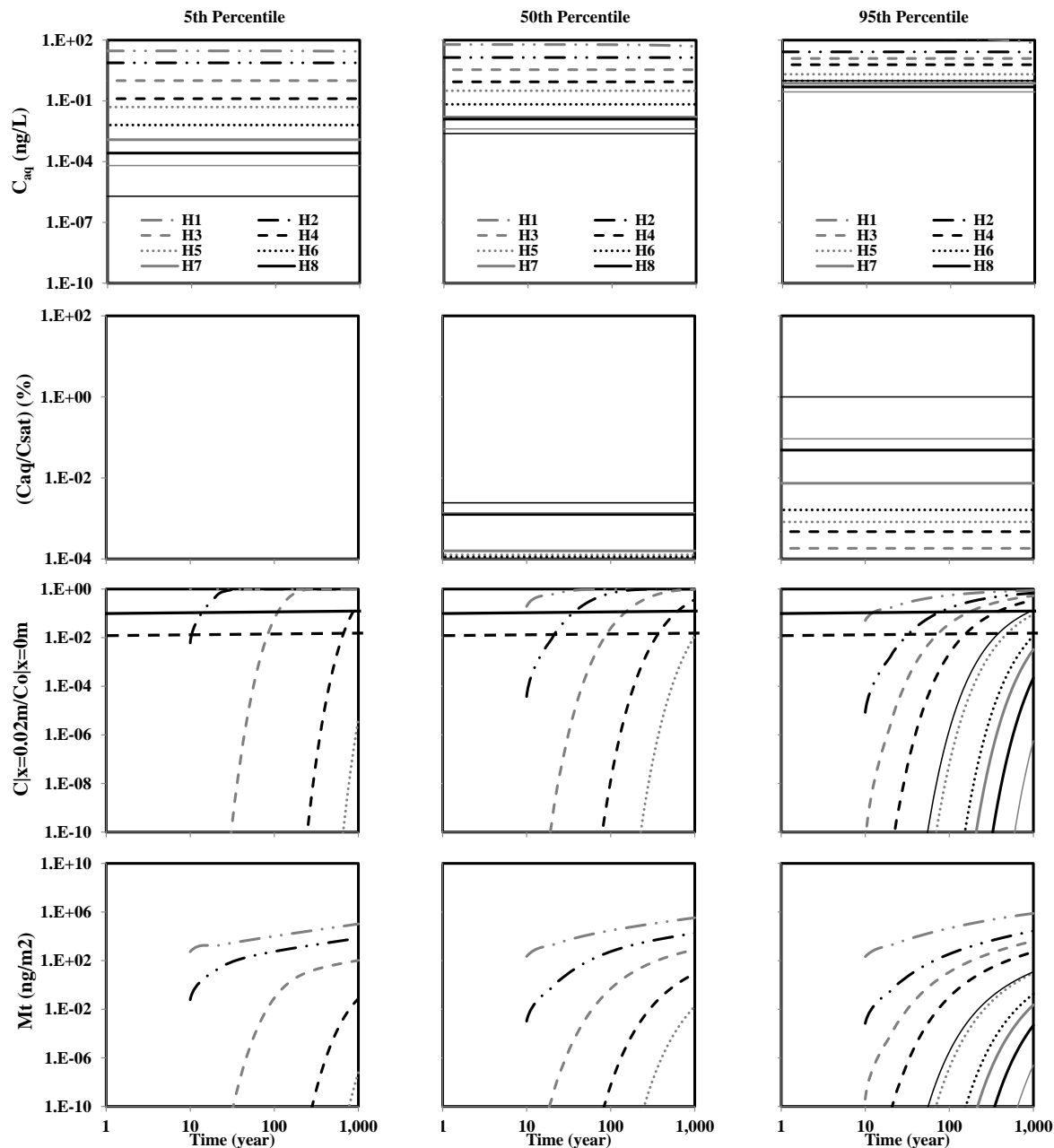


Figure D5.5h: Predicted PBDE aqueous phase concentration under local equilibrium assumption (C_{aq}), ratio of aqueous phase concentration to saturation concentration (C_{aq}/C_{sat}), ratio of aqueous phase concentration at sediment boundary layer to homogenous aqueous phase concentration ($C|_{x=0.02m}/C_0|_{x=0m}$), and mass leaving the sediment boundary layer (M_t) under advection-diffusion with organic carbon only sorption (A(OC)) shown in row1 through 4, respectively as predicted by the 5th, 50th, and 95th percentile transport parameters values shown in column 1 through 3, respectively in core AFR for 50th percentile initial concentration values (60 ng/g).

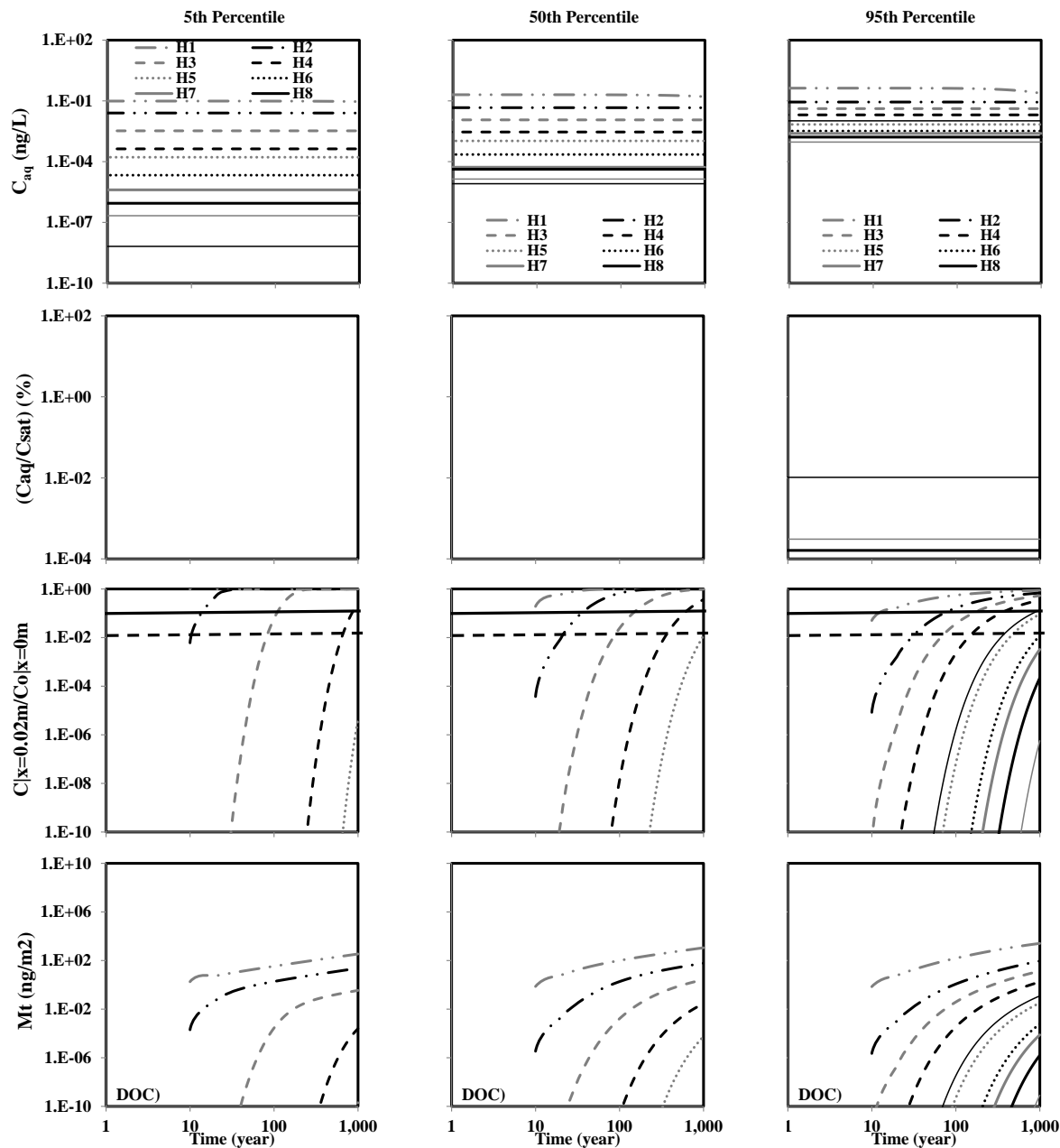


Figure D5.5i: Predicted PBDE aqueous phase concentration under local equilibrium assumption (C_{aq}), ratio of aqueous phase concentration to saturation concentration (C_{aq}/C_{sat}), ratio of aqueous phase concentration at sediment boundary layer to homogenous aqueous phase concentration ($C_{|x=0.02m}/C_{|x=0m}$), and mass leaving the sediment boundary layer (M_t) under advection-diffusion with organic carbon only sorption (A(OC)) shown in row1 through 4, respectively as predicted by the 5th, 50th, and 95th percentile transport parameters values shown in column 1 through 3, respectively in core AFR for 5th percentile initial concentration values (0.2 ng/g).

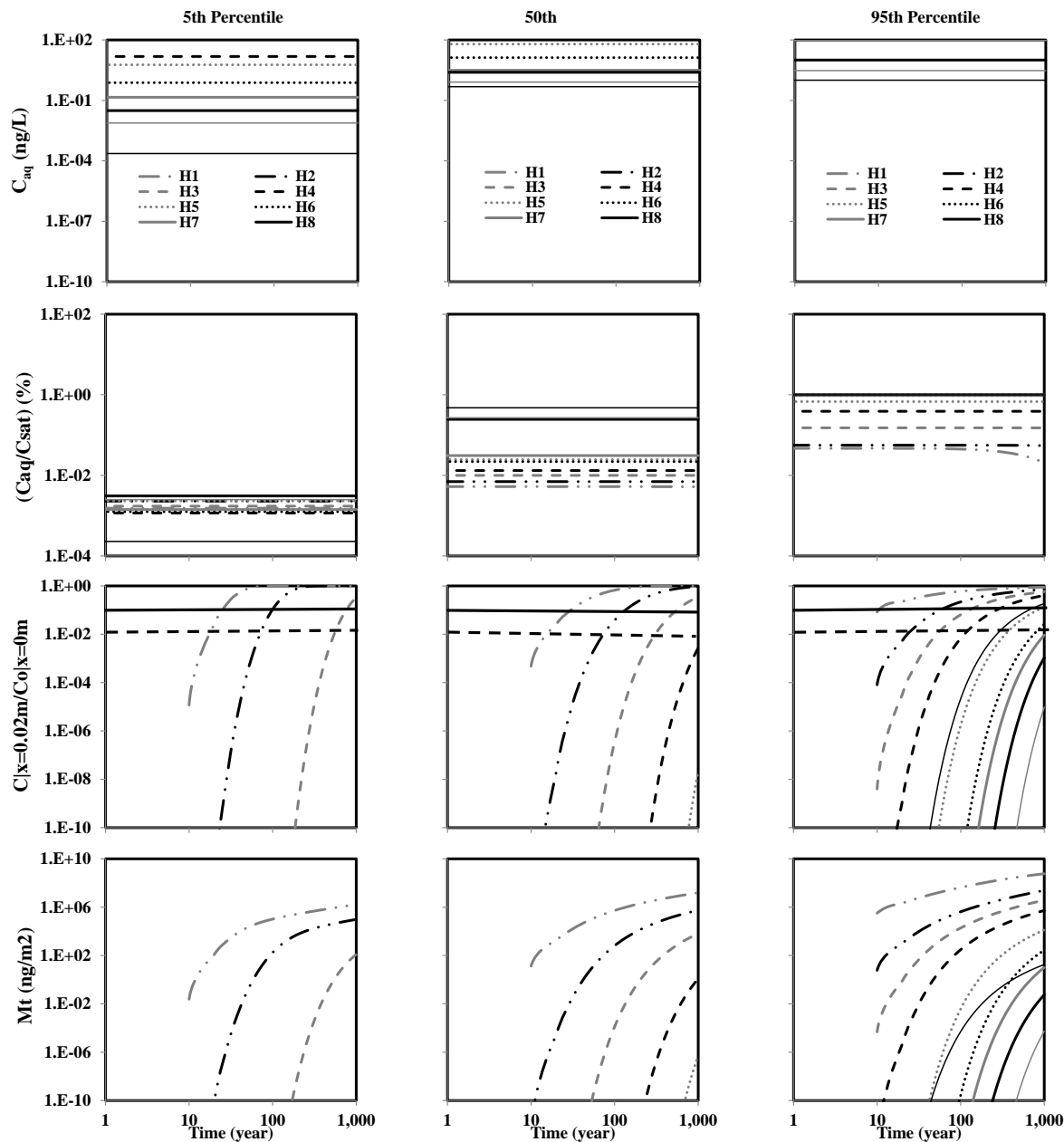


Figure D5.5j: Predicted PBDE aqueous phase concentration under local equilibrium assumption (C_{aq}), ratio of aqueous phase concentration to saturation concentration (C_{aq}/C_{sat}), ratio of aqueous phase concentration at sediment boundary layer to homogeneous aqueous phase concentration ($C_{|x=0.02m}/C_{|x=0m}$), and mass leaving the sediment boundary layer (M_t) under advection-diffusion with organic carbon only sorption (A(OC)) shown in row1 through 4, respectively as predicted by the 5th, 50th, and 95th percentile transport parameters values shown in column 1 through 3, respectively in core AJL for 95th percentile initial concentration values (36100 ng/g).

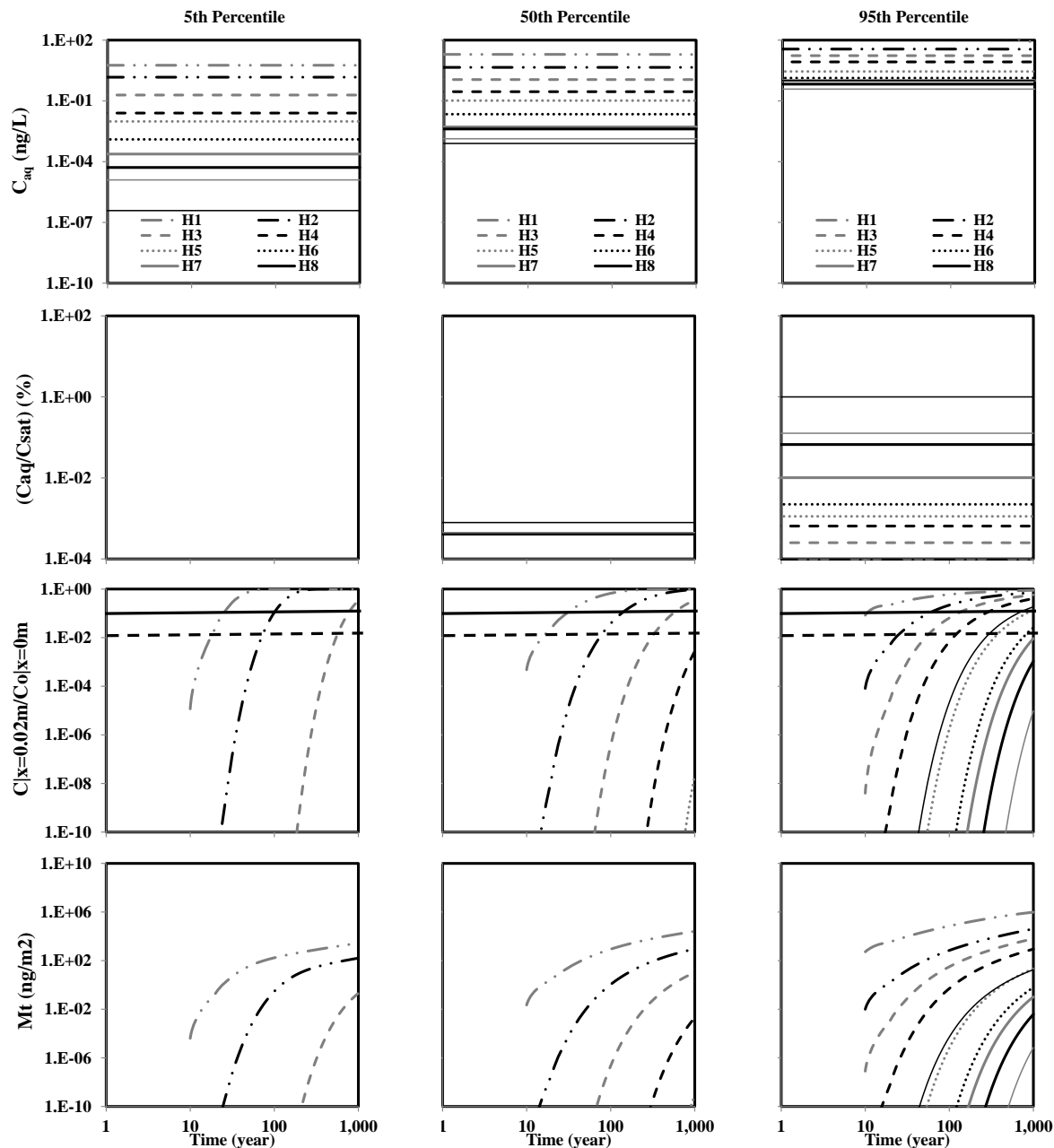


Figure D5.5k: Predicted PBDE aqueous phase concentration under local equilibrium assumption (C_{aq}), ratio of aqueous phase concentration to saturation concentration (C_{aq}/C_{sat}), ratio of aqueous phase concentration at sediment boundary layer to homogenous aqueous phase concentration ($C_{|x=0.02m}/C_{|x=0m}$), and mass leaving the sediment boundary layer (M_t) under advection-diffusion with organic carbon only sorption ($A(OC)$) shown in row1 through 4, respectively as predicted by the 5th, 50th, and 95th percentile transport parameters values shown in column 1 through 3, respectively in core AJL for 50th percentile initial concentration values (60 ng/g).

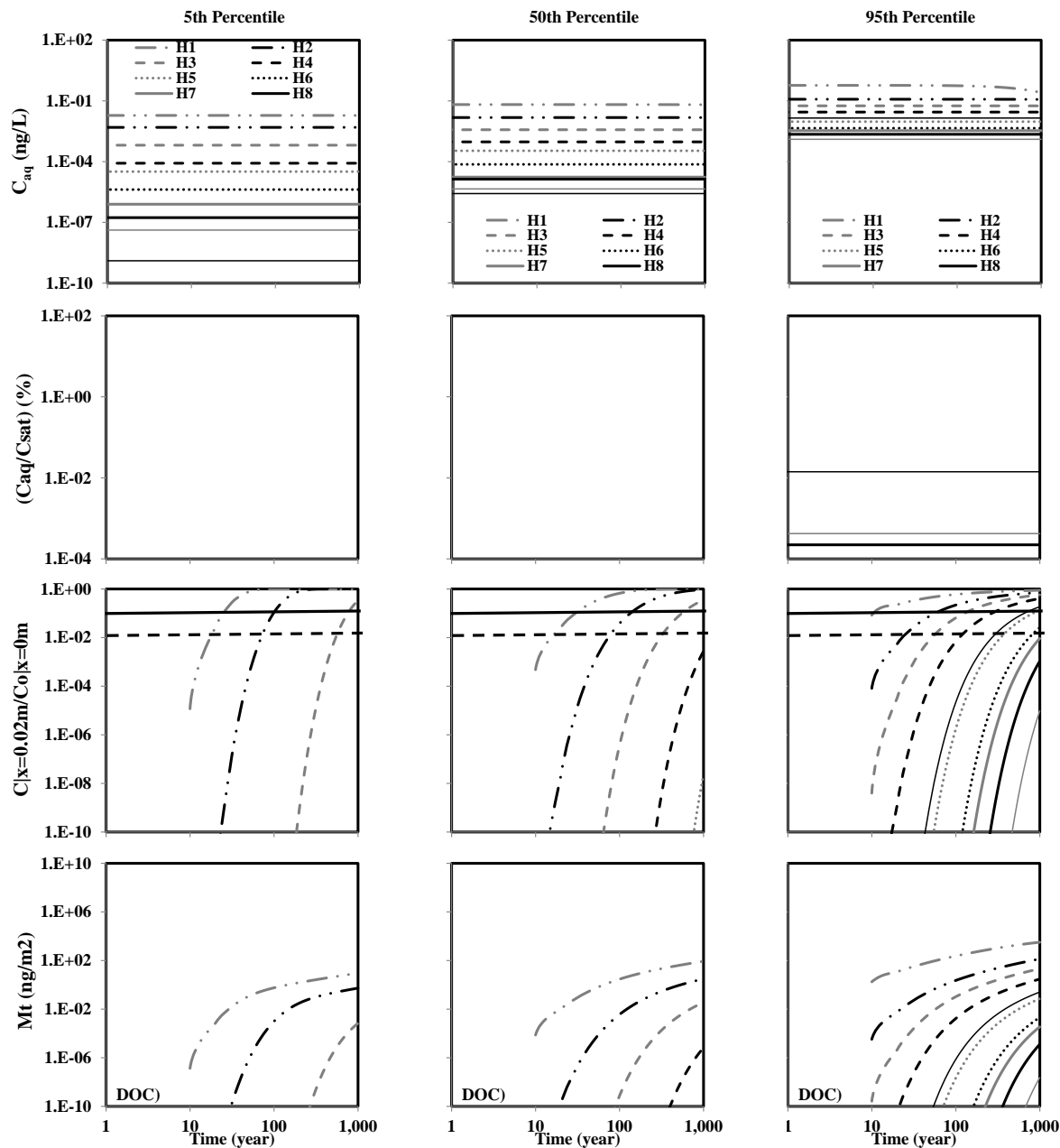


Figure D5.51: Predicted PBDE aqueous phase concentration under local equilibrium assumption (C_{aq}), ratio of aqueous phase concentration to saturation concentration (C_{aq}/C_{sat}), ratio of aqueous phase concentration at sediment boundary layer to homogenous aqueous phase concentration ($C_{|x=0.02m}/C_{|x=0m}$), and mass leaving the sediment boundary layer (M_t) under advection-diffusion with organic carbon only sorption ($A(OC)$) shown in row1 through 4, respectively as predicted by the 5th, 50th, and 95th percentile transport parameters values shown in column 1 through 3, respectively in core AJL for 5th percentile initial concentration values (0.2 ng/g).

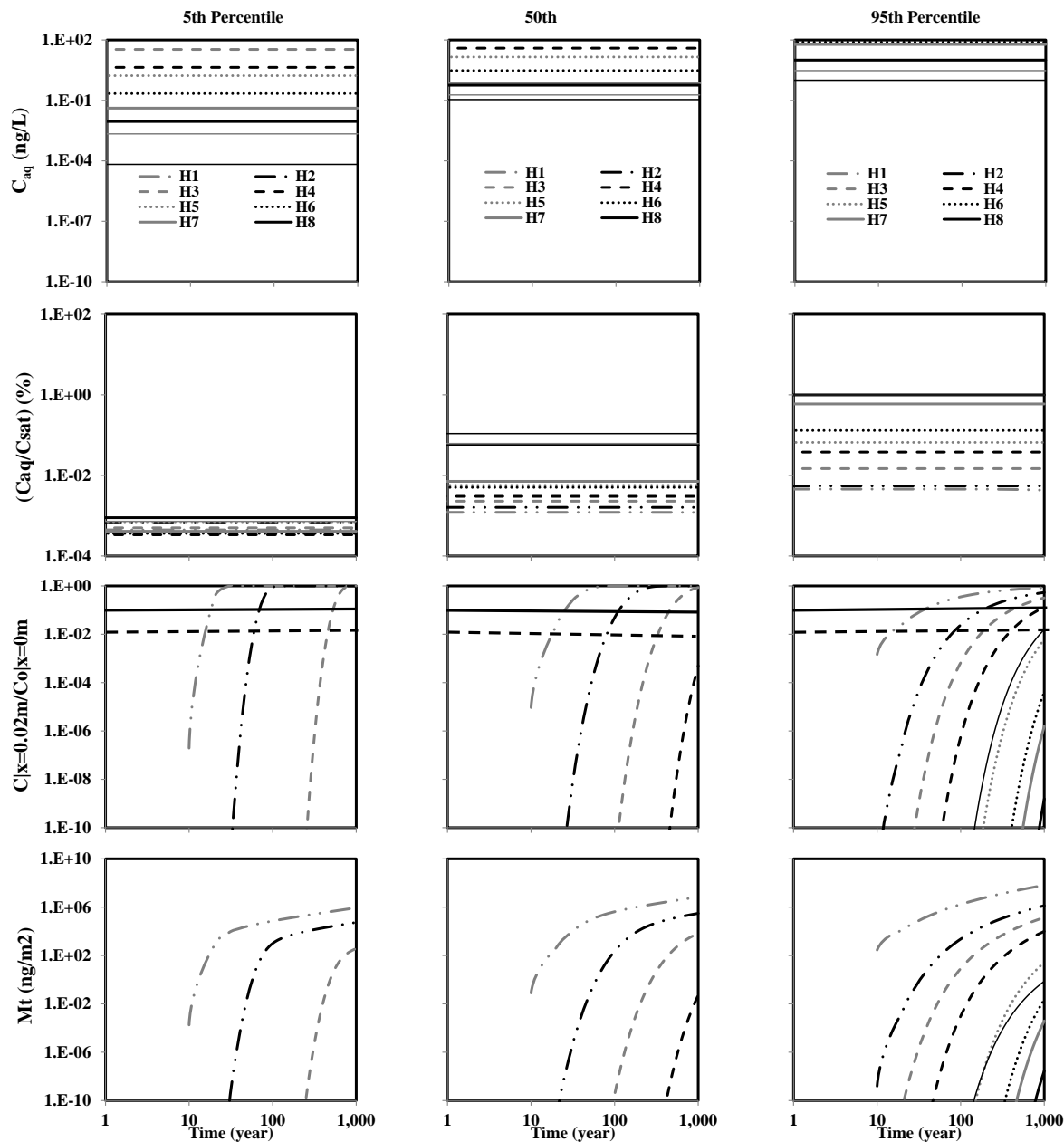


Figure D5.5m: Predicted PBDE aqueous phase concentration under local equilibrium assumption (C_{aq}), ratio of aqueous phase concentration to saturation concentration (C_{aq}/C_{sat}), ratio of aqueous phase concentration at sediment boundary layer to homogeneous aqueous phase concentration ($C_{|x=0.02m}/C_{|x=0m}$), and mass leaving the sediment boundary layer (M_t) under advection-diffusion with organic carbon only sorption (A(OC)) shown in row1 through 4, respectively as predicted by the 5th, 50th, and 95th percentile transport parameters values shown in column 1 through 3, respectively in core AMW for 95th percentile initial concentration values (36100 ng/g).

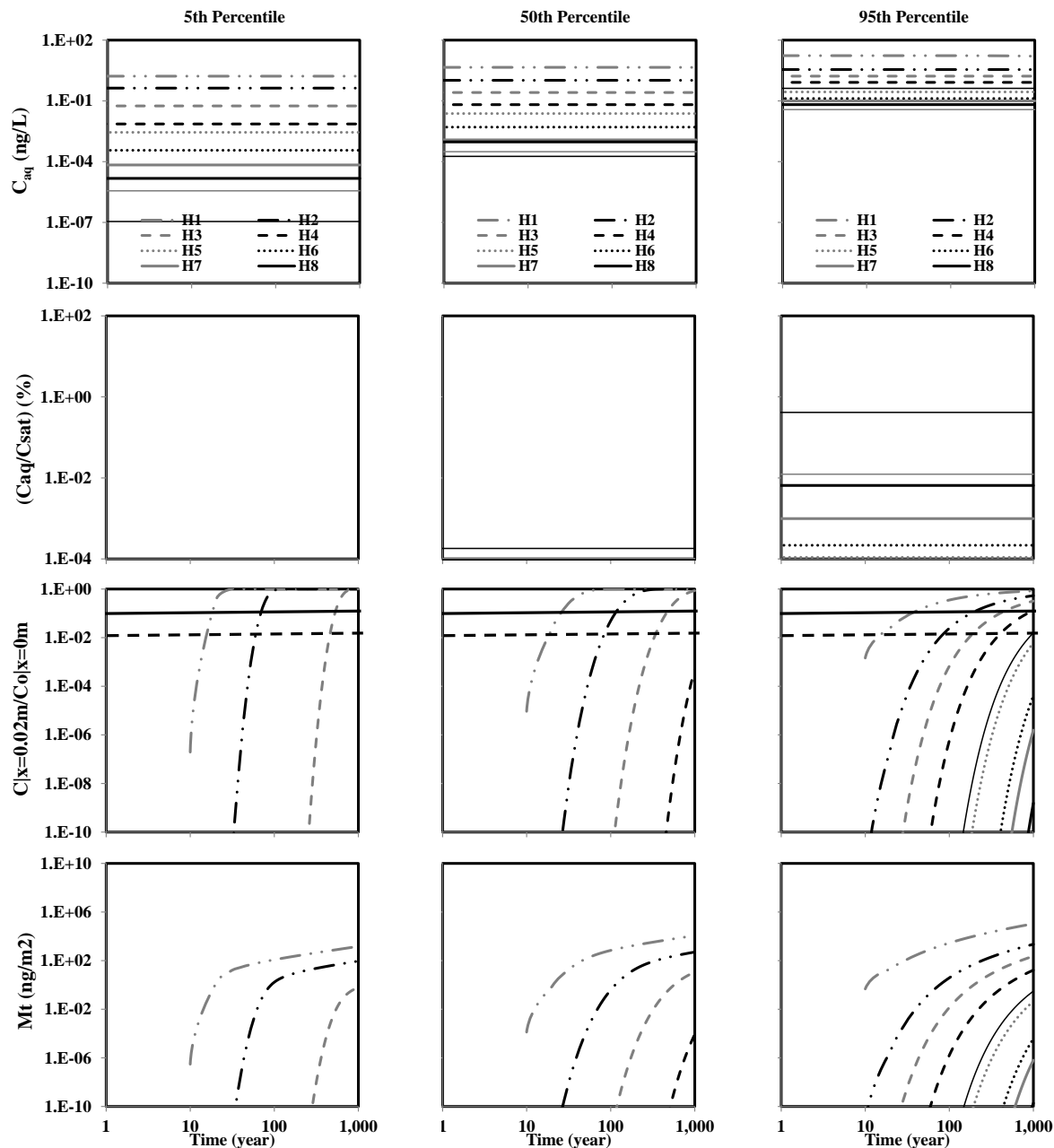


Figure D5.5n: Predicted PBDE aqueous phase concentration under local equilibrium assumption (C_{aq}), ratio of aqueous phase concentration to saturation concentration (C_{aq}/C_{sat}), ratio of aqueous phase concentration at sediment boundary layer to homogenous aqueous phase concentration ($C|x=0.02m/C|x=0m$), and mass leaving the sediment boundary layer (M_t) under advection-diffusion with organic carbon only sorption (A(OC)) shown in row1 through 4, respectively as predicted by the 5th, 50th, and 95th percentile transport parameters values shown in column 1 through 3, respectively in core AMW for 50th percentile initial concentration values (60 ng/g).

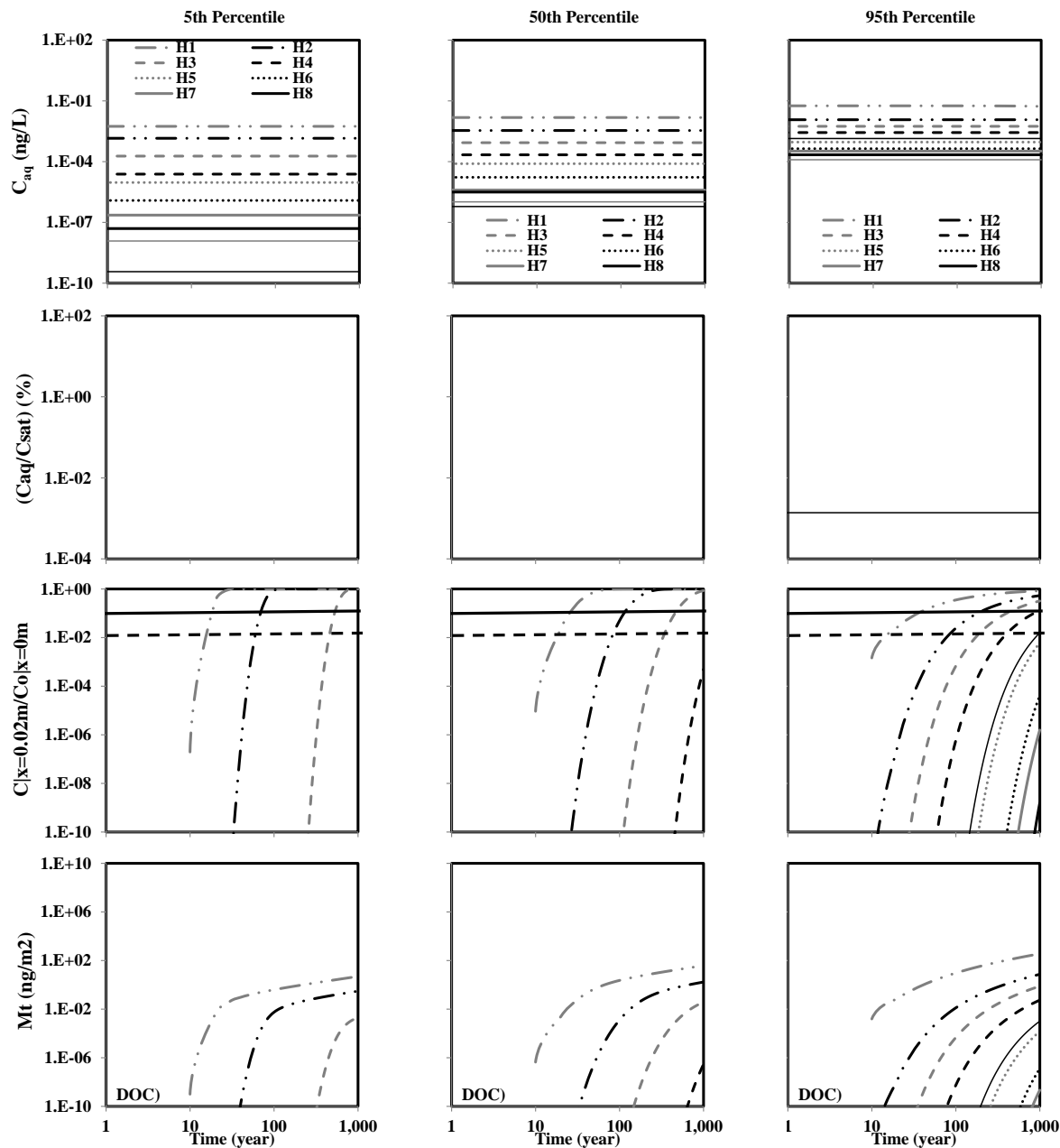


Figure D5.5o: Predicted PBDE aqueous phase concentration under local equilibrium assumption (C_{aq}), ratio of aqueous phase concentration to saturation concentration (C_{aq}/C_{sat}), ratio of aqueous phase concentration at sediment boundary layer to homogeneous aqueous phase concentration ($C_{|x=0.02m}/C_{|x=0m}$), and mass leaving the sediment boundary layer (M_t) under advection-diffusion with organic carbon only sorption (A(OC)) shown in row1 through 4, respectively as predicted by the 5th, 50th, and 95th percentile transport parameters values shown in column 1 through 3, respectively in core AMW for 5th percentile initial concentration values (0.2 ng/g).

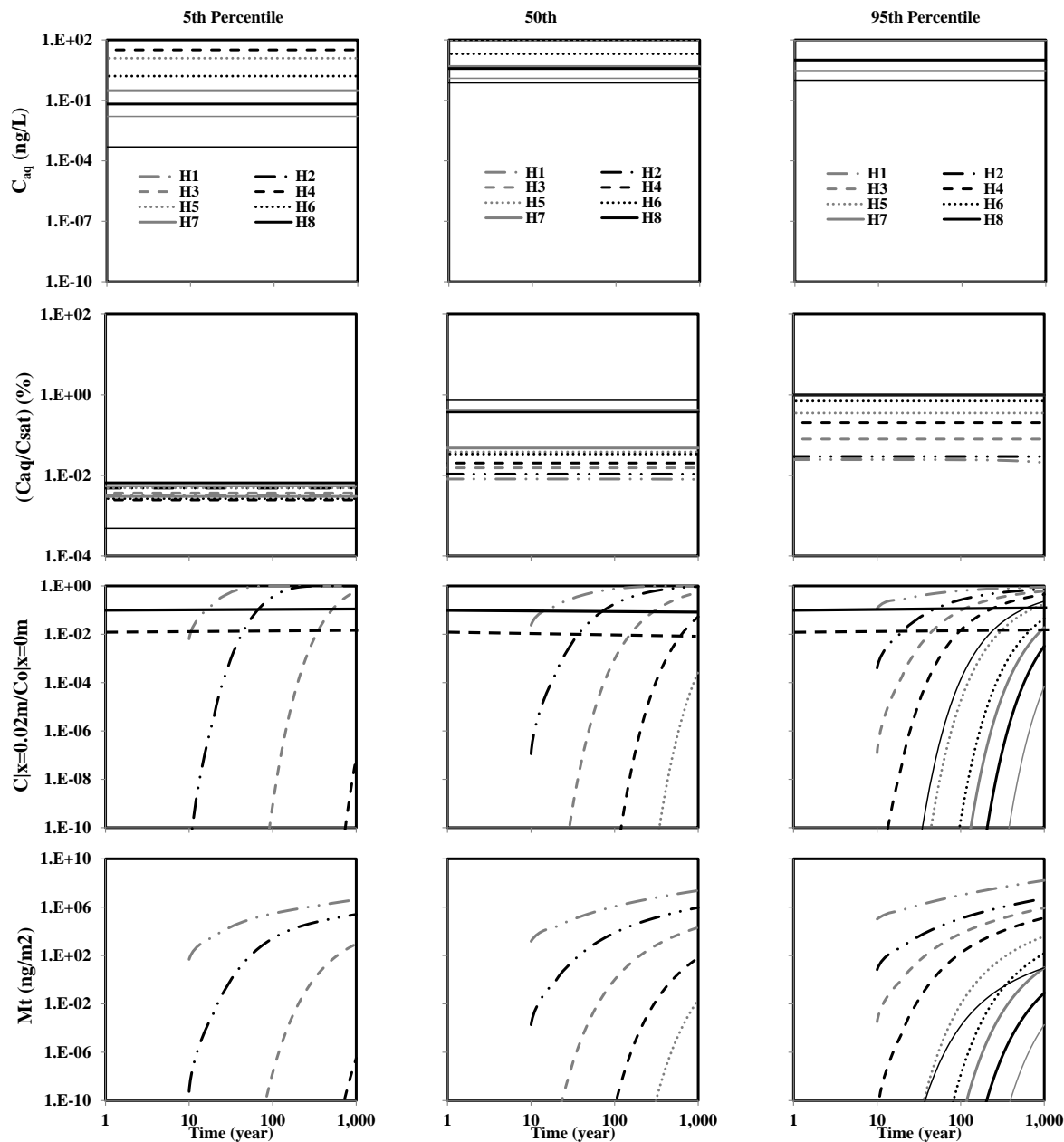


Figure D5.5p: Predicted PBDE aqueous phase concentration under local equilibrium assumption (C_{aq}), ratio of aqueous phase concentration to saturation concentration (C_{aq}/C_{sat}), ratio of aqueous phase concentration at sediment boundary layer to homogeneous aqueous phase concentration ($C_{|x=0.02m}/C_{|x=0m}$), and mass leaving the sediment boundary layer (M_t) under advection-diffusion with organic carbon only sorption ($A(OC)$) shown in row1 through 4, respectively as predicted by the 5th, 50th, and 95th percentile transport parameters values shown in column 1 through 3, respectively in core AOT for 95th percentile initial concentration values (36100 ng/g).

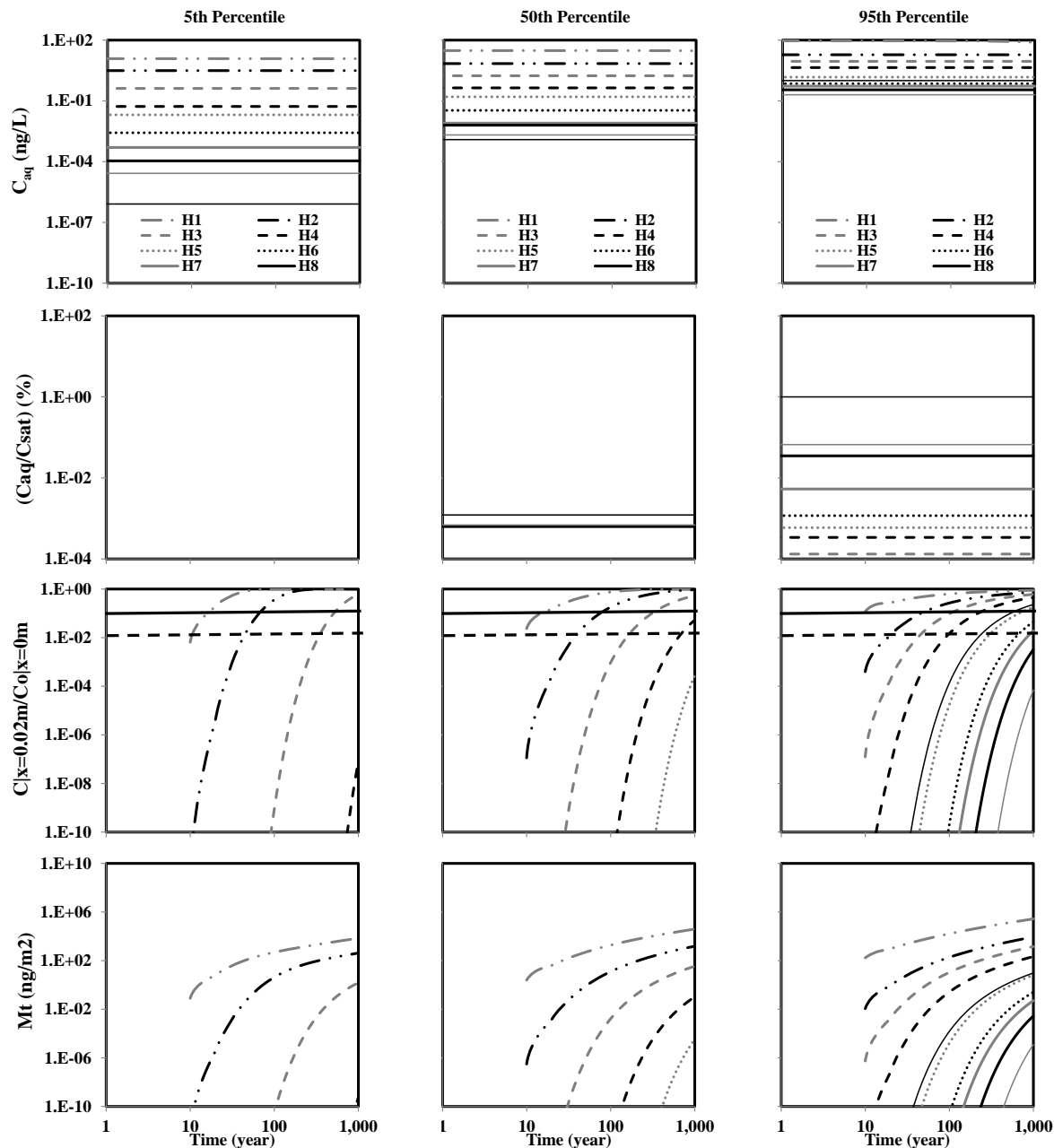


Figure D5.5q: Predicted PBDE aqueous phase concentration under local equilibrium assumption (C_{aq}), ratio of aqueous phase concentration to saturation concentration (C_{aq}/C_{sat}), ratio of aqueous phase concentration at sediment boundary layer to homogenous aqueous phase concentration ($C_{|x=0.02m}/C_{|x=0m}$), and mass leaving the sediment boundary layer (M_t) under advection-diffusion with organic carbon only sorption (A(OC)) shown in row1 through 4, respectively as predicted by the 5th, 50th, and 95th percentile transport parameters values shown in column 1 through 3, respectively in core AOT for 50th percentile initial concentration values (60 ng/g).

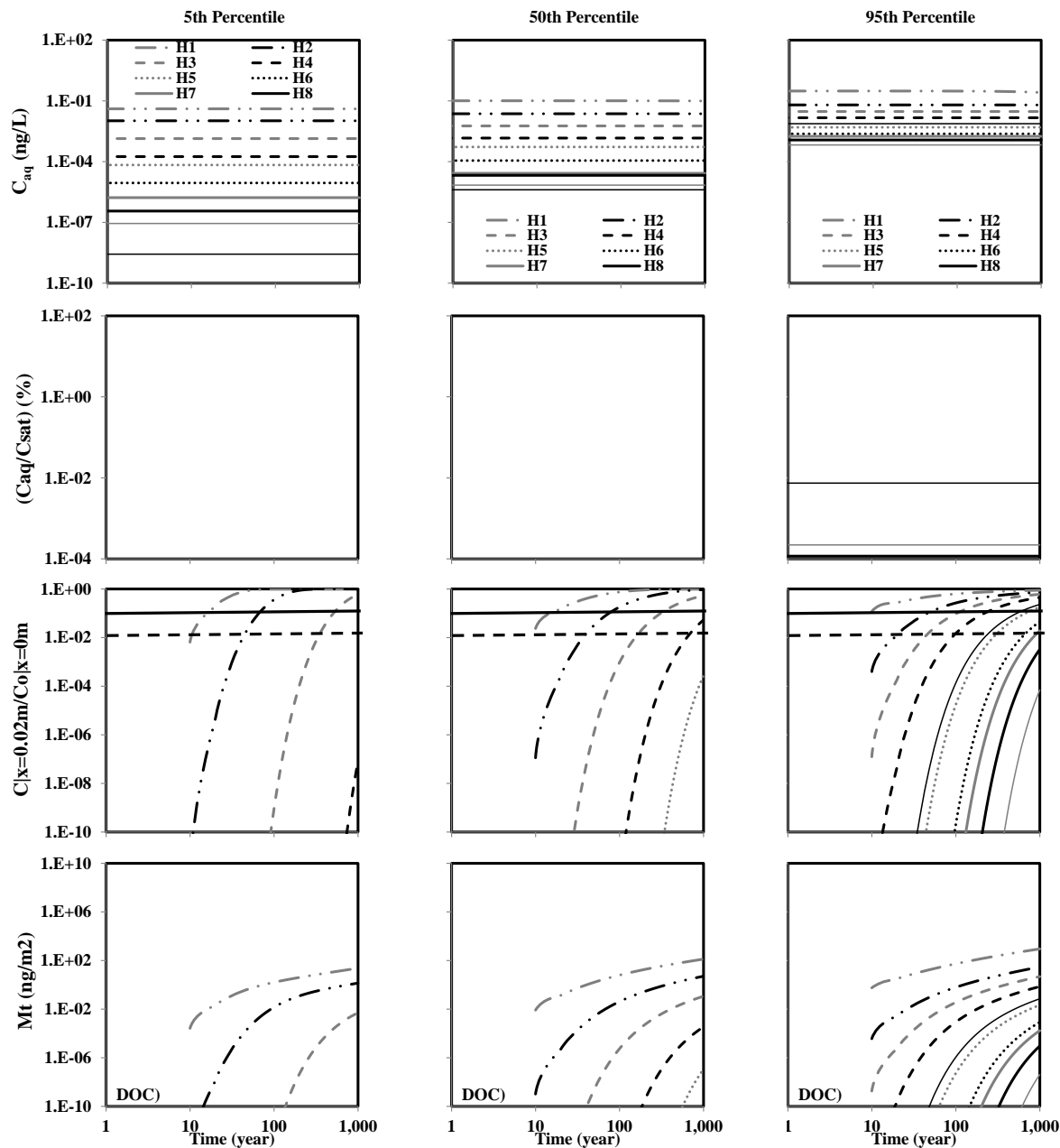


Figure D5.5r: Predicted PBDE aqueous phase concentration under local equilibrium assumption (C_{aq}), ratio of aqueous phase concentration to saturation concentration (C_{aq}/C_{sat}), ratio of aqueous phase concentration at sediment boundary layer to homogeneous aqueous phase concentration ($C_{|x=0.02m}/C_{|x=0m}$), and mass leaving the sediment boundary layer (M_t) under advection-diffusion with organic carbon only sorption (A(OC)) shown in row1 through 4, respectively as predicted by the 5th, 50th, and 95th percentile transport parameters values shown in column 1 through 3, respectively in core AOT for 5th percentile initial concentration values (0.2 ng/g).

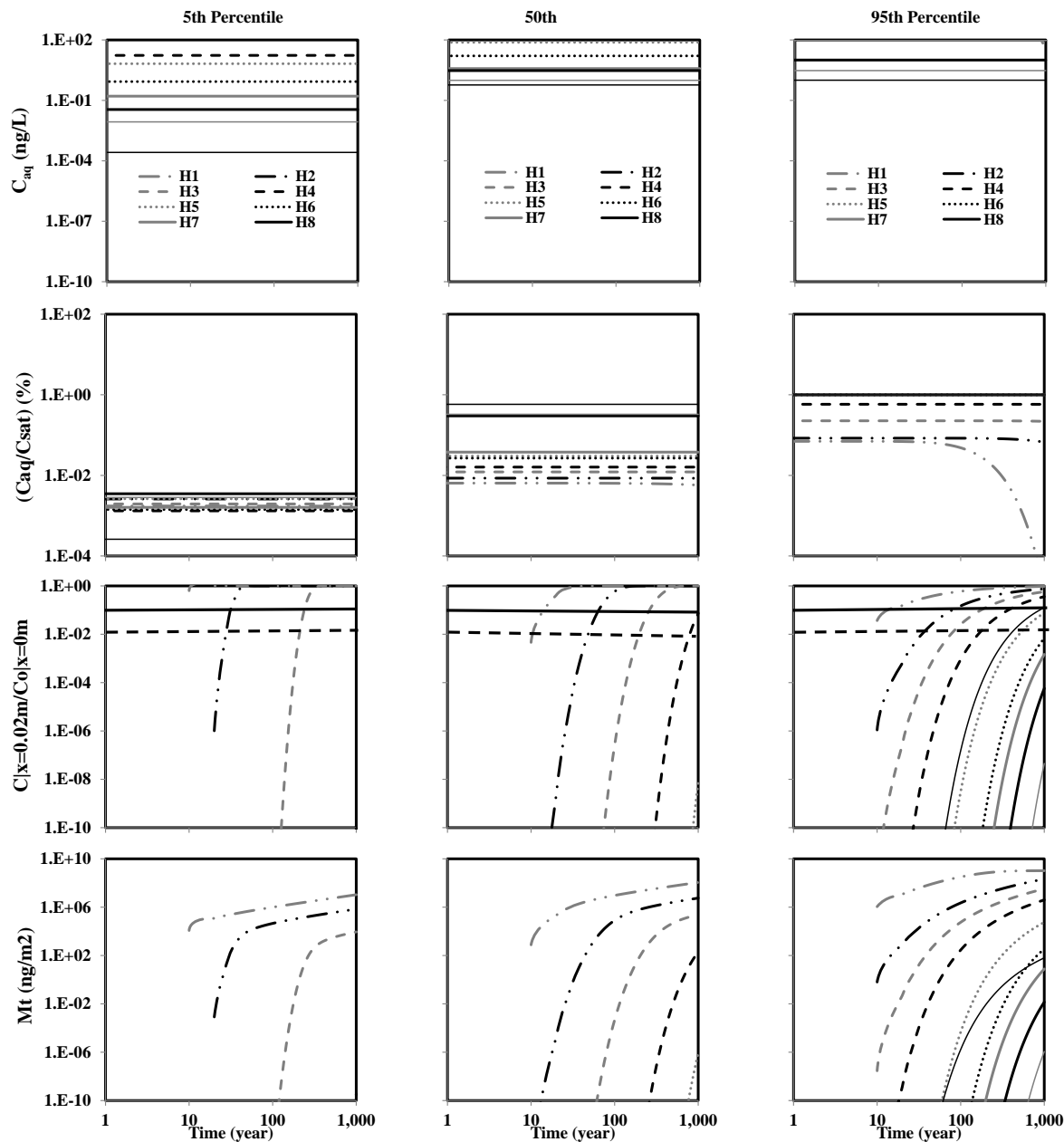


Figure D5.5s: Predicted PBDE aqueous phase concentration under local equilibrium assumption (C_{aq}), ratio of aqueous phase concentration to saturation concentration (C_{aq}/C_{sat}), ratio of aqueous phase concentration at sediment boundary layer to homogeneous aqueous phase concentration ($C_{|x=0.02m}/C_{|x=0m}$), and mass leaving the sediment boundary layer (M_t) under advection-diffusion with organic carbon only sorption (A(OC)) shown in row1 through 4, respectively as predicted by the 5th, 50th, and 95th percentile transport parameters values shown in column 1 through 3, respectively in core CBC for 95th percentile initial concentration values (36100 ng/g).

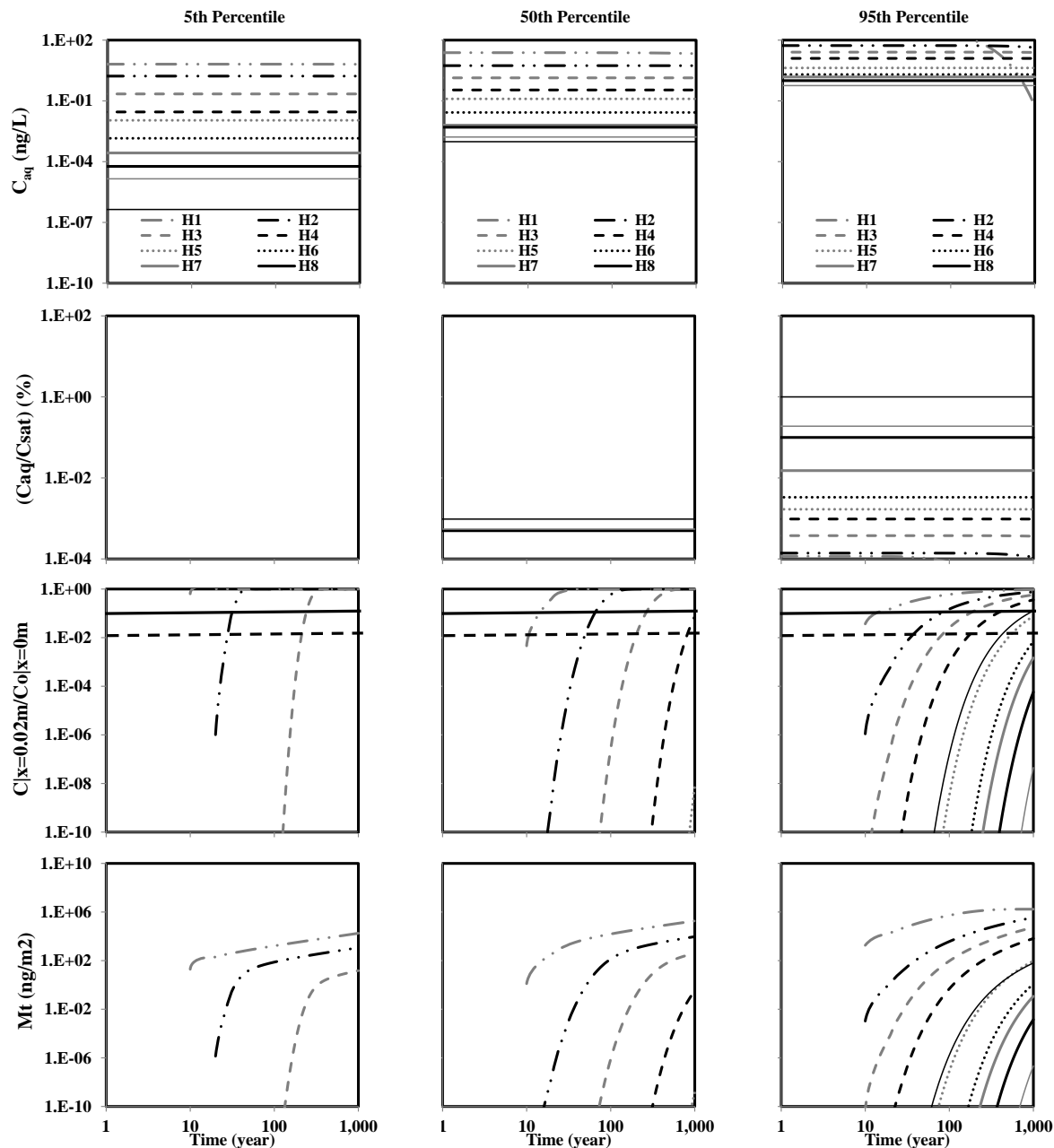


Figure D5.5t: Predicted PBDE aqueous phase concentration under local equilibrium assumption (C_{aq}), ratio of aqueous phase concentration to saturation concentration (C_{aq}/C_{sat}), ratio of aqueous phase concentration at sediment boundary layer to homogenous aqueous phase concentration ($C_{|x=0.02m}/C_{|x=0m}$), and mass leaving the sediment boundary layer (M_t) under advection-diffusion with organic carbon only sorption (A(OC)) shown in row1 through 4, respectively as predicted by the 5th, 50th, and 95th percentile transport parameters values shown in column 1 through 3, respectively in core CBC for 50th percentile initial concentration values (60 ng/g).

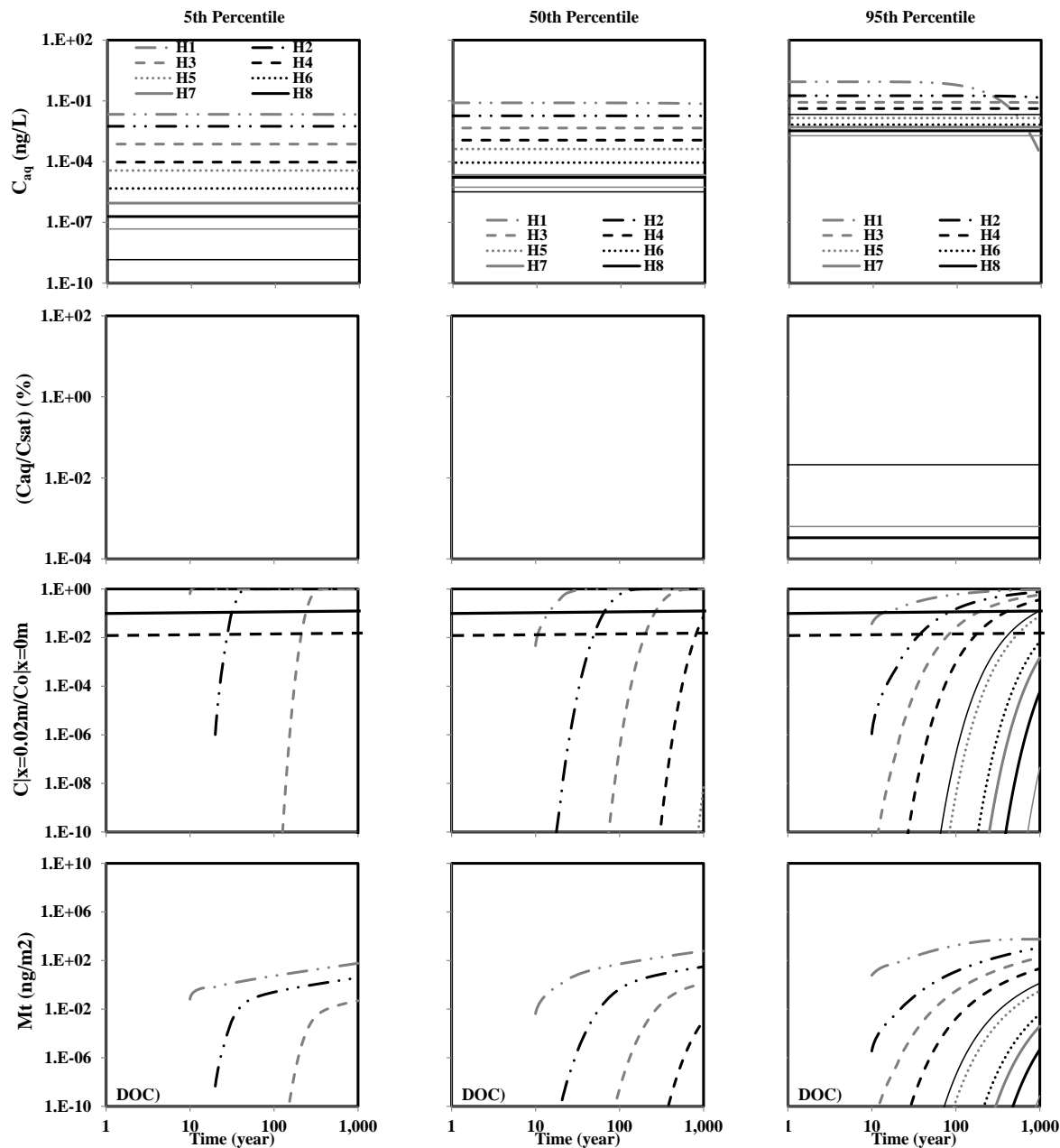


Figure D5.5u: Predicted PBDE aqueous phase concentration under local equilibrium assumption (C_{aq}), ratio of aqueous phase concentration to saturation concentration (C_{aq}/C_{sat}), ratio of aqueous phase concentration at sediment boundary layer to homogenous aqueous phase concentration ($C_{|x=0.02m}/C_{|x=0m}$), and mass leaving the sediment boundary layer (M_t) under advection-diffusion with organic carbon only sorption (A(OC)) shown in row1 through 4, respectively as predicted by the 5th, 50th, and 95th percentile transport parameters values shown in column 1 through 3, respectively in core CBC for 5th percentile initial concentration values (0.2 ng/g).

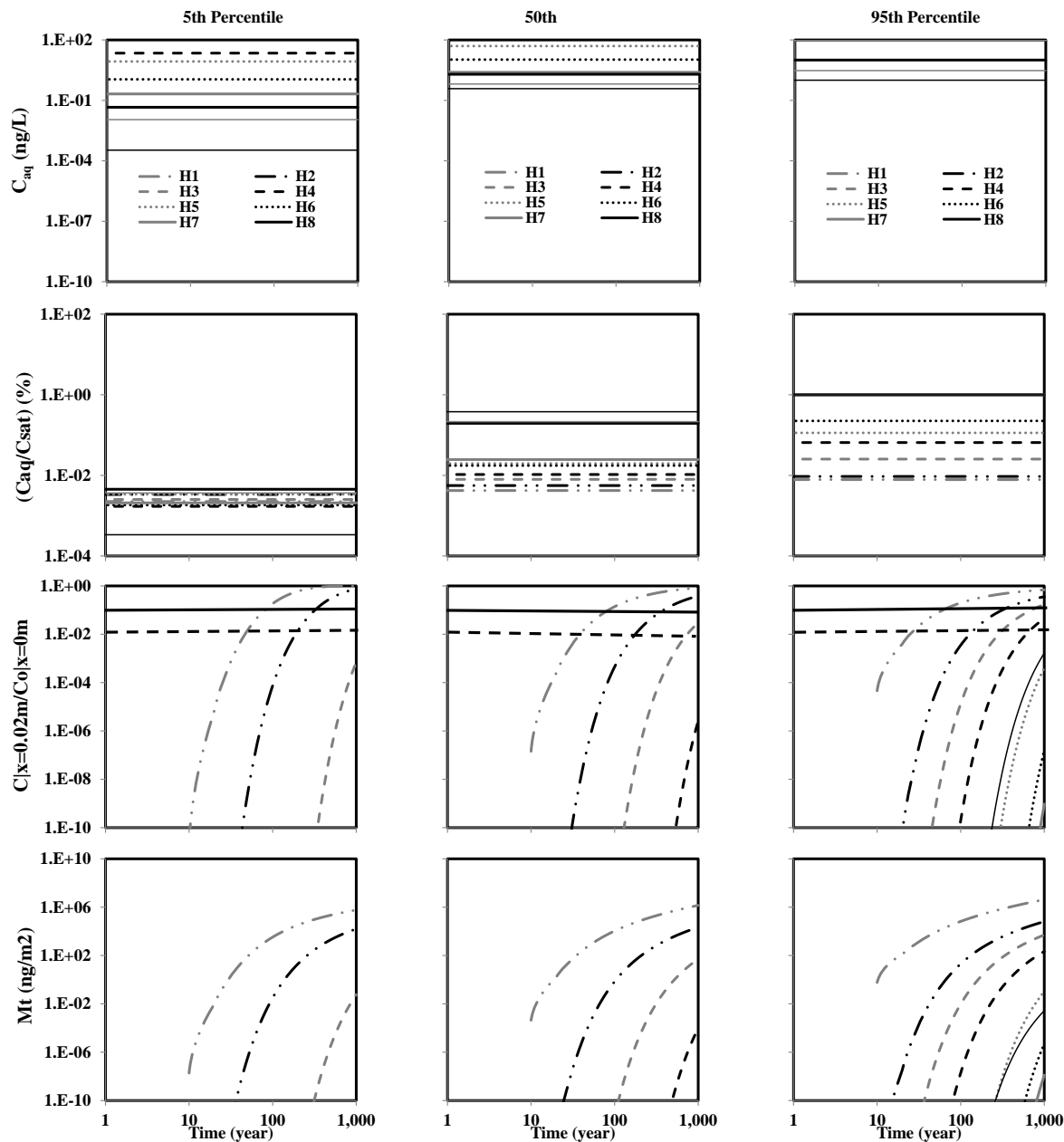


Figure D5.5v: Predicted PBDE aqueous phase concentration under local equilibrium assumption (C_{aq}), ratio of aqueous phase concentration to saturation concentration (C_{aq}/C_{sat}), ratio of aqueous phase concentration at sediment boundary layer to homogeneous aqueous phase concentration ($C_{|x=0.02m}/C_{|x=0m}$), and mass leaving the sediment boundary layer (M_t) under advection-diffusion with organic carbon only sorption (A(OC)) shown in row1 through 4, respectively as predicted by the 5th, 50th, and 95th percentile transport parameters values shown in column 1 through 3, respectively in core CLC for 95th percentile initial concentration values (36100 ng/g).

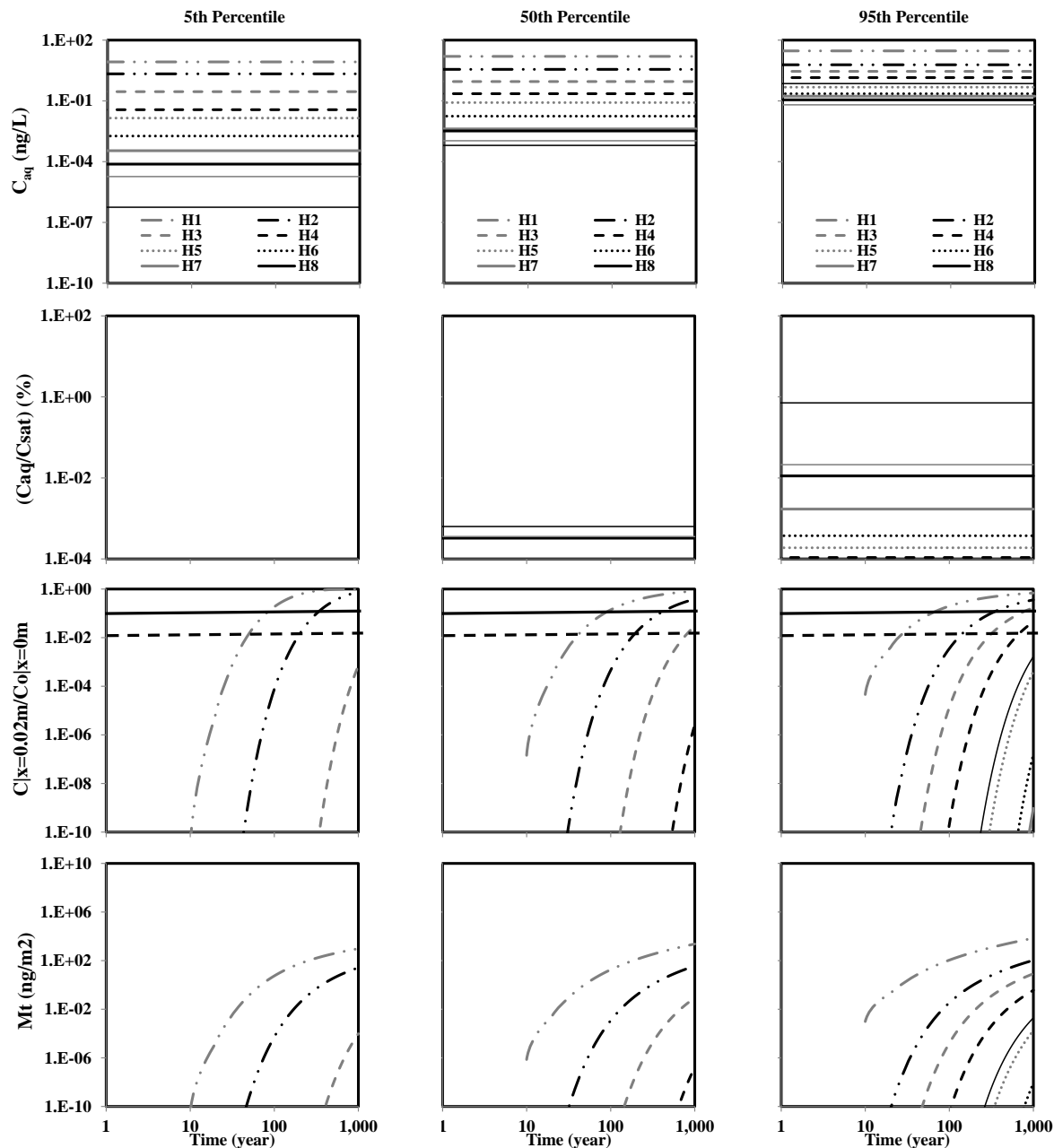


Figure D5.5w: Predicted PBDE aqueous phase concentration under local equilibrium assumption (C_{aq}), ratio of aqueous phase concentration to saturation concentration (C_{aq}/C_{sat}), ratio of aqueous phase concentration at sediment boundary layer to homogenous aqueous phase concentration ($C_{|x=0.02m}/C_{|x=0m}$), and mass leaving the sediment boundary layer (M_t) under advection-diffusion with organic carbon only sorption (A(OC)) shown in row1 through 4, respectively as predicted by the 5th, 50th, and 95th percentile transport parameters values shown in column 1 through 3, respectively in core CLC for 50th percentile initial concentration values (60 ng/g).

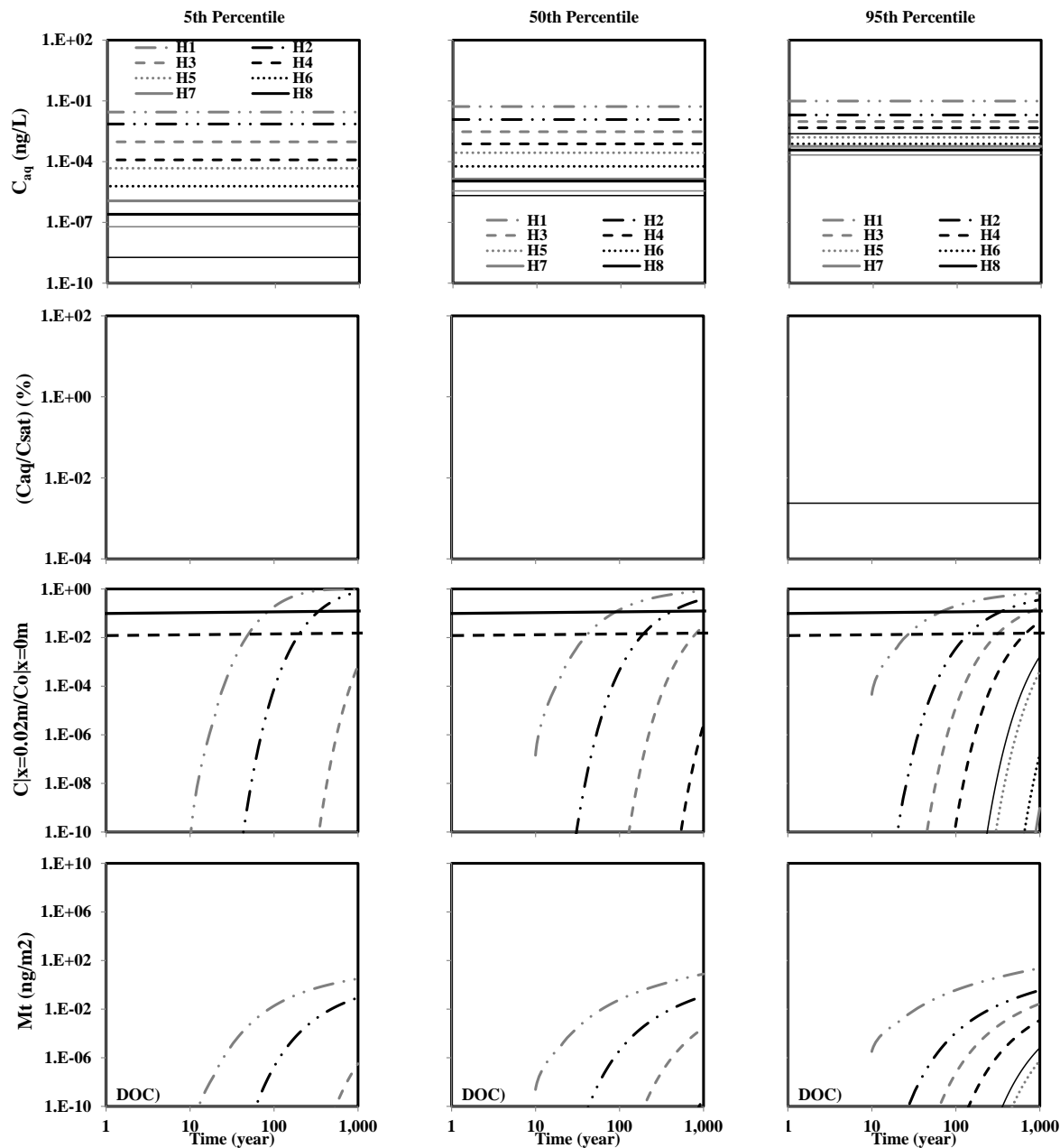


Figure D5.5x: Predicted PBDE aqueous phase concentration under local equilibrium assumption (C_{aq}), ratio of aqueous phase concentration to saturation concentration (C_{aq}/C_{sat}), ratio of aqueous phase concentration at sediment boundary layer to homogeneous aqueous phase concentration ($C_{|x=0.02m}/C_{|x=0m}$), and mass leaving the sediment boundary layer (M_t) under advection-diffusion with organic carbon only sorption (A(OC)) shown in row1 through 4, respectively as predicted by the 5th, 50th, and 95th percentile transport parameters values shown in column 1 through 3, respectively in core CLC for 5th percentile initial concentration values (0.2 ng/g).

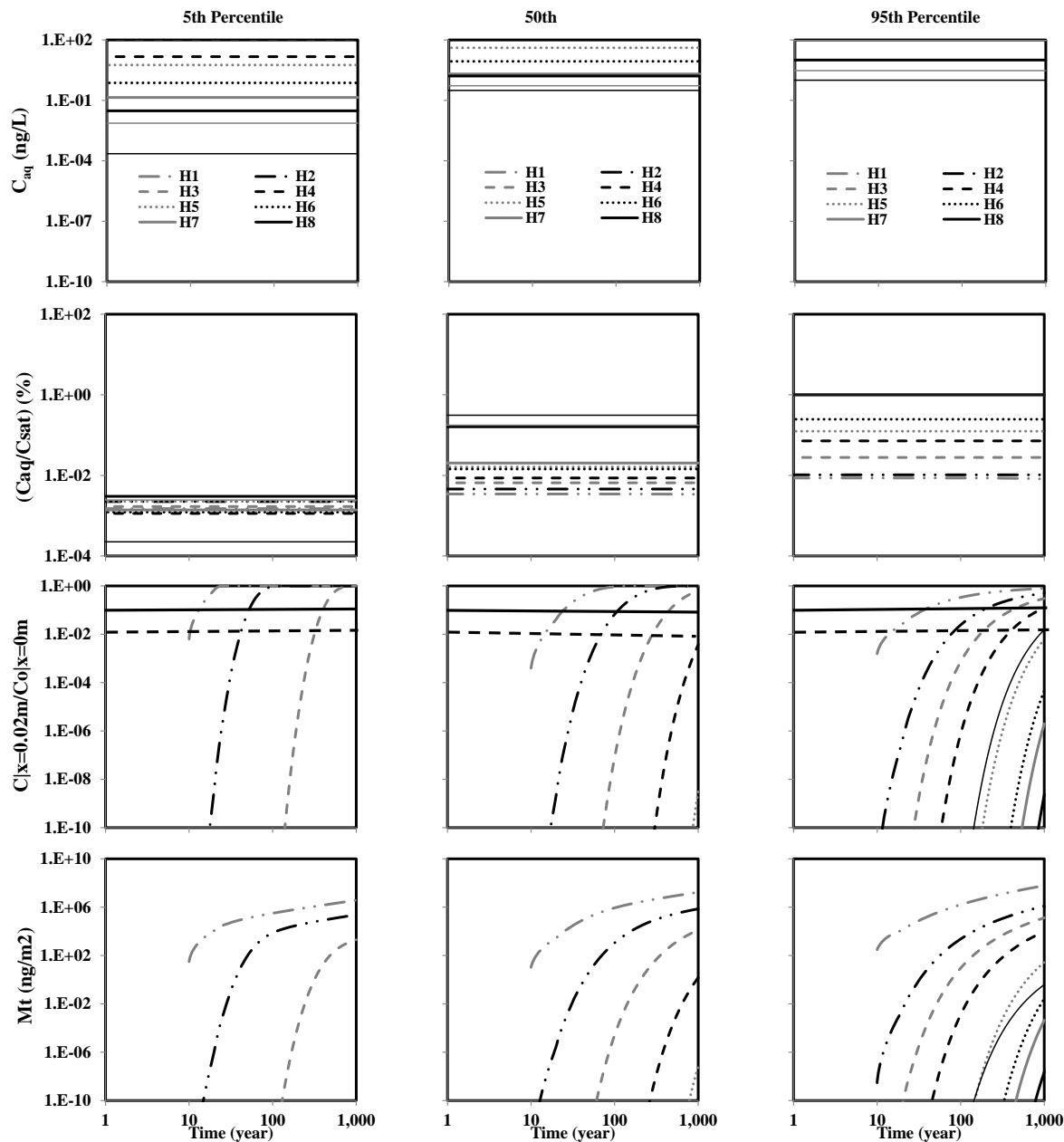


Figure D5.5y: Predicted PBDE aqueous phase concentration under local equilibrium assumption (C_{aq}), ratio of aqueous phase concentration to saturation concentration (C_{aq}/C_{sat}), ratio of aqueous phase concentration at sediment boundary layer to homogenous aqueous phase concentration ($C_{|x=0.02m}/C_{|x=0m}$), and mass leaving the sediment boundary layer (M_t) under advection-diffusion with organic carbon only sorption (A(OC)) shown in row1 through 4, respectively as predicted by the 5th, 50th, and 95th percentile transport parameters values shown in column 1 through 3, respectively in core CWP for 95th percentile initial concentration values (36100 ng/g).

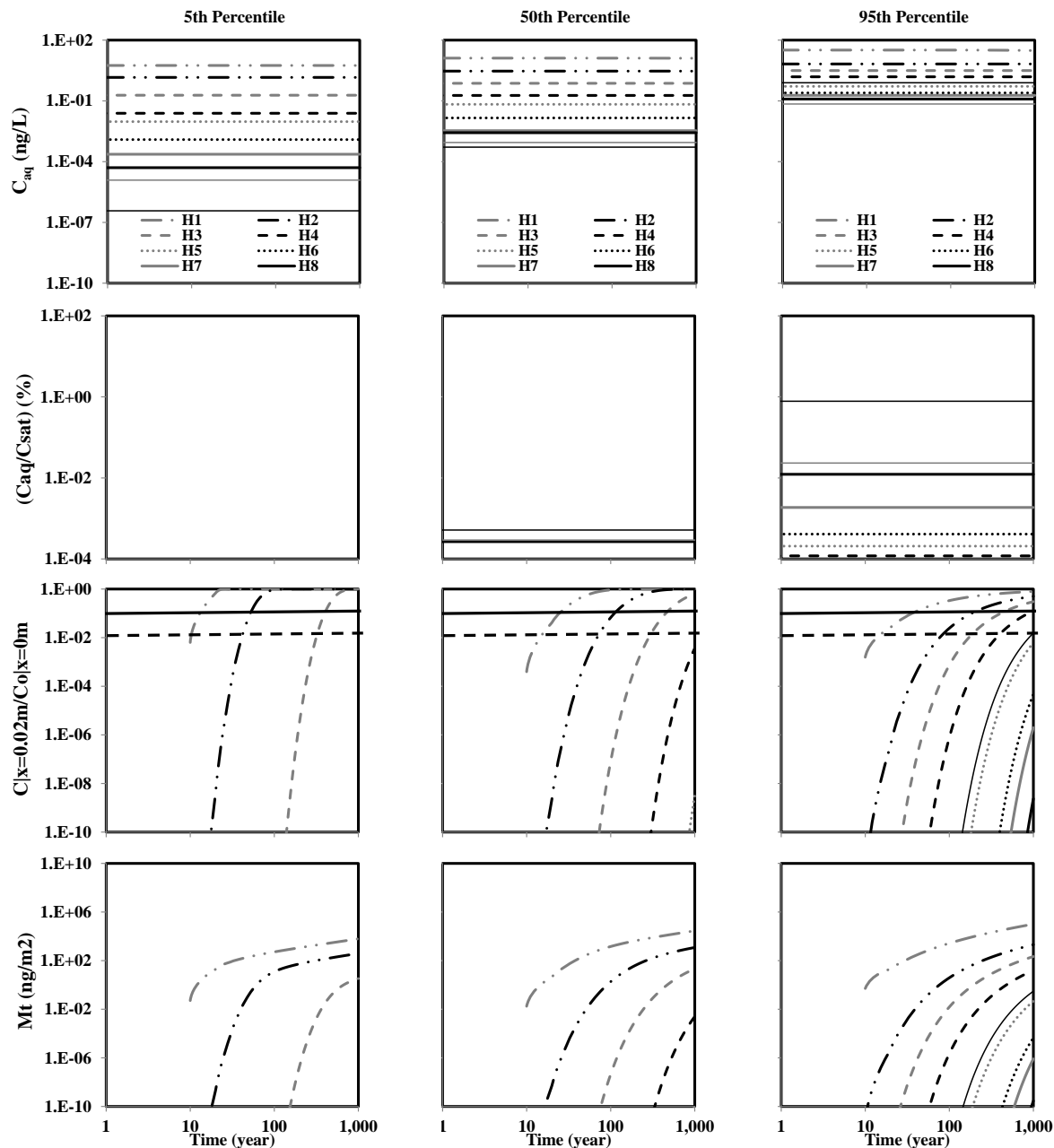


Figure D5.5z: Predicted PBDE aqueous phase concentration under local equilibrium assumption (C_{aq}), ratio of aqueous phase concentration to saturation concentration (C_{aq}/C_{sat}), ratio of aqueous phase concentration at sediment boundary layer to homogenous aqueous phase concentration ($C|_{x=0.02m}/C|_{x=0m}$), and mass leaving the sediment boundary layer (M_t) under advection-diffusion with organic carbon only sorption (A(OC)) shown in row1 through 4, respectively as predicted by the 5th, 50th, and 95th percentile transport parameters values shown in column 1 through 3, respectively in core core CWP for 50th percentile initial concentration values (60 ng/g).

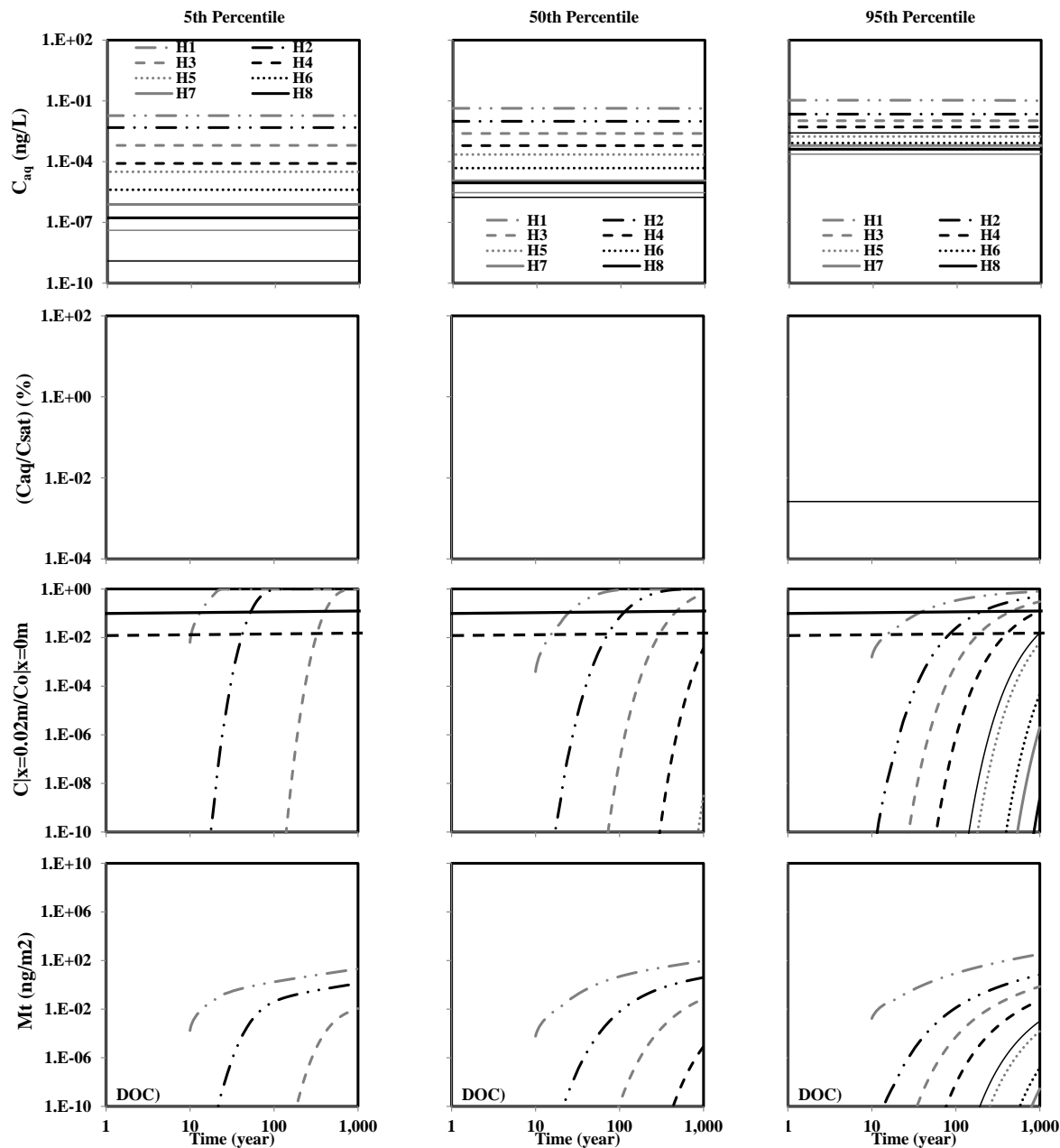


Figure D5.5aa: Predicted PBDE aqueous phase concentration under local equilibrium assumption (C_{aq}), ratio of aqueous phase concentration to saturation concentration (C_{aq}/C_{sat}), ratio of aqueous phase concentration at sediment boundary layer to homogeneous aqueous phase concentration ($C_{|x=0.02m}/C_{|x=0m}$), and mass leaving the sediment boundary layer (M_t) under advection-diffusion with organic carbon only sorption (A(OC)) shown in row1 through 4, respectively as predicted by the 5th, 50th, and 95th percentile transport parameters values shown in column 1 through 3, respectively in core CWP for 5th percentile initial concentration values (0.2 ng/g).

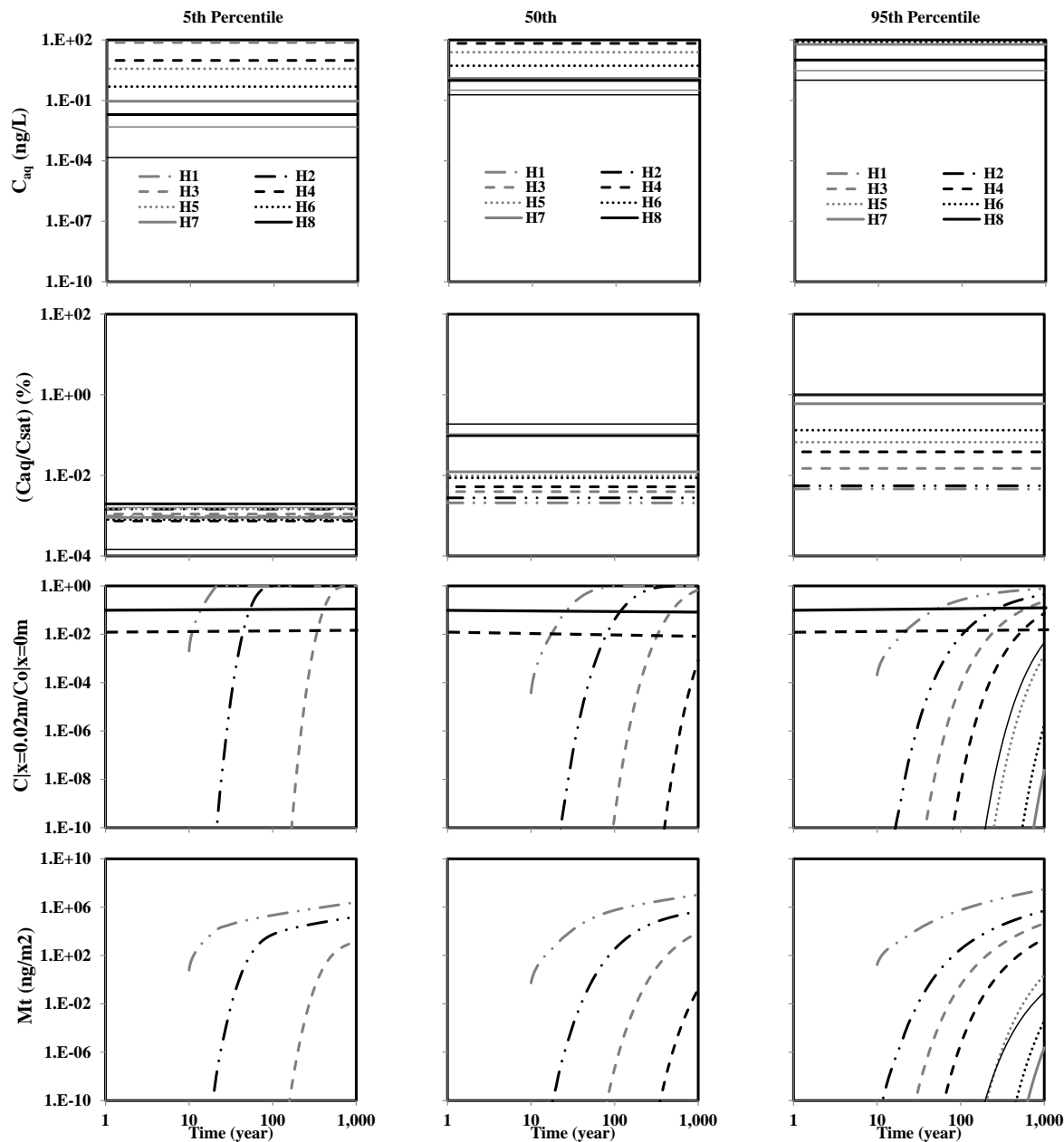


Figure D5.5ab: Predicted PBDE aqueous phase concentration under local equilibrium assumption (C_{aq}), ratio of aqueous phase concentration to saturation concentration (C_{aq}/C_{sat}), ratio of aqueous phase concentration at sediment boundary layer to homogenous aqueous phase concentration ($C_{|x=0.02m}/C_{|x=0m}$), and mass leaving the sediment boundary layer (M_t) under advection-diffusion with organic carbon only sorption (A(OC)) shown in row1 through 4, respectively as predicted by the 5th, 50th, and 95th percentile transport parameters values shown in column 1 through 3, respectively in core IGC09 for 95th percentile initial concentration values (36100 ng/g).

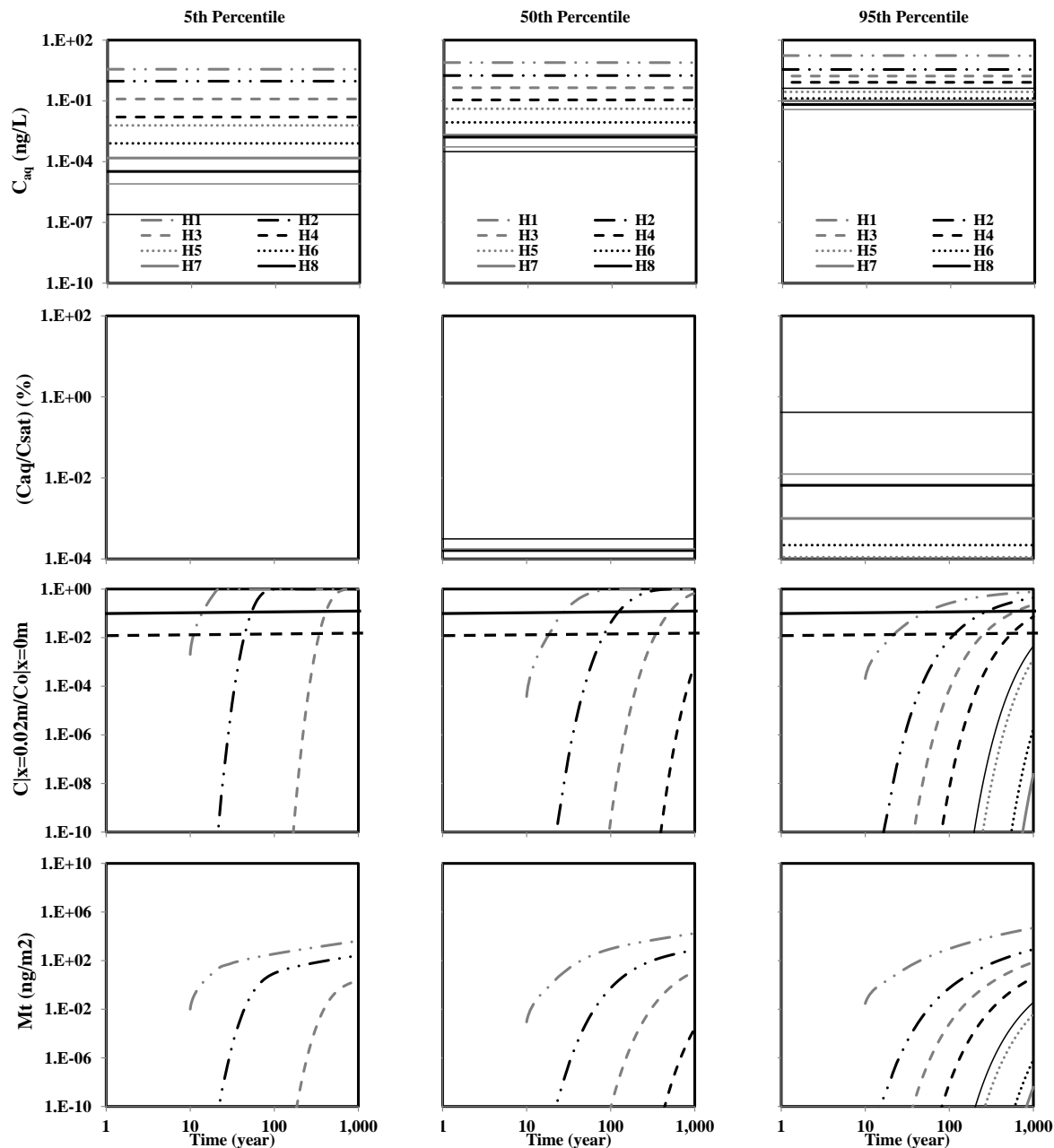


Figure D5.5ac: Predicted PBDE aqueous phase concentration under local equilibrium assumption (C_{aq}), ratio of aqueous phase concentration to saturation concentration (C_{aq}/C_{sat}), ratio of aqueous phase concentration at sediment boundary layer to homogenous aqueous phase concentration ($C_{|x=0.02m}/C_{|x=0m}$), and mass leaving the sediment boundary layer (M_t) under advection-diffusion with organic carbon only sorption (A(OC)) shown in row1 through 4, respectively as predicted by the 5th, 50th, and 95th percentile transport parameters values shown in column 1 through 3, respectively in core IGC09 for 50th percentile initial concentration values (60 ng/g).

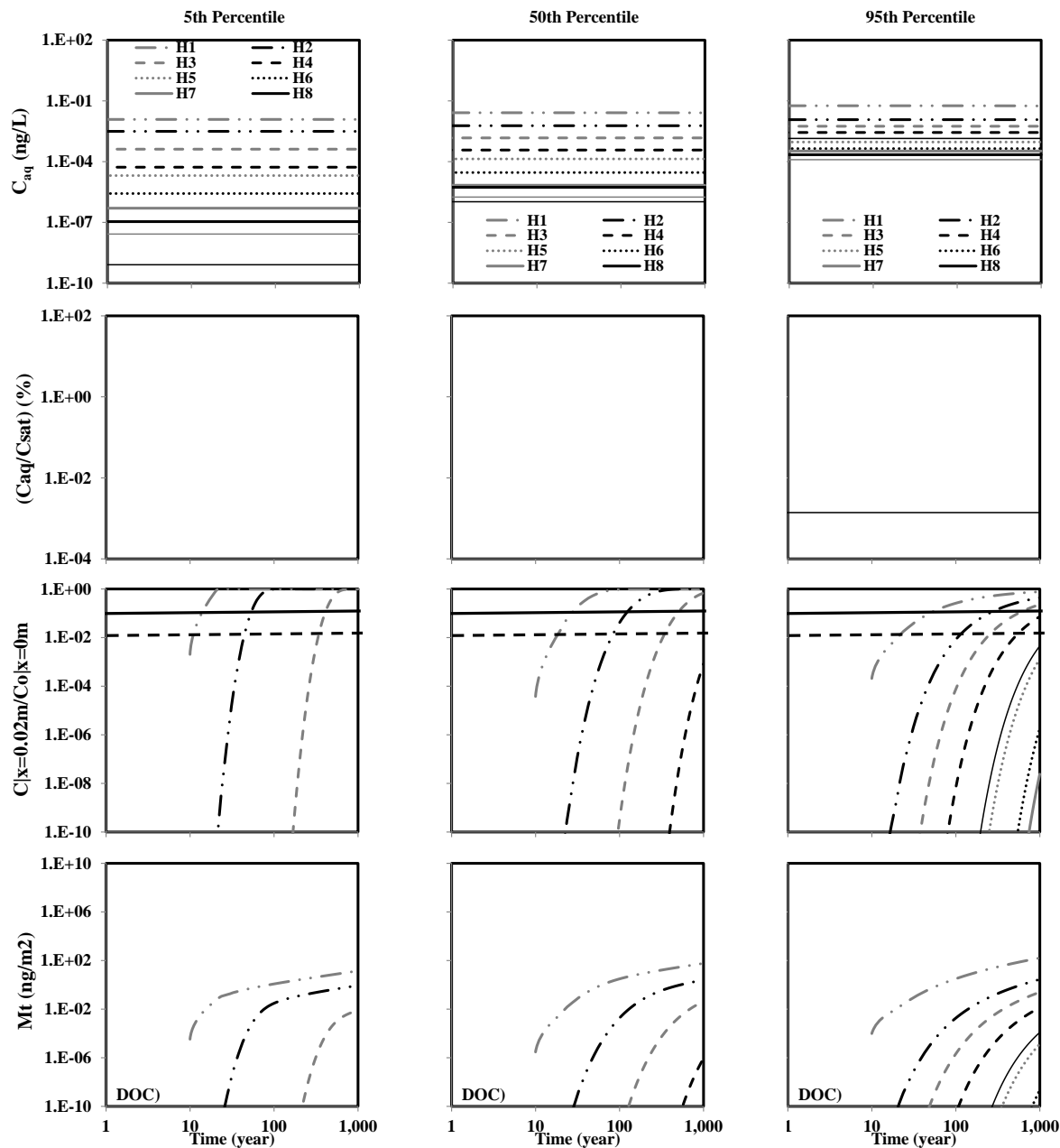


Figure D5.5ad: Predicted PBDE aqueous phase concentration under local equilibrium assumption (C_{aq}), ratio of aqueous phase concentration to saturation concentration (C_{aq}/C_{sat}), ratio of aqueous phase concentration at sediment boundary layer to homogeneous aqueous phase concentration ($C_{|x=0.02m}/C_{|x=0m}$), and mass leaving the sediment boundary layer (M_t) under advection-diffusion with organic carbon only sorption (A(OC)) shown in row1 through 4, respectively as predicted by the 5th, 50th, and 95th percentile transport parameters values shown in column 1 through 3, respectively in core IGC09 for 5th percentile initial concentration values (0.2 ng/g).

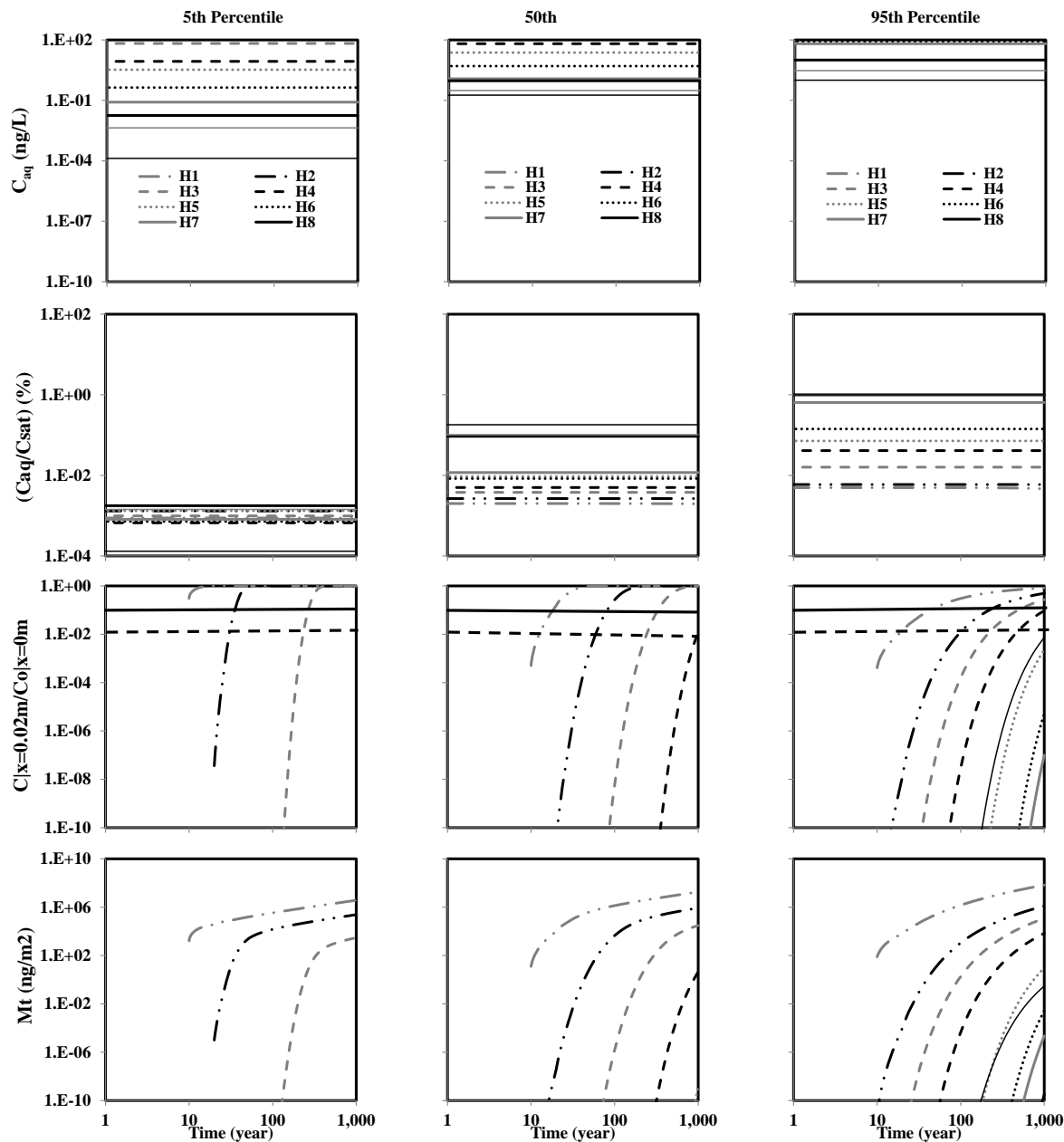


Figure D5.5ae: Predicted PBDE aqueous phase concentration under local equilibrium assumption (C_{aq}), ratio of aqueous phase concentration to saturation concentration (C_{aq}/C_{sat}), ratio of aqueous phase concentration at sediment boundary layer to homogeneous aqueous phase concentration ($C_{|x=0.02m}/C_{|x=0m}$), and mass leaving the sediment boundary layer (M_t) under advection-diffusion with organic carbon only sorption (A(OC)) shown in row1 through 4, respectively as predicted by the 5th, 50th, and 95th percentile transport parameters values shown in column 1 through 3, respectively in core IGC13 for 95th percentile initial concentration values (36100 ng/g).

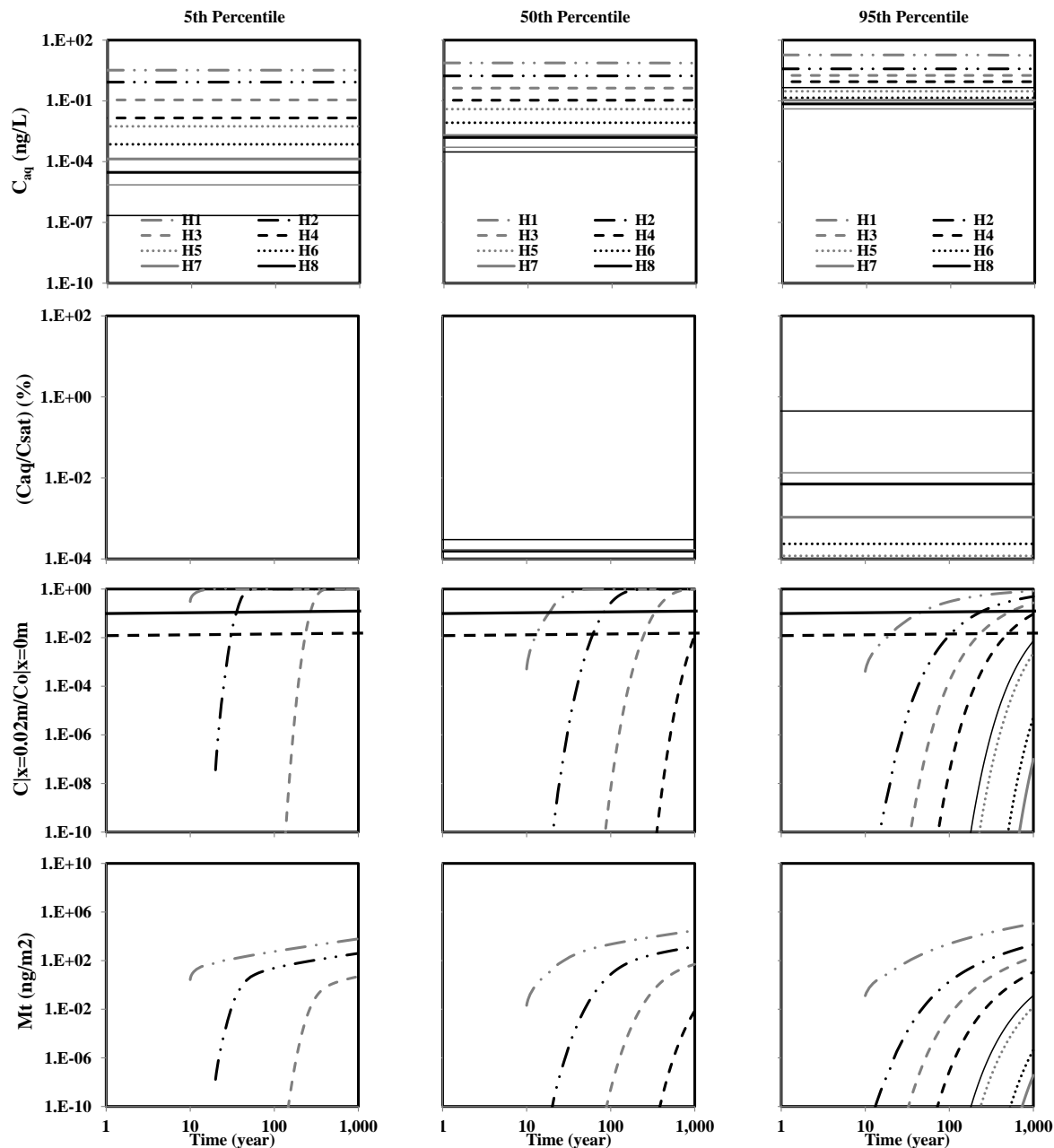


Figure D5.5af: Predicted PBDE aqueous phase concentration under local equilibrium assumption (C_{aq}), ratio of aqueous phase concentration to saturation concentration (C_{aq}/C_{sat}), ratio of aqueous phase concentration at sediment boundary layer to homogenous aqueous phase concentration ($C_{|x=0.02m}/C_{0|x=0m}$), and mass leaving the sediment boundary layer (M_t) under advection-diffusion with organic carbon only sorption ($A(OC)$) shown in row1 through 4, respectively as predicted by the 5th, 50th, and 95th percentile transport parameters values shown in column 1 through 3, respectively in core IGC13 for 50th percentile initial concentration values (60 ng/g).

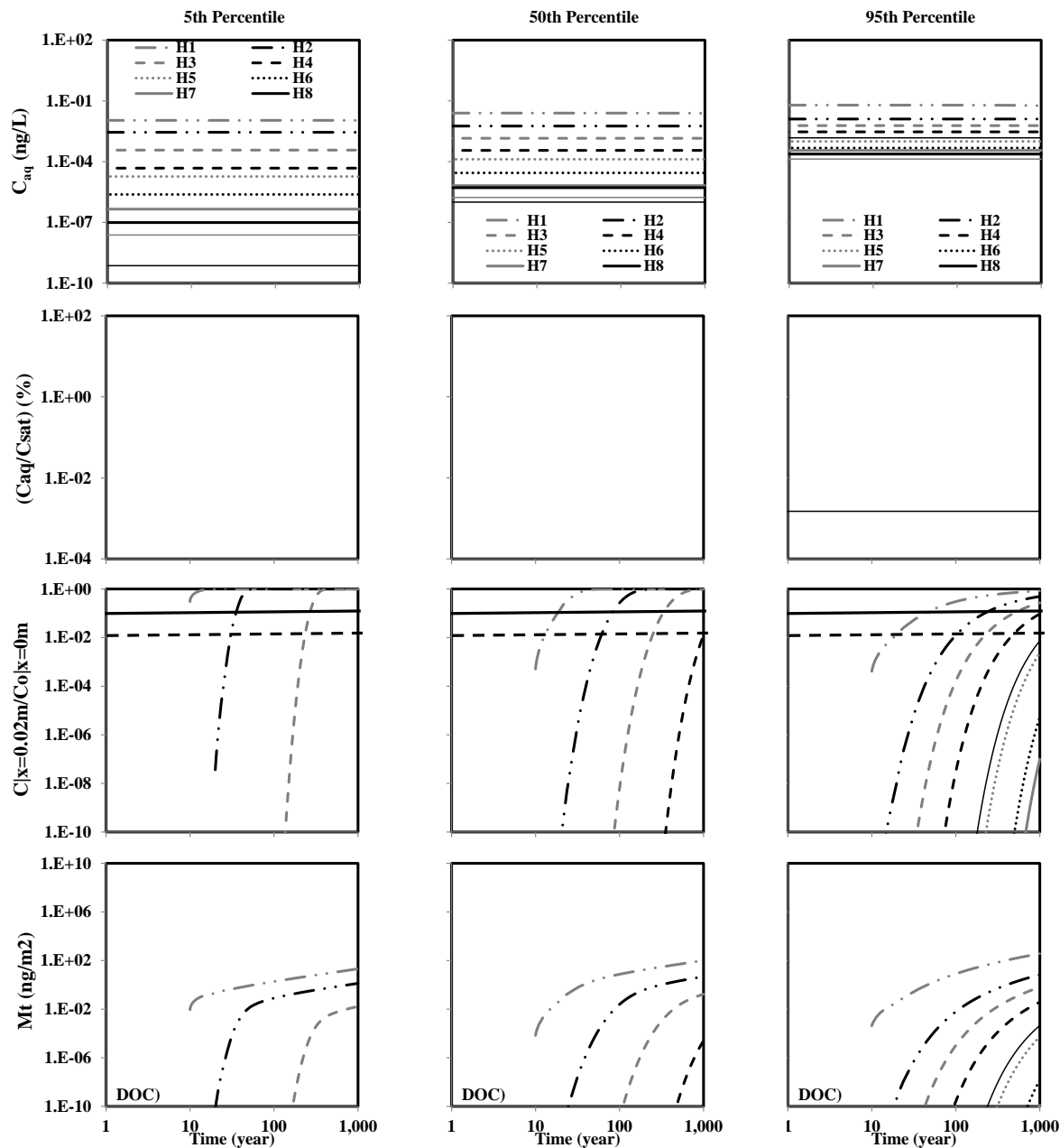


Figure D5.5ag: Predicted PBDE aqueous phase concentration under local equilibrium assumption (C_{aq}), ratio of aqueous phase concentration to saturation concentration (C_{aq}/C_{sat}), ratio of aqueous phase concentration at sediment boundary layer to homogeneous aqueous phase concentration ($C_{|x=0.02m}/C_{|x=0m}$), and mass leaving the sediment boundary layer (M_t) under advection-diffusion with organic carbon only sorption (A(OC)) shown in row1 through 4, respectively as predicted by the 5th, 50th, and 95th percentile transport parameters values shown in column 1 through 3, respectively in core IGC13 for 5th percentile initial concentration values (0.2 ng/g).

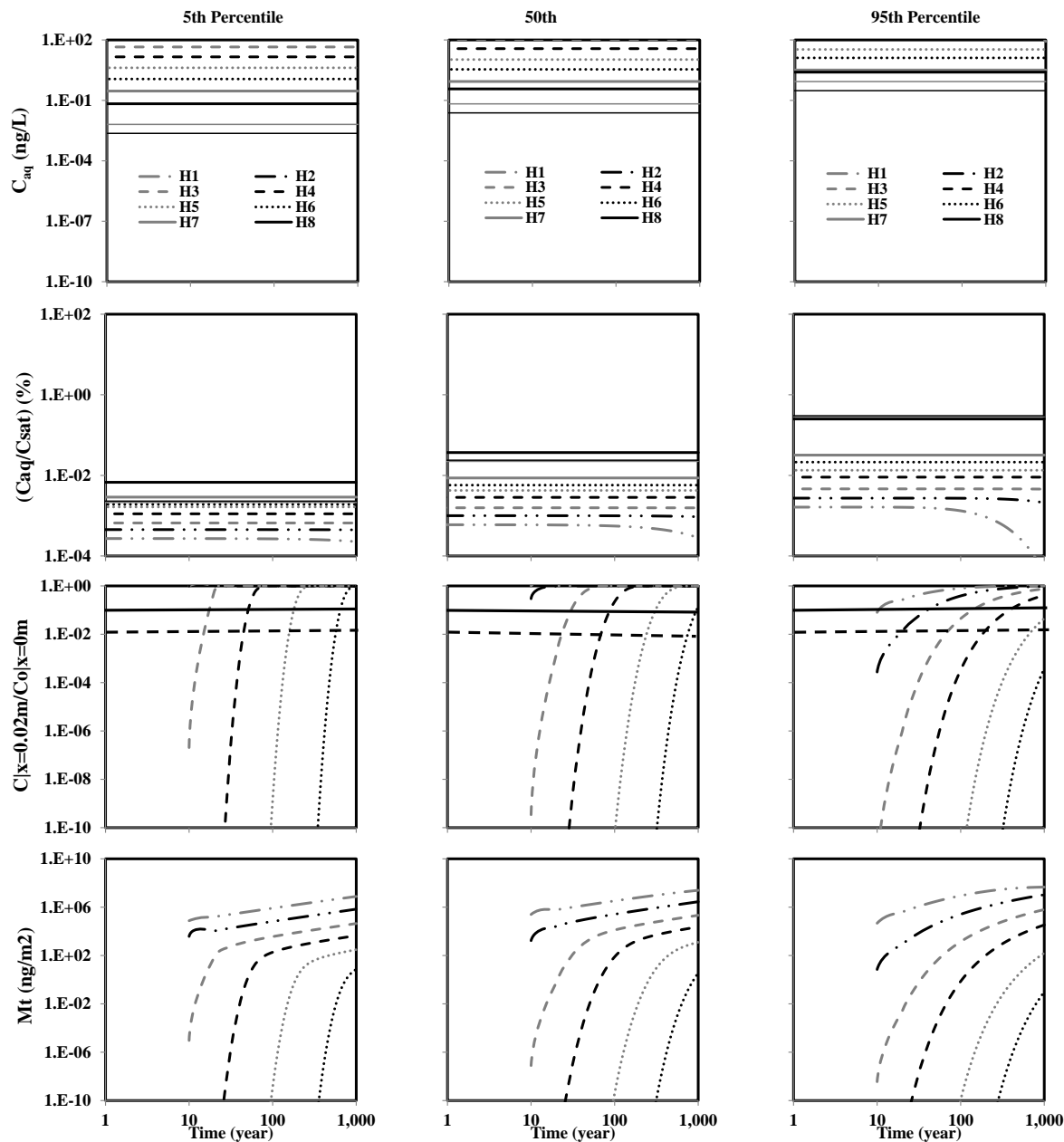


Figure D5.5ah: Predicted PCB aqueous phase concentration under local equilibrium assumption (C_{aq}), ratio of aqueous phase concentration to saturation concentration (C_{aq}/C_{sat}), ratio of aqueous phase concentration at sediment boundary layer to homogeneous aqueous phase concentration ($C|x=0.02m/C|x=0m$), and mass leaving the sediment boundary layer (M_t) under advection-diffusion with organic carbon only sorption ($A(OC)$) shown in row1 through 4, respectively as predicted by the 5th, 50th, and 95th percentile transport parameters values shown in column 1 through 3, respectively in core ACL for 95th percentile initial concentration values (1640 ng/g).

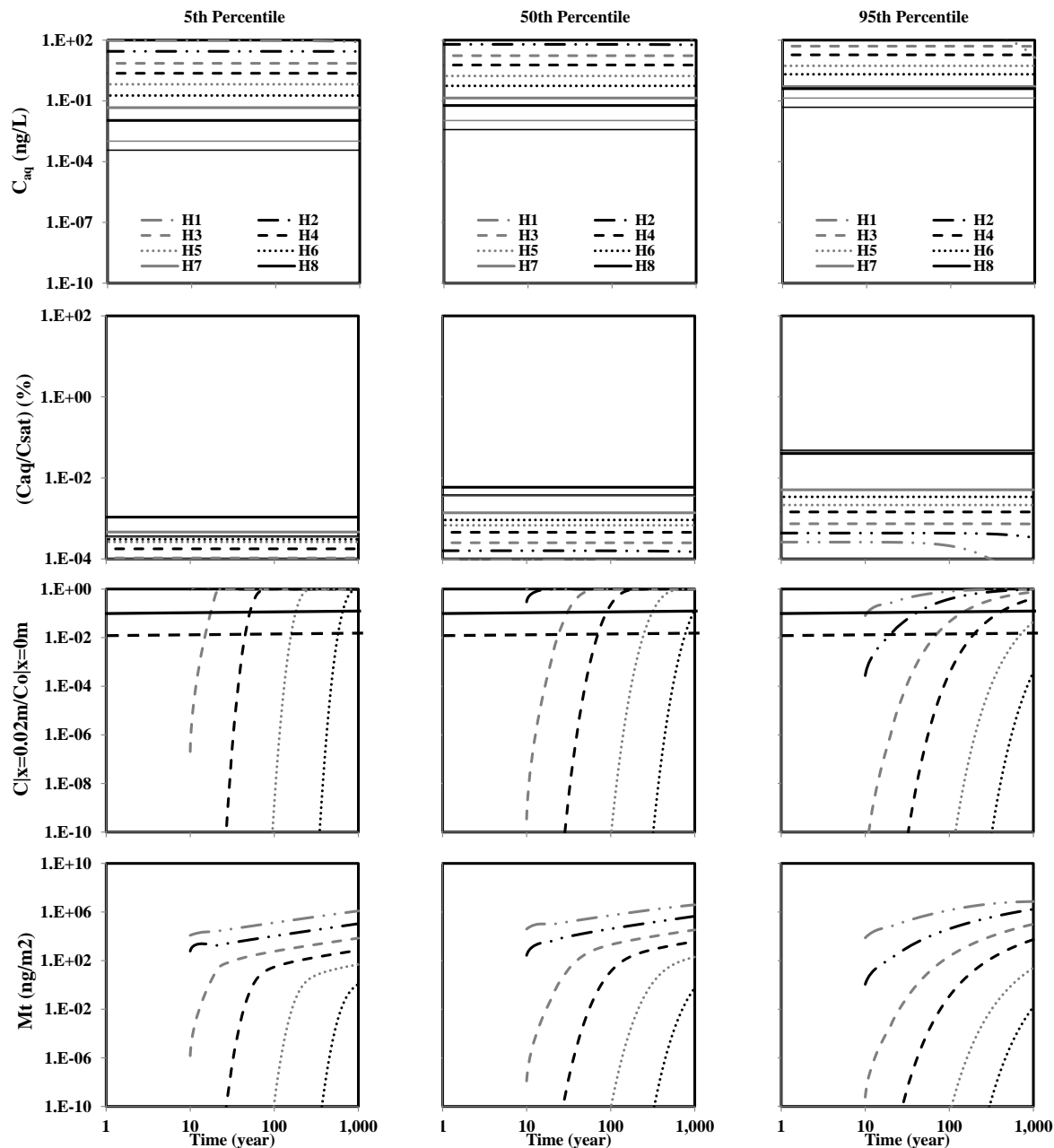


Figure D5.5ai: Predicted PCB aqueous phase concentration under local equilibrium assumption (C_{aq}), ratio of aqueous phase concentration to saturation concentration (C_{aq}/C_{sat}), ratio of aqueous phase concentration at sediment boundary layer to homogenous aqueous phase concentration ($C|x=0.02m/C|x=0m$), and mass leaving the sediment boundary layer (M_t) under advection-diffusion with organic carbon only sorption (A(OC)) shown in row1 through 4, respectively as predicted by the 5th, 50th, and 95th percentile transport parameters values shown in column 1 through 3, respectively in core ACL for 50th percentile initial concentration values (262 ng/g).

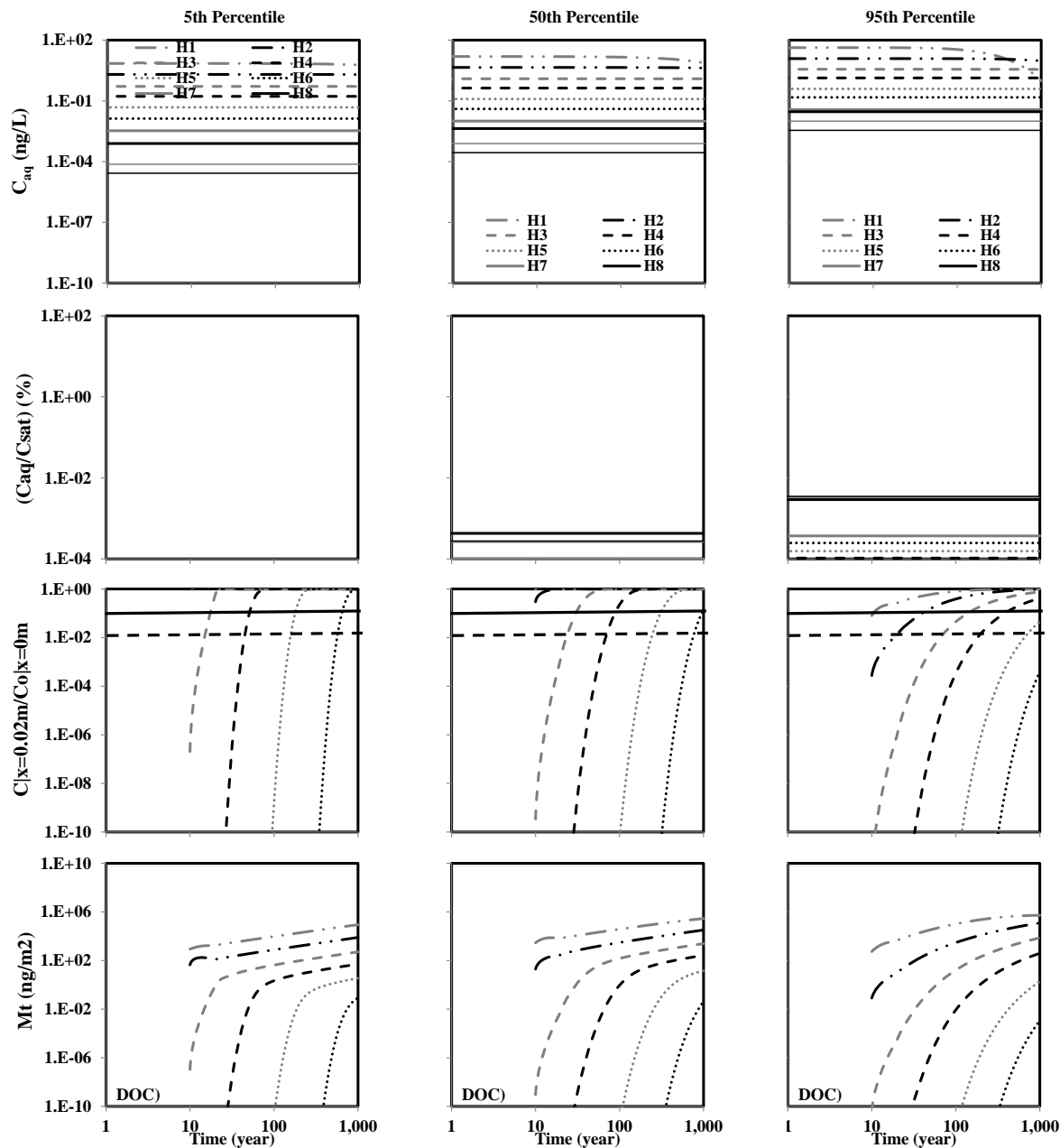


Figure D5.5aj: Predicted PCB aqueous phase concentration under local equilibrium assumption (C_{aq}), ratio of aqueous phase concentration to saturation concentration (C_{aq}/C_{sat}), ratio of aqueous phase concentration at sediment boundary layer to homogeneous aqueous phase concentration ($C|x=0.02m/C|x=0m$), and mass leaving the sediment boundary layer (M_t) under advection-diffusion with organic carbon only sorption ($A(OC)$) shown in row1 through 4, respectively as predicted by the 5th, 50th, and 95th percentile transport parameters values shown in column 1 through 3, respectively in core ACL for 5th percentile initial concentration values (19 ng/g).

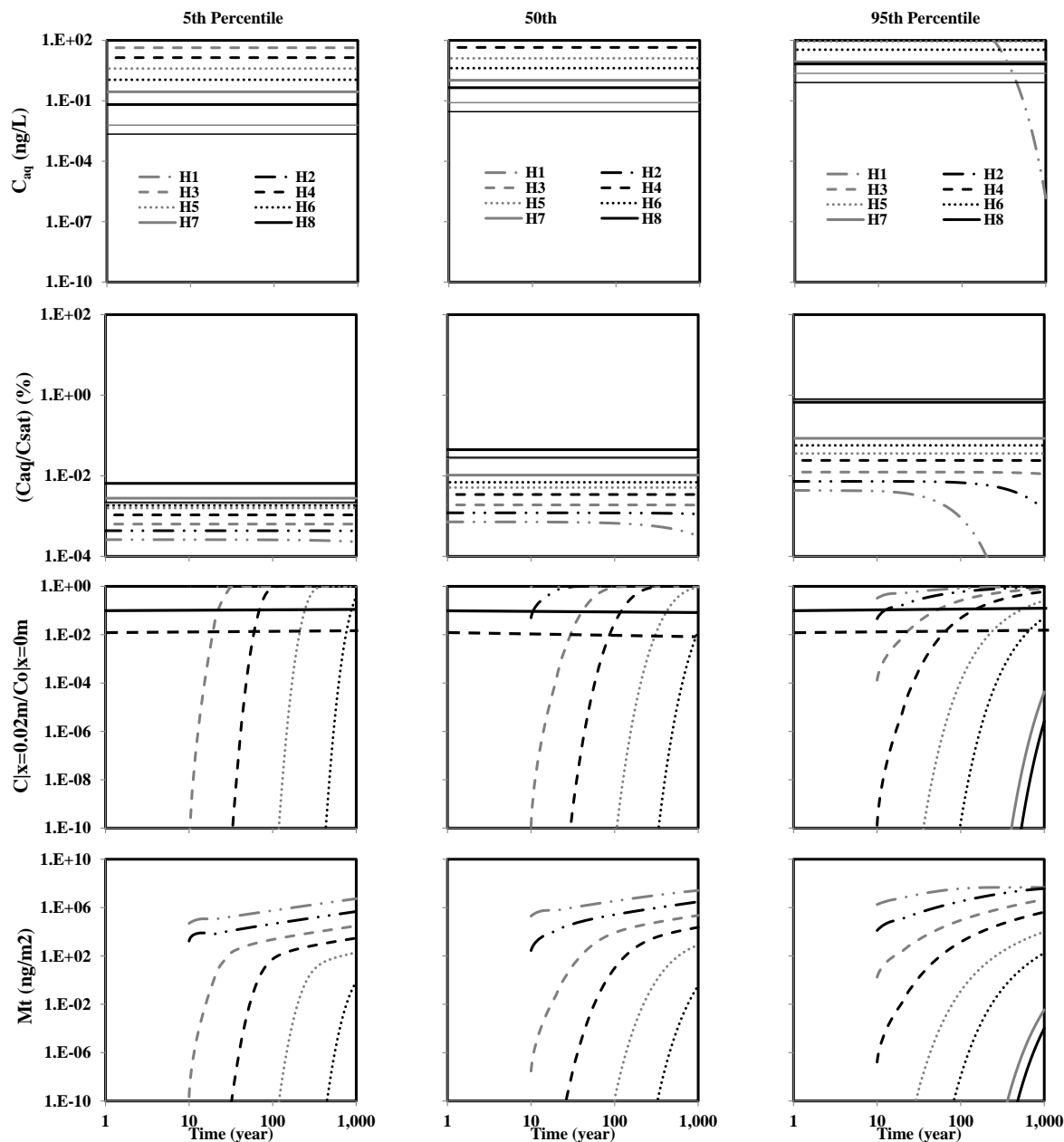


Figure D5.5ak: Predicted PCB aqueous phase concentration under local equilibrium assumption (C_{aq}), ratio of aqueous phase concentration to saturation concentration (C_{aq}/C_{sat}), ratio of aqueous phase concentration at sediment boundary layer to homogeneous aqueous phase concentration ($C|x=0.02m/C|x=0m$), and mass leaving the sediment boundary layer (M_t) under advection-diffusion with organic carbon only sorption (A(OC)) shown in row1 through 4, respectively as predicted by the 5th, 50th, and 95th percentile transport parameters values shown in column 1 through 3, respectively in core AED for 95th percentile initial concentration values (1640 ng/g).

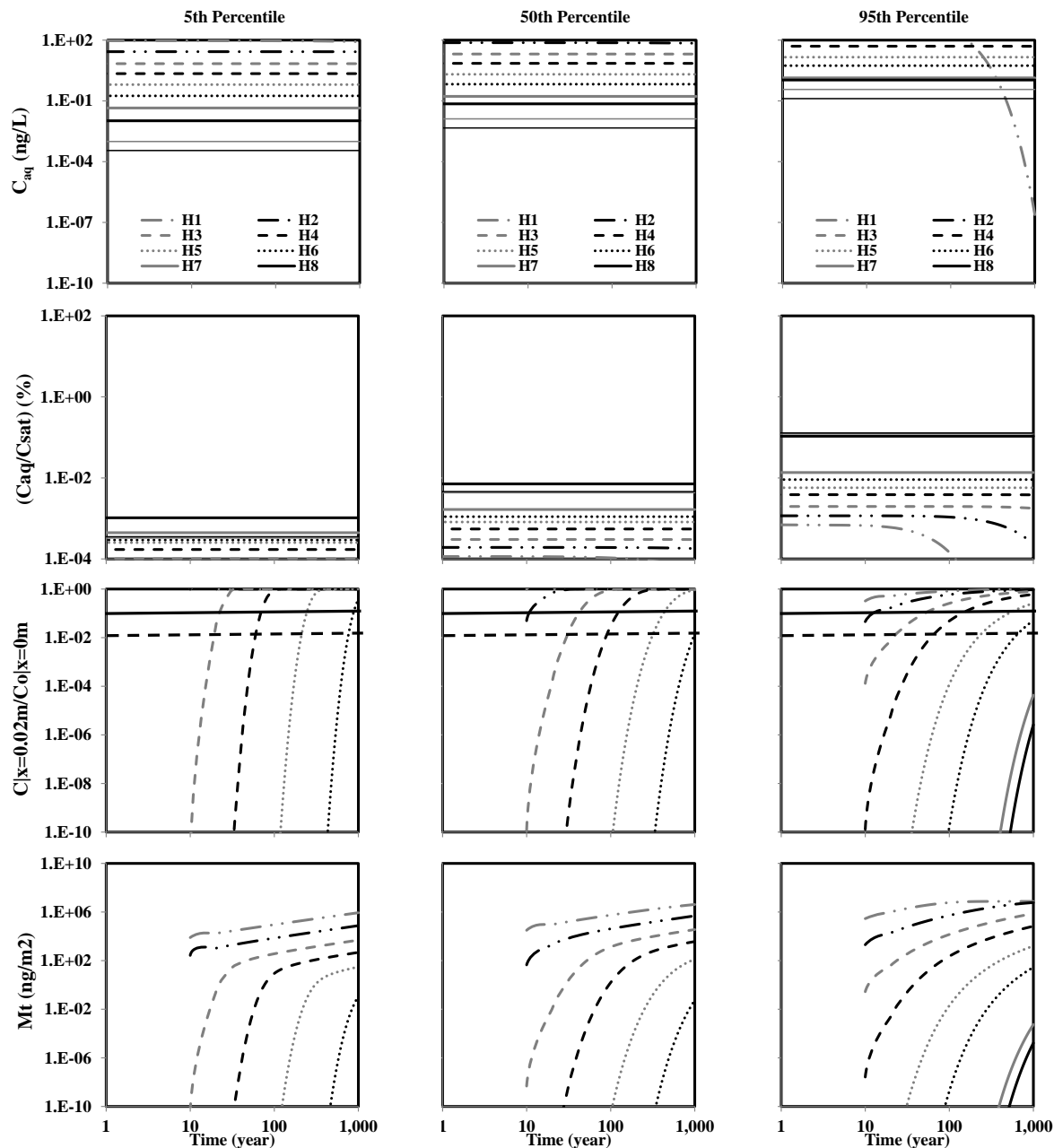


Figure D5.5al: Predicted PCB aqueous phase concentration under local equilibrium assumption (C_{aq}), ratio of aqueous phase concentration to saturation concentration (C_{aq}/C_{sat}), ratio of aqueous phase concentration at sediment boundary layer to homogenous aqueous phase concentration ($C|x=0.02m/C|x=0m$), and mass leaving the sediment boundary layer (M_t) under advection-diffusion with organic carbon only sorption ($A(OC)$) shown in row1 through 4, respectively as predicted by the 5th, 50th, and 95th percentile transport parameters values shown in column 1 through 3, respectively in core AED for 50th percentile initial concentration values (262 ng/g).

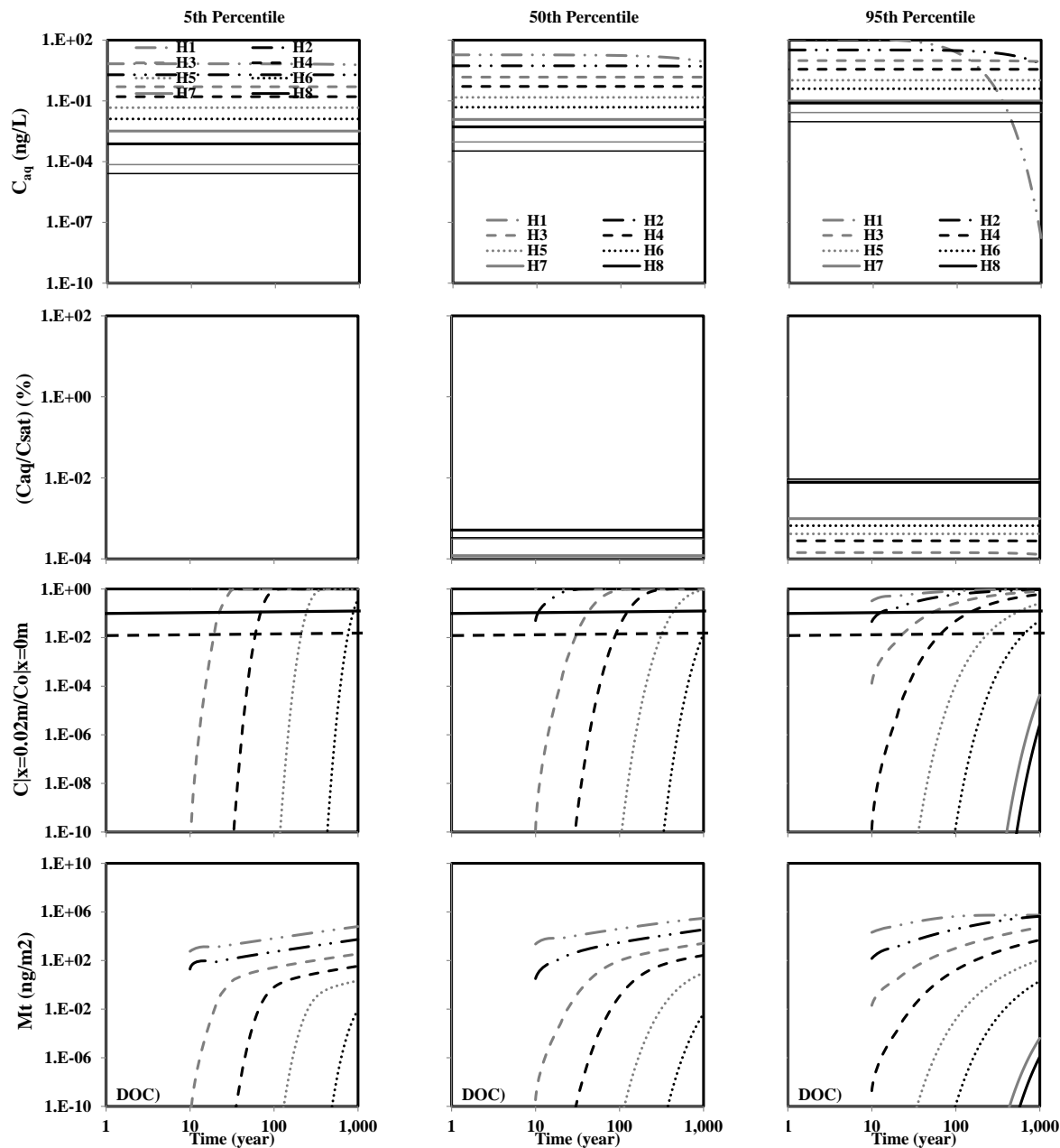


Figure D5.5am: Predicted PCB aqueous phase concentration under local equilibrium assumption (C_{aq}), ratio of aqueous phase concentration to saturation concentration (C_{aq}/C_{sat}), ratio of aqueous phase concentration at sediment boundary layer to homogenous aqueous phase concentration ($C|x=0.02m/C|x=0m$), and mass leaving the sediment boundary layer (M_t) under advection-diffusion with organic carbon only sorption (A(OC)) shown in row1 through 4, respectively as predicted by the 5th, 50th, and 95th percentile transport parameters values shown in column 1 through 3, respectively in core AED for 5th percentile initial concentration values (19 ng/g).

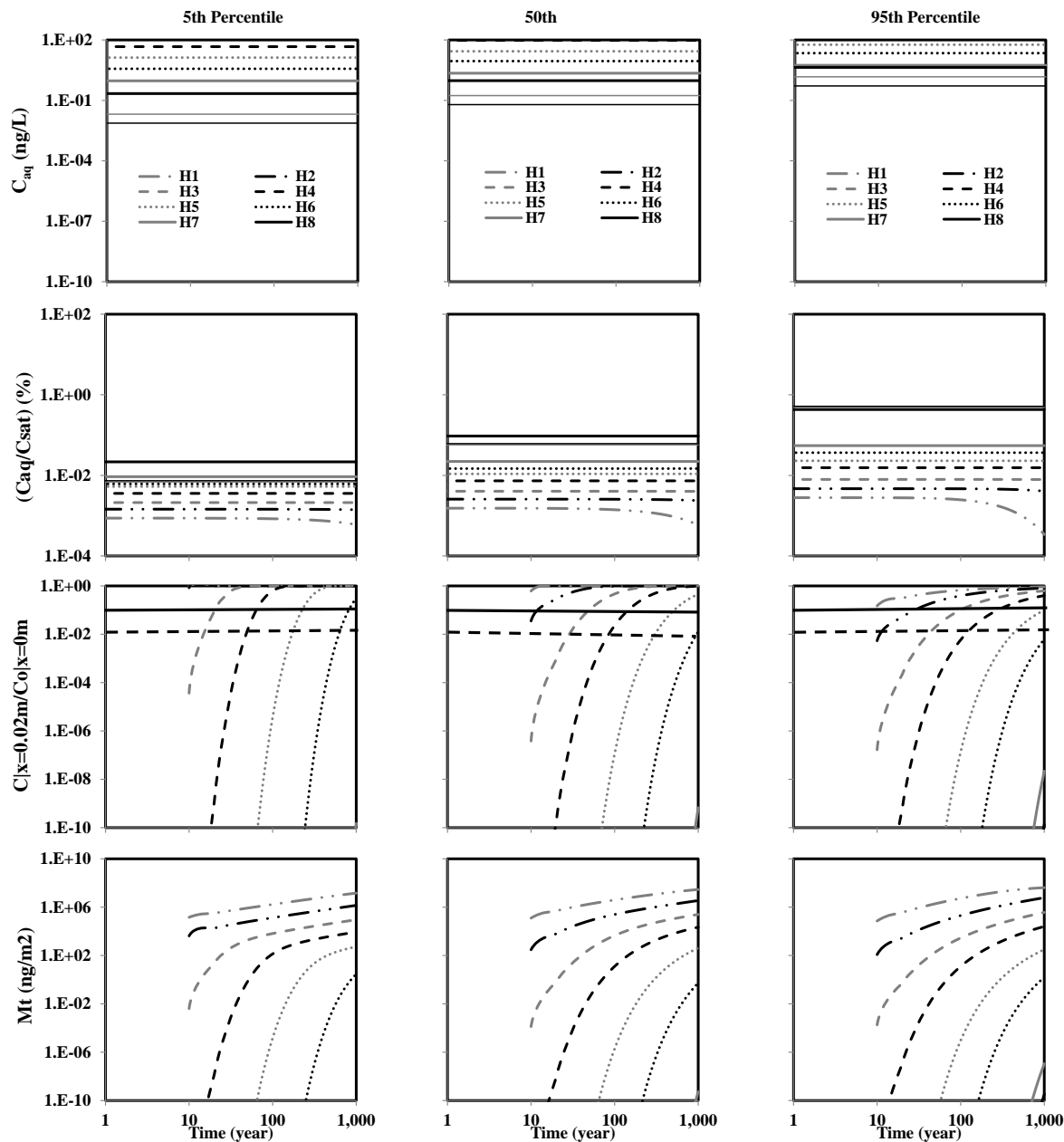


Figure D5.5an: Predicted PCB aqueous phase concentration under local equilibrium assumption (C_{aq}), ratio of aqueous phase concentration to saturation concentration (C_{aq}/C_{sat}), ratio of aqueous phase concentration at sediment boundary layer to homogeneous aqueous phase concentration ($C|x=0.02m/C|x=0m$), and mass leaving the sediment boundary layer (M_t) under advection-diffusion with organic carbon only sorption (A(OC)) shown in row1 through 4, respectively as predicted by the 5th, 50th, and 95th percentile transport parameters values shown in column 1 through 3, respectively in core AFR for 95th percentile initial concentration values (1640 ng/g).

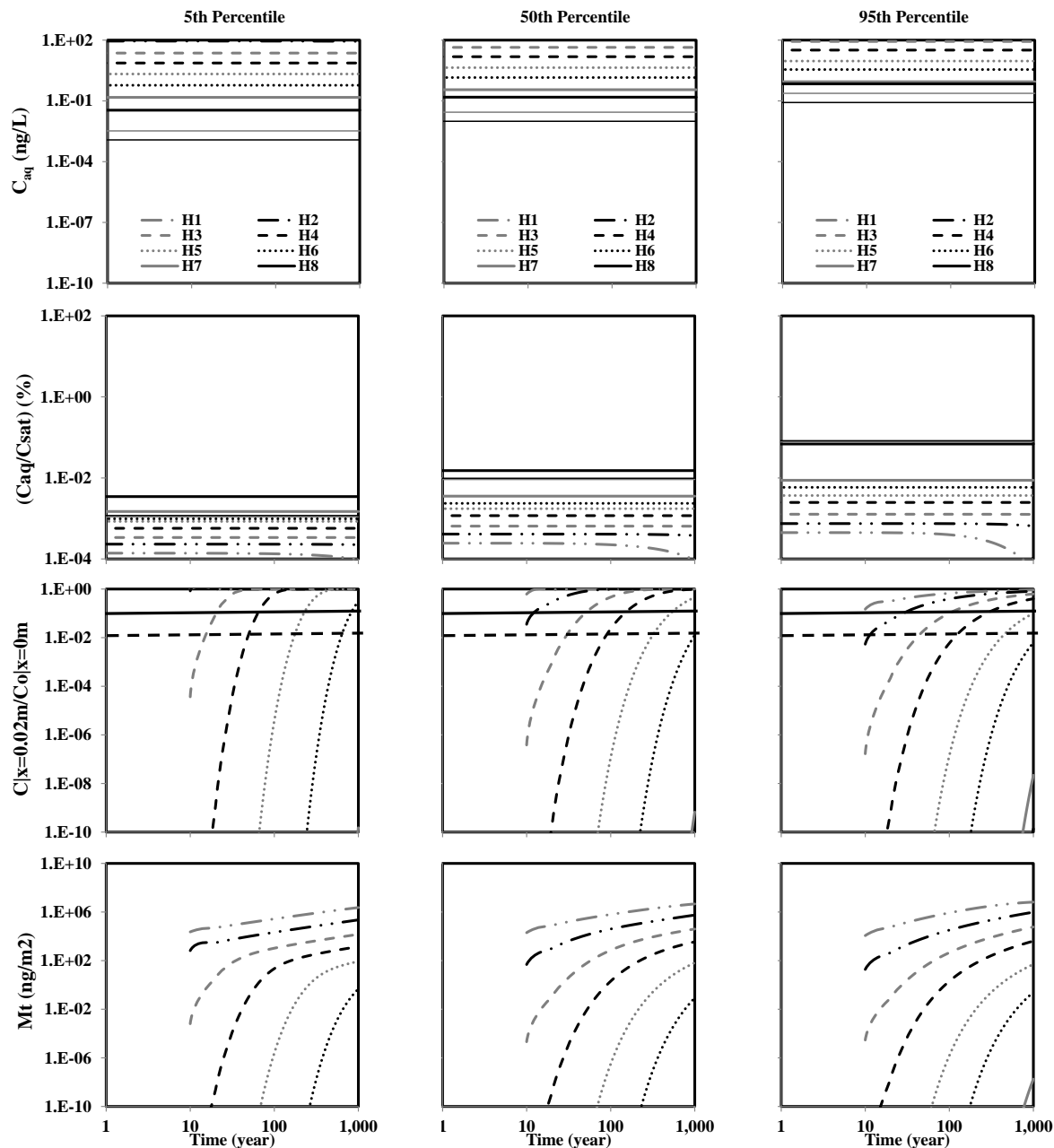


Figure D5.5ao: Predicted PCB aqueous phase concentration under local equilibrium assumption (C_{aq}), ratio of aqueous phase concentration to saturation concentration (C_{aq}/C_{sat}), ratio of aqueous phase concentration at sediment boundary layer to homogenous aqueous phase concentration ($C|x=0.02m/C|x=0m$), and mass leaving the sediment boundary layer (M_t) under advection-diffusion with organic carbon only sorption (A(OC)) shown in row1 through 4, respectively as predicted by the 5th, 50th, and 95th percentile transport parameters values shown in column 1 through 3, respectively in core AFR for 50th percentile initial concentration values (262 ng/g).

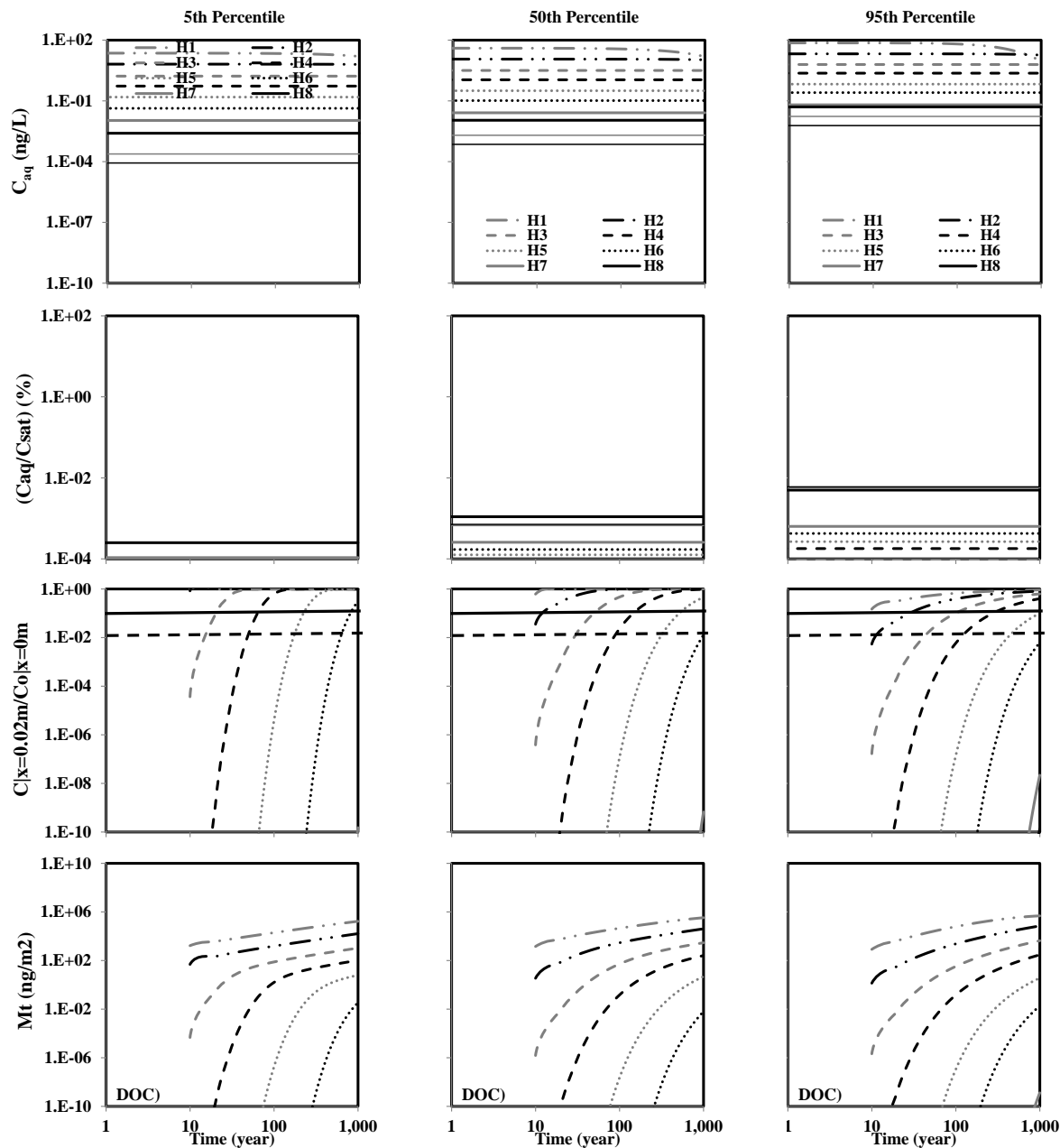


Figure D5.5ap: Predicted PCB aqueous phase concentration under local equilibrium assumption (C_{aq}), ratio of aqueous phase concentration to saturation concentration (C_{aq}/C_{sat}), ratio of aqueous phase concentration at sediment boundary layer to homogeneous aqueous phase concentration ($C|x=0.02m/C|x=0m$), and mass leaving the sediment boundary layer (M_t) under advection-diffusion with organic carbon only sorption ($A(OC)$) shown in row1 through 4, respectively as predicted by the 5th, 50th, and 95th percentile transport parameters values shown in column 1 through 3, respectively in core AFR for 5th percentile initial concentration values (19 ng/g).

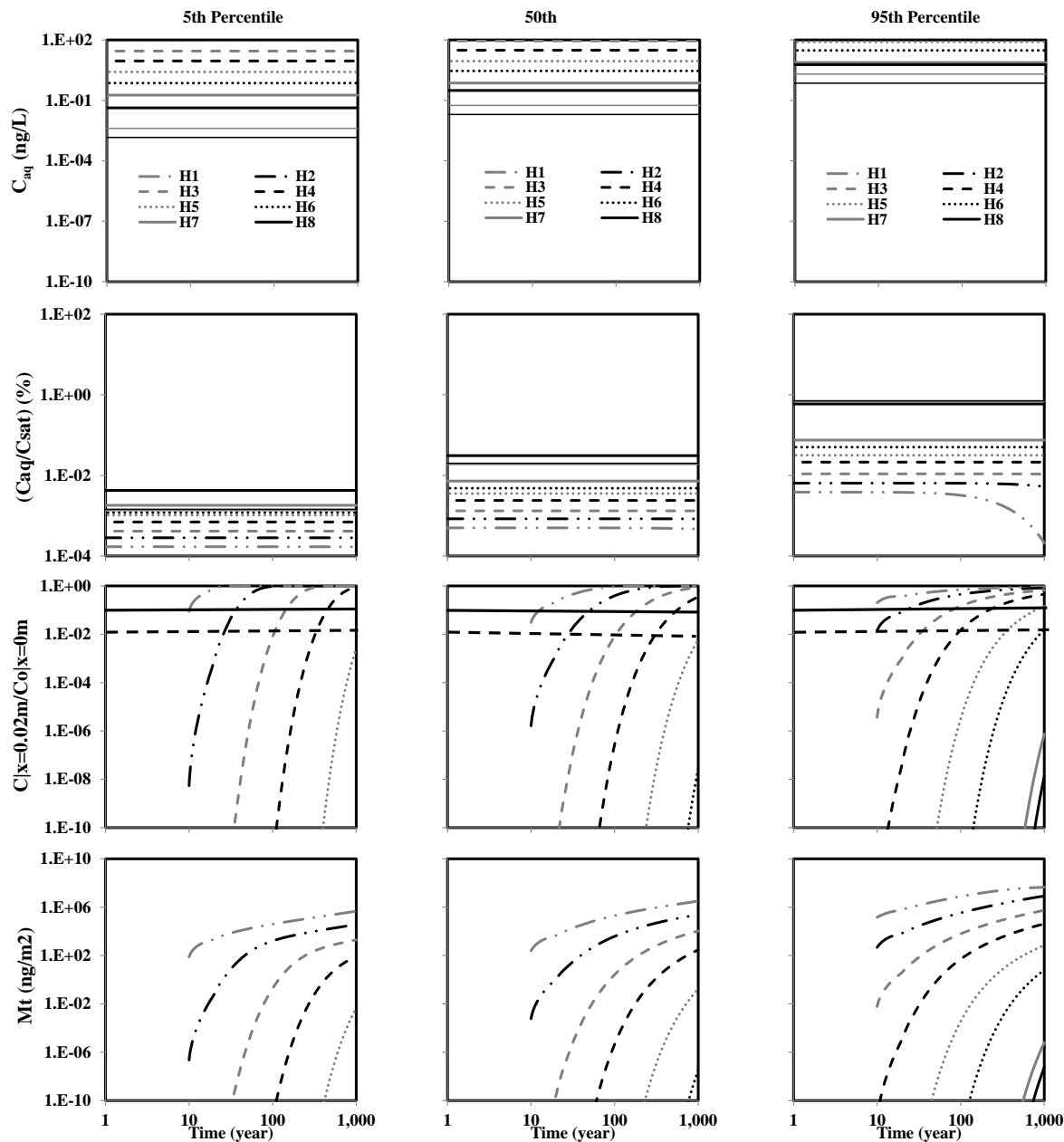


Figure D5.5aq: Predicted PCB aqueous phase concentration under local equilibrium assumption (C_{aq}), ratio of aqueous phase concentration to saturation concentration (C_{aq}/C_{sat}), ratio of aqueous phase concentration at sediment boundary layer to homogeneous aqueous phase concentration ($C|x=0.02m/C|x=0m$), and mass leaving the sediment boundary layer (M_t) under advection-diffusion with organic carbon only sorption (A(OC)) shown in row1 through 4, respectively as predicted by the 5th, 50th, and 95th percentile transport parameters values shown in column 1 through 3, respectively in core AJL for 95th percentile initial concentration values (1640 ng/g).

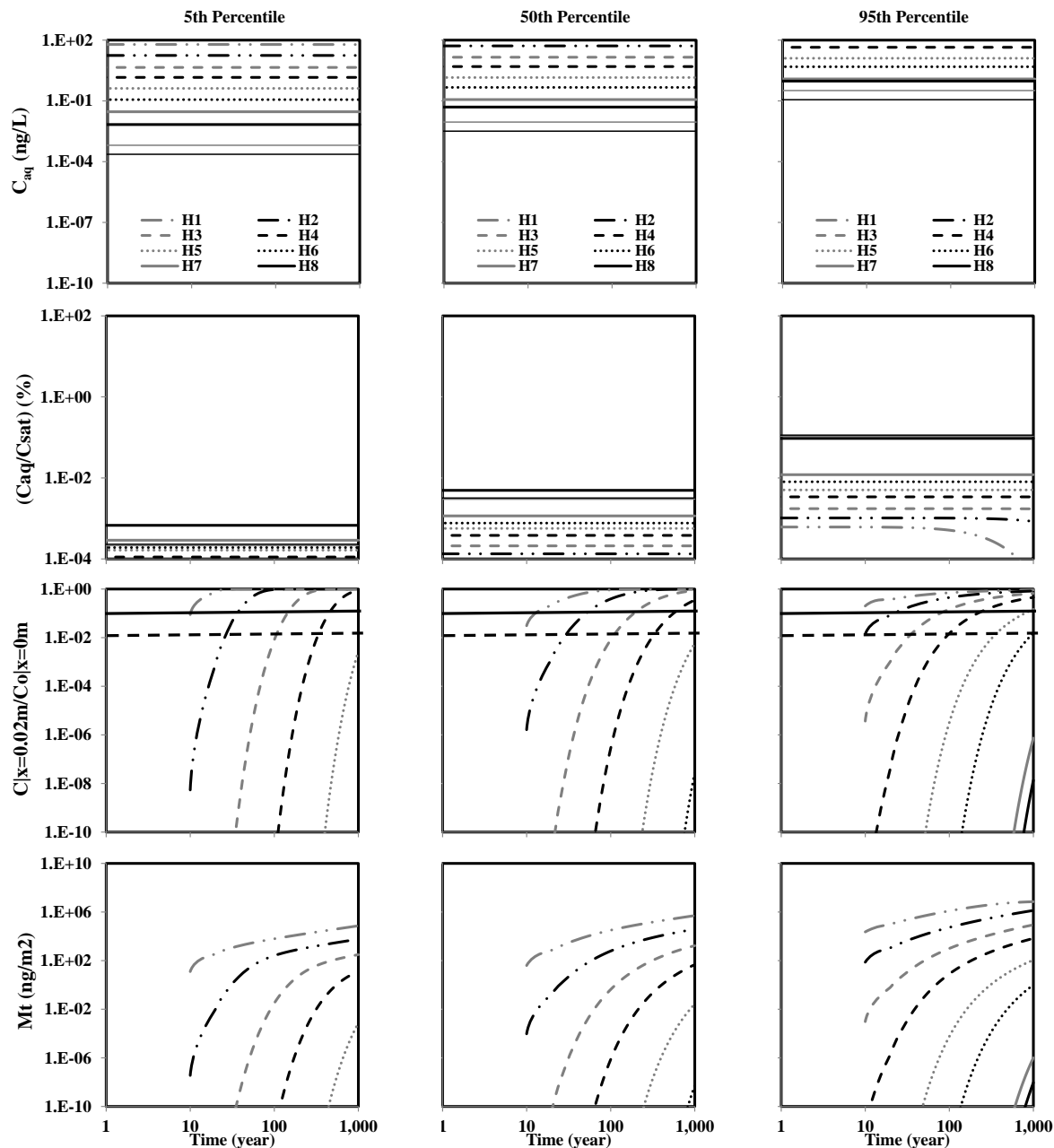


Figure D5.5ar: Predicted PCB aqueous phase concentration under local equilibrium assumption (C_{aq}), ratio of aqueous phase concentration to saturation concentration (C_{aq}/C_{sat}), ratio of aqueous phase concentration at sediment boundary layer to homogenous aqueous phase concentration ($C|x=0.02m/C|x=0m$), and mass leaving the sediment boundary layer (M_t) under advection-diffusion with organic carbon only sorption (A(OC)) shown in row1 through 4, respectively as predicted by the 5th, 50th, and 95th percentile transport parameters values shown in column 1 through 3, respectively in core AJL for 50th percentile initial concentration values (262 ng/g).

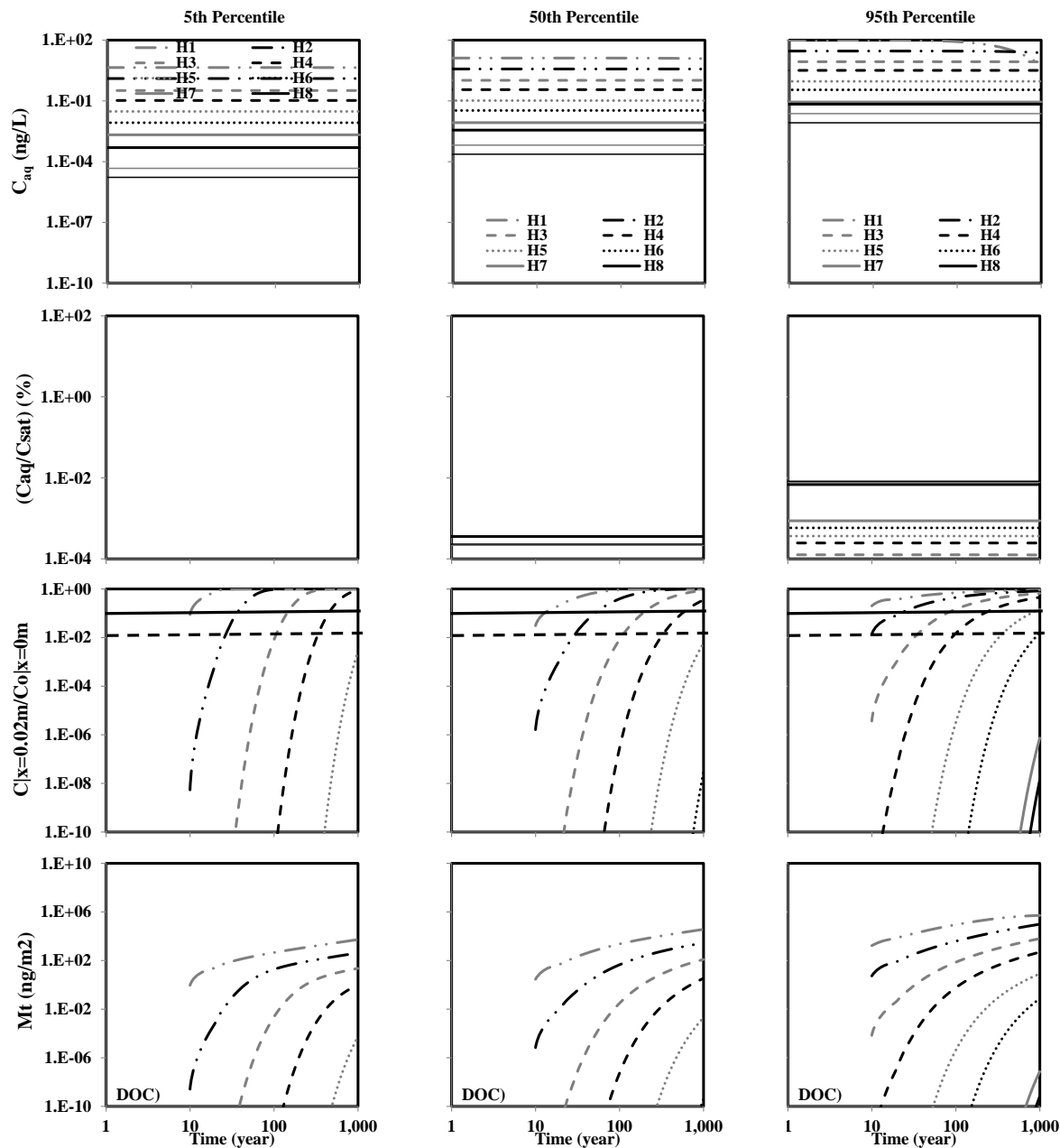


Figure D5.5as: Predicted PCB aqueous phase concentration under local equilibrium assumption (C_{aq}), ratio of aqueous phase concentration to saturation concentration (C_{aq}/C_{sat}), ratio of aqueous phase concentration at sediment boundary layer to homogenous aqueous phase concentration ($C|x=0.02m/C|x=0m$), and mass leaving the sediment boundary layer (M_t) under advection-diffusion with organic carbon only sorption ($A(OC)$) shown in row1 through 4, respectively as predicted by the 5th, 50th, and 95th percentile transport parameters values shown in column 1 through 3, respectively in core AJL for 5th percentile initial concentration values (19 ng/g).

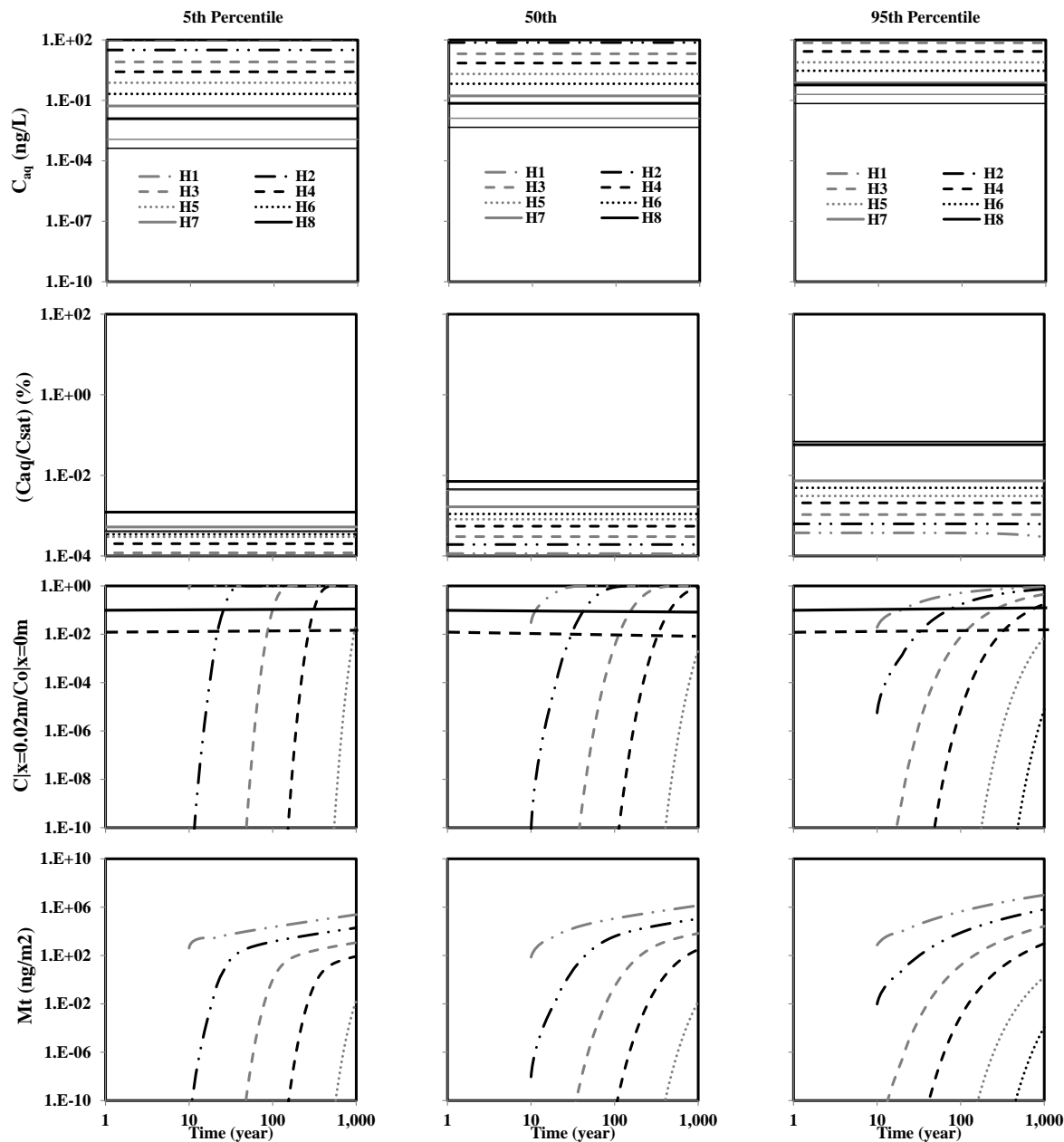


Figure D5.5at: Predicted PCB aqueous phase concentration under local equilibrium assumption (C_{aq}), ratio of aqueous phase concentration to saturation concentration (C_{aq}/C_{sat}), ratio of aqueous phase concentration at sediment boundary layer to homogeneous aqueous phase concentration ($C|x=0.02m/C|x=0m$), and mass leaving the sediment boundary layer (M_t) under advection-diffusion with organic carbon only sorption ($A(OC)$) shown in row1 through 4, respectively as predicted by the 5th, 50th, and 95th percentile transport parameters values shown in column 1 through 3, respectively in core AMW for 95th percentile initial concentration values (1640 ng/g).

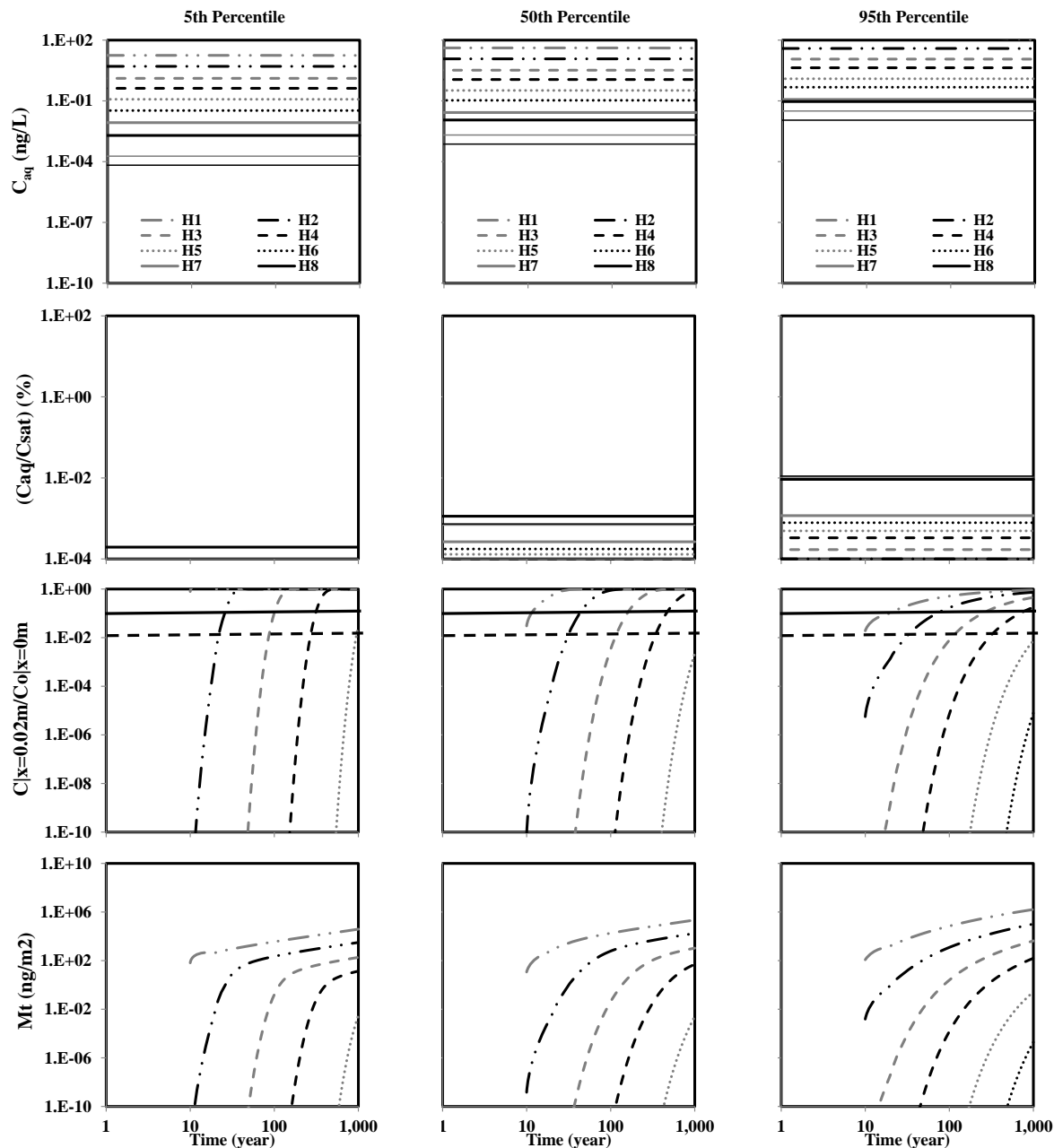


Figure D5.5au: Predicted PCB aqueous phase concentration under local equilibrium assumption (C_{aq}), ratio of aqueous phase concentration to saturation concentration (C_{aq}/C_{sat}), ratio of aqueous phase concentration at sediment boundary layer to homogenous aqueous phase concentration ($C|x=0.02m/C|x=0m$), and mass leaving the sediment boundary layer (M_t) under advection-diffusion with organic carbon only sorption (A(OC)) shown in row1 through 4, respectively as predicted by the 5th, 50th, and 95th percentile transport parameters values shown in column 1 through 3, respectively in core AMW for 50th percentile initial concentration values (262 ng/g).

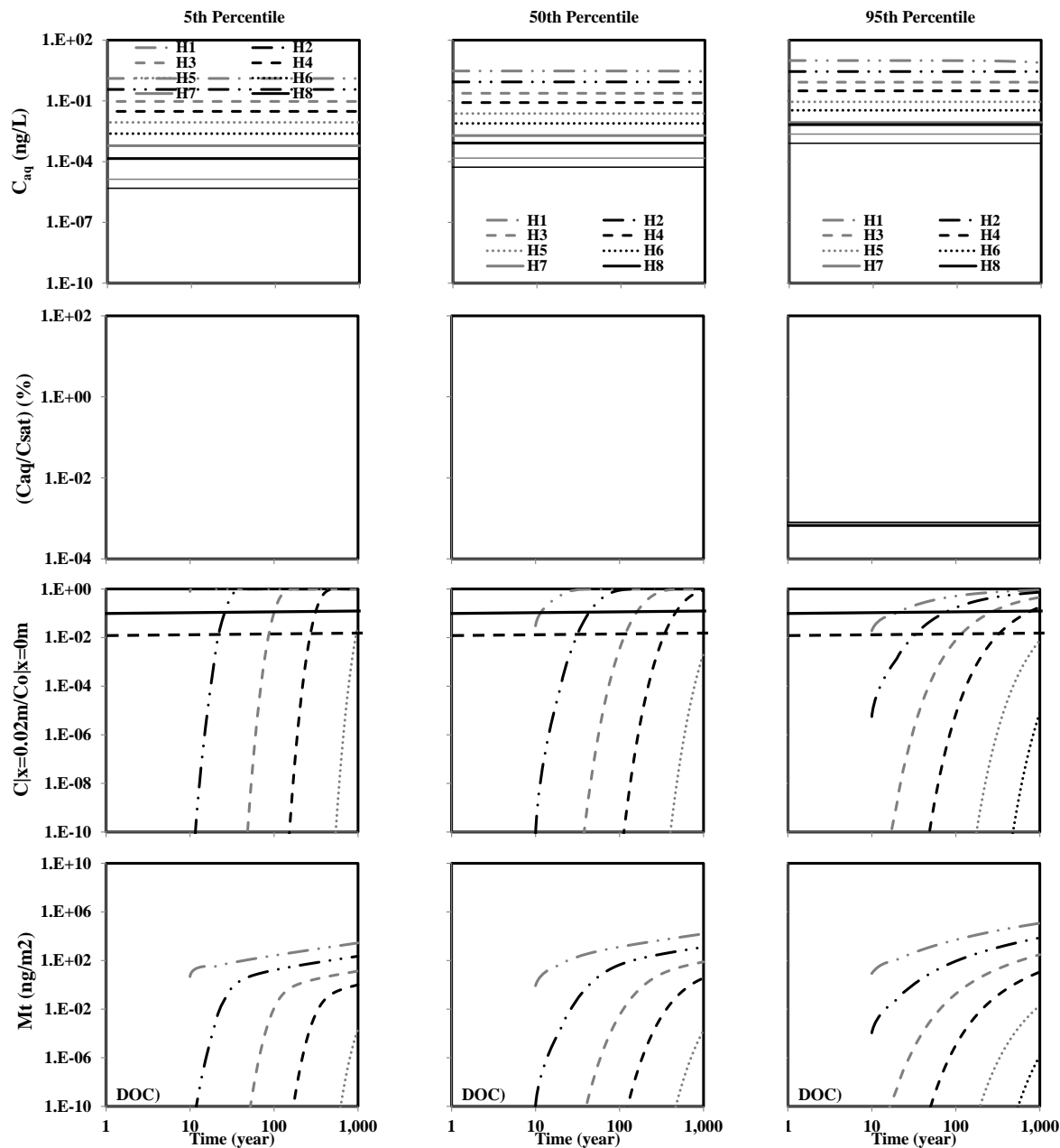


Figure D5.5av: Predicted PCB aqueous phase concentration under local equilibrium assumption (C_{aq}), ratio of aqueous phase concentration to saturation concentration (C_{aq}/C_{sat}), ratio of aqueous phase concentration at sediment boundary layer to homogenous aqueous phase concentration ($C|x=0.02m/C|x=0m$), and mass leaving the sediment boundary layer (M_t) under advection-diffusion with organic carbon only sorption ($A(OC)$) shown in row1 through 4, respectively as predicted by the 5th, 50th, and 95th percentile transport parameters values shown in column 1 through 3, respectively in core AMW for 5th percentile initial concentration values (19 ng/g).

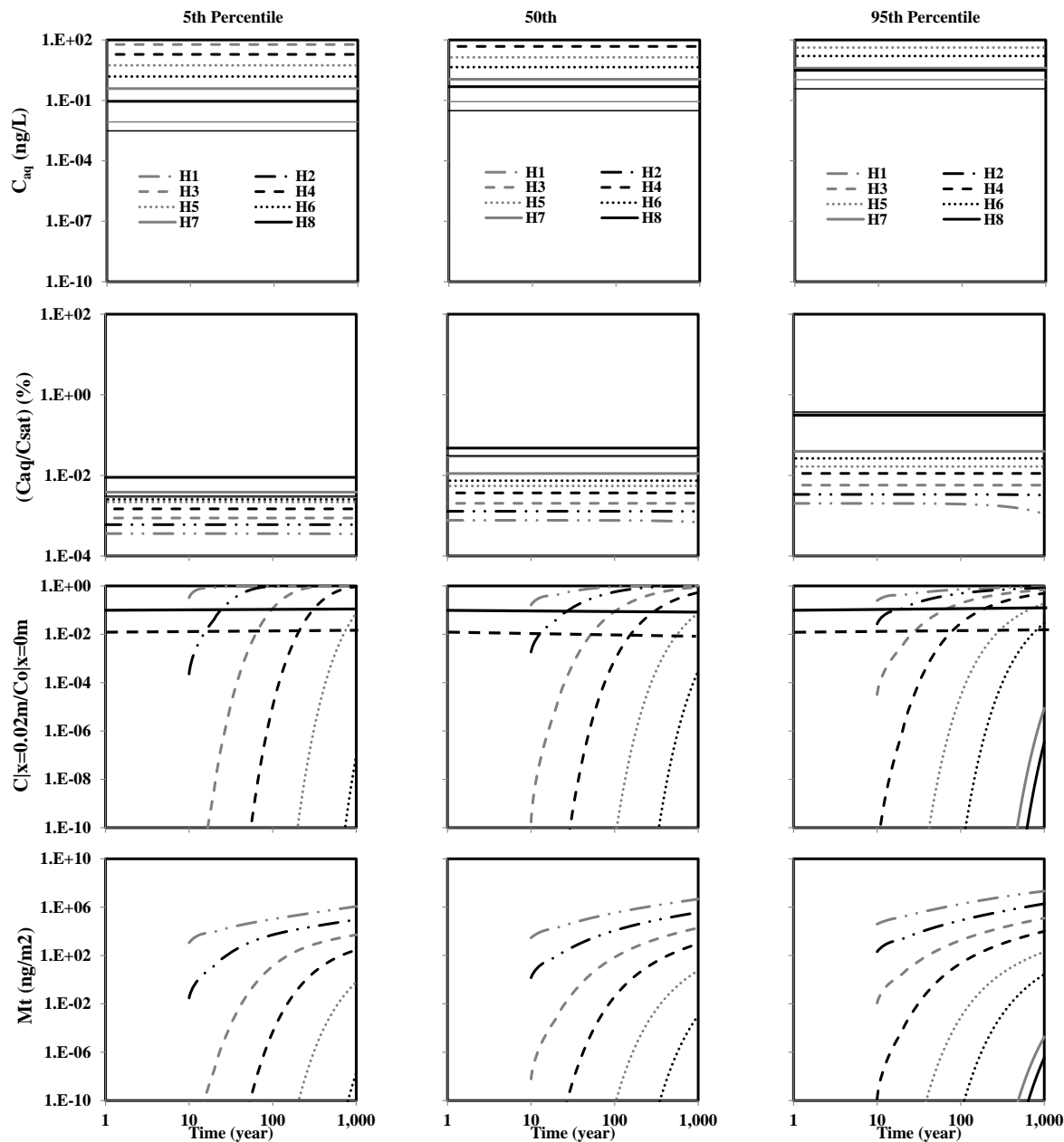


Figure D5.5aw: Predicted PCB aqueous phase concentration under local equilibrium assumption (C_{aq}), ratio of aqueous phase concentration to saturation concentration (C_{aq}/C_{sat}), ratio of aqueous phase concentration at sediment boundary layer to homogenous aqueous phase concentration ($C|x=0.02m/C|x=0m$), and mass leaving the sediment boundary layer (M_t) under advection-diffusion with organic carbon only sorption ($A(OC)$) shown in row1 through 4, respectively as predicted by the 5th, 50th, and 95th percentile transport parameters values shown in column 1 through 3, respectively in core AOT for 95th percentile initial concentration values (1640 ng/g).

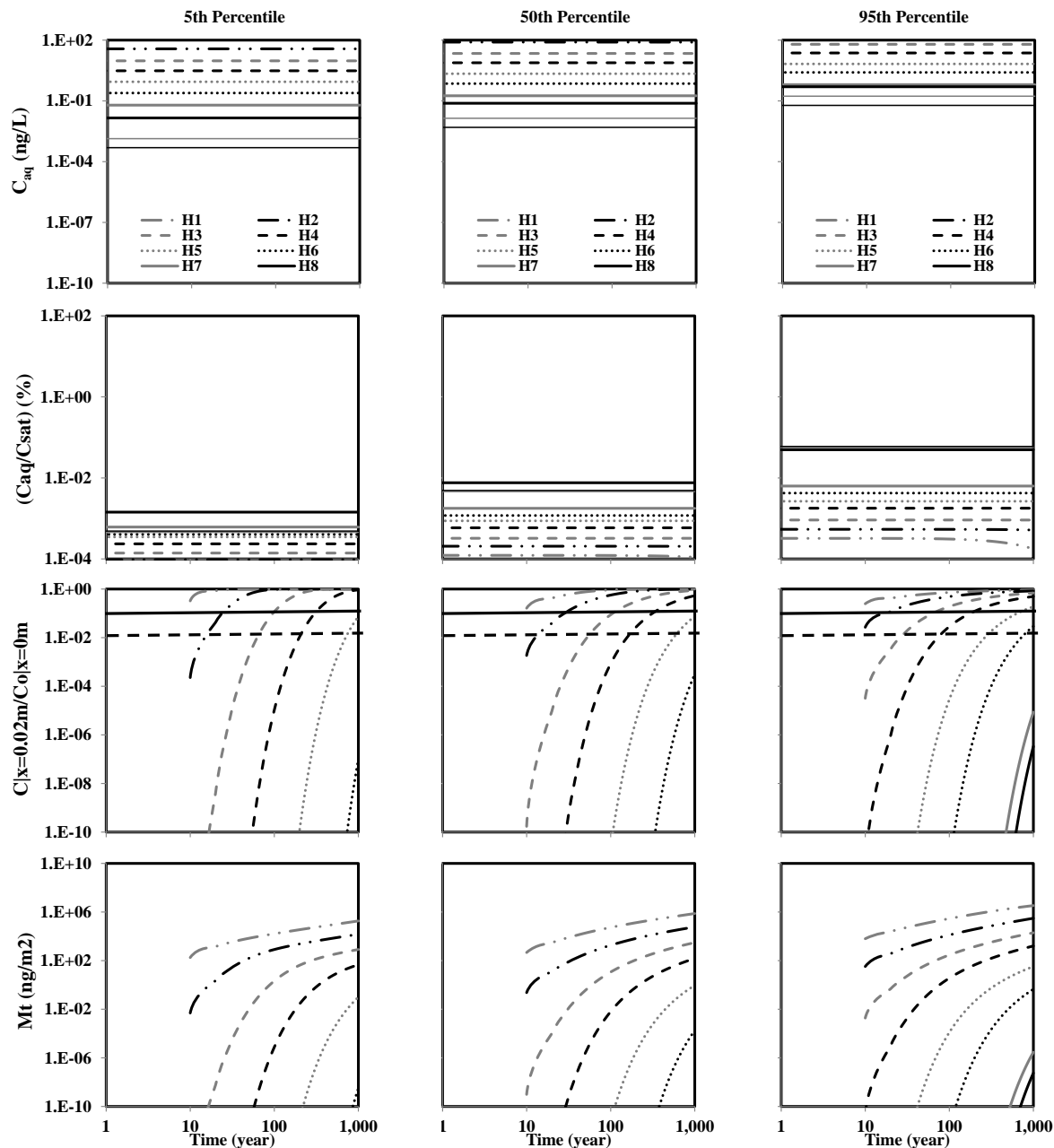


Figure D5.5ax: Predicted PCB aqueous phase concentration under local equilibrium assumption (C_{aq}), ratio of aqueous phase concentration to saturation concentration (C_{aq}/C_{sat}), ratio of aqueous phase concentration at sediment boundary layer to homogenous aqueous phase concentration ($C|x=0.02m/C_0|x=0m$), and mass leaving the sediment boundary layer (M_t) under advection-diffusion with organic carbon only sorption (A(OC)) shown in row1 through 4, respectively as predicted by the 5th, 50th, and 95th percentile transport parameters values shown in column 1 through 3, respectively in core AOT for 50th percentile initial concentration values (262 ng/g).

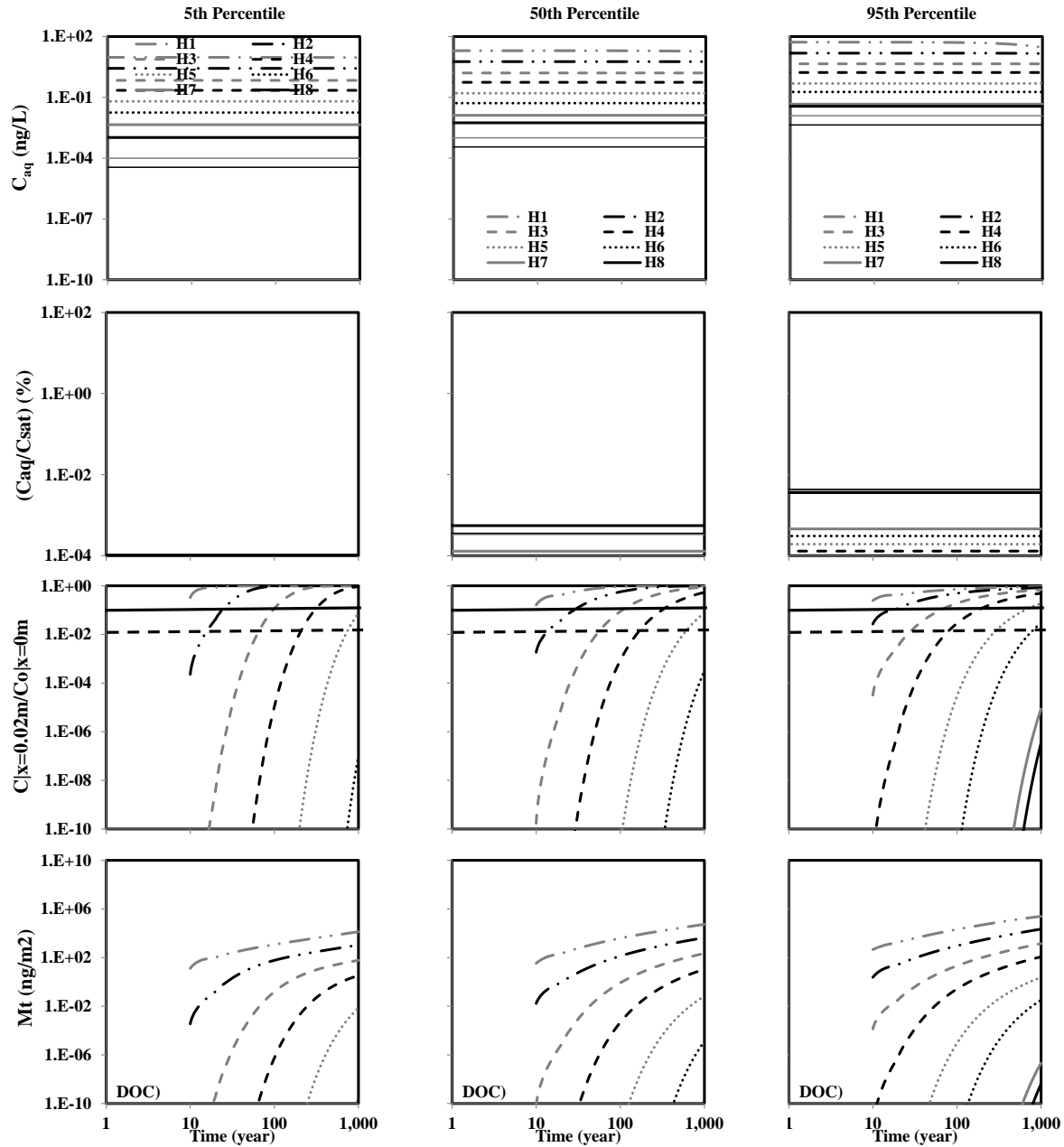


Figure D5.5ay: Predicted PCB aqueous phase concentration under local equilibrium assumption (C_{aq}), ratio of aqueous phase concentration to saturation concentration (C_{aq}/C_{sat}), ratio of aqueous phase concentration at sediment boundary layer to homogeneous aqueous phase concentration ($C|x=0.02m/C|x=0m$), and mass leaving the sediment boundary layer (M_t) under advection-diffusion with organic carbon only sorption ($A(OC)$) shown in row1 through 4, respectively as predicted by the 5th, 50th, and 95th percentile transport parameters values shown in column 1 through 3, respectively in core AOT for 5th percentile initial concentration values (19 ng/g).

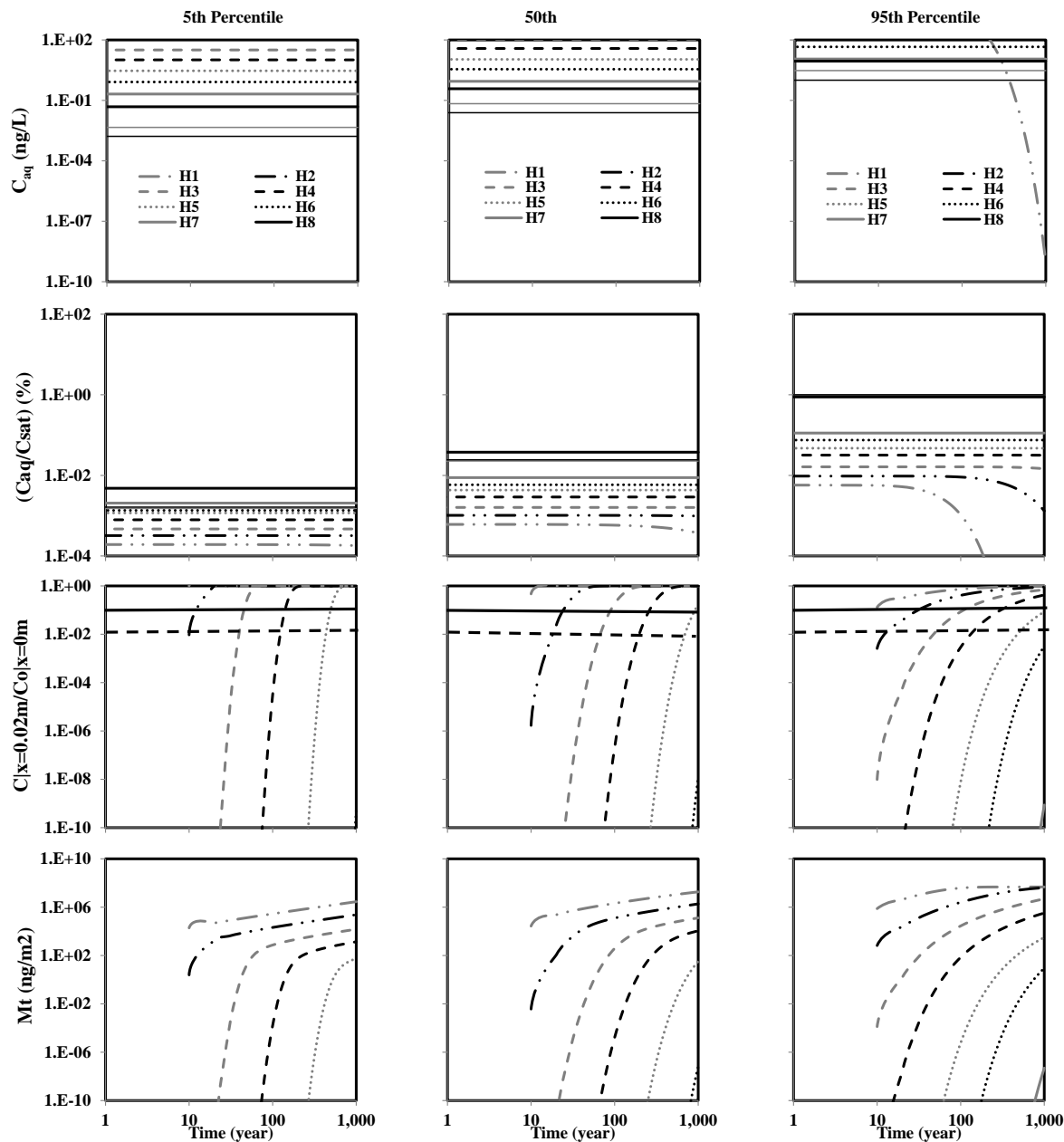


Figure D5.5az: Predicted PCB aqueous phase concentration under local equilibrium assumption (C_{aq}), ratio of aqueous phase concentration to saturation concentration (C_{aq}/C_{sat}), ratio of aqueous phase concentration at sediment boundary layer to homogeneous aqueous phase concentration ($C|x=0.02m/C|x=0m$), and mass leaving the sediment boundary layer (M_t) under advection-diffusion with organic carbon only sorption (A(OC)) shown in row1 through 4, respectively as predicted by the 5th, 50th, and 95th percentile transport parameters values shown in column 1 through 3, respectively in core CBC for 95th percentile initial concentration values (1640 ng/g).

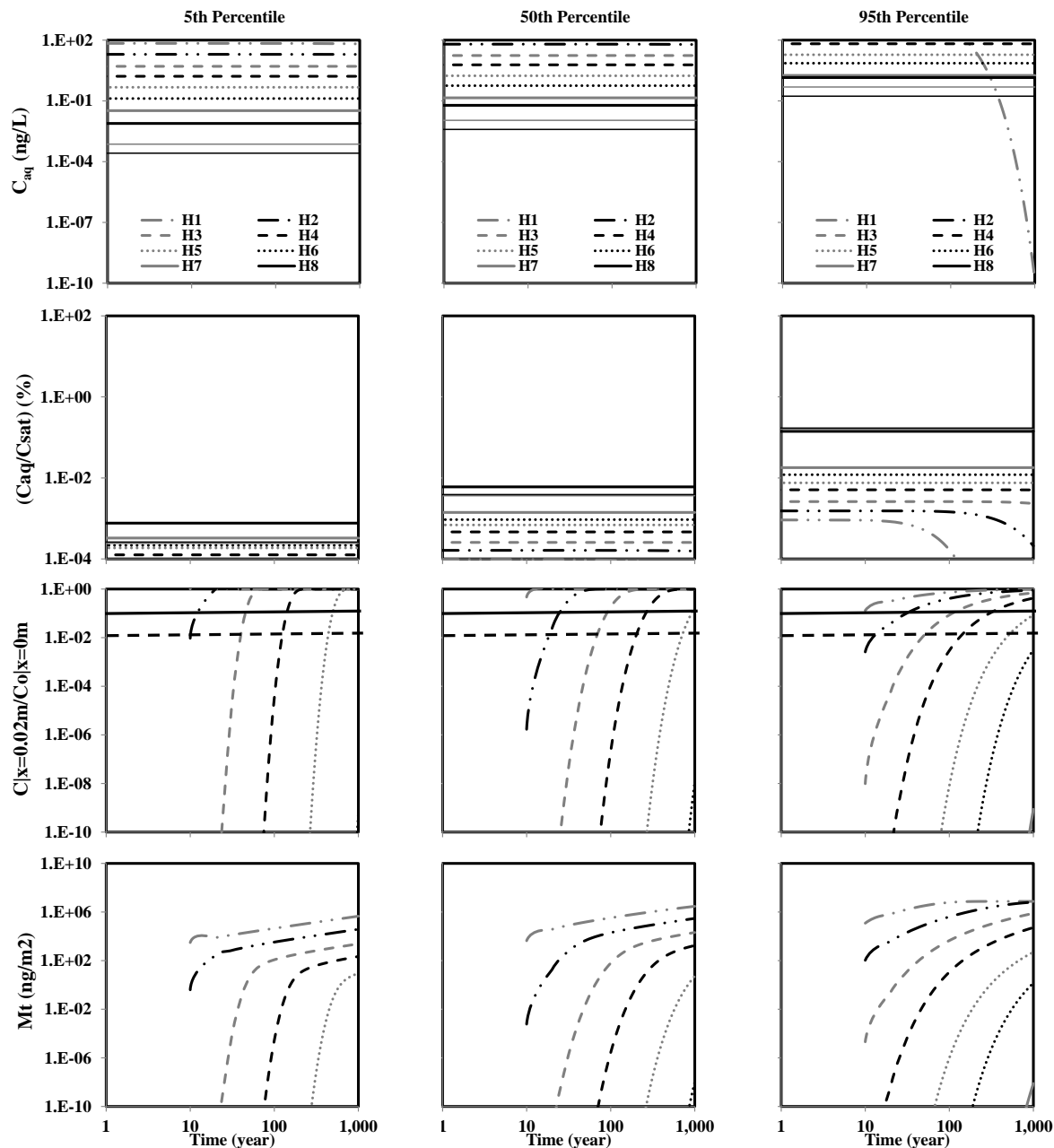


Figure D5.5ba: Predicted PCB aqueous phase concentration under local equilibrium assumption (C_{aq}), ratio of aqueous phase concentration to saturation concentration (C_{aq}/C_{sat}), ratio of aqueous phase concentration at sediment boundary layer to homogenous aqueous phase concentration ($C|x=0.02m/C|x=0m$), and mass leaving the sediment boundary layer (M_t) under advection-diffusion with organic carbon only sorption ($A(OC)$) shown in row1 through 4, respectively as predicted by the 5th, 50th, and 95th percentile transport parameters values shown in column 1 through 3, respectively in core CBC for 50th percentile initial concentration values (262 ng/g).

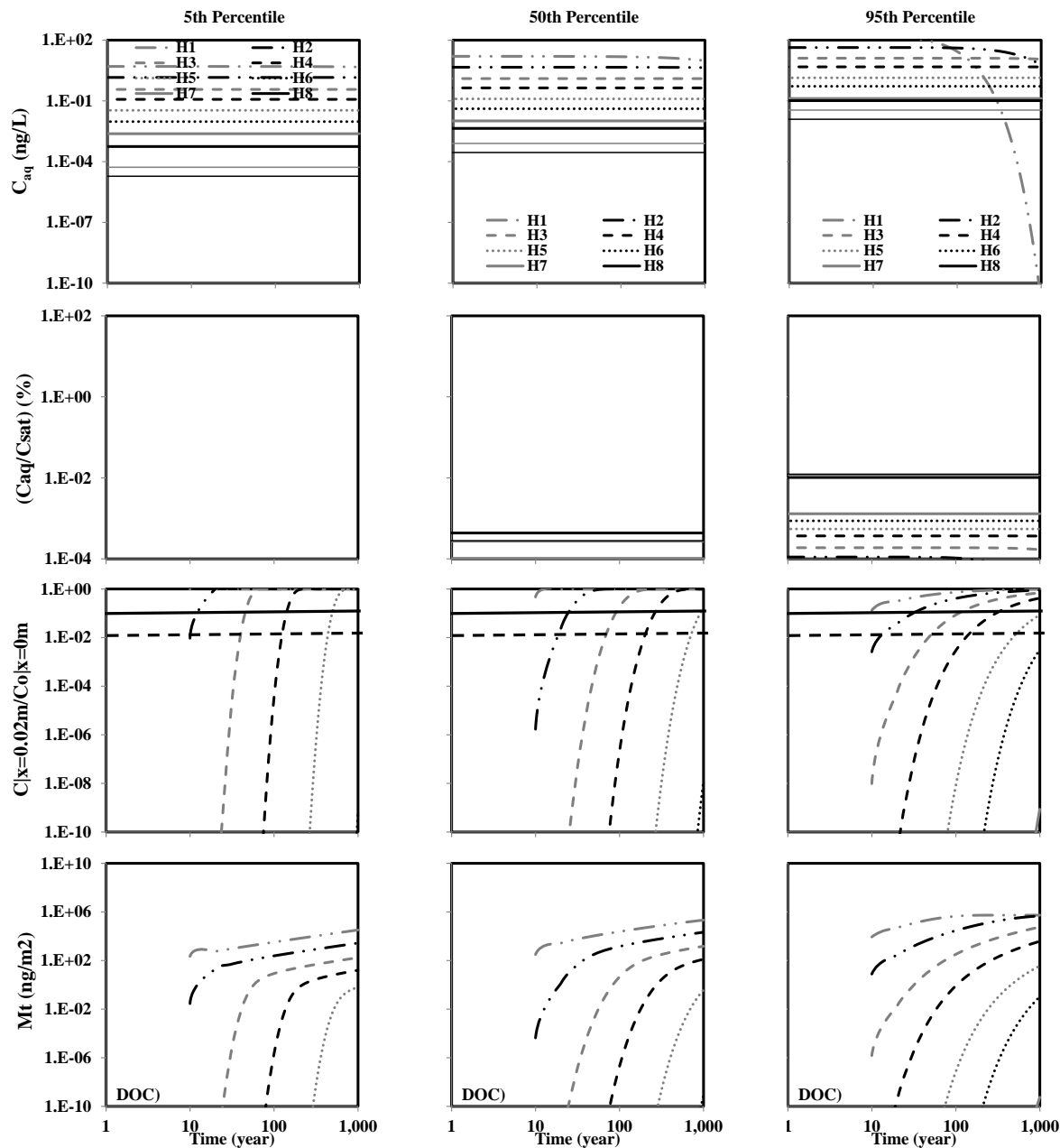


Figure D5.5bb: Predicted PCB aqueous phase concentration under local equilibrium assumption (C_{aq}), ratio of aqueous phase concentration to saturation concentration (C_{aq}/C_{sat}), ratio of aqueous phase concentration at sediment boundary layer to homogeneous aqueous phase concentration ($C|x=0.02m/C|x=0m$), and mass leaving the sediment boundary layer (M_t) under advection-diffusion with organic carbon only sorption ($A(OC)$) shown in row1 through 4, respectively as predicted by the 5th, 50th, and 95th percentile transport parameters values shown in column 1 through 3, respectively in core CBC for 5th percentile initial concentration values (19 ng/g).

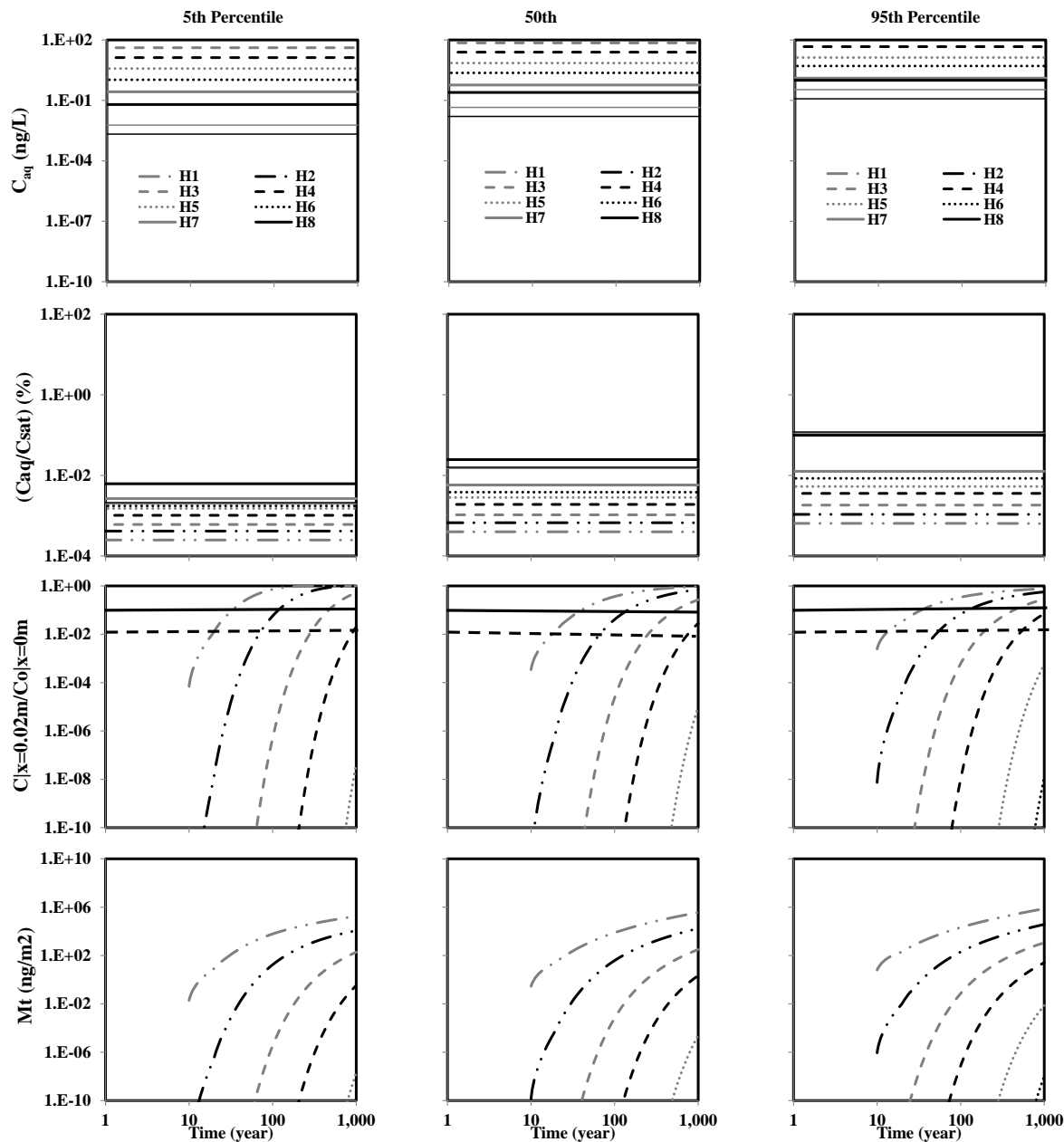


Figure D5.5bc: Predicted PCB aqueous phase concentration under local equilibrium assumption (C_{aq}), ratio of aqueous phase concentration to saturation concentration (C_{aq}/C_{sat}), ratio of aqueous phase concentration at sediment boundary layer to homogeneous aqueous phase concentration ($C|x=0.02m/C|x=0m$), and mass leaving the sediment boundary layer (M_t) under advection-diffusion with organic carbon only sorption ($A(OC)$) shown in row1 through 4, respectively as predicted by the 5th, 50th, and 95th percentile transport parameters values shown in column 1 through 3, respectively in core CLC for 95th percentile initial concentration values (1640 ng/g).

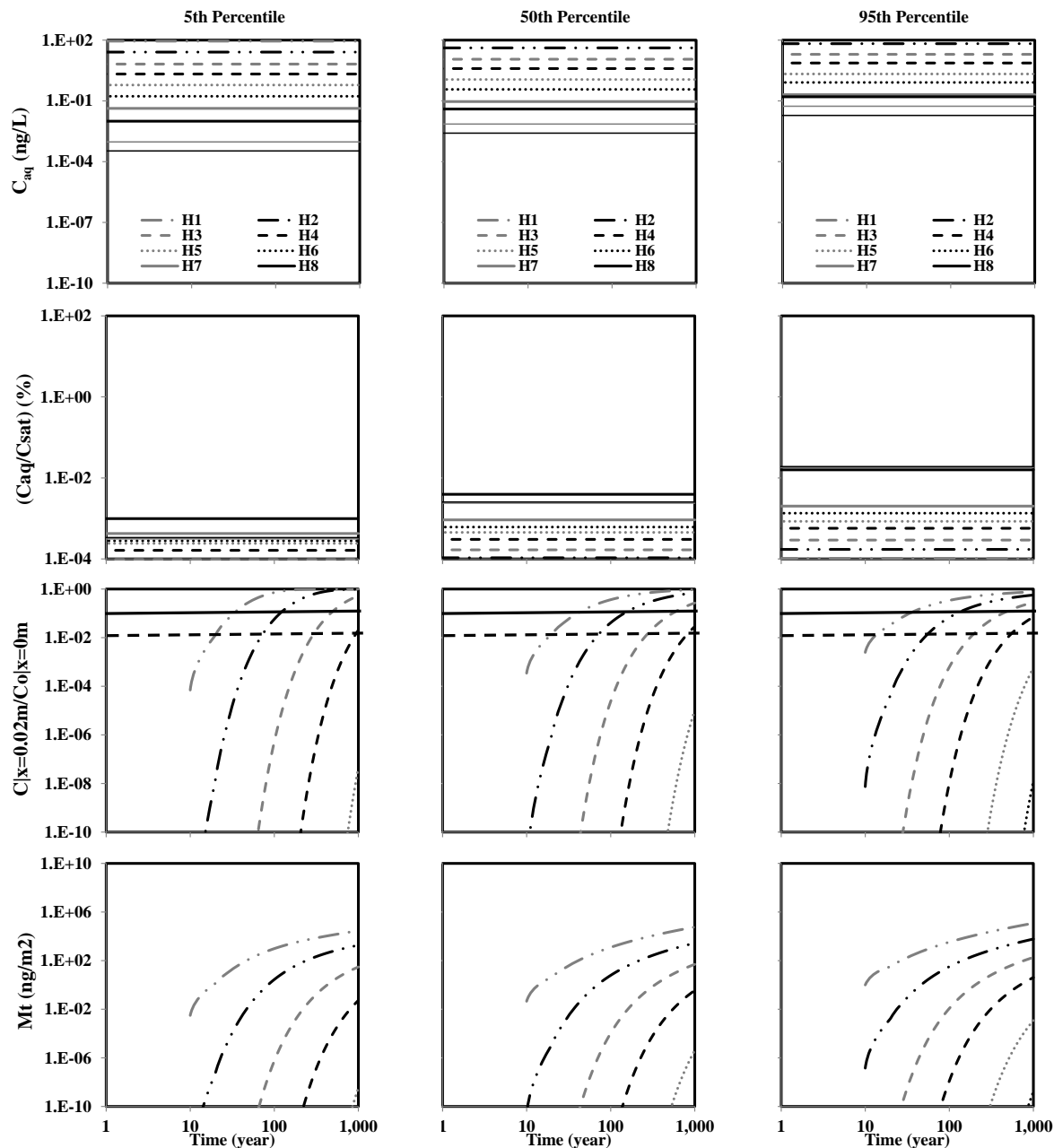


Figure D5.5bd: Predicted PCB aqueous phase concentration under local equilibrium assumption (C_{aq}), ratio of aqueous phase concentration to saturation concentration (C_{aq}/C_{sat}), ratio of aqueous phase concentration at sediment boundary layer to homogenous aqueous phase concentration ($C|x=0.02m/C|x=0m$), and mass leaving the sediment boundary layer (M_t) under advection-diffusion with organic carbon only sorption ($A(OC)$) shown in row1 through 4, respectively as predicted by the 5th, 50th, and 95th percentile transport parameters values shown in column 1 through 3, respectively in core CLC for 50th percentile initial concentration values (262 ng/g).

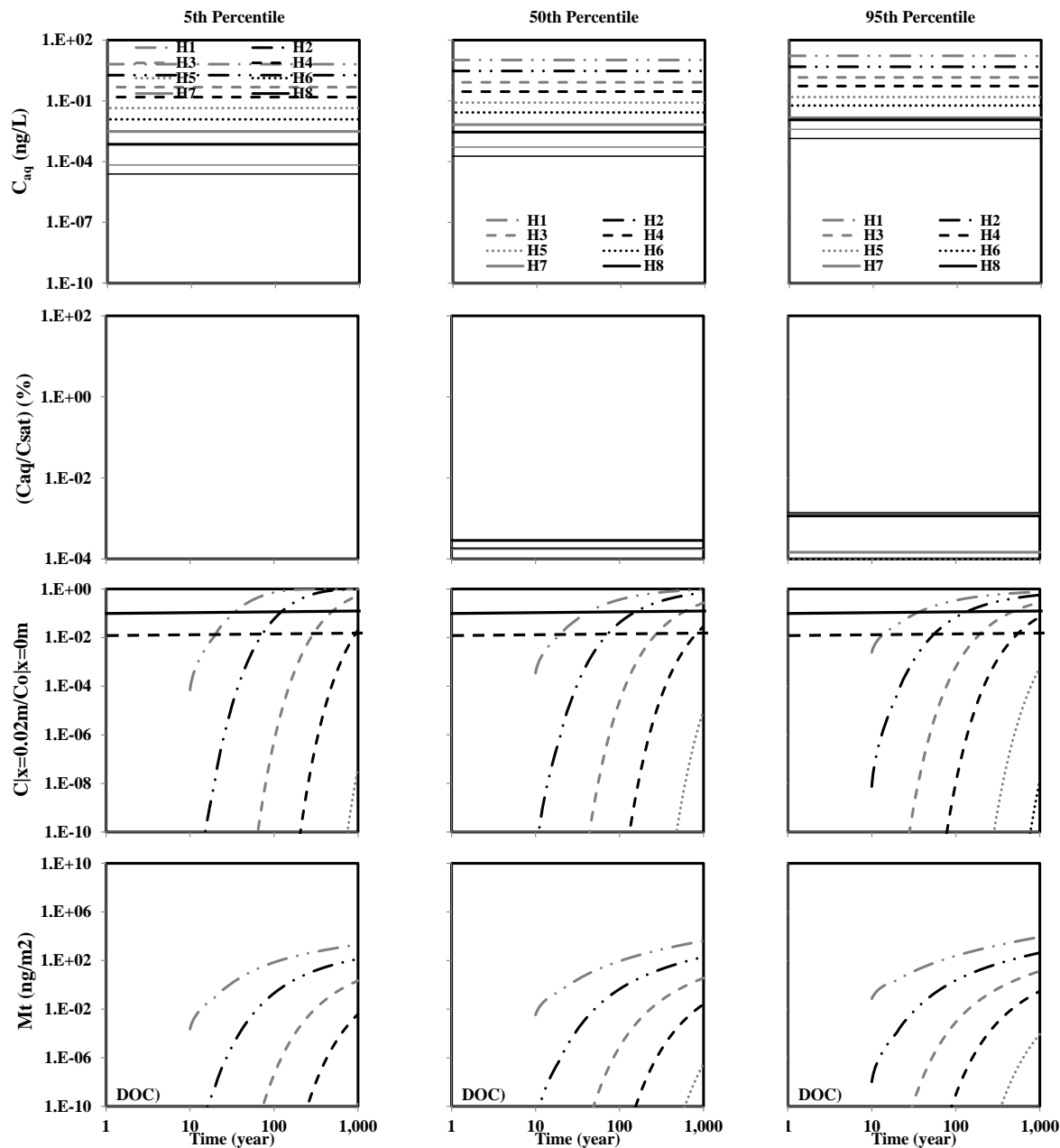


Figure D5.5be: Predicted PCB aqueous phase concentration under local equilibrium assumption (C_{aq}), ratio of aqueous phase concentration to saturation concentration (C_{aq}/C_{sat}), ratio of aqueous phase concentration at sediment boundary layer to homogenous aqueous phase concentration ($C|x=0.02m/C|x=0m$), and mass leaving the sediment boundary layer (M_t) under advection-diffusion with organic carbon only sorption ($A(OC)$) shown in row1 through 4, respectively as predicted by the 5th, 50th, and 95th percentile transport parameters values shown in column 1 through 3, respectively in core CLC for 5th percentile initial concentration values (19 ng/g).

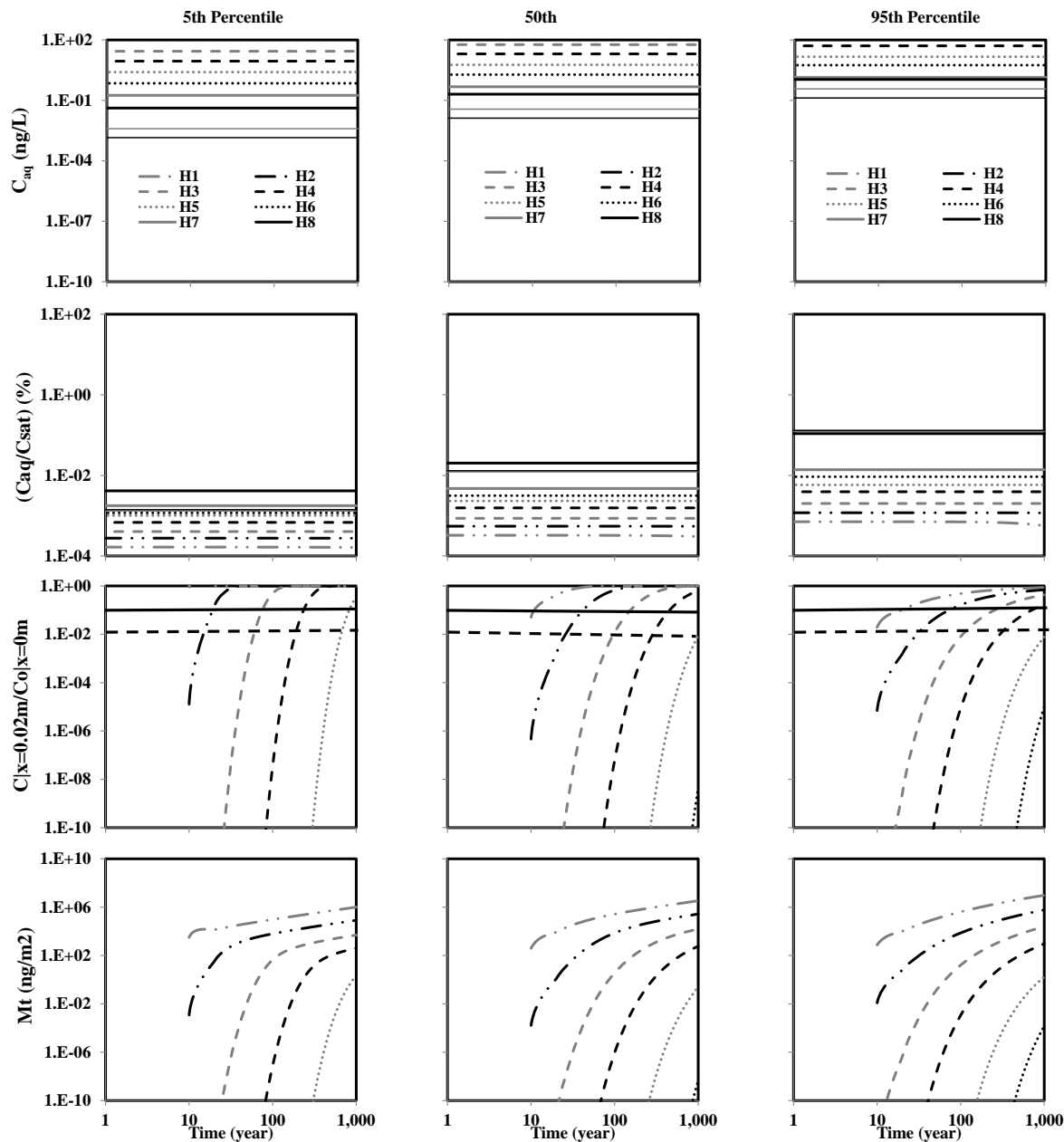


Figure D5.5bf: Predicted PCB aqueous phase concentration under local equilibrium assumption (C_{aq}), ratio of aqueous phase concentration to saturation concentration (C_{aq}/C_{sat}), ratio of aqueous phase concentration at sediment boundary layer to homogeneous aqueous phase concentration ($C|x=0.02m/C|x=0m$), and mass leaving the sediment boundary layer (M_t) under advection-diffusion with organic carbon only sorption (A(OC)) shown in row1 through 4, respectively as predicted by the 5th, 50th, and 95th percentile transport parameters values shown in column 1 through 3, respectively in core CWP for 95th percentile initial concentration values (1640 ng/g).

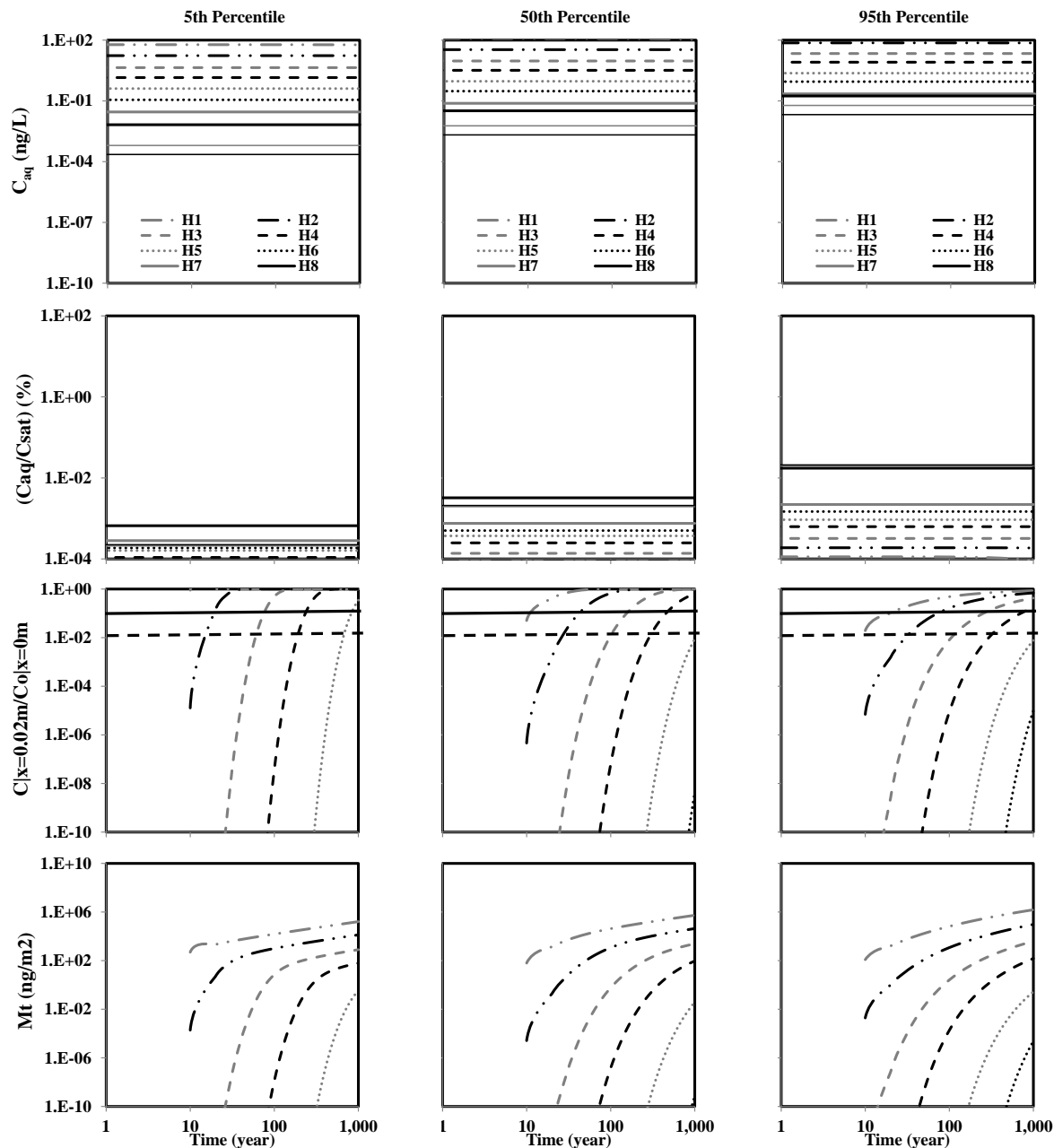


Figure D5.5bg: Predicted PCB aqueous phase concentration under local equilibrium assumption (C_{aq}), ratio of aqueous phase concentration to saturation concentration (C_{aq}/C_{sat}), ratio of aqueous phase concentration at sediment boundary layer to homogeneous aqueous phase concentration ($C|x=0.02m/C|x=0m$), and mass leaving the sediment boundary layer (M_t) under advection-diffusion with organic carbon only sorption (A(OC)) shown in row1 through 4, respectively as predicted by the 5th, 50th, and 95th percentile transport parameters values shown in column 1 through 3, respectively in core CWP for 50th percentile initial concentration values (262 ng/g).

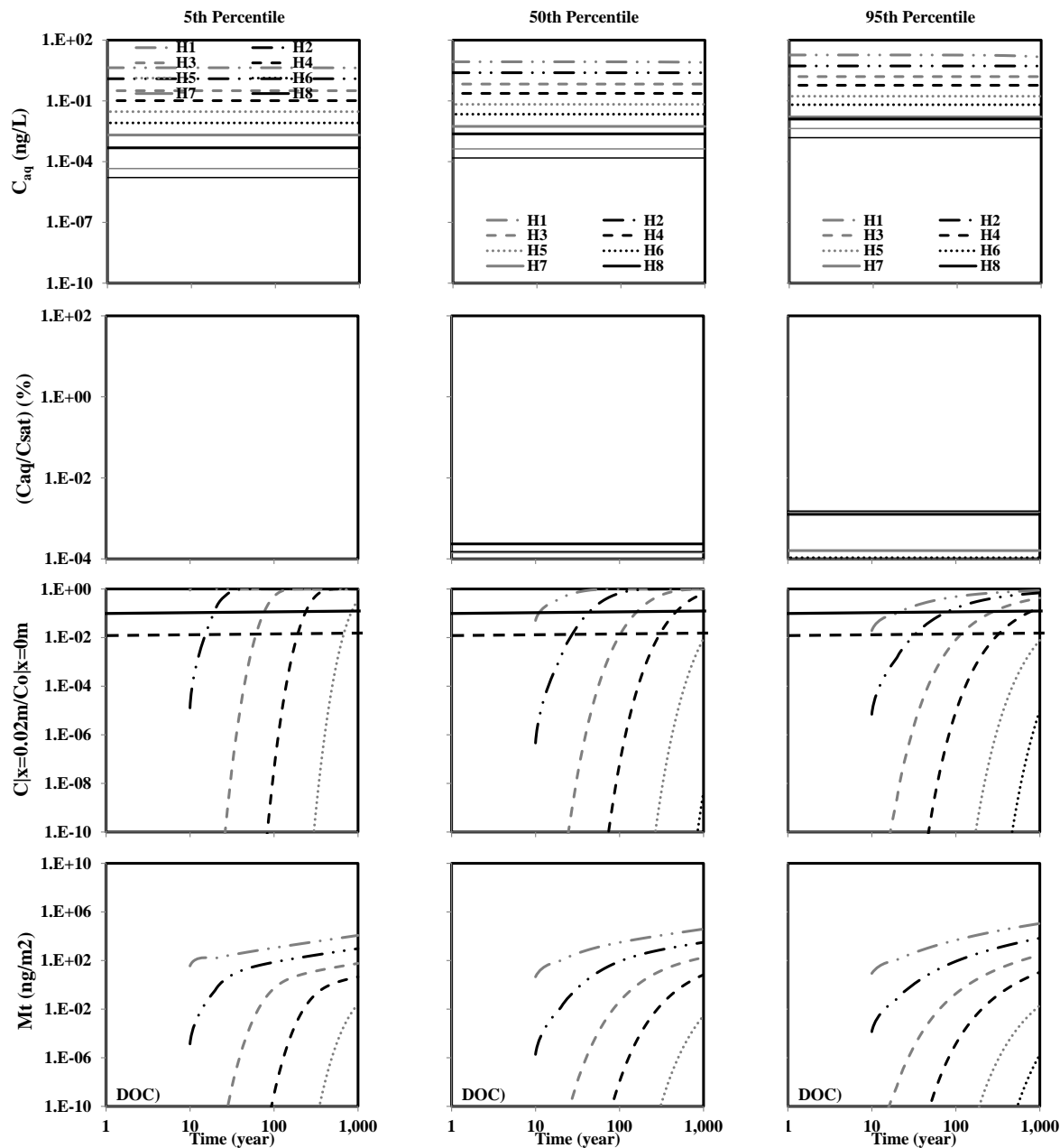


Figure D5.5bh: Predicted PCB aqueous phase concentration under local equilibrium assumption (C_{aq}), ratio of aqueous phase concentration to saturation concentration (C_{aq}/C_{sat}), ratio of aqueous phase concentration at sediment boundary layer to homogeneous aqueous phase concentration ($C|x=0.02m/C|x=0m$), and mass leaving the sediment boundary layer (M_t) under advection-diffusion with organic carbon only sorption ($A(OC)$) shown in row1 through 4, respectively as predicted by the 5th, 50th, and 95th percentile transport parameters values shown in column 1 through 3, respectively in core CWP for 5th percentile initial concentration values (19 ng/g).

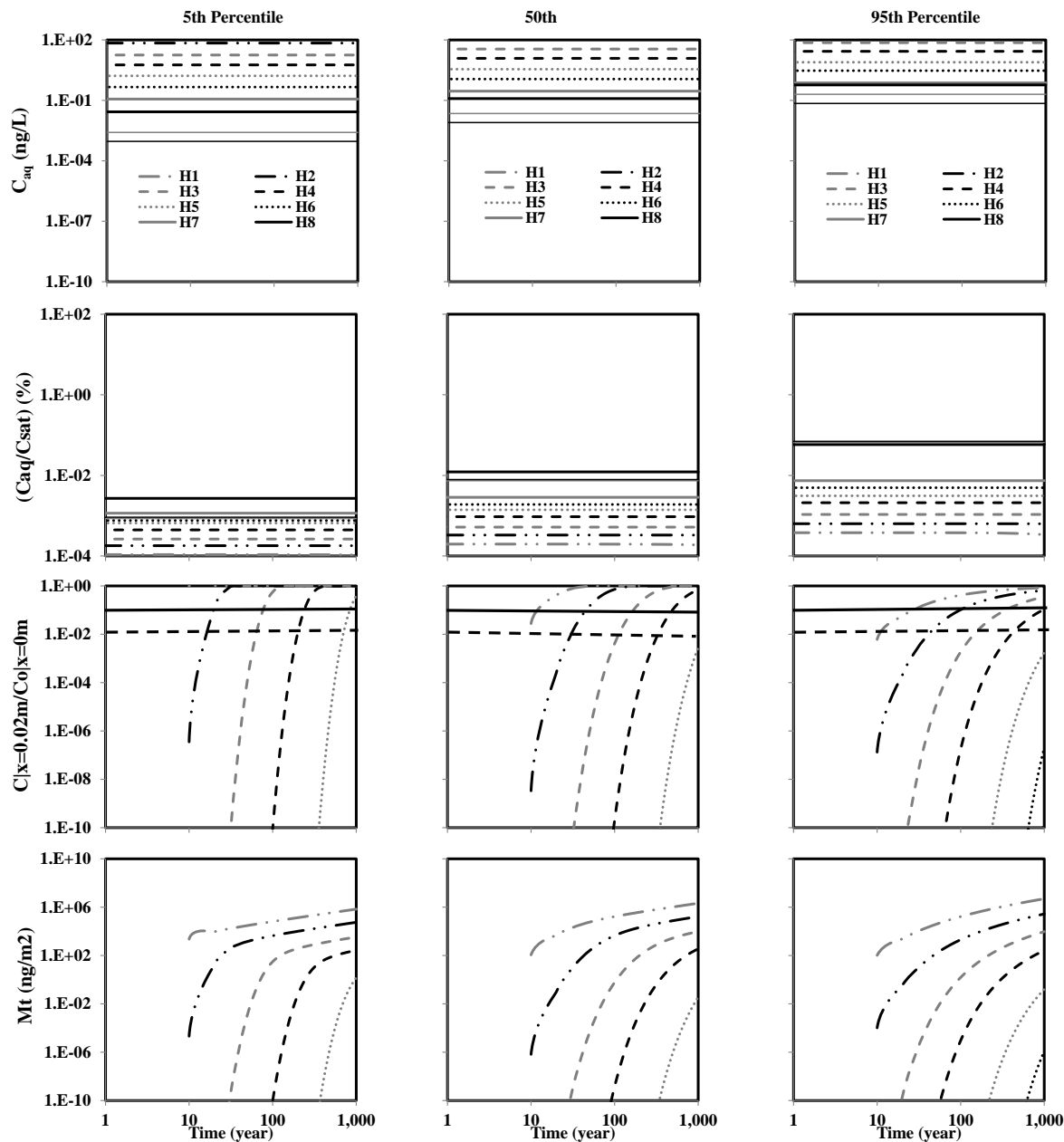


Figure D5.5bi: Predicted PCB aqueous phase concentration under local equilibrium assumption (C_{aq}), ratio of aqueous phase concentration to saturation concentration (C_{aq}/C_{sat}), ratio of aqueous phase concentration at sediment boundary layer to homogeneous aqueous phase concentration ($C|x=0.02m/C|x=0m$), and mass leaving the sediment boundary layer (M_t) under advection-diffusion with organic carbon only sorption ($A(OC)$) shown in row1 through 4, respectively as predicted by the 5th, 50th, and 95th percentile transport parameters values shown in column 1 through 3, respectively in core IGC09 for 95th percentile initial concentration values (1640 ng/g).

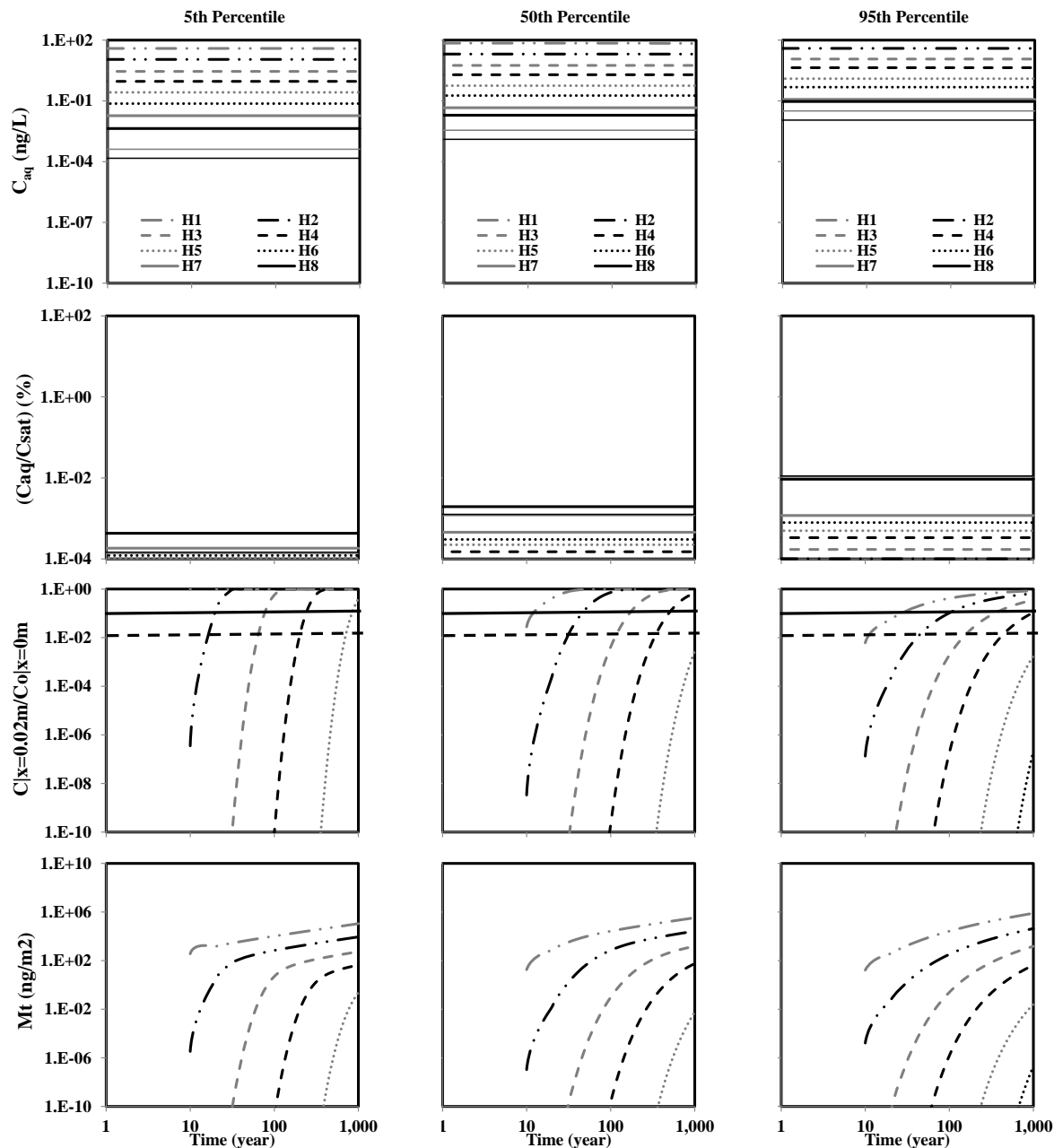


Figure D5.5bj: Predicted PCB aqueous phase concentration under local equilibrium assumption (C_{aq}), ratio of aqueous phase concentration to saturation concentration (C_{aq}/C_{sat}), ratio of aqueous phase concentration at sediment boundary layer to homogenous aqueous phase concentration ($C|x=0.02m/C|x=0m$), and mass leaving the sediment boundary layer (M_t) under advection-diffusion with organic carbon only sorption ($A(OC)$) shown in row1 through 4, respectively as predicted by the 5th, 50th, and 95th percentile transport parameters values shown in column 1 through 3, respectively in core IGC09 for 50th percentile initial concentration values (262 ng/g).

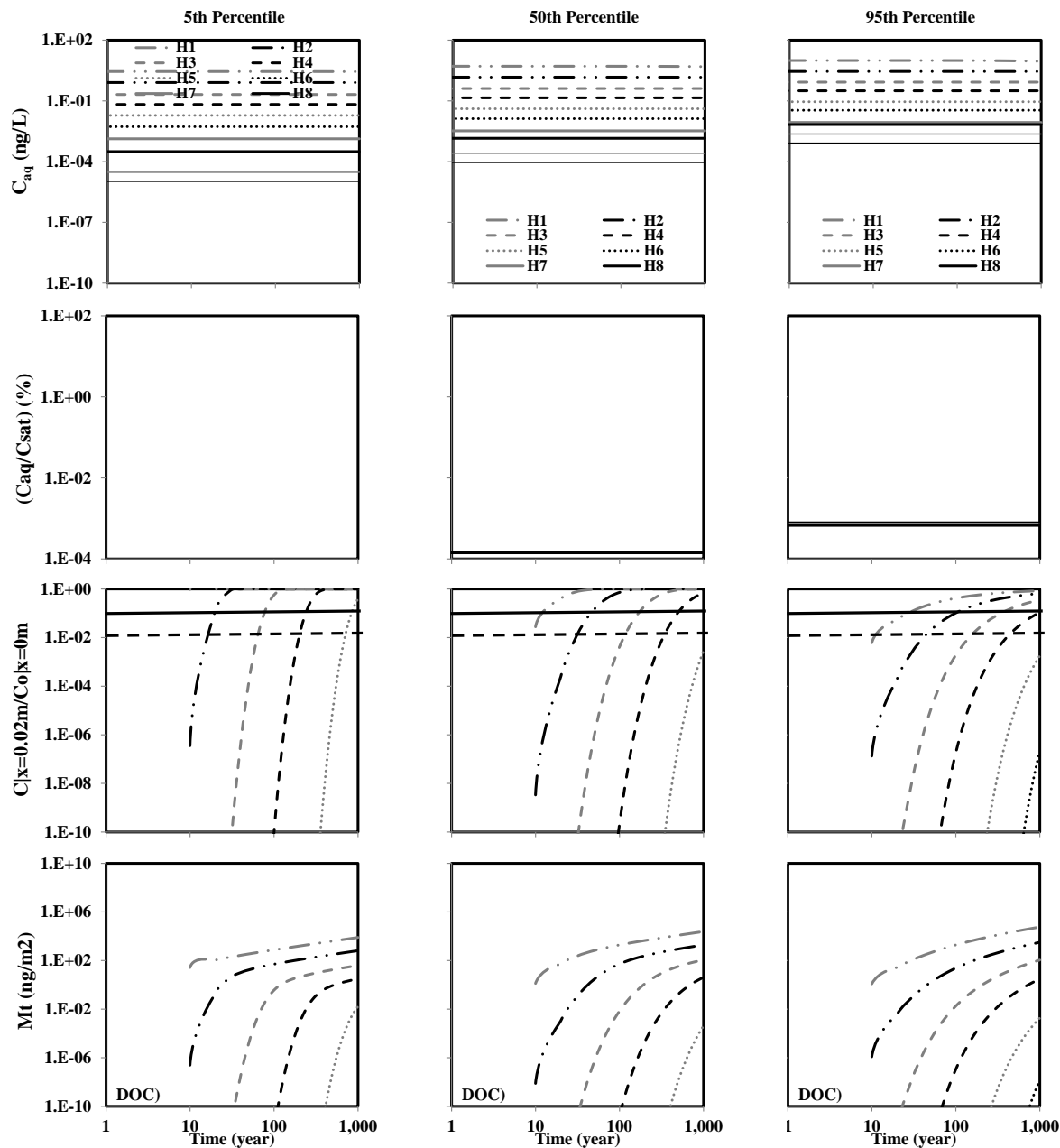


Figure D5.5bk: Predicted PCB aqueous phase concentration under local equilibrium assumption (C_{aq}), ratio of aqueous phase concentration to saturation concentration (C_{aq}/C_{sat}), ratio of aqueous phase concentration at sediment boundary layer to homogeneous aqueous phase concentration ($C|x=0.02m/C|x=0m$), and mass leaving the sediment boundary layer (M_t) under advection-diffusion with organic carbon only sorption ($A(OC)$) shown in row1 through 4, respectively as predicted by the 5th, 50th, and 95th percentile transport parameters values shown in column 1 through 3, respectively in core IGC09 for 5th percentile initial concentration values (19 ng/g).

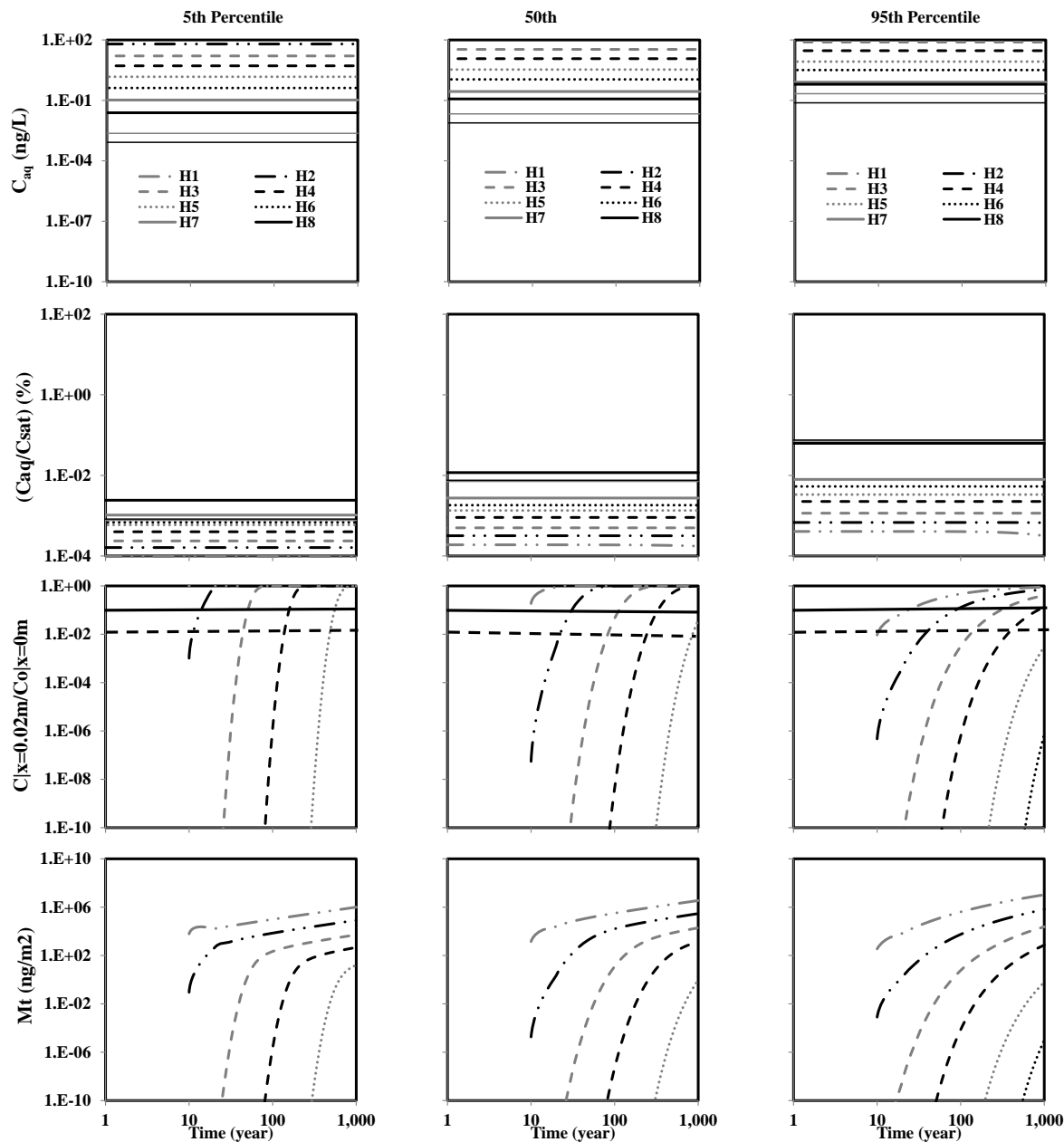


Figure D5.5bl: Predicted PCB aqueous phase concentration under local equilibrium assumption (C_{aq}), ratio of aqueous phase concentration to saturation concentration (C_{aq}/C_{sat}), ratio of aqueous phase concentration at sediment boundary layer to homogeneous aqueous phase concentration ($C|x=0.02m/C|x=0m$), and mass leaving the sediment boundary layer (M_t) under advection-diffusion with organic carbon only sorption (A(OC)) shown in row1 through 4, respectively as predicted by the 5th, 50th, and 95th percentile transport parameters values shown in column 1 through 3, respectively in core IGC13 for 95th percentile initial concentration values (1640 ng/g).

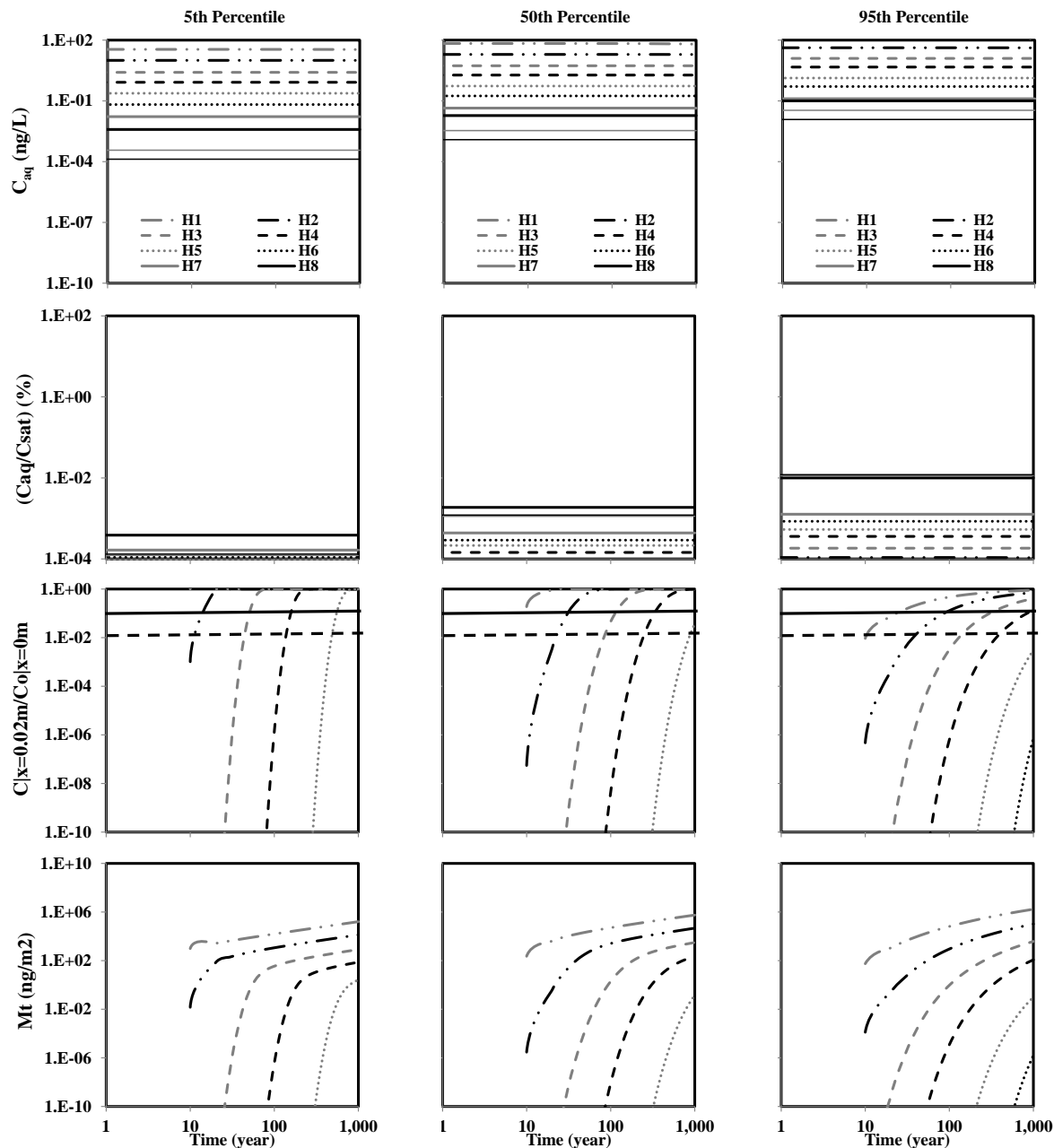


Figure D5.5bm: Predicted PCB aqueous phase concentration under local equilibrium assumption (C_{aq}), ratio of aqueous phase concentration to saturation concentration (C_{aq}/C_{sat}), ratio of aqueous phase concentration at sediment boundary layer to homogeneous aqueous phase concentration ($C|x=0.02m/C|x=0m$), and mass leaving the sediment boundary layer (M_t) under advection-diffusion with organic carbon only sorption (A(OC)) shown in row1 through 4, respectively as predicted by the 5th, 50th, and 95th percentile transport parameters values shown in column 1 through 3, respectively in core IGC13 for 50th percentile initial concentration values (262 ng/g).

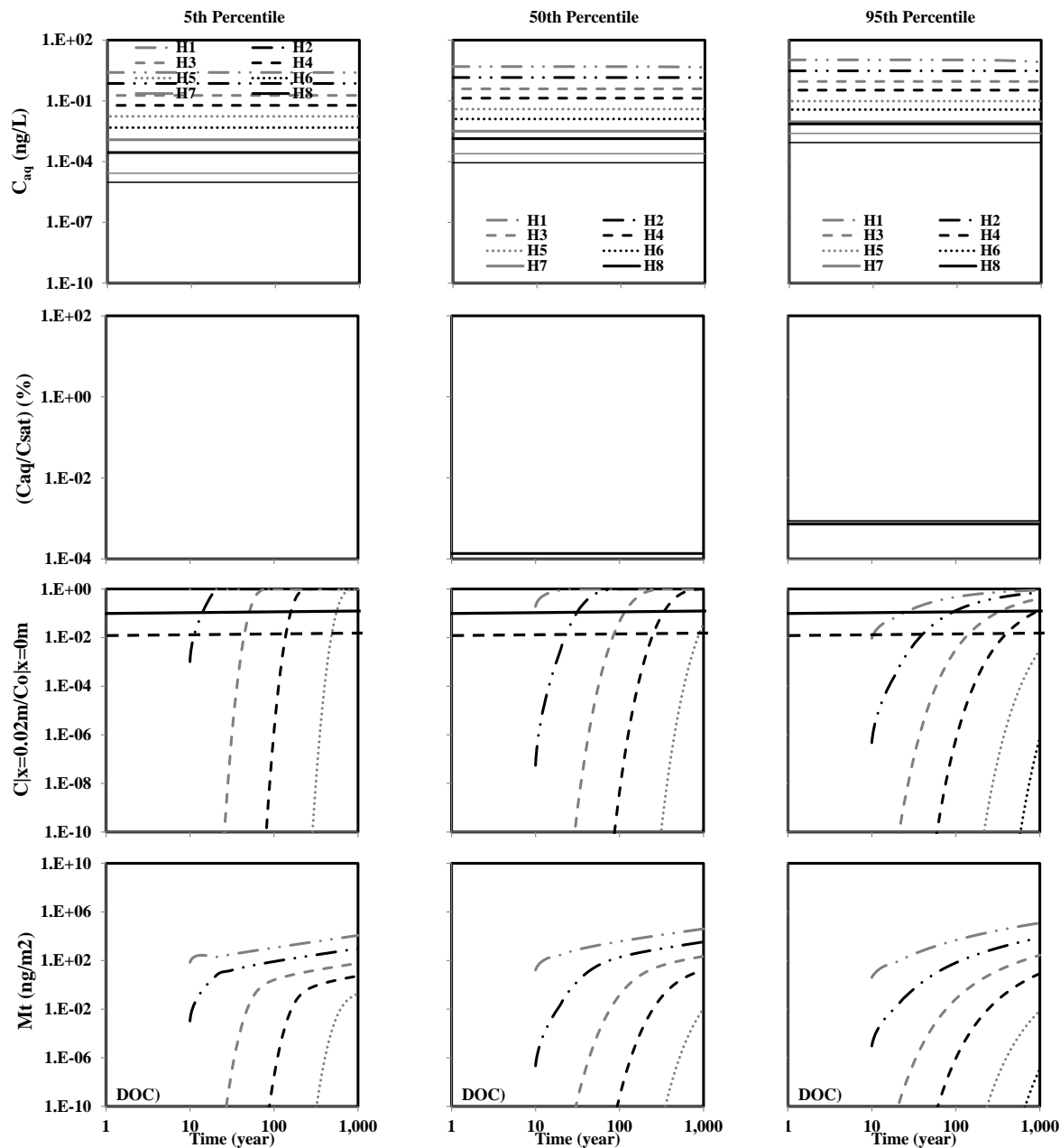


Figure D5.5bn: Predicted PCB aqueous phase concentration under local equilibrium assumption (C_{aq}), ratio of aqueous phase concentration to saturation concentration (C_{aq}/C_{sat}), ratio of aqueous phase concentration at sediment boundary layer to homogeneous aqueous phase concentration ($C|x=0.02m/C|x=0m$), and mass leaving the sediment boundary layer (M_t) under advection-diffusion with organic carbon only sorption ($A(OC)$) shown in row1 through 4, respectively as predicted by the 5th, 50th, and 95th percentile transport parameters values shown in column 1 through 3, respectively in core IGC13 for 5th percentile initial concentration values (19 ng/g)

CURRICULUM VITAE

Azivy Che Aziz

526 Michigan Avenue, 2N, Evanston, IL 60202
Cell Number: 224-422-0625; Email: acheaz2@uic.edu

EDUCATION

University of Illinois in Chicago (January 2009 to current)

PhD in Civil Engineering, Environmental and Water Resources Program (Expected Graduation: May 2014, CGPA: 4.00/4.00)

MS in Civil Engineering, Environmental and Water Resources Program (Dec 2011, CGPA: 4.00/4.00)

- 2011 Christopher B. and Susan S. Burke Civil Engineering Professional Advisory Council Award.
- 2010 Illinois Section American Society of Civil Engineers for the Environmental Engineering and Water Resources Technical Group Student Scholarship Award.

University of Wisconsin - Madison (August 2003 to December 2007)

BS in Chemical Engineering (Dec 2007, CGPA: 3.62/4.00)

- Majlis Amanah Rakyat (MARA) Malaysia Full Scholarship for Undergraduate Study.
- Kowalke-Harr Award For Teamwork in Operations and Process Laboratory, Chemical and Biological Engineering Department - University of Wisconsin-Madison.
- Dean's Honor List in the Chemical and Biological Engineering Department - University of Wisconsin-Madison.

WORK EXPERIENCE

Environmental Technology Internship (Jun 2012 to current) ExxonMobil Upstream Research Company, Safety, Health and Environment Function-Houston, TX.

- Streamlined an ecosystem services framework to systematically identify region-specific environmental sensitivities and assessed framework efficacy in addressing diverse operating environments.
- Adapted evaluation methodology to optimize framework benefits to augment and inform existing environmental risk management structure.
- Evaluated opportunity to integrate stakeholder engagement methodology into framework through pilot study with simulated stakeholder group of regulatory agencies, non-government organizations and industries representatives.
- Demonstrated ecosystem services framework capability through assessment of realistic operating scenarios case studies to internal clients by leading an informational workshop.
- Published newsletter article to promote ecosystem services framework utility in facilitating different business needs to meet increasing and evolving environmental regulatory expectations.

Graduate Research Assistant (Jan 2009 to current) Applied Environmental and Biotechnology Laboratory, Civil and Materials Engineering Department - University of Illinois in Chicago.

- Coordinated logistic arrangement with the Arkansas Department of Environmental Quality for a 10 days sampling trip in El Dorado and Little Rock, AR.
- Researched and performed physical, chemical and biological characterization of sediment and water samples impacted by flame retardants. Applied environmental forensic techniques to identify 'contaminant fingerprints'. Self-taught 2 statistical software (SPSS and ORIGIN) and programming language (PERL) to aid large volume data analysis.
- Provided visual and graphical aid to interpret research data by incorporating NOAA wind monitoring data into ArcGIS to map atmospheric deposition route
- Wrote technical manuals and standard operating procedures documents for the operations, maintenance and troubleshooting of the CE Elantech Flash EA1112 Elemental Analyzer and Dionex

IC25 Anion Chromatograph units. Led the analysis software upgrade and provided technical assistance for chromatograms interpretation.

- Prepared proposal manuscripts, budget plans, annual reports and papers for funding organizations and publications in peer reviewed journals.
- **Chemical Hygiene Officer (May 2011 to June 2012) Applied Environmental and Biotechnology Laboratory, Civil and Materials Engineering Department - University of Illinois in Chicago.**
- Volunteered to obtain certification for Occupational Safety and Health Administration general industry training (OSHA 10). Completed annual Laboratory Safety and Chemical Waste Management training, and Hazardous Material Shipping and Receiving certifications.
- Ensure laboratory personnel comply with laboratory safety regulations, maintain chemical inventory, update material safety datasheet information and track delivery of hazardous chemicals.
- Liaison with the Environmental Health and Safety Office on hazardous waste removal from satellite area and safety training for laboratory personnel. Initiated laboratory participation in the Chemical Redistribution Program to minimize waste from unused chemical agents.

Undergraduate Research Assistant (August 2006 to December 2007). Civil and Environmental Engineering Department - University of Wisconsin-Madison.

- Quantified microbial antibiotic resistance genes in water samples by performing DNA extraction and amplification (PCR and qPCR).
- Independently developed analytical methods for DNA extraction from fish food pellets. Contribution acknowledged in publication.

Wastewater Engineering Intern (May 2005 to August 2005) Indah Water Konsortium, Malaysia.

- Investigated feasible methods to transport municipal wastewater from a newly developed residential area in rural Malaysia. Recommended two methods based on financial considerations, ease of implementation and company's available technical resources.
- Evaluated the long term sustainability by assessing environmental and community impact of both methods using life cycle analysis method.
-

Staff Consultant (May 2004 to August 2005) Academic and Computer Resources - University of Wisconsin-Madison.

- Assisted students with hardware and software related problems in university computer facilities.
- Organized the Peer Education Program by matching qualified tutors in the Science, Technology and Mathematics subjects to prospective students.

TEACHING EXPERIENCE

Teaching Assistant (Spring 2009, Fall 2011, Spring 2012). Civil and Materials Engineering Department - University of Illinois in Chicago.

- Conducted 3 fluid dynamics laboratory sessions per week for 60 students. Graded and provided constructive feedbacks on technical laboratory reports. Aided 60 senior civil engineering designed final year projects reviewed at the University of Illinois Chicago Research Forum.
- Developed lecture plans (notes, assignment and short projects) to aid students in the application of advanced Excel and SYSTAT for multidisciplinary engineering design project.

Substitute Teacher (May 2005 to August 2005). Setiu High School - Kuala Terengganu, Malaysia.

- Taught trigonometry and English courses to 4 classes of approximately 30 students each.
- Coordinated English Language Week. Incorporated students' theatrical performances to encourage conversation in English.

VOLUNTEER EXPERIENCE

Graduate Student Council Representative and Steward for the Civil and Materials Engineering Department (2011 to June 2012) University of Illinois in Chicago.

- Resolved graduate students related issues such as employment, campus safety and commuting. Communicated information on travel grants, project awards and social outreach activities from the Graduate College.

Mentor for the local chapter of Women in Science and Engineering and Society of Women Engineers (2010 to June 2012) University of Illinois in Chicago.

- Advised Civil Engineering undergraduates on available career track options after graduation.
- Promoted available undergraduate research opportunities in the department.

COMPUTER SKILLS

EES, Maple, Mathlab, MS Office, ORIGIN, Perl, R, SPSS, SYSTAT, ArcGIS.

PROFESSIONAL MEMBERSHIPS

Society of Women Engineers, Women In Science and Engineering, American Society of Civil Engineers, Water Environment Federation, American Society of Chemical Engineers.

PUBLICATION/PRESENTATION

Wei, H.; Aziz-Schwanbeck, A.; You, Z.; Corcoran, M.; Poghosyan, A.; Li, A.; Rockne, K.J.; Christensen, E.R. and Sturchio, N.C. (2012) Polybromodiphenyl Ethers and Decabromodiphenyl Ethane in Aquatic Sediments from Southern and Eastern Arkansas, United States. Environmental Science and Technology, 46(15),pp 8017-8024.

Aziz, A.; Rockne, K.J.; Christensen, E.R.; Li, A. and Wei, H. (2011) Sediment Physical Characteristics as a Biological Indicator for Microbial Reductive Debromination of Polybrominated Diphenyl Ethers (PBDEs) . Batelle Sixth International Conference On Remediation of Contaminated Sediments, New Orleans, February 7-10.

Zou, Y.; Christensen, E.R.; Li,A.; Wei, H.,Rockne, KJ and Aziz, A. (2011) Polybrominated Diphenyl Ethers Sources in Sediments of Bubbly Creek and Calumet Pond , Chicago Determined by Positive Matrix Factorization. Batelle Sixth International Conference On Remediation of Contaminated Sediments, New Orleans, February 7-10.

Aziz, A.; Granberg, K.J. and Rockne, K.J (2010) Sources, Releases, and Fate of the Emerging Pollutant Polybrominated Diphenyl Ethers (PBDEs) in Urban Aquatic Systems In: Summit Conference National Academy of Engineers. April 21st 2010.

Aziz, A.; Granberg, K.J. and Rockne, K.J (2010) Sources, Releases, and Fate of the Emerging Pollutant Polybrominated Diphenyl Ethers (PBDEs) in Urban Aquatic Systems In: Summit Conference National Academy of Engineers. April 21st 2010.

Aziz, A.; Granberg, K.J. and Rockne, K.J. (2010) Sources, Releases, and Fate of the Emerging Pollutant Polybrominated Diphenyl Ethers (PBDEs) in Urban Aquatic Systems In: University of Illinois at Chicago Student Research Forum. April 20th 2010.

Li,A.; Rockne, K.J.; Wei, H. and Aziz, A. (2010). Year-2 Progress Report. Collaborative Research: Debromination of PBDEs in Aquatic Sediments. Submitted to NSF. February 13,2010.

Li,A.; Rockne, K.J.; Wei, H. and Aziz, A. (2009). Year-1 Progress Report. Collaborative Research: Debromination of PBDEs in Aquatic Sediments. Submitted to NSF. February 13,2009.

Li,A.; Wei, H.; Aziz, A.;Rockne, K.J. , Christensen,E.R.; Sturchio,N.; Sietsema, M.; Wang,Y. and Jiang, G.(2009). Long Term Variation of PBDE Congener Pattern in Aquatic Sediments and its Implications. The Society of Environmental Toxicology and Chemistry (SETAC) North America Annual Meeting. New Orleans, November 19-23, 2009.

Christensen,E.R.; Zou,Y.;Li,A.;Rockne,K.J.; Wei, H. and Aziz, A. (2008) Modellling PAH, PCB, and PBDE Sources And Degradation In Aquatic Sediments Based On Factor Analysis With Nonnegative Constraints. Proceedings, International Conference On Water Scarcity, Global Changes, and Groundwater Management Responses. December 1-5, Irvine, CA.

